Green Energy and Technology



S. Sumathi
L. Ashok Kumar
P. Surekha

Solar PV and Wind Energy Conversion Systems

An Introduction to Theory, Modeling with MATLAB/SIMULINK, and the Role of Soft Computing Techniques

Springer

Green Energy and Technology

More information about this series at http://www.springer.com/series/8059

S. Sumathi • L. Ashok Kumar • P. Surekha

Solar PV and Wind Energy Conversion Systems

An Introduction to Theory, Modeling with MATLAB/SIMULINK, and the Role of Soft Computing Techniques

Springer

S. Sumathi
Electrical and Electronics Engineering
PSG College of Technology
Coimbatore, Tamil Nadu, India

L. Ashok Kumar
Electrical and Electronics Engineering
PSG College of Technology
Coimbatore, Tamil Nadu, India

P. Surekha
Electrical and Electronics Engineering
PES University
Bangalore, Karnataka, India

ISSN 1865-3529 ISSN 1865-3537 (electronic)
Green Energy and Technology
ISBN 978-3-319-14940-0 ISBN 978-3-319-14941-7 (eBook)
DOI 10.1007/978-3-319-14941-7

Library of Congress Control Number: 2015930263

Springer Cham Heidelberg New York Dordrecht London
© Springer International Publishing Switzerland 2015
This work is subject to copyright. All rights are reserved by the Publisher, whether the whole or part of the material is concerned, specifically the rights of translation, reprinting, reuse of illustrations, recitation, broadcasting, reproduction on microfilms or in any other physical way, and transmission or information storage and retrieval, electronic adaptation, computer software, or by similar or dissimilar methodology now known or hereafter developed.
The use of general descriptive names, registered names, trademarks, service marks, etc. in this publication does not imply, even in the absence of a specific statement, that such names are exempt from the relevant protective laws and regulations and therefore free for general use.
The publisher, the authors and the editors are safe to assume that the advice and information in this book are believed to be true and accurate at the date of publication. Neither the publisher nor the authors or the editors give a warranty, express or implied, with respect to the material contained herein or for any errors or omissions that may have been made.

Printed on acid-free paper

Springer International Publishing AG Switzerland is part of Springer Science+Business Media (www.springer.com)

Preface

Solar PV and wind energy is an integral part of different renewable energy resources, in general, and, in particular, it is the main and continuous input variable from the practically inexhaustible sun. Solar energy is expected to play a very significant role in the future especially in developing countries, but it also has potential in developed countries. Over the past few years, wind energy has shown the fastest rate of growth of any form of electricity generation with its development stimulated by concerns of national policy makers over climate change, energy diversity and security of supply. The material presented in this book has been chosen to provide a comprehensive account of solar energy modeling methods based on MATLAB/SIMULINK.

The book is intended for later year undergraduate, post-graduate and research students interested in understanding the modeling and control of large wind turbine generators based on MATLAB/SIMULINK. It starts with a review of the principles of operation, modeling and control of the common solar energy and wind generation systems and then moves on to discuss grid compatibility, power quality issues and hybrid models of solar PV and Wind Energy Conversion Systems. MATLAB/SIMULINK models of fuel cell technology and their converters are discussed in detail. The impact of soft computing techniques such as neural networks, fuzzy logic, and genetic algorithms in the area of solar and wind energy is explained with practical implementation using MATLAB/SIMULINK models.

Coimbatore, India S. Sumathi

Acknowledgement

The authors are always thankful to the Almighty for perseverance and achievements.

The authors owe their gratitude to Mr. L. Gopalakrishnan, Managing Trustee, PSG Institutions, and Dr. R. Rudramoorthy, Principal, PSG College of Technology, Coimbatore, for their whole-hearted cooperation and great encouragement given in this successful endeavour.

Dr. Sumathi owes much to her daughter, S. Priyanka, who has helped a lot in monopolizing her time on book work and substantially realized the responsibility. She feels happy and proud for the steel frame support rendered by her husband, Mr. Sai Vadivel. Dr. Sumathi would like to extend whole-hearted thanks to her parents who have reduced the family commitments and for their constant support. She is greatly thankful to her brother Mr. M. S. Karthikeyan who has always been a "Stimulator" for her progress. She is pertinent in thanking her parents-in-laws for their great moral support.

Dr. L. Ashok Kumar would like to take this opportunity to acknowledge those people who helped me in completing this book. This book would not have come to its completion without the help of my students, my department staff and my institute. My sincere gratitude and thanks are due to our Management and to our Principal Dr. R. Rudramoorthy for providing me such a wonderful platform to perform. I am thankful to all my students who are doing their project and research work with me. But the writing of this book is greatly possible mainly because of the support of my family members, parents and sisters.

Most importantly, I am very grateful to my wife, Y. Uma Maheswari, for her constant support during writing, and without her all these things would not be possible. I would like to express my special gratitude to my daughter, A. K. Sangamithra, for her smiling face and support, this helped a lot in completing this book work even there is any backlog and the writing of this book has taken a significant amount of my play time with her.

Dr. P. Surekha would like to thank her parents, husband, Mr. A. Srinivasan, and daughter, Baby. S. Saisusritha, who shouldered a lot of extra responsibilities during the months this was being written. They did this with the long-term vision, depth of character, and positive outlook that are truly befitting of their name.

The authors wish to thank all their friends and colleagues who have been with them in all their endeavours with their excellent, unforgettable help and assistance in the successful execution of the work.

About This Book

Solar and wind energy are expected to play a very significant role in the future especially in developing countries, but it also has potential in developed countries. The material presented in this book has been chosen to provide a comprehensive account of solar and wind energy modeling methods. For this purpose, explanatory background material has been introduced with MATLAB based simulation models with the intention that engineers and scientists can benefit on the subject both from application and research points of view. In practical implementation, the efficiency of solar PV and wind energy conversion systems is less, hence converters are used to improve the efficiency. Converters are designed using MATLAB/SIMULINK models thus increasing the efficiency and providing several applications in the research perspective. Recent trends in solar and wind energy based on soft computing techniques are also provided with practical examples and Simulink models.

Salient Features

The salient features of this book include:

- Detailed description of solar PV and their components.
- Theory and practical applications of wind energy conversion systems.
- MATLAB/SIMULINK based models of solar and wind energy conversion systems.
- Hybrid energy systems, power quality issues and grid integration techniques.
- Applications of solar and wind energy conversion systems based on soft computing.
- Implementation of soft computing based solar PV and wind energy conversion systems using MATLAB/SIMULINK.
- Principle of fuel cell, converters used in fuel cell and architecture models for high power and high voltage applications.

Organization of the book

Chapter 1 describes the basic concepts of renewable energy systems, i-implications of renewable energy and their availability in India and the World, basic terminologies used in the renewable energy systems, grid integration issues while integrating renewable energy systems, schemes, policies and funds available for renewable energy systems, and the role of MATLAB/SIMULINK and soft computing techniques in renewable energy systems.

Chapter 2 provides an understanding of basic components of solar PV system and its merits and demerits, involvement of power electronic devices in solar PV components, MATLAB/SIMULINK model of different control strategies of power conditioning unit, importance of MATLAB/SIMULINK model in improving the efficiency of the overall solar PV system, characteristics of solar PV panel and its MATLAB/SIMULINK model, and characteristics and MATLAB/SIMULINK model of solar PV power conditioning unit.

Chapter 3 discusses the importance of soft computing techniques such as neural networks, fuzzy logic and genetic algorithms in solar PV system. Soft computing techniques used in MPPT of solar PV system and its MATLAB/SIMULINK model, prediction of solar irradiance using soft computing techniques and parameter estimation of solar PV module using genetic algorithms are delineated in this chapter.

Chapter 4 focuses on the characteristics of wind energy and components of wind energy conversion systems. The types of wind turbine generators based on their electrical configuration are described. The power converter topologies used for wind turbine generators are elaborated in detail. The MATLAB/SIMULINK models for wind turbine and types of wind turbine generators are developed and the simulation results are analyzed. The concept of grid connection with SIMULINK model is presented in this chapter.

In Chap. 5, importance of soft computing techniques in WECS, prediction of power factor using soft computing techniques, fuzzy based pitch angle control, soft computing based MPPT in WECS, and economic dispatch of WECS using soft computing algorithms are discussed.

In Chap. 6, a detailed description of hybridizing solar PV module with wind energy system and diesel system is provided. Further, the MATLAB/SIMULINK model of hybrid solar PV and wind energy conversion system, converters used for hybrid solar PV and wind energy conversion system, and fuzzy logic controller for hybrid power systems are also elaborated.

Chapter 7 explains the grid issues in integrating renewable energy systems, converters used for grid integration techniques and their control strategy. MATLAB/SIMULINK models of Synchronous Reference Frame PLL (dq PLL), Stationary Reference Frame PLL (αβ PLL), Decoupled Synchronous Reference Frame PLL (DSRF PLL), Decoupled Stationary Reference Frame PLL (Dαβ PLL) and Hybrid Dαβ PLL, and Filters used for grid integration techniques and its control strategy are provided.

Chapter 8 gives the basic concepts of harmonics and power quality issues, reactive power compensation using custom power devices such as DSTATCOM, DVR and UPQC, power quality problems and standards associated with power quality issues. The procedure for measurement of power quality in PV system and harmonic reduction in wind energy conversion systems with power quality issues are explained in detail.

Chapter 9 enlightens the need for fuel cells and types of fuel cells, comparative analysis and characteristic behavior of fuel cells, MATLAB/SIMULINK implementation of fuel cell model, types of converters and their implementation using MATLAB/SIMULINK, series architecture, DC bus distribution architecture, high frequency AC (HFAC) distribution architecture, multilevel architecture models for high power and high voltage applications.

Contents

1 Introduction 1
1.1 What Is Energy? 1
1.1.1 The Energy Scenario 2
1.1.2 Energy Crisis: Global and Indian 4
1.2 Energy Efficiency 6
1.2.1 Efficient Energy Use 7
1.3 Classification of Energy Sources 7
1.4 Solar Photovoltaics 8
1.4.1 Solar Radiation 11
1.4.2 Measurement of Solar Radiation 12
1.5 Wind Energy 13
1.5.1 Renewable Energy in the 12th Five-Year Plan (2012–2017) 14
1.5.2 Barriers to Achieving Higher Growth 15
1.6 Benefits of Renewable Energy Sources 18
1.7 Trends in Energy Consumption 19
1.7.1 Annual Energy Consumption 24
1.7.2 RES in INDIA 25
1.7.3 National Policy Measures Supporting Renewables 26
1.7.4 Renewable Energy Law 27
1.7.5 Generation Based Incentive (2009–2012) 28
1.7.6 Renewable Energy Certificate Scheme 29
1.7.7 National Clean Energy Fund 30
1.7.8 Other Initiatives: Renewable Regulatory Fund Mechanism 30
1.7.9 Land Allocation Policy 31
1.7.10 Grid Integration Issues 31
1.7.11 Grid Transmission Planning Process 32
1.7.12 Interconnection Standards 33

1.7.13 Green Energy Corridor 33
1.7.14 India Smart Grid Task Force 33
1.8 Worldwide Potentials of Renewable Energy Sources 34
1.9 Need for New Energy Technologies 41
1.10 Introduction to Matlab and Simulink 44
1.11 Introduction to Soft Computing 44
1.11.1 Soft Computing Techniques 45
1.11.2 Applications of Soft Computing Techniques in Solar Energy 52
1.11.3 Applications of Soft Computing (AI) Techniques in Wind Energy 54
1.12 Summary 55
Bibliography 55

2 Application of MATLAB/SIMULINK in Solar PV Systems 59
2.1 Basics of Solar PV 60
2.2 PV Module Performance Measurements 61
2.2.1 Balance of System and Applicable Standards 62
2.2.2 Photovoltaic Systems Total Costs Overview 65
2.3 Types of PV Systems 66
2.3.1 Grid-Connected Solar PV System 66
2.3.2 Stand-Alone Solar PV System 67
2.3.3 PV-Hybrid Systems 69
2.3.4 Stand-Alone Hybrid AC Solar Power System with Generator and Battery Backup 69
2.4 MATLAB Model of Solar PV 71
2.4.1 SIMULINK Model of PV Module 79
2.4.2 SIMULINK Model for PV Array 81
2.4.3 SIMULINK Model to Find Shading Effect 82
2.5 Charge Controller 83
2.5.1 Batteries in PV Systems 84
2.5.2 Battery Types and Classifications 85
2.5.3 Battery Charging 85
2.5.4 Battery Discharging 86
2.5.5 Battery Gassing and Overcharge Reaction 88
2.5.6 Charge Controller Types 88
2.5.7 Charge Controller Selection 94
2.5.8 Operating Without a Charge Controller 95
2.5.9 Using Low-Voltage “Self-Regulating” Modules 95
2.5.10 Using a Large Battery or Small Array 96
2.6 MATLAB Model of SOC 96
2.6.1 SIMULINK Model 98
2.7 MATLAB Model of Charge Controller 100
2.8 Inverter 103
2.8.1 Centralized Inverters 104
2.8.2 String Inverters 106

2.8.3 Multi-string Inverters . . . 107
2.8.4 Module Integrated Inverter/Micro-inverters . . . 107
2.8.5 Inverter Topology . . . 108
2.9 MATLAB/SIMULINK Model of Inverter . . . 108
2.9.1 SIMULINK Model . . . 109
2.10 Maximum Power Point Tracking . . . 110
2.10.1 MPPT Techniques . . . 115
2.10.2 MATLAB/SIMULINK Implementation of Perturb and Observe Method . . . 130
2.10.3 MATLAB/SIMULINK Model of the Incremental Conductance Method . . . 130
2.10.4 PV Module with MPPT Techniques . . . 130
2.11 Summary . . . 140
Bibliography . . . 140

3 Soft Computing Techniques in Solar PV . . . 145
3.1 Introduction . . . 145
3.2 MPPT Using Fuzzy Logic . . . 146
3.2.1 Implementation . . . 147
3.2.2 Description and Design of FLC . . . 148
3.2.3 Simulation and Results . . . 151
3.3 Neural Networks for MPP Tracking . . . 152
3.3.1 Background of Neural Networks . . . 154
3.3.2 Implementation . . . 156
3.3.3 Algorithm for ANN Based MPPT . . . 159
3.3.4 Simulation Results . . . 160
3.4 Neuro-Fuzzy Based MPPT Method . . . 162
3.4.1 Fuzzy Neural Network Hybrids . . . 164
3.4.2 Theoretical Background of ANFIS . . . 164
3.4.3 Architecture of Adaptive Neuro-Fuzzy Inference System . . . 168
3.4.4 Hybrid Learning Algorithm . . . 170
3.4.5 Neuro-Fuzzy Network Model and Calculation Algorithm . . . 173
3.4.6 ANFIS Network Specifications . . . 175
3.4.7 Algorithm for Neuro-Fuzzy Based MPPT . . . 175
3.4.8 Results for Neuro-Fuzzy Based MPPT . . . 178
3.5 Fuzzy Based Solar Tracking . . . 181
3.5.1 Design Process of the Fuzzy Controller . . . 185
3.5.2 SIMULINK Model . . . 186
3.5.3 Simulation Results of Solar Tracking System . . . 188
3.6 MATLAB/SIMULINK Model of Two Axis Sun Tracker Using Fuzzy Logic . . . 193
3.6.1 Sensors . . . 194
3.6.2 Design of FLC for Sun Tracking System . . . 196
3.6.3 SIMULINK Model and Results of FLC Based Sun Tracker System . . . 199

3.7 FLC for Solar Powered Energy 199
3.7.1 Methodology 201
3.7.2 Theoretical Explanation 201
3.7.3 SIMULINK Model of FLC Blocks 204
3.7.4 Simulation Results 206
3.8 Fuzzy Optimization for Solar Array System 206
3.8.1 Photovoltaic Systems 211
3.8.2 Peak-Power-Transfer Search 213
3.8.3 Fuzzy Logic Based Solar Array Controller 216
3.8.4 Experimental Results 222
3.9 Forecasting of Solar Irradiance Using ANN 222
3.9.1 Relation Between Solar Irradiance and Weather Variations 224
3.9.2 Reconstruction for the Input Vector of the Forecasting Model 226
3.9.3 ANN Forecasting Model Using Statistical Feature Parameters 229
3.10 Parameter Identification of Solar Cell Using Genetic Algorithm 232
3.10.1 Method of Determining the Parameters of Solar Cell Using Genetic Algorithms 235
3.11 Application of Neuro-Fuzzy Technique for Prediction of Solar Radiation 238
3.11.1 Neuro-Fuzzy Predictor (NFP) 238
3.11.2 Error Metrics 241
3.11.3 Neural Networks Training 241
3.11.4 Prediction Results with NNP 242
3.12 Summary 243
Bibliography 244

4 Wind Energy Conversion Systems 247
4.1 Introduction 247
4.2 Wind Characteristics 249
4.3 Wind Turbine 250
4.3.1 Fixed-Speed Wind Turbines 251
4.3.2 Variable-Speed Wind Turbines 252
4.4 Components of WECS 252
4.4.1 Description of Components 253
4.5 Types of Wind Turbine Generators 256
4.5.1 Type 1 WTG 258
4.5.2 Type 2 WTG 258
4.5.3 Type 3 WTG 260
4.5.4 Type 4 WTG 261
4.5.5 Type 5 WTG 262

4.6 Power Converter Topologies for Wind Turbine Generators 262
4.6.1 Permanent Magnet Synchronous Generators 262
4.6.2 Doubly Fed Induction Generators 267
4.6.3 Induction Generators 272
4.6.4 Synchronous Generators 273
4.7 Economics of Wind Energy Conversion Systems 274
4.8 Grid Connection 276
4.8.1 Unique Configurations for Linking Wind Turbines on the Grid 276
4.9 Modeling of Wind Turbine Using MATLAB/SIMULINK 280
4.9.1 SIMULINK Models 280
4.9.2 Simulation and Results 287
4.10 MATLAB/SIMULINK Model of Type 1 WTG 290
4.10.1 Pitch Angle Control System 291
4.10.2 Parameters 291
4.11 MATLAB/SIMULINK Model of Type 2 WTG 292
4.12 MATLAB/SIMULINK Model of Type 3 WTG 294
4.13 MATLAB/SIMULINK Model of Type 4 WTG 296
4.14 MATLAB/SIMULINK Model of Grid Connection 298
4.15 Summary 305
Bibliography 306

5 Soft Computing Techniques in Wind Energy Conversion Systems . . . 309
5.1 Prediction of Wind Turbine Power Factor 310
5.1.1 Problem Formulation 310
5.1.2 Artificial Neural Networks 312
5.1.3 Adaptive Neuro-fuzzy Inference System (ANFIS) 315
5.1.4 Description of Profile Types 322
5.1.5 Design of the ANN 322
5.1.6 ANFIS for Prediction of Power Factor 323
5.1.7 Estimation of the Optimal Power Factor 324
5.2 Pitch Angle Control 326
5.2.1 Problem Definition 327
5.2.2 Fuzzy Logic Controllers 327
5.2.3 Genetic Algorithms 328
5.2.4 Conventional Pitch Angle Control 329
5.2.5 Fuzzy Logic for Pitch Control 331
5.2.6 Genetic Algorithm Controller for Pitch Angle Control . 333
5.3 MPPT for WECS 334
5.3.1 Fuzzy Logic Based MPPT Controller 336
5.4 Economic Dispatch for Wind Power System 339
5.4.1 Mathematical Model of Economic Dispatch for Power System Based on Wind Energy 339
5.4.2 Quantum Genetic Algorithm (QGA) for Economic Dispatch of Wind Power System 341
5.4.3 Strength Pareto Evolutionary Algorithm (SPEA) Approach 345

5.5 SEIG Driven by WECS 346
5.5.1 Mathematical Model for SEIG Driven by WECS 347
5.5.2 Controllers 349
5.5.3 Fuzzy Logic Controller 349
5.5.4 Genetic Algorithm 352
5.6 FLC Based STATCOM 355
5.6.1 Modeling of STATCOM 355
5.6.2 MATLAB/SIMULINK Model 356
5.6.3 Simulation Results 360
5.7 FLC Based Wind Energy Production System 361
5.7.1 Wind/Battery Energy Production System 361
5.7.2 The Wind Turbine Model 362
5.7.3 Battery Model 363
5.7.4 Fuzzy Logic Controller 363
5.7.5 MATLAB SIMULINK Model 369
5.7.6 Simulation Results 369
5.8 Prediction of Wind Speed Based on FLC 374
5.8.1 Controller Model 376
5.8.2 Experimental Results 376
5.9 Fuzzy Logic Controlled SPWM Converter for WECS 379
5.9.1 Components of Standalone WECS 380
5.9.2 MATLAB/SIMULINK Model 383
5.9.3 Simulation Results 383
5.10 Summary 388
Bibliography 388

6 Hybrid Energy Systems 391
6.1 Need for Hybrid Energy System 391
6.2 Hybrid Solar PV/Wind Energy System Using MATLAB/SIMULINK 392
6.2.1 Architecture of Solar-Wind Hybrid System 393
6.2.2 Implementation Using MATLAB/SIMULINK 393
6.2.3 Small Domestic Power Grid Based on Hybrid Electrical Power 395
6.2.4 Small Industrial Power System Based on Hybrid Renewable Energy 397
6.3 Hybrid Model of Solar PV and Wind Energy System Using Cuk-Sepic Converter 402
6.3.1 Objectives 403
6.3.2 Hybrid Power System 403
6.3.3 Cuk: SEPIC Based Converter on Source Side 404
6.3.4 Model for Hybrid Wind and Solar Power Plant 407
6.3.5 Three Phase Uncontrolled AC-DC Bridge Rectifier . . . 407
6.3.6 Total Harmonic Distortion 410
6.3.7 Test Simulation and Results 410

6.4 Hybrid Model of Solar PV and Diesel Energy System 415
6.4.1 Need for Solar PV Diesel Hybrid System 415
6.4.2 Photovoltaic Diesel Hybrid System 415
6.4.3 Components of the Photovoltaic Diesel Hybrid System 416
6.4.4 MATLAB/SIMULINK Model of Solar PV/Diesel Hybrid System 418
6.5 Fuzzy Logic Controller for Hybrid Power System 418
6.5.1 FLC for HPS 421
6.5.2 Description of the Model 422
6.5.3 Implementation in MATLAB 426
6.6 Fuzzy Logic Based MPPT for Hybrid Solar and WECS 435
6.6.1 Methodology 438
6.6.2 Design Considerations 442
6.6.3 Intelligent Controller 446
6.6.4 Fuzzy Logic Controller Based MPPT for HPS 450
6.6.5 PID Controller 451
6.6.6 Simulation of Solar PV Under Atmospheric Conditions 453
6.6.7 Simulation of FLC Based MPPT 458
6.7 Summary 468
Bibliography 469

7 Grid Integration Techniques in Renewable Energy Systems 471
7.1 Introduction 471
7.1.1 Integration of Small Scale Generation into Distribution Grids 472
7.1.2 Different Types of Grid Interfaces 472
7.1.3 Issues Related to Grid Integration of Small Scale Generation 472
7.1.4 Integration of Large Scale Renewable Energy Generation 477
7.2 MATLAB Model of Grid Integration 479
7.2.1 Photovoltaic Module 480
7.2.2 Boost Converter 480
7.2.3 SIMULINK Model of Boost Converter 482
7.2.4 Implementation of Grid Integration Using MATLAB 485
7.3 Phase Locked Loop for Grid Connected Power System 489
7.3.1 Challenges Imposed on an Inverter-Based DG Interface 491
7.3.2 Requirements for Establishing a Grid Connection 492
7.3.3 Grid Synchronization Algorithms 494
7.3.4 PLLs for Three Phase Systems 496

7.4 Grid Connected Inverters 503
7.4.1 Inverters 503
7.4.2 Pulse Width Modulation Control 504
7.4.3 Grid Filter 508
7.5 Current Controllers for PWM Inverters 510
7.5.1 SRF PI Current Controller 510
7.5.2 Cascaded Deadbeat and PI Controller 513
7.6 SIMULINK Model of PLL Grid Connected Power System 515
7.6.1 SIMULINK Model of a Synchronous Reference Frame PLL 515
7.6.2 SIMULINK Model of a Synchronous Reference Frame PLL During Unbalanced Fault 516
7.6.3 SIMULINK Model of a DSRF PLL 518
7.6.4 SIMULINK Model of a DSRF PLL Under an Unbalanced Fault 518
7.6.5 SIMULINK Model of αβPLL 522
7.6.6 SIMULINK Model of a αβPLL During Unbalanced Fault 524
7.6.7 SIMULINK Model of a Dαβ PLL 524
7.6.8 SIMULINK Model of a Dαβ PLL Under an Unbalanced Fault 526
7.6.9 SIMULINK Model of a Decoupled Double Synchronous Reference Frame PLL(DDSRF PLL) 528
7.6.10 SIMULINK Model of a DDSRF PLL During an Unbalanced Fault 532
7.6.11 SIMULINK Diagram of Grid Synchronization of the Inverter Using the Hybrid Dαβ PLL 534
7.6.12 SIMULINK Model of SRF PI Controlled Voltage Source Inverter 536
7.6.13 SIMULINK Diagram of Grid Synchronization of the Inverter Using Cascaded Deadbeat and PI Controller 536
7.6.14 Comparison of Current THD of SRF PI and Cascaded Deadbeat and PI Controllers 538
7.7 Summary 541
Bibliography 542

8 Harmonic Reduction Techniques in Renewable Energy Systems 545
8.1 Introduction 545
8.2 Power Quality Issues 547
8.3 Sources and Effects of Power Quality Problems 549
8.4 Standards Associated with Power Quality 550
8.4.1 IEEE Standards 550
8.4.2 SEMI International Standards 551

8.5 Measurement of Power Quality in Solar PV Systems 552
8.5.1 System Description 552
8.5.2 Measurement Procedure for Power Quality in PV System 553
8.5.3 Assessment Procedure for Power Quality in PV Systems 554
8.5.4 Description of Case Studies 555
8.5.5 Problem Evaluation and Solution Description 556
8.6 Distribution Static Compensator 557
8.6.1 SIMULINK Model of DSTATCOM 558
8.6.2 Simulation Results 558
8.7 Dynamic Voltage Restorer 561
8.7.1 Equations Related to DVR 561
8.7.2 SIMULINK Model of DVR 563
8.7.3 Results and Discussion 566
8.8 Unified Power Quality Conditioner 568
8.8.1 UPQC with PV Array 569
8.8.2 SIMULINK Model of UPQC 570
8.8.3 Simulation Results 570
8.9 Harmonic Reduction in WECS 573
8.9.1 Power Quality Standards and Issues 574
8.9.2 Power Curtailment or Wind Turbine Disconnection . . . 575
8.9.3 Coordination with Other Generating Plants 576
8.9.4 Load Control 576
8.9.5 Reactive Compensation and Voltage Control 577
8.10 Power Quality in WECS- A Case Study 581
8.10.1 Topology for Power Quality Improvement 584
8.10.2 SIMULINK Model of Grid Connected WECS 587
8.10.3 SIMULINK Model of Grid Connected WECS with STATCOM 587
8.10.4 FFT Analysis 587
8.11 Summary 592
Bibliography 593

9 Fuel Cell and Converters 597
9.1 Introduction 597
9.2 Fuel Cell Technology 598
9.2.1 Importance of Fuel Cell 599
9.2.2 Types of Fuel Cells 600
9.2.3 Electrical Behaviour of Fuel Cell 603
9.2.4 Need for Power Electronic Converters 605
9.2.5 DC-DC Converters 607
9.2.6 Conventional Boost Converter 608
9.2.7 Cascaded Boost Converter 611
9.2.8 Interleaved Boost Converter 614

9.2.9 Isolated Converters 620
9.2.10 Flyback Converter 621
9.2.11 Forward Converter 622
9.2.12 Push-Pull Converter 623
9.2.13 Half Bridge Converter 625
9.2.14 Full Bridge Converter 626
9.3 Inverters 627
9.3.1 Single Phase Inverter 627
9.3.2 Half-Bridge Configuration 628
9.3.3 Half Bridge with Resistive Load 628
9.3.4 Half Bridge with RL Load 628
9.3.5 Full Bridge Configuration 630
9.3.6 Full Bridge with Resistive Load 631
9.3.7 Full Bridge with Resistive Load 631
9.3.8 Three Phase Inverter 632
9.3.9 Z-Source Inverter 635
9.3.10 LLCC Resonant Inverter 637
9.4 Fuel Cell System with Motor Load 639
9.5 Architecture of Multiple Fuel Cells for High Voltage/High Power Applications 640
9.5.1 Series Architecture 642
9.5.2 DC Bus Distribution Architecture 643
9.5.3 HFAC Distribution Architecture 645
9.5.4 Multilevel Architecture 646
9.6 Summary 648
Bibliography 649

Appendix I. Models Used to Assess the Performance of Solar PV Systems 651

Appendix II. Research Projects 665

Appendix III. SIMULINK Block Sets 689

Appendix IV. Data for Case Study 747

Index 783

About the Authors

Dr. S. Sumathi, was born on 31.01.1968, completed B.E. degree in Electronics and Communication Engineering and master's degree in Applied Electronics at Government College of Technology, Coimbatore, Tamil Nadu. The Author got her Ph.D. degree in the area of data mining, and is currently working as Associate Professor in the Department of Electrical and Electronics Engineering, PSG College of Technology, Coimbatore, with teaching and research experience of 16 years.

The Author received the prestigious Gold Medal from the Institution of Engineers Journal Computer Engineering Division – Subject Award for the research paper titled, "Development of New Soft Computing Models for Data Mining" 2002–2003, and also Best Project Award for UG Technical Report titled, "Self Organized Neural Network Schemes: As a Data Mining Tool", 1999. She received Dr. R. Sundramoorthy award for Outstanding Academic of PSG College of Technology in the year 2006. The author has guided a project which received Best M. Tech Thesis award from Indian Society for Technical Education, New Delhi.

In appreciation of publishing various technical articles, the Author has received National and International Journal Publication Awards, 2000–2003. She prepared Manuals for Electronics and Instrumentation Lab and Electrical and Electronics Lab of EEE Department, PSG College of Technology, Coimbatore, and also organized the second National Conference on Intelligent and Efficient Electrical Systems in the year 2005 and conducted Short Term Courses on "Neuro Fuzzy System Principles and Data Mining Applications", November 2001 and 2003. Dr. Sumathi has published several research articles in national and international journals/conferences and guided many UG and PG projects. She has also published the following books: *Introduction to Neural Networks with MATLAB*, *Introduction to Fuzzy Systems with MATLAB*, *Introduction to Data Mining and Its Applications*, *LabVIEW based Advanced Instrumentation Systems* and *Evolutionary Intelligence: An Introduction to Theory and Applications using MATLAB*. She reviewed papers in national/international journals and conferences. His research interests include

neural networks, fuzzy systems and genetic algorithms, pattern recognition and classification, data warehousing and data mining, operating systems and parallel computing etc.

Dr. L. Ashok Kumar was born on 7 April 1976 in Coimbatore, India. He completed his graduate programme in Electrical and Electronics Engineering. He did his post-graduation with Electrical Machines as his major. He completed his MBA with specialization in HRD in 2008. He has completed his Ph.D. on Wearable Electronics. He has been a teaching faculty at PSG College of Technology, India, since 2000. Presently he is working as a Professor, Dept. of EEE at PSG College of Technology, Coimbatore. After the completion of UG degree, he joined as Project Engineer in Serval Paper Boards Ltd., Coimbatore (now renamed as ITC unit, Kovai).

He has been actively involved in numerous Government Sponsored Research Projects funded by DRDO, DSIR, CSIR, DST, L-RAMP, Villgro and AICTE. He has published 81 technical papers in reputed national and international journals and presented 136 research articles in National and International Conferences. He has visited many countries for presenting his research work. He has been selected as the Visiting Professor in University of Arkansas, USA. He got trained in Germany for installing Grid connected and stand-alone solar PV systems. He is a registered Charted Engineer from IE (India). Dr. L. Ashok Kumar is a recipient of many National Awards from IE, ISTE, STA, NFED, etc. He is a member of various national and international technical bodies like IE, ISTE, IETE, TSI, BMSI, ISSS, SESI, SSI, CSI and TAI.

The author has received several awards namely, Young Engineer Award from IE, India, Dr. Triguna Charan Sen Prize from the Institution of Engineers, P.K. Das Memorial Best Faculty Award 2013- EEE, Prof. K Arumugam National Award from the Indian Society for Technical Education, and Best Researcher Award from Science & Technology, New Delhi. His research areas include: wearable electronics, solar PV and wind energy systems, textile control engineering, smart grid, energy conservation and management, and power electronics and drives.

Dr. P. Surekha born on May 1, 1980, has completed her B.E. degree in Electrical and Electronics Engineering in PARK College of Engineering and Technology, Coimbatore, Tamil Nadu, and master's degree in Control Systems at PSG College of Technology, Coimbatore, Tamil Nadu. She has obtained her Ph. D. degree in the faculty of Electrical Engineering, Anna University, Chennai, Tamil Nadu. Her current research work includes computational intelligence. Presently, she is working as an Associate Professor in the Department of Electrical and Electronics Engineering, PES University, Bangalore. She was a Rank Holder in both B.E. and M.E. degree programmes. She has received Alumni Award for best performance in curricular and co-curricular activities during her master's degree programme. She has presented papers in national conferences and journals. She has also published books such as: *Computational Intelligence Paradigms: Theory and Applications using MATLAB*, *Virtual Instrumentation Systems using LabVIEW* and *Evolutionary Algorithms using MATLAB*. Her areas of interest include: robotics, virtual instrumentation, mobile communication, and computational intelligence.

Chapter 1
Introduction

Learning Objectives
On completion of this chapter, the reader will have knowledge on:

- Basic concepts of renewable energy systems.
- Implications of renewable energy and their availability in India and World.
- Basic terminologies used in the renewable energy systems.
- Grid integration issues while integrating renewable energy systems.
- Schemes, Policies and funds available for renewable energy systems.
- Role of MATLAB/SIMULINK and Soft computing techniques in renewable energy systems.

1.1 What Is Energy?

Prior to discussing global energy production and consumption, it is prudent to have a look at the physics associated with energy. Although many people are familiar with the term *energy*, surprisingly only a few people can appreciate energy's true nature. In everyday language, the word *energy* is used very slackly; words like *work*, *power*, *fuel* and *energy* are often used interchangeably and erroneously. Energy forms the basis of human life. There is hardly any activity that is independent of energy. In olden days man used muscle power, then fire and animal power. Later, man learnt to harness energy, convert it to useful form and put it to various uses. Over the past few decades, energy has become the backbone of technology and economic development. Not counting men, machines and money, 'energy' is now the fourth factor of production. Without energy, no machine will run and electricity has become a necessity. Hence, the energy requirements have increased in the years following the industrial revolution. This tremendous increase in use of energy has created troubles of 'demand and supply'. If this mounting world energy demand is to be met

© Springer International Publishing Switzerland 2015

S. Sumathi et al., *Solar PV and Wind Energy Conversion Systems*,
Green Energy and Technology, DOI 10.1007/978-3-319-14941-7_1

with fossil fuels, they will not be available for energy production in few years. It is a need of today's world to concentrate on renewable energy sources to satisfy the demand and conserve our finite natural resources for the generations to come. This is an endeavor to present an overview of the concerns about energy demand and supply ratio and how to conserve energy as well how to make best use of renewable energy.

Energy is vital in the entire process of evolution, growth and survival of all living beings. Energy plays a fundamental role in the socio-economic development and human welfare of a country. The term *strategic commodity* is commonly used in countries to define energy. Any ambiguity in the supply of energy would cause a pressure to the economy of the country. Such energy security is important not only to the country's economic growth, but also for the vision of a country with reference to the activities related to human development. These activities include removal of poverty, providing employment and satisfying the Millennium Development Goals (MDGs). The issues related to the demand in energy are related to energy demand, energy poverty and environmental effects of energy growth. In this chapter, we will discuss the energy scenario, global and Indian energy crisis, energy efficiency, classification of energy sources, solar energy, wind energy, benefits of renewable energy, trends in energy consumption, worldwide potentials of renewable energy sources, and the need for new energy technologies. In addition an introduction to MATLAB and SIMULINK is provided with application of soft computing techniques in solar and wind energy generation systems.

1.1.1 The Energy Scenario

World population is expected to grow at around 1 % while GDP (Gross Domestic Product) is expected to grow around 3 %. GDP per capita can be considered a reasonable proxy for global energy demand. Demand for natural gas is expected to rise significantly, especially due to its use in power generation. Liquefied Natural Gas (LNG) becomes a significant energy carrier globally.

Fossil fuel based thermal power, hydro-electric, and nuclear constitute the conventional sources of power. Taking into consideration the profile of energy sources in India, coal has a dominant position. Coal constitutes about 51 % of India's primary energy resources followed by Oil (36 %), Natural Gas (9 %), Nuclear (2 %) and Hydro (2 %). Non-conventional sources are less than 5 % of total installed capacity in India. The present installed capacity (as in March 2006) is about 1, 25,000 MW, consisting of coal based plants (56 %), gas based plants (10 %), hydro-electric (26 %), nuclear (3 %) non-conventional (5 %). For next few decades, India would need to exploit all possible options to create reasonably large capacity base on the energy side. It needs to increase the coal generation, extract oil and gas reserves through all conceivable means wherever possible. It ought to additionally depend on import of coal, procure coal and gas reserves abroad and exploit completely the huge hydro electric potential which is over 1,50,000 MW. So far about 32,000 MW i.e. 20 % of the hydroelectric potential has been exploited.

An increase in the capacity of power generation based on the coal reserves of the nation, which are of the order of 200 billion tones is inexorable. Atomic projects have ended up being successful and effective. Atomic power plants are one of the essential choices that India is seeking since mid-1980s and early 1990s. India has immense gas holds, both on the Western, and all the more especially, around the Eastern coast. In addition, various LNG terminals have likewise been created and are, no doubt created with the goal that the utilization of gas could be supplemented through import of Liquefied Natural Gas. India is one of the minority countries which has been successful in employing wind turbine technology and today of the total capacity of 1,25,000 MW in the country about 5 % is constituted by the various non-conventional sources of generation, wind being the largest contributor.

India has the least per capita energy consumption among other countries in the world. The consumption of energy by India is 540 kgoe in 2008, whereas 1,803 kgoe is consumed by the world, 4,560 kgoe by OECD nations, and 1,600 kgoe by China. India's energy use productivity for creating Gross Domestic Product in Purchasing Power Parity is superior to numerous nations and even contrasted with the world normal. It is normal that with a development rate of 9 %, TPES necessity for India in 2021–2022 will be around 1,192 mtoe which will further expand to around 2,043 mtoe by the year 2031–2032. The power utilization per capita for India is only 566 Kwh and is far below most nations on the earth. Despite the fact that 85 % of towns are supplied with electricity, around 57 % of the domestic units in the country and 12 % of urban families, i.e. 84 million family units in the nation, don't have accessibility to electric power. Power utilization in India is required to ascent to around 2,280 Bkwh by 2021–2022 and around 4,500 Bkwh by 2031–2032. The Human Development Index (HDI) is figured from the literacy rate, infant mortality rate and GDP plotted against per capita power utilization. It is observed that for consumption over 4,000 kWh/per person the curve plateaus out and straightens. Power capacity has risen at a rate of 5.87 % per annum over the last 25 years. The aggregate supply of power has climbed at the rate of 7.2 % for every annum over the same period. This reflects a change in Plant Load Factor (PLF). In any case, the utilization is still compelled as force deficiencies proceed with torment to the nation. Availability Based Tariffs (ABT) and unscheduled exchange charges of force presented since 2003 for interstate offer of power has narrowed down the fluctuations in voltage and frequency. The deficiencies are additionally ascribed to insufficient ventures in distribution and transmission. Expanding the generation capacity has attracted wide range of investment. Aggregate Technical and Commercial (AT&C) misfortunes which incorporate theft of electricity, non billing, wrong billing, inefficient transmission and distribution losses surpassed 40 % for the nation in general in 2005. Hence, the State Electricity Boards remain monetarily sick and are unable to draw in accounts for venture. The degree of power deficiency differs from state to state.

The Planning Commission of India has set a focus of including more than 78,000 mw in a five year plan starting from 2007. Historically the plan targets have been missed and actually for this five year plan the target is likely going to be missed as capacity addition till February 2011 was just 40,000 MW. At last, the

historical backdrop of attention on speculation in power generation brings about stacking more power on a deficient transmission and distribution (T&D) system. Industrial and commercial units have been forced to look for standby generation to meet their demand on a 24×7 support.

The division is commanded by vast state imposing business models at both federal and state levels. Private distribution of electric power has been acquainted, yet it is confined to specific regions. An uneven playing field saturates the commercial center wherein the Central Power Sector Unit get ensured post-government forms of 14–16 % with full installment supported by the GOI. State Power Sector Utilities (SPSUs) are given zero or low returns by Regulators who are under consistent pressure not to raise tariffs, which are as of now around the most astounding on the planet in PPP terms for mechanical, business and family customers. The power tariffs are framed based on the premise of industrial users cross subsidizing agricultural and domestic power users. In almost all the states, the farmers are provided with un-metered power and in turn they pay an exceptionally high amount towards the horse power of their pumps. This prompts a zero peripheral expense of power which promotes wasteful use and over abuse of ground water. The local division likewise has an extent of subsidies depending upon the level of utilization including vigorously financed force for the poorest fragment wherein families pay a low amount aggregate added towards month to month billing.

1.1.2 Energy Crisis: Global and Indian

The entire world rely on coal, oil and gas (the fossil fuels) for over 80 % of the current energy needs – a situation which shows little sign of changing over the medium-term without drastic policy changes. Energy demand is expected to increase by 50 % during the following two decades. Naturally this is creating panic that our energy assets are beginning to run out, with obliterating outcomes for the worldwide economy and worldwide personal satisfaction. Created nations, no more strangers to intermittent power outages, are agonized over security of energy supply. In the creating scene, almost 2.4 billion individuals still depend on customary biomass powers, while 1.6 billion individuals – around a quarter of humankind – have no accessibility to electricity. In particular Africa suffers severely. In 2005, nearly two-thirds of Africa's 891 million people had no access to electricity. Nearly every aspect of development – from reducing poverty to improving healthcare – requires reliable access to modern energy services.

The potential for emergency in the event that we use energy is quite genuine however there is still time before that happens. In the previous two decades, demonstrated gas reserves have expanded by 70 % and demonstrated oil reserves by 40 %. At needed rates of interest development we have enough for 30 years supply. The International Energy Agency (IEA) says the world's energy needs could be 50 % higher in 2030 than they are today. The security of global energy supplies continues to be problematic. Today, oil and gas reserves are in the hands of

a small group of nations, several of which are considered political unstable or have testy relationships with large consuming countries. Eighty percent of the world's oil reserves are spotted in only three locales throughout the world: Africa; Russia and the Caspian Basin; and the Persian Gulf. While more than 50 % of the world's remaining gas reserves exist in Russia, Iran, and Qatar.

Policymakers have been prompted to seek autonomy from foreign sources of energy due to the distress about energy security. In Europe, new coal-terminated force stations are again on the political motivation, incompletely on the grounds that Russia is no more seen as a dependable supplier of gas. In the US, home-developed bio-fuels have been pushed by progressive organizations as an elective to Middle Eastern oil imports, in spite of being more costly. These responses are a characteristic outcome. The more the governments can extricate themselves from the reliance on outside energy assets, the more secure they feel.

The recent accessibility of power in India has both expanded and enhanced yet request has constantly overwhelmed supply and generous energy and top deficiencies rose in 2009–2010. There are additionally different assessments of 25,000–35,000 MW of power being processed by diesel generation to meet the shortages. Power lack is not by any means the only issue, its spread is a similarly genuine issue. Indeed, the individuals who have access to power also experience the ill effects of deficiencies in power. Industrial equipments often harmed because of the inconsistent power supply. Added to these is the expense of unmoving labor and misfortune of processing when power supply is interfered. Previously, the determination of an energy asset for power generation was overwhelmed by discovering the least expensive power generating plant. Despite the fact that such a methodology is crucial, there is a concern about different aspects of power generation such as, social, environmental, and technological consequences of selection of energy source. It could be noticed that coal has the most extreme potential next to Natural Gas and other sources of energy. Hence, it needs to be re-emphasized that for developing countries like India, the expense of transforming power is a main concern while anticipating the sort of plant to be introduced and requisitioned and all the more so with inexhaustible supply of coal. On the other hand, in the long run assuming that we produce the results of the contaminations on human health environment and cost and in addition exertions required to enhance or adjust the way of corruption, the initial expense of utilizing renewable assets for processing energy may not be too huge. A high level of alert is likewise required as rising economies in countries like India may not at present have the financial aid to jump specifically to cleaner systems of energy. Since a worldwide temperature alteration is a global wonder and it has no limits, there is an urgent necessity for the exchange of engineering and advancement of proper monetary instruments to countries that are as of now attempting to discover their legitimate spots. No contention is required to comprehend that the world is today confronting the issue of a dangerous atmospheric change because of fast industrialization and urbanization accompanied by the western world. According to the per capita value India is 145th on the earth with an annual discharge of 1.25 t CO_2.

1.2 Energy Efficiency

It is either impractical or prohibitively expensive to install comprehensive sub-metering and so it is necessary to estimate the energy consumption of various terms of plant and equipment. It is a difficult process to estimate the equipment energy consumption, which relies on skill and judgment. Nevertheless, it is relatively easy to establish an upper limit for energy consumption by using (1.1):

$$\text{Annual energy consumption (kWh)} = \frac{Q_{out}}{\eta} \times T_h \tag{1.1}$$

where Q_{out} is the plant power output (kW), η is the efficiency of plant and T_h is the number of operating hours per year. Equation (7.1) provides only an upper limit on the plant's energy consumption rather than the actual operating energy consumption. Such kind of a drawback can be avoided by first monitoring the actual energy consumption of the plant using energy meters for a short duration and then multiplying the average measured load by the annual operating time. Simple measuring instruments such as the clamp-on meter is a suitable device for performing the monitoring operation. The energy consumed in producing domestic hot water can be determined; if the cold feed water is metered, by using (1.2):

$$\text{Annual energy consumption (kWh)} = \frac{m_{\text{cf}} \times c_p \times (t_s - t_{\text{cf}})}{\eta_s \times 3,600} \tag{1.2}$$

where m_{cf} is the mass of cold feed water used annually (kg), c_p is the specific heat capacity of water (i.e. 4.19 kJ/kg K), t_s is the hot water storage temperature (e.g. 60 °C), t_{cf} is the cold feed water temperature (e.g. 10 °C) and η_s is the seasonal efficiency of system. The seasonal efficiencies for various domestic hot water – producing systems are given in Table 1.1.

It is possible to estimate the energy consumed in producing hot water, if the cold feed water consumption is not known by using (1.3):

$$\text{Annual energy consumption (kWh)} = 0.024 \times q_{\text{hws}} A_f N_w \tag{1.3}$$

where q_{hws} is the mean power requirement (W/m^2), A_f is the floor area (m^2) and N_w is the number of working days.

Table 1.1 Seasonal efficiencies for water heating systems

System type	Seasonal efficiency
Gas heater with storage cylinder	52
Gas or oil fired boiler with storage cylinder	56
Hot water cylinder with immersion heater using off-peak electricity	80
Instantaneous gas multi-point heater	62
District heating with local calorifiers	60
District heating with central calorifiers and distribution	56

1.2.1 Efficient Energy Use

Utilizing energy as effectively as could be expected under the circumstances is the most financially savvy approach to oversee energy interest, and accordingly to address carbon emissions. In most nations, regulations and budgetary motivating forces are presently set up to empower energy effectiveness yet their impact is humble and national energy utilization figures keep on rising year on year. Saving energy is much easier than producing it. Energy efficiency can be improved by adopting the following strategies:

- The demand on gas and electricity distribution networks can be reduced, energy efficiency will improve the security and resilience of these networks and reduce dependence on imported fuels.
- By decreasing the energy bills, energy efficiency will help businesses to be more productive and competitive.
- The domestic energy standards can be improved thus reducing the cost spent on fuel.

To increase sales and profits, increasing energy end use efficiency is unattractive for energy companies driven by commercial imperative. Regulations can be put in place for example that requires utilities to encourage customers to use electricity efficiently. A more revolutionary methodology imagines the utility being converted into a supplier of energy administrations, owning apparatus use in individuals' homes and hence being propelled to augment the productivity of these machines. Whatever methodology is at long last received, the essentialness of diminishing energy utilization ought to be the foundation of any CO_2 mitigation programme.

1.3 Classification of Energy Sources

By contrast to fossil fuels which are quickly being drained, renewable energy sources, for example, sunlight and wind are regularly recharged and accordingly reasonable. Environmental change, coupled with worries about high oil and energy costs, is driving a worldwide pattern towards the expanded utilization of renewable energy. Undoubtedly, it is the apparent idea of manageability that is driving governments far and wide to present enactment pushing the utilization of renewable energy. Most wellsprings of renewable energy begin either straight forwardly or in a roundabout way from the sun. For example, both wind and wave power derives their energy indirectly from the sun. When solar radiation is absorbed by the Earth it is dissipated around the globe in the form of winds and ocean currents. In addition, solar energy promotes evaporation of water from the oceans. This airborne water ultimately falls as rain, creating rivers which may be dammed to produce hydroelectric power. Furthermore, solar energy drives the photosynthesis necessary for the plants that are used to create biofuels. Currently,

Table 1.2 Renewable forms of energy

Energy	Percent of renewable resources	Product
Bio mass	Burning of plant materials and animal wastes	Heat and gas
Hydro power	Water flowing from higher to lower elevations through dams	Electricity
Wind	Capture of wind by turbines	Electricity
Geothermal	Tapping steam and hot water from the Earth's mantle	Heat and electricity
Solar	Absorbing and storing heat from the Sun	Heat and electricity
Emerging technologies		
Hydrogen fuels	Burning hydrogen gas	Power for movement
Nanotechnology	Using the unique properties of materials on the size scale of molecules or atoms	Electricity
Ancient technologies		
Wind	Water wheels, dams, weight	Power motion
Water	Windmills, sails	Power motion
Movement(kinetic energy)	Animals, human exertion	Power motion

only about 18 % of the world's energy demand is supplied from renewable energy sources. However, there is a great potential to increase this contribution. Indeed, it has been estimated that the technical potential of renewable energy is more than 18 times that of current global primary energy demand. This assessment, on the other hand, does not take into account budgetary and ecological imperatives and is accordingly to some degree misdirecting. So as to endeavor renewable wellsprings of energy it is regularly important to make an impressive capital financing. This is especially the case with huge framework activities, for example, hydroelectric or tidal blast plans. To be financially feasible, such ventures must assimilate substantial capital expenses and still have the capacity to contend on cost with universal wellsprings of energy – something which as a rule is challenging to do. Moreover, substantial base undertakings, for example, hydroelectric dams and tidal floods may make ecological issues. Hence, there are significant restraints to the boundless abuse of renewable energy. The various renewable forms of energy are shown in Table 1.2.

1.4 Solar Photovoltaics

In 2010, among the world's total power, the contribution of solar PV was a very small fraction. However a rapid growth is observed in the installation of solar PV and would continue to increase in the upcoming years. In the New Policies Scenario, power generated from solar PV in 2035 is over 26-times that of 2010,

expanding from 32 Twh to 846 Twh. The energy from installed solar PV would increase from 67 GW in 2011 to 600 GW in 2035, on account of decreasing expenses and government aids.

Based on the historical comparison, this is found to be an extremely rapid increase since the global solar PV capacity was just 1 GW in 2000. Throughout the span of 2011, solar PV capacity expanded by 30 GW, a 75 % increment. Around 60 % of the augmentations were in Germany and Italy, the world pioneers in solar PV, with 25 GW and 13 GW of installed capacity at the end of 2011. The European Union records for over 75 % of worldwide solar PV capacity in 2011. During the Outlook period, the EU capacity has expanded to exactly 146 GW, representing 5 % of its power generation in 2035 (up from 1 % in 2010). In the United States, capacity increments from 4 GW in 2011 to 68 GW in 2035. Different nations expected with huge solar PV capacity in 2035 are China (113 GW), India (85 GW) and Japan (54 GW). Speculation in solar PV establishments has been energized as of late by generous falls in solar PV costs, which resulted largely from widespread deployment and substantial oversupply (Spotlight). Between the first quarter of 2010 and the first quarter of 2012, expenses to generate energy from solar PV decreased by 44 % (Frankfurt School UNEP Collaborating Centre and Bloomberg New Energy Finance, 2012). Solar PV expenses keep on falling over the projection period, despite the fact that at lower level rates, the oversupply circumstance is revised. The increment in solar PV installations in European Union nations is utilized wholly to feeding tariffs, which impressively reduce the project risk as returns are ensured, regularly for a period of 10–20 years. These tariffs have been exceptionally liberal in a few cases and were not balanced rapidly enough to reflect the quickly falling expenses of solar PV. Subsequently, the returns offered were closer to those ordinarily connected with high-chance speculations and prompted huge financing in solar PV installations. In some countries, governments responded quickly by reducing feed-in tariffs to levels that better reflected costs. As the costs of feeding tariffs are passed on to consumers in most cases, it is essential to design incentives which attract sufficient investment while yet permitting adjustment of subsidies for new capacity additions as technology costs fall, to avoid unnecessary increases in electricity prices and maintain public acceptance. Solar PV cell generating capacity has become faster due to booming demand, at first in OECD nations, where request initially developed, and later in China, which stretched assembling limit hugely to help trades. During the recent years, capacity has expanded more significantly than genuine interest for solar PV panels. Since 2008, there has been a quite sharp fall in the expense of purged silicon, a key resource for production. Alongside expense diminishments from technical knowledge, these two factors have determined the fall in expense of PV frameworks (IEA, 2011b). The solar PV installers and final consumers have gained benefits due to the decrease in solar PV cost, while the solar PV manufacturers, especially in USA and Europe have faced several financial difficulties. Thus measures have been taken to reduce the cost and hence becoming more competitive. During April 2012 a few huge organizations have effectively gone bankrupt, for example, Germany's Q-Cells – the biggest solar unit producer in Europe – in April 2012. Exchange strains have emerged

between the United States, Europe and China, bringing about the burden of import duties by the United States in 2012 on sun based boards from China.

Difficulties are prone to persevere in the short term, while the lopsidedness between supply and interest continues. How rapidly the parity is restored depends on the rate of development of interest for sun powered PV. China speaks to a substantial potential business, yet its interest for sun oriented PV in the fleeting is questionable. In the New Policies Scenario, the oversupply proceeds over the short term.

India is blessed with plentiful sun powered energy, which is fit for processing 5,000 trillion kilowatts of clean energy. Nation is honored with around 300 sunny days in a year and sun based insolation of 4–7 kwh for every Sq. m for every day. In the event that this energy is tackled effectively, it can undoubtedly diminish the country's energy deficiency situation and with no carbon emissions. Solar Energy is the requirement for creating nation like India where huge segment of nation's populace is basically spotted in provincial ranges and needs access to power. The distribution infrastructure is not well established in the rural areas in India and hence developing such systems would lead to a major cost and such high cost cannot be upheld by the utilities existing in the present scenario.

The Government of India has initiated the Jawaharlal Nehru National Solar Mission, a significant activity with dynamic investment from States to promote environmentally sustainable development thus addressing the country's energy security challenge. It assumes a significant part in India's commitment to battle against the issues of environmental change which is an enormous concern over the globe. The goal of the Jawaharlal Nehru National Solar Mission is to build India as a worldwide pioneer in sunlight based energy, by making the strategy conditions for its substantial scale dispersion the nation over as fast as could be expected under the circumstances. The Mission embraced a 3-stage methodology, spreading over the time of the eleventh Plan and first year of the twelfth Plan (up to 2012–2013) as Phase 1, the remaining 4 years of the twelfth Plan (2013–2017) as Phase 2 and the thirteenth Plan (2017–2022) as Phase 3. During the end of each plan, and mid-term throughout the twelfth and thirteenth Plans, there will be an assessment of advancement, audit of limit and focuses for resulting stages, taking into account rising expense and engineering patterns, both local and worldwide. The point might be to ensure Government from subsidy introduction in the event that the normal expense decrease does not emerge or is more quick than anticipated. The quick point of the Mission was to concentrate on setting up an empowering environment for solar innovation in the nation both at a centralized and decentralized level. The principal phase (up to 2013) kept tabs on catching of the low hanging choices in solar; on pushing off-network frameworks to serve the populace without access to business energy and unobtrusive capacity expansion in grid based frameworks. In the second stage, based on the knowledge of from recent years, capacity will be combatively increased to make conditions for up scaled and competitive solar energy entrance in the nation. The mission National Solar mission under the brand name "Sun powered India" set a driven focus of including 20 GW of Grid connected and 2 GW of Off-grid capacity by 2022 in three stages.

1.4.1 Solar Radiation

Solar radiation is one of the brilliant energy emitted by the sun, especially electromagnetic energy. About a large portion of the radiation is in the visible short-wave path of the electromagnetic range. The other half is generally in the close infrared part, with some in the ultraviolet a piece of the range. The allotment of this ultraviolet radiation that is not ingested by the air transforms a suntan or sunburn on individuals who have been in daylight for longer duration of time.

Sunshine span is the period of time that the ground surface is illuminated by immediate sun based radiation (i.e., daylight arriving at the world's surface straightforwardly from the sun). World Meteorological Organization characterized daylight span as the period throughout which administered sunlight based irradiance surpasses a capacity quality of 120 W/m^2. This worth is identical to the level of sunlight based irradiance not long after day break or in a matter of seconds before dusk without cloud conditions. It was dictated by looking at the daylight span recorded utilizing a Campbell-Stokes daylight recorder with the real control sun powered irradiance. Campbell-Stokes daylight recorders and Jordan daylight recorders have long been utilized as instruments to measure daylight term, and are invaluable in that they have no moving parts and oblige no electric force. Their hindrances are that the qualities of the recording paper or photosensitized paper utilized within them influence estimation precision, contrasts between onlookers may emerge in deciding the event of daylight, and the recording paper must be swapped after dusk. As daylight is characterized quantitatively at present, a mixed collection of photoelectric daylight recorders have been produced and are utilized as a part of spot of these instruments. As the threshold limit for the event of daylight is characterized regarding immediate sunlight based irradiance, it is additionally conceivable to watch daylight term with a pyrheliometer.

In Solar PV framework it is important to know the measure of daylight accessible at a specific area at a given time. The two basic systems which describe sun based radiation are the solar radiance (or radiation) and solar insolation. The solar radiance is an instantaneous power density in units of kw/m^2. The solar radiance shifts for the duration of the day from 0 kw/m^2 during the evening to a greatest of about 1 kw/m^2. The solar radiance is emphatically dependant on area and neighborhood climate. Solar radiance estimations comprise of worldwide or immediate radiation estimations taken intermittently for the duration of the day. The estimations are taken utilizing either a pyranometer (measuring worldwide radiation) or a pyrheliometer (measuring immediate radiation). In overall built areas, this information has been gathered for more than 20 years. An elective system for measuring sunlight based radiation, which is less faultless additionally less unmanageable, is utilizing a daylight recorder. These daylight recorders (otherwise called Campbell-Stokes recorders), measure the amount of hours in the day throughout which the daylight is above a certain level (commonly 200 mw/cm^2). Information gathered along these lines might be utilized to focus

the solar insolation by looking at the measured number of daylight hours to those dependent upon computations and including a few rectification components. A last technique to gauge solar insolation is shadiness information taken from existing satellite pictures.

1.4.2 Measurement of Solar Radiation

Everything in nature transmits electromagnetic energy, and sun based radiation is energy emitted by the sun. The energy of extraterrestrial sun oriented radiation is disseminated over a wide persistent range running from ultraviolet to infrared beams. In this range, sun oriented radiation in short wavelengths (0.29–3.0 μm) represents something like 97 % of the aggregate energy.

Solar radiation is part of the way retained, scattered and reflected by atoms, mist concentrates, water vapor and mists as it passes through the climate. The immediate sunlight based shaft arriving specifically at the world's surface is called immediate sun powered radiation. The aggregate sum of sunlight based radiation falling on a level surface (i.e. the immediate sunlight based shaft in addition to diffuse sun powered radiation on a flat surface) is alluded as worldwide sun oriented radiation. Direct sun oriented radiation is watched from dawn to nightfall, while worldwide sun based radiation is watched in the dusk before day break and after nightfall, in spite of its reduced power at these times.

While sun powered irradiance is most generally measured, a more regular type of radiation information utilized as a part of framework outline is the solar insolation. The solar insolation is the aggregate sum of sun powered energy gained at a specific area throughout a specified time period, regularly in units of kwh/(m^2 day). While the units of solar insolation and sun powered irradiance are both a force thickness (for solar insolation the "hours" in the numerator are a period estimation as is the "day" in the denominator), solar insolation is truly unique in relation to the sun based irradiance as the solar insolation is the quick solar irradiance arrived at the midpoint of over a given time period. Solar insolation information is usually utilized for straightforward PV framework configuration while sun based brilliance is utilized as a part of additional confounded PV framework execution which ascertains the framework execution at each one point in the day. Solar insolation can likewise be communicated in units of Mj/m^2 for every year. For a given region the solar radiation can be presented in different ways such as:

- Average data for a year in a particular location.
- Average daily, monthly or yearly solar insolation for a specific location.
- Global isoflux contours either for a full year, a quarter year or a particular month.
- Sunshine hours data.
- Solar Insolation Based on Satellite Cloud-Cover Data.
- Calculations of Solar Radiation.

1.5 Wind Energy

The 2012 worldwide wind energy market developed by more than 10 % contrasted with 2011, and almost 45 GW of new wind power carried speculations of about € 56 billion. By 2020, the IEA's New Policies Scenario infers that aggregate limit might achieve 587 GW, supplying something like 6 % of worldwide power; yet the GWEO Moderate situation recommends that this could achieve 759 GW, supplying 7.7–8.3 % of worldwide power supply. The Advanced situation recommends that with the right arrangement help wind force could arrive at more than 1,100 GW by 2020, supplying between 11.7 % and 12.6 % of worldwide power, and sparing about 1.7 billion tons of CO_2 discharges.

China the biggest business for wind since 2009, saw a slower showcase, which implied that the US recovered the top spot in 2012. Yet establishments in Asia still headed worldwide markets, with North America a second place, and Europe not far behind. In 2012, wind-produced energy in China added up to 100.4 billion kwh, representing 2 % of the nation's aggregate power yield a year ago, up from 1.5 % in 2011. The Japanese business sector saw new establishments of 88 MW in 2012 to achieve a combined capacity of 2,614 MW. This speaks to around 0.5 % of the aggregate power supply in Japan. The Government of South Korea has made "green development" one of its national improvement necessities. In spite of the fact that wind force is still a generally junior energy generation innovation in South Korea, there was 76 MW of new inland establishments in 2012, which carried the aggregate introduced ability to 483 MW. Pakistan requisition its first extensive scale business wind homestead of 50 MW in the territory of Sindh. The aggregate introduced capacity arrived at 56 MW by the end of 2012. In 2012, wind energy was the biggest wellspring of new US power generation, giving practically 42 % of all new capacity. Truth be told, 2012 was a strong year for all renewable energy sources, as together they gave over 55 % of new generation capacity in the nation. Canada saw 935 MW of new wind capacity come online, making it the ninth biggest market in 2012. Contrasted with 1,267 MW in 2011, Canada's wind force business saw a slight log jam in 2012, however it was still the second best year ever. Wind energy spoke to 26 % of new EU power capacity introduced a year ago, and speculations of between €12.8 billion and €17.2 billion. Wind is currently meeting 7 % of Europe's power interest, up from 6.3 % at the end of 2011 and 4.8 % in 2009. The United Kingdom has the best wind assets in Europe, and introduced 1,897 MW in 2012–2016 % of new wind capacity in Europe, 1,043 MW inland and 854 MW seaward. This puts the UK second as far as new organization a year ago and the UK's wind energy yield expanded by 33 % in 2012 contrasted with the past year. In general wind energy created 5.5 % of the UK's power needs in 2012, up from 4 % in 2011. Italy now has an aggregate introduced capacity of 8,144 MW, up from 6,737 MW in 2011; and is the seventh biggest wind showcase all around. Brazil headed Latin America with 1,077 MW of new capacity, pulling the nation into the little club of wind energy markets with yearly establishments of over 1 GW comprehensively. Brazil has a solid pipeline of nearly 7 GW to be finished by 2016.

The Australian business sector included 358 MW in 2012 (up from 234 MW in 2011), carrying the aggregate introduced capacity up to 2,584 MW.

In an undeniably tight market, with enormous descending weight on costs through oversupply in the turbine market; furious rivalry with "modest" gas; and a wave of descending modifications to help systems in a starkness driven monetary scene; the industry keeps on being tested to contend on a value premise straightforwardly with intensely sponsored fossil fuel and atomic energy plants. Having said that, all the basic drivers for wind power improvement still hold, and there is a necessity around the globe for new power generation, which is clean, reasonable, indigenous, dependable and speedy to install.

In 2012, notwithstanding an abating worldwide economy, India's power interest kept on rising. Power deficiencies were basic, and over 40 % of the populace has no right to gain entrance to up to date energy services. India's power interest is anticipated to more than three times between 2005 and 2030. As of National Electricity Plan (2012), the Central Electricity Authority anticipated the necessity for 350–360 GW of aggregate generation capacity by 2022. Regardless of significant capacity increases over later decades, power supply battles to stay aware of interest. India had an alternate record year of new wind energy establishments between January and December 2011, introducing more than 3 GW of new capacity despite any precedent to the contrary to achieve what added up to 16,084 MW. As of March 2012, renewable energy represented 12.2 % of aggregate introduced capacity, up from 2 % in 1995. Wind energy represents 70 % of this introduced capacity. Toward the end of August 2012, wind power establishments in India had arrived at 17.9 GW. Under the New Policies Scenario of the World Energy Outlook (2011), aggregate force capacity in India might achieve 779 GW in 2035. To achieve 779 GW in 2035, capacity must develop at a CAGR of 5.9 %, or over 20 GW for every year from 2009 through 2035. The biggest expansion for every year is almost 18 GW throughout monetary year 2011–2012; this scale of extension could represent a test for the legislature (IEA 2012) without a noteworthy part for renewable energy. Throughout financial year 2011–2012 wind energy alone conveyed over 3 GW to India's new introduced generation capacity, representing over 16.5 % of aggregate capacity.

1.5.1 Renewable Energy in the 12th Five-Year Plan (2012–2017)

Generally, wind energy has met and frequently surpassed the target set for it under both the tenth Plan (2002–2007) and eleventh Plan (2007–2012) periods. Throughout the tenth Plan period the target set was of 1,500 MW though the genuine establishments were 5,427 MW. Additionally throughout the eleventh Plan period the updated target was for 9,000 MW and the genuine establishments were much higher at 10,260 MW. The report of the sub-bunch for wind power improvement named by

the Ministry of New and Renewable Energy to create the methodology for the twelfth Plan period (April 2012 to March 2017) settled a reference focus of 15,000 MW in new capacity increases, with an inspirational focus of 25,000 MW. Significantly the report prescribes the continuation of the Generation Based Incentive plan throughout the twelfth Plan period. The report additionally prioritized the issue of transmission, which was a powerless connection in the quality chain up to this point. A joint gathering of the MNRE, the Ministry of Power, the Central Electricity Authority and the Power Grid Corporation of India is taking a gander at this issue. Notwithstanding, for India to achieve its potential and to support the essential financing in renewable energy it will be key to present far reaching, stable and long haul help approaches, painstakingly intended to guarantee that they work in agreement with existing state level instruments to abstain from lessening their adequacy.

Presently, India has an introduced power generation capacity of 207.8 GW, of which renewable record for about 25 GW, and wind makes up a greater part of this introduced capacity. In 2011 the state-run Centre for Wind Energy Technology reassessed India's wind power potential as 102,778 MW at 80 m tower height at 2 % area accessibility, up from the prior evaluation of surmised 49,130 MW at 50 m, likewise at 2 % area accessibility. Assuming that the assessed potential of 102 GW were completely created, wind might produce 8 % of the anticipated power request in 2022 and 5 % in 2032 (LBNL, 2012). Over the previous year other exploration associations have assessed wind potential utilizing diverse models for mapping the wind asset. In one such study directed by the Lawrence Berkeley National Laboratory (LBNL), expecting a turbine thickness of 9 Mw/km^2, the aggregate wind potential in India with a base capacity variable of 20 % ranges from 2,006 GW at 80-m center tallness to 3,121 GW at 120-m center stature 10 (LBNL, 2012). These exploration studies require ground level acceptance through long haul wind estimations at 80 and 120-m center tallness. By the by their discoveries may have a huge effect on India's renewable energy methodology as it endeavors to adapt to a generous and unending lack of power. In a positive advancement the Ministry of New and Renewable Energy (MNRE), has now marked a Memorandum of Understanding with the Lawrence Berkeley Lab to team up on a few issues identified with the estimation of wind asset potential and matrix reconciliation.

1.5.2 Barriers to Achieving Higher Growth

The eleventh Plan had meant to make 78.7 GW of extra capacity for lattice associated power however real acknowledgment was around 50 GW. The twelfth Plan imagines introducing 100 GW of new capacity of which 30 GW is anticipated to hail from Renewable Energy Sources, of which wind might represent 15 GW. Generally the Indian wind energy division has met and sometimes surpassed its designated target.

During FY 2011–2012, India introduced a record 3.1 GW of new wind power capacity. For this scale of development to be looked after and heightened it is fundamental that the industry is upheld by a stable arrangement and nature's turf. India had introduced just about 18 GW of wind force capacity by August of 2012 (MNRE). With C-WET's overhauled wind power potential numbers and the development towards advertising seaward wind advancement, there is a ton more that could be attained in the nation.

Based on the twelfth Plan report, a GDP development rate of 9 % for every year over the Plan period will oblige energy supply to develop at around 6.5 % for every year. The capacity to take care of this energy demand relies on upon the nation's capability to stretch household preparation in basic energy sub areas on a critical premise. Power generation (utilities + hostage) developed at 5.8 % for every annum throughout the 20-year period from 1990–1991 to 2010–2011. Wind force is a full grown and versatile clean energy innovation where India holds a domestic advantage. India has a yearly assembling capacity for over 9.5 GW of wind turbines today. The nation is seeing about 3 GW in 12-month establishments under the twelfth Plan target. This unobtrusive pace of use of the nation's wind energy assembling and asset potential so far is attributable to a few components, including absence of a proper administrative structure to encourage purchase of renewable energy from outside the host state, deficient framework connectivity, high wheeling and open access charges in a few states, and defers in securing land and acquiring statutory clearances. The more extensive worldwide financial log jam has reduced the desires for the monetary year 2012–2013 from the wind division, which is even now adapting to the decrease of the Accelerated Depreciation profit from 80 % to 35 % in the first year of a wind turbine's operation. Additionally, there are other potential restraints to attain higher development rates in the short to medium term. Throughout the most recent decade the national government has offered three key motivations to be specific the Accelerated Depreciation (AD), the Generation Based Incentive (GBI) since 2009 and the Renewable Energy Certificates (REC) component since 2010. A basic purpose behind the development of wind area had been the accessibility of the AD profit. With the quantum of this profit reduced under the current Plan (from first April 2012), the other elected plan called the GBI has now turned into an indispensable motivator for the wind segment. In spite of the fact that liable to be resuscitated in not so distant future, at present the GBI is additionally in suppression. The GBI in its initial couple of years of operation has not attracted Independent Power Producers as imagined, since the investors were of the slant that the current rate of INR 0.5/kwh (~1 Us$ cent) was not sufficient or not standard with the monetary profit offered under the Accelerated Depreciation plan; as the two keep on being fundamentally unrelated.

The state-wise Renewable Purchase Specification (RPS) targets and the tradable Renewable Energy Certificates (REC) give further support to the division. However there are no motivators in the existing skeleton, particularly for state utilities in wind-energy rich states, to embrace RPSs higher than the levels inferred by the National Action Plan on Climate Change. Additionally the REC Mechanism, because of its constrained time allotment (5 years) confronts the test of

acknowledgement as an income stream by the money related establishments. Both the GBI and REC are at an early stage of implementation and require learning and capacity building for all stakeholders especially before the REC markets mature. Further, the multitudes of regulatory agencies add to the confusion. The electricity regulatory framework consists of the Central Electricity Regulatory Commission (CERC) at the federal level and a State Electricity Regulatory Commission (SERC) at the state level.

The CERC issues rules for deciding the food in-tax for renewable energy based power generation and these are material to central government power generating stations and the individuals who transmit control in the between state passage. On the other hand, this is material to a quite little number of force makers and the dominant part is still secured by the tariff dictated by the SERCs. This duality is not of service, as the tariff controlled by the SERCs could conceivably be equal to that of CERC tariffs. Tariffs differ over the states and remain settled for a more extended control period, this could affect the returns for new undertakings requisitioned under this tax administration and contrarily affect new extend improvement action. In FY 2011–2012 a portion of the state utilities, such as Tamil Nadu, postponed FIT installments to wind power generators by over a year. This unfavorably influences mogul certainty in the area. Inadequate lattice foundation is an alternate key issue that needs to be addressed immediately. Over the majority of the states with noteworthy wind potential, the grid does not have sufficient ability to have to empty regularly expanding measures of wind energy. Thus, the state appropriation utilities are hesitant to acknowledge more wind energy generation and typically have a tendency to favor warm power generation. Consequently, there is an urgent requirement to expand general lattice capacity. This obliges better gauging of energy request the country over, and a modernization of the grid. In most states, accessibility of area for wind ranches is a quarrelsome issue. Regardless of the fact that private grounds are accessible, transformation of area use from farming to commercial is a long term process. In addition, if the area is near a secured territory or forest land then getting freedom from the corresponding authorities for utilizing the forestland for wind power generation is prolonged.

One more hindrance to the development of the wind sector is the high borrowing expenses. In India, a huge larger part of wind energy undertakings are considered with a 70:30 debt-equity ratio as a venture financing strategy. The high investment rates (at present >13 %) make for exceptionally costly obligation under intense macroeconomic conditions. Further it might be helpful for the little and medium endeavors to have admittance to concessional financing to hold up under the dangers identified with preparation limit growth, particularly for segment producers. Ultimately India's wind part has enormous employment creation potential as the domesticated business develops. There is prone to be higher interest for prepared labor and likewise, the specialized curriculum and educational system over the States may need to be upgraded.

1.6 Benefits of Renewable Energy Sources

A few benefits are connected with the consumption of renewable energy technologies, including quite low or no greenhouse-gas emissions, making them a key segment in any environmental change moderation methodology (IPCC, 2011). In the New Policies Scenario, absolute CO_2 investment funds over all parts from renewable are 4.1 Gigatonnes (Gt) in 2035. In the power sector, renewable-based generation reduces emissions when it displaces power generation from the combustion of fossil fuels. Relative to the emissions that would be generated if the growing electricity demand of the New Policies Scenario were to be supplied using the electricity generation mix of 2010, renewable help to reduce CO_2 emissions in the power sector by 3.6 Gt in 2035. These savings represent some 10 % of the level of emissions reached in 2035, with more than 40 % of the savings coming from increased wind generation. Although hydropower generation increases by about two-thirds over the projection period, its share of total generation declines in many regions, therefore its contribution to CO_2 savings is more limited than other renewable. Heat produced from renewable sources, as in wood pellet or solar heat boilers for example, reduce CO_2 emissions by 150 million tons in 2035 by displacing heat from boilers using coal, oil or gas. Biofuels reduce emissions from oil in the transport sector by an estimated 0.4 Gt in 2035 but only so long as their production does not result in increases in emissions from direct or indirect land-use changes. This aspect of biofuels has come under close scrutiny in recent years. Sugarcane ethanol and advanced biofuels have the highest potential to reduce emissions (IEA, 2011a). Biofuels have also been criticized for competing with food supply and contributing to deforestation. The negative impacts of biofuels, however, can be minimized or avoided if the right policies are established and enforced. Renewable energy is largely a domestic source of energy (although some proportion of biofuels and other bioenergy is traded internationally). When it dislodges foreign made powers, it helps more amazing national energy security and specifically decreases import bills, which in turn aid to an equitably noteworthy rate of GDP in numerous importing nations and frequently help an exchange shortfall. Biofuels have the possibility to diminish these impacts fundamentally. In addition, more utilization of renewable energy could in a roundabout way put descending weight on oil and gas costs and decrease value unpredictability. In the electricity sector, renewable mainly reduce the need to import gas or coal, as oil use is limited in this sector.

The use of fossil fuels gives rise to several pollutants that worsen ambient air quality and have a negative impact on human health. Two of the most important of these pollutants are sulphur dioxide (SO_2) and nitrogen oxides (NOx); SO_2 coming mainly from burning coal but also from diesel fuel, while NOx come from burning all types of fossil fuels. They cause various ecological issues, for example, corrosive rain and ground-level ozone creations. Their effect is neighborhood and local. Air contamination is a significant issue in a few vast urban communities in non-OECD nations (and in a few urban areas in the OECD). Mix of air quality and renewable energy arrangements might be more powerful than divide

movements. A few sorts of renewable energy innovations for power generation require fundamentally less water for their operation than fossil fuel-based and atomic force plants. Solar PV and wind power do not use water to produce electricity and require only small amounts for cleaning purposes. If the significant use of water during the extraction of fossil fuels and uranium is taken into consideration, the differences in water use are even greater. Use of solar PV and wind power also avoids thermal pollution and contamination that may be caused by the discharge of cooling water for thermal power plants.

1.7 Trends in Energy Consumption

Worldwide energy utilization has relentlessly expanded in the course of recent years from 3,826.6 mtoe in 1965 to 10,878.5 mtoe in 2006. This is graphically represented in Fig. 1.1, which demonstrates the breakdown of worldwide energy utilization, based on the type of fuel. From these information it could be seen that in spite of the fact that development was moderately relentless over the period 1965–2000, there was a noteworthy increment (i.e. 1,315.3 mtoe) in utilization from 2000 to 2005. Moreover, it could be seen that over the period 1965–2005, development happened for all fuel types, with none declining in notoriety. While worldwide energy utilization has relentlessly expanded lately, in local terms this development has been sort of uneven. From Fig. 1.2 it could be seen that energy utilization in North America has expanded by just a modest measure, while that in Europe has really fallen. By examination, energy utilization in Asia has risen with

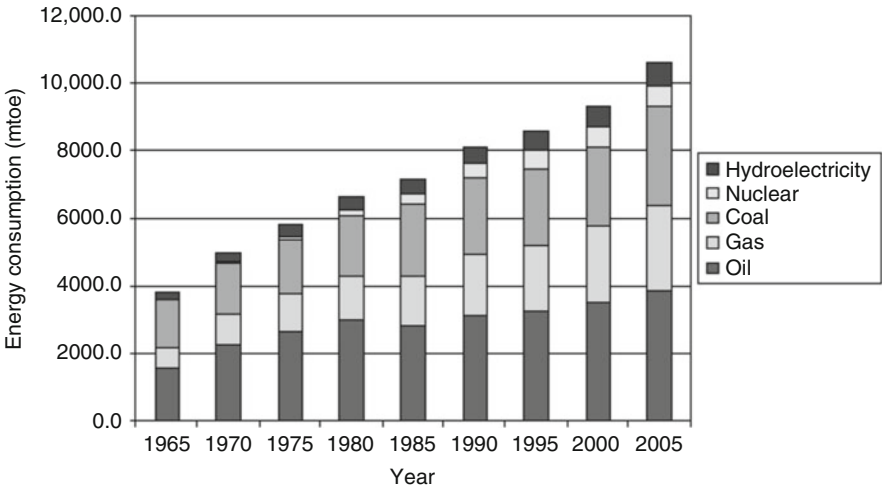


Fig. 1.1 Global energy consumption by fuel type (1965–2005)

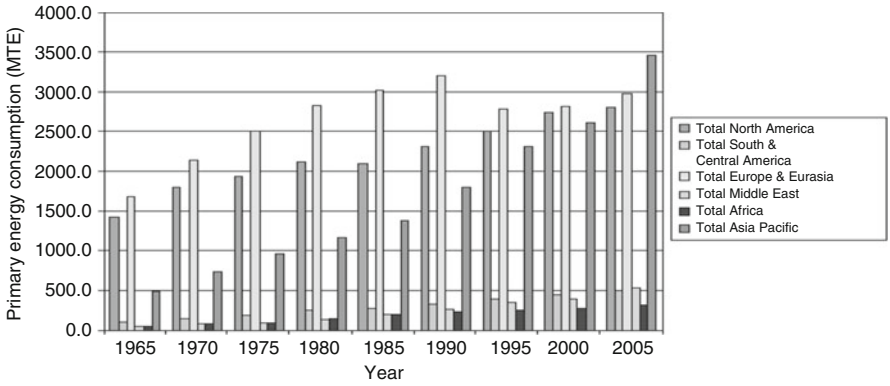


Fig. 1.2 Primary energy consumption by region (1965–2005)

the industrialization of China and India, so now that area consumes more energy than either Europe or North America.

Worldwide energy utilization information for 2006 is displayed in Table 1.3. These information give a nitty gritty breakdown of energy utilization on a nation by-nation and fuel-by fuel groundwork. It might be seen from Table 1.3 that in 2006 worldwide energy utilization was more or less 10,879 mtoe. Of this aggregate, just 51.1 % is devoured in the OECD nations, with 21.4 % expended in the USA and 15.8 % in the EU. While this implies that over a large portion of the world's energy is still expended in the OECD nations, it speaks to a noteworthy movement from the position in 1999, where 59.1 % was devoured by the OECD economies. This lessening reflects the fast industrialization that has happened in China and India in recent years – a process that has been determined, to some extent, by the outsourcing of assembling ability to these nations by numerous corporate associations in Europe, Japan and North America. In 2006, China and India represented 15.6 % and 3.9 % separately of worldwide utilization. From Table 1.3 it might be seen that the fuel blend and subsequently the carbon intensity changes incredibly area wise. In the USA, for instance, the proportion of coal to regular gas utilization is 1.00:1.00, while in UK the degree is 1.00:1.87, whereas in China the proportion is just 1.00:0.04 and in India it is 1.00:0.15. These figures reflect, firstly, the movement far from coal towards regular gas that happened in the UK throughout the 1990s and, besides, the substantial dependence on coal in China and India. The Energy Information Administration (EIA) in the USA predicts that in the twenty-first century there will be significant expand in energy interest, built for the most part with respect to fossil fills. This is relied upon to happen principally due to investment development in the creating economies of Asia and South America. In creating nations, energy and monetary development have a tendency to move in parallel. Financial advancement is an energy escalated methodology which eventually raises living norms and encourages expansive access to power and mechanized transportation.

Table 1.3 Global energy consumption data for 2006

Country	Oil (mtoe)	Natural gas (mtoe)	Coal (mtoe)	Nuclear energy (mtoe)	Hydroelectric (mtoe)	Total consumption (mtoe)	Percentage of total (%)
USA	938.8	566.9	567.3	187.5	65.9	2,326.4	21.39
Canada	98.8	87.0	35.0	22.3	79.3	322.3	2.96
Mexico	86.9	48.7	9.3	2.5	6.8	154.2	1.42
Total North America	1,124.6	702.5	611.6	212.3	152.0	2,803.0	25.77
Argentina	21.1	37.6	0.9	1.7	9.7	71.0	0.65
Brazil	92.1	19.0	13.1	3.1	79.2	206.5	1.90
Chile	11.4	6.8	3.0	–	6.7	27.9	0.26
Colombia	10.3	6.6	2.4	–	9.6	28.9	0.27
Ecuador	8.1	0.2	–	–	1.9	10.3	0.09
Peru	7.5	1.6	0.9	–	4.1	14.1	0.13
Venezuela	26.1	25.8	*	–	18.4	70.4	0.65
Other South & Central America	59.8	19.9	1.5	–	18.3	99.5	0.91
Total South & Central America	236.5	117.5	21.8	4.9	147.9	528.6	4.86
Austria	14.2	8.5	3.0	–	8.1	33.7	0.31
Azerbaijan	4.7	8.6	*	–	0.6	13.9	0.13
Belarus	8.0	17.6	0.1	–	*	25.7	0.24
Belgium & Luxembourg	41.0	15.3	6.1	11.0	0.6	73.9	0.68
Bulgaria	5.0	2.7	7.4	4.4	0.8	20.3	0.19
Czech Republic	9.8	7.6	19.4	5.9	0.7	43.5	0.40
Denmark	9.5	4.6	5.5	–	*	19.6	0.18
Finland	10.6	3.8	5.2	5.4	2.6	27.6	0.25
France	92.8	40.6	13.1	102.1	13.9	262.6	2.41

(continued)

Table 1.3 (continued)

Country	Oil (mtoe)	Natural gas (mtoe)	Coal (mtoe)	Nuclear energy (mtoe)	Hydroelectric (mtoe)	Total consumption (mtoe)	Percentage of total (%)
Germany	123.5	78.5	82.4	37.9	6.3	328.5	3.02
Greece	22.1	2.9	8.8	–	1.4	35.2	0.32
Hungary	7.4	11.3	2.9	3.0	*	24.7	0.23
Iceland	1.0	–	0.1	–	1.6	2.7	0.02
Republic of Ireland	9.3	4.0	1.8	–	0.2	15.4	0.14
Italy	85.7	69.4	17.4	–	9.7	182.2	1.67
Kazakhstan	10.6	18.2	29.7	–	1.8	60.3	0.55
Lithuania	2.8	2.9	0.2	2.0	0.2	8.0	0.07
Netherlands	49.6	34.5	7.5	0.8	*	92.3	0.85
Norway	10.0	4.0	0.4	–	27.1	41.5	0.38
Poland	23.1	12.3	58.4	–	0.7	94.5	0.87
Portugal	16.8	3.7	3.7	–	2.7	26.7	0.25
Romania	10.5	15.3	7.6	1.3	4.2	38.8	0.36
Russian Federation	128.5	388.9	112.5	35.4	39.6	704.9	6.48
Slovakia	3.9	5.0	3.8	4.1	1.0	17.8	0.16
Spain	78.1	30.0	18.3	13.6	5.7	145.8	1.34
Sweden	14.9	0.8	2.2	15.4	14.0	47.3	0.43
Switzerland	12.6	2.7	0.1	6.3	7.4	29.0	0.27
Turkey	28.5	27.4	28.8	–	9.9	94.7	0.87
Turkmenistan	5.2	17.0	–	–	–	22.3	0.20
Ukraine	15.0	59.8	39.6	20.4	2.9	137.8	1.27
United Kingdom	82.2	81.7	43.8	17.0	1.9	226.6	2.08
Uzbekistan	6.9	38.9	1.1	–	1.6	48.5	0.45
Other Europe & Eurasia	26.5	13.2	22.0	1.9	17.2	80.8	0.74

Total Europe & Eurasia	970.1	1,031.7	552.9	287.8	184.6	3,027.2	27.83
Iran	79.3	94.6	1.1	–	3.8	178.8	1.64
Kuwait	14.0	11.6	–	–	–	25.6	0.24
Qatar	4.4	17.6	–	–	–	21.9	0.20
Saudi Arabia	92.6	66.3	–	–	–	158.9	1.46
United Arab Emirates	19.7	37.5	–	–	–	57.2	0.53
Other Middle East	70.2	32.7	7.8	–	1.1	111.8	1.03
Total Middle East	280.1	260.3	8.9	–	4.9	554.2	5.09
Algeria	11.5	21.4	0.6	–	*	33.5	0.31

* Data not available

Economic improvement of the foundation likewise causes development in energy escalated assembling commercial ventures. As opposed to the creating nations, in exceptional industrialized nations the connection between monetary development and energy utilization is generally frail, with energy request development falling behind budgetary development. In praiseworthy economies for every capita the utilization of energy has a tendency to be moderately stable, with old energy serious machines and gear regularly being swapped by current energy effective supplies. Hence it is anticipated that the rate development in energy interest will be significantly lower in the developed nations in contrast to the developing nations. It is anticipated by the EIA that the pattern towards the expanded utilization of regular gas in the 1990s will proceed in the twenty-first century. This is on account of regular gas is progressively observed as the fuel of decision for power generation: it has much lower carbon force than coal; the power generation procedure is more effective; it is free from the streamlined debates which are frequently connected with coal preparation; and it is much less expensive and snappier to develop gas-terminated force plants. Oil interest is anticipated to develop with the expanded utilization of mechanized transport in creating nation.

1.7.1 Annual Energy Consumption

Presumably the least complex investigation that might be attempted is to process a cost breakdown of 12-month energy utilization and expense information. This is a handy method which empowers the general energy execution of a building rapidly and effortlessly to be evaluated. The examination of yearly energy utilization ought to be executed as follows:

(i) Convert all the energy consumption data into standard units (usually the kWh).
(ii) Produce percentage breakdowns of the total consumption and cost of each energy type, and determine the average unit cost per kWh.
(iii) Compile a table similar to the total annual energy consumption, cost and percentage breakdown of each fuel type.
(iv) Produce pie charts to show the energy and cost contributions graphically for each energy type.
(v) Where historical energy data are available, comparisons should be made in order to identify the trends, as illustrated in Table 1.4.

Table 1.4 Changes in annual energy use

Year	Consumption (kWh)	Change (%)
1994–1995 (base)	201,456.4	NA
1995–1996	197,562.2	−1.9
1996–1997	203,216.2	+0.9
1997–1998	220,403.5	+9.4
1998–1999	236,800.0	+17.5

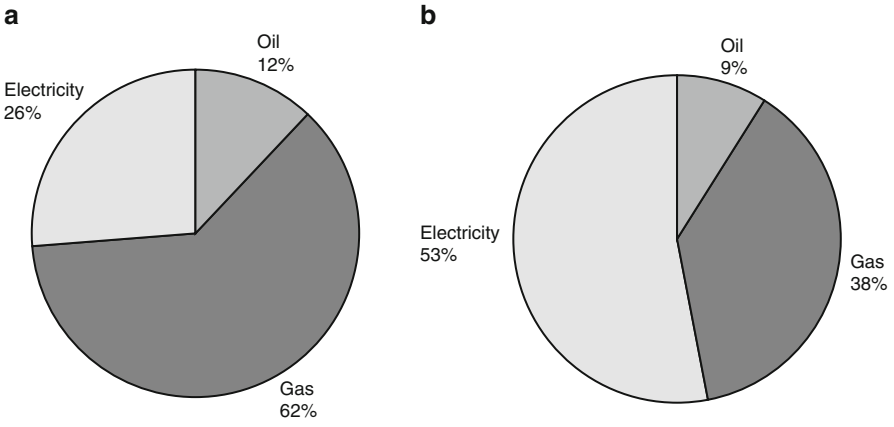


Fig. 1.3 (**a**) Energy consumption (**b**) Cost estimation

It is critical to note that in spite of the fact that the straightforward examination portrayed above may generate energy cost breakdowns and distinguish conceivable patterns, no recompenses have been made for uneven variables, for example, the climate, which may impact the energy execution of the office. It ought to thus be seen as a noticeably unrefined dissection system, and ought not be utilized when looking at the energy execution of one building against an alternate (Fig. 1.3).

1.7.2 RES in INDIA

India confronts a huge test in giving access to satisfactory, competitive and clean wellsprings of energy, particularly cooking fuel to a substantial area of the populace who live in rural ranges. According to the 2011 Census, just about 85 % of rural family units were reliant on accepted biomass fills for their cooking energy pre-requisites. National Sample Survey 2009–2010 uncovers the proceeded reliance on kindling in country ranges for cooking, with rate of families relying upon kindling staying at 76.3 % in 2009–2010 with a drop of just 2 rate since 1993–1994, despite the fact that the rate utilizing LPG has expanded from something like 2–11.5 % over the same period. Then again, the frequency of reliance on kindling for cooking in urban ranges has tumbled from about 30 % to 17.5 % between 1993–1994 and 2009–2010 a drop of more than 12 rate and the occurrence of reliance on lamp oil has plunged from 23.2 % to 6.5 % throughout the same period which records to 72 % lessening, while the rate of urban family units utilizing LPG has multiplied from 30 % to 64.5 %. At the end of the day, the development in pervasiveness of utilization of LPG in urban regions has been adjusted by a real decrease in usage of oil lamps accompanied by kindling and chips. In rural ranges, the ascent in LPG use

has been mostly from fertilizer cake, emulated by lamp fuel. Further, according to the NSSO Reports (55th, 61st and 66th Rounds), there has been an expansion in biomass fuel use as far as total amount expended over the previous decade around rural family units. This is a zone of concern given the respectable health effects of smoldering biomass powers separated from being a deterrent to accomplishing developmental objectives, i.e. guaranteeing a base expectation for everyday life. In this manner, a move to cleaner manifestations of energy regarding access to power and other up to date energy structures might have suggestions on energy security, as well as for empowering sexual orientation balance and achieve more terrific improvement and social advancement. It is in this connection that the part of renewable energy requirements is to be considered. It is no more "interchange energy", however will progressively turn into a key some piece of the answer for the country's energy needs.

India has an immense supply of renewable energy assets, and it has one of the biggest projects on the planet for conveying renewable energy items and frameworks. Renewable energy has been a paramount part of India's energy arranging procedure since a long while. The conversion of renewable energy sources to a supportable energy base was distinguished in the early 1970s. At the Government level, political responsibility to renewable energy showed itself in the station of the first Department of Non-Conventional Energy Sources in 1982, which was then updated to a full-fledged Ministry of Non-Conventional Energy Sources (MNES) in 1992 accordingly renamed as Ministry of New and Renewable Energy (MNRE). Truth be told, India is the main nation on the planet to have a service only for renewable energy advancement. MNRE is the nodal Ministry of the Government of India at the Federal level for all matters relating to new and renewable energy. Ever since its inception, the Ministry has been launching many ambitious programs on renewable energy, facilitating the implementation of broad spectrum programs including harnessing renewable power, renewable energy to rural areas for lighting, cooking and motive power, use of renewable energy in urban, industrial and commercial applications and development of alternate fuels and applications. The Ministry has also been involving in activities such as encouraging research, designing and developing products and services related with renewable energy trends.

In view of the fast changing energy scenario both domestically and internationally, and the important role expected to be played by new and renewable energy (NRE) sources, it is imperative to take stock of the progress achieved so far adopt a more focused approach than hitherto fore and chart out a clear strategy for accelerated growth of the NRE sector over the short, medium and long term.

1.7.3 National Policy Measures Supporting Renewables

Enactment preceding the Electricity Act, 2003 (EA 2003) had no particular procurements that might promote renewable or nonconventional resources of energy. Notwithstanding this weakness, the Ministry for New and Renewable Energy has

worked towards supporting the sector by proposing policy guidelines since 1994–1995, with blended outcomes. On the other hand, the EA 2003 changed the legitimate and administrative schema for the renewable energy area in India. The EA 2003 orders strategy plan to push renewable wellsprings of energy by the national government, the State governments and the individual organizations inside their locales. The SERCs focus the duty for all renewable energy ventures over the States, and the state-possessed force Distribution Companies (DISCOMs) guarantee framework connectivity to the renewable energy venture destinations, which for the most part are arranged in remote areas far from real load focuses. The order, which is known as a Renewable Purchase Specification (RPS), shifts from 0.5 % to 10 % in different states in excess of 2012–2013. A coordinated energy approach schema in India, the first endeavor at pulling together an umbrella energy arrangement approached after just about 60 years of the nation's freedom. The Planning Commission carried out the 'Coordinated Energy Policy: Report of the Expert Committee' (IEP) in October 2006, which gave a wide framework to all systems administering the preparation, dispersion, use and so on of diverse energy sources. In spite of the fact that the report of the master advisory group has been accessible since 2006, political duty to it has been restricted. After analyzing the IEP report absolutely from the viewpoint of the help it gives to renewable, which accentuated the necessity to move far from capital subsidies towards execution motivators for pushing renewable sources. The IEP report consigned a constrained part to power generation from renewable energy sources even as late as 2032, with just 5.2 % of renewable source based generation in the framework.

1.7.4 Renewable Energy Law

One of the basic prerequisites for India is to create and receive a coordinated energy skeleton that has a long haul vision, a period bound arrangement and an executing order that supports India's exertions for accomplishing clean, secure and all inclusive energy access for its kin. Today, most nations with progressed levels of wind force advancement have this structure set up, normally as a renewable energy law. Such a skeleton, if received, can help to address not just the concerns of moguls in connection to unstable strategy environment and business chances additionally convey indigenous power supply free from the fuel value danger connected with fossil energizes.

India will need to put resources into alternatives that give energy security as well as give practical equipments to destroying energy destitution no matter how they are focused, in the following decade. As a piece of commitments to the United Nations Climate Convention (UNFCCC), India discharged a National Action Plan on Climate Change (NAPCC) in June 2008 that laid out the legislature's vision for a maintainable and clean energy future.

The NAPCC could be actualized through the foundation of eight national missions. Two energy related missions are incorporated, to be specific the National

Solar Mission and the National Mission for Enhanced Energy Efficiency. Other significant thing about NAPCC is it doesn't have induction devoted to wind power. The NAPCC stipulates that an element least renewable buy focus of 5 % (of aggregate lattice buy) may be endorsed in 2009–2010 and this ought to build by 1 % every year for a time of 10 years. As per NAPCC by 2020, India ought to be obtaining 15 % of its energy from renewable energy sources.

1.7.5 Generation Based Incentive (2009–2012)

In 2009, for lattice associated wind force ventures, Government actualized a Generation Based Incentive (GBI) plan. A GBI of INR 0.50 for every kwh (1 US $ penny), with a top of roughly $29,000 for every MW for every year, totaling $116,000 for every MW over 10 years of an undertaking's life was offered under this plan. Between March 2010 and October 2012, 2,021.29 MW capacity of wind activities had benefitted themselves of the GBI profit and 1,830.43 MW undertakings of AD profits. The GBI plan incorporates hostage wind force ventures, yet prohibits outsider bargain, for instance, dealer force plants. GBI and AD profits are totally unrelated. The GBI is far beyond the duty sanction by separate Sercs and dispensed on a half yearly support through the Indian Renewable Energy Development Agency (IREDA). At first this plan was appropriate to wind force ventures dispatched before 31st March 2012. Not long ago the MNRE proposed that the GBI proceed over the twelfth Plan period, with a conceivable amendment of the motivating force. The last support from the Cabinet is pending as of October 2012.

GBI plan was not alluring enough to draw designers far from AD in its unique structure. As per gauges by IREDA, at the predominating duties in 2010, the IRR (post-charge) for wind holdings might be higher by 1.2–1.5 % if there should be an occurrence of AD profits over all key states other than Maharashtra. Likewise, the low capacity figures in the vast majority of the states implied that the present GBI might not have made an extend more possible in correlation to AD. Then again, the GBI does not restrict wind power makers from entering the REC market. The administration activity to move far from duty subsidy backing to execution impetus backing of INR 0.50 for every kwh has not discovered an excited emulating to a great extent because of the low esteem of the motivating force and the tops on the guaranteed sum.

Continuation of the GBI conspire in its prior structure is questionable. For the advancement of wind undertakings from an assessment arranging measure to a energy arranging instrument, the GBI plan might need to be further improved. Industry masters in India infer that developing the plan to incorporate hostage and third–party bargains, and in addition multiplying the impetus to INR 1.0 for every kwh or evacuating the top of INR 6.2 million ($116,000) for every MW could help support the advance of the plan.

1.7.6 Renewable Energy Certificate Scheme

The Electricity Act 2003 proposed required Renewable Purchase Specification (RPS) for all the states. So far till date, 26 states have specified focuses for the uptake of power from renewable energy sources. With the presentation of the Renewable Energy Certificate (REC) conspire in 2010, states are currently satisfying the RPSs under this procurement by securing comparable RECs. REC is a tradable authentication of verification that a renewable energy plant has created 1 Mwh of power. Under this schema, renewable energy generators can exchange RECs through a force trade stage that permits business sector based value revelation, inside a value reach controlled by the Central Electricity Regulatory Commission. The particular value points of confinement are called forbearance price and floor cost and their qualities are computed independently for solar based and non solar based sources (i.e. wind, biomass, little hydro). While the CERC has stipulated floor and abstinence costs for RECs; the true cost of a REC might be resolved at the force trades dependent upon predominating power supply and interest circumstances.

The exchanging of RECs in the Indian market started in February 2011. So as to meet all requirements for RECs, venture designers necessity to enroll with the National Load Dispatch Centre. The issued RECs are exchanged at qualified force trades inside the capacity set by the floor cost and abstinence cost, as controlled by the CERC. For wind power generation, as of April 2012, the amended extent is between INR 1,400 (~$26) to INR 3,480 (~$65) for every Mwh. By mid-October in 2012 the national REC registry had issued 3,384,257 RECs of which 3,381,714 were non-sunlight based RECs. Of the aggregate authorize venture capacity recorded by the national REC registry, wind represented over 56 % or 1993.46 MW of the capacity by October 2012. The quick expand in volume recommends that more research engineers are entering the REC market and the system is welcoming premium yet feeble authorization of RPSs at the State level is prompting climbing amounts of unsold RECs in the business. In September 2012, dealers offered to offer 7, 11, 171 (non sun oriented) RECs, however just 2,64,446 were purchased, and that too, at the floor cost of INR 1,40,030. Throughout September 2012, no state-possessed power Distribution Company (DISCOMs) approached to purchase the testaments, in spite of the fact that they are all ‘committed elements’. This is because of absence of authorization of their commitments. The RPS is material on the Distribution Companies (DISCOMs), open access buyers and hostage power clients consistently. On the other hand, the present RPS system is discovered needing in viable agree ability and implementation at the State level. Also the hostage power clients in states like Gujarat, Rajasthan and Orissa are not extremely quick to buy renewable based force for gathering the RPS and have tested the RPS regulations. The configuration of the REC instrument is continuously enhanced with endeavors being made to handle the execution issues as they emerge and there is expanded taking in the business sector. A portion of the states have forced punishments for rebelliousness with RPO focuses on the

generators or utilities. Activities are continuously anticipated creating a voluntary REC showcase likewise.

Making REC a generally acknowledged instrument and an income stream for the undertaking financing group still remains a test in India. Further there is a necessity for an element RPS setting methodology with incessant upward amendment to meet the 15 % renewable energy target set under the NAPCC by 2020.

1.7.7 National Clean Energy Fund

The legislature proposed the formation of the National Clean Energy Fund (NCEF) in the Union Budget 2010–2011 by forcing a clean energy charge (cess) of INR 50 (~$1) for every term. The Ministry of Finance, through the Clean Energy Cess principles 2010, set rules for the gathering and appraisal of this duty by the Revenue Department. From there on an inter-ministerial assembly was set up in the Ministry to support tasks and qualification necessities for entering stores from the NCEF. However since its commencement in July 2010, few data on the operationalization of the NCEF has been discharged in general society realm other than the rules and requisition structure for recommendations. A study directed by WISE gauges that at the current expense rate and the normal coal utilization rates, an aggregate of INR 670 billion (~$12.5 billion) could gather to the trust by 2022. This store could help network and other framework improvement to take into account more excellent departure of force produced from renewable energy sources. The store could likewise be utilized for exploration, advancement and sending of clean and renewable energy innovations. The proposals presented by national Ministries were lacking quality and were not innovative, thus failing to meet the objectives of NCEF. In addition, the large amount of NCEF funds remains unutilised. Thus it is required to modify the rules of NCEF thus utilizing the funds for gathering customary budgetary deficits of Ministries. Financing to help different Ministries' customary exercises ought to be met from the suitable sources accessible inside the existing financing structure of the general Budget. In spite of the fact that admissible under the rules, there has been constrained contribution of Indian industry and examination establishments to date in the proposal advancement process. This prescribes constrained cognizance around Indian exploration foundations and industry on the NCEF subsidizing opportunity.

1.7.8 Other Initiatives: Renewable Regulatory Fund Mechanism

The Indian Electricity Grid Code (IEGC) was received in April 2010 and supercedes the Indian Electricity Grid Code, 2006. It gives itemized rules on the

part of different players included in the operation of a power system. Under Clauses 5 and 7 of the IEGC, unscheduled exchange charges because of the variety in real generation by wind and solar ought to be imparted around all the States through the 'Renewable Regulatory Charge' to be worked through the 'Renewable Regulatory Fund' instrument. This might have made gauging and planning of wind and solar power generation compulsory with impact from January 2012 with the introductory execution of the RRF component. However this still stays to be presented, despite the fact that the point by point methods presented by National Load Dispatch Centre were analyzed by CERC and the changed strategies were distributed on eighteenth February 2011.

The execution of Renewable Regulatory Fund system is postponed because of a few ground level issues; including an absence of coordination between the CERC directives and auspicious agreeability by different SERCs. Determining the concerns on both sides through early and preemptive involvement of stakeholders including different Regional and State Load Dispatch Centers, the MNRE and wind farm designers is critical. This might help in guaranteeing more level abridgement and higher generation numbers from both wind and solar power plants.

1.7.9 Land Allocation Policy

In perspective of the developing number of wind force establishments in the nation and the expanding scarce of permissible area with wind potential, the MNRE, through its correspondence dated fifteenth May 2012, has asked for state governments to inspect their property strategy for wind power establishments and figure an approach for area designation on a "footprint" hypothesis. The MNRE is working towards executing the best practices in this respect.

1.7.10 Grid Integration Issues

India's transmission system has a two-level structure: interstate networks that are overseen by the Power Grid Corporation of India (PGCIL) and the nearby lattices, which are overseen by the State Transmission Utilities. India still needs to make an interlinked and joint by combining its nearby, territorial and national networks. Frequently insufficient and frail lattices go about as a hindrance to smoother reconciliation of power generation from renewable sources. India's energy transmission framework is partitioned into five local matrices: northern, northeastern, eastern, southern and western districts. Since August 2006, four local lattices have been completely incorporated except for the southern matrix that is to be synchronized with these networks by 2014.

The variability of wind power can create problems for the traditional grids in maintaining a supply and demand balance. Most of the wind farms in India are

located in remote areas that are quite far away from load centers. Due to a weak transmission and distribution network, it is difficult to transmit the power from wind farms to the load dispatch centers. This is one of the key constraints for the future of wind power development in the country. In the past, with vertically integrated utilities, a single organization was responsible for the planning and operation of networks and giving access to generators, and therefore the technical requirements did not have to be particularly clearly defined or codified. Now, with increased ownership separation between grid operators and power generators the need for defining the technical requirements governing the relationship between them becomes essential. Renewable energy generation further complicates the process of evacuation and dispatch.

1.7.11 Grid Transmission Planning Process

Lack of adequate power evacuation capacity in the state grids is a major concern in transmission planning. Unless the transmission capacity planning process incorporates a long term vision of planned wind power additions and involves wind sector players at the planning stage, bottlenecks related to evacuation capacity are expected to remain. The remedy is more procedural than technical and requires administrative will rather than advanced technical understanding. The Ministry of Power (MOP) has recently constituted a committee chaired by the Joint Secretary of the MOP to work on accelerated development of RE through legislative and policy changes. One of the suggestions to streamline transmission planning for renewable energy is to have a separate sub-division in the Central Electricity Authority (CEA) and across all the state utilities for transmission planning of all renewable energy power plants. India's local distribution systems are weak and would require substantial augmentation or laying of parallel power evacuation infrastructure, which will invariably add not only to the costs but also to construction time. The issue is further muddled by stipulations identified with expense imparting of building this extra infrastructure. It is particularly valid for state-claimed utilities (DISCOMs) that are seriously impoverished. An alternate real concern is that of constrained power outage (curtailment) due to powerless local grid, which brings about considerable generation loss for the investing organization. In addition, intricacies related to institutional learning, ground level information and deficiency of expertise knowledge in grid integration and comprehensive power evacuation planning are adding to the postponement. For utilities that are usual to the customary model of concentrated power generation, these issues are prone to wait for some more years. In India, past regulations under the electricity grid code (IEGC) did not permit renewables based power to associate with the inter-state transmission system, bringing about interconnection of wind force tasks to a powerless State transmission or dispersion system prompting constrained blackout of generation, particularly throughout the crest wind season. The need to allow power evacuation at higher voltages in the inter-state grid of the Central transmission utility (PGCIL 36) is critical for the growth of the sector. The CERC recently allowed projects with

capacities of over 50 MW to connect directly to the central transmission network subject to scheduling requirements. This allowance has addressed one long-standing concern of investors by reducing the threat of curtailment.

1.7.12 Interconnection Standards

Grid stability is the primary consideration in interconnecting any new system to an existing grid. The conventional electricity network tuned to conventional generation's radial mode of power flow and wind power poses new challenges related to safety, reliability and efficiency of the interconnected systems. Because of the variable nature of wind power, the aim of developing an interconnection standard would be enable the grid to sustain the variability without affecting the power quality adversely. Under (IEGC) 2010, wind and solar assignments have been offered 'must-run' status. The IEGC unites a solitary set of specialized and business guidelines, incorporating all the utilities that are joined with or utilize the inter-state transmission system.

1.7.13 Green Energy Corridor

Recently, the MNRE and CERC has commissioned the Power Grid Corporation of India (PGCIL) to study and distinguish transmission infrastructure for renewable energy capacity expansion throughout the twelfth plan period. Based on extensive conferences, conclusions were drawn with different stakeholders including the State Nodal Agencies, the last report called 'Environmentally friendly power Energy Corridors' was discharged in September 2012. It examines issues of inter-state and intra-state transmission framework, for example, strengthening and augmentation, foundation of a Renewable Energy Management Centre, enhanced anticipation addressing variability viewpoints and also lattice reconciliation issues of huge scale renewable energy generation. A venture of roughly $8 billion (~INR 42,557 crores) is continuously anticipated the advancement of this hall by 2017. Among the total sum allotted, $3.8 billion (INR 20,466 crores) is liable to be invested in intra-state grid system and roughly $4 billion (INR 21,867 crores) is prone to be invested in strengthening the inter-state transmission framework. This activity if executed effectively could be a significant driver for the improvement of the renewable energy division in India.

1.7.14 India Smart Grid Task Force

Particularly after the presentation of the IEGC, grids over the nation are obliged to tackle power generated from nonconventional energy sources under different plans

(RPSs and RECs). The Ministry of Power (MOP) took the first step towards lattice changes when it set up the 'India Smart Grid Task Force' (ISGTF) in June 2010. The ISGTF is an inter-ministerial group that serves as the administration point of convergence for arrangements identified with Smart Grid improvement in India. MOP's vision of a smart grid was to unite the fields of correspondences, IT and the power segment to build an extensive power grid framework. Henceforth the requirement to redo and modernize the national/regional and nearby frameworks must be one of the essential territories of speculation and advancement. Further, on the interest side it imagined giving a decision to the purchaser to choose the timing and measure of power utilization based upon the constant costs in the power market. Further, under one of the missions of the NAPCC, called the National Mission for Enhanced Energy Efficiency, India's Bureau of Energy Efficiency partnered with the IT firm IBM to create the country's first smart grid project in May 2011. The focus of the analysis will be determining India's readiness for deploying smart grid technologies. It will also develop a framework for adopting new smart grid technologies and identifying regulatory frameworks. The analysis will calculate return on investment for a range of smart grid projects planned across India. The ISGTF has set up five working gatherings, including 'Trials on new innovations' and 'Transmission misfortune decrease and robbery, information social affair and investigation'. In the interim, in view of the proposals of the Indian Smart Grid Forum, the MOP is supporting 14 pilot venture suggestions worth nearly $72 million (INR 400 crores) for smart grid pilot projects across different areas. These suggestions concentrate on assorted ranges of the force area, including incorporation of renewable energy sources with the framework and bringing down of total specialized and business losses. On the other hand for this basic activity to be successful, it is vital that different elected services, for example, the Ministry of Power, the Ministry of New and Renewable Energy, the Ministry of Communications and Information Technology and the Ministry of Environment and Forests, and their state level partners must meet up to develop a regular movement plan. Further, both state and national grid administrators and their related electricity regulatory commissions must start community exchange across the country towards characterizing a basic comprehension of a genuinely brilliant network framework for India. A top down prescriptive report from the focal government through the ISGTF could prompt costly postponements, which might bring about the speculators and power producers proceeding towards other financing chances.

1.8 Worldwide Potentials of Renewable Energy Sources

The Earth's energy framework seen by the occupants is overwhelmed by the environmental heat associated with the nursery the impact initiated via carbon dioxide (CO_2) accumulation, which captures solar energy and stores it inside a surface sheet of topsoil and air around the Earth. Just 0.02 % of this energy

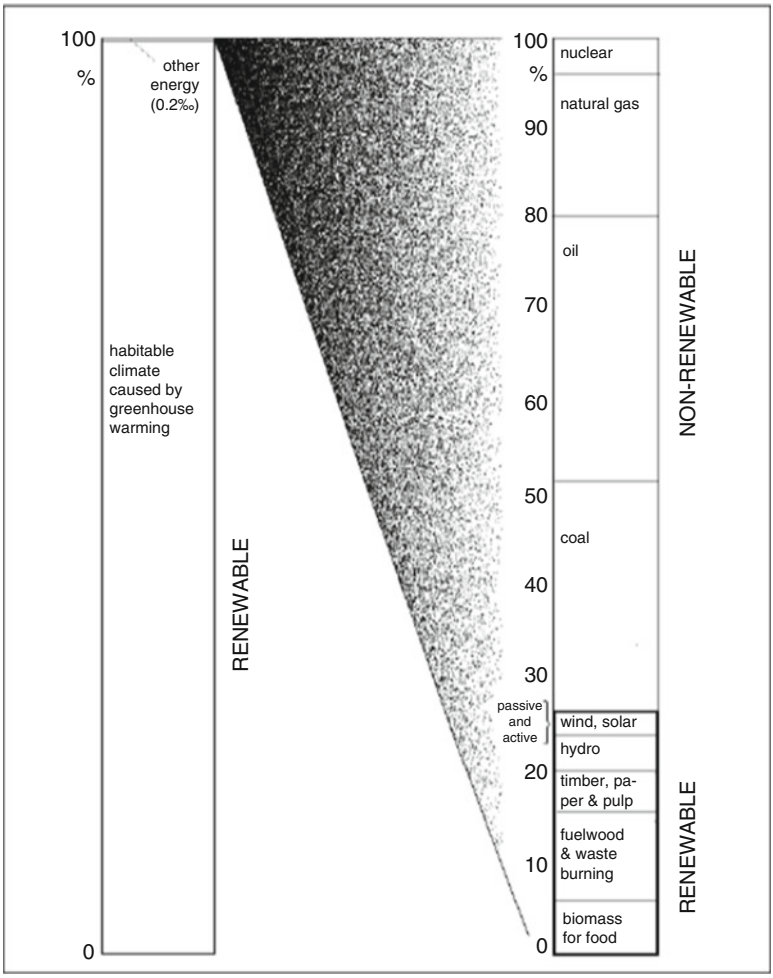


Fig. 1.4 Renewable energy in the global energy system

framework is right now overseen by human culture, as delineated in Fig. 1.4. Inside this financially managed part of the energy sector, renewable energy sources as of now give around 25 % of the energy supplied. According to Fig. 1.4, a vast a piece of this renewable energy is biomass energy, either in food crops or in managed forestry supplying wood to streamlined purposes or for incineration. The moreover misused wellsprings of renewable energy incorporate hydro, wind and sun powered. Hydropower is a considerable source; however its utilization is no more developing because of ecological cutoff points distinguished in numerous areas with potential hydro assets. Passive solar warming is a key characteristic of building design all over the world, yet active solar warming power panels are still at an extremely moment level of penetration. Wind energy has a both passive and

active role, inactive utilization of wind energy for ventilation of structures assumes a critical part, and active power generation by wind turbines is today a quickly developing energy innovation in numerous parts of the world. The elevated penetration reaching at almost 20 % of aggregate power produced is found in Denmark, the nation pioneering present day wind innovation. As demonstrated in Fig. 1.4, the predominant energy sources are still fossil fills, notwithstanding the way that they are depletable and a reason for regular national clashes, because of the crisscross between their specific topographical accessibility and interest examples. Further renewable energy innovations, so far with little worldwide penetration, incorporate biofuels, for example, biogas and geothermal power and heat will start to exist.

Current renewable energy markets contain purchaser markets, markets determined by government show programmes and business sector invigorating subsidy plans. The explanation behind the initialization is in part modern arrangement, pointed at kicking new industry ranges off, the expected energy commercial ventures are not completely paying for the negative ecological effects initiated by their items. This is a complex issue, part of the way on account of the challenge in careful determination of outside expenses. Partly due to the fact that most nations recently require tariff on energy items that may to some extent be helping towards paying for the natural damage. Active use of renewable energy have been penetrating recently, in national energy frameworks, and the Figs. 1.5, 1.6, 1.7, 1.8, 1.9, 1.10, 1.11, 1.12, 1.13, 1.14, and 1.15 show the qualities for year 2000, which may serve as a source of perspective year for surveying up to date information. In situations where the development rate is specifically high, its 12-month quality is specified indicating the national appropriation of businesses.

The national average values of wind power generation for year 2000 are indicated in Fig. 1.5 based upon BTM (2001) and an average capacity factor of 0.3. The world average for the year 2000 is 0.92 W/cap. The development in cumulated introduced capacity from 2000 to 2001 was 35 % (BTM 2002). A few eyewitnesses anticipate that the development will moderate throughout the accompanying years,



Fig. 1.5 Wind power production (Courtesy: NCEP-NCAR, 1998)

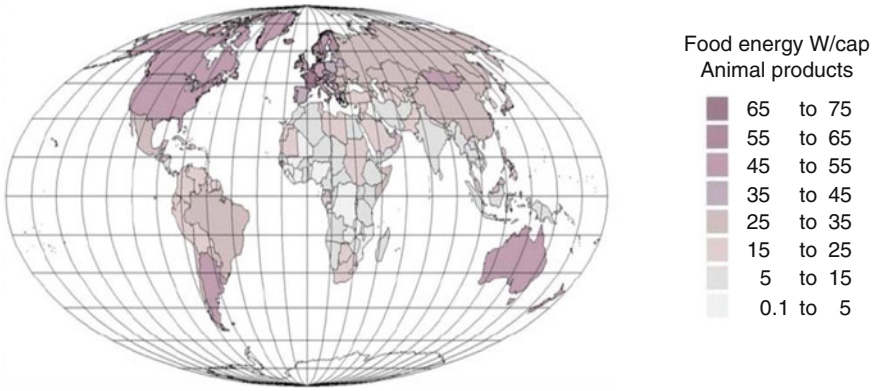


Fig. 1.6 Illustrates biomass energy contained in time-averaged food intake of animal products (Courtesy: NCEP-NCAR, 1998)

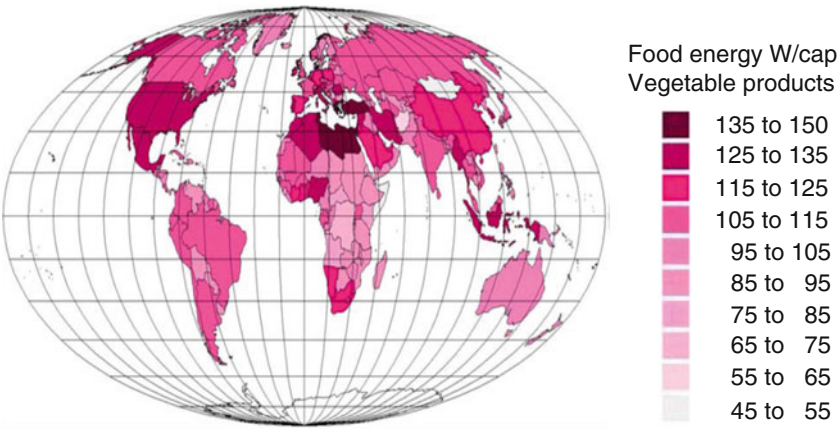


Fig. 1.7 Shows biomass energy contained in human time averaged food intake of vegetable products (Courtesy: FAO, 2003)

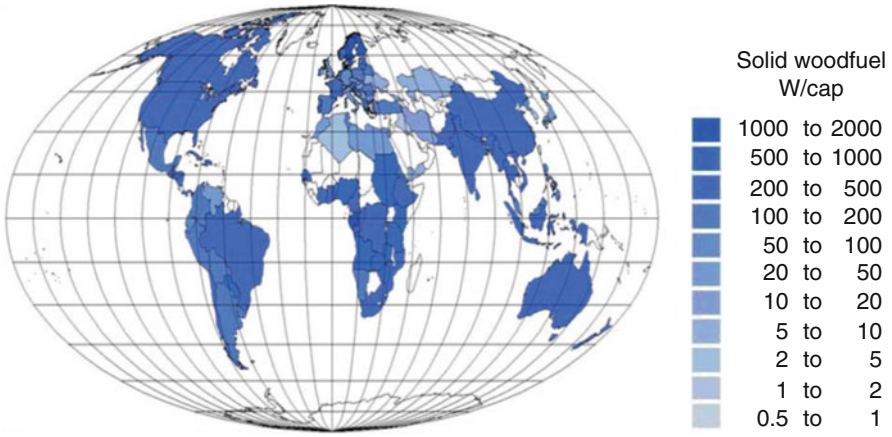


Fig. 1.8 Shows biomass energy contained in wood fuel (Courtesy: OECD/IEA 2002a; 2002b)



Fig. 1.9 Shows energy in biomass waste (refuse) utilised for power or heat production (Courtesy: OECD/IEA 2002a; 2002b)



Fig. 1.10 Shows energy of liquid biofuels namely ethanol and biodiesel (Courtesy: OECD/IEA 2002a; 2002b)

for monetary and political reasons, however then to continue development (Wind Control Monthly 2003).

The average animal based food consumption for the year 2000 is 22.2 W/cap. The national average values for year 2000 are shown in Fig. 1.6 (FAO 2003).

National average Values for year 2000 are shown in Fig. 1.7. The world average vegetable food intake for year 2000 is 113.7 W/cap.

National average values of biomass energy held in wood fuel for year 2000 are indicated in Fig. 1.8. The world normal wood-fuel use in year 2000, inferred by the



Fig. 1.11 Shows energy in biogas (Courtesy: OECD/IEA 2002a; 2002b)

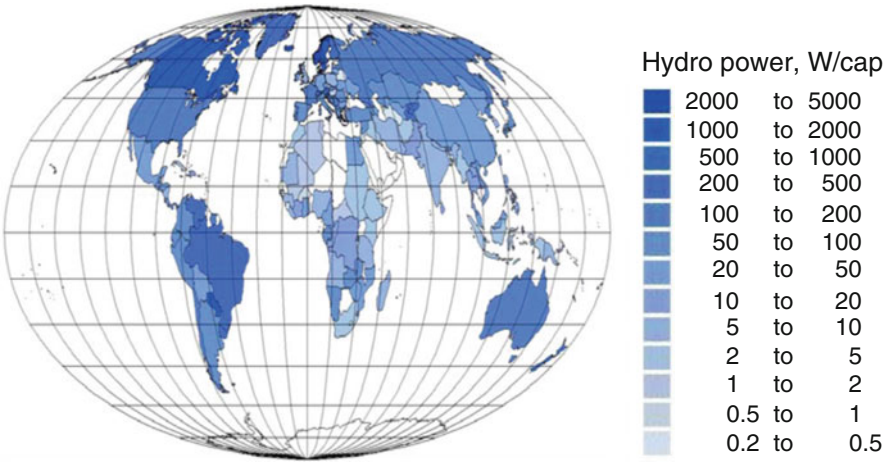


Fig. 1.12 Energy in hydropower (Courtesy: OECD/IEA 2002a; 2002b)

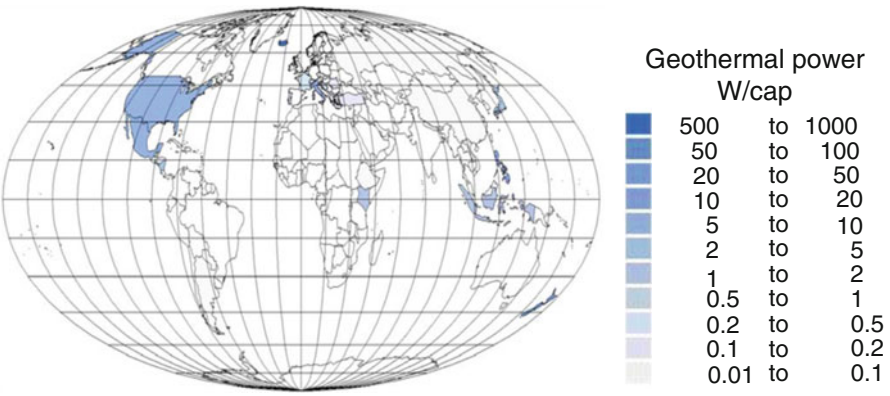


Fig. 1.13 Energy in geothermal power (Courtesy: OECD/IEA 2002a; 2002b)



Fig. 1.14 Energy of solar power (Courtesy: OECD/IEA 2002b)



Fig. 1.15 Energy in solar heat (Courtesy: IEA PVPS 2001)

information, is 221.9 W/cap. No wood fuel utilization is accounted for Russia, while other nations are not secured by the information source.

National average values for year 2000 are shown in Fig. 1.9 based upon OECD/IEA. The world average for year 2000 is 3.7 W/cap.

National average values for year 2000 are shown in Fig. 1.10, based upon EC-ATLAS (2003) and OECD/IEA. The world average for year 2000 is 2.3 W/cap.

National average values for year 2000 are demonstrated in Fig. 1.11, based on converting the amount of units (FAO-Asia 2003), with an assumption that for every family unit a biogas production of half that of an optimally working unit fed manure from the equivalent of 2.5 cows and producing 1,736 W of biogas. The information is obtained from OECD/IEA. The world normal for year 2000 is 2.8 W/cap.

National average values for year 2000 are shown in Fig. 1.12, based upon OECD/IEA and installed power data from Aqua-Media (1997) for countries not covered by IEA, using estimated capacity factors of 0.2–0.4. The world average for year 2000 is 50 W/cap.

National average values for year 2000 are shown in Fig. 1.13 based upon either 10 % of heat input given in OECD/IEA or 60 % of installed power from Barbier (1999). The world average for year 2000 is 9.3 W/cap.

National average values for year 2000 are shown in Fig. 1.14 based upon OECD/IEA or an average energy production equal to 10 % of the installed capacity given in IEA-PVPS (2001). The world average for year 2000 is 0.007 W/cap. The growth rate from 2000 to 2001 was 35 %.

National average values for year 2000 are shown in Fig. 1.15, based upon IEA-PVPS. Both building-integrated and central district heating thermal systems are included. The world average for year 2000 is 0.11 W/cap.

The conventional utilization of biomass for combustion is still the commanding utilization of renewable energy. The utilization of nourishment energy in biomass of creature or vegetable cause is marginally less (146 W/cap). Next comes to hydropower (50 W/cap) and after that geothermal force, which could be considered partially renewable (as numerous steam repositories are abused at a rate that will deplete the store over times of decades). Deciphering OECD information (OECD 2002) to energy units, the current entire bargain cost of grains, for example, rice or wheat are around 70 c/kwh, while the entire deal cost of normal meat and dairy items are about 100 c/kwh. Nonetheless, the quickest developing markets are those of wind and sunlight based force, both right now including 35 % of introduced power every year. Just specific gourmet items get higher costs in the commercial center. Purchaser retail costs are commonly five times higher than the mass costs recently cited. This is more than 30 times the current buyer cost of a kwh of power generated from fossil fills. Wholesale market costs for biomass waste and fuel wood range from about 1 c/kwh (of "blazing quality", i.e. energy of ignition) in India (FAO-Asia 2003) to around 2 c/kwh in industrialized nations (e.g. straw, wood chips 1.6 c/kwh and wood pellets 1.9 c/kwh, Danish Energy Agency, 1996. For correlation, the expense of coal before acknowledging externalities is 0.5 c/kwh (Danish Energy Agency 2002). The generation expense of biogas is 3.6–7 c/kwh (Danish Energy Agency 1992). While that of wind force is 3–7 c/kwh, contingent upon wind conditions and that of photovoltaic solar energy is 40–130 c/kwh (IEA-PVPS 2002). The photovoltaic business revels in generous open start-up subsidies to industry (frequently as financing client ventures or offering engaging purchase back rates for overabundance sun based force). This is the situation in nations, for example, Germany, Japan, and in Switzerland the business has to a great extent been made by commercial enterprises purchasing PV (Photovoltaic's) for reasons of feel or picture greening.

1.9 Need for New Energy Technologies

The IEA's most recent observations on global energy are as follows:

- All current energy trends are not sustainable.
- Oil will likely remain the leading energy source.

- Oil fields have declined, so undiscovered oil reserves will be needed to sustain current consumption.
- Countries must cooperate on holding the average global temperature rise to 3.6 °F (2 °C).
- Arresting current global temperature rise requires lowering emissions in both industrialized and non industrialized regions.

For hydropower, improvement is required to be generally confined to arrangement with ecological and social effects. This could prompt accentuation on smaller, falling plans rather than the exact extensive dam establishments seen previously. Still, the basic technology must be considered as fully developed, and the cost of environmentally sound hydro schemes is rarely lower than that of fossil fuels, the expansion rate of hydropower globally has narrowed to nearly zero. There are still possible new sites available, and if social acceptance can be regained after the disasters of the past, then environmentally integrated hydro could add a further substantial amount to global renewable energy supply. On account of wind turbines, a further advancement with present patterns, especially in materials, will permit bigger flat pivot turbines to be assembled. In spite of the fact that other wind change methods could get practical, the achievement of the flat hub idea is liable to keep it in a heading position. Modification in blade profile and regulation characteristics of the blades are prone to be accompanied by the broad investment in offshore wind. Currently, the same turbines are sold for deployment on land and at sea. However, the wind conditions at sea are so different, that the land design typically chosen to optimize total annual production at good sites on land, far from the same turbine which is placed off-shore. But these concerns still involve only small adjustments to a technology which is already close to maturity, with different blade designs for different locations, and for control of pitch. The later is applied in commercial turbines and gives a few percent improvement in average efficiency. Thus, the main challenge in wind turbines is improvement of materials, particularly for blades and also for cost reduction of foundations. Such advances in blade construction will allow turbines with rated power larger than the 2–3 MW which is typical at present. Furthermore, with any mature technology continued small improvements in cost per produced kWh with time can be expected. Entirely new concepts could be imagined for harvesting, still higher wind power levels are found at open sea, i.e. much further offshore than exploited by current machines standing on the sea floor. These could be consolidated wave and wind-capturing gadgets, drifting however kept inside a limited region by praiseworthy navigation framework. The wind turbines could be covered or ducted developments, while the wave energy part is liable to utilize double air turbines. No improvements in this bearing have been fruitful so far. Wave energy devices for near-shore employment have not successfully struck the balance between the necessary strength and economic power production, and no large mid-ocean wave converters have reached interesting sizes for energy production.

Various biomass change routines are close enough to guide investment practicality for the incorporation of backhanded matters of trade and profit in expense

correlations to make them adequate. This is valid for biogas plants, especially on a mutual scale and as a major aspect of general waste administration plans. Gasification plans accompanied by hydrogen or fluid biofuel creation are additionally getting suitable, contingent upon the valuation utilized for the externalities of current fuel-based energy frameworks. Without contemplations of backhanded matters of trade and profit, such plans are not presently practical, as showed by the endeavors to generate vaporous and fluid fills from coal and sugar crops. However, in addition to altering the economic valuation, there is certainly room for technology improvements in gasification, cleaning and chemical reaction steps, involving device construction and possibly use of new pathways are possible. The entire bioenergy field may be in for a radical restructuring if the current trends of valuing high food quality continues and spreads to regions not currently being concerned. This may alter agricultural practices, both for plant and animal production, and lead to new concepts of integrated food and energy production based upon ecological principles, such as distinct from the concept of dedicated energy crops. Geothermal resources used in a sustainable way can be a stable source of low-temperature heat, and cost already appears acceptable. The market for such geothermal solutions depends on the viability of district heating. New projects of district heating by geothermal energy are coming on-line, e.g. the Amager plant serving the existing Copenhagen heat network. If the full potential for making existing and new buildings highly energy-efficient is realized, there will be very few locations in the world, where distinct heating is economically attractive (probably only city centre's with dense high-rise buildings).

As regards solar energy, the thermal applications are in some, not too high-latitude regions, economically viable in an assessment including externalities for conventional solutions. But also this depends on whether the building is energy-efficient in the first place. A large heat requirement in winter is little compatible with solar coverage, but if the passive and active efficiency features of the building are optimal, the heat load may be dominated by hot water use, which is more amenable to solar supply. This is especially for niche markets, for example, vacation areas (e.g. in the Mediterranean area or comparable spots) where there may be loads of building space being possessed just throughout the summer season. For solar power, the circumstances is diverse, as the current expenses of photovoltaic force frameworks are still excessively high even with liberal thought of circuitous expenses. On the other hand, the specialized improvement is fast here, and novel results under present advancement for customary solar cells may achieve financially engaging results in the following one or two decades. Likewise, there is a nearly infinite amount of novel systems for changing over solar energy that could assume a conclusive part later on. The utilization of natural colors, right now in its early stages, with characteristic low productivity and short lifetimes could pick up new force by supplanting Tio_2 materials and ruthenium-based colors with ideas dependent upon polymers and natural colors or the developing three-dimensional photonic crystalline carbon structures, which would conceivably permit a built station of suitable properties.

1.10 Introduction to Matlab and Simulink

MATLAB is numerical computation and simulation software that was developed as a commercial tool with an easy to use interface based on the earlier numerical libraries such as LINPACK and EISPACK, which were initially composed in the FORTRAN customizing dialect. Rather than the well-known computer algebra programs, for example, MAPLE or MATHEMATICA, which are fit for performing typical operations and accordingly, ascertaining numerical comparisons as an individual would ordinarily do with paper and pencil. MATLAB has the capability to perform absolute numerical estimations. Computer algebra programs oblige complex information structures that include muddled syntax structure for the standard client and complex projects for the programmer. Anyhow MATLAB, basically includes a single information structure, whereupon all its operations are based. This is the numerical field, or, as such, the matrix. This is reflected in the name: MATLAB is an abbreviation for Matrix Laboratory. MATLAB is not only a numerical instrument for assessment of equations, however is likewise a free customizing dialect fit for treating complex issues and is provided with all the key builds of a higher modifying dialect. Since the MATLAB summon interface includes a supposed translator and MATLAB is a mediator dialect, all summons might be completed straightforwardly. This makes the testing of specific programs much easier.

In addition, MATLAB 7 is furnished with a very well conceived editor with debugging functionality, which simplifies the development and error analysis of large MATLAB programs. One of the major advantage is the interaction with the special toolbox SIMULINK, which is used for building and creating simulation models based on a graphical interface similar to block diagrams. The simulation runs under MATLAB and the interconnection between MATLAB and SIMULINK is guaranteed.

SIMULINK is a tool for simulating dynamic systems derived from the terms **Simu**lation and **Link**. It is available in the form of a toolbox which is an integral part of the MATLAB environment. SIMULINK is linked with MATLAB with a graphical user interface and also includes a comprehensive library of a number of linear, non-linear, continuous, and discrete functions available in block form. The goal of this book is to introduce simple manipulations related to solar PV and wind energy conversion systems with SIMULINK blocksets.

1.11 Introduction to Soft Computing

Numerous human mental exercises, for example, composing PC projects, performing arithmetic calculations, logical thinking, comprehension dialect, and even driving a car demand “intelligence”. Over the past few decades, a few PC frameworks have been assembled, that can perform complex tasks. Exclusively,

there are machine frameworks that can diagnose illnesses, arrange the combination of complex natural synthetic mixes, compute differential mathematical equations in symbolic structure, dissect electronic circuits, understand constraints in problems, or compose mini PC projects to meet formal requirements. Such frameworks possess a certain level of Soft computing. Most of the above mentioned intelligent work has occurred in the field called Soft computing (AI). Several AI projects are truly perplexing complex tasks and mastering their multifaceted nature is a major research objective.

Such kind of intelligent techniques are required in several areas and in this book the authors provide different AI methods in solar and wind energy applications. Solar energy provisions incorporate the estimation of solar radiation, solar heating, solar PV systems, MPPT models and numerous others. While wind energy includes power factor calculation, pitch angle control in wind turbines, and MPPT controllers. The major objectives of AI research are:

- Understand human cognition.
- Cost-effective automation replaces humans in intelligent tasks.
- Cost-effective intelligent amplification builds systems to help humans think better, and faster.
- Superhuman intelligence builds programs to exceed human intelligence.
- General problem-solving solves a broad range of problems.
- Coherent discourse communicates with people using natural language.
- Autonomy has intelligent systems acting on own initiative.
- Training of the system should be able to gather own data.
- Store information and know how to retrieve it.

1.11.1 Soft Computing Techniques

AI techniques have the potential for making better, quicker and more practical predictions than any of the traditional methods. AI consists of several branches such as artificial neural network (ANN), fuzzy logic (FL), Adaptive Network based Fuzzy Inference System (ANFIS) and Data Mining (DM).

1.11.1.1 Artificial Neural Networks (ANN)

Artificial Neural Networks are relatively crude electronic models based on the neural structure of the brain. The brain basically learns from experience. It is natural proof that some problems that are beyond the scope of current computers are indeed solvable by small energy efficient packages. This brain modeling also promises a less technical way to develop machine solutions. This new approach to computing also provides a more graceful degradation during system overload than its more traditional counterparts.

These biologically inspired methods of computing are thought to be the next major advancement in the computing industry. Even simple animal brains are capable of functions that are currently impossible for computers. Computers do rot things well, like keeping ledgers or performing complex math. But computers have trouble recognizing even simple patterns much less generalizing those patterns of the past into actions of the future.

Now, advances in biological research promise an initial understanding of the natural thinking mechanism. This research shows that brains store information as patterns. Some of these patterns are very complicated and allow us the ability to recognize individual faces from many different angles. This process of storing information as patterns, utilizing those patterns, and then solving problems encompasses a new field in computing. This field, as mentioned before, does not utilize traditional programming but involves the creation of massively parallel networks and the training of those networks to solve specific problems. This field also utilizes words very different from traditional computing, words like behave, react, self-organize, learn, generalize, and forget.

Basically, all artificial neural networks have a similar structure or topology as shown in Fig. 1.16. In this structure some of the neurons interfaces to the real world to receive its inputs. Other neurons provide the real world with the network's outputs. This output might be the particular character that the network thinks that it has scanned or the particular image it thinks is being viewed. All the rest of the neurons are hidden from view.

But a neural network is more than a bunch of neurons. Some early researchers tried to simply connect neurons in a random manner, without much success. Now, it is known that even the brains of snails are structured devices. One of the easiest

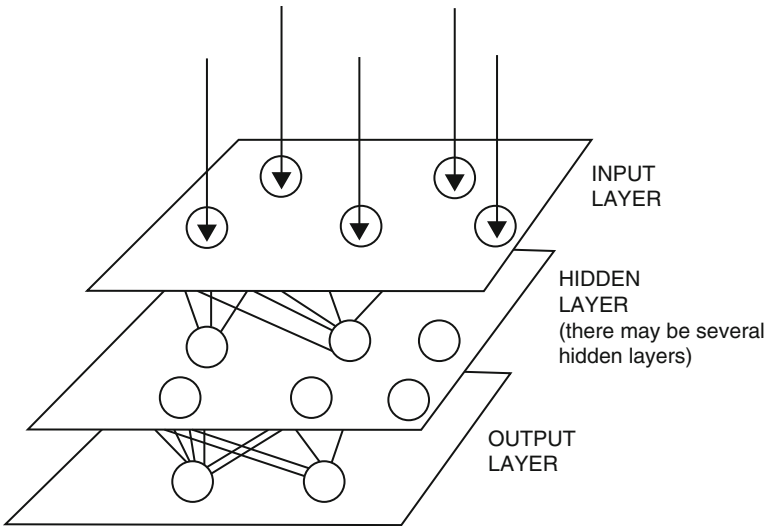


Fig. 1.16 A simple neural network diagram

ways to design a structure is to create layers of elements. It is the grouping of these neurons into layers, the connections between these layers, and the summation and transfer functions that comprises a functioning neural network. The general terms used to describe these characteristics are common to all networks.

Although there are useful networks, which contain only one layer, or even one element, most applications require networks that contain at least the three normal types of layers – input, hidden, and output. The layer of input neurons receives the data either from input files or directly from electronic sensors in real-time applications. The output layer sends information directly to the outside world, to a secondary computer process, or to other devices such as a mechanical control system. Between these two layers can be many hidden layers. These internal layers contain many of the neurons in various interconnected structures. The inputs and outputs of each of these hidden neurons simply go to other neurons.

In most networks each neuron in a hidden layer receives the signals from all of the neurons in a layer above it, typically an input layer. After a neuron performs its function it passes its output to all of the neurons in the layer below it, providing a feed-forward path to the output. These lines of communication from one neuron to another are important aspects of neural networks. They are the connections, which provide a variable strength to an input. There are two types of these connections. One causes the summing mechanism of the next neuron to add while the other causes it to subtract. In more human terms one excites while the other inhibits. Another type of neural network connection is feedback. This is where the output of one layer routes back to a previous layer. An example of this is shown in Fig. 1.17.

The way that the neurons are connected to each other has a significant impact on the operation of the network. In the larger, more professional software development packages the user is allowed to add, delete, and control these connections at will. By "tweaking" parameters these connections can be made to either excite or inhibit.

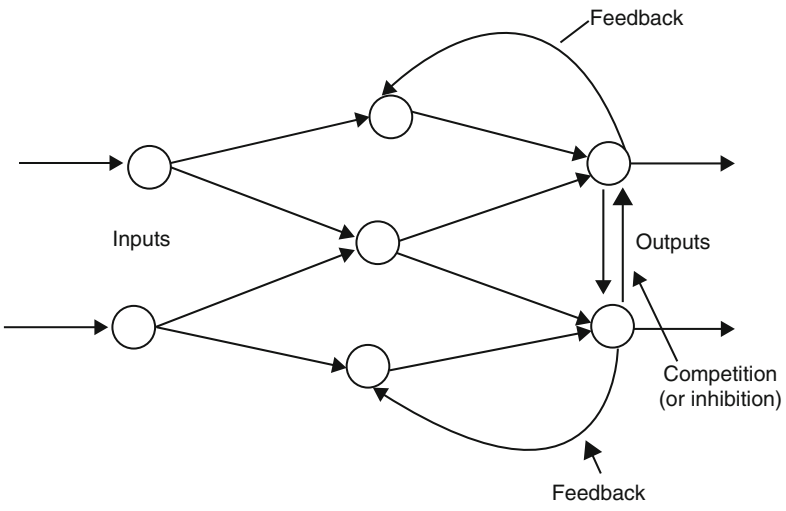


Fig. 1.17 Simple network with feedback and competition

Once a network has been structured for a particular application, that network is ready to be trained. To start this process the initial weights are chosen randomly. Then, the training, or learning, begins. There are two approaches to training – supervised and unsupervised. Supervised training involves a mechanism of providing the network with the desired output either by manually "grading" the network's performance or by providing the desired outputs with the inputs. Unsupervised training is where the network has to make sense of the inputs without outside help.

Neuron connection weights are not just modified in one pass. The process by which neuron weights are modified occurs over iterations. The neural network is presented with training data, and then the results are observed. These results must in some way change the connection weights in order for the neural network to be learn. The exact process by which this happens is determined by the learning algorithm.

1.11.1.2 Fuzzy Logic (FL)

Fuzzy Logic was initiated in 1965 by Lotfi A. Zadeh, professor for computer science at the University of California in Berkeley. Basically, Fuzzy Logic (FL) is a multivalued logic that allows intermediate values to be defined between conventional evaluations like true/false, yes/no, high/low, etc. These intermediate values can be formulated mathematically and processed by computers, in order to apply a more human like way of thinking. Based on Aristotle and other later mathematicians, the so called "Laws of Thought" was posited. One of these, the "Law of the Excluded Middle," states that every proposition must either be True or False. Even when Parminedes proposed the first version of this law (around 400 B. C.) there were strong and immediate objections: for example, Heraclitus proposed that things could be simultaneously True and not True. It was Plato who laid the foundation for what would become fuzzy logic, indicating that there was a third region (beyond True and False) where these opposites "tumbled about." Other, more modern philosophers echoed his sentiments, notably Hegel, Marx, and Engels. But it was Lukasiewicz who first proposed a systematic alternative to the bi – valued logic of Aristotle. Even in the present time some Greeks are still outstanding examples for fussiness and fuzziness. Fuzzy Logic has emerged as a profitable tool for the controlling and steering of systems and complex industrial processes, as well as for household and entertainment electronics, as well as for other expert systems and applications like the classification of SAR data. A few features of fuzzy logic are listed below:

- *Fuzzy logic is conceptually easy to understand*. The mathematical concepts behind fuzzy reasoning are very simple. Fuzzy logic is a more intuitive approach without the far reaching complexity.
- *Fuzzy logic is flexible*. With any given system, it is easy to add on more functionality without starting again from scratch.

- *Fuzzy logic is tolerant of imprecise data*. Everything is imprecise on a closer look, but more than that, most things are imprecise even on careful inspection. Fuzzy reasoning builds this understanding into the process rather than tacking it on to the end.
- *Fuzzy logic can model nonlinear functions of arbitrary complexity*. A fuzzy system can be created to match any set of input-output data. This process is made particularly easy by adaptive techniques like Adaptive Neuro-Fuzzy Inference Systems (ANFIS), which are available in Fuzzy Logic Toolbox software.
- *Fuzzy logic can be built on top of the experience of experts*. In direct contrast to neural networks, which use training data and generate opaque, impenetrable models, fuzzy logic lets the user rely on the experience of people who already understand the system.
- *Fuzzy logic can be blended with conventional control techniques*. Fuzzy systems don't necessarily replace conventional control methods. In many cases fuzzy systems augment them and simplify their implementation.
- *Fuzzy logic is based on natural language*. The basis of fuzzy logic is human communication. This observation underpins many of the other statements about fuzzy logic. Because fuzzy logic is built on the structures of qualitative description used in everyday language, fuzzy logic is easy to use (MATLAB Fuzzy logic toolbox user's guide).

A fuzzy expert system shown in Fig. 1.18 consists of four components namely, the fuzzifier, the inference engine, and the defuzzifier, and a fuzzy rule base.

In the fuzzifier, crisp inputs are fuzzified into linguistic values to be associated to the input linguistic variables. After fuzzification, the inference engine refers to the fuzzy rule base containing fuzzy IF-THEN rules to derive the linguistic values for the intermediate and output linguistic variables. Once the output linguistic values are available, the defuzzifier produces the final crisp values from the output linguistic values.

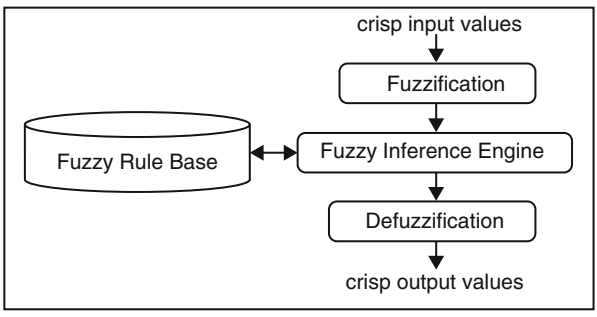


Fig. 1.18 Fuzzy expert system model

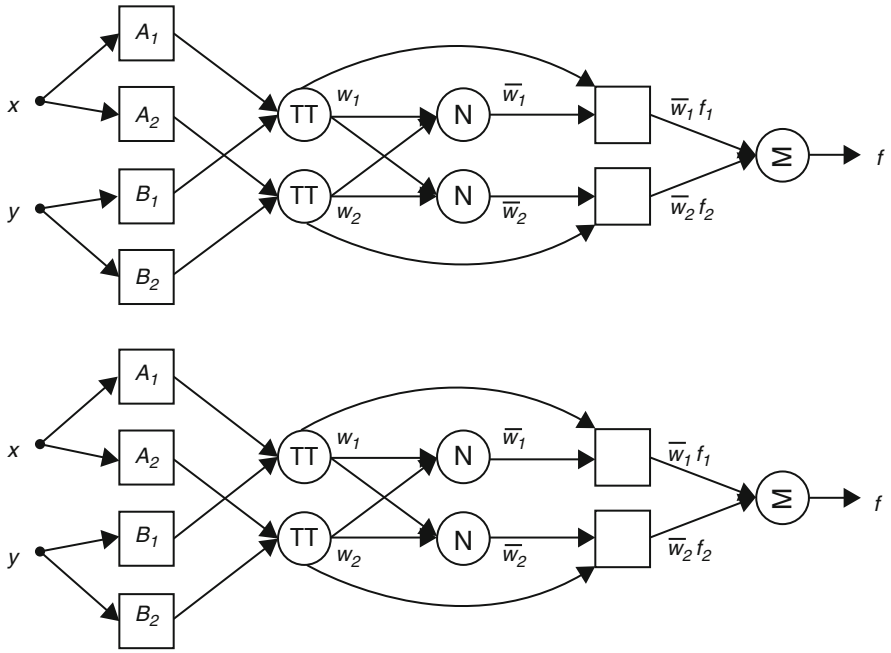


Fig. 1.19 ANFIS architecture

1.11.1.3 Adaptive Network Based Fuzzy Inference System (ANFIS)

ANFIS implements a Takagi Sugeno FIS and has a five layered architecture as shown in Fig. 1.19. The first hidden layer is for fuzzification of the input variables and T-norm operators are deployed in the second hidden layer to compute the rule antecedent part. The third hidden layer normalizes the rule strengths followed by the fourth hidden layer where the consequent parameters of the rule are determined. Output layer computes the overall input as the summation of all incoming signals. ANFIS uses backpropagation learning to determine premise parameters (to learn the parameters related to membership functions) and least mean square estimation to determine the consequent parameters. A step in the learning procedure has got two parts: In the first part the input patterns are propagated, and the optimal consequent parameters are estimated by an iterative least mean square procedure, while the premise parameters are assumed to be fixed for the current cycle through the training set. In the second part the patterns are propagated again, and in this epoch, backpropagation is used to modify the premise parameters, while the consequent parameters remain fixed. This procedure is then iterated.

The functionality of nodes in ANFIS can be summarized as follows:

- *Layer 1*: Nodes are adaptive; membership functions (MFs) of input variables are used as node functions, and parameters in this layer are referred to as antecedent or premise parameters.
- *Layer 2*: Nodes are fixed with outputs representing the firing strengths of the rules.

1.11.1.4 Genetic Algorithms (GA)

The Genetic Algorithm (GA) is a model of machine learning which derives its behavior from a metaphor of some of the mechanisms of evolution in nature. This is done by the creation within a machine of a population of individuals represented by chromosomes, in essence a set of character strings that are analogous to the base-4 chromosomes. The individuals in the population then go through a process of simulated "evolution". Genetic algorithms are used for a number of different application areas. An example of this would be multidimensional optimization problems in which the character string of the chromosome can be used to encode the values for the different parameters being optimized.

In practice, the genetic model of computation can be implemented by having arrays of bits or characters to represent the chromosomes. Simple bit manipulation operations allow the implementation of crossover, mutation and other operations. Although a substantial amount of research has been performed on variable-length strings and other structures, the majority of work with genetic algorithms is focused on fixed-length character strings. The users should focus on both this aspect of fixed-length and the need to encode the representation of the solution being sought as a character string, since these are crucial aspects that distinguish genetic programming, which does not have a fixed length representation and there is typically no encoding of the problem.

The genetic algorithm is implemented by evaluating the fitness of all of the individuals in the population. Then a new population is created by performing operations such as crossover, fitness-proportionate reproduction and mutation on the individuals whose fitness has just been measured. The old population is discarded and the iteration continues using the new population. A single iteration of this cycle is referred to as a generation. There is no theoretical reason for this as an implementation model. Indeed, behavior in populations in nature is not found as a whole, but it is a convenient implementation model.

The first generation (generation 0) of this process operates on a population of randomly generated individuals. From there on, the genetic operations, in concert with the fitness measure, operate to improve the population.

The pseudocode of GA is given as follows:

```
// start with an initial time
  t := 0;
// initialize a usually random population of individuals
  initpopulation P (t);
// evaluate fitness of all initial individuals of population
  evaluate P (t);
// test for termination criterion (time, fitness, etc.)
  while not done do
   // increase the time counter
        t := t + 1;
   // select a sub-population for offspring production
        P' := selectparents P (t);
   // recombine the "genes" of selected parents
        recombine P' (t);
   // perturb the mated population stochastically
        mutate P' (t);
   // evaluate its new fitness
        evaluate P' (t);
   // select the survivors from actual fitness
        P := survive P,P' (t);
 od
end GA.
```

1.11.2 Applications of Soft Computing Techniques in Solar Energy

Soft computing (SC) techniques have been used by various researchers in solar energy applications. This section deals with an overview of these applications and some examples on the use of SC techniques in the solar energy applications are summarized in Table 1.5. ANNs are used to predict and estimate local and global solar radiation. The energy consumption can be predicted using ANNs in solar building and also in modeling solar steam generators. Efficiency of solar flat PV collectors can be estimated using appropriate ANN models. Fuzzy logic is applied in photovoltaic solar energy systems, solar tracking system, to predict solar radiation and in solar powered energy. Fuzzy logic controllers are applied to control solar air-conditioning system, for maximum power point tracking, and in charge controllers. Combination of neural networks and fuzzy logic are applied as ANFIS systems to predict solar radiation and temperature. The ANFIS systems are also applied to model the power supply of PV systems. Genetic Algorithms are used as optimization tools in solar PV based systems in the areas such as solar tracking, solar irradiation, parameter identification in solar cells, and for temperature control in solar water heating systems.

Table 1.5 Summary of SC applications in solar energy

Soft computing technique	Area
Artificial neural networks	Prediction of solar radiation
	Modeling of solar steam-generator
	Estimation of global solar radiation
	Prediction of the energy consumption of a passive solar building
	Characterization of PV modules
	Efficiency of flat-plate solar collectors
	Heating controller for solar buildings
	Modeling of a solar air heater
	MPPT controller
	Prediction of solar energy potential
Fuzzy logic	Photovoltaic solar energy systems
	Sun tracking system
	Solar powered energy
	Prediction of solar radiation
	Control of solar buildings
	Controller of solar air-conditioning system
	Sizing of PV systems
	MPPT controller
	Solar tracking system
	Charge controller
	Solar heating
	Solar irradiance
Adaptive network based fuzzy inference system	Prediction of solar radiation and temperature
	Modeling of photovoltaic power supply
Genetic algorithms	Photovoltaic solar energy systems
	Solar irradiation
	Determination of Angstrom equation coefficients
	Solar water heating systems
	Hybrid solar–wind system
	PV-diesel hybrid system
	Solar cell
	Solar tracking
	Parameter identification in solar cells
	Sizing of a solar thermal electricity plant
	Sizing of solar water heaters
	Solar thermal energy storage
	Flat plate solar air heater

1.11.3 Applications of Soft Computing (AI) Techniques in Wind Energy

Recent researches report the application of Soft computing techniques such as neural networks, fuzzy logic, and genetic algorithms in wind energy. Several SC applications in different areas of wind energy are presented in Table 1.6. ANNs have been applied to forecast wind energy, to predict online wind power, to predict short term wind speed, to predict power ratio in wind turbine and to detect and identify faults in wind turbine systems. These networks are also applied to the controllers such as PID in the wind energy conversion systems. Fuzzy logic has been successfully applied to MPPT control and pitch angle control of wind turbines. In addition, they are also used to predict power generation and parameters in wind turbines. ANFIS systems have been applied to forecast regional wind generation and to forecast wind power. They have produced capable results in predicting power factor of wind turbines. Optimization of power factor, wind blade chord, twist angle, and pitch angle of wind turbines can be effectively performed using GAs. The parameters of wind turbine can also be tuned to their optimal values using genetic algorithms.

Table 1.6 Summary of SC applications in wind energy

Soft computing technique	Area
Artificial neural networks	Controllers for grid connected wind turbine
	PID control of wind energy conversion systems
	Wind energy forecasting
	Online prediction of wind power
	Wind turbine flicker calculation
	Short term wind speed prediction
	Prediction of the power ratio in wind turbine
	Wind turbine siting
	Fault detection and identification for wind turbine systems
Fuzzy logic	MPPT control for wind turbines
	Pitch angle control of wind turbines
	Predicting wind turbine power generation
	Wind speed forecasting
	Prediction of wind turbine parameters
Adaptive network based fuzzy	Forecasting of regional wind generation
	Wind power forecasting
Inference system	Prediction of wind turbine power factor
Genetic algorithms	Wind turbine siting
	Optimization of wind turbine energy and power factor
	Modeling of wind energy systems
	Pitch angle control for wind turbines
	Wind blade chord and twist angle optimization
	Tuning of wind turbine controller

1.12 Summary

Energy plays a fundamental role in the socio-economic development and human welfare of a country. Energy demand is expected to increase by 50 % during the following two decades. Naturally this is creating panic that our energy assets are beginning to run out, with eliminating the outcomes for the worldwide economy and worldwide personal satisfaction. This chapter discussed the energy scenario, global and Indian energy crisis, energy efficiency, classification of energy sources, solar energy, wind energy, benefits of renewable energy, trends in energy consumption, worldwide potentials of renewable energy sources, and the need for new energy technologies. In addition an introduction to MATLAB and SIMULINK is provided with application of soft computing techniques in solar and wind energy generation systems.

Review Questions

1. What is the DC electrical output of PV cells?
2. How are PV cells configured to produce large amount of usable power?
3. How reliable are the PV modules? Discuss their lifetime.
4. What are the factors to be considered while choosing PV cells?
5. State the differences between solar irradiance and solar insolation.
6. Collect a few sources where solar radiation data is available.
7. Discuss about system commissioning, inspection and operation.
8. How does a solar water-heating system work?
9. Can a solar water heater replace an electric or gas water heater?
10. Discuss a few applications of renewable energy systems based on soft computing techniques.

Bibliography

Adzic E, Ivanovic Z, Adzic M, Katic V (2009) Maximum power search in wind turbine based on fuzzy logic control. Acta Polytech Hung 6(1):131–149

Ahmed MM, Sulaiman M (2003) Design and proper sizing of solar energy schemes for electricity production in Malaysia. National Power and Energy Conference 2003, pp 268–271

Alameda Lozada JI (2008) Las Energías Renovables: ¿Solución a la Crisis Económica?, Seminario de Energía: Opciones Energéticas para el Comercio, 24 de Abril 2008

Ardente F, Beccali G, Cellura M (2004) Life cycle assessment of a solar thermal collector. Science Direct

AVA Solar website (2008) IEEE standard for interconnecting distributed resources with electric power systems, New York: IEEE, IEEE Std.1547–2003. http://www.avasolar.com. Accessed June 2008.

Azar C, Schneider S (2002) Are the economic costs of stabilizing the atmosphere prohibitive? Ecol Econ, Science Direct

Basso TS, DeBlasio RD (2003) IEEE P1547-series of standards for interconnection. IEEE, New York

Bergmann A, Colombo S, Hanley N (2006) Rural versus Urban preferences for renewable energy developments. Science Direct.
Bernal-Agustin J, Dufo-Lopez R (2005) Economical and environmental analysis of grid connected photovoltaic systems in Spain. Science Direct
Bode GH, Loh PC, Newman MJ, Holmes DG (2005) An improved robust predictive current regulation algorithm. IEEE Trans Ind Appl 41(6):1720–1733
Borowy BS, Salameh ZM (1996) Methodology for optimally sizing the combination of a battery bank and PV array in a wind/PV hybrid system. IEEE Trans Energy Conv 11(2):367–375
Brini S, Abdallah HH, Ouali A, Economic dispatch for power system included wind and solar thermal energy. Leonardo J Sci (14):204–220
Bryan J, Duke R, Round S (2003) Distributed generation – nanogrid transmission and control options. Int Power Eng Conf 1:341–346
Castro I, Silveira J (2006) Ecological efficiency in thermoelectric power plants. Science Direct
Chaudhari M, Frantzis L, Hoff TE (2004) PV grid connected market potential under a cost breakthrough scenario. Navigant Consulting, Sept 2004. http://www.ef.org/documents/EF-Final-Final2.pdf. Accessed June 2008
Chowdhury AA, Koval DO (2005) Impact of photovoltaic power sources on a power system's capacity reliability levels. I&CPS
Chowdhury BH, Rahman S (1988) Is central power station photovoltaic power dispatchable? IEEE Trans Energy Convers 3(42):747–754
Clean energy project analysis: RETSCREEN® engineering & cases textbook, [Online]. www.retscreen.net. Accessed June 2008
Connor H (2006) Strategies for development in islands: assessing the need for a paradigm shift. IEEE Paper
Conti S, Raiti S, Tina G, Vagliasindi U (2003) Integration of multiple PV units in urban power distribution systems. Sol Energy 75:87–94
Corzine KA, Wielebski MW, Peng FZ, Wang J (2004) Control of cascaded multilevel inverter. IEEE Trans Power Electron 19(3):732–738
Davidson J, The new solar electric home, 20th printing 2001
Duffie JA, Beckman WA (2006) Solar engineering of thermal processes, 3rd edn. Wiley, New York
Dunlop JP (1997) Batteries and charge control in stand alone photovoltaic systems, Jan 1997
Energy Information Administration website. http://www.eia.doe.gov. Accessed June 2008
Estimating PV system size and cost, [Online]. www.InfinitePower.org. Accessed Apr 2007
Griese H, Stobbe L, Reichl H (2005) Eco-design and beyond-key for a global sustainable development. IEEE Paper
Haghbin S, Khan K (2010) Integrated chargers for EV's and PHEV's: examples and new solutions. In: Proceedings of ICEM, pp 1–6, Sept 2010
Hammad AE (1995) Comparing the voltage source capability of present and future var compensation techniques in transmission systems. IEEE Trans Power Deliv 1(1)
Hart DW (1997) Introduction to power electronics. Prentice Hall, New Jersey
Houck CR, Joins JA.A genetic algorithm for function optimization: a matlab implementation
http://www.ren21.net. Accessed June 2008
Hyman D (1988) Modern microeconomics, 2nd edn, pp 148–149
Jäger-Waldau A (2007) PV status report 2007: research, solar cell production and market implementation of photovoltaics. European Commission Directorate General Joint Research Center. http://re.jrc.ec.europa.eu/refsys/pdf/PV_StatusReport_2007.pdf. Accessed June 2008
Jenkins N (1995) Photovoltaic systems for small scale remote power supplies. Power Eng J 9 (2):89–96
Jing W, Jia-hai Y (2006) Green cost of electricity concept and preliminary account system. IEEE Paper
Kannan R, Leong K, Osman R (2005) "Life Cycle Assessment" study of solar PV systems: an example of a 2.7 kWp distributed solar PV system in Singapore. Science Direct

Karki S, Mann M, Salehfar H (2006) Substitution and price effects of carbon tax on CO_2 emissions reduction from distributed energy sources. IEEE Paper
Kleinkauf W, Cramer G, Ibrahim M (2005) PV systems technology: state of the art developments and trends in remote electrification. SMA Technologies AG
Komor P (2004) Renewable energy policy. iUniverse, New York
Li C, Yu Cheng, Zhang L (2008) Research of externality of electricity generation in electricity market. IEEE Paper
Lin C-T, Lee CSG (1996) Neural fuzzy systems: a neuro-fuzzy synergism to intelligent systems. Prentice-Hall, Upper Saddle River
Marquez C, Ryan F (2007) New Fomento open for business. Caribbean Business, Thursday, 12 Apr 2007. http://www.pridco.org/. Accessed Nov 2007
Marxuach SM (2005) Restructuring the Puerto Rico Electricity Sector, vol 3, White paper. Center for the New Economy, San Juan
Mashford K (2007) Unearthly mess. IEEE Paper
Moran D, Wackernagel M, Kitzes J (2007) Measuring sustainable development nation by nation. Science Direct, Ecol Econ
Mortensen J (2008) Factors associated with photovoltaic system costs, NREL/TP.620.29649. http://www.doe.gov/bridge. Accessed June 2008
National Fire Protection Association, National Electrical Code, 1990 Edition
Naval Facilities Engineering Command, Maintenance and Operation of Photovoltaic Power Systems, NAVFAC MO-405.1
Navigant Consulting (2006) A review of PV inverter technology cost and performance projections NREL/SR-620-38771, Jan 2006. www.nrel.gov. Accessed June 2008
NFPA 70-1999, National Electrical Code
NREL (2008) Planning for PV: the value and cost of solar electricity, DOE/GO-102008-2555 Jan 2008. www.eere.energy.gov. Accessed June 2008
Olivier J, Harms T, Esterhuyse D (2007) Technical and economic evaluation of the utilization of solar energy at South Africa's SANAE IV base in Antarctica. Science Direct
Pacca S, Sivaraman D (2007) Parameters affecting the life performance of PV technologies and systems. Science Direct
PREPA (2007) Puerto Rico Electric Power Authority official statement. Apr 2007
Puerto Rican Census website. http://www.gobierno.pr/Censo/
Puerto Rican Government website. http://www.gobierno.pr. Accessed Dec 2007
Puerto Rico Electric Power Authority website. http://www.prepa.com
Puerto Rico Industrial Economic Incentives Law (Law 73), May 2008
Puerto Rico Renewable Energy Incentives Law, Aug 2008
PV system installation and grid-interconnection guidelines in selected IEA countries, Task V, Report IEA PVPS T5-04:2001
Ramakumar R (1993) Photovoltaic systems. Proc IEEE 81(3):365–376
Ramos-Robles CA (2005) Determination of favorable conditions for the development of a wind power farm in Puerto Rico. Master of Science thesis, Department of Electrical and Computer Engineering, University of Puerto Rico, Mayagüez Campus
Rashid MH (2006) Power electronics devices, circuits and applications. Academic Press, San Diego
Renewable energy technology characterizations, Dec 1997, TR-109496. www.nrel.gov/docs/gen/fy98/24496.pdf. Accessed June 2008
RETScreen software online user manual: photovoltaic project model, [Online]. www.retscreen.net. Accessed June 2008
RETScreen International, Clean Energy Decision Support Center, Photovoltaic project analysis. Minister of Natural Resources Canada 2001–2004
Rolf F, Grosskopf S, Pasurka C (2007) Pollution abatement activities and traditional productivity. Ecol Econ, Science Direct

Secretaria Auxiliar de Relaciones Exteriores, Datos Basicos sobre Puerto Rico website. www.estado.gobierno.pr/datos_basicos.htm

Solar Electric Power Association (2001) TEAM-UP final reports: six reports documenting the TEAM-UP program, and the experiences and data collected from the 35 TEAM- UP ventures, Dec 2001. http://www.solarelectricpower.org. Accessed June 2008

Solero L (2001) Nonconventional on-board charger for electric vehicle propulsion batteries. IEEE Trans Veh Technol 50:144–149

Soytas U, Sari R (2007) Energy consumption, economic growth, and carbon emissions: challenges faced by an EU candidate member. Science Direct

Stand-alone photovoltaic systems – a handbook of recommended design practices, Sandia National Laboratories, SAND87-7023, revised Nov 1991

Stoppato A (2006) Life cycle assessment of photovoltaic electricity generation. Science Direct

Surface meteorology and solar energy: a renewable energy resource web site (release 6.0). http://eosweb.larc.nasa.gov/sse/RETScreen/

Svrzek M, Sterzinger G (2005) Solar PV development: location of economic activity. Renewable Energy Policy Report

The Delphi Group (2007) Overview of renewable electricity costs and cost variation final report. Prepared For: The Commission for Environmental Cooperation

Udo H, Heijungs R (2007) Life cycle assessment for energy analysis and management. Science Direct

Vachon S, Menz F (2006) The role of social, political, and economic interests in promoting state green electricity policies. Science Direct

Valarmathi R, Palaniswami S, Devarajan N (2012) Simulation and analysis of wind energy and photo voltaic hybrid system. Int J Soft Comput Eng 2(2):193–200, ISSN: 2231-2307

Waldau A (2007) PV status report 2007_Research, solar cell production and market implementation of photovoltaics

Wiles J (2006) Photovoltaic systems and the 2005 National Electrical Code: suggested practices. Sandia National Laboratories

Wiser R, Bolinger M, Cappers P, Margolis R (2008) Letting the sun shine on solar costs: an empirical investigation of photovoltaic cost trends in California, NREL/TP-620-39300. http://eetd.lbl.gov/EA/EMP. Accessed June 2008

Zhang C, Zhao Z, Han J (2007) Renewable energy in China: an strategic imperative. IEEE Paper

Chapter 2
Application of MATLAB/SIMULINK in Solar PV Systems

Learning Objectives
On completion of this chapter, the reader will have knowledge on:

- Basic components of Solar PV system and its merits and demerits.
- Involvement of power electronic devices in Solar PV components.
- MATLAB/SIMULINK model of different control strategies of power conditioning unit.
- Importance of MATLAB/SIMULINK model in improving the efficiency of the overall solar PV system.
- Characteristics of Solar PV panel and its MATLAB/SIMULINK model.
- Characteristics and MATLAB/SIMULINK model of Solar PV power conditioning unit.

MATLAB and Power electronics application ranges from power supplies to robotic controls, industrial automation, automotive, industrial drives, power quality, and renewable energy systems. In particular, before the installation of power plant, MATLAB finds applications in selecting the system based on the requirements and to choose particular components for the Solar PV application. This chapter is to explore the role and possibility of MATLAB along with its tool boxes in Solar PV Systems to promote Modeling, and Simulation with emphasis on Analysis, and Design. In renewable energy systems applications, MATLAB helps for selecting the matrix manipulations in the converters to grid inverter, plotting of functions and data, implementation of MPPT algorithms, creation of user interfaces for monitoring the Solar PV modules and for interfacing with inverters and converters, wherein which control algorithms would be written in other languages. As a result of the MATLAB simulation of the components of the solar PV system one can benefit from this model as a photovoltaic generator in the framework of the MATLAB/SIMULINK toolbox in the field of solar PV power conversion systems. In addition,

© Springer International Publishing Switzerland 2015

S. Sumathi et al., *Solar PV and Wind Energy Conversion Systems*,
Green Energy and Technology, DOI 10.1007/978-3-319-14941-7_2

such models discussed in this chapter would provide a tool to predict the behavior of solar PV cell, module and array, charge controller, SOC battery, inverter, and MPPT, under climate and physical parameters changes.

2.1 Basics of Solar PV

A photovoltaic system is made up of several photovoltaic solar cells. An individual small PV cell is capable of generating about 1 or 2 W of power approximately depends of the type of material used. For higher power output, PV cells can be connected together to form higher power modules. In the market the maximum power capacity of the module is 1 kW, even though higher capacity is possible to manufacture, it will become cumbersome to handle more than 1 kW module. Depending upon the power plant capacity or based on the power generation, group of modules can be connected together to form an array.

Solar PV systems are usually consists of numerous solar arrays, although the modules are from the same manufactures or from the same materials, the module performance characteristics varies and on the whole the entire system performance is based on the efficiency or the performance of the individual components. Apart from the solar PV module the system components comprises a battery charge controller, an inverter, MPPT controller and some of the low voltage switchgear components. Presently in the market, power conditioning unit consists of charge controller, inverter and MPPT controller. A Balance-of-System (BoS) includes components and equipments that convert DC supply from the solar PV module to AC grid supply. In general, BOS of the solar PV system includes all the components of the system except the Solar PV modules. In addition to inverters, this includes the cables/wires, switches, enclosures, fuses, ground fault detectors, surge protectors, etc. BOS applies to all types of solar applications (i.e. commercial, residential, agricultural, public facilities, and solar parks).

In many systems, the cost of BOS equipment can equal or exceed the cost of the PV modules. When examining the costs of PV modules, these costs do not include the cost of BOS equipment. In a typical battery based solar PV system the cost of the modules is 20–30 % of the total while the remaining 70 % is the balance of systems (BOS). Apart from the 50 % of the system BOS costs a lot more maintenance expense is also required for proper maintenance of the BOS. By controlling the balance-of-system components, increase efficiency, and modernize solar PV systems can be maintained. BOS components include the majority of the pieces, which make up roughly 10–50 % of solar purchasing and installation costs, and account for the majority of maintenance requirements. Thus, suitable integration of the BOS is vital for the proper functionality and the reliability of the solar PV system. However it is often completely overlooked and poorly integrated. Costs are steadily decreasing with regard to solar panels and inverters.

As per the statistics, the Solar PV module world market is steadily growing at the rate of 30 % per year. The reasons behind this growth are that the reliable

production of electricity without fuel consumption anywhere there is light and the flexibility of PV systems. Also the solar PV systems using modular technology and the components of Solar PV can be configured for varying capacity, ranging from watts to megawatts. Earlier, large variety of solar PV applications found to be in industries but now it is being used for commercial as well as for domestic needs.

One of the hindrance factor is the efficiency of the solar PV cell, in the commercial market a cell efficiency of up to 18.3 % is currently obtained, depending on the technology that is used. When it is related to the module efficiency, it is slightly lower than the cell efficiency. This is due to the blank spaces between the arrays of solar cells in the module. The overall system efficiency includes the efficiency and the performance of the entire components in the system and also depends on the solar installation. Here there is another numerical drop in value when compared to the module efficiency, this being due to conductance losses, e.g., in cables. In the case of inverter, it converts the DC output from the Solar PV module to the AC grid voltage with a certain degree of efficiency. It depends upon conversion efficiency and the precision and quickness of the MPP tracking called tracking efficiency. MPP tracking which is having an efficiency of 98–99 % is available in the market, each and every MPPT is based on a particular tracking algorithm.

Current research states that all materials have physical limits on the electricity that they can generate. For example, the maximum efficiency of crystalline silicon is only 28 %. But tandem cells provide immense scope for development in coming years. Efficiency of existing laboratory cells has already achieved efficiency values of over 25 %. PV Modules with BOS components known as an entire PV system. This system is usually sufficient to meet a particular energy demand, such as powering a water pump, the appliances and lights in a home, and electrical requirements of a community.

In the cost of PV systems and in consumer acceptance, reliability of PV arrays is a crucial factor. With the help of fault-tolerant circuit design, reliability can be improved using various redundant features in the circuit to control the effect of partial failure on overall module yield and array power degradation. Degradation can be limited by dividing the modules into a number of parallel solar cell networks. This type of design can also improve module losses caused by broken cells. The hot-spots in the Solar PV module can be avoided by having diodes across each cell and that is called as bypass diodes. Practically a solar PV module consists of one bypass diode for 18 cells to mitigate the effects of local cell hot-spots.

2.2 PV Module Performance Measurements

Peak watt rating is a key performance measurement of PV module. The peak watt (W_p) rating is determined by measuring the maximum power of a PV module under laboratory Standard Test Conditions (STC). These conditions related to the maximum power of the PV module are not practical. Hence, researchers must use the

NOCT (Nominal Operating Cell Temperature) rating. In reality, either of the methods is designed to indicate the performance of a solar module under realistic operating conditions. Another method is to consider the whole day rather than "peak" sunshine hours and it is based on some of the factors like light levels, ambient temperature, and air mass and also based on a particular application.

Solar arrays can provide specific amount of electricity under certain conditions. In order to determine array performance, following factors to be considered: (i) characterization of solar cell electrical performance (ii) degradation factors related to array design (iii) assembly, conversion of environmental considerations into solar cell operating temperatures and (iv) array power output capability. The following performance criteria determines the amount of PV output.

Power Output Power output is represented in watts and it is the power available at the charge controller/regulator specified either as peak power or average power produced during one day.

Energy Output Energy Output indicates the amount of energy produced during a certain period of time and it is represented in Wh/m^2.

Conversion Efficiency It is defined as energy output from array to the energy input from sun. It is also referred as power efficiency and it is equal to power output from array to the power input from sun. Power is typically given in units of watts (W), and energy is typical in units of watt-hours (Wh).

To ensure the consistency, safety and quality of Solar PV system components and to increase consumer confidence in system performance IEEE, Underwriters Laboratories (UL), International Electrotechnical Commission (IEC), AM0 Spectrum (ASTM) are working on standards and performance criteria for PV systems.

2.2.1 Balance of System and Applicable Standards

The market access requirements for PV equipment are segmented into safety and performance. UL is a global leader in energy product testing and certification. The focus of the UL standards is in providing requirements for materials, construction and the evaluation of the potential electrical shock, fire safety hazard and also testing and certification according to the appropriate energy standard. UL certifies that PV equipment complies with the safety, environmental and other performance requirements of the appropriate standards.

IEC focus on the requirements in terms and symbols, testing, design qualification and type approval. UL supports manufacturers with the compliance to both the UL and the IEC requirements. In addition, UL provides balance of systems equipment certification to the standards identified in the diagram. These certifications include materials (such as polymeric used for back sheets, encapsulates, and adhesives), components (like junction boxes and connectors) and end-products (for example, inverters and meters). Even though the design of solar PV system

Table 2.1 UL standards used for the BOS components

Description	UL standards
PV modules testing and certification	UL 1703
	IEC/EN 61215, IEC/EN 61646
	IEC 61730/UL 790 (Fire Test)
	UL-SU 8703 (CPV)
Mounting system	UL-SU 1703 –A
Tracking system	UL-SU 9703
Combiner box	UL 1741
Inverter	UL 1741
	IEC 62109
Batteries	UL 1989, UL 2054
	UL-SU 2580, UL-SU 1973

components can be done with the help of mathematical calculations or by using dedicated software, there are certain protocols and standards in selecting the BOS components which should be adhered to while installing a PV system. The UL standards used for the corresponding BOS components of the Solar PV system are as shown in Table 2.1 above.

As these issues might seem insignificant during the installation, they affect the system performance, efficiency, reliability, maintenance cost and aesthetics in the long run. The BOS components can be divided into the following categories based on their basic functions: (i) Mounting Structure (ii) Power Conditioning Units (iii) Cables/Protection devices and (iv) Storage devices.

2.2.1.1 Mounting Structure

The PV module should be designed in such a way that it can withstand rain, hail, wind and other adverse conditions. The common made mistakes in selection of the mounting structures are (i) Durability of the design (ii) Tilt angle (iii) Orientation and (iv) PV array shading. Tilting angle optimally varies the efficiency of the solar PV module so, the mounting structure also serves as a PV module tilting structure which tilts the PV arrays at an angle determined by the latitude of the site location, to maximize the solar insolation falling on the panels. The optimum tilt angle required to maximize the solar insolation changes as the position of the sun varies every month.

Similarly, shading has a significant effect on PV generation. Partial shading can reduce the system production up to 90 %. Thus, it is essential that the PV arrays to be installed at a suitable location without any difficulties. To identify the shading levels at any location, software and online tools are available. Some of commonly used tools are – Sun path, Eco tech, Celeste lite etc. For PV array installation with multiple rows the shading de-rate factor should account for losses that may occur when a row shades an adjacent row.

2.2.1.2 Power Conditioners

In the off-grid inverter in a battery based PV system, it is important to review the efficiency and the self-power consumption of the inverter along with the capacity, power quality and surge rating. Generally inverter is normally sized to support the load, power factor and surge. For the efficient operation of the inverter, it should have low self consumption to increase the battery life. A high self consumption inverter, continuously drains the battery which results in lower back up and decrease the battery life cycle due to increased discharge. Further, as the efficiency of the inverter changes with respect to the load, it is good practice to design the load on average efficiency rather than the peak efficiency. In a typical inverter, the peak efficiency is mostly between 20 % and 30 % of the total capacity.

2.2.1.3 Cables and Protection Devices

The main purpose of cabling is to allow a safe passage of current. Appropriate cable sizing allows the current to be transferred within an acceptable loss limit to ensure optimal system performance. In order to establish connection between solar PV modules, charge controller, battery etc., cables are needed. The size of the cable determined based on the transmission length, voltage, flowing current and the conductor. The commonly found mistakes in installation sites are the undersized or inappropriate selection of cables. The cables can be appropriately sized with the help of several tools – such as mathematical formula, voltage drop tables and online calculators. In addition to the appropriate sizing, selection of relevant type of wire is also important in the case of solar PV application. For outdoor applications UV stabilized cable must be used, while normal residential cables can be used in indoors. This ensures the long term functioning of the cable and hence reduction in the system ongoing maintenance.

2.2.1.4 Storage

For off-grid and critical applications, storage systems are required, the most common medium of storage are the lead acid batteries. Presently researches are going on in the field of Li-ion batteries and to implement the concept of fuel cells in Solar PV Systems. One of the most expensive components in the PV system is the battery. Under sizing the batteries will become more costly as the battery life cycle is significantly reduced at higher Depth of Discharge (DOD%). At a higher depth of discharge, expected average number of charge–discharge cycles of a battery reduced. Further, a higher current discharge than the rating will dramatically reduce the battery life. This can be avoided by carefully sizing of the battery according to the ‘C-rating’ during the system design. It signifies the maximum amount of current that can be safely withdrawn from the battery to provide adequate back up and without causing any damage. A discharge more than the C-ratings, may cause

irreversible capacity loss due to the fact that the rate of chemical reactions taking place in the batteries cannot keep pace with the current being drawn from them.

The de-rating factor of the BOS plays a significance role in boosting up the overall efficiency of the solar PV system. The de-rating factor can be calculated by multiplying the BOS components de-rate factor. As per the survey, the overall de-rating factor is 84.5 % at STC. With good selection and installation practice the overall losses from BOS can be limited to 15.5 % at STC. With poor practice the overall de-rate factor can be 54.7 % or even less, which means the losses can account for more than 46 %.

2.2.2 *Photovoltaic Systems Total Costs Overview*

The PV industry is drawing attention because of worldwide environmental concerns and of its immense energy production potential due to the widely available free solar resource. It is important to understand the factors that directly and indirectly affect the system costs and viability (Table 2.2).

Table 2.2 Factors affecting PV system costs and feasibility

Factors	Facts
Grid connection	Grid-connected systems do not need batteries which reduces initial capital costs
	For a comparable load, grid-tied systems use smaller PV arrays than stand-alone systems
Distance to nearest utility grid	Stand-alone systems tend to become feasible in locations which are far from electrical distribution networks
	Grid extensions can cost thousands of dollars per mile of transmission line
Solar resource	Solar resource will not affect capital costs but the availability of solar energy does affect the cost of producing energy, hence the payback period for the investment
	Location is considered the second important factor affecting PV system cost performance. It can have influence on shading patterns, soiling, operating temperature and solar resource variations
BOS (tracking)	Balance of system components is estimated to represent 30–50 % of the total costs of a PV system
	Local safety codes or regulations can require additional balance of system costs for the installation
Type of installation, mounting, size and space	Commercial and industrial clients prefer horizontal Installation to maximize flat roof utilization and to lower mounting expenses
	Retrofit installations tend to be more expensive than those planned for new buildings
	Large scale systems tend to be less expensive on a per watt basis
	Due to capital cost restrictions, stand-alone systems tend to be smaller or used for smaller loads
	Grid-tied systems tend to be larger because they provide lower capital costs and energy costs for larger loads
	Typically larger systems tend to have lower cost per kW

(continued)

Table 2.2 (continued)

Factors	Facts
Module technology	Modules account for 40–50 % of total system costs. These determine the total area needed to install the system. Less area per watt is desired to maximize roof or land use
O&M	Grid tied PV systems do not have notable O&M costs
	Most small scale grid-tied systems do not have moving parts and therefore maintenance is minimal
	Large-scale systems may use tracking systems and therefore may require more work
	Battery assisted systems may require acid refills when valve regulated batteries are not used
	Some arrays will require regular cleaning. This could represent additional costs especially for large scale systems
Energy use and cost	System size depends mostly on energy use, solar resource and component efficiency
	Reducing energy consumption greatly reduces the initial capital cost investment necessary
	PV systems can be cost competitive in locations with high energy prices and Net metering programs. The assumption that PV is expensive is therefore relative to the solar resource and utility energy prices in a location
Indirect benefits	Emissions reductions provide a wide range of economic, environmental and health benefits. These are difficult to quantify, yet they cannot be ignored

2.3 Types of PV Systems

Based on the electric energy production, PV modules can be arranged into arrays to increase electric output. Solar PV systems are generally classified based on their functional and operational requirements, their component configurations. It can be classified into grid-connected and stand-alone systems.

2.3.1 Grid-Connected Solar PV System

The primary component of grid-connected PV systems is power conditioning unit (PCU). The PCU converts the DC power produced by the PV array into AC power as per the voltage and power quality requirements of the utility grid. A bi-directional interface is made between the PV system AC output circuits and the electric utility network, typically at an on-site distribution panel or service entrance. This allows the AC power produced by the PV system to either supply on-site electrical loads or to back-feed the grid when the PV system output is greater than the on-site load demand. This safety feature is required in all grid-connected

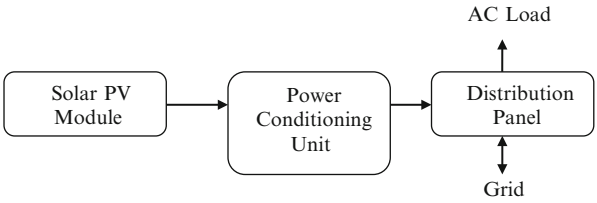


Fig. 2.1 Bock diagram of grid-connected solar PV system

PV systems, and ensures that the PV system will not continue to operate and feed back into the utility grid when the grid is down for maintenance or during grid failure state. Figure 2.1 shows the general block diagram of the grid connected solar PV system. In grid-connected systems, switching of AC power from the standby generator and the inverter to the service bus or the connected load is accomplished by internal or external automatic transfer switches.

One of the important components of a grid-connected system is *net metering*. Standard service meters are odometer-type counting wheels that record power consumption at a service point by means of a rotating disc, which is connected to the counting mechanism. The rotating discs operate by an electro physical principle called *eddy current*. Digital electric meters make use of digital electronic technology that registers power measurement by solid-state current and voltage-sensing devices that convert analog measured values into binary values that are displayed on the meter using liquid crystal display (LCD) readouts.

Inverters are the main difference between a grid-connected system and a stand-alone system. Inverters must have line frequency synchronization capability to deliver the excess power to the grid. Net meters have a capability to record consumed or generated power in an exclusive summation format. The recorded power registration is the net amount of power consumed—the total power used minus the amount of power that is produced by the solar power cogeneration system. Net meters are supplied and installed by utility companies that provide grid-connection service systems. Net metered solar PV power plants are subject to specific contractual agreements and are subsidized by state and municipal governmental agencies.

2.3.2 Stand-Alone Solar PV System

Stand-alone PV systems or direct coupled PV systems are designed and sized to supply DC and/or AC electrical loads. It is called direct coupled systems because, the DC output of a PV module or array is directly connected to a DC load. There is no electrical energy storage (batteries) in direct-coupled systems as because of that, the load only operates during sunlight hours. The maximum power point tracker

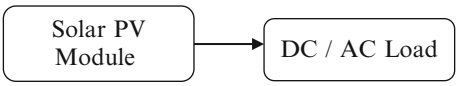


Fig. 2.2 Direct coupled solar PV system

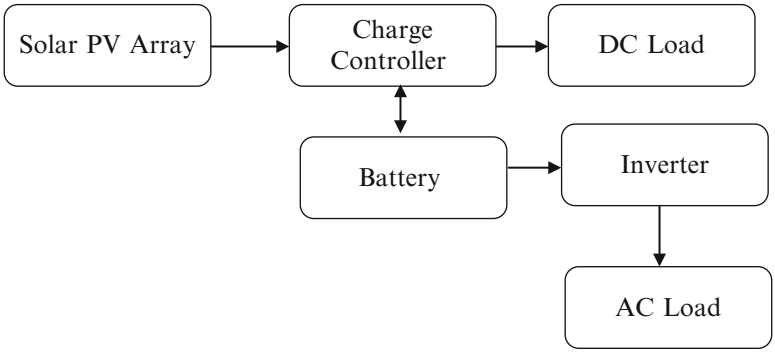


Fig. 2.3 Block diagram of stand-alone PV system with battery storage

(MPPT) is used between the array and load to help better utilize the available array maximum power output and also for matching the impedance of the electrical load to the maximum power output of the PV array. Figure 2.2 shows the general block diagram of the stand alone solar PV system.

An example of direct coupled solar PV systems is in agriculture applications, solar PV module can be directly connected to run the pump. Depending upon the capacity of the pump, the module can be connected in series/parallel configurations. In such application, surge protector is needed to be connected between the positive and negative supply provides protection against lightning surges. Batteries are used for energy storage in many stand-alone PV systems. Figure 2.3 shows the block diagram of a typical stand-alone PV system powering DC and AC loads with battery storage option.

The solar PV array configuration, a DC load with battery backup, is essentially the same as the one without the battery except that there are a few additional components that are required to provide battery charge stability. PV panels are connected in series to obtain the desired increase in DC voltage, such as 12, 24, or 48 V. The charge controller regulates the current output and prevents the voltage level from exceeding the maximum value for charging the batteries. The output of the charge controller is connected to the battery bank by means of a dual DC cutoff disconnect. Apart from this a cutoff switch can be provided, when turned off for safety measures, disconnects the load and the PV arrays simultaneously.

During the sunshine hours, the load is supplied with DC power while simultaneously charging the battery. The controller will ensure that the DC power output

from the PV arrays should be adequate to sustain the connected load while sizing the batteries. Battery bank sizing depends on a number of factors, such as the duration of an uninterrupted power supply to the load when there is less or no radiation from the sun. The battery bank produces a 20–30 % power loss due to heat when in operation, which also must be taken into consideration. When designing a solar PV system with a battery backup, the designer must determine the appropriate location for the battery racks and room ventilation.

2.3.3 PV-Hybrid Systems

Hybrid systems generally refers to the combination of any two input sources, here solar PV can be integrated with Diesel Generator, Wind Turbines, Bio-mass or any other renewable on non-renewable energy sources. Solar PV systems will generally use battery bank to store energy output from the panels to accommodate a pre-defined period of insufficient sunshine, there may still be exceptional periods of poor weather when an alternative source is required to guarantee power production. PV-hybrid systems combine a PV module with another power sources - typically a diesel generator, but occasionally another renewable supply such as a wing turbine. The PV generator would usually be sized to meet the base load demand, with the alternate supply being called into action only when essential. This arrangement offers all the benefits of PV in respect of low operation and maintenance costs, but additionally ensures a secure supply.

Hybrid systems can also be sensible approach in situations where occasional demand peaks are significantly higher than the base load demand. It makes little sense to size a system to be able to meet demand entirely with PV if, for example, the normal load is only 10 % of the peak demand. By the same token, a diesel generator-set sized to meet the peak demand would be operating at inefficient part-load for most of the time. In such a situation a PV-diesel hybrid would be a good compromise. Figure 2.4 shows the block diagram of Solar PV hybrid system.

2.3.4 Stand-Alone Hybrid AC Solar Power System with Generator and Battery Backup

A stand-alone hybrid solar PV configuration is essentially identical to the DC solar power system. In this alternating current inverters are used to convert DC into AC. The output of inverter is square waves, which are filtered and shaped into sinusoidal AC waveforms. Any waveform, when analyzed, essentially consists of the superimposition of many sinusoidal waveforms known as harmonics. The first

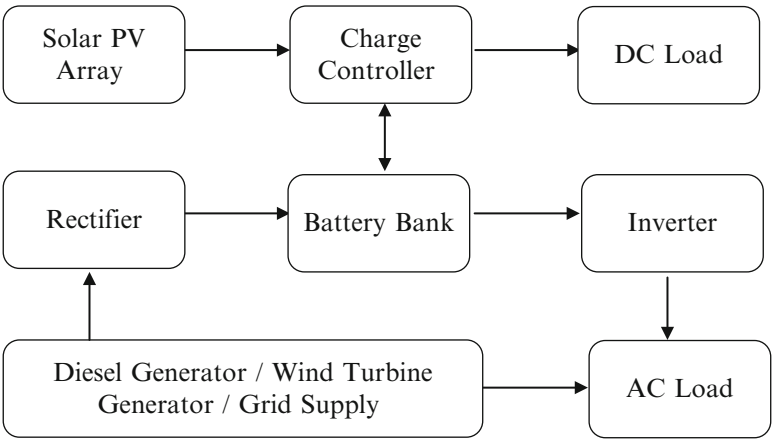


Fig. 2.4 Block diagram of photovoltaic hybrid system

harmonic represents a pure sinusoidal waveform. Additional waveforms with higher frequencies, when superimposed on the base waveform, add or subtract from the amplitude of the base sinusoidal waveform.

The combination of base waveform and higher harmonics produce a distorted wave shape that resembles a distorted sinusoidal wave. Converted DC output, derived from the solar power, is considered to be a numerous superimposition of odd and even numbers of harmonics. To obtain a relatively clean sinusoidal output, most inverters employ electronic circuitry to filter a large number of harmonics. Filter circuits consist of specially designed inductive and capacitor circuits to block certain unwanted harmonics. In general, DC-to-AC inverters are intricate electronic power conversion equipment designed to convert direct current to a single or three-phase current that replicates the regular electrical services provided by utilities.

Most inverters, in addition to PV module input power, accept auxiliary input power to form a standby generator, used to provide power when battery voltage is dropped to a minimum level. A special type of inverter, referred to as the *grid-connected* type, incorporates synchronization circuitry that allows the production of sinusoidal waveforms in harmony with the electrical service grid. When the inverter is connected to the electrical service grid, it can effectively act as an AC power generation source. Grid-type inverters used in grid-connected solar power systems are strictly regulated by utility agencies that provide net metering. Some inverters incorporate an internal AC transfer switch that is capable of accepting an output from an AC-type standby generator. In such designs, the inverters include special electronics that transfer power from the generator to the load.

2.4 MATLAB Model of Solar PV

As shown in Fig. 2.5, the solar system configuration consists of a required number of solar photovoltaic cells, commonly referred to as PV modules, connected in series or in parallel to attain the required voltage output.

The basic equation from the theory of semiconductors that mathematically describes the *I–V* characteristic of the ideal PV cell is

$$I = I_{pv,cell} - I_{0,cell}\left[\exp\left(\frac{qV}{\alpha kT}\right) - 1\right] \tag{2.1}$$

The basic (2.1) of the elementary PV cell does not represent the *I–V* characteristic of a practical PV array. Cells connected in parallel increase the current and cells connected in series provide greater output voltages. Practical arrays are composed of several connected PV cells and the observation of the characteristics at the

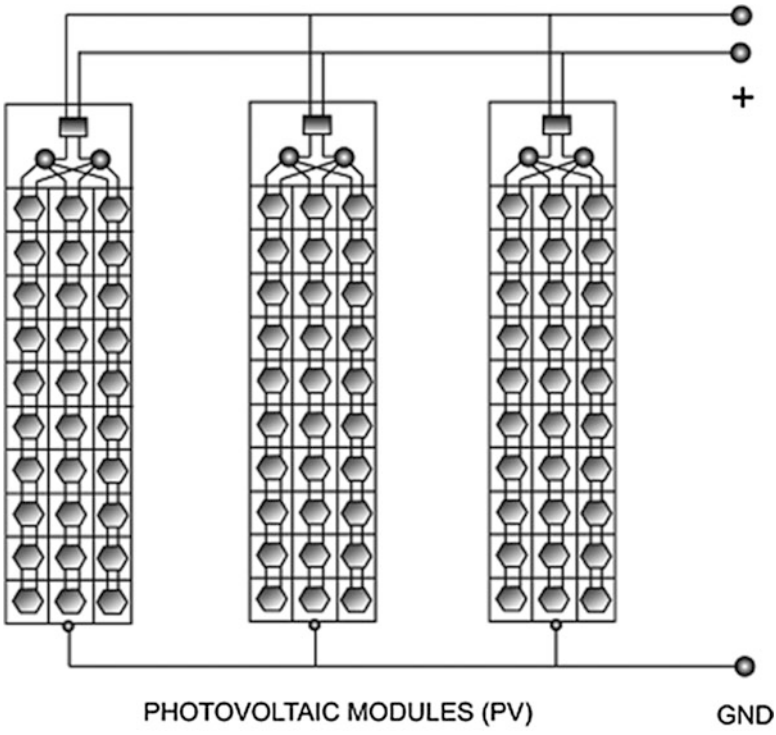


Fig. 2.5 Solar array diagram

terminals of the PV array requires the inclusion of additional parameters to the basic equation

$$I = I_{pv} - I_0\left[\exp\left(\frac{V + R_s I}{V_t \alpha}\right) - 1\right] - \frac{V + R_s I}{R_P} \tag{2.2}$$

All PV array datasheets bring basically the nominal open-circuit voltage ($V_{oc,n}$), the nominal short-circuit current ($I_{sc,n}$), the voltage at the MPP (V_{mp}), the current at the MPP (I_{mp}), the open-circuit voltage/temperature coefficient (K_V), the short circuit current/temperature coefficient (K_I), and the maximum experimental peak output power ($P_{max,e}$). This information is always provided with reference to the nominal condition or standard test conditions (STC's) of temperature and solar irradiation. The practical PV device has a series resistance R_s whose influence is stronger when the device operates in the voltage source region and a parallel resistance R_p with stronger influence in the current source region of operation.

The assumption $I_{sc} \approx I_{pv}$ is generally used in the modeling of PV devices because in practical devices the series resistance is low and the parallel resistance is high. The diode saturation current is given by

$$I_0 = \frac{I_{sc,n} + K_I \Delta_T}{\exp\left(\dfrac{V_{oc,n} + K_V \Delta_T}{\alpha V_t}\right) - 1} \tag{2.3}$$

The saturation current I_0 is strongly dependent on the temperature so that the net effect of the temperature is the linear variation of the open-circuit voltage according to the practical voltage/temperature coefficient. This equation simplifies the model and cancels the model error at the vicinities of the open-circuit voltages, and consequently, at other regions of the I–V curve.

$$I_{pv} = \left(I_{pv,n} + K_I \Delta_T\right)\frac{G}{G_n} \tag{2.4}$$

The relation between R_s and R_p, the only unknowns of (2.2) may be found by making $P_{max,m} = P_{max,e}$ and solving the resulting equation for R_s, as shown

$$\begin{aligned} P_{max,m} &= V_{mp}\left\{I_{pv} - I_0\left[\exp\left(\frac{q}{kT}\frac{V_{mp} + R_s I_{mp}}{\alpha N_s}\right) - 1\right] - \frac{V_{mp} + R_s I_{mp}}{R_P}\right\} \\ &= P_{max,e} \end{aligned} \tag{2.5}$$

$$R_p = \frac{V_{mp} + I_{mp} R_s}{\left\{V_{mp} I_{pv} - V_{mp} I_0 \exp\left[\dfrac{\left(V_{mp} + I_{mp} R_s\right)}{N_s \alpha}\dfrac{q}{kT}\right] + V_{mp}\, I_0 - P_{max,e}\right\}} \tag{2.6}$$

Equation 2.6 means that for any value of R_s there will be a value of R_p that makes the mathematical I–V curve cross the experimental (V_{mp}, I_{mp}) point. The goal is to

find the value of R_s (and hence, R_p) that makes the peak of the mathematical P–V curve coincide with the experimental peak power at the (Vmp, Imp) point. This requires several iterations until $P_{max,m} = P_{max,e}$. Each iteration updates R_s and R_p toward the best model solution.

$$I_{pv,n} = \frac{R_P + R_S}{R_P} I_{sc,n} \tag{2.7}$$

The initial value of R_s may be zero. The initial value of R_p may be given by

$$R_{p,\min} = \frac{V_{mp}}{I_{sc,n} - I_{mp}} - \frac{V_{oc,n} - V_{mp}}{I_{mp}} \tag{2.8}$$

Equation 2.8 determines the minimum value of R_p, which is the slope of the line segment between the short-circuit and the maximum-power *remarkable points*. Although R_p is still unknown, it surely is greater than $R_{p,min}$ and this is a good initial guess.

According to Tables 2.3 and 2.4, along with Figs. 2.6 to 2.8, the developed model and the experimental data are exactly matched at the nominal *remarkable points* of the I–V curve (flowchart is shown in Fig. 2.6), and the experimental and

Table 2.3 Parameters of KC200GT solar array at 25 °C, 1,000 W/m^2

I_{mp}	7.61 A
V_{mp}	26.3 V
$P_{max,e}$	200.143 W
I_{sc}	8.21 A
V_{oc}	32.9 V
K_V	−0.1230 V/K
K_I	0.0032 A/K
N_S	54

Table 2.4 Parameters of the adjusted model of the KC200GT solar array at nominal operating conditions

I_{mp}	7.61 A
V_{mp}	26.3 V
$P_{max,e}$	200.143 W
I_{sc}	8.21 A
V_{oc}	32.9 V
$I_{0,n}$	$9.825*10^{-8}$ A
I_{pv}	8.214 A
α	1.3
R_P	415.405 Ω
R_S	0.221 Ω

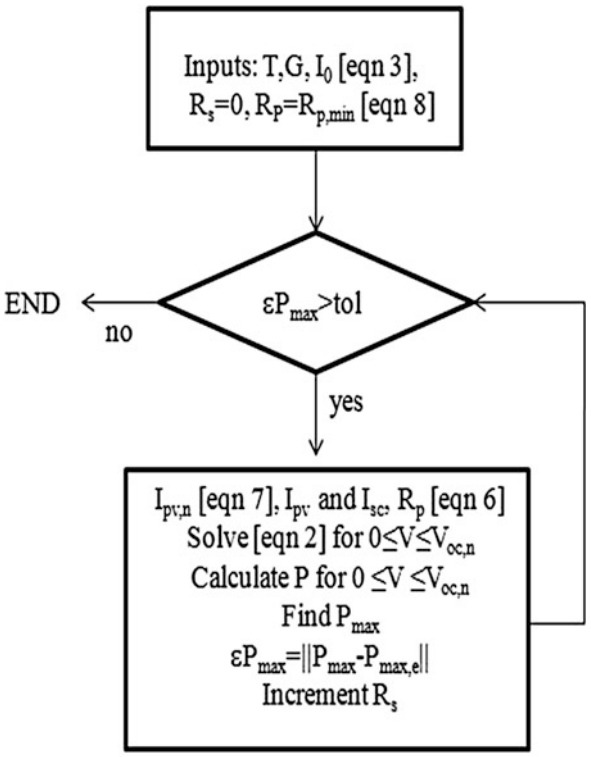


Fig. 2.6 Algorithm of the method used to adjust the *I–V* model

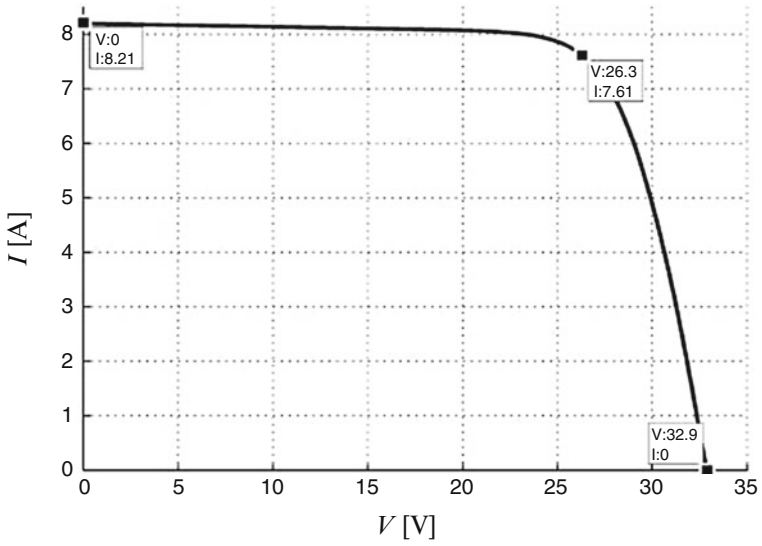


Fig. 2.7 I-V curve adjusted to three remarkable points

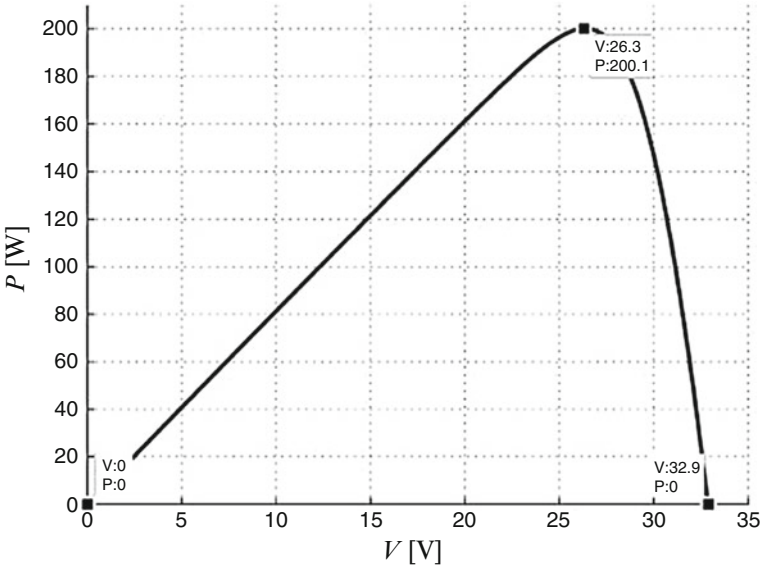


Fig. 2.8 P-V curve adjusted to three remarkable points

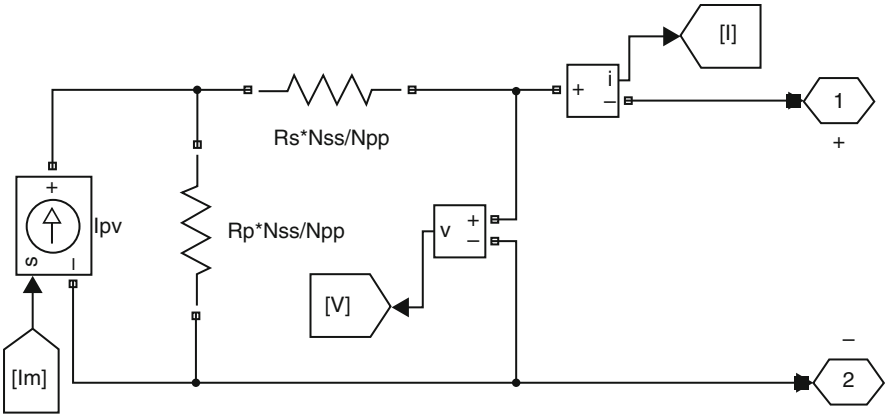


Fig. 2.9 Basic SIMULINK model of equivalent PV module

mathematical maximum peak powers coincide. The objective of adjusting the mathematical *I–V* curve at the three *remarkable points* was successfully achieved. The PV array can be simulated with an equivalent circuit model based on the PV model of Fig. 2.9. The circuit model composed of only one current source. The value of the current is obtained by numerically solving the *I–V* equation. For every value of V, a corresponding I that satisfy the *I–V* (2.2) is obtained.

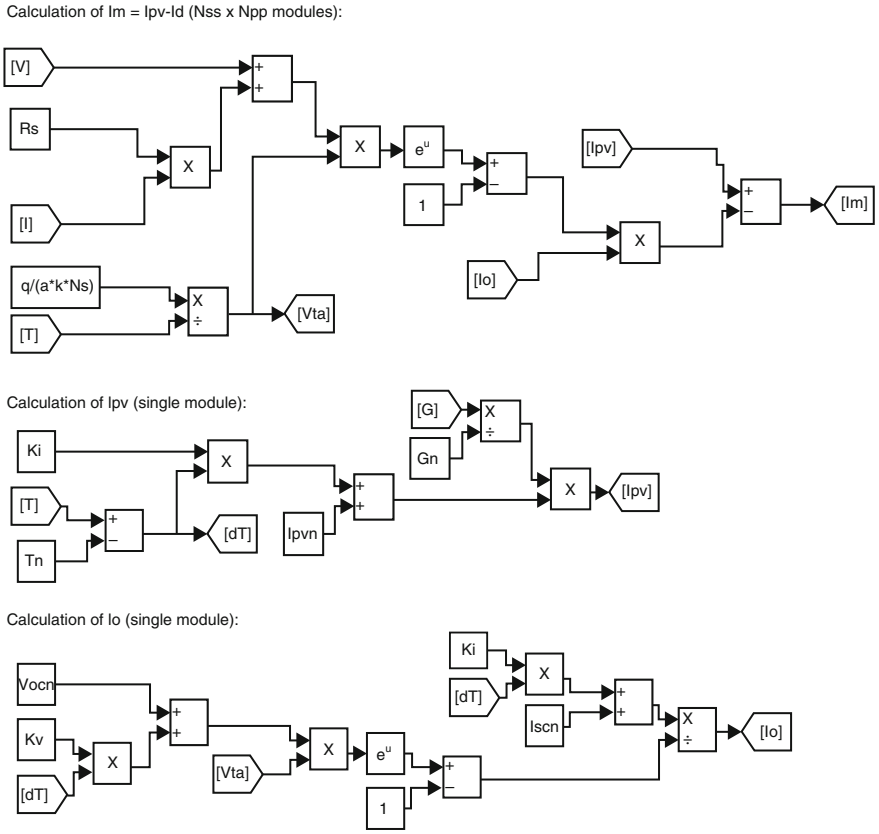


Fig. 2.10 SIMULINK model of the PV equations

The model of the PV array was designed and the calculation of Im, Ipv and Io are presented as separate sub-systems in Fig. 2.10.

The parameters required for simulation are initialized by the following script file

```
%% Information from the KC200GT solar array datasheet
 Iscn = 8.21;      %Nominal short-circuit voltage [A]
Vocn = 32.9;      %Nominal array open-circuit voltage [V]
Imp = 7.61;       %Array current @ maximum power point [A]
Vmp = 26.3;       %Array voltage @ maximum power point [V]
Pmax_e = Vmp*Imp;    %Array maximum output peak power [W]
Kv = -0.123;      %Voltage/temperature coefficient [V/K]
Ki = 3.18e-3;     %Current/temperature coefficient [A/K]
Ns = 36;          %Nunber of series cells
```

```
%% Constants

k = 1.3806503e-23;  %Boltzmann [J/K]
q = 1.60217646e-19; %Electron charge [C]
a = 1.3;       %Diode constant

%% Nominal values

Gn = 1000;      % Nominal irradiance [W/m^2] @ 25oC
Tn = 25 + 273.15;  % Nominal operating temperature [K]

%% Adjusting algorithm

% The model is adjusted at the nominal condition
T = 25 + 273.15;
G =800;

Vtn = k * Tn / q;          %Thermal junction voltage (nominal)
Vt = k * T / q;           %Thermal junction voltage (current temperature)

Ion = Iscn/(exp(Vocn/a/Ns/Vtn)-1);  % Nominal diode saturation current

Io = Ion;

% Reference values of Rs and Rp
Rs_max = (Vocn - Vmp)/ Imp;
Rp_min = Vmp/(Iscn-Imp) - Rs_max;

% Initial guesses of Rp and Rs
Rp = Rp_min;
Rs = 0;

tol = 0.001; % Power mismatch Tolerance

P=(0);

error = Inf; %dummy value

% Iterative process for Rs and Rp until Pmax,model = Pmax,experimental

while (error>tol)

% Temperature and irradiation effect on the current
dT = T-Tn;
Ipvn = (Rs+Rp)/Rp * Iscn;     % Nominal light-generated current
Ipv = (Ipvn + Ki*dT) *G/Gn;    % Actual light-generated current
Isc = (Iscn + Ki*dT) *G/Gn;    % Actual short-circuit current

% Increments Rs
Rs = Rs + .01;

% Parallel resistance
Rp = Vmp*(Vmp+Imp*Rs)/(Vmp*Ipv-Vmp*Io*exp((Vmp+Imp*Rs)/Vt/Ns/a)+Vmp*Io-Pmax_e);

% Solving the I-V equation for several (V,I) pairs
clear V
clear I
```

```
V = 0:.1:50;       % Voltage vector
I = zeros(1,size(V,2));  % Current vector

for j = 1 : size(V,2) %Calculates for all voltage values

% Solves g = I - f(I,V) = 0 with Newntonn-Raphson

g(j) = Ipv-Io*(exp((V(j)+I(j)*Rs)/Vt/Ns/a)-1)-(V(j)+I(j)*Rs)/Rp-I(j);

while (abs(g(j)) > 0.001)

g(j) = Ipv-Io*(exp((V(j)+I(j)*Rs)/Vt/Ns/a)-1)-(V(j)+I(j)*Rs)/Rp-I(j);
glin(j) = -Io*Rs/Vt/Ns/a*exp((V(j)+I(j)*Rs)/Vt/Ns/a)-Rs/Rp-1;
I_(j) = I(j) - g(j)/glin(j);
I(j) = I_(j);

end

end % for j = 1 : size(V,2)

 % Calculates power using the I-V equation
 P = (Ipv-Io*(exp((V+I.*Rs)/Vt/Ns/a)-1)-(V+I.*Rs)/Rp).*V;

 Pmax_m = max(P);

 error = (Pmax_m-Pmax_e);

end % while (error>tol)

%% Outputs

fprintf('Model info:\n');
fprintf(' Rp_min = %f',Rp_min);
fprintf('\n   Rp = %f',Rp);
fprintf('\n Rs_max = %f',Rs_max);
fprintf('\n   Rs = %f',Rs);
fprintf('\n   a = %f',a);
fprintf('\n   T = %f',T-273.15);
fprintf('\n   G = %f',G);
fprintf('\n Pmax,m = %f (model)',Pmax_m);
fprintf('\n Pmax,e = %f (experimental)',Pmax_e);
fprintf('\n  tol = %f',tol);
fprintf('\nP_error = %f',error);
fprintf('\n  Ipv = %f',Ipv);
fprintf('\n  Isc = %f',Isc);
fprintf('\n  Ion = %f',Ion);
```

The characteristics of PV cell are a combination of current source and diode. The current source V-I characteristics are considered separately and the diode V-I characteristics are determined separately. Here these two elements are in parallel connection so by adding currents the PV array characteristics are achieved.

The simulation results for the single PV cell are shown W/m^2 in Figs. 2.11 and 2.12. The V-I characteristics and V-P characteristics for different temperatures such as 25°, 50° and 75° are presented. It is observed that as the temperature increases the open circuit voltage decreases without any considerable change in the short circuit current. As a result, the maximum power from the cell is decreasing. Similarly, the

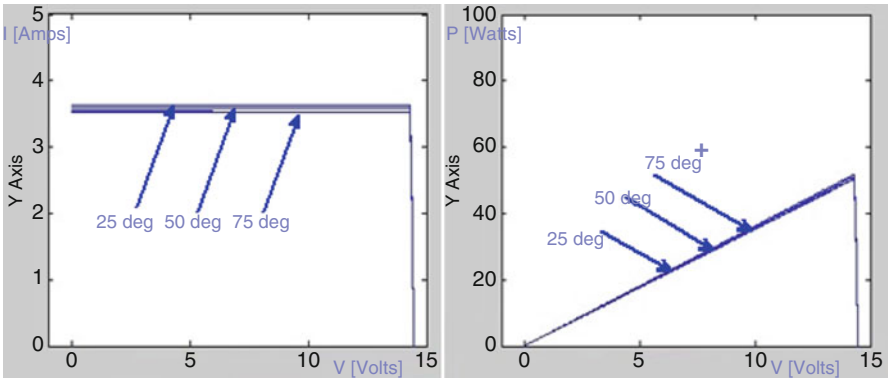


Fig. 2.11 V-I and V-P characteristics to the variation in temperature

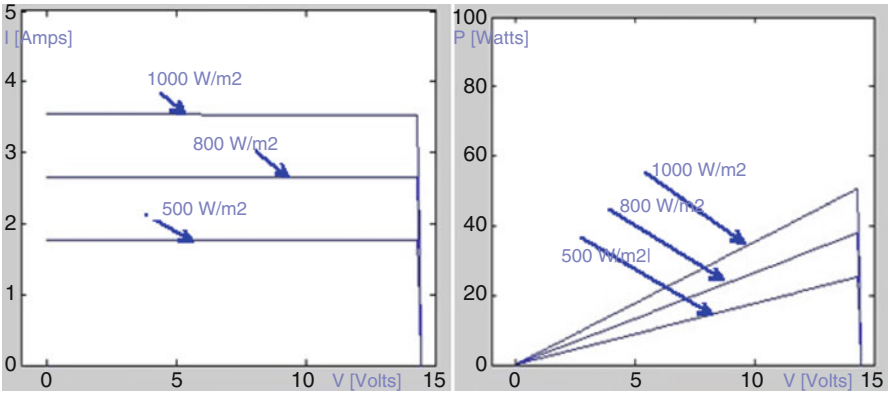


Fig. 2.12 V-I and V-P characteristics to the variation in solar radiations

V-I and V-P characteristics for radiations 500, 800, and 100 W/m^2 are given. For low values of solar radiations the short circuit current is reducing considerably but the change in open circuit voltage is very less, thus proving that the maximum power from the module is dropping.

2.4.1 SIMULINK Model of PV Module

This model contains an external control block permitting an uncomplicated variation of the models' parameters. In this model, 36 PV cells are interconnected in series to form one module. As a result, the module voltage is obtained by multiplying the cell voltage by the cells number while the total module current is the same as the cell's current.

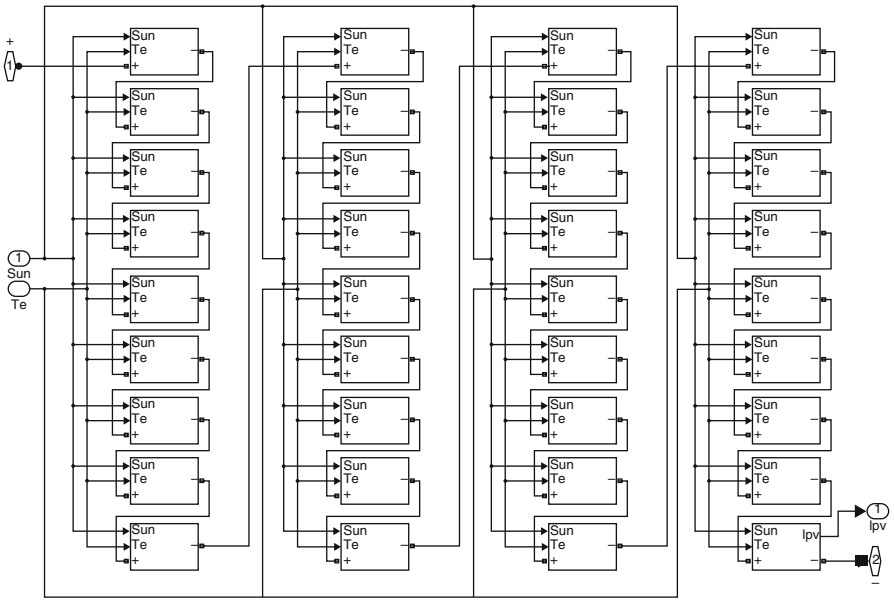


Fig. 2.13 Proposed PV module SIMULINK model

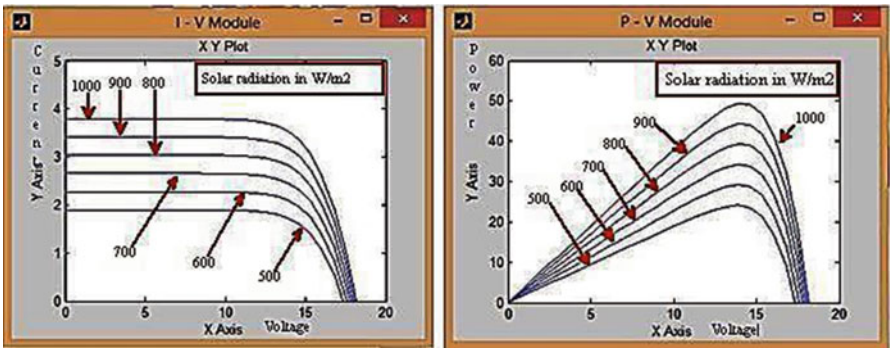


Fig. 2.14 (**a**) P – V characteristics of PV module (**b**) I – V characteristics of PV module

Figure 2.13 shows the PV module with 36 cells connected in series in order to obtain an increased voltage level. Each cell is a sub-system based on Figs. 2.9 and 2.10. Simulation results for the proposed PV module based on P-V and I-V characteristics under different solar radiations are shown in Fig. 2.14.

Simulation results for the proposed PV module based on P-V and I-V characteristics for different values of cell temperatures are shown in Fig. 2.15.

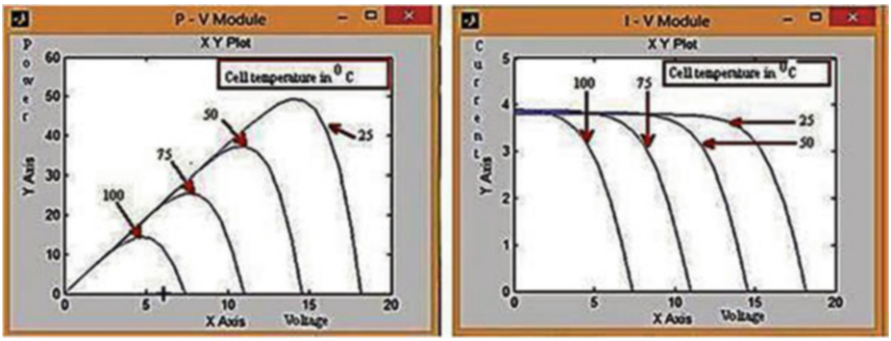


Fig. 2.15 (**a**) P – V characteristics of PV module (**b**) I – V characteristics of PV module

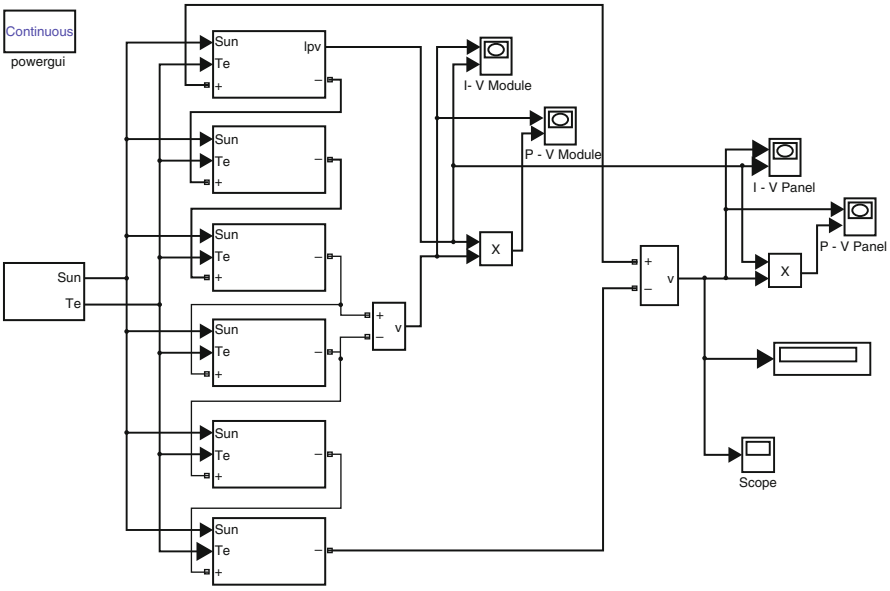


Fig. 2.16 Proposed PV array SIMULINK model

2.4.2 SIMULINK Model for PV Array

An array of 6 PV modules has been constructed based on Fig. 2.9. The PV modules were interconnected in series and all of them are connected to the external control block as shown in Fig. 2.16. The PV array model was simulated similarly to the model of the PV module and the results obtained are shown in Figs. 2.17 and 2.18.

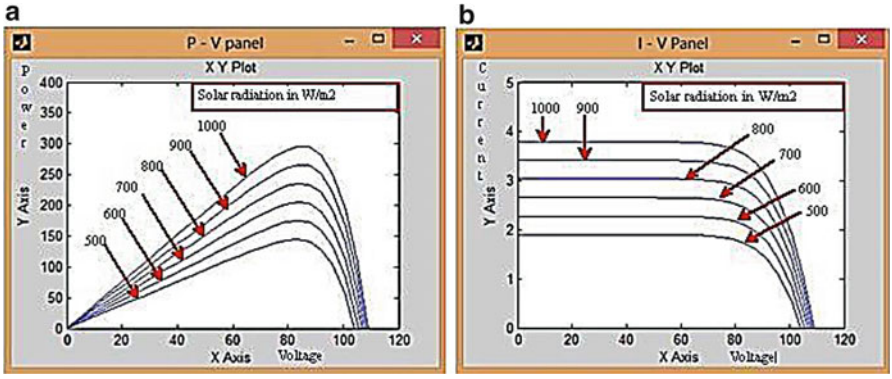


Fig. 2.17 (**a**) P – V characteristics of PV array (**b**) I – V characteristics of PV array

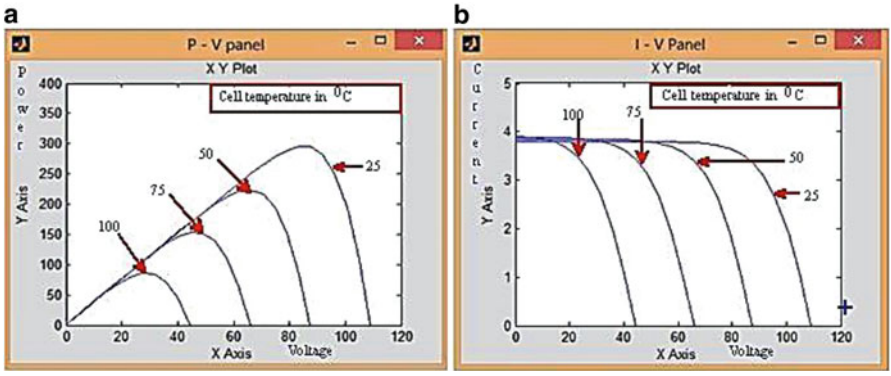


Fig. 2.18 (**a**) P – V characteristics for PV array (**b**) I – V characteristics for PV array

2.4.3 SIMULINK Model to Find Shading Effect

This section describes the procedure used for simulating the I–V and P–V characteristics of a partially shaded PV array. It is important to understand how the shading pattern and the PV array structure are defined in MATLAB (Fig. 2.19) using the proposed scheme. The PV array is configured as a combination of six series of PV modules connected in three parallel connections. Each set of PV modules operate under different solar radiations and different cell temperatures. The first set is under solar radiation of 800 W/m^2 and cell temperature of 750 °C, second set is under solar radiation of 600 W/m^2 and cell temperature of 250 °C, and third set is under solar radiation of 700 W/m^2 and cell temperature of 500 °C. Based on these conditions the simulations illustrating the PV characteristics is shown in Fig. 2.20 with three different multiple peaks. The maximum peak is called as global peak and the remaining two peaks are called as the local peaks.

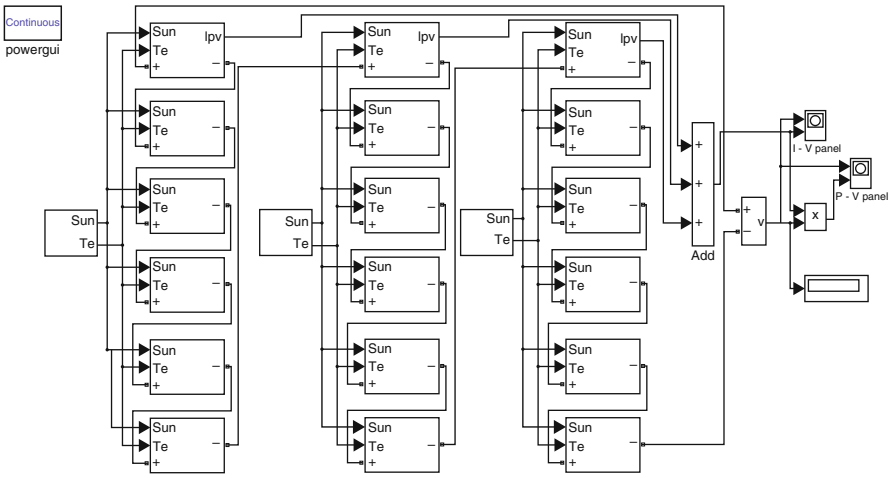


Fig. 2.19 Proposed SIMULINK model PV arrangement to find shading effect

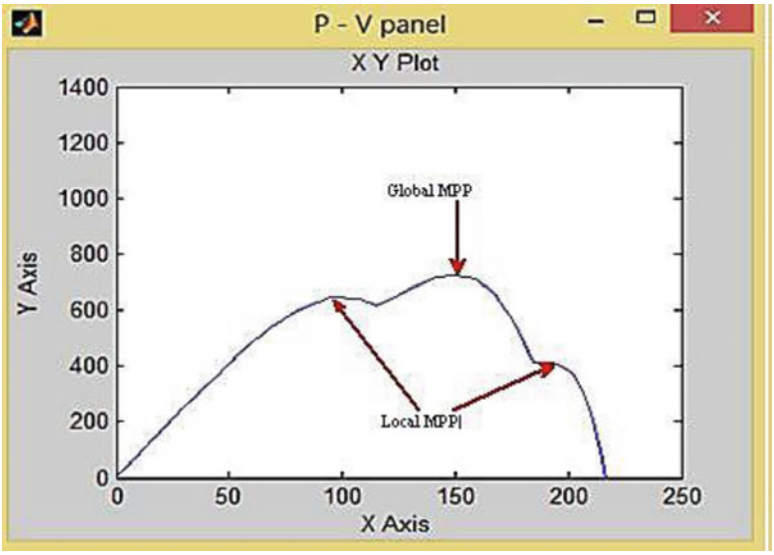


Fig. 2.20 *P–V* curves under shaded conditions

2.5 Charge Controller

A charge controller, charge regulator or battery regulator limits the rate at which electric current is added to or drawn from electric batteries. It prevents overcharging and may prevent against overvoltage, which can reduce battery performance or lifespan, and may pose a safety risk. To protect battery life, charge

controller may prevent battery from deep discharging or it will perform controlled discharges, depending on the battery technology. The terms "charge controller" or "charge regulator" may refer to either a stand-alone device, or to control circuitry integrated within a battery pack, battery-powered device, or battery recharger.

Solar Charge Controllers are the controllers which regulate the power output or the DC output voltage of the solar PV panels to the batteries. Charge controllers take the DC output voltage as the input voltage converts it into same DC voltage required for battery charging. These are mostly used in off grid scenario and uses Maximum Power Point Tracking scheme which maximizes the output efficiency of the Solar PV Panel. In battery charging system, the output voltage regulation is an important factor as batteries require specific charging method with various voltage and current levels for specific stage. These charging processes enhance battery performance and battery life. Standard Charge controllers are used where the solar panel voltage used as input are higher than the output voltage. Thus keeping the current constant, the voltage will be reduced by the controller but it results in loss of power. MPPT based solar charge controllers use microcontrollers based techniques to compute highest possible power output at any given time i.e. voltage will be monitored and regulated without power loss. The Controller will lower the voltage simultaneously increase the current, thereby increasing the power transfer efficiency. To know much about the charge controller, it is better to discuss about the batteries used in the PV system.

2.5.1 Batteries in PV Systems

Selecting the suitable battery for a PV application depends on many factors. Specific decisions on battery selection depend on physical properties, while other decisions will be much more difficult and may involve making tradeoffs between desirable and undesirable battery features. With the proper application of this knowledge, designers should be able to differentiate among battery types and gain some application experience with batteries they are familiar with. Considerations in battery subsystem design include the number of batteries is series and parallel, over-current and disconnect requirements, and selection of the proper wire sizes and types.

The energy output from the Solar PV systems is generally stored in a battery or in a battery bank deepening upon the requirements of the system. Mostly batteries or used in the stand-alone system and in the case of grid connected system, batteries are used as a backup system. The primary functions of the battery in a PV system are:

(a) **Energy Storage Capability and Autonomy:** to store electrical energy when it is produced by the PV array and to supply energy to electrical loads as needed or on demand.
(b) **Voltage and Current Stabilization:** to supply power to electrical loads at stable voltages and currents, by suppressing or 'smoothing out' transients that may occur in PV systems.
(c) **Supply Surge Currents:** to supply surge or high peak operating currents to electrical loads or appliances.

2.5.2 Battery Types and Classifications

Even batteries from the same manufactures differ in their performance and its characteristics. Different manufacturers have variations in the details of their battery construction, but some common construction features can be described for almost all batteries. Batteries are generally mass produced; it consists of several sequential and parallel processes to construct a complete battery unit. The manufacturing is an intensive, heavy industrial process involving the use of hazardous and toxic materials. After production, initial charge and discharge cycles are conducted on batteries before they are shipped to distributors and consumers.

Different types of batteries are manufactured today, each with specific design for particular applications. Each battery type or design has its individual strengths and weaknesses. In solar PV system predominantly, *lead-acid* batteries are used due to their wide availability in many sizes, low cost and well determined performance characteristics. For low temperature applications *nickel-cadmium* cells are used, but their high initial cost limits their use in most PV systems. The selection of the suitable battery depends upon the application and the designer. In general, electrical storage batteries can be divided into two major categories, *primary* and *secondary* batteries.

2.5.2.1 Primary Batteries

Primary batteries are non rechargeable but they can store and deliver electrical energy. Typical carbon-zinc and lithium batteries commonly used primary batteries. Primary batteries are not used in PV systems because they cannot be recharged.

2.5.2.2 Secondary Batteries

Secondary batteries are rechargeable and they can store and deliver electrical energy. Common *lead-acid* batteries used in automobiles and PV systems are secondary batteries.

The batteries can be selected based on their design and performance characteristics. The PV designer should consider the advantages and disadvantages of the batteries based on its characteristics and with respect to the requirements of a particular application. Some of the important parameters to be considered for the selection of battery are lifetime, deep cycle performance, tolerance to high temperatures and overcharge, maintenance and many others.

2.5.3 Battery Charging

In a stand-alone PV system, the ways in which a battery is charged are generally much different from the charging methods battery manufacturers use to rate battery

performance. The battery charging in PV systems consists of three modes of battery charging; *normal or bulk charge, finishing or float charge* and *equalizing charge*.

Bulk or Normal Charge: It is the initial portion of a charging cycle performed at any charge rate and it occurs between 80 % and 90 % state of charge. This will not allow the cell voltage to exceed the gassing voltage.

Float or Finishing Charge: It is usually conducted at low to medium charge rates. When the battery is fully charged, most of the active material in the battery has been converted to its original form, generally voltage/current regulation are required to limit the overcharge supplied to the battery.

Equalizing Charge: It consists of a current-limited charge to higher voltage limits than set for the finishing or float charge. It is done periodically to maintain consistency among individual cells. An equalizing charge is typically maintained until the cell voltages and specific gravities remain consistent for a few hours.

2.5.4 Battery Discharging

Depth of Discharge (DOD): The battery DOD is defined as the percentage of capacity that has been withdrawn from a battery compared to the total fully charged capacity. The two common qualifiers for depth of discharge in PV systems are the *allowable* or *maximum DOD* and the a*verage daily DOD* and are described as follows:

Allowable DOD: The maximum percentage of full-rated *capacity* that can be withdrawn from a battery is known as its allowable depth of discharge. The allowable DOD is the maximum discharge limit for a battery, generally dictated by the *cut off voltage* and *discharge rate*. In standalone PV systems, the *low voltage load disconnect* (LVD) set point of the battery charge controller dictates the allowable DOD limit at a given discharge rate.

Depending on the type of battery used in a PV system, the design allowable depth of discharge may be as high as 80 % for deep cycle, motive power batteries, to as low as 15–25 %. The allowable DOD is related to the *autonomy*, in terms of the *capacity* required to operate the system loads for a given number of days without energy from the PV array.

Average Daily DOD: The average daily depth of discharge is the percentage of the full-rated *capacity* that is withdrawn from a battery with the *average daily load* profile. If the load varies seasonally, the average daily DOD will be greater in the winter months due to the longer nightly load operation period. For PV systems with a constant daily load, the average daily DOD is generally greater in the winter due to lower battery temperature and lower rated capacity. Depending on the *rated capacity* and the *average daily load* energy, the average daily DOD may vary between only a few percent in systems designed with a lot of autonomy, or as high as 50 % for marginally sized battery systems. The average daily DOD is inversely related to autonomy; meaning that systems designed for longer autonomy periods (more capacity) have a lower average daily DOD.

State of Charge (SOC): The state of charge (SOC) is defined as the amount of energy as a percentage of the energy stored in a fully charged battery. Discharging a battery results in a decrease in state of charge, while charging results in an increase in state of charge. A battery that has had three quarters of its capacity removed, or been discharged 75 %, is said to be at 25 % state of charge.

Autonomy: Generally autonomy refers to the time a fully charged battery can supply energy to the systems loads when there is no energy supplied by the PV array. Longer autonomy periods generally result in a lower average daily DOD and lower the probability that the allowable (maximum) DOD or minimum load voltage is reached.

Self-Discharge Rate: In open-circuit mode without any charge or discharge current, a battery undergoes a reduction in state of charge, due to internal mechanisms and losses within the battery. Different battery types have different self-discharge rates, the most significant factor being the active materials and grid alloying elements used in the design.

Battery Lifetime: Battery lifetime is dependent upon a number of design and operational factors, including the components and materials of battery construction, temperature, frequency, depth of discharges, and average state of charge and charging methods.

Temperature Effects: For an electrochemical cell such as a battery, temperature has important effects on performance. As the temperature increases by 10 °C, the rate of an electrochemical reaction doubles, resulting in statements from battery manufacturers that battery life decreases by a factor of two for every 10 °C increase in average operating temperature. Higher operating temperatures accelerate corrosion of the positive plate grids, resulting in greater gassing and electrolyte loss. Lower operating temperatures generally increase battery life. However, the capacity is reduced significantly at lower temperatures, particularly for lead-acid batteries. When severe temperature variations from room temperatures exist, batteries are located in an insulated or other temperature-regulated enclosure to minimize battery.

Effects of Discharge Rates: The higher the discharge rate or current, the lower the capacity that can be withdrawn from a battery to a specific allowable DOD or cut off voltage. Higher discharge rates also result in the voltage under load to be lower than with lower discharge rates, sometimes affecting the selection of the low voltage load disconnects set point. At the same battery voltage the lower the discharge rates, the lower the battery state of charge compared to higher discharge rates.

Corrosion: The electrochemical activity resulting from the immersion of two dissimilar metals in an electrolyte, or the direct contact of two dissimilar metals causing one material to undergo oxidation or lose electrons and causing the other material to undergo reduction, or gain electrons. Corrosion of the grids supporting the active material in a battery is an ongoing process and may ultimately dictate the battery's useful lifetime. Battery terminals may also experience corrosion due to the action of electrolyte gassing from the battery, and generally require periodic cleaning and tightening in flooded lead-acid types. Higher temperatures and the flow of electrical current between two dissimilar metals accelerate the corrosion process.

2.5.5 *Battery Gassing and Overcharge Reaction*

When the battery is nearly fully charged gassing occurs in a battery during charging. At this point, essentially all of the active materials have been converted to their fully charged composition and the cell voltage rises sharply. The gas products are either recombined internal to the cell as in sealed or valve regulated batteries, or released through the cell vents in flooded batteries. In battery, the overcharge or gassing reaction is irreversible and it results in water loss. All gassing reactions consume a portion of the charge current which cannot be delivered on the subsequent discharge, thereby reducing the battery charging efficiency.

2.5.6 *Charge Controller Types*

There are two basic charge controller (i) Shunt Controller and (ii) Series Controller

2.5.6.1 Shunt Controller

Shunt controllers consists of a blocking diode in series between the battery and the shunt element to prevent the battery from short-circuiting when the module is regulating. This type of charge controllers are limited to use in Solar PV systems with PV module currents less than 20 A. Shunt controller require a heat sink to dissipate the power because of the voltage drop between the module and controller and due to wiring and resistance of the shunt element, the module is never entirely short circuited, resulting in some power dissipation within the controller. Figure 2.21 below shows the diagram of shunt controller.

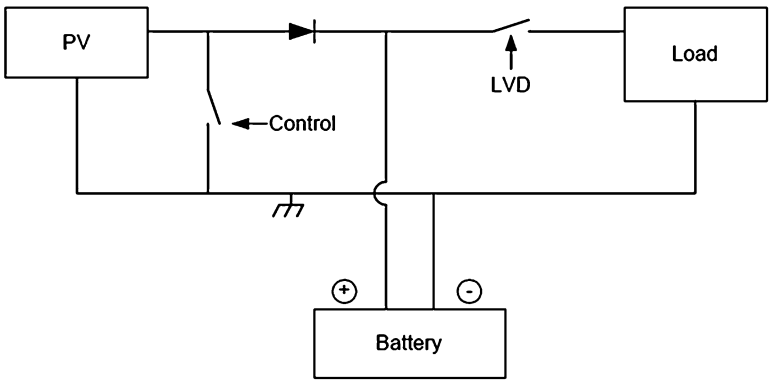


Fig. 2.21 Diagram of shunt controller

2.5.6.2 Shunt-Interrupting Design

The shunt-interrupting controller completely disconnects the array current in an interrupting or on-off fashion when the battery reaches the voltage regulation set point. When the battery decreases to the array reconnect voltage, the controller connects the array to resume charging the battery. This cycling between the regulation voltage and array reconnect voltage is why these controllers are often called on-off or pulsing controllers. Shunt-interrupting controllers are widely available and are low cost, however they are generally limited to use in systems with array currents less than 20 A due to heat dissipation requirements. In general, on-off shunt controllers consume less power than series type controllers that use relays, so they are best suited for small systems where even minor parasitic losses become a significant part of the system load. Shunt-interrupting charge controllers can be used on all battery types; however the way in which they apply power to the battery may not be optimal for all battery designs. In general, constant-voltage, PWM or linear controller designs are recommended by manufacturers of gelled and AGM lead-acid batteries. However, shunt-interrupting controllers are simple, low cost and perform well in most small stand-alone PV systems.

2.5.6.3 Shunt-Linear Design

Once a battery becomes nearly fully charged, a shunt-linear controller maintains the battery at near a fixed voltage by gradually shunting the array through a semiconductor regulation element. In some designs, a comparator circuit in the controller senses the battery voltage, and makes corresponding adjustments to the impedance of the shunt element, thus regulating the array current. In other designs, simple Zener power diodes are used, which are the limiting factor in the cost and power ratings for these controllers. There is generally more heat dissipation in a shunt-linear controller than in shunt-interrupting types. Shunt-linear controllers are popular for use with sealed VRLA batteries. This algorithm applies power to the battery in a preferential method for these types of batteries, by limiting the current while holding the battery at the regulation voltage.

2.5.6.4 Series Controller

In a series controller, a relay or solid-state switch either opens the circuit between the module and the battery to discontinuing charging, or limits the current in a series-linear manner to hold the battery voltage at a high value. In the simpler series interrupting design, the controller reconnects the module to the battery once the battery falls to the module reconnect voltage set point. Figure 2.22 shows the diagram of series controller.

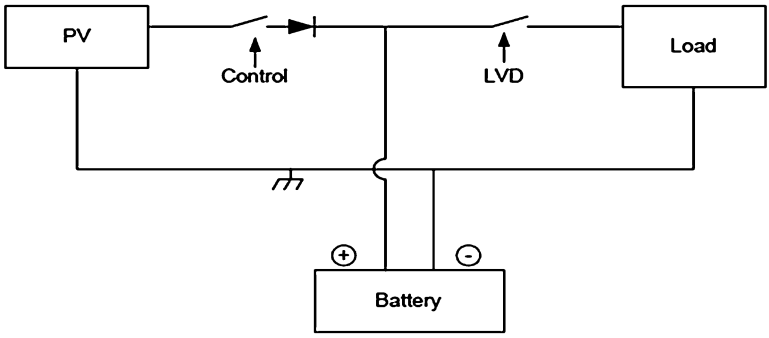


Fig. 2.22 Diagram of series controller

2.5.6.5 Series-Interrupting Design

The most simple series controller is the series-interrupting type, involving a one-step control, turning the array charging current either on or off. The charge controller constantly monitors battery voltage, and disconnects or open-circuits the array in series once the battery reaches the regulation voltage set point.

After a pre-set period of time, or when battery voltage drops to the array reconnect voltage set point, the array and battery are reconnected, and the cycle repeats. As the battery becomes more fully charged, the time for the battery voltage to reach the regulation voltage becomes shorter each cycle, so the amount of array current passed through to the battery becomes less each time. In this way, full charge is approached gradually in small steps or pulses, similar in operation to the shunt-interrupting type controller. The principle difference is the series or shunt mode by which the array is regulated. Similar to the shunt-interrupting type controller, the series-interrupting type designs are best suited for use with flooded batteries rather than the sealed VRLA types due to the way power is applied to the battery.

2.5.6.6 Series-Interrupting, 2-Step, Constant-Current Design

This type of controller is similar to the series-interrupting type, however when the voltage regulation set point is reached, instead of totally interrupting the array current, a limited constant current remains applied to the battery. This "trickle charging" continues either for a pre-set period of time, or until the voltage drops to the array reconnect voltage due to load demand. Then full array current is once again allowed to flow, and the cycle repeats. Full charge is approached in a continuous fashion, instead of smaller steps as described above for the on-off type controllers. A load pulls down some two-stage controls increase array current immediately as battery voltage. Others keep the current at the small trickle charge level until the battery voltage has been pulled down below some intermediate value (usually 12.5–12.8 V) before they allow full array current to resume.

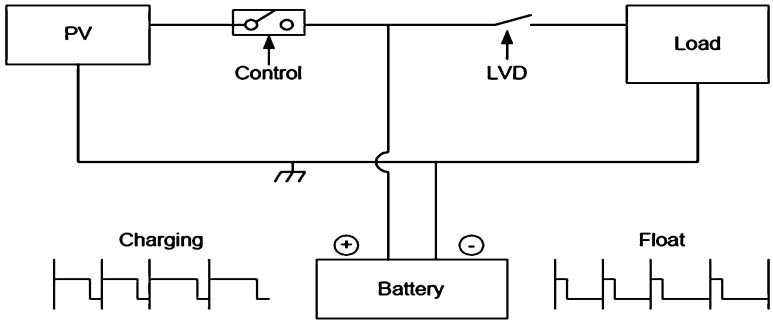


Fig. 2.23 Pulse width modulation (PWM)

2.5.6.7 Pulse-Width Modulation (PWM)

This method uses solid state switches to apply pulses of current at a reasonably high frequency (e.g., 300 Hz), but with a varying duty cycle, such that the battery receives a constant voltage charge from the array. This type of controller, shown in a series configuration in Fig. 2.23, can also be configured in the shunt topology. Although similar to the series linear and shunt linear controller in function, power dissipation is reduced with PWM topology compared to series linear control.

Overcharge Protection

In a 12 V battery system the voltage vary between 10.5 and 14.4 V, depending on the actual state of charge of the battery, charge current, discharge current, type and age of the battery. When a normal full loaded battery and no charging or discharging current is flowing than the battery voltage is about 12.4–12.7 V, when charging current is flowing the voltages jump to a higher level e.g. 13.7 V (depending on the current), when loads are switched on the voltage drops down to a lower lever e.g. 12.0 V or 11.8 V (also depending on the current). The PV module produces energy and the current is flowing into the battery so voltage level increases up to the range of 14.4 V. Then the overcharge protection starts the work. When the battery voltage level is 14.4 V, the charge controller is switched off the charging current or reduced it (by pulse wide modulation). To disconnect the system loads once the battery reaches a low voltage or low state of charge condition.

If the voltage of the system falls below 11.5 V for a period of minimum 20 s than the charge controller will be switched off for minimum 30 s. All loads which are connected to the controller is off. If the battery voltage increase above 12.5 V for more than 20 s than the charge controller will be switched ON the loads again for a minimum time of 30 s. The delay of 30 s is integrated to protect the system against a swinging situation.

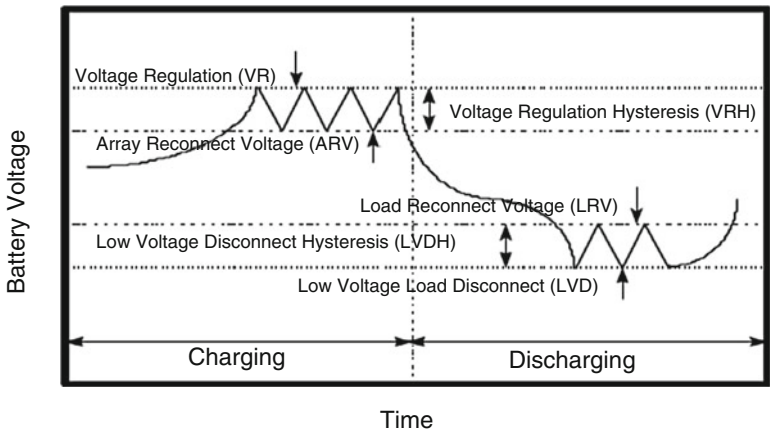


Fig. 2.24 Charge controller set points

Charge Controller Set Points

Controller set points are the battery voltage levels at which a charge controller performs control or switching functions. Four basic control set points are defined for most charge controllers that have battery overcharge and over-discharge protection features. The voltage regulation (VR) and the array reconnect voltage (ARV) refer to the voltage set points at which the array is connected and disconnected from the battery. The low voltage load disconnect (LVD) and load reconnect voltage (LRV) refer to the voltage set points at which the load is disconnected from the battery to prevent over discharge. Figure 2.24 shows the basic controller set points on a simplified diagram plotting battery voltage versus time for a charge and discharge cycle. A detailed discussion of each charge controller set point follows.

High Voltage Disconnect (HVD) Set Point

The high voltages disconnect (HVD) set point is one of the key specifications for charge controllers. The voltage regulation set point is the maximum voltage that the charge controller allows the battery to reach, limiting the overcharge of the battery. Once the controller senses that the battery reaches the voltage regulation set point, the controller will either discontinue battery charging or begin to regulate the amount of current delivered to the battery.

Array Reconnect Voltage (ARV) Set Point

In interrupting (on-off) type controllers, once the module or array current is disconnected at the voltage regulation set point, the battery voltage will begin

to decrease. If the charge and discharge rates are high, the battery voltage will decrease at a greater rate when the battery voltage decreases to a predefined voltage, the module is again reconnected to the battery for charging. The voltage at which the module is reconnected is defined as the array reconnects voltage (ARV) set point.

Deep Discharge Protection

When a battery is deeply discharged, the reaction in the battery occurs close to the grids, and weakens the bond between the active materials and the grids. When we deep discharge the battery repeatedly, loss of capacity and life will eventually occur. To protect battery from deep discharge, most charge controllers include an optional feature.

2.5.6.8 Voltage Regulation Hysteresis (VRH)

The voltage differences between the high voltages disconnect set point and the array reconnect voltage is often called the voltage regulation hysteresis (VRH). The VRH is a major factor which determines the effectiveness of battery recharging for interrupting (on-off) type controller. If the hysteresis is too big, the module current remains disconnected for long periods, effectively lowering the module energy utilization and making it very difficult to fully recharge the battery. If the regulation hysteresis is too small, the module will cycle on and off rapidly. Most interrupting (on-off) type controllers have hysteresis values between 0.4 and 1.4 V for nominal 12 V systems.

2.5.6.9 Low Voltage Load Disconnect (LVD) Set Point

Deep discharging the battery can make it susceptible to freezing and shorten its operating life. If battery voltage drops too low, due to prolonged bad weather or certain non-essential loads are connected the charge controller disconnected the load from the battery to prevent further discharge. This can be done using a low voltage load disconnect (LVD) device is connected between the battery and non-essential loads. The LVD is either a relay or a solid-state switch that interrupts the current from the battery to the load.

2.5.6.10 Load Reconnect Voltage (LRV) Set Point

The battery voltage at which a controller allows the load to be reconnected to the battery is called the load reconnect voltage (LRV). After the controller disconnects the load from the battery at the LVD set point, the battery voltage rises to its

open-circuit voltage. When the PV module connected for charging, the battery voltage rises even more. At some point, the controller senses that the battery voltage and state of charge are high enough to reconnect the load, called the load reconnect voltage set point. LRV should be 0.08 V/cell (or 0.5 V per 12 V) higher than the load-disconnection voltage. Typically LVD set points used in small PV systems are between 12.5 and 13.0 V for most nominal 12 V lead-acid battery. If the LRV set point is selected too low, the load may be reconnected before the battery has been charged.

2.5.6.11 Low Voltage Load Disconnect Hysteresis (LVLH)

The voltage difference between the low voltage disconnect set point and the load reconnect voltage is called the low voltage disconnect hysteresis. If the low voltage disconnect hysteresis is too small, the load may cycle on and off rapidly at low battery state-of-charge (SOC), possibly damaging the load or controller, and extending the time it required to charge the battery fully. If the low voltage disconnect hysteresis is too large the load may remain off for extended periods until the array fully recharges the battery.

2.5.7 Charge Controller Selection

Charge controllers are used in Solar PV systems to allow high rates of charging up to the gassing point, and then limit or disconnect the PV current to prevent overcharge. The highest voltage that batteries are allowed to reach depends on how much gassing occurs. To limit gassing, proper selection of the charge controller voltage regulation set point is critical in PV systems. Both under and overcharging will result in premature battery failure and loss of load in stand-alone PV systems. The selection and sizing of charge controllers in PV systems involves the consideration of several factors, depending on the complexity and control options required. While the primary function is to prevent battery overcharge, many other functions may also be used, including low voltage load disconnect, load regulation and control, control of backup energy sources, diversion of energy to and auxiliary load, and system monitoring. The designer must decide which options are needed to satisfy the requirements of a specific application.

The charge controller must not only be able to handle typical or rated voltages and currents, but must also be sized to handle expected peak or surge conditions from the PV array or required by the electrical loads that may be connected to the controller. It is extremely important that the controller be adequately sized for the intended application. The sizing of the charge controller can be determined by multiplying the short-circuit current of the solar PV module and the safety factor.

2.5.8 Operating Without a Charge Controller

Charge controller is an essential part in stand-alone PV systems. However there are special circumstances where a charge controller may not be needed in small systems with well-defined loads. By eliminating the need for the sensitive electronic charge controller, the design is simplified, at lower cost and with improved reliability. There are two cases where battery charge regulation may not be required: (1) when a low voltage "self-regulating module" is used in the proper climate; and (2) when the battery is very large compared to the array. Each of these cases are discussed next.

2.5.9 Using Low-Voltage "Self-Regulating" Modules

A Self-regulating system consists of a low voltage solar PV module, battery and load. Solar PV module is used to charge a 12 V battery. In the case self-regulating modules without battery charge regulation, the array current falls off sharply as the voltage increases above the maximum power point. In a "self-regulating" low voltage PV module, there are generally only 28–30 silicon cells connected in series, resulting in an open-circuit voltage of about 18 V and a maximum power voltage of about 15 V at 25 °C. For every 1 °C increase in temperature, module voltage decreases by 2.3 mV. For self-regulation and no battery overcharge to occur, the following three conditions must be met:

1. ***The load must be used daily.*** Every day the battery will receive excessive charge, even if the module is forced to operate beyond the "knee" at current levels lower than its Imp. If the load is used daily, then the amp-hours produced by the module are removed from the battery, and this energy can be safely replaced the next day without overcharging the battery. So for a system to be "self-regulating", the load must be consistent and predictable.
2. ***The climate cannot be too cold.*** If the module stays very cool, the "knee" of the IV curve will not move down in voltage enough, and the expected drop off in current will not occur, even if the battery voltage rises as expected. Often "self-regulating modules" are used in arctic climates for lighting for remote cabins for example, because they are the smallest and therefore least expensive of the power modules, but they are combined with a charge controller or voltage dropping diodes to prevent battery overcharge.
3. ***The climate cannot be too warm.*** If the module heats up too much, then the drop off in current will be too extreme, and the battery may never be properly recharged. The battery will sulfate, and the loads will not be able to operate. A "self-regulating system" design can greatly simplify the design by eliminating the need for a charge controller, however these type of designs are only appropriate for certain applications and conditions. In most common stand-alone PV system designs, a battery charge controller is required.

2.5.10 Using a Large Battery or Small Array

A charge controller may not be needed if the charge rates delivered by the array to the battery are small enough to prevent the battery voltage from exceeding the gassing voltage limit when the battery is fully charged and the full array current is applied. In certain applications, a long autonomy period may be used, resulting in a large amount of battery storage capacity. In these cases, the charge rates from the array may be very low, and can be accepted by the battery at any time without overcharging. These situations are common in critical application requiring large battery storage, such as telecommunications repeaters in alpine conditions or remote navigational aids. It might also be the case when a very small load and array are combined with a large battery, as in remote telemetry systems. In general a charging rate of C/100 or less is considered low enough to be tolerated for long periods even when the battery is fully charged. This means that even during the peak of the day, the array is charging the battery bank at the 100 h rate or slower, equivalent to the typical trickle charge rate that a controller would produce anyway.

2.6 MATLAB Model of SOC

The implementation of State of charge battery using MATLAB/SIMULINK is presented in this section. This simulation focuses on knowing the state of charge of a battery by connecting it to a load with constant charging and discharging.

Assumptions

- The internal resistance is maintained constant during the charge and the discharge cycles and does not vary with the amplitude of the current.
- The parameters of the model are deduced from discharge characteristics and assumed to be the same for charging.
- The capacity of the battery doesn't change with the amplitude of current (No Peukert effect).
- The model doesn't take the temperature into account.
- The Self-Discharge of the battery is not represented. It can be represented by adding a large resistance in parallel with the battery terminals.
- The battery has no memory effect.

Limitations

The minimum no-load battery voltage is 0 V and the maximum battery voltage is equal to $2*E_0$. The minimum capacity of the battery is 0 Ah and the maximum capacity is Qmax. The equivalent circuit of a generic dynamic battery model parameterized to represent most popular types of rechargeable batteries is shown in Fig. 2.25.

In this section, Nickel-Cadmium and Nickel-Metal-Hydride model is implemented using SIMULINK. The corresponding equations for charge and discharge model are represented according to the following equations.

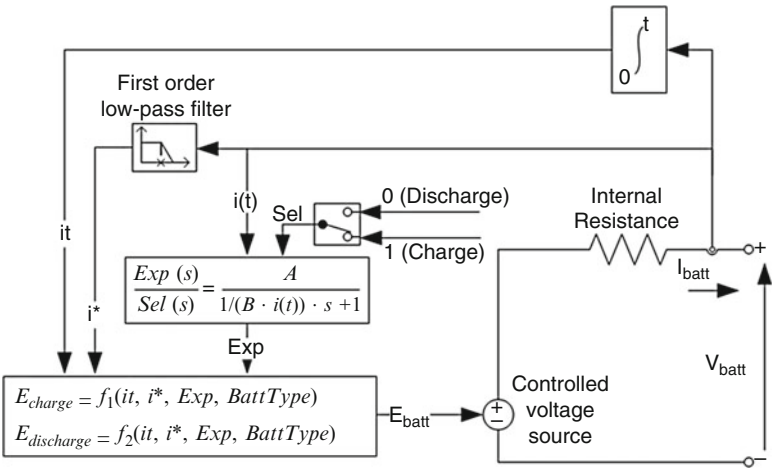


Fig. 2.25 Equivalent circuit of battery

Charge model ($i^* < 0$)

$$f_2(it, i^*, i, Exp) = E_0 - K \cdot \frac{Q}{|it| + 0.1Q} \cdot i^* - K.\frac{Q}{Q - it} \cdot it + Laplace^{-1}\left(\frac{Exp(s)}{Sel(s)} \cdot \frac{1}{s}\right) \tag{2.9}$$

Discharge model ($i^* > 0$)

$$f_1(it, i^*, i, Exp) = E_0 - K \cdot \frac{Q}{Q - it} \cdot i^* - K \cdot \frac{Q}{Q - it} \cdot it + Laplace^{-1}\left(\frac{Exp(s)}{Sel(s)} .0\right) \tag{2.10}$$

where

E_0 = Constant voltage (V)
Exp(s) = Exponential zone dynamics (V)
Sel(s) = Represents the battery mode. Sel(s) = 0 during battery discharge, Sel(s) = 1 during battery charging.
K = Polarization constant (Ah^{-1}) or Polarization resistance (Ohms)
i^* = Low frequency current dynamics (A)
i = Battery current (A)
it = Extracted capacity (Ah)
Q = Maximum battery capacity (Ah)

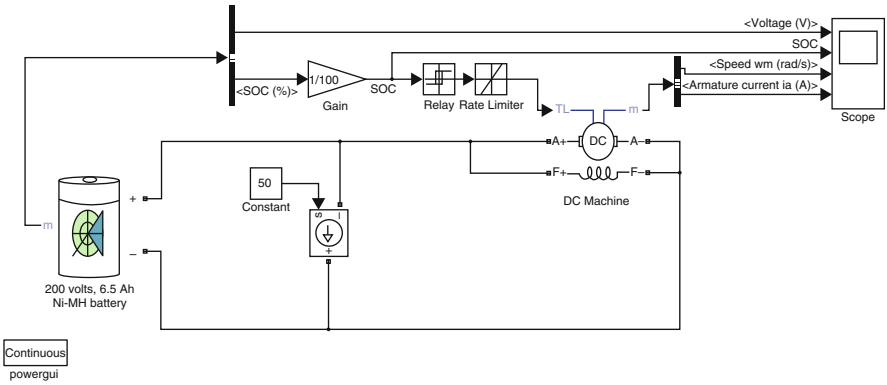


Fig. 2.26 SIMULINK model of state of charge estimation of a battery

2.6.1 SIMULINK Model

The power battery example illustrates a 200 V, 6.5 Ah NiMH battery connected to a constant load of 50 A as shown in Fig. 2.26. The DC machine is connected in parallel with the load and operates at no load torque. When the State-Of-Charge (SOC) of the battery goes under 0.4 (40 %), a negative load torque of 200 Nm is applied to the machine so it acts as a generator to recharge the battery. When the SOC goes over 80 %, the load torque is removed so only the battery supplies the 50 amps load.

The battery is discharged by the constant DC load of 50 A. When the SOC drops under 0.4, a mechanical torque of −200 Nm is applied so the machine acts as a generator and provides a current of 100 amps, among which 50 amps is consumed by the load and 50 amps consumed to recharge the battery. When the SOC goes over 0.8, the mechanical torque is removed and the machine operates freely to repeat the cycle of operation.

2.6.1.1 Blockset Used

The dialog box and the parameters for the battery model are shown in Fig. 2.27.

Battery Type
Provides a set of predetermined charge behavior for four types of battery such as Lead-Acid, Lithium-Ion, Nickel-Cadmium, and Nickel-Metal-Hydride.

Nominal Voltage (V)
The nominal voltage (*Vnom*) of the battery (volts). The nominal voltage represents the end of the linear zone of the discharge characteristics.

Rated Capacity (Ah)
The rated capacity (*Qrated*) of the battery in ampere-hour. The rated capacity is the minimum effective capacity of the battery.

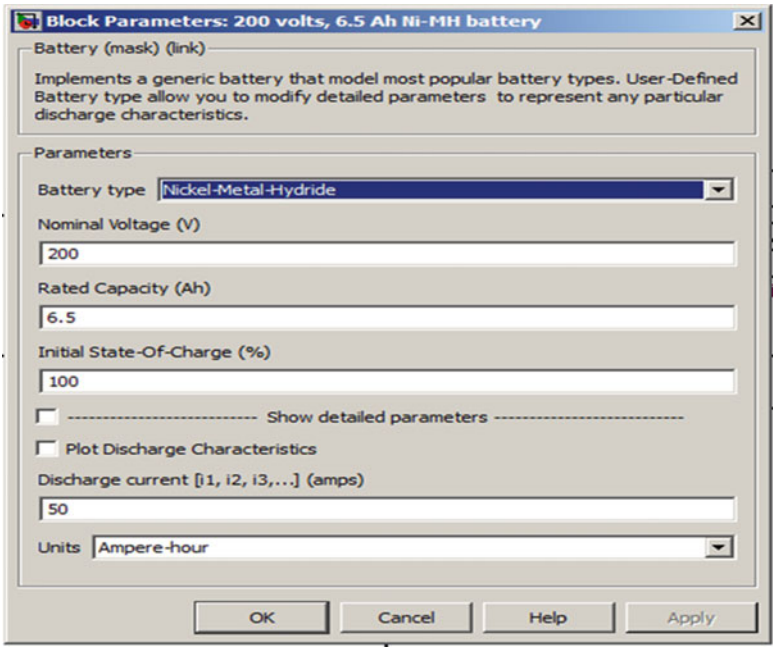


Fig. 2.27 Block parameters for Ni-MH battery

Initial State-of-Charge (%)
The initial State-Of-Charge (SOC) of the battery. 100 % indicates a fully charged battery and 0 % indicates an empty battery. This parameter is used as an initial condition for the simulation and does not affect the discharge curve (when the option **Plot Discharge Characteristics** is used).

Use Parameters Based on Battery Type and Nominal Values
Load the corresponding parameters in the entries of the dialog box, depending on the selected **Battery type**, the **Nominal Voltage** and the **Rated Capacity**. When a preset model is used, the detailed parameters cannot be modified. If the user wants to modify the discharge curve, select the desired battery type to load the default parameters, and then uncheck the **Use parameters based on Battery type and nominal values** checkbox to access the detailed parameters.

Discharge Characteristics
The simulation result of the SOC model for Ni-MH battery is shown in Fig. 2.28. Here the first graph represents the battery terminal voltage under charge and discharge conditions of the battery. The second graph represents the state of charge of the battery, due to the presence of the generator when state of charge crosses below the 40 % mark, the battery is charged by the generator and when it drops below the 80 % mark, the battery starts to discharge as indicated by the

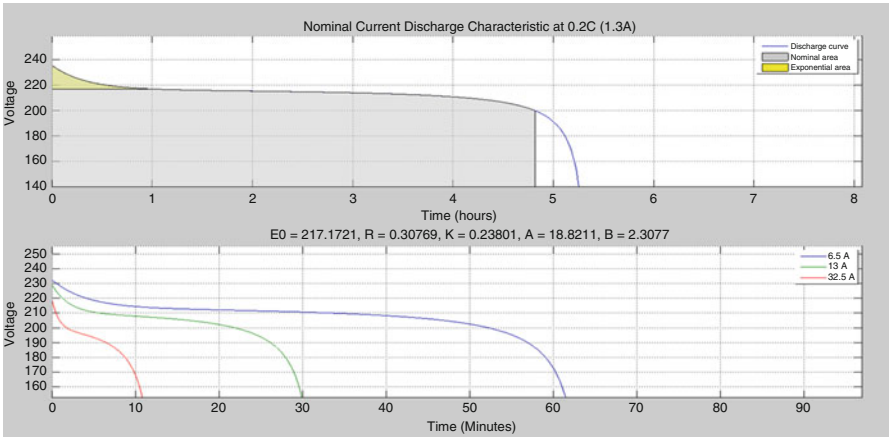


Fig. 2.28 Discharge characteristics of battery

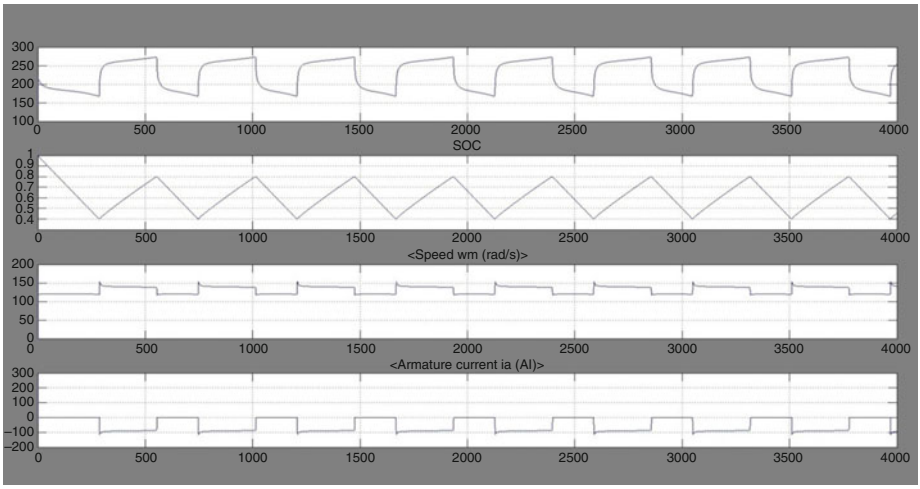


Fig. 2.29 Simulation results for Ni-MH SOC battery

graph. The third graph represents the speed of the DC machine which alters with respects to charge and discharge of the battery. The final graph shown in Fig. 2.29 represents the armature current output of the machine.

2.7 MATLAB Model of Charge Controller

The main function of a charge controller in a PV system is to regulate the voltage and current from PV solar panels into a rechargeable battery. The minimum function of a PV charge controller is to disconnect the array when the battery is

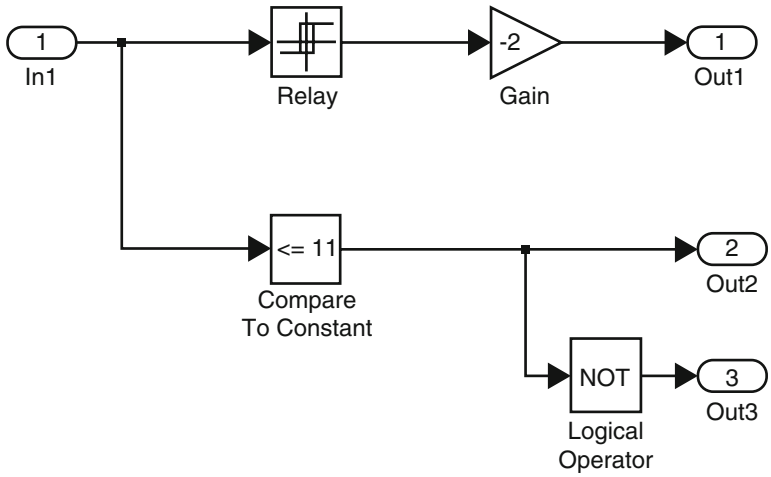


Fig. 2.30 Internal circuit of charge controller

fully charged and keep the battery fully charged without damage. A charge controller is important to prevent battery overcharging, excessive discharging, reverse current flow at night and to protect the life of the batteries in a PV system. Power electronics circuit is used in a PV charge-controller to get highest efficiency, availability and reliability. The use of power electronics circuits such as various DC to DC converters topologies like buck converter, boost converter, buck-boost converter and others converter topology as power conditioning circuitry enables the effective flow of desired current to charge the battery.

A PV array with 17 subsystems was developed to implement the charge controller model. The charge controller unit is designed according to Fig. 2.30 based on the battery voltage level, which was considered to be 12 V and with a current level of 1 Amphr. The function of charge controller is as follows: if the battery voltage reaches the more than 13 V, battery disconnected from the PV-array, and if the voltage drops lesser than 10 V then it has to be connected to PV array, so if voltage of battery in between 10 and 13 V then only connection between PV-array and battery exist. This logic is implemented by taking considering the hysteresis relay. If the voltage of battery is between 11 and 13 V, normal load is connected else dummy load is connected to battery. The block parameters of the SIMULINK blocks used in this example are shown in Figs. 2.31 and 2.32.

The complete circuit involving the PV array, charge controller and battery is illustrated in Fig. 2.33. The battery voltage and the load voltage are represented in the form of waveforms in Fig. 2.34.

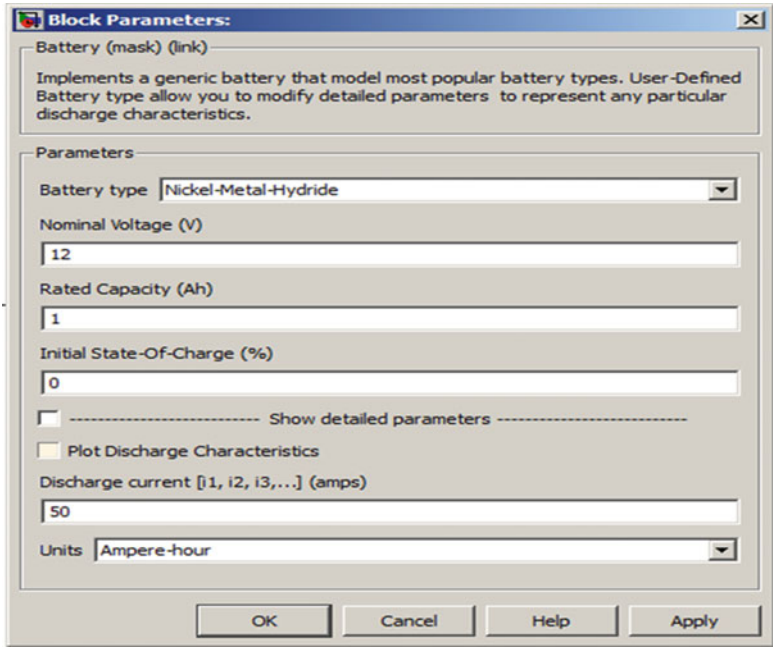


Fig. 2.31 Block parameters of Ni-MH battery

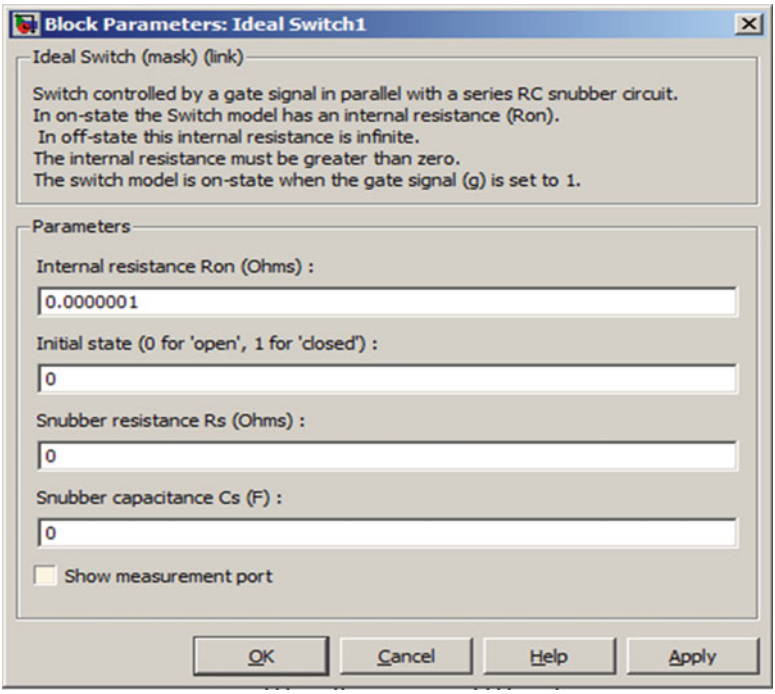


Fig. 2.32 Block parameters of ideal switch

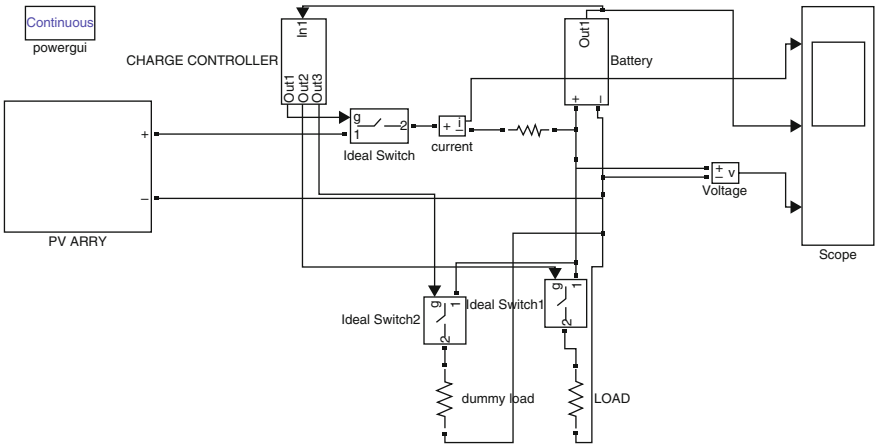


Fig. 2.33 Complete circuit

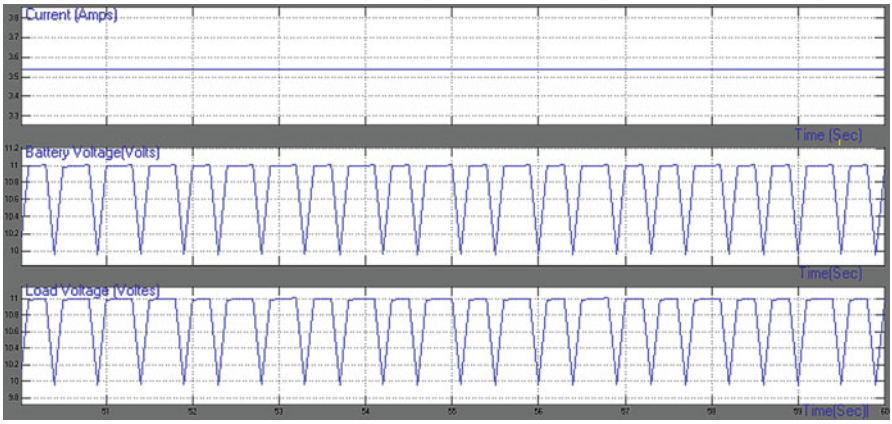


Fig. 2.34 Scope wave forms of complete circuit

2.8 Inverter

Inverters are used to convert DC current into AC currents in PV systems. Different types of inverters produce a different "quality" of electricity. So, the user must match the power quality required by your loads with the power quality produced by the inverter. Major discrepancies exist between power generation with PV modules and the requirements of the public grid. The job of the inverter is to connect the systems with each other and to feed the solar power into the grid with the highest possible efficiency.

The simplest inverter can be accomplished with a circuit similar to that shown in Fig. 2.35. The ideal switches in the circuit can be selected depending on the power

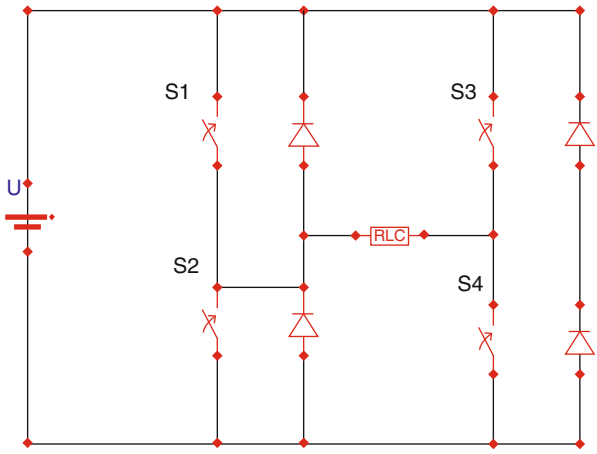


Fig. 2.35 Simple inverter circuit

and voltage requirements. A simple control strategy to get the inverter output is to turn on and off the switches at the required AC frequency to obtain a square wave voltage but it consists of high harmonic currents and voltages. It can be reduced by using high frequency pulse width modulation techniques to diminish harmonic distortion and provide load voltage control. Because, harmonic content can cause overheating in the case of motor loads due to higher copper losses as well as uneven magnetic fields affecting overall operation. Sensitive electronic loads may also display erratic operation. Today, advanced control schemes and creative topologies allow the creation of AC with very low harmonic distortion; three phase designs are also possible by incorporating additional switches.

The efficiency indicates the percentage of the available solar power that is actually converted and fed into the utility grid. Modern inverters currently consume between 4 % and 8 % of the converted energy in the conversion process, which corresponds to an overall efficiency of 92–94 %. Further reducing this already low energy consumption is a major technical challenge, and one which can only be achieved with new and innovative designs. The solar PV inverters can be classified into (i) Centralized inverters (ii) String inverters (iii) Multi string inverter and (iv) Module integrated inverter.

2.8.1 Centralized Inverters

Earlier centralized inverters are the most common form of power electronics used in PV systems. In this model a single, large inverter is connected to many PV modules wired in series to form strings with up to 600 V/1,000 V of open-circuit voltage. All the solar PV modules are connected in strings, generating a sufficient high voltage to avoid amplification and the strings are connected in parallel to support high power to output. The conversion efficiency of many central inverters is

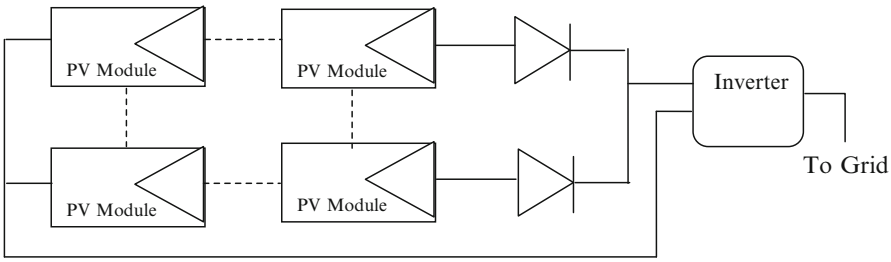


Fig. 2.36 Centralized inverters

95 % or higher, and they feature a relatively low unit cost per watt. However, central inverters have multiple drawbacks.

This main disadvantage of this topology is the involvement of high voltage DC cable from the strings to the inverter and losses in string diodes. This structure is also limited from Maximum Power Point (MPP) Tracking and controlling mismatch between strings so individual PVs, resulting in low efficiency and reliability. This topology is not flexible and this makes it less appealing in mass production. With all these issues, this technology is not used in new solar PV systems installation. Central inverters (Fig. 2.36) cannot monitor the performance of individual PV modules, so damaged or otherwise compromised modules often go undetected. Finally, central inverters limit the design and site selection of PV systems, particularly in residential applications. They require co-planar module layouts and a lack of partial shading from chimneys, trees, vent pipes, etc. PV installers may opt out of half or more of potential sites due to these restrictions.

The conversion efficiency of many central inverters is 95 % or higher, and they feature a relatively low unit cost per watt. Generally for high voltage PV systems central inverters are preferred mainly because for systems ranging from 5 kW to 1 MW, incentives are provided by government agencies. Certain centralized inverters uses common MPPT and IGBT based topology for enhancing power quality. In some power plants, central inverters were arranged in master slave configurations in order to use the most efficient combination of inverters according to total PV array output. Presently central inverters can be installed along with the DC-DC Optimizers. DC-DC optimizers supplement a central inverter with individual DC-DC converters installed for each PV module (Fig. 2.37). DC-DC optimizers can be wired serially in strings and also it can be wired in parallel. The central inverter still converts the combined DC output from across the array to grid-compatible AC power, but the DC-DC optimizers perform MPPT at the module level. This allows each module to produce its full output without being held back by any under-performing modules in the array. DC-DC optimizers also permit module-level communications and performance monitoring. However, DC-DC optimizers retain a key disadvantage of central inverters–a failure of the central inverter still results in a complete loss of system output. Furthermore, some DC-DC optimizer systems also require a separate command-and-control device to operate, creating one more point of potential system failure in addition to the central

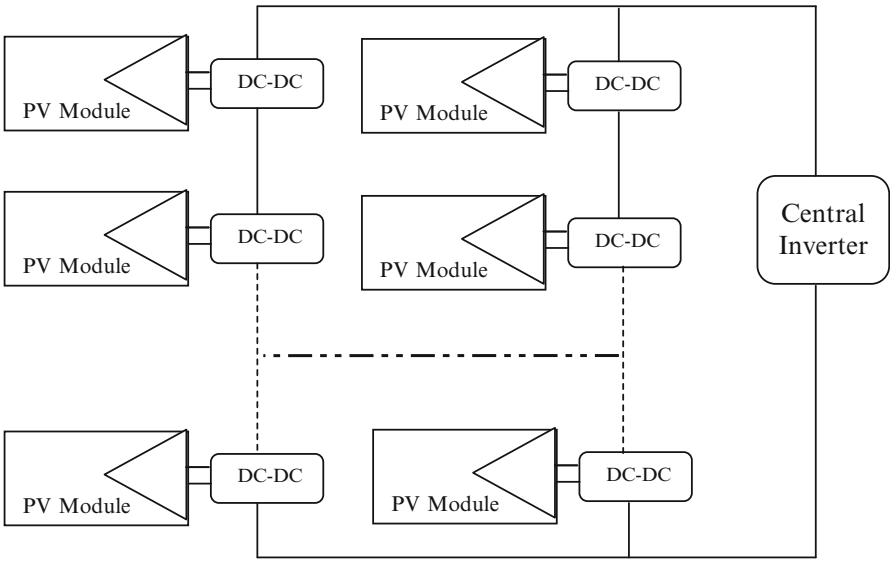


Fig. 2.37 Central inverter with one DC-DC optimizer per module

inverter. With additional equipment to purchase and install, DC-DC optimizers add to the initial cost of a PV system. The added module-level hardware also imposes a penalty on overall system-level efficiency by introducing an additional stage of loss power conversion.

2.8.2 String Inverters

This topology having been introduced to the market for about 10 years, this structure remains a favorite structure in new installation. However, in a common scenario of partial shading, MPP tracking may still not be sufficient to achieve a certain efficiency requirement. Currently, the most successful technology is the string inverter. Most of these inverters use either Metal Oxide Field Effect Transistors (MOSFET) or Insulated Gate Bipolar Transistor (IGTB) semiconductors instead of thyristors to perform self-commutated switching actions. High input voltages are possible to avoid voltage amplification stages, yet smaller voltages are possible (e.g. AC module) by incorporating additional DC-DC conversion or line frequency transformers at the output. Figure 2.38 has a string of inverters connected in series with an AC module. While still avoiding high voltage amplification, this structure has improved performance with no diode loss in series, separate MPP tracking for each string and lower cost with mass productions. It is possible to have less PVs in string with voltage amplification by DC-DC converter or a line frequency transformer, which increases total area.

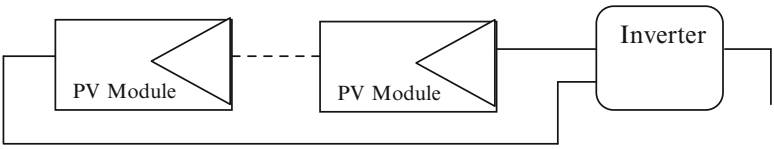


Fig. 2.38 String inverters

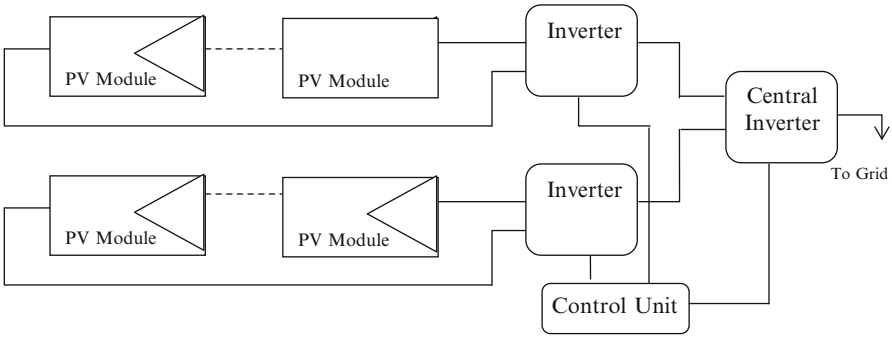


Fig. 2.39 Multi-string inverters

2.8.3 Multi-string Inverters

In this structure as shown in Fig. 2.39, DC-DC converter is implemented for each string for MPP tracking and power combination of different string to a DC bus. Multi-string inverter features the optimal MPP tracking for a single string of PVs. A big power stage works as a grid connected half bridge inverter without transformer. The multi-string inverter is useful when PV strings of different rated power, different orientation are combined. The DC-DC part can be implemented with high-frequency pulse width modulation (PWM) converter to reduce implementation area.

2.8.4 Module Integrated Inverter/Micro-inverters

Micro inverters (Fig. 2.40) are a complete, environmentally protected unit consisting of solar cells, optics, inverter, and other components, designed to generate AC power when exposed to sunlight. Module-level micro-inverters were first introduced to the PV market in the 1990s but now they progressed to the point and it became the alternative solution to the central inverters most commonly used today in PV systems. It is predicted that within a few years most PV modules will feature some form of module-level power electronics. The micro-inverter,

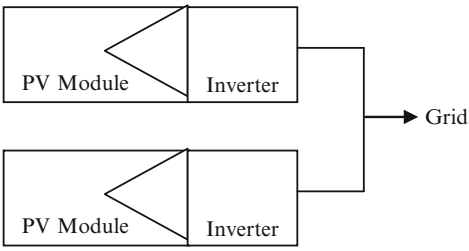


Fig. 2.40 Micro-inverters

also called AC module is the integration of PV and inverter into one electrical device. In an AC module, a micro-inverter is directly integrated with a PV panel, yielding a module that natively generates grid-compatible AC power. Micro inverter simplify system design, allowing any number and combination of modules to connect directly to the grid, and provide enhanced safety by eliminating all exposed DC wiring from the system altogether.

2.8.5 Inverter Topology

Inverters can be classified by their output waveform in four categories: square wave, modified square wave, also called quasi-square wave, multilevel and sine wave (synthesized from a high frequency PWM). The square and quasi-square wave inverters are not recommended due to their poor quality waveform. Multilevel and sine wave inverters are considered the state of the art technology. The Multilevel inverter is based on low frequency and the sine wave inverter is based on high switching frequency. Multilevel inverters are the best available solution for high power applications. However, for medium and low power applications, there is not a clear tradeoff to make it more appealing than sine wave inverters, or vice versa. High frequency inverters favor compactness and reduced cost, while low frequency ones are claimed to have the best efficiency and robustness. The final choice of one inverter instead of the other better depends on the application. In our application of stand-alone renewable energy systems (SARES), multilevel inverters have great potential with its reliability, surge power capacity and efficiency.

2.9 MATLAB/SIMULINK Model of Inverter

For a solar PV output of 2.7 V DC, we design a boost converter with output voltage = 8 V, supply current = 1 A. Switching Frequency = 25 Khz such that the variation in inductor current is not more than 40 % of average inductor current for all operating conditions. The output ripple should be not more than 2 %.

DC-DC Converter (Boost)
In a boost converter, the output voltage is related to input voltage by the formula

$$v_o = \frac{V_{IN}}{(1-k)}$$

Switching frequency = 25 kHz
V_{in} = 2.7 V To obtain an output of 8 V and load current of 1 A,

$$8 = \frac{2.7}{(1-k)} \qquad \text{K} = 0.6$$

$$\Delta V_{C=} \frac{I_O K}{CF} \qquad \Delta I = \frac{V_S * K}{LF}$$

The tolerable limits of voltage and current ripple are 20 % and 40 % respectively.

$$I_0 = 0.44\ A \qquad \Delta V_C = 0.02 * 8 = 0.16, \qquad \Delta I = 0.40$$

$$c = \frac{I_o * K}{\Delta V_C * F} = \frac{0.44 * 0.66}{16 * 25K} = 72.6\ \mu\text{F} \qquad L = \frac{V_S * K}{\Delta \text{I} * F} = \frac{2.7 * 0.66}{0.40 * 25K} = 0.2\ \text{mH}$$

Single-Phase Inverter
Input Voltage = 8 V DC
Reference Wave:
Amplitude = 1 V
Frequency = 50 Hz
= 2*3.14*50
= 314 radians
Carrier Wave:
Time period = [0 0.25e-4 0.5e-4 0.75e-4 1e-4]
Amplitude = [0 1.2 0–1.2 0]

2.9.1 SIMULINK Model

For inverter development, the power system blockset provides the required components such as a full-bridge, batteries, resistors, inductors, capacitors etc. The pulse generation circuit is modeled as shown in Fig. 2.41.

The single phase inverter designed using IGBT, diode and ideal switch is presented in Fig. 2.42. The block parameters used in this SIMULINK implementation are illustrated in Figs. 2.43, 2.44, 2.45, and 2.46. The input voltage was set to 2.7 V based on the design specifications in the DC voltage source block. The internal resistance of the ideal switch was set to 0.001 Ω with the initial state 'open'. The diode's internal resistance was also maintained at 0.001 Ω with a forward voltage of 0.8 V.

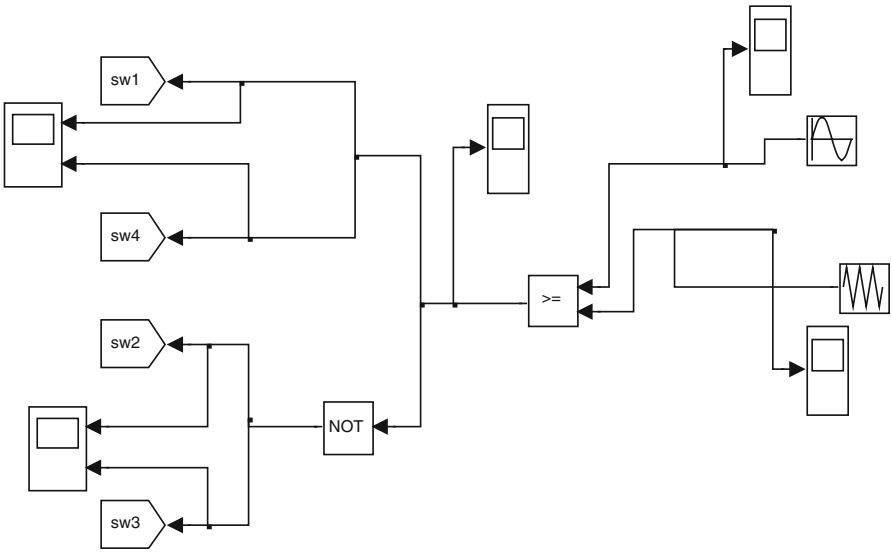


Fig. 2.41 Pulse generation circuit

The output voltage waveform is shown in Fig. 2.47. The boost converter was designed for a 2.7 V input from solar PV panel with L = 0.2 mH and C = 72.6 μF. A single phase full-bridge inverter (PWM) circuit was used to convert the boosted DC voltage to alternating voltage. The above model can be conveniently used for integrating the Solar PV system to grid system. The inverter system modeled with MATLAB/SIMULINK was achieved using the power system and standard SIMULINK block sets. The system was analyzed by sending the required signal to scopes and the workspace, which allowed for analysis and design of the inverter model.

2.10 Maximum Power Point Tracking

Maximum Power Point Tracking, frequently referred to as MPPT, operates Solar PV modules in a manner that allows the modules to produce all the power they are capable of generating. MPPT is not a mechanical tracking system but it works on a particular tracking algorithm and it based on a control system. MPPT can be used in conjunction with a mechanical tracking system, but the two systems are completely different. MPPT algorithms are used to obtain the maximum power from the solar array based on the variation in the irradiation and temperature. The voltage at which PV module can produce maximum power is called 'maximum power point' (or peak power voltage). Maximum power varies with solar radiation, ambient temperature and solar cell temperature.

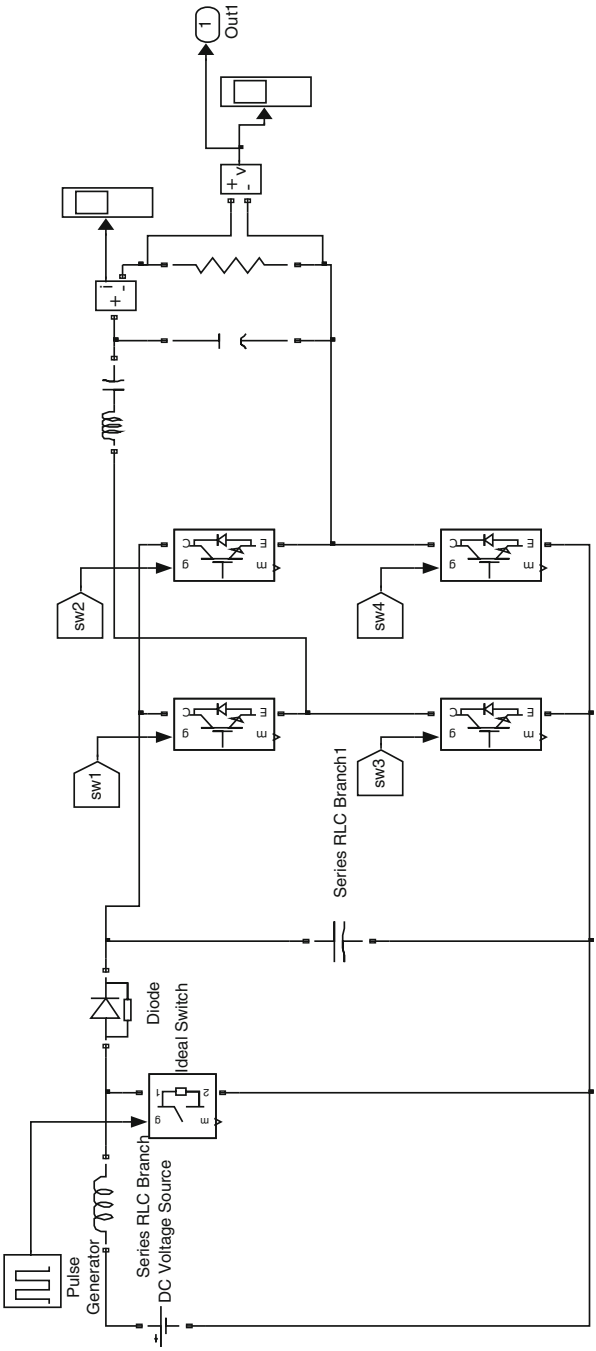


Fig. 2.42 Boost converter and single-phase inverter circuit

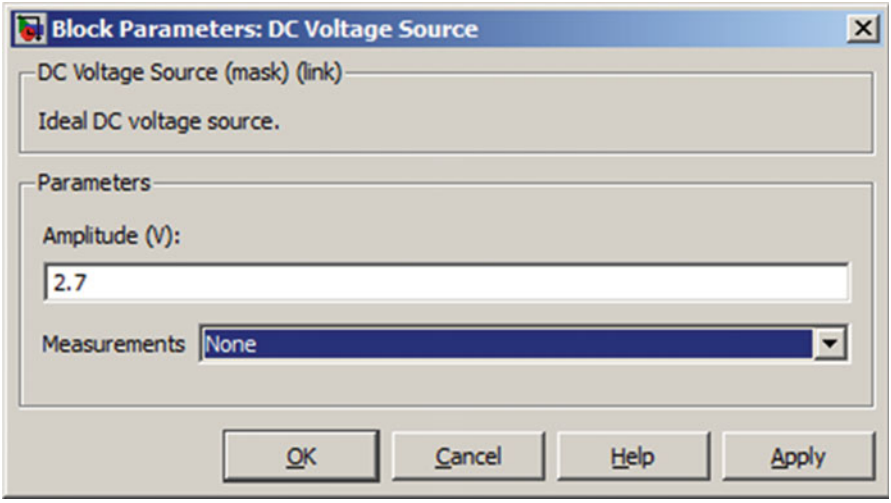


Fig. 2.43 Block parameters of DC voltage source

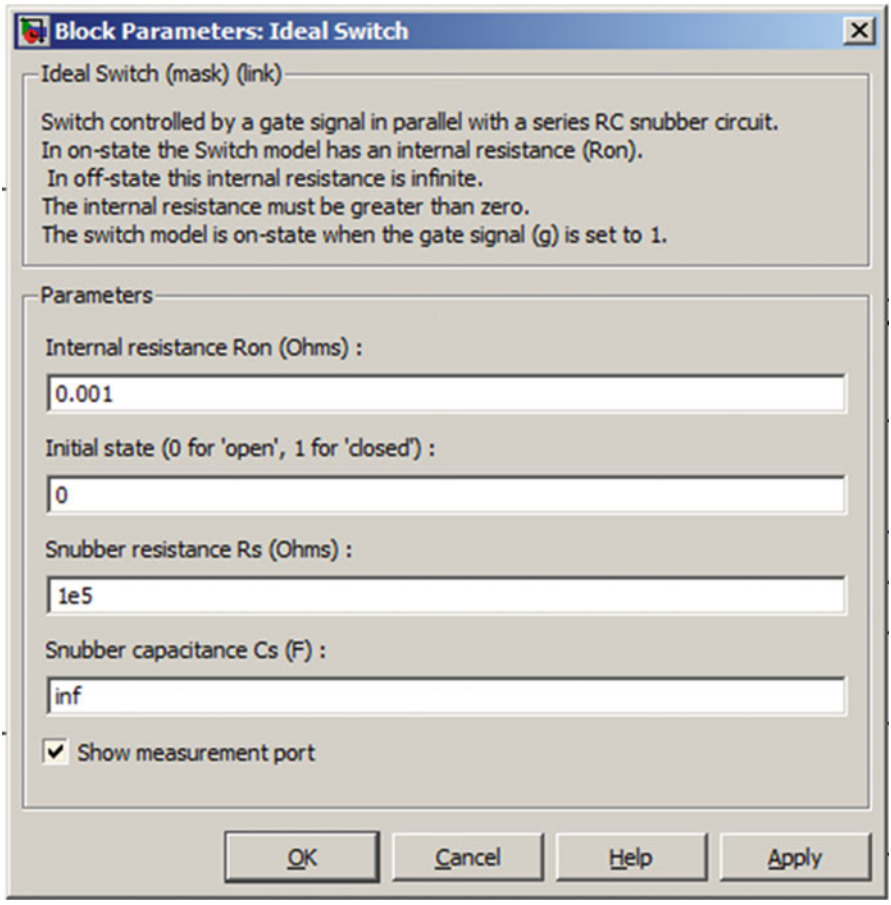


Fig. 2.44 Block parameters of ideal switch

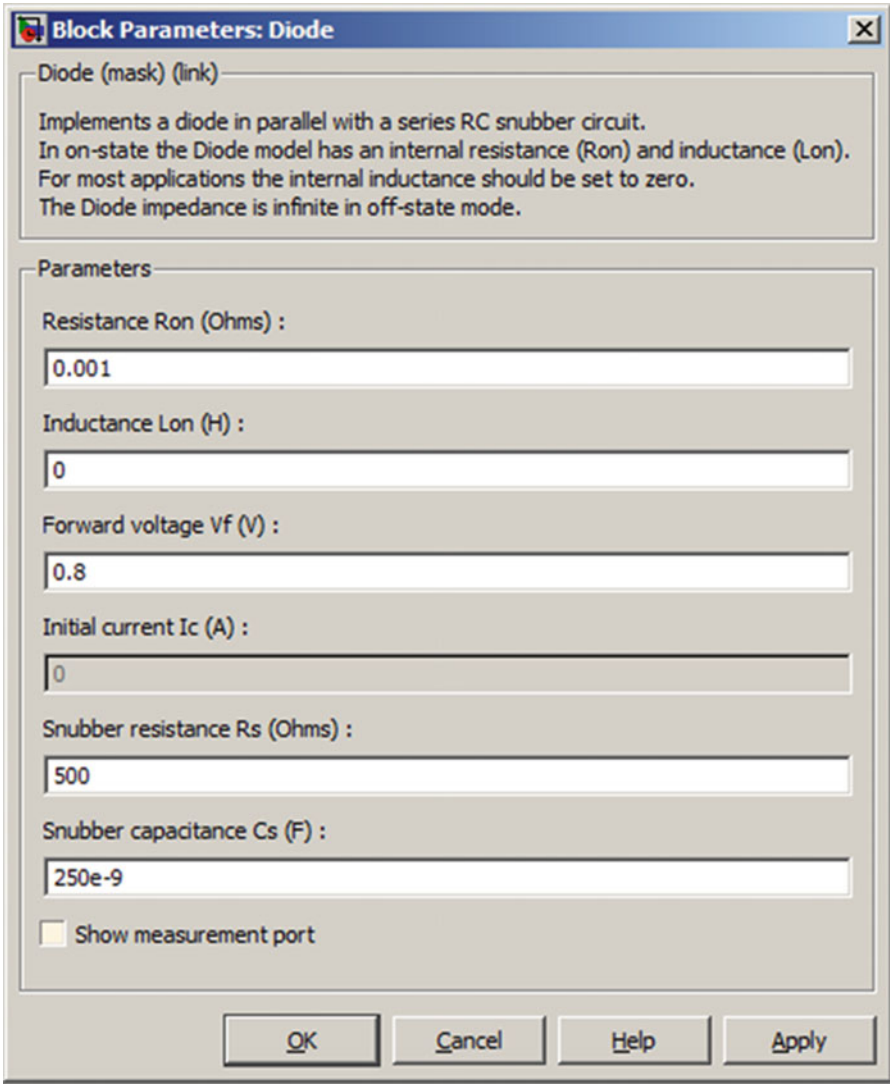


Fig. 2.45 Block parameters of diode

Typical PV module produces power with maximum power voltage of around 17 V when measured at a cell temperature of 25 °C, it can drop to around 15 V on a very hot day and it can also rise to 18 V on a very cold day. The major principle of MPPT is to extract the maximum available power from PV module by making them operate at the most efficient voltage. MPPT Algorithm is based on the simple logic that, MPPT calculates the output of PV module, compares it to battery voltage then

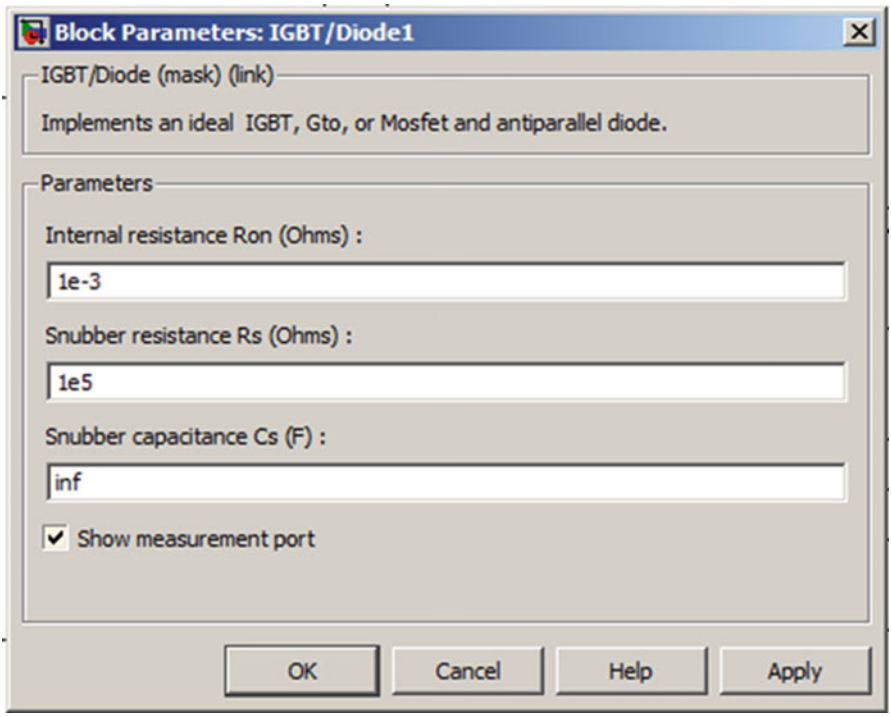


Fig. 2.46 Block parameters of IGBT

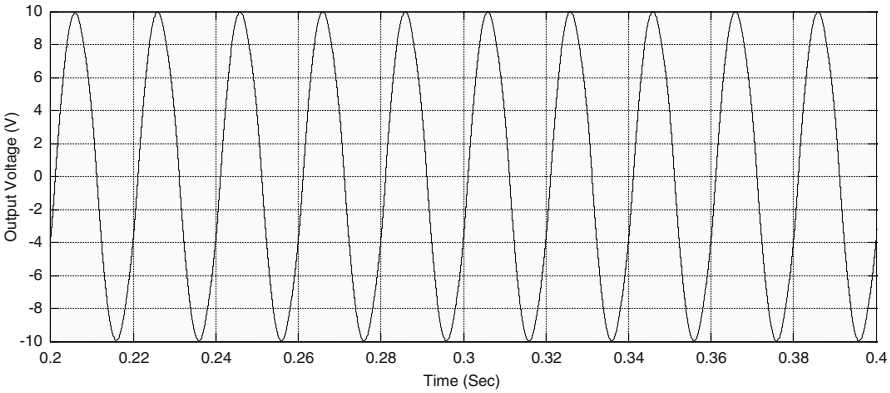


Fig. 2.47 Scope output for inverter model

fixes what is the optimum power that PV module can produce to charge the battery and converts it to the optimum voltage to get maximum current into battery. It can also supply power to a DC load, which is connected directly to the battery. MPPT is mostly useful during cloudy days and when the battery is deeply discharged.

2.10.1 MPPT Techniques

Over the past decades many methods to find the MPP have been developed. These techniques differ in many aspects such as required sensors, complexity, cost, range of effectiveness, convergence speed, correct tracking when irradiation and/or temperature change, hardware needed for the implementation or popularity, among others. Some of the most popular MPPT techniques are:

1. Perturb and Observe (hill climbing method).
2. Incremental Conductance method.
3. Fractional short circuit current.
4. Fractional open circuit voltage.
5. Fuzzy logic.
6. Neural networks.
7. Ripple Correlation Control.
8. Current Sweep.
9. DC-link capacitor droop control.
10. Load current or load voltage maximization.
11. dP/dV or dP/dI Feedback control.

Among several techniques mentioned, the Perturb and Observe (P&O) method and the Incremental Conductance (InCond) algorithms are the most commonly applied algorithms. Other techniques based on different principles include fuzzy logic control, neural network, fractional open circuit voltage or short circuit current, current sweep, etc. Most of these methods yield a local maximum and some, like the fractional open circuit voltage or short circuit current, give an approximated MPP, rather than an exact output. In normal conditions the V-P curve has only one maximum. However, if the PV array is partially shaded, there are multiple maxima in these curves. Both P&O and InCond algorithms are based on the "hill-climbing" principle, which consists of moving the operation point of the PV array in the direction in which the power increases. Hill-climbing techniques are the most popular MPPT methods due to their ease of implementation and good performance when the irradiation is constant. The advantages of both methods are simplicity and requirement of low computational power. The drawbacks are: oscillations occur around the MPP and they get lost and track the MPP in the wrong direction during rapidly changing atmospheric conditions.

2.10.1.1 Perturb and Observe

In the P&O method only one voltage sensor is used to sense the PV array voltage and hence the cost of implementation is less. The algorithm involves a perturbation on the duty cycle of the power converter and a perturbation in the operating voltage of the DC-link between the PV array and the power converter. Perturbing the duty cycle of the power converter implies modifying the voltage of the DC-link

between the PV array and the power converter. In this method, the sign of the last perturbation and the sign of the last increment in the power are used to decide the next perturbation. As can be seen in Fig. 2.48, on the left of the MPP incrementing the voltage increases the power whereas on the right decrementing the voltage decreases the power. If there is an increment in the power, the perturbation should be kept in the same direction and if the power decreases, then the next perturbation should be in the opposite direction. Based on these facts, the algorithm is implemented as show in the flowchart in Fig. 2.49 and the process is repeated until the MPP is reached. The operating point oscillates around the MPP.

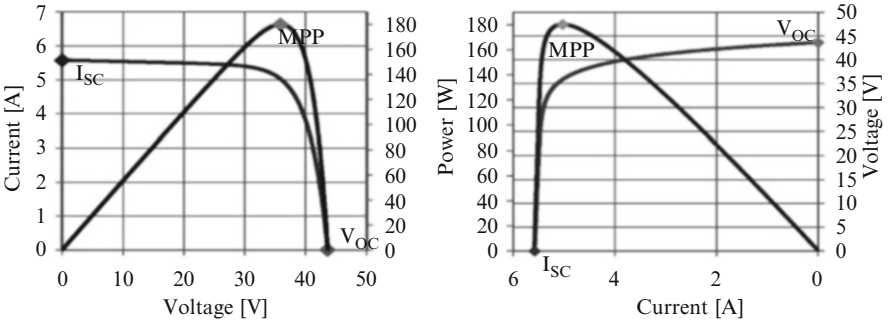


Fig. 2.48 PV panel characteristic curves

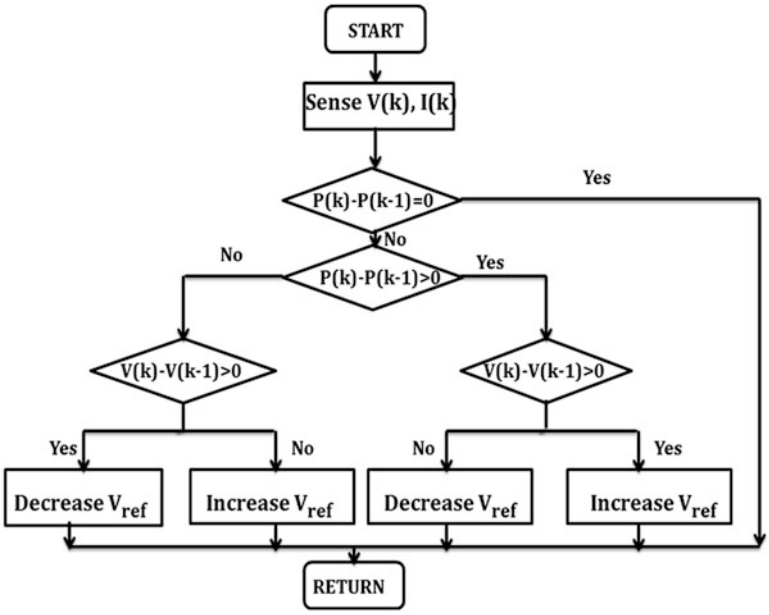


Fig. 2.49 Flowchart of the perturb and observe algorithm

The time complexity of this algorithm is very less but on reaching very close to the MPP it doesn't stop at the MPP and keeps on perturbing on both the directions. To avoid such a condition, an appropriate error limit can be set or a wait function can be used to stop the increase in time complexity of the algorithm. However the method does not take account of the rapid change of irradiation level (due to which MPPT changes) and considers it as a change in MPP due to perturbation and ends up calculating the wrong MPP. To avoid this problem we can use incremental conductance method.

2.10.1.2 Incremental Conductance

The incremental conductance algorithm uses two voltage and current sensors to sense the output voltage and current of the PV array. In incremental conductance method the array terminal voltage is always adjusted according to the MPP voltage it is based on the incremental and instantaneous conductance of the PV module.

Figure 2.50 shows that the slope of the P-V array power curve is zero at The MPP, increasing on the left of the MPP and decreasing on the Right hand side of the MPP. The basic equations of this method are as follows.

$$\begin{aligned} \frac{dI}{dV} &= -\frac{I}{V} && \text{At MPP} \\ \frac{dI}{dV} &> -\frac{I}{V} && \text{Left of MPP} \\ \frac{dI}{dV} &< -\frac{I}{V} && \text{Right of MPP} \end{aligned} \tag{2.11}$$

where I and V are P-V array output current and voltage respectively. The left hand side of equations represents incremental conductance of P-V module and the right hand side represents the instantaneous conductance. When the ratio of change in output conductance is equal to the negative output conductance, the solar array

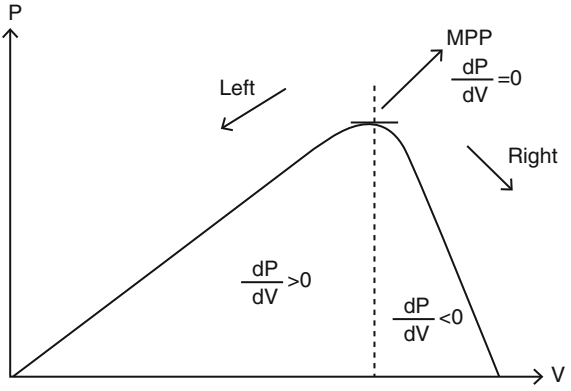


Fig. 2.50 Basic idea of incremental conductance method on a P-V curve of solar module

will operate at the maximum power point. This method exploits the assumption of the ratio of change in output conductance is equal to the negative output Instantaneous conductance. We have,

$$P = VI$$

Applying the chain rule for the derivative of products yields to

$$\partial P/\partial V = [\partial(VI)]/\partial V \tag{2.12}$$

At MPP, as $\partial P/\partial V = 0$

The above equation could be written in terms of array voltage V and array current I as

$$\partial P/\partial V = -I/V \tag{2.13}$$

The MPPT regulates the PWM control signal of the DC – to – DC boost converter until the condition: $(\partial I/\partial V) + (I/V) = 0$ is satisfied. In this method the peak power of the module lies at above 98 % of its incremental conductance. The Flow chart of incremental conductance MPPT is shown in Fig. 2.51.

In both P&O and InCond schemes, the speed of occurrence of MPP depends on the size of the increment of the reference voltage. The drawbacks of these

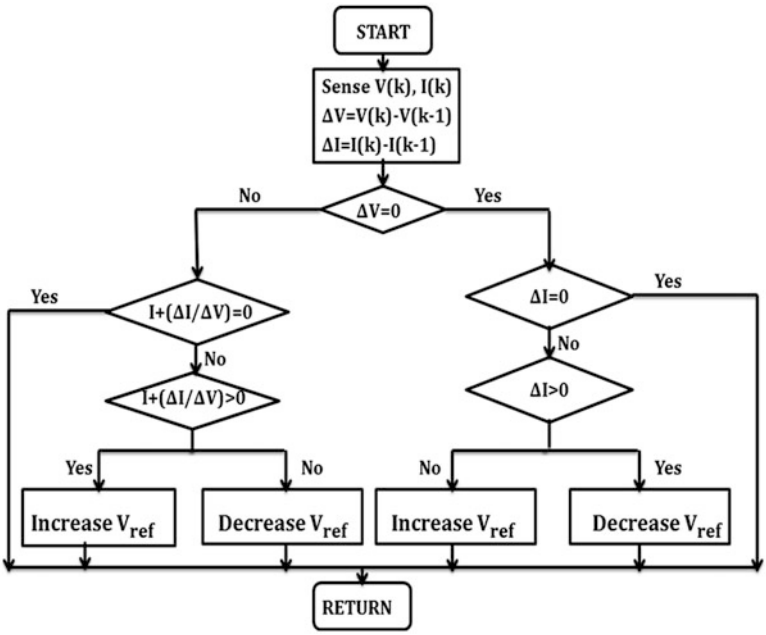


Fig. 2.51 Flow chart for incremental conductance algorithm

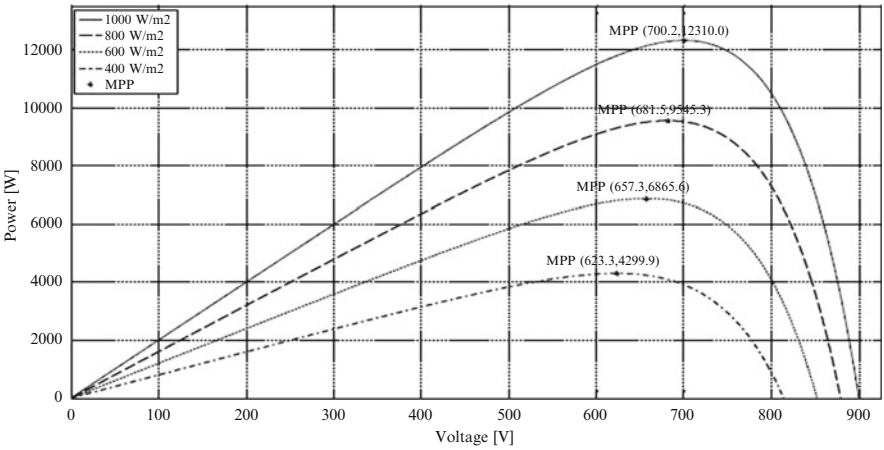


Fig. 2.52 P-V curve depending on the irradiation

techniques are: The first drawback is that they can easily lose track of the MPP if the irradiation changes rapidly. In case of step changes they track the MPP very well, because the change is instantaneous and the curve does not keep on changing. However, when the irradiation changes following a slope, the curve in which the algorithms are based changes continuously with the irradiation, as can be seen in Fig. 2.52, so the changes in the voltage and current are not only due to the perturbation of the voltage. As a consequence it is not possible for the algorithms to determine whether the change in the power is due to its own voltage increment or due to the change in the irradiation.

The other drawback of both methods is the oscillations of the voltage and current around the MPP in the steady state. This is due to the fact that the control is discrete and the voltage and current are not constantly at the MPP but oscillating around it. The size of the oscillations depends on the size of the rate of change of the reference voltage. The greater the oscillation, higher is the amplitude of the oscillations. However, speed of the MPP occurrence also depends on this rate of change and this dependence is inversely proportional to the size of the voltage increments. The traditional solution is a trade off: if the increment is small the oscillations decrease, then the MPP is reached slowly and vice versa, so a compromise solution has to be found.

2.10.1.3 Fractional Open-Circuit Voltage

The near linear relationship between V_{MPP} and V_{OC} of the PV array, under varying irradiance and temperature levels, has given rise to the fractional V_{OC} method.

$$V_{MPP} \approx k_1 V_{OC} \tag{2.14}$$

where k_1 is a constant of proportionality. Since k_1 is dependent on the characteristics of the PV array being used, it usually has to be computed beforehand by empirically determining V_{MPP} and V_{OC} for the specific PV array at different irradiance and temperature levels. The factor k_1 has been reported to be between 0.71 and 0.78. Once k_1 is known, V_{MPP} can be computed using (2.14) with V_{OC} measured periodically by momentarily shutting down the power converter. However, this incurs some disadvantages, including temporary loss of power. To prevent this, pilot cells are used from which V_{OC} can be obtained. These pilot cells must be carefully chosen to closely represent the characteristics of the PV array. Once V_{MPP} has been approximated, a closed loop control on the array power converter can be used to asymptotically reach this desired voltage. Since (2.14) is only an approximation, the PV array technically never operates at the MPP. Depending on the application of the PV system, this can sometimes be adequate. Even if fractional V_{OC} is not a true MPPT technique, it is very easy and cheap to implement as it does not necessarily require DSP or microcontroller control. However, k_1 is no more valid in the presence of partial shading (which causes multiple local maxima) of the PV array and proposes sweeping the PV array voltage to update k_1. This obviously adds to the implementation complexity and incurs more power loss.

2.10.1.4 Fractional Short-Circuit Current

Fractional I_{SC} results from the fact that, under varying atmospheric conditions, I_{MPP} is approximately linearly related to the I_{SC} of the PV array.

$$I_{MPP} \approx k_2 I_{SC} \tag{2.15}$$

where k_2 is a proportionality constant. Just like in the fractional VOC technique, k_2 has to be determined according to the PV array in use. The constant k_2 is generally found to be between 0.78 and 0.92. Measuring I_{SC} during operation is problematic. An additional switch usually has to be added to the power converter to periodically short the PV array so that I_{SC} can be measured using a current sensor. This increases the number of components and cost. Power output is not only reduced when finding I_{SC} but also because the MPP is never perfectly matched as suggested by (2.15). The variable k_2 can be compensated such that the MPP is better tracked while atmospheric conditions change. To guarantee proper MPPT in the presence of multiple local maxima, the PV array voltage from open-circuit to short-circuit periodically sweeps to update k_2. Most of the PV systems using fractional I_{SC} in the literature use a DSP, while a few systems use a simple current feedback control loop instead.

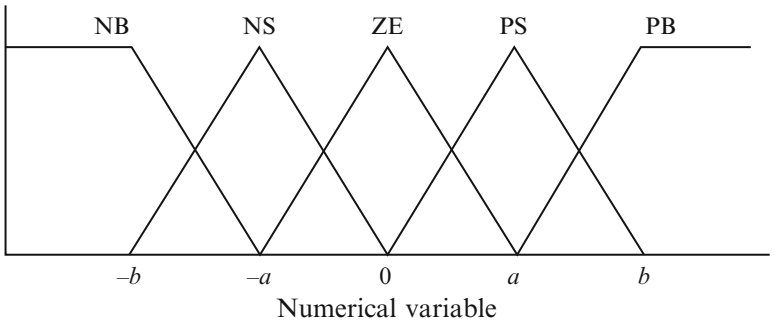


Fig. 2.53 Membership function for inputs and output of fuzzy logic controller

2.10.1.5 Fuzzy Logic Control

Microcontrollers have made using fuzzy logic control popular for MPPT over last decade. Fuzzy logic controllers have the advantages of working with imprecise inputs, not needing an accurate mathematical model, and handling nonlinearity. Fuzzy logic control generally consists of three stages: fuzzification, rule base table lookup, and defuzzification. During fuzzification, numerical input variables are converted into linguistic variables based on a membership function similar to Fig. 2.53. In this case, five fuzzy levels are used: NB (Negative Big), NS (Negative Small), ZE (Zero), PS (Positive Small), and PB (Positive Big).

In some cases seven fuzzy levels are also used probably for more accuracy. In Fig. 2.53, a and b are based on the range of values of the numerical variable. The membership function is sometimes made less symmetric to give more importance to specific fuzzy levels. The inputs to a MPPT fuzzy logic controller are usually an error E and a change in error ΔE. The user has the flexibility of choosing how to compute E and ΔE. Since dP/dV vanishes at the MPP, approximation can be applied as follows,

$$E(n) = \frac{P(n) - P(n-1)}{V(n) - V(n-1)} \tag{2.16}$$

and

$$\Delta E(n) = E(n) - E(n-1) \tag{2.17}$$

Equivalently, $e = I/V + dI/dV$ is often used. Once E and ΔE are calculated and converted to the linguistic variables, the fuzzy logic controller output, which is typically a change in duty ratio ΔD of the power converter, can be looked up in a rule base table such as Table 2.5. The linguistic variables assigned to ΔD for the different combinations of E and ΔE are based on the power converter being used and also on the knowledge of the user. The rule base shown in Table 2.5 is based on a boost converter. If for example, the operating point is far to the left of the MPP,

Table 2.5 Fuzzy rule base

	ΔE				
E	NB	NS	ZE	PS	PB
NB	ZE	ZE	NB	NB	NB
NS	ZE	ZE	NS	NS	NS
ZE	NS	ZE	ZE	ZE	PS
PS	PS	PS	PS	ZE	ZE
PB	PB	PB	PB	ZE	ZE

that is E is PB, and ΔE is ZE, then we want to increase the duty ratio largely, that is ΔD should be PB to reach the MPP. In the defuzzification stage, the fuzzy logic controller output is converted from a linguistic variable to a numerical variable still using a membership function as shown in Fig. 2.53. This provides an analog signal that will control the power converter to the MPP. MPPT fuzzy logic controllers have been shown to perform well under varying atmospheric conditions. However, their effectiveness depends a lot on the knowledge of the user or control engineer in choosing the right error computation and coming up with the rule base table.

2.10.1.6 Neural Network

Along with fuzzy logic controllers another technique of implementing MPPT are the neural networks, which are also well adapted for microcontrollers. Neural networks commonly have three layers: input, hidden, and output layers as shown in Fig. 2.54. The number nodes in each layer vary and are user-dependent. The input variables can be PV array parameters like V_{OC} and I_{SC}, atmospheric data like irradiance and temperature, or any combination of these. The output is usually one or several reference signal(s) like a duty cycle signal used to drive the power converter to operate at or close to the MPP. How close the operating point gets to the MPP depends on the algorithms used by the hidden layer and how well the neural network has been trained. The links between the nodes are all weighted. The link between nodes i and j is labeled as having a weight of wij in Fig. 2.54. To accurately identify the MPP, the wij's have to be carefully determined through a training process, whereby the PV array is tested over months or years and the patterns between the input(s) and output(s) of the neural network are recorded. Since most PV arrays have different characteristics, a neural network has to be specifically trained for the PV array with which it will be used. The characteristics of a PV array also change with time, implying that the neural network has to be periodically trained to guarantee accurate MPPT.

2.10.1.7 Ripple Correlation Control

When a PV array is connected to a power converter, the switching action of the power converter imposes voltage and current ripple on the PV array. As a consequence, the PV array power is also subject to ripple. Ripple correlation control (RCC) makes use of ripple to perform MPPT. RCC correlates the time derivative of

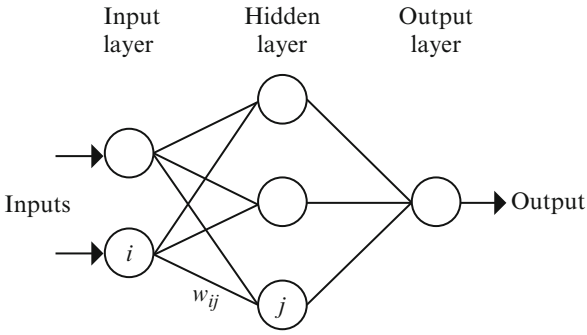


Fig. 2.54 Example of neural network

the time-varying PV array power p with the time derivative of the time-varying PV array current i or voltage v to drive the power gradient to zero, thus reaching the MPP. Based on the PV array characteristics, if v or i is increasing ($v > 0$ or $i > 0$) and p is increasing ($p > 0$), then the operating point is below the MPP ($V < V_{MPP}$ *or* $I < I_{MPP}$). On the other hand, if v or i is increasing and p is decreasing ($p < 0$), then the operating point is above the MPP ($V > V_{MPP}$ *or* $I > I_{MPP}$). Combining these observations, we see that $\dot{p}\dot{v}$ or $\dot{p}\dot{i}$ are positive to the left of the MPP, negative to right of the MPP, and zero at the MPP. When the power converter is a boost converter, increasing the duty ratio increases the inductor current, which is the same as the PV array current, but decreases the PV array voltage. Therefore, the duty ratio control input is

$$d(t) = -k_3 \int \dot{p}\dot{v}\, dt \tag{2.18}$$

or

$$d(t) = k_3 \int \dot{p}\dot{i}\, dt \tag{2.19}$$

where k_3 is a positive constant. Controlling the duty ratio in this fashion assures that the MPP will be continuously tracked, making RCC a true MPP tracker. The derivatives in (2.18) and (2.19) are usually undesirable, the AC-coupled measurements of the PV array current and voltage can be used instead since they contain the necessary phase information. The derivatives can also be approximated by high-pass filters with cutoff frequency higher than the ripple frequency. A different and easy way of obtaining the current derivative in (2.19) is to sense the inductor voltage, which is proportional to the current derivative. The non-idealities in the inductor (core loss, resistance) have a small effect since the time constant of the inductor is much larger than the switching period in a practical converter. Equation (2.19) can fail due to the phase shift brought about by the intrinsic capacitance of the PV array at high switching frequencies. However, correlating power and voltage as in (2.18) is barely affected by the intrinsic capacitance.

2.10.1.8 Current Sweep

The current sweep method uses a sweep waveform for the PV array current such that the *I-V* characteristic of the PV array is obtained and updated at fixed time intervals. The V_{MPP} can then be computed from the characteristic curve at the same intervals. The function chosen for the sweep waveform is directly proportional to its derivative as in (2.20),

$$f(t) = k_4 \frac{df(t)}{dt} \tag{2.20}$$

where k_4 is the proportionality constant. The PV array power is thus given by

$$p(t) = v(t)i(t) = v(t)f(t) \tag{2.21}$$

At the MPP,

$$\frac{dp(t)}{dt} = v(t)\frac{df(t)}{dt} + f(t)\frac{dv(t)}{dt} = 0 \tag{2.22}$$

Substituting (2.20) in (2.22) gives

$$\frac{dp(t)}{dt} = \left[v(t) + k_4 \frac{dv(t)}{dt}\right]\frac{df(t)}{dt} = 0 \tag{2.23}$$

The differential equation in (2.20) has the following solution

$$f(t) = Ce^{t/k_4} \tag{2.24}$$

C is chosen to be equal to the maximum PV array current Imax and k_4 to be negative, resulting in a decreasing exponential function with time constant $\tau = -k_4$. Equation (2.24) leads to

$$f(t) = I_{\max} e^{-t/\tau} \tag{2.25}$$

The current in (2.25) can be easily obtained by using some current discharging through a capacitor. Since the derivative of (2.25) is nonzero, (2.23) can be divided throughout by $df(t)/dt$ and, with $f(t) = i(t)$, (2.23) simplifies to

$$\frac{dp(t)}{di(t)} = v(t) + k_4 \frac{dv(t)}{dt} = 0 \tag{2.26}$$

Once V_{MPP} is computed after the current sweep, (2.26) can be used to double check whether the MPP has been reached. In literature it is been observed that the current sweep takes about 50 ms, implying some loss of available power.

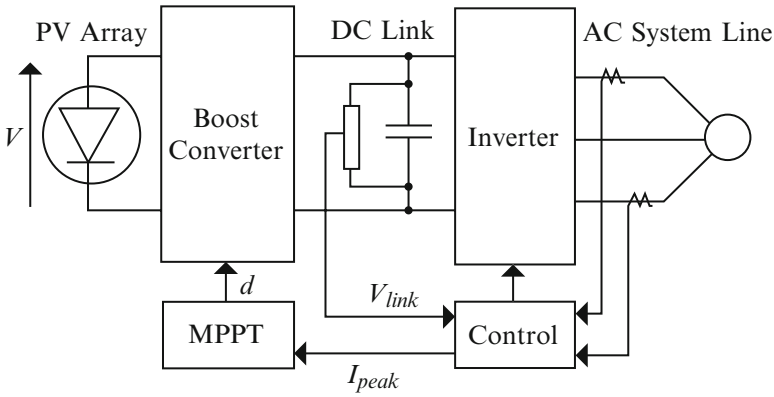


Fig. 2.55 Topology for DC-link capacitor droop control

2.10.1.9 DC Link Capacitor Droop Control

DC-link capacitor droop control is a MPPT technique that is specifically designed to work with a PV system that is connected in parallel with an AC system line as shown in Fig. 2.55. The duty ratio of an ideal boost converter is given by

$$d = 1 - V/V_{link} \tag{2.27}$$

where V is the voltage across the PV array and V_{link} is the voltage across the DC-link. If V_{link} is kept constant, increasing the current going in the inverter increases the power coming out of the boost converter and consequently increases the power coming out of the PV array. While the current is increasing, the voltage V_{link} can be kept constant as long as the power required by the inverter does not exceed the maximum power available from the PV array. If that is not the case, V_{link} starts drooping. Right before that point, the current control command I_{peak} of the inverter is at its maximum and the PV array operates at the MPP. The AC system line current is feedback to prevent V_{link} from drooping and d is optimized to bring I_{peak} to its maximum, thus achieving MPPT. DC-link capacitor droop control does not require the computation of the PV array power, but its response deteriorates when compared to a method that detects the power directly; this is because its response directly depends on the response of the DC voltage control loop of the inverter. This control scheme can be easily implemented with analog operational amplifiers and decision making logic units.

2.10.1.10 Load Current or Load Voltage Maximization

The purpose of MPPT techniques is to maximize the power coming out of a PV array. When the PV array is connected to a power converter, maximizing

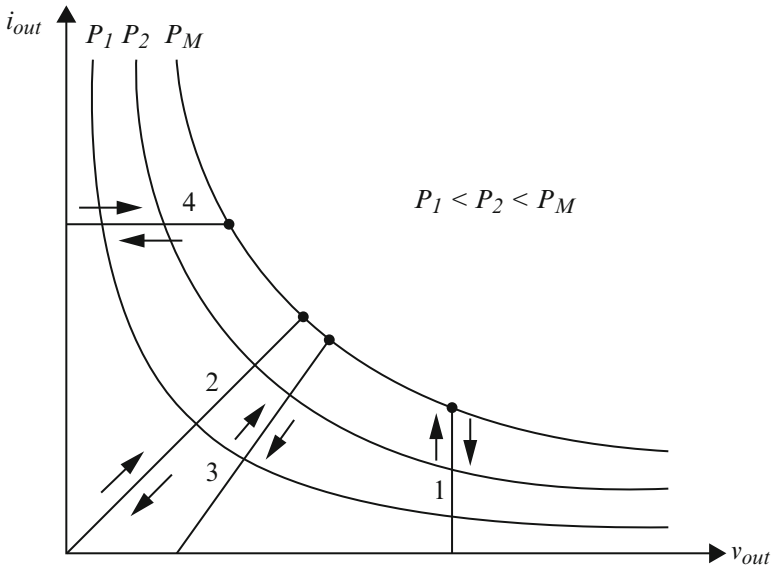


Fig. 2.56 Different load types: *1*-voltage-source, *2*-resistive, *3*-resistive and voltage-source, *4*-current-source

the PV array power also maximizes the output power at the load of the converter. Conversely, maximizing the output power of the converter should maximize the PV array power, assuming a lossless converter. Most loads can be of voltage source type, current-source type, resistive type, or a combination of these, as shown in Fig. 2.56. From this figure, it is clear that for a voltage-source type load, the load current i_{out} should be maximized to reach the maximum output power *PM*. For a current-source type load, the load voltage v_{out} should be maximized. For the other load types, either i_{out} or v_{out} can be used. This is also true for nonlinear load types as long as they do not exhibit negative impedance characteristics. Therefore, for almost all loads of interest, it is adequate to maximize either the load current or the load voltage to maximize the load power. Consequently, only one sensor is needed. In most PV systems, a battery is used as the main load or as a backup. Since a battery can be thought of as a voltage-source type load, the load current can be used as the control variable. A positive feedback can also be used to control the power converter such that the load current is maximized and the PV array operates close to the MPP. Operation exactly at the MPP is almost never achieved because this MPPT method is based on the assumption that the power converter is lossless.

2.10.1.11 dP/dV or dP/dI Feedback Control

With DSP and microcontroller being able to handle complex computations, an obvious way of performing MPPT is to compute the slope (*dP*/*dV* or *dP*/*dI*) of the

PV power curve and feed it back to the power converter with some control to drive it to zero. There are several methods to compute the slope. dP/dV can be computed and its sign can be stored for the past few cycles. Based on these signs, the duty ratio of the power converter is either incremented or decremented to reach the voltage-source, 4-current-source. A dynamic step size is used to improve the transient response of the system. Linearization based method can also be used to compute dP/dV. Sometimes sampling and data conversion with subsequent digital division of power and voltage are also applied to approximate dP/dV. dP/dI can then be integrated together with an adaptive gain to improve the transient response. The PV array voltage is periodically incremented or decremented and $\Delta P/\Delta V$ is compared to a marginal error until the MPP is reached. Convergence to the MPP was shown to occur in tens of milliseconds.

With so many MPPT techniques available to PV system users, it might not be obvious for the latter to choose which one better suits their application needs. The main aspects of the MPPT techniques to be taken into consideration are highlighted in the following subsections.

Implementation

The ease of implementation is an important factor in deciding which MPPT technique to use. However, this greatly depends on the end-users' knowledge. Some might be more familiar with analog circuitry, in which case, fractional I_{SC} or V_{OC}, RCC, and load current or voltage maximization are good options. Others might be willing to work with digital circuitry, even if that may require the use of software and programming. Then, their selection should include hill-climbing/P&O, IncCond, fuzzy logic control, neural network, and dP/dV or dP/dI feedback control. Furthermore, a few of the MPPT techniques only apply to specific topologies. For example, the DC-link capacitor droop control works with the system shown in Fig. 2.55 and the OCC MPPT works with a single-stage inverter.

Sensors

The number of sensors required to implement MPPT also affects the decision process. Most of the time, it is easier and more reliable to measure voltage than current. Moreover, current sensors are usually expensive and bulky. This might be inconvenient in systems that consist of several PV arrays with separate MPP trackers. In such cases, it might be wise to use MPPT methods that require only one sensor or that can estimate the current from the voltage. It is also uncommon to find sensors that measure irradiance levels, as needed in the linear current control and the I_{MPP} and V_{MPP} computation methods.

Multiple Local Maxima

The occurrence of multiple local maxima due to partial shading of the PV array (s) can be a real hindrance to the proper functioning of a MPP tracker. Considerable power loss can be incurred if a local maximum is tracked instead of the real MPP. As mentioned previously, the current sweep and the state-based methods should track the true MPP even in the presence of multiple local maxima. However, the other methods require an additional initial stage to bypass the unwanted local maxima and bring operation to close the real MPP.

Costs

It is hard to mention the monetary costs of every single MPPT technique unless it is built and implemented. However, a good costs comparison can be made by knowing whether the technique is analog or digital, whether it requires software and programming, and the number of sensors. Analog implementation is generally cheaper than digital, which normally involves a microcontroller that needs to be programmed. Eliminating current sensors considerably drops the costs.

Applications

Different MPPT techniques discussed above will suit different applications. For example, in space satellites and orbital stations that involve large amount of money, the costs and complexity of the MPP tracker are not as important as its performance and reliability. The tracker should be able to continuously track the true MPP in minimum amount of time and should not require periodic tuning. In this case, hill climbing/P&O, IncCond, and RCC are appropriate. Solar vehicles would mostly require fast convergence to the MPP. Fuzzy logic control, neural network, and RCC are good options in this case. Since the load in solar vehicles consists mainly of batteries, load current or voltage maximization should also be considered. The goal when using PV arrays in residential areas is to minimize the payback time and to do so, it is essential to constantly and quickly track the MPP. Since partial shading (from trees and other buildings) can be an issue, the MPPT should be capable of bypassing multiple local maxima. Therefore, the two-stage IncCond and the current sweep methods are suitable. Since a residential system might also include an inverter, the OCC MPPT can also be used. PV systems used for street lighting only consist in charging up batteries during the day. They do not necessarily need tight constraints; easy and cheap implementation might be more important, making fractional V_{OC} or I_{SC} viable. Table 2.6 summarizes the major characteristics of all the MPPT techniques.

Table 2.6 Characteristics of MPPT techniques

MPPT technique	PV array dependent?	True MPPT?	Analog or digital?	Periodic tuning?	Convergence speed	Implementation complexity	Sensed parameters
Hill-climbing/P&O	No	Yes	Both	No	Varies	Low	Voltage, current
IncCond	No	Yes	Digital	No	Varies	Medium	Voltage, current
Fractional V_{OC}	Yes	No	Both	Yes	Medium	Low	Voltage
Fractional I_{SC}	Yes	No	Both	Yes	Medium	Medium	Current
Fuzzy logic control	Yes	Yes	Digital	Yes	Fast	High	Varies
Neural network	Yes	Yes	Digital	Yes	Fast	High	Varies
RCC	No	Yes	Analog	No	Fast	Low	Voltage, current
Current sweep	Yes	Yes	Digital	Yes	Slow	High	Voltage, current
DC-link capacitor droop control	No	No	Both	No	Medium	Low	Voltage
Load I or V maximization	No	No	Analog	No	Fast	Low	Voltage, current
dP/dV or dP/dI feedback control	No	Yes	Digital	No	Fast	Medium	Voltage, current
Array reconfiguration	Yes	No	Digital	Yes	Slow	High	Voltage, current
Linear current control	Yes	No	Digital	Yes	Fast	Medium	Irradiance
I_{MPP} & V_{MPP} computation	Yes	Yes	Digital	Yes	N/A	Medium	Irradiance, temperature
State-based MPPT	Yes	Yes	Both	Yes	Fast	High	Voltage, current
OCC MPPT	Yes	No	Both	Yes	Fast	Medium	Current
BFV	Yes	No	Both	Yes	N/A	Low	None
LRCM	Yes	No	Digital	No	N/A	High	Voltage, current
Slide control	No	Yes	Digital	No	Fast	Medium	Voltage, current

2.10.2 MATLAB/SIMULINK Implementation of Perturb and Observe Method

The detailed block diagram of the P&O algorithm mentioned above is constructed using MATLAB/SIMULINK and the model is shown in Fig. 2.57. Here the voltage and current inputs are sensed to compute power as shown. A saturation limit is set to monitor the increase or decrease in voltage in order to avoid oscillations in the MPP.

2.10.3 MATLAB/SIMULINK Model of the Incremental Conductance Method

The MATLAB/SIMULINK model of the incremental conductance method is shown in Fig. 2.58.

The duty cycle in both P&O and the InCond algorithms can be adjusted as shown in Fig. 2.59.

2.10.4 PV Module with MPPT Techniques

The SIMULINK model for the MPPT algorithm using incremental conductance (If P&O algorithm is required the block can be replaced accordingly) is shown in Fig. 2.60. The PV module is added from Fig. 2.9.

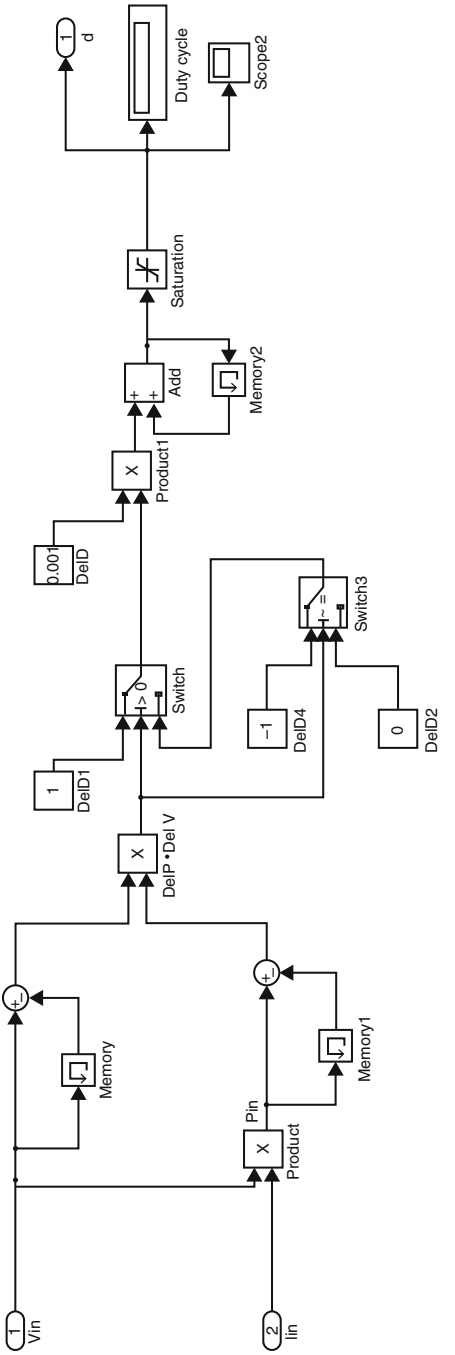


Fig. 2.57 SIMULINK model of the perturb and observe method

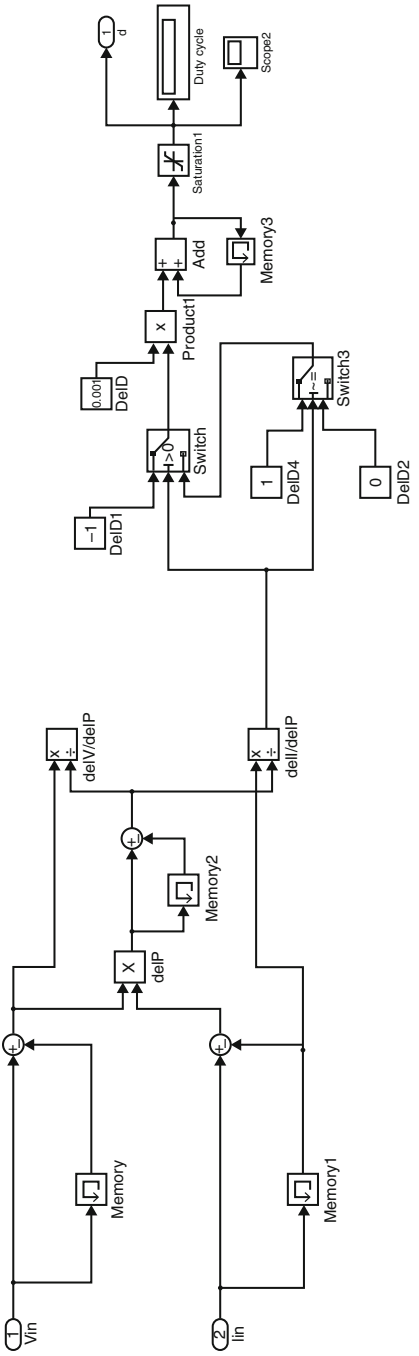


Fig. 2.58 SIMULINK model of incremental conductance method

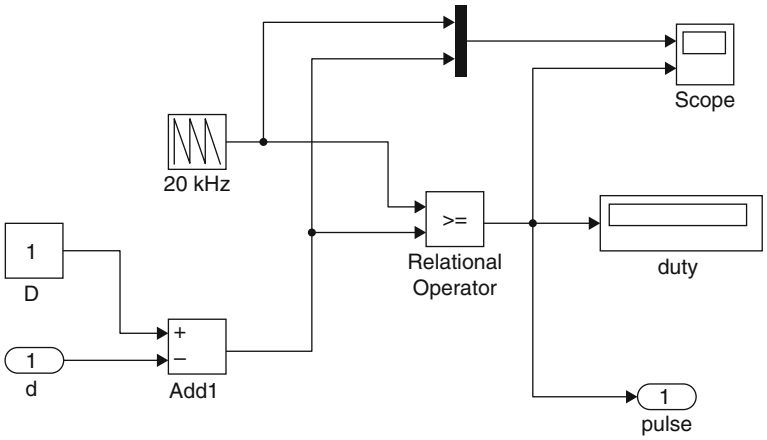


Fig. 2.59 SIMULINK model for adjusting the duty cycle

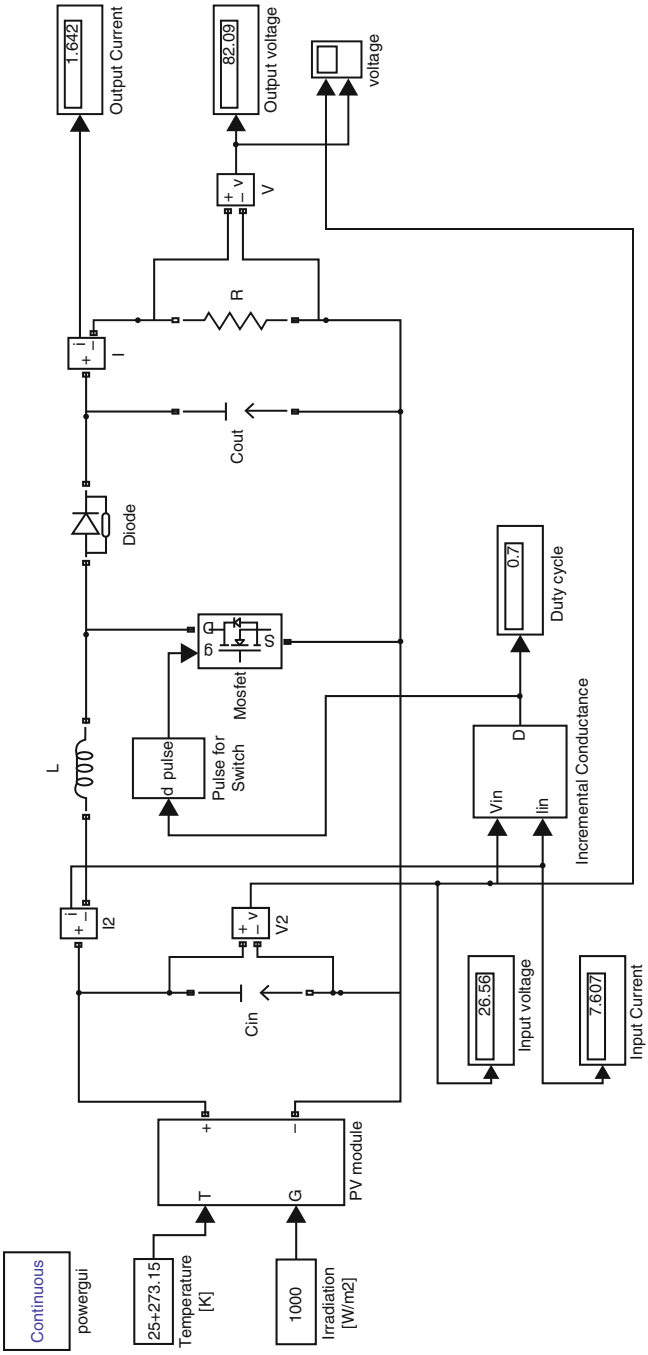
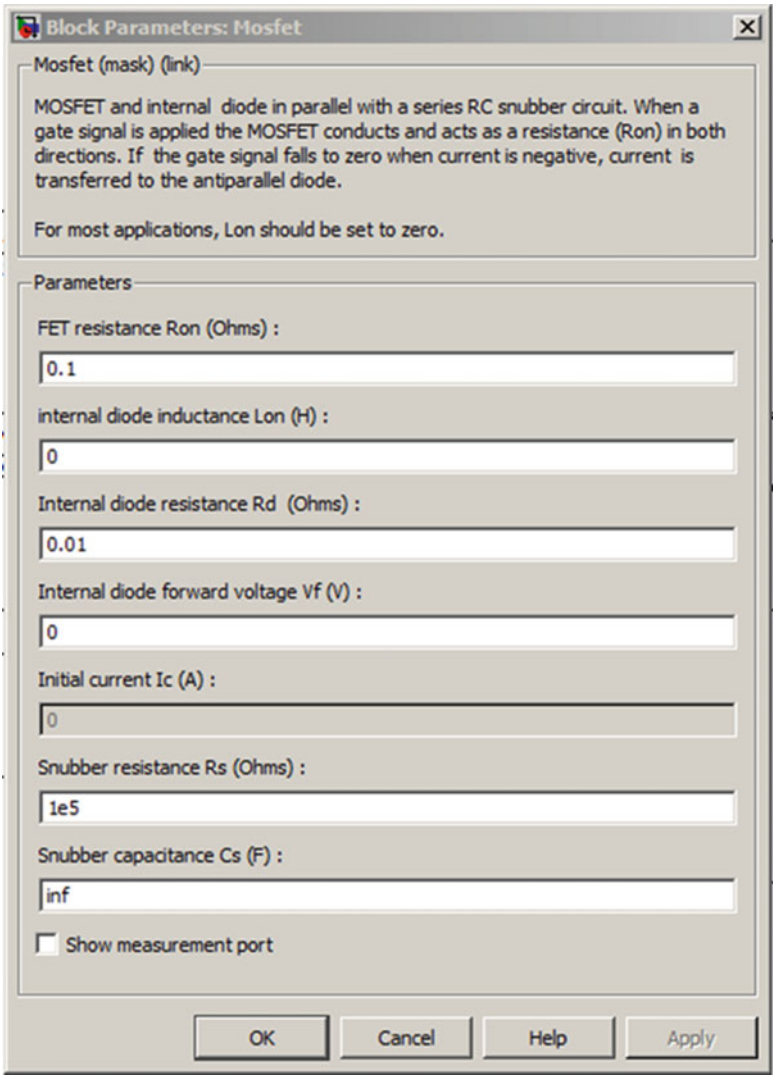


Fig. 2.60 Overall SIMULINK model

2.10.4.1 Blockset Used

MOSFET Block

The properties of the MOSFET block are shown below. The FET resistance is set to 0.1 Ω and the internal diode resistance is 0.01 Ω.



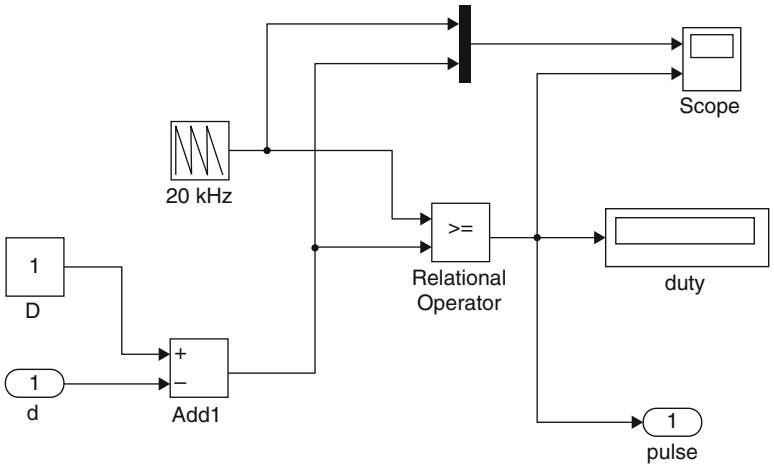


Fig. 2.61 Pulse to switch module

Pulse for Switch

The pulse for switch module is constructed using relational operator as shown in Fig. 2.61.

The parameters used in the model has the following specifications

Parameters	Value
C_{in}	1,000 μF
L	0.011 H
C_{out}	60 μF
R	50 Ω
Switching frequency, F_s	20 kHz

2.10.4.2 Simulation Results

Figures 2.62 and 2.63 show the voltage versus time curve without the MPPT technique at temperature 25 °C with irradiation levels 1,000 W/m^2 and 600 W/m^2. It is inferred that the output voltage obtained without MPPT technique had perturbations before obtaining the required output and the output voltage was not of the desired value. The P&O method was applied and the output was observed as shown in Figs. 2.64 and 2.65 for irradiation levels 1,000 W/m^2 and 600 W/m^2. It is inferred that using the perturb and observe technique, when the irradiation is constant, it oscillates around the MPP value. The amplitude of the oscillations depends directly on the size of increment in the reference voltage, $\Delta Vref$. Also, when the irradiation is constant, the corresponding MPP voltage is reached after a delay, which depends on the size of $\Delta Vref$. The P&O block was replaced using the

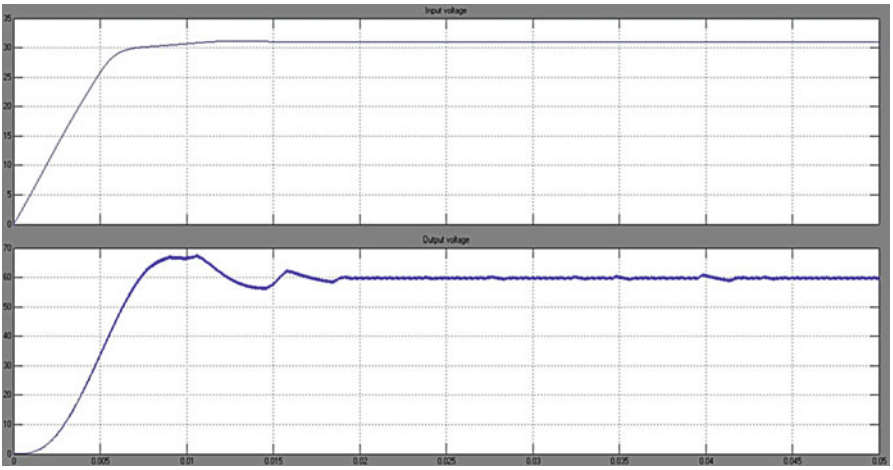


Fig. 2.62 Voltage versus time curve without MPPT technique at temperature 25 °C and irradiance 1,000 W/m^2

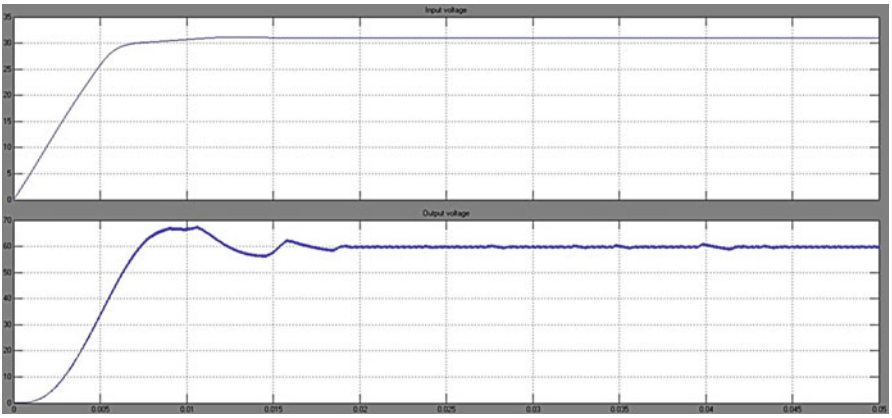


Fig. 2.63 Voltage versus time curve without MPPT technique at temperature 25 °C and irradiance 600 W/m^2

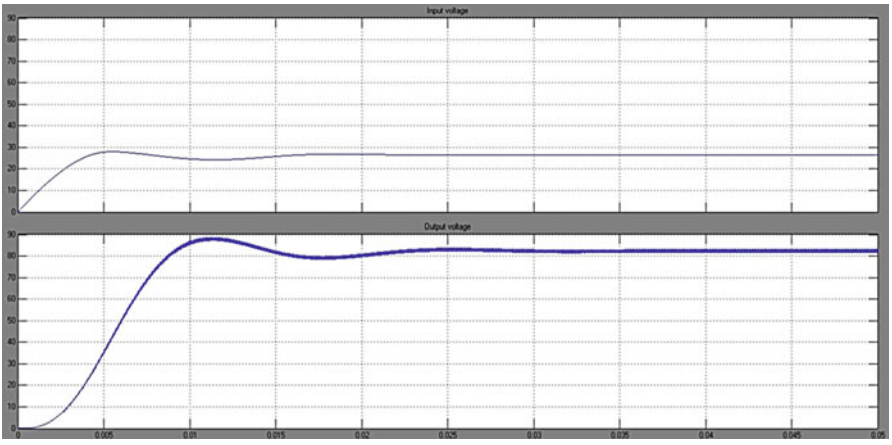


Fig. 2.64 Voltage versus time curve with P&O MPPT technique with temperature 25 °C and irradiance 1,000 W/m^2

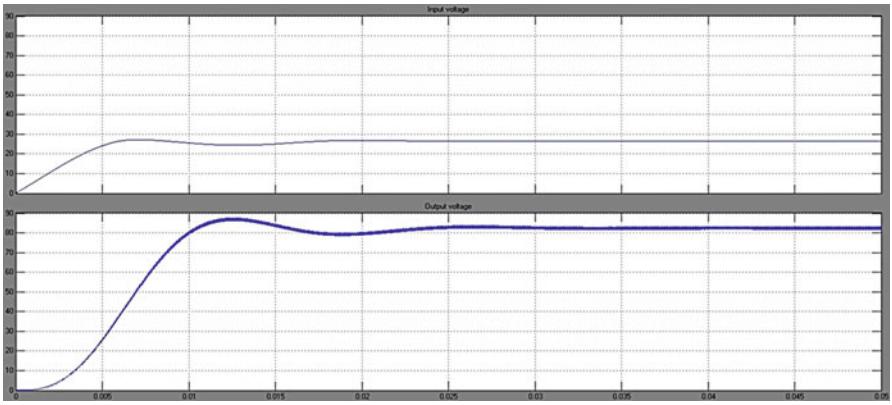


Fig. 2.65 Voltage versus time curve with P&O MPPT technique with temperature 25 °C and irradiance 600 W/m^2

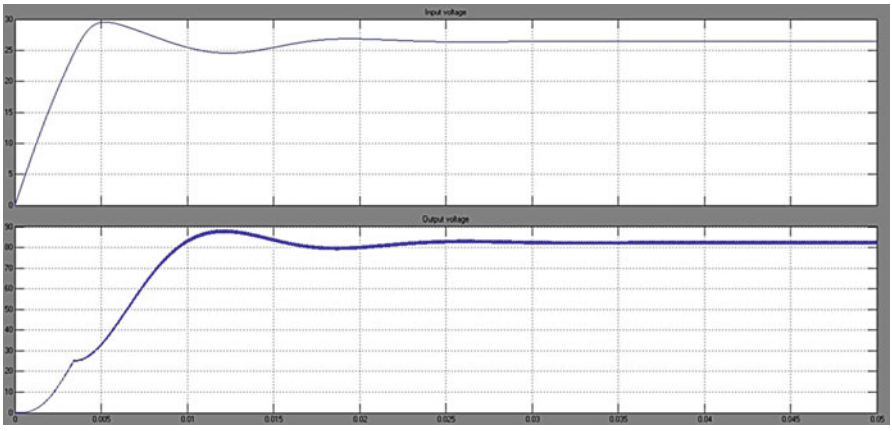


Fig. 2.66 Voltage versus time curve with In Cond MPPT technique with temperature 25 °C and irradiance 1,000 W/m^2

InCond technique and the output was observed as shown in Figs. 2.66 and 2.67. The results are almost practically the same. Simulations were carried out by varying the irradiation levels from 1,000 W/m^2 to 600 W/m^2. Figure 2.68 shows the Voltage versus Time curve with P&O MPPT technique and Fig. 2.69 shows the Voltage versus Time curve with In Cond MPPT technique. In this case the tracking is adequate, which demonstrates that irradiation step changes do not pose a challenge to the hill-climbing algorithms and are not suitable for testing MPPT. As expected, the convergence speed, i.e. how fast the steady state is reached, and the amplitude of the oscillations are a trade off, as both cannot be improved at the same time: if one is reduced the other increases, because both depend directly on the size of the voltage increment.

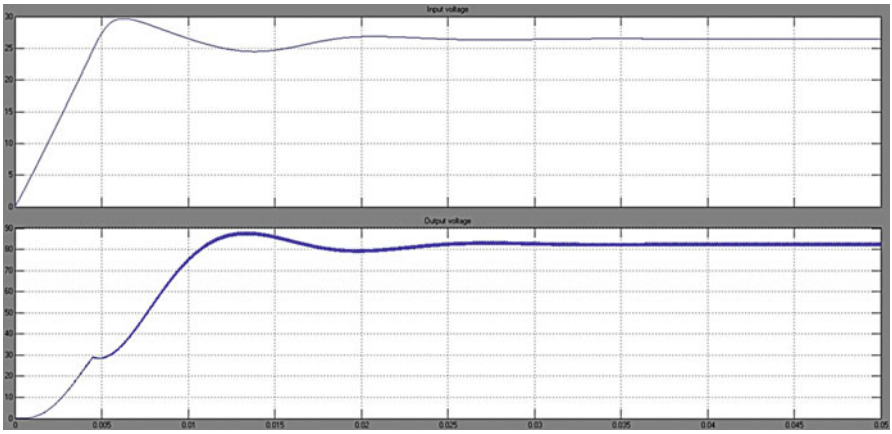


Fig. 2.67 Voltage versus time curve with In Cond MPPT technique with temperature 25 °C and irradiance 600 W/m^2

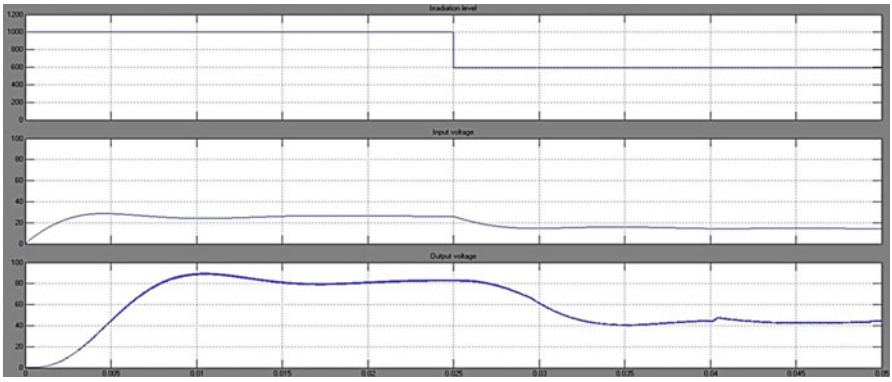


Fig. 2.68 Voltage versus time curve with P&O MPPT technique with temperature 25 °C and variation in irradiation from 1,000 W/m^2 to 600 W/m^2

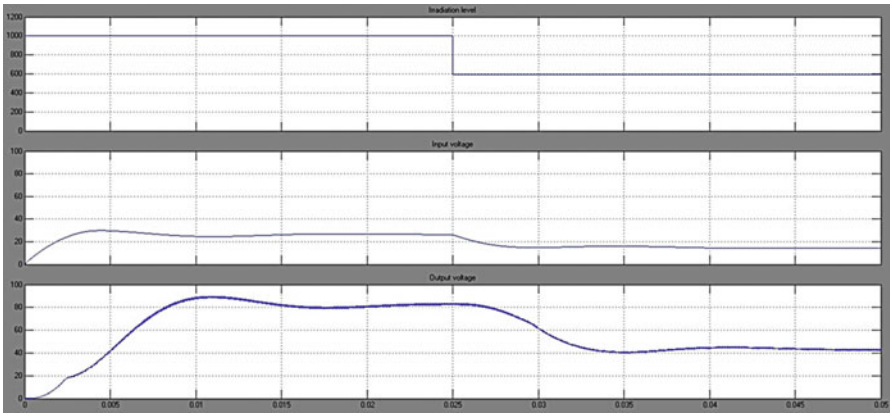


Fig. 2.69 Voltage versus time curve with In Cond MPPT technique with temperature 25 °C and variation in irradiation from 1,000 W/m^2 to 600 W/m^2

2.11 Summary

Solar PV is used primarily for grid-connected electricity to operate residential appliances, commercial equipment, lighting and air conditioning for all types of buildings. Through stand-alone systems and the use of batteries, it is also well suited for remote regions where there is no electricity source. Solar PV panels can be ground mounted, installed on building rooftops or designed into building materials at the point of manufacturing. This chapter discussed the solar PV array, batteries, charge controllers, inverters, power conditioning unit and MPPT techniques along with their MATLAB/SIMULINK modules. The future will see everyday objects such as clothing, the rooftops of cars and even roads themselves turned into power-generating solar collectors.

Review Questions

1. Mention the major components of a PV system.
2. Differentiate between grid connected and stand-alone PV systems.
3. What is the need for batteries in stand-alone PV systems?
4. What are the considerations for installing PV arrays on rooftops?
5. List the consequences of shading in PV arrays.
6. How are stand-alone PV systems sized?
7. Differentiate between PWM charge controller and MPPT charge controller.
8. Develop a MATLAB/SIMULINK model for a PV system using micro inverters.
9. Design a full bridge inverter using MATLAB/SIMULINK.
10. Design and simulate a PV module using fuzzy based MPPT algorithm using MATLAB/SIMULINK.

Bibliography

Ahmed MM, Sulaiman M (2003) Design and proper sizing of solar energy schemes for electricity production in Malaysia. National Power and Energy Conference 2003, pp 268–271

Akhter R, Hoque A (2008) Analysis of a PWM boost inverter for solar home application. World Acad Sci Eng Technol 23

Anegawa T (2010) Characteristics of CHAdeMO quick charging system. In: Proceedings of the EVS-25 Shenzhen, 5–9 Nov 2010

Ardente F, Beccali G, Cellura M (2004) Life cycle assessment of a solar thermal collector. Science Direct

Atlas H, Sharaf AM (2007) A photovoltaic array simulation model for matlab-simulink GUI environment. In: Proceeedings of IEEE international conference on clean electrical power, ICCEP 2007, Capri

AVA Solar website (2008) IEEE standard for interconnecting distributed resources with electric power systems, New York: IEEE, IEEE Std.1547–2003. http://www.avasolar.com. Accessed June 2008.

Ayob SM, Yee CH, Muhamad ND, Jusoh A (2005) A new hybrid multilevel inverter topology with harmonics profile improvement. IEEE Trans Power Electron Drives Syst, ISSN: 0-7803-9296-5/05, pp 999–1002

Baldsing et al (1991) Lead-ácid batteries for remote area energy storage. CSIRO Australia, Jan 1991

Banerjee S, Jeevananathan (2010) Modeling of PV array and performance enhancement by MPPT algorithm. Int J Comput Appl 7:35–39 (0975–8887)

Bechtel National (1980) Handbook for battery energy storage in photovoltaic power systems, Final report, SAND80-7022, Feb 1980

Borowy BS, Salameh ZM (1996) Methodology for optimally sizing the combination of a battery bank and PV array in a wind/PV hybrid system. IEEE Trans Energy Conv 11(2):367–375

"Buck Converter Design Example", Microchip WebSeminor, Microchip Technology Incorporated. All Rights Reserved (2006). Microchip Web Sites: www.microchip.com/smps

Calais M, Agelidis V (1998) Multilevel converters for single phase grid connected photovoltaic systems, an overview. IEEE Int Symp Ind Electron 7–10:224–229

Cavalcanti MC, de Oliveira KC, Neves FAS, Azevedo GMS (2010) Modulation techniques to eliminate leakage currents in transformer less three-phase photovoltaic systems. IEEE Trans Ind Electron 57(4)

Chang HC, Liaw CM (2009) Development of compact switched reluctance motor drive for EV propulsion with voltage-boosting and PFC charging capabilities. IEEE Trans Veh Technol 58:3198–3215

Chen A, He X (2006) Research on hybrid-clamped multilevel inverter topologies. IEEE Trans Ind Electron 53(6):1898–1906

Chowdhury AA, Koval DO (2005) Impact of photovoltaic power sources on a power system's capacity reliability levels. I&CPS

Chowdhury BH, Rahman S (1988) Is central power station photovoltaic power dispatchable? IEEE Trans Energy Convers 3(42):747–754

Conti S, Raiti S, Tina G, Vagliasindi U (2003) Integration of multiple PV units in urban power distribution systems. Sol Energy 75:87–94

Corzine KA, Wielebski MW, Peng FZ, Wang J (2004) Control of cascaded multilevel inverter. IEEE Trans Power Electron 19(3):732–738

Davidson J, The new solar electric home, 20th printing 2001

Duffie JA, Beckman WA (2006) Solar engineering of thermal processes, 3rd edn. Wiley, New York

Dunlop JP (1997) Batteries and charge control in stand alone photovoltaic systems, Jan 1997

Dunlop J, Bower W, Harrington S (1991) Performance of batter charge controllers: first year test report. In: Proceedings of the 22nd IEEE photovoltaic specialists conference, Las Vegas, Nevada, 7–11 Oct 1991

Egan MG, O'Sullivan DL, Hayes JG (2007) Power-factor-corrected single-stage inductive charger for electric vehicle batteries. IEEE Trans Ind Electron 54:1217–1226

Enslin JHR, Snyman DB (1991) Combined low-cost, high-efficient inverter, peak power tracker and regulator for PV applications. IEEE Tran Power Electron 6(1):73–82

Esram T, Chapman PL (2007) Comparison of photovoltaic array maximum power point tracking techniques. IEEE Trans Energy Convers 22(2):439–449

Exide Management and Technology Company (1981) Handbook of secondary storage batteries and charge controllers in photovoltaic systems – final report, for Sandia National Laboratories, SAND81-7135, Aug 1981

Ghani ZA, Hannan MA, Mohamed A (2012) Simulation model linked PV inverter implementation utilizing dSPACE DS1104 controller. Elsevier

Gounden NA, Peter SA, Nallandula H, Krithiga S (2009) Fuzzy logic controller with MPPT using line-communicated inverter for three-phase grid-connected photovoltaic systems. Renew Energy 34:909–915

Haghbin S, Khan K (2010) Integrated chargers for EV's and PHEV's: examples and new solutions. In: Proceedings of ICEM, pp 1–6, Sept 2010

Haiwen Liu, Leon M Tolbert, Surin Khomfoi, Burak Ozpineci, Zhong Du (2008) Hybrid cascaded multievel inverter with PWM control method. IEEE, pp 162–166

Harrington S, Dunlop J (1992) Battery charge controller characteristics in photovoltaic systems. In: Proceedings of the 7th annual battery conference on advances and applications. Long Beach, California, 21 Jan 1992

Hart DW (1997) Introduction to power electronics. Prentice Hall, New Jersey

http://inventors.about.com/od/pstartinventions/ss/photovoltic_cel_8.htm

http://www.solarbuzz.com/Technologies.htm

http://www.ren21.net. Accessed June 2008

Huan-Liang Tsai, Ci-Siang Tu, Yi-Jie Su *Member, IAENG* (2008) Development of generalized photovoltaic model using MATLAB/SIMULINK. In: Proceedings of the world congress on engineering and computer science 2008 WCECS, 22–24 Oct 2008

Hussein KH, Muta I, Hoshino T, Osakada M (1995) Maximum photovoltaic power tracking: an algorithm for rapidly changing atmospheric conditions. IEE Proc Gener Trans Distrib 142 (1):59

IEEE recommended practice for utility interface of photovoltaic system, IEEE Std. 929–2000

Institute of Electrical and Electronics Engineers (1987) IEEE recommended practice for installation and operation of lead-acid batteries for photovoltaic (PV) systems. ANSI/IEEE Std. 937–1987, New York

Institute of Electrical and Electronics Engineers (1990) IEEE recommended practice for installation and operation of nickel-cadmium batteries for photovoltaic (PV) systems. ANSI/IEEE Std. 1145–1990, New York

International Rectifier Application Note AN-978

IR2112 Datasheet

Jäger-Waldau A (2007) PV status report 2007: research, solar cell production and market implementation of photovoltaics. European Commission Directorate General Joint Research Center. http://re.jrc.ec.europa.eu/refsys/pdf/PV_StatusReport_2007.pdf. Accessed June 2008

Jenkins N (1995) Photovoltaic systems for small scale remote power supplies. Power Eng J 9 (2):89–96

Jewell WT, Uaruh TD (1990) Limits on cloud-induced fluctuations in photovoltaic generation. IEEE Trans Energy Convers 5(1):8–14

Jiang A et al (2005) Maximum power tracking for photovoltaic power systems. Tamkang J Sci Eng 8(2):147–153

Jianye Rao, Yongdong Li (2008) High-performance control strategies and applications of a new hybrid cascaded multilevel inverter. ISSN: 978-14244-2279-1/08, pp 1–5

Kannan R, Leong K, Osman R (2005) "Life Cycle Assessment" study of solar PV systems: an example of a 2.7 kWp distributed solar PV system in Singapore. Science Direct

Kern EC, Gulachenski EM, Kern GA (1989) Cloud effects on distributed photovoltaic generation: slow transients at the Gardner, Massachusetts photovoltaic experiment. IEEE Trans Energy Convers 4(2):184–190

Khomfoi S, Aimsaard C (2009) A 5-level cascaded hybrid multilevel inverter for interfacing with renewable energy resources. IEEE, 978-1-4244-3388-9

Khomfoi S, Praisuwanna N (2010) A hybrid cascaded multilevel inverter for interfacing with renewable energy resources. IEEE, 978-1-4244-5393-1/10/2010

Kiehne HA (1989) Battery technology handbook. Marcel Dekker, New York

Kleinkauf W, Cramer G, Ibrahim M (2005) PV systems technology: state of the art developments and trends in remote electrification. SMA Technologies AG

Koutroulis E et al (2001) Development of a microcontroller-based photovoltaic maximum power tracking control system. IEEE Trans Power Electron 16(1):46–54

Kutkut NH, Divan DM, Novotny DW, Marion RH (1998) Design considerations and topology selection for a 120-kW IGBT converter for EV fast charging. IEEE Trans Power Electron 13:169–178

Ladner-Garcia HP, O'Neill-Carrillo E(2008) Demonstrative PV systems for an isolated system. In: Proceedings of the 10th IASTED international conference on power and energy systems
Liang TJ, Kuo YC, Chen JF (2001) Single-stage photovoltaic energy conversion system. Proc Inst Elect Eng 148(4):339–344
Linden D (1984) Handbook of batteries and fuel cells. McGraw Hill, New York
Luque A, Hegedus S (2003) Handbook of photovoltaic science and engineering. Wiley, New York
Maimone G (2010) Application note. Selecting L and C components in the power stage of the MC34700 switching regulators. Freescale Semiconductor, AN4067 Rev. 1.0, 11/2010
Markvart T, Castañer L (2003) Practical handbook of photovoltaics: fundamentals and applications. Elsevier Advanced Technology, Oxford
Musavi F, Eberle W, Dunford WG (2010) Efficiency evaluation of single-phase solutions for AC-DC PFC boost converters for plug-inhybrid electric vehicle battery chargers. In: Proceedings of IEEE VPPC, pp 1–6, Sept 2010
Navigant Consulting (2006) A review of PV inverter technology cost and performance projections NREL/SR-620-38771, Jan 2006. www.nrel.gov. Accessed June 2008
Orosco R, Vazquez N (2000) Discrete sliding mode control for DC/DC converters. Power Electronics Congress 231–236
Ozpineci B, Chinthavali MS, Tolbert LM, Kashyap A, Mantooth HA (2009) A 55 kW three-phase inverter with Si IGBTs and SiC Schottky diodes. IEEE Trans Ind Appl 45(1):278–285
Qin YC, Mohan N, West R, Bonn R (2002) Status and needs of power electronics for photovoltaic inverters. SAND2002-1535, Unlimited Release, June 2002
Ramakumar R (1993) Photovoltaic systems. Proc IEEE 81(3):365–376
Rashid MH (2006) Power electronics devices, circuits and applications. Academic Press, San Diego
Saravana Ilango G, Srinivasa Rao P, Karthikeyan A, Nagamani C Single-stage sine-wave inverter for an autonomous operation of solar Photo voltaic energconversion system
Solero L (2001) Nonconventional on-board charger for electric vehicle propulsion batteries. IEEE Trans Veh Technol 50:144–149
Teodorescu R, Blaabjerg F, Pedersen JK, Cengelci E, Enjeti PN (2002) Multilevel inverter by cascaded industrial VSI. IEEE Trans Ind Electron 49(4):832–834
Vinal GW (1954) Storage batteries, 4th edn. Wiley, New York
Waldau A (2007) PV status report 2007_Research, solar cell production and market implementation of photovoltaics
Xue Y, Chang L, Kjaer S, Bordonau J, Shiminizu T (2004) Topologies of single-phase inverters for small distributed power generators: an overview. IEEE Trans Power Electron 19(5):1305–1314

Chapter 3
Soft Computing Techniques in Solar PV

Learning Objectives
On completion of this chapter, the reader will have knowledge on:

- Importance of soft computing techniques such as neural networks, fuzzy logic and genetic algorithms in solar PV system.
- Soft computing techniques used in MPPT of Solar PV system and its MATLAB/SIMULINK model.
- Prediction of solar irradiance using soft computing techniques.
- Parameter estimation of Solar PV module using Genetic Algorithms.

3.1 Introduction

Problems that are computationally difficult to solve are known as NP-Complete/NP-Hard problems. Traditional algorithms take a very long time to determine solutions for these problems. The basic example of such kind of a problem is the Travelling Salesman Problem (TSP). Such problem cannot be solved using conventional deterministic process and hence stochastic process is required to handle them encompassing uncertainties. Soft computing techniques comprises of those paradigms in AI that relate to some kind of biological or naturally occurring system. General consensus suggests that these paradigms are neural networks, evolutionary computing, and fuzzy systems. Neural networks are based on their biological counterparts in the human nervous system. Similarly, evolutionary computing draws heavily on the principles of Darwinian evolution observed in nature. Genetic Algorithms are part of evolutionary computing algorithms. Finally, human reasoning using imprecise, or fuzzy, linguistic terms is approximated by fuzzy systems.

During the recent years, these soft computing techniques are commonly applied for designing, modeling, predicting, optimizing, and forecasting of renewable

© Springer International Publishing Switzerland 2015

S. Sumathi et al., *Solar PV and Wind Energy Conversion Systems*,
Green Energy and Technology, DOI 10.1007/978-3-319-14941-7_3

energy systems. In addition, innovative models, environmentally benign processes, etc. used in renewable energy systems are computationally-intensive, non-linear and complex as well as involve a high degree of uncertainty. Soft computing techniques are most suitable in handling the noise, imprecision, and uncertainty in the data, and in turn achieve robust, low-cost solutions. Hence, soft computing paradigms and intelligent algorithms are increasingly applied in the study of renewable energy systems. This chapter describes the application of fuzzy logic and neural networks for MPP tracking in solar PV arrays, fuzzy based solar powered energy, genetic algorithms for parameter identification in solar cells, and neural networks for forecasting of solar irradiance.

3.2 MPPT Using Fuzzy Logic

The application of fuzzy logic for MPPT has become more popular with the utilization of microcontrollers. Fuzzy logic controllers have the benefits of operating with general inputs, not needing associate correct mathematical model and handling nonlinearities. mathematical logic management typically consists of three stages: fuzzification, rule base table operation, and defuzzification. Throughout fuzzification, numerical input variables are regenerated into linguistic variables supported by a membership operate almost like Fig. 3.1. Fuzzy levels used are of the type: NB (Negative Big), NS (Negative Small), ZE (Zero), PS (Positive Small), and lead (Positive Big). In Fig. 3.1a, b are the membership values of the numerical variable.

The inputs to a MPPT fuzzy logic controller (FLC) are usually an error E and a change in error ΔE. The user has the flexibility of choosing how to compute E and ΔE. Since dP/dV vanishes at the MPP, the following approximation is used.

$$E(n) = P(n) - P(n-1)/V(n) - V(n-1) \tag{3.1}$$

$$\Delta E(n) = E(n) - E(n-1) \tag{3.2}$$

Once E and ΔE are the calculated and deviated change applied to the linguistic variables, the symbolic logic controller output, that is often an amendment in duty quantitative relation ΔD of the ability convertor, is researched in an exceedingly rule base table like Table 3.1. The linguistic variables assigned to ΔD for the various combos of E and ΔE based on the data of the user. Consider an example, the in operation purpose is much to the left of the MPP, that's E is metal, and

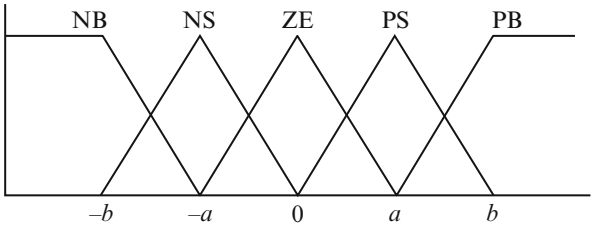


Fig. 3.1 Membership function for input and output of FLC

Table 3.1 Fuzzy rule base table

	ΔE				
E	NB	NS	ZE	PS	PB
NB	ZE	ZE	NB	NB	NB
NS	ZE	ZE	NS	NS	NS
ZE	NS	ZE	ZE	ZE	PS
PS	PS	PS	PS	ZE	ZE
PB	PB	PB	PB	ZE	ZE

ΔE is ZE, then the duty quantitative relation is basically accumulated, that's ΔE is metal to achieve the MPP.

In the defuzzification stage, the fuzzy logic controller output is regenerated from a linguistic variable to a numerical variable still employing a membership operation as in Fig. 3.1. This provides an analog signal which will manage the facility device to the MPP. MPPT fuzzy logic controllers have shown to perform well below variable atmospherical conditions. However, their effectiveness depends on the data of the user or management engineer in selecting the correct error computation and bobbing up with the rule base table.

3.2.1 Implementation

To beat a percentage of the disservices mentioned in past MPPT strategies, fuzzy logic controller is utilized for most extreme force following the PV Panel. The primary distinction from the past routines is that the correct depiction of the framework to be controlled is not needed. Fuzzy logic permits the determination of the principle base by etymological terms and consequently, the tuning of the controller is an extremely basic way which is qualitatively not quite the same as accepted configuration systems. Moreover, fuzzy control is nonlinear and versatile in nature, which provides strong execution under parameter variety, load and supply voltage. Fuzzy logic is progressively utilized within present times as a helpful device to model control frameworks which are nonlinear in nature, in the same way as the solar based PV exhibit to track the greatest force. The control inputs to the fuzzy logic controller are lapse and change of failure, while the yield is the change of control indicator for the band width adjustment generator. A band width modulator is utilized to supply a band train to the exchanging MOSFET. The MOSFET is inclined into a directing state when the beat voltage is high and into a non-leading state when the beat voltage is low.

The obligation cycle of the beat decides the powerful impedance seen by the sun oriented cell. Therefore by basically modifying the obligation cycle of the switch, the current stream to the battery may be controlled. A suitable charge controller to attain the control portrayed above is a DC-to-DC controller with beat width balance control. A buck sort converter, which steps down cell voltage to an easier quality, is indicated in Fig. 3.2.

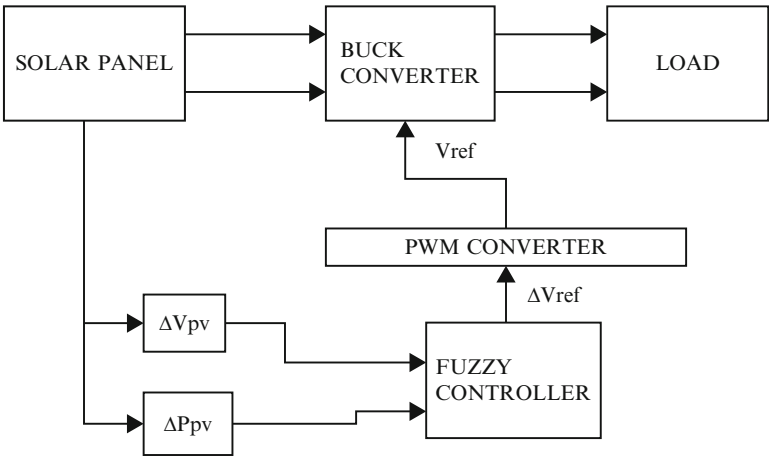


Fig. 3.2 Block diagram of the scheme

The inputs to the fuzzy controller are change in PV power (ΔPpv) and change in PV show voltage (ΔVpv) relating to the two inspecting time moments. The two inputs are prepared by the fuzzy controller and the yield of the fuzzy controller is the incremental reference voltage (ΔVref), which shifts in size and extremity relying upon which region of the Ipv × Vpv curve, the framework is working on. This yield is given to PWM generator, which yields the reference voltage to the buck converter. The fuzzy based plan utilized yields an incremental reference voltage of fitting extremity and variable greatness. In this way throughout transient conditions the fuzzy logic controller yields a bigger incremental reference voltage to accelerate the transient reaction however yields practically zero incremental reference voltage close to the top power locale to diminish motions about the MPP.

3.2.2 Description and Design of FLC

Fuzzy model of the framework is planned based on master information of the fuzzy framework. The fuzzy logic controller is partitioned into four segments: Fuzzification, rule base, inference and defuzzification. The inputs to the fuzzy logic controller are change in PV array power (ΔPpv) and change in PV array voltage (ΔVpv) and the output is the change in reference voltage (ΔVref) (Fig. 3.3).

3.2.2.1 Fuzzification

The fuzzy model is developed on a trial-and-error basis to meet the desired performance criteria.

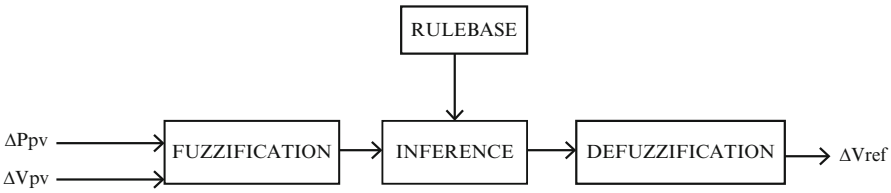


Fig. 3.3 Block diagram of the FLC

The universe of discourse for input variable 1 (ΔPpv) is divided into seven Fuzzy sets: PL (Positive Large), PM (Positive Medium), PS (Positive Small), Z (Zero), NS (Negative Small), NM (Negative Medium) and NL (Negative Large). Here, the Fuzzy set PS assumes a membership value greater than zero beginning at the origin, in order to speed up the start-up process and at the same time prevent variation of the reference voltage at the MPP. Additional Fuzzy sets PM and NM has been added to improve the control surface.

The universe of discourse for input variable 2 (ΔVpv) is divided into seven fuzzy sets: PL (Positive Large), PM (Positive Medium), PS (Positive Small), Z (Zero), NS (Negative Small), NM (Negative Medium) and NL (Negative Large). The universe of discourse for the output variable (ΔVref) is divided into seven fuzzy sets: PL (Positive Large), PM (Positive Medium), PS (Positive Small), Z (Zero), NL (Negative Large), NM (Negative Medium) and NS (Negative Small). The membership functions for the input and output variables are shown in Fig. 3.4. The membership functions for the input and output variables are designed to model the unsymmetrical nature of the PV panel Ipv × Vpv curve. The membership functions are denser at the center to provide greater sensitivity in the region near the MPP. Input membership functions are normalized and suitable tuning gains are used to match the inputs to the respective universe of discourse.

3.2.2.2 Rule Base

The Fuzzy algorithm tracks the maximum power based on the rule-base: If the last change in the reference voltage (Vref) has caused the power to increase keep changing the reference voltage in the same direction; else if it has caused the power to drop, move it in the opposite direction. A rule base consisting of 49 rules is designed as shown in Table 3.2.

3.2.2.3 Inference Method

The Inference technique decides the yield of the fuzzy controller. Mamdani's inference system is utilized within the recognized framework alongside the max-min creation strategy. This is on the grounds that this system is computationally more proficient and has preferable interpolative properties over techniques dependent upon other suggestion capacities. Henceforth, Mamdani's deduction system is normally prominent for most control building provisions.

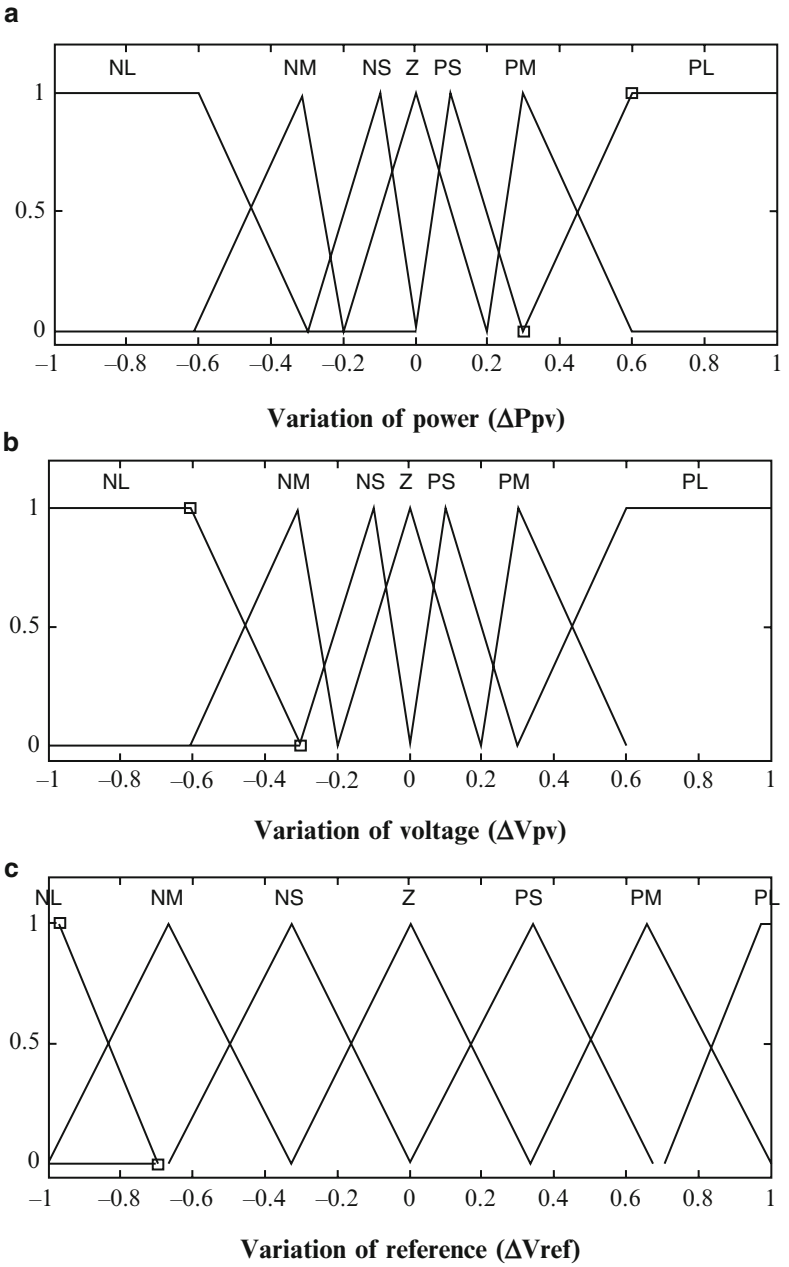


Fig. 3.4 Membership functions for the fuzzy model (**a**) input ΔPpv, (**b**) Input ΔVpv (**c**) output ΔVref

Table 3.2 Rule base for the fuzzy model

	ΔP_{pv}						
ΔV_{pv}/	NL	NM	NS	Z	PS	PM	PL
NL	PL	PL	PL	PL	NM	Z	Z
NM	PL	PL	PL	PM	PS	Z	Z
NS	PL	PM	PS	PS	PS	Z	Z
Z	PL	PM	PS	Z	NS	NM	NL
PS	Z	Z	NM	NS	NS	NM	NL
PM	Z	Z	NS	NM	NL	NL	NL
PL	Z	Z	NM	NL	NL	NL	NL

3.2.2.4 Defuzzification

The output of the fuzzy controller is a fuzzy variable. However a crisp quantity is needed. Thus the output of the fuzzy controller ought to be defuzzified. The centroid method of defuzzification is one of the normally utilized defuzzification routines and is the one being utilized for the framework. This system has great averaging properties and recreation effects have demonstrated that it gives the best outcome.

3.2.3 Simulation and Results

The SIMULINK model of fuzzy logic based maximum power tracking for a solar panel with 60 W is shown in Fig. 3.5. The performance of the SIMULINK model is validated with a PV panel,, buck converter and a resistive load. The objective of the modeled FLC using SIMULINK is to track maximum power irrespective of panel voltage variations. Accordingly FLC uses two input variables: change in PV array Power (ΔPpv) and change in PV array voltage (ΔVpv) corresponding to the two sampling time instants. Equations (3.3, 3.4, and 3.5) determine the required power, change in array voltage and reference variable. The change in control variable (ΔVref) is considered as the output variable. (ΔVref) is integrated to achieve desired Vref value. The duty cycle of the DC-DC converter is determined using the reference voltage Vref.

$$\Delta P_{pv} = \left[P_{pv}(k) - P_{pv}(k-1)\right] * K1 \tag{3.3}$$

$$\Delta V_{pv} = \left[V_{pv}(k) - V_{pv}(k-1)\right] * K2 \tag{3.4}$$

$$\Delta V_{ref} = \left[V_{ref}(k) - V_{ref}(k-1)\right] * K3 \tag{3.5}$$

where K1, K2, K3 denote the gain coefficients and k is a time index. The crisp inputs and output are converted to linguistic variables to determine FLC output value. In order to perform this conversion fuzzy membership functions are used. Here, all membership functions are defined between −1 and 1 interval by means of input scaling factors K1 and K2 and the output scaling factor K3. Thus, since simple

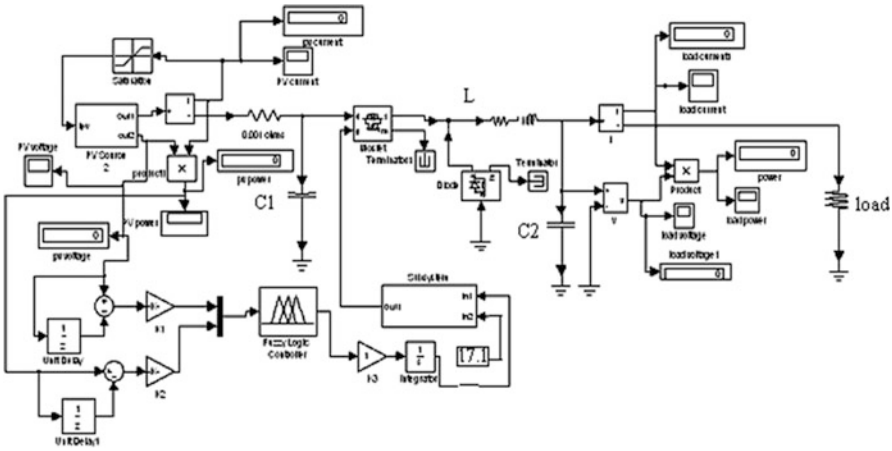


Fig. 3.5 FLC SIMULINK model

numbers are now processed in controller after scaling, fuzzy computation is performed in a shorter time. The linguistic terms for input and output values are represented by seven membership functions as shown in Fig. 3.4. The two inputs (ΔPpv) and (ΔVpv) are processed by the FLC and outputs a control variable (ΔVref) based on the control rules as shown in Table 3.2. The fuzzy output is given to the PWM generator which outputs the reference voltage to the buck converter. Fundamentally, the operating principle of PWM generator is based on the comparison of two signals. One of the signals is a triangular waveform and the other one is fixed linear signal, which represents time equivalent of triggering voltage.

Consequently, reference voltage time signal and triangular signal are U1 and U2 variables of 'IF' block used in simulation model as shown in Fig. 3.5. The output of the pulse width modulator is used to supply a pulse train to the switching MOSFET. The MOSFET is biased into a conducting state when the pulse voltage is high and into a non-conducting state when the pulse voltage is low. Thus the fuzzy algorithm tracks the maximum power based on the defined rules. The PV source block and the sub-system block are shown in Figs. 3.6 and 3.7 respectively.

Fuzzy logic controller model is simulated in MATLAB/SIMULINK environment to track the maximum power point and the value of the maximum power tracked is 59.9 W as shown in Fig. 3.8.

3.3 Neural Networks for MPP Tracking

The human brain mainly inspires artificial neural networks. This doesn't mean that Artificial Neural Networks are exact simulations of the biological neural networks inside our brain because the actual working of human brain is still a mystery. Neural

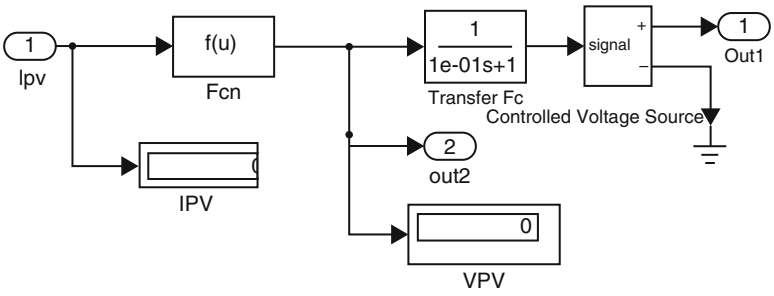


Fig. 3.6 PV source block

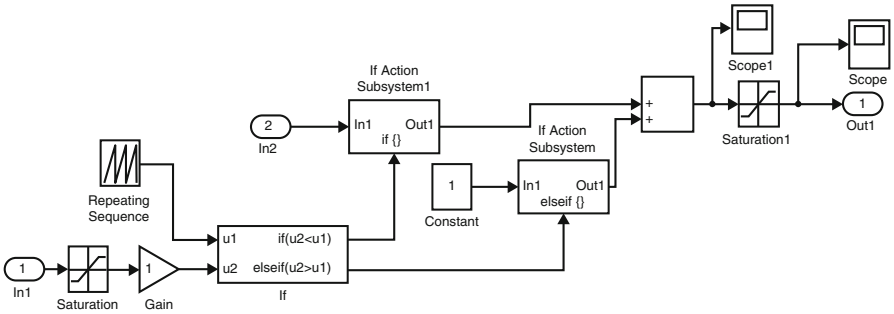


Fig. 3.7 Subsystem block

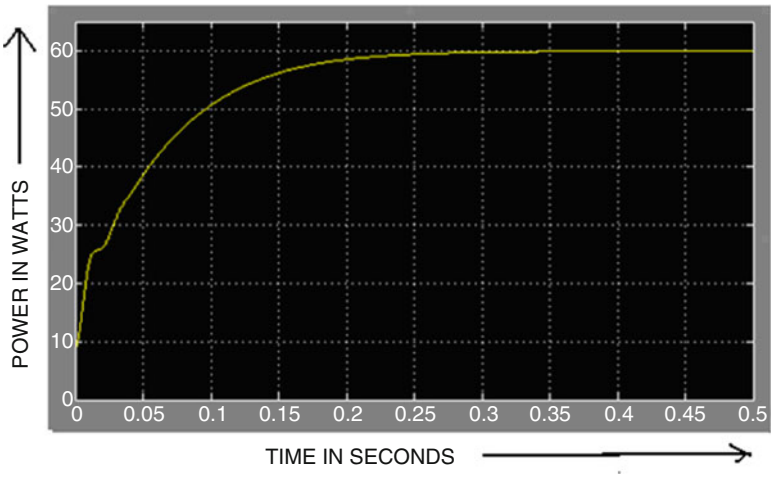


Fig. 3.8 Power characteristic curve with FLC

Network is a machine that is designed to model the way to which the brain performs a particular task. The network is implemented using electronic components or is simulated in software on digital computer. Neural networks perform usual computations through process of learning.

3.3.1 Background of Neural Networks

Neural network is a massively parallel distributed processor made up of simple processing units, which has a natural property of storing experimental knowledge and making it available for use. It resembles the brain in two respects:

– Knowledge is acquired by the network from its environment through learning process.
– The interneuron connection strengths, known as synaptic weights are used to store the acquired knowledge.

The primary significance of the neural network is the ability of the network to learn from its environments and to improve its performance through learning. It learns about its environment through an interactive process of adjustments applied to its synaptic weights and biases. The network becomes more knowledgeable about its environment after each iteration of learning process. The definition of learning process implies the sequence of events:

- The neural network is stimulated by an environment.
- Neural network undergoes changes in its parameters.
- Neural network responds in a new way to the environment because of the changes that have occurred in its internal structure.

The fundamental processing element of a neural network is a neuron. This building block of human awareness encompasses a few general capabilities. Basically, a biological neuron receives inputs from other sources, combines them in some way, performs a generally nonlinear operation on the result, and then outputs the final result. Figure 3.9 shows the relationship of these four parts.

Within humans there are many variations on this basic type of neuron, further complicating man's attempts at electrically replicating the process of thinking. Yet, all natural neurons have the same four basic components. These components are known by their biological names – dendrites, soma, axon, and synapses. Dendrites are hair-like extensions of the soma, which act like input channels. These input channels receive their input through the synapses of other neurons. The soma then processes these incoming signals over time. The soma then turns that processed value into an output, which is sent out to other neurons through the axon and the synapses.

But currently, the goal of artificial neural networks is not the grandiose recreation of the brain. On the contrary, neural network researchers are seeking an understanding of nature's capabilities for which people can engineer solutions to

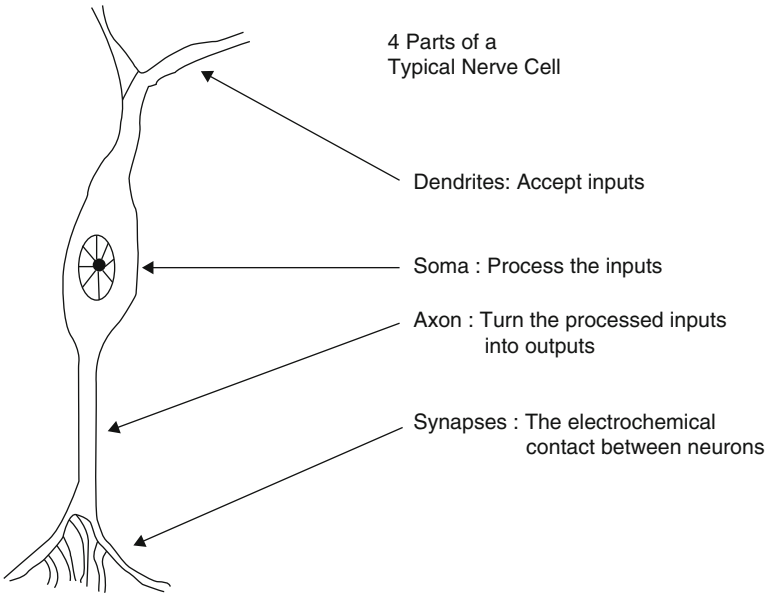


Fig. 3.9 A simple neuron

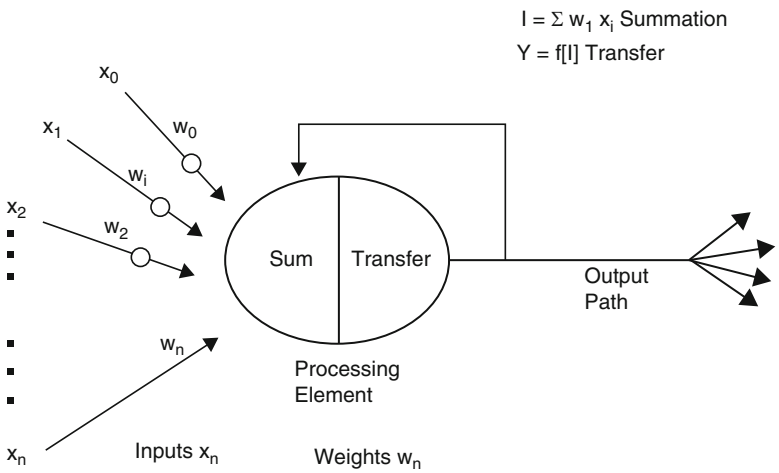


Fig. 3.10 A basic artificial neuron

problems that have not been solved by traditional computing. To do this, the basic unit of neural networks, the artificial neurons, simulate the four basic functions of natural neurons. Figure 3.10 shows a fundamental representation of an artificial neuron.

In Fig. 3.10, various inputs to the network are represented by the mathematical symbol, x(n). Each of these inputs are multiplied by a connection weight. These weights are represented by w(n). In the simplest case, these products are simply summed, fed through a transfer function to generate a result, and then output. This process lends itself to physical implementation on a large scale in a small package. This electronic implementation is still possible with other network structures, which utilize different summing functions as well as different transfer functions.

3.3.2 Implementation

A three layered feed forward network is created using newff command in MATLAB. The network is created with two neurons in the input layer, 50 neurons in the hidden layer and one neuron in the output layer. The two inputs to the network are the insolation and the temperature. Totally 23 sets of input data samples are given to the network for training. The targets of the network are specified to be the values of voltages that are obtained from modeling for a particular input set among training sets. The activation functions used at the input and output layers are tansig and purelin functions respectively. The tansig activation function calculates its output according to:

$$\text{tansig}(\text{n}) = 2/(1 + \exp(-2 * \text{n})) - 1 \tag{3.6}$$

The purelin activation function calculates its output according to:

$$\text{purelin}(\text{n}) = \text{n} \tag{3.7}$$

The basic structure of the neural network is shown below in Fig. 3.11.

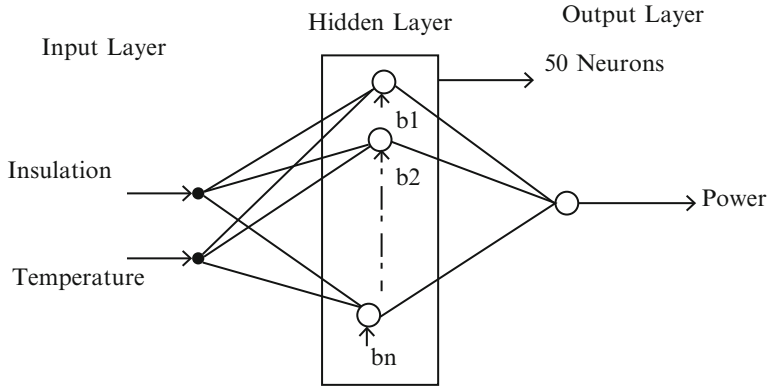


Fig. 3.11 Basic structure of neural network

The error criterion that is considered for training is Mean Square Error. The learning function is taken to be trainlm. "Trainlm" is a network training function that updates weight and bias values according to Levenberg-Marquardt (LM) optimization. This is one of the most popularly used algorithms which are a type of numerical optimization technique that has many advantages over its counterparts. The main advantage of this algorithm is that it requires less number of data for training the network and achieves accurate results. The other advantage of using LM optimization method is that it produces accurate results even if the system is not completely controllable and observable. Also it need not compute the Hessian matrix. When the performance function has the form of a sum of squares, then the Hessian matrix is approximated as

$$\mathrm{H} = \mathrm{J}^{\mathrm{T}}\mathrm{J} \ldots . \tag{3.8}$$

and the gradient is computed as

$$\mathrm{g} = \mathrm{J}^{\mathrm{T}}\mathrm{e} \ldots . \tag{3.9}$$

The Jacobian matrix(J) is computed through a standard back-propagation (BP) that is much less complex than computing the Hessian matrix. The LM method uses this approximation to the Hessian matrix in the following Newton-like update as follows.

$$x_{k+1} = x_k - \left[J^T J + \mu I\right]^{-1} J^T e \tag{3.10}$$

When the scalar μ is zero, this is just Newton's method, using the approximate Hessian matrix. When μ is large, this becomes gradient descent with a small step size. Newton's method is faster and more accurate near an error minimum, so the aim is to shift towards Newton's method as quickly as possible. Thus, μ is decreased after each successful step (reduction in performance function) and is increased only when a tentative step would increase the performance function. In this way, the performance function will always be reduced at each iteration of the algorithm. The error BP learning is implemented for updating the weights of the network in order to minimize the mean square error. The BP algorithm consists of two passes.

- Forward pass.
- Backward pass.

In the forward pass, 23 pairs of insolation and temperature are given to the network. As these are given all at a time, this type of training is called Batch training. These inputs propagate through the network layer-by-layer and the output voltage is generated. These inputs are used for computing the gradient and updating the network weights and biases. Now the output voltage is compared with the corresponding target value and then the error which is the difference between these

two values is propagated through the network in the backward pass. During this process, the weights of the network are updated recursively. The BP algorithm uses the following rule for updating the weights of the network.

$$w(k+1) = w(k) - \eta g(k) \tag{3.11}$$

where η------learning rate

g(k)-----gradient vector

The gradient vector is computed in the backward pass by applying the chain rule. The training parameters for trainlm are epochs, show, goal, time, min_grad, max_fail, mu, mu_dec, mu_inc, mu_max. Training occurs according to the trainlm's training parameters as shown below.

net.trainParam.epochs ---------- Maximum number of epochs to train
net.trainParam.goal ---------- Performance goal
net.trainParam.max_fail -------- Maximum validation failures
net.trainParam.mem_reduc------ Factor used for memory/speed purpose
net.trainParam.min_grad ------- Minimum performance gradient
net.trainParam.mu ---------- Initial Mu
net.trainParam.mu_dec---------- Mu decrease factor
net.trainParam.mu_inc---------- Mu increase factor
net.trainParam.mu_max --------- Maximum Mu
net.trainParam.show ---------- Epochs between showing progress
net.trainParam.time ---------- Maximum time to train in seconds.

The performance goal is specified as 0.15. The maximum number of epochs are set to 30. This is done on trial basis. When the epoch number is mentioned to be low than this number, training is stopped without reaching the performance. Maximum validation failures is kept as 5. Mu decrease factor is mentioned as 0.01. The time interval for showing the Epoch's progress is set to 50. This shows the training curve for every 50 epochs. The other parameters are set to their default values. The default values for these parameters are shown below.

net.trainParam.mu_inc ---------10
net.trainParam.mu_max ------- 1e-10
net.trainParam.mem_reduc---- 1
net.trainParam.min_grad ------ 1e-25

The parameter mu is the initial value for μ. This value is multiplied by mu_dec whenever the performance function is reduced by a step. It is multiplied by mu_inc whenever a step would increase the performance function. If mu becomes larger than mu_max, the algorithm is stopped. The trained network thus obtained is tested using nine sets of data.

3.3.3 *Algorithm for ANN Based MPPT*

Step-1: Construct the network and initialize the synaptic weights with random values.

Step-2: Apply the input sets to the network.

Step-3: Set the parameters of the network and calculate the corresponding output values by training the network.

Step-4: Compare the actual outputs with the desired outputs and determine a measure of the error.

Step-5: Determine the amount by which each weight is to be changed and make corrections to each weight.

Step-6: Repeat Step-3 to Step-4 until the error for the sets in the training set is reduced to an acceptable value.

Step-7: Validate the so formed network using testing sets.

A neural network SIMULINK block is generated using gensim (net) command. After the network is generated, nine sets of insolation and temperature are given to the network for validating the network. Each data set is given to the network at different instances of time with an interval of 1 s. The network is simulated. The curves for voltage, current and power are obtained. The overall SIMULINK model is shown in Fig. 3.12.

The structure of neural network is shown below in Fig. 3.13. It consists of two layers. The structures of the first and the second layers are shown in Figs. 3.14 and 3.15 respectively.

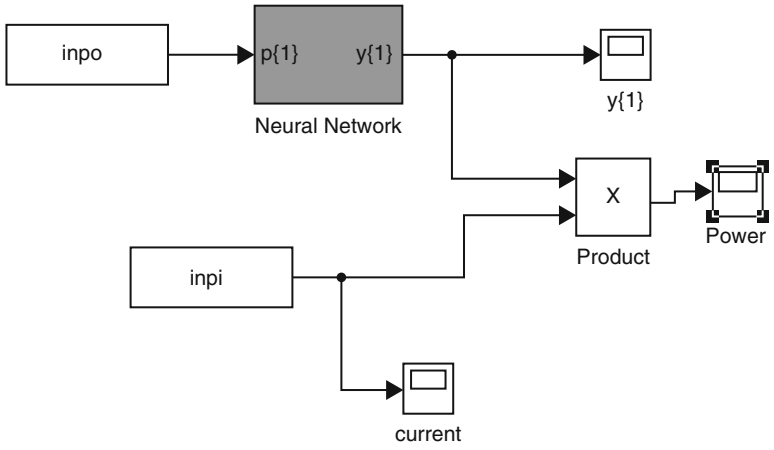


Fig. 3.12 Overall SIMULINK model

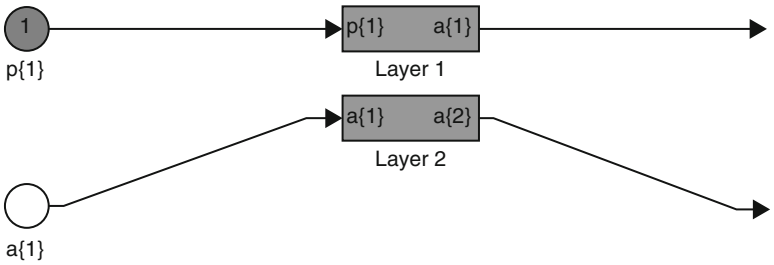


Fig. 3.13 Structure of neural network

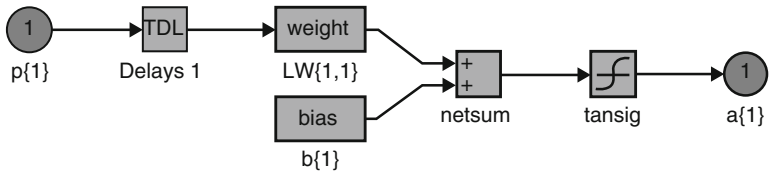


Fig. 3.14 Structure of first layer of neural network

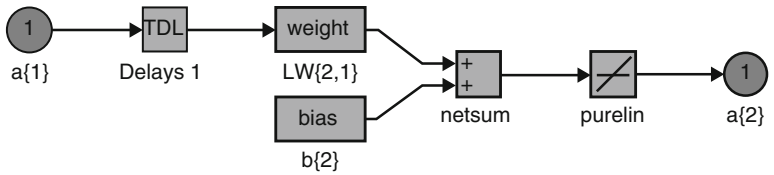


Fig. 3.15 Structure of second layer of neural network

3.3.4 Simulation Results

The training data used is shown below. These training sets were chosen to cover all the typical input space in order to get good performance where temperature ranges from −40 °C to 52 °C and solar irradiation ranged from 50 to 1,000 W/m^2. The first column shows the various values of insolation, second column corresponds to various temperatures and the third column corresponds to the target voltages.

Training data:		
50	50	16.15
100	−40	7.95
100	0	11.82
180	30	15.69
200	10	13.75
220	40	17.04

(continued)

Training data:		
600	52	19.45
700	42	18.58
770	47	19.15
830	35	18
850	50	19.68
900	10	15.41
910	12	15.6
920	13	18.17
950	23.75	16.96
955	23.87	16.97
960	24	16.96
965	24.12	16.96
970	24.25	17.02
975	24.37	17.02
980	24.5	17.08
985	24.62	17.13
995	24.87	17.14

The results are shown in Table 3.3. Training is completed for 25 epochs and the performance goal is met. The Mean Square error after training is 0.146852. The training curve is shown in Fig. 3.16.

The trained network is validated with the following nine sets of insolation and temperature conditions. The corresponding voltages and powers are tabulated in Table 3.3.

The curves for voltage, current and Power are shown below in Figs. 3.17, 3.18, and 3.19 respectively.

Table 3.3 Results of ANN based MPPT method

Insolation (W/m^2)	Temperature (°C)	Target voltage obtained from modeling (V)	Power obtained from modeling (W)	Voltage obtained from ANN based MPPT method (V)	Power obtained from ANN based MPPT method (W)
960	24	16.96	56.84	16.9698	56.8380
175	5	13.1	7.892	12.04	7.6394
1,000	25	17.1	59.9159	17.0862	59.8885
700	42	18.52	44.82	19.2	44.8192
965	24.125	16.96	57.21	16.98	57.2030
930	12	16.6	48.64	16.5	48.6104
995	24.87	17.14	59.41	17.0674	59.4013
820	40	18.46	53.14	18.05	52.9013
980	24.5	17.08	58.31	17.02	58.3007

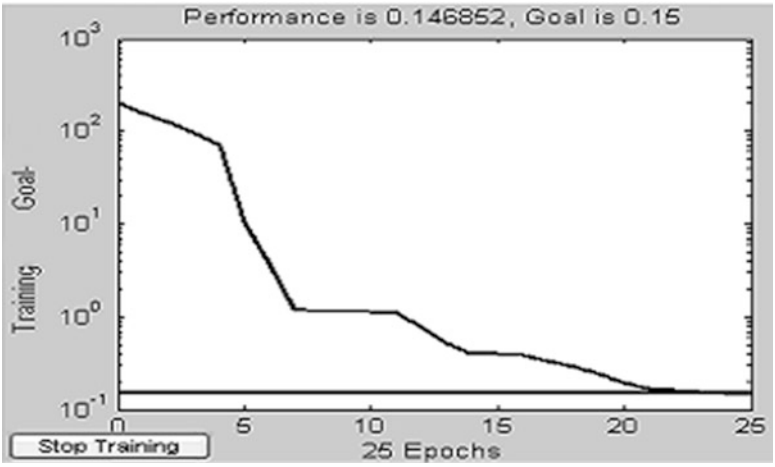


Fig. 3.16 Training curve

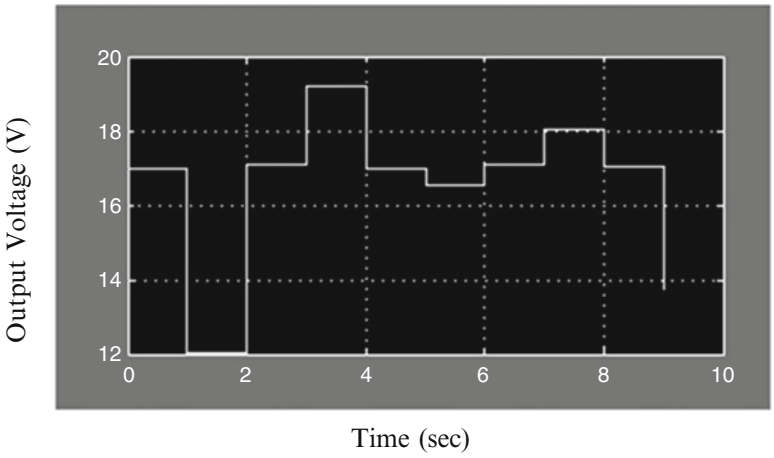


Fig. 3.17 Voltage curve for neural network based MPPT method

3.4 Neuro-Fuzzy Based MPPT Method

Over the previous decades there has been a solid resurgence in the field of information based nonlinear framework demonstrating and distinguishing proof including specialists from different orders. This present reality power framework issues might not, one or the other fit the presumptions of a solitary system nor be successfully explained by the qualities and competencies of a solitary procedure. One methodology to manage the complex true issues is to incorporate the utilization of two or more systems with a specific end goal to consolidate their distinctive

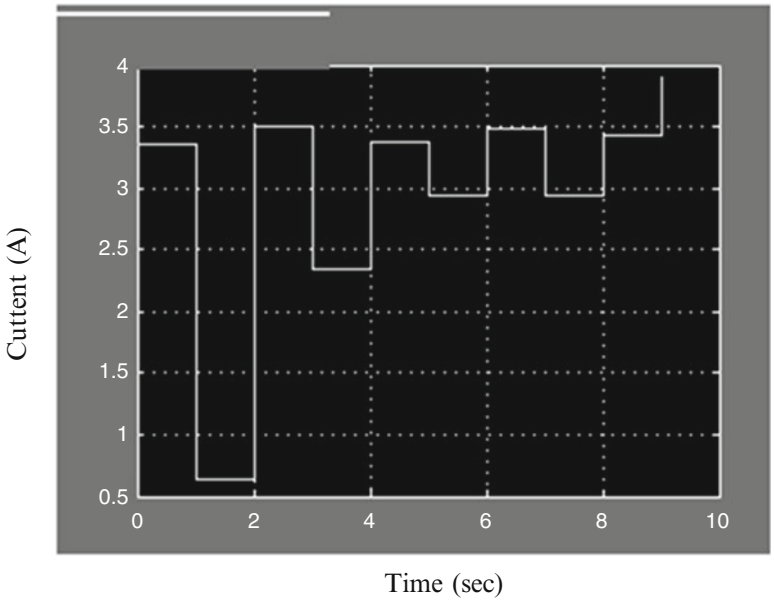


Fig. 3.18 Current curve for neural network based MPPT method

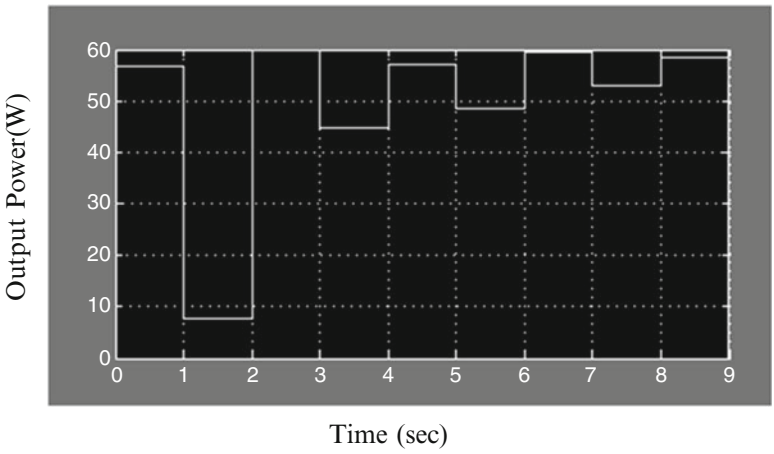


Fig. 3.19 Power curve for neural network based MPPT method

qualities and overcome one another shortcoming to produce cross breed results. Fuzzy Logic is the compelling apparatus for displaying uncertainty and approximate reasoning; however the presence of an expert is the most important part of the design. Master less outline obliges information which must blanket all the potential outcomes of operation. Neural systems are the best learning machines in the field. Adaptive Neuro Fuzzy Inference Systems joins the point of interest of fuzzy logic

and neural systems in one bundle and gives an enhanced fuzzy derivation framework installing the entire learning of the framework conduct (following operation). PV cells carry on as non-straight sources relying upon climatic parameters. Insolation and Temperature are the most paramount variables affecting the greatest force conveyed from the PV exhibit. Here, a cross breed system that joins fuzzy logic and neural systems is connected to recognize the greatest force point.

3.4.1 Fuzzy Neural Network Hybrids

In Engineering, a class of neural systems is ended up being equipped for speaking to a class of obscure nonlinear input–output mappings with self-assertive little rough guess lapse competence. The preference of the FL methodology is its logicality and transparency, where it is not difficult to consolidate from the earlier learning around a framework into an express fuzzy guideline base. A Neuro-Fuzzy hypothesis brings the plans of ANN and FL together in a binding schema, such that the resultant model has structure for learning properties and is connected with a fuzzy tenet base about the produced information. Neuro-fuzzy frameworks join together the regular etymological/typical transparency of fuzzy frameworks with the provable learning and representation ability of the ANN weights. The combo of qualitative based thinking through fuzzy logic and quantitative versatile numeric/information handling by means of ANN, is a possibly compelling idea, since it permits inside a solitary schema clever qualitative and quantitative thinking is attained. Really savvy frameworks must make utilization of all accessible learning: numerical, master or heuristic standards and referred to practical connections, for example, physical laws. Neuro-fuzzy frameworks permit all these. There are two methodologies to fuzzy neural structural planning which are alluded to as neuro-driven and fuzzy driven. The neuro-driven methodology offers power to the neural side of the depiction. Fuzzy math is utilized as a method for enhancing neuronal and/or whole system conduct. Then again, in the fuzzy driven methodology, neural systems are utilized as auxiliary apparatuses either to focus participation capacities, or to change the set of standards adaptively.

3.4.2 Theoretical Background of ANFIS

If X is a superset of n multi-class predictor maps X_i (i = 1 to n), each containing m patterns, then the strength of x_{ij}, the j^{th} (j = 1 to m) pattern on the i^{th} predictor map X_i, as an indicator of a target mineral deposit-type can be estimated in terms of class score (cs_{ij}), which is defined as:

$$cs_{ij} = w_i \ x \ w_{ij} \quad \left(\forall x_{ij} \in X_i\right) \tag{3.12}$$

where w_i is the map weight of the i^{th} predictor map and w_{ij} is the class weight of the j^{th} pattern on the i^{th} predictor map. The procedure for assigning class weights and map weights is based on the class scores of predictor patterns, n fuzzy sets $\tilde{A}_i^1$ (i = 1 to n) in X, containing 'favorable indicators of target mineral deposit-type,' can be defined as:

$$\tilde{A}_i^1 = \left\{ \left(x_{ij}, \mu_{\tilde{A}_i^1}(x_{ij}) \right) \ \forall x_{ij} \in X_i \right\} \tag{3.13}$$

where the fuzzy membership function $\mu_{\tilde{A}} i^1$ for estimating the fuzzy membership value of x_{ij} in $\tilde{A}_i^1$ is defined as:

$$\mu_{\tilde{A}_i^1}(x_{ij}) = e^{\frac{-\left(cs_{ij}-c_{i1}\right)^2}{2\sigma_{i1}}} \quad (\forall xij \in X_i) \tag{3.14}$$

where c_{i1} (i = 1 to n) and σ_{i1} (i = 1 to n) are the parameters that, respectively, define the center and the spread of the Gaussian function and cs_{ij} is the class score of x_{ij}.

Similarly, n fuzzy sets $\tilde{A}_i^2$(i = 1 to n) in X, containing 'unfavorable indicators of target mineral deposit-type,' can be defined as follows:

$$\tilde{A}_i^2 = \left\{ \left(x_{ij}, \mu_{\tilde{A}_i^2}(x_{ij}) \right) \ \forall x_{ij} \in X_i \right\} \tag{3.15}$$

where the fuzzy membership function $\mu_{\tilde{A}_i^2}$ for estimating the fuzzy membership value of x_{ij} in $\tilde{A}_i^2$ is defined as:

$$\mu_{\tilde{A}_i^2}(x_{ij}) = e^{\frac{-\left(cs_{ij}-c_{i2}\right)^2}{2\sigma_{i2}}} \quad (\forall xij \in X_i) \tag{3.16}$$

where c_{i2} (i = 1 to n) and σ_{i2} (i = 1 to n) are the parameters that, respectively, define the center and the spread of the Gaussian function and cs_{ij} is the class score of x_{ij}.

In the context of a hybrid neuro-fuzzy model, each unique combination of spatially-coincident predictor patterns is considered a vector of predictor features (or a feature vector). Because each predictor map is represented by one, and only one, pattern in a feature vector, the number of components (or dimensions) of the feature vector is equal to the number of predictor maps. The favorability of a feature vector with respect to target mineral deposit-type is estimated as follows. Consider, for simplicity, a two-dimensional feature vector $T = [x_{1j}, x_{2j}]$, where x_{1j} and x_{2j} are the patterns representing, respectively, the predictor maps X_1 and X_2 in the feature vector. The membership values of x_{1j} in the fuzzy sets $\tilde{A}_i^1$ and $\tilde{A}_i^2$ are estimated using the fuzzy membership functions $\mu_{\tilde{A}_i^1}$ (3.14) and $\mu_{\tilde{A}_i^2}$ (3.16), respectively.

A typical fuzzy if-then rule in a generalized Takagi-Sugeno type fuzzy inference system has the following form:

$$\text{IF } x \text{ is } a \text{ AND } y \text{ is } b \text{ THEN } z = f(x, y)$$

where x and y are input variables, a and b are fuzzy membership values of x and y, respectively, in the antecedent part of the fuzzy if-then rule and $z = f(x, y)$ is a crisp function in the consequent part of the rule. Usually, $f(x, y)$ is a polynomial in the input variables x and y, but it can be any function as long as it can appropriately describe the output of the system. When $f(x, y)$ is a first-order polynomial, the resulting fuzzy inference system is called a first-order Takagi-Sugeno type fuzzy inference system, which was originally proposed by Takagi and Sugeno. When $f(x, y)$ is a constant, the resulting fuzzy inference system is called a zero-order Takagi-Sugeno type fuzzy inference system. The higher the order of the polynomial functions, in a fuzzy inference system, the larger is the number of the function parameters and, consequently, the larger is the number of training samples required for a robust estimation of these parameters. Therefore, the order of a fuzzy inference system used in an application is largely determined by the number of available training samples. In the case of the feature vector T, there are two input predictor patterns, x_{1j} and x_{2j}, and four membership functions, $\mu_{\tilde{A}_1^1}$, $\mu_{\tilde{A}_1^2}$, $\mu_{\tilde{A}_2^1}$ and $\mu_{\tilde{A}_2^2}$, which can be combined using a first-order Takagi-Sugeno type fuzzy inference system based on the following fuzzy if-then rules:

1. IF x_{1j} is $\mu_{\tilde{A}_1^1}(x_{1j})$ AND x_{2j} is $\mu_{\tilde{A}_2^1}(x_{2j})$ THEN $F_1 = P_{10} + P_{11}x_{1j} + P_{12}x_{2j}$
2. IF x_{1j} is $\mu_{\tilde{A}_1^1}(x_{1j})$ AND x_{2j} is $\mu_{\tilde{A}_2^2}(x_{2j})$ THEN $F_2 = P_{20} + P_{21}x_{1j} + P_{22}x_{2j}$
3. IF x_{1j} is $\mu_{\tilde{A}_2^1}(x_{1j})$ AND x_{2j} is $\mu_{\tilde{A}_2^1}(x_{2j})$ THEN $F_3 = P_{30} + P_{31}x_{1j} + P_{32}x_{2j}$
4. IF x_{1j} is $\mu_{\tilde{A}_1^2}(x_{1j})$ AND x_{2j} is $\mu_{\tilde{A}_2^2}(x_{2j})$ THEN $F_4 = P_{40} + P_{41}x_{1j} + P_{42}x_{2j}$

where P_{ki} (k = 1 to 4, i = 0 to 2) is the parameter of the polynomial function in the consequent part of the k^{th} fuzzy if-then rule. The above fuzzy inference system is characterized by four fuzzy if-then rules, each of which contains, in the consequent part, a first-order polynomial function characterized by three parameters. Therefore, a first-order Takagi- Sugeno type fuzzy inference system with two input predictor maps and two fuzzy membership functions for each map results in $2^2(=4)$ fuzzy if-then rules and $2^2(2+1)(=12)$ function parameters. In general, a first-order Takagi- Sugeno type fuzzy inference system with n predictor maps and 2^n fuzzy membership functions contains 2^n fuzzy if-then rules and $2^n(n+1)$ function parameters.

Even for a moderately-large n, robust estimation of the function parameters would require a large number of training samples of known mineral deposits, which may not always be available. In such cases, it is preferable to use a zero-order Takagi-Sugeno type fuzzy inference system, which, in the case of the feature vector T, comprises the following fuzzy if-then rules:

1. IF x_{1j} is $\mu_{\tilde{A}_1^1}(x_{1j})$ AND x_{2j} is $\mu_{\tilde{A}_2^1}(x_{2j})$ THEN $F_1 = P_1$
2. IF x_{1j} is $\mu_{\tilde{A}_1^1}(x_{1j})$ AND x_{2j} is $\mu_{\tilde{A}_2^2}(x_{2j})$ THEN $F_2 = P_2$
3. IF x_{1j} is $\mu_{\tilde{A}_2^1}(x_{1j})$ AND x_{2j} is $\mu_{\tilde{A}_2^1}(x_{2j})$ THEN $F_3 = P_3$
4. IF x_{1j} is $\mu_{\tilde{A}_1^2}(x_{1j})$ AND x_{2j} is $\mu_{\tilde{A}_2^2}(x_{2j})$ THEN $F_4 = P_4$

where P_k (k = 1 to 4) is the parameter of the constant function in the consequent part of the k^{th} fuzzy if-the rule. The number of function parameters is reduced to $2^2(=4)$ for the zero-order Takagi-Sugeno fuzzy inference system from $2^2(2+1)(=12)$ for the first-order Takagi-Sugeno fuzzy inference system. In general, a zero-order Takagi-Sugeno type fuzzy inference system with n predictor maps and 2^n fuzzy membership functions contains 2^n fuzzy if-then rules and 2^n function parameters. The firing strengths s_i (i = 1 to 4) of the above fuzzy if-then rules are calculated using prod t-norm operator as follows:

$$\begin{aligned} s_1 &= \mu_{\tilde{A}_1^1}\left(x_{1j}\right) \times \mu_{\tilde{A}_2^1}\left(x_{2j}\right) \\ s_2 &= \mu_{\tilde{A}_1^1}\left(x_{1j}\right) \times \mu_{\tilde{A}_2^2}\left(x_{2j}\right) \\ s_3 &= \mu_{\tilde{A}_1^2}\left(x_{1j}\right) \times \mu_{\tilde{A}_2^1}\left(x_{2j}\right) \\ s_4 &= \mu_{\tilde{A}_2^1}\left(x_{1j}\right) \times \mu_{\tilde{A}_2^2}\left(x_{2j}\right) \end{aligned} \tag{3.17}$$

As a matter of fact, other t-norm operators that perform generalized AND can also be used for combining the fuzzy membership values in order to determine the firing strengths of the fuzzy if-then rules. The output, O_k, of the k^{th} (k = 1 to 4) fuzzy if-then rule is:

$$O_k = s_k.F_k \tag{3.18}$$

where F_k *(k = 1 to 4)* is the value of the function in the consequent part of the k^{th} fuzzy if-then rule. The overall output of the fuzzy inference system is the weighted average of the output of all the four fuzzy if-then rules:

$$Overall\ output = \frac{\sum_{k=1}^{4} O_k}{\sum_{k=1}^{4} s_k} \tag{3.19}$$

The overall output is a measure of combined favorability of the feature vector T with respect to a target mineral deposit-type. The above procedure can be easily extended for estimating the favorability of a feature vector comprising more than two predictor maps. In a simple Takagi-Sugeno type fuzzy inference system, the parameters of fuzzy membership functions and consequent polynomial functions are estimated heuristically. However, in a hybrid neuro-fuzzy model, an ANFIS is used for estimating these parameters.

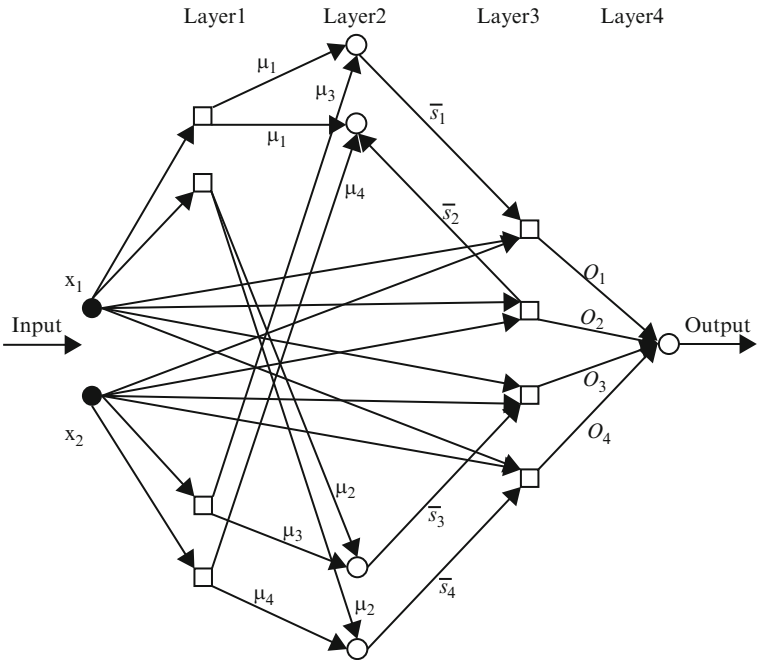


Fig. 3.20 Simplified ANFIS for mineral potential mapping. Square and circular nodes contain, respectively, adaptive and fixed functions

3.4.3 Architecture of Adaptive Neuro-Fuzzy Inference System

The fundamental construction modeling of an ANFIS embodies a Takagi-Sugeno sort fuzzy deduction framework in a five-layer food forward system. Figure 3.20 demonstrates the rearranged four-layer ANFIS structural engineering utilized within a crossover neuro fuzzy model for mineral potential mapping. The essential usefulness of each one layer is outlined in the accompanying sections.

3.4.3.1 Layer 1

There are 2^n (=the number of fuzzy sets defined in the superset X) nodes in this layer. One half of the nodes (=n) contain the adaptive Gaussian fuzzy membership function defined in (3.14), each of which receives one component (a predictor pattern x_{ij} encoded as a class score cs_{ij}) of an incoming n-dimensional feature vector and returns its membership value in the fuzzy set $\tilde{A}_i^1$(i = 1 to n) containing 'favorable indicators of target mineral deposit type'. The other half of the nodes (=n) contain the adaptive Gaussian fuzzy membership function defined in (3.16), each of which also receives one component of the incoming feature vector and

returns its membership value in the fuzzy set $\tilde{A}_i^2$ (i = 1 to n) containing 'unfavorable indicators of target mineral deposit-type'.

The parameters c and σ, which control the shape of a node function, and therefore output fuzzy membership values, are referred to as premise parameters.

3.4.3.2 Layer 2

Each of the 2^n (=the number of fuzzy if-then rules) nodes in this layer contains a prod t-norm operator as a node function, which synthesizes information transmitted by Layer 1 and returns a firing strength for each of the fuzzy if-then rules:

$$s_k = \mu_{\tilde{A}_1^q}(x_{1j}) \;\; x \;\; \mu_{\tilde{A}_2^q}(x_{2j}) \;\; x.....x \;\; \mu_{\tilde{A}_n^q}(x_{nj}) \tag{3.20}$$

where q = 1 or 2, depending on whether $\mu_{\tilde{A}_1^q}$ defines fuzzy membership value of x_{ij} in the fuzzy set $\tilde{A}_i^1$ or in the fuzzy set $\tilde{A}_i^2$ (i = 1 to n). The output of each node is the normalized firing strength $\overline{s}_k$(k = 1 to 2^n) of the k^{th} fuzzy if-then rule given by:

$$\overline{s}_k = \frac{s_k}{\sum_{k=1}^{2^n} s_k} \tag{3.21}$$

3.4.3.3 Layer 3

Each of the 2^n (=the number of fuzzy if-then rules) nodes in this layer, contains the following adaptive function:

$$O_k = s_k.F_k = s_k\left(P_{k0} + P_{k1}x_{1j} + P_{k2}x_{2j} + ... + P_{kn}x_{nj}\right) \tag{3.22}$$

where O_k is the output of the k^{th} fuzzy if-then rule. The parameters P_{ki} (k = 1 to 2^n, i = 0 to n) are referred to as consequent parameters. In the case of a zero-order Takagi-Sugeno type fuzzy inference system, $F_k = P_{k0}$.

3.4.3.4 Layer 4

The single node in this layer synthesizes information transmitted by Layer 3 and returns the overall output using the following fixed function:

$$Overall\ Output = \sum_{k=1}^{2^n} O_k \tag{3.23}$$

3.4.4 Hybrid Learning Algorithm

Assuming that an ANFIS has two input variables, x_1 and x_2, the overall output is (based on 3.22 and 3.23):

$$\begin{aligned} O_1 + O_2 &= \overline{s}_1(P_{10} + P_{11}x_1 + P_{12}x_2) + \overline{s}_2(P_{20} + P_{21}x_1 + P_{22}x_2) \\ &= \overline{s}_1 P_{10} + \overline{s}_1 x_1 P_{11} + \overline{s}_1 x_2 P_{12} + \overline{s}_2 P_{20} + \overline{s}_2 x_2 P_{21} + \overline{s}_2 x_2 P_{22} \end{aligned} \tag{3.24}$$

which is linear in the consequent parameters P_{ki}, if the premise parameters and, therefore, the firing strengths s_k of the fuzzy if-then rules are fixed. ANFIS uses a hybrid learning procedure for estimation of the premise and consequent parameters. The hybrid learning procedure estimates the consequent parameters (keeping the premise parameters fixed) in a forward pass and the premise parameters (keeping the consequent parameters fixed) in a backward pass. In the forward pass, the information propagates forward until Layer 3 where the consequent parameters are estimated by the least square estimator method. In the backward pass, the error signals propagate backwards and the premise parameters are updated by a gradient descent method. The following description of the hybrid learning procedure is drawn from Jang and Sun.

3.4.4.1 Forward Pass: Least Square Estimator Method

For 2^n fuzzy if-then rules and Q n-dimensional training vectors (where n is the number of input predictor maps), (3.24) can be expressed as:

$$\mathrm{B} = AX \tag{3.25}$$

where B is a column vector containing output values of training vectors, A is matrix containing one row for each training vector and X is an unknown vector whose elements are the consequent parameters P_{ki}. As the number of consequent parameters is $2^n(n+1)(=M$, say), the dimensions of A, X and B are $Q \times M$, $M \times 1$ and $Q \times 1$, respectively.

A least square estimate of X, denoted by X*, can be used to minimize squared error $\|AX\text{-}B\|^2$. It can be computed as below:

$$X* = \left(A^T A\right)^{-1} A^T B \tag{3.26}$$

where A^T is the transpose of A and $(A^T A)^{-1} A^T$ is the pseudo-inverse of A, if $A^T A$ is non-singular. The above equation is expensive in computation when dealing with matrix inversion and, moreover, becomes ill defined if $A^T A$ is singular. ANFIS uses a recursive least-square method for estimating X as follows.

If a_q^T is the qth row vector of A and b_q^T is the qth element of B, then X can be calculated iteratively as follows:

$$X_{q+1} = X_q + \sum\nolimits_{q+1} a_{q+1}\left(b_{q+1}^T - a_{q+1}^T X_q\right) \tag{3.27}$$

$$\sum\nolimits_{q+1} = \sum_q - \frac{\sum_q a_{q+1} a_{q+1}^T \sum_q}{1 + a_{q+1}^T \sum_q a_{q+1}} \left(for\ q = 0, 1, \ldots\ldots\ldots\ldots.., Q-1\right) \tag{3.28}$$

where $\sum$ is called covariance matrix and the least square estimate X^* is equal to X_q. The initial conditions are $X_0 = 0$ and $\sum 0 = \gamma I$, where γ is a large positive number and I is an identity matrix of $M \times M$ dimensions.

3.4.4.2 Backward Pass: Back-Propagation Method

Premise parameters of ANFIS are estimated iteratively by using a modified back-propagation learning rule along with the chain rule as follows. In (3.25), if the estimated output of the qth row vector, a_q, of the matrix A is o_q and the actual output is b_q, the qth element of B, then an error margin for the q^{th} training vector a_q can be defined as:

$$E_q = \left(b_q - o_q\right)^2 \tag{3.29}$$

If E_q is zero, then the actual output exactly matches the estimated output. Thus, the objective is to minimize an overall error measure, which is defined as $\sum_{q=1}^{Q} E_q$, where Q is the total number of training vectors. In order to use the gradient descent method to minimize the error measure, a gradient vector is required to be calculated. It should be noted that a small change in the premise parameters (c or σ) will affect the output of the node containing the parameters, which, in turn, will affect the output of the single node in Layer 4 and, hence, the error measure will also change. Therefore in order to calculate the gradient vector of the parameters, a form of derivative information has to be passed, starting from Layer 4 and traveling back to Layer 1.

An error signal, $\varepsilon_{l,i}$, can be defined as the ordered derivative of the error measure E_q with respect to the output of node i in Layer l (l = 1 to 4) as follows

$$\varepsilon_{l,i} = \frac{\partial + E_q}{\partial o_{l,i}} \tag{3.30}$$

where $o_{l,i}$ is the output of the i^{th} node of Layer l. The error signal for the single output node of Layer 4 can be calculated as:

$$\varepsilon_4 = \frac{\partial + E_p}{\partial o_{(4,1)}} = \frac{\partial E_p}{\partial o_{(4,1)}} = -2\left(b_q - o_q\right) \tag{3.31}$$

For the i^{th} node of Layer $l(l = 1 \text{ to } 3)$, the error signal can be derived using the chain rule:

$$\varepsilon_{l,i} = \frac{\partial + E}{\partial o_{(l,i)}} = \sum_{m=1}^{N_{(l+1)}} \frac{\partial + E}{\partial o_{(l+1,m)}} \frac{\partial f_{(l+1,m)}}{\partial o_{(l,i)}} = \sum_{m=1}^{N_{(l+1)}} \varepsilon_{(l+1,m)} \frac{\partial f_{(l+1,m)}}{\partial o_{(l,i)}} \tag{3.32}$$

where $N_{(l+1)}$ is the number of nodes in Layer $(l+1)$, $o_{(l+1,m)}$ is the output of the m^{th} node in Layer $(l+1)$, $f_{(l+1,m)}$ is the nodal function of the m^{th} node in Layer $(l+1)$, $o(l,i)$ is the output of the i^{th} node in Layer l and $\varepsilon(l+1,m)$ is the error signal at the mth node of Layer $(l+1)$. In other words, the error signal of an internal node at Layer l can be expressed as a linear combination of the error signal of the nodes at Layer $(l+1)$. Therefore, for the ith node of Layer 1, the error signal, ε (1,i), can be obtained by first applying (3.31) once to get error signals at the Layer 4 and then applying (3.32) iteratively until Layer 1 is reached.

Because the consequent parameters are fixed in the backward pass, the gradient vector is defined as the derivative of the error measure with respect to each of the two premise parameters, c and ε, which reside in the nodes of Layer 1. The chain rule is applied to determine the gradient vectors as follows:

$$\frac{\partial^+ E_p}{\partial c_i} = \frac{\partial^+ E_p}{\partial o_{(1,i)}} \frac{\partial^+ \mu_{1,i}}{\partial c_i} = \varepsilon_{(1,i)} \frac{\partial^+ \mu_{(1,i)}}{\partial c_i} \tag{3.33}$$

and

$$\frac{\partial^+ E_p}{\partial \sigma_i} = \frac{\partial^+ E_p}{\partial o_{(1,i)}} \frac{\partial^+ \mu_{1,i}}{\partial \sigma_i} = \varepsilon_{(1,i)} \frac{\partial^+ \mu_{(1,i)}}{\partial \sigma_i} \tag{3.34}$$

In the above equations c_i and σ_i are, respectively, center and spread of the Gaussian membership function $\mu_{(1,i)}$ in the i^{th} node of layer 1.

The derivative of the overall error measure E with respect to c_i is:

$$\frac{\partial^+ E}{\partial c_i} = \sum_{q=1}^{Q} \frac{\partial^+ E_q}{\partial c_i} = \sum_{q=1}^{Q} \varepsilon_{(1,i)} \frac{\partial^+ \mu_{(1,i)}}{\partial c_i} \tag{3.35}$$

where Q is the total number of training vectors. The update expression for the parameter c_i is given by:

$$\Delta c_i = -\eta \frac{\partial^+ E}{\partial c_i} \tag{3.36}$$

where η is the learning rate, which can be expressed as follows:

$$\eta = \frac{\kappa}{\sqrt{\sum_{i=1}^{N(1)} \left(\frac{\partial E}{\partial c}\right)^2}} \tag{3.37}$$

where $N(1)$ is the total number of nodes in Layer 1 and κ is the step size or the length of each transition along the gradient direction in the parameter space. Similarly, the derivative of the overall error measure E with respect to σ_i is:

$$\frac{\partial^+ E}{\partial \sigma_i} = \sum_{q=1}^{Q} \frac{\partial^+ E_q}{\partial \sigma_i} = \sum_{q=1}^{Q} \varepsilon_{(1,i)} \frac{\partial^+ \mu_{(1,i)}}{\partial \sigma_i} \tag{3.38}$$

where Q is the total number of training vectors. The update expression for the parameter σ_i is given by:

$$\Delta \sigma_i = -\eta \frac{\partial^+ E}{\partial \sigma_i} \tag{3.39}$$

where η is the learning rate, which can be expressed as follows:

$$\eta = \frac{\kappa}{\sqrt{\sum_{i=1}^{N(1)} \left(\frac{\partial E}{\partial \sigma}\right)^2}} \tag{3.40}$$

where $N(1)$ is the total number of nodes in Layer 1 and κ is the step size or the length of each transition along the gradient direction in the parameter space.

The above learning procedures were implemented using the software and procedure described by Jang and Gulley.

3.4.5 *Neuro-Fuzzy Network Model and Calculation Algorithm*

Fuzzy logic methodology is utilized to figure out the greatest force purpose of PV cells. Fitting decision of the parameters and thorough acceptance of decision are

involved to fulfill a faultless representation. In the event of critical levels of missed perceptions, the choice of the sort and estimations of the parameters of participation is not simple. In these circumstances, determination is focused around the qualities of information/yield information. By using neuro-fuzzy methods it is conceivable to learn data about the information set so that the parameters of the enrollment capacities are processed in such a path, to the point that the related fuzzy inference framework maps the given info/yield information legitimately. ANFIS frameworks join together the coherent impact force of fuzzy frameworks and the numerical force of neural systems. The connected ANFIS display for this situation is a first request Takagi-Sugeno model. The first stage is a direct synthesis of data variables in addition to a steady term and the last yield is the weighted normal of each one guideline's yield.

ANFIS utilizes a half breed learning calculation to distinguish subsequent parameters of Sugeno sort fuzzy induction frameworks. It applies a synthesis of the minimum squares technique and Back-propagation system for preparing fuzzy surmising framework enrollment capacities parameters to imitate a given set.

This method of Neuro-fuzzy system owes much from the feed forward neural network with supervised learning capability. Figure 3.21 shows the fuzzy inference system while Fig. 3.22 shows the equivalent ANFIS system.

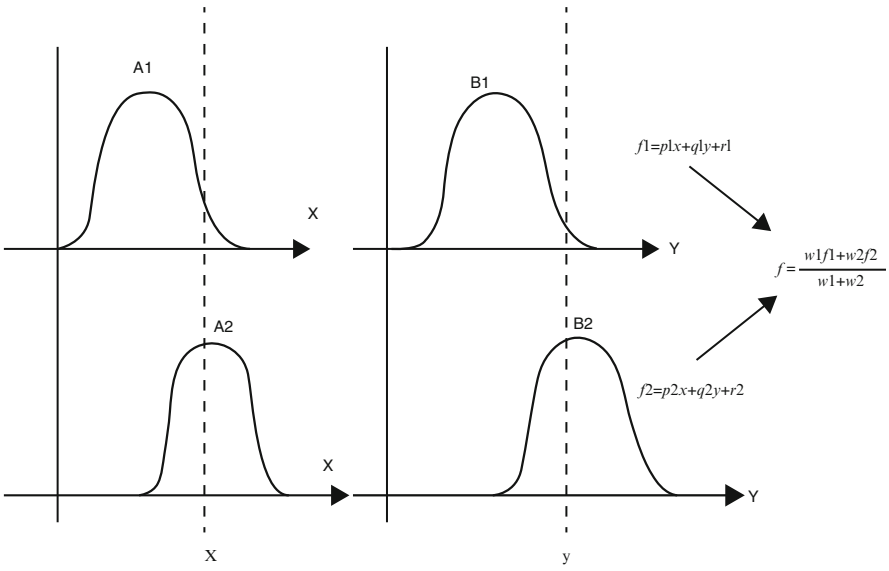


Fig. 3.21 Fuzzy inference system

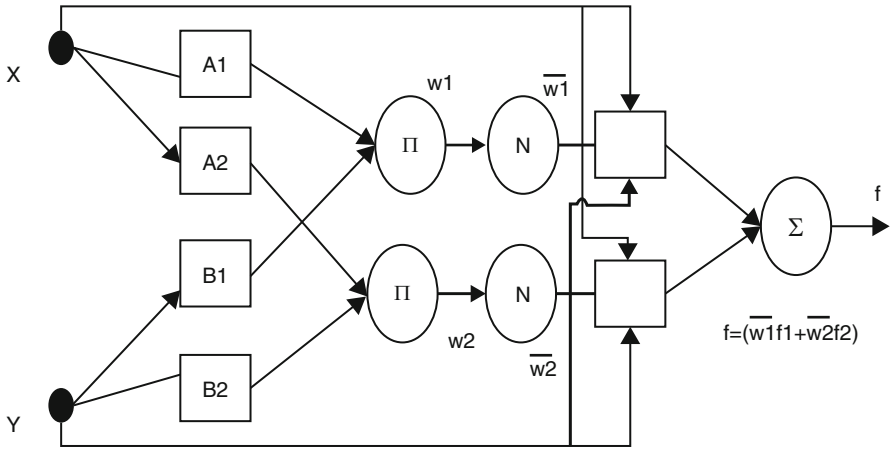


Fig. 3.22 ANFIS equivalent system

3.4.6 ANFIS Network Specifications

- Inputs: Insolation (G), Temperature (T).
- Output: Maximum power point Voltage.
- Number of Membership functions:

  Three (3) for Insolation
  Three (3) for Temperature

- Number of Rules: 9 (Sugeno FIS).

3.4.7 Algorithm for Neuro-Fuzzy Based MPPT

Step 1: Fuzzification Step (Input Step) in the first layer:

The ANFIS architecture is shown in Fig. 3.23. This layer is a fundamental fuzzification layer where the crisp inputs are apportioned to relative fuzzy qualities. The membership functions are bell shaped. The output of the first layer ith membership function is computed as:

$$O_i^1 = \mu A_i(G) = e^{\left\{-\left(\frac{x-c_i}{a_i}\right)^2\right\}^{b_i}} \tag{3.41}$$

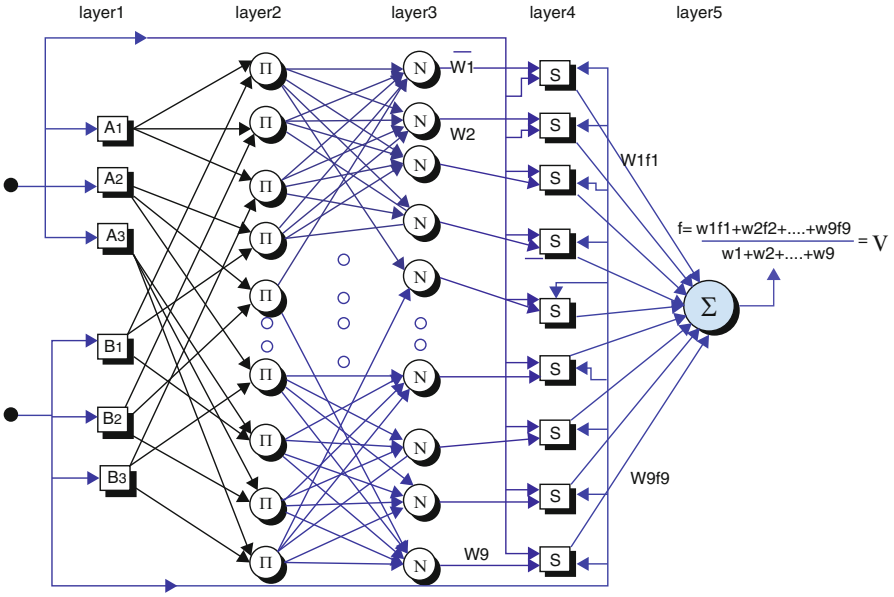


Fig. 3.23 ANFIS architecture for the system implemented

$$O_i^1 = \mu B_i(T) = e^{\left\{-\left(\frac{y-c_i}{a_i}\right)^2\right\}^{b_i}} \tag{3.42}$$

where O_i^1 is the output of the first layer, G is the insolation and T is the temperature (crisp values) for this application. A_i and B_i are linguistic variables characterized by appropriate membership functions, $\{a_i, b_i, c_i\}$ are the premise parameters described from the characteristics of bell shaped function. These premise parameters are fixed in the forward pass and are updated in the adaptation process by gradient descent method in the backward pass.

Step 2: Calculation of rules (or) generalization of firing strengths in the second layer:

The degree to which a piece of fuzzy rule is fulfilled and it shapes the respective output function is known as the firing strength. The intelligent administrator is the logical AND operator which is connected to acquire the output for every defined rule. The product inference principle is utilized at fuzzification level to yield values at this level. The yields at this hub are named as a consequence of increase of inputs from the layer one hubs.

$$O_i^2 = W_i = \mu A_i(G) \times \mu B_i(T) \tag{3.43}$$

where i = 1,2,. . .9

The value of node output represents the strength of the rule.

Step 3: Calculation of the ratio of firing strengths in the third layer.

The nodes in this layer are represented by circular nodes labeled N. The main objective of this step is to calculate the ratio of each ith rule's firing strength to the sum of all rule's firing strength, which is also called as normalized firing strength with the output O_i^3 at this step.

$$O_i^3 = \overline{W_i} = \left\{ \frac{W_i}{\sum_i W_i} \right\} \text{ where } i = 1, 2, \ldots., 9 \tag{3.44}$$

Step 4: Contribution of each rule: The fourth layer

Calculation of the contribution of each ith rule towards the total output O_i^4 is formed at this step.

$$O_i^4 = \overline{W_i}(p_i T + q_i G + r_i) \text{ where } i = 1, 2, \ldots 9 \tag{3.45}$$

where W_i is the output of layer 3 and $\{p_i,q_i,r_i\}$ are consequent parameters which are updated on forward pass by least square estimates and are fixed in backward pass. This layer establishes the relation between weight based premise parameters and linear summation based consequent part of the adapted ANFIS structure.

Step 5: Summation Step (Defuzzification Step) in the fifth layer:

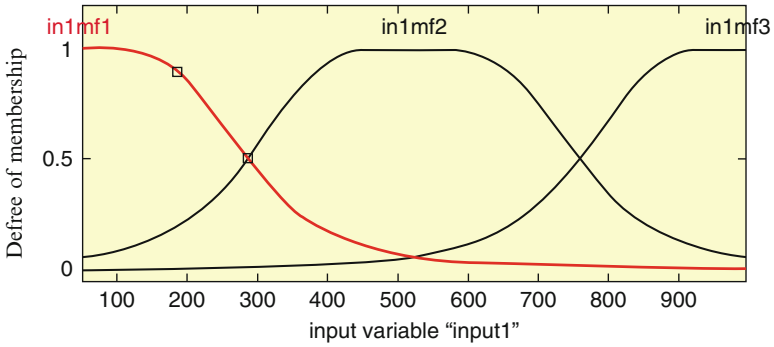
Each rule's fuzzy results are transformed into a crisp output O_i^5 at this step. The single output node in this layer sums up all the outputs of the previous layer as the output of ANFIS in this case is the maximum power point voltage of the PV cells.

$$K_p = \sum_i \overline{W_i} f_i = \sum_i \left\{ \frac{W_i f_i}{W_i} \right\} \text{ where } i = 1, 2, \ldots 9 \tag{3.46}$$

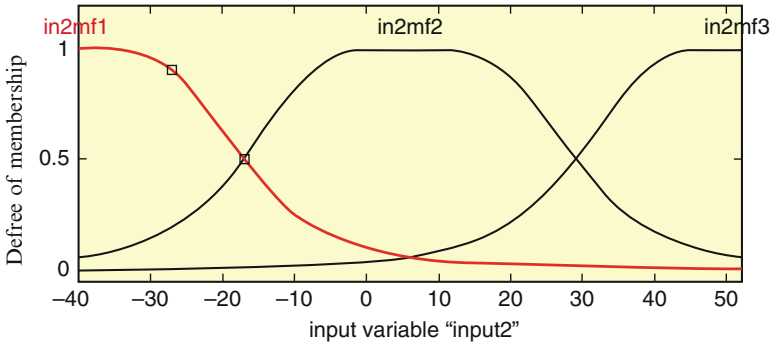
3.4.8 *Results for Neuro-Fuzzy Based MPPT*

3.4.8.1 Network Training

A set of 25 training patterns was presented to the network, while another set of nine points were randomly chosen as the testing data points which were not utilized for training . These training patterns were uniformly distributed to cover all the typical input space in order to get good performance where temperature ranges from −40 °C to 50 °C and solar irradiation ranged from 0 to 1,000 W/m^2. The implementation of Neuro-Fuzzy based MPPT for maximum power point tracking using MATLAB is done. Initial Memberships of the temperature T and Irradiation G are shown in Fig. 3.24 while Fig. 3.25 presents the final membership functions after ANFIS training. Figure 3.27 presents the ANFIS architecture obtained.



Original membership function for irradiation



Original membership function of temperature

Fig. 3.24 Original memberships of T and G before training

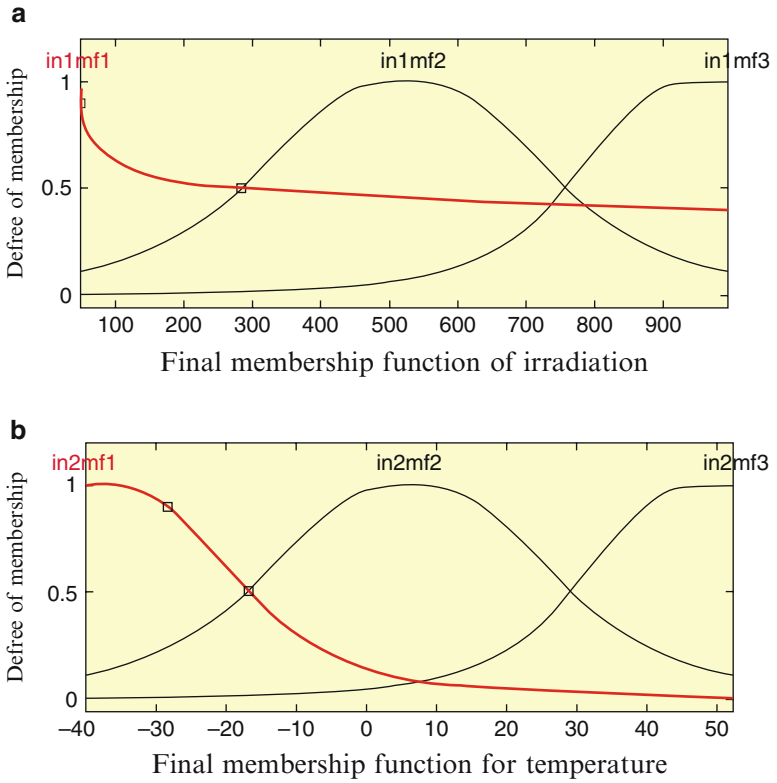


Fig. 3.25 Final memberships of T and G after training

3.4.8.2 Training Data for Neuro-Fuzzy Controller

1)	900	10	16.16
2)	830	35	8.75
3)	910	12	16.39
4)	850	50	20.36
5)	920	13	16.57
6)	600	52	20
7)	770	47	19.9
8)	700	42	19.9
9)	950	23.75	17.7
10)	980	24.5	17.89
11)	985	24.62	17.8
12)	995	24.87	18
13)	180	30	13.51

(continued)

14)	220	40	16.77
15)	825	20.6	17.1
16)	925	18	17.4
17)	940	20	17.68
18)	930	23	17.7
19)	650	16	16
20)	955	23.87	17.7
21)	960	24	17.8
22)	970	24.25	17.9
23)	975	24.37	17.8
24)	100	−40	7.8995
25)	100	0	11.74

3.4.8.3 Root Mean Square Error

Root mean square error evaluates the magnitude of deviations between the measured values and actual predictions.

$$RMSE = \left[\sum_{i=1}^{n} \frac{(m_i - z_i)^2}{n}\right]^{0.5} \tag{3.47}$$

where m_i – measurements, z_i – model outputs and N – number of observations.

3.4.8.4 Validation of the Model

The accuracy of the model is tested using a set of data different from training and the ANFIS controller gives accurate results and is able to closely mimic the actual values. The original and final membership functions of T and G are shown in Figs. 3.24 and 3.25 respectively. The RMSE of the training data with respect to training epoch is shown in Fig. 3.26. The ANFIS model with insolation and temperature as inputs and voltage as output is shown in Fig. 3.27. The accuracy of the obtained model is validated using testing data. Figure 3.28 show the variations of *VPP* (*V*) for various insolation and temperature conditions. The obtained model designed and trained has shown a very fast convergence with little number of memberships.

Table 3.4 summarizes the Neuro-Fuzzy controller output values for various insolation and temperature conditions.

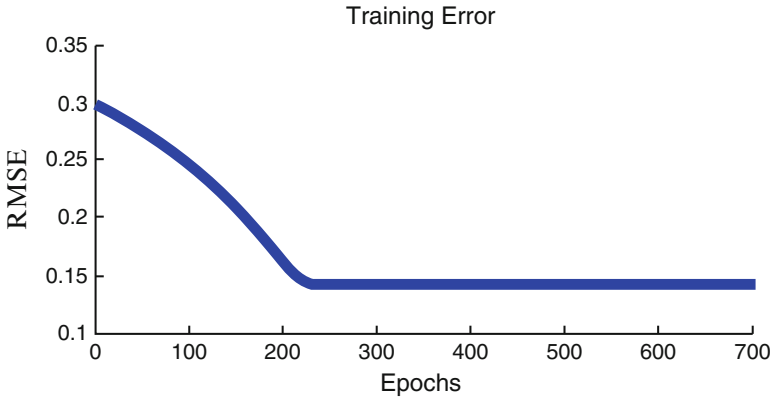


Fig. 3.26 RMSE of the training data with respect to training epoch

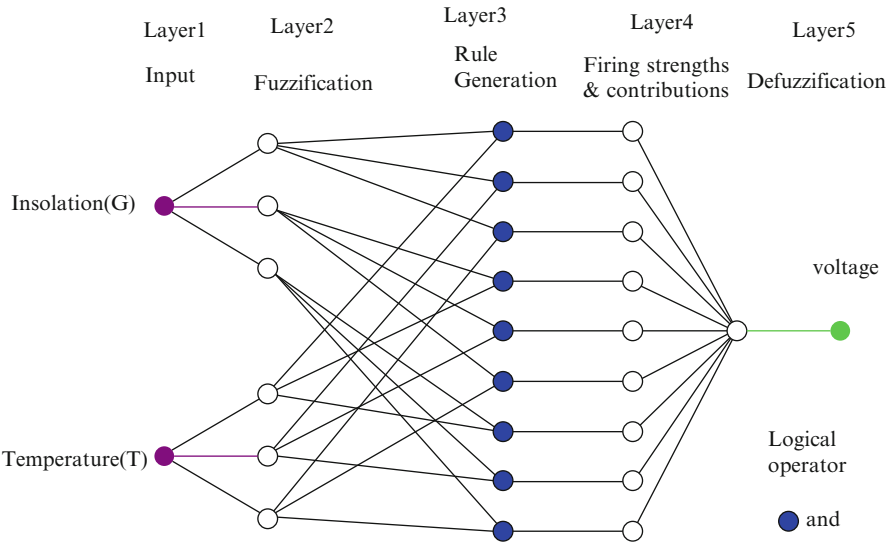


Fig. 3.27 ANFIS architecture

3.5 Fuzzy Based Solar Tracking

A solar tracking system is configured to optimize the functioning of solar energy receiving system. If solar receivers are installed appropriately with a tracking system, then additional solar energy can be accumulated throughout the day. In this section, a solar tracking system is simulated by applying MATLAB/SIMULINK and a fuzzy logic control is developed for the control of this system. The combination of the generated controller with the solar tracking system is realized with the fuzzy logic controller in the MATLAB/SIMULINK environment.

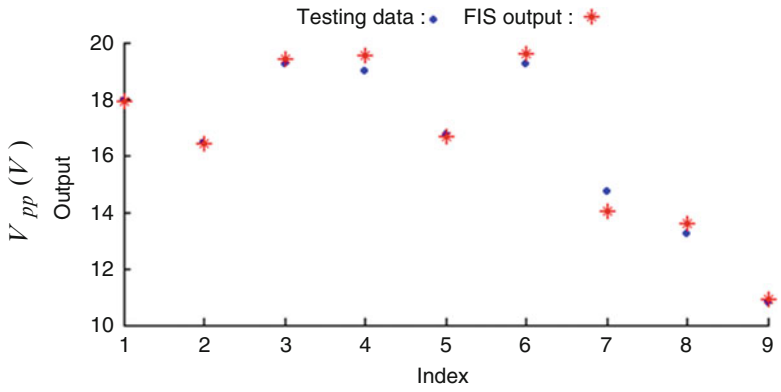


Fig. 3.28 Vpp plotted for various values of insolation and temperature

Table 3.4 Output of neuro-fuzzy controller

Insolation (W/m^2)	Temperature (°C)	Maximum power tracked by neuro-fuzzy controller
1,000	25	59.91
930	12	51.45
700	40	45.45
500	46	32.091
950	15	53.7
820	40	53.46
200	20	9.74
100	−10	3.48

Concurrently, PI control is implemented to the system and the solutions found using the PI control are compared with those obtained using fuzzy logic.

In order to obtain optimal efficiency, solar panels ought to be orthogonal according to the sunlight where the illumination is heaviest. Nevertheless, as the focus of sunlight shifts naturally throughout the day, and from season to season, a superior solar tracking system that performs better can maximize utilization of the panels. This scheme is comprised of two permanent magnet DC (PMDC) motors, two directional light detecting circuits and two amplifiers to drive the motors. The two drive motors are uncoupled, i.e. the rotation angle of one motor does not influence that of the other motor, therefore reducing control problems. Such kind of implementation minimizes the power consumption of the system during its operation thus increasing the efficiency and the total quantity of electricity yielded. The light detecting circuit of design comprises of four light sensitive devices, namely LDR, photodiodes or phototransistors, mounted on the solar panel and placed in an enclosure. The quadruplet light detectors are blocked out form one another by opaque surfaces. The sensing elements are designed in a sense that LDR1 and LDR2 are accustomed to track the sun horizontally, meantime LDR3 and LDR4 allow tracking the sun vertically. As one experiences more light than the

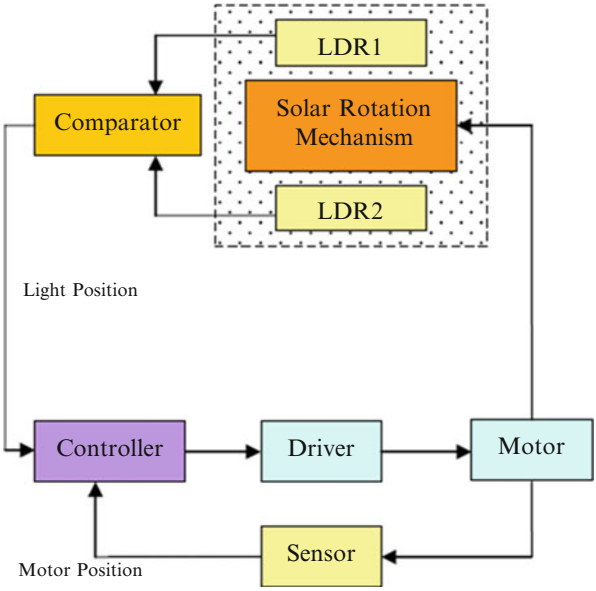


Fig. 3.29 Solar tracking control architecture for one direction (vertical or horizontal)

other, the panel is not coordinated properly and therefore an error voltage occurs. The error voltage is used as a command to an amplifier circuit to drive the motor and align the panel to be orthogonal to the light beam. In Fig. 3.29, the architecture of unidirectional solar tracking control is shown.

Photo Detecting Circuit and Amplifier

The photo detecting circuit and amplifier supply an electrical thrust to the motor which is proportional to the rotational misalignment of the panels to the light source. The photo detecting circuit and amplifier can be considered as a single variable K, where K is proportionality constant with units of volts per radian. The value of K constitutes the gain of the "photo detector" circuit and the "gain adjust" circuit.

Permanent Magnet DC Motor

Two permanent magnet DC (PMDC motors) are used to actuate the solar panel. The design of a PMDC motor for MATLAB/SIMULINK GUI Environment is discussed in this section. The PMDC motors are applicable in a wide range of low-power applications in which the field winding is a permanent magnet. Some of the benefits of PMDC are: they don't require external excitation, they require less space and they are cheaper. The equivalent circuit of PMDC motor is shown in Fig. 3.30 and the equations governing the model are given by (3.48, 3.49, 3.50, and 3.51). The MATLAB/SIMULINK model for PMDC motor is shown in Fig. 3.31.

The motor winding is a resistor connected in series with an inductor. When the motor has a nonzero speed, there is back emf voltage generated. The back emf voltage is proportional to the speed. According to Kirchoff's Voltage Law:

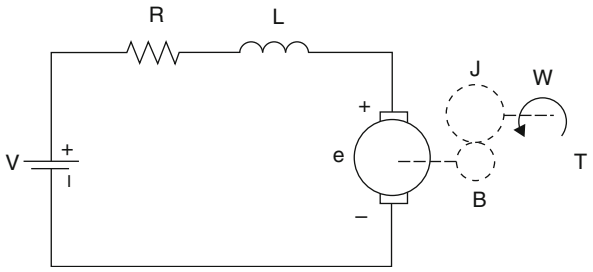


Fig. 3.30 Equivalent circuit of a PMDC motor

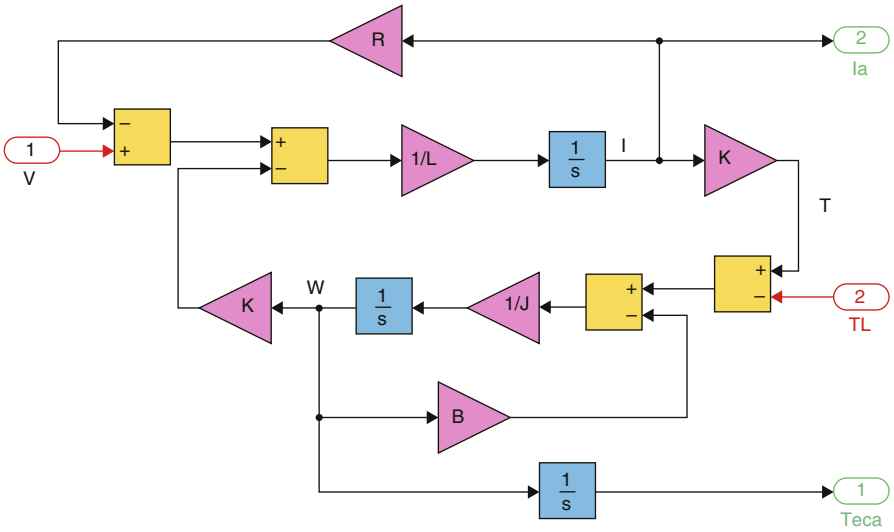


Fig. 3.31 MATLAB/SIMULINK model for PMDC motor

$$V(t) = R \cdot i(t) + L \cdot \frac{di(t)}{dt} + E(t) \tag{3.48}$$

where V is the voltage applied to the motor and

$$E(t) = K \cdot \omega(t) \tag{3.49}$$

The torque generated by the motor is proportional to the current. According to Newton's second law (rotational version):

$$T(t) - T_f(t) - T_L(t) = J \cdot \frac{d\omega(t)}{dt} \tag{3.50}$$

where T_L is the load torque and

$$T(t) = K \cdot i(t) \; and \; T_f(t) = B \cdot \omega(t) \tag{3.51}$$

Equations 3.48 and 3.50 describe the dynamic behaviour of the motor. Equations 3.48, 3.49, 3.50, and 3.51 can be re-arranged as in (3.52) and (3.53) for construction of the block diagram.

$$\frac{di(t)}{dt} = \frac{1}{L} \cdot (V(t) - R \cdot i(t) - K \cdot \omega(t)) \tag{3.52}$$

$$\frac{d\omega(t)}{dt} = \frac{1}{J} \cdot (K \cdot i(t) - T_L(t) - B \cdot \omega(t)) \tag{3.53}$$

Differential equations (3.52) and (3.53) for armature current and angular speed can be arranged as state space equations in (3.54).

$$\begin{bmatrix} \dot{i}(t) \\ \dot{\omega}(t) \end{bmatrix} = \begin{bmatrix} -\frac{R}{L} & -\frac{K}{L} \\ \frac{K}{J} & -\frac{B}{J} \end{bmatrix} \cdot \begin{bmatrix} i(t) \\ \omega(t) \end{bmatrix} + \begin{bmatrix} \frac{1}{L} & 0 \\ 0 & -\frac{1}{J} \end{bmatrix} \cdot \begin{bmatrix} V(t) \\ T_L(t) \end{bmatrix} \tag{3.54}$$

3.5.1 *Design Process of the Fuzzy Controller*

For most investigations performed so far, a fuzzy controller system is frequently thought of which emulates an individual pro. However, the feeling of the individual driver can be put in the type of a set of fuzzed lingual policies. These kinds of principles would green goods an approximate decision the identical way a human could complete. The structural plan of the fuzzy logic technique is shown in Fig. 3.32 with the design mechanism.

The fuzzified control comprises the subsequent four aspects. These include fuzzification, rule base, inference system along with defuzzification. Some sort of fuzzification program changes the particular highly detailed crisp inputs into the fuzzified values which have been framed in the rule base so that the user can execute these associated principles making sure that an output may be generated. Any principle base is made up of rule base including details related to the device. The inference process emulates throughout interpretation as well as making use of know-how about computers and how to manage the levels. A defuzzification interface converts the findings with the inference procedure into curt advices with the practice. The particular ideals regarding problem (e(k)) as well as alter (Δe(k)) transpiring through the surgery on the program form the fresh inputs of the method.

$$e(k) = r(k) - y(k) \tag{3.55}$$

$$\Delta e(k) = e(k) - e(k-1) \tag{3.56}$$

r(k), y(k) and k are expressed as the reference input, the actual output of the system and the sampling step respectively. The design of FLC in the MATLAB/

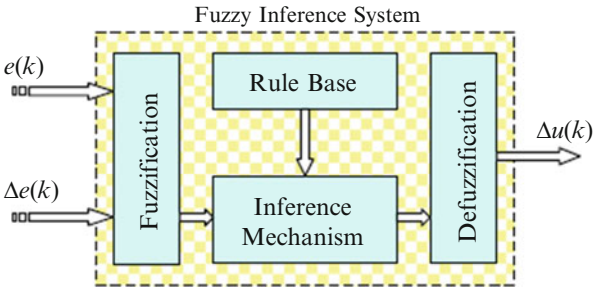


Fig. 3.32 The basic structure of fuzzy logic based controller

SIMULINK environment is discussed following the expressions. The basic elements of the FLC are the fuzzy membership functions which are available in the modeling of the controller. In several applications, different types of membership functions such as triangle, trapezoid, bell, Gaussian, sigmoid and sinusoid are used. The approach used to design FLC in this section uses triangular membership function given the following equation (10).

$$\mu(x) = \max\left[\min\left(\frac{x - x_1}{x_2 - x_1}, \frac{x_3 - x}{x_3 - x_2}\right), 0\right] \tag{3.57}$$

3.5.2 SIMULINK Model

Figure 3.33 shows the SIMULINK model of the triangular fuzzy membership function where x_1, x_2, and x_3 are the crisp values which in turn define the location and shape of the triangle. The input x is the crisp variable whose membership value on this triangle fuzzy subset is the output mu(x).

The crisp inputs e(k) and Δe(k) are converted to fuzzy membership values on the fuzzy subsets NB, NS, ZZ, PS and PB. The fuzzy inference mechanism has the structure as in verbal expression (3.58).

$$\textit{If}\ \text{e is A}\ \textit{and}\ \Delta\text{e is B}\ \textit{then}\ \Delta\text{u is}\ C. \tag{3.58}$$

In the general rule, parameters A, B and C in (3.58) denote any one of the fuzzy subsets NB, NS, ZZ, PS and PB. The input space in (3.58) is the part that represented by the expression (e is A ***and*** Δe is B). The connector "and" represents the Boolean operator "min". The weight coefficient required for each rule is determined by using the Boolean operator "min" (min(μA(x), μB(x))). Therefore, the membership values of each variable in the output space are obtained. The process of fuzzification with 9 rules with respect to the input is shown in Fig. 3.34.

These weight coefficients which are shown as mu1, mu2, . . ., mu9 are multiplied by the crisp values of each corresponding fuzzy subset in the output space Δu.

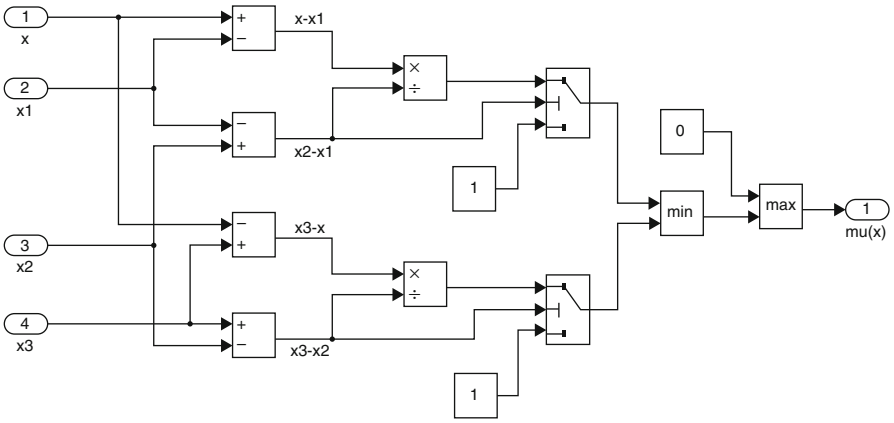


Fig. 3.33 SIMULINK model of the triangular fuzzy membership function

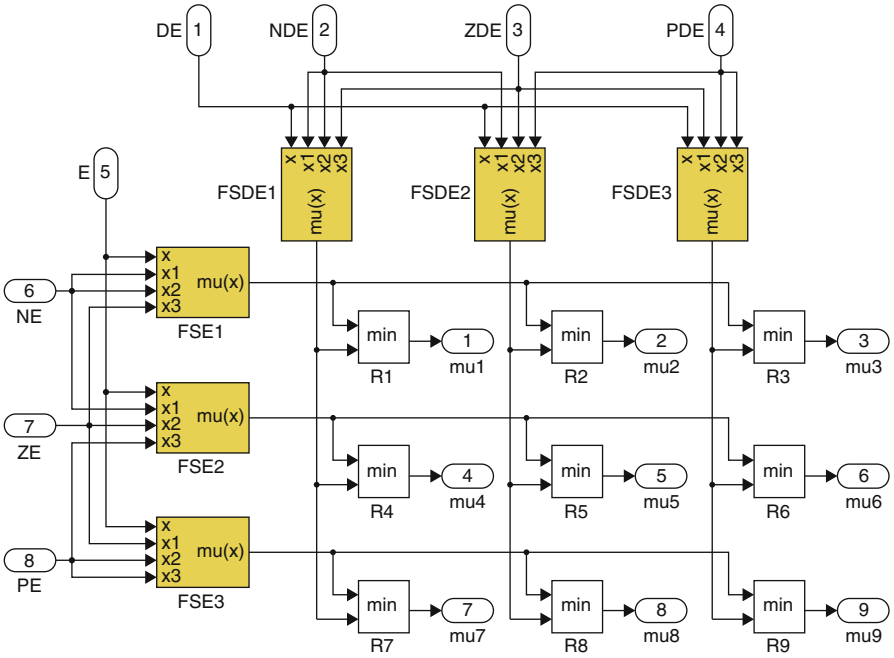


Fig. 3.34 The SIMULINK model of the verbal expression

These crisp values indicate the peak locations of the triangular fuzzy subsets. This multiplication process represents the products in the denominator of defuzzification method called the centre of area. Then the sum of these products is divided by the sum of membership values obtained as in Fig. 3.35.

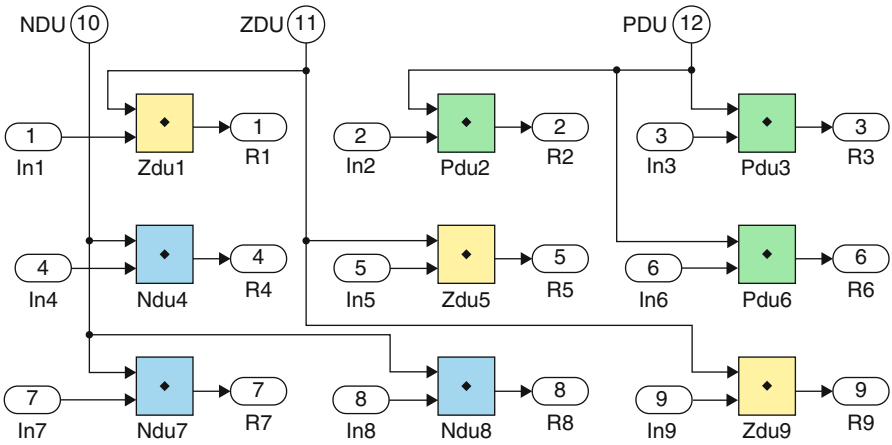


Fig. 3.35 The SIMULINK model of the fuzzy rules

Though different types of defuzzification methods are applied, the most commonly used in fuzzy logic control applications is the center of area method. The center of area method is given the following equation (3.59).

$$\Delta U(k) = \frac{\sum_{i=1}^{n} \mu_i(\Delta u_i) \cdot \Delta u_i}{\sum_{i=1}^{n} \mu_i(\Delta u_i)} \tag{3.59}$$

ΔU(k) is the final crisp output. The center of area method as shown in (3.59) is implemented in MATLAB/SIMULINK. A general overlooked view of the FLC is given in Fig. 3.36 where the processes from inputs e and Δe to output Δu are shown. The input data blocks to represent fuzzy membership functions for the error e, error change Δe and the controlled output change Δu are shown in Fig. 3.37. The user is able to edit and change the parameters of the membership functions on this stage without going into the detail of the FLC.

3.5.3 Simulation Results of Solar Tracking System

The model of solar tracking system is simulated using both FLC and PI controllers for comparison and validation purposes using MATLAB/SIMULINK models. The proportional gain (K_P) set to 1.55 and the integral gain (K_I) set to 0.02. Figure 3.38 shows the MATLAB/SIMULINK model of the developed system.

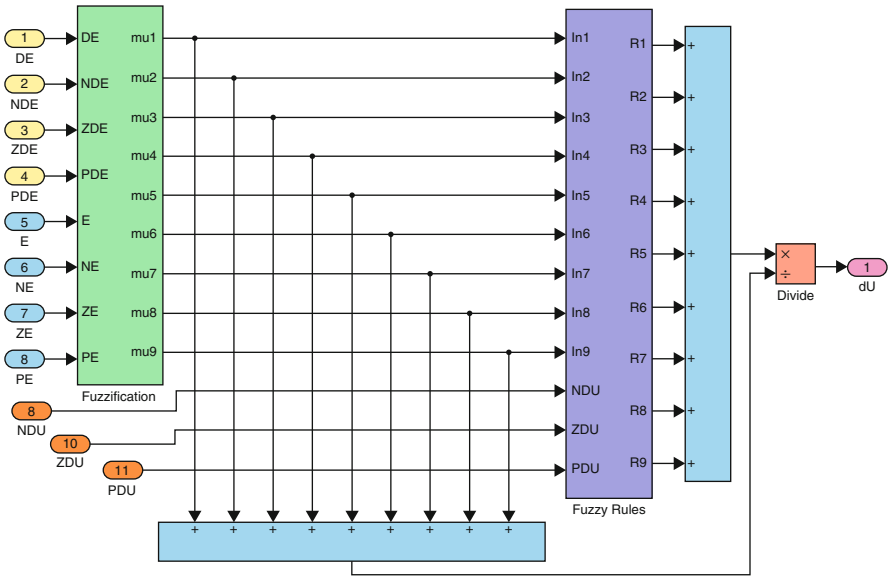


Fig. 3.36 Fuzzy reasoning representing the process from fuzzification to defuzzification

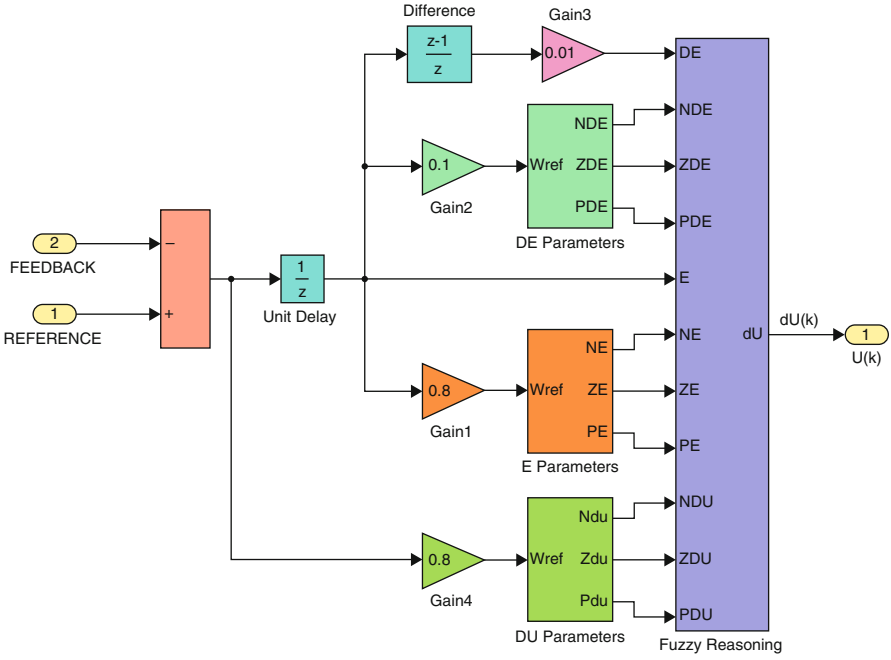


Fig. 3.37 The input and output units of the FLC

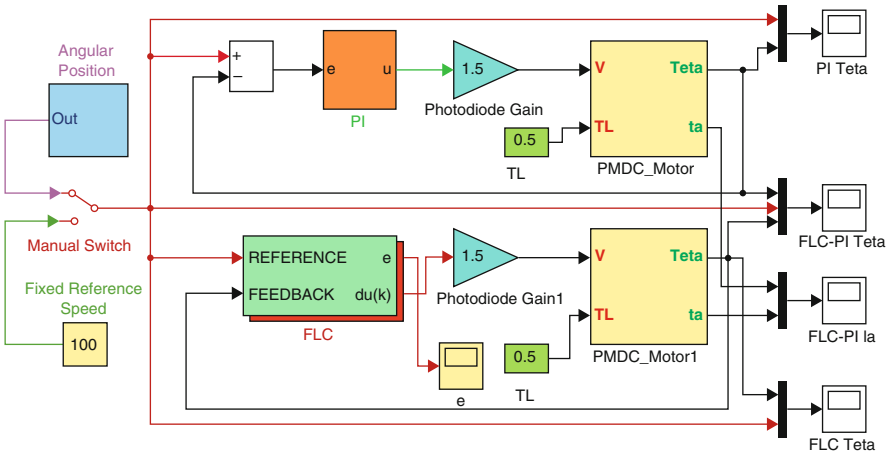


Fig. 3.38 MATLAB/SIMULINK model for the solar tracking system

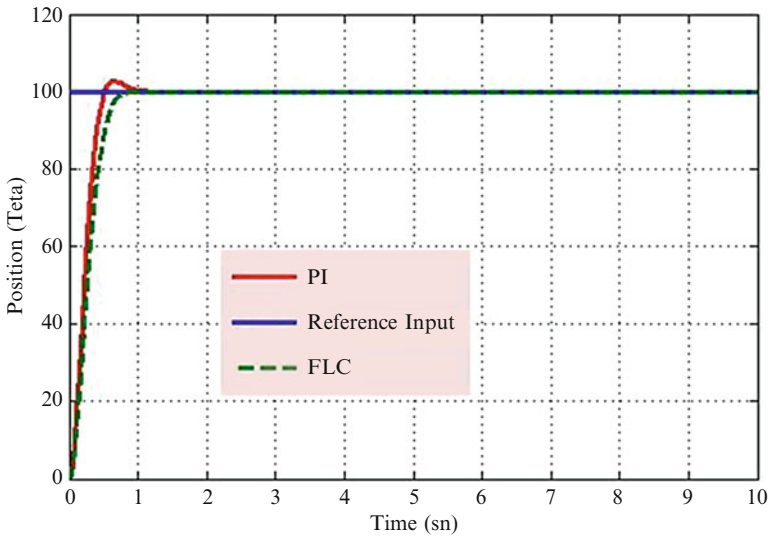


Fig. 3.39 The output of the system for FL and PI controllers

Figure 3.39 shows the system responses for FL and PI controllers. Comparatively, it is noted that the FLC gives faster response and less overshoot than PI controller.

Figure 3.40 shows the change of the error in fixed reference input for FL controller. It is observed that the error falls to zero quickly when compared with the reference input.

According to variable angular position applied to the system, the system responses from both FL and PI controllers are shown in Fig. 3.41.

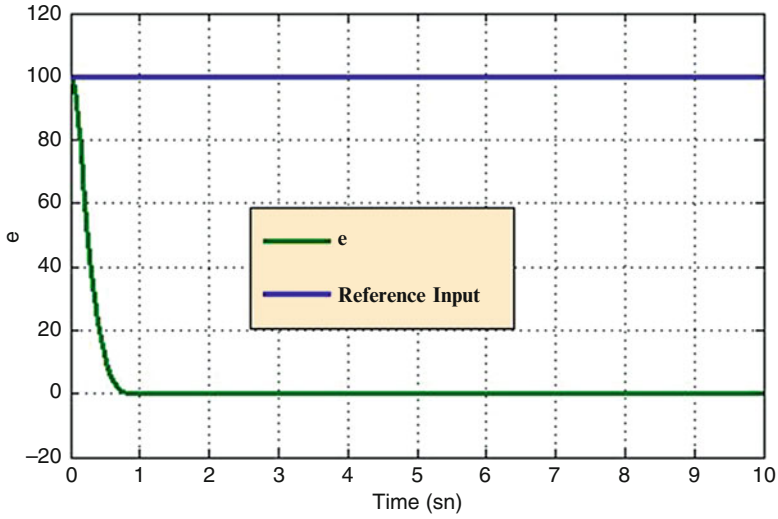


Fig. 3.40 The change of the error in fixed reference input for FL controller

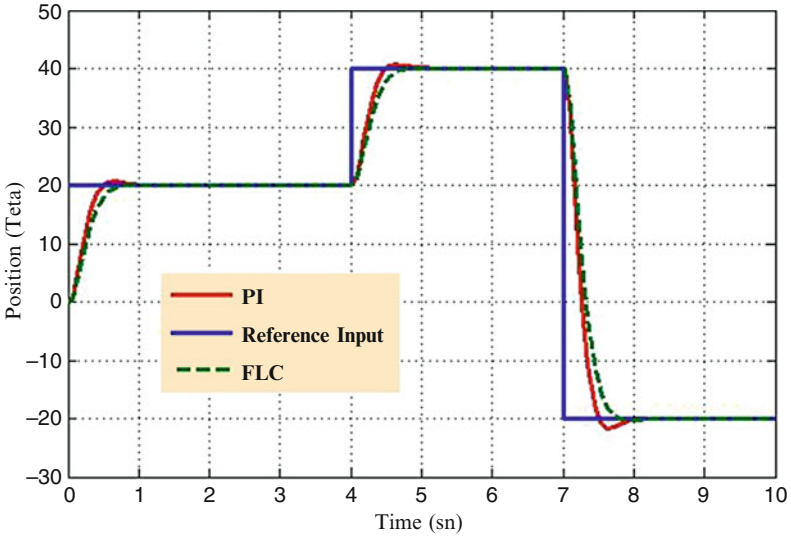


Fig. 3.41 The outputs of the system from both FL and PI controller for variable angular position

Although there are some differences during the transient period of position, both controllers follow variable reference input. The position response from FLC seems to be slower than that of obtained with PI when step changes occur in reference position input level. If a load of 0.5 N is applied to the motor shaft, the system responses from both FL and PI controllers for variable reference input are shown in Fig. 3.42.

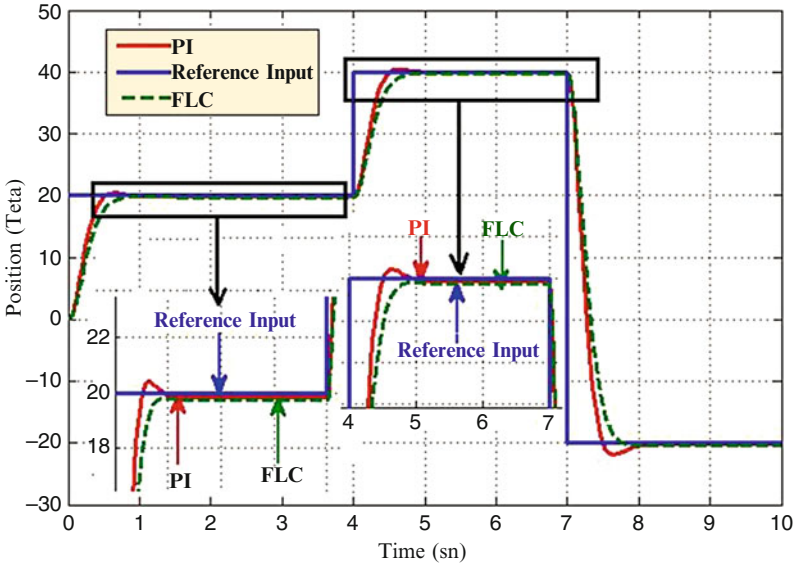


Fig. 3.42 The output of the system from both controllers for a load of 5 N

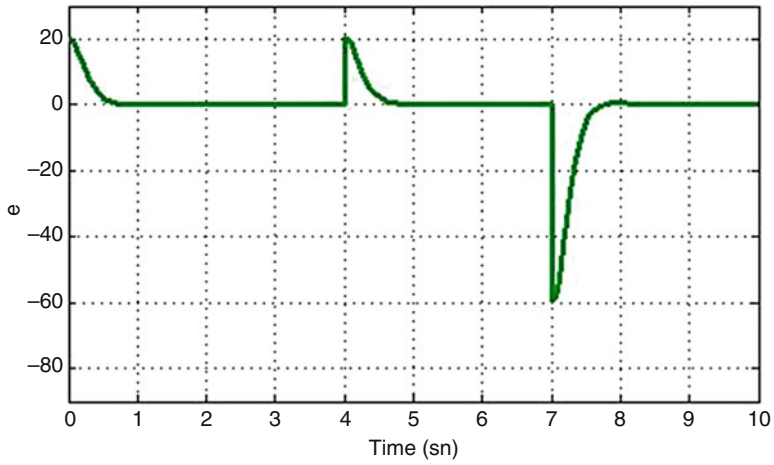


Fig. 3.43 The change of the error in variable reference input for FL controller

It is seen from Fig. 3.42 that when a load is applied to the motor shaft, FLC gives better results than PI controller. Because, in Fig. 3.42, PI controller is occurred overshoot more than FLC but PI controller has less steady-state error. As the load applied to the motor shaft increases, the error of the system also increases. The change of the error in variable reference input for FL controller is shown in Fig. 3.43.

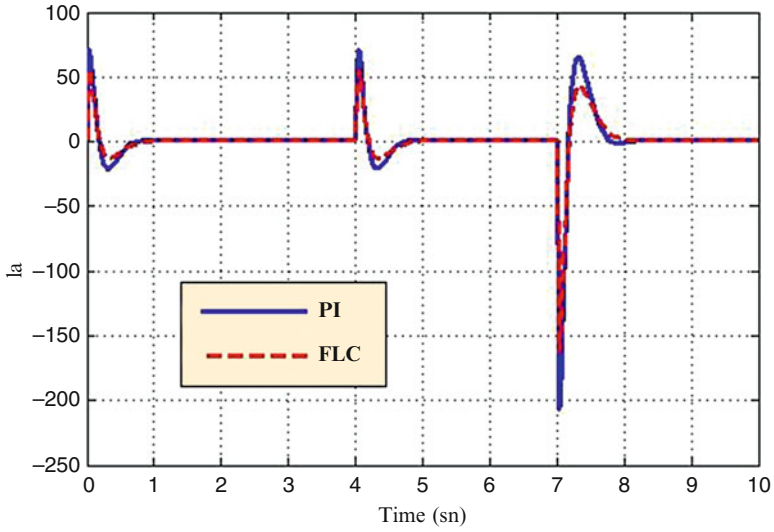


Fig. 3.44 The motor current from both controllers for a load of 5 N

However, each controller gives different current responses during the transients. As depicted in Fig. 3.44, the current has less ripple magnitudes during the transients with FLC than it has with the PI controller. In this section, a solar tracking system was designed for MATLAB/SIMULINK environment and a control method was developed for this system. The results from the FLC are compared with those obtained using PI controller. The results from simulations showed good and acceptable performances for the FLC. It was observed that both FLC and PI have almost the same settling time but the FLC show less overshoot. The most important advantage of this control has less ripple magnitudes during the transient. Practically obtained results show that using such controller increases speed of the time response.

3.6 MATLAB/SIMULINK Model of Two Axis Sun Tracker Using Fuzzy Logic

In this section, a two axis solar tracking system which uses two stepper motors as the drive source to rotate the solar panel is delineated. The basic structural model is shown in Fig. 3.45. The positioning of the sunlight is ascertained by applying a tracking sensor, the sensor interpretation is changed from analog to digital signal, and then it is passed to a fuzzy logic controller implemented on PIC microcontroller. The output of the FLC is linked to the driver of the stepper motor to rotate PV panel in one axis until it faces the sun.

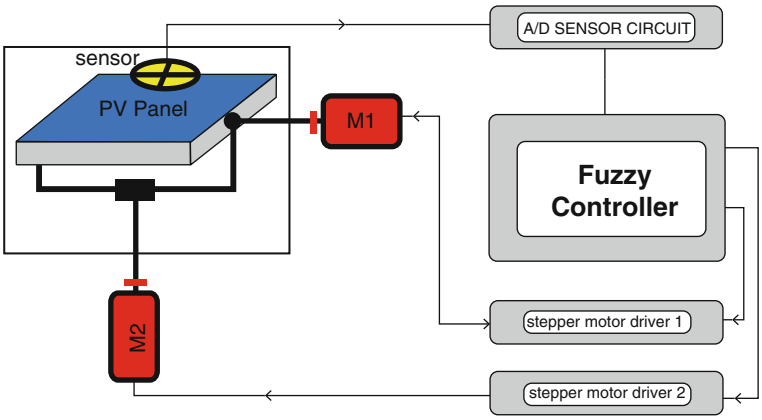


Fig. 3.45 Block diagram for the sun tracker system

3.6.1 Sensors

The solar tracking system discussed in this section uses two sensors namely the photo sensor and the position sensor.

3.6.1.1 Photo Sensor

Light dependent resistors (LDR) are applied to fabricate the sensor, since they are the most authentic sensor that can be exploited for light detection. LDR is fundamentally a resistor whose electric resistance changes based on the intensity of light, hence more intensity leads to less resistance. Several LDR sensors can be obtained in the market. The largest size is applied to fabricate the sensor since larger the area of the sensor leads to larger sensitivity or lesser the time taken for output to change according to the changes in the input.

3.6.1.2 Tracking Sensor Design

The tracking sensor is composed of four LDR sensors, which are located based on directions such as east, west, south, and north to detect the light source intensity. The LDR sensor casts a 45° angle based on the light source. In the LDR sensor positions, brackets are available to insulate the brightness from extra orientations to attain a wide-angle search and promptly decide the sun's positioning.

To sense the positioning of sun in one axis say east/west, two LDR sensors are mounted on the solar panel and placed in an enclosing. The response of this approach is similar to that of a human eye. The LDR sensors in east and west directions compare the intensity of received light. Based on the changes in the sun's

position, here the light source intensity level accepted by the sensors is dissimilar; the system gets signals from the sensors' output voltage in the two orientations. The system then ascertains the level of intensity received by the sensor based on the sensor yield voltage measure represented by voltage type A/D converter. Thus the system drives the stepper motor towards the orientation of this sensor. When the output measures of the two sensors are equal, the difference yielded at the output is zero and the motor's drive voltage is zero, which implies that the system has tracked the current position of the sun.

3.6.1.3 Position Sensor

Position sensors are accustomed to find out the location of the PV panel, thus preventing the panel from the shock while it arrives at the edges, and to get the PV panel to the beginning point at the night. This sensor employed a varying resistor (potentiometer) placed with the rotor of the motor and rotates with it, and the value of the resistor (R) changes with the rotary motion as shown in Fig. 3.46. While the position sensor achieves the measures at the PV at the edges, the controller blocked off the motor and exempt it from rotating in this direction. During night the LDRs sensors' measures are very large. In such a position the controller goes to night procedure to rotate the PV panel until the position sensor attains the starting point value.

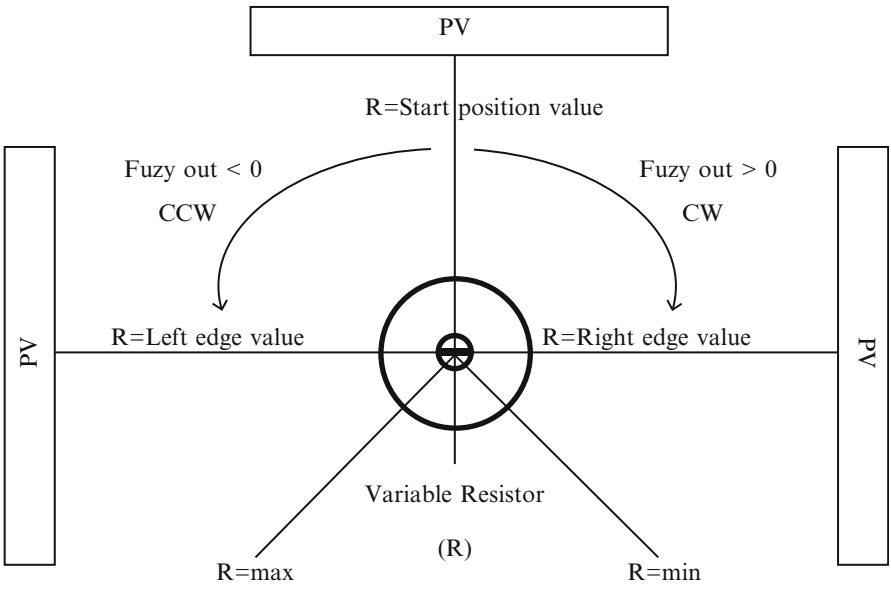


Fig. 3.46 Position sensor

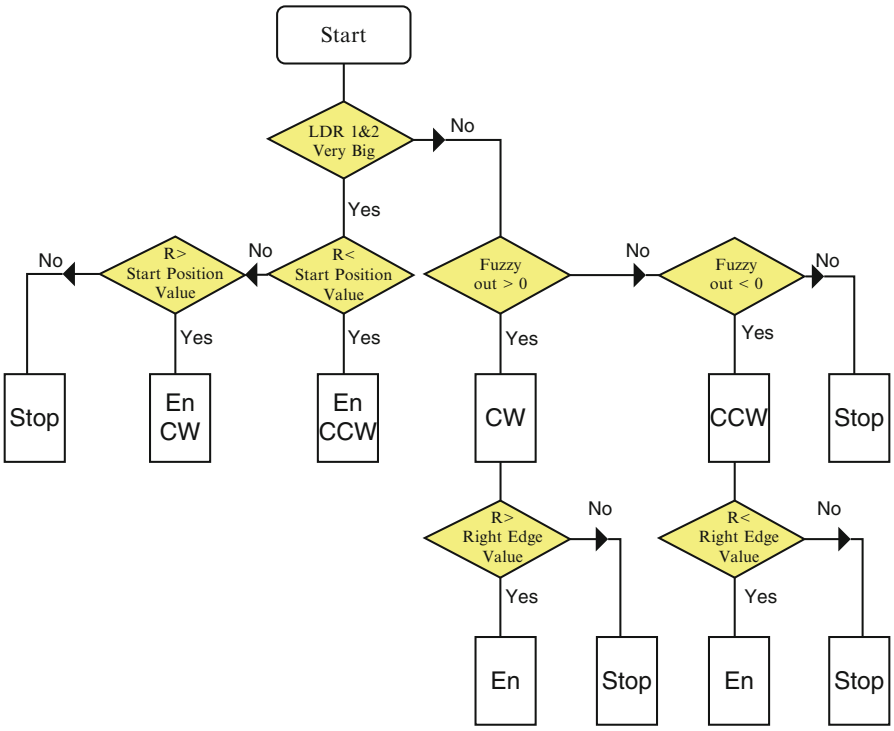


Fig. 3.47 Motor control signals algorithm

The algorithm for extracting the motor control signals based on the reading obtained from the sensors and the output of the controller is shown in Fig. 3.47. Here, R is the value of the position sensor, and En is the enable signal to rotate the motor.

3.6.2 Design of FLC for Sun Tracking System

Figure 3.48 shows the block diagram of the FLC for the sun tracker system.

3.6.2.1 FLC Design

The two inputs to the FLC are: error and the change in error. Only one output is used which feed the stepper motor driver. Though Mamdani and Sugeno approaches are applied for FLCs, in this section Mamdani based model is used to construct the fuzzy controller. The FLC contains three basic parts: Fuzzification, Base rule, and Defuzzification.

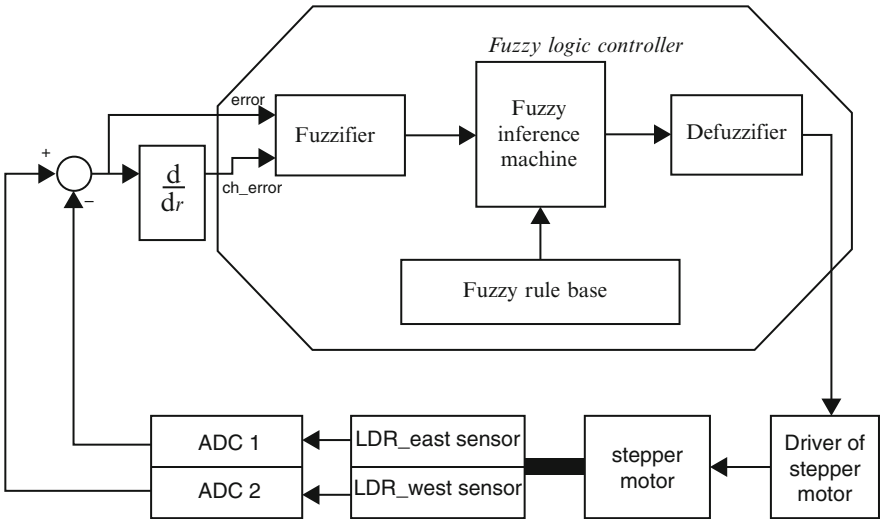


Fig. 3.48 FLC controller for the sun tracker system

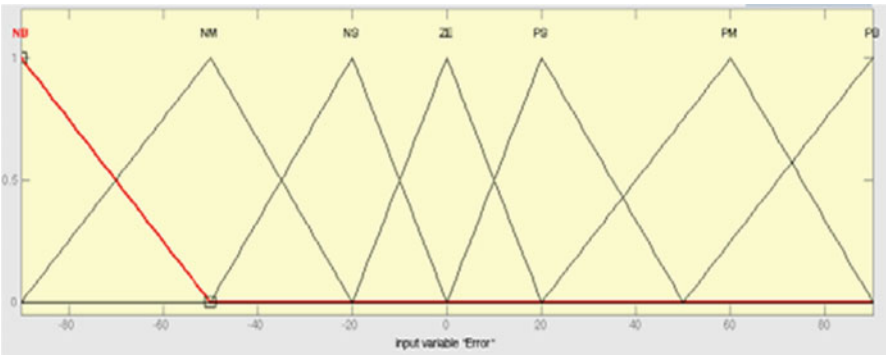


Fig. 3.49 Error fuzzy set of FLC

3.6.2.2 Fuzzification

Figure 3.49 illustrates the fuzzy set of the Error input which contains seven Triangular memberships.

Figure 3.50 illustrates the fuzzy set of the Change of Error input which contains seven Triangular memberships.

Figure 3.51 illustrates the fuzzy set of the output which contains seven Triangular memberships.

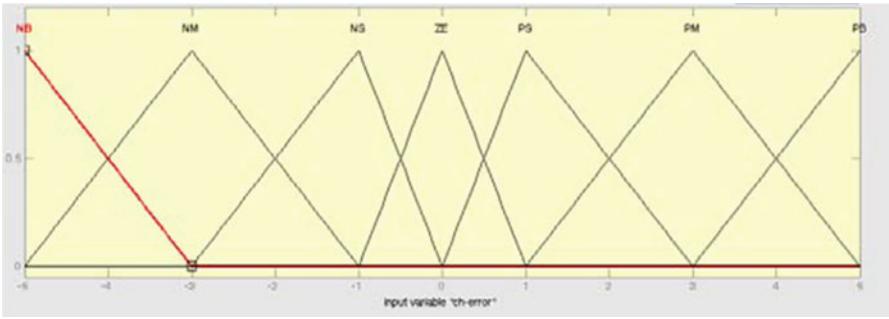


Fig. 3.50 Change in error fuzzy set of FLC

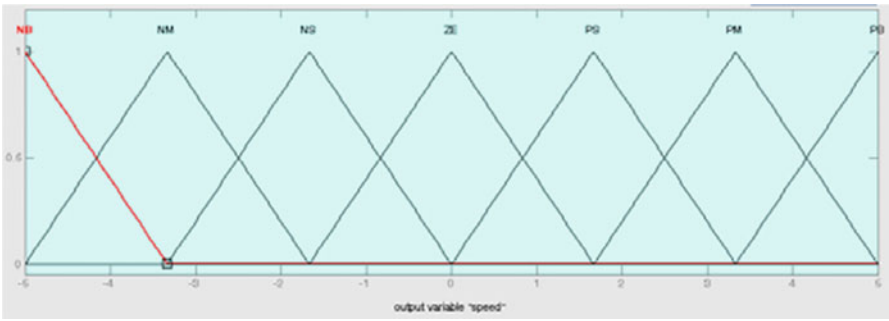


Fig. 3.51 Fuzzy set of FLC output entering to stepper motor driver

Table 3.5 Control rule base for fuzzy controller

	CE						
Er	NB	NM	NS	ZE	PS	PM	PB
NB	NB	NB	NB	NB	NM	NS	ZE
NM	NB	NB	NM	NM	NS	ZE	PS
NS	NB	NM	NS	NS	ZE	PS	PM
ZE	NB	NM	NS	ZE	PS	PM	PB
PS	NM	NS	ZE	PS	PS	PM	PB
PM	NS	ZE	PS	PM	PM	PB	PB
PB	ZE	PS	PM	PB	PB	PB	PB

3.6.2.3 Control Rule Base

The knowledge base is defined by the rules for the desired relationship between the input and output variables in terms of the membership functions illustrated in Table 3.5. The control rules are evaluated by an inference mechanism, and represented as a set of:

IF Error is . . . and Change of Error is . . . THEN the output will . . ..

For example: Rule 1: IF Error is NS and Change of Error is ZE THEN the output is NS.

The linguistic variables used are:

NB: Negative Big.
NM: Negative Medium.
NS: Negative Small.
ZE: Zero.
PS: Positive Small.
PM: Positive Medium.
PB: Positive Big.

3.6.2.4 Defuzzification

The centre of gravity method is widely used in Mamdani approach which has been selected in this section to compute the output of the FLC, which is the motor speed as:

$$Speed = \frac{\sum_{i=1}^{n} S_i \cdot \mu(S_i)}{\sum_{i=1}^{n} \mu(S_i)} \tag{3.60}$$

3.6.3 SIMULINK Model and Results of FLC Based Sun Tracker System

Figure 3.52 illustrates the SIMULINK block diagram for the Fuzzy controller for sun tracker system.

The controller has been tested using SIMULINK motor module in MATLAB, by applying the step input and initial degree of the rotor is -10°. The output step response is shown in Fig. 3.53. The range from -10 to 0° takes five steps since each step in our motor is 1.8°, so $(10/1.8) = 5$ steps.

3.7 FLC for Solar Powered Energy

Solar powered electric schemes comprise of several components to be controlled individually. As the generated power is a function based on varying environmental factors, it demands additional care to design controllers that deal with such unpredictable issues and sustain effective load matching power. Here, a photovoltaic (PV) solar array model is designed using MATLAB/SIMULINK GUI environment and controlled using a fuzzy logic controller (FLC), which is also designed in the GUI environment. Additionally, the FLC is applied to maintain the DC load bus voltage at a constant value and to control the speed of a PMDC motor as one of the loads being

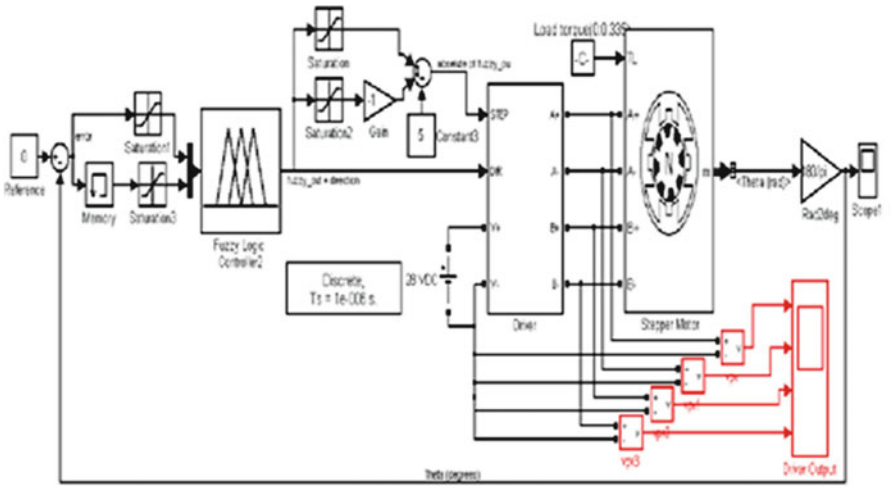


Fig. 3.52 Testing the FLC in the sun tracker system using MATLAB/SIMULINK

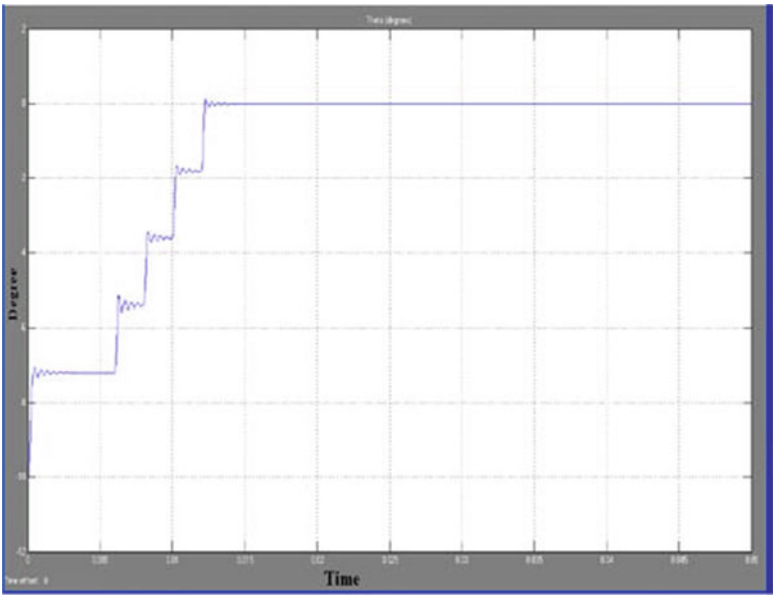


Fig. 3.53 Output degree

fed. This FLC controller has common design criteria's therefore it can easily be altered and expanded for controlling several systems. The modeled FLC is applicable for three different parts of the PVA stand alone utilization scheme: (i) the speed control of the PMDC load (ii) controlling the DC load bus voltage, (iii) maximum power point (MPP) tracking control, which is used to operate the PVA at its available maximum power as the solar insulation and ambient temperature change.

3.7.1 Methodology

The application of modern effective photovoltaic solar cells (PVSCs) has risen out as a crucial solution in energy conservation and demand-side direction during the past few decades. Due to their initial high costs, PVSCs have not as yet been an attractive mutually exclusive for electricity users who are able to buy less expensive electrical energy from the utility grid. All the same, they have been applied extensively for water pumping and air conditioning in distant and detached areas wherever substitute power is not available or is excessively unaffordable to transport. Though solar cell (SC) costs have reduced substantially during the last years owed to modern growths in the film engineering and fabricating technique, PV arrays are even believed quite expensive compared with the utility fossil fuel generated electrical energy costs. Subsequently building up such an expensive renewable energy system, the user by nature prefers to control the PV array at its maximum conversion efficiency by endlessly utilizing the utmost acquirable output power of the array. The electrical system powered by solar cells necessitates exceptional design circumstances due to the changing nature of the solar power generated resulting from irregular changes in weather conditions which affect the solar radiation level as well as the cell operating temperature. Different schemes to solve the problems on maximum power point tracking (MPPT) have been an all time active topic for PVA employment systems.

PVA operational strategies comprise of primarily four different controlled parts as MPP tracking controller, backup battery charge regulator and controller, load bus voltage controller, and special load controllers. A PVA system must be weighed as a complete unit of measurement because each of these parts are attached up collectively and need to be controlled together. Separate circumstance commonly leads to the failure of required process and affect the efficiency of the system. Hence the PVA system here consists of three controllers for MPP tracking, load bus voltage and the special load controller such as PMDC motor speed control. The battery backup unit controller is combined with the MPP tracking controller and is not treated separately.

3.7.2 Theoretical Explanation

3.7.2.1 PVA Utility System

Based on Fig. 3.54, the PVA utility system comprises of a PVA, a PMDC motor driving a fan type load, a constant R-L load, a switch able R-L load, a MPPT unit consisting of a switch capable of back-up battery unit, and a filter circuit. A PMDC motor speed controller unit, a voltage controller unit, and a MPP tracking controller unit are accumulated to the system. A DC load bus is made using the electric voltage kept constant by using a controlled DC chopper. Basically more DC buses

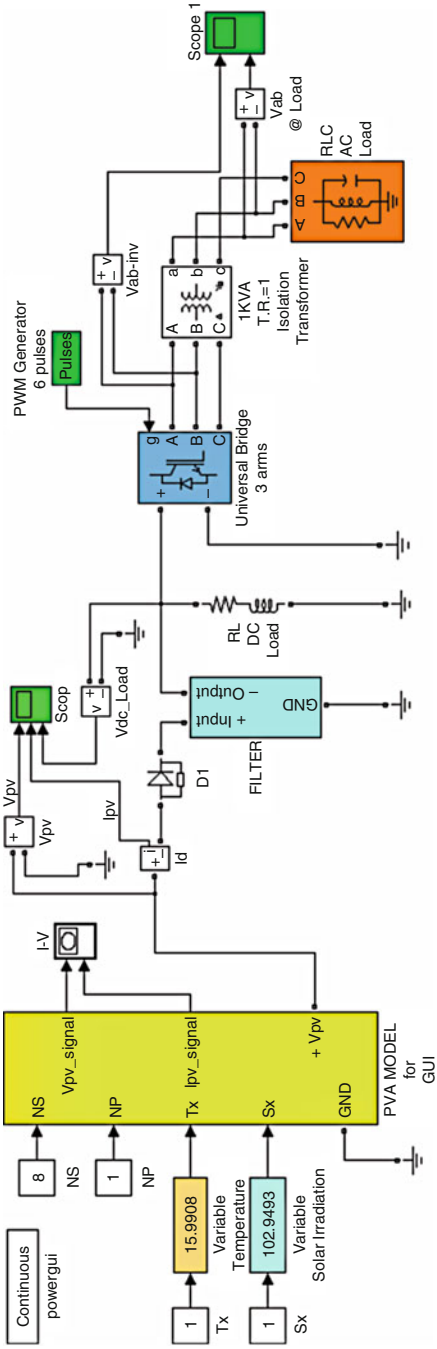


Fig. 3.54 Operational functional block diagram of the PVA model

can be produced with assorted voltage values which unbroken continuous using a DC chopper for every single DC bus given that the total load power stays between upper and lower power limitations plus the PVA MPPT operating voltage is the same as or more as opposed to voltages with the load buses. The particular potential drop in weight jalopy can be retained frequent considering that the lots are often built to end up being controlled from the user definite ranked voltage pertaining to more secure procedure. Additional operating conditions are required such as the PMDC motor as shown in Fig. 3.54. Here, the PMDC motor is actually operated on various speeds. As a result yet another controller is utilized for speed control of the PMDC generator. The load is characterized by a R-L load connected to the load bus which in turn is handled on constant voltage without any control strategy. The PMDC motor and the R-L loads are believed to be the loads fed at all times. Additional loads can be characterised by switching R-L loads connected either in series or parallel. The entire load power has to match the PVA output power.

3.7.2.2 GUI Modeling of the PVA

An over-all block diagram of the PVA model for GUI environment using SIMULINK is presented in Fig. 3.54. The PVA block in the GUI is the last stage on the model. The other stages of PVA are masked as functional subsystem blocks in the last stage shown in Fig. 3.54. The first stage in the PVA modeling is depicted in Fig. 3.55 in which the mathematical model of a single PV cell is represented with the block known as Equation 1. Another block representing the impacts of solar

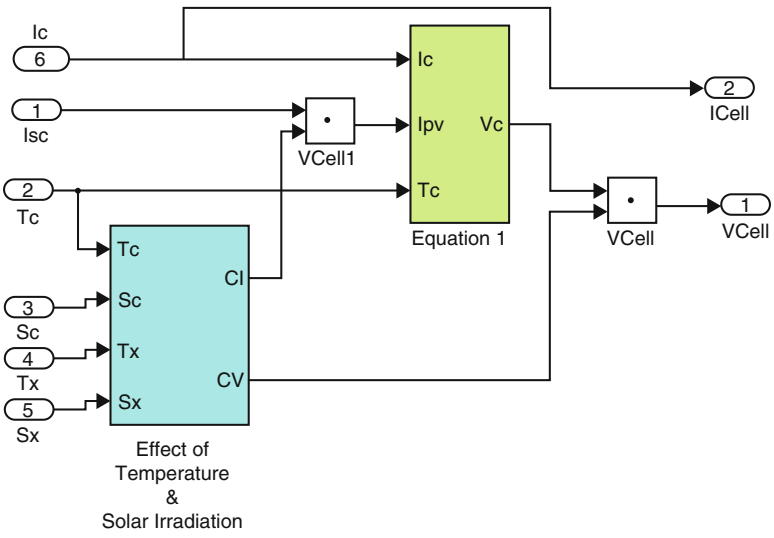


Fig. 3.55 Modeling stage 1

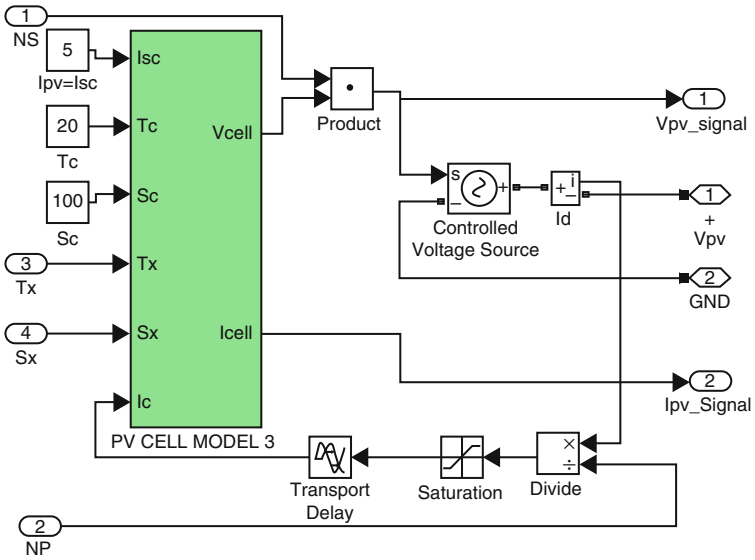


Fig. 3.56 Modeling stage 2

insulation and operating temperatures are also built into Fig. 3.56, a sub-mask of the stage 2, given in Fig. 3.56.

3.7.3 SIMULINK Model of FLC Blocks

The blocks of an FLC such as: fuzzification, rule base inference, and defuzzification are explained in this section.

The crisp inputs e(k) and Δe(k) are converted to fuzzy membership values on the fuzzy subsets Negative Big (NB), Negative Small (NS), Zero (Z), Positive Small (PS), and Positive Big(PB). Each fuzzy subset (FS) is represented by a triangular membership function. The letters E and DE are used to indicate whether the elements belong to error or its change DE, respectively.

The Boolean operator "*min*" is used with the verbal connector "*and*" to simulate the *input space of the rules* that have the structure as in expression;

If e is PB ***and*** Δe is NB ***then*** Δu1 is NB.

The input space in above expression is the part that represented by the expression (e is PB ***and*** Δe is NB). Therefore the min operator in SIMULINK Block Library is used to model the input spaces of 25 rules used by FLC. The outputs of the "*min*" operators indicate the strength (membership degree) of the rules in the output space Δu1. The implementation of the rule input space by the expression (e is PB ***and*** Δe is NB) is nothing but the fuzzification of the two crisp inputs e and Δe for all the

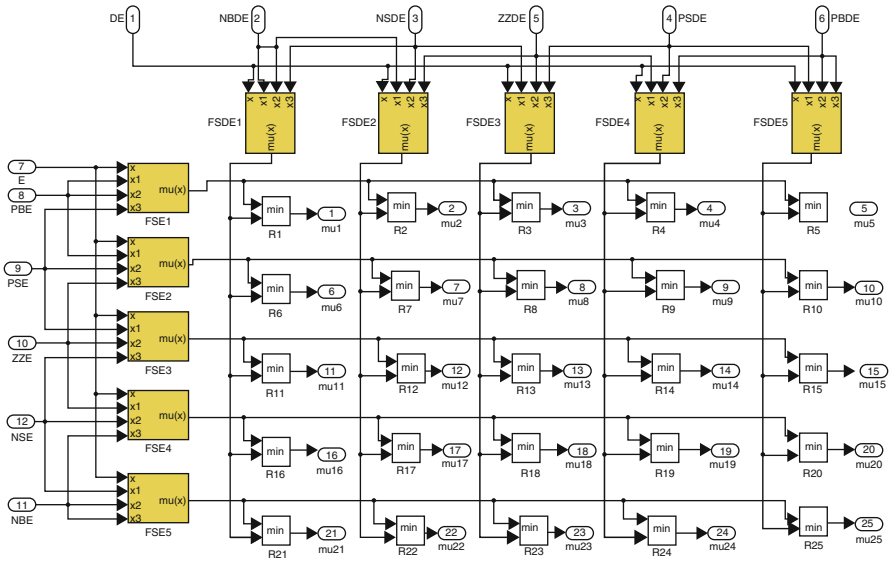


Fig. 3.57 The SIMULINK model of the fuzzification process

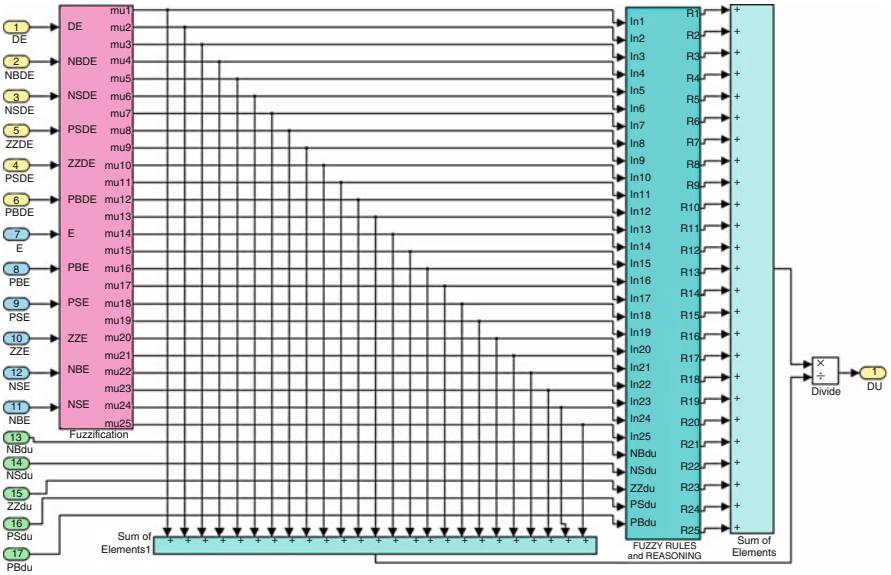


Fig. 3.58 The process from fuzzification to defuzzification in the FLC block

rules. The process of fuzzification of the input space with 25 rules is shown in Fig. 3.57. Simulation model of the *centre of area* method for defuzzification and reasoning is depicted in Fig. 3.58. This is the final stage of the FLC to generate the required change in control signal for the current k*th* sampling.

3.7.4 Simulation Results

The MPP tracking controller is tested by simulating the machine given in Fig. 3.54. The pace in the PMDC motor along with the load bus voltage are also controlled using a fuzzy logic controller just like the one explained above. Since rated voltage in the PMDC motor is 36 V, the strain bus voltage is kept constant at 40 V. The average importance of the output voltage on the chopper is weighed against 40 V reference voltages along with the difference utilized from the controller to get the desired chopper duty cycle in order that the DC bus voltage is kept at 40 V. The duty cycle in the chopper for PMDC motor speed control depends on final results controller, which is used to maintain the motor speed at 200 rad/s. The total current drawn by each of the loads and backup batteries being charged would be the current drawn from the PVA. This total current is divided by the number of cells in parallel to get the current of any single cell so that it enables to simulate PV cell model to build a voltage, which is then multiplied by the number of cells in series to discover the PVA output voltage.

A novel MATLAB/SIMULINK based unified Functional Block Model is presented above and a novel but simple FLC model for use in MATLAB/SIMULINK GUI environment. The nature of maximum power point MPP-Search and Detection algorithm is dynamic and operates without any required measurement or forecasted PV array information about the irradiation and temperature. The FLC GUI model can be used in different stages of the PVA scheme to control both MPP trackers, load bus voltage and load motor speed. Simulation results in Figs. 3.59, 3.60, 3.61, and 3.62 show acceptable MPP tracking as well as voltage and speed control responses.

3.8 Fuzzy Optimization for Solar Array System

During the recent years there has been an ever rising energy demand, owing to industrial development and population growth, motivating research and technological investments related to improved energy efficiency and generation. The reduced life cycle and upkeep of alternative resources can complement hydropower, fossil fuel and nuclear power generation. Solar photovoltaic power can be a prime candidate in many countries, where the solar power density with direct overhead incidence is 1 kW/m^2. Regardless of the high initial solar installation costs plus a low cell conversion efficiency (from 12 % on ordinary units up to and including maximum of 29 % on very special ones) the costs with the solar cells and power electronics are sharply decreasing, and that is supposed to aid the acceptance of such systems. The solar array is usually associated with an electricity storage system, that may consist of a method of batteries, fuel cells, flywheels or perhaps the distribution mains. The solar power is subjected to varying solar intensity and alterations in environmental temperature which, in turn, get a new maximum power

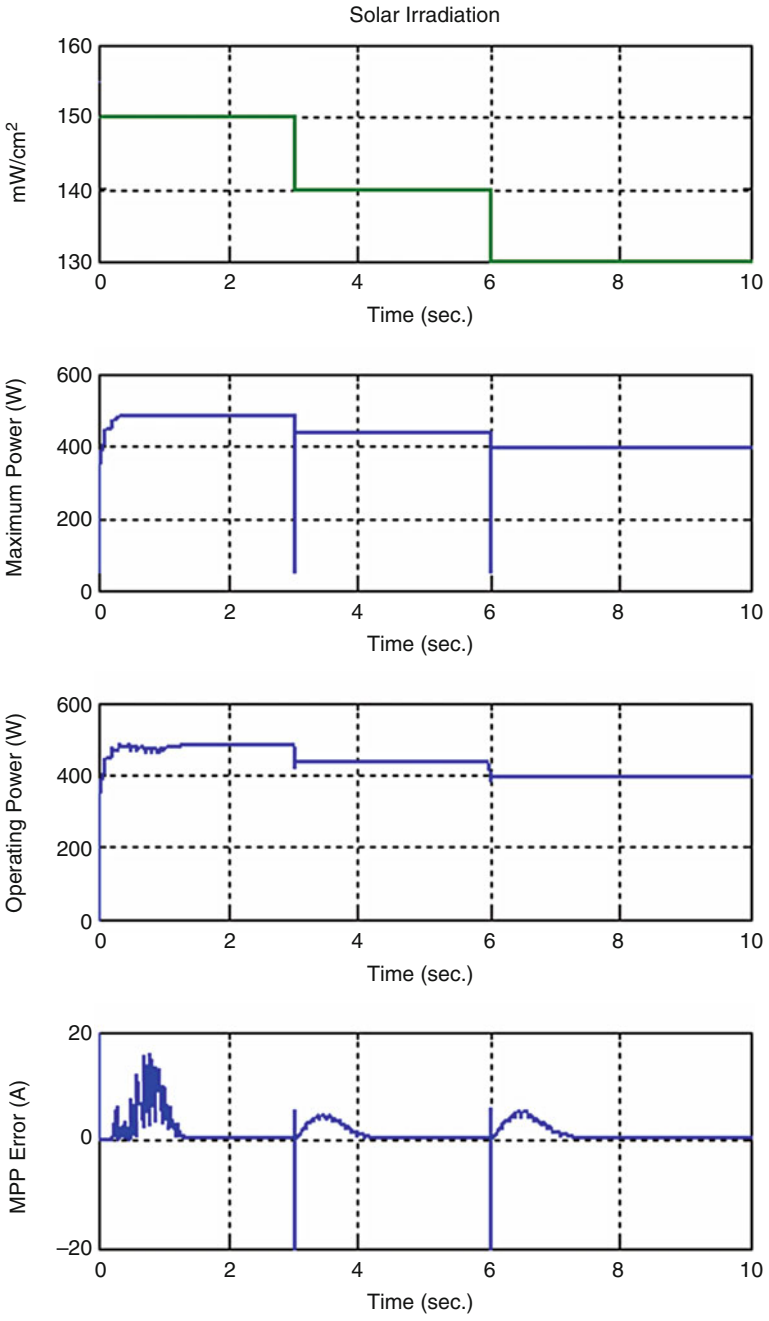


Fig. 3.59 Variations of the PVA power quantities as the solar irradiation level decreases

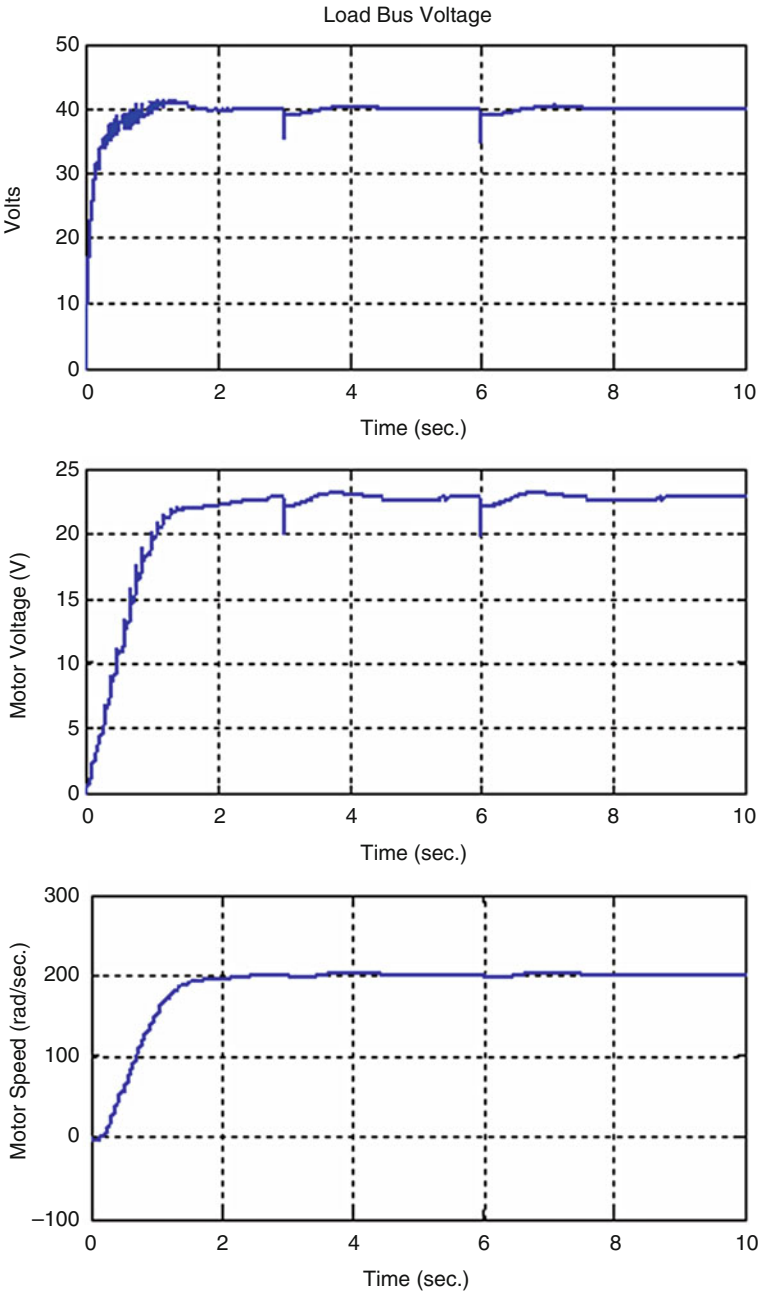


Fig. 3.60 Variations of the DC load bus voltage, PMDC motor voltage, and the motor speed as the solar irradiation level decreases

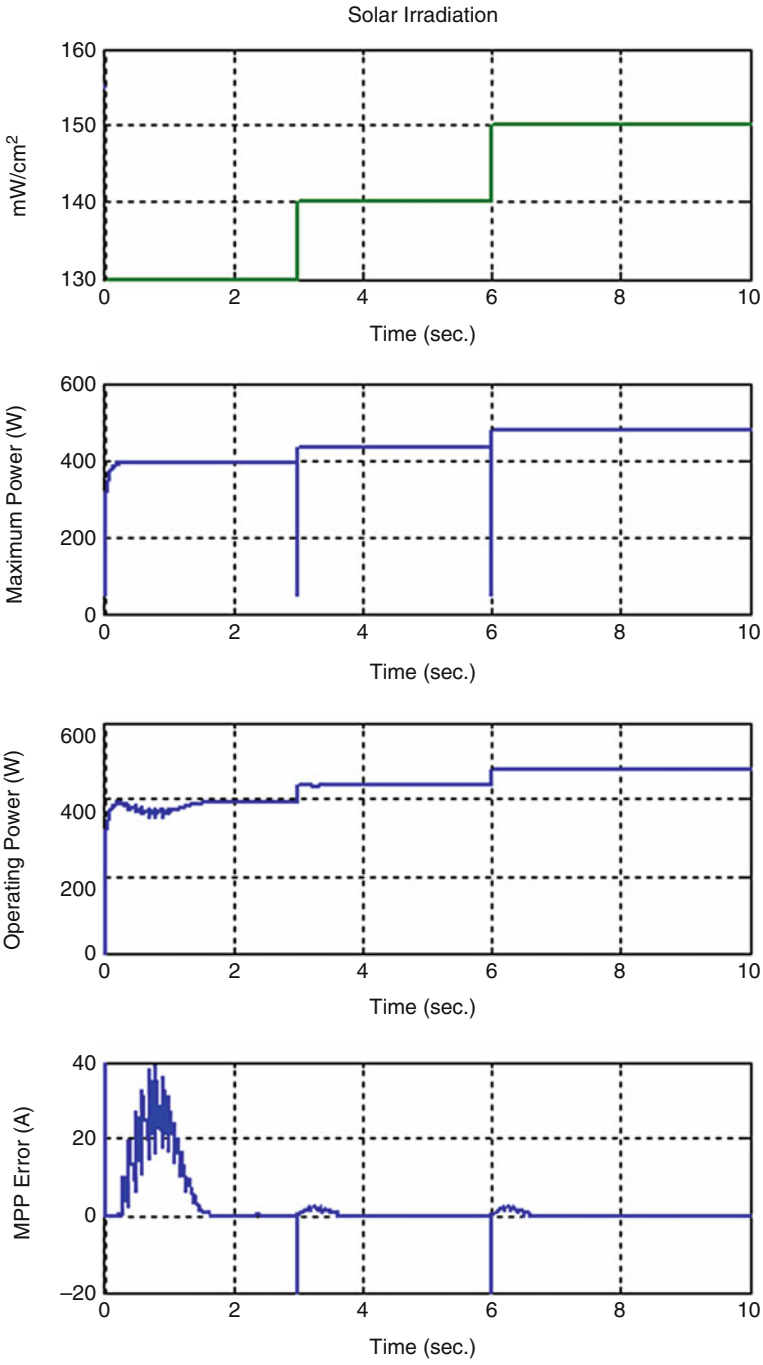


Fig. 3.61 Variations of the PVA power quantities as the solar irradiation level increases

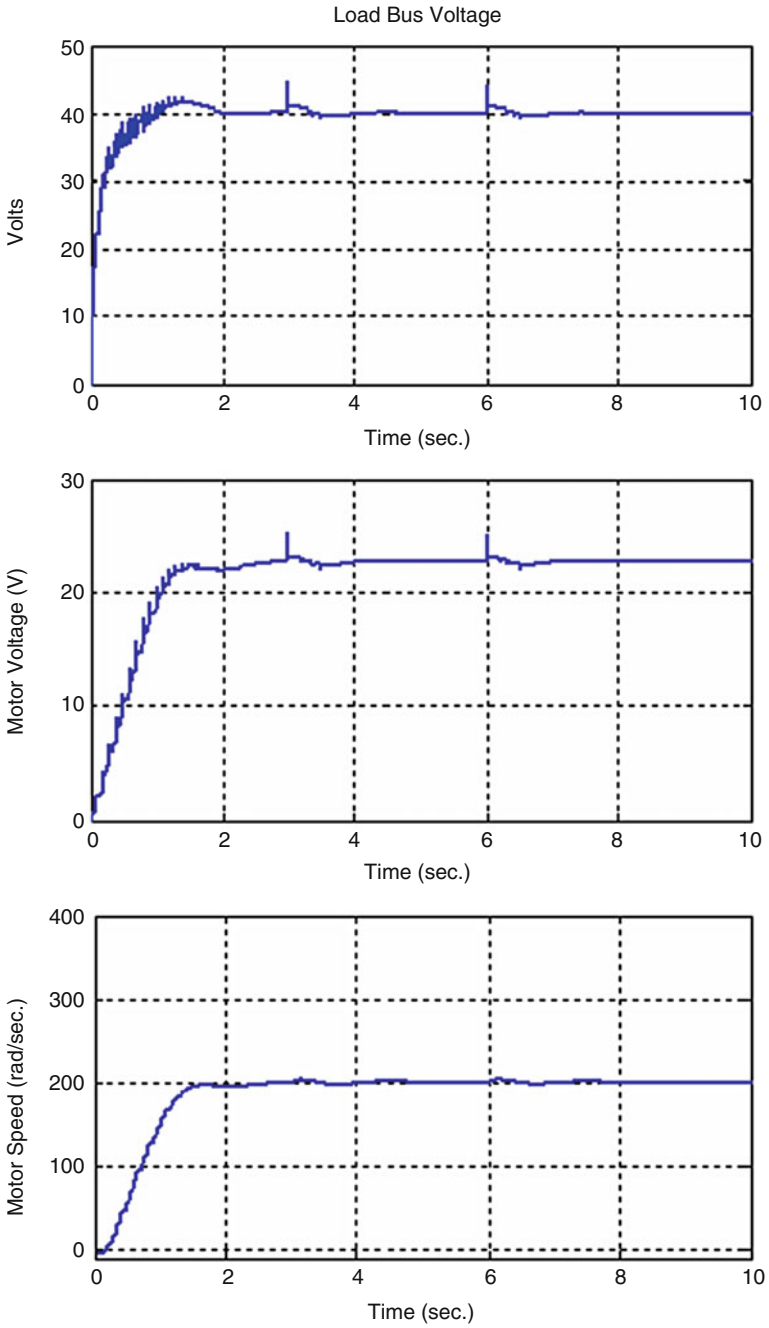


Fig. 3.62 Variations of the dc load bus voltage, PMDC motor voltage, and the motor speed as the solar irradiation level decreases

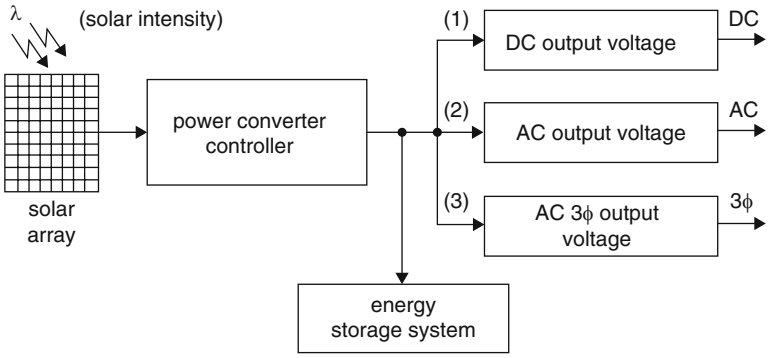


Fig. 3.63 Photovoltaic system block diagram

operating point. So as to increase the amortization of installation costs, it is essential to extract the utmost power available on continuous basis.

A few prominent abilities of fuzzy system are: online adaptive search of maximum power, robustness to solar intensity and temperature variation, does not require external sensors for solar intensity and temperature measurements. In this section, the system have been analyzed simulated and implemented by a low cost RISC microcontroller. The rig is modular, that permits paralleling for higher power installations.

3.8.1 Photovoltaic Systems

A typical photovoltaic system is shown in Fig. 3.63. The solar panel receives the sunlight and converts it to electricity by means of a power converter which possesses a peak-power tracking controller. A power storage system and possible connections with a single phase or three phase utility may also be provided. Usually the storage system is connected by way of a DC-link, but very recently, AC links using lossless resonant power converters have demonstrated promise. Several schemes are available for photovoltaic systems for residential applications and solar powered vehicles and various different control strategies for instance online conductance optimizers that keep the power factor near to unity, dynamic modeling for power maximization and fuzzy PI controllers to interchange conventional PI controllers inside feedback circuit. Special power electronic inverter circuits have also been suggested for photovoltaic systems. Solar arrays are already modeled for mathematical optimization, with emphasis on their physical properties.

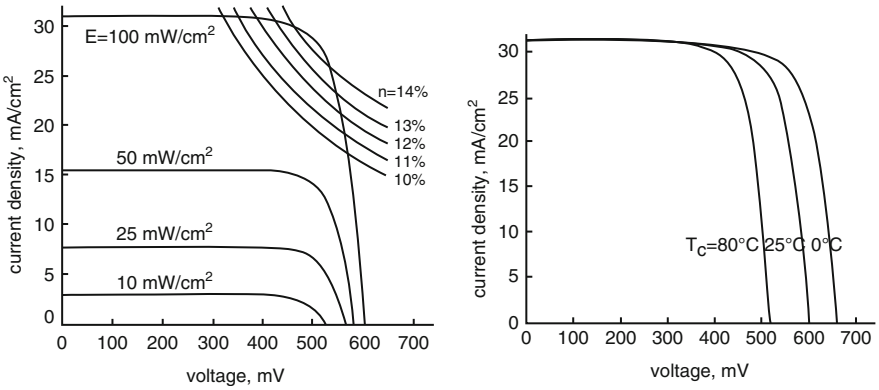


Fig. 3.64 Operating curves

3.8.1.1 Photovoltaic Array System Modeling

Solar panels are devices that convert photons into electrical potential in a p-n silicon junction. Due to the complex physical structure in the photovoltaic cell, manufacturers generally present a family of operating curves (I-V) shown in Fig. 3.64, with solar incidence and temperature as parameters. For each condition there is a unique point located in the knee with the I-V curve, where the solar cell will generate maximum power. Figure 3.64 also demonstrates the cell current density which is a function of voltage, and that the curves could be displaced vertically by solar intensity and horizontally by temperature variation. The model equations are listed below:

$$J = k1 \cdot \lambda - k2 \cdot e^{\alpha V - \beta T - \gamma} \tag{3.61}$$

$$\upsilon = \frac{1}{\alpha}\left(\ln\left(\lambda\frac{k1}{k2} - \frac{i_p}{k2 \cdot S}\right) + \beta T + \gamma\right) \tag{3.62}$$

$$\upsilon_p = \sum_{j=1}^{N_{cel}} \upsilon_j - N_{cel} \cdot R_s \cdot i_p \tag{3.63}$$

The parameters k1 (non-dimensional), k2 (m A/cm^2), α (voltage coefficient, v^{-1}), β (temperature coefficient, °C^{-1}) and γ (non-dimensional) are adjusted on the manufacturer's curves having a multi-rectilinear regression algorithm, to be able to minimize a quadratic error function. Figure 3.65 shows a PWM power-boost converter that steps in the array voltage to a higher DC bus voltage operating in continuous conduction mode (CCM). Equations 3.64, 3.65, and 3.66 provide dynamic equations, which in turn govern the boost converter operation

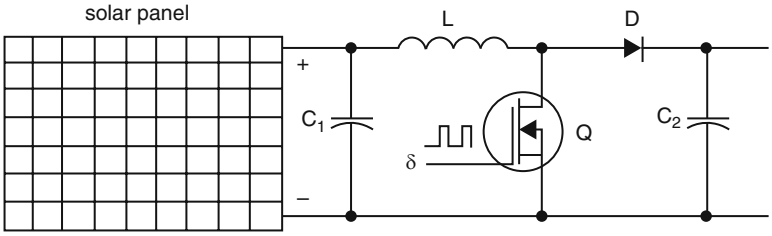


Fig. 3.65 Solar array driven by a boost converter

$$\frac{di}{dt} = -\frac{R_L + (1-\delta)(R_L/R_C)}{L} i - \frac{(1-\delta)R}{L(R+R_C)} \upsilon + \frac{\upsilon_p}{L} \tag{3.64}$$

$$\frac{d\upsilon}{dt} = -\frac{(1-\delta)(R)}{(R+R_C)C} i - \frac{\upsilon}{(R+R_C)C} \tag{3.65}$$

$$\upsilon_0 = (1-\delta)(R_L/R_C) + \frac{R}{(R+R_C)} \upsilon \tag{3.66}$$

3.8.1.2 Open Loop Simulation Studies

The system depicted in Fig. 3.65 is implemented in MATLAB/SIMULINK using the above equations. A thirty-cell solar array supplied voltage to the boost converter which, in turn, delivered power to an equivalent output load. Initially the system will operate in open-loop mode, in order to determine the behavior for various combinations of input variables and conditions. Figure 3.66, 3.67, 3.68, 3.69, 3.70, 3.71, and 3.72 show the system static characteristics for three temperatures (0 °C, 25 °C, 60 °C) with a fixed load resistance of 100 Ω and the solar intensity λ, varying gradually, from 10 mW/cm^2 up to the maximum of 100 mW/cm^2.

The shift of the peak power operating point is evident in such figures, as seen by the different duty-cycle, δ, values for the peak power. Figure 3.73 shows the power for three different load resistance values, at a fixed temperature (T = 25 °C) and solar intensity showing that the duty cycle, where the power is maximum also changes with the equivalent load resistance.

3.8.2 Peak-Power-Transfer Search

Figure 3.74 shows the solar array current/voltage curves superimposed with a set of constant power curves, indicating the region of maximum power delivery for nominal solar intensity and temperature, °C. The produced instantaneous power emerged with the product from the DC-link voltage with the DC-link current plus

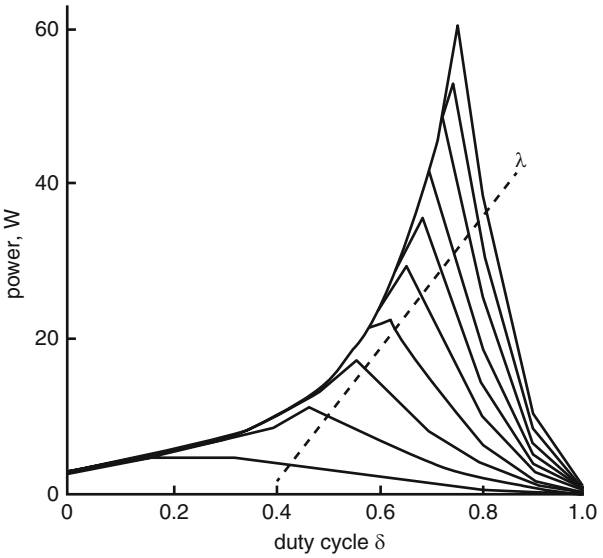


Fig. 3.66 Photovoltaic system output for λ from 10 to 100 mW/m^2 at T = 0 °C

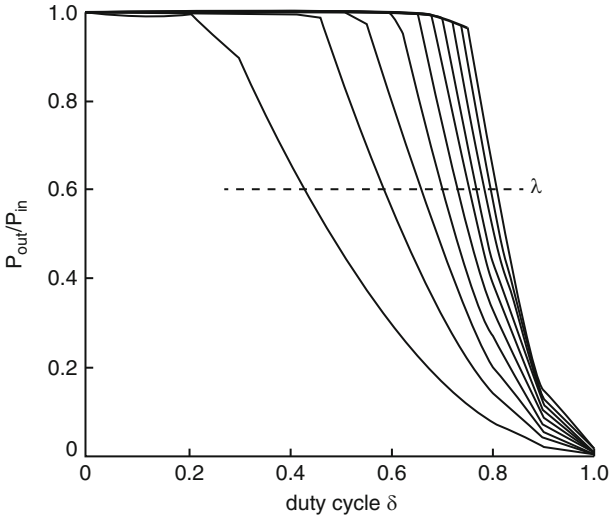


Fig. 3.67 Photovoltaic system efficiency P_{out}/P_{in} for λ from 10 to 100 mW/m^2 at T = 0 °C

the power used in the DC-link equals the solar-array power (assuming a stable-state lossless system). This means that, for that specific parameters, the obligation cycle from the boost power converter might be varied to vary the load-line slope, i.e. the solar-array impedance.

During the steady-state operation, it can be desirable to modify Z^{-1} so the peak-array power is available. This algorithm may be based on a look-up table, which

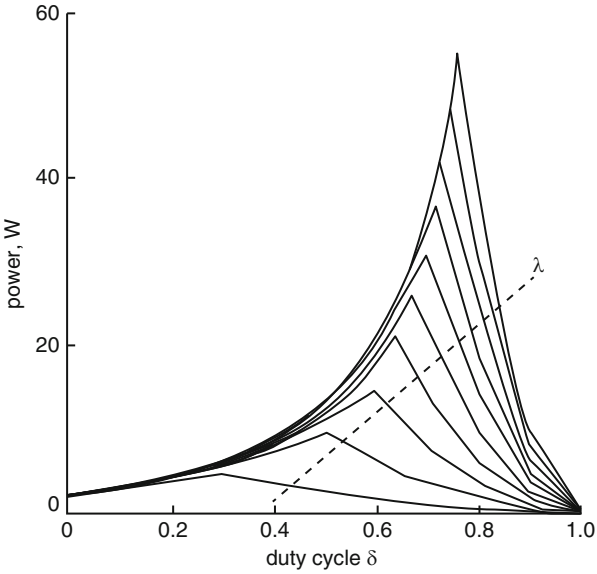


Fig. 3.68 Photovoltaic system output for λ from 10 to 100 mW/m^2 at T = 25 °C

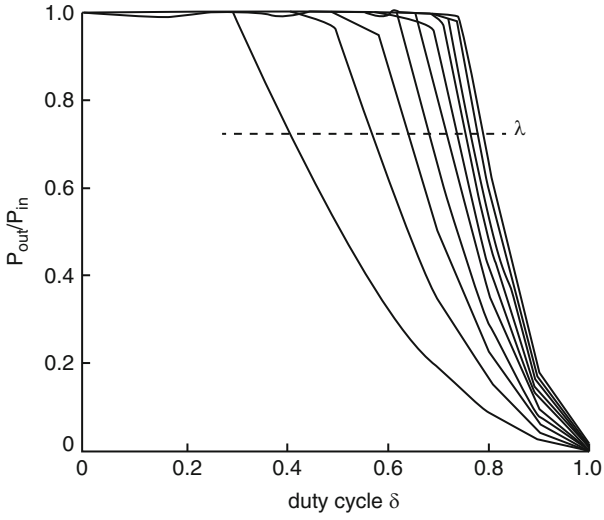


Fig. 3.69 Photovoltaic system efficiency P_{out}/P_{in} for λ from 10 to 100 mW/m^2 at T = 25 °C

would either need an exact solar-array parameter estimation, or a step-by-step duty-cycle alteration. The step-by-step duty cycle alteration is less favorable, since it may create a time-consuming search and a low-frequency oscillation towards the optimum point.

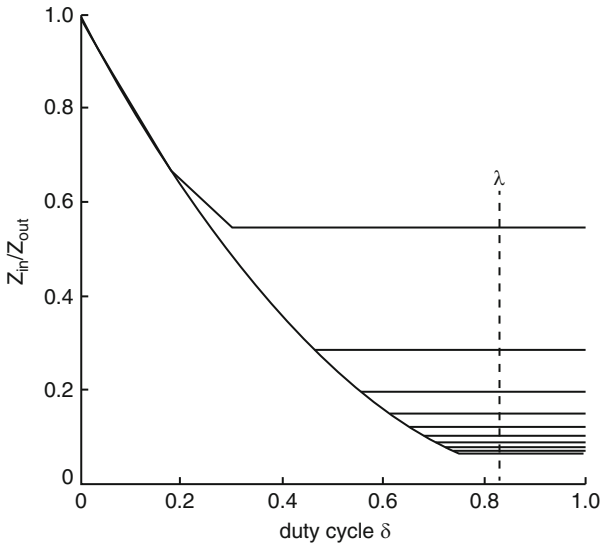


Fig. 3.70 Photovoltaic system normalized array impedance for λ from 10 to 100 mW/m^2 at T = 0 °C

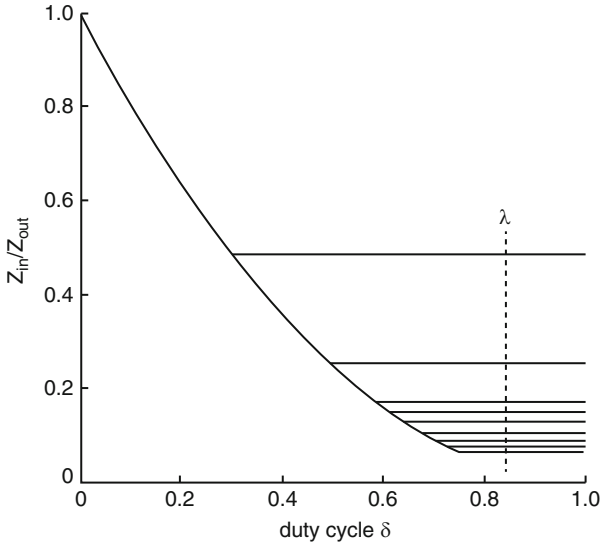


Fig. 3.71 Photovoltaic system normalized array impedance for λ from 10 to 100 mW/m^2 at T = 25 °C

3.8.3 Fuzzy Logic Based Solar Array Controller

The block diagram of the complete system is shown in Fig. 3.75. The solar array and the boost-power converter can be modeled according to (3.61, 3.61, 3.62, 3.63, 3.64, and 3.66), while the fuzzy control algorithm is based on rules written and fine tuned by simulations in the SIMULINK/MATLAB environment. The fuzzy algorithm searches for the maximum power heuristically, using the meta-rule:

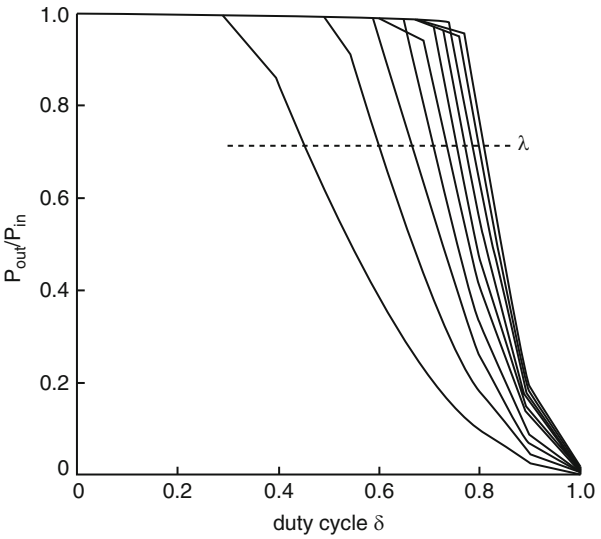


Fig. 3.72 Photovoltaic system efficiency P_{out}/P_{in} for λ from 10 to 100 mW/m^2 at T = 60 °C

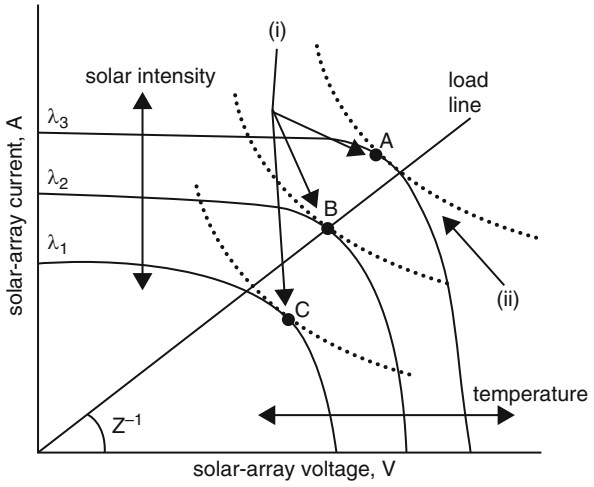


Fig. 3.73 Curves for solar intensity and temperature variation (i) Maximum peak power points, (ii) Maximum power hyperbola

If the last change in the duty-cycle (DC) has caused the power to go up, then exercise the duty (DC) in the same direction; otherwise, when it is mainly responsible for the power dropping, move it in the opposite direction.

The control logic, described above being a simple sentence, is translated using the following fuzzy control rules:

- IF ΔDC_k is P AND ΔP_k is PB THEN ΔDC_{k+1} is PB.
- IF ΔDC_k is P AND ΔP_k is PS THEN ΔDC_{k+1} is PM.
- IF ΔDC_k is N AND ΔP_k is PB THEN ΔDC_{k+1} is NB.

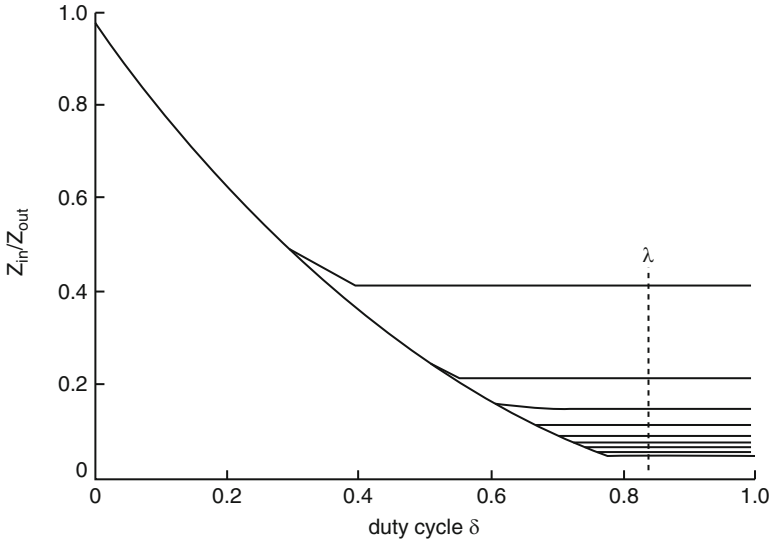


Fig. 3.74 Photovoltaic system normalized array impedance for λ from 10 to 100 mW/m^2 at T = 60 °C

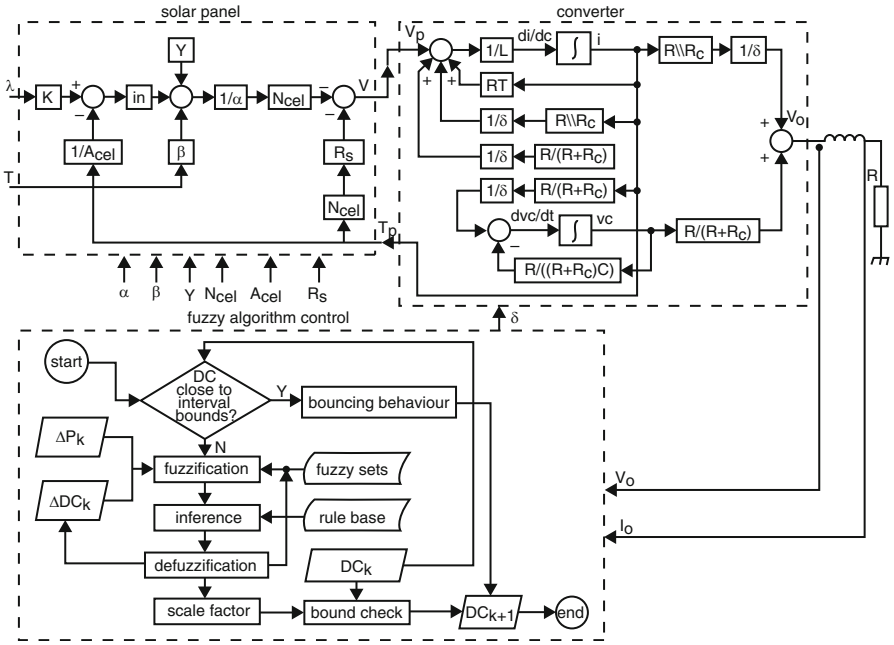


Fig. 3.75 Fuzzy logic based solar array controller

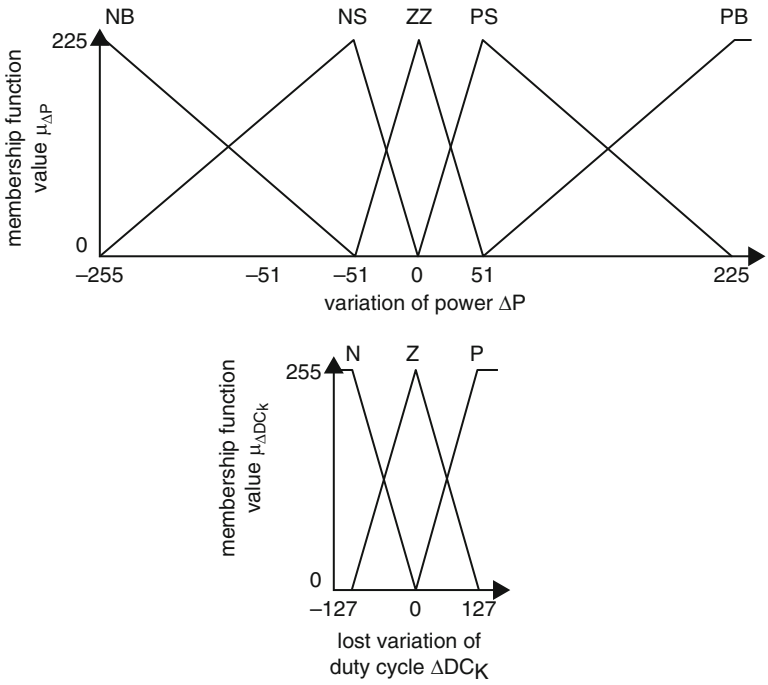


Fig. 3.76 Membership functions for fuzzy search controller

- IF ΔDC_k is N AND ΔP_k is PS THEN ΔDC_{k+1} is AM.
- IF ΔDC_k is P AND ΔP_k is NB THEN ΔDC_{k+1} is NB.
- IF ΔDC_k is P AND ΔP_k is NS THEN ΔDC_{k+1} is NM.
- IF ΔDC_k is N AND ΔP_k is NB THEN ΔDC_{k+1} is PB.
- IF ΔDC_k is N AND ΔP_k is NS THEN ΔDC_{k+1} is PM.

The two inputs used in this approach namely the variation-of-duty-cycle (DC) and variation–of-power (P) are represented by fuzzy sets as shown in Fig. 3.76. Additionally, other rules are also required, due to the fact that the characteristic curves might change with temperature and sunlight level, leading to an overall shift of the optimum point. In order to keep track of this situation, the system must have the following rules:

- IF ΔDC_k is Z AND ΔP_k is PB THEN ΔDC_{k+1} is PM.
- IF ΔDC_k is Z AND ΔP_k is PS THEN ΔDC_{k+1} is PS.
- IF ΔDC_k is Z AND ΔP_k is NB THEN ΔDC_{k+1} is AM.
- IF ΔDC_k is Z AND ΔP_k is NS THEN ΔDC_{k+1} is NS.

From the simulation studies it is observed that a vital feature to provide an artificial inertia is required, in order to keep it from stopping whenever a zero-crossing of the power is detected, resulting in a curve for ongoing motion for some

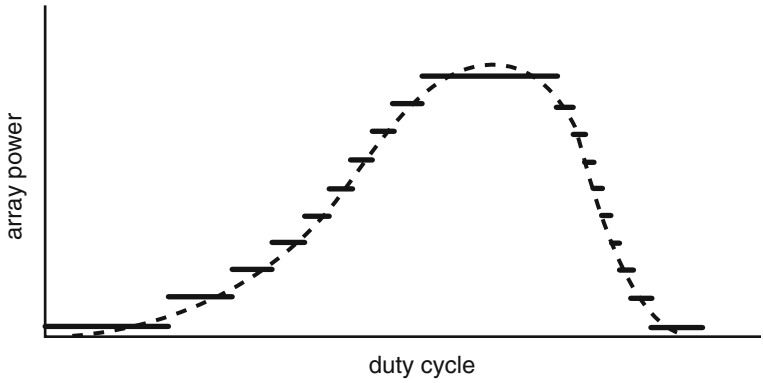


Fig. 3.77 Quantization effect on power search

cycles. The usefulness in this group of rules becomes clear when one considers the quantization effect shown in Fig. 3.77. Considering that the input signals are digitized, the continuous curve is broken down into a series of plateaus. Clearly, the steeper the curve, the shorter the plateau. Since the optimum point tends to match the condition, it might recognize any large plateau to be a maximum power region. The subsequent rules are actually identified for avoiding the stabilizing effect inside a region other than that of true peak power:

- IF ΔDC_k is P AND ΔP_k is ZZ THEN ΔDC_{k+1} is PS.
- IF ΔDC_k is N AND ΔP_k is ZZ THEN ΔDC_{k+1} is NS.

At last, it is required to provide the system with a rule that stabilizes the point of operation at a peak power point:

- IF ΔDC_k is Z AND ΔP_k is ZZ THEN ΔDC_{k+1} is ZZ.

According to Fig. 3.76, the membership functions for ΔP and ΔDC are more dense towards the centre, thus providing more sensitivity as the changes in power approaches zero. The implementation of fuzzy-algorithm is shown in the block diagram of Fig. 3.78. The duty-cycle parameter (ΔDC) is internal to the PWM routine, which is stored as a floating point number in order to increase control resolution; ΔDC_k is a feedback parameter, stored as an 8-bit value (1 sign bit, 7-bit absolute value); ΔP_k is a calling parameter, stored as a 9-bit value (1 sign bit, 8-bit absolute value); DC is obtained as a floating point value, in order to allow precise scaling at the end of the process; however, it is converted to an integer at the end of the sampling-time routine.

The duty cycle is bound by upper and lower limits (90 % and 10 %) as a safety measure; if DC is close enough to one of the ends of the interval, the fuzzy algorithm is overridden and the DC is 'bounced' back to the centre of the interval. The same safety reasons apply to the bound check that is performed at the end of the

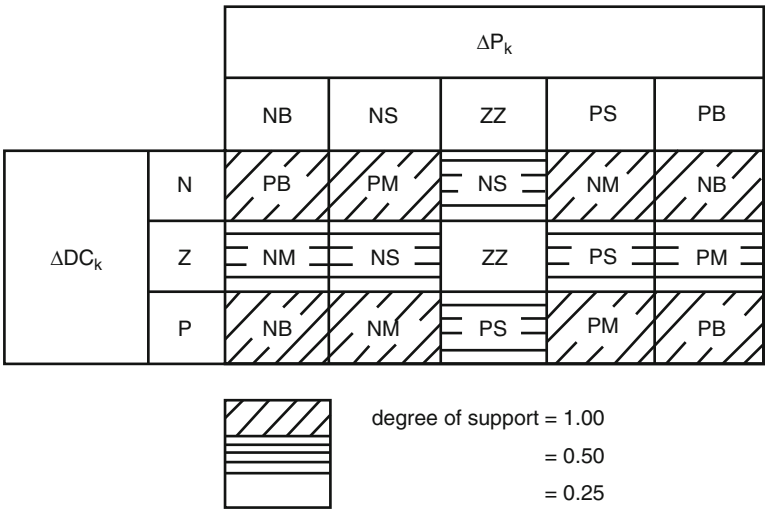


Fig. 3.78 Fuzzy rule base with different degree of support

control cycle; if the new duty cycle ($\Delta DC_k + S.\ \Delta DC_{k+1}$, where S is a scaling factor) ends up being outside the specified interval, it is reduced to the closest bound. Once these exceptions have been accounted for, the fuzzy algorithm is run. The first task is to perform the fuzzification of the input parameters, indicated by the fuzzy sets shown in Fig. 3.76. Following this, the fuzzy inference engine applies the control rule base described above.

The user can find several rule weights to satisfy different conditions. The strongest condition needs to be the one corresponding towards the first band of rules, since the task represented by them describes the conventional system operation. The other and third sets deal with special conditions thereby have a lower strength. They are active only when certain specific conditions apply. A final list of rules, activated whenever the device reaches the optimum point, only need an easy weight. The quantization effect on power search is illustrated in Fig. 3.77. These varying strengths are implemented with different degrees of support on the corresponding rules, as shown by Fig. 3.78.

Once all the rules have been evaluated, then the final stage of FLC, defuzzification is performed. Here, the centre of gravity method of defuzzification is employed, thus presenting the result in floating-point format. The usefulness of utilizing the time and memory consuming floating-point format becomes clear when the user considers the precision that the scaling factor S needs to be tuned. After the effect can result in defuzzified and scaled, it can be placed on the present DC and fed returning to the following control cycle, by making $\Delta DC_k = \Delta DC_{k+1}$.

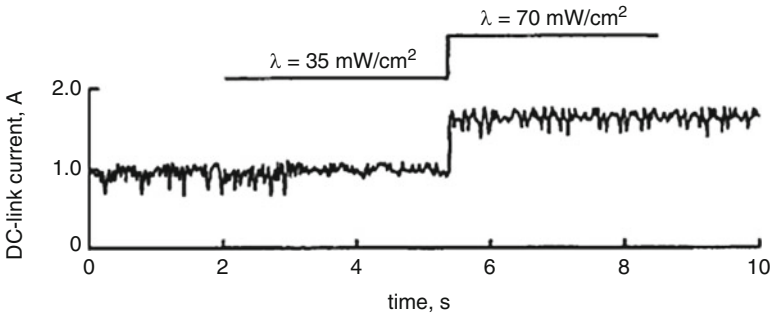


Fig. 3.79 Solar intensity variation and the corresponding DC-link current change with fuzzy duty cycle search

3.8.4 Experimental Results

The hardware model of the system shown in Fig. 3.75 was implemented in the laboratory with a RISC microcontroller type PIC16C74. A few notable features in this chip include, inbuilt PWM, input compare capture functions, serial and parallel interfaces and can be programmed with only 35 instructions. The simulation study was carried out in MATLAB/SIMULINK and the software was written in an assembler, on the basis of the block diagram in Fig. 3.75. The complete peak-power tracking system with the solar array was connected in the laboratory to charge the batteries, using variable illumination supplied by tungsten halogen lamps.

Experiments also included the application of sunlight, with a protective screen to produce a variable shade to the solar array. Figure 3.79 shows a step response for illumination level variation, showing that the DC-link current flowing to the batteries quickly establishes the new operating condition after the solar intensity has been varied from $\lambda = 35$ mW/cm^2 to $\lambda = 70$ W/cm^2.

An entire fuzzy logic solar array peak power tracking controller have been simulated, designed and implemented from the laboratory. The power circuit based on a boost converter, and the controller, which has a fuzzy algorithm that results in optimum duty cycle and transfers the peak power from the solar array into a charger. The major advantages of the fuzzy controller are that the control algorithm gives fast convergence and robust performance against parameter variation, and can accept noisy and inaccurate signals. It was found to reliably stabilize the utmost power transfer in all types of operating conditions.

3.9 Forecasting of Solar Irradiance Using ANN

Solar irradiance forecasting could be the foundation of power prediction of PV generation. While using the fast development of photovoltaic generation in recent times, there's an increasing desire for more precise and applicable modeling,

forecasting and prediction of solar irradiance. The possible computational models include linear regression models, satellite data based models and ANN models using meteorological parameters. A regressive model to the estimation from the hourly diffuse solar irradiation under all environmental conditions will depend on the sigmoid function and applies the clearness index and also the relative optical mass as predictors. Several solar irradiance forecasting models were applied in the past. Such models could be classified into two main groups: physical models and statistical models. The physical models depend on mathematical equations which define the physical state and dynamic motion of the atmosphere. These physical models are extremely complex non-linear equations which require strong computing power to solve them. Numerical methods were applied to obtain the approximate solutions of the equations, and they are also often known as numerical weather predictions (NWP) models. NWP can be used in forecasting but it's not available commonly.

The difficulties of solar irradiance forecast based on NWP vary significantly and rely on the different climate and dynamic motion of the atmosphere in the study location. The statistical models include time series models, satellite data based models, sky images based models, ANN and wavelet analysis based models. The statistical models depending on satellite data and sky images detect the motion of cloud structures using motion vector fields. The motion of cloud structures is determined from two consecutive cloud index images from satellite data or sky camera images. The errors of satellite data and sky images based forecasts proposed in the literature increase drastically under low sun elevations, high spatial variability and low irradiance conditions.

Usually, the statistical models are less complex than physical models simply because they require less input information and shorter computation time for the forecast. Two basic features must be looked into in order to evaluate the models: the foremost is the supply of information to be applied as input by the models and the second would be the accuracy and complexity on the forecasting model. Satellite data, sky images and NWP aren't always intended for various occasions. However, common meteorological parameters including ambient temperature, relative humidity, wind speed, wind direction, sunshine duration and clearness index are instantly available in most instances, hence the conventional solar irradiance forecasting model is created with all the input on the historical measured data of solar irradiance as well as other meteorological parameters.

Based on the technical specifications in the State Grid Corporation of China, the time scale of solar irradiance forecasting includes ultra short-term (around 4–6 h ahead) and short-term (up to 24–72 h ahead) forecasting. The forecast as much as 24 h ahead or maybe more should be used for the power dispatching plans along with the optimization operations of grid-connected PV plants and also the coordination charge of energy storage devices. The most prevalent short-term forecast horizon is 24 h overnight. Solar irradiance forecasting models on different time scales according to ANN using meteorological parameters without NWP and satellite data show good

performance and could be classified into three differing types. The first estimates the solar irradiance based on some meteorological parameters, the other one allows forecasting the future solar irradiance in line with the past observed data of solar irradiance, a final one combines both the previous models. These approaches need some meteorological parameters as input from the ANN model, but the meteorological data aren't always available. So as to overcome this challenge, a fairly easy method for forecasting 24 h ahead solar irradiance using multilayer perceptron may be applied. It shows good performance in forecasting solar irradiance except under unstable conditions including fast variations or violent fluctuations.

The constituents of the input vector determine the adequacy and sufficiency on the input information. Based on the input vector dimensions, excessive components could make the model structure become too complex, which enhances the difficulty of modeling, but not enough components will result in the lack of info that cause the model not to ever reflect truth variation. Merely a reasonable balance between model complexity and information absence can settle the condition of the determination with the dimensions of input vector. Through the mindset from the introduced forms with the pieces of input vector, most ANN models directly utilize original data number of meteorological parameters as being the input vector on the model. This may import much information redundancy minimizing the generalization ability in the ANN forecasting model. To overcome these shortcomings and improve forecast accuracy, in this particular section the ANN model is improved upon by 50 % aspects: firstly, effective input components are constructed while using the few available meteorological parameters under the input dimension limits to extract more features on the existing data, secondly, CV is applied to the ANN model structure to optimize the amount of neurons along with other model parameters.

3.9.1 Relation Between Solar Irradiance and Weather Variations

The definition for solar irradiance is follows: The amount electromagnetic energy incident on a surface per unit time and per unit area is defined as solar irradiance. The energy emitted from the Sun passes through space until it can be intercepted by planets, other celestial objects, or interstellar gas and dust. The concentration of solar radiation striking these objects is dependent upon an actual law known as the inverse square law. Just about 40 % (general level) from the solar panel technology intercepted near the top of Earth's atmosphere passes to the symptoms. The proportion takes a different approach under different conditions: this proportion is greater than 40 % in sunny days, approximately equal to 40–50 % in cloudy days and fewer than 40 % in overcast days. The solar constant GSC is the sunshine, per unit time received over a unit division of surface perpendicular for the direction in

the Sun's rays, at mean Earth-Sun distance, away from atmosphere. The planet Metrological Organization suggests a value of 1,367 W/m^2.

The parameters of solar irradiance are extraterrestrial irradiance G_0 and surface irradiance G_s. Extraterrestrial irradiance refers to the upper bound irradiance and that is not affected by the aerosphere and weather conditions but is dependent upon planet earth's rotation and revolution. Surface irradiance is related to the latitude, the sun's rays elevation angle, date plus the time of the day. Ignoring some minor factors like polar motion, the precession of the planet's axis and leap years, extraterrestrial irradiance changes yearly. For the certain location, with the connection between different day's 12 months and different time of just 1 day, the corresponding extraterrestrial irradiance G_0 might be calculated as,

$$G_0 = G_{SC}\left(1 + 0.33\cos\frac{360n}{365}\right)(\cos\delta\cos\varphi\cos\omega + \sin\delta\sin\varphi)$$

where G_{SC} is solar constant, n is the date sequence number in 1 year, $n \in [1,365]$, δ is solar declination, φ is latitude, ω is solar hour angle. While the solar radiation transmits from the upper bound to the Earth's surface, a certain amount of attenuation occurs due to the absorption, scattering and reflection of the atmosphere. This degree of attenuation is related to various factors such as the amount of clouds, cloud form, cloud thickness, water vapor, and aerosols. Hence the surface irradiance at few locations is less than its corresponding extraterrestrial irradiance. The changes in surface irradiance occur randomly which in turn are closely related to the atmospheric motion. The difference between G_0 extraterrestrial irradiance and G_s surface irradiance G_d (hereinafter referred to as solar irradiance difference $G_d = G_0 - G_s$) can reflect the weather conditions. The measured data of surface solar irradiance G_s (from 2010.03.09 to 2010.03.12, Kunming, Yunnan, China), corresponding extraterrestrial solar irradiance G_0 and solar irradiance difference G_d are shown in Fig. 3.80.

From Fig. 3.80, it can be observed that the solar irradiance difference G_d is small and has similar shape under sunny days (20100311, 20100312). As opposed, G_d is larger and contains more inflections on cloudy days (20100309, 20100310) than sunny days. Quite simply, it means the change of G_d is closely related to weather conditions. The analysis of G_d related to different weather conditions often leads and allow us to extract more information from the measured data of surface solar irradiance G_s plus the calculated data of corresponding extraterrestrial solar irradiance G_0 by finding and selecting suitable mathematic parameters which can reflect these correlative variation characteristics. Due to the strong correlation between a few meteorological parameters and irradiance, these meteorological parameters are directly influenced by irradiance. Thus these parameters can reflect the alterations of irradiance which enable it to consider due to the input in the ANN forecasting model. Such parameters include ambient temperature, relative humidity, etc.

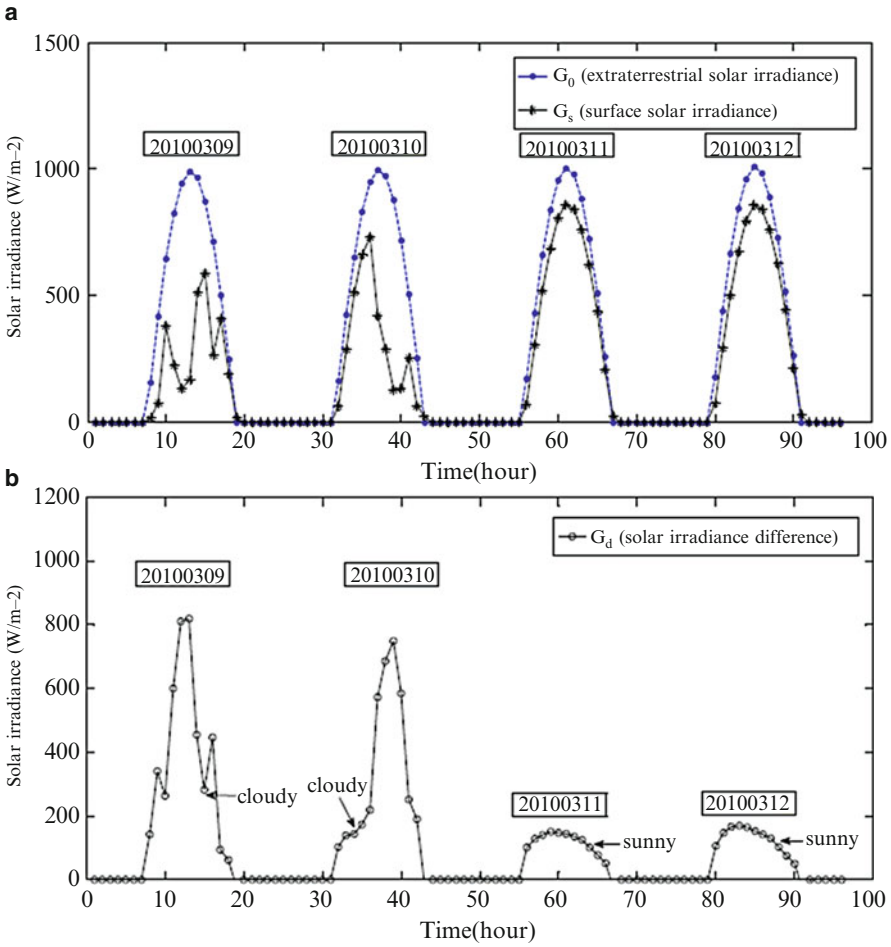


Fig. 3.80 Extraterrestrial irradiance, surface irradiance and solar irradiance difference; (**a**) Extraterrestrial irradiance and surface irradiance; (**b**) Solar irradiance difference

3.9.2 Reconstruction for the Input Vector of the Forecasting Model

The components of forecasting model input vector are classified as forecasting factors, whose selection is significant towards performance in the model. Generally, forecasting factors with the ANN model are selected from two classes of historical data: solar irradiance itself along with the meteorological parameters associated with solar irradiance. Two aspects should be considered in the selection: exactly what data must be selected and what form these data can be imported in. Generally in most from the current ANN solar irradiance forecasting models, multi-

dimensional historical data combination of solar irradiance in just a stretch of time is employed as forecasting factors, it can be shown as:

$$I_G = [G_{t-1}, G_{t-2}, \ldots, G_{t-m}]$$

where I_G is the input vector of the ANN forecasting model, G_{t-i} ($i = 1,\ldots,m$) is the historical data of solar irradiance, m is embedding dimension. The time choice of the historical results are dependant on m and sampling interval. Usually, m is more than 8.

Under varying conditions, the symptoms of solar irradiance changes randomly. The outer lining solar irradiance is zero during the period of time between sunset and sunrise even as it varies constantly between sunrise and sunset, utilizing the unprocessed multi-dimensional historical data compilation of solar irradiance as forecasting factors will import a lot of repeated information and produce high dimensions with the input vector with the model which can make the modeling tougher and complicated. Therefore, as opposed to the historical data series of solar irradiance, the statistical indicators of the historical data inside a period of time can be taken as the new forecasting factors, so effective information in the historical data will probably be fully extracted and utilized. Meanwhile, the size and style of input vector will likely be decreased. Moreover, because solar irradiance difference G_d reflect varying weather conditions, it can be viewed as forecasting factors in appropriate forms, so that accurate weather condition information can be obtained to the model along with the forecasting. The symptoms irradiance G_s is discrete sampling data and extraterrestrial irradiance G_0 is corresponding calculated value, thus G_d is a discrete multi-dimensional data series. Taking into consideration the restriction on the input vector dimensions, we could take some mathematical parameters in the data combination of G_d as forecasting factors.

Usually, the derivative is a proper index of the variation tendency of the corresponding variable. The measured data of surface solar irradiance G_s (from 2010.02.18 to 2010.02.23, Kunming, Yunnan, China), corresponding extraterrestrial solar irradiance G_0, the 1st-order, second-order and third-order derivative of solar irradiance difference are calculated and shown in Fig. 3.81. It follows through the mathematical definition that derivatives of solar irradiance difference are related to the fluctuation of climate. In Fig. 3.81, it could be seen that each one order derivatives (1st, 2nd and 3rd order) of solar irradiance difference are positively correlated towards fluctuations power of surface solar irradiance. Further research indicated that third-order derivative of solar irradiance difference (TOD = d3Gd/dt3) is obviously in excess of additional two derivatives (1st and 2nd order) while you will discover mutations from the curve of G_s meaning fast variation and violent fluctuation were took place the weather.

The comparisons of the derivatives shown in Fig. 3.81a have been illustrated here. Therefore, third-order derivative of solar irradiance difference is usually selected just as one appropriate measure to explain the variation and fluctuation of weather conditions. To achieve more significant, clear and description for several climate conditions of merely 1 day, the ideal price of TOD denoted by TODmax is

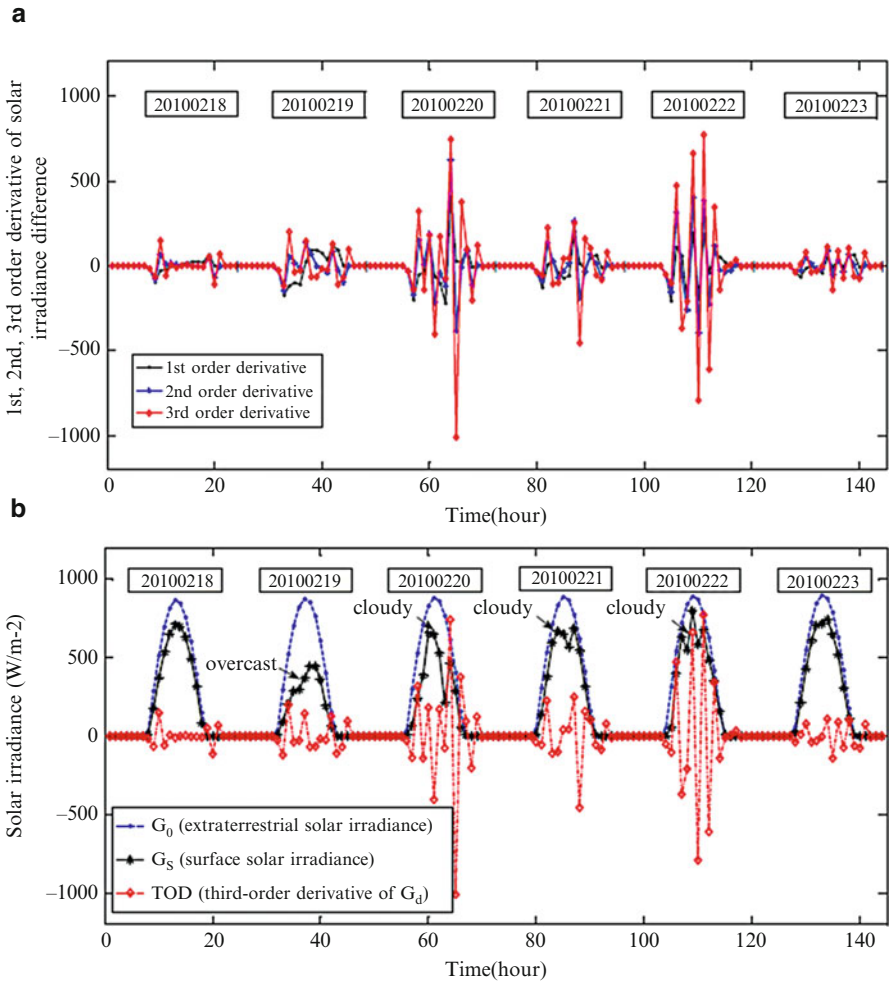


Fig. 3.81 Solar irradiance and the derivatives of solar irradiance difference; (**a**) First-order, second-order and third-order derivative of solar irradiance difference; (**b**) Extraterrestrial solar irradiance, surface solar irradiance and *TOD*

selected being an index to the weather changing characteristics. From another angle, we can notice that is very important distinction between surface irradiance G_s and extraterrestrial irradiance G_0 is closely related to the alteration inside the conditions, which is relatively smaller in sunny days when compared to cloudy or overcast days. To make clear comparison in the difference between surface irradiance and extraterrestrial irradiance, the irradiance value are normalized using (3.67) to eliminate the impact of numerous amplitude of the actual irradiance data:

$$G_{0N,i} = \frac{G_{0,i}}{\max\limits_{i=1,2,\ldots,k} G_{0,i}} \times 100 \qquad G_{sN,i} = \frac{G_{s,i}}{\max\limits_{i=1,2,\ldots,k} G_{s,i}} \times 100 \tag{3.67}$$

where $G_{0N,i}$ is normalized extraterrestrial irradiance, $G_{sN,i}$ is normalized surface irradiance ($i = 1,2,\ldots,k$), k is the number of the irradiance data. Later, the normalized discrete difference (NDD) of solar irradiance is defined in (3.68) as a specific index to describe the difference between surface irradiance and extraterrestrial irradiance:

$$NDD = \sqrt{\frac{1}{k}\sum_{i=1}^{k} (G_{0N,i} - G_{sN,i})^2} \tag{3.68}$$

Based on the definition, the first and normalized value of solar irradiance, the NDD index for each day (k = 24) towards the same irradiance data in Fig. 3.81 are calculated and shown in Fig. 3.82.

In Fig. 3.82, NDD2 = 9.00 (overcast day), NDD3 = 14.40 (cloudy day), NDD4 = 5.59 (cloudy day), NDD5 = 9.76 (cloudy day), it may be seen that NDD index during these 4 days are significantly above from the other sunny days. Out of this, the NDD index is used to measure different conditions. Together with TODmax and NDD, another component that is highly recommended is the date sequence number n a single year, n ∈ [1, 365]. Determined by these three factors, the typical surface irradiance Gsavg and the average ambient temperature Tavg of 1 day may also be given to the input vector. The last input vector in the new ANN forecasting model is composed of five components and shown as,

$$I_{ANN} = \left[G_{savg}, TOD_{\max}, NDD, T_{avg}, n\right] \tag{3.68a}$$

where I_{ANN} is the new input vector of the ANN forecasting model.

3.9.3 ANN Forecasting Model Using Statistical Feature Parameters

ANN is used as the modeling of solar irradiance forecast in line with the input vector consisting of statistical feature parameters. The time scale of short-term forecast is 24–72 h ahead. Some time interval of input and output solar irradiance series is depended on the actual situation. In line with the reconstruction for that input vector simply 3 above, a brief-term forecasting model depending on ANN using statistical feature parameters (ANN-SFP) is presented. This ANN model consists of four layers i.e., input layer, hidden layer 1, hidden layer 2 and output layer, the model is shown in Fig. 3.83.

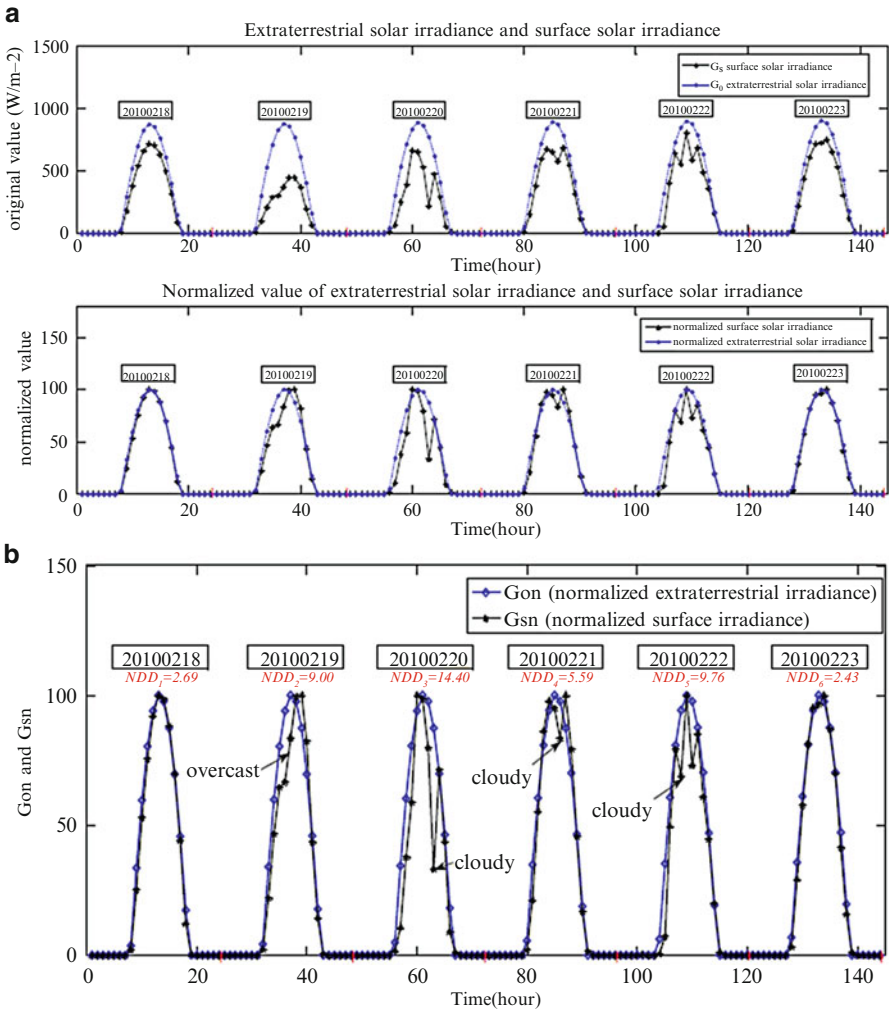


Fig. 3.82 Original value, normalized value and *NDD* of solar irradiance; (**a**) Original and normalized value of solar irradiance; (**b**) Normalized discrete difference of solar irradiance

The input vector relies on 3.68a, including three statistical feature parameters of irradiance Gsavg (n), TODmax(n) and NDD(n), one statistical feature parameter of ambient temperature Tavg(n), and also the date sequence number n. The output vector includes 24 components represent the surface irradiance from the next day (i.e., the date sequence number is n + 1). Any time resolution is 1 h for the components of output vector. The two hidden layers in the ANN model, and also the volume of neurons in hidden layer 1 and hidden layer 2 are p, q respectively. Levenberg-Marquardt Algorithm (LMA) is used rather than conventional BP algorithm. LMA combines the feature of Gauss-Newton algorithm along with the

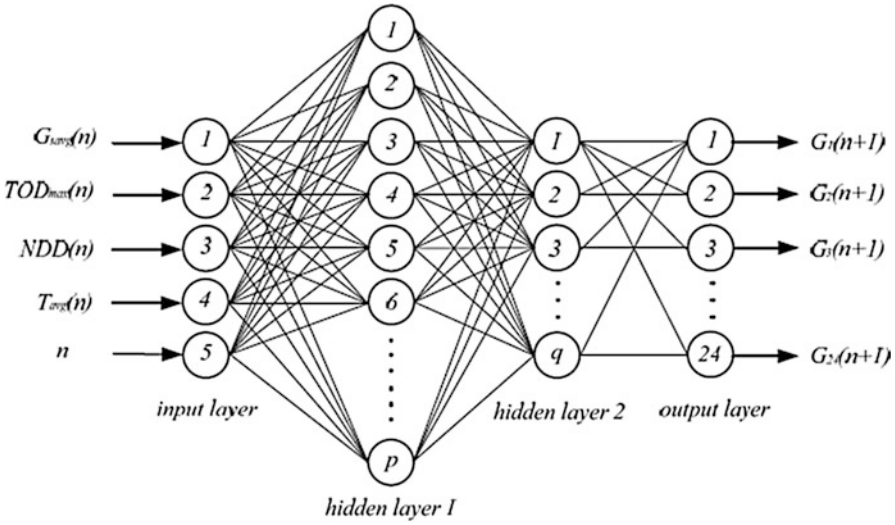


Fig. 3.83 ANN forecast model using statistical feature parameters

gradient descent algorithm. LMA might be more robust than Gauss-Newton algorithm since it finds an alternative whether or not it starts very far from the last minimum. In a large distance from the function minimum, the steepest descent strategy is utilized to provide steady and convergent progress toward the solution. As the solution approaches the minimum, damping parameter is adaptively decreased, the LMA approaches the Gauss-Newton algorithm, and the solution typically converges rapidly to the minimum.

The connection weights are adjusted by the LMA according to (3.69):

$$\Delta\omega = -\left[\mu I + \sum_{p=1}^{P} J^P(\omega)^T J^p(\omega)\right]^{-1} \nabla E(\omega) \tag{3.69}$$

where ω is connection weights, $\Delta\omega$ is weight correction, $E(\omega)$ is learning error, $J(\omega)$ is the Jacobian matrix of error vector, μ is damping parameter, I is identity matrix, P is the number of sample data. Three different error statistical indicators including mean absolute percentage error (MAPE), root mean square error (RMSE) and mean absolute bias error (MABE) are selected to evaluate the forecast accuracy of the models, these error statistical indicators can be computed according to the following formulas:

$$MAPE = \frac{1}{N}\sum_{i=1}^{N}\left(\left|\frac{G_{f,i} - G_{m,i}}{G_{m,i}}\right|\right) \times 100 \tag{3.70}$$

$$RMSE = \sqrt{\frac{1}{N}\sum_{i=1}^{N}\left(G_{f,i} - G_{m,i}\right)^2} \tag{3.71}$$

$$MABE = \frac{1}{N}\sum_{i=1}^{N}\left(\left|G_{f,i} - G_{m,i}\right|\right) \tag{3.72}$$

where $G_{f,i}$ is forecasted value, $G_{m,i}$ is measured value, $(i = 1,2,\ldots,N)$, N is the number of the solar irradiance data. The benefit of the traditional ANN-HDS model is that it might be simply built only through the use of historical data compilation of solar irradiance. One main problem with ANN-HDS model is usually that the high dimension with the input vector, which will bring about more complex model that is hard to build and train. A result of the absence of the opposite related parameters except solar irradiance, another disadvantage to ANN-HDS model is the information inside the input vector is incomplete this also can lead to the losses of precision.

The solar irradiance of adjacent sunny days shows strong similarity and regularity and as a consequence perfect prediction can be performed through the common ANN-HDS forecasting model. Under changeable climate conditions, solar irradiance show irregular complex changes caused by a volume of meteorological factors, and therefore the ANN-HDS forecast model has stopped being applicable. The input vector in the ANN forecast model is reconstructed, and few statistical feature parameters are selected to change the multi-dimensional historical data group of solar irradiance. The input vector dimension is reduced plus the main information about the variation of climate might be effectively extracted through such improvement. The info redundancy and multiple coupling between input components are reduced inside the ANN-SFP forecast model.

3.10 Parameter Identification of Solar Cell Using Genetic Algorithm

The comparison of the voltage–current characteristic I(V) of a solar PV cell is dead set utilizing hereditary calculations focused around segregated purposes of the trademark got tentatively. The mathematical expressions involve a PV model with seven parameters. The basic model consists of a current source in parallel with a diode, as shown in Fig. 3.84. The sunlight makes the cell dynamic, delivering an electrical current denoted as photocurrent Iph. The output current I relies on the estimation of diode current I_D.

The basic scheme in Fig. 3.84 is extended with two resistors as shown in Fig. 3.85: RD is connected in parallel while RS is connected in series. RP shapes the crystal defects leading to less currents passing through the p-n junction. For well constructed solar cells, these defects are minor, such that RP is moderately high. The safety resistance RS is of a very small value.

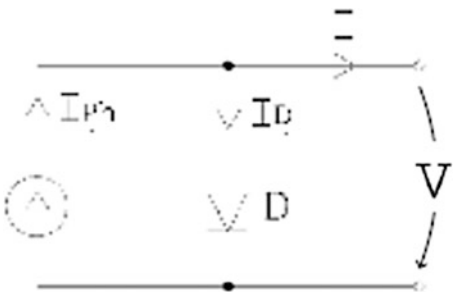


Fig. 3.84 Simplified conceptual model, with one diode, for a photovoltaic/ solar cell

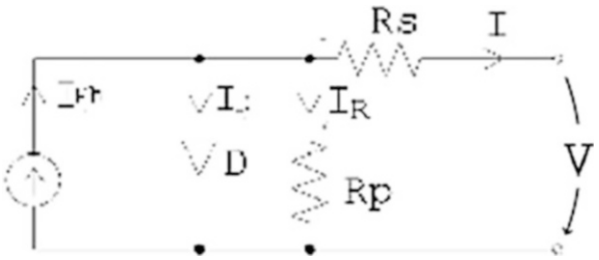


Fig. 3.85 Extended conceptual model, with one diode, for a photovoltaic/ solar cell

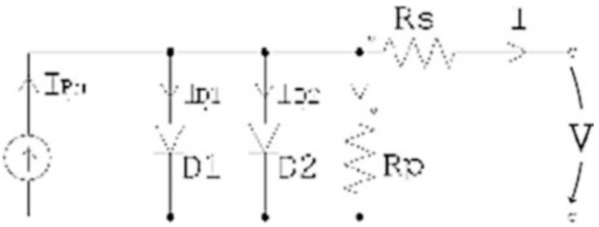


Fig. 3.86 Conceptual model with a two diodes for a photovoltaic/solar cell

An additional diode D2 is used in Fig. 3.86. The real diode effect is provided by this diode which is visible in the I(V) characteristics especially for $V < 0$ and partially for $V > 0$.

The model shown in Fig. 3.86 holds default *I(V)* characteristics and it works as follows.

$$I = I_{ph} - I_{D1} - I_{D2} - \frac{V + IR_s}{R_p} \tag{3.73}$$

Considering for I_{D1} and I_{D2} the same expressions as for Shockley diodes, the equality (3.73) becomes:

$$I = I_{ph} - I_{01}\left(e^{\frac{V+IR_s}{V_{T1}}} - 1\right) - I_{02}\left(e^{\frac{V+IR_s}{V_{T2}}} - 1\right) - \frac{V + IR_s}{R_p} \tag{3.74}$$

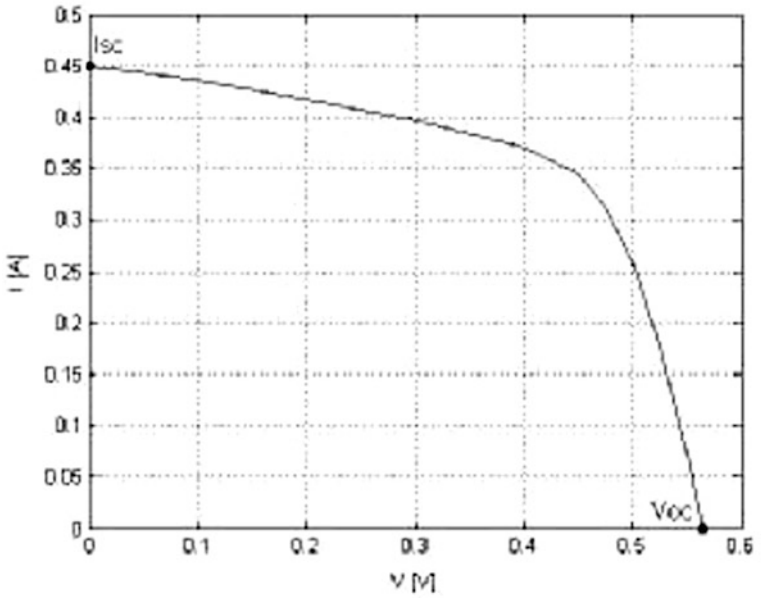


Fig. 3.87 Solar cell *I(V)* characteristic for constant solar radiation

The parameters such as I_{ph}, I_{01}, I_{02}, R_p, R_s are known in (3.74). Apart from these, two more parameters namely V_{T1} and V_{T2}. serve to model the non-linear influence of the temperature on the diode effect. V_{T1} and V_{T2} can be approximated by the relationship:

$$V_{T1} = \frac{n_1 \cdot k \cdot T_1}{q} \qquad V_{T2} = \frac{n_2 \cdot k \cdot T_2}{q} \tag{3.75}$$

where n_1 and n_2 are diode ideality factors for diode D_1 and D_2 respectively, k is the Boltzmann constant, T_1 and T_2 are the temperature of diode D_1 and D_2 respectively expressed in °K, and q is the elementary electrical charge. The functional part of the I(V) characteristic of the solar cell characteristic curve cold also "direct voltage" area is shown in Fig. 3.87. This in turn is equivalent to the values $V \geq 0, I \geq 0$ of the I-V curve and is bounded by the short circuit points ($V = 0$, $I = I_{SC}$), and open circuit point ($V = V_{OC}$, $I = 0$). The short circuit and open circuit points can be determined experimentally. With the assumption that V_{OC} and I_{SC} are known from measurements, the open circuit point and short circuit point imposed two links between the seven parameters.

$$0 = I_{ph} - I_{01}\left(e^{\frac{V_{OC}}{V_{T1}}} - 1\right) - I_{02}\left(e^{\frac{V_{OC}}{V_{T2}}} - 1\right) - \frac{V_{OC}}{R_p} \tag{3.76}$$

$$I_{SC} = I_{ph} - I_{01}\left(e^{\frac{I_{SC}R_S}{V_{T1}}} - 1\right) - I_{02}\left(e^{\frac{I_{SC}R_S}{V_{T2}}} - 1\right) - \frac{I_{SC}R_S}{R_p} \tag{3.77}$$

Assuming known the values of I_{01}, I_{02}, R_S, V_{T1} and V_{T2}, (3.76) and (3.77) make possible to obtain the parameters R_P and I_{ph} with the formulas

$$R_p = \frac{V_{OC} - I_{SC}R_S}{I_{SC} - I_{01}\left(e^{\frac{V_{OC}}{V_{T1}}} - e^{\frac{I_{SC}R_S}{V_{T1}}}\right) - I_{02}\left(e^{\frac{V_{OC}}{V_{T2}}} - e^{\frac{I_{SC}R_S}{V_{T2}}}\right)} \tag{3.78}$$

$$I_{ph} = I_{01}\left(e^{\frac{V_{OC}}{V_{T1}}} - 1\right) - I_{02}\left(e^{\frac{V_{OC}}{V_{T2}}} - 1\right) - \frac{V_{OC}}{R_p} \tag{3.79}$$

Hence, identification of expression given in (3.74), implies the determination of the following:

- seven parameters if the relations (3.75, 3.76, and 3.77) are not used;
- five parameters if only relation (3.75) is used;
- three parameters if all relations (3.75, 3.76, 3.77, 3.78, and 3.79) are used.

3.10.1 *Method of Determining the Parameters of Solar Cell Using Genetic Algorithms*

Identification of the expression in the I(V) characteristic curve leads to determination of seven parameters namely, I_{Ph}, I_{01}, I_{02}, R_S, R_P, V_{T1} and V_{T2}. Let us assume that R_P and I_{ph} can be calculated with formulas given by (3.78) and (3.79), while V_{T1} and V_{T2} are estimated with the formula given in (3.75). This leads to determination of remaining three parameters I_{01}, I_{02} and R_S. Let us refer this as Case I.

If relation (3.75) is not used, then five parameters such as V_{T1}, V_{T2}, I_{01}, I_{02} and R_S are determined. Let us refer this situation as *case II*.

Here Genetic Algorithms are applied to identify the parameters in both cases I and II. In Case I, an individual is defined by the vector (I_{01}, I_{02}, R_S), and in case II by the vector (V_{T1}, V_{T2}, I_{01}, I_{02}, R_S). The fitness function is framed as follows:

$$fitness = \sqrt{\sum_{k=1}^{12} c_k^2 \left(I_{meas}(V_k) - I_{calc}(V_k)\right)^2} \tag{3.80}$$

where $I_{meas}(V_k)$ is the measured current when $V = V_k$ and $I_{calc}(V_k)$ is the value calculated for voltage $V = V_k$.

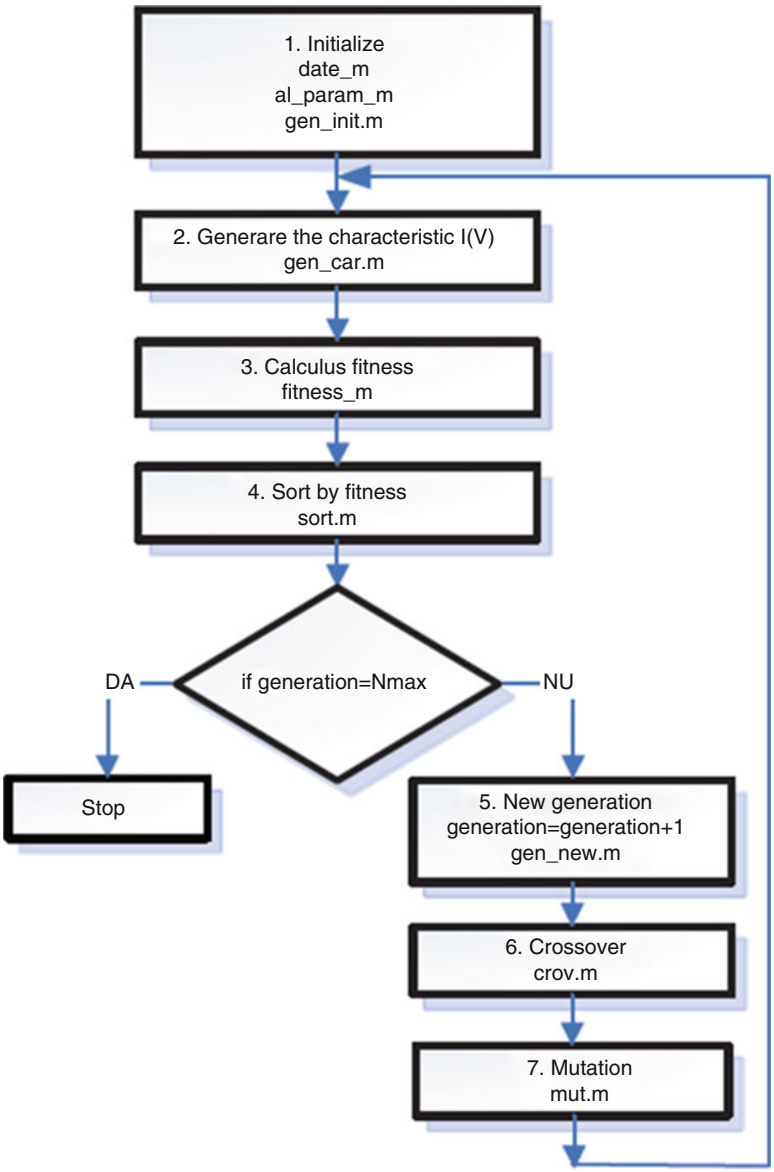


Fig. 3.88 Flowchart for parameter identification based on GA

The approach used in *case I* is depicted in the form of a flow chart as shown in Fig. 3.88. The MATLAB model of the program uses the following m files:

- *date.m* for the measured data {*Vk, Imeas(Vk)*};
- *al_param.m* for parameters as the cell surface or cell temperature;
- *gen_init.m* for the initial generation of genetic algorithms;

- *gen_car.m* for computing of the characteristic *Icalc(Vk)* of an individual;
- *fitness.m* for fitness computing of an chromosome / individual; descending order of fitness values;
- *gen_new.m* for a new generation;
- *crov.m* and *mut.m* for crossover, respectively mutation operations.

The steps illustrated in the flow chart are explained below:

Step 1: The parameters such as (V_{k_meas}, I_{k_meas}) are introduced; V_{T1} and V_{T2} are calculated using (3.75); With these inputs, the starting value for the parameters I_{01}, I_{02}, R_S are estimated. The initial population is formed in a random manner with 20 chromosomes in the form of vectors (I_{01}, I_{02}, R_S). The values are formed within a range of 20 % of the starting values. The parameters R_P and I_{Ph} of each chromosome in the population are computed using (3.78) and (3.79). The initial population is configured as the current generation.

Step 2: For each individual in the population, the characteristics $I_{calc}(V_{k_meas})$ of current generation is calculated.

Step 3: The fitness function is evaluated for all the individuals in the current generation according to (3.80).

Step 4: Based on the fitness values, the individuals of the current population are ordered in descending order.

Step 5: Stopping condition – If the number of iterations does not exceed N_{max} on proceed to step 6, otherwise Stop.

Step 6: Based on the ordering with respect to the fitness function, a new population is formed with the best 10 individuals of the current population.

Step 7: The crossover operator is applied. The new population expands and continues to grow based on crossover operation. The growing of the new generation is continued using the crossover operation. The type of crossover operator is based on roulette wheel followed by a intermediary crossover to generate two offspring. The descendent value is generated randomly within the zone Z in Fig. 3.89. After applying crossover, R_P and I_{Ph} are calculated with formulas (3.78) and (3.79).

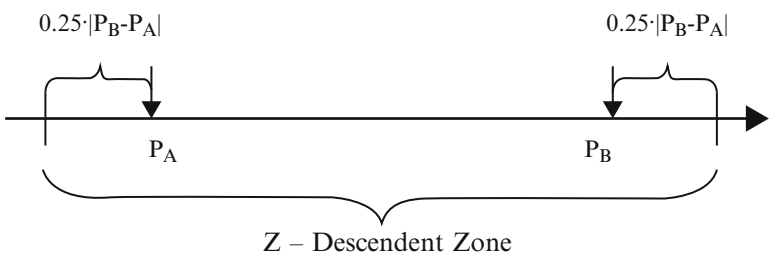


Fig. 3.89 Intermediary crossover

Step 8: The mutation operator is applied on a randomly chosen individual, by modifying one or more parameters. For each modified parameter the value of the descendent maintained in range of 20 % of the choice parameter. R_P and I_{Ph} are calculated as in step 7.

The same flowchart is followed for case II with changes in Step 1 of the algorithm. In Step 1, the starting value is estimated for the parameters such as V_{T1}, V_{T2}, I_{01}, I_{02}, R_S.

A maximum of 120-200 generations is required for the fitness function to stabilize. The stabilization of the fitness function is based on the following:

- the impact of intervention in panel because of the availability of several cells;
- the positive influence of higher surface of the cells from panel on the starting value estimations of parameters.

A method to identify the parameters of the external characteristics I(V) of the solar PV cells is discussed in this section. The methodology is based on genetic algorithms.

3.11 Application of Neuro-Fuzzy Technique for Prediction of Solar Radiation

The prediction is incredibly beneficial in solar powered energy applications since it permits to estimate solar data for locations where measurements aren't available. The developed artificial intelligence models predict the solar radiation time series better compared to the conventional procedures based on the clearness index. The forecasting ability of some models may very well be further enhanced with the aid of additional meteorological parameters. After having simulated a variety of structures of neural networks and trained using measurements as training data, the most beneficial structures were selected in order to evaluate their performance with regards using the performance of a neuro-fuzzy system. Since the alternative system, ANFIS neuro-fuzzy system was considered, because doing so combines fuzzy logic and neural network techniques which might be found in order to get more efficiency.

3.11.1 Neuro-Fuzzy Predictor (NFP)

The method for prediction system design based on fuzzy logic presents three characteristics: simplicity, a one-pass operation on the numerical input–output pairs to extract the rules and fast computational time. Suppose we are given N input output samples:

$$\left(x_1^{(p)}, x_2^{(p)}, \ldots\ldots, x_M^{(p)}; y^{(p)}\right) y^{(p)} \in R \qquad p = 1, 2, \ldots, N$$

where x_i = inputs, M = the number of inputs, y = the output.

This kind of is made up of the subsequent five steps as shown in Fig. 3.90. ANFIS is really a way of automatically tuning (Back propagation algorithm) TS-type fuzzy inference system based on some bunch of input–output data. The ANFIS predictor uses first-order TS-type systems, single output derived by weighted defuzzification and membership function type this is a generalized bell curve (MATLAB). Another method for solving forecasting tasks could be the combination of neural net predictors called committee machine. The committee machine is usually a static structure. In this particular technique the predictors are combined using a mechanism that does not involve the input. The outputs of four different predictors are nonlinearly combined to create an optimum prediction as shown in Fig. 3.91. Here, the nonlinear mechanism could be the neuro-fuzzy system ANFIS that is trained because of the output data from predictors. For simplicity, the NNP will likely be known as IL-HL-OL network, corresponding to the variety of nodes in each layer (IL: Input Layer, HL: Hidden layer and OL: Output layer). In iteration (time step) n, the nth training example is presented towards the network. The symbol Zi(n) refers back to the prediction signal appearing in the output of NNPi. The symbol Y (n) refers to the final prediction at iteration n.

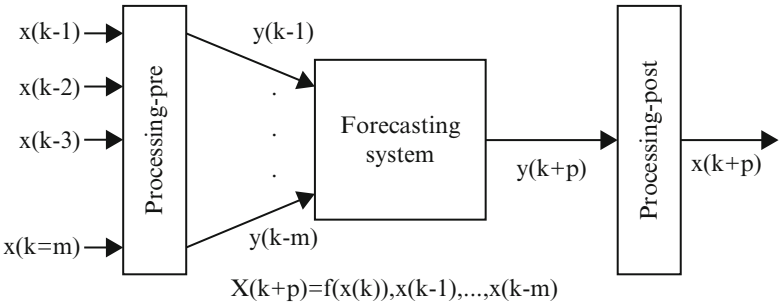


Fig. 3.90 Basic structure of the forecasting system

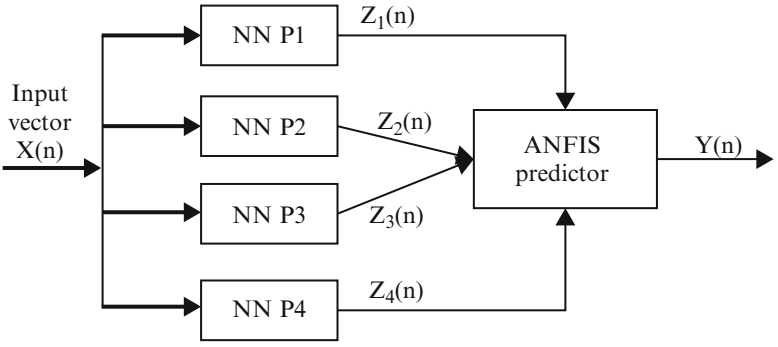


Fig. 3.91 A typical architecture of the non-linear mechanism of ANFIS model

Step 1: Divide the input and output spaces into fuzzy regions: Assume that the input xi and the output y lie in the domain intervals [xilmin, xilmax] and [ymin, ymax,] respectively. Each interval is then divided into 2z + 1 fuzzy regions and each region is assigned a symmetrical triangular fuzzy set.

Step 2: Data-generated fuzzy rules: The mth numerical data pair ((m) (m) (m) (m)) 1 2 M x,x,. . .,x;y is chosen from the training set. The membership grades are calculated for each data pair in the attributed fuzzy sets. The highest membership degree from the respective grades is chosen for each variable. A rule is formed based on the m training pair as follows:

Rm : IF x_1^m is A_1^m AND. . ..AND x_M^m is A_M^m THEN y^m is C^m

where A_i^m and C^m are fuzzy sets. These sets are attributed in the condition and conclusion parts of the rule and m is the index of the rule. Especially, li(i = 1,. . ., M) fuzzy sets are defined A_i^q, q = 1,. . .li for each input xi where lo represents the number of membership functions in the output space.

The fuzzy set A_i^m is one of the A_i^q's. Generally, in real applications we give, in the fuzzy sets linguistic names, like "big", "very positive".

Step 3: Assign a degree to each rule: Because there are usually many data pairs and as a consequence many rules generated, there exists high odds of conflict. That is certainly, rules who have the same IF part as well as a different then part. To settle this issue would be to assign a Truth Degree (TD) to each rule and accept merely the rule that has the biggest truth degree. We utilize following product strategy:

$$TD(m) = \mu_{A_1^m}\left(x_1^{(m)}\right).....\mu_{A_M^m}\left(x_M^{(m)}\right).\mu_{C^m}\left(y^{(m)}\right) \tag{3.81}$$

Step 4: Create a combined fuzzy rule base: The maximum number of rules that can be generated is l1 · l2 · . . . · lM. Through the 3rd step the reduction of the amount of rules is achieved. The generated rules determine a combined fuzzy rule base.

Step 5: Determine a mapping based on the combined fuzzy rule base: Determine the entire continuous fuzzy predictive model. Using the combined rule base with K fuzzy rules, the goods inference engine, the singleton fuzzifier as well as the center-average defuzzifier, the subsequent fuzzy technique is obtained:

$$y = f(x) = \frac{\sum_{j=1}^{K} y_c^j \left(\prod_{i=1}^{M} \mu_{A_i^j}(x_i)\right)}{\sum_{j=1}^{K} \left(\prod_{i=1}^{M} \mu_{A_i^j}(x_i)\right)} \tag{3.82}$$

where y_c^j is the centre of Cj. The output variable y is based on the inputs (x1, x2,. . ., xM). Methods to train object is always to minimize the mean square error between the predictions plus the real values. To find the most appropriate training algorithm, there is developed a small neural network 3-10-1, with sigmoid

activation function from the nodes in the hidden layer plus it was simulated for normalized data in the community 0.1–0.9 for 13 different algorithms using the neural network toolbox of MATLAB. Five error metrics were used in order to find the best algorithm: MSE, RMSE, AME, NDEI, ρ. The algorithms based on metrics used are as follows:

3.11.2 Error Metrics

$$MSE = \frac{1}{n}\sum_{k=1}^{n}\left(x(k) - \hat{x}\,(k)\right)^2 \tag{3.83}$$

$$RMSE = \sqrt{\frac{1}{n}\sum_{k=1}^{n}\left(x(k) - \hat{x}\,(k)\right)^2} \tag{3.84}$$

$$AME = \frac{1}{n}\sum_{k=1}^{n}\left|x(k) - \hat{x}\,(k)\right| \tag{3.85}$$

$$NDEI = \frac{RMSE}{\sigma} = \sqrt{\frac{\sum_{k=1}^{n}\left(x(k) - \hat{x}\,(k)\right)^2}{\sum_{k=1}^{n}x^2(k)}} \tag{3.86}$$

$$\rho = \frac{\sum_{k=1}^{n}\left(x(k) - \overline{x}\right).\left(\hat{x}\,(k) - \overline{x}\right)}{\sqrt{\sum_{k=1}^{n}(x(k) - \overline{x})^2.\sum_{k=1}^{n}(\hat{x}\,(k) - \overline{x})^2}} \tag{3.87}$$

where, x(k) is the real value in time instance k, $\hat{x}\,(k)$ is the prediction of the model, and N is the number of test data used for prediction. It must be mentioned which the most characteristic error criterion showing the caliber of prediction was proved really do the correlation coefficient criterion (ρ). As the prediction improves, ρ is getting close to 1.

3.11.3 Neural Networks Training

After having trained and tested all of the different cases and structures of neural networks while using the different in normalization and type meteorological time-

series, they are compared good above error criteria in order to result in the most suitable neural predictor's structure for every single different time-series:

- To start with there was clearly chosen the best four neural networks for every different form of normalization.
- Next there are chosen the most beneficial four neural network predictors for every single different type of meteorological time-series.
- Finally there were made choice of the most effective neural network predictor for each and every different time-series just to be capable to compare its results with ANFIS or any other system created.

The best neural network predictors for any different time-series using Sigmoid Activation Function (SAF) are introduced.

Mean daily solar radiation: 5-15-1, normalized inside the range 0.1–0.9, using SAF.

Mean daily temperature: 5-10-1, normalized within the range 0.1–0.9, using SAF.

'Best' neural network predictors Vs ANFIS: To the training and testing of knowledge there seemed to be made a first TS type system composed of seven inputs. A combination of fuzzy logic with neural networks turned out to have good results about the daily solar radiation and temperature forecasting. Below there is presented an assessment is presented relating to the 'best' N.N. predictors and ANFIS, with the four different time series, using as criterion the metric that turned out to be probably the most accurate, which is the correlation coefficient (ρ). With the global prediction scheme we split the collected data into two categories. The set includes the temperature on the first 5 years (1991–1995), while the test set includes the rest of the 5-years (1996–2000). Choosing four inputs to make the TS method case-dependent. For that numerical fuzzy approach 125 rules were obtained. In the table of comparison the computational time has already been recorded.

3.11.4 Prediction Results with NNP

The key object would be to create many different structures of neural network predictors and train and test them out while using meteorological data available in order to summarize the top plus more efficient topology for forecasting solar radiation and temperature. For the meteorological time series utilized in these studies, one hidden layer is proper and sufficient. These cases of structures of neural networks are created and simulated:

Inputs: 2,3,5,7 previous daily measurements for the 12 different time series created (real and normalized data),
Number of hidden layers: 1,
Number of nodes of hidden layer: 2,3,5,10,15,
Output: 1 (One day prediction),

Activation Functions used in neurons:

Hidden layer: sigmoid, linear,
Output layer: linear.

After having trained and tested all the various cases and structures of neural networks with the different in normalization and type meteorological time-series, they've been compared good above error criteria so that the most appropriate neural predictors' structure for different time-series. The optimum neural network predictors for different time-series are introduced.

Daily mean solar radiation: 5-15-1, normalized in the range 0.1–0.9, using SAF.
Daily mean temperature: 5-10-1, normalized in the range 0.1–0.9, using SAF.

Concerning neuron-fuzzy predictors plus more specifically ANFIS it can be proved which the combined linguistic rules of fuzzy logic while using training algorithm utilised in neural networks, contribute in very qualitative prediction results, which approach the 'best' neural predictor's results. The structure from the TS fuzzy model is identified having a method which permits to determine the optimal structure on automatic manner while being based on the calculation in the incredible importance of the policies in the calculation on the model output. However, the linear parameters are estimated with the WLS algorithm along with the non-linear parameters are estimated while using the TS method. Additionally, an assessment is completed between identified TS fuzzy model. The obtained results show that this identified TS fuzzy model provides satisfactory performances. So, we conclude which the fuzzy systems can be used as an alternative approach to generate solar data for locations where measurements will not be available.

3.12 Summary

In this chapter, the basic concepts of soft computing techniques such as neural networks, fuzzy logic, genetic algorithms, hybrid model of neural networks and fuzzy logic are discussed. The importance of soft computing techniques such as neural networks, fuzzy logic and genetic algorithms in solar PV system is delineated. MATLAB/SIMULINK models have been developed for ANN, fuzzy and ANFIS based MPPT of Solar PV system, fuzzy based solar powered energy and optimization in solar PV array. The approach to predict solar irradiance using soft computing techniques and parameter estimation of Solar PV module using Genetic Algorithms is explained in detail.

Review Questions

1. State the different types of Artificial Neural Networks.
2. Mention the differences between biological and artificial neurons.
3. What are considerations to take into account while choosing a neural network?

4. Define uncertainty and imprecision with respect to fuzzy logic.
5. What do you mean by fuzzification?
6. Discuss the different methods available for defuzzification.
7. State the step by step procedure for Genetic Algorithms.
8. Define crossover and mutation probability.
9. What is the role of soft computing techniques in Solar PV systems?
10. Develop a MATLAB/SIMULINK model for MPPT control using Genetic Algorithms.
11. Discuss optimization in Solar PV systems using soft computing techniques.
12. Describe solar cell parameter extraction using Artificial Neural NetwoSIMULINK mode/SIMULINK model.
13. How is ANFIS applied to solar irradiance forecasting?
14. State and explain applications of solar PV using Fuzzy logic control.

Bibliography

Ahmed MM, Sulaiman M (2003) Design and proper sizing of solar energy schemes for electricity production in Malaysia. National Power and Energy Conference 2003, pp 268–271

AL-Ismail FS, Abido MA (2011) The impact of statcom based stabilizers on power system stability, using intelligent computational optimization approach. Innovative Smart Grid Technologies Asia (ISGT), 2011 IEEE PES, pp 1–13

Altas IH, Sharaf AM (2007) A novel GUI modeled fuzzy logic controller for a solar powered energy utilization scheme. The 13th international conference on emerging nuclear energy systems (ICENES2007), Istanbul, 3–8 June 2007

Attia A-F, Soliman H, Sabry M (2006) Genetic algorithm based control system design of a self-excited induction generator. Acta Polytech 46(2):11–22

Banerjee S, Jeevananathan (2010) Modeling of PV array and performance enhancement by MPPT algorithm. Int J Comput Appl 7:35–39 (0975–8887)

Brini S, Abdallah HH, Ouali A, Economic dispatch for power system included wind and solar thermal energy. Leonardo J Sci (14):204–220

El-Moghany MS, Hamed BM (2012) Two axes sun tracker using fuzzy controller via PIC16F877A. The 4th international engineering conference –towards engineering of 21st century, 2012

Houck CR, Joins JA.A genetic algorithm for function optimization: a matlab implementation

http://www.ren21.net. Accessed June 2008

Hussein KH, Muta I, Hoshino T, Osakada M (1995) Maximum photovoltaic power tracking: an algorithm for rapidly changing atmospheric conditions. IEE Proc Gener Trans Distrib 142 (1):59

Karthika S, Rathika P, Devaraj D (2013) Fuzzy logic based maximum power point tracking designed for 10 kW solar photovoltaic system. Int J Comput Sci Manag Res 2(2):1421–1427

Koutroulis E et al (2001) Development of a microcontroller-based photovoltaic maximum power tracking control system. IEEE Trans Power Electron 16(1):46–54

Lin C-T, Lee CSG (1996) Neural fuzzy systems: a neuro-fuzzy synergism to intelligent systems. Prentice-Hall, Upper Saddle River

Petcuţ F-M, Dragomir TL (2010) Solar cell parameter identification using genetic algorithms. Control Eng Appl Inf 12(1):30–37

Rahoma WA, Ali Rahoma U, Hassan AH (2011) Application of neuro-fuzzy techniques for solar radiation. J Comput Sci 7(10):1605–1611

Simoes MG, Franceschetti NN (1999) Fuzzy optimization based control of a solar array system. IEE Proc Electr Power Appl 146(5)

Usta MA, Akyaz Ö, Altaş İH (2011) Design and performance of solar tracking system with fuzzy logic controller. 6th international advanced technologies symposium (IATS'11), Elazığ, 16–18 May 2011

Valarmathi R, Palaniswami S, Devarajan N (2012) Simulation and analysis of wind energy and photo voltaic hybrid system. Int J Soft Comput Eng 2(2):193–200, ISSN: 2231-2307

Wang F, Mi Z, Su S, Zhao H (2012) Short-term solar irradiance forecasting model based on artificial neural network using statistical feature parameters. Energies 5:1355–1370

Chapter 4
Wind Energy Conversion Systems

Learning Objectives
On completion of this chapter, the reader will have knowledge on:

- Characteristics of Wind Energy.
- Basic components of Wind Energy Conversion systems.
- Types of Wind Turbine Generator Configurations.
- Power Converter Topologies for Wind Turbine Generator.
- MATLAB/SIMULINK model of Wind Turbine.
- MATLAB/SIMULINK model of different types of turbines in WECS.
- Grid Integration and MATLAB/SIMULINK model of Grid Connected WECS.

4.1 Introduction

The wind is a free, clean, and inexhaustible type of solar powered energy. Winds originate from the uneven heating in the atmosphere from the sun, the irregularities from the earth's surface, and rotation of the earth. Wind flow patterns are modified through the land terrain, environmental conditions and buildings. This wind flow, or motion energy, when harvested by modern wind turbines, enable to generate electricity. The terms wind energy or wind generation describes the task where the wind is utilized to come up with mechanical power or electricity. Wind turbines convert the kinetic energy inside wind turbine into mechanical power. This mechanical power may be used for grinding grain or pumping water or perhaps a generator can convert this mechanical power into electricity energy. Wind turbines exactly like the aircraft propeller blades, converts the linear motion in the air into circular motion and powers a power generator that supplies a current. The wind turns the blades, high torque, low speed of the wind will result in low torque, high

© Springer International Publishing Switzerland 2015

S. Sumathi et al., *Solar PV and Wind Energy Conversion Systems*,
Green Energy and Technology, DOI 10.1007/978-3-319-14941-7_4

speed using gearbox and through a shaft, which connects to a generator and in turn produces electricity. Wind turbines can be bought in different sizes, and as a consequence different power ratings. Utility-scale turbines home in size from 50 to 750 kW. Single small turbines, below 50 kW can be used for domestic applications. Wind turbines will often be grouped together in a single wind generation plant, alias wind energy facility. Electricity out there turbines is fed in to a utility grid and distributed to customers, just like conventional power plants.

The wind has been utilized to power wind-surfing ships for almost all centuries. Many international locations owed their success on their science in sailing. No doubt, wind was about the only actual power source intended for ships until W invented the water engine inside the actual 1700s. The first recorded English generator is dated at 1191. In this generation, the initial corn-grinding windmill was integrated. There were quite a few technological developments on the centuries, and furthermore during 1600 the most popular windmill was the actual tower mill. This phrase mill refers to the operation of grinding or milling texture. Based on this application, wind generators were categorised as windmills regardless in the event that these people moved water or performed some other work. Denmark was the primary country to work with the wind pertaining to generation of electrical energy. Denmark was the leading country to operate the wind for multiplication of electricity.

During 1925, commercial wind-electric plants using a couple of- and three-bladed propellers appeared for the American market. The most commonly encountered brands were Wincharger (200–1,200 W) as well as Jacobs (1.5–3 kW). These were applied to farms to charge hard drive batteries which were then used to operate receivers, lights, and small devices with voltage ratings involving 12, 32, or 110 volts. A good collection of 32 Vdc appliances was made by industry to meet this demand. Then the Rural Electric Administration (REA) was established by Congress in 1936. Low interest rate loans were provided and so the necessary transmission and circulation lines could be made to supply farmers using electricity. In the conception of the REA, approximately during 1940, electricity could follow supplied to the outlying customer at a tariff of 3–6 cents per kWh. The equivalent cost of wind created electricity was 12–30 cents per kWh when interest, accounting allowance, and maintenance were incorporated. After 1940, the price of utility generated electricity carried on a slow decline, sinking under 3 cents per kWh in the beginning 1970s. This ended up by using larger and more useful generating plants.

The Federal Wind Energy Program got its beginning in 1975 when a joint Solar technology Panel of the National Science Foundation (NSF) as well as the National Aeronautics and Space Administration (NASA) recommended that will wind energy be created to broaden the Region's energy options achievable energy sources. With 1973, NSF was given the responsibility for this Federal Solar Energy Plan, of which wind vitality was a part. The actual Lewis Research Center, any Federal Laboratory controlled by simply NASA, was selected to deal with the technology development and also initial deployment of prominent wind turbines. Early in 1974, NASA was financed by NSF to (1) design, build, and operate a wind turbine for research purposes, designated the MOD-0, initiate scientific studies of wind turbines pertaining to utility application, and (three or more) undertake a

program involving supporting research and engineering development for wind turbines. In 1975, the liability within the Federal governing for wind turbine development was assigned to the actual newly created Energy Analysis and Development Administration (ERDA). ERDA was after that by the United states doe (DOE) in 1977. The actual NASA Lewis Research Center continued to direct the technology development of prominent turbines during this time.

In this chapter, the characteristics of Wind energy and components of Wind energy conversion systems are discussed. The types of wind turbine generators based on their electrical configuration are described. The power converter topologies used for wind turbine generators are elaborated in detail. The MATLAB/SIMULINK models for wind turbine and types of wind turbine generators are developed and the simulation results are analyzed. The concept of grid connection with SIMULINK model is presented in this chapter.

4.2 Wind Characteristics

> The wind blows to the south and goes round to the north; round and round goes the wind, and on its circuits the wind returns. Ecclesiastes 1:6

The earth's air can be modeled as a gigantic heat engine. The item extracts energy from the sun in addition to delivers heat to yet another reservoir at a cheaper temperature (space).In the procedure, work is done within the gases in the ambiance and upon the ground-atmosphere boundary. There will likely be regions where the atmospheric pressure is temporarily higher or perhaps lower than average. That difference in air pressure causes atmospheric gases or perhaps wind to flow through the region of higher press to that of reduced pressure. These regions are normally hundreds of kilometers in diameter. The wind relocating counter clockwise in the particular cyclone experiences a strain gradient force fp inward, a Coriolis force fc outward, and a centrifugal force fg outward. For wind to go on moving in a antagonistic clockwise direction parallel for the isobars, the forces have to be balanced, so the stress gradient force for A cyclone is $fp = fc + fg$. The pressure force inward is balanced well by the sum from the Coriolis and centrifugal aids. The wind that runs in such a product is called the gradient wind flow.

Mechanical designing of gears, shafts and brakes is performed. They possess effect on minimum energy required to start the equipment, cut-in-speed, potential to absorb variation within rotor torque by keeping in the form of strain energy, shaft rigidity for non-useful a good deal and flexibility for beneficial loads. Structural design is carried out for knives, root, hub, support anatomical structure, tower and foundation according to static, dynamic and tiredness loading. Blade root will be subjected to loads together with moments in all several direction. Further they change through-out the lifetime of the machine even whether it's in a shut-down condition. Soft designing techniques like coning and teetering of rotor works extremely well in rotor design. Collection of tower is also important in wind machine design the way it slows down the breeze and also imparts innervation loads on the device. Natural frequencies of distinct wind machine

components ought to be carefully designed considering how often these excitation loads exist. The wind machine also needs to be designed considering the requirements of transport and installation. Direct smooth highways are required to carry long blades and installation equipment to the installation site usually in remote parts. Similarly, heavy, sophisticated along with costlier material handling products are required to handle heavy and unwieldy machine pieces at site.

Characteristic parameters for wind machine are

- Rated power of the machine, is the maximum power developed by the rotor and is also the generator rating.
- Cut-in speed, u_c is the minimum wind speed at which the machine starts rotating.
- Rated speed, u_R is the minimum wind speed at which the machine develops rated power. This is the speed at which the blade regulation become active.
- Furling speed, u_F is the maximum wind speed at which the machine develops power. The machine is stopped beyond this speed.

4.3 Wind Turbine

The principle of wind turbines in power generation is transformation of the air kinetic energy into rotating mechanical power of the turbine rotor blades. At this moment soon enough the most common secondary wind turbine is the particular horizontal-axis propeller having 2 or 3 blades mounted on the top of a tower. The selection of number of blades of the wind turbine is not an easy design choice. Three blade systems cost in excess of two blade systems, yet two blade wind generators have to operate on higher rotational speeds than three blade ones. This way the individual blades of the two bladed wind generator need to be lighter and have bigger awkwardness and are therefore more pricey. The basic formulation for the power in the wind in a location A, perpendicular to the wind blowing direction is given by the formula:

$$P = \frac{1}{2}.\rho.A.C_p.v^3 \tag{4.1}$$

where P is the power, ρ is the air density, v is the wind speed and Cp is the power coefficient, which describes the fraction of the wind captured by a wind turbine. According to Betz rules, the value of the power coefficient features a theoretic limit connected with 59.7 %.

Most wind power internet sites experience large wind speeds only for the few hours per evening. Hence different forms of power regulating schemes are necessary to be designed which in turn are cost effective. The design of wind mill elements is regulated by the ability to withstand physical loads. There are two basic aerodynamical blades types, which make it possible to reduce those loads. The wind generation can end up being regulated possibly by not function-regulation – scheming the knives to begin sleek stall above a specific wind speed level or even by message-control –

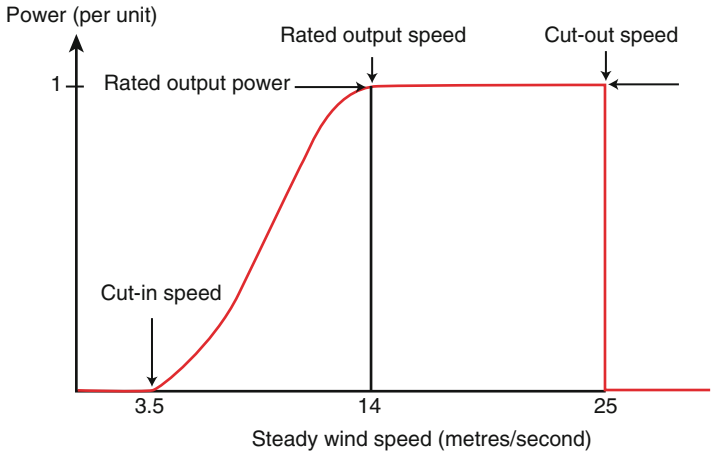


Fig. 4.1 Power from a pitch-regulated wind turbine

designing the rotor blades to generate the unnecessary power. A benefit involving stall-regulation is a simplified mechanized design of the rotor, that enables the blades for being affixed rigidly the generator hub. Additionally, stall-rules will definitely not permit strength excursions by very robust and gusty winds to pass on the thrust train. Additionally, it features disadvantages, as well: the requirement of a rotor coil brake, technological difficulties involving aerodynamic blades stall design, motor powered start along with stronger aerodynamic noise.

Figure 4.1 shows a comfortable wind speeding – power contour, which demonstrates the controlled power accomplishable from the particular wind generator. At very low wind rates of speed the developed power is too low to end up being utilized. With typical models the wind generators are started out when the wind swiftness exceeds three or more than four thousand. The turbine is started out at the cut-in wind pace and it's power will increase with another power on the wind rate, for the moment once the rated breeze speed is reached. On wind rates of speed range by 12 m/s around about 25 min the electricity is restricted to the ranked power on the wind turbine with the assistance of stall-regulations or pitch-control methods. When this wind pace exceeds 20–25 m/s the particular wind generators are commonly brought to be able to standstill avoiding high mechanically skillful loads within the turbine components. This wind flow speed is called the shortened-out breeze speed.

4.3.1 Fixed-Speed Wind Turbines

In early prototypes involving "fixed-speed wind turbines" "synchronous machines" have already been used, nevertheless the generalization machine was more broadly adopted to its lower charge, better environmental durability along with superior hardware compatibility along with rapid wind changes. That is why in preset-speed wind turbines, the power generator used may be the induction electrical generator type, connected towards the grid. Inside the majority associated with wind generators

designs the actual generator is definitely connected while using the hub using blades via a gearbox. They are placed within a nacelle on the top of the turbine system. The gear box is needed to change the lower rotational speed of the particular turbine to a high rotational speed within the generator. The rotational speed of induction power generators is typically 1,000 or even 1,500 revolutions. The rate of this turbine relies on their rotor dimension. For exercise a 330 kW turbine carries a rotational speed of around 18 – 1 out of 3 rpm, while rotational pace of the 1,670 kW turbine is around 10–19 rpm. A set-speed windmill is created to obtain greatest efficiency with one winding speed that will give this optimum tip speed with wind velocity ratio with the rotor aerofoil. To be able to capture far more wind energy, some set-speed wind turbines have a couple of different rotational speeds. This is achieved practically by positioning two power generators in this nacelle or by a single generator obtaining two freestanding windings.

4.3.2 Variable-Speed Wind Turbines

There are many similarities in variable speed wind turbine with respect to the components of fixed-speed wind turbines. These wind generators operating with a narrow variable-speed variety. Fixed-speeding wind mills operating inside a narrow velocity range unremarkably use a double-fed induction generator and possess a converter coupled to the rotor setup. The spinning speed on the double-fed induction motor is nearly 1,000 or 1,500 rpm, so a gear box implementation is necessary.

To reduce the nacelle design and style an unmediated-driven generator is employed. A unmediated-driven source using a huge turbine rotor blades diameter may operate for a very lower speeds and need a gearbox fitted to boost to pace. The usage of frequency convertor is to use a principal-driven power generator, so wind generators operating inside a broad adjustable-speed variety are equipped with a frequency converter. In the conventional fixed-speed wind generator, the gear box and the actual generator must be mounted on the stiff your bed plate and also aligned specifically in respect to each other. A direct driven generator can end up being integrated with the entire nacelle, so the generator unit and support structure can also be the main parts in the nacelle structure.

4.4 Components of WECS

Wind energy can follow harnessed with a wind power conversion organization, composed of wind generator blades, a generator, an power electronic converter tools and the related control system. Figure 4.2 indicates the block diagram involving different parts of WECS. Different WECS options based on synchronous or asynchronous machines, and stalling-regulated or even pitch controlled systems are available. The sensible objective of those systems is identical: converting the wind kinetic energy into electricity and inserting this energy into a utility grid.

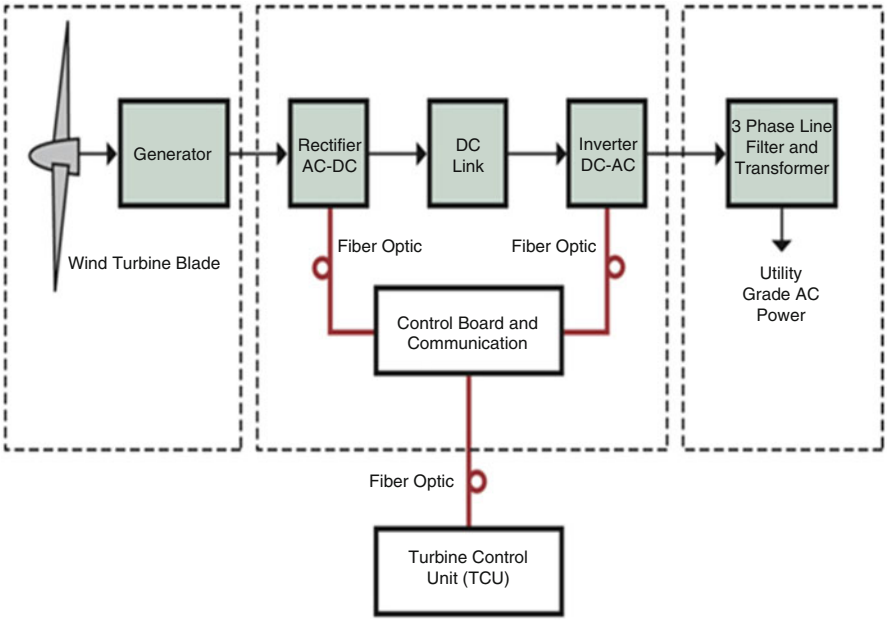


Fig. 4.2 Typical block diagram for a wind turbine power generation system

Figure 4.2 shows the normal block diagram of typical wind power generation system. The actual block demonstrates the wind generator and source selection represents a huge part in this wind energy conversion. Modern wind generators fall straight into two fundamental groups: the horizontal-axis wind turbine, like the original wind generator used for pumping water, and the vertical-axis wind turbine, like an eggbeater-fashion Darrieus product, named right after its France inventor. Many large modern-day wind mills are horizontal-axis wind generators.

Wind generators have being mounted in place where wind power is ample. Wind speed is higher up in the sky than the ground. The optimal site needs to be far by tall structures to keep off turbulences, which are the link between changing speed of wind when it hits the actual obstacles. Horizontal axis wind turbines harvest the wind energy against the actual direction associated with wind.

4.4.1 Description of Components

Horizontal turbine components include:

- blade or rotor, which converts the energy in the wind to rotational shaft energy;
- a drive train, usually including a gearbox and a generator;
- a tower that supports the rotor and drive train; and

- Other equipment, including controls, electrical cables, ground support equipment, and interconnection equipment.

4.4.1.1 Rotor

The area of the wind generator that accumulates energy on the wind is known as the blades. The rotor coil usually is made of two or even more wooden, fiberglass or steel blades which usually rotate an axis (horizontal or vertical) at a rate determined by the wind velocity and the design of your blades. The blades are attached to the center, which consequently is attached to the main base.

4.4.1.2 Drag Design

Knife designs run by using either drag or lift. With the drag design and style, the wind literally promotes the blades out of the way. Drag powered wind generators are seen as slower rotational speeds as well as high torque capabilities. They may be useful with the pumping, cutting or grinding work that will Dutch, grow and similar "work-equine" windmills perform. For exercise, a village-type wind turbine must develop high twisting at commence-up so as to pump, or lift, water system from the deep ground.

4.4.1.3 Lift Design

This lift edge design engages the same principle that makes it possible for airplanes, kites and also birds to fly. The particular blade is essentially control surface, or annex. When air travel flows past the blade, some sort of wind speed and force differential is produced between the top and lower blade section. The demand at the lower surface is greater and thus acts to be able to "lift" the blade. While blades attach to a main axis, like a wind turbine rotor, the lift is actually translated into rotational motions. Lift-power wind generators have much higher rotational data transfer speeds than move types and as a consequence well designed for electricity generation.

4.4.1.4 Tip Speed Ratio

The tip-speed would be the ratio in the rotational pace of the blade towards the wind speed. The greater this percentage, the more quickly the turning of the actual wind turbine rotor at the given winding speed. Energy generation calls for high rotational speeds. Lift-type wind generators have maximal tip-swiftness ratios of around 10, while drag-type ratios are generally approximately. Given this high rotational speed demands of electrical generators, it's clear that this lift-type wind turbine is almost practical due to its application.

4.4.1.5 Number of Blades

The volume of blades comprises the total number of blades and the total area they will cover to aid wind generator performance. For a lift-type rotor to function effectively, the wind ought to flow effortlessly over this blades. In order to avoid turbulence, spacing between blades should be greater so that particular blade is not going to encounter the actual disturbed blade. Due to this reason, most of the wind turbines have only two or three blades on their rotors.

4.4.1.6 Generator

The generator converts the particular rotation of wind turbines blades directly into electricity. Inside this constituent, coils regarding wire tend to be rotated in the magnetic field to create electricity. Generator models produce often alternating current (AC) or perhaps direct current (DC), and they're available within a large range of output electrical power ratings. The generator's standing, or size of it, is influenced by the length of the wind generator blades. Generators that generate AC usually are equipped along with features to generate the accurate voltage (a 100 V and 20 V or 240 V) as well as constant consistency (50 series) of power, even if the wind speed is varying. DC power generators are normally used in battery pack charging applications and for operating Digicam appliances in addition to other equipments. They also can be used to produce Air conditioning electricity by using an inverter, which converts Direct current to Air conditioning.

4.4.1.7 Transmission

The amount of revolutions per minute (rpm) of wind turbine rotor range between 45 rpm along with 400 rpm, depending on the model plus the wind velocity. Generators generally require rpm's of just 200 to at least 800. Consequently, most wind turbines require some sort of gear-pack transmission to raise the rotation of the generator to the speeds necessary for efficient electricity production. A few DC-form wind turbines do not use transmissions. Instead, they have a direct online link between the particular rotor and generator. These are generally known as direct thrust systems. While transmission is not performed, wind turbine complexity and maintenance specifications are decreased, but a larger turbine is necessary to deliver the identical power output in this AC-type wind turbines.

4.4.1.8 Towers

The structure on which usually a wind generator is installed is not just a support framework. It in addition raises the particular wind turbine so that it is blades safely and securely clears the floor and then it can attain the stronger winds at increased elevations. Maximum tower level is optional in many cases, except in which zoning restrictions apply. Deciding exactly what height tower system should be mounted will be based on the cost regarding taller towers versus the amount of the increase in power production caused by their work. Studies have established that the added cost connected with increasing podium height is often justified through the added power generated in the stronger gusts of wind. Larger wind generators are unremarkably mounted about towers between 40 and 70 m tall. Podiums for small wind methods are generally "guyed" styles. This means that there are guy wires anchored to the floor on 3 or 4 sides of the tower to carry it erect. These podiums cost lower than freestanding systems, but require more acreage to ground tackle the man wires. A few of these guyed towers are built by tilting them upwards. This function can possibly be quickly achieved using just a winch. This shortens not only installation, but maintenance as well. Towers could be constructed of a simple tubing, a wood pole or a lattice connected with tubes, supports, and angle bracket. Large wind generators may be mounted in lattice towers, tube towers or guyed aim-up systems. Installers can suggest the better type connected with tower on wind turbine. It must be strong and ample to offer the wind turbine and to be able to sustain shake, wind packing and the complete weather components for the lifetime of the wind generator. Tower expenses will change widely as being a function associated with design as well as height. A few wind turbines are marketed complete having tower. More often, however, podiums are marketed separately.

Advantages of the Horizontal axis Wind turbine:

- Higher efficiency,
- Ability to turn the blades, and
- Lower cost-to-power ratio.

Disadvantages of horizontal-axis:

- Generator and gearbox should be mounted on a tower, thus restricting servicing, and
- More complex design required due to the need for yaw or tail drive.

4.5 Types of Wind Turbine Generators

Over four decades the advancement of wind generation conversion engineering has generated development of several different adjustments of wind generators, which employ a wide selection of electric turbines. The group of most popular electric source types utilized in megawatt variety wind energy conversion systems (WECS) is presented in Fig. 4.3.

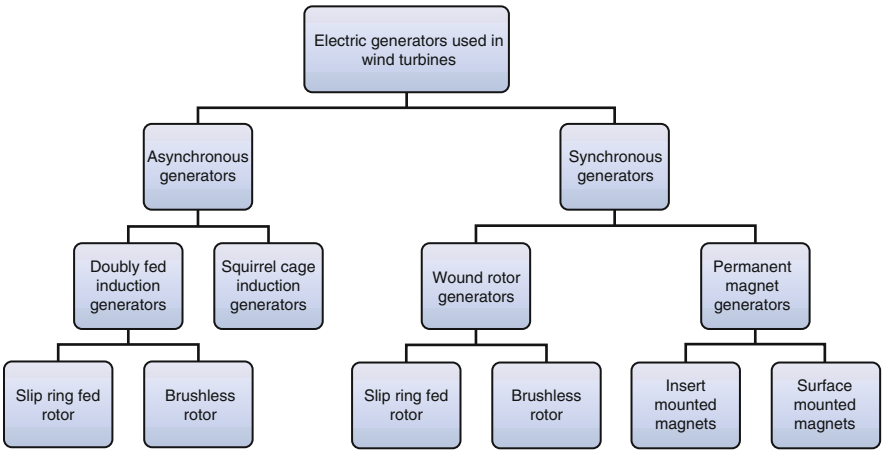


Fig. 4.3 Types of generators in WECS

Nowadays the direct current generators are usually found in low-voltage and very low-power standalone systems with small size wind strength applications. The alternating stream generators existing in present scenario are the most common solution for large scale wind flow energy conversion process systems. This alternating current generators are usually divided in two main groups, depending on the construction along with operating theory: synchronous generators (SG) and also the induction generators (IG). Each synchronous and induction generators can always be constructed using wounded rotors, that is fed with slip rings through hair brushes or by way of brushless electro-magnetic exciter. In the matter of non-harmed induction generator rotor designs, the rotor coil alternating current needs to develop the magnetic field from a different source compared to externally given current. With regards to the generalization generators it is performed via induction phenomena. The most commonly used induction generator through the years is the squirrel cage induction turbine. If the particular induction power generator rotor gets injured, it becomes doubly fed induction generator (DFIG), becoming one of the extremely commonly utilized generator used in wind generators applications. In case there is synchronous turbines the rotor magnetic flux can be also created because of the rotor rotation and also through the usage of permanent magnets mounted on the blades. This results in permanent magnet synchronous generator (PMSG). A few types regarding permanent magnet synchronous generators can be distinguished, determined by how the magnets are mounted on the rotor: wound rotor generators, permanent magnet generators. The classification of generators used in WECS is shown in Fig. 4.3.

4.5.1 Type 1 WTG

Squirrel-cage Induction generator (SCIG) connected directly to the step up transformer is referred to as the Type I Wind Turbine Generator. The turbine speed is fixed (or practically fixed) towards electrical grid frequency. The item generates real power when the turbine shaft rotates faster than the electrical grid frequency developing a negative (positive slip and power is due to motoring convention). For any given wind flow speed, the actual operating velocity of the turbine under steady problems is a practically linear purpose of torsion. For abrupt changes within wind speed, the kinetic inertia with the drive will control the pace of change in electrical output. Figure 4.4 shows the standard configuration connected with type 1 wind turbine generators.

Figure 4.5 shows the power flow on the SCIG terminals. Since there is a deviation in the output due to the slip of the machine, Type 1 generators typically work at or perhaps very close to a rated speed. An important drawback in the induction generator is the reactive energy it consumes for its excitation subject and the massive currents the machine can bring when running "across-the-line." To remove these outcomes the turbine typically engages a delicate starter in addition to discrete ways of capacitor banks from the turbine.

4.5.2 Type 2 WTG

Wound rotor motor induction generators are connected to the WTG step-up transformer in a way similar to Type 1 with respect to the machines stator coil circuit, but also include a variable resistor in the actual rotor signal as found in Fig. 4.6. This can be accomplished with a set of resistors and power electronics components added external to the rotor along with currents going between the resistors as well as rotor through slip rings. Alternately, the resistors as well as electronics components can be mounted within the rotor, eradicating the slip rings. The variable resistors are generally connected to the rotor routine softly and can control the rotor voltages quite quickly, thus maintaining continuous power.

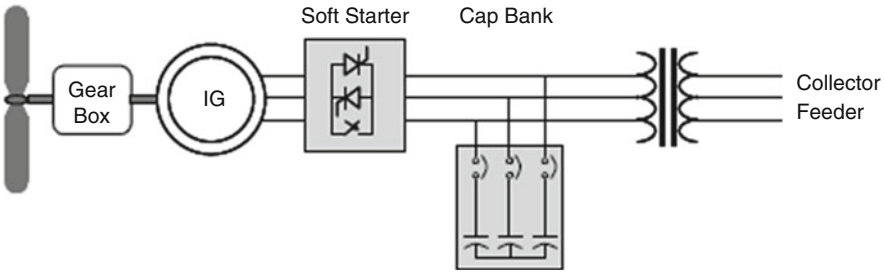


Fig. 4.4 Configuration of Type 1 WTG

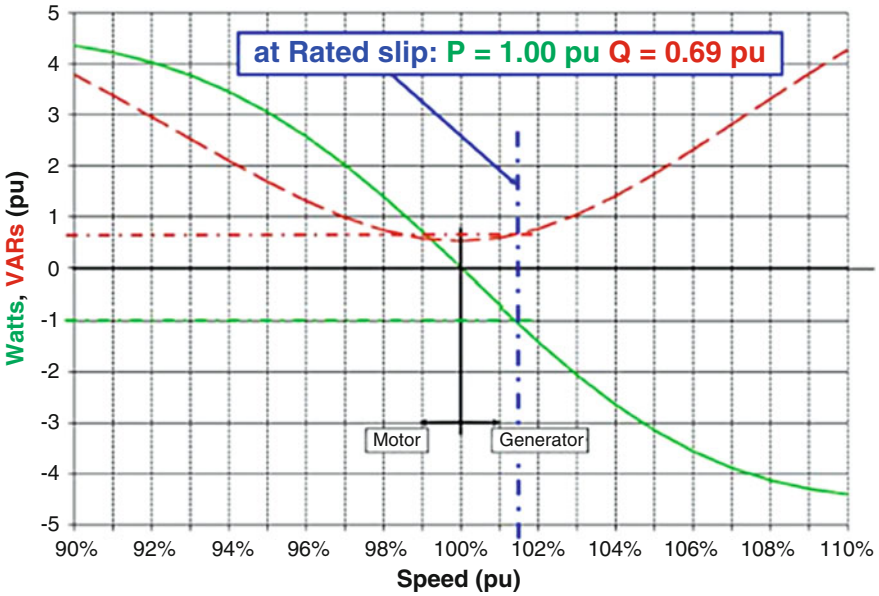


Fig. 4.5 Variation of real and reactive power for SCIG

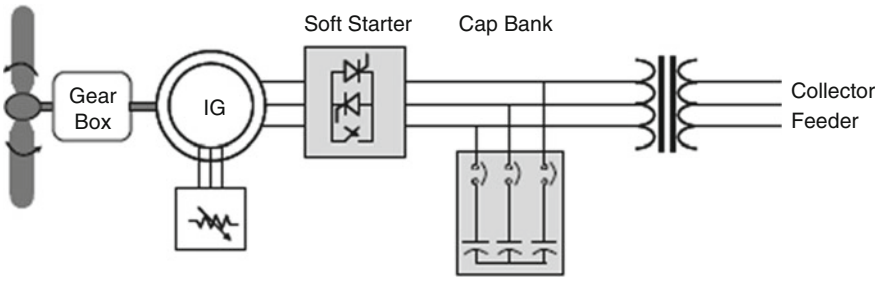


Fig. 4.6 Configuration of type 2 WTG

By including resistance for the rotor signal, the actual power curve can become varied on the higher slip and speed ranges as shown in Fig. 4.7. The generator should spin faster to create the very same output strength, for an added rotor opposition. This allows some ability to control the pace, with the particular blades' pitching mechanisms and also move the actual turbines based on tip-speed ratio to achieve the best energy output. It is typical in which speed versions of nearly 10 % tend to be possible, taking into account some degree of freedom towards energy capture and self protective torque control.

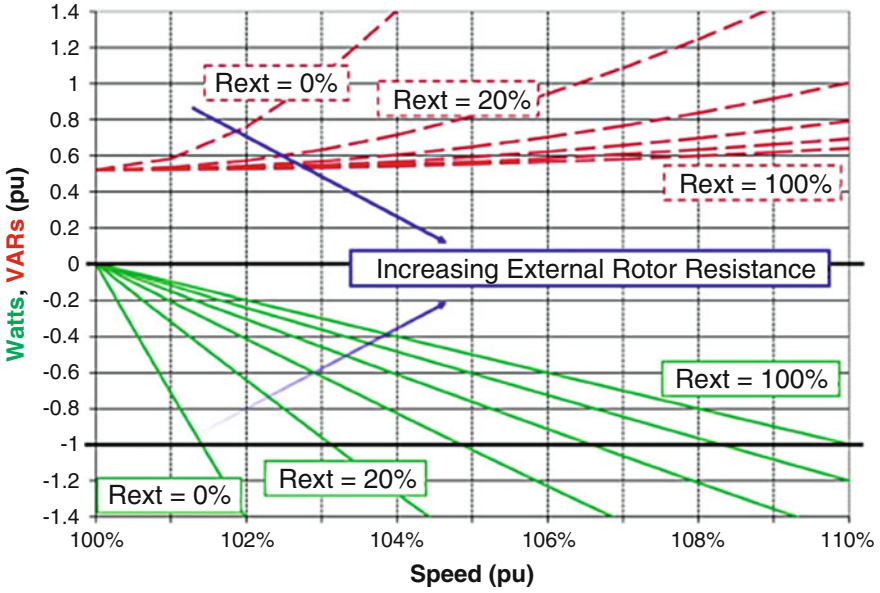


Fig. 4.7 Variation of real and reactive power with an external rotor resistor in a type 2 WTG

4.5.3 Type 3 WTG

The Type 3 turbine, known normally as the Doubly Fed Induction Generator (DFIG) or Doubly Fed Asynchronous Generator (DFAG), improves the type 2 design to one stage further, by adding or changing frequency to the AC excitation (instead of purely resistance) to the actual rotor circuit shown in Fig. 4.8. The extra rotor excitation is supplied via slip happens to be by a latest regulated, voltage-resource converter, which in turn adjust the windmill currents' magnitude and phase. This rotor-side converter is connected back-to-rear with a grid side converter, that exchanges power immediately with the grid.

A small volume of power is injected into the rotor circuit to make a large difference in the control of power in the stator circuit. This is a major advantage in the DFIG. A great deal of control of the output is available with the presence of user to set converters that commonly are only 30 % of the status of the machine. In addition on the real power that is certainly delivered to this grid from this generator's stator circuit, power will be delivered to the grid through the grid-connected inverter when the generator is shifting faster than synchronous speed. When the particular generator is going slower than synchronal speed, electricity flows from the grid, through the two converters, and via rotor to stator. These two modalities, made possible from the four-quadrant nature of the two converters, allows a significantly wider speed array, both in addition to below synchronous velocity by an increase of 50 %, although smaller ranges are more widespread.

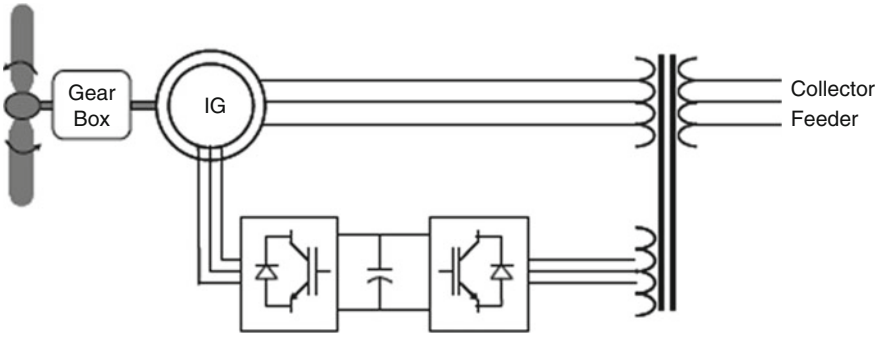


Fig. 4.8 Configuration of type 3 WTG

The major benefit from the DFIG, is it offers separate real and reactive power controller, much like a regular synchronous generator, even though being able to run asynchronously. The industry has produced as well as matured the ideas of vector or field oriented control over induction machines. Using these control techniques, the torque providing components of this rotor flux can be created to respond fast enough that the appliance remains under control, even for the duration of significant grid disturbances. Indeed, cost is higher than the Type 1 or 2 machines, the Type 3 is turning into popular due to its advantages.

4.5.4 Type 4 WTG

The Type 4 turbine offers a great deal of flexibility in design and style and operation because the output of the rotating machine will be sent to the grid through a complete-scale back-to be able to-back frequency ripping tools as shown in Fig. 4.9. The turbine is permitted to rotate at its optimal aerodynamic speed, resulting in a "wild" AC productivity from the machine. In addition, the gearbox may always be eliminated, such that the machine spins for the slow turbine rate and generates an electric frequency well at a lower place that of the grid. The rotating machines of this type have been made as wound rotor synchronous machines, comparable to conventional generators seen in hydroelectric plants together with control of area of current and higher pole numbers, equally permanent magnet synchronous machines, or seeing that squirrel cage induction machines. However, based on the ability of the machine, an inverter is used to control real and reactive power flow. Advances in power electronic devices as well as controls in the last decade have built the converters both equally responsive and useful. It does carry mentioning, however, that this power electronic converter have to get sized to pass the entire output of the spinning machine, plus any kind of capacity to provide for reactive compensation.

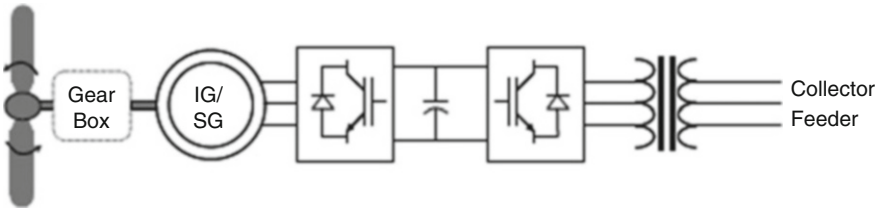


Fig. 4.9 Configuration of type 4 WTG

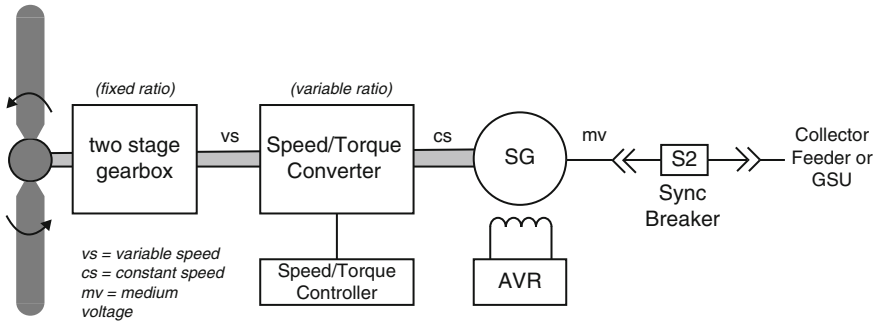


Fig. 4.10 Configuration of type 5 WTG

4.5.5 Type 5 WTG

Type 5 turbines consist of a regular WTG variable-speed drive train attached to a Speed/Torque converter coupled with a synchronous generator as shown in Fig. 4.10. The Speed/Torque converter alters the variable pace of the rotor head to a continuous output shaft speed. The closely coupled synchronous generator, functioning at a set speed (corresponding to the grid frequency), might be directly attached to the grid through any synchronizing circuit breaker. The synchronous source can be designed appropriately for virtually any desired speed (commonly 6 pole as well as 4 pole) and also voltage (typically moderate voltage for greater capacities). This approach requires speed in addition to torque control with the Speed/Torque convertor along with the average voltage regulator (AVR), synchronizing process, and generator protection system using a grid-connected synchronous generator.

4.6 Power Converter Topologies for Wind Turbine Generators

4.6.1 Permanent Magnet Synchronous Generators

Permanent magnet excitation is generally popular in newer smaller scale turbine types, since it enables higher efficiency in addition to smaller wind generator blade

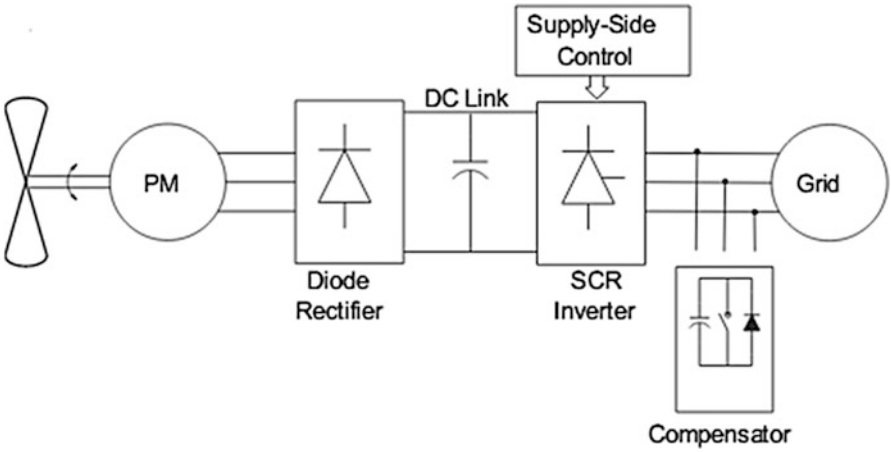


Fig. 4.11 Configuration of thyristor supply-side inverter

diameter. Though recent research has considered larger scale patterns, the economics of huge volumes of large volume material has constrained their practical use. The primary benefit from permanent magnet synchronal generators (PMSG) is that they do not require any external excitement current. A major cost benefit in using the PMSG is a diode bridge rectifier that may be used at the generator devices since no external excitation current should be used. A variety of research has been performed using a diode rectifier.

4.6.1.1 Thyristor Supply-Side Inverter

On applying thyristor-based grid-side inverter as shown in Fig. 4.11, continuous control on the inverter firing angle, regulating the turbine speed is possible with the DC-link voltage; hence, capturing optimum energy. Advantages with this scheme include cheaper device cost and improved power than hard-switching inverters. A major drawback in this inverter is the need for an active compensator for the reactive power demand and to reduce harmonic distortions. A voltage source converter (VSC) can be used for the compensator and the error signal between the reference and compensator is utilized to drive the actual pulse width modulated (PWM) controller.

4.6.1.2 Hard-Switching Supply-Side Inverter

A recommended control involves the particular manipulation of the modulation index in the reference sinusoidal signal applied to the particular PWM generator. This is achieved by determining the actual DC-link voltage by an electrical power mapping technique which has the maximum electricity versus DC-link

characteristic. The control system is additionally improved by using a derivative control around the stator frequency, mainly because it also changes along with change in DC-link voltage. This control is compared to maximum power point tracking (MPPT), which includes an anemometer, a wind prediction scheme and a fixed-voltage scheme. The anemometer measures the actual wind speed along with aids in providing the wind power reference to the MPPT controlled. The reference electrical power is compared with the actual DC energy extracted and the result is used to determine the new operating DC voltage drop. The current control loop of this inverter receives the brand new operating DC voltage and outputs a great instantaneous driving indication for the PWM. In breeze prediction methods, autoregressive statistical types are commonly utilized. The system views energy captured within the previous time shape to predict the actual wind speed importance for the next time frame set. With reference to the fixed voltage the voltage on the inverter is fixed at a precise optimum wind velocity. In comparing some control methods, the fixed voltage output was used as the reference. The actual MPPT with wind gage setup proved being superior, obtaining 56–63 % of energy available.

4.6.1.3 Intermediate DC/DC Converter Stage

The use of a voltage source inverter (VSI) that has a DC/DC converter is depicted in Fig. 4.12. This kind of setup is also compared to the converter shown in Fig. 4.13. Incorporating an extra DC/DC convertor gives the following advantages:

1. control over generator-side Power-voltage through deviation of the switching ratio,
2. retains appropriate inverter-side DC-voltage,

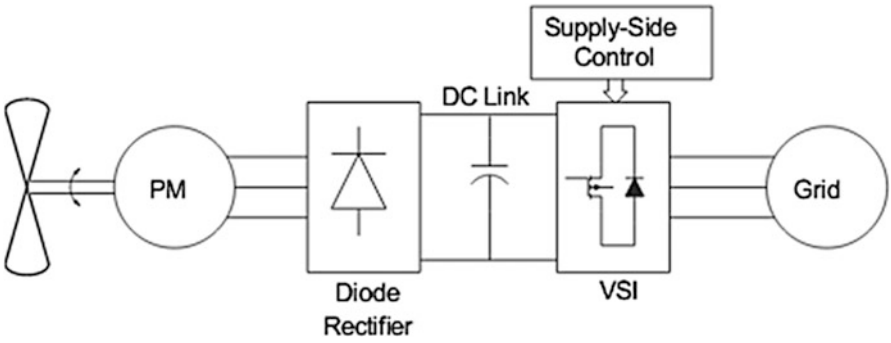


Fig. 4.12 Configuration of VSI using DC/DC converter

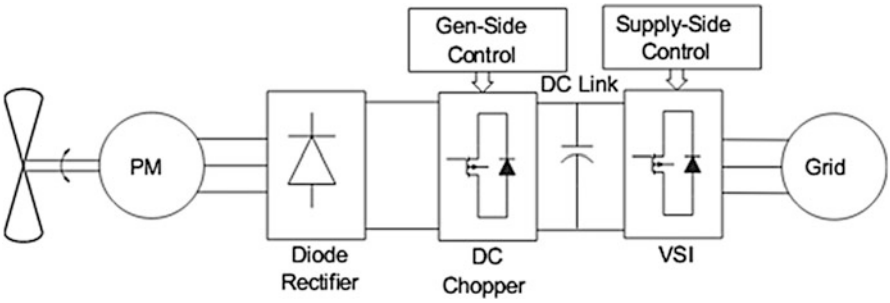


Fig. 4.13 Configuration using VSI

3. allows for selective harmonic elimination (SHE) switching, resulting in reduced losses,
4. inverter no longer needs to command DC-voltage, possesses more flexible power.

The inverter control can be achieved by regulating the particular magnitude of the basic line current and the phase angle between line current and also line voltage. The controller can be configured such that the VSI is switched at the absolute frequency of the three-sided carrier signal and its output harmonics are well defined. For each shaft speed, optimal values of electric voltage can be recognized corresponding to the most available turbine power. The DC/AC voltage percentage and power are used while control variables which can be tuned to control the power are used upon necessity. The inverter handle can also possibly be implemented to keep the DC-link continuous and vary the active power in a fashion so that it attains maximum real power transfer towards grid. Effects show that the thyristor-based inverter with active compensator is most suitable for strong HVAC systems since the inverter relies on the device to ensure substitution. However, the two VSI and Direct current/DC–VSI devices are capable of integrating with equally strong AC systems. Various other control strategies have been also adopted for this convertor. The specific DC/AC inverter can control the active as well as reactive power brought to the grid by means of control of the q-axis in addition to the existing d-axis. The q-axis reference point current is determined by the error inside DC-link voltage, and is subsequently compared with the current. The phase angle of this utility, used in power factor command, is detected using phase locked loop (PLL) mechanism in a d–q synchronous reference frame. Power factor control makes the d-axis of rotation as the reference current, thus it can be compared while using the actual d-axis current. The error in both coordinate system currents are utilized to create the d–q-axis voltages used inside space vector PWM control. While using voltage equation control a boost-controlled DC/DC chopper and a proportional–integral (PI) controlled, the duty ratio of the chopper switch may be determined for any kind of specific optimum location. The inverter-side DC-link voltage remains constant set by the actual grid voltage giving the advantage of involving flexible

transfer of active and reactive power to the particular grid. A bit of a modification to the particular DC-link is included by means of including a battery power. The battery allows charging during night when load demand is usually lower. An advantage due to the continuous DC-link voltage, leads to controlling the chopper output to its maximum value thus resulting output power. To perform the control, a human relationship between the output power and duty cycle of this chopper is utilized. Starting from an arbitrary point, the obligation cycle can become continuous and slow adjusted between a unique ranges searching to the maximum power distributor point. It is found that the system began losing efficiency at large speeds; this had been due to the phase lag relating to the DC current in addition to duty ratio.

4.6.1.4 Back-to-Back PWM Converters

The use of, 6-switch, hard-switched converters, with a DC-link capacitor, had been existing so far. The source side rectifier is definitely controlled through a PI controller in ways that the d-axis current is held to zero to obtain maximum electrical torsion with minimum stream. A MPPT is used in determining this optimum rotor speed for each winding speed to get maximum rotor power. In contrast, this grid side inverter controls the line current to end up being sinusoidal through a hysteresis controller. The DC-link voltage is also controlled by a PI controller, via the grid side inverter.

Recently a converter using two B-4 converters and two DC-link capacitors has been developed, shown in Fig. 4.14. Yet again MPPT calculates the actual output power involving the generator by measurement the DC-link current and potential drop, and then alters the operating point through increasing or decreasing the reference current magnitude. The MPPT control is performed on the generator side rectifier. The error in current is used to drive the inverter switching responses. A PLL is employed on each section to ensure power factor is maintained throughout the complete system.

4.6.1.5 Unconventional Schemes

A rather unconventional scheme using a PMSG has been recently discussed. The system relies on a rotary phase shifter (RPS) as a frequency converter. This RPS can adjust the angular velocity of the turbine at a affordable price in comparison into a power electronic device. A flywheel is also used as an electricity stabilizer; it includes a lifetime that is just not limited unlike the use of a battery. Recently, researches have been performed in order to resolve DC-link voltage problems under low wind speed ailments. By placing 3 switches between the diode rectifier and middle point on the DC-link capacitor, the voltage at low winds might be increased.

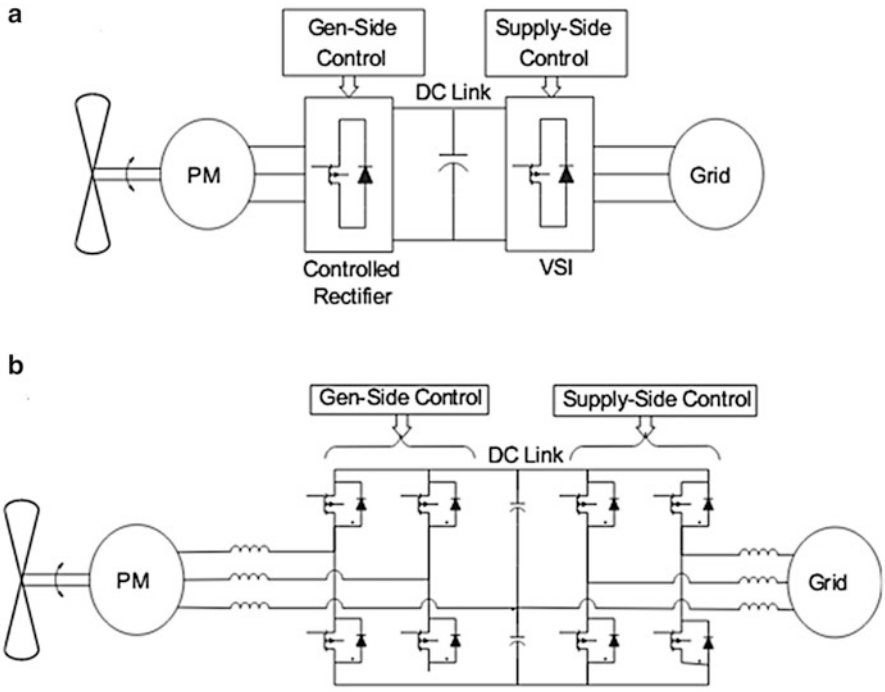


Fig. 4.14 PMSG with back-to-back PWM converter schemes

During reduced wind speeds, the switches are switched on and off instead, keeping the program symmetrical while increasing the voltage. The knobs are not utilized during high winds to avoid haunt over-voltages. Another modification to converter system is presented in Fig. 4.12, can be done to ensure constant flow from generator to grid by placing a straightforward diode in between capacitive DC-link and the inverter, flow of energy is restricted as a result of reverse blocking functions of the diode.

4.6.2 Doubly Fed Induction Generators

As the PMSG has acquired much attention throughout wind energy transformation, the doubly fed induction generator has brought just as very little consideration. If a wound rotor induction unit is used, the user will be able to control the generator by accessing this rotor circuits. A tremendous advantage in utilizing doubly fed generalization generators (DFIG) could be the ability to produce output more than their rated power without getting overheated. It is able to transfer maximum power over a wide space range in the two modes of operation. The DFIG along with

induction generators are extremely useful for high power applications in particular in the MW range. Furthermore, converter power evaluation is reduced since it is connected to the actual rotor, while almost all of the power flows through the stator.

4.6.2.1 Static Kramer Drive and SCR Converter Methods

The stable Kramer drive is made up of diode rectifier within the rotor side and a line commutated inverter connected to the supply side as shown in Fig. 4.15. With this converter, a sliding mode control is developed which provides the ideal compromise between alteration efficiency and smoothing of torque oscillation. The controller regulates the thyristor inverter discharge angle to attain the ideal compromise. This sliding mode control law forces the generator torque to become linear function with the generator speed across the operating point of maximum power transfer. This converter is only able to provide power from each stator and windmill circuits, under excellent-synchronous operation. To solve this problem, methods replace this diode rectifier using thyristor rectifier (SCR). The supplement of a minute SCR allows the particular generator reactive power demand to be satisfied by the rotor-side converter system. When coupled to the wind turbine, it is shown that ideal performance is attained by adjusting the apparatus ratio, of the gear box, to the optimum value. In comparison for the Kramer drive, this product produces more power due to the lack of reactive power available with a diode rectifier. More descriptive control of the two rectifiers is succumbed. A variety of both firing angles for each mode of operation is given like a plot showing the particular optimum firing angle at different the wind speeds resulting in ideal power transfer. It is discovered that between 7.5 as well as 8.5 m/hydrates, maximum

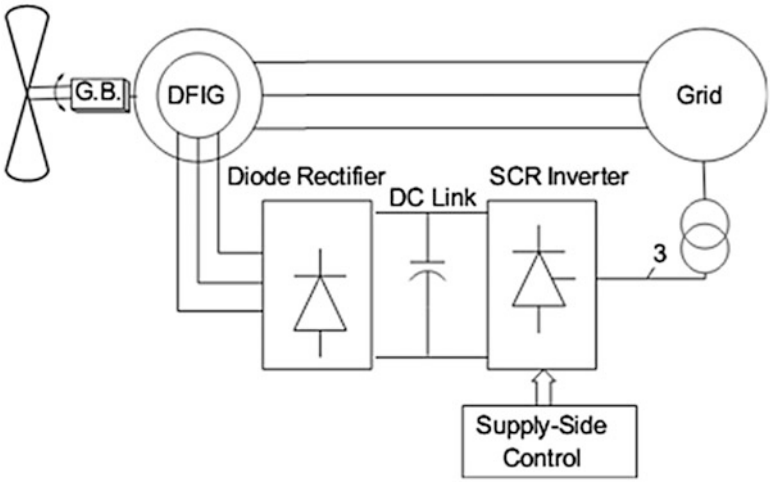


Fig. 4.15 DFIG with static Kramer drive

power is usually generated in both sub-and super-synchronous modes. Major drawbacks on this approach include firing off and commutation problems with the rotor-side converter and consonant distortion to the grid, created with the supply-side thyristor converter.

4.6.2.2 Back-to-Back PWM Converters

A more highly advanced method applying back-to-back converters has also been developed, as shown in Fig. 4.16. Although the convertor used in most of these works are extremely similar, great differences lie within the control strategy and complexity. One option is to employ vector control on the supply-side ripper tools, with a frame of reference orientated with the actual d-axis along the stator voltage vector. The supply-side converter is definitely controlled to maintain the DC-link electric potential constant through regulation of the d-axis current. It can be responsible for reactive power control by means of alteration of the actual q-axis stream. As for the rotor side, choosing decoupled control in the electrical torque in addition to the rotor excitation current is displayed. The machine is controlled in a very synchronously rotating coordinate system with the n-axis orientated over the stator-flux transmitter, providing maximum power transfer. Conversely, inwards, the rotor coil current was decomposed into d–q components, in which the d-axis current is used to manage the electromagnetic torque and the q-axis current controls the power factor. Both kinds of rotor-side convertor control are used in the application of PI controllers. PWM switching techniques can be utilized, or additionally space vector machine (SVM) is found to obtain a better inflection index.

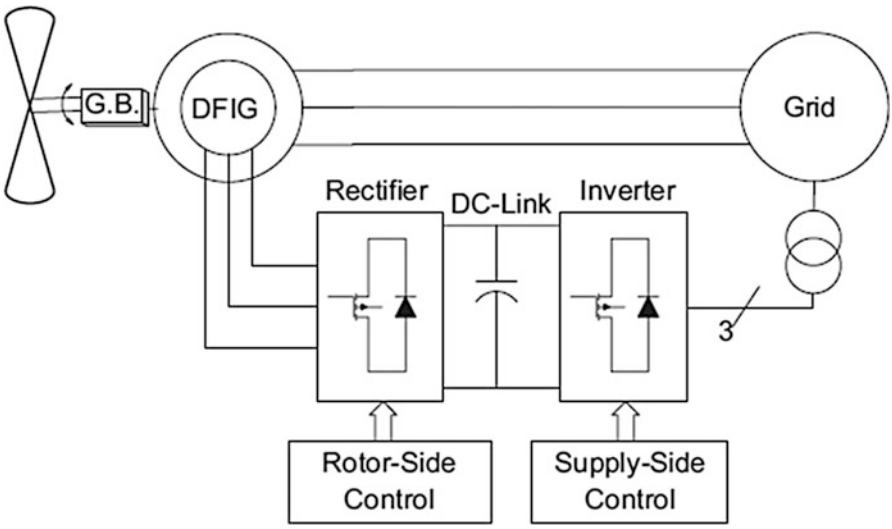


Fig. 4.16 DFIG with back-to-back PWM converters

Typically control schemes aided by a windmill speed encoder attain excellent tracking outcomes. However these encoders are high priced and the charge due to dropped accuracy without the encoder may not be as large as possible. The application of speed sensors has been described. To go along with the capacitor within the DC-link, a cell may be employed as a storage device. With the additional storage device, the supply-side converter controls the movement of real energy between the power grid and the battery, as the DC-link voltage is at this point is fixed. The supply side controller comprises three PI controllers, one for outside loop power control, and the other two for the d–q-axis inner current controller loop. Energy can be stored during large winds and is exported to the actual grid during silent conditions to compensate for the drop in the stator power. Throughout long periods connected with high or lower wind speeds, the control algorithm will be modified to manage the bus current until the ailments change. In this example, the rotor-side converter is used to control the real and reactive power of the equipment. Another different pick for rotor command has been identified. The algorithmic rule searches for the peak power by means of varying the rotor coil speed, and the actual peak power factors are recognized with zero slopes for the power-speed shape. The control algorithm works continuously, as a substantial shift in power causes the controller to shift the rate at which it causes the power to shift once more. Once the alternation in power no change exceeds the minimal set value, the particular controller takes no more further action. Once again, d–q-axis control is utilized to control the real and reactive power of the machine. It is crucial that the user ensures that this dynamics of the speed controller are not necessarily extremely fast, more large transients with generator torque may occur. The standard control objectives identified above can end up being attained through handle theory based on voltage space vectors (VSV). The use of certain voltage vectors may accelerate the rotor flux, in addition to increase the lively power generated by the stator. Other voltage vectors may also increase or decrease the actual rotor flux value, resulting in a reduction in the reactive power drawn by the stator and an increased power factor. The direct power command method requires a series of tables to determine which of the six sectors the operator is operating on. From the choice of sector, the employed voltage vectors can be discovered from a controller table. A concluding control scheme, with the back-to-back again PWM converter plan, uses information on base speed and turbine output power to estimate the wind speed. This turbine output power can be described as a function of TSR. The sources of the equation are solved to look for the optimum TSR in a specific range. Using the estimated wind velocity and optimal TSR, the revolutionary reference of the particular generator output power and shaft speed is obtained. The machine is commanded towards desired shaft pace and the production power is over again measured, regurgitating the control. This control is applied to a brushless DFIG, giving reduced cost when compared with machines with brushes and slip-rings.

4.6.2.3 Matrix Converter

The matrix converter is capable of converting the variable quantity AC from the generator into continous AC to the actual grid in a single stage (Fig. 4.17). Two distinct advantages arise from this type of topology, the converter requires no bulky energy storage or perhaps DC-link in addition to control. The simply using a matrix converter with a DFIG has already been explored. The use of stator–flux oriented control was applied to the rotor coil matrix converter. This type of d-axis current was aligned with the entire stator–flux linkage vector. Simple PI controllers can be used to control the–d-axis currents. The regulation of the actual d-axis steady current allows for control of the stator-part reactive power flow, where as the q-axis current helps regulate the stator-side dynamical power.

A recent option is to control the rotor winding voltage, that therefore manipulates the power factor of the DFIG. The particular matrix converter incorporates nine bi-directional switches (18 in total), arranged in a fashion such that an input cycle could possibly be connected to virtually almost any output phase according to the user need. Each specific switch is capable of connecting with correction and upending. The matrix converter is controlled making use of double space vector PWM, employing use of input current along with output voltage SVM. One of the major drawbacks associated with the matrix converter is that 18 total switches are required, creating an increase in the converter semiconductor cost.

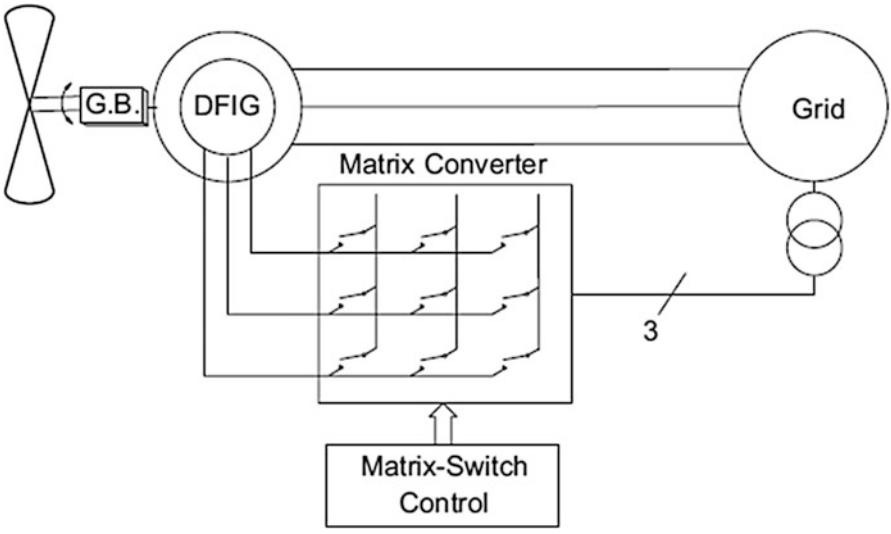


Fig. 4.17 DFIG with matrix converter

4.6.3 Induction Generators

The use of induction generators (IG) is advantageous since they are usually relatively inexpensive, and they call for low maintenance. The type of IG can be unlike that associated with PMSG, they have to possess bi-directional power flow in the particular generator-side convertor since the induction generator requires external reactive power assitance from the grid. The use of back-to-back PWM converters (Fig. 4.18), along with the implementation of one or more fuzzy logic remote controls is a constant converter-control combination. The advantages of fuzzy logic command are parameter insensitivity, fast convergence as well as acceptance of imprecise and inaccurate alerts. A PI based fuzzy logic operator takes in the DC voltage error and change in DC voltage error. The controller outputs the d-axis reference current used in actual power flow control. In a similar manner, the Q-axis current is definitely kept zero to maintain unity power element. A control program using three fuzzed logic controllers has been investigated. The first controller tracks the generator speed with the actual wind velocity to be able to extract maximum power. The second controller programs the machine flux for lighting load efficiency progress. More specifically, the rotor flux might be reduced from the particular rated value to lessen the core losses and thereby improve the efficiency. The rotor coil flux may be reduced by constantly decreasing the magnetizing current until the maximum power output is obtained. The third controller gives robust speed control versus wind gust and turbine oscillatory torque. Unlike the second controller, the third fuzzy logic controller is always effective.

In another control strategy, a PI controller is additionally used; nevertheless, rotor slot harmonics (RSH) cause speed estimation. The rotor slots get connected to the magnetizing element of the air-space magneto-motive force (MMF), generating harmonics that are dependent on the rotational speed. Once the algorithmic program locates the consistency of the RSH through a look-up table, the rotational speed can be found through a series of calculations. While using RSH, the control system also utilizes sensor-less command through a model reference adaptive

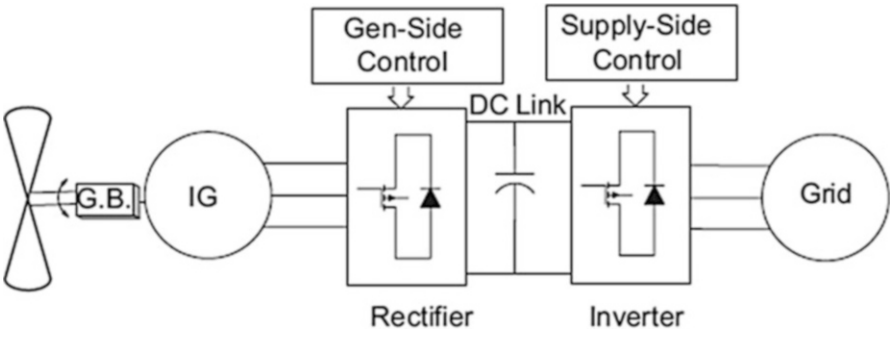


Fig. 4.18 Induction generator with back-to-back converter

system (MRAS) based observer to help estimate the spinning speed. Some sort of control option to the supply-side convertor includes real along with reactive power control. A reference shape orientated along the supply voltage rotating vector allows for real power control via d-axis current control and Q-axis manipulation regulates the reactive power. The above mentioned control results in rotational speed with high accuracy, a positive characteristic for methods employing a stall controlled wind turbine. This control protocol can react speedily to wind gusts and will be utilized to manage the amount regarding mechanical power in addition to torque input to the generator. They are common concerns intended for stall controlled wind turbines as operation over rated power could potentially cause damage to this generator and power electronic converter. Rather than the usual back-to-back PWM converters scheme, the generators use a fixed-capacitor thyristor-governed reactor and a static Volt-ampere compensator at the actual generator terminals to manage its voltage. The mechanical input power is controlled while using blade pitch angle. The design methods used for this control systems are based on the state infinite linearized model of the system. Two remote controls, a state feedback controller and output feedback controller are designed. The output feedback control is preferred since each of the output signals are available for measurement and the observer is not needed due to their state feedback control. A comparison between the wound rotor induction machine plus a caged rotor induction machine, both regarding identical size, has been performed. Both the squirrel cage induction motor and wound rotor six pole slip ring generalization machine have a rated voltage of 415 V. The coupled generators are identically rated for 300 kW and have a rated speed of 1,000 rpm. The comparison ensures validity with the use of identical converter sorts in each of the systems. The separate designs were tested individually under the exact variable wind problems. A variable wind speed profile was made to model an area with a normal wind speed of 12 m/s for the duration of peak wind period. It is found, under the like wind conditions, which the wound rotor induction machine outputs 35 kWh of electricity over 10 min, while the caged induction machine produces only 28.5 kWh inside 10 min. The higher cost of the injure rotor induction machine, due to potential need of slip rings, is reimbursed by the reduction in the sizing of the power converters along with the increase in electricity output. The DFIG is more advanced than the caged induction machine, due to its ability to create above rated power.

4.6.4 Synchronous Generators

Finally, the application of synchronous generators (SG) in residential wind power generation has also recently been researched. A brief description of one possible converter-command scheme is given for a small wind energy the conversion process system. The application of a diode rectifier along with a DC/DC boost stage and inverter as an energy electronic interface pertaining to grid connection

have been discussed. The converter is similar to, except a SG replaces the actual PMSG. In this particular scheme, the DC-link voltage is actually controlled while using the amplitude of the three-phase inverter voltages and the particular phase displacement angle of the inverter. The linearized currents and DC-link potential drop of the inverter can always be obtained by ways of state equations. Controller performance improvements are usually achieved over the original power angle control. For low power systems, the existence on a winding circuit in the rotor coil may be a drawback as compared to PMSG. Although PMSG are frequently used for low-electricity application, larger systems utilize SG. In big systems, the energy from the SG is most often converted through back-to-back PWM voltage source inverters, similar to Fig. 4.18. The supply side PWM inverter allows control of genuine and reactive power transferred to the actual grid. The source side converter is utilized for electromagnetic torque regulation. The controllers found in these systems are designed to achieve maximum power transfer to the grid. These generation devices have a large efficiency since the full stator current is utilized during electromagnetic torque production. Another advantage is the minimization of stator current over the direct control of generator power. In comparison to IG, the application of SG is useful since they are generally self-excited machines and the magnetic pole pitch of the machine can be more compact. As a result both DFIG and SG are preferred for high power applications.

A comparison of different generator converter topologies available for the Wind Energy Conversion Systems is summarized in Table 4.1.

4.7 Economics of Wind Energy Conversion Systems

The cost-effective goal of maximizing the energy output per dollar of expenditure has been pointed out several times. We have discussed the matter of determining the entire capital investment along with operating cost intended for wind electric power generators, so that we can determine the device cost of power. The fuel wind may be no cost, but the equipment essential to use the fuel tends to be expensive, so economic scientific tests are quite important. The unit expense of electricity can be determined in an easy manner from knowledge of capital investment and operating expenses. The value on the electricity is fairly more difficult to view, but must end up being calculated before capital investment decisions can be achieved. The value ought to exceed the cost before the purchase of wind equipment can be validated. The ratio of worth to cost need to be as good equally that for choice sources of power before wind is usually justified over these kind of alternatives. The price of wind generated electrical power to an electric utility is driven by its fuel savings and also its capacity credit ratings. When the breeze is blowing, less oil and coal need to be burned, which represents a savings on the utility. Also, when the utility is able to delete or delay payments on some new traditional generation as a consequence of adding wind devices, then this represents additional savings to the utility.

Table 4.1 Summary of generator converter topologies

Generator	Converter options	Control schemes
PMSG (kW)	Diode bridge/SCR inverter/compensator	Simple firing angle control of one converter
	SCR rectifier/SCR inverter	Simple firing angle control of both converters
	Diode bridge/hard-switching inverter	Power mapping technique including stator frequency derivative control MPPT, wind prediction control
	Diode bridge/DC boost/ hard-switching inverter	Vector control of supply side inverter DC Voltage control via chopper duty ratio
	Back-to-back hard-switching inverters	MPPT, vector control of both converters
	Back-to-back hard-switching inverters (reduced switch)	Generator controlled through MPPT inverter current controlled through PI controllers
DFIG (kW–MW)	Diode bridge/SCR inverter	Sliding mode control
	SCR rectifier/SCR inverter	Dual thyristor firing angle control
	Back-to-back hard-switching inverters	Vector control of rotor and supply side space vector modulation or PWM MPPT, space vector control
	Matrix converter	Vector control of rotor and supply side double space vector PWM switching
IG (kW–MW)	Back-to-back hard-switching inverters	Vector control, use fuzzy logic controllers use rotor slot harmonics and model reference adaptive system
SG (kW–MW)	Diode bridge/DC boost/ hard-switching inverter	Phase angle displacement control supply voltage control
	Back-to-back hard-switching inverters	Supply real and reactive power control generator electromagnetic torque control

There are nearly one thousand million people living in scattered rural regions of developing countries inside continents of Japan, Africa, and South USA who have very poor living conditions. Most of these conditions are explaining a massive exodus to the elegant slums, which helps make the overall situation more painful in many conditions. Most of the developing countries are poor in ceremonious fossil fuel resources and have to import them making use of their meager foreign exchange reserves. There are only two feasible solutions from a technical perspective to their energy problems. One is a commitment to use large central atomic power plants and an electrical transmission and distribution network. The other is a decentralized system of PV and wind gear installed at the village level. A tough estimate of the energy needs of a typical village of 190 families is as follows: 88,500 kWh per calendar year for cooking food, 1,000 kWh per class for pumping water, and 26,000 kWh per year for lighting. The specific average 315 kWh per 24 h, most of which should be delivered during a few hour period at night. The energy needed for cooking food is about three-fourths in the total, and just about any resource must be able to satisfy the load even in case all the villagers choose to cook at the same time

frame. The most noticeable solution is a diesel engine and 100-kW or 150-kW generator, even so the cost of gas makes this unaccepted. This energy consumption style also puts many difficult constraints about solar or wind systems that will be used. The production of a solar panel will be nearly zero by the time of the optimum load and the winding may be quiet at that time period also. Thus it is necessary to store satisfactory energy to meet one days requirement. This storage can be in the way of storage batteries regarding wind and solar electric systems.

Yet another possibility for the power system is biogas. Plant, animal, and human waste materials can be accustomed to produce methane, which may be stored and used directly for cookery. It is not functional to use methane directly with regard to lighting so the actual methane can use in a car engine driving a generator to supply electricity for lights. The investment is very less but requires extensive labor to maintain biogas facility along with the operating internal combustion engine. The real amount of electricity consumed per person is not large, so costs every kWh can follow relatively high but still be acceptable. One problem is that people look at the costs of gear, the lack connected with transportation, the insufficient trained people, as well as the centuries-old cultures and customs in addition to conclude that it isn't economically feasible to supply electricity to these kinds of villages. The towns are left in poverty and hopelessness. City slums are perceived as being a better location to live, with enormous migrations of individuals. The country grows more unstable and ripe for revolution as this process continues. It can be concluded that the genuine costs to the developing country and in many cases to the human race community of international locations is greater if these basic electricity needs are certainly not met than when they are required. An enhancing standard of coping with the rural areas would relieve quite a lot of human misery and also improve the political stability of the planet.

4.8 Grid Connection

4.8.1 Unique Configurations for Linking Wind Turbines on the Grid

The association of the windmill to the grid depends on the electrical generator as well as power electronic converters used. Based about the application of PE converters in the WECS, the turbine configurations can be divided into a few topologies: directly connected to the grid without any PE converter, connected via full-scale the PE converter, and connected via partially-rated PE converter. In the following, the generator in addition to power electronic converter configurations most widely used in wind turbine systems are discussed.

As a basic, robust and reasonably low-cost program, a squirrel-cage induction generator (SCIG), as an asynchronous machine, will be connected directly towards the grid, as represented in Fig. 4.19. For a good induction generator, using a gearbox

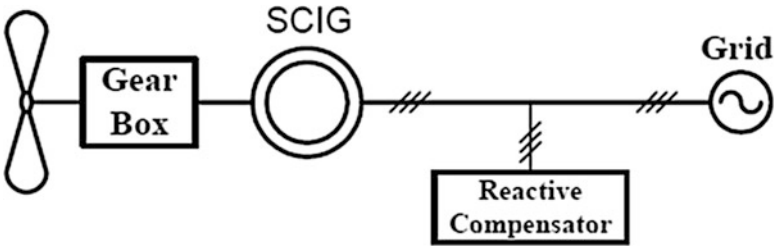


Fig. 4.19 Wind turbine system with SCIG

is required in order to interface the turbine speed and generator speed. The electrical condenser bank (for responsive power compensation) as well as soft-starter (regarding smooth grid link) are also necessary. The speed and also power are minimal aerodynamically by stall or pitch handle. The variation of slip is within the range of 1 %–2 %, but there are several wind turbines determined by SCIG in marketplace with increased rotor resistance and, thus, increased slip (2 %–3 %). This program is used to allow for a little bit of speeding up for the duration of wind gusts in order to reduce the physical stresses. However, the configuration based with almost fixed pace is not suitable for a windmill in an increased power range as well as for locations together with widely varying the wind velocity.

Three wind turbine systems based on induction generators, while using the capability of variable-speed operation are shown in Fig. 4.20. The wind turbine system in Fig. 4.20a uses a wound-rotor induction turbine (WRIG). The concept of this model is the rotor resistance might be varied electronically having a variable external rotor resistance and a PE converter. Simply by controlling the rotor coil resistance, the output of the unit will be improved over a 10 % range (speed range 2–4 %). In normal operations, the rotor level of resistance is low, related to low slip, yet during wind gusts the rotor opposition is increased to allow speeding up. Figure 4.20b shows a setting employing a Doubly-Fed Induction Source (DFIG) and power electronic converters that connects this rotor winding towards grid directly. On this configuration, it is quite possible to extend the speed range further without affecting the efficiency. The reason behind speed control without having loss of productivity is that fall power can follow back to the grid by the particular converter instead to be wasted in the rotor resistance. Note that the power standing of the electrical power converter is sPnom, where 's' would be the maximum possible elusion and Pnom would be the nominal power in the machine. The windmill slip (s) is usually positive or adverse because the rotor coil power can stay positive or negative, due to the bidirectional nature connected with power electronic ripper tools. For example, when the power rating from the converter is 12 % of the electricity rating of the generator, the speed control range is definitely from 90 % to 110 % of the synchronous speed. It implies at 110 % rate, $s = -0.1$ and power can be fed from this rotor to the particular grid, whereas from 90 % speed, your slip is $s = +0.1$, as well as 10 % of the energy is fed on the grid to the rotor through the converter. With these kind of attributes, a larger control range

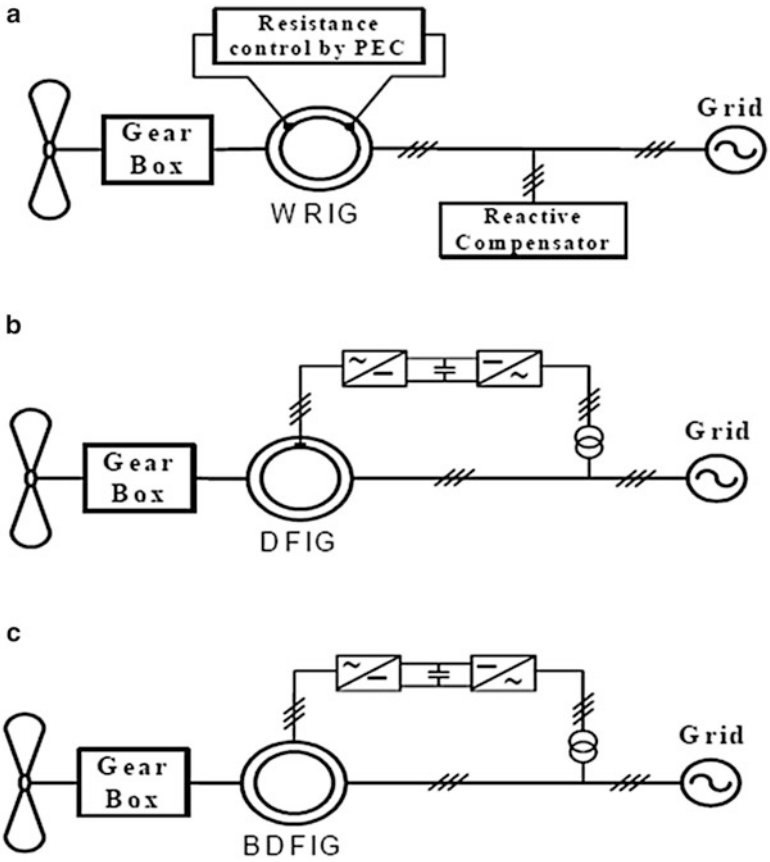


Fig. 4.20 Wind turbine systems based on induction generator with capability of variable-speed operation: (**a**) Wound-Rotor, (**b**) Doubly-Fed, and (**c**) Brushless Doubly-Fed induction generators

and more compact losses, the shape in Fig. 4.20b is a lot more attractive than this configuration in Fig. 4.20(a).

In the configurations shown in Fig. 4.20a, b, together with wound-rotor induction generator, the access to the rotor is achievable through the slip rings and brushes. Slip rings as well as brushes cause hardware problems and electric losses. In order to solve the difficulties of using get rings and brushes one alternative is utilizing the Brushless Doubly-Fed induction generator (BDFIG), shown in Fig. 4.20c. In this scheme, the stator coil windings (main winding) are directly connected to the grid, while three-phase auxiliary winding is connected on the electrical grid by having a PE converter. When using the appropriate control within the auxiliary winding, the user possibly can control the trigger machine at any speed virtually.

In this category, the electro-mechanical machine is coupled to the electrical grid using a fully-rated converter. It means that this whole power interchanged between the particular wind turbine and also the electrical grid has to be passed through any

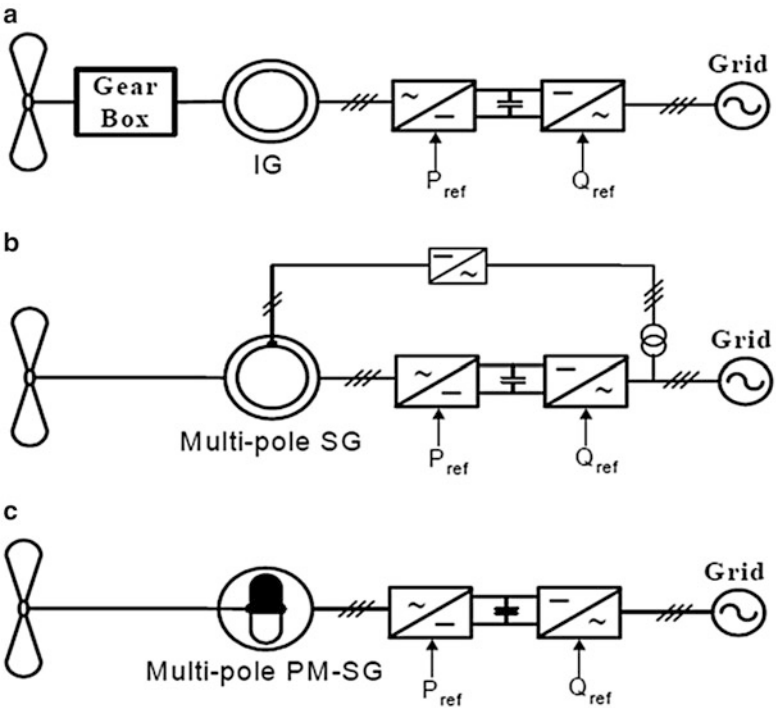


Fig. 4.21 Wind turbine systems with fully-rated power converter between generator terminals and the grid: (**a**) induction generator with gearbox, (**b**) synchronous and, (**c**) PM synchronous generator

PE converter. This suggests extra losses in the power conversion. Nonetheless this configuration can improve the technological performance. In this kind of configuration, as an electrical machine, it may be possible to use induction machine or synchronous machine, as demonstrated in Fig. 4.21. Note the system of Fig. 4.21a uses a gear box together with a SC induction generator. The systems associated with Fig. 4.21b, c use synchronous machines without a gear case. In Fig. 4.21b the synchronous generator needs power electronic converter tools for field excitement, and slip speed. An advantage of utilizing the synchronous generator is the chance of eliminating the gear case in the wind generator (direct-drive turbine). Direct drive machines essentially have a big diameter due to the high torque. Within gearless drives, induction machines cannot supply because of the excitation losses in these large machines as a result of large air break. However, synchronous machines can be utilized in direct-drive wind turbines, with either electrically excited or permanent-magnet blade structures (Fig. 4.21c). Direct-drive systems with permanent magnet excitation are more costly, because of the high price regarding magnets, but results in lower losses. Nowadays, the price connected with permanent magnets is definitely decreasing dramatically. Yet another disadvantage of using permanent magnet synchronous machine is the actual uncontrollability of their

excitation. All configurations shown in Fig. 4.21 have the same control characteristics because the power converter relating to the generator and the grid enables fast control of lively and reactive electrical power. Also, the power generator is isolated through the grid by a new DC-link capacitor. But, using fully-rated power automated converter is the particular disadvantage of these configurations. Different wind turbine manufacturers produce different configurations. Comparing different systems from various points of check out shows a trade-off between price and performance.

4.9 Modeling of Wind Turbine Using MATLAB/ SIMULINK

This section presents the simulation of a wind turbine connected to a synchronous generator and a rectifier. The torque of the wind turbine is given as the input to the synchronous generator and the three phase AC output is given to the rectifier. The electromagnetic torque, stator current and the base speed of the synchronous generator are also analyzed.

4.9.1 SIMULINK Models

The SIMULINK blocks of the permanent magnate synchronous machine, wind turbine and asynchronous machine are discussed below:

4.9.1.1 Permanent Magnet Synchronous Machine

Model the dynamics of three-phase permanent magnet synchronous machine with sinusoidal or trapezoidal back electromotive force (back EMF). The sinusoidal machine is modelled in the dq rotor reference frame and the trapezoidal machine is modelled in the abc reference frame. Stator windings are connected in wye to an internal neutral point.

Library

The Permanent Magnet Synchronous Machine block shown in Fig. 4.22 is available in the ***Machines*** library.

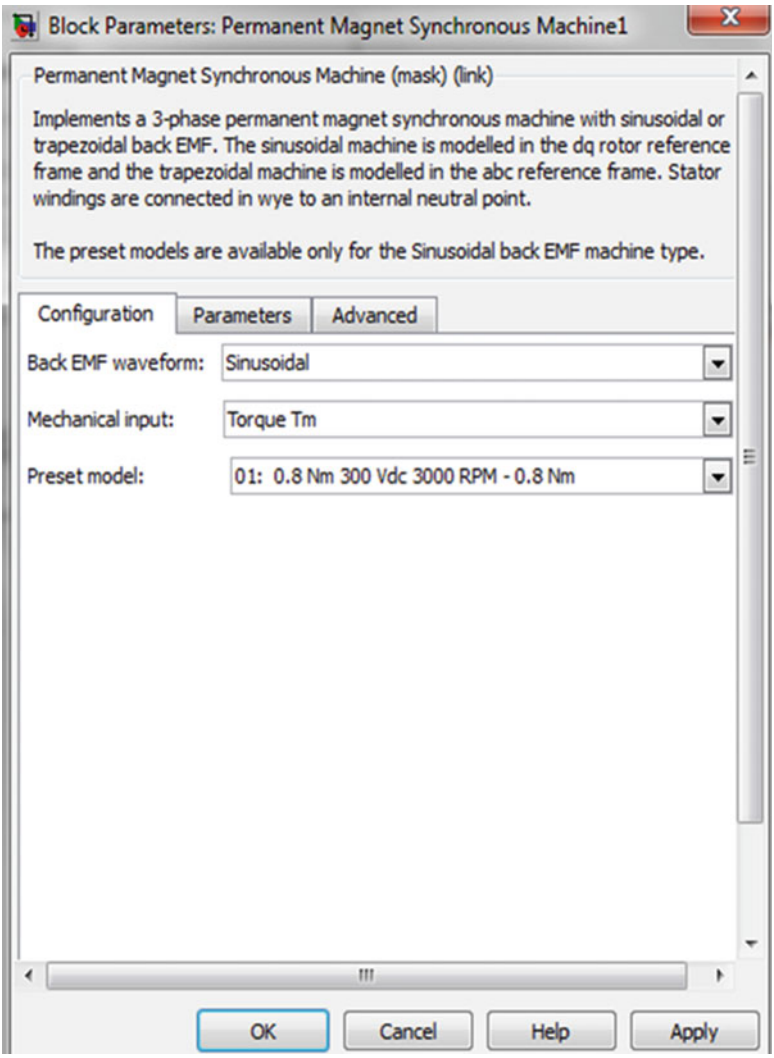


Fig. 4.22 Permanent magnet synchronous machine block

Description

The Permanent Magnet Synchronous Machine block operates in either generator or motor mode. The mode of operation is dictated by the sign of the mechanical torque (positive for motor mode, negative for generator mode). The electrical and mechanical parts of the machine are each represented by a second-order state-space model. The sinusoidal model assumes that the flux established by the permanent magnets in the stator is sinusoidal, which implies that the electromotive forces are sinusoidal. For the trapezoidal machine, the model assumes that the winding distribution and flux established by the permanent magnets produce three trapezoidal back EMF waveforms.

Table 4.2 Parameters of the permanent magnet synchronous machine block

Parameters	Value
Stator phase resistance Rs (ohm)	2.8750
Inductance Ld(H)	8.5e-3
Inductance Lq(H)	8.5e-3
Flux linkage established by magnets (V.s)	0.175
Voltage constant V-peak (V)	126.966
Torque constant	1.05
Inertia J(kg.m^2)	0.0008
Friction factor F(N.m.s)	0.001

Parameters

The parameters of the Permanent Magnet Synchronous Machine block for sinusoidal back emf machine are shown in Table 4.2:

4.9.1.2 Wind Turbine

This block implements a variable pitch wind turbine model. The performance coefficient Cp of the turbine is the mechanical output power of the turbine divided by wind power and a function of wind speed, rotational speed, and pitch angle (beta). Cp reaches its maximum value at zero beta. Select the wind-turbine power characteristics display to plot the turbine characteristics at the specified pitch angle.

The first input is the generator speed in per unit of the generator base speed. For a synchronous or asynchronous generator, the base speed is the synchronous speed. For a permanent-magnet generator, the base speed is defined as the speed producing nominal voltage at no load. The second input is the blade pitch angle (beta) in degrees. The third input is the wind speed in m/s.

The output is the torque applied to the generator shaft in per unit of the generator ratings. The turbine inertia must be added to the generator inertia.

Library

The wind turbine block shown in Fig. 4.23 is available in the Distributed Resources/Wind Generation library.

Description

The model is based on the steady-state power characteristics of the turbine. The stiffness of the drive train is infinite and the friction factor and the inertia of the turbine must be combined with those of the generator coupled to the turbine.

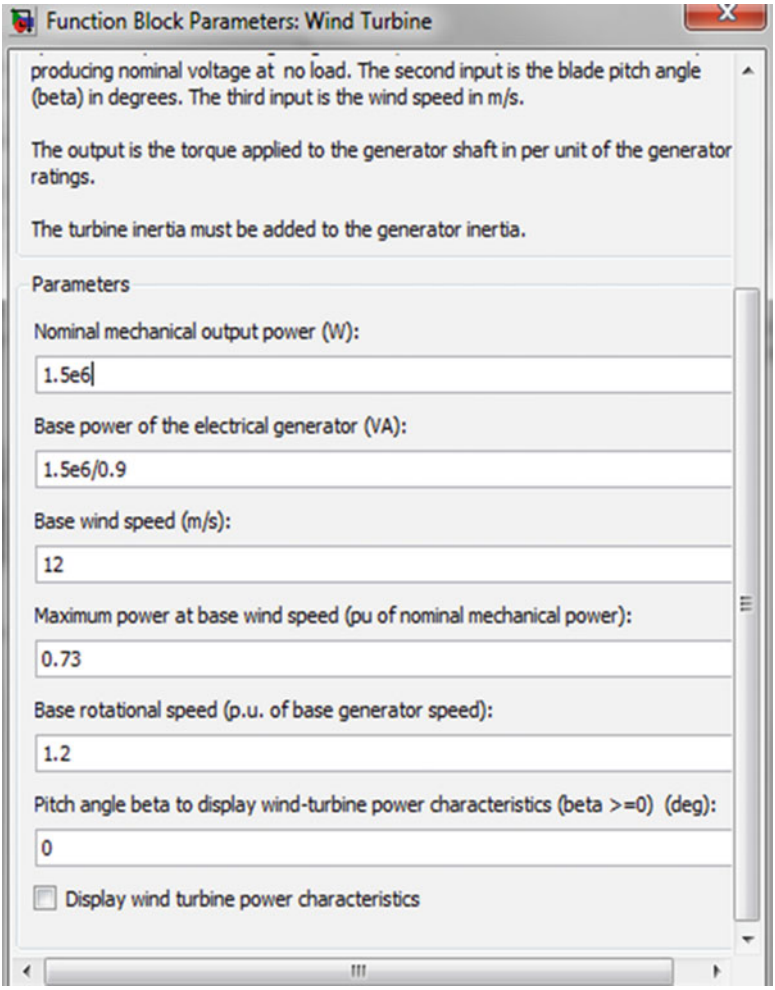


Fig. 4.23 Wind turbine block

Parameters

The parameters of the Wind Turbine block are shown in Table 4.3.

The SIMULINK model of the turbine is illustrated in the following Fig. 4.24. The three inputs are the generator speed (ωr_pu) in pu of the nominal speed of the generator, the pitch angle in degrees and the wind speed in m/s. The tip speed ratio λ in pu of $\lambda_{_nom}$ is obtained by the division of the rational speed in pu of the base rotational speed (defined below) and the wind speed in pu of the base wind speed. The output is the torque applied to the generator shaft. The parameters are described below:

Nominal Mechanical Output Power
The nominal output power in watts (W).

Table 4.3 Parameters of the wind turbine block

Parameters	Value
Nominal mechanical output power (W)	1.5e6
Base power of the electrical generator (VA)	1.5e6/0.9
Base wind speed (m/s)	12
Maximum power at base wind speed (pu of Nominal mechanical power)	0.73
Base rotational speed (kpu of base generator speed)	1.2

Base Power of the Electrical Generator
The nominal power of the electrical generator coupled to the wind turbine, in VA. This parameter is used to compute the output torque in pu of the nominal torque of the generator.

Base Wind Speed
The base value of the wind speed, in m/s, used in the per unit system. The base wind speed is the mean value of the expected wind speed. This base wind speed produces a mechanical power which is usually lower than the turbine nominal power.

Maximum Power at Base Wind Speed
The maximum power at base wind speed in pu of the nominal mechanical power. This parameter is the power gain k_p already defined.

Base Rotational Speed
The rotational speed at maximum power for the base wind speed. The base rotational speed is in pu of the base generator speed.

Pitch Angle Beta to Display Wind Turbine Power Characteristics
The pitch angle beta, in degrees, used to display the power characteristics. Beta must be greater than or equal to zero.

Display Wind Turbine Power Characteristics
If this parameter is checked, the turbine power characteristics are displayed for different wind speeds and for the specified pitch angle beta.

4.9.1.3 Inputs and Outputs

Generator Speed (pu)

SIMULINK input of the generator speed in pu based on the nominal speed of the generator.

Pitch Angle (deg)

SIMULINK input of the pitch angle.

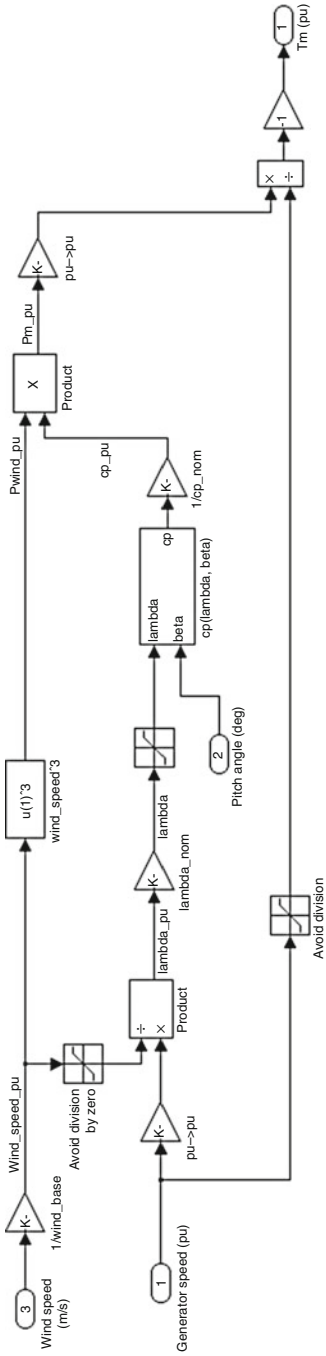


Fig. 4.24 SIMULINK model of the turbine

Wind Speed (m/s)

SIMULINK input of the wind speed in m/s.

Tm (pu)

SIMULINK output of the mechanical torque of the wind turbine, in pu of the nominal generator torque. The nominal torque of the generator is based on the nominal generator power and speed.

4.9.1.4 Characteristics of Wind Turbine

A wind turbine as power source leads to special conditions. The shaft speed power function is pre-determined because aerodynamic efficiency of the turbine depends on the ratio between the blade tip speed and the wind speed, called tip speed ratio. Maximum aerodynamic efficiency is obtained at a fixed tip speed ratio. To keep the turbine efficiency at its maximum, the speed of the turbine should be changed linearly with the wind speed. The wind power is proportional to the cube of the wind speed. If a turbine control program that is designed to optimize the energy production is used the wind speed turbine power function is also a cubic function. The turbine power curve is shown in Fig. 4.25 together with the turbine speed curve. In this report the turbine speed is assumed to be controllable above the rated wind speed by blade pitch control. The generator speed can then be considered nearly constant at wind speeds above the rated wind speed. An ordinary wind turbine has a rated wind speed of about 13–14 m/s but the median wind speed is much lower, about 5–7 m/s. Therefore, the power of the turbine is most of the time considerably less than the rated power.

It can be seen that the wind speed usually is about half of the rated wind speed. Only during a small fraction of the time, less than 10 % of the year, the turbine

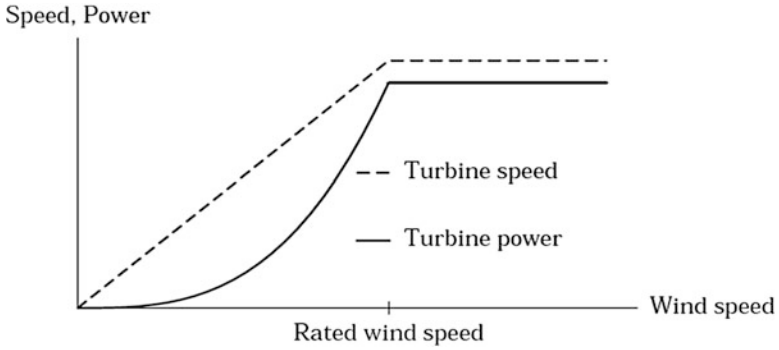


Fig. 4.25 Wind turbine characteristics

produces rated power. Therefore, a generator system for a wind turbine benefits more of low losses at low power than it does of low losses at rated power. At high power a variable-speed generator and converter have higher losses than what a similar generator connected directly to the network has. However, at low power the variable-speed system can have lower losses than the network-connected generator. Therefore, the annual average efficiency can be almost the same for both the systems.

4.9.1.5 Asynchronous Machine

Model the dynamics of three-phase asynchronous machine, also known as induction machine.

Library

The Asynchronous Machine block with corresponding parameters and their values is shown in Fig. 4.26. This block is available in the Machines library.

Description

The Asynchronous Machine block (Fig. 4.26) operates in either generator or motor mode. The mode of operation is dictated by the sign of the mechanical torque. If T_m is positive, the machine acts as a motor and if T_m is negative, the machine acts as a generator. The stator terminals of the Asynchronous Machine block are identified by the A, B, and C letters. The rotor terminals are identified by a, b, and c letters. The electrical part of the machine is represented by a fourth-order state-space model and the mechanical part by a second-order system. All electrical variables and parameters are referred to the stator. The input to the block is the mechanical Torque T_m. The output is the rotor speed in p.u.

4.9.2 Simulation and Results

The SIMULINK model of a wind energy system with AC/DC converter is constructed as shown in Fig. 4.27. The output of the model is obtained in terms of DC output voltage, stator current, and rotor speed and the curves are plotted with respect to time as shown in Figs. 4.28, 4.29 and 4.30. The wind turbine is connected with a three-phase load (Fig. 4.31) and the DC output voltage and rotor speed are shown in Figs. 4.32 and 4.33.

This section presents a novel conversion method of wind energy for achieving maximum benefits from the inverters when installed in three-phase four-wire

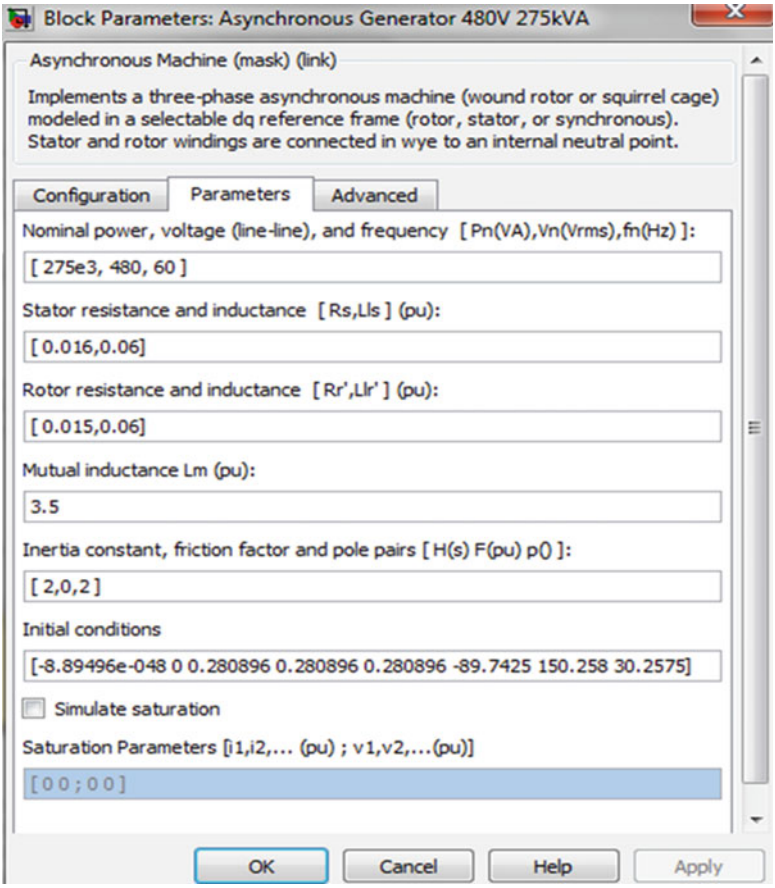


Fig. 4.26 Asynchronous machine block

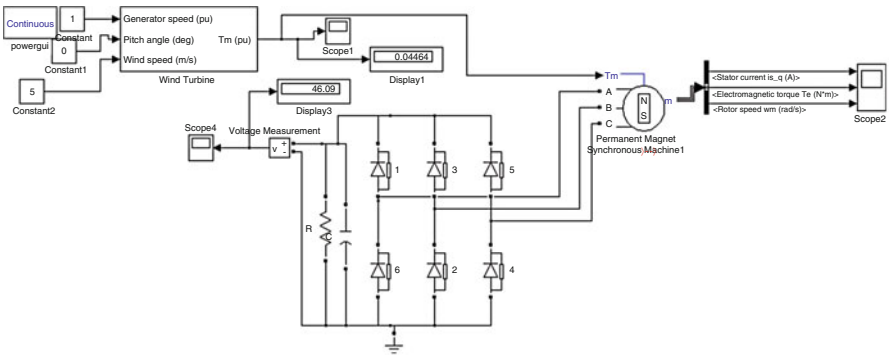


Fig. 4.27 SIMULINK model of wind energy system with AC/DC converter

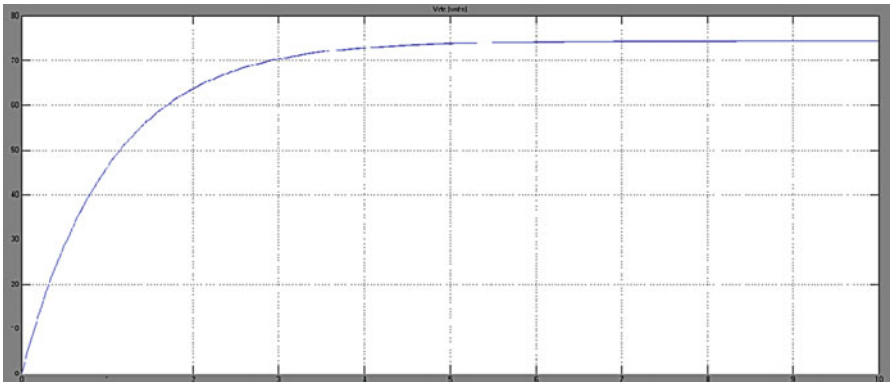


Fig. 4.28 DC output voltage (v_{dc}) versus time

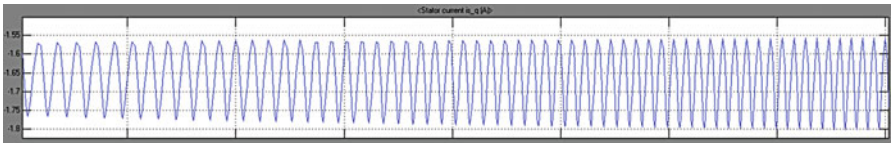


Fig. 4.29 Stator current versus time

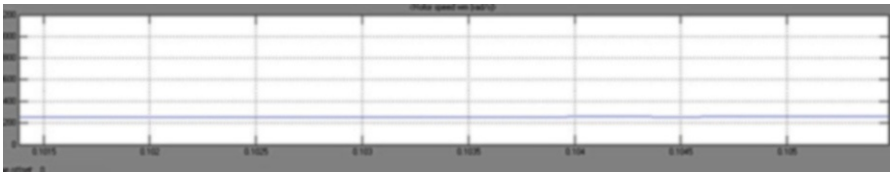


Fig. 4.30 Rotor speed versus time

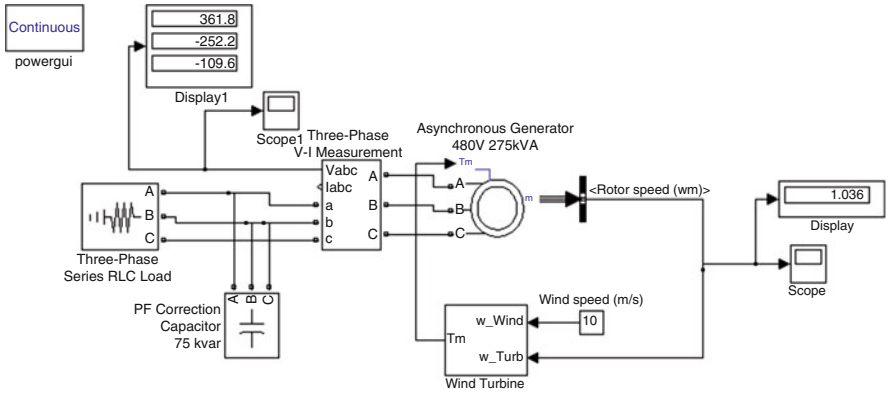


Fig. 4.31 SIMULINK model of wind energy system with three phase load

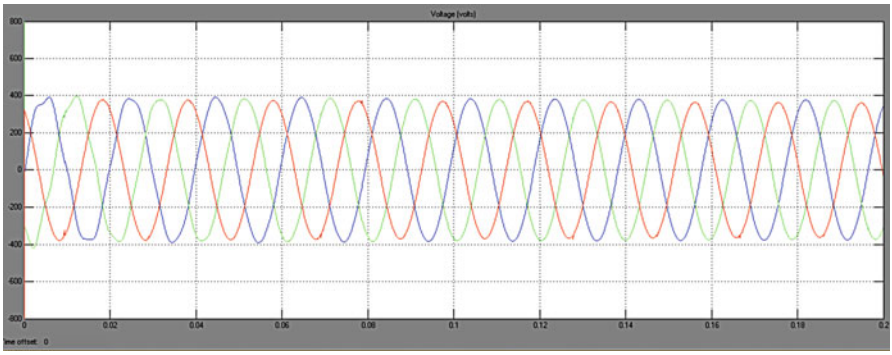


Fig. 4.32 Output voltage (v_{dc}) versus time

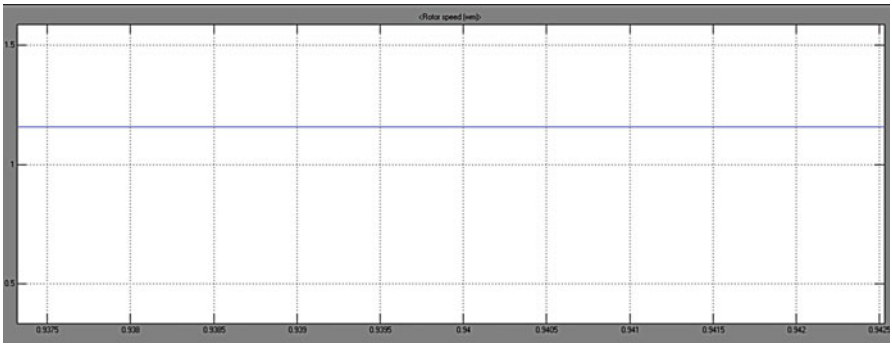


Fig. 4.33 Rotor speed versus time

distribution systems in the grid connected wind conversion system. The inverter can thus be utilized as: power converter to inject power generated from RES to the grid. All of these functions may be accomplished either individually or simultaneously. With such a control, the combination of grid-interfacing inverter and the three-phase four-wire linear/non-linear unbalanced load at point of common coupling appears as balanced linear load to the grid. This new control concept is demonstrated with extensive MATLAB/SIMULINK simulation and its results.

4.10 MATLAB/SIMULINK Model of Type 1 WTG

The stator winding of generator is connected directly to the grid and the rotor is driven by the wind turbine model. The power captured by the wind turbine is converted into electrical power by the induction generator and is transmitted to the grid by the stator winding. The pitch angle is controlled in order to limit the generator output power to its nominal value for high wind speeds. In order to

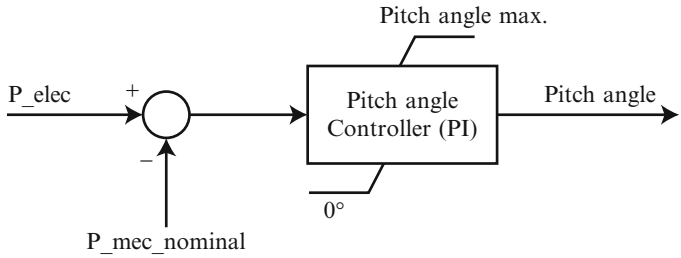


Fig. 4.34 Model of PI controller

generate power the induction generator speed must be slightly above the synchronous speed. But the speed variation is typically so small that the WTIG is considered to be a fixed-speed wind generator. The reactive power absorbed by the induction generator is provided by the grid or by some devices like capacitor banks, SVC, STATCOM or synchronous condenser.

4.10.1 Pitch Angle Control System

A Proportional-Integral (PI) controller shown in Fig. 4.34 is used to control the blade pitch angle in order to limit the electric output power to the nominal mechanical power. The pitch angle is kept constant at zero degree when the measured electric output power is under its nominal value. When it increases above its nominal value the PI controller increases the pitch angle to bring back the measured power to its nominal value.

4.10.2 Parameters

The parameters to be considered are the nominal power in VA, the nominal line-to-line voltage in Vrms, the nominal system frequency in hertz, the stator resistance Rs, leakage inductance Lls in pu based on the generator ratings. The rotor resistance Rr' and leakage inductance Llr', both referred to the stator, in pu based on the generator ratings. The magnetizing inductance Lm in pu based on the generator ratings. Combined generator and turbine inertia constant H in seconds, combined viscous friction factor F in pu based on the generator ratings and number of pole pairs p. The initial slip s, electrical angle Θ in degrees, stator current magnitude in pu and phase angle in degrees. Figure 4.35 shows the SIMULINK model of type 1 wind turbine generator. The generation and transmission of power in the wind farm model is simulated.

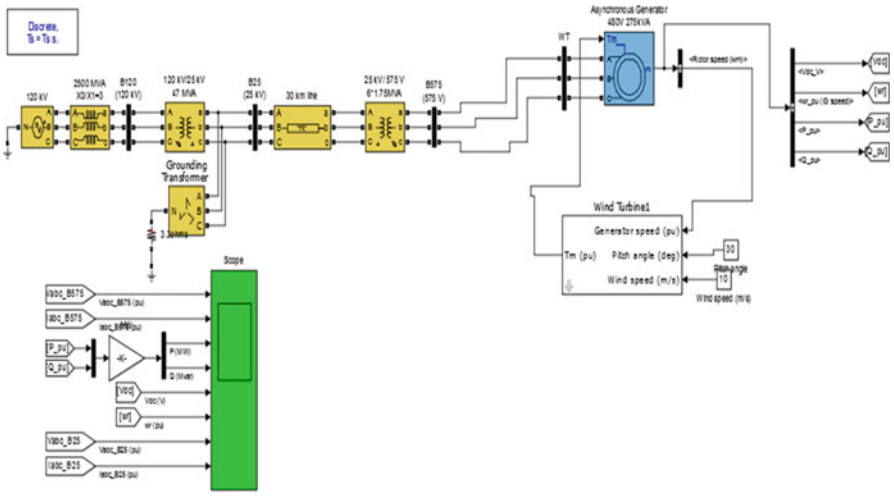


Fig. 4.35 SIMULINK model of type 1 WTG

The wind turbine is operated with a constant wind speed (13 m/s). This wind speed is chosen to be the rated value. Voltage sag on the grid is simulated, and the real and reactive power response of the wind turbine is observed. The grid voltage drops from 1 to 0.8 p.u. at $t = 15$ s, and the sag persists for 18 cycles (0.3 s). The intent of the test is to show that the model does indeed respond to events occurring in the dynamic timescale and that the response of the machine to this event is realistic. The grid voltage, rotor speed, real power, and reactive power during the event are shown. As expected, the step changes in the grid voltage magnitude when the sag begins and ends cause an immediate response. Note that the speed does not change by much (approximately 2 %), as expected from a fixed-speed wind turbine. The real power and reactive power outputs experience a disturbance too, and the outputs show that a mechanical oscillation occurs after the sag ends, and that the oscillation eventually damps out.

Figure 4.36 shows the simulation result obtained from the type 1 WTG. Three phase power is supplied to the load the output power is maintained nearly constant with respect to time.

4.11 MATLAB/SIMULINK Model of Type 2 WTG

The basic principle behind the IM operation is electromagnetic induction. Voltages applied to a multiphase AC stator winding result in currents which produce a rotating magnetic field. This field induces voltages (and therefore currents) in the rotor circuit. The interaction between the stator produced field and the rotor induced currents produces torque. If the induction machine is driven by a prime mover at a

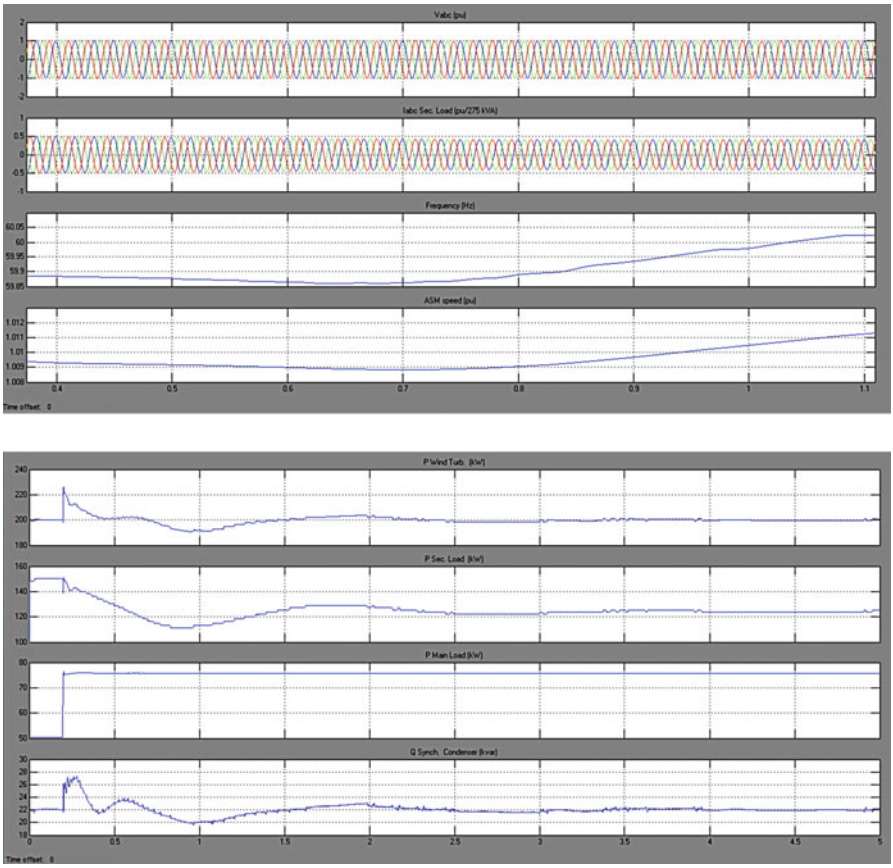


Fig. 4.36 Simulation results of type 1 WTG

speed greater than its synchronous speed, it acts as a generator. The rotor circuit may consist of bars short-circuited through end rings in the case of squirrel cage machines, or in the case of wound-rotor machines, multiphase windings accessible through slip rings and brushes. Only wound-rotor machines are used widely in all applications. Since the rotor windings are accessible, modifications to the rotor circuit are possible. One of these possible modifications is changing the rotor resistance. Revisiting the induction machine equivalent circuit is necessary to evaluate the impact of changing the rotor resistance on the torque and power associated with the machine.

Control of power output of a Type-2 turbine can be accomplished by varying the rotor resistance. The MATLAB/SIMULINK model is shown in Fig. 4.37. The objective of a rotor resistance controller in this situation is to seek the operating point at which power extraction from the wind is maximized, and also prevent the power extracted from exceeding the machine's ratings. The wind turbine is operated with a constant wind speed (13 m/s). This wind speed was chosen to be the

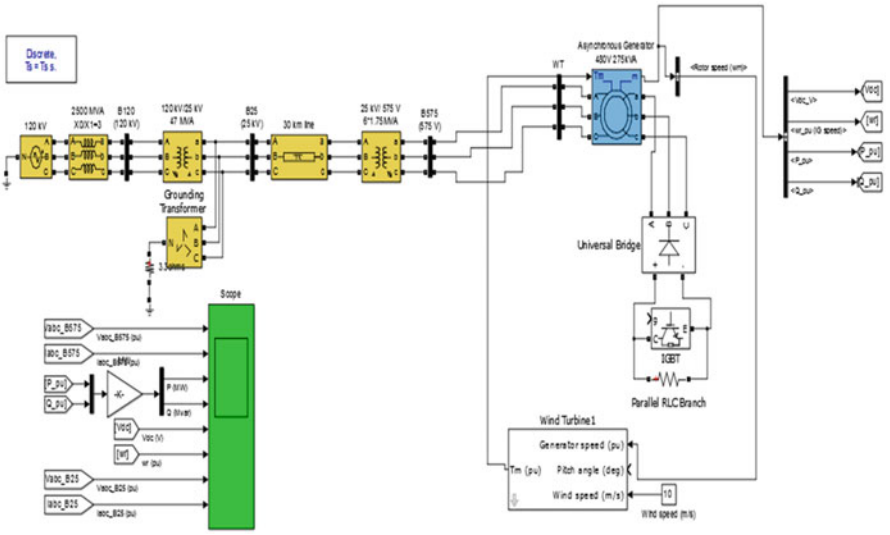


Fig. 4.37 SIMULINK model of type 2 WTG

rated value. Voltage sag on the grid was simulated, and the real and reactive power response of the wind turbine was observed. The grid voltage drops from 1 to 0.8 p.u. at t = 15 s, and the sag persists for 18 cycles (0.3 s). The grid voltage, rotor speed, real power, and reactive power during the event are shown in Fig. 4.38. As expected, the step changes in the grid voltage magnitude when the sag begins and ends cause an immediate response. Note that the speed experiences a greater change (approximately 5 %) as compared to the fixed-speed wind turbine. The real power and reactive power outputs experience a disturbance too; however, the disturbance is once again qualitatively and quantitatively different from the response of the fixed speed wind turbine due to the rotor resistance controller. As in the previous case, the outputs also show that a mechanical oscillation occurs after the sag ends, and that the oscillation eventually damps out.

4.12 MATLAB/SIMULINK Model of Type 3 WTG

Type 3 is the model with generic doubly-fed induction generator (DFIG) for a wind turbine. A set of three-phase currents is injected into the grid such that the real and reactive power of the generator can be independently controlled. The behavior of a DFIG control system to independently control the real and reactive power allows the use of a regulated current source in the dynamic model to represent the induction generator and power electronics. The main concern is to ensure that the model was suitably general and since the ultimate purpose of the model is use in load flow and dynamic stability studies, a highly detailed representation of the

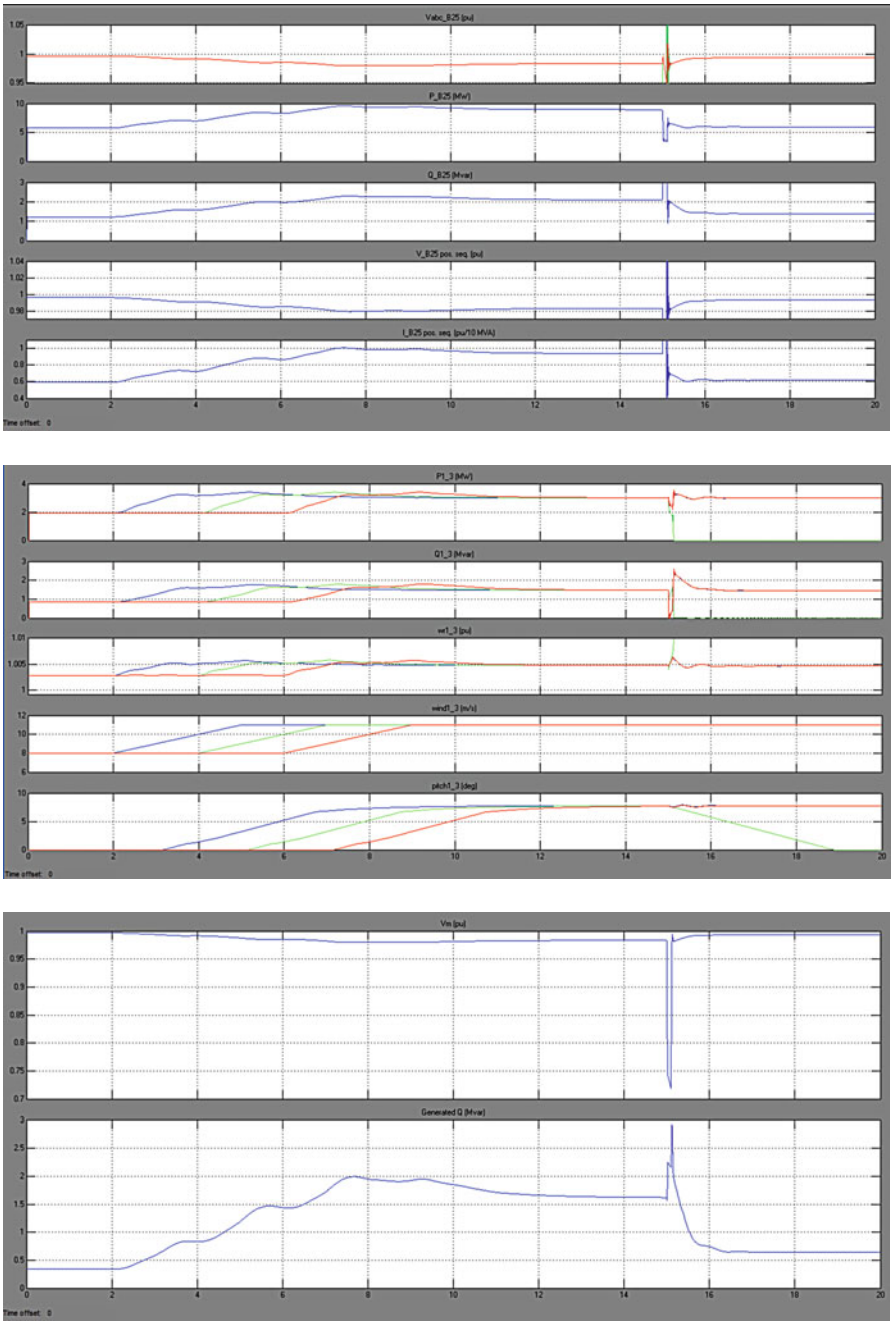


Fig. 4.38 Simulation results of type 2 WTG

machine and converter is not necessary. This subsection presents the analysis behind the approximations of using a regulated current source representation instead of explicitly modeling the generator and power electronics. A simplified model of the device dynamics is adequate. The mechanical modeling of the system has also been considerably simplified, with a one-mass model being used to represent the numerous rotating masses (the turbine, gearbox, and generator). Let the wound rotor induction machine be represented in a synchronously rotating qd0 reference frame. The currents flowing in the stator are assumed to be balanced. These currents produce a resultant stator magnetic field which has a constant magnitude and is rotating at synchronous speed. Since the angular speeds of 39 the stator magnetic field and the qd0 rotating frame are identical, the vector of the stator magnetic field is fixed with respect to the q- and d- axes of the qd0 rotating frame. In an actual WPP, a local grid collects the output from each wind turbine into a single point of connection on the grid. As a WPP is usually made up of several identical machines, it is a reasonable approximation to parallel all the turbines into a single equivalent large turbine behind single equivalent impedance. The rated power rating of the single equivalent wind turbine is equal to the combined rated power ratings of all wind turbines. The model developed is a simplified generic model intended for bulk power system studies where a detailed representation of a wind turbine generator is not required. The model is intended for transient stability analysis of grid disturbances. The actual device dynamics have been greatly simplified. To be specific, the very fast dynamics involved with the control of the generator-converter have been modeled as algebraic approximations of their response. This makes the generator-converter dynamics instantaneous.

Simplified turbine mechanical controls along with blade aerodynamic characteristics are included in the model. Generator-Converter sub-system: The generator-converter system is represented by a regulated voltage source. It injects three-phase voltage into the power system in response to the control commands from the Converter Control sub-system. Converter Control sub-system consists of the Reactive Power Control and Real Power Control sub-systems. These subsystems emulate power electronics controllers in regulating real and reactive power. Wind Turbine sub-system is represented by a single-mass model and it determines the mechanical input power and the angular speed of the wind turbine based on the specified pitch angle. Pitch Control sub-system is used to determine the desired blade pitch angle based on desired angular speed and real power. Figure 4.39 shows the SIMULINK model of type 3 WTG and Fig. 4.40 shows the corresponding simulation results obtained from MATLAB/SIMULINK model.

4.13 MATLAB/SIMULINK Model of Type 4 WTG

Full Converter Wind Turbine (FCWT) effectively decouples the generator from the grid, improving fault response. It allows the turbine to operate over a wide speed range, leading to improved power extraction from the wind. The converter

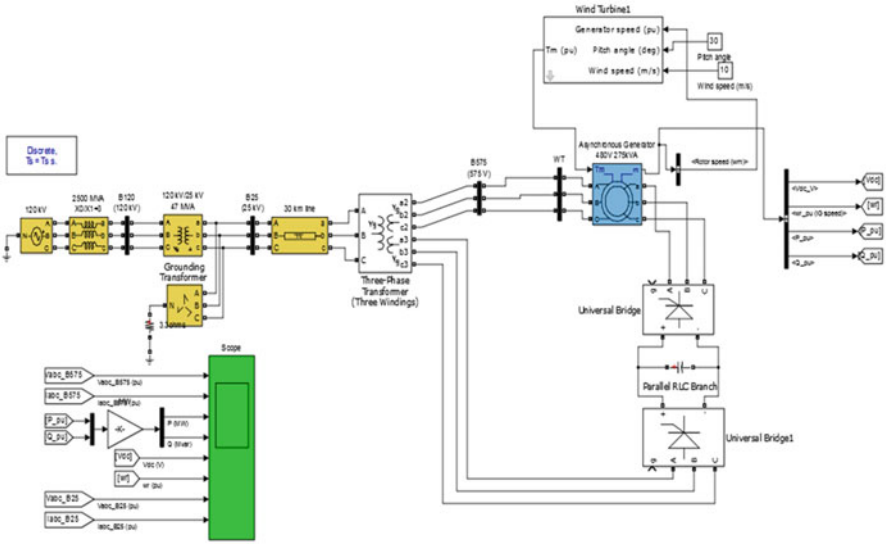


Fig. 4.39 SIMULINK model of type 3 WTG

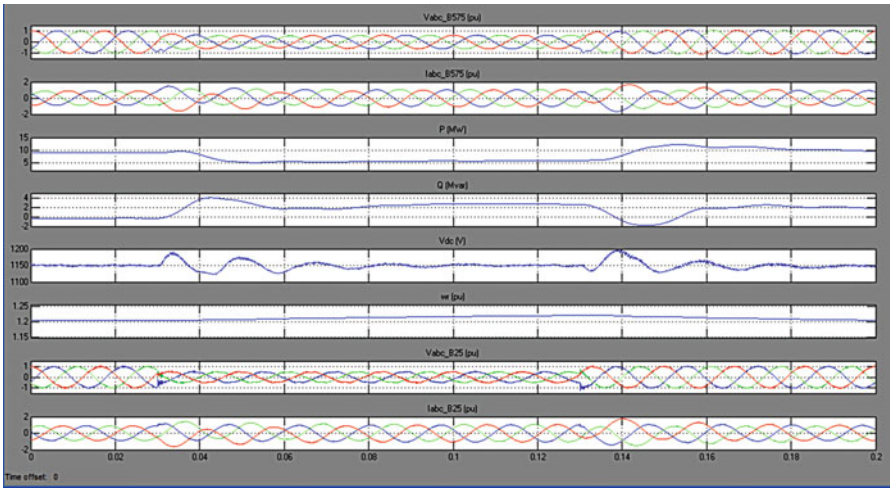


Fig. 4.40 Simulation results of type 3 WTG

interfacing the turbine to the grid has to handle the entire output of the generator (unlike in a DFIG turbine where the converter handles only 30–40 % of the generator output) and hence is more costly and lossy, but also provides more headroom to supply reactive power to the grid. The Permanent Magnet Alternator (PMA) itself has no rotor windings, reducing excitation losses and reducing the size of the generating unit with respect to competing technologies. Absence of rotor slip

rings reduces maintenance requirements. This combination of factors is driving the increasing penetration of FCWTs, especially for offshore wind power plants. The popularity of FCWTs has led to a search for reliable models to evaluate the impacts of integrating these FCWTs into the existing grid. The model presented in this report is a generic, manufacturer-independent model for a PMA-based FCWT, with no restrictions on its use. The PMA is interfaced to the grid through an AC-DC-AC conversion system. The AC-DC converter is comprised of a diode-bridge rectifier and a buck-boost converter which controls the DC-link voltage. The DC-AC conversion is accomplished using a current-controlled inverter which controls the real and reactive output power. Universal bridge is used for conversion purpose in the MATLAB model.

Figure 4.41 shows the SIMULINK model of type 4 WTG. Converter model is included in between for voltage conversion. Figure 4.42 shows the simulation results obtained for type 4 WTG.

4.14 MATLAB/SIMULINK Model of Grid Connection

The turbine rotor, gear box and generator are the main three components for energy conversion. The rotor, being the driving component in the conversion system, converts the wind energy into mechanical energy. In case of variable speed wind turbines also an electronic inverter absorbs the mechanical power from the rotor, converting it into electrical energy, which is then fed into a supply grid. The gear box us used to adapt the rotor speed to the generator speed, if it is necessary. The main components of the grid for connection of the wind turbines are the transformer and the substation with safety equipment (circuit breaker) and the electricity meter inside. Due to relatively high losses in low voltage lines, each of the turbines in the wind farm has its own transformer, converting the voltage level of the turbine to the medium voltage line of the distribution system. To avoid long low voltage cabling the transformers are located directly beside the turbine. Only in case of small wind turbines it is possible to connect them directly to the low voltage level of the grid without using a transformer. A wind farm of small wind turbines can use one transformer to connect to the grid. For very large wind farms with high powers a separate substation is necessary for transformation from the medium voltage system to the high voltage system. Between a single wind turbine or a wind farm and the grid, at the point of common coupling (PCC), a circuit breaker has to be installed to provide disconnection possibility in case a fault. The circuit breaker is usually located at the medium voltage system side, inside a substation, together with the electricity meter. The meter has its own voltage and current transformers. Depending on the individual conditions of the existing supply system the connection to the grid can be performed as a radial feeder or as a ring feeder (Fig. 4.43).

Figure 4.44 shows the generation part of the wind form. The generator is a wound rotor induction machine. The stator winding is directly connected to the grid. The rotor supply is connected through an AC-DC-AC converter for the P and

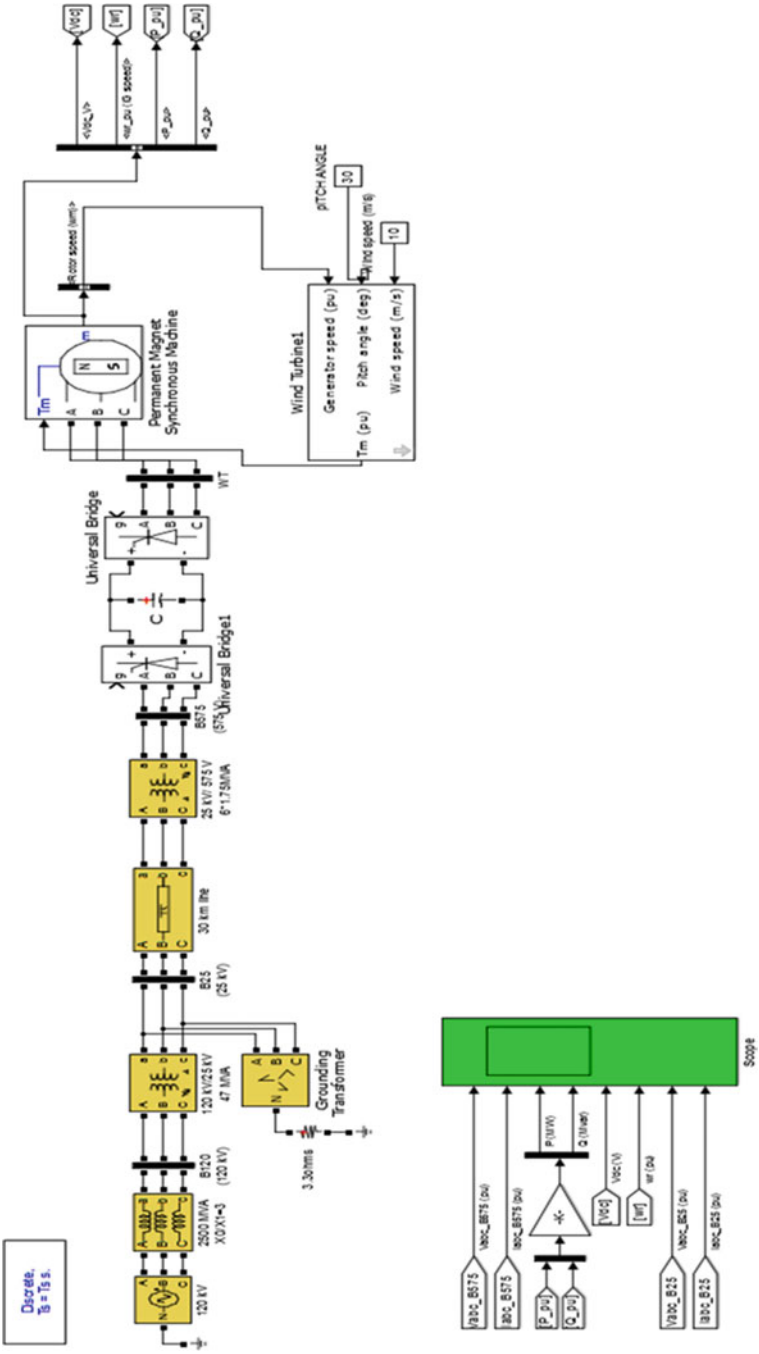


Fig. 4.41 SIMULINK model of type 4 WTG

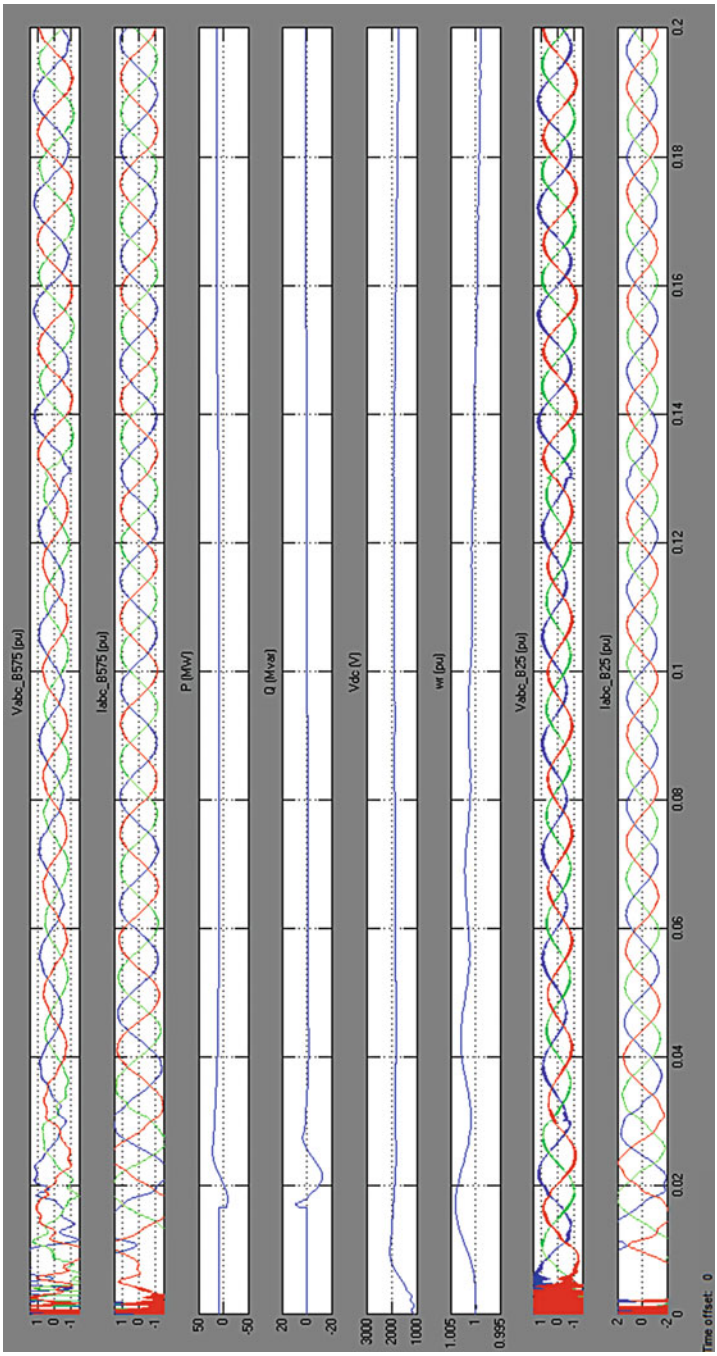


Fig. 4.42 Simulation results of type 4 WTG

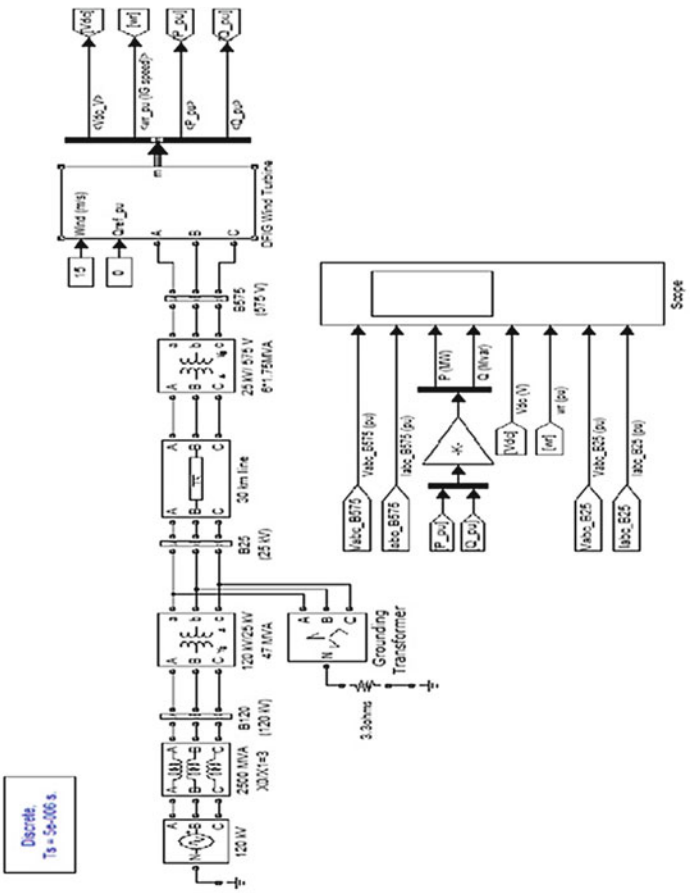


Fig. 4.43 SIMULINK model of grid connection

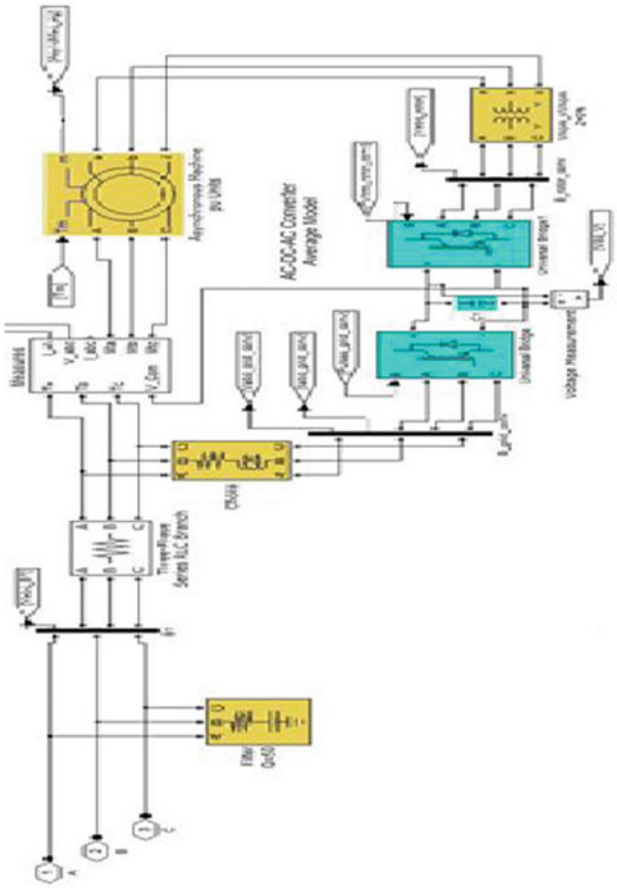


Fig. 4.44 SIMULINK model of the generating system

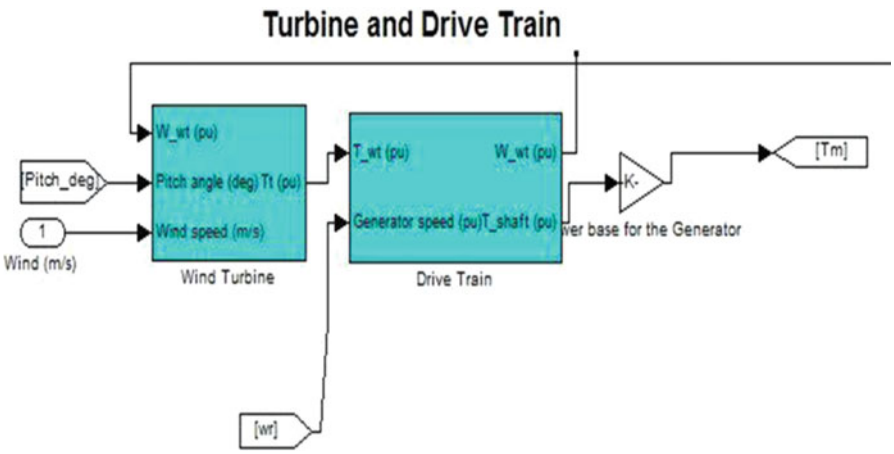


Fig. 4.45 Simulation diagram of the turbine and drive train

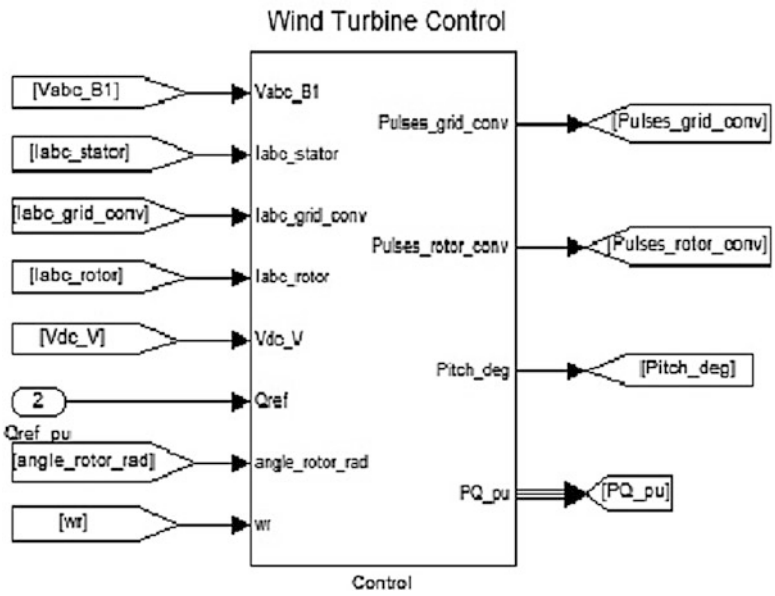


Fig. 4.46 Model of the wind turbine control

Q levels control. The two converters will get the control pulses from respective controllers i.e. grid side converter. Figure 4.45 shows the SIMULINK model of the turbine and drive train. Turbine control plays a major role in effective power generation. Figure 4.46 shows the Wind turbine control SIMULINK model.

Figures 4.47, 4.48, 4.49, and 4.50 shows the simulation results obtained for grid connected wind farm for variable speed. The grid is a 25 kv system. That shows the generation at one end which is step up to the grid voltage by using the step up transformer. The fault protection also provided with a grounding transformer.

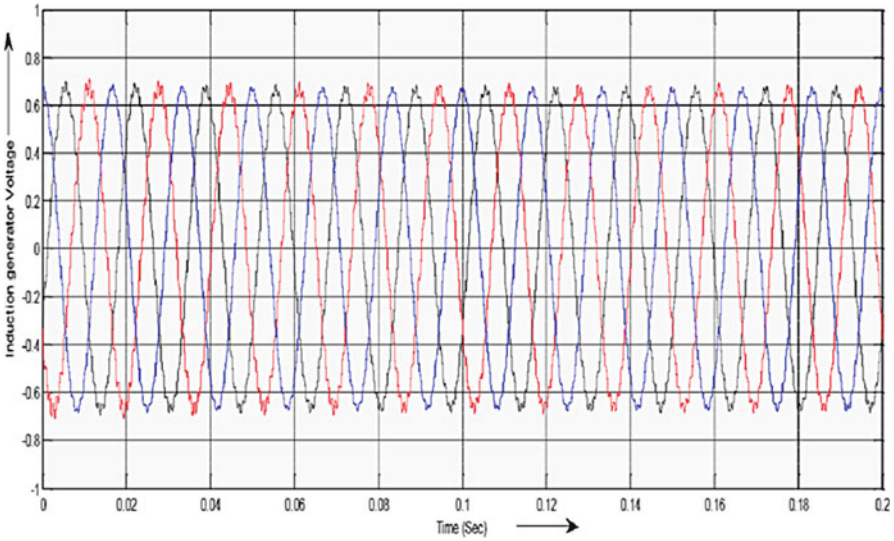


Fig. 4.47 Three phase voltage waveforms from Induction generator

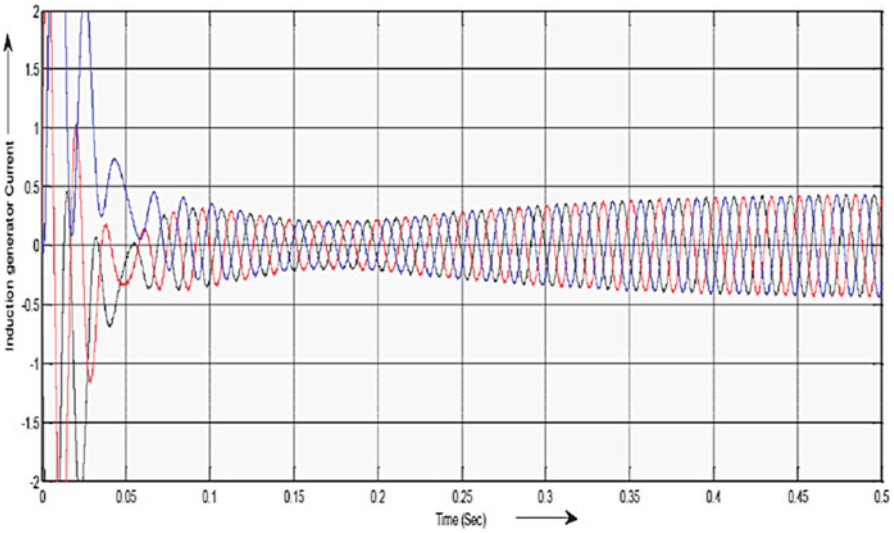


Fig. 4.48 Three phase current waveforms from Induction generator

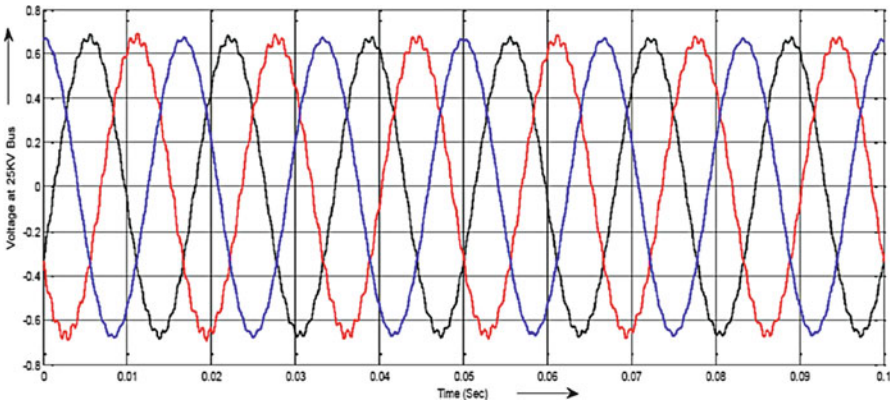


Fig. 4.49 Three phase voltage waveforms at 125KV Bus

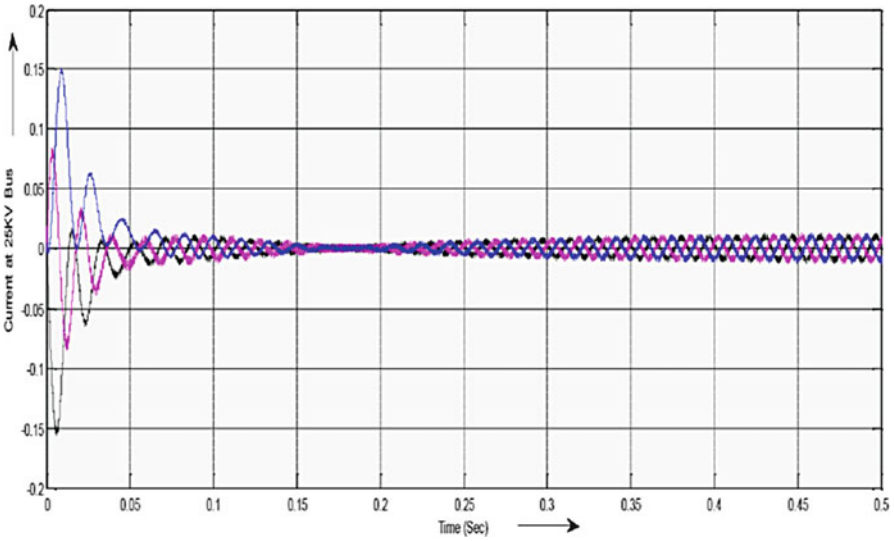


Fig. 4.50 Three phase current waveforms at 125KV Bus

4.15 Summary

Wind energy generation has become a highly researched area. A concise review of various WECS has been achieved through this chapter. Converter topologies used in combination with PMSG, DFIG, IG and SG, along with different control schemes has been described in detail. All control methods described, attempt to obtain maximum energy transfer from the wind turbine to the grid. There is a continuing effort to make converter and control schemes more efficient and cost

effective in hopes of an economically viable solution to increasing environmental issues. Wind power generation has grown at an alarming rate in the past decade and will continue to do so as power electronic technology continues to advance. In addition, development of MATLAB/SIMULINK models has aided to practical implementation of the models discussed in this chapter.

Review Questions

1. During high wind speeds, what are the approaches to regulate the power?
2. How is the energy in the wind captured?
3. What are the different types of anemometers used to measure wind?
4. How much electricity can one wind turbine generate?
5. How many turbines does it take to make one megawatt (MW)?
6. The wind doesn't blow all the time. How much can it really contribute to a utility's generating capacity?
7. What are the environmental benefits of wind power?
8. A wind turbine is being operated in a variable speed mode with an optimum load. If the wind speed doubles, what is the change in (a) output power? (b) torque? (c) rotor speed?
9. A three-phase load draws 250 kW at a power factor of 0.707 lagging from a 440-V line. In parallel with this load is a three-phase capacitor bank which draws 60 kVA. Find the magnitude of the line current and the overall power factor.
10. A 500-kW Darrieus wind turbine is equipped with a synchronous generator rated at 480 V line to line and 625 kVA at 0.8 power factor. Rated current is flowing and the current leads the voltage by 40°. What are the real and reactive powers being supplied to the load?
11. What are the economic obstacles to greater wind power usage?
12. Differentiate between back-to-back inverter with matrix inverter used for DFIG based WTG?
13. How are power quality issues addressed in WECS?
14. Develop a MATLAB/SIMULINK model for Hard switching inverter with vector control of supply side inverter DC voltage control using chopper duty ratio.
15. Develop a MATLAB/SIMULINK model for Matrix inverter for DFIG WTG.

Bibliography

Amei K, Takayasu Y, Ohji T, Sakui M (2002) Amaximum power control of wind generator system using a permanent magnet synchronous generator and a boost chopper circuit. Proc Power Conv 3:1447–1452

Borowy BS, Salameh ZM (1996) Methodology for optimally sizing the combination of a battery bank and PV array in a wind/PV hybrid system. IEEE Trans Energy Conv 11(2):367–375

"Buck Converter Design Example", Microchip WebSeminor, Microchip Technology Incorporated. All Rights Reserved (2006). Microchip Web Sites: www.microchip.com/smps

Casadei D, Angelo T (2000) Implementation of a direct torque control algorithm for induction motors based on discrete space vector modulation. IEEE Trans Power Electron 15(4):769–777

Chang HC, Liaw CM (2009) Development of compact switched reluctance motor drive for EV propulsion with voltage-boosting and PFC charging capabilities. IEEE Trans Veh Technol 58:3198–3215

http://www.ren21.net. Accessed June 2008

Hussein KH, Muta I, Hoshino T, Osakada M (1995) Maximum photovoltaic power tracking: an algorithm for rapidly changing atmospheric conditions. IEE Proc Gener Trans Distrib 142 (1):59

International Rectifier Application Note AN-978

IR2112 Datasheet

Kouro S, Bernal R, Miranda H, Silva CA, Rodriguez J (2007) High-performance torque and flux control for multilevel inverter fed induction motors. IEEE Trans Power Electron 22(6):2116–2123

Ramos-Robles CA (2005) Determination of favorable conditions for the development of a wind power farm in Puerto Rico. Master of Science thesis, Department of Electrical and Computer Engineering, University of Puerto Rico, Mayagüez Campus

Rashid MH (2006) Power electronics devices, circuits and applications. Academic Press, San Diego

Remli A, Aouzellag D, Ghedamsi K (2011) Study and control of wind energy conversion system based permanent magnet synchronous generator connected to the grid. Int J R Rev Comput Eng 1(1)

Sandip RV, Vijay Sridhar, Saikumar S (2011) Modelling and control of a wind turbine using permanent magnet synchronous generator. Int J Eng Sci Technol 3(3):2377–2384, ISSN: 0975-5462

Soliman HF, Attia AA, Mokhymar SM, Badr MAL. Fuzzy algorithm for supervisory control of self-excited induction generator. JKAU: Eng Sci 17(2):19–40

Takahashi I, Nouguchi T (1986) A new quick response and high efficiency control strategy for an induction motor. IEEE Trans Ind Appl IA-22(5):820–827

Tang L, Zhong L, Rahman MF, Hu Y (2003) A novel direct torque control for interior permanent-magnet synchronous machine drive with low ripple in torque and flux-a speed-sensor less approach. IEEE Trans Ind Appl 39(6):1748–1756

Wood J, Wollenberg BF (1996) Power generation operation an control, 2nd edn. Wiley, New York

Chapter 5
Soft Computing Techniques in Wind Energy Conversion Systems

Learning Objectives
On completion of this chapter, the reader will have knowledge on:

- Importance of soft computing techniques in WECS.
- Prediction of power factor using soft computing techniques.
- Fuzzy based Pitch angle control.
- Soft computing based MPPT in WECS.
- Economic dispatch of WECS using soft computing algorithms.

The influence of soft computing on the different aspects of wind power systems especially in the field of operation and maintenance has received great focus during the recent years. This chapter reviews, analyses, discusses and summarizes the recent research, development and trends in the applications of soft computing in the field of wind power systems. This chapter provides the state of the art of soft computing techniques in wind energy conversion systems as a good guidance for future research work. Based on the observations from several applications, soft computing techniques are adequate for solving the different challenges at different phases of the life cycle processes of wind power systems. Soft computing can enhance the efficiency and effectiveness of the operation and maintenance of offshore wind power systems through improving the availability levels, thus, providing secure, sustainable and competitive energy supply for the future.

Soft computing is a collection of computational techniques which intend to complement each other. The aim of soft computing is to exploit the tolerance for imprecision, uncertainty, approximation, and partial truth to achieve tractability, robustness, and low solution cost. Components of soft computing include: fuzzy logic, neural computing, evolutionary computing and probabilistic computing. Applications based on soft computing such as evolutionary computation, neural networks and fuzzy logic for components of wind energy conversion systems are illustrated in this chapter.

© Springer International Publishing Switzerland 2015

S. Sumathi et al., *Solar PV and Wind Energy Conversion Systems*,
Green Energy and Technology, DOI 10.1007/978-3-319-14941-7_5

5.1 Prediction of Wind Turbine Power Factor

Wind energy conversion systems (WECS) are arising as smart alternative for electricity generation. The basic components of a typical wind energy conversion system include a wind turbine, a generator, interconnection apparatus, and control systems. The design of such components has great focus during recent years. The wind turbine is the most important part of the WECS, which transforms the wind kinetic energy into mechanical or electric energy. The wind turbine comprises of a blade, a mechanical part and an electric engine coupled to each other. The kinematical energy of wind is the function of wind speed, the specific mass of air, the area of air space where the wind is captured and the height at which the rotor is placed. The power generated by each wind turbine depends on parameters such as turbine type, the number of blades and the power factor. The power factor is also called blade yield and can be obtained from blade and wind properties. In this section, power factor of wind turbine is predicted using Artificial Neural Networks (ANN) and Adaptive Neuro-Fuzzy Inference System (ANFIS).

5.1.1 Problem Formulation

The definition of power factor is the ratio between the power in turbine shaft (Pp) and the wind power (Pr) due to its kinetic energy right before the turbine plane, which yields

$$C_p = \frac{P_p}{P_r} \tag{5.1}$$

The wind power, P_r, in the air flow passing through the circle with a radius of R immediately before the turbine plane can be defined as;

$$P_r = \frac{1}{2}\rho\pi R^2 V_r^3 \tag{5.2}$$

where ρ is the density of the air and Vr is the wind speed. In general, the maximum power factor of the wind turbine is 59.26 % known as the Betz limit and the practical value can be 45 % of the maximum. This decrease is due to the losses involved in practical systems such as profile losses, end losses, eddy losses, and blade number losses.

5.1.1.1 Profile Losses

This loss can be considered using

$$\eta_{profile} = 1 - (\lambda_A/\varepsilon) \tag{5.3}$$

where λ_A is the tip speed ratio and ε is the number of slip (Slide) and expressed as

$$\varepsilon = \frac{C_L}{C_D} \tag{5.4}$$

where C_L is the coefficient of lift force of chosen profile and C_D is the coefficient of drag force.

5.1.1.2 End Losses

In the end of a blade, airflow from the lower side of the profile to the upper side takes place. Coupling with the airflow coming towards the blade, this airflow widens gradually. In the calculations, this can be considered as

$$\eta_{end} = 1 - (1.84/z\lambda_A) \tag{5.5}$$

where z is the number of turbine blade.

5.1.1.3 Eddy Losses

There is no change in the wind before and after the turbine plate, based on the Betz theory. But the air mass encountering the blade changes its direction.

5.1.1.4 Blade Number Losses

If the turbine has more than four blades, the movement of air through the blades becomes complex, and hence theoretical analysis is difficult. Thus, the theory of Glauert-Shmitz previously applies to the turbines with four or less wind turbine blade.

Including the losses mentioned in the above sections, the power factor can be re-expressed as

$$C_p = f\left(A, \lambda_A, C_{pschmitz}, \eta_{end}, \eta_{profile}, \eta_{eddy}, \eta_{blade\ number}\right) \tag{5.6}$$

where A represents the type of profile used, λ_A is the tip speed ratio, $C_{pshmitz}$ is Shmitz coefficient and the η values are the associate losses. Based on the above equation, assessment of the power factor is quite cumbersome, for which an effective procedure is needed. Thus soft computing techniques are applied to predict the power factor in WECS.

5.1.2 *Artificial Neural Networks*

The typical back-propagation network has an input layer, an output layer, and at least one hidden layer. There is no theoretical limit on the number of hidden layers but typically there is just one or two. Some work has been done which indicates that a minimum of four layers (three hidden layers plus an output layer) are required to solve problems of any complexity. Each layer is fully connected to the succeeding layer, as shown in Fig. 5.1.

The in and out layers indicate the flow of information during recall. Recall is the process of putting input data into a trained network and receiving the answer. Back-propagation is not used during recall, but only when the network is learning a training set.

The number of layers and the number of processing element per layer are important decisions. These parameters to a feedforward, back-propagation topology are also the most ethereal. There are only general rules picked up over time and followed by most researchers and engineers applying this architecture of their problems.

Rule One: As the complexity in the relationship between the input data and the desired output increases, then the number of the processing elements in the hidden layer should also increase.

Rule Two: If the process being modeled is separable into multiple stages, then additional hidden layer(s) may be required. If the process is not separable into stages, then additional layers may simply enable memorization and not a true general solution.

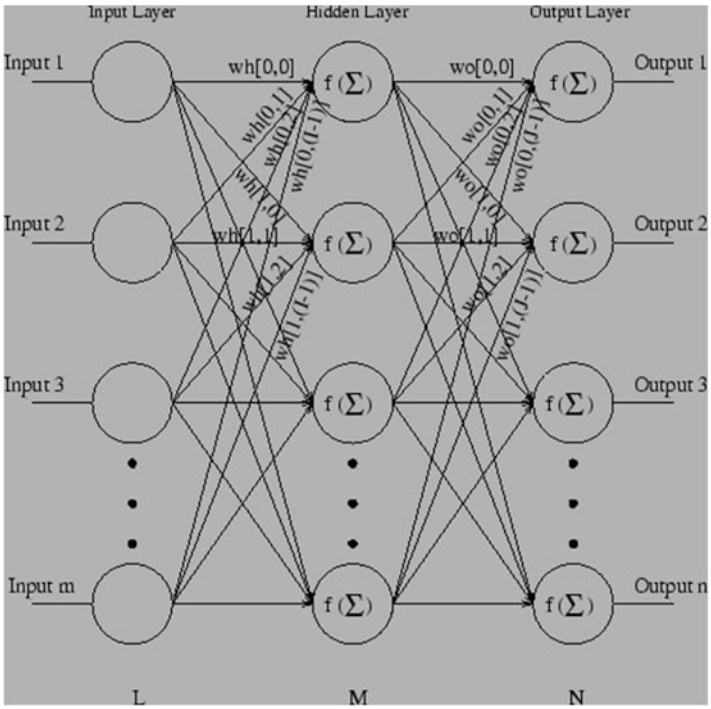


Fig. 5.1 Back-propagation network

Rule Three: The amount of training data available sets an upper bound for the number of processing elements in the hidden layers. To calculate this upper bound, use the number of input output pair examples in the training set and divide that number by the total number of input and output processing elements in the network. Then divide that result again by a scaling factor between 5 and 10. Larger scaling factors are used for relatively noisy data. Extremely noisy data may require a factor of 20 or even 50, while very clean input data with an exact relationship to the output might drop the factor to around 2. It is important that the hidden layers have few processing elements. Too many artificial neurons and the training set will be memorized. If that happens then no generalization of the data trends will occur, making the network useless on new data sets.

5.1.2.1 Training Algorithm

The training algorithm of back propagation involves four stages, viz.

1. Initialization of weights.
2. Feed forward.
3. Back propagation of errors.
4. Updation of the weights and biases.

During first stage, which is the initialization of weights, some small random values are assigned.

During feed forward stage each input unit (X_i) receives an input signal and transmits this signal to each of the hidden units $z_1 \ldots z_p$. Each hidden units then calculates the activation function and sends its signal z_j to each output unit. The output unit calculates the activation function to form the response of the net for the given input pattern.

During back propagation of errors, each output unit compares its computed activation y_k with its target value t_k to determine the associated error for that pattern with that unit. Based on the error, the factor δ_k ($k = 1,\ldots m$) is computed and is used to distribute the error at output unit y_k back to all units in the previous layer. Similarly the factor δ_j ($j = 1,\ldots p$) is computed for each hidden unit z_j.

During final stage, the weight and biases are updated using the δ factor and the activation.

5.1.2.2 Parameters

The various parameters used in the training algorithm is as follows:

x: Input training vector $x = (x_1,\ldots x_i,\ldots x_n)$
t: Output target vector $t = (t_1,\ldots t_k,\ldots t_m)$.
δ_k = error of output unit y_k
δ_j = error of output unit z_j
α = learning rate
v_{oj} = bias on hidden unit j
z_j = hidden unit j
w_{oK} = bias on output unit k
y_k = output unit k

The pseudocode of the training algorithm of the back propagation network is as follows. The algorithm is given with the various phases:

Initialization stage:
Initialize weights v and w to small random values
Initialize Learning rate
While not stopping condition for phase I **Do**
For each training pair
Feed forward stage:
Each input unit receives the input signal x_i and transmits to all units in the hidden layer
Each hidden unit (z_j, j=1,…,p) sums its weighted input signals

$$z_{inj} = v_{oj} + \sum_{i=1}^{n} x_i v_{ij}$$

applying activation function
$Zj = f(z_{inj})$
and sends this signal to all units.
Each output unit (y_k, k=1,…,m) sums its weighted input signals

$$y_{ink} = w_{ok} + \sum_{j=1}^{p} z_j w_{jk}$$

applies its activation function to calculate output signals
$Y_k = f(y_{ink})$
Back propagation of errors:
Each output unit (y_k, k=1,…, m) receives a target pattern corresponding to an input pattern, error information term is calculated as

$$\delta_k = (t_k - y_k) f(y_{ink})$$

Each hidden unit (z_j, j=1,…,p) sums its delta inputs from units in the layer above

$$\delta_{inj} = \sum_{k=1}^{m} \delta_j w_{jk}$$

The error information is calculated as
$\delta_j = \delta_{inj}\ f(z_{inj})$
Updation of weights and biases:
Each output unit (y_k, k=1,…,m) updates its bias and weights (j=0,…,p)
The weight correction term is given by

$$\Delta W_{jk} = \alpha \delta_k z_j$$

The bias correction term is given by

$$\Delta W_{ok} = \alpha \delta_k$$

$W_{jk(new)} = W_{jk(old)} + \Delta W_{jk}$, $W_{ok(new)} = W_{ok(old)} + \Delta W_{ok}$
Each hidden unit (z_j, j=1,…,p) updates its bias and weights (i=0,…,n)
The weight correction term

$$\Delta V_{ij} = \alpha \delta_j x_i$$

The bias correction term

$$\Delta V_{oj} = \alpha \delta_j$$

$V_{ij\ (new)} = V_{ij(old)} + \Delta V_{ij}$, $V_{oj(new)} = W_{oj(old)} + \Delta V_{oj}$
End For
Test the stopping condition
End while
End

The stopping condition may be the minimization of the errors, number of epochs etc.

5.1.3 Adaptive Neuro-fuzzy Inference System (ANFIS)

Both fuzzy logic systems and neural networks are natural complementary tools in building intelligent systems. Neural networks are basically low-level computational structures that perform well when dealing with raw data, fuzzy logic deals with reasoning on a higher level. However, fuzzy systems lack the ability to learn and cannot adjust themselves. A neuro-fuzzy system is, in fact, a neural network that is functionally equivalent to a fuzzy inference model.

The hybrid neuro-fuzzy model for potential mapping described here is a Takagi-Sugeno type fuzzy inference system, which is implemented in the framework of adaptive neural networks. It is an adaptation of "adaptive network-based fuzzy inference system" for mineral potential mapping. A typical fuzzy if-then rule in a generalized Takagi-Sugeno type fuzzy inference system has the following form:

$$\text{IF } x \text{ is } a \text{ AND } y \text{ is } b \text{ THEN } z = f(x, y)$$

where x and y are input variables, a and b are fuzzy membership values of x and y, respectively, in the antecedent part of the fuzzy if-then rule and $z = f(x, y)$ is a crisp function in the consequent part of the rule. Usually, $f(x, y)$ is a polynomial in the input variables x and y, but it can be any function as long as it can appropriately describe the output of the system. When $f(x, y)$ is a first-order polynomial, the resulting fuzzy inference system is called a first-order Takagi-Sugeno type fuzzy inference system, which was originally proposed by Takagi and Sugeno. When $f(x, y)$ is a constant, the resulting fuzzy inference system is called a zero-order Takagi-Sugeno type fuzzy inference system. The higher the order of the polynomial functions, in a fuzzy inference system, the larger is the number of the function parameters and, consequently, the larger is the number of training samples required for a robust estimation of these parameters. Therefore, the order of a fuzzy inference system used in an application is largely determined by the number of available training samples. In the case of the feature vector T, there are two input predictor patterns, x_{1j} and x_{2j}, and four membership functions, $\mu_{\tilde{A}_1^1}$, $\mu_{\tilde{A}_1^2}$, $\mu_{\tilde{A}_2^1}$ and $\mu_{\tilde{A}_2^2}$, which can be combined using a first-order Takagi-Sugeno type fuzzy inference system based on the following fuzzy if-then rules:

1. IF x_{1j} is $\mu_{\tilde{A}_1^1}(x_{1j})$ AND x_{2j} is $\mu_{\tilde{A}_2^1}(x_{2j})$ THEN $F_1 = P_{10} + P_{11}x_{1j} + P_{12}x_{2j}$
2. IF x_{1j} is $\mu_{\tilde{A}_1^1}(x_{1j})$ AND x_{2j} is $\mu_{\tilde{A}_2^2}(x_{2j})$ THEN $F_2 = P_{20} + P_{21}x_{1j} + P_{22}x_{2j}$
3. IF x_{1j} is $\mu_{\tilde{A}_2^1}(x_{1j})$ AND x_{2j} is $\mu_{\tilde{A}_2^1}(x_{2j})$ THEN $F_3 = P_{30} + P_{31}x_{1j} + P_{32}x_{2j}$
4. IF x_{1j} is $\mu_{\tilde{A}_1^2}(x_{1j})$ AND x_{2j} is $\mu_{\tilde{A}_2^2}(x_{2j})$ THEN $F_4 = P_{40} + P_{41}x_{1j} + P_{42}x_{2j}$

where P_{ki} (k = 1 to 4, i = 0 to 2) is the parameter of the polynomial function in the consequent part of the k^{th} fuzzy if-then rule. The above fuzzy inference system is characterized by four fuzzy if-then rules, each of which contains, in the consequent part, a first-order polynomial function characterized by three parameters. Therefore, a first-order Takagi- Sugeno type fuzzy inference system with two input predictor

maps and two fuzzy membership functions for each map results in $2^2(=4)$ fuzzy if-then rules and $2^2(2+1)(=12)$ function parameters. In general, a first-order Takagi- Sugeno type fuzzy inference system with n predictor maps and 2n fuzzy membership functions contains 2^n fuzzy if-then rules and $2^n(n+1)$ function parameters.

Even for a moderately-large n, robust estimation of the function parameters would require a large number of training samples of known mineral deposits, which may not always be available. In such cases, it is preferable to use a zero-order Takagi-Sugeno type fuzzy inference system, which, in the case of the feature vector T, comprises the following fuzzy if-then rules:

1. IF x_{1j} is $\mu_{\tilde{A}_1^1}(x_{1j})$ AND x_{2j} is $\mu_{\tilde{A}_2^1}(x_{2j})$ THEN $F_1 = P_1$
2. IF x_{1j} is $\mu_{\tilde{A}_1^1}(x_{1j})$ AND x_{2j} is $\mu_{\tilde{A}_2^2}(x_{2j})$ THEN $F_2 = P_2$
3. IF x_{1j} is $\mu_{\tilde{A}_2^1}(x_{1j})$ AND x_{2j} is $\mu_{\tilde{A}_2^1}(x_{2j})$ THEN $F_3 = P_3$
4. IF x_{1j} is $\mu_{\tilde{A}_1^2}(x_{1j})$ AND x_{2j} is $\mu_{\tilde{A}_2^2}(x_{2j})$ THEN $F_4 = P_4$

where P_k (k = 1 to 4) is the parameter of the constant function in the consequent part of the k^{th} fuzzy if-the rule. The number of function parameters is reduced to $2^2(=4)$ for the zero-order Takagi-Sugeno fuzzy inference system from $2^2(2+1)(=12)$ for the first-order Takagi-Sugeno fuzzy inference system. In general, a zero-order Takagi-Sugeno type fuzzy inference system with n predictor maps and 2n fuzzy membership functions contains 2^n fuzzy if-then rules and 2^n function parameters. The firing strengths s_i (i = 1 to 4) of the above fuzzy if-then rules are calculated using prod t-norm operator as follows:

$$\begin{aligned} s_1 &= \mu_{\tilde{A}_1^1}(x_{1j}) \, x \, \mu_{\tilde{A}_2^1}(x_{2j}) \\ s_2 &= \mu_{\tilde{A}_1^1}(x_{1j}) \, x \, \mu_{\tilde{A}_2^2}(x_{2j}) \\ s_3 &= \mu_{\tilde{A}_1^2}(x_{1j}) \, x \, \mu_{\tilde{A}_2^1}(x_{2j}) \\ s_4 &= \mu_{\tilde{A}_2^1}(x_{1j}) \, x \, \mu_{\tilde{A}_2^2}(x_{2j}) \end{aligned} \tag{5.7}$$

As a matter of fact, other t-norm operators that perform generalized AND can also be used for combining the fuzzy membership values in order to determine the firing strengths of the fuzzy if-then rules. The output, O_k, of the k^{th} (k = 1 to 4) fuzzy if-then rule is:

$$O_k = s_k . F_k \tag{5.8}$$

where F_k *(k = 1 to 4)* is the value of the function in the consequent part of the k^{th} fuzzy if-then rule. The overall output of the fuzzy inference system is the weighted average of the output of all the four fuzzy if-then rules:

$$\textit{Overall output} = \frac{\sum_{k=1}^{4} O_k}{\sum_{k=1}^{4} s_k} \tag{5.9}$$

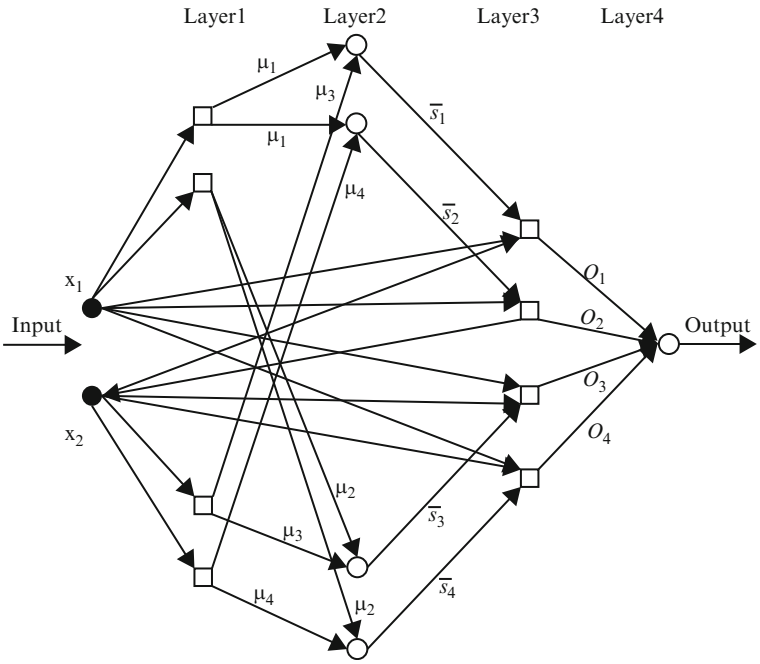


Fig. 5.2 Simplified ANFIS for mineral potential mapping. *Square* and *circular nodes* contain, respectively, adaptive and fixed functions

The overall output is a measure of combined favorability of the feature vector T with respect to a target mineral deposit-type. The above procedure can be easily extended for estimating the favorability of a feature vector comprising more than two predictor maps. In a simple Takagi-Sugeno type fuzzy inference system, the parameters of fuzzy membership functions and consequent polynomial functions are estimated heuristically. However, in a hybrid neuro-fuzzy model, an ANFIS is used for estimating these parameters.

The basic architecture of an ANFIS comprises a Takagi-Sugeno type fuzzy inference system in a five-layer feed-forward network. Figure 5.2 shows the simplified four-layer ANFIS architecture used in a hybrid neuro fuzzy model for mineral potential mapping. The basic functionality of each layer is summarized in the following paragraphs.

5.1.3.1 Layer 1

There are 2n (= the number of fuzzy sets defined in the superset X) nodes in this layer. One half of the nodes (= n) contain the adaptive Gaussian fuzzy membership function defined in Eq. 5.3, each of which receives one component (a predictor pattern x_{ij} encoded as a class score cs_{ij}) of an incoming n-dimensional feature vector and returns its membership value in the fuzzy set $\tilde{A}_i^1$ (i = 1 to n) containing 'favorable indicators of

target mineral deposit type'. The other half of the nodes (= n) contain the adaptive Gaussian fuzzy membership function, each of which also receives one component of the incoming feature vector and returns its membership value in the fuzzy set $\tilde{A}_i^2$ (i = 1 to n) containing 'unfavorable indicators of target mineral deposit-type'.

The parameters c and σ, which control the shape of a node function, and therefore output fuzzy membership values, are referred to as premise parameters.

5.1.3.2 Layer 2

Each of the 2^n (= the number of fuzzy if-then rules) nodes in this layer contains a prod t-norm operator as a node function, which synthesizes information transmitted by Layer 1 and returns a firing strength for each of the fuzzy if-then rules:

$$s_k = \mu_{\tilde{A}_1^q}(x_{1j}) \;\; x \;\; \mu_{\tilde{A}_2^q}(x_{2j}) \;\; x.....x \;\; \mu_{\tilde{A}_n^q}(x_{nj}) \tag{5.10}$$

where q = 1 or 2, depending on whether $\mu_{\tilde{A}_1^q}$ defines fuzzy membership value of x_{ij} in the fuzzy set $\tilde{A}_i^1$ or in the fuzzy set $\tilde{A}_i^2$ (i = 1 to n). The output of each node is the normalized firing strength $\overline{s}_k$ (k = 1 to 2^n) of the k^{th} fuzzy if-then rule given by:

$$\overline{s}_k = \frac{s_k}{\sum_{k=1}^{2^n} s_k} \tag{5.11}$$

5.1.3.3 Layer 3

Each of the 2^n (= the number of fuzzy if-then rules) nodes in this layer, contains the following adaptive function:

$$O_k = s_k.F_k = s_k\left(P_{k0} + P_{k1}x_{1j} + P_{k2}x_{2j} + ... + P_{kn}x_{nj}\right) \tag{5.12}$$

where O_k is the output of the k^{th} fuzzy if-then rule. The parameters P_{ki} (k = 1 to 2^n, i = 0 to n) are referred to as consequent parameters. In the case of a zero-order Takagi-Sugeno type fuzzy inference system, $F_k = P_{k0}$.

5.1.3.4 Layer 4

The single node in this layer synthesizes information transmitted by Layer 3 and returns the overall output using the following fixed function:

$$Overall\ Output \;=\; \sum_{k=1}^{2^n} O_k \tag{5.13}$$

The following description of the hybrid learning procedure is drawn from Jang and Sun.

Forward Pass: Least Square Estimator Method

For 2^n fuzzy if-then rules and Q n-dimensional training vectors (where n is the number of input predictor maps), Eq. 5.13 can be expressed as:

$$B = AX \tag{5.14}$$

where B is a column vector containing output values of training vectors, A is matrix containing one row for each training vector and X is an unknown vector whose elements are the consequent parameters P_{ki}. As the number of consequent parameters is $2^n(n+1)(=M$, say), the dimensions of A, X and B are $Q \times M$, $M \times 1$ and $Q \times 1$, respectively.

A least square estimate of X, denoted by X*, can be used to minimize squared error $\|AX - B\|^2$. It can be computed as below:

$$X^* = \left(A^T A\right)^{-1} A^T B \tag{5.15}$$

where A^T is the transpose of A and $(A^T A)^{-1} A^T$ is the pseudo-inverse of A, if $A^T A$ is non-singular. The above equation is expensive in computation when dealing with matrix inversion and, more over, becomes ill defined if $A^T A$ is singular. ANFIS uses a recursive least-square method for estimating X *as follows*.

If a_q^T is the q^{th} row vector of A and b_q^T is the qth element of B, then X can be calculated iteratively as follows:

$$X_{q+1} = X_q + \sum\nolimits_{q+1} a_{q+1} \left(b_{q+1}^T - a_{q+1}^T X_q\right) \tag{5.16}$$

$$\sum\nolimits_{q+1} = \sum\nolimits_q - \frac{\sum\nolimits_q a_{q+1} a_{q+1}^T \sum\nolimits_q}{1 + a_{q+1}^T \sum\nolimits_q a_{q+1}} \left(for\ q = 0, 1, \ldots\ldots\ldots.., Q-1\right) \tag{5.17}$$

where $\sum$ is called covariance matrix and the least square estimate X^* is equal to X_q. The initial conditions are $X_0 = 0$ and $\sum 0 = \gamma I$, where γ is a large positive number and I is an identity matrix of $M \times M$ dimensions.

Backward Pass: Back-Propagation Method

Premise parameters of ANFIS are estimated iteratively by using a modified back-propagation learning rule along with the chain rule as follows. In Eq. 5.14, if the estimated output of the qth row vector, a_q, of the matrix A is o_q and the actual output is b_q, the qth element of B, then an error margin for the q^{th} training vector a_q can be defined as:

$$E_q = \left(b_q - o_q\right)^2 \tag{5.18}$$

If E_q is zero, then the actual output exactly matches the estimated output. Thus, the objective is to minimize an overall error measure, which is defined as $\sum_{q=1}^{Q} E_q$, where Q is the total number of training vectors. In order to use the gradient descent method to minimize the error measure, a gradient vector is required to be calculated. It should be noted that a small change in the premise parameters (c or σ) will affect the output of the node containing the parameters, which, in turn, will affect the output of the single node in Layer 4 and, hence, the error measure will also change. Therefore in order to calculate the gradient vector of the parameters, a form of derivative information has to be passed, starting from Layer 4 and traveling back to Layer 1.

An error signal, $\varepsilon_{l,i}$, can be defined as the ordered derivative of the error measure E_q with respect to the output of node i in Layer l (l = 1 to 4) as follows

$$\varepsilon_{l,i} = \frac{\partial + E_q}{\partial o_{l,i}} \tag{5.19}$$

where $o_{l,i}$ is the output of the i^{th} node of Layer l. The error signal for the single output node of Layer 4 can be calculated as:

$$\varepsilon_4 = \frac{\partial + E_p}{\partial o_{(4,1)}} = \frac{\partial E_p}{\partial o_{(4,1)}} = -2\left(b_q - o_q\right) \tag{5.20}$$

For the i^{th} node of Layer $l(l = 1$ to $3)$, the error signal can be derived using the chain rule:

$$\varepsilon_{l,i} = \frac{\partial + E}{\partial o_{(l,i)}} = \sum_{m=1}^{N_{(l+1)}} \frac{\partial + E}{\partial o_{(l+1,m)}} \frac{\partial f_{(l+1,m)}}{\partial o_{(l,i)}} = \sum_{m=1}^{N_{(l+1)}} \varepsilon_{(l+1,m)} \frac{\partial f_{(l+1,m)}}{\partial o_{(l,i)}} \tag{5.21}$$

where $N_{(l+1)}$ is the number of nodes in Layer $(l+1)$, $o_{(l+1,m)}$ is the output of the m^{th} node in Layer $(l+1)$, $f_{(l+1,m)}$ is the nodal function of the m^{th} node in Layer $(l+1)$, $o_{(l,i)}$ is the output of the i^{th} node in Layer l and ε(l + 1,m) is the error signal at the mth node of Layer (l + 1). In other words, the error signal of an internal node at Layer l can be expressed as a linear combination of the error signal of the nodes at Layer (l + 1). Therefore, for the ith node of Layer 1, the error signal, ε (1,i), can be obtained by first applying Eq. 5.20 once to get error signals at the Layer 4 and then applying Eq. 5.21 iteratively until Layer 1 is reached.

Because the consequent parameters are fixed in the backward pass, the gradient vector is defined as the derivative of the error measure with respect to each of the two premise parameters, c and ε, which reside in the nodes of Layer 1. The chain rule is applied to determine the gradient vectors as follows:

$$\frac{\partial^+ E_p}{\partial c_i} = \frac{\partial^+ E_p}{\partial o_{(1,i)}} \frac{\partial^+ \mu_{1,i}}{\partial c_i} = \varepsilon_{(1,i)} \frac{\partial^+ \mu_{(1,i)}}{\partial c_i} \tag{5.22}$$

and

$$\frac{\partial^+ E_p}{\partial \sigma_i} = \frac{\partial^+ E_p}{\partial o_{(1,i)}} \frac{\partial^+ \mu_{1,i}}{\partial \sigma_i} = \varepsilon_{(1,i)} \frac{\partial^+ \mu_{(1,i)}}{\partial \sigma_i} \tag{5.23}$$

In the above equations c_i and σ_i are, respectively, center and spread of the gaussian membership function $\mu_{(1,i)}$ in the i^{th} node of layer 1.

The derivative of the overall error measure E with respect to c_i is:

$$\frac{\partial^+ E}{\partial c_i} = \sum_{q=1}^{Q} \frac{\partial^+ E_q}{\partial c_i} = \sum_{q=1}^{Q} \varepsilon_{(1,i)} \frac{\partial^+ \mu_{(1,i)}}{\partial c_i} \tag{5.24}$$

where Q is the total number of training vectors. The update expression for the parameter c_i is given by:

$$\Delta c_i = -\eta \frac{\partial^+ E}{\partial c_i} \tag{5.25}$$

where η is the learning rate, which can be expressed as follows:

$$\eta = \frac{\kappa}{\sqrt{\sum_{i=1}^{N(1)} \left(\frac{\partial E}{\partial c}\right)^2}} \tag{5.26}$$

where $N(1)$ is the total number of nodes in Layer 1 and κ is the step size or the length of each transition along the gradient direction in the parameter space. Similarly, the derivative of the overall error measure E with respect to σ_i is:

$$\frac{\partial^+ E}{\partial \sigma_i} = \sum_{q=1}^{Q} \frac{\partial^+ E_q}{\partial \sigma_i} = \sum_{q=1}^{Q} \varepsilon_{(1,i)} \frac{\partial^+ \mu_{(1,i)}}{\partial \sigma_i} \tag{5.27}$$

where Q is the total number of training vectors. The update expression for the parameter σ_i is given by:

$$\Delta \sigma_i = -\eta \frac{\partial^+ E}{\partial \sigma_i} \tag{5.28}$$

where η is the learning rate, which can be expressed as follows:

$$\eta = \frac{\kappa}{\sqrt{\sum_{i=1}^{N(1)} \left(\frac{\partial E}{\partial \sigma}\right)^2}} \tag{5.29}$$

where $N(1)$ is the total number of nodes in Layer 1 and κ is the step size or the length of each transition along the gradient direction in the parameter space.

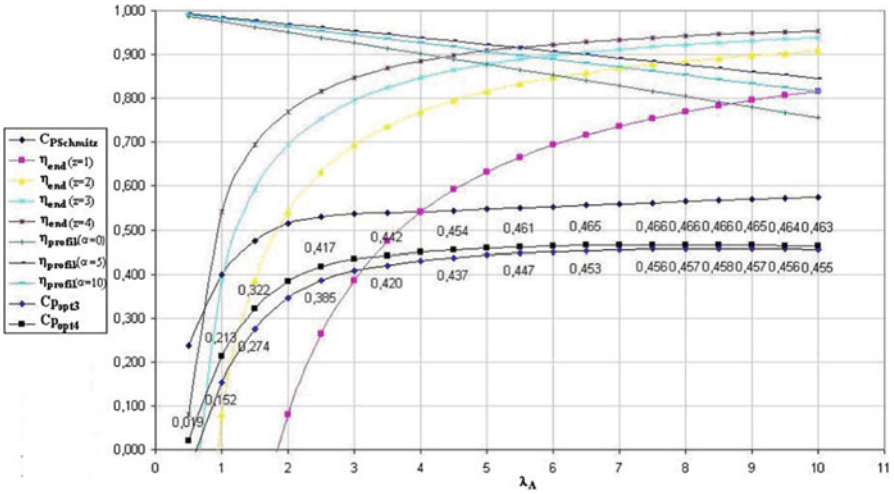


Fig. 5.3 Plot of the values of the profile type NACA 4415

5.1.4 Description of Profile Types

The experimental procedure based on ANN and ANFIS for optimum power factor prediction for three-blade and four-blade turbines. To carry out the analysis, the profile types such as LS-1 and NACA 4415 are considered. The properties of these profiles are presented Figs. 5.3 and 5.4. The input parameters are taken according to the Eq. 5.6 without considering the eddy losses. The blade number losses are not directly taken as an input parameter but considered during the preparation of training data.

5.1.5 Design of the ANN

The design process for estimating power factor using the ANN includes the following steps:

(i) Preparation of suitable training data.
(ii) Selection of a suitable ANN structure.
(iii) Training of the ANN.
(iv) Evaluation of the trained network.

The design process in ANN is an iterative procedure. If the user is not satisfied with the results, the selection of the ANN structure can be changed according to problem and then the network has to be retrained. Sometimes even a trained network may fail while testing the network. Even in such situations, the network structure should be changed and network is retrained and tested.

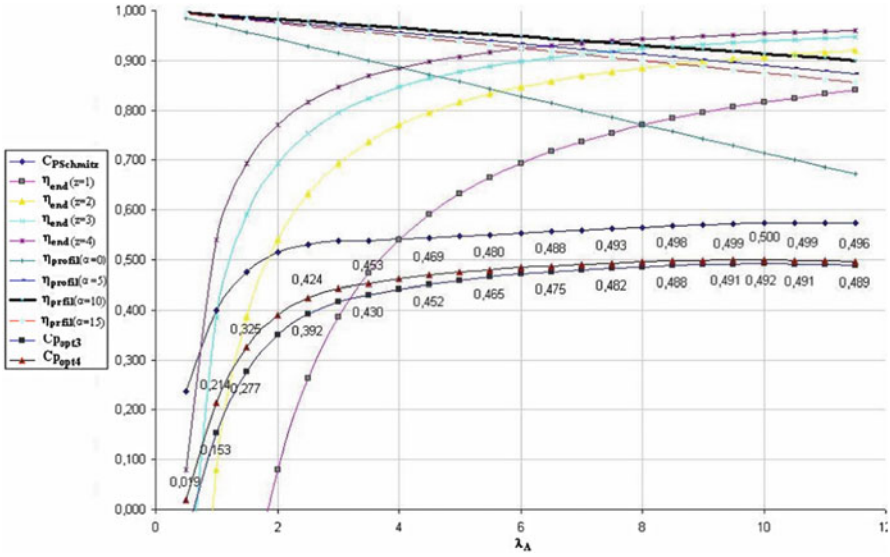


Fig. 5.4 Plot of the values of the profile type LS-1

The training patterns presented to the ANN structure should contain all the necessary information to generalize the problem. After collecting all the required data, normalization of data is mandatory, and this is usually done in the range [0,1]. Normalisation is done for both training and testing data. The testing data is usually chosen as a random percentage of the training sample.

The choice of type of neural network depends upon the number of layers, type of transfer function, number of nodes in the input, hidden and output layer. Based on previous research on neural networks, it is observed that a three-layer feed-forward network can model complex-mapping functions reasonably well and, therefore, is adopted for power factor prediction for the above mentioned profile types. The arbitrary shaped functions requires sigmoid non-linear mapping for modeling. The number of neurons in the input layer and hidden layers are decided by experimentation which involves training and testing different network configurations.

Training of the selected network is done using the training patterns and back propagation algorithm. Training is stopped when the mean squared error between actual outputs and desired outputs stops improving. However, at that point, if the designer is not satisfied with the training and performance of the ANN, the training data and structure of the ANN are modified and the design process is repeated.

5.1.6 ANFIS for Prediction of Power Factor

While implementing the ANFIS model in MATLAB, the basic parameters such as the number of inputs; the number of membership functions (MFs) and their type/shape; and the number of training epochs are to be defined. A small change

in any one of these parameters, can affect the system's operation thus leading to inefficient results. The major advantages of ANFIS are:

- ANFIS uses the neural network's ability to classify data and find patterns.
- A fuzzy expert system is more transparent to the user and also less likely to produce memorization errors than a neural network.
- ANFIS maintains the advantages of a fuzzy expert system, thus reducing the need for an expert.

In general, ANFIS requires a large amount of training data to develop an accurate system. In complex data analysis, fuzzy logic reduces the difficulty in modeling and behaves like a human in including the aspects in terms of its mapping rules. Likewise, ANNs are also more popular in identifying models of complex systems. Thus, ANNs and FL are combined, referred to as ANFIS, to take advantage of the learning capabilities of ANNs and modeling superiority of FL.

The model is designed to predict the power factor of wind turbines according to the following steps:

(i) the input and output data were divided into two groups for training and testing;
(ii) a fuzzy model was created using the ANFIS editor and data training was carried out;
(iii) the test data were utilized for the validation of the model.

A hybrid ANFIS algorithm based on the Sugeno system improved by Jang is used for acquiring optimal output data in the experiment. The algorithm consists of the least-squares method and the back-propagation algorithm. The first method was used for optimizing the consequent parameters, while the second method in relation to fuzzy sets was employed to arrange the premise parameters. The input parameters in the application are

– type of profile
– Schmitz coefficient
– end losses
– profile type losses based on the type of profile

The output parameter is the power factor. The experiment was conducted for two different profile types namely, LS-1 and NACA4415. The training and testing data used for ANFIS model were formed from the characteristic values shown in Figs. 5.3 and 5.4 for the two profile types considered. The membership function of the model outputs was selected to be Gaussian (gaussmf). A separate data set, not included in the training set, was employed for verifying the ANFIS model generalization capabilities.

5.1.7 Estimation of the Optimal Power Factor

The ANN and ANFIS approaches are applied to profile types, LS-1 and NACA4415. The number of input neurons was chosen as seven inputs and the input variables are described according to

$$x(t) = A, \lambda_A, C_{pschmitz}, \eta_{end}, \eta_{profile}, \eta_{eddy}, \eta_{blade\ number}, \tag{5.30}$$

where A is an integer number representing the type of profile, 1 for LS-1 and 2 for NACA4415; λ_A is the tip speed ratio, $C_{pschmitz}$ is the Schmitz coefficient mentioned previously; η_{end} represents the end losses for 3 and 4 blade turbines. $\eta_{profile}$ is the profile type losses for the type of profiles considered, LS-1 and NACA4415. On the other hand, the output variables take the form:

$$y(t) = \left[C_{popt3}, C_{popt4}\right], \tag{5.31}$$

where C_{popt3}, C_{popt4} are the power factors for the wind turbines with 3 and 4 blades. The appropriate ANN structure, back propagation is chosen and the network is formed by presenting the inputs to the network. The network is then trained to verify of the structure is efficient in producing the output variables from the given inputs. From the chosen profile, for all input and output variables 30 training samples were formed from the characteristic values given in Figs. 5.3 and 5.4.

The observations of the ANFIS and ANN methods in terms of power factors are presented in Tables 5.1 and 5.2. The performance of the network is satisfactory with

Table 5.1 Comparison of power factor obtained by ANFIS and conventional method

	ANFIS		Conventional method			
Test no	C_{popt3}	C_{popt4}	C_{popt3}	C_{popt4}	Error (%)	
1	0.4530	0.4650	0.4528	0.4646	−0.04	−0.08
2	0.4576	0.4665	0.4576	0.4665	0.00	0.00
3	0.4550	0.4630	0.4553	0.4627	−0.06	−0.06
4	0.3515	0.3893	0.3510	0.3900	−0.14	0.17
5	0.4520	0.4690	0.4520	0.4690	0.00	0.00
6	0.4641	0.4800	0.4650	0.4800	0.19	0.00
7	0.4895	0.4970	0.4890	0.4960	0.01	−0.20
8	0.3695	0.3896	0.3700	0.3890	0.13	−0.15
9	0.3309	0.3381	0.3320	0.3390	0.33	0.26

Table 5.2 Comparison of power factor obtained by ANN and conventional method

	By ANN		By CM			
Test no	Cp_{opt3}	Cp_{opt4}	Cp_{opt3}	Cp_{opt4}	Error (%)	
1	0.4531	0.4664	0.4528	0.4646	−0.06	−0.38
2	0.4576	0.4676	0.4576	0.4665	0.00	−0.23
3	0.4566	0.4649	0.4553	0.4627	−0.28	−0.47
4	0.3525	0.3888	0.3510	0.3900	−0.42	0.30
5	0.4505	0.4702	0.4520	0.4690	0.33	−0.25
6	0.4637	0.4808	0.4650	0.4800	0.27	−0.16
7	0.4890	0.4991	0.4890	0.4960	0.00	−0.62
8	0.3689	0.3916	0.3700	0.3890	0.29	−0.66
9	0.3298	0.3374	0.3320	0.3390	0.66	0.47

small deviation from the values obtained from the curves given in Figs. 5.3 and 5.4. The conventional values are also presented for computation of the percentage of error.

Therefore, it can be stated that the presented methodology provides more detailed values in an attempt to obtain the optimal power factor wind turbines rather than using the small number of data obtained from the curves whose derivations require rather complicated process. The results indicate that both ANN and ANFIS models can give good predictions of the power factor. However, the ANFIS model performs better than ANN model.

5.2 Pitch Angle Control

Generally, wind turbines are capable of operating with either fixed speed or variable speed. The variable-speed wind turbines involving pitch adjustment have become more dominant during the recent years. The reasons for the increase in choice of variable speed wind turbines during the recent years are the reduction of both the mechanical structure stresses and acoustic stresses, and the possibility to control active and reactive power. In fact, variable speed operation increases the energetic efficiency and reduces the drive train torque and the energy of generating flow unsteadiness. Thus pitch angle control is necessary when the rotational speed is kept constant. Very small changes in the pitch angle can lead to a massive change on the output power. Pitch angle control is expressed as:

1. Optimization of power output: Below rated wind speed, the pitch setting should be at its optimum value to give maximum power.
2. Prevention of input mechanical power from exceeding design limits: Above rated wind speed, pitch angle control provides a very effective means of regulating the aerodynamic power and loads produced by the rotor.
3. Minimizing fatigue loads of the turbine mechanical component.

While designing the pitch angle controller, the effect on loads must be considered and the controller should ensure that excessive loads will not result from the control action. For explicit design of the controller with the objective of reducing the effect of soft-computing methodologies, such as artificial intelligence and genetic algorithms are proving to be more effective during recent years. In this section, conventional pitch angle control strategy, using the proportional and integral (PI) controller is discussed. In addition, fuzzy logic and genetic algorithms are applied for pitch angle control since these intelligent algorithms do not need a well known system and are potential for the system with strong non-linearity.

5.2.1 Problem Definition

The power in the wind is proportional to the cube of the wind speed and may be expressed as

$$P = 0.5\rho A\nu_w^3 \tag{5.32}$$

where ρ is air density, A is the area swept by blades and ν_w is wind speed. A wind turbine can only extract part of the power from the wind, which is limited by the Betz limit (maximum 59 %). This fraction is described by the power coefficient of the turbine, Cp, which is a function of the blade pitch angle and the tip speed ratio. Therefore the mechanical power of the wind turbine extracted from the wind is

$$P_w = 0.5C_p(\beta, \lambda)\rho A\nu_w^3 \tag{5.33}$$

where Cp is the power coefficient of the wind turbine, β is the blade pitch angle and λ is the tip speed ratio. The tip speed ratio is defined as the ratio between the blade tip speed and the wind speed

$$\lambda = \frac{\Omega R}{\nu_w} \tag{5.34}$$

where Ω is the turbine rotor speed and R is the radius of the wind turbine blade.

Thus any change in the rotor speed or the wind speed induces change in the tip speed ratio leading to power coefficient variation. In this way, the generated power is affected.

5.2.2 Fuzzy Logic Controllers

The ability to model the fuzzy, or imprecise, membership of an element to a set enables inference based on linguistic terms. Production rules governing a fuzzy controller can be described using words or simple sentences in natural language as opposed to formal predicate calculus statements. This enables a domain expert, who typically would not have an advanced knowledge of first-order predicate logic, to describe the rules that govern a given system using domain specific linguistic terms, which may be better understood. Figure 5.5 outlines a simple architecture for a fuzzy controller consisting of three primary components. First, the condition interface, which is responsible for converting outputs from the system into a fuzzy form, hence the term fuzzifier, utilized by the fuzzy inference engine. Next, the engine performs inference, based on linguistic rules, to determine an appropriate control action. Finally, the action interface is responsible for interpreting the output of the inferencing process and converting it back into system specific actions

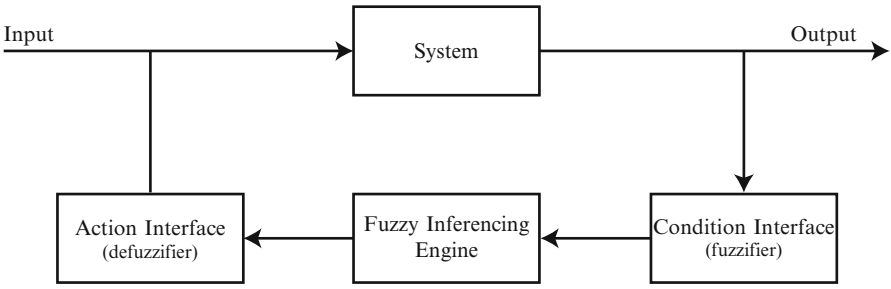


Fig. 5.5 Fuzzy controller architecture

through a process known as defuzzification. Thus, a feedback loop is realized where the controller constantly monitors the system while effecting control actions on the system according to its rule base.

After fuzzifying the inputs, the next step is to perform inferencing using the fuzzy rule base. Typically, the rule base is made up of a list of rules of the form:

$$if\ antecedent \rightarrow consequent \tag{5.35}$$

where the *antecedent* consists of one or more fuzzy sets combined using the operators to form a logical expression. In the case of a Mamdani controller, the *consequent* consists of a single target fuzzy set. The value of the antecedent, also known as the firing strength of the rule, determines the degree of membership to the target set in the *consequent*.

5.2.3 Genetic Algorithms

Genetic Algorithms (GAs) are adaptive heuristic search algorithm premised on the evolutionary ideas of natural selection and genetic. The basic concept of GAs is designed to simulate processes in natural system necessary for evolution, specifically those that follow the principles first laid down by Charles Darwin of survival of the fittest. As such they represent an intelligent exploitation of a random search within a defined search space to solve a problem. First pioneered by John Holland in 1960s, Genetic Algorithms has been widely studied, experimented and applied in many fields in engineering worlds. Not only does GAs provide alternative methods to solving problem, it consistently outperforms other traditional methods in most of the problems link. Many of the real world problems involved finding optimal parameters, which might prove difficult for traditional methods but ideal for GAs. However, because of its outstanding performance in optimization, GAs has been wrongly regarded as a function optimizer. In fact, there are many ways to view genetic algorithms. Perhaps most users come to GAs looking for a problem solver, but this is a restrictive view.

GAs are used as problem solvers, as challenging technical puzzle, as basis for competent machine learning, as computational model of innovation and creativity, as computational model of other innovating systems and for guiding philosophy.

GAs were introduced as a computational analogy of adaptive systems. They are modeled loosely on the principles of the evolution via natural selection, employing a population of individuals that undergo selection in the presence of variation-inducing operators such as mutation and recombination (crossover). A fitness function is used to evaluate individuals, and reproductive success varies with fitness.

5.2.3.1 The Algorithms

1. Randomly generate an initial population.
2. Compute and save the fitness for each individual in the current population.
3. Define selection probabilities for each individual in so that is proportional to the fitness.
4. Generate the next population by probabilistically selecting individuals from current population to produce offspring via genetic operators.
5. Repeat step 2 until satisfying solution is obtained.

The paradigm of GAs described above is usually the one applied to solving most of the problems presented to GAs. Though it might not find the best solution. more often than not, it would come up with a partially optimal solution.

5.2.4 Conventional Pitch Angle Control

Under strong wind speeds, the performance of the wind turbine can be regulated by adjusting the pitch angle of the blades. During normal operation, the expected blade pitch adjustments are rotational speeds of approximately 5–10 %. Here the chosen pitch rate is 8°/s which avoids excessive loads during normal regulation procedures. The conventional blade pitch angle control strategies are shown in Fig. 5.6. The pitch angle reference, β_{ref}, is controlled by the input values, such as the wind speed, generator rotor speed and the generator power described as follows:

1. Wind speed (Refer Fig. 5.6a). In general the pitch angle reference can be obtained by plotting a curve between pitch angle and wind speed. This type of pitch angle control strategy is simple since the wind speed is measured directly. This method does not measure the wind speed directly and hence it is not an appropriate procedure.
2. Generator rotor speed (Refer Fig. 5.6b). The difference between the rotor speed and reference is determined. The error signal is then sent to the PI controller and produces the reference value of the pitch angle, β_{ref}.
3. Generator power (Refer Fig. 5.6c). The error signal of the generator power is sent to a PI controller. The PI controller produces the reference pitch angle β_{ref}.

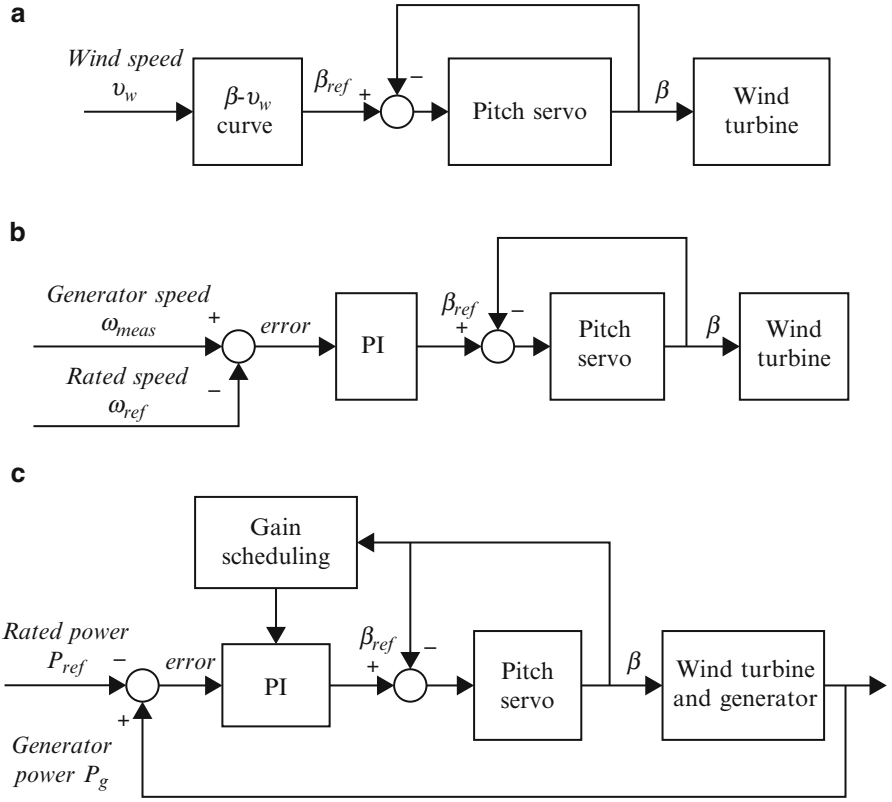


Fig. 5.6 Pitch angle control strategy. (**a**) Wind speed; (**b**) generator rotor speed; (**c**) generator power

The variation of the pitch angle and wind speed during large wind speeds is non-linear in fashion and hence requires a non-linear control strategy. For a wind speed close to the rated speed, the sensitivity of aerodynamic torque to pitch angle is very small. Hence a larger controller gain is required. A very small change in pitch can have a large effect on torque. Frequently the torque sensitivity changes almost linearly with pitch angle, and so can be compensated by varying the overall gain of the controller linearly in inverse proportion to the pitch angle. This process of modifying the gain with operating point is termed as gain scheduling. This type of conventional pitch angle control strategy with gain scheduling is best suitable when the system dynamic is not strong. On the other hand, the sensitivity of aerodynamic torque to pitch angle varies in a different way which is treated as linear variation in gain scheduling, and because of its effect on turbine dynamics which couples strongly with the pitch controller, it may be necessary to modify the gain scheduling further to ensure good performance.

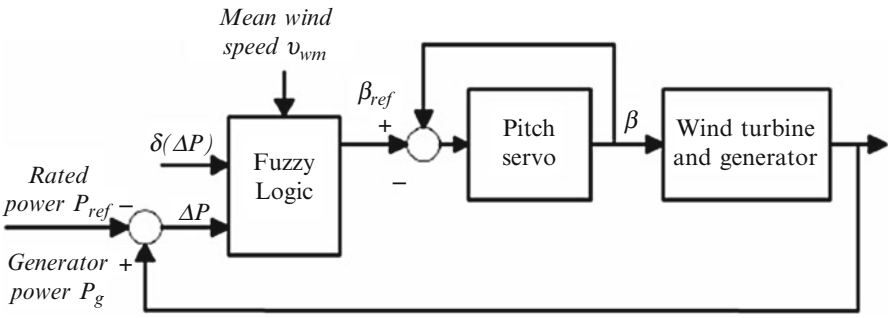


Fig. 5.7 Fuzzy logic control strategy

5.2.5 *Fuzzy Logic for Pitch Control*

The major steps in designing a pitch control strategy based on fuzzy logic consists of determining the inputs, setting up the rules and designing a method to convert the fuzzy result of the rules into output signal, known as defuzzification. The fuzzy logic controller for pitch control should be modeled in order to reduce the fatigue loads. The model for pitch angle control based on fuzzy logic system is shown in Fig. 5.7. For both input and output triangular symmetrical membership functions are more suitable, since they are capable of providing more sensitivity especially as variables approach to zero value. The width of variation can be adjusted according to the system parameters.

As shown in Fig. 5.7, the proposed fuzzy logic controller is based on the power deviation from its reference value ΔP, its variation during a sampled time $\delta(\Delta P)$ as follows:

$$\begin{cases} \Delta P = P_{ref} - P_g \\ \delta(\Delta P) = \Delta P_n - \Delta P_{n-1} \end{cases} \tag{5.36}$$

where *Pref* is the rated power of the system and *Pg* is the measured generator power. The mean wind speed ν_{wm}, used as the third input variable, is useful to compensate the non-linear sensitivity of pitch angle to the wind speed. Table 5.3 lists the control rules for the input and output variable. In the proposed fuzzy system, nine fuzzy sets have been considered for variables: negative large (NL), negative medium large (NML), negative medium (NM), negative small (NS), zero (ZE), positive small (PS), positive medium (PM), positive medium large (PML), positive large (PL). At lower mean wind speed, the low sensitive of the pitch angle control means that a large reaction of pitch angle to the control variants will be needed than at higher mean wind speed.

Table 5.3 Rules of fuzzy logic controller

υ_m	PS					PM					PL				
ΔP	NL	NS	ZE	PS	PL	NL	NS	ZE	PS	PL	NL	NS	ZE	PS	PL
δΔP															
NL	NL	NML	NM	NM	PS	NL	NM	NM	NS	PS	NML	NM	NS	NS	PS
NS	NL	NM	NS	PS	PM	NML	NM	NS	PS	PM	NML	NM	NS	ZE	PS
ZE	NML	NS	ZE	PS	PML	NM	NS	ZE	PS	PM	NM	NS	ZE	PS	PM
PS	NM	NS	PS	PM	PL	NM	NS	PS	PM	PML	NS	ZE	PS	PM	PML
PL	NS	PM	PM	PML	PL	NS	PS	PM	PM	PL	NS	PS	PS	PM	PML

The fuzzy rule base is defined based on Table 5.3. An immediate and easy understanding of the controller logic can be obtained as following considerations:

1. If ΔP and $\delta(\Delta P)$ are negative large, the output power angle is too large and its amplitude is growing, consequently current pitch angle must be fast decreased.
2. If ΔP is negative large and $\delta(\Delta P)$ is positive large, the output power is higher than its reference, but since its amplitude is decreasing, pitch angle variation must be small.
3. If ΔP is small pitch angle variation must be smoothed because too large variations excite oscillatory modes.

5.2.6 *Genetic Algorithm Controller for Pitch Angle Control*

Genetic algorithms (GA) are commonly used as optimization techniques, thus providing high quality solutions. In this section, the GAs are used as controllers rather than optimizers. The proposed Genetic algorithm controller approach can be better explained by considering the turbine power curves shown in Fig. 5.8.

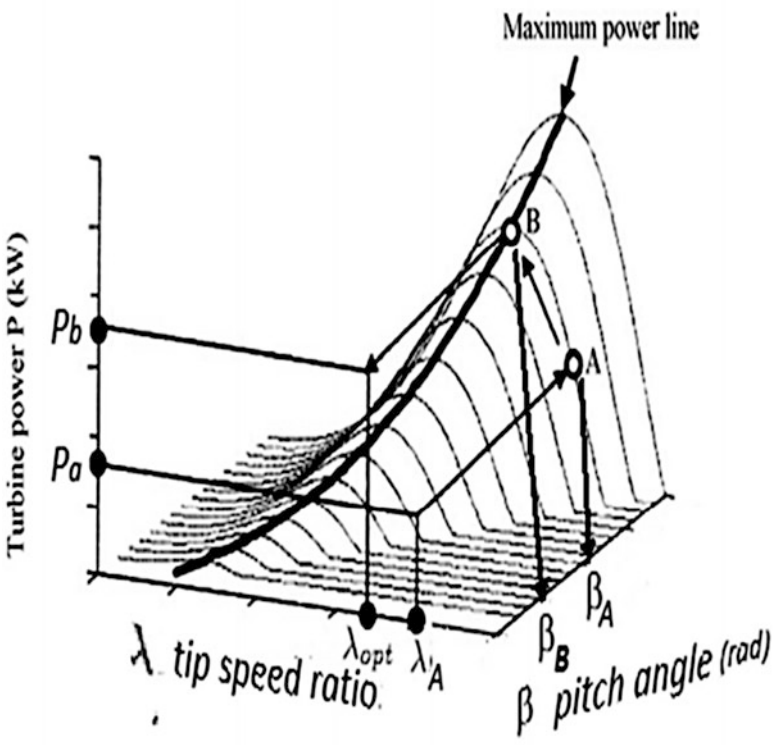


Fig. 5.8 Turbine power curves

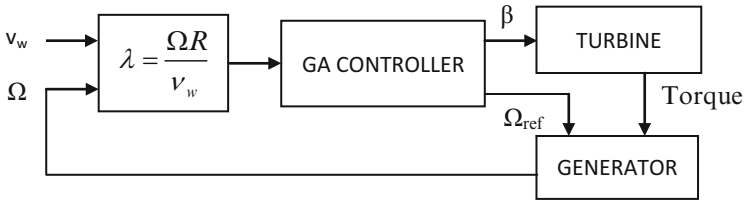


Fig. 5.9 Genetic algorithm based pitch control

Assuming that the wind turbine operates initially at point A, the fuzzy control system from measured speed ratio $\lambda_A = \frac{\Omega_A R}{v_w}$ and β_A pitch angle, turbine power P_w can derive the corresponding optimum operating point B, giving the desired rotor speed reference $\lambda_B = \frac{\Omega_B R}{v_w}$ and send a control signal for new β_B. The GA based pitch control strategy is shown in Fig. 5.9. Therefore, the generator speed will be controlled in order to reach the speed Ω_A and β allowing the extraction of the maximum power from the turbine.

Pitch angle control is the most common means to control the aerodynamic power generated by the wind turbine rotor. Pitch angle control also has an effect on the aerodynamic loads which may be controlled by the controller to achieve lower torque peak as well as lower fatigue loads. The conventional pitch angle control strategy using different controlling variables can be implemented. However, fuzzy logic and genetic algorithm pitch angle control strategy need not well know about the wind turbine dynamics and these algorithms are more suitable when wind turbine contains strong non-linearities. The soft computing techniques can results in lowest fatigue loads and lower torque peak and lower power peak. The pitch angle of the fuzzy logic controller is less active than conventional pitch angle control with power or wind speed controlling variable, which causes less dynamic torque.

5.3 MPPT for WECS

MPPT controllers are used for extracting maximum power from the WECS using different generators such as permanent magnet synchronous generators (PMSG), squirrel cage induction generators (SCIG) and doubly fed induction generator (DFIG). The MPPT controllers can be classified into three main control methods, namely tip speed ratio (TSR) control, power signal feedback (PSF) control and hill-climb search (HCS) control. The energy produced from wind source depends upon the accuracy with which the peak power points are tracked by the MPPT controller of the WECS control system irrespective of the type of generator used. Based on the control schemes, the maximum power extraction algorithms are tip speed ratio (TSR) control, power signal feedback (PSF) control and hill-climb search (HCS) control.

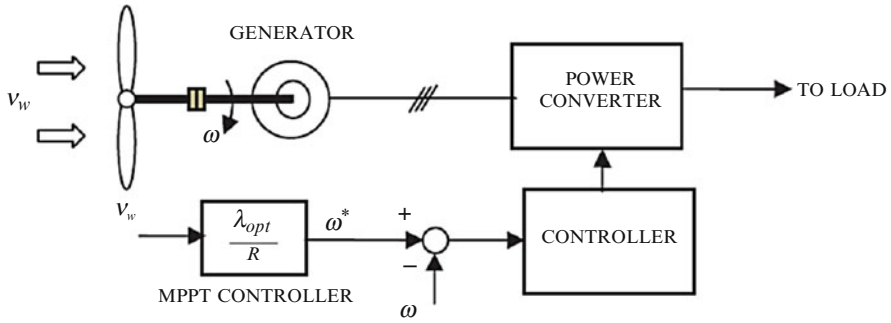


Fig. 5.10 Tip speed ratio control of WECS

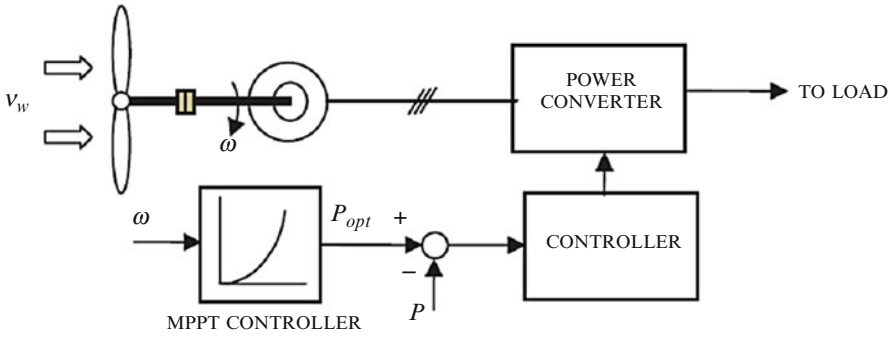


Fig. 5.11 Power signal feedback control

In the TSR control method, the rotational speed of the generator is regulated in order to maintain the tip speed ratio to an optimum value during which the power extracted attains the maximum. In this method in order to obtain the maximum output power, the speed from both wind and the turbine are required along with the optimal value of the TSR of the turbine. The block diagram of a WECS with TSR control is shown in Fig. 5.10.

In PSF control, it is required to have the knowledge of the wind turbine's maximum power curve, and track this curve through its control mechanisms. The maximum power curves need to be obtained via simulations or off-line experiment on individual wind turbines. In this method, reference power is generated either using a recorded maximum power curve or using the mechanical power equation of the wind turbine where wind speed or the rotor speed is used as the input. Figure 5.11 shows the block diagram of a WECS with PSF controller for maximum power extraction.

The HCS control algorithm continuously searches for the peak power of the wind turbine. It can overcome some of the common problems normally associated with the other two methods. The tracking algorithm, depending upon the location of the operating point and relation between the changes in power and speed, computes

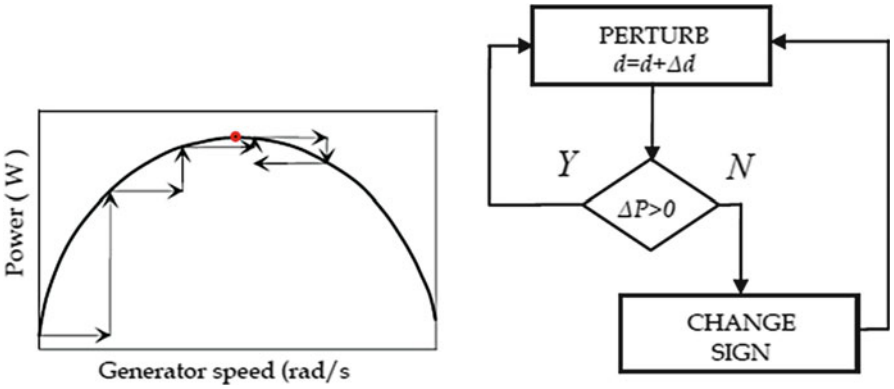


Fig. 5.12 HCS control principle

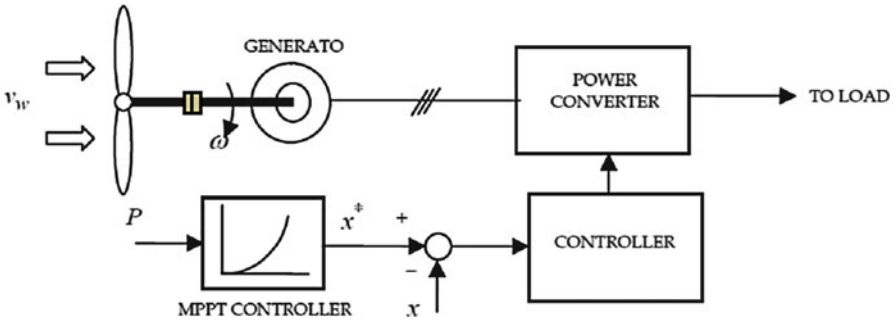


Fig. 5.13 WECS with hill climb search control

the desired optimum signal in order to drive the system to the point of maximum power. Figure 5.12 shows the principle of HCS control and Fig. 5.13 shows a WECS with HCS controller for tracking maximum power points.

5.3.1 Fuzzy Logic Based MPPT Controller

Though the implementation of the traditional hill climb search algorithm is simple and independent of turbine characteristics, the selection of step size is a very important concern. MPP values can be tracked with a large step size at a faster rate, but leads to severe oscillations around the maximum power point. A small value of step size is capable of decreasing the oscillations around the MPP to a much minimum value, but the MPPT process slows down during varying wind speeds. Thus fuzzy logic control algorithms with variable step size are used recently for tracking the MPP effectively and smoothly.

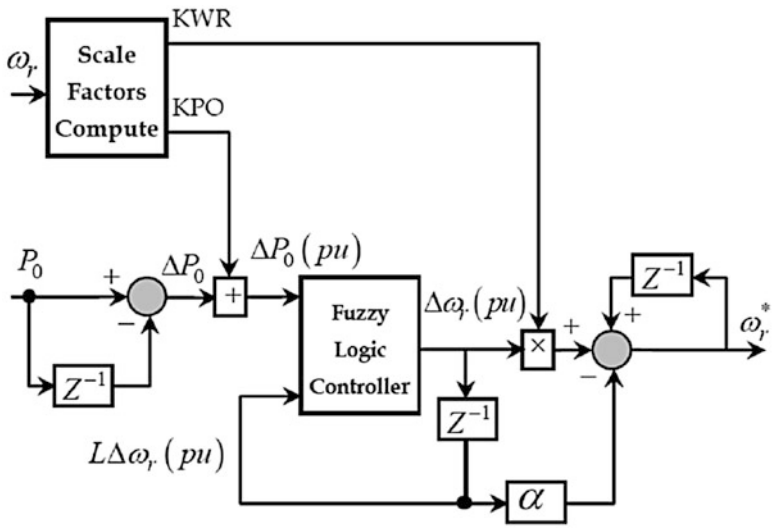


Fig. 5.14 Block diagram of fuzzy logic MPPT controller

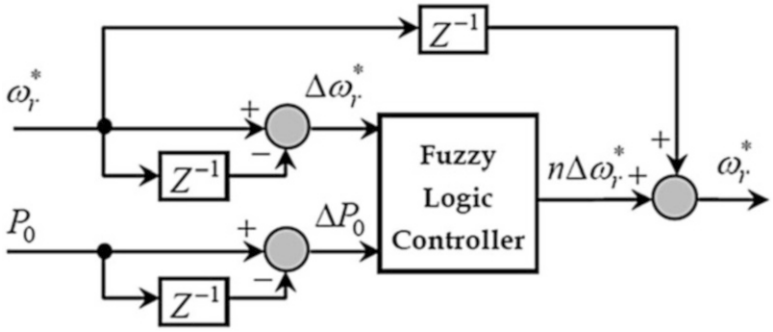


Fig. 5.15 Fuzzy MPPT controller

The fuzzy logic controller is used in MPPT to perturb the generator reference speed and to estimate the corresponding change of output power *P0*. The decision process is based on the output power. The searching process continues in the same direction, if the output power increases with the last increment. Vice versa, if the output power reduces with the last increment, then the direction of search is reversed. The block diagram of the fuzzy logic controller is shown in Fig. 5.14. The fuzzy logic controller is efficient to track the maximum power point, especially in case of frequently changing wind conditions. Two inputs $\Delta\omega_r^*$, Δw_{ref} and ΔP_0 in Fig. 5.15 are used as the control input signals and the output of the controller is the new speed reference speed which, after adding with previous speed command, forms the present reference speed.

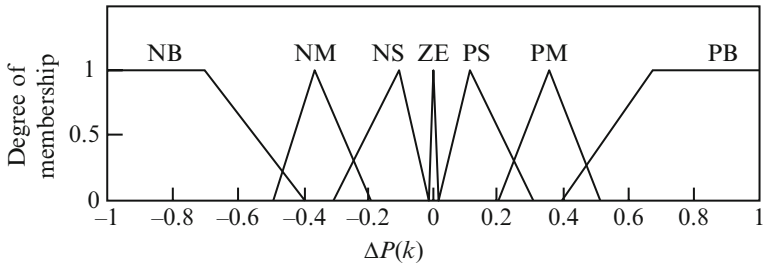


Fig. 5.16 Member functions of input variables $\Delta P(k)$

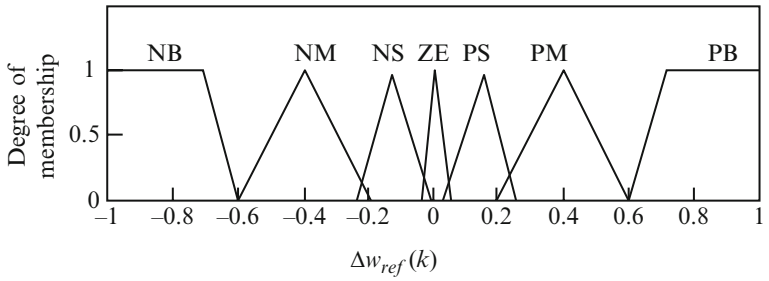


Fig. 5.17 Member functions of output variable $\Delta w_{ref}(k)$

The membership functions corresponding to the input variable ΔP(k) for the implemented FLC is defined as follows (Figs. 5.16 and 5.17): PB (positive big), PM (positive medium), PS (positive small), ZE (zero), NS (negative small), NM (negative medium), and NB (negative big), respectively; the member functions corresponding to the input variable Δw(k) are P (positive), Z (zero), and N (negative), respectively.

The member functions of output variable $\Delta w_{ref}(k)$, are PB, PM, PS, ZE, NS, NM, NB, respectively almost similar to that of the input variable. The following equations define the relationship between turbine mechanical power and turbine rotational speed depending on the $P - w$ curve.

$$dP/dw > 0, \ (w < w_{mpp})$$
$$dP/dw = 0, \ (w = w_{mpp})$$
$$dP/dw < 0, \ (w > w_{mpp})$$

where w_{mpp} denotes the turbine rotational speed corresponding to the MPP value. The fuzzy rule base is formed based on properties of wind turbine, as shown in Table 5.4. The reference rotational speed is updated according to $w_{ref}(k) = w(k-1) + \Delta w(k)$. Thus the FLC is capable of changing the step size dynamically based on the wind speed, thus enabling the turbine to track the MPP efficiently.

Table 5.4 Rules for the fuzzy logical controller

	$\Delta P(k)$						
$\Delta w(k)$	NB	NM	NS	ZE	PS	PM	PB
N	PB	PM	PS	NS	NS	NM	NB
Z	NM	NS	NS	ZE	PS	PS	PM
P	NB	NM	NS	PS	PS	PM	PB

5.4 Economic Dispatch for Wind Power System

The increased rate of power consumption has lead to development of alternate energy source. Several renewable energy sources are responsible for today's electric network. The characteristics of these energy resources are based on operational costs and reliability. In this section, Economic Environmental Dispatching (EED) of power system including wind energy is discussed based on evolutionary algorithms. Renewable energy resources depend on the data of the climate such as the wind speed for wind energy, solar radiation and the temperature for solar thermal energy. The problem focuses on minimizing the cost and reducing of the emissions of the polluting gases.

In traditional power systems, power can be dispatched economically using static and dynamic methods. The static optimal dispatch only seeks to achieve an optimal objective for the power system at a specific time, but will not take into account of the intrinsic link between system at different time moments; while the dynamic optimal dispatch takes into account of the coupling effect of system at different time moments, such as the limit on the climbing rate of a generator. Thus the computation process is more complex in the dynamic dispatch while the computation results are more in line with actual requirements.

Moreover, economic dispatch of power systems containing wind power farms adopts dynamic models due to the random changes in wind speed. In addition, dynamic economic dispatch requires the knowledge of output data of the wind power farm at every moment in the optimal duration. Thus artificial intelligent methods have been developed to minimize the error of predicting output for a wind power farm, thus reducing the difficulty for economic dispatch. In this section, techniques such as Quantum Genetic Algorithm (QGA) and Strength Pareto Evolutionary Algorithm (SPEA) are adopted to solve the problem.

5.4.1 Mathematical Model of Economic Dispatch for Power System Based on Wind Energy

The wind power consumed from nature has to dispatched immediately, since there is no fuel consumption in wind power systems. The economic dispatch of power

systems containing wind energy is to minimize the cost of generating power using a traditional power generator group. The objective function is defined as:

$$Min\ F_T = \min \sum_{t=1}^{T} \sum_{i=1}^{N} F_{it}(P_{Git}) + F_{cp} \tag{5.37}$$

where F_T is the total cost for generating power; T is the number of hours in the research period; N is the total number of conventional generators within the system; P_{Git} is the output of active power for the i^{th} generator at time t; $F_{it}(P_{Git})$ is the corresponding cost of consumption and is usually expressed using the following polynomial equation:

$$F_i(P_{Gi}) = a_i + b_i P_{Gi} + ciP_{Gi}^2 \tag{5.38}$$

where a_i, b_i, and c_i are the coefficients for the cost function $F_{it}(P_{Git})$, F_{cp} is the environmental cost function. In considering the emission characteristics of thermal generating unit in the economic dispatch model of electricity market, the environmental cost of thermal generating units is added on top of the cost of generating electricity for these units. This added cost:

$$F_{cp} = \sum_{i=1}^{n} M_{cpi} \times f_{di} \tag{5.39}$$

where M_{cpi} is the environmental cost coefficient, f_{di} is the emission amount of the ith thermal generating unit, n is the number of thermal generating units in the system. From the point of view of environmental protection, the emission characteristics for each unit can be represented by emission per unit time converting to the weight of the amount of NOx discharged. The emission equation:

$$f_{di} = \alpha_i + \beta_i P_{Gi} + \gamma_i P_{Gi}^2 + \delta_i \times \exp(\theta_i \times P_{Gi}) \tag{5.40}$$

where $\alpha_i, \beta_i, \gamma_i, \delta_i$ *and* θ_i are the emission characteristics coefficients for the i^{th} thermal generating unit, which can be measured.

5.4.1.1 Constraints

Power conservation constraint is given as

$$\sum_{i=1}^{N} P_{Git} + \sum_{j=1}^{N_w} P_{Gjt}^{w} = P_{Dt} + P_L \tag{5.41}$$

where N_w is the total number of wind power plants in the system; P_{Gjt}^{w} is the output of active power for the jth wind power plant at time t; P_{Dt} is the load at time t.

$$P_L = \sum_{i=1}^{N_G}\sum_{j=1}^{N_G} P_{Gi}B_{ij}P_{Gj} + \sum_{i=1}^{N_G} B_{0i}P_{Gi} + B_{00} \tag{5.42}$$

where P_L is the line loss, B_{ij}, B_{0i} and B_{00} are the loss parameters also known as the B parameters.

Operation constraints are given by

$$P_{Git}^{\min} \leq P_{Git} \leq P_{Git}^{\max} \tag{5.43}$$

where $P_{Git}^{\min}$ and $P_{Git}^{\max}$ are the minimum and maximum generator limits corresponding to the i^{th} unit.

5.4.2 Quantum Genetic Algorithm (QGA) for Economic Dispatch of Wind Power System

QGA embeds the concept of quantum bit and quantum superposition state into traditional genetic algorithm to form Quantum genetic algorithm. The chromosomes are encoded using quantum bits and quantum chromosomes are generated using quantum encoding. The quantum probability amplitude implies that a quantum chromosome carries information about multiple states, a chromosome will be in a quantum superposition state of many determined states before an observation is made on it. Therefore, generating a new object through the quantum probability amplitude, the deciding variable, in a sense, is no longer fixed information; rather, it has become a kind of information carrying a superposition of different information. Thus it can bring a richer population than the simplistic application of genetic method. In addition, mutations can be induced with the information of current best individual object so that the population will evolve toward a good schema with high probability to speed up the convergence and, at the same time, prevent it from being trapped in a local optimal solution effectively and prevent the premature phenomenon from occurring.

5.4.2.1 Step 1: Initialize Population

Quantum Bit The smallest information unit in QGA is a quantum bit. The state of a quantum bit can be either 0 or 1, which can be represented as:

$$|\psi\rangle = \alpha|0\rangle + \beta|1\rangle \tag{5.44}$$

where α, β, represent two complex numbers representing the probability of occurrence for the corresponding state: $\left(|\alpha|^2 + |\beta|^2\right) = 1$, $|\alpha|^2 and\ |\beta|^2$ represent the probability of the quantum bit in the state of 0 and 1 respectively.

Quantum Chromosome Frequently used coding methods in EA are binary, decimal, and symbolic coding. In QGA, a new coding method based on quantum bit is adopted, i.e. using a pair of complex numbers to define a quantum bit. A system with m quantum bits can be described as

$$\left[\begin{array}{c|c|c|c} \alpha_1 & \alpha_2 & \ldots & \alpha_m \\ \beta_1 & \beta_2 & \ldots & \beta_m \end{array}\right] \tag{5.45}$$

This representation method can be used to express any linear superposition of states.

5.4.2.2 Step 2: Perform Coding and Individual Measurement for the Generating Units in the Population

QGA is a probabilistic algorithm similar to EA. The algorithm flowchart is shown in Fig. 5.18. $H(t) = \left\{Q_1^t, Q_2^t, \ldots Q_h^t, \ldots Q_l^t\right\}$, (h = 1, 2,. . ., l) where h is the size of the population, $Q_l(t) = \left\{q_1^t, q_2^t, \ldots q_j^t, \ldots q_n^t\right\}$, where n is the number of generator unit, t is the evolution generation, q_j^t is the binary coding of the generation volume of the jth generator unit. Its chromosome is defined as follows:

$$q_j^t = \left[\begin{array}{c|c|c|c} \alpha_1^t & \alpha_2^t & \ldots & \alpha_m^t \\ \beta_1^t & \beta_2^t & \ldots & \beta_m^t \end{array}\right] \tag{5.46}$$

For (j = 1, 2,. . ., n) (m is the length of the quantum chromosome).

During the "initialization of H(t)," if α_i^t, β_i^t (i = 1, 2,. . ., m) in $Q_l(t)$ and all the q_j^t are initialized, it means that all the possible linear superposition states will occur with the same probability. During the step of "generating S(t) from H(t)", a common solution set S(t) is generated by observing the state of H(t), where in the t^{th} generation, $S(t) = \left\{P_1^t, P_2^t, \ldots P_h^t, \ldots P_l^t\right\}, P_l = \left\{x_1^t, x_2^t, \ldots x_j^t, \ldots x_n^t\right\}$, every x_j^t (j = 1, 2,. . ., n) is a series, (x_1, x_2,. . ., x_i. . ., x_m), of length m, which are obtained from the amplitude of quantum bit $|\alpha_i^t|^2$ or $|\beta_i^t|^2$, (i = 1, 2,. . ., m). The corresponding process in the binary situation is to generate a [0, 1] number randomly. Take "1" if it is larger than $|\alpha_i^t|^2$ take "0" otherwise.

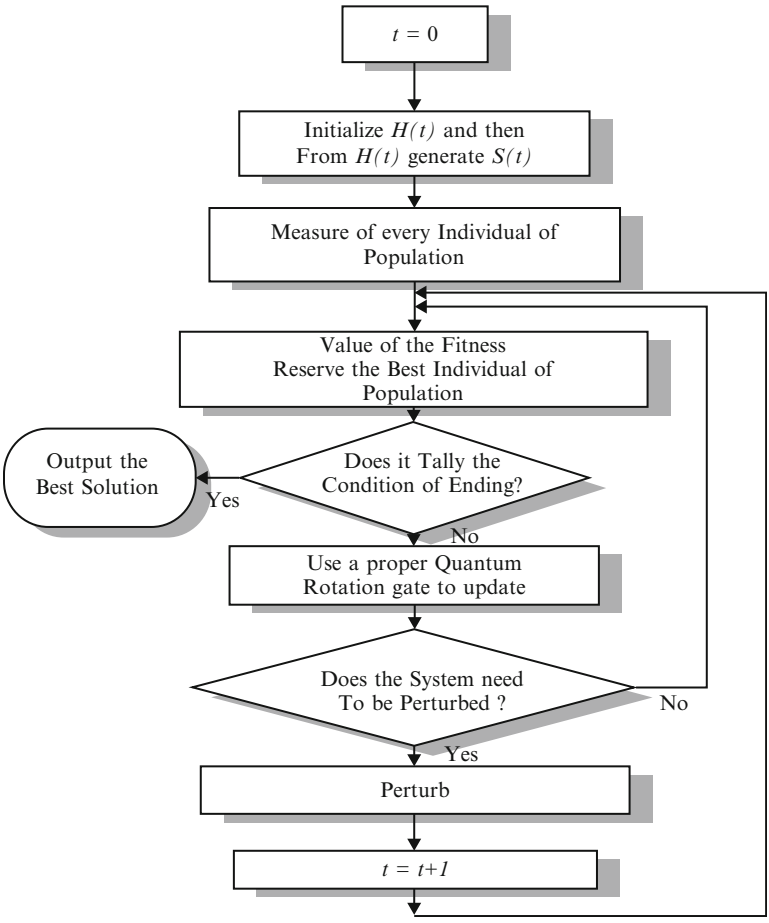


Fig. 5.18 Flowchart of QGA

5.4.2.3 Step 3: Perform Individual Measurement to Each Object in S(t)

Use a fitness evaluation function to evaluate each individual object in S(t) and keep the best object in the generation. If a satisfactory solution is obtained, stop the algorithm; otherwise, continue to the fourth step.

5.4.2.4 Step 4: Use a Proper Quantum Rotation gate U(t) to Update S(t)

The traditional genetic algorithm uses mating, mutation, etc. operations to maintain the diversity of the population. Quantum genetic algorithm applies logic gate to the probability amplitude of quantum state to maintain the diversity of the population. Therefore, the update method using a quantum gate is the key to the quantum

genetic algorithm. In the traditional genetic algorithm, binary system, adaptation values, and probability amplitude comparison method are used for update using a quantum gate. This update method using a quantum gate is suitable to find solutions for combinatorial optimization problems with known optimal solution in principle. However, for the actual optimization problems, in particular, those multi-variable continuous function optimization problems, their optimal solutions are not known beforehand in principle. Therefore, here a quantum rotation gate of quantum logic gate is adopted for the new quantum genetic algorithm.

$$U = \begin{bmatrix} \cos\theta & \sin\theta \\ \sin\theta & \cos\theta \end{bmatrix} \tag{5.47}$$

where θ is the quantum gate rotation angle. Its value is taken as,

$$\theta = k.f(\alpha_i, \beta_i) \tag{5.48}$$

$$k = \pi.\exp\left(-\frac{t}{iter_{\max}}\right) \tag{5.49}$$

We define k as a variable related to the generation of the evolution so that it will adjust the size of the grid self-adaptively. Where t is the evolution generation, p is an angle, $\text{iter}_{\max}$ is a constant depending on the complexity of the optimization problem. The purpose of the function $f(\alpha_i, \beta_i)$ is to make the algorithm search along the optimal direction. Its principle is to make the current search solution approach the optimal solution gradually and thereby, determine the direction of the quantum rotation gate. In this way, the procedure for applying quantum rotation gate to all probability amplitude for individual object in the population, i.e. using quantum rotation gate U(t) to update S(t), in quantum genetic algorithm can be expressed as:

$$S(t+1) = U(t) \times S(t) \tag{5.50}$$

In the above equation: t is the evolution generation, U(t) is the t^{th} generation quantum rotation gate, S(t) is the t^{th} generation probability amplitude of a certain object, S(t + 1) is the $(t + 1)^{th}$ generation probability amplitude of the corresponding object.

5.4.2.5 Step 5: Perturbation

In order to solve the QGA problem being prone to be trapped in local extreme value better, we perturb the population. It is found that by using the QGA analysis that when the best individual of the current generation is a local extreme value, it is very hard for the algorithm to extricate itself. Therefore, when the best individual does not change in successive generations, the algorithm is trapped in the local extreme. At this point of time, a perturbation should be applied to the population to extricate itself out of the local optimal and start a new search.

5.4.3 Strength Pareto Evolutionary Algorithm (SPEA) Approach

Zitzler and Thiele developed an elitist evolutionary approach to solve a multi objective problem called Strength Pareto Evolutionary Algorithm (SPEA). The elitism in SPEA is introduced by an external Pareto set. The external set stores the non-dominant solutions funded during the resolution of the problem. In order to reduce the size of the external set, an average linkage based on hierarchical clustering algorithm is used without destroying the characteristics of the trade-off front.

The notations are denoted as:

P: the current population.
P_t: the external population.
N_{pop}: the size of current population.
F_i the fitness of an individual i.
S_i the strength of an individual i.

The assignment procedure to calculate the fitness values is the following:

Step 1: For each individual $i \epsilon P_t$ is assigned a reel value $S_i \epsilon (0, 1)$ called strength. S_i is proportional to the number of individuals in the current population dominated by the individual i in the external Pareto set. It can be calculated as follows:

For an individual $j \epsilon P_t$

$$S_i = \frac{|\{j/j \in P_t \ \ and \ \ individual \ \ j \ \ is \ \ dominated \ \ by \ \ i\}|}{N_{pop} + 1} \tag{5.51}$$

The strength of a Pareto solution is also its fitness: $F_i = S_i$

Step 2: The fitness of an individual $j \epsilon P_t$ is the sum of the strengths of all external Pareto individuals $i \epsilon P_t$ dominated by $j \epsilon P_t$. We add one in odder to guarantee that Pareto solutions are most likely to be produced.

$$F_j = 1 + \sum_{i \in P_t, i \ \ dominate \ \ j} S_i \tag{5.52}$$

where $F_j \epsilon (1, N_{pop})$

The clustering algorithm is described by the following steps:

Step 1: To initialise clustering set C; each individual $i \epsilon P_t$ constitutes a distinct cluster:

$$C = Y_{i \in P_t}\{i\} \tag{5.53}$$

Step 2: If the number of cluster is lower or equal to maximum size of external set (N_{pop}), go to step 5. Else, go to step 3.

Step 3: Calculate the distance between each pair of clusters. The distance d_c between two clusters c_1 and $c_2 \epsilon\, C$ is defined as the average distance between two pairs of individuals from each cluster:

$$d_c = \frac{1}{n_1 n_2} \sum_{i_1 \in c_1,\, i_2 \in c_2} d_{i_1, i_2} \tag{5.54}$$

n_1 and n_2 are respectively the numbers of individuals in clusters c_1 and c_2.

Step 4: Find the pair of clusters corresponding to the minimal distance d_c between them and return to step 2.

Step 5: Find the centroid of each cluster. Select the nearest individual in this cluster to the centroid as a representative individual and remove all other individuals from the cluster.

Step 6: Thus, the reduced Pareto set P_{t+1} is computed by uniting these representatives:

$$P_{t+1} = Y_{c \in C} c. \tag{5.55}$$

In this section, a method allowing the resolution of the problem of the Environmental Economic Dispatching of an electrical network including wind energy based on QGA and SPEA was discussed. The optimization was performed without auxiliary elements to extract the maximum of power from the random wind energy and to distribute the remainder of the power on the power stations.

5.5 SEIG Driven by WECS

Various research work and case studies were investigated in self-excited induction generators (SEIG) since 1935. SEIG have been commonly applied due to the basic advantages such as lower maintenance costs, better transient performance, lack of a DC power supply for field excitation, and brushless construction (squirrel-cage rotor), etc. In general, induction generators have been commonly used to operate as wind-turbine generators and small hydroelectric generators of isolated power systems since they can be easily connected to large power systems, to inject electric power.

The generator action takes place, when the rotor speed of the induction generator is greater than the synchronous-speed of the air-gap-revolving field. This section concentrates on the dynamic performance of an isolated SEIG, driven by wind

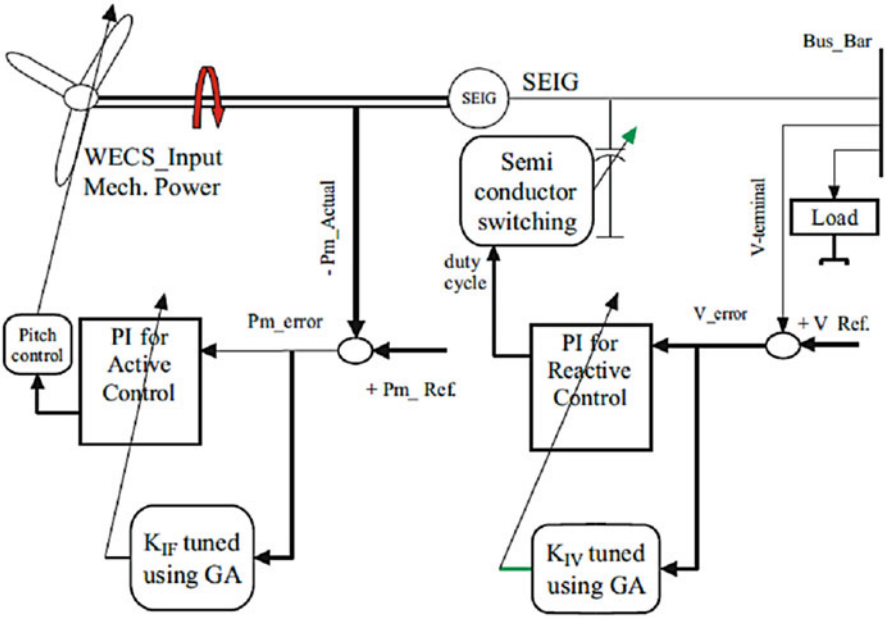


Fig. 5.19 SEIG driven by WECS

energy, to supply an isolated static load. A D-Q axis equivalent circuit model based on various reference frames, extracted from fundamental machine theory, is created to study SEIG performance in dynamic case. The performance of the SEIG, when equipped with a switching capacitor bank is discussed with a controller based on Genetic Algorithm (GA). GA is used to adjust the duty cycle and the stator frequency via the pitch control.

5.5.1 Mathematical Model for SEIG Driven by WECS

The *d-q* axis equivalent-circuit model without any load for a three-phase symmetrical induction generator is presented in Fig. 5.19. The stator and rotor voltage equations are derived based on Krause transformation, with a stationary reference frame.

5.5.1.1 Reactive Power Control and Switching Capacitor Bank Technique

Switching

During the past decades, the switching of capacitors has been neglected due to the practical difficulties such as the occurrence of voltage and current transients.

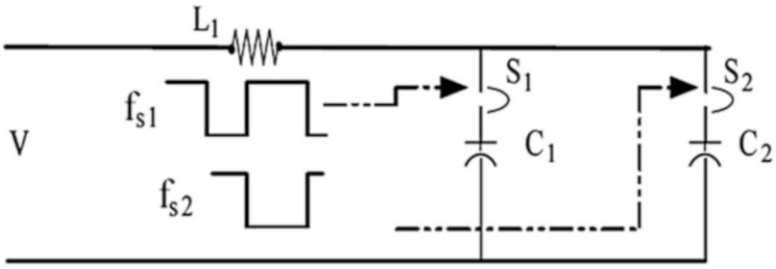


Fig. 5.20 Semi conductor switches (S1, S2) circuit for capacitor bank

Discussions in the literature prove that current 'spikes', would inevitably exceed the maximum current rating as well as the (di/dt) value of a particular semiconductor switch. To overcome this drawback, a semiconductor switch is designed to withstand the transient value at the switching instant. The equivalent circuit in Fig. 5.20 shows the application of switching capacitor bank due to duty cycle. In this circuit, the operation of the switches are in anti-phase, i.e., the switching function fs2 which controls switch S2 is the inverse function of fs1 which controls switch S1. In simple terms, switch S2 is closed when switch S1 is open and vice versa.

Reactive Power Control

The error in voltage is taken as the input to the controller and the output is the duty cycle (λ). The computed λ is applied as an input to the semiconductor switches to change the value of the capacitor bank. The input is applied based on the requirement of the excitation. The terminal voltage in turn is controlled by adjusting the self-excitation through automatic switching of the capacitor bank.

Active Power Control

Active power control is applied by adjusting the pitch angle of the wind turbine blades. Such control strategy is used to maintain the constant and steady operation of SEIG thus reducing the effect of the speed annoyance. The pitch angle is usually a function of the power coefficient "Cp" of the wind turbine WECS. The best optimal value of pitch angle leads to improved mechanical power regulation, which, in turn, achieves a better frequency adaptation of the overall system. Thus the active power control regulates the mechanical power of the wind turbine.

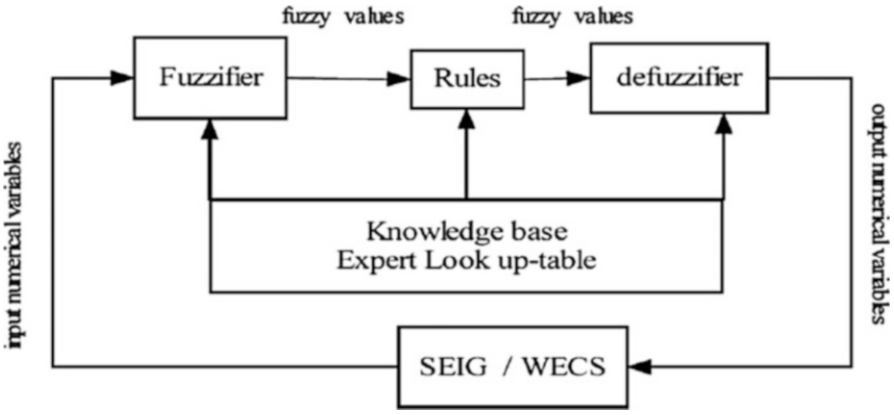


Fig. 5.21 FLC with SEIG driven WECS

5.5.2 Controllers

With SEIGs in this section, two different types of controller strategies have been discussed. The application of GA and FLC controllers are used to adjust the value of KI for both active and reactive controllers.

5.5.3 Fuzzy Logic Controller

With the information on artificial decision making in a closed loop environment, a fuzzy logic controller is designed using knowledge base. Figure 5.21 shows the basic construction of the FLC. The FLC is designed using input fuzzy sets, fuzzy rules and output fuzzy sets. The relation between the input and output variables are governed by a set of rules. The rules are formed based on prior knowledge base of the system. Each parameter in the input and output variable set has a corresponding membership function. The better adaptation of fuzzy set parameters leads to fine tuning of the fuzzy output. The FLC is used to compute and adapt the variable integral gain KI of PI controller.

The fuzzy input vector corresponding to reactive control consists of two variable; the terminal voltage deviation eV and the change of the terminal voltage deviation ΔeV. Table 5.5 shows the linguistic variables formed for both the inputs. The membership functions for voltage deviation and change in voltage deviation are shown in Figs. 5.22 and 5.23 respectively. Similarly, mechanical power deviation eF and the change of the mechanical power deviation ΔeF are chosen as the fuzzy inputs and five linguistic variables are defined. While, the output variable fuzzy set is shown in Fig. 5.24 and Fig. 5.25 shows the fuzzy surface. The linguistic variables are defined as follows: for example PB is Positive Big and NS is Negative

Table 5.5 Look up table

	Voltage deviation change (Δe_v)				
Voltage deviation (e_v)	NB	NS	AV	PS	PB
NB	NB	NB	NB	NS	AV
NS	NB	NB	NS	AV	PS
AV	NB	NS	AV	PS	PB
PS	NS	AV	PS	PB	PB
PB	AV	PS	PB	PB	PB

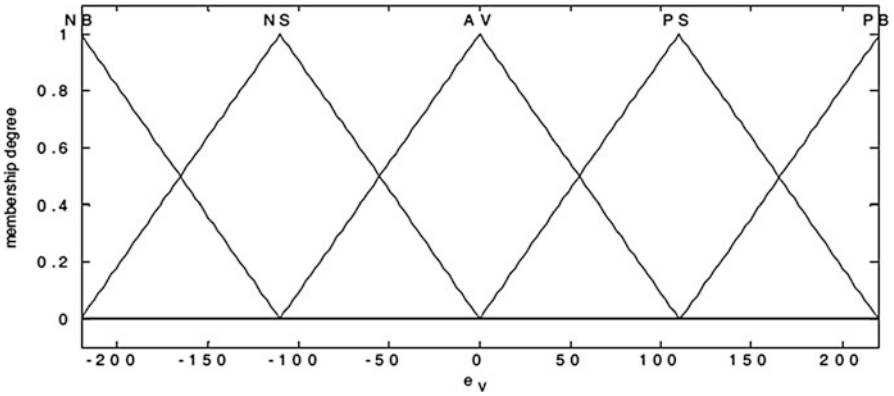


Fig. 5.22 Membership function of voltage error e_v

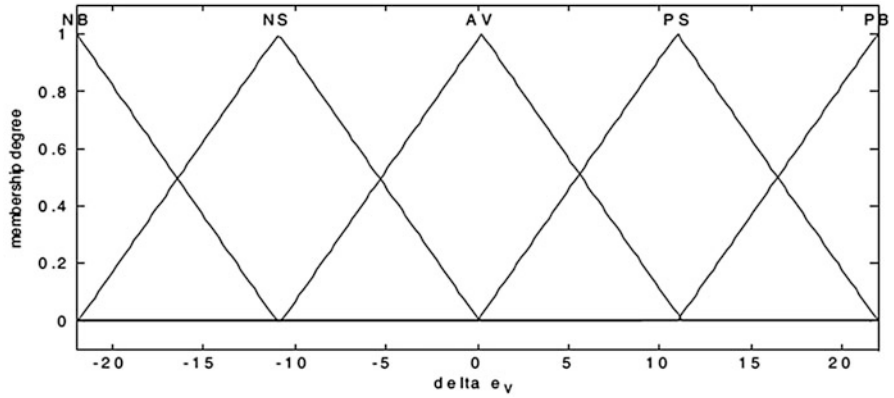


Fig. 5.23 Membership function of change in voltage error e_v

Small . . ..etc. Once the linguistic variables for the input and output variables are defined, the set of rules are developed, also known as the look-up table (Table 5.5). The rule base states the relation between the input variables, eV, eF, ΔeV and ΔeF and the output variable of the fuzzy logic controller. The integral gain value KI is the output of the fuzzy controller further applied in the PI controller.

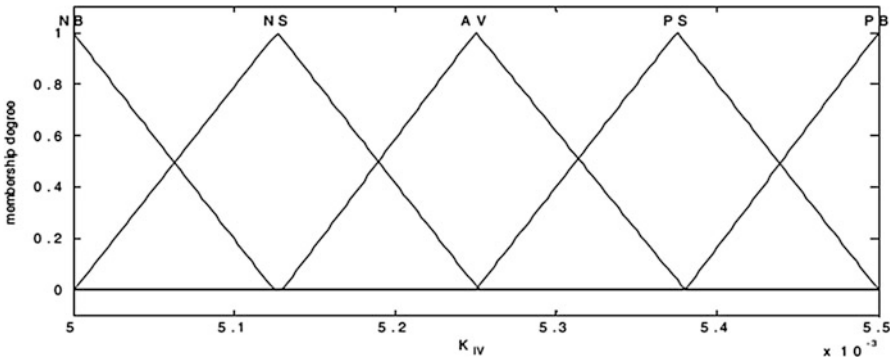


Fig. 5.24 Membership function of variable K_{IV}

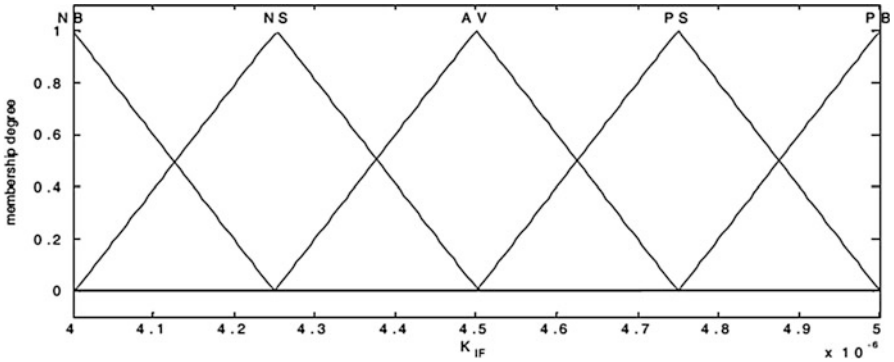


Fig. 5.25 Membership function of variable K_{IF}

The Defuzzification process is performed using the minimum of maximum method to determine the output from the fuzzy rules. This method, in general represents a polyhedron map. Initially, the minimum membership grade is computed from the intersection between two input variables, say x_1 and x_2. The min value is computed to rescale the output rule, and then the max value is computed. Finally, the centroid or center of area is used to compute the fuzzy output, which is defined as follows:

$$KI = \frac{\int y\mu(y)dy}{\int \mu(y)dy} \tag{5.56}$$

Thus, two FLCs are used to represent the reactive power and active power. The first controller is applied to tune the KI value of PI controller, using the terminal voltage error (eV) and its rate of change (ΔeV) as input variables. The second controller is

used to regulate the mechanical power via the blade angle adaptation of the wind turbine. The terminal voltage error (eV) varies between (−220 and 220) and its change (ΔeV) varies between (−22 and 22), and the output of the FLC is the KIV which changes between (5e-003 and 5.5e-003). The same technique is applied for active power controller where the two inputs for FLC are the mechanical power error (eF) which varies between (−1 and 1) and its change (ΔeF) varies between (−0.1 and 0.1). The output of the FLC is the KIF which changes between (4e-006 and 5e-006). The output of the PIFLC in the active controller adapts the pitch angel value to enhance the stator frequency.

The FLCs can be applied to active and reactive power controls of the system under study to enhance its dynamic performance. The FLC is used to regulate the duty cycle of the switched capacitor bank to adjust the terminal voltage of the induction generator. Another FLC is applied to regulate the blade angle of the wind energy turbine to control the stator frequency of the overall system.

5.5.4 Genetic Algorithm

The integral gain of the second PI controller is optimized based on the Genetic Algorithm. GA is used to calculate the optimum value of the variables based on the best dynamic performance and a domain search of the variable. The objective function used in the GA technique is $F = 1/(1 + J)$, where J is the minimum cost function. GA uses its operators and functions to find the values of *KIV* and *KIF* of the PI controllers to achieve better dynamic performance of the overall system. These values of gains lead to the optimum value of gains for which the system achieves the desired values by improving the P. O. S, rising time and oscillations. The main aspects of the proposed GA approach for optimizing the gains of PI controllers, and the flowchart procedure for the GA optimization process, are shown in Fig. 5.26.

5.5.4.1 Solution Representation

The PI gains are formulated using the GA approach, where all the gains are represented in a chromosome. The chromosome representation determines the GA structure. The parameter gains are encoded in a chromosome. The PI controller gains are initially started using minimum values of the domain search for PI gains. Based on the simulation results given in the previous sections, the values of [*KIV*max, *KIV*min] are shown in Fig. 4, while the values of [*KIF*max, *KIF*min] are shown in Fig. 11. The acceptable domain search for each gain is defined as [*KIV*max, *KIV*min] and [*KIF*max, *KIF*min] based on five times less and five times more than the gains obtained using the Ziegler-Nichols rule to satisfy minimum cost function J, as given in the following equation:

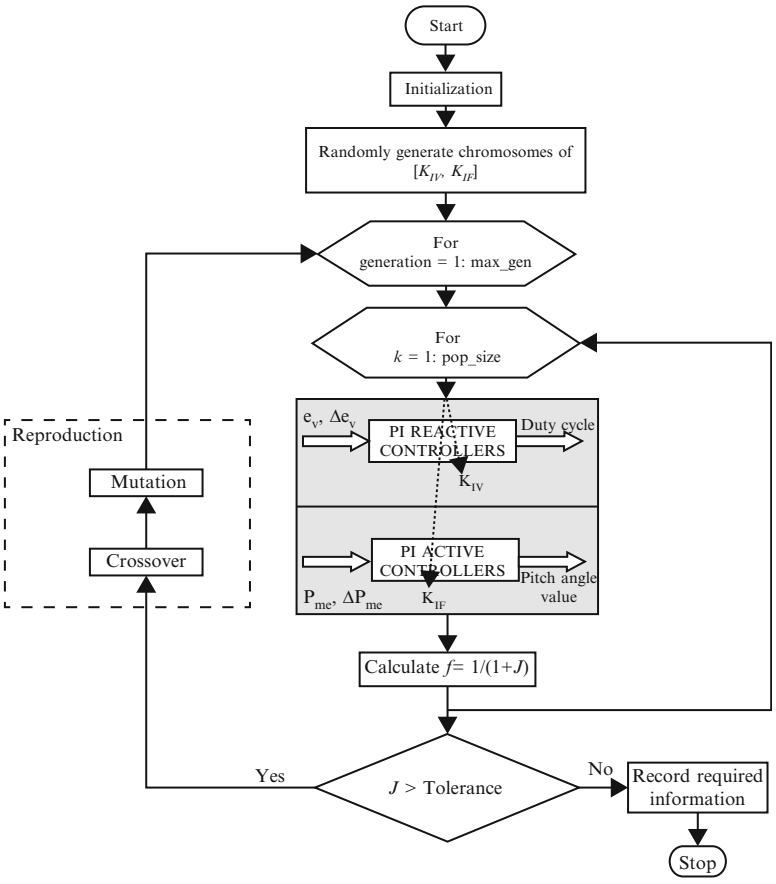


Fig. 5.26 Flowchart of GA approach for optimizing PIC gains

$$J = \int_0^T \left(\alpha_1 |e(t)| + \beta_1 \left|e^{'}(t)\right| + \gamma_1 \left|e^{''}(t)\right|\right) dt \tag{5.57}$$

where; $e(t)$ is equal to eV or Pme; eV is the voltage error used for the reactive power control and Pme is the mechanical power error used for active power control, as shown in Fig. 1. The parameters α_1, β_1, and λ_1 are weighting coefficients.

5.5.4.2 Coding of PI Controller Gains

The coded parameters are arranged on the basis of their constraints, as shown in Fig. 5.27, to form a chromosome of the population. The binary representation, given in Fig. 5.27, is the coded form for parameters with chromosome length equal

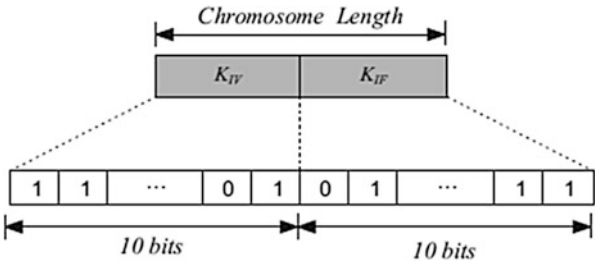


Fig. 5.27 Coded parameters of PI controller gains

to the sum of the bits for all parameters. In binary coding, the relation between the bit length L_i and the corresponding bit resolution R_i is given in the following equation:

$$R_i = \frac{UB_i - LB_i}{2^{L_i} - 1}, \tag{5.58}$$

where *UBi* and *LBi* are the upper and lower bounds of parameter *i*, respectively. In the present case study, we assume bit resolution $R = 10^5$ for all parameters. Figure 5.27 shows the coded parameters of the PI controller gains for reactive and active power controllers, respectively. The chromosome length used in this paper was 20 bits, where the bit length of *KIV* equal 10 bits and the bit length of *KIF* equals 10 bits.

5.5.4.3 Selection Function

The selection strategy decides how to select individuals to be parents for new '*children*'. The selection usually applies some selection pressure by favoring individuals with better fitness. After procreation, the suitable population consists, for example, of L chromosomes, which are all initially randomized. Each chromosome has been evaluated and associated with fitness, and the current population undergoes the reproduction process to create the next population. Then, the "roulette wheel" selection scheme is used to determine the member of the new population. The chance on the roulette-wheel is adaptive and is given as $P_\ell / \sum P_\ell$, where P_ℓ is defined as:

$$P_\ell = \frac{1}{J_\ell}, \ell \in \{1, \ldots, L\} \tag{5.59}$$

and J_ℓ is the performance of the model encoded in the chromosome measured in the terms used in Eq. 5.56. Maximizing the fitness function of each chromosome, which is inversely proportional to the performance criteria, Eq. 5.56 will damp the overshoot or the oscillations.

5.5.4.4 Crossover and Mutation Operators

The mating pool is formed, and crossover is applied. Then the mutation operation is applied, followed by the proposed GA approach. Finally, after these three operations, the overall fitness of the population is improved. The procedure is repeated until the termination condition is reached. The termination condition is the maximum allowable number of generations, or a certain value of J. This procedure is shown in the flowchart given in Fig. 5.26.

This section provided a GA based approach to optimize the PI controller gains in order to improve the dynamic response of the overall system. Optimal gains for the PI controller were determined using the GA procedure. The two types of controllers improve the dynamic performance when tested against various types of disturbances.

5.6 FLC Based STATCOM

Reactive power compensation is an important issue in the control of electric power system. Reactive power from the source increases the transmission losses and reduces the power transmission capability of the transmission lines. Moreover, reactive power should not be transmitted through the transmission line to a longer distance. Hence Flexible AC Transmission Systems (FACTS) devices such as static compensator (STATCOM) unified power flow controller (UPFC) and static volt-ampere compensator (SVC) are used to alleviate these problems.

5.6.1 Modeling of STATCOM

The STATCOM is based on the principle that a voltage source inverter generates a controllable AC voltage source behind a transformer leakage reactance so that the voltage difference across the reactance produces active and reactive power exchange between the STATCOM and the transmission network. By injecting a current of variable magnitude in quadrature with the line voltage, the STATCOM can inject reactive power into the power system which is done by making the inverter output voltage greater than the bus voltage. At the same time it will absorb the reactive power from the power system when the inverter output voltage is less than the bus voltage. The STATCOM does not employ capacitor or reactor banks to produce reactive power as does the SVC, but instead uses a capacitor to maintain a constant DC voltage for the inverter operation. The DC capacitor voltage can be adjusted by controlling the phase angle difference between line voltage and VSC voltage. The angle of line voltage is taken as reference. If the phase angles ‘α’ is slightly advanced, beyond the system bus voltage the STATCOM injected voltage

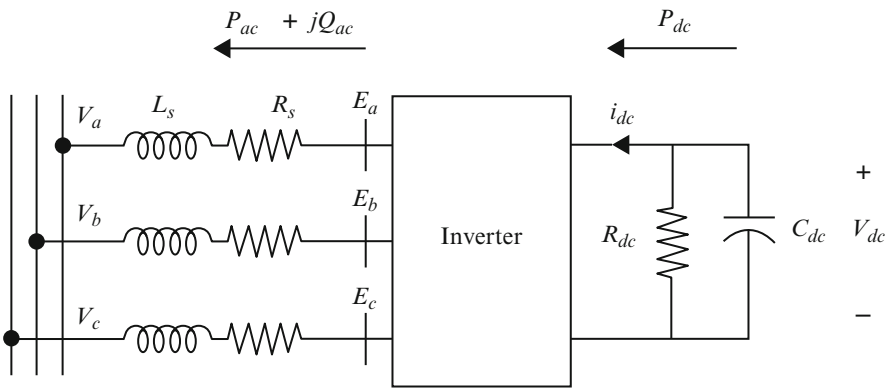


Fig. 5.28 Equivalent circuit model of STATCOM

decreases and reactive power flows into STATCOM. Conversely, if the phase angle 'α' is slightly delayed, the STATCOM injected voltage increases and STATCOM supplies reactive power to the bus. By controlling the phase angles of VSC, the reactive power can be generated from or absorbed by STATCOM and the voltage regulation can be achieved. The DC voltage maintained by the Cdc will act as voltage source for the VSC and it is connected to the transmission line through a shunt transformer. Figure 5.28 shows the equivalent circuit of the STATCOM. The loop equations for the circuit may be written in vector form as

$$\frac{d}{dt}i_{abc} = -\frac{R_s}{L_s}i_{abc} + \frac{1}{L_s}(E_{abc} - V_{abc}) \tag{5.60}$$

where R_s and L_s represent the STATCOM transformer resistance and inductance respectively, E_{abc} are the inverter AC side phase voltages, V_{abc} are the system-side phase voltages, and i_{abc} are the phase currents. The output of the STATCOM is given by

$$E_a = KV_{dc}\cos(\omega t + \alpha) \tag{5.61}$$

where V_{dc} is the voltage across the DC capacitor, K is the modulation index, and 'α' is the injected voltage phase angle. Figure 5.29 consists of one IGBT based intelligent power module (IPM) which acts as VSC, three phase transformer as AC source, display and sensing unit, RL loads, LC filters, and dSPACE kit with PC.

5.6.2 MATLAB/SIMULINK Model

Figure 5.29 shows the SIMULINK diagram of the PI controller part of the STATCOM. The real time performance analysis of STATCOM with PI controller

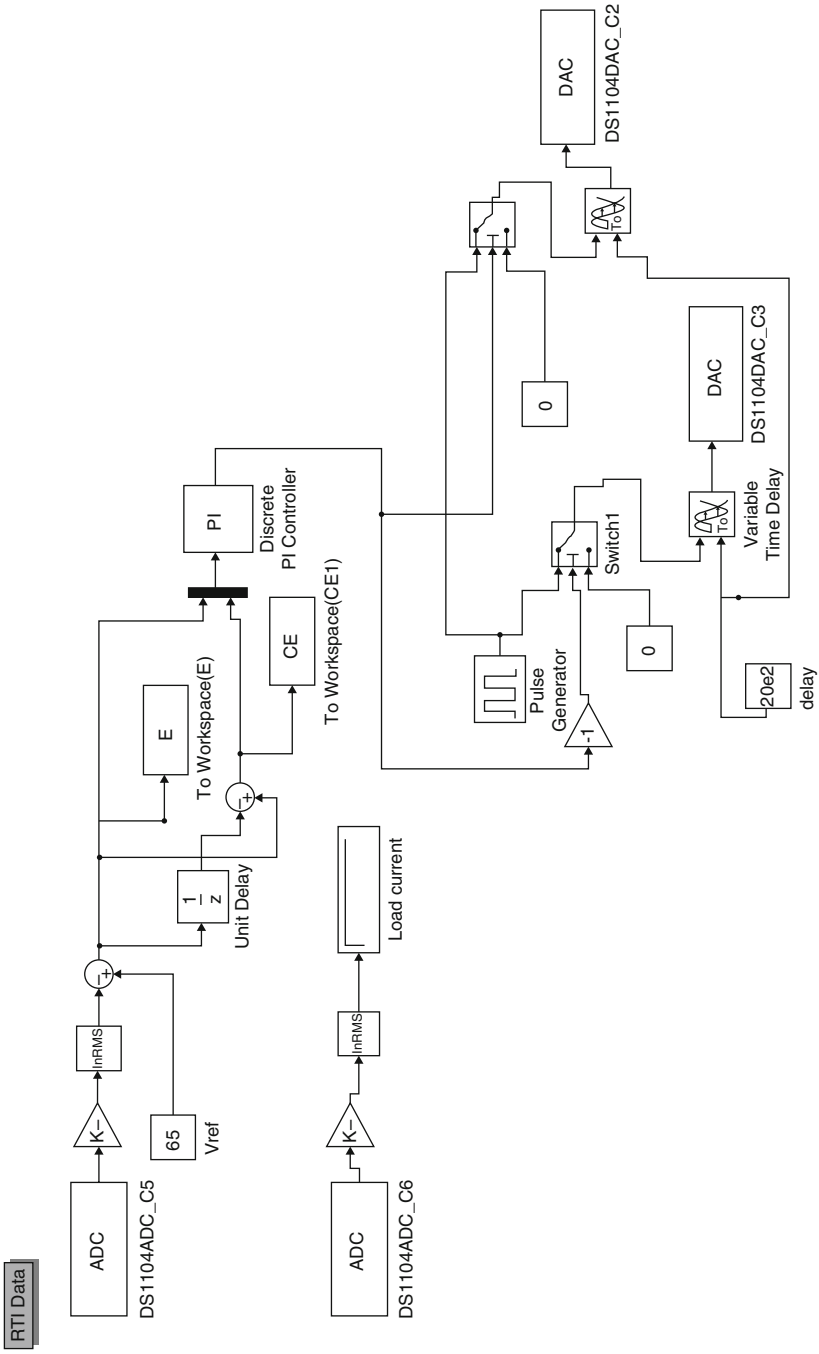


Fig. 5.29 SIMULINK diagram of the PI controller part of the STATCOM

is done by giving a load disturbance. In order to control V_{pcc}, its value is received in the dSPACE environment through one ADC. The command to change the phase angle 'α' so as to change the V_{pcc} is given to the I/O pins of the dedicated DSP TMS320F2407 through DAC from the dSPACE. Once the PI controller for STATCOM has been built in SIMULINK block-set, machine codes are generated by the dSPACE controller that runs on the inbuilt DSP processor. While the experiment is running, the dSPACE DS1104 provides a reference Vpcc as knob for the user to change its value online. Thus, it is possible for the user to view the process in real time, while the experiment is in progress. The Vpcc and the load current value have been taken from the ADCs. The reference value of Vpcc is set as 70v. The PI controller gives the output to DAC which is used to change the phase angle of the injected voltage by STATCOM till it reaches the reference value. Kp and Ki values are 0.1 and 500 respectively in the PI controller.

Fuzzy logic is used in STATCOM control loop. The V_{pcc} is fed back and is compared with the V_{pccref}. After comparison, the error and the change in error are calculated and are given as input to fuzzy controller. In this work, the error is normalized to one with V_{pccref}. This helps in using the fuzzy controller for any reference V_{pcc}. The fuzzy controller will attempt to reduce the error to zero by giving the pulse to S1 or S2. Figure 5.30 shows the SIMULINK diagram of the fuzzy controller part.

5.6.2.1 Sugeno Fuzzy Controller

There are two types of fuzzy controllers, viz., Mamdani and Sugeno type fuzzy controllers. In this work, Sugeno fuzzy controller is used. It uses singleton membership functions for the output variables. The Sugeno type controller is used because it can be easily implemented in any embedded system and reduces calculations. Furthermore, the reduction in calculation can result in real-time operation.

5.6.2.2 Fuzzification

In the present work, the error and change in error of Vpcc are fuzzified. Seven linguistic fuzzy sets with triangular membership function are used. The seven sets used for fuzzy variables 'error' and 'change in error' are negative big (NB), negative medium (NM), negative small (NS), zero (Z), positive big (PB), positive medium (PM), and positive small (PS).

5.6.2.3 Defuzzification

The reverse of fuzzification is called defuzzification. Weighted average method of defuzzification suitable for Sugeno type controllers is used in this work. The defuzzified output is the duration of the pulse.

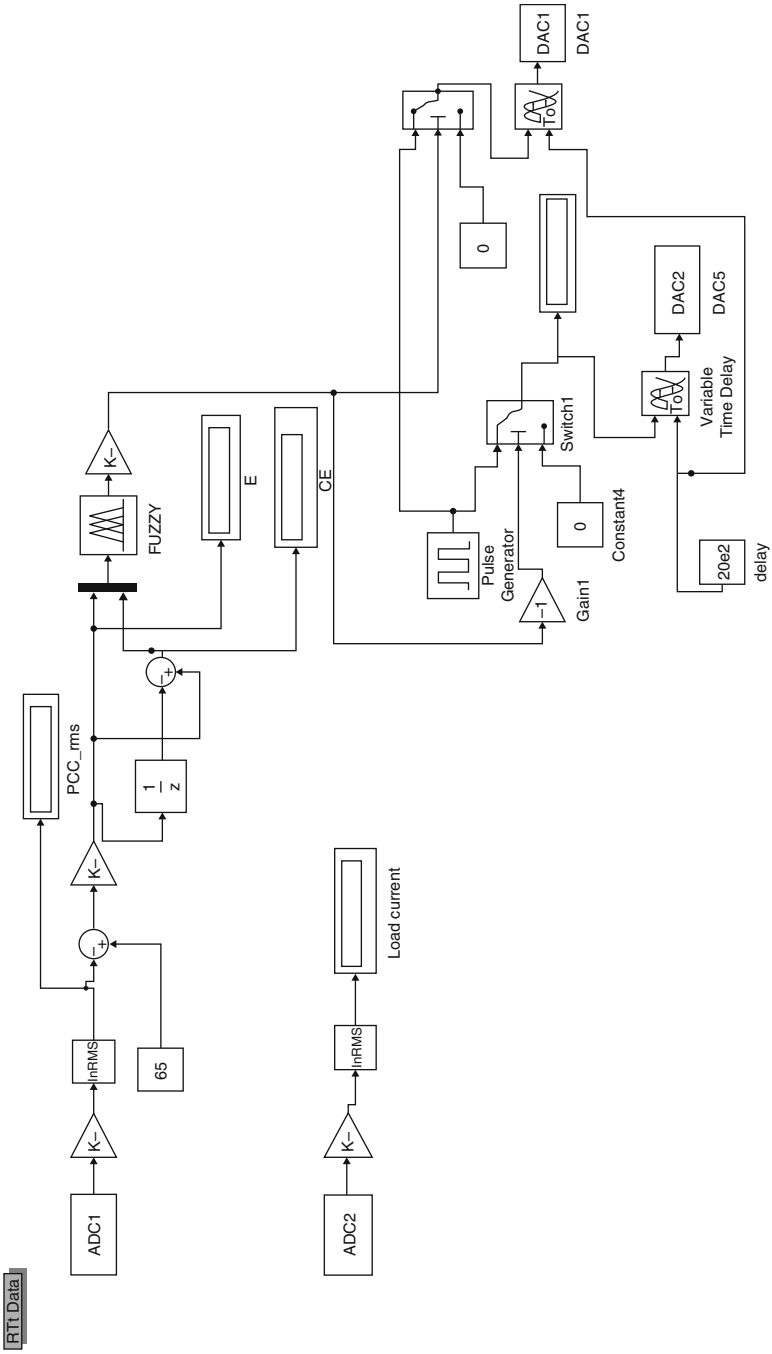


Fig. 5.30 SIMULINK diagram of the fuzzy controller part of the STATCOM

5.6.2.4 Rule Base

The fuzzy rules used in the design are in the general "If–Then" format. If error is Ai, and change in error is Bi, then output is Ci . Here the "if" part of a rule is called the rule-antecedent and is a description of a process state in terms of a logical combination of fuzzy linguistic sets. The "then" part of the rule is called the rule consequent and is a description of the control output in terms of logical combinations of fuzzy sets. The designed fuzzy controller increases the pulse duration when the error is positive and decreases the same when the error is negative. Figure 8 shows the fuzzy membership function.

5.6.3 Simulation Results

Simulation results of the fuzzy controller is presented in this section. Figure 5.31 shows the Active power, reactive power, power factor and current in the load side. The DC-link voltage regulation during sudden voltage changes is presented in Fig. 5.32. The active power, reactive power and power factor on the source side are shown in Fig 5.33.

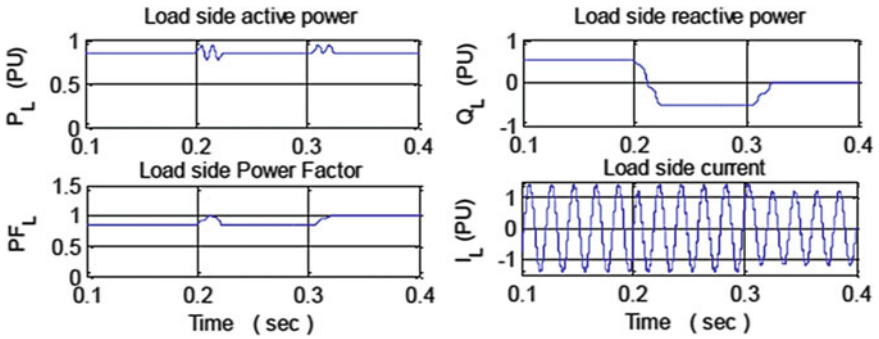


Fig. 5.31 Active power, reactive power, power factor and current in the load side

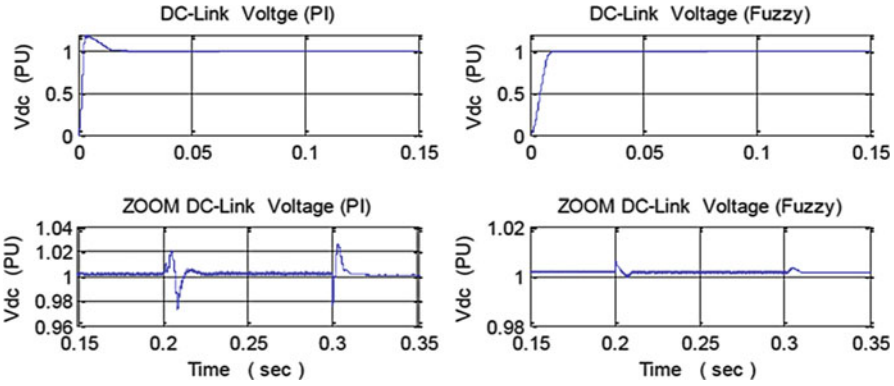


Fig. 5.32 DC-link voltage regulation during sudden voltage changes

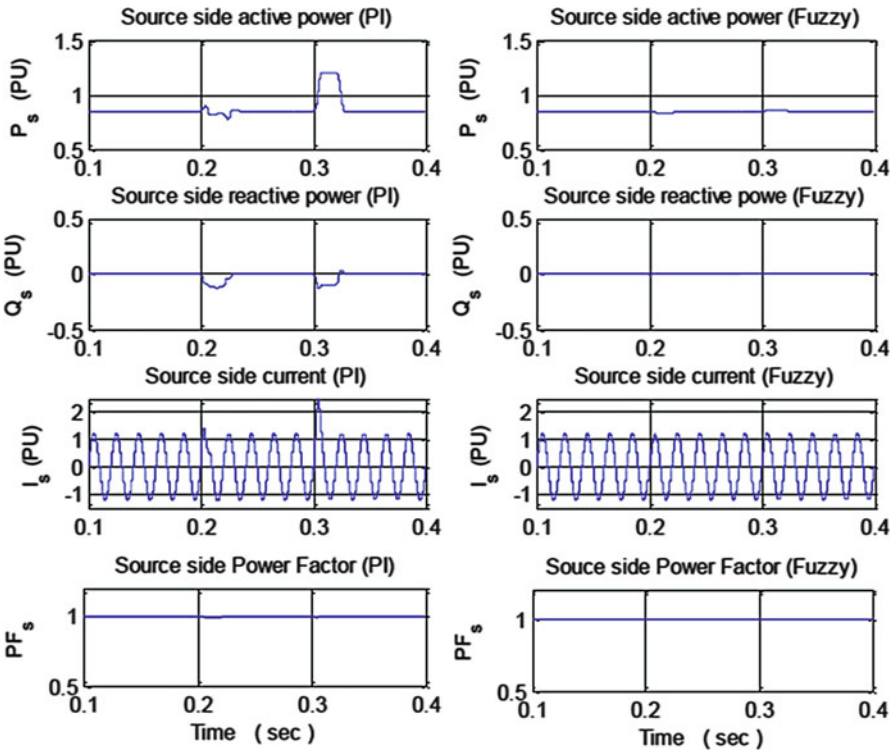


Fig. 5.33 Monitored results in the source side

5.7 FLC Based Wind Energy Production System

In this section, the fixing of voltage amplitude at a constant value of 380 V by using a controller for the loads supplied from a wind/battery energy production system is explained. The wind speed was continuously changed and the behavior of the system was analyzed. For the controller, both a PI controller and a fuzzy logic controller (FLC) were used; the results were compared. The quality of the energy was observed by taking measurements of the loads frequently. The value of the total harmonic distortion (THD) was held at the standard intervals. The entire system and all of its subcomponents were designed in a MATLAB/SIMULINK environment.

5.7.1 Wind/Battery Energy Production System

The overall system structure, consisting of a three-phase load, wind/battery hybrid energy system, interfacing converters, filters, and control unit, is shown in Fig. 5.34. When the wind speed is sufficient, the whole system is supplied by the wind turbine; otherwise, the batteries are turned on to supply the system. The direct-current (DC) voltage produced by the wind/battery system is converted to alternative-

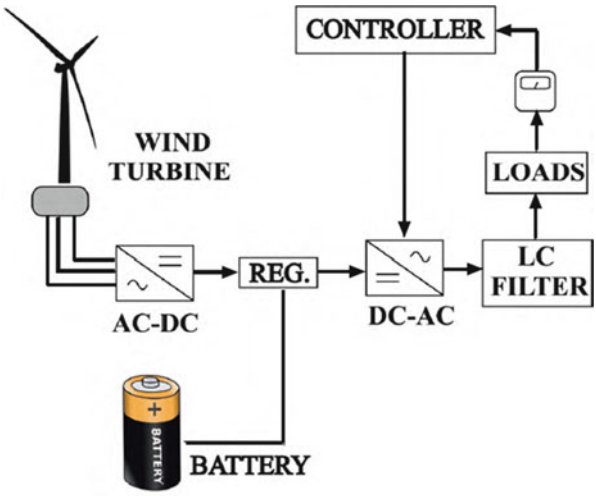


Fig. 5.34 PV/battery renewable source

current (AC) voltage using a three-phase inverter in order to supply power to the three-phase load. The voltage output of the inverter is controlled to keep the voltage at 380 V, line to line, at a fixed frequency of 50 Hz. The three-phase voltages are converted to d-q axis layouts as direct-axis voltage Vd and quadrature voltage Vq, to be used by the PI controller and the FLC. The output of the controller is then used to generate a pulse-width modulated (PWM) signal, which is used to control the output voltage of the inverter. The frequency of the inverter is controlled and kept constant at 50 Hz through a phase-locked loop (PLL) process.

The filters in the system are used to supply clean AC voltage to the loads. The value of the THD in the system was measured and compared with the correct standard values. All of the subsystem components (wind turbine, batteries, FLC, PI controller, inverter, three-phase load, regulator, and filters) were sub modeled individually using the MATLAB/SIMULINK GUI (graphical user interface) environment and were combined to establish the overall system model. The simulation of the proposed scheme was done in MATLAB/SIMULINK/SimPower to establish model validation and component compatibility. The used regulator is a device that measures the wind speed. This controller is a mechanism that uses an on-off control technique. When the wind speed is less than a specific value, it cannot supply the guaranteed power to the system; the system then turns off the wind turbine and turns on the batteries. In this study, a wind/battery system supplying power to three-phase AC loads was examined. To fix the voltage on the loads at 380 V, both a PI controller and a FLC were used, and the results were compared.

5.7.2 The Wind Turbine Model

Wind turbines convert mechanical energy produced by the wind to electrical energy. To use this electrical energy, voltage and frequency regulation are needed.

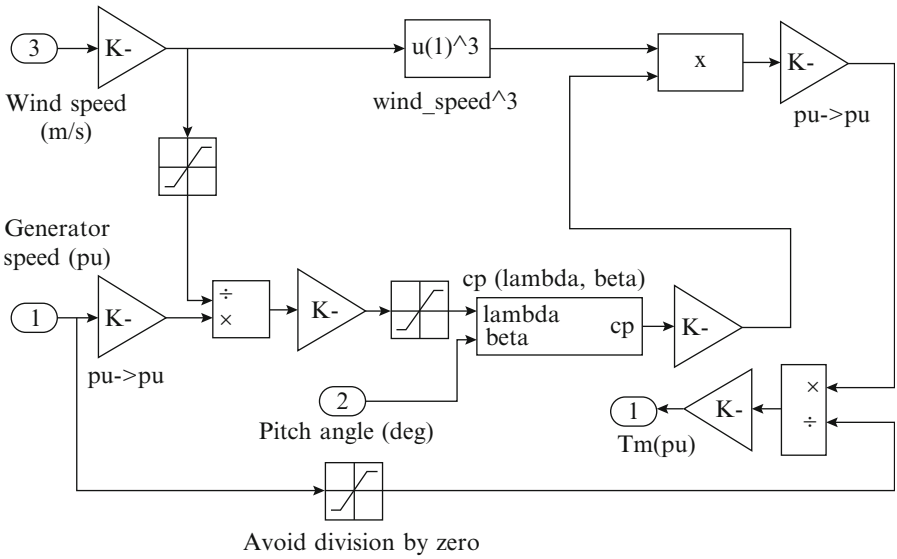


Fig. 5.35 Wind turbine model

The model of a wind turbine is developed on the basis of the steady-state power characteristics of the turbine. The SIMULINK model of the studied wind turbine is shown in Fig. 5.35.

5.7.3 Battery Model

The nickel-metal hydride battery was modeled using a simple controlled voltage source in a series with constant resistance, as shown in Fig. 5.36. This model assumes the same characteristics for the charge and the discharge cycles. The open voltage source was calculated with a nonlinear equation based on the actual state of charge (SOC) of the battery.

5.7.4 Fuzzy Logic Controller

The FLC's input values are generally the control error and the variation of this error in one sampling time. According to these variables, a rule table is produced in the FLC's rule-base unit.

The holding of the voltage and the amplitude of the load at the desired values of 380 V and 50 Hz is done by the FLC. The three-phase voltage is transferred from

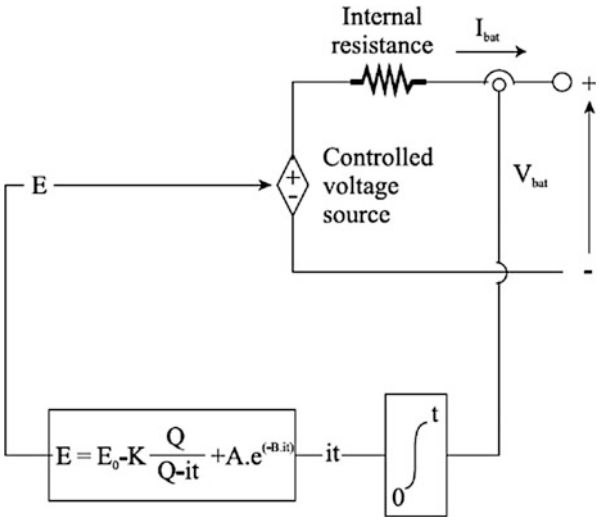


Fig. 5.36 Nonlinear battery model

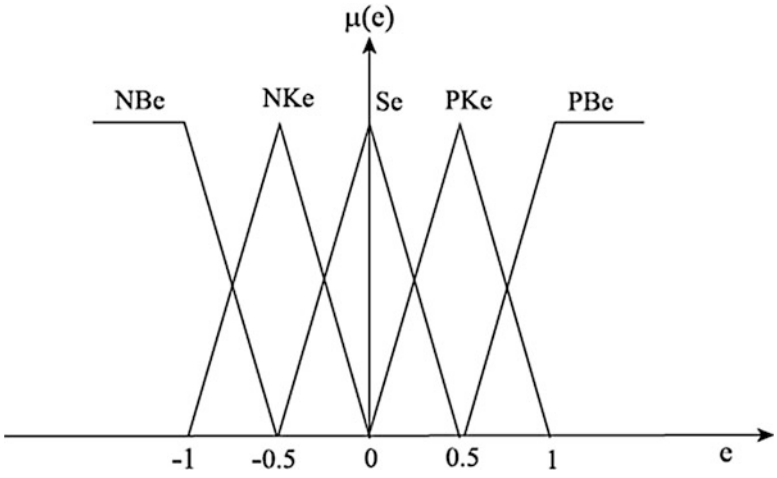


Fig. 5.37 Error membership functions

the a-b-c axes to the d-q axes first. The voltage divides into its components, which are controlled separately. At the output of the control, the voltage is transferred in reverse, from the d-q axes to the a-b-c axes, and, at the end, the PWM is driven by that voltage. These controls are done in the regulator block.

In Figs. 5.37 and 5.38, the error and the error variation of the input data of the FLC's input variables are shown. Triangle membership functions were used. These functions are called NB, NK, S, PK, and PB, and the data vary between –1 and 1.

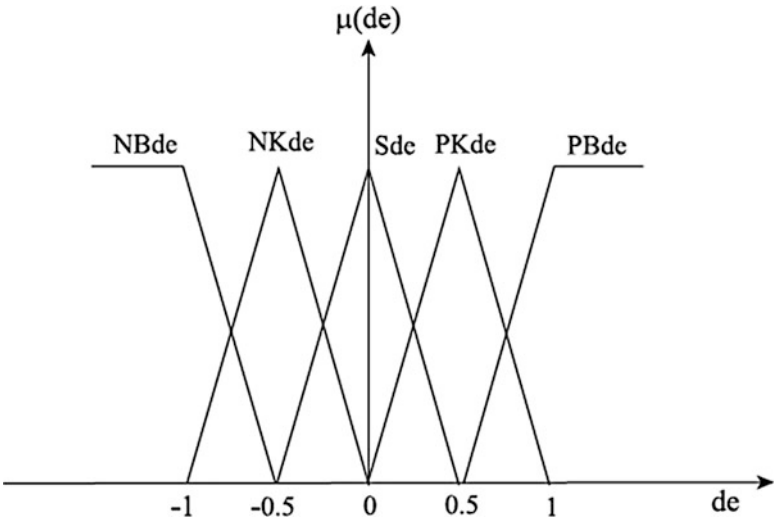


Fig. 5.38 Variation of error membership functions

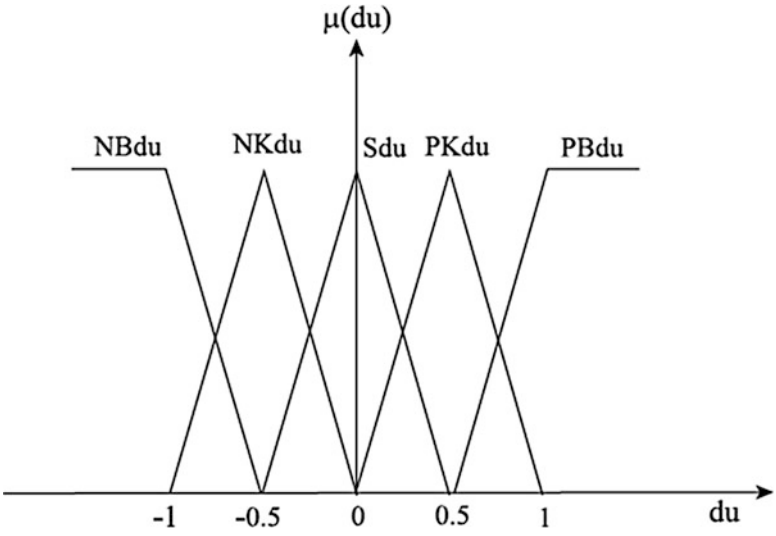


Fig. 5.39 Output space

In Fig. 5.39, the output space of the FLC is shown. These data also vary between –1 and 1. These subsystems are shown in Figs. 5.40, 5.41, 5.42 and 5.43. The triangle membership function is defined in Eq. 5.61, and its SIMULINK subsystem is shown in Fig. 5.40.

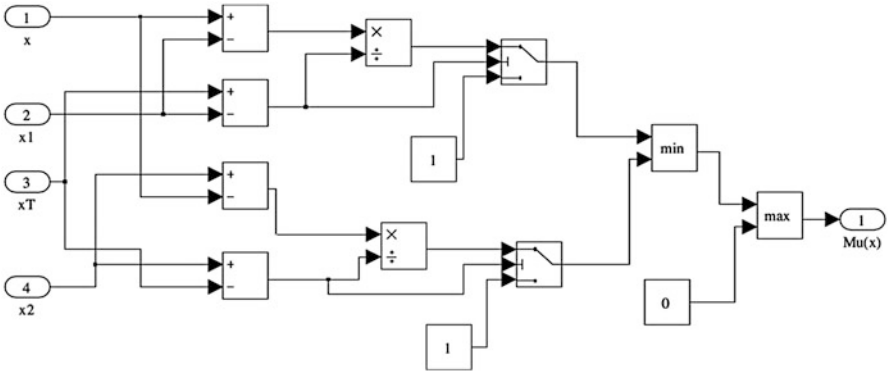


Fig. 5.40 Triangular membership function

Table 5.6 Fuzzy rules

e/de	NB	NK	S	PK	PB
NB	NB	NB	NK	NK	S
NK	NB	NK	NK	S	PK
S	NK	NK	S	PK	PK
PK	NK	S	PK	PK	PB
PB	S	PK	PK	PB	PB

$$\mu_{MU}(x) = \max\left(\min\left(\frac{x - x_1}{x_T - x_1}, \frac{x_2 - x_1}{x_2 - x_T}\right), 0\right) \tag{5.62}$$

In Fig. 5.41, the fuzzification unit is shown, with five rules. The minimums of the error and its variations according to the input variables are calculated here. In Table 5.6, the rules of the FLC are given. Due to the 5-ruled input variables, there are 25 rules in total. The unit for the rule processing is seen in Fig. 5.42.

In Fig. 5.43, certain variables are obtained with defuzzification by using the center of the area method. In Eq. 5.62, the mathematical expression of this method is shown.

$$z_0 = \frac{\sum_{j=1}^{n} \mu_C(z_j).z_j}{\sum_{j=1}^{n} \mu_C(z_j)} \tag{5.63}$$

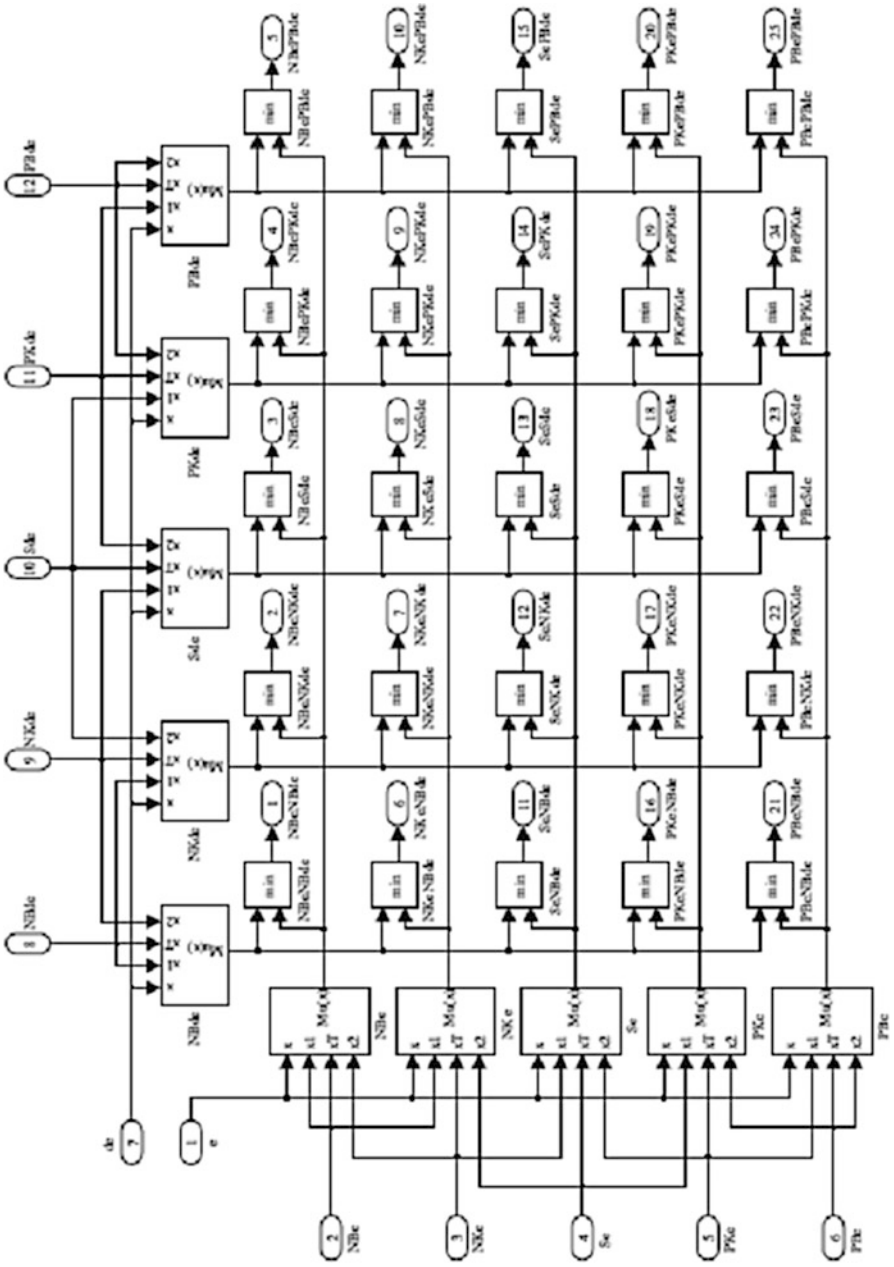


Fig. 5.41 Fuzzification unit

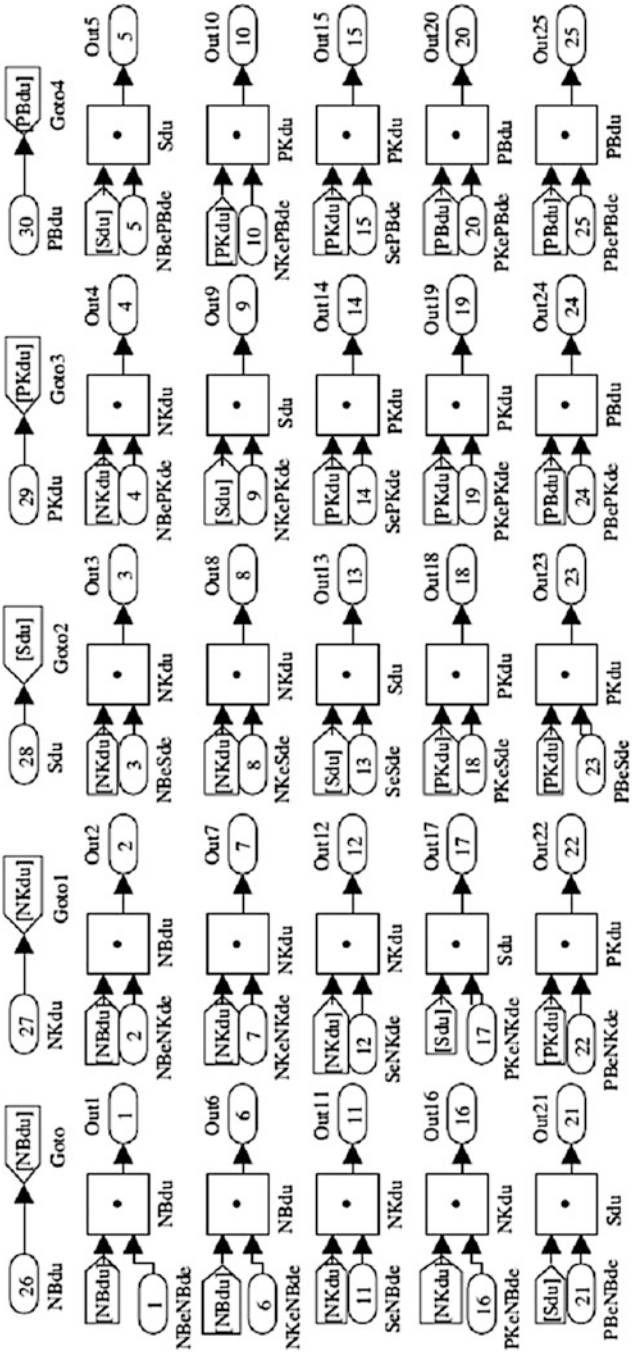


Fig. 5.42 Fuzzy rules in SIMULINK

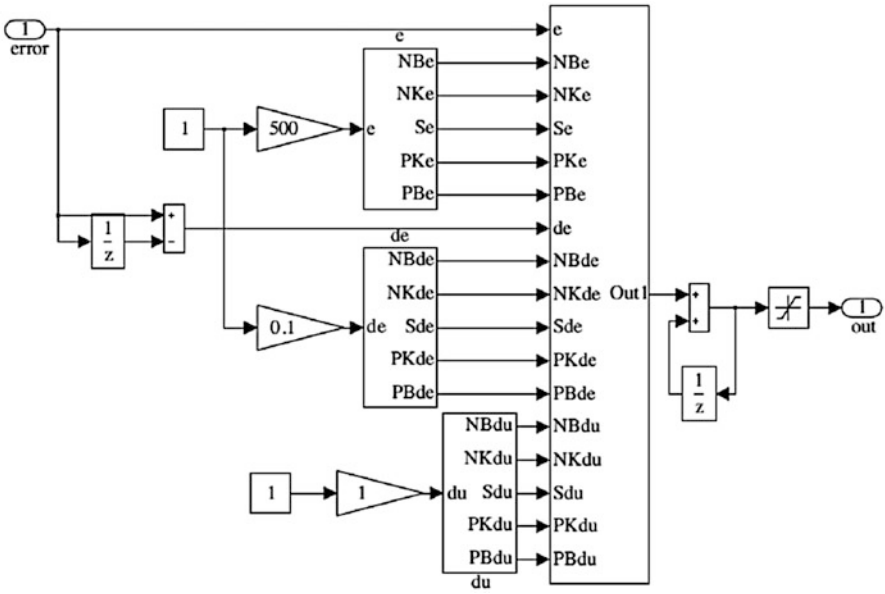


Fig. 5.43 FLC with input and output values

5.7.5 MATLAB SIMULINK Model

The wind turbine is affected by the wind speed. The simulated system is shown in Fig. 5.44. The system includes a 60-kW wind turbine and induction machine, a 55-kW battery, a regulator, an inverter, filters, a total 50-kW load, measuring units, switches, and controllers. During the simulation process, the voltages on the loads are fixed at the values of 380 V and 50 Hz.

5.7.6 Simulation Results

The PWM used in the system's inverter has a 2-kHz switching frequency. Therefore, in the simulation, discrete time control is done at a sampling time of 2 μs. The alternative voltage obtained from the wind turbine is converted to direct current by passing it through a rectifier and then filtering it. The direct current is also connected to the battery unit. It is converted to the three-phase voltage by an inverter and then filtered again, and the loads are supplied by this voltage. To investigate the system's behavior at different loads, first a 10-kW and then a 20-kW load is added to the 20-kW reference load. The total load is 50 kW. In the system, the regulator decides when the loads will be supplied by the wind turbine or by the battery unit. According to the decision, the signals are sent to the switches that turn

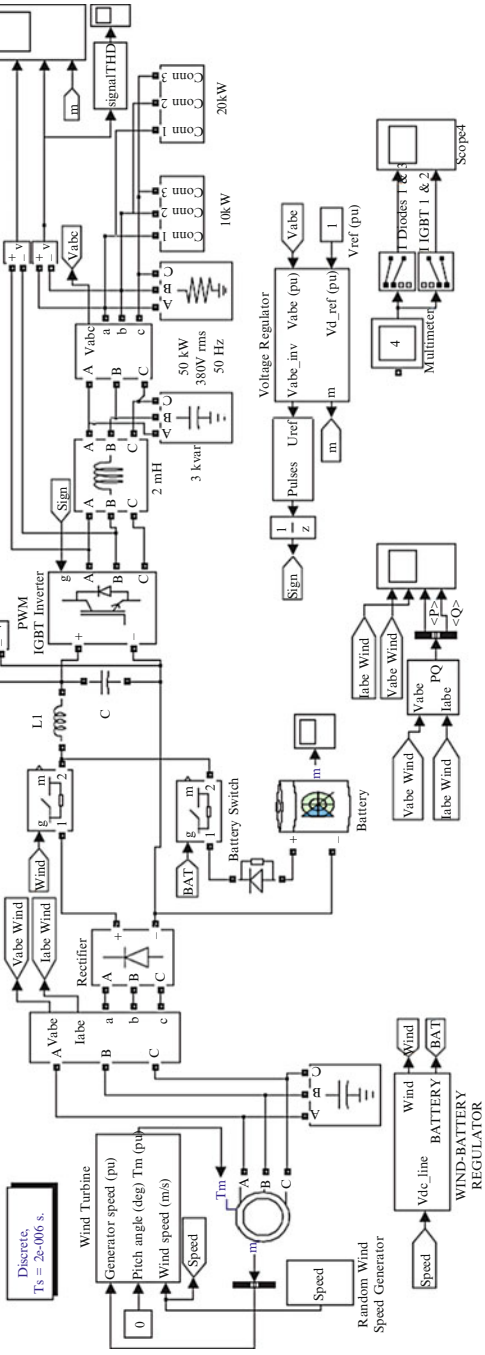


Fig. 5.44 Main system

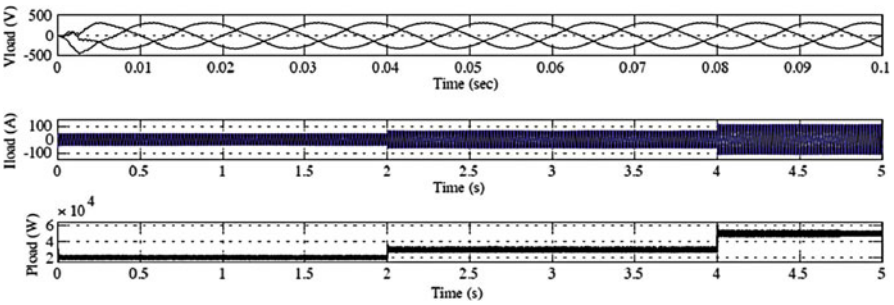


Fig. 5.45 Power on the load with a PI controller

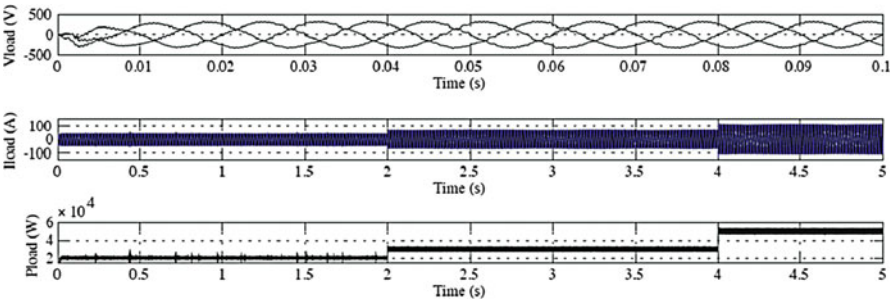


Fig. 5.46 Power on the load with FLC

on and off the wind turbine and the battery unit. This process is conducted in the wind-battery block.

The voltage regulator block is the place where the control process occurs. Here, as explained before, the transfer process is done from the a-b-c axes to the d-q axes. The voltage is divided into its d and q components, which are controlled separately, and, in the output of the controller, these data are converted to the a-b-c axes from the d-q axes. The PWM is driven by that voltage.

By taking some measurements from every point, data about the system's current, voltage, and power can be examined. By changing the wind speed between 0 and 12 m/s, a simulation close to reality is undertaken.

In Figs. 5.45 and 5.46, the active power, current, and voltage on the load with both a PI controller and a FLC are shown. The increase of the loads can be seen clearly. First a 20-kW, then a 10-kW, and finally a 20-kW load were added to the system. As a result, a total load of 50 kW is supplied by the system.

In Fig. 5.47, the voltage on the load reaches a value of 380 V at 2 s with the PI controller. The maximum overshoot voltage that can be reached is 392 V. The three-phase THD value is less than 10 % at the steady situation. In Fig. 5.48, the results derived from the control done by using the FLC are shown, along with the DC output voltage, the inverter's output voltage between the a and b phases, the

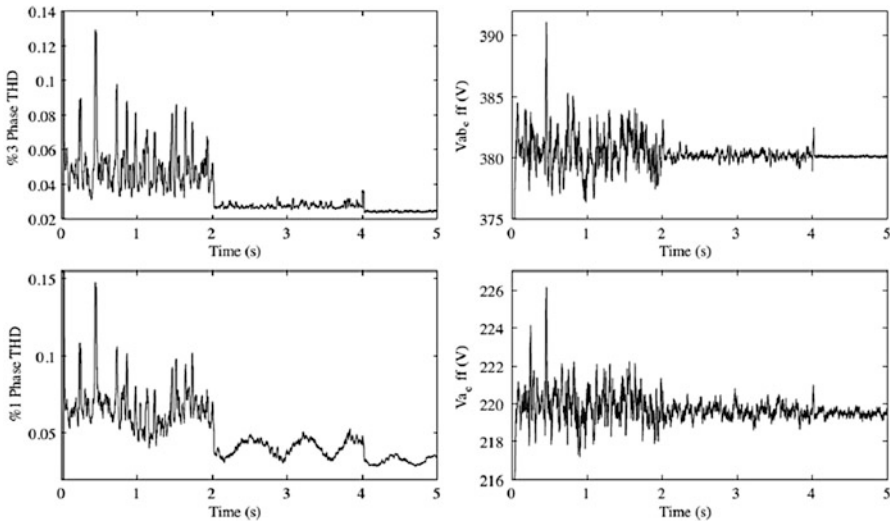


Fig. 5.47 PI controller results

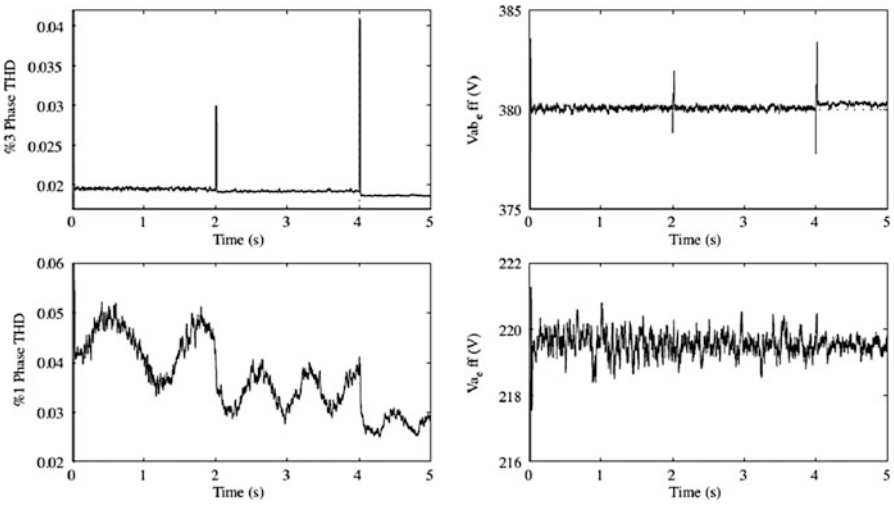


Fig. 5.48 FLC results

load voltage between the a and b phases, and the variation of the modulation indexes. The voltage on the load reaches a value of 380 V at 0.05 s with the FLC. The maximum overshoot value is 384 V. The three-phase THD value is less than 2 % at the steady situation.

In Figs. 5.49 and 5.50, the variation of the voltage between the a and b phases done in simulations with the PI controller and FLC in sequence are shown. As can be seen from the THD values, the FLC has a less harmonic and a clean sinus wave.

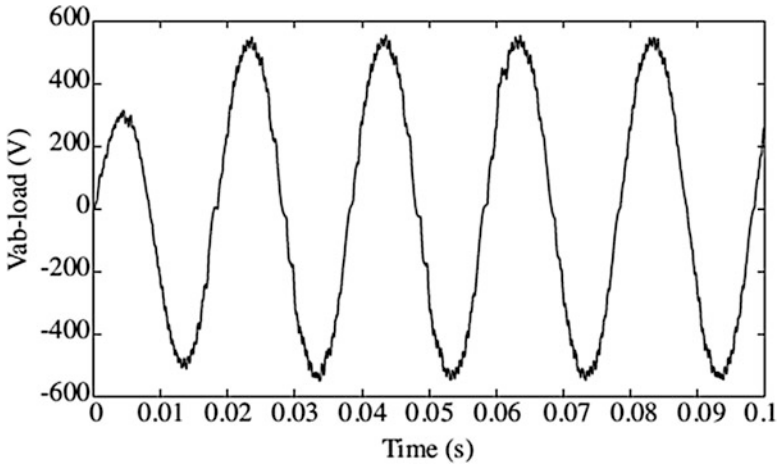


Fig. 5.49 V*ab* – *load* variation for PI controller

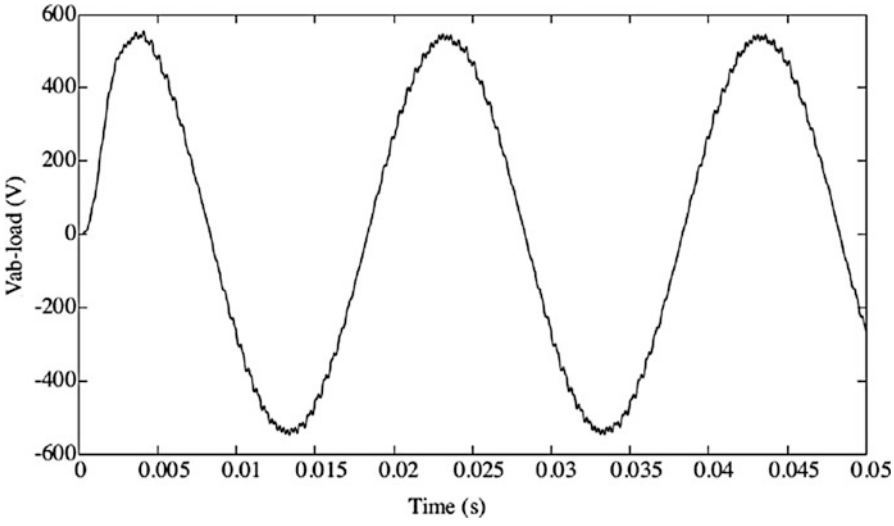


Fig. 5.50 V*ab* – *load* variation for the FLC

The waveform of the loads was very similar to the sinus wave form using both the PI and fuzzy logic controllers. The system can fix the voltage on the loads at a constant value of 380 V regardless of effects from the variations of the wind speed. The system frequency value is steady at 50 Hz. According to the value of the wind speed, the used regulator works effectively by turning on and off the batteries. The maximum overshoot and settling time values of the FLC were much better than those of the PI controller. The PI controller maximum overshoot voltage that can be

reached is 392 V. This value is 384 V with the FLC system. The PI controller's setting time was 2 s; this value was 0.05 s for the FLC. When the THD values are compared, it is seen that both controllers had values in the standard ranges. However, the FLC's value was better than the PI's, as was its sinus wave form. When the produced energy is greater and the loads are low, the wind turbine must be arranged to recharge the batteries. This can be done by the management of the energy. When there is no wind, the loads are supplied only with batteries. When the batteries are empty, the loads will have no energy supply. To prevent this situation, a diesel generator can be added to the system or the system can be supplied with energy by the main network.

5.8 Prediction of Wind Speed Based on FLC

Fuzzy logic controller (FLC) is used in order to achieve maximum power delivery for each wind speed and to have more robustness. Maximum output power operating point deviates from the maximum torque point. The torque follows the square-law characteristics and the output power follows the cube law. This means that under light load conditions, additional generator magnetic flux controller is needed in order to achieve more power efficiency, by reducing the iron losses. The optimum fuzzy logic control of an induction generator require controller which will track wind speed in order to achieve λopt and thus extract maximum power.

The product of torque and speed gives turbine power, and by assuming a steady state lossless system it is equal to the grid power. The curves in Fig. 5.51 show the grid power pO in dependence of generator speed ωr in terms of wind velocities vw.

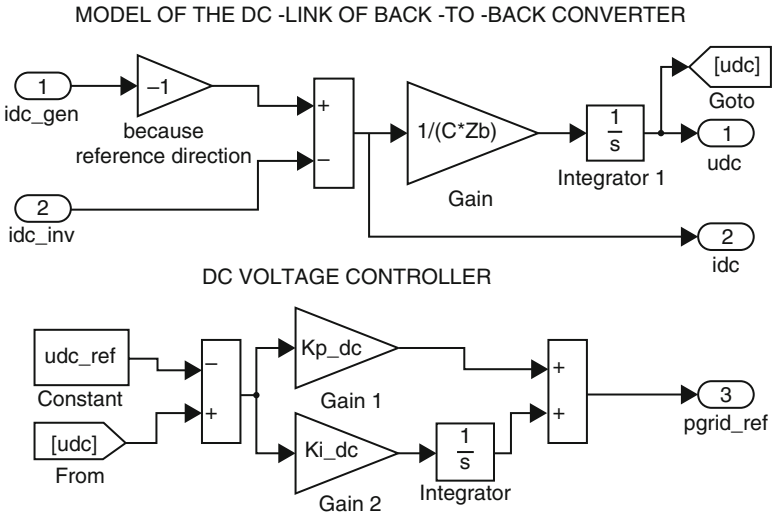


Fig. 5.51 MATLAB/SIMULINK model of the DC-link and DC voltage controller

What is the exact task of fuzzy controller it could be best seen from these set of power curves.

For a particular value of wind velocity, the function of the fuzzy controller FLC is to seek the generator speed in steps until the system settles down at the maximum output power operating point. For example, at a wind velocity of *Vw4*, the output power will be at point A if the generator speed is *ωr1*. The FLC will change the speed in steps until it reaches the speed *ωr2*, where the output power is maximized at point B. If the wind velocity increases to *Vw2*, the output power will jump to point C, and then FLC will bring the operating point to D by searching the generator speed to *ωr4*. The strategy for decrease of wind velocity is similar. If wind velocity decreases to *Vw3*, output power is altered and settled at operating point E. FLC will now decrease generator speed to the optimum value *ωr3* (point F) where output power is at maximum.

Therefore, the principle of the fuzzy controller is to increment or decrement the generator speed in accordance with the corresponding increment or decrement of the estimated output power *pO*. If *ΔpO* is positive with the last positive *Δωr*, the search is continued in the same direction. If, on the other hand, positive *Δωr* causes negative change *ΔpO*, the direction of search is reversed. So, during these step changes of generator speed, controller observes changes in turbine output power and due to this it keeps searching generator speed for which this change of output power would be zero. That would be the maximum power delivery point. If *ωr1* is far from *ωr2*, controller could give greater value of generator speed increments, *Δωr*, for faster convergence to the maximum delivery point. Similar, if current generator speed is close to the *ωr2* controller must give smaller value of speed increments, *Δωr*, to avoid oscillations and ensure stable system. Descriptive rules like this could be applied converting the system into the fuzzy system. Actual values that indicates input variables, here change of output power, *ΔpO,* and last change of generator speed, *LΔωr*, are initially converted into the correspondent fuzzy sets with human descriptive and intuitive values such are terms BIG, MEDIUM, SMALL, ZERO. This is done in the "fuzzification block", where the variables *ΔpO* (variation of output power), *Δωr* (variation of generator speed) and *LΔωr* (last variation of generator speed) are described by membership functions. Afterwards, it is possible to apply descriptive rules of reasoning like "if the last change of output power *ΔpO* during maximum power searching was POSITIVE and BIG and the last change of desired generator speed *LΔωr* was POSITIVE then keep tracking the maximum power in the same POSITIVE direction with BIG increment *Δωr*". Rules like this are involved in block "rules table", and they are given in Table 5.7. Finally, the fuzzy set of output reference change of generator speed *Δωr* is back "deffuzified" to convert it to the actual value. That means the output values such are BIG, MEDIUM, SMALL are translated to numbers which indicates a measurable (but normalized) value of the generator speed. It could be also noticed the output of controller *Δωr* is added by some amount of *LΔωr* in order to avoid local minima in characteristics *Cp(λ)* due to the changes of wind speed. value. That means the output values such are BIG, MEDIUM, SMALL are translated to numbers which indicates a measurable (but normalized) value of the

Table 5.7 Fuzzy rules

	$\Delta\omega_r$		
ΔP_o	*P*	*ZE*	*N*
PVB	*PVB*	*PVB*	*NVB*
PBIG	*PBIG*	*PVB*	*NBIG*
PMED	*PMED*	*PBIG*	*NMED*
PSMA	*PSMA*	*PMED*	*NSMA*
ZE	*ZE*	*ZE*	*ZE*
NSMA	*NSMA*	*NMED*	*PSMA*
NMED	*NMED*	*NBIG*	*PMED*
NBIG	*NBIG*	*NVB*	*PBIG*
NVB	*NVB*	*NVB*	*PVB*

generator speed. It could be also noticed the output of controller $\Delta\omega r$ is added by some amount of $L\Delta\omega r$ in order to avoid local minima in characteristics $Cp(\lambda)$ due to the changes of wind speed.

5.8.1 Controller Model

The controller operates on a per unit basis so that the response is insensitive to system variables and the algorithm is universal to any system. Membership functions of FLC controller are implemented by using MATLAB/SIMULINK fuzzy control toolbox. In Fig. 5.52 realized model of fuzzy logic controller is shown. Heart of the controller is block of fuzzy logic controller from MATLAB/SIMULINK fuzzy control toolbox. With this powerful tool it is possible to define the fuzzy controller in relatively easy way using graphical interface and intuitive dialogs, which is obvious from Figs. 13 and 14. The scale factors *KPO* and *KWR* are functions of the generator speed, so that control becomes somehow insensitive to speed variation. The scale factors are generated by fuzzy computation realized in *MATLAB*/*SIMULINK* as shown in Fig. 5.53. Their values are generated partly empirically, and partly taking into account dependence of wind turbine power related to wind speed in terms of different generator speed. The membership functions are scaled using MATLAB editor shown in Fig. 5.54.

In order to verify control principle, detailed model of the system in MATLAB/SIMULINK has been developed. The system data are shown in Table 5.8.

5.8.2 Experimental Results

Simulation results shown in Fig. 5.55 illustrate performance of wind turbine with fuzzy controller which tracks the maximum power delivery operating point. They are given for the case of wind velocity decrease from nominal to 80 % of nominal

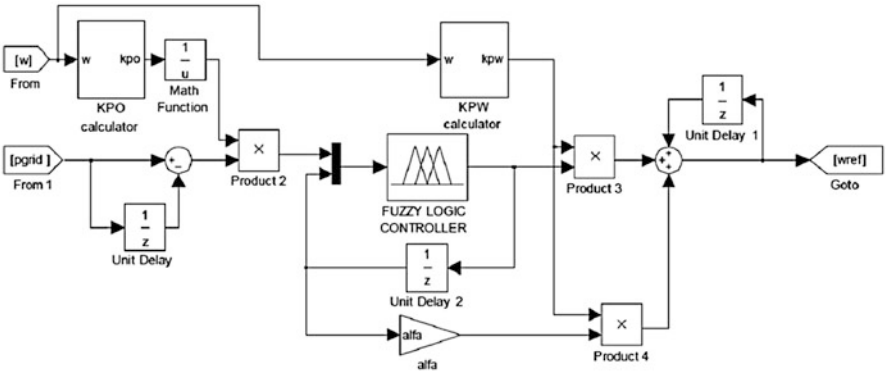


Fig. 5.52 MATLAB SIMULINK model of FLC

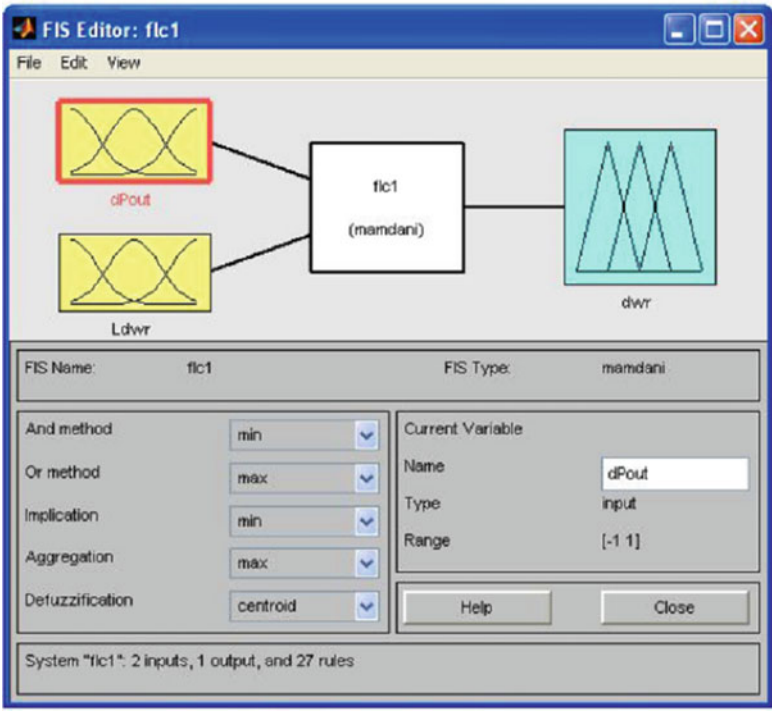


Fig. 5.53 MATLAB graphical editor for defining of fuzzy logic controller

value. It could be noticed that before disturbance ($t < 5$ *s*) all variables are settled at nominal values. After wind velocities decrease power fed to the grid gradually decrease to value around 50 % of nominal, which is expected because turbine power follows the cube law. Reference value of q current component i_{sq} also drops, and

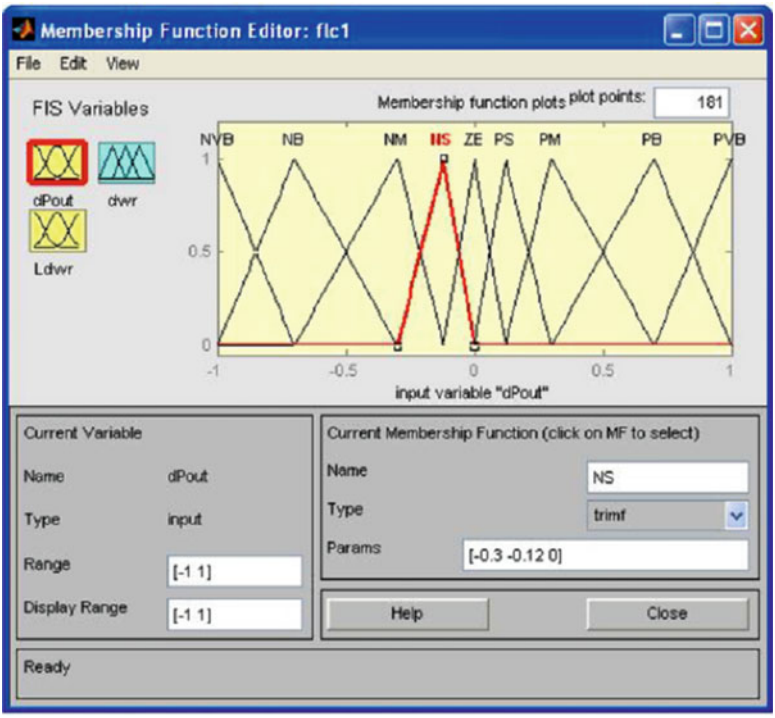


Fig. 5.54 MATLAB graphical editor for defining membership functions

Table 5.8 The system parameters used in simulation

Stator resistance, *rS* 7.7 m (p.u.)
Rotor resistance, *rR* 9.0 m (p.u.)
Stator reactance, *xS* 3.56 (p.u.)
Rotor reactance, *xR* 3.53 (p.u.)
Magnetization reactance, *xM* 3.47 (p.u.)
Leakage coefficient, σ 41 m (p.u.)
Grid resistance, *rGRID* 6.4 m (p.u.)
Grid reactance, *xGRID* 40 m (p.u.)
Fuzzy controller sampling per., *Tflc* 0.014 s
Capacitance of DC-link, *C* 1,000 μF
Based impendance, *ZB* 16 Ω
Turbine power coefficient, *CpMAX* 0.4639
Based angular speed, ωB $100 \cdot \pi$ rad/s

thus the value of electromagnetic torque. *D* current component *isd* remain the same, so the magnetic flux is unchanged. DC-link voltage is maintained constant which means that all generated power is transferred to the grid. Generator rotational speed is changing consistent with changes of wind velocity. Speed response is without overshoot and abrupt transients, as a consequence of fuzzy controller usage.

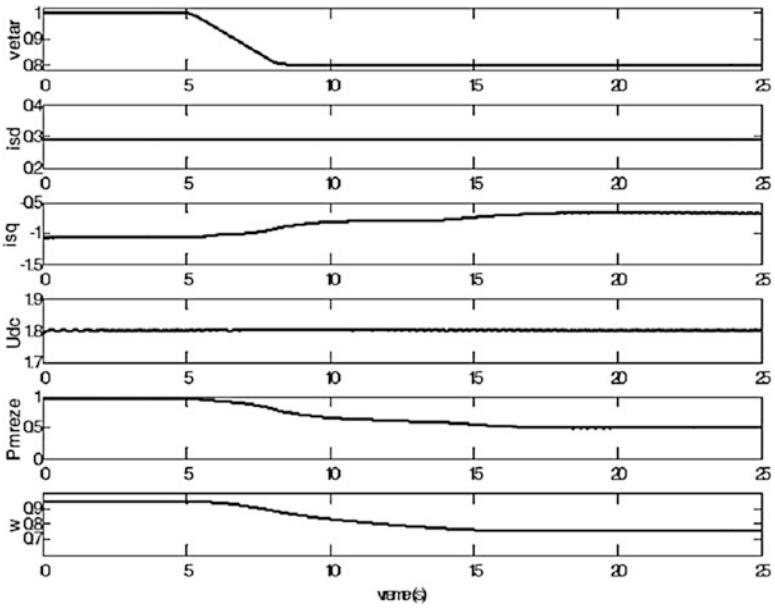


Fig. 5.55 Simulation results. From up to down: wind velocity *Vw*, *d* grid current component *isd*, *q* grid current component *isq*, DC-link voltage *UDC*, grid power *PO*, and generator speed *ωr*

In order to verify that maximum power is extracted from the available wind, power coefficient *Cp(λ)* has to be observed. In Fig. 5.56, *Cp(λ)* is shown during the change of wind velocity. It could be noticed that during the change of wind velocity, power coefficient *Cp(λ)* differs from optimum value. Deviation is relatively small, but after the transient period which lasts around 10 s, it settles at the optimum value.

In this section optimum fuzzy control of wind turbine in order to extract maximum power is described and verified through the simulation. The main goal of implemented fuzzy controller is to continuously adapt the rotational speed of the generator to the wind speed in a way that the turbine operates at its optimum level of aerodynamic efficiency. The advantages of using fuzzy controller are universal control algorithm, fast response, and parameter insensitivity. Implemented system has satisfactory dynamic and static performances.

5.9 Fuzzy Logic Controlled SPWM Converter for WECS

A novel sinusoidal PWM switched AC/DC/AC converter interface scheme using real novel tri-loop voltage error tracking fuzzy logic controller (FLC), to stabilize the stand alone Wind Energy Conversion Scheme (WECS) using an induction generator is presented in this section. The novel Sinusoidal Pulse Width Modulator

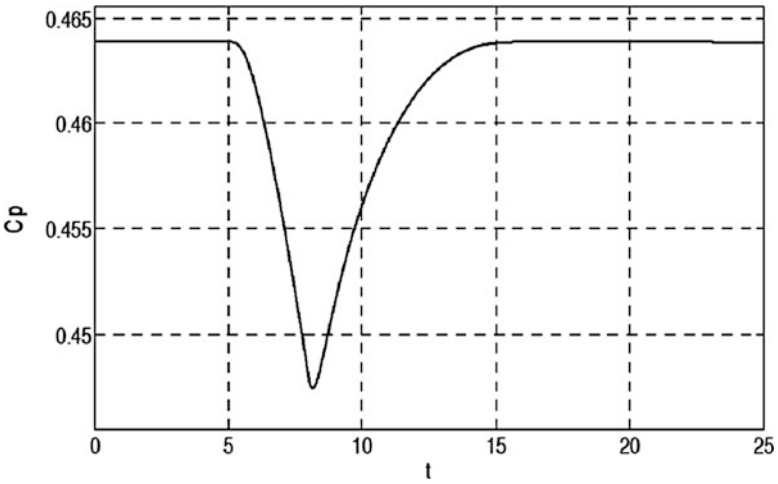


Fig. 5.56 Power coefficient *Cp(λ)* during simulation

(SPWM) switched (AC/DC/AC) converter (diode rectifier and 6-pulse IGBT inverter) interface scheme serves as a combined voltage stabilization regulator and maximum wind energy utilization and enhancement compensator.

5.9.1 Components of Standalone WECS

The standalone WECS connected to the local load bus over a radial transmission line comprising the following main components, as shown in Fig. 5.57.

- Wind turbine.
- Gear box.
- Step up and step down transformers.
- Distribution power lines.
- Induction generator.
- Stabilization interface scheme and stabilization controller.
- The hybrid electric load.

Each component of the proposed WECS shown in Fig. 5.57 is modeled in MATLAB/SIMULINK environment. The hybrid composite linear, nonlinear and motorized loads are shown in Fig. 5.58.

The parameters of the proposed controller are selected by a guided trial and error off-line simulation to ensure the minimum induction load and generator voltage excursion for any large wind and load variation. The standalone WECS sample study system unified AC system model parameters, comprising the induction

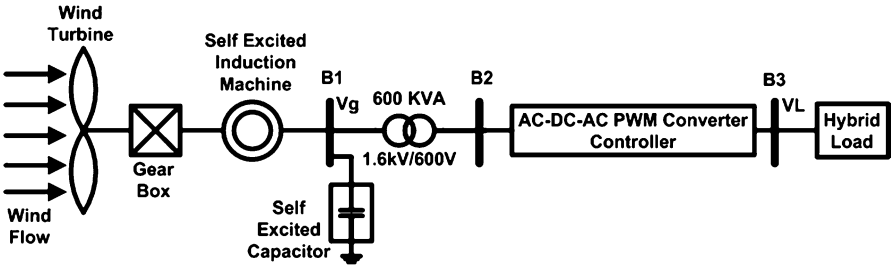


Fig. 5.57 Sample study 600 kVA wind energy conversion scheme

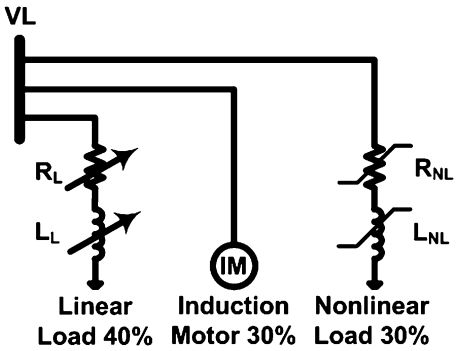


Fig. 5.58 Hybrid composite linear, nonlinear and motorized load model

generator, wind turbine, combined hybrid load, and controller parameters are all given below.

5.9.1.1 Simple Wind Turbine Model (Quasi-static Model)

$$T_W = \frac{1}{2\lambda}\rho A R C_P V_W^2 = \frac{1}{2\omega_W}\rho A C_P V_W^3 = k\frac{V_W^3}{\omega_W}$$

where

ρ is the specified density of air (1.25 kg/m^2)
A is the area swept by the blades
R is the radius of the rotor blades
C_P is power conversion coefficient
λ is the tip speed ratio
ω_W is the wind turbine velocity in rpm
k is equivalent coefficient in per unit (0.745)

Induction Generator

Three phase, two pairs of poles, $V_g = 1.6$ kV (L-L), Sg = 600 KVA, Cself = 150 uF/Phase

$$R_s = 0.016, L_{ls} = 0.06, R_r^{'} = 0.015, L_{lr}^{'} = 0.06$$
$$L_m = 3.5, H = 2, F = 0, p = 2$$

Combined Hybrid AC Load Model (@ V = 1.0 pu)

Linear PQ Load (40 %)

$$P_L = 0.4pu, Q_L = 0.4pu$$

Nonlinear (Voltage-Dependent Type) PQ Load (30 %)

$$P = P_o\left(\frac{V_g}{V_{go}}\right)^{\alpha},\ Q = Q_o\left(\frac{V_g}{V_{go}}\right)^{\alpha}$$
$$P_o = 0.3pu, Q_o = 0.3pu, V_{go} = 1.0pu,$$
$$\alpha = 2 - 3, \beta = 2 - 3\,(Nonlinearity\ \ order)$$

Three Phase Squirrel Cage Induction Motor Inrush Type PQ Load (30 %)

Power: $S_M = 0.3pu$
Stator resistance and leakage inductance: $R_s = 0.0201pu, L_{ls} = 0.0349pu$
Rotor resistance and leakage inductance:$R_r = 0.0377pu, L_{lr} = 0.0349pu$
Magnetizing inductance: $L_m = 1.2082pu$
Pole pairs: 2

Per Unit Base Values Used

S_{base} = 600KVA, V_{base} = 1.6 kV (L-L)

DC-Link RLC Filter Parameters

$$R_f = 0.1\Omega,\ \ L_f = 0.2mH,\ \ C_f = 5000uF$$

Weight Factors

$$\gamma_{vg} = 10, \ \gamma_{vdc} = 10, \ \gamma_{vload} = 0.1$$

SPWM Switching Frequency

$$f_{sw} = 2kHz, \ 6 pulse IGBT \ operation$$

5.9.2 MATLAB/SIMULINK Model

The MATLAB/SIMULINK functional model of full AC study system is given in Fig. 5.59.

The sample WECS standalone scheme was subjected to severe combined sequence of load switching/load variation/load excursion and wind speed variation and gusting. The novel tri-loop dynamic voltage tracking and FLC control scheme is shown in Fig. 5.60. The control signal adjusts the sinusoidal pulse width modulated IGBT six pulse inverter. The system real time dynamic response for a combined load/wind excursion time sequence as follows:

t = 0.03 s Linear Load excursion applied, +30 %
t = 0.04 s Linear Load excursion removed, +30 %
t = 0.05 s Linear Load excursion applied, −30 %
t = 0.06 s Linear Load excursion removed, −30 %
t = 0.07 s Wind Speed excursion applied, −30 %
t = 0.08 s Wind Speed excursion removed, −30 %
t = 0.09 s Wind Speed excursion applied, +30 %
t = 0.10s Wind Speed excursion removed, +30 %

5.9.3 Simulation Results

The WECS dynamic performance is compared for the two cases, with and without the AC/DC/AC PWM converter based on the novel tri-loop dynamic voltage tracking tri-loop FLC. Fig. 5.61 shows the system dynamic response including generator voltage (RMS), load voltage (RMS), DC-link voltage, generator current (RMS), average generator power, the voltage-current two-dimensional phase portraits for the wind energy system controller interface system as shown in Fig. 5.61.

This section discussed a novel low cost dynamic voltage error tri-loop fuzzy logic controller and sinusoidal PWM driven IGBT inverter scheme for stand alone wind energy system. This PWM power converter scheme is extremely effective in ensuring voltage stabilization and enhancing power/energy utilization under severe

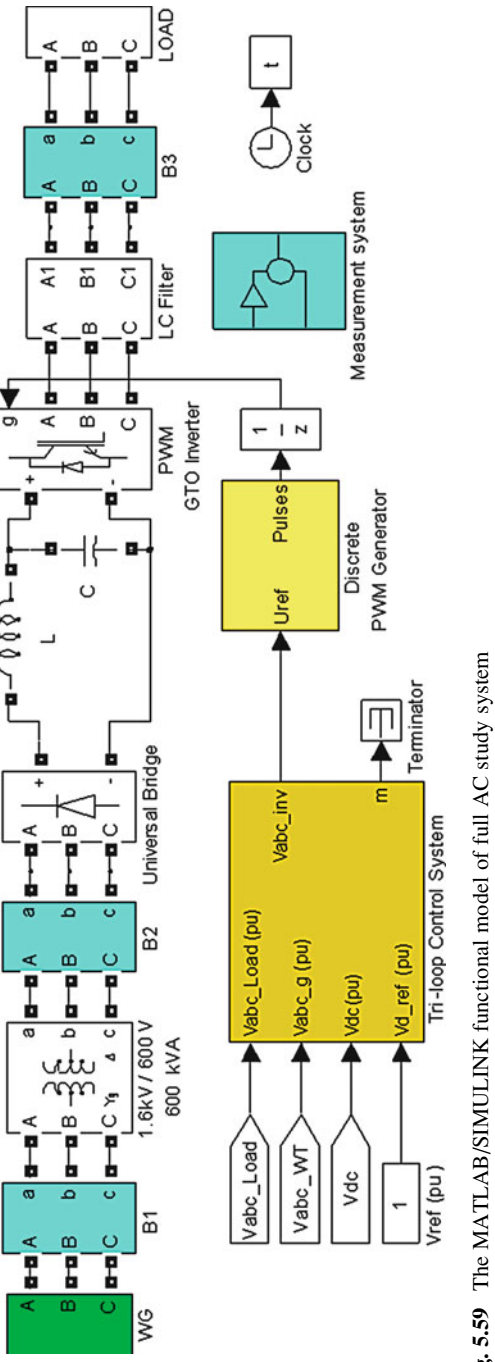


Fig. 5.59 The MATLAB/SIMULINK functional model of full AC study system

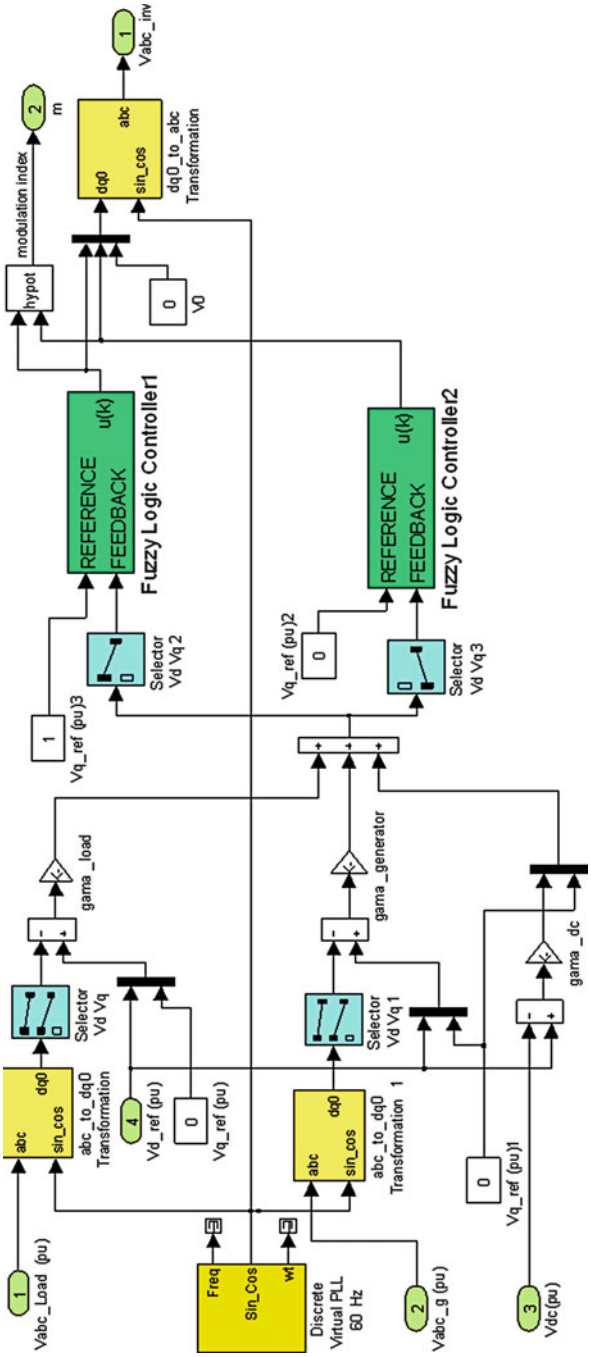


Fig. 5.60 Dynamic tri-loop global voltage error tracking FL controlled scheme for voltage stabilization at generator, load and inverter buses

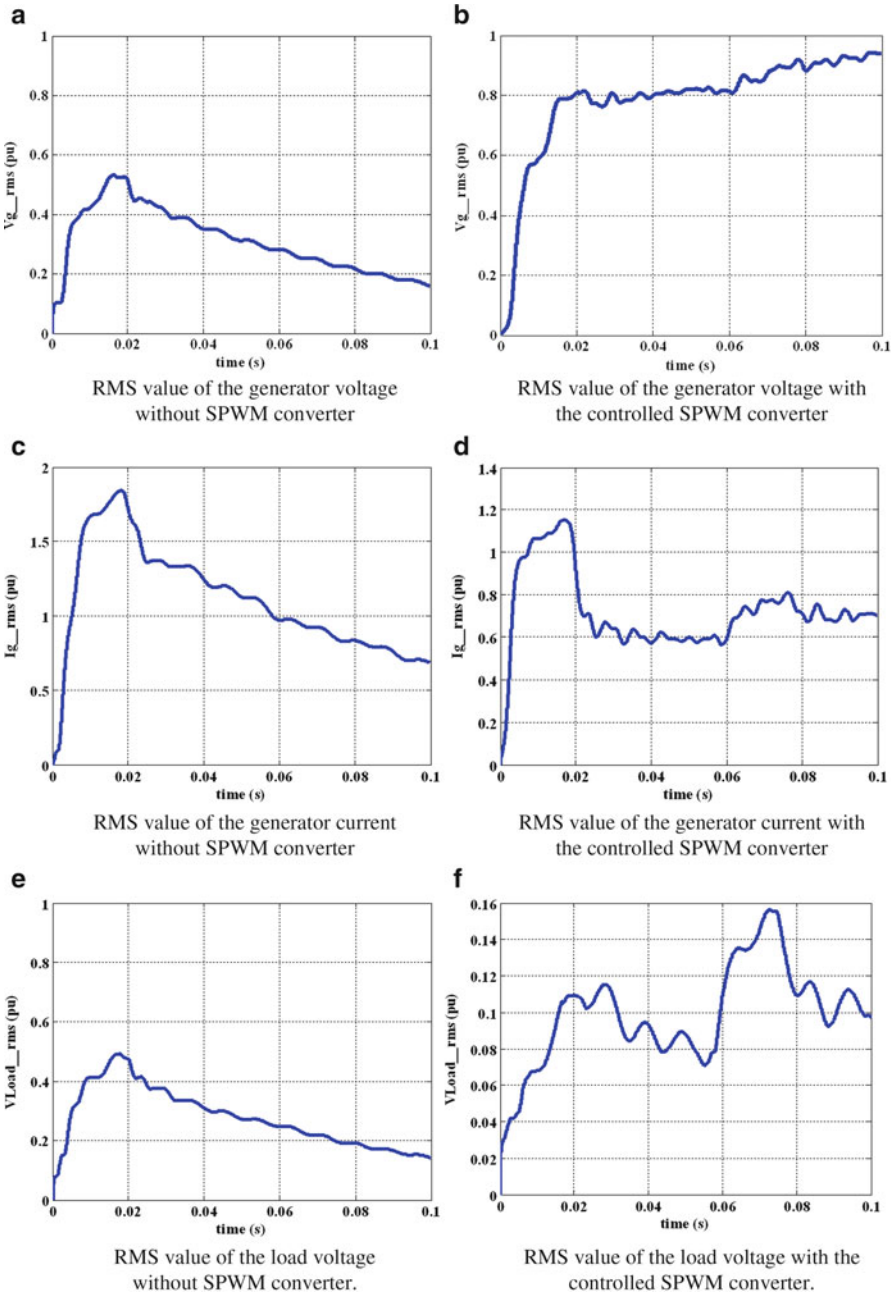
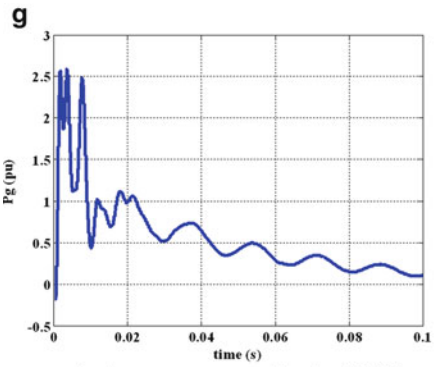
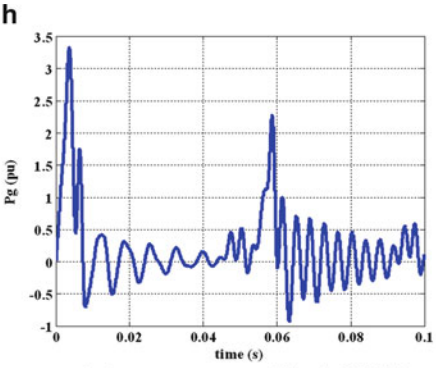


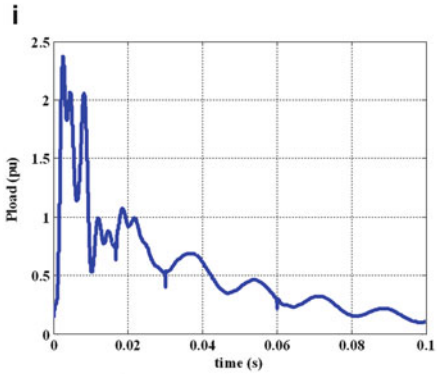
Fig. 5.61 WECS performance without and with the SPWM converter for a combined excursion sequence



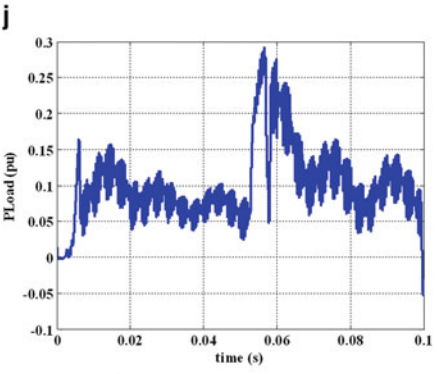
Active power generated by the WECS without SPWM converter.



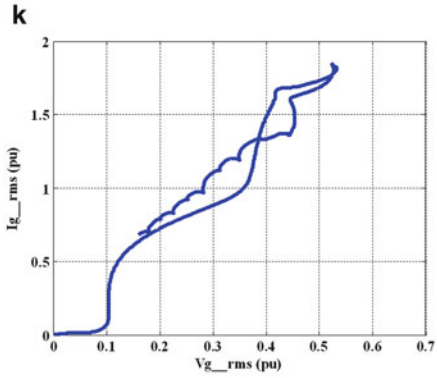
Active power generated by the WECS with the controlled SPWM converter.



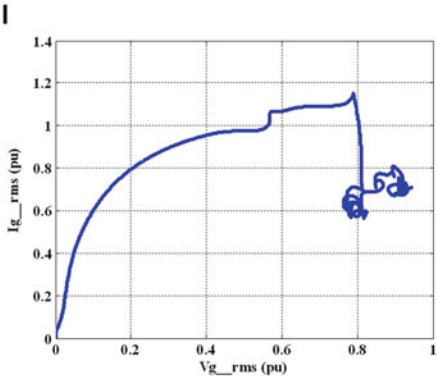
Active power dissipated by the load without SPWM converter.



Active power dissipated by the load with the controlled SPWM converter.



RMS current-voltage trajectory at generator terminals without SPWM converter.



RMS current-voltage trajectory at generator terminals with SPWM converter.

Fig. 5.61 (continued)

load and wind prime mover/wind velocity excursion. A tri-loop dynamic error driven Fuzzy Logic Controller is designed and employed in this application. The use of tri-loop dynamic error signal to the controller ensures that all changes, excursions or variations in WECS, in Loads, and in DC interface system are included in the controller.

5.10 Summary

This chapter reviewed and discussed the recent research, development and trends in the field of wind energy conversion systems based on soft computing tools. A theoretical knowledge based on the methodology involved in applications to wind energy power factor, pitch angle control, MPPT, economic dispatch for wind energy, and SEIG driven WECS based on artificial neural networks, ANFIS, fuzzy logic and genetic algorithms were summarized. MATLAB/SIMULINK models for several practical applications were provided with the simulation results for easy understanding and development. It has been observed that soft computing tools can enhance the efficiency and effectiveness of the operation and maintenance of wind power systems. In addition, the state of the art of soft computing techniques in wind energy conversion systems were provided to serve as guidance for future research work.

Review Questions

1. Develop a MATLAB/SIMULINK model for optimizing the wind blade chord and twist angle using Genetic Algorithm.
2. Explain the procedure involved in Fuzzy logic based Pitch Angle Control. Develop a suitable SIMULINK model and discuss the results.
3. How is wind turbine flicker calculated? Briefly discuss the application of Artificial Neural Network in wind turbine flicker computation.
4. How are ANNs applied to detect and identify faults in Wind Turbine Systems?
5. Develop a SIMULINK model for tuning of wind turbine using PI, and PID controllers using Genetic Algorithms.
6. Develop a DSTATCOM model using SIMULINK and compare the results with a fuzzy based design.

Bibliography

Adzic E, Ivanovic Z, Adzic M, Katic V (2009) Maximum power search in wind turbine based on fuzzy logic control. Acta Polytech Hung 6(1):131–149

AL-Ismail FS, Abido MA (2011) The impact of statcom based stabilizers on power system stability, using intelligent computational optimization approach. Innovative Smart Grid Technologies Asia (ISGT), 2011 IEEE PES, pp 1–13

Amei K, Takayasu Y, Ohji T, Sakui M (2002) Amaximum power control of wind generator system using a permanent magnet synchronous generator and a boost chopper circuit. Proc Power Conv 3:1447–1452

Attia A-F, Soliman H, Sabry M (2006) Genetic algorithm based control system design of a self-excited induction generator. Acta Polytech 46(2):11–22

Belghazi O, Cherkaoui M (2012) Pitch angle control for variable speed wind turbines using genetic algorithm controller. J Theor Appl Inf Technol 39(1):6–10

Brini S, Abdallah HH, Ouali A, Economic dispatch for power system included wind and solar thermal energy. Leonardo J Sci (14):204–220

Chang HC, Liaw CM (2009) Development of compact switched reluctance motor drive for EV propulsion with voltage-boosting and PFC charging capabilities. IEEE Trans Veh Technol 58:3198–3215

Chen Y-M, Liu Y-C, Lin S-H (2003) Double-input PWM DC/DC converter for high/low voltage sources. In: Proceedings of the IEEE international telecommunications energy conference, pp 27–32

Dhal PK, Christober Asir Rajan C (2012) Transient stability improvement using neuro-fuzzy controller design for STATCOM. IEEE – international conference on advances in engineering, science and management (ICAESM – 2012), March 2012, pp 510–515

Goel N, Patel RN, Chacko ST (2010) Genetically tuned STATCOM for voltage control and reactive power compensation. Int J Comput Theor Eng 2(3)

Houck CR, Joins JA.A genetic algorithm for function optimization: a matlab implementation

http://www.ren21.net. Accessed June 2008

Hui J (2008) An adaptive control algorithm for maximum power point tracking for wind energy conversion systems. Department of Electrical and Computer Engineering, Queen's University

Hussein KH, Muta I, Hoshino T, Osakada M (1995) Maximum photovoltaic power tracking: an algorithm for rapidly changing atmospheric conditions. IEE Proc Gener Trans Distrib 142 (1):59

Jianzhong Zhang, Ming Cheng, Zhe Chen, Xiaofan Fu (2008) Pitch angle control for variable speed wind turbines. DRPT2008 6-9. Nanjing China

Lai Y-S, Lin J-C (2003) New hybrid fuzzy controller for direct torque control induction motor drives. IEEE Trans Power Electron 18(5):1211–1219

Lee J-C, Lin W-M, Liao G-C, Tsao T-P (2011) Quantum genetic algorithm for dynamic economic dispatch with valve-point effects and including wind power system. Int J Electr Power Energy Syst 33:189–197

Lin C-T, Lee CSG (1996) Neural fuzzy systems: a neuro-fuzzy synergism to intelligent systems. Prentice-Hall, Upper Saddle River

Luo A, Tang C, Shuai Z (2009) Fuzzy-PI-based direct-output-voltage control strategy for the STATCOM used in utility distribution systems. IEEE Trans Ind Electron 56(7):2401–2411

Mengi OO, Altas IH (2012) Fuzzy logic control for a wind/battery renewable energy production system. Turk J Electr Eng Comput Sci 20(2):187–206

Mienski R, Pawelek R (2004) Shunt compensation for power quality improvement using a STATCOM controller: modeling and simulation. IEEE Proc Gener Trans Distrib 151(2):274

Rasit ATA (2007) Neural prediction of power factor in wind turbines. J Electr Electron Eng 7 (2):431–438

Rasit ATA (2009) An adaptive neuro-fuzzy inference system approach for prediction of power factor in wind turbines. J Electr Electron Eng 1(9):905–912

Saetieo S, Torrey DA (1998) Logic control of a space-vector PWM current regulator for three-phase power converters fuzzy. IEEE Trans Power Electron 13(3):419–426

Shathiand B, Natatajan SP (2009) Comparative study on various unipolar PWM strategies for single phase five level cascaded inverter. Int J Power Electron 2(1):36–50

Soliman HF, Attia AA, Mokhymar SM, Badr MAL. Fuzzy algorithm for supervisory control of self-excited induction generator. JKAU: Eng Sci 17(2):19–40

Valarmathi R, Palaniswami S, Devarajan N (2012) Simulation and analysis of wind energy and photo voltaic hybrid system. Int J Soft Comput Eng 2(2):193–200, ISSN: 2231-2307

Xing-Peng Li, Wen-Lu Fu, Qing-Jun Shi, Jian-Bing Xu, Quan-Yuan Jiang (2013) A fuzzy logical MPPT control strategy for PMSG wind generation systems. J Electron Sci Technol 11(1)

Chapter 6
Hybrid Energy Systems

Learning Objectives
On completion of this chapter, the reader will have knowledge on:

- Basic knowledge on Hybridizing solar PV module with wind energy system and diesel system.
- MATLAB/SIMULINK model of hybrid solar PV and wind energy conversion system.
- Converters used for hybrid solar PV and wind energy conversion system.
- Fuzzy logic controller for hybrid power systems.

6.1 Need for Hybrid Energy System

Instead of utilizing power from wind energy alone or solar energy alone, combining both wind and solar provides a better and reliable system. Both sources together can supply power and if any decrease in power occurs, in any one, the other source can compensate for the first. Also both system together can supply higher loads if required. Whenever the generated power is in excess, it can also be stored in a battery.

For reliable supply of power in remote locations or inaccessible rural areas, it is necessary to design and set up hybrid system, which combined the advantage of two different energy technologies. These could be either two renewable technologies or a renewable and a conventional energy or fossil fuel technology. A hybrid system would ensure that power supply can be maintained at an optimum level during cloudy days for a PV system and at low wind conditions for wind electric generators. According to many renewable energy experts, a small hybrid electric system that combines wind energy system and solar PV technology offers several advantages over either single system. In this chapter solar PV module is hybridized with

© Springer International Publishing Switzerland 2015

S. Sumathi et al., *Solar PV and Wind Energy Conversion Systems*,
Green Energy and Technology, DOI 10.1007/978-3-319-14941-7_6

wind energy system and diesel system. The MATLAB/SIMULINK model is developed for the hybrid combination and the results are presented.

6.2 Hybrid Solar PV/Wind Energy System Using MATLAB/SIMULINK

This section presents the modeling of a solar-wind-hydroelectric hybrid system using MATLAB/SIMULINK. The application applicable for analysis and also simulation of a genuine hybrid solar-wind-hydroelectric system connected to a public grid. Application is built on modular architecture to facilitate quick study of each and every component module impact. Blocks like wind model, solar product, hydroelectric model, energy conversion and load are implemented. The simulation results of model are also discussed. As an exercise, one of the key studies is the behavior of hybrid process which allows employing renewable and adjustable in time powers while providing a continuous supply.

The custom modeling rendering, simulation and analysis of a prominent variety of techniques based on electrical power and to manage these systems, MATLAB was broadened with the RegenSim library. This library was made not only to implement the previously mentioned functions for crossbreed systems based on renewable energy options, but also to interface the components interfacing together with components from different libraries, particularly those of MATLAB SimPowerSystems library. Basic components of RegenSim library tend to be: Wind generators, PV generators, Hydro generation devices and Storage equipment. Each of these elements was basically sculptured on studies regarding mathematical models and possesses associated specific guidelines. The interfacing with MATLAB libraries parts was realized to make a thorough study of the modeled hybrid system by local automatic control systems to the centralized operational supervision system. Apart from the storage device component, each of the remaining three components has, input boundaries, the specific primary source of energy and, interconnection with different sorts of measurement blocks of MATLAB, voltages, currents, powers and energy flows from it, depending on the nature of the customer. The Storage product component was made with the primary, serving as a buffer to store the energy made by renewable sources, looking at the terminals being directly supplied to the DC consumers and the AC through this inverter blocks. On the batteries level can be monitored by making use of measure and present blocks from MATLAB, the shape and state regarding battery charge (SOC), the critical voltage or voltages absorbed by consumers. One of the major advantage of MATLAB software is the fact that libraries offer a variety of basic components intended for modeling according to the problem under consideration. Thus, it is usually modeled for both single phase and three phased consumers with some other powers, nature and also types (e.g.: resistive, capacitive or perhaps inductive consumers).

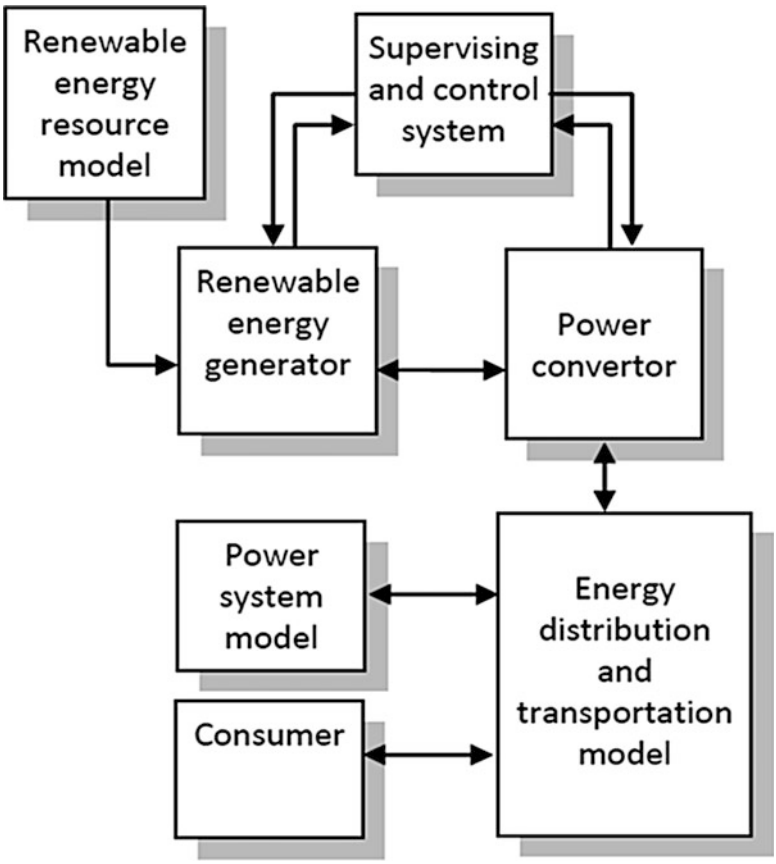


Fig. 6.1 Simulation model architecture based on RegenSim library

6.2.1 Architecture of Solar-Wind Hybrid System

The simulation model was implemented according to the system architecture presented in Fig. 6.1. Employing this architecture we could model any system determined by alternative energy. Several forms of primary sources with various parameters, different energy and power converters with specific parameters, different topologies from the local distribution system and as a final point a variety of consumers with linear or nonlinear characteristic is usually chosen within the simulation model, with respect to the version that is certainly intended as studied.

6.2.2 Implementation Using MATLAB/SIMULINK

With all the RegenSim library blocks an alternative energy hybrid system shown in Fig. 6.2 was developed. As shown, the simulation system contains power

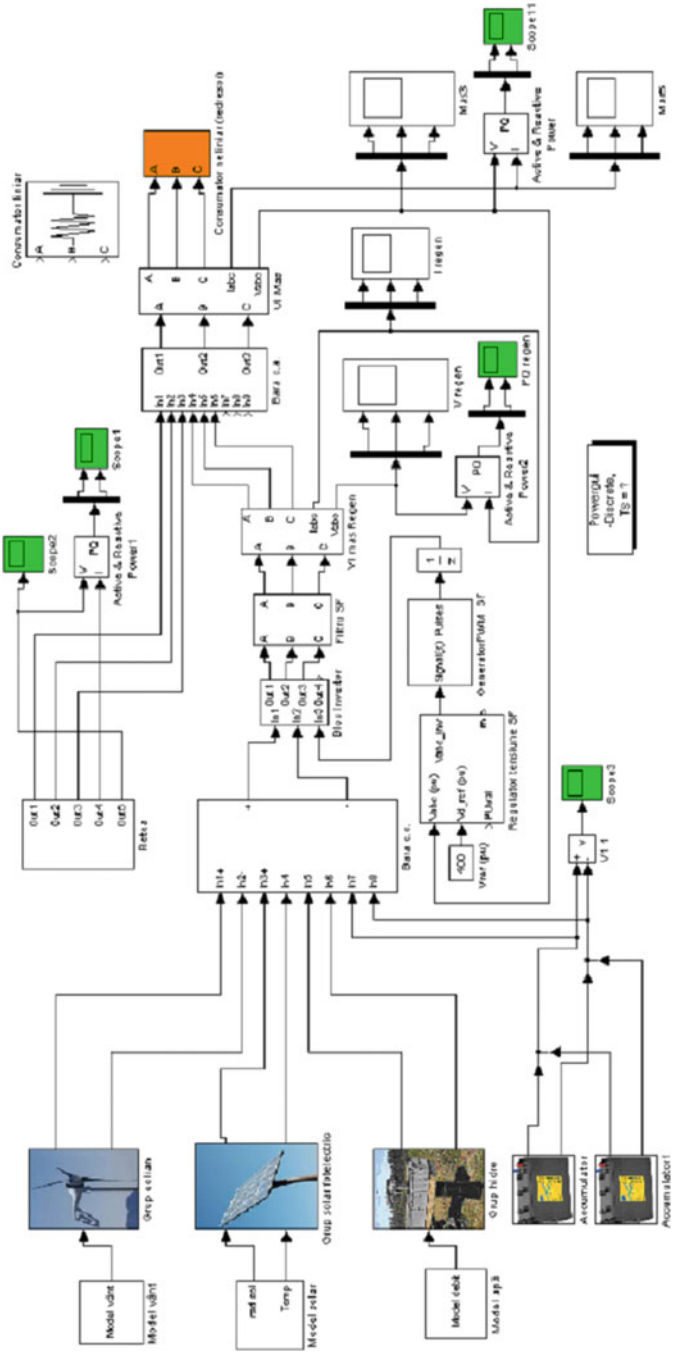


Fig. 6.2 MATLAB/SIMULINK simulation model of a hybrid system based on renewable energy

generation blocks from renewable energy sources including sun, wind or water, battery blocks (providing the energy storage), measurements blocks for electrical parameters (voltage, current, power), inverter blocks (for power generation in DC voltage), voltage regulator block, AC and DC voltage bus bars and AC and DC consumers blocks. It should also be specified that each with the power generation simulated blocks could be sized which enable it to operate independently providing energy within the system, but they might be also interconnected, a correct sizing of the batteries (dependant upon configuration) being mandatory.

The simulation model was primarily suitable for the means analysis of renewable energy resources usage, for its management in the design phase and for the study of issues that may occur as a result of the adopted solution. The adopted solution concerns the management solutions that could be adopted, but additionally the monitoring, control and command of renewable energy sources as well as the consumer. Beyond just the above functions, the model was created and developed to the study of real-time system operation and then for power quality analysis of the studied system. After running with the simulation, power flow graphs among hybrid system determined by renewable sources and the public power network and instantaneous voltages and currents graphics might be obtained.

Inside performed study were considered different configurations and situations of renewable energy sources availability for different sorts of consumers. Within this paper the alternative energy resource availability was taken within the choice of 0.8–3 kWh/m^2 for solar resource, a variable wind speed from 2 to 20 m/s along with a water flow and drainage between 30 and 100 l/s at 50 m level difference through the hydro resource. A linear plus a nonlinear consumer (Pi = 33 kW) were also considered.

6.2.3 Small Domestic Power Grid Based on Hybrid Electrical Power

In Fig. 6.3 is presented the active power variation in the power network. It might be noted that in case the force storage elements are loaded at given parameters from the sustainable energy availability, the device provides about two fifths of the electricity stated in utility network. If the energy storage elements are certainly not loaded at rated capacity it might be noted that, by the point of their fully recharge, energy is absorbed from the public network. In Fig. 6.4 is presented the reactive power variation in the local power network. It might be observed that the sustainable energy hybrid system can be used to produce reactive energy. The most favorable situation would be the use of all alternative energy in addition to all energy storage devices.

In Figs. 6.5 and 6.6 the active and reactive power created by renewable energy sources are presented. It might be noticed that the power generated from alternative energy is utilized for charging the vitality storage devices, with the consumers as well

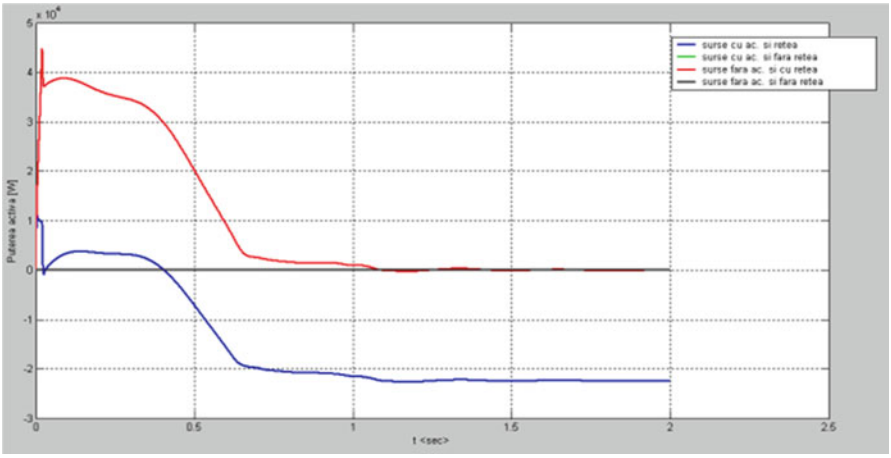


Fig. 6.3 Evolution of active power transit between the hybrid system based on renewable energy sources and the public network

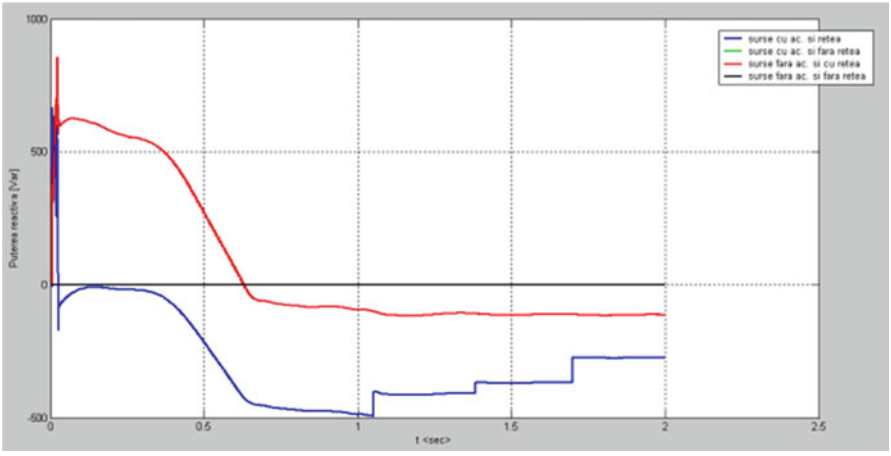


Fig. 6.4 Evolution of reactive power transit between the hybrid system based on renewable energy sources and the public network

as to cover losses plus the surplus is injected to the local public network. When the consumer is isolated power evolution is stabilized following an equivalent constant level in line with consumer power and losses. If consumer is isolated, the presence of reactive power is caused by nonlinear elements utilized in the simulation model: power transformers and power converters determined by electronic switching components. Confirmation for the above is shown in Figs. 6.7 and 6.8 that is definitely the active and reactive power at consumer terminals.

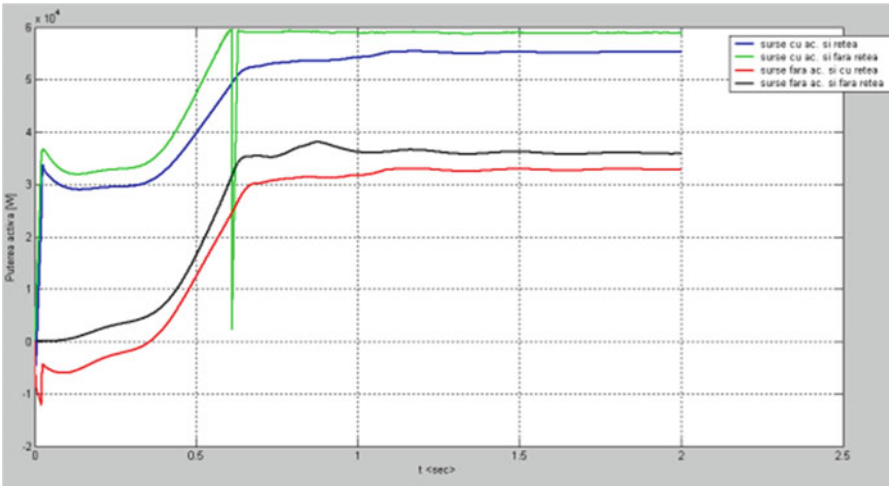


Fig. 6.5 Renewable energy sources active power variation

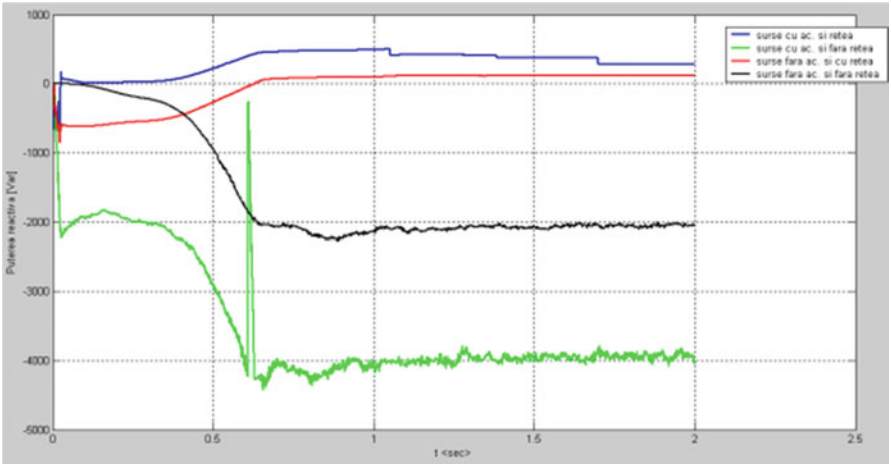


Fig. 6.6 Renewable energy sources reactive power variation

6.2.4 Small Industrial Power System Based on Hybrid Renewable Energy

In practice, individual drives are employed in variable speed drive applications. This drives consists of controlled rectifiers, whose speed varies according to the temperature, this has to modeled. In Fig. 6.9 is presented the active power variation in the local power network. It is usually noted that when the force storage elements are loaded at given parameters through the alternative energy availability, the

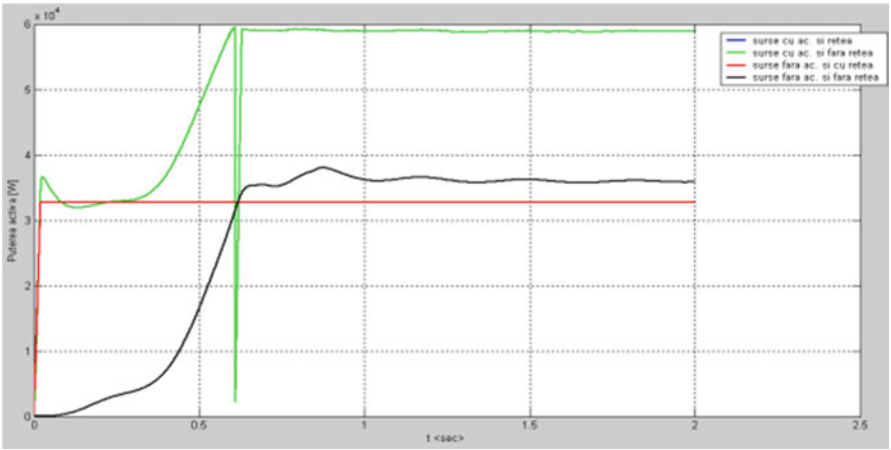


Fig. 6.7 Consumer active power variation

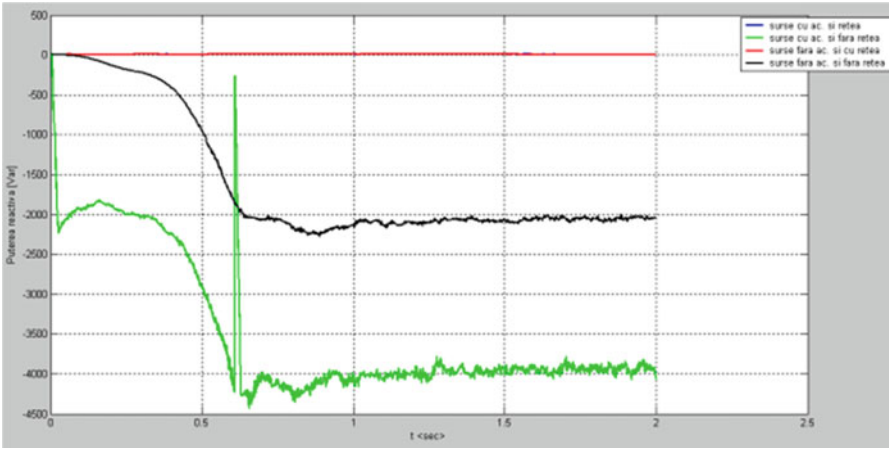


Fig. 6.8 Consumer reactive power variation

machine provides produced energy in the public network. When the energy storage elements are certainly not loaded at rated capacity it might be noted that, at the point when they are fully recharge, energy is absorbed from the public network. In Fig. 6.9 can even be seen the highly nonlinear nature of the consumer. Dark and green characteristics correspond to situation the location where the consumer is isolated.

In Fig. 6.10 is presented the reactive power variation from the power network. It could be observed that the renewable power hybrid system enables to produce reactive energy in the considered cases. In Figs. 6.11 and 6.12 the active and reactive power produced by renewable energy sources are presented. It could be

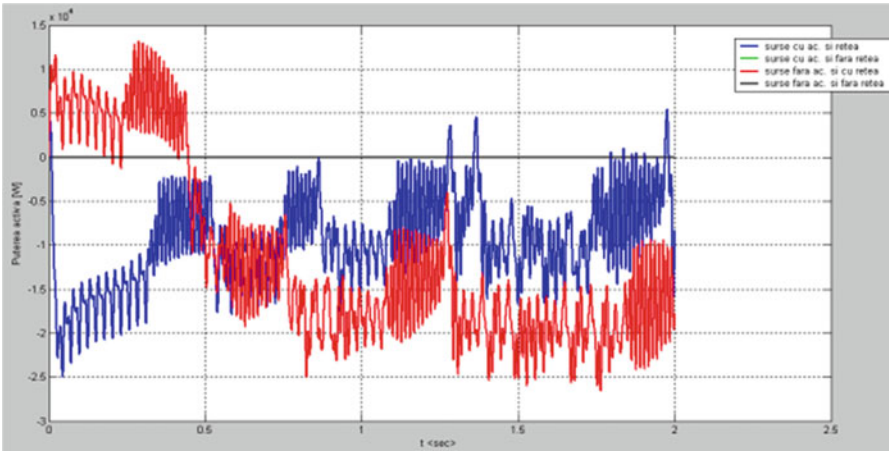


Fig. 6.9 Evolution of active power transit between the hybrid system based on renewable energy sources and the public network

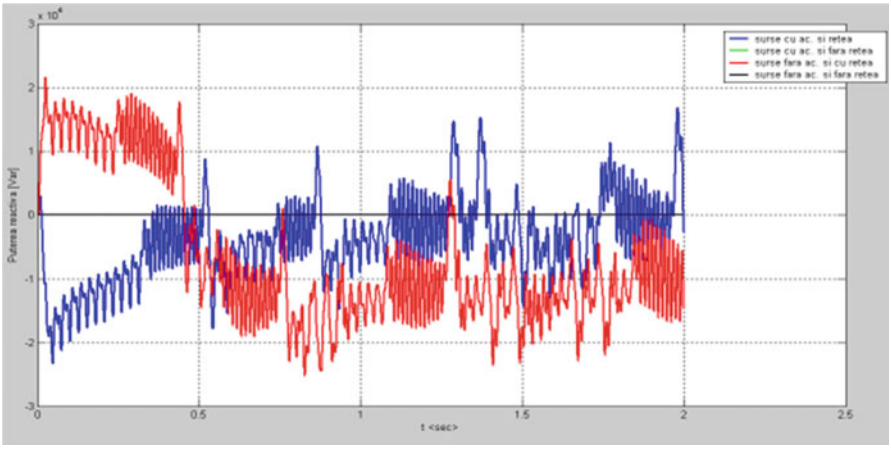


Fig. 6.10 Evolution of reactive power transit between the hybrid system based on renewable energy sources and the public network

seen that the power generated from renewable energy sources is employed for charging the force storage devices, for the consumers or to cover losses and also the surplus is injected to the local public network.

If the consumer is isolated, the presence of reactive power is due to nonlinear elements employed in the simulation model: power transformers and power converters based on electronic switching components, but is usually attributable to the highly nonlinear nature of the consumer as mentioned in Fig. 6.12. Confirmation in

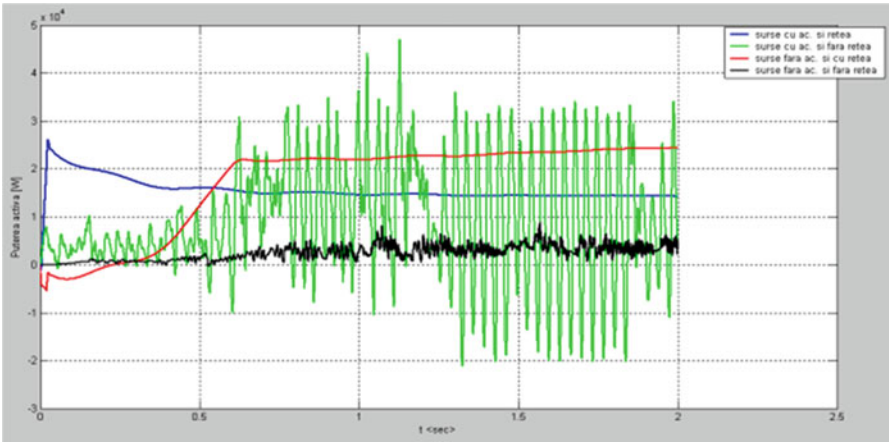


Fig. 6.11 Renewable energy sources active power variation

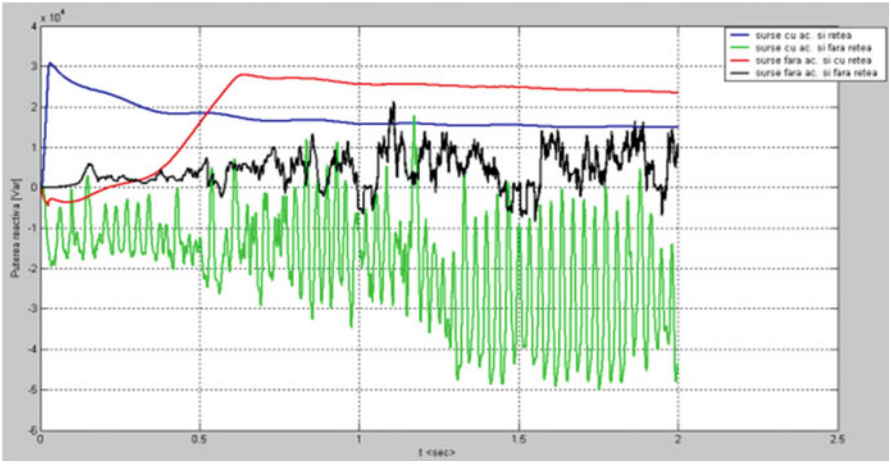


Fig. 6.12 Renewable energy sources reactive power variation

the above is shown in Figs. 6.13 and 6.14 that presents the active and reactive power at consumer terminals.

This section presents a pretense model helpful for the study of small power programs dependant on sustainable energy. To the simulation model advancement an accumulation objects organized in a very new MATLAB/SIMULINK library named RegenSim was created. The realized simulated model in line with the new RegenSim selection is compatible and may be interconnected along with aspects of the dedicated SimPowerSystems library that is used for power techniques functioning, simulation, acting and analysis. The particular simulation model in this particular section is quite useful in the present circumstances allowing research

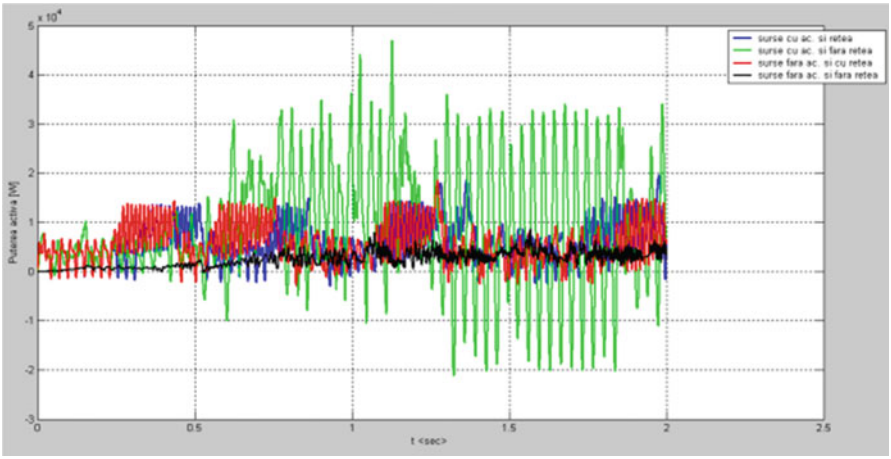


Fig. 6.13 Consumer active power variation

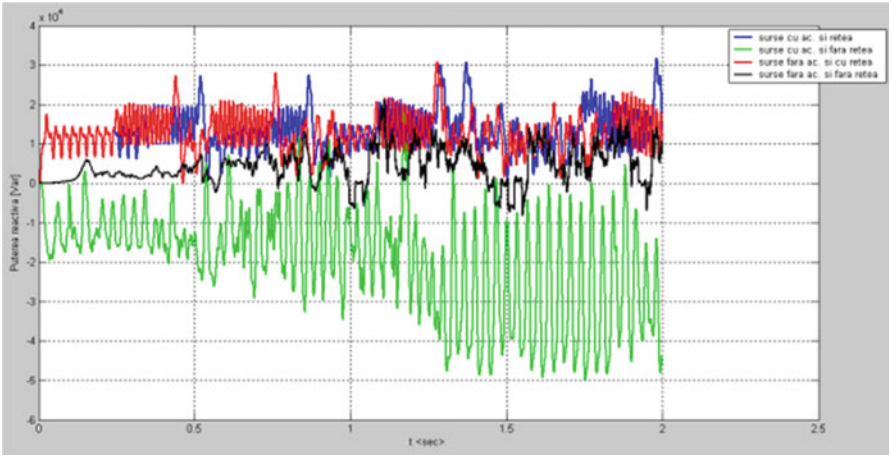


Fig. 6.14 Consumer reactive power variation

considering the identification, any type of usage opportunity as well as the implementation for might systems dependant on renewable energies available within a certain area. In order to exemplify this attribute the Mureş State area was thought to be and performed a work with the appropriateness employing solar, wind along with hydro resources available here. Other significant studies allowed because of the developed simulation product consider steady or passing regimes, using the potential for active and responsive power flowing progress.

6.3 Hybrid Model of Solar PV and Wind Energy System Using Cuk-Sepic Converter

Power supply system all over the world is facing challenging situations where they have to be extremely flexible, reliable and expandable. Existing grids have to be modified due to the growing proportion of distributed and renewable energy sources. Power electronic inverters are the key components to couple different energy conversion systems and to manage their operation. To fulfill the changing demands of the growing smart grid needs, new concepts for inverter design are needed. In this section an innovative concept for future oriented power systems – the modular inverter design – is detailed. A modular inverter design is presented for a modern power system which inputs power from both AC and DC Renewable resources. The Converter is the combination of Cuk-Sepic converters, the input from the source can be either buck or boosted or stabilized at the particular value, the inductor in circuit further provides the function of filter reducing Harmonics. The Inverter is the combination of two kinds of Inverters and it supports both symmetric and asymmetric loads. System works on the presence of both or any one of the Renewable resources, Furthermore; existing systems can be changed, rescaled and expanded easily. The system senses the load (symmetric or asymmetric) and switches between the Inverters (Three leg inverter or three leg inverter with Neutral point) according to the loads.

Due to the increasing awareness about climate change and global warming, the research in the electrical energy sector is geared towards making use of renewable energy sources (RES) for electricity generation. The renewable energy system can be constructed as a stand-alone system for the domestic applications or grid-connected system to supply the AC power to utility system. Both Solar and wind energy sources have great potential for power generation. The Photovoltaic (PV) and fuel cell systems generate DC power which needs to be converted to single- or three-phase AC for utility connection. The wind, micro-turbine systems generate variable frequency AC output which needs to be converted into 50/60 Hz AC for the utility connection.

The Wind and Solar energy systems are highly unreliable due to their unpredictable nature. None of these are available round the clock. Thus hybridizing solar and wind power sources provide a more reliable source of power generation. When any of the two sources is unavailable or insufficient in meeting the load demands, the other energy source can compensate for the difference. The main requirement of power electronic interfaces for the PV systems is to convert the generated DC voltage into a suitable AC for consumer use and utility connection.

6.3.1 Objectives

Several hybrid Wind/PV power systems with Maximum Power Point Tracking (MPPT) control have been proposed earlier. A separate DC/DC buck and buck boost converter connected in fusion with the rectifier stage has been used to perform the MPPT control for each of the renewable energy power sources. Most of the systems uses boost converter for this purpose. In this project, a Cuk-SEPIC converter for grid connected PV/Wind hybrid system has been used. MPPT control of PV source is implemented on Cuk converter. The Cuk-SEPIC fused converters have the capability to eliminate the high frequency current harmonics. So no additional input filters are needed. Fusion of Cuk-SEPIC converter works well for individual as well as for simultaneous operation.

6.3.2 Hybrid Power System

Hybrid Power System (HPS) is to provide an economical and sustainable power for the rural electrification. HPS use a combination of non renewable energy sources like fossil fuel, nuclear energy or a combination of renewable energy sources like solar and wind energy. This is clean and abundantly available in nature. The advantages over non renewable fossil fuel based power generation systems, such as low pollution, high efficiency. The Hybrid power system is classified as follows:

(i) Stand alone/off-grid/islanding HPS (Fig. 6.15).
(ii) Grid connected HPS.

The power units commonly used for PV panels (dc source), Wind Power (WP) and Diesel Generators (ac sources). Batteries are used for storage and backup. The control system for HPS configurations should minimize fuel consumption by maximising power by the variability of the renewable energy, which cause disturbances that can affect the quality of the power delivered to the load. The major constraint in the synchronization of the inverters and ac sources to maintain the voltage and frequency of the system. The undesired harmonics introduced into the system by the use of inverters increases the level of power quality problems. Both buses are connected through a bidirectional converter that permits power flow between two buses. This arrangement increases the system power reliability and supply continuity.

In centralized ac bus Fig. 6.16a, the sources and battery are all installed in one place and are connected to a main bus bar before connecting to the grid. This system is centralized in the sense that the power delivered by all the energy conversion systems and battery is fed to the grid through a single point. In distributed ac-bus Fig. 6.16b, the power sources do need not be installed close to each other, and they do need not be connected to main bus. The sources are connected to the grid

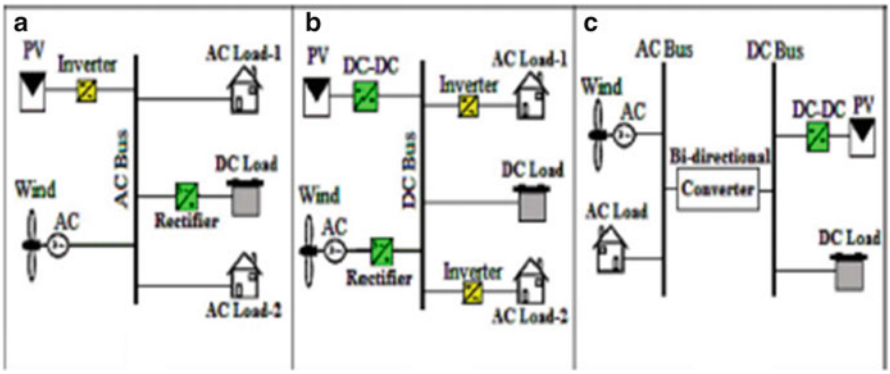


Fig. 6.15 Standalone HPS (**a**) DC sources needed to have an inverters to convert dc to ac before connecting to ac bus. (**b**)AC sources needed to have rectifiers to convert ac to dc before connecting to dc bus. (**c**)The ac and dc sources and loads are connected to ac and dc bus

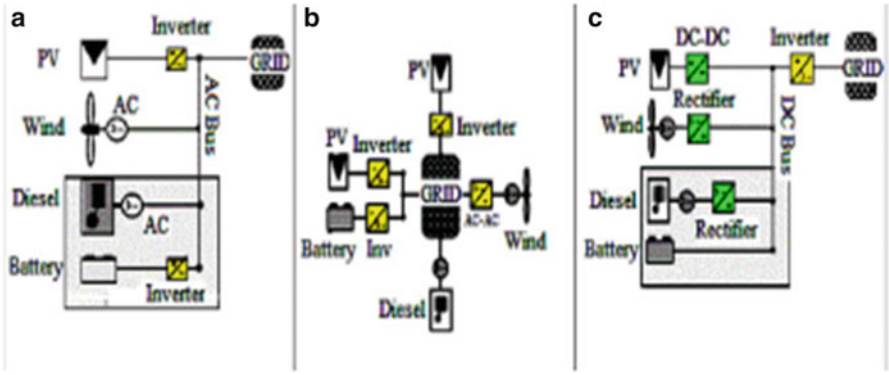


Fig. 6.16 GRID connected HPS

separately. The main drawback of this arrangement is the difficulty of controlling the system. The centralized ac-dc bus Fig. 6.16c utilizes a main centralized dc bus bar. So the energy conversion system that produce ac power, deliver to rectifiers to be converted into dc before connecting to the main dc bus bar. A main inverter takes the responsibility of feeding the ac grid from this dc bus.

6.3.3 Cuk: SEPIC Based Converter on Source Side

Hybridising solar and wind power sources provides a realistic form of power generation. A modular inverter is designed for a modern power system which inputs power from both AC (wind) and DC (solar) Renewable resources. The Inverter is the

combination of two kinds of Inverters and it supports both symmetric and asymmetric loads. System works on the presence of both or any one of the Renewable resources. The features of the presented topology are: (1) the inherent nature of these two converters eliminates the need for separate input filters for PFC (2) it can support step up/down operations for each renewable source (can support wide ranges of PV and wind input); (3) System works on the presence of both or any one of the Renewable resources; (4) individual and simultaneous operation is supported.

One of the inputs is connected to the output of the PV array and the other input connected to the output of a generator. The fusion of the two converters is achieved by reconfiguring the two existing diodes from each converter and the shared utilization of the cuk output inductor by the SEPIC converter. This configuration shown in Fig. 6.17 allows each converter to operate normally individually in the event that one source is unavailable. Figure 6.18 illustrates the case when only the wind source is available. In this case, $D1$ turns off and D2 turns on; the proposed circuit becomes a SEPIC converter. On the other hand, if only the PV source is available, then D2 turns off and $D1$ will always be on and the circuit becomes a Cuk converter as shown in Fig. 6.19.

In both cases, both converters have step-up/down capability, which provide more design flexibility in the system if duty ratio control is utilized to perform MPPT control. If the turn on duration of M1 is longer than M2, then the switching states will be state I, III. Similarly, the switching states will be state I, II, III if the switch conduction periods are vice versa. To provide a better explanation, the inductor current waveforms of each switching state are given as follows assuming that $d2 > d1$; hence only states I, II, III are discussed in this example. In the following, Ii, PV is the average input current from the PV source; Ii, W is the RMS input current after the rectifier (wind case); and Idc is the average system output current.

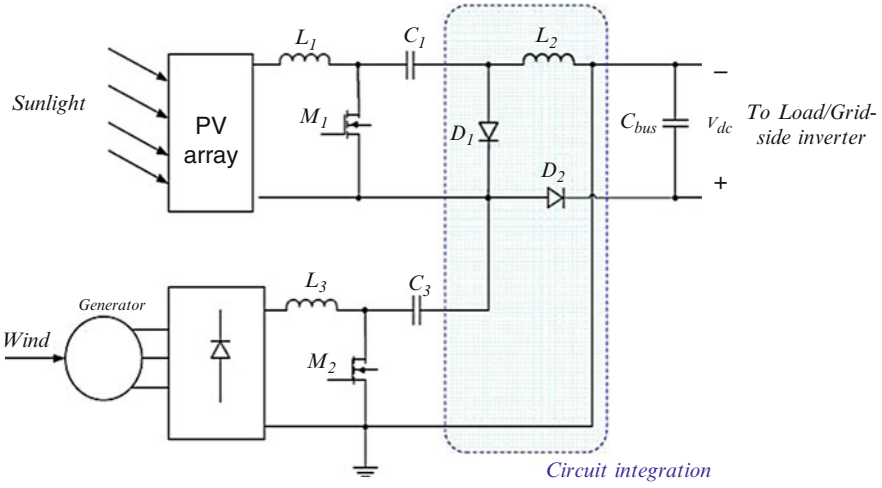


Fig. 6.17 A system diagram of the proposed rectifier stage of hybrid energy system

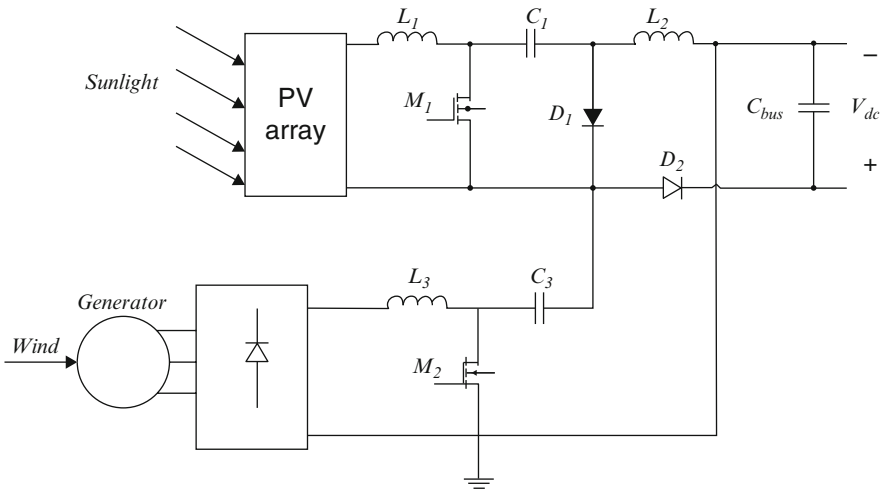


Fig. 6.18 SEPIC converter (wind source available)

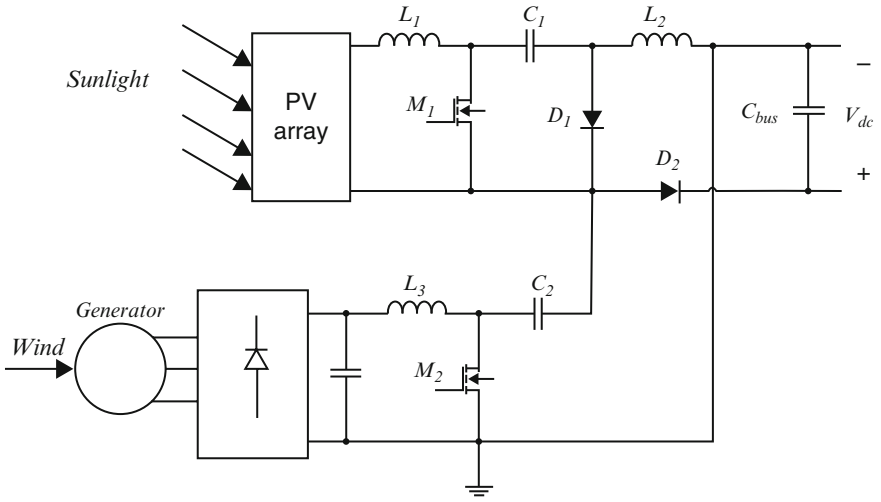


Fig. 6.19 CUK converter (PV source available)

State I (M_1 on, M_2 on)

$$i_{L1} = I_{i,PV} + \frac{V_{PV}}{L_1}t \qquad 0 < t < d_1 T_s$$

$$i_{L2} = I_{dc} + \left(\frac{v_{c1} + v_{c2}}{L_2}\right)t \qquad 0 < t < d_1 T_s$$

$$i_{L3} = I_{i,W} + \frac{V_W}{L_3}t \qquad 0 < t < d_1 T_s$$

State II (M_1 off, M_2 on)

$$i_{L1} = I_{i,PV} + \left(\frac{V_{PV} - v_{c1}}{L_1}\right)t \qquad d_1 T_s < t < d_2 T_s$$

$$i_{L2} = I_{dc} + \frac{v_{c2}}{L_2}t \qquad d_1 T_s < t < d_2 T_s$$

$$i_{L3} = I_{i,W} + \frac{V_W}{L_3}t \qquad d_1 T_s < t < d_2 T_s$$

State III (M_1 off, M_2 off)

$$i_{L1} = I_{i,PV} + \left(\frac{V_{PV} - v_{c1}}{L_1}\right)t \qquad d_2 T_s < t < T_s$$

$$i_{L2} = I_{dc} - \frac{V_{dc}}{L_2}t \qquad d_2 T_s < t < T_s$$

$$i_{L3} = I_{i,W} + \left(\frac{V_W - v_{c2} - V_{dc}}{L_3}\right)t \qquad d_2 T_s < t < T_s$$

6.3.4 Model for Hybrid Wind and Solar Power Plant

The model of a hybrid wind and solar power plant is shown in Fig. 6.20.

6.3.5 Three Phase Uncontrolled AC-DC Bridge Rectifier

The three-phase AC-DC rectifier using six diodes is shown in Fig. 6.21. The diodes are arranged in three legs. Each leg has two series connected diodes. Upper diodes D1, D3, D5 are the positive group of diodes. The lower diodes D2, D4, D6 are the negative group of diodes. The positive group of diodes are conducted when the supply voltage is most positive anode. The negative group of diodes are conducted when the voltage is most negative anode. The output waveforms for the AC-DC bridge rectifier are shown in Figs. 6.22 to 6.24.

Conduction of Positive Group Diodes

Diode D1 conducts during the interval $\omega t = 30^\circ$ to 150°.
Va is more positive than the voltages Vb,Vc
Diode D3 conducts during the interval $\omega t = 150^\circ$ to 270°.
Vb is more positive than compared to Va,Vc
Diode D5 conducts during the interval $\omega t = 270^\circ$ to 390°.
Vc is more positive than the voltages Va,Vb

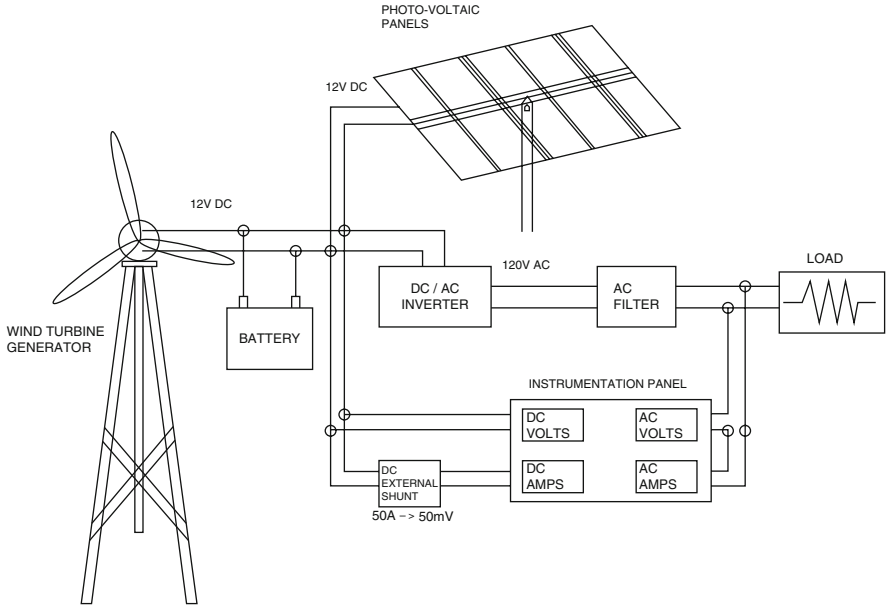


Fig. 6.20 Model representation of hybrid wind and solar power system

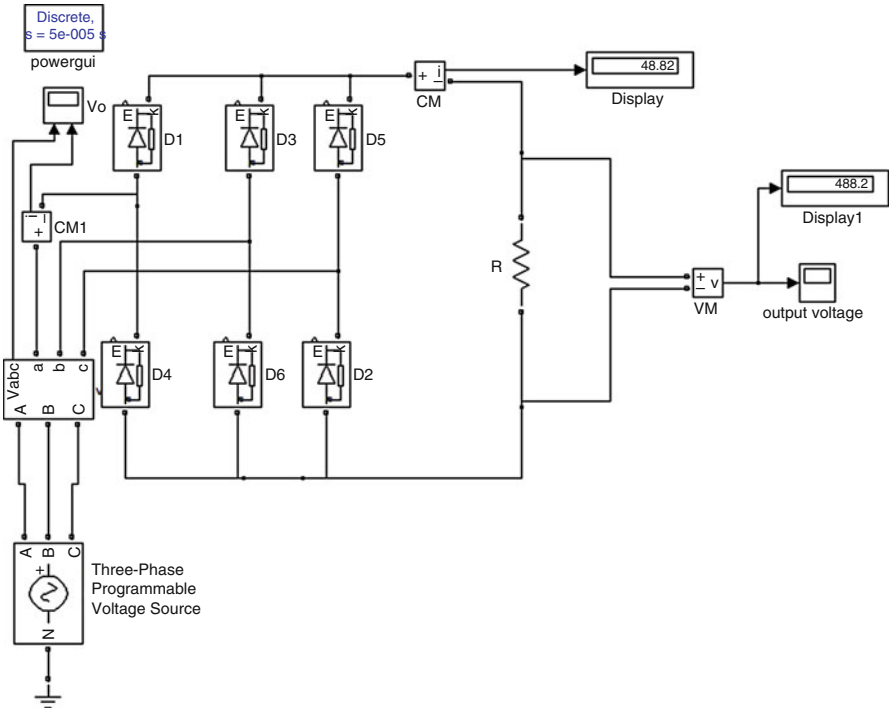


Fig. 6.21 Three phase uncontrolled AC-DC rectifier using MATLAB

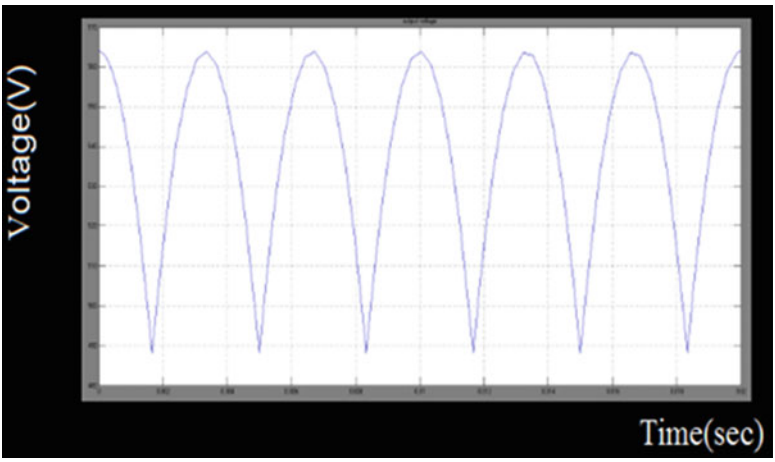


Fig. 6.22 Output voltage waveform for AC-DC bridge rectifier

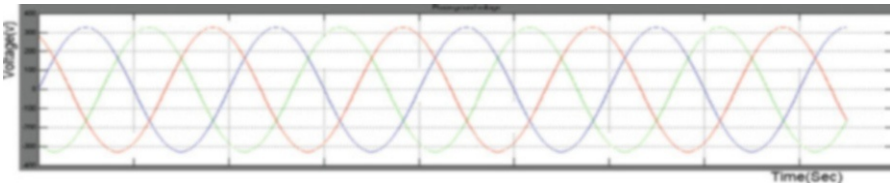


Fig. 6.23 Phase to ground voltage waveform for AC-DC bridge rectifier

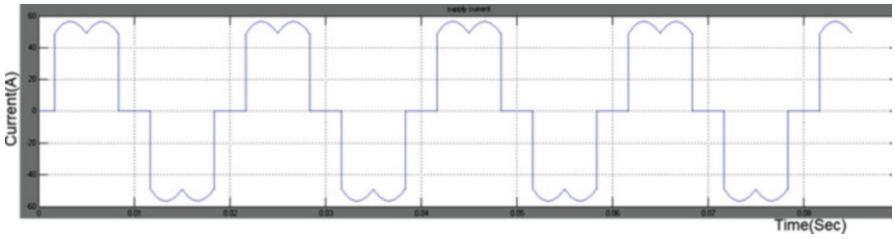


Fig. 6.24 Supply current waveform for AC-DC bridge rectifier

Conduction of Negative Group Diodes

Diode D2 conducts during the interval $\omega t = 90^\circ$ to 210°.
Vc is most negative than the voltages Vb,Va
Diode D4 conducts during the interval $\omega t = 210^\circ$ to 330°.
Va is more negative than compared to Vb,Vc
Diode D6 conducts during the interval $\omega t = 330^\circ$ to 450°.
Vb is more negative than the voltages Va,Vc

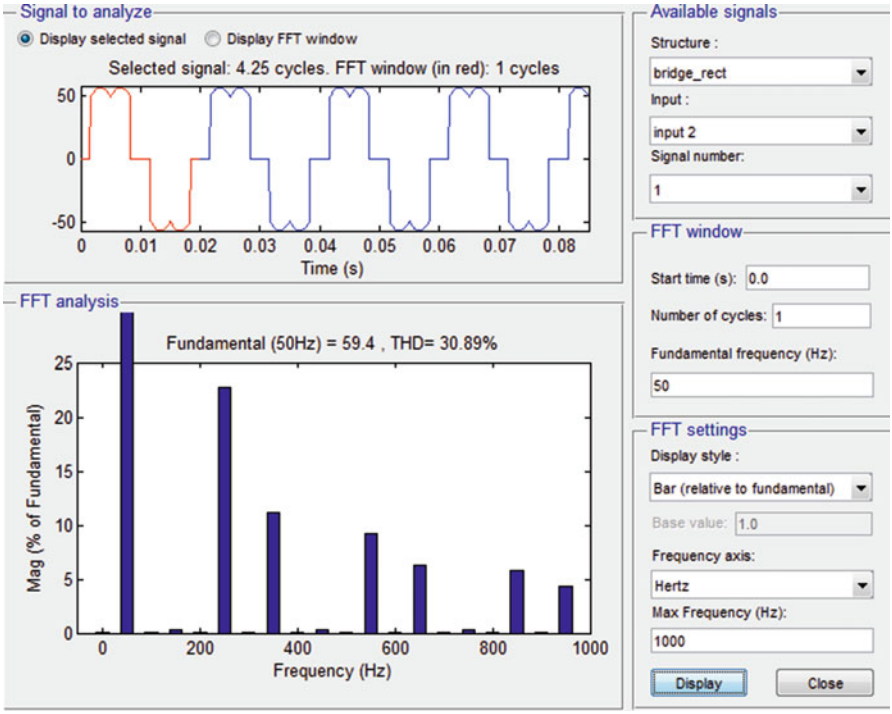


Fig. 6.25 THD analysis for AC-DC bridge rectifier

6.3.6 Total Harmonic Distortion

The first and foremost power quality parameter is the Total Harmonic Distortion (THD). The as the ratio of the sum of the squared individual harmonic amplitudes to the fundamental frequency (or) the root mean square (RMS) value of the total harmonics of the signal, divided by the RMS value of its fundamental signal. The signal can be a measured voltage or current as shown in Fig. 6.25.

6.3.7 Test Simulation and Results

The MATLAB/SIMULINK model of the wind power system using a permanent magnet synchronous machine is shown in Fig. 6.26. The parameters such as generator speed, pitch angle, wind speed, and the solar power system are set according to Table 6.1. Figure 6.27 represents the voltage waveform of the wind power model. The MATLAB/SIMULINK model of the solar power system, the parameters and their settings and the output voltage waveform are shown in Fig. 6.28, Table 6.2 and Fig. 6.29 respectively. In this hybrid model a cuk-sepic converter is used and its MATLAB/SIMULINK model is provided in Fig. 6.30. Table 6.3 provides the parameters and their settings for the cuk-sepic converter.

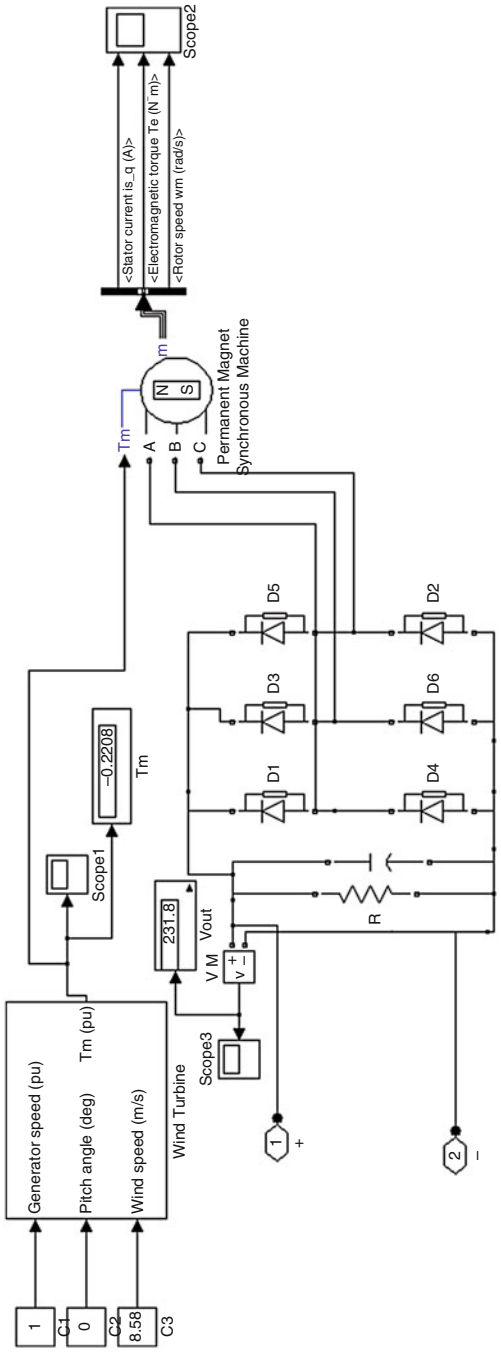


Fig. 6.26 Wind power system using MATLAB

Table 6.1 Parameters used in wind power system

Sl. No.	Parameters	Description
1	No. of bridge arms	3
2	Generator speed	1 (pu)
3	Pitch angle	0
4	Wind speed	8.58 (m/s)
5	Resistor	1k (Ω)
6	Capacitor	1000e-6 (F)

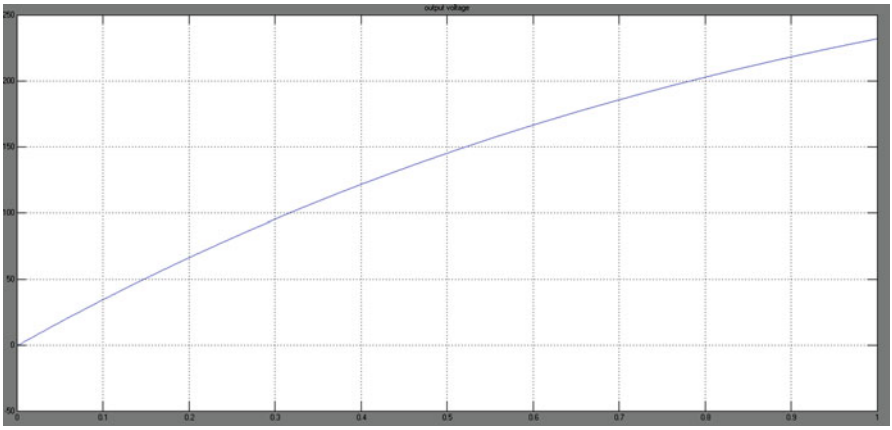


Fig. 6.27 Output voltage waveform for wind power system

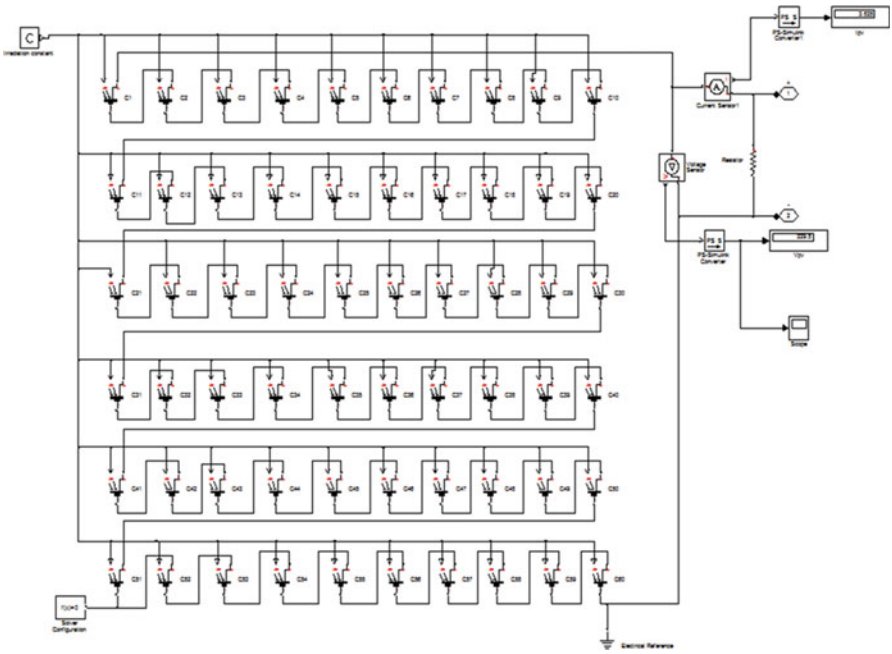


Fig. 6.28 Solar power system using MATLAB

Table 6.2 Parameters used in solar cell

Sl. No.	Parameters	Description
1	Short circuit current (Isc)	7.65 (A)
2	Open circuit voltage (Voc)	3.86 (V)
3	Irradiance (Iro)	1,000
4	Quality factor (N)	7.5
5	Resistor (R)	60 (Ω)

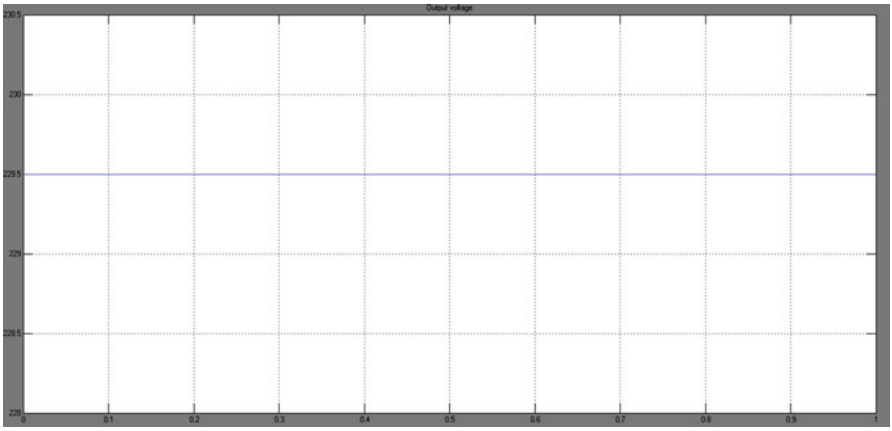


Fig. 6.29 Output voltage waveform for solar power system

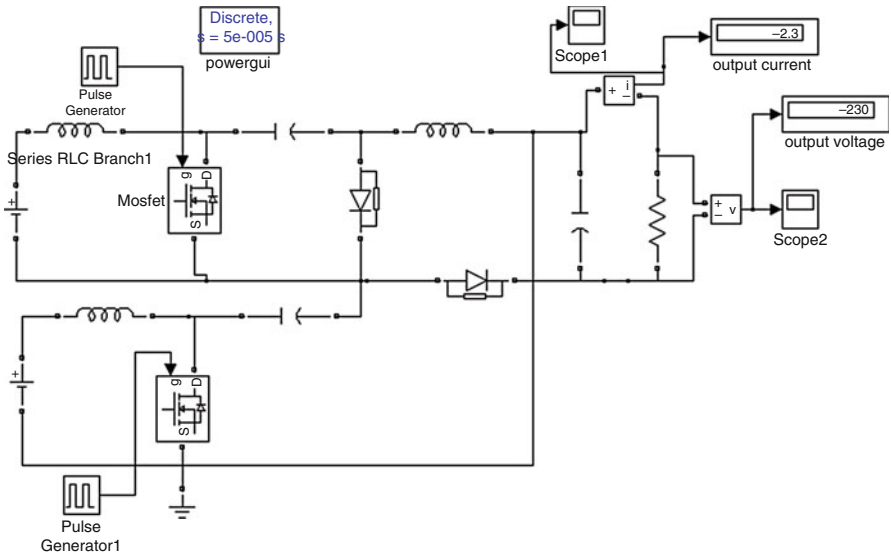


Fig. 6.30 Cuk-SEPIC converter

Table 6.3 Parameters used for cuk-SEPIC converter

Sl. No.	Parameters	Description
1	Pulse generator	–
2	Power electronic device	MOSFET, DIODE
3	Inductor	218e-6 (H)
4	Capacitor	1000e-6 (F)
5	Resistor	100 (Ω)

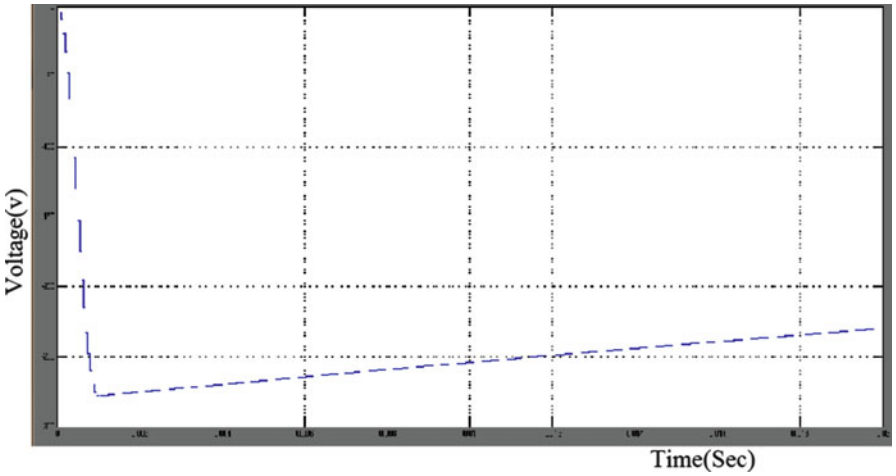


Fig. 6.31 Output voltage waveform for cuk-SEPIC converter

Here the two inputs are shown as taken from a dc source of 230 V each, but in practical condition they are the outputs from the wind and the solar which is shown in Figs. 6.31 and 6.32. In order to get the harmonics free output various carrier modulation techniques such as multiple pulse width modulation and single pulse width modulation is used in the inverter in the power system.

Thus the hybrid wind and solar power system is successfully done and the outputs are verified. The topology allows the two sources to supply the load separately or simultaneously depending on the availability of the energy sources. The output voltage obtained from the hybrid system is the sum of the inputs of the Cuk and SEPIC converters. Two PV arrays each of 5 kW is simulated in MATLAB/SIMULINK. PV 1 is the input to the Cuk converter and PV 2 is the input to the SEPIC converter. The converters are fused together by reconfiguring the two existing diodes from each converter and the sharing the Cuk output inductor by the SEPIC converter. This configuration allows each converter to operate individually in the event that one source is unavailable. MPPT has been realized to extract maximum power from PV source using perturb and observe (P&O) method.

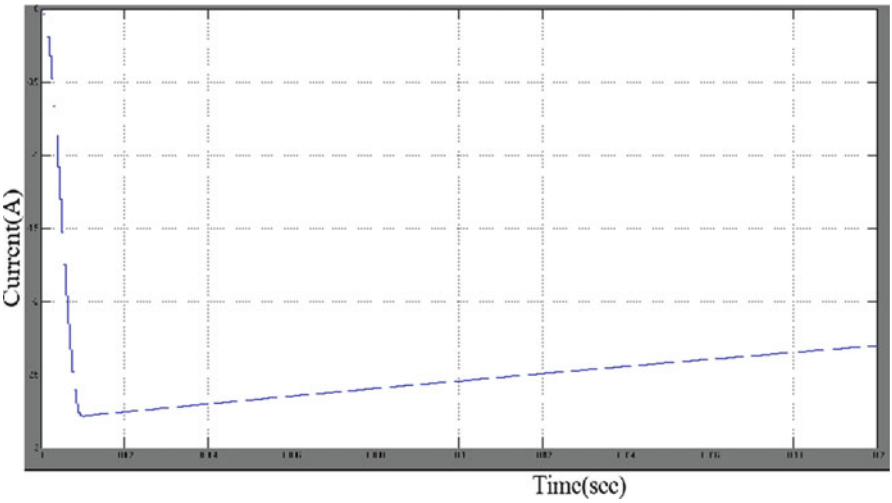


Fig. 6.32 Output current waveform for cuk-SEPIC converter

6.4 Hybrid Model of Solar PV and Diesel Energy System

6.4.1 Need for Solar PV Diesel Hybrid System

Over several areas of the world, power grids are either inadequate or non-existent. Due to this, industrial consumers usually ensure the availability of power all time using diesel gensets. Worldwide statistics have shown that 500 GW of power are generated from diesel gensets for electricity in industrial companies. In addition, fuel costs for the gensets continue to increase rapidly, due to the rising price of diesel. Moreover, if fuel has to be transported to remote regions, then the effective costs increase even more as a result of the necessary storage. In contrast, the cost for PV system has decreased more than 50 % during the last 5 years, hence proving to be the most economical alternate energy for remote regions throughout the world. Thus is it sensible to combine PV and diesel systems so that solar irradiation – which is both abundant and free – can profitably be used as an energy source in industrial applications. Besides, nearly 450,000 l of diesel can be saved per year and significantly reduce CO_2 emissions while using hybrid combination.

6.4.2 Photovoltaic Diesel Hybrid System

A "hybrid" is one approach that is modeled by combining two different components that develop the same or maybe similar results. A photovoltaic diesel hybrid system a mix of both system ordinarily is made up of PV system, diesel gensets and intense

management to be sure that the amount of solar energy fed into the technique exactly matches the demand at that instant.

6.4.2.1 Working

Fundamentally, the Photo voltaic system complements the diesel gensets. It might supply additional strength when loads are high or minimize the genset to minimize its fuel use. From the potential, excess energy may optionally be kept in batteries, making this practical for the actual hybrid system to utilize more solar might even at night time. Intelligent management of various system components guarantees optimal fuel economic climate and minimizes CO_2 emissions.

6.4.2.2 Advantages

In contrast to power supply systems using diesel gensets, and despite their higher initial cost, PV systems can be amortized in as little as 4–5 years, depending on the site and system size, and they have low operating costs.

In addition, PV systems are flexible and can be expanded on a modular basis as the energy demand grows. Compared to pure genset systems, a photovoltaic diesel hybrid system provides numerous advantages:

- Lower fuel costs.
- Reduced risk of fuel price increases and supply shortages, thanks to optimized planning.
- Minimal CO_2 emissions (protects the environment and facilitates CO_2 certificate trading).

6.4.3 Components of the Photovoltaic Diesel Hybrid System

6.4.3.1 PV Inverters

Inverters would be the central components and are designed specifically for use in weak utility grids, they may be well suited for high profile and frequency fluctuations. In addition they remain extremely productive in harsh ambient conditions, including heat, moisture and salty air, a few. A centralized PV system contains one string right into a central point, where DC is converted to alternating electric current. In a decentralized PV system, the PV power is put into many strings, which can be converted to AC by a few inverters. The selection between a centralized or decentralized system is dependent upon many factors. Both system installation costs and operating costs have to be considered. One example is, maintenance work on a decentralized strategy is not complicated, even in

inaccessible areas. If service is needed, local electricians can replace individual inverters. However, remote monitoring is very simple for just a centralized system structure.

6.4.3.2 PV Array

The solar energy is generated inside PV modules, which can be placed on the soil or on the roof, dependant upon local conditions. Inverters chosen must work with all PV module types and technologies available in the marketplace.

6.4.3.3 Diesel Genset

In grid-remote regions, pure diesel systems often provide the energy for industrial applications. They constitute the local grid, ensuring a constant power supply to all connected users. Because the gensets require a constant fuel supply, they are often the system's highest operating cost. In regions with weak utility grids, diesel gensets often serve as a backup during grid power outages.

6.4.3.4 Genset System House

The Genset consists of the monitoring and control systems required for the working of the diesel gensets. The genset system home is the central terminal and point of common coupling.

6.4.3.5 Optional Storage Batteries

In order to increase the efficiency of the entire energy supply system, it is necessary to include a storage battery. During darkness, when solar irradiation is insufficient, the storage battery supplies the required energy, ensuring optimal hybrid system operation.

6.4.3.6 Industrial Loads

Application-specific load profiles, such as heavy-duty industrial loads for mining or processing raw materials as well as for agricultural use, are generally characterized by loads with high starting currents and widely fluctuating load curves. Intelligent system management ensures that generation and load are perfectly matched. It achieves constant system stability by reacting quickly to generation and load performance spikes, such as when a conveyor belt is turned on.

For industrial, large-scale loads in remote regions, complementing diesel gensets with photovoltaics is the ideal solution under the following conditions:

1. When the effective cost of diesel increases.
2. When intelligent communication between the genset and PV systems facilitates demand-oriented use of PV power.
3. When local solar irradiation conditions allow the use of PV.

6.4.4 MATLAB/SIMULINK Model of Solar PV/Diesel Hybrid System

The hybrid model of solar PV and Diesel generator system is implemented using MATLAB/SIMULINK as shown in Fig. 6.33. The subsystem of the diesel generator and diesel engine are shown in Figs. 6.34 and 6.35. The user can simulate the model and analyze the results in terms of output voltage Va.

Photovoltaic diesel hybrid systems (MATLAB model is shown in Fig. 6.36) can be amortized especially quickly in sunny regions, with little or no grid access. For industries such as mining, raw material processing, agriculture (such as flower farms and water desalinization systems), and tourism (facilities with a high energy demand), low power generation costs, quick operational readiness, maximum reliability and availability are fundamental. The environmental benefits are also convincing: CO_2 emissions and noise pollution are significantly reduced, minimizing the environmental impact.

6.5 Fuzzy Logic Controller for Hybrid Power System

The wind and solar among the renewable resources are the most preferred option as they are readily available at all places and anyone can utilize it easily. Combining both the wind and solar forms a better option. This is because, if even one resource

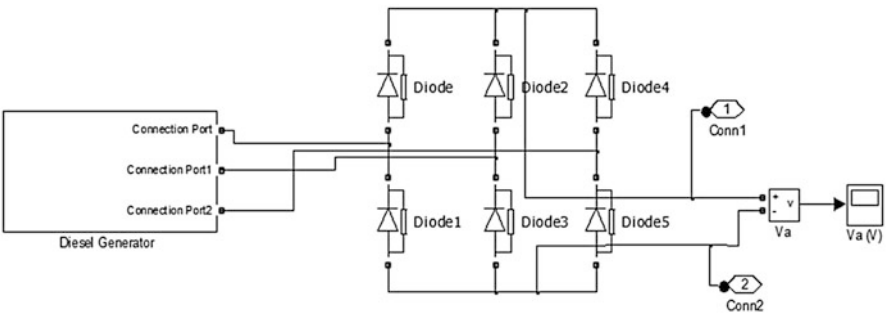


Fig. 6.33 MATLAB/SIMULINK model of diesel generator

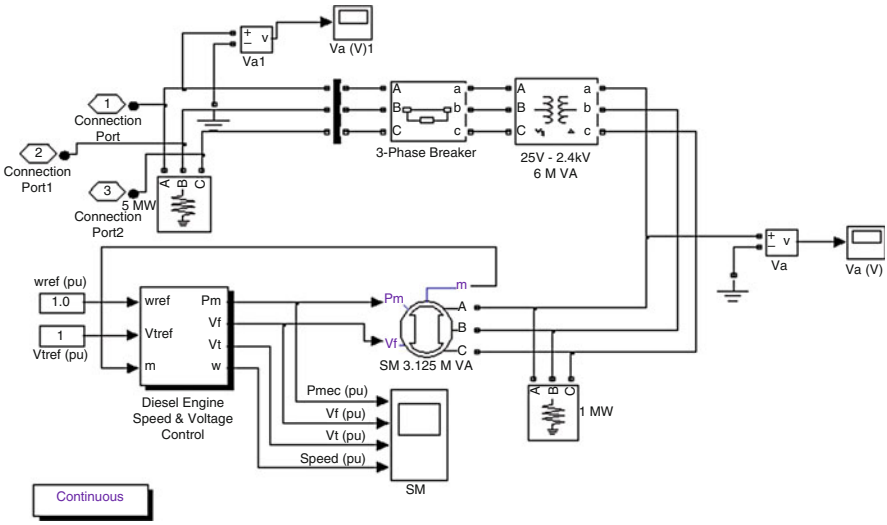


Fig. 6.34 Subsystem of diesel generator

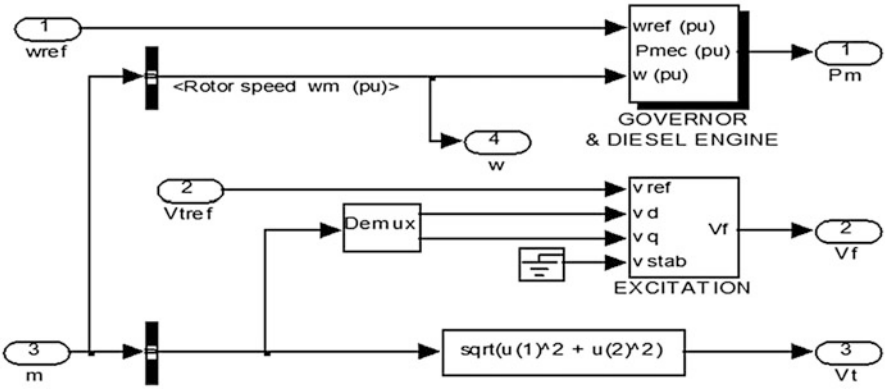


Fig. 6.35 Subsystem of diesel engine

becomes less, we can manage the system with the other resource. But still the hybrid wind and solar energy system also requires a backup, as decrease in both the resources at the same time may happen. Usually a constant reliable source of supply is required with the renewable energy sources. The system can operate well on wind and solar energy and when there is a insufficient supply of wind and solar power, the batteries can provide power to the system.

Multi-source HPS with proper control has a higher potential for providing better quality and more reliable power to utilities than a system based on a single resource.

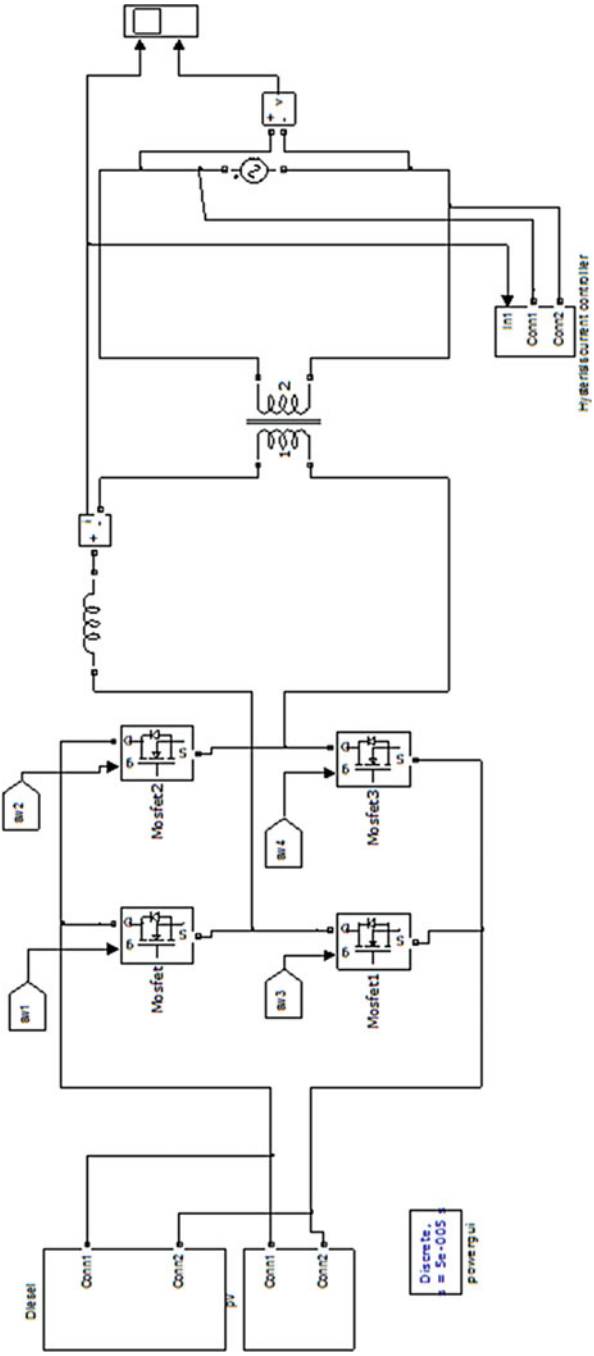


Fig. 6.36 Solar PV and diesel hybrid system

The hybrid system can be utilised to power individual domestic loads and the industries that require more power could be supplied from power stations. The wind generates an AC and a solar generates a DC. Therefore we need to convert any one power to the other so as to interconnect them. Here wind generated AC power is converted to DC with the help of rectifier and paralleled with solar energy system. Converting AC to DC is more preferred when boosting the voltage.

For any system there is a need of a controller. Controller is required so that the system becomes more reliable and stable. There is always a possibility that the voltage in the system may be fluctuating. Hence maintaining a constant voltage and frequency is required and hence a controller is required. The most commonly used controller is the Proportional Integral Derivative (PID) controller or a Proportional Integral (PI) control. But after the advent of fuzzy logic, FLC is preferred nowadays. FLC is compared to the conventional controllers are cheaper to develop and also cover a wider range of operating conditions. FLC allows for rapid prototyping because the system designer doesn't need to know everything about the system before starting and it can achieve steady state in a shorter time interval. A fuzzy controller can automatically refine an initial approximate set of fuzzy rules and hence a FLC is more preferred.

As both the wind and solar power are of fluctuating type, employing a FLC makes the system more reliable. Thus a constant DC voltage is obtained from the system. This DC power can be used to charge a battery or can be used to supply a DC load. The same can be inverted and can be supplied to an AC load also. Thus a hybrid wind and solar energy system which a load of 200 kW can be designed and implemented.

The objective of this section is designing a hybrid wind and solar energy system and controlling it by means of a FLC for domestic loads of about 100–200 kW. The main goal is to develop a new simple, cost-effective grid connected hybrid wind and solar power system. The developed system should also enable further enlargements with a less or no modification. A future expansion of the system should not put any constraints on the existing system. By doing so, a flexible design with high efficiency, and low cost is achieved. In more detail, the objective of this work is as follows:

1. Development of hybrid wind and solar power generating system.
2. Development of a controller for the overall system.

6.5.1 FLC for HPS

The modelling of Solar PV, Wind Turbine (WT), Fuzzy logic Controller (FLC), Inverter and the overall modelling of the system work done is explained in this section.

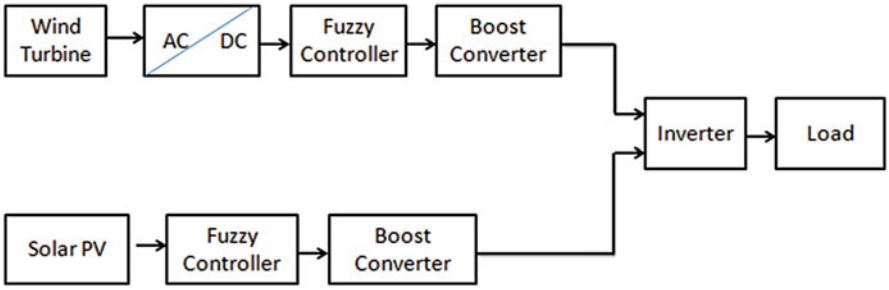


Fig. 6.37 Hybrid wind and solar power generation system

The overall system shown in Fig. 6.37 consists of a solar PV panel, Wind Turbine (WT), rectifier (AC-DC), battery, charge controller, Fuzzy logic controller (FLC), Inverter and loads. Individually the solar PV system and Wind energy system are controlled and their outputs are connected in parallel.

The output of the solar PV module is DC and the output of wind turbine is AC, before combining these two output of sources converted into any one of the source. Hence the output of wind turbine is AC is converted into DC by using rectifier. The fuzzy logic controller is introduced between rectifier, solar PV output and boost converter. FLC is used to maintain constant voltage and power throughout the system. The output of FLC is duty cycle which is given to the gate pulse of MOSFET switch which is used in boost converter.

6.5.2 Description of the Model

Initially a Solar PV is designed and is simulated in MATLAB/SIMULINK and analyzed. The Solar PV is then connected to a boost converter for getting the required output voltage. Then the Solar PV along with boost converter is connected to the FLC for getting a constant output voltage.

Similarly a Wind Turbine system is taken and analyzed. The Output from the WT is AC and hence is rectified and then boosted to the required level by means of a boost converter. Then this system is also connected to a FLC to get a constant output voltage.

Then both the Solar PV and the Wind Turbine system are connected together in parallel and the combined output is taken.

6.5.2.1 Equivalent Circuit of Solar PV Module

A solar cell (also called a photovoltaic cell) is an electrical device that converts the energy of light directly into electricity by the photovoltaic effect. It is a form of photoelectric cells in that its electrical characteristics. e.g. current, voltage, or

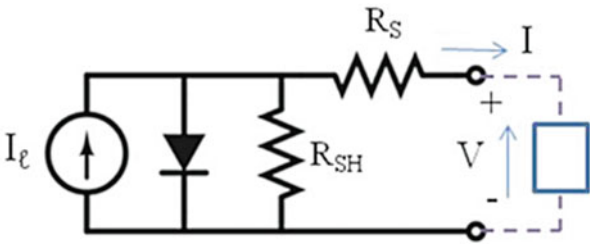


Fig. 6.38 Equivalent circuit of solar cell

resistance vary when sunlight is falls on solar cell its generated charge carriers that produces electrical current without being attached to any external voltage source. The group of solar cell is called solar PV module. The amount of power generated by solar cell is very small. So, the cells are to be arranged in series and parallel to produce useful range of electrical power. The efficiency of solar PV depends on environmental and operating conditions such as irradiation and temperature.

A solar cell as a parallel combination of a current source, exponential diode and parallel resistor R_P, that are connected in series with a resistance R_S. The equivalent circuit of solar cell is shown Fig. 6.38. The solar PV array consists of several photovoltaic cells in series and parallel connections. Series connections are responsible for increasing the voltage of the module whereas the parallel connection is responsible for increasing the current in the array. The value of series resistance is very low and the shunt resistance value is infinity.

The output current of solar cell is given by,

$$\mathbf{I = Iph - Is * e\hat{}[(V + I * Rs)/(N * Vt) - 1]}$$

where

Iph – is the actual photon generated current (A)
Is – diode saturation current (A)
Rs – series resistance (Ω)
N – quality factor
Vt – thermal voltage (V)

The short circuit current I_{SC} corresponds to the short circuit condition when the impedance is low and is calculated when the voltage is 0.

$$\text{I (at V} = 0) \;=\; \text{I}_{\text{SC}}$$

$$I_{sc} = \left\{ I_s \left[\exp\left(\frac{qV}{KT}\right) - 1 \right] - I_{ph} \right\} \text{ at V} = 0$$

The open circuit voltage (V_{OC}) occurs when there is no current passing through the solar cell, V (at I = 0) = V_{OC}

$$V_{oc} = \frac{K_B T}{q} \ln\left[\frac{I_{ph}}{I_s} + 1\right] \cong \frac{K_B T}{q} \ln\left[\frac{I_{ph}}{I_s}\right]$$

where

q – is the electron charge [$1.60217646 \times 0^{-19}$ C]
k – is the Boltzmann constant [$1.3806503 \times 10^{-23}$ J/K]
T – is the temperature of the p-n junction [K]

$$P_{MAX} = V_{MP} \times I_{MP}$$

P_{MAX} is the maximum power (W)
V_{MP} is the Array voltage at maximum power point (V)
I_{MP} is the Array Current at maximum power point (A)

6.5.2.2 WECS

The Inputs to the wind turbine are,

1. The generator speed in per units is 1.p.u.
2. The pitch angle is chosen to be zero.
3. The wind speed is chosen to be 12 m/s.

The pitch angle is the angle at which the wind turbine blade surface contacts the wind. It's chosen to be zero for our convenience. The output of Wind Turbine is mechanical torque (Tm).

The output power of wind turbine is given by the following equation,

$$P_m = \frac{C_p(\lambda, \beta).\rho.A.v^3}{2}$$

where

P_m – mechanical output power of the turbine (W)
Cp – performance coefficient of the turbine
ρ – Air density (kg/m^3)
A – turbine swept area (m^2)
β – blade pitch angle
λ – tip speed ratio of the rotor blade tip speed to the wind speed

The output waveform from the PMSG is an Alternating Current (AC) output waveform. The Alternating output is rectified using a rectifier. A high value of resistor is connected between the PMSG and the rectifier circuit. The rectifier used is a basic diode bridge rectifier. The rectified voltage is again boosted and controlled by means of a FLC.

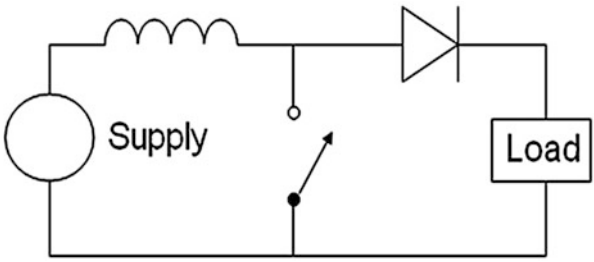


Fig. 6.39 Schematic diagram of boost converter

The output of wind power is ac, which is given to the input of the uncontrolled bridge rectifier. The wind turbine output is given to the permanent magnet synchronous machine. The rectifier is used to convert ac into dc. The Permanent Magnet Synchronous Machine operates in either generator or motor mode. The mode of operation is dictated by the sign of the mechanical torque (positive for motor mode, negative for generator mode).

6.5.2.3 Three Phase Uncontrolled AC-DC Rectifier

The three-phase AC-DC rectifier using six diodes. The diodes are arranged in three legs. Each leg has two series connected diodes. The upper diodes are the positive group of diodes. The lower diodes are the negative group of diodes. The positive group of diodes are conducted when the supply voltage is most positive anode. The negative group of diodes are conducted when the voltage is most negative anode.

6.5.2.4 Boost Converter

A boost converter, also called a step-up converter, is a DC-DC power converter with an output voltage greater than its input voltage. It is a class of Switched-Mode Power Supply (SMPS) containing at least two semiconductor switches (a diode and a transistor) and at least one energy storage element, a capacitor, inductor, or the two in combination. Filters made of capacitors (sometimes in combination with inductors) are normally added to the output of the converter to reduce output voltage ripple.

Power for the boost converter can come from any suitable DC sources, such as batteries, solar panels, rectifiers and DC generators.

The key principle that drives the boost converter is the tendency of an inductor to resist changes in current. In a boost converter, the output voltage is always higher than the input voltage. A schematic of a boost power stage is shown in Fig. 6.39.

When the switch is ON, inductor stores energy and current through the load would increases from I_1 to I_2 as shown in Fig. 6.40. With switch ON, the source voltage is applied to inductor, $V_L = V_{in}$.

When the switch is OFF, the output stage receives energy from the inductor as well as from the input. The inductor current cannot comes down instantaneously;

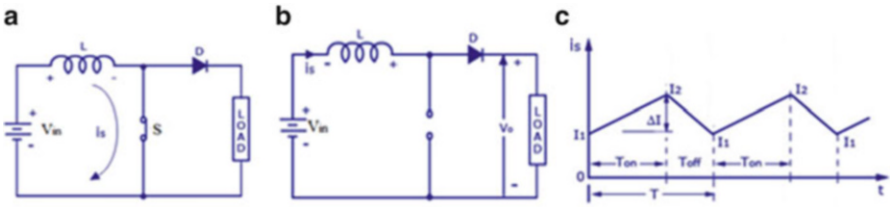


Fig. 6.40 Boost converter operation

this current is forced to flow through the diode and load for a time T_{off}. As the current tends to fall from I_2 to I_1 and polarity of the emf induced in L is reversed. As a result voltage across the load exceeds the input voltage which is given by, $V_o = V_{in} + L\frac{di}{dt}$.

Design of Boost Converter
$V_{i=}$ 25 V, $V_{0=}$ 90 V, f = 20 KHZ

1. **Duty cycle, D = 1-(Vs/Vo)**

   D = 1-(25/90)
   D = 0.7

2. **Ripple current, ΔIL** $= \frac{VS * D}{Lf}$

   ΔIL is 1 % of load current
   ΔIL = 0.01

3. **Inductance, L** $= \frac{VS * D}{\Delta IL * f}$

   L = 0.011H

4. **Ripple voltage, ΔVc** $= \frac{I0 * D}{cf}$

   ΔVc is 2 % of output voltage
   ΔVc = 0.02

5. **Capacitance, C** $= \frac{I0 * D}{\Delta VC * f}$

   C = 60uF

6.5.3 Implementation in MATLAB

6.5.3.1 Solar PV System

The Solar panel as per our requirement is designed in MATLAB. The MATLAB simulated model of the PV panel is shown in the Fig. 6.41.

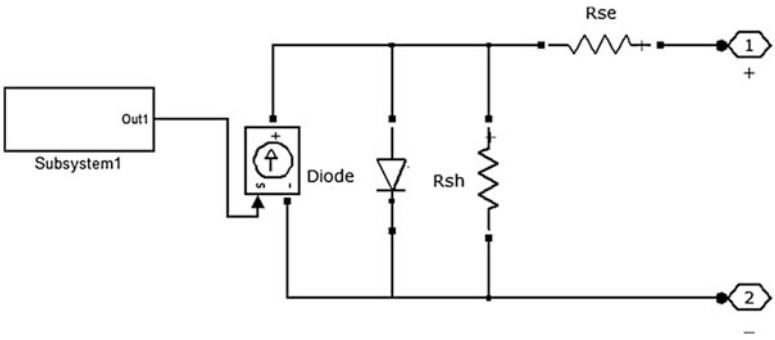


Fig. 6.41 Simulation model of the single PV cell

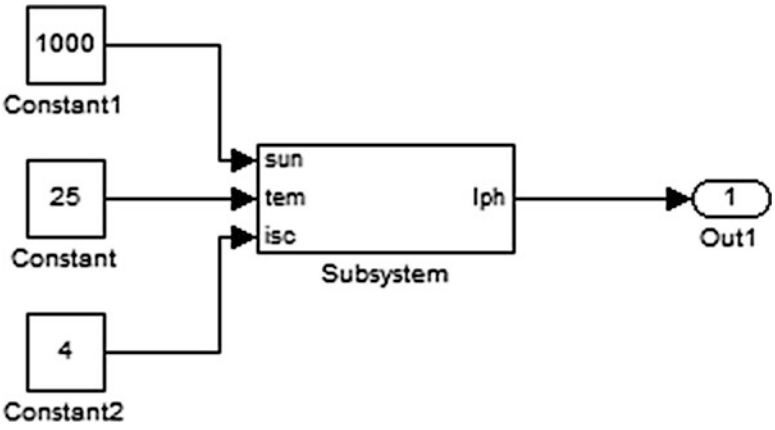


Fig. 6.42 Subsystem of the solar PV cell

The PV panel that is simulated has a subsystem connected to it. The solar irradiation, temperature and short circuit current are given as input to subsystem and current is taken as output from the subsystem. This current is given to the controlled current source which is connected to an inverted diode and two resistors one connected in parallel and other in series in the circuit as shown in the Fig. 6.41.

The value of the shunt resistance connected in parallel to the cell is selected as 1,000 Ω and the value of series resistance connected in series with the solar cell as 0.001 Ω.

The constant 1,000 given as input to the sun is the irradiation considered in W/m^2. The constant 25 given to the input term in Fig. 6.42, is the temperature considered in deg Celsius. The Constant 4 is the short circuit current of the solar PV. The subsystem of Fig. 6.41 is shown in Fig. 6.42.

The irradiation of 1,000 W/m^2 and temperature of 25 °C is considered to be standard testing condition. The system is simulated with various range of resistors

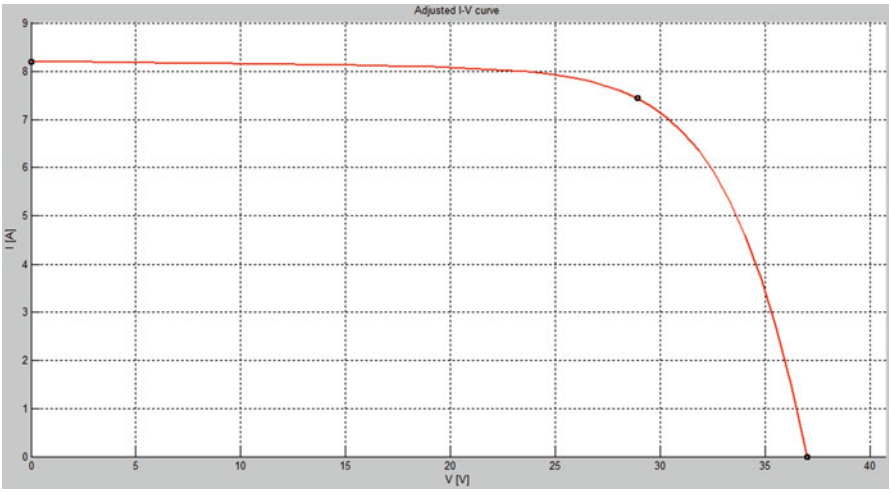


Fig. 6.43 I-V characteristic of single solar PV module

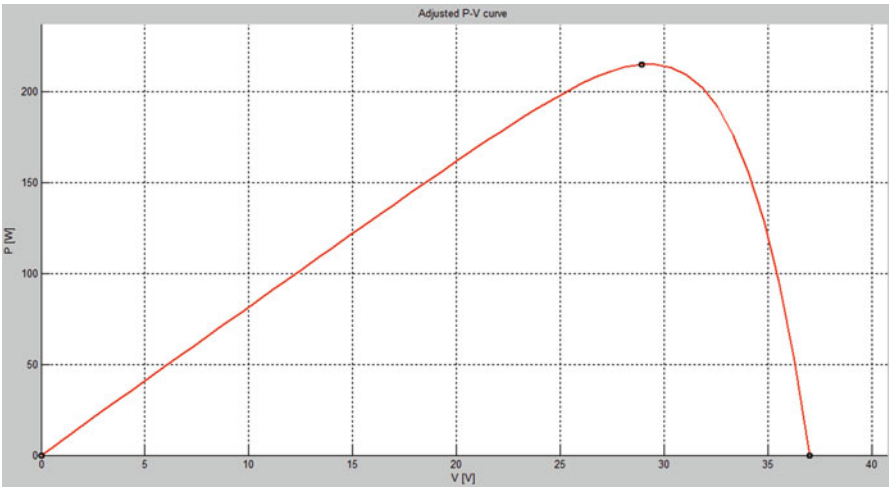


Fig. 6.44 P-V characteristic of single solar PV module

connected to it, in this condition. A single solar PV module parameters values are written in MATLAB M-File coding and get the following output characteristics.

The I–V characteristic of the photovoltaic device depends on the internal characteristics of the device (R_s, R_p) and an external influence such as irradiation level and temperature.

When the voltage and the current characteristics are multiplied we get the P-V characteristics as shown in Fig. 6.44. The Maximum Power Point (MPP) is the point at which the panel power output is maximum.

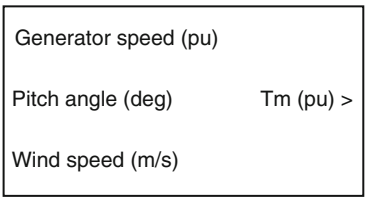


Fig. 6.45 WT subsystem used in wind energy system simulation

6.5.3.2 WECS in MATLAB

Initially a Wind Turbine (WT) system is simulated in MATLAB/SIMULINK and output is analyzed. An inbuilt wind turbine is taken from MATLAB and the output torque of the wind turbine is connected to a Permanent Magnet Synchronous Generator (PMSG). The inbuilt function of WT used is shown in Fig. 6.45.

6.5.3.3 Fuzzy Logic Controller (FLC)

The mathematical system that analyzes analogue input values in terms of logical variables that take on continuous values between 0 and 1, in contrast to classical or digital logic, which operates on discrete values of either 1 or 0. A fuzzy can deal with non-linearity and more robust than conventional logic controller.

FLC can be classified into four steps:

1. Fuzzification
2. Membership Functions
3. Rule base
4. Defuzzification

Fuzzy inputs are error (E) and change in error (CE), the output is duty cycle (D). FIS editor is shown in Fig. 6.46. The corresponding rule base is provided in Table 6.4.

The Output from the FLC is compared with a repeating sequence of 5 kHz frequency. The compared output is given to the MOSFET of the boost converter which is connected to the system and the output voltage is accordingly boosted as required.

6.5.3.4 Simulation of Photo-voltaic Array for Different Atmospheric Conditions

The single solar PV module consists of series and parallel solar cell, which is used to increasing the voltage and current. The maximum current is given to the input of a current controlled source. The output power of solar PV is 100 kW.

The PV array results can be varied according to the different atmospheric conditions such as constant irradiation and varying temperature. The value of constant irradiance is 1,000 (W/m^2) and temperature varying from 20 to 70 (K).

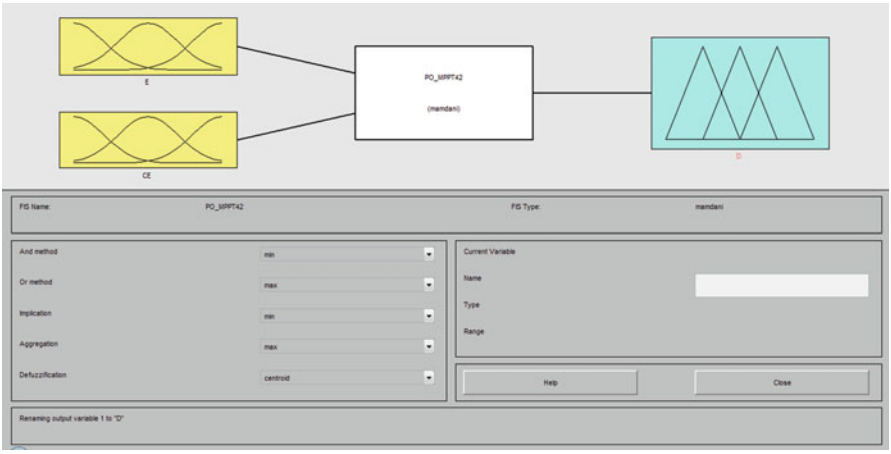


Fig. 6.46 FIS editor

Table 6.4 Fuzzy rule table

	E				
CE	NB	NS	ZE	PS	PB
NB	ZE	ZE	PB	PB	PB
NS	ZE	ZE	PS	PS	PS
ZE	PS	ZE	ZE	ZE	NS
PS	NS	NS	NS	ZE	ZE
PB	NS	NB	NB	ZE	ZE

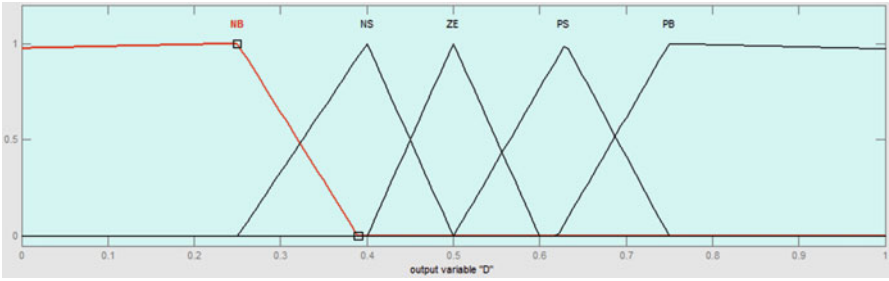


Fig. 6.47 FLC output

Inference The output voltage of PV module is gradually increasing and output current and Power is varied according to the constant irradiance and changing temperature.

The solar PV module contains 250 series cells and 100 parallel cells. A single solar cell has the voltage of 0.5 V and has the short circuit current value is 8A, which produces the power of 4 W. The total power produced by solar PV module is 100 kW due to the radiation of 1,000 W/m^2 and the temperature of 25 °C.

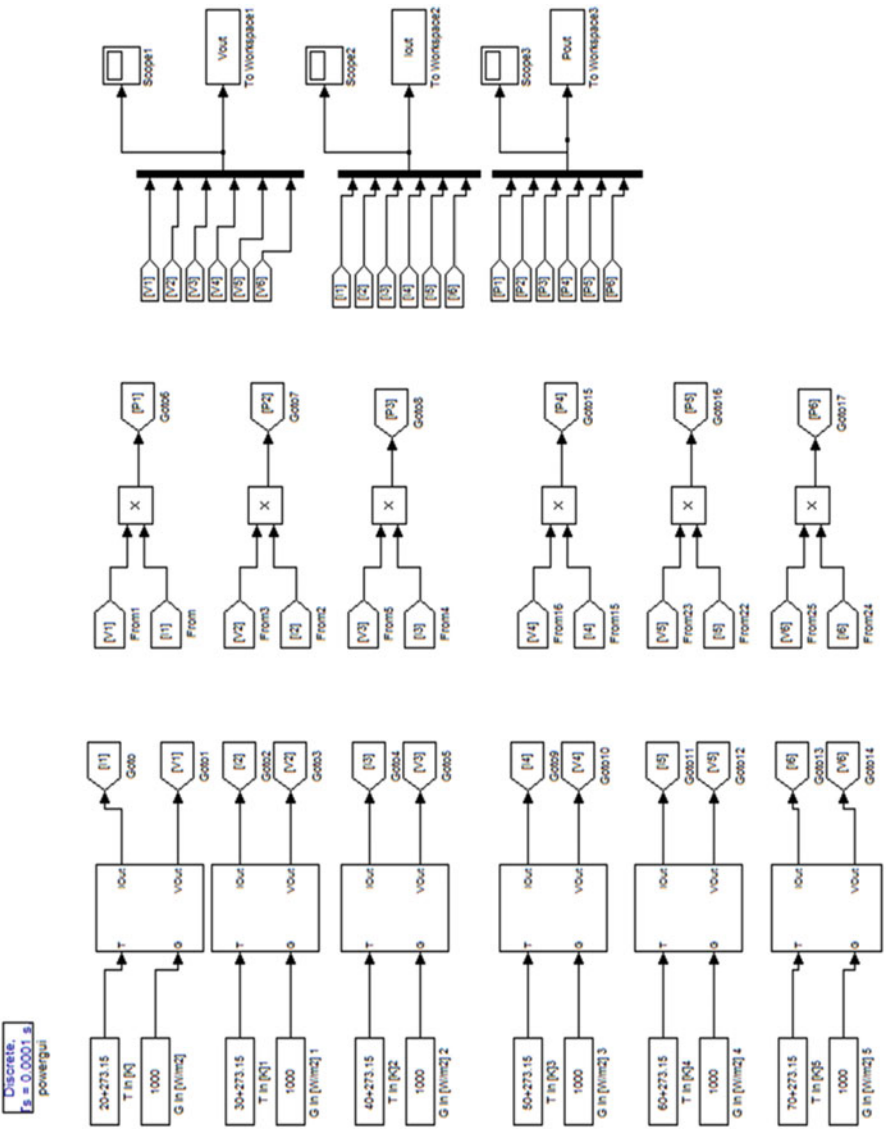


Fig. 6.48 Simulation of PV array for different atmospheric conditions

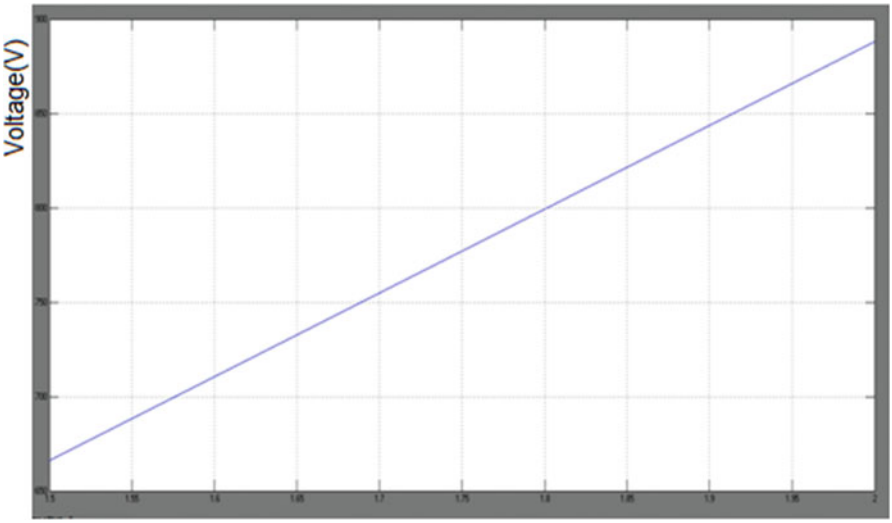


Fig. 6.49 Output voltage of single PV module

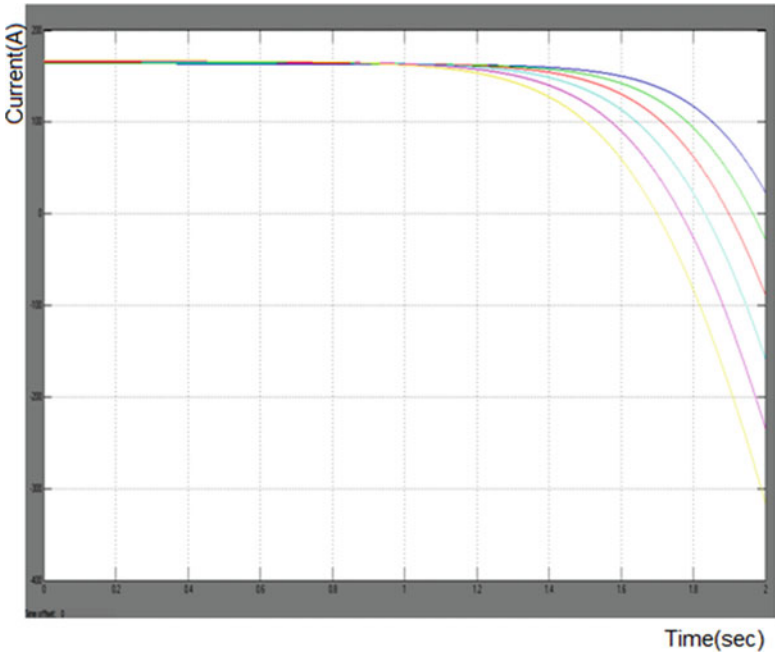


Fig. 6.50 Output current of single PV module

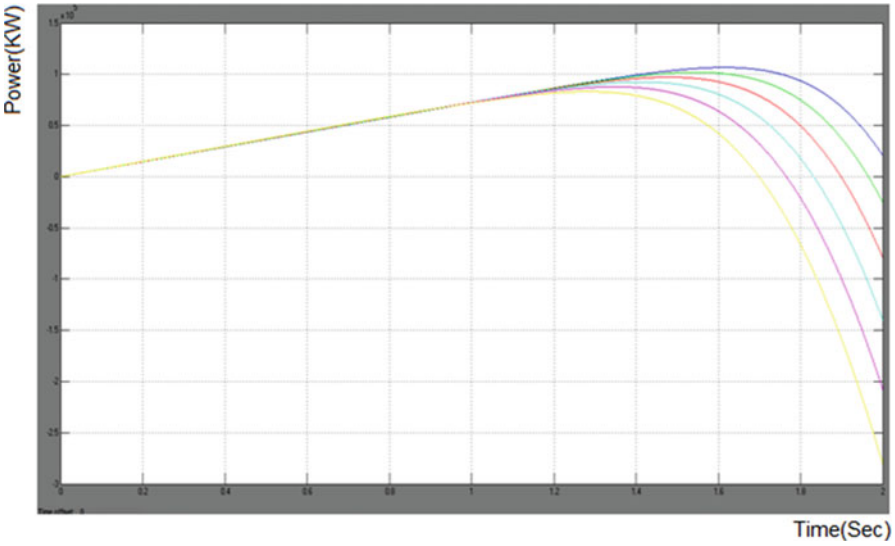


Fig. 6.51 Output power of single PV module

Inference The Output power of solar PV module can be varied according to the different values of radiation and fixed PV panel temperature.

Inference The input voltage is increased from 25 to 90 V. The output voltage is greater than that of an input voltage.

6.5.3.5 AC-DC Rectifier

The input supply ac source is converted into dc using rectifier. The three phase uncontrolled ac-dc rectifier using six diodes.

The first and foremost power quality parameter is the Total Harmonic Distortion (THD). The ac-dc rectifier supply current waveform is distorted. THD analysis can be done for one cycle.

The output of WT is given to an input of PMSG. If the output of mechanical torque is negative the PMSG works as generator and if the torque is positive the PMSG operating in motor mode. The ac is converted into dc by using rectifier.

Inference The output power of wind energy system is fluctuated. So the controller is needed to maintain the output voltage and power.

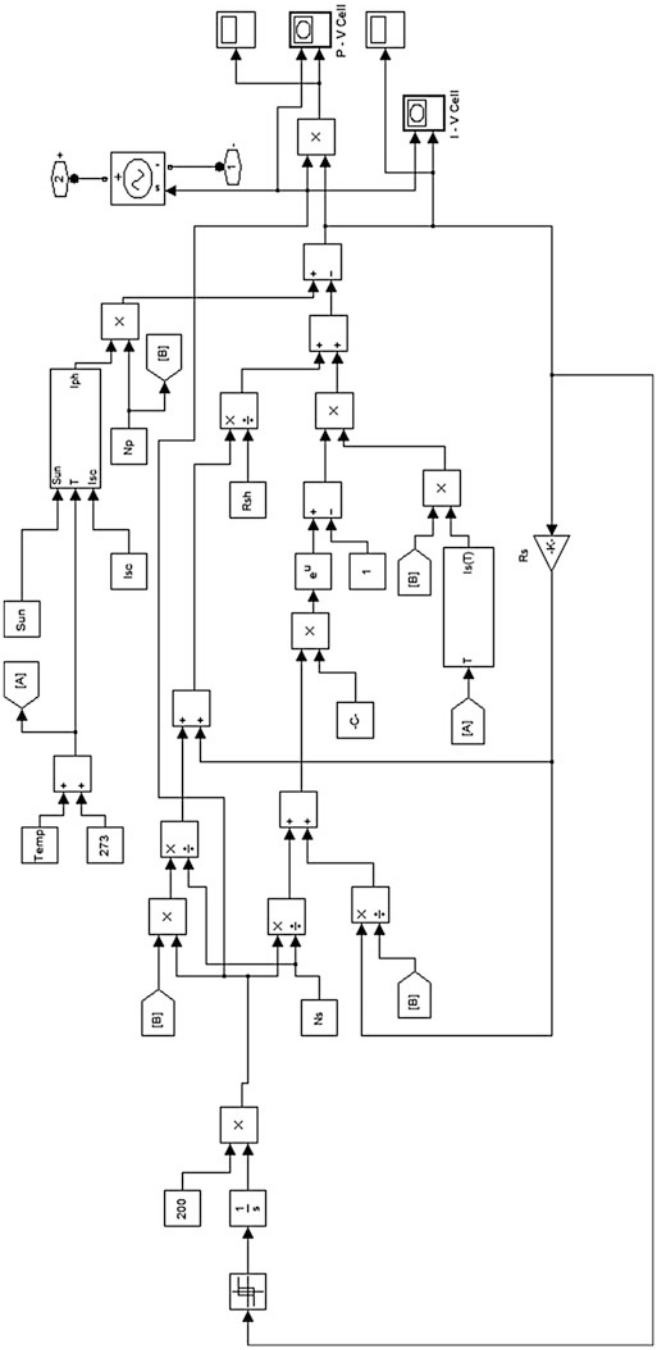


Fig. 6.52 Simulation of solar PV module

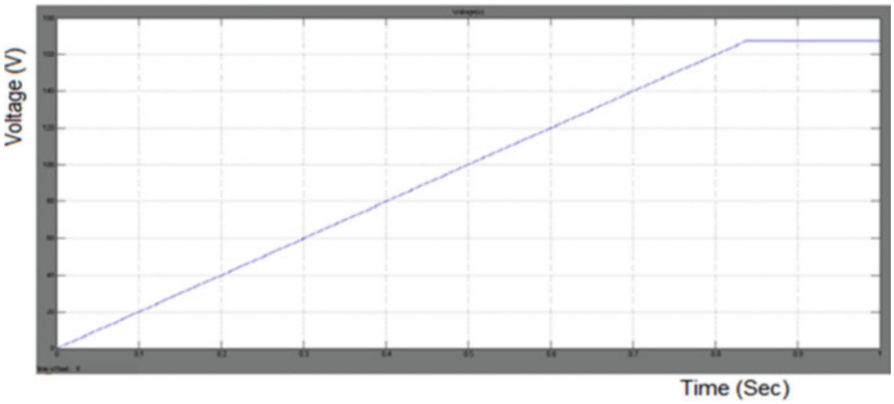


Fig. 6.53 Output voltage for solar PV module

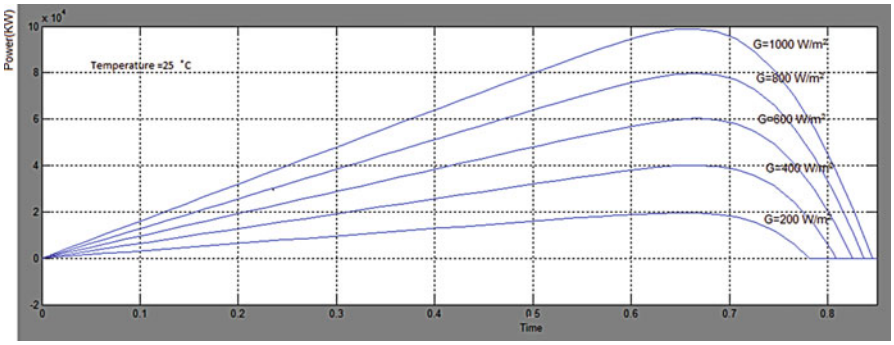


Fig. 6.54 Output power for different values of solar radiation G (W/m^2) and fixed temperature T = 25 °C

6.6 Fuzzy Logic Based MPPT for Hybrid Solar and WECS

According to many renewable energy experts, a small hybrid electric system that combines wind energy system and solar PV system offers several advantages over either single system. Combining the renewable energy generation with the conventional diesel power generation will enable the power generated from renewable energy sources to be more reliable and affordable.

Due to the non-availability of solar PV and wind energy at all times, it is necessary to model a system that would give reliable source of power. When a direct connection is made between the source (Solar PV, Wind) and load, the operating point is not optimal. In order to track MPP and make the output voltage constant, two stage of DC-DC conversion is required. Hence, MPPT Controllers with DC-DC converters is designed to obtain an efficient output for all operating

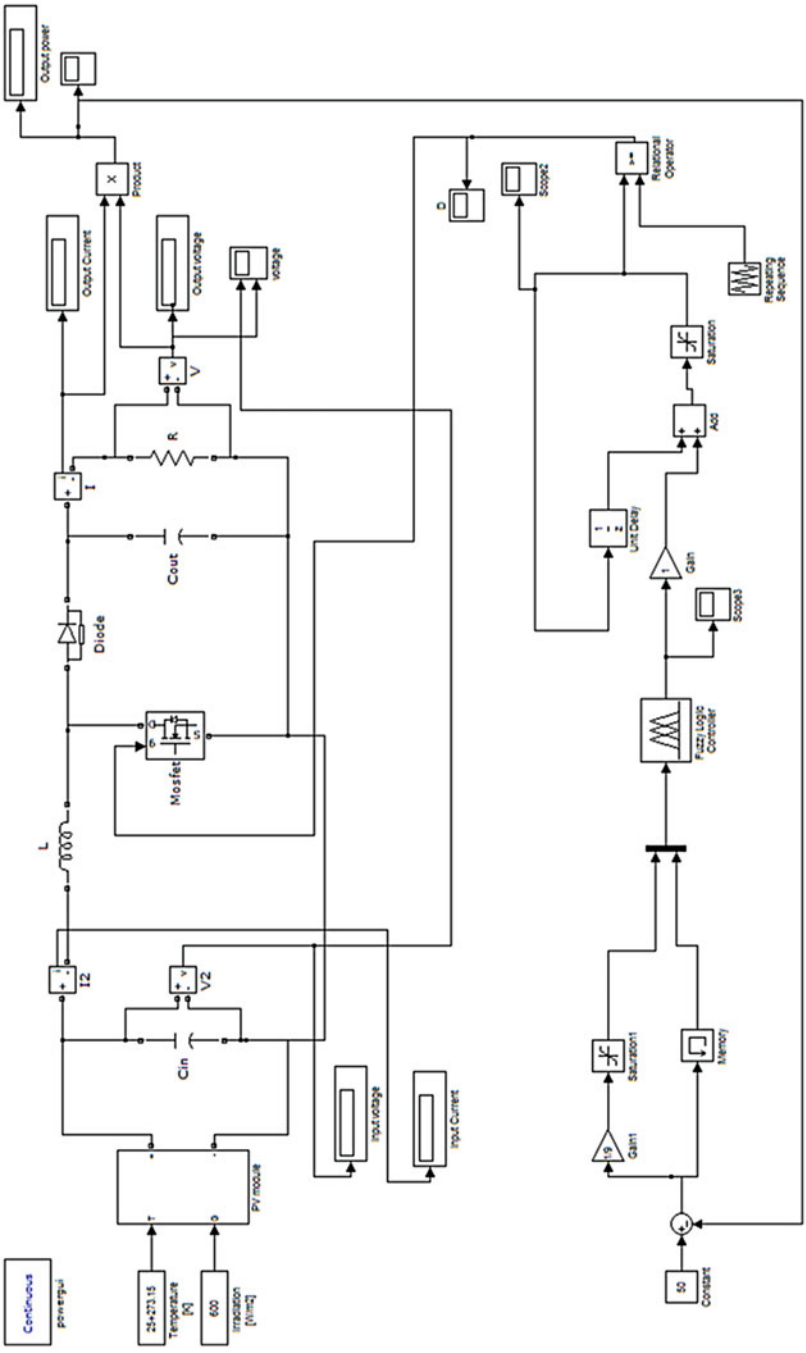


Fig. 6.55 Closed loop control of single solar cell

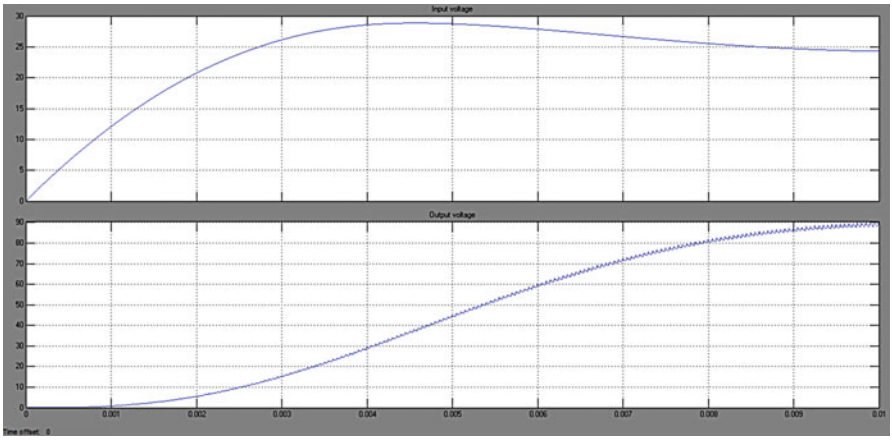


Fig. 6.56 Voltage waveform of boost converter

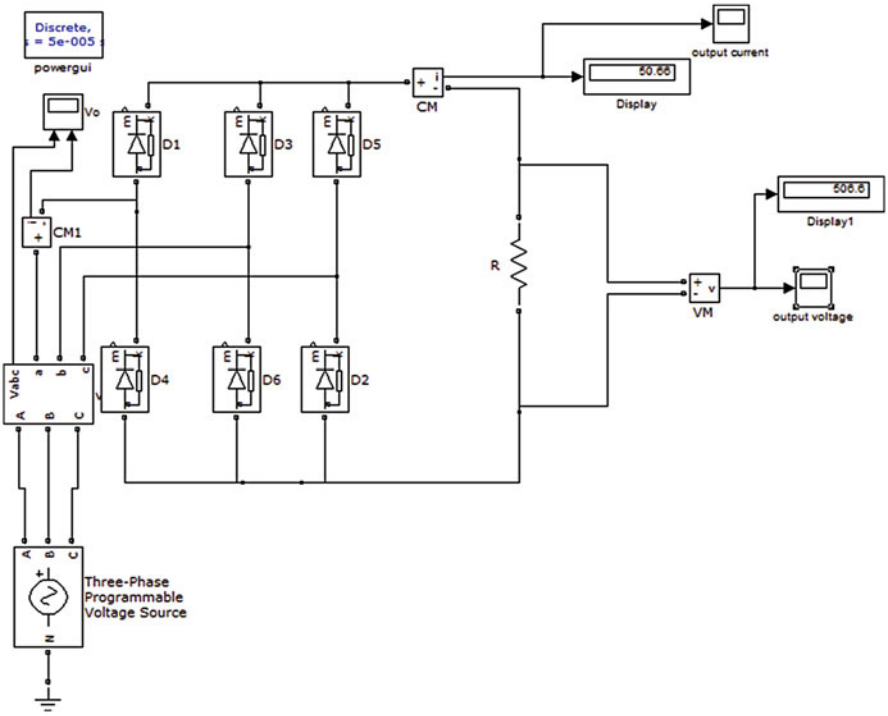


Fig. 6.57 Three phase uncontrolled ac-dc rectifier

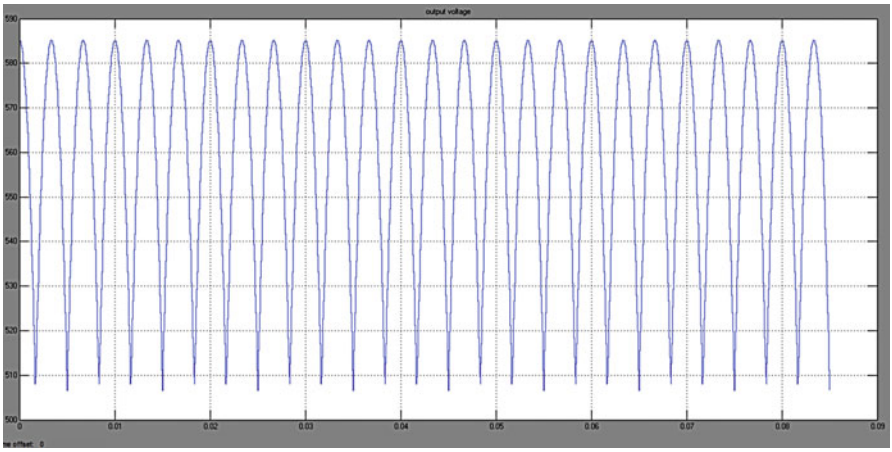


Fig. 6.58 Output voltage for ac-dc uncontrolled rectifier

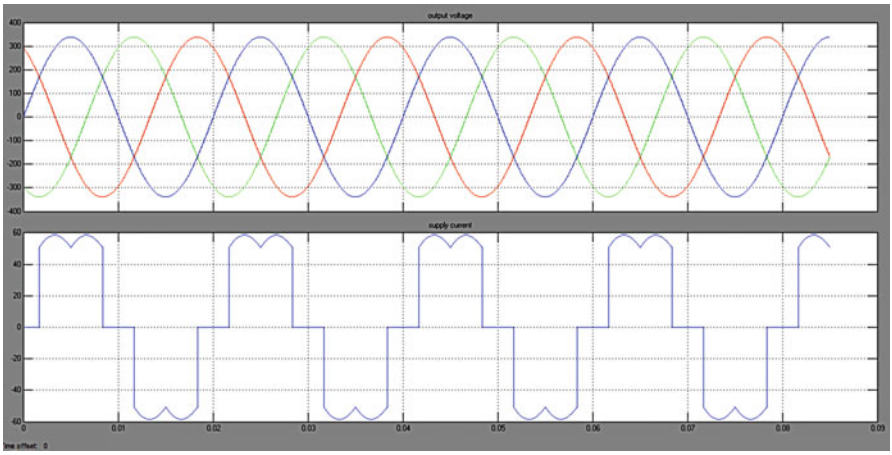


Fig. 6.59 Phase to ground voltage and supply current of ac-dc rectifier

conditions. As most of the consumer end applications are based on AC supply, the DC output obtained from the DC-DC converter are fed into the inverter for conversion into AC output filter is also designed to reduce the THD levels.

6.6.1 Methodology

In this section, a fuzzy logic based MPPT is proposed. The proposed fuzzy logic based MPPT can track the maximum power point faster and it can also minimize

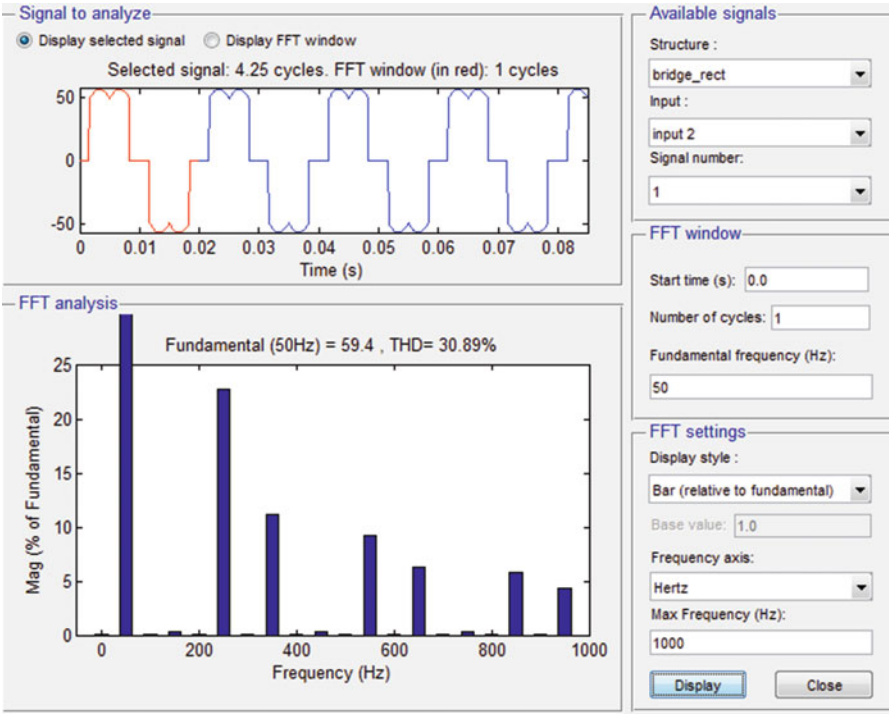


Fig. 6.60 THD analysis of source current in AC-DC rectifier

the voltage fluctuation after MPP has been recognized. In solar system the MPPT which depends on the atmospheric conditions such as solar cell temperature and irradiation conditions. When the MPPT will be implemented in wind, the maximum power can be extracted by varying the duty cycle of DC-DC Boost converter.

A fuzzy logic based MPPT has been implemented for both solar and wind energy system. MPPT control technique is implemented to generate the optimal voltage from PV and wind energy system by modulating the duty cycle and applied to the DC-DC boost converter. The output power from Solar PV and wind energy system are fluctuating. So the controller is required to make the DC bus voltage constant. PI controller has been implemented for DC-DC Buck-boost converter, which is used to vary the duty cycle and to maintain a constant voltage in DC-link capacitor. DC bus voltage is converted to AC by using PWM inverter, which is given to the AC load. The low harmonic distortion of the voltage and current at the output of the inverter is reduced by using an output L-filter.

The objective of the work is to design a hybrid wind and solar energy system and controlling it by means of a Fuzzy Logic Controller for domestic loads of about 100–200 kW. The main goal is to develop a simple, cost-effective stand alone

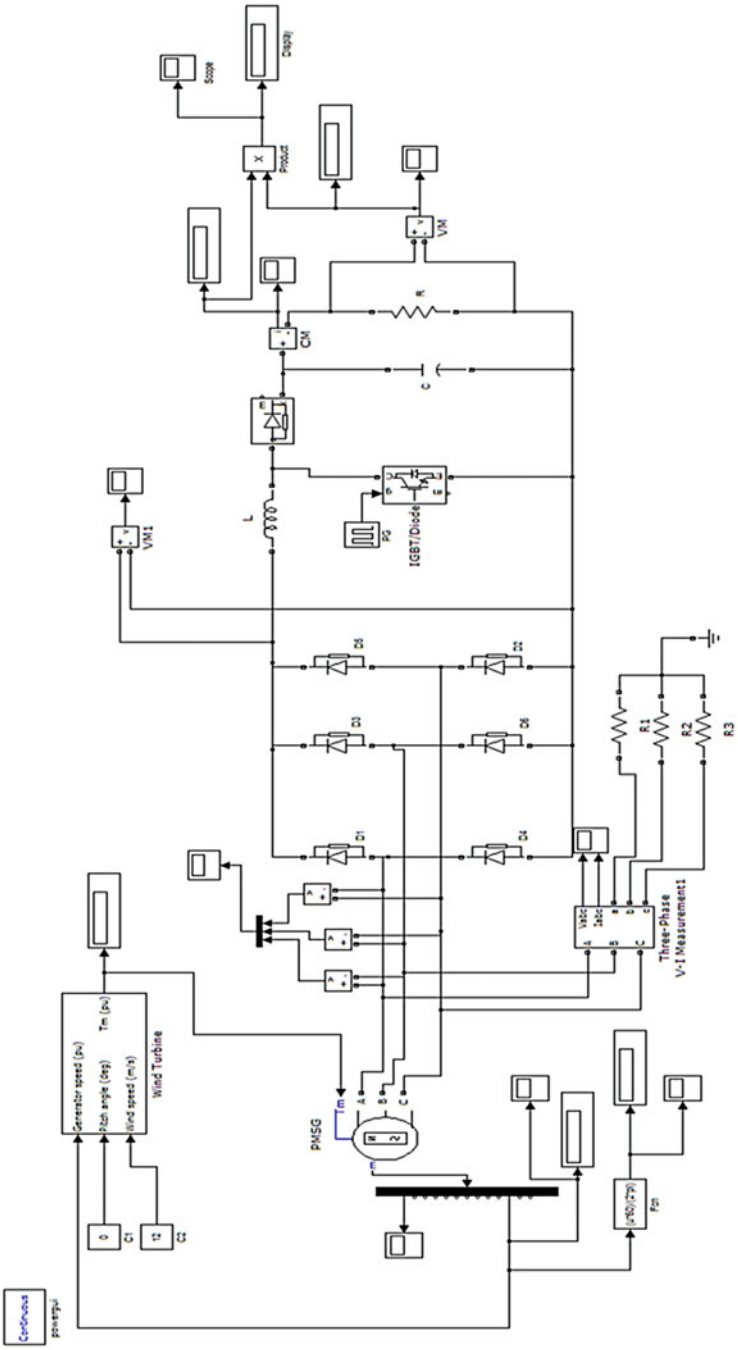


Fig. 6.61 Simulation of wind energy system with boost converter

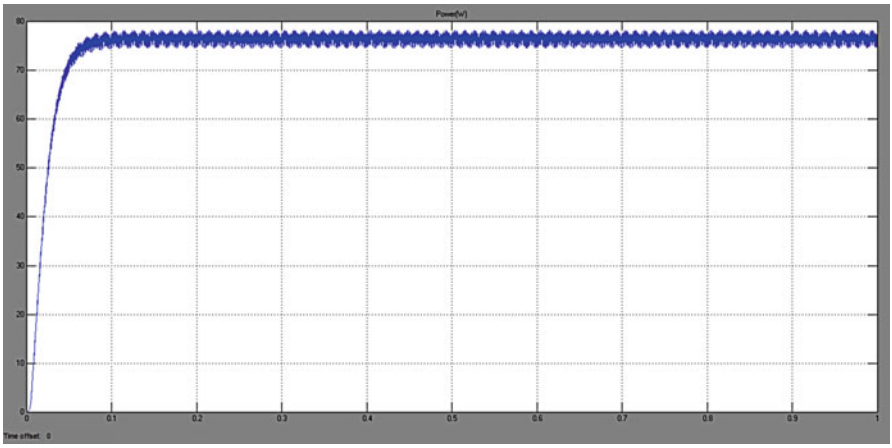


Fig. 6.62 Output power of wind energy system

hybrid wind and solar PV power system. In more detail, the objective of this work is as follows:

1. Development of a standalone hybrid wind and solar power generating system.
2. Design of FLC based MPPT for both Solar and Wind power system.
3. Development of a controller for the DC bus voltage.
4. Design of three phase PWM Inverter.
5. Design a low pass filter for an Inverter.

The Hybrid Power System (HPS) consists of solar PV module, Variable speed Wind Turbine (WT), AC-DC Diode bridge rectifier, DC-DC Boost converter, PWM Inverter and load are shown in Fig. 6.63. Individually the solar system and wind energy system are controlled and their outputs are connected in parallel.

The output of solar PV module is DC and the output of Wind energy system is AC, before combining these two output sources, they are converted to anyone of the source. Hence the output of WECS is converted into DC by using Diode Bridge Rectifier. Converting AC to DC is more preferred when boosting the voltage. The voltage applied by the PV array does not have constant values; it fluctuates according to the atmospheric conditions such as solar irradiation and temperature.

Here, Boost converter and Buck-boost converter are used. The Boost converter is used for increasing the output voltage magnitude obtained from solar PV module is shown in Fig. 6.63. The Boost converter is used to regulate a chosen level of the solar photovoltaic module output voltage and to keep the system at the maximum possible power from solar panels at all times. Buck-boost converter that has an output voltage magnitude that is either greater than or less than the input voltage magnitude. The output voltage is varied according to the duty cycle. They can produce a range of output voltages from an output voltage much larger than the input voltage. A fuzzy logic based MPPT control technique is implemented to

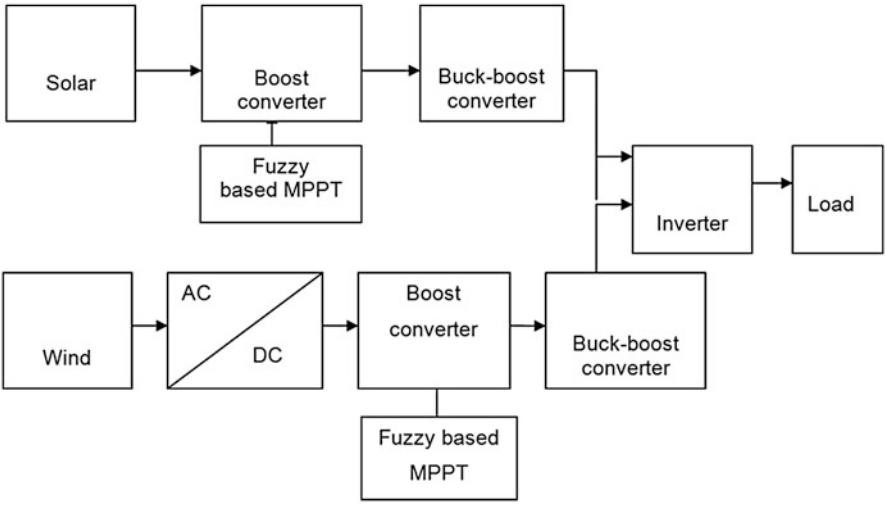


Fig. 6.63 Hybrid solar and wind power generation system

generate the optimal voltage from the PV system by modulating the duty cycle which is applied to the Boost converter. The Boost converter is used to regulate a chosen level of the solar photovoltaic module output voltage and keeps the system at the maximum possible power from solar panels and wind turbine at all times. The fuzzy logic based MPPT can track the Maximum Power Point (MPP) faster and can also minimize the voltage fluctuation after MPP has been recognized. According to V_{ref}, FLC boost converter forces the terminal voltage of PV array and wind energy systems to operate at its maximum power point. The boost converter output voltage is fluctuating, in order to make the DC bus voltage constant, two stage of DC-DC conversion is required. The DC bus voltage is converted into AC by using PWM inverter, which is given to AC load.

6.6.2 Design Considerations

Since the theoretical explanation for Solar PV module, wind turbine and rectifier are discussed in Sect. 6.5, we directly move on to the design considerations.

6.6.2.1 Design of Boost Converter

The parameters of Boost converter for solar and wind generation system values are calculated by using the following formulae tabulated in Tables 6.5 and 6.6.

Input voltage, $V_s = 150–950$ V, Output voltage, $V_o = 230–1{,}120$ V, Switching frequency, $F_s = 20$ kHz, ΔI_L is 3 % of output current, ΔV_c is 4 % of output voltage.

Table 6.5 Parameters of boost converter for solar PV system

Parameter	Symbol	Formula	Value
Duty cycle	K	$k = 1 - \frac{V_s}{V_0}$	0.727
Inductance	L	$L = \frac{Vs * k(1-k)}{\Delta I_L * f}$	8.9 mH
Capacitance	C	$C = \frac{Vs * k(1-k)}{8Lf^2 \Delta V_C}$	57 μF

Table 6.6 Parameters of boost converter for wind generation system

Parameter	Symbol	Formula	Value
Duty cycle	K	$k = 1 - \frac{V_s}{V_0}$	0.85
Inductance	L	$L = \frac{Vs * k(1-k)}{\Delta I_L * f}$	7.4 mH
Capacitance	C	$C = \frac{Vs * k(1-k)}{8Lf^2 \Delta V_C}$	86 μF

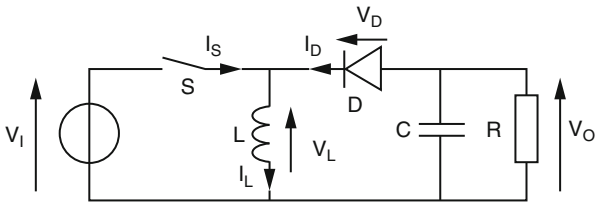


Fig. 6.64 Schematic diagram of buck-boost converter

Input voltage, $V_s = 120–925$ V, Output voltage, $V_o = 400–1{,}000$ V, Switching frequency, $F_s = 20$ kHz, ΔI_L is 2 % of output current, ΔV_c is 3 % of output voltage.

6.6.2.2 Design of Buck-Boost Converter

The Buck-boost converter is a case of DC-DC converter that has an output voltage magnitude that is either greater than or less than the input voltage magnitude. The yield voltage is of the contrary polarity as the input. This is the switched mode power supply with a similar circuit topology to the boost converter and the Buck converter. The output voltage is changeable based on the duty cycle of the switching transistor. The schematic diagram of Buck-boost Converter is shown in Fig. 6.64.

When the switch is turned ON as shown in Fig. 6.65, the input voltage source is directly connected to the inductor (L). This results in accumulating energy in inductor. In this stage, the capacitor supplies energy to the output load.

When the switch is opened as shown in Fig. 6.66, the inductor supplies current to the load through the diode D. While in the OFF state, the inductor is connected to the output load and capacitor, so energy is transferred from inductor to Capacitor, and resistor.

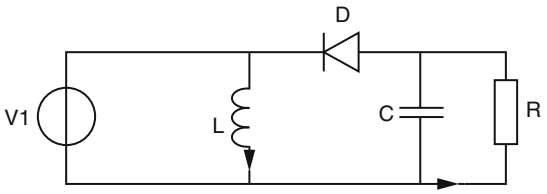


Fig. 6.65 Buck–boost converter-ON state

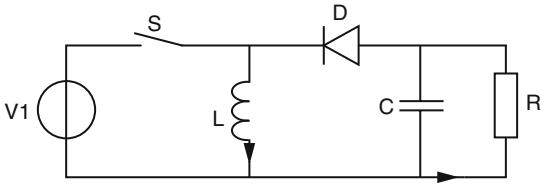


Fig. 6.66 Buck-boost converter-OFF state

Compared to the Buck and boost converters, the characteristics of the Buck–boost converter are mainly:

1. Opposite Polarity of the output voltage compared to that of the input.
2. The output voltage can vary continuously from 0 to $-\infty$ (for an ideal converter). The output voltage ranges for buck and boost converter are respectively 0 to V_i, and V_i to ∞.

6.6.2.3 Design of Buck-Boost Converter

The Buck-boost Converter parameter values are calculated by using the following formulae.

Input voltage, $V_s = 160$–$1{,}100$ V, Output Voltage, $V_o = 850$ V, Switching frequency, $F_s = 20$ kHz, ΔI_L is 2 % of Output current, ΔV_c is 4 % of Output voltage.

1. Duty Cycle, $k = \frac{V_0}{V_0 + V_S}$

$$= 850/(850 + 1{,}100)$$
$$k = 0.435$$

2. Inductance, $L = \frac{V_S * k}{\Delta I_L * f}$

$$= (160*0.4)/(0.17*20e^3)$$
$$L = 8 \text{ mH}$$

3. Capacitance, $C = \frac{I_0 * k}{\Delta V_C * f}$

$$= (0.17*0.4)/(34*20e^3)$$
$$C = 85\ \mu\text{F}$$

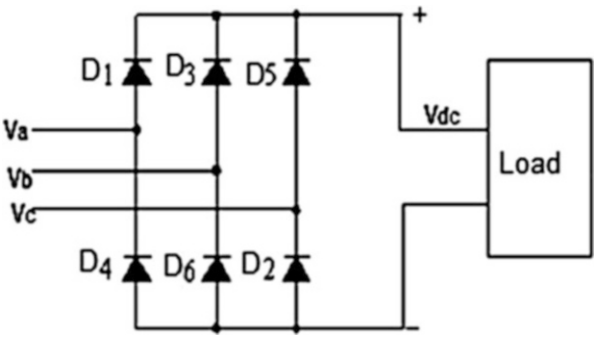


Fig. 6.67 Schematic diagram of diode bridge rectifier

6.6.2.4 Diode Bridge Rectifier

A Diode Bridge Rectifier circuit converts AC input voltage into fixed DC voltage. Semiconductor diodes are used extensively in power electronic circuits for the conversion of power from AC to unidirectional DC. A rectifier circuit shown in Fig. 6.67 employing diodes is called an uncontrolled rectifier, because its average output voltage is a fixed DC voltage. The output voltage from the PMSG based WECS is a three phase AC voltage and it has to be rectified into a DC voltage. For rectification, a diode bridge rectifier is used and it rectifies the three phase AC to DC respectively. The diode bridge consists of six diodes from D1 to D6 as shown in Fig. 6.67.

The impedance of the diodes is neglected assuming to be very small values. The output rectified voltage from the diode bridge rectifier is boosted as required voltage.

The three phase circuit consists of two groups of diodes, positive group and negative group. The positive group of diodes are turned on when the supply voltages are positive and negative group diodes are turned on when the supply voltages are negative. If D1 is triggered at a particular instant, it can conduct provided there is a return path for the current. Since phase B is the maximum negative, the return path should be to phase B which means D5 must be triggered simultaneously with D1.

6.6.2.5 Three Phase PWM Inverter

An inverter is converted fixed DC voltage to a variable AC voltage. The output may be variable voltage and variable frequency. The output voltage from the PMSG is a three phase AC voltage and it has to be rectified into a DC voltage. For rectification a diode bridge rectifier is used and it rectifies the three phase AC to DC respectively. Pulse Width modulation is the process of modifying the width of pulses in a pulse train in direct proportion to a small control signal. Three phase inverters are normally used for high power applications.

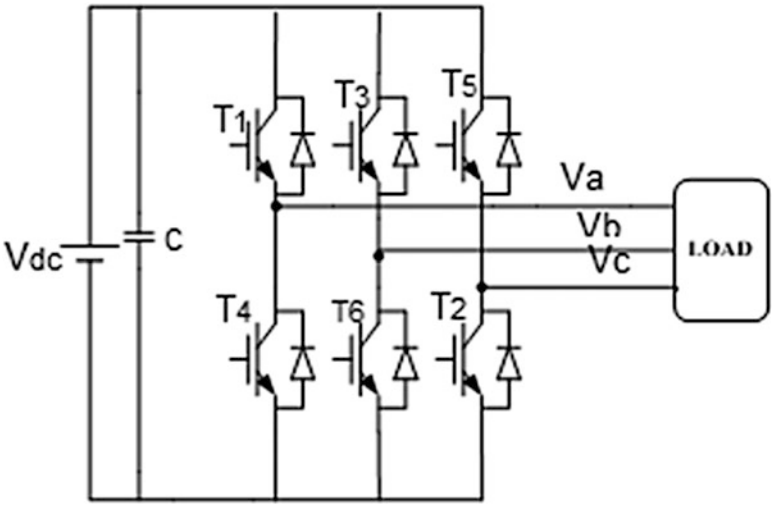


Fig. 6.68 Three phase PWM inverter

Three Phase inverter output can be obtained from topology having six transistor and six diodes as shown in Fig. 6.68. When transistor T1 is switched ON, terminal a is connected to the particular positive terminal from the DC input potential. When transistor T4 is started up, terminal a is actually brought to the actual negative terminal on the DC source. Switches of any kind of leg of this inverter (T1 & T4, T3 & T6, and T5 & T2) can not be switched simultaneously; this could result in a brief short circuit across the actual DC-link current supply. Similarly, in order to avoid undefined states therefore undefined AC line voltages, the switches of virtually any leg of the actual inverter cannot end up being switched off concurrently because this could result in changes in the voltages with respect to the current polarity.

If two changes: one upper then one lower conduct concurrently such that the actual output voltage is +Vs or −Vs, the switch point out is 1, although if these switches are off at the same time, the switch state is 0. To generate a given wave form, the inverter goes from one point out to another condition. The output of current has harmonics; hence your L filter is employed to reduce this harmonics in output current.

6.6.3 Intelligent Controller

Intelligent control describes the discipline where control methods are developed that attempt to emulate important characteristics of human intelligence. An intelligent controller system has the ability to act appropriately in an uncertain

environment, where an appropriate action is that which increases the probability of success. In intelligent control problems, which are most often complex and challenging, there may not be a clear separation of the plant and the controller; the control laws may be defined and be part of the system to be controlled.

6.6.3.1 Fuzzy Logic Control

A fuzzy control system is based on a mathematical system that will analyzes analog insight values in regards to logical variables which take on continuous values between 2 and 1, contrary to classical or electronic digital logic, which is run on discrete values associated with either 1 or perhaps 0 (true or false, respectively). Using fuzzy logic command has become well-liked over the final decade because it could deal with imprecise inputs, does not need an accurate model and can handle nonlinearity. Microcontrollers in addition have helped in your popularization of fluffy logic control.

Fuzzy logic seems closer to the way regarding human brains employment. We aggregate the information and form a number of partial truths which we aggregate further into higher realities which in switch, when certain thresholds exceeds the range. Fuzzy logic continues to be extended to take care of the concept connected with partial truth, where the truth value whitethorn range between completely accurate and completely mistaken.

6.6.3.2 Fuzzy Logic Controlled Design

P&E method for MPPT tracking is not going to respond quickly in order to rapid changes in temperature or irradiance. And so the Fuzzy Logic Control (FLC) algorithm is definitely capable of increasing the tracking performance. The FLC is intended for rapid prototyping because the system designer doesn't need to know every little thing about the program before starting this will achieve steady condition in a quicker time interval. FLC can handle non-linearity and it does not demand the exact model of the system and more lustiness than conventional judgement controller.

FLC can be classified into four steps:

1. Fuzzification
2. Membership function
3. Inference
4. Defuzzification

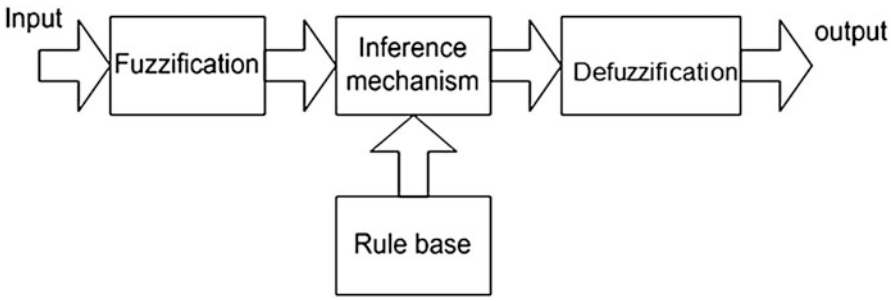


Fig. 6.69 Block diagram of fuzzy logic controller

Fuzzification

The operation of converting a crisp input value into right fuzzy value is termed "fuzzification". The input variables inside a fuzzy control system are in general mapped by sets of membership functions is known as "fuzzy sets". The membership function values are assigned towards linguistic variables using seven fuzzy subset called as Negative Big (NB), Negative Medium (NM), Negative Small (NS), Zero (ZE), Positive Small (PS), Positive Medium (PM), Positive Big (PB).

Membership Function

The membership function is often a curvature that describes each point of membership value from the input space. The volume of membership functions used will depend on the mandatory accuracy in the controller. The fuzzy logic based MPPT technique the error (E) and difference in error (CE) are taken as input variables which might be as below for Kth sample time.

$$E(K) = \frac{dp}{dv} = \frac{P_K - P_{K-1}}{V_K - V_{K-1}}$$
$$CE(K) = E(K) - E(K-1)$$

where Error E(k) is the load operation point at the instant k is located on right or left of MPPT. The Change of Error, CE(k) expresses the moving direction of MPPT. The input variable of Error E(k), Change in Error CE(k) are shown in Figs. 6.70 and 6.71, respectively. The output variable of V_{ref} is shown in Fig. 6.72.

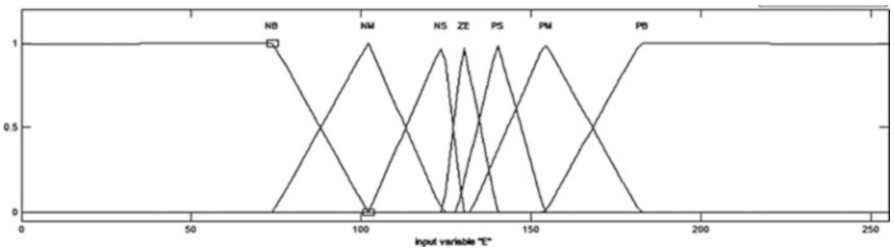


Fig. 6.70 Membership function of input variable 'error'

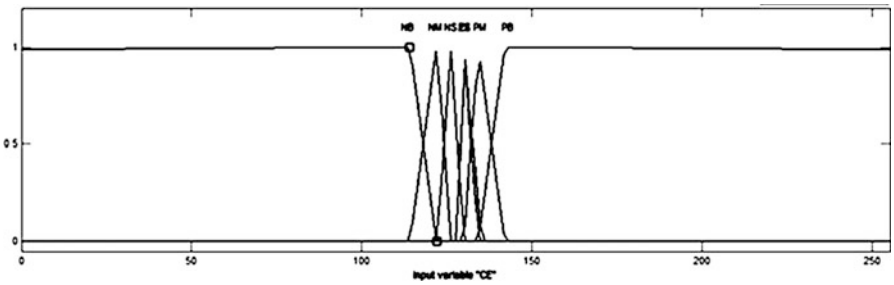


Fig. 6.71 Membership function of input variable 'change in error'

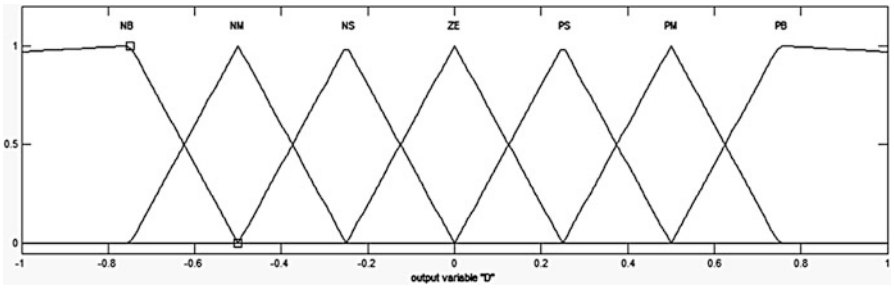


Fig. 6.72 Membership function of output variable 'V_{ref}'

Inference

Fuzzy rule base is an accumulation if-then rules which has all the info for the controlled parameters. A fuzzy inference method, Mamdani's strategy is used with Max-Min operation fuzzy combination. Fuzzy inference is founded on fuzzy rule base system. Rules are framed in inference block. The common strategy is MAX-MIN. The output membership function of every rule is given by MIN (Minimum) operator and MAX (Maximum) operator. The behaviour of the control surface which relates the input and output variables with the strategy is governed with a list of rules.

Defuzzification

Defuzzification is the procedure of conversion of fuzzy value into crisp value. The output of fuzzy controller can be a fuzzy subset. Because actual system requires a non fuzzy importance of control, hence the defuzzication is necessary. There are numerous methods for sale to defuzzification. Probably the most prevalent one is Centroid method, which utilizes the following formula:

$$\int \frac{x\mu(x)dx}{\mu(x)dx}$$

where μ is the membership degree of output x.

6.6.4 *Fuzzy Logic Controller Based MPPT for HPS*

P&O means for MPPT tracking will not respond quickly to rapid changes in photovoltaic cell temperature or irradiance. Meaning that the fuzzy control algorithm is competent at enhancing the tracking performance. A FLC makes for rapid prototyping for the reason that system designer doesn't have to recognize everything regarding the system before commencing this will achieve steady state in a shorter interval. FLC can take care of non-linearity also it does not require the precise mathematical model of the system and more robustness than conventional logic controller.

A Fuzzy based MPPT and DC-DC Boost converter are proposed within this project. Conventional Controller put in at home are straightforward to implement, however it contains the disadvantage to dependence system parameters especially in photovoltaic and WECS with massive amount uncertainties as being a sequence of changing wind speed and solar irradiance.

Due to inherent robustness and uncertainties in fuzzy logic controller, it can be used effectively in solar PV and WECS. The Maximum Power Point Tracking (MPPT) extracts the maximum power from the (wind turbine from cut in to rated wind velocity by sensing the output DC power of the wind generator.

The maximum power can be extracted at a certain operating point, with coordinates of V_{MPP} and I_{MPP} as shown in Fig. 6.73. Since the MPP depends on solar irradiation, cell temperature and Wind speed, it is never constant over time, thereby MPPT should be used to track its changes. Some of the advantages of FLC are

- Allows for rapid prototyping because the system designer doesn't need to know everything about the system before starting.
- Rule base or fuzzy sets are easily modified.
- Relates input to output in linguistic terms, making it easy to understand.
- Cheaper because they are easier to design.
- Increased robustness.
- It can achieve less overshoot and oscillation.
- It can achieve steady state in a shorter time interval.

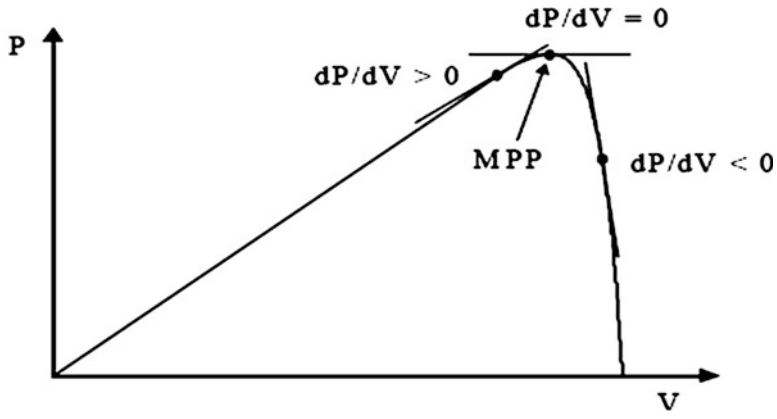


Fig. 6.73 P-V characteristics

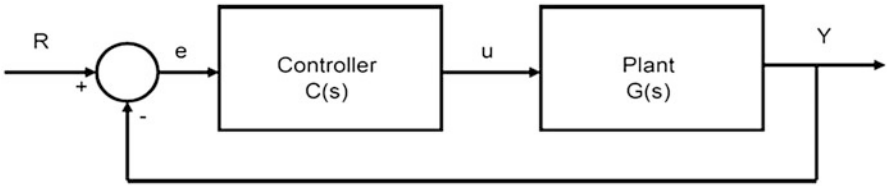


Fig. 6.74 Structure of PID controller

6.6.5 PID Controller

PID controller is a control loop feedback mechanism (controller) widely used in industrial control systems.

A PID controller calculates a problem value as the visible difference between a scored process variable and a desired set level. The controller tries to minimize the error in outputs aside adjusting the physical process control inputs.

The particular PID controller criteria involves three distinct constant parameters, and is accordingly sometimes referred to as three term command the proportional, integral and derivative prices denoted P, i, and D; i.e., these beliefs can be interpreted in terms of your energy: P depends within the present error, My partner and i on the accumulation of past errors, and D is a prediction of foreseeable future errors, based about current rate involving change.

By tuning the three guidelines in the PID controller algorithmic rule, the controller offers control action designed for the specific method requirements. The response of the control can be explained in terms with the responsiveness of the particular controller to a blunder, the degree this agreement the controller overshoots the arranged point, and the degree of system cycle. PI controllers tend to be fairly common, since derivative action is sensitive to rating noise. The

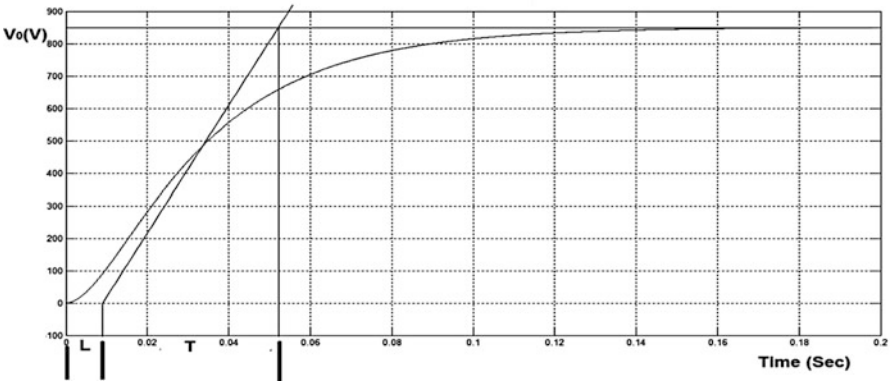


Fig. 6.75 S-shaped reaction curve method

essential term is proportional to both magnitude of the error and the continuance of the fault.

The S-shaped reaction curve can be characterized by two constants as shown in Fig. 6.75, delay time L and time constant T, which are determined by drawing a tangent line at the inflection point of the curve and finding the intersections of the tangent line with the time axis and the steady-state level line.

The proportional and integral gain values can be calculated by using the following formulae,

$$\text{Proportional gain, } K_P = 0.9 * \frac{T}{L}$$

$$\text{Integral gain, } K_I = 0.27 * \frac{T}{L^2}$$

where T is the time constant and L is the delay time constant.

6.6.5.1 Characteristics of PID Controllers

A proportional controller (Kp) will have the issue of lowering the rise time and will reduce but never remove the steady-state error. A integral control (Ki) could have the issue of eliminating the steady-state error for a constant or step input, nevertheless it will make the transient response slower. A derivative controller (Kd) will have the issue of helping the stability of the system, lowering the overshoot, and increasing the transient response.

The effects of each of controller parameters and on a closed-loop system are summarized in the Table 6.7.

Typical steps for designing a PID controller:

1. Determine what characteristics of the system need to be improved.
2. Use K_p to decrease the rise-time.

Table 6.7 PID controller rules

Response	Rise-time	Overshoot	Settling-time	Steady-state error
$\mathbf{K_P}$	Decrease	Increase	No change	Decrease
$\mathbf{K_I}$	Decrease	Increase	Increase	Eliminate
$\mathbf{K_D}$	Decrease	Increase	Increase	No change

Table 6.8 Ziegler–Nichols tuning rule table

Controller	K_P	K_I	K_D
P	$\frac{T}{L}$	0	0
PI	$0.9 * \frac{T}{L}$	$0.27 * \frac{T}{L^2}$	0
PID	$1.2 * \frac{T}{L}$	$0.6 * \frac{T}{L^2}$	0.6 T

3. Use K_d to reduce the overshoot and settling-time.
4. Use k_i to eliminate the steady-state error.

6.6.5.2 Ziegler-Nichols Tuning Rule Table

Using the parameters L and T, one can set the values of K_P, K_I and K_D according to the formulae as shown in the Table 6.8.

These parameters will typically give the response with an overshoot about 25 % and good Settling-time. The Ziegler-Nichols tuning rule is suitable reaction curve method when initial estimate of parameters are known. The proportional and integral gain control is determined by using the formulae as shown in Table 6.8. PI Controller is designed to control the output of Buck-boost converter based on Ziegler-Nichols tuning method.

6.6.6 Simulation of Solar PV Under Atmospheric Conditions

The single solar PV module consists of series and parallel solar cells, which is used to increasing the voltage and current. The maximum current is given to the input of a current controlled source. The maximum output power of solar PV is 100 kW. The amount of produced power is generated by solar cell is very small. So the cells are arranged in series and parallel to produce the useful range of electric power.

Figures 6.76 and 6.77 which represent the I-V and P-V characteristics of solar cell TITANS6_60 which is written in M-file coding.

The solar PV module consists of 24 modules connected in series and 20 strings connected in Parallel. The specifications of solar cell TITANS6_60 considered for simulation are tabulated in Table 6.9. In the event the modules are wired together in series, their voltage rating is increased while the current remains constant. In the event the modules are wired in parallel, their current is increased even though the voltage remains constant. The absolute maximum power can be had by varying

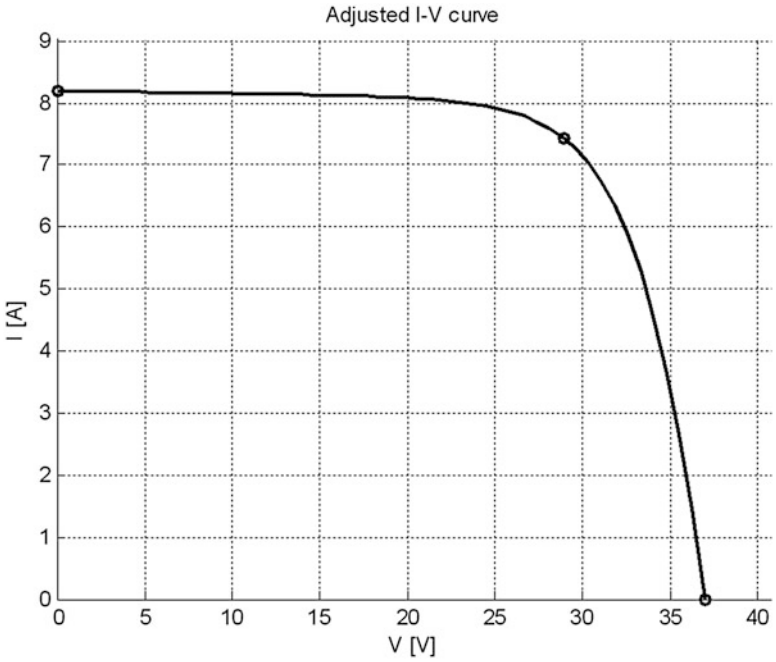


Fig. 6.76 I-V characteristics of solar PV system

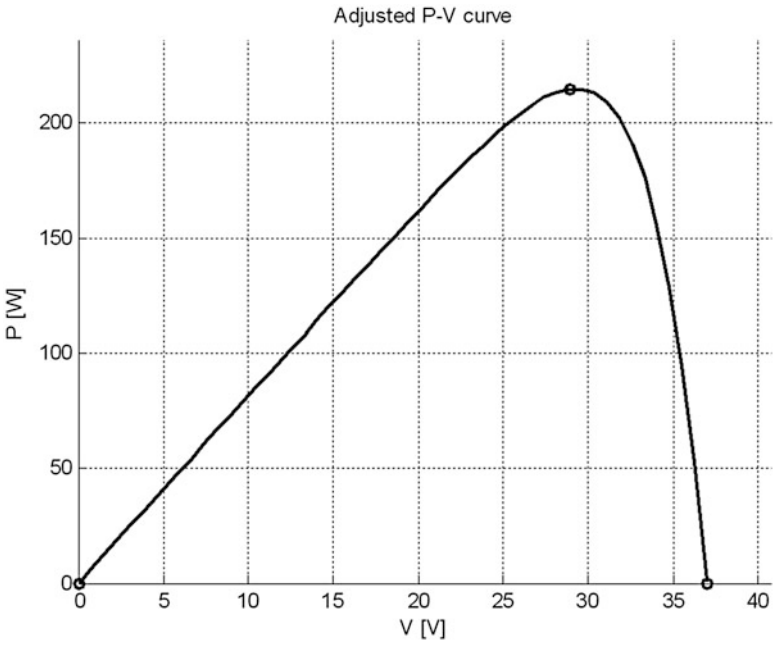


Fig. 6.77 P-V characteristics of solar PV system

Table 6.9 Parameters of the TITANS6_60 PV module at 25 °C and 1,000 W/m^2

Parameter	Symbol	Value
Peak power	P_{MPP}	215.015 W
Peak power voltage	V_{MPP}	28.9 V
Peak power current	I_{MPP}	7.44 A
Open circuit voltage	V_{OC}	37 V
Short circuit current	I_{SC}	8.21 A
Temperature coefficient of current	K_i	3.183e^{-3} mA/°C
Temperature coefficient of voltage	K_v	−0.123 mV/°C
Number of series cells	N_s	60

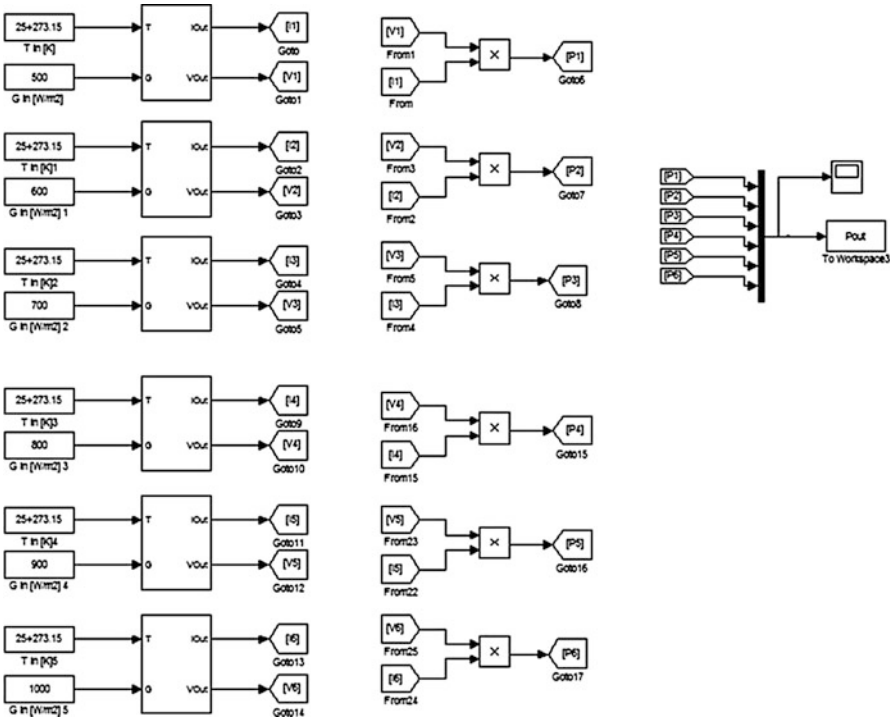


Fig. 6.78 Solar PV array for different values of solar irradiance and fixed cell temperature

the solar cell temperature and solar irradiance. The photovoltaic module is simulated for different values of solar irradiance and fixed cell temperature as shown in Fig. 6.78.

The maximum power can be obtained from solar PV module in the voltage range from 700 to 800 V as shown in Fig. 6.79.

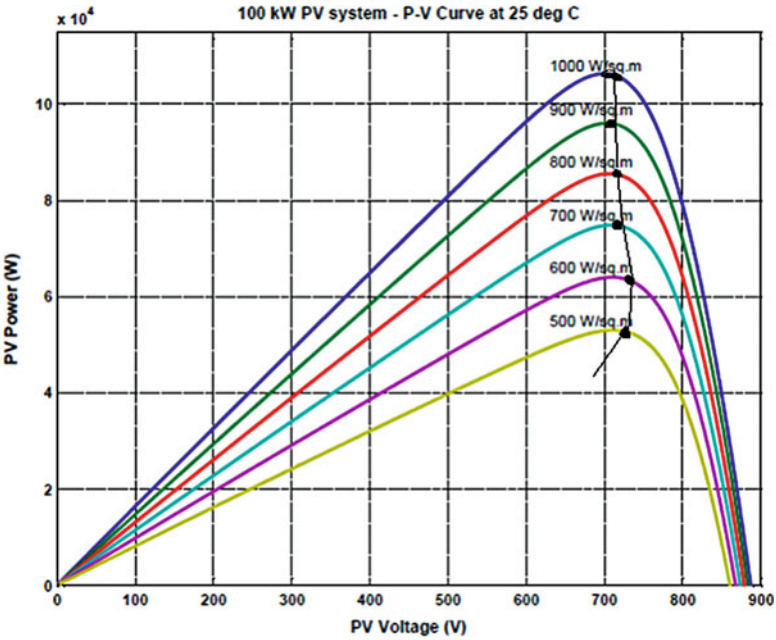


Fig. 6.79 P-V characteristics of solar PV module-different solar irradiance & fixed cell temperature

Table 6.10 Output power for different operating conditions

Sl. No.	Irradiance (W/m^2)	Output power (kW)
1	500	55
2	600	64
3	700	78
4	800	85
5	900	98
6	1,000	110

The solar PV output power is obtained according to the variable irradiance levels between (500–1,000 W/m^2) and fixed solar cell temperature of 25 °C as shown in Table 6.10. The solar PV voltage and current are varied corresponding to the solar irradiance as shown in Fig. 6.80.

The maximum power is obtained according to different solar irradiance levels between 200 and 1,000 W/m^2 as shown in Fig. 6.81. The maximum solar PV output power is 100 kW which is obtained at the solar irradiance of 1,000 W/m^2 as shown in Table 6.11.

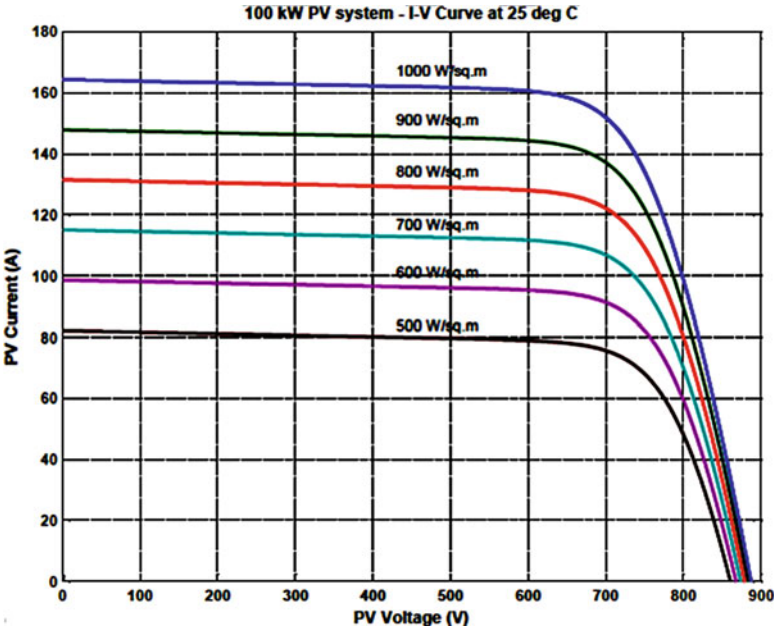


Fig. 6.80 I-V characteristics of solar PV module-different solar irradiance & fixed cell temperature

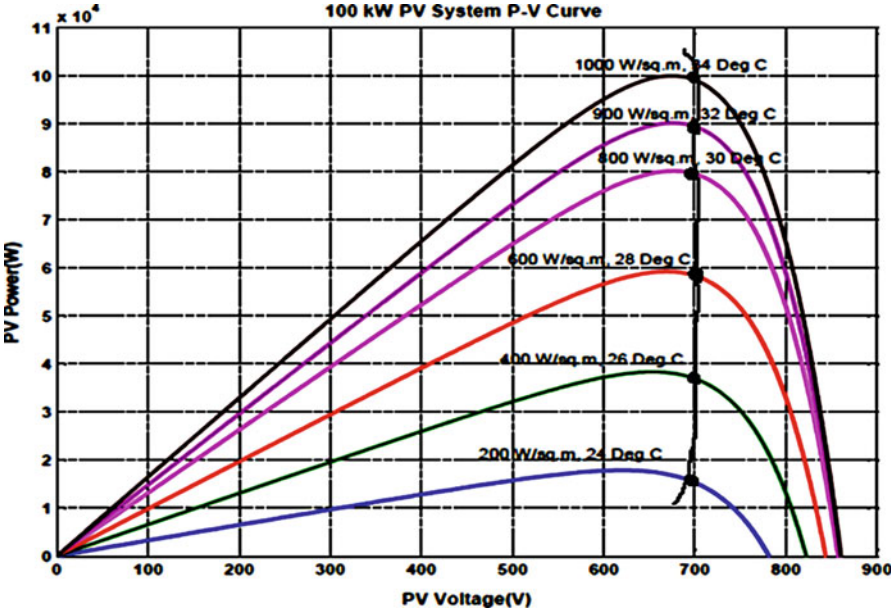


Fig. 6.81 P-V characteristics of solar PV module-different cell temperature & solar irradiance

Table 6.11 Output power for different solar irradiance conditions

Sl. No.	Irradiance (W/m^2)	Output power (kW)
1	200	20
2	400	38
3	600	60
4	800	80
5	900	90
6	1,000	100

6.6.7 Simulation of FLC Based MPPT

The simulations are carried out in MATLAB/SIMULINK environment and the results are discussed in this section.

6.6.7.1 Solar PV

The solar PV system model consists of FLC based MPPT, DC-DC converters and load. The system is simulated in MATLAB/SIMULINK environment at cell temperature of 25 °C and Solar Irradiance of 1,000 W/m^2.

The Solar output voltage and current are measured and fed to the fuzzy based MPPT control circuit for MPP tracking. Based on the change of power with respect to change of voltage dp/dv and Δdp/dv, fuzzy control determines the voltage reference from solar PV system by modulating the duty cycle in the boost converter.

When the solar PV output power is positive, the system will keep the perturbation in same direction. The system will change the perturbation in reverse direction, when the change of power is negative.

6.6.7.2 DC-DC Converters

A fuzzy logic based MPPT control technique is implemented to generate the optimal voltage from the PV system by modulating the duty cycle is applied to the boost converter switch. Buck-boost converter is used to maintain the constant DC-link capacitor voltage which is controlled by PI controller. Thus a constant DC voltage is obtained from the PV system as shown in Fig. 6.83. This DC power is supplied to DC load. The same power is inverted and it is supplied to AC load.

The PV module has variable irradiance and fixed cell temperature. For analysis purpose, irradiance levels of 200, 1,000, and 850 W/m^2 are considered. The PV module output power is 40, 100, and 87 kW are shown in Fig. 6.83.

The Buck-boost converter output voltage is maintained at constant 850 V as shown in Fig. 6.84. The Buck-boost Converter and PI Controller parameter values are shown in Table 6.12.

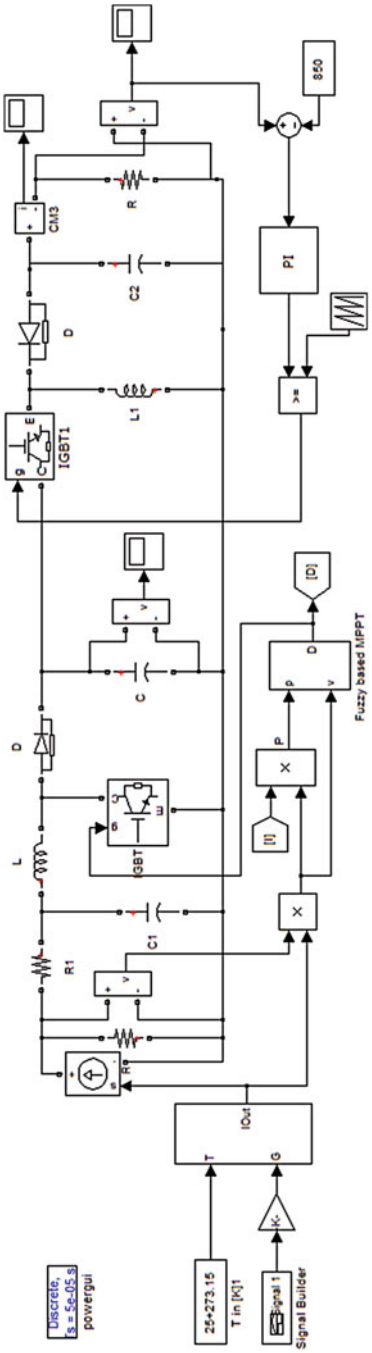


Fig. 6.82 Simulation of solar PV system

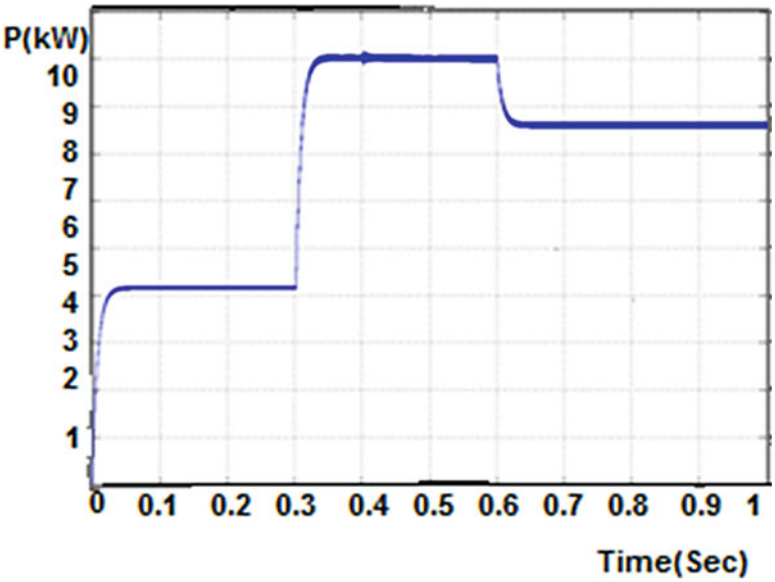


Fig. 6.83 Output power of solar PV system

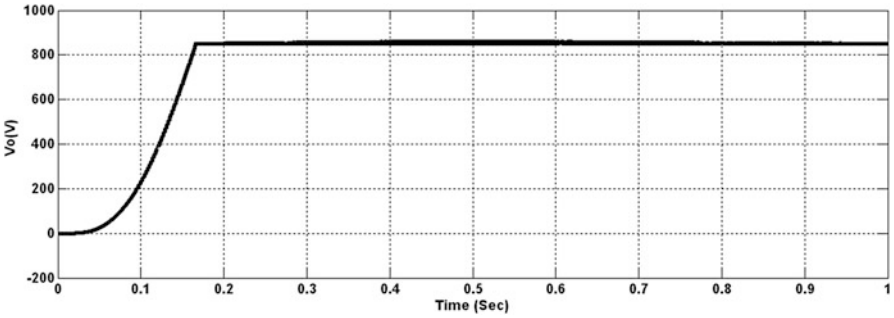


Fig. 6.84 Output voltage of buck-boost converter

6.6.7.3 Wind Generation System

The wind energy system has been developed and simulated in MATLAB/SIMULINK as shown in Fig. 6.85. The maximum output power of Wind generation is 200 kW. The Wind generation system has Wind turbine, two mass Drive Train, PMSG. By running the wind turbine generator in variable speed mode, the maximum power can be extracted at low and medium wind speeds. The output of wind turbine is Mechanical torque (T_m), which is not directly connected to PMSG, T_m is given to PMSG through Drive train.

Table 6.12 Parameters of buck-boost converter and PI controller

Parameter	Symbol	Value
Input voltage	Vs	350–1,200 V
Output voltage	V_0	850 V
Switching frequency	F_s	20 kHz
Inductance	L	8 mH
Capacitance	C	85 μF
Proportional gain	K_p	2
Integral gain	K_i	50

The PMSG converts the mechanical power from the wind turbine into output power of AC, which is then converted into DC power through a converter with DC-link voltage is supplied to DC load. The mechanical power converted from the turbine is a function of the rotational speed, and the converted power is maximized at the particular rotational speed for various wind speeds. The fuzzy logic based MPPT can track the MPP faster and it can also minimize the voltage fluctuation after MPP has been recognized. The Buck-boost converter is used to maintain the constant voltage and it is done by controlling with PI Controller. The DC voltage source is converted to AC and it can be supplied to AC load.

The maximum output power 200 kW is obtained at the wind speed of 11 m/s. The output power is varied according to the rotor speed variation as shown in Fig. 6.86 and Table 6.13.

The 200 kW Wind Generation system parameters and their values are tabulated in Table 6.14. The specification of ITALTECH 200 kW wind turbine is considered for simulation.

The maximum power is extracted at pitch angle of 0° and wind velocity of 11 m/s. The RMS line voltage is 500 V and output power of wind generation system is 200 kW, obtained at wind velocity of 11 m/s as shown in Fig. 6.87.

The Buck-boost converter output voltage is maintained at 850 V as constant and it is shown in Fig. 6.88. The parameter values of Buck-boost converter and PI Controller as mentioned in Table 6.15.

6.6.7.4 Hybrid Solar and Wind Generation System

The solar PV system is integrated with the wind energy system to form the hybrid system as shown in Fig. 6.89. The hybrid renewable energy system ensures continuous power flow to the load. The proposed fuzzy based MPPT for hybrid system comprises of a Wind turbine and a Solar PV system to the load. The only adaptation needed is the requirement to maintain the DC bus voltage constant. Both Solar PV and Wind are connected in parallel to a common PWM inverter through their individual AC-DC rectifier and DC-DC converters. The Fuzzy logic based MPPT can track the maximum power point faster and it can also minimize the voltage fluctuation. The Solar PV and Wind turbine voltage are measured and controlled

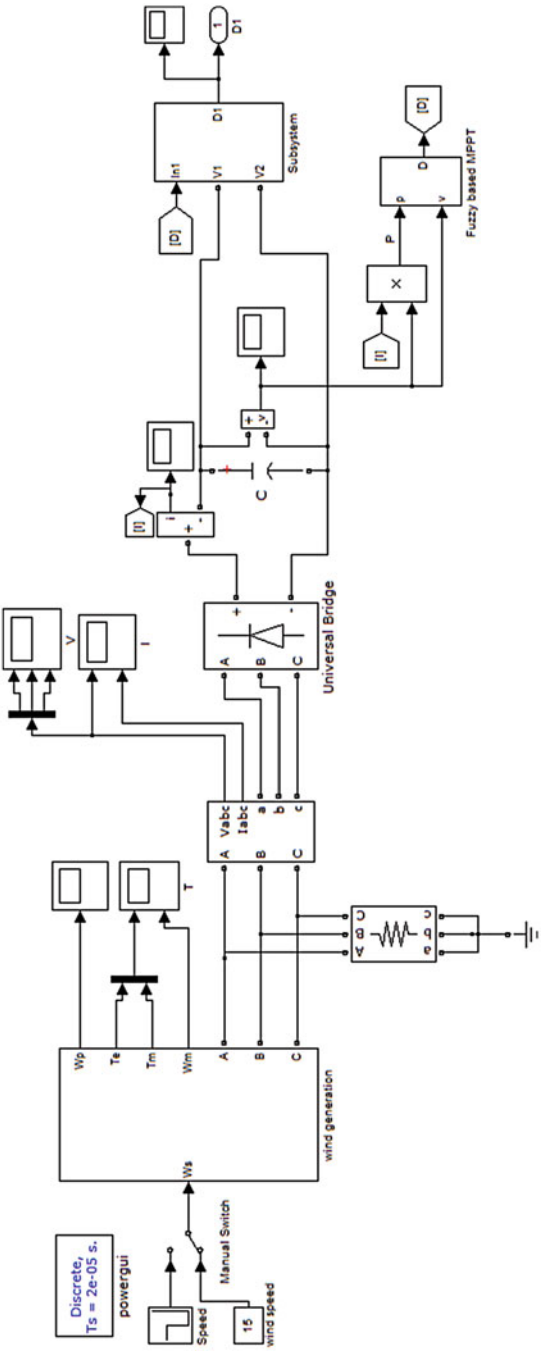


Fig. 6.85 Simulation of wind generation system

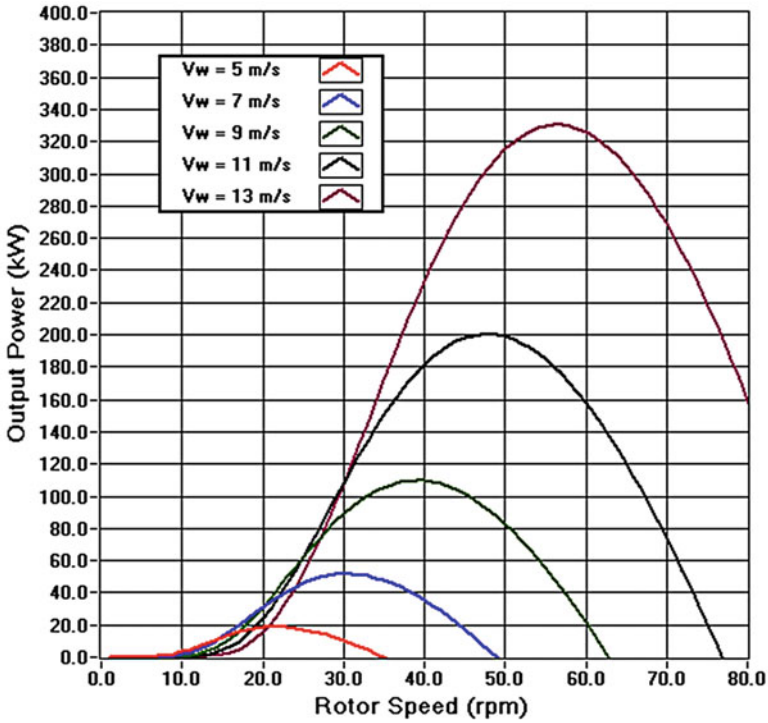


Fig. 6.86 Output power versus speed characteristics of wind generation system

Table 6.13 Output power of wind generation system

Wind speed (m/s)	Output power (kW)
5	30
7	60
9	110
11	200
13	325

based on the error signal. The error is fed into the controller, to generate the pulses for DC-DC Boost converter. The Boost Converter output voltage is varied corresponding to the MPP output by varying the duty cycle. Hence, DC-DC Buck-boost converter has been implemented to maintain the output voltage constant. The DC bus voltage is converted into AC by using inverter.

The function of the inverter is to transfer the maximum power to the load. The low harmonic distortion of the voltage and current at the output of the inverter is achieved by using an output filter. The filter is the most favourable one for the attenuation of the harmonics of the inverter. The PWM inverter is connected to the load through a low pass L-filter. The operating values of three phase PWM inverter is tabulated in Table 6.16.

Table 6.14 Parameters of wind generation of 200 kW system

Permanent magnet synchronous generator		
Parameter	Symbol	Value
Stator resistance	R_s	0.005 Ω
Armature inductance	L_a	0.000835 H
Static friction	T_f	0.54 N-m
Flux linkage	ϕ	0.283 Wb
Moment of inertia	J	0.1197 kg-m^2
Viscous damping	F	0.1189 N-m
Pole pairs	P	24

Wind turbine model		
Parameter	Symbol	Value
Mechanical output power	P_m	200 kW
Base wind speed	V_w	11 m/s
Maximum power at base wind speed	P_{max}	0.9 pu
Pitch angle	β	0°

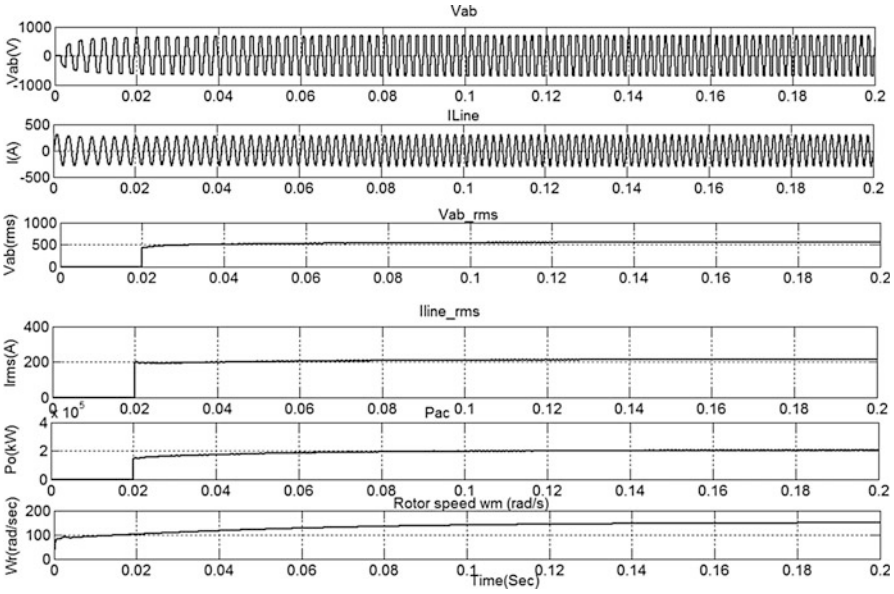


Fig. 6.87 Output waveforms of PMSG

The three phase RMS output voltage is 415 V and it is shown in Fig. 6.91. The THD spectrums for output current without and with filter are shown in Figs. 6.92 and 6.93, respectively. The Peak Voltage of Three Phase PWM Inverter is 586 V and it is shown in Fig. 6.90.

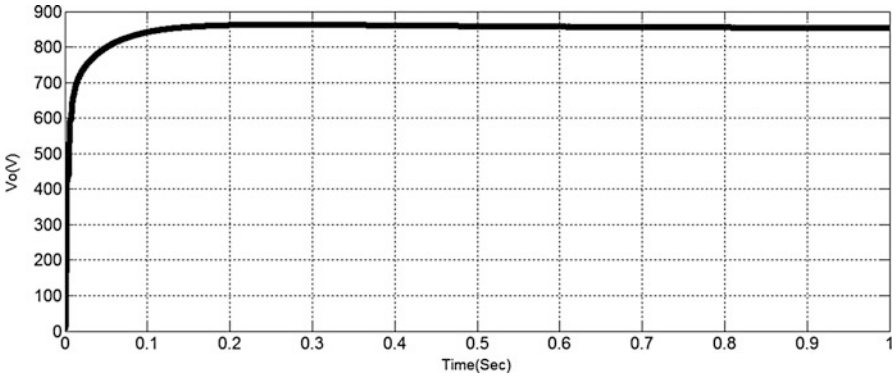


Fig. 6.88 Output voltage of buck-boost converter

Table 6.15 Parameters of buck-boost converter and PI controller

Parameter	Symbol	Value
Input voltage	Vs	300–1,100 V
Output voltage	V_0	850 V
Switching frequency	F_s	20 kHz
Inductance	L	9 mH
Capacitance	C	57 μF
Proportional gain	K_p	3.86
Integral gain	K_i	500

The output current of three phase inverter without filter has 51.82 % THD, which is shown in Fig. 6.92. By using L-filter, the current harmonic is reduced to 1.6 % THD as shown in Fig. 6.93.

The stand-alone 100 kW Solar PV and Wind Energy Systems are designed, simulated for a load of 100–200 kW. The proposed fuzzy logic based MPPT technique can track the maximum power point faster than the conventional controller. It has the ability of reducing the voltage fluctuation after MPP has been recognised. The Solar PV and wind energy system not only boosts up the voltage but also produce a signal, free from transient noise. Hence the performance of the closed loop system has been improved by using FLC.

The synchronized hybrid Solar and Wind energy systems are simulated in MATLAB/SIMULINK. After obtaining the constant output voltage, from both Wind and Solar energy systems, they are connected in parallel. The DC source from hybrid power system is converted to AC by using PWM inverter. In order to produce a pure sine wave output with low harmonics, an L-filter is used. The output current of the inverter has 1.6 % THD which is lower than the IEEE-519-1992 standard. The hybrid power system can be utilized either for remote generation plants or it can be utilized for grid integration.

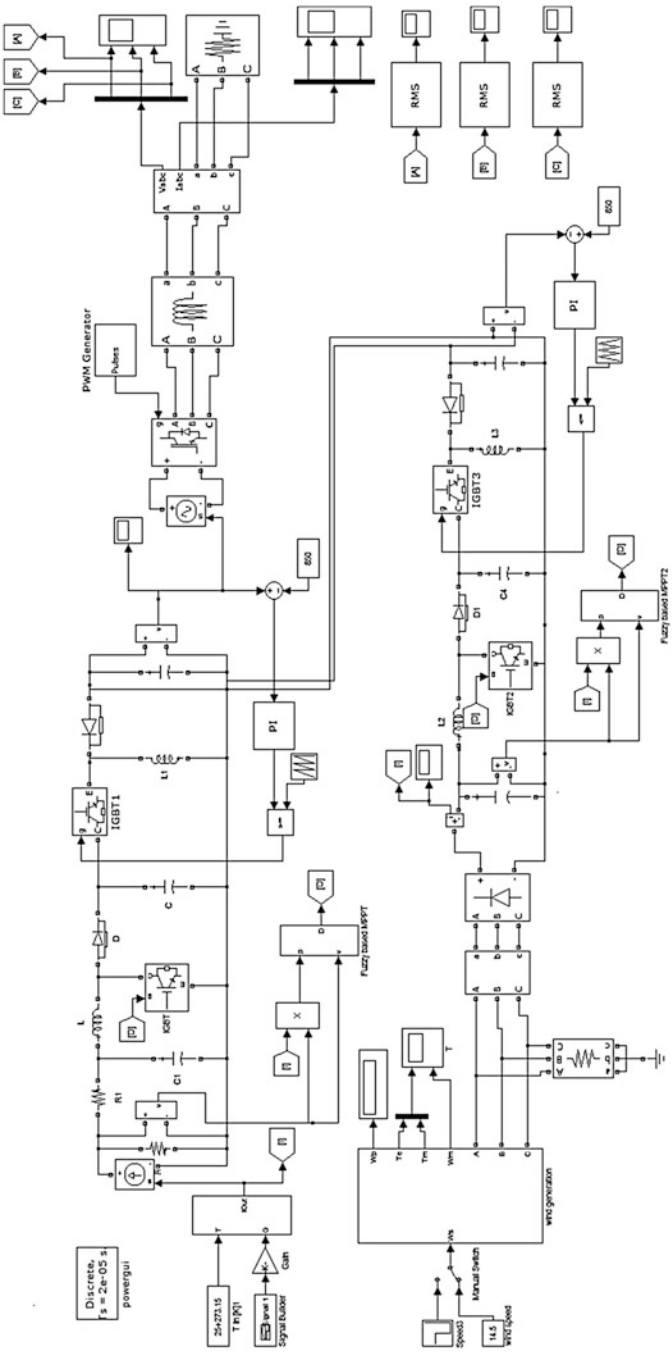


Fig. 6.89 Hybrid solar PV and wind generation system

Table 6.16 Operating values of three phase PWM inverter

Parameter	Symbol	Value
DC input voltage	V_s	850 V
AC input voltage	V_0	415 V
Carrier frequency	F_c	10 kHz
Modulation index	m	0.9
Filter inductance	L	4 mH

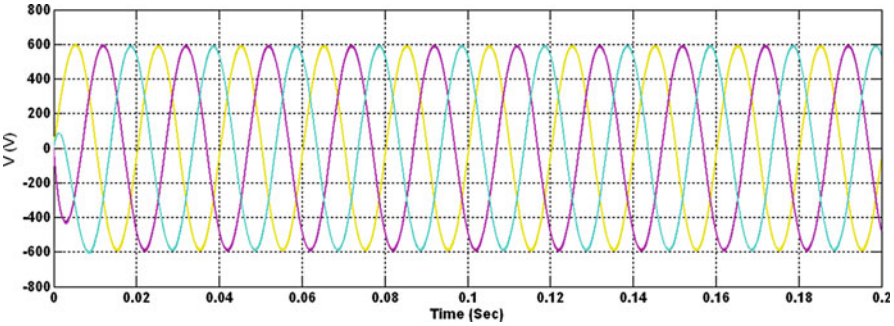


Fig. 6.90 Output voltage of three phase inverter

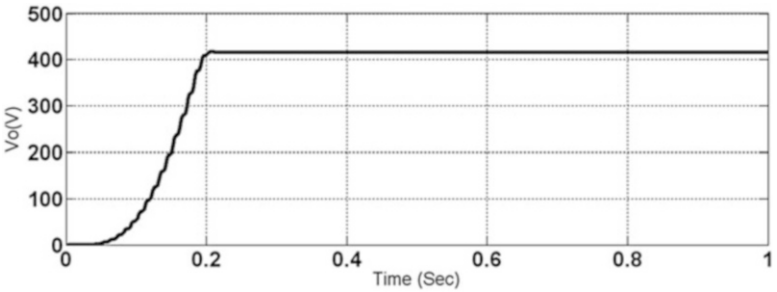


Fig. 6.91 RMS voltage of three phase inverter

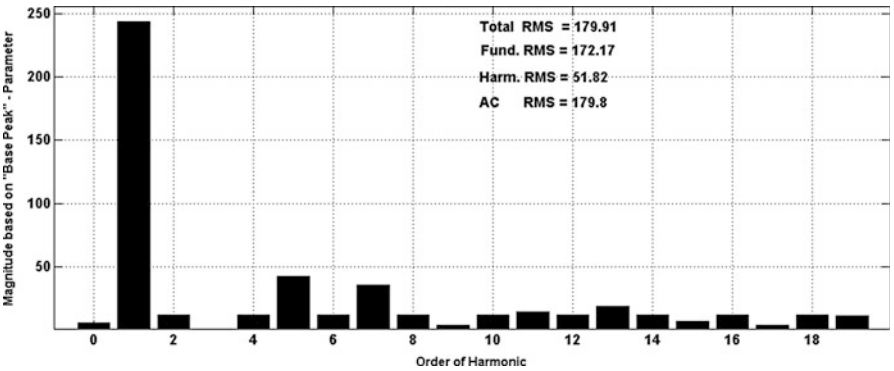


Fig. 6.92 THD spectrum of output current without filter

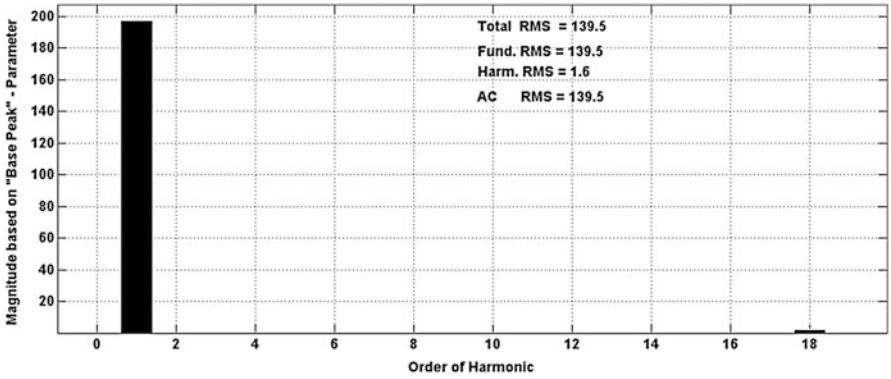


Fig. 6.93 THD spectrum of output current with filter

6.7 Summary

Hybrid energy system including several (two or more) energy sources with appropriate energy conversion technology connected together to feed power to local load/grid. Since, it is coming under distributed generation umbrella, there is no unified standard or structure. It receives benefits in terms of reduced line and transformer losses, reduced environmental impacts, relived transmission and distribution congestion, increased system reliability, improved power quality, peak shaving, and increased overall efficiency. HES allow wide variety of primary energy sources, frequently renewable sources generation as the stand alone system for rural electrification where grid extension is not possible or uneconomic. The hybrid combination of Solar PV and Wind energy conversion system, along with solar PV with diesel energy are discussed in this chapter. Suitable MATLAB/SIMULINK models and their results are also presented. Design and development of various HES components has more flexibility for future extension and growth. Device can be added as the need arises and assure the promising operation with existing system.

Review Questions

1. What are the advantages of hybrid solar PV with diesel over hybrid solar PV with wind energy conversion systems?
2. Discuss the different types of converters used for hybridising solar PV and wind energy conversion systems.
3. What is the need for agentification in hybrid energy systems?
4. Mention the need for filters in the modelling of HES.
5. State the design considerations involved in Buck Boost converter.
6. Discuss the challenges involved while integrating hybrid energy system with grid connected system.

7. Develop a MATLAB/SIMULINK model of PV/wind hybrid system using cuk-sepic converter.
8. Define THD. Analyse the performance of converters used in HES based on THD.
9. Develop a MATLAB/SIMULINK model for MPPT control in HES using Artificial Neural Networks and Genetic Algorithms.

Bibliography

Abbey C, Joos G (2005) Energy management strategies for optimization of energy storage in wind power hybrid system. In: Proceedings of the 36th IEEE power electronics specialists conference, pp 2066–2072

Basso TS, DeBlasio RD (2003) IEEE P1547-series of standards for interconnection. IEEE, New York

Borowy BS, Salameh ZM (1996) Methodology for optimally sizing the combination of a battery bank and PV array in a wind/PV hybrid system. IEEE Trans Energy Conv 11(2):367–375

Davidson J, The new solar electric home, 20th printing 2001

Dursun E, Kilic O (2012) Comparative evaluation of different power management strategies of a stand- alone PV/Wind/PEMFC hybrid power system. Electr Power Energy Syst 34:81–89, Elsevier

Haiwen Liu, Leon M Tolbert, Surin Khomfoi, Burak Ozpineci, Zhong Du (2008) Hybrid cascaded multievel inverter with PWM control method. IEEE, pp 162–166

Hart DW (1997) Introduction to power electronics. Prentice Hall, New Jersey

IEC 61000-3-6:1996 Electromagnetic compatibility (EMC) – Part 3: Limits – Section 6: Assessment of emission limits for distorting loads in MV and HV power systems. Basic EMC publication

IEEE recommended practice for utility interface of photovoltaic system, IEEE Std. 929–2000

Jain S, Agarwal V (2008) An integrated hybrid power supply for distributed generation applications fed by nonconventional energy sources. IEEE Trans Energy Convers 23:622–631

Jiang Z (2006) Agent-based control framework for distributed energy resources micro grids. In: Proceedings of the IEEE International conference on intelligent agent technology, pp 646–652

Kalantar M, Mousavi SMG (2010) Dynamic behaviour of a stand-alone hybrid power generation system of wind turbine microturbine, solar array and battery storage. Appl Energy 87:3051–3064, Elsevier

Kern EC, Gulachenski EM, Kern GA (1989) Cloud effects on distributed photovoltaic generation: slow transients at the Gardner, Massachusetts photovoltaic experiment. IEEE Trans Energy Convers 4(2):184–190

Kouro S, Bernal R, Miranda H, Silva CA, Rodriguez J (2007) High-performance torque and flux control for multilevel inverter fed induction motors. IEEE Trans Power Electron 22(6):2116–2123

Lagorse J, Simoes MG (2009) Multiagent fuzzy-logic-based energy management of hybrid systems. IEEE Trans Ind Appl 45(6):2123–2129

Musavi F, Edington M, Eberle W, Dunford WG (2011) Evaluation and efficiency comparison of front end AC-DC plug-in hybrid charger topologies. IEEE Trans Smart Grid 1–9

Nirmala Jyothi J, Sateesh S (2012) MATLAB/SIMULINK model of grid connected PV system With Maximum power point tracking. Int J Emerg Trends Eng Dev 7(2)

Pairodamonchai P, Sangwongwanich S (2009) Design and implementation of a hybrid output EMI filter for high frequency common-mode voltage compensation in PWM inverters. IEEE Trans Ind Appl 45(5):1647–1659

Rashid MH (2006) Power electronics devices, circuits and applications. Academic Press, San Diego

Rech C, Pinheiro H, Grundling HA, Hey HL, Pinheiro JR (2002) Analysis and comparison of hybrid multilevel voltage source inverters. ISSN: 0-7803-7262-x/02, pp 491–496

Schekulin D (1999) Grid-connected photovoltaic system. Germany Patent DE197 32218 Cl; Mar 1999

Sreedevi M, Paul PJ (2011) Fuzzy PI controller based grid-connected PV system. Int J Soft Comput 6:11–15

Zhong J (2006) PID controller tuning: a short tutorial. Mechanical Engineering, Purdue University, Spring

Chapter 7
Grid Integration Techniques in Renewable Energy Systems

Learning Objectives
On completion of this chapter, the reader will have knowledge on

- Grid Issues in integrating renewable energy systems.
- Converters used for grid integration techniques and its control strategy.
- MATLAB/SIMULINK models of Synchronous Reference Frame PLL (dq PLL), Stationary Reference Frame PLL (αβ PLL), Decoupled Synchronous Reference Frame PLL (DSRF PLL), Decoupled Stationary Reference frame PLL (Dαβ PLL) and Hybrid Dαβ PLL.
- Filters used for grid integration techniques and its control strategy.

7.1 Introduction

Depending on the scale of generation, the renewable energy can be integrated into the utility grid either at the transmission level or at the distribution level. Wind farms which are a part of large renewable energy generation can be directly interconnected to the transmission system whereas the small scale distributed generation is generally interconnected to the medium or low voltage distribution systems. Before designing the system for both the types of interconnections a detailed analysis have to be made to face the different challenges in it. The most common issues encountered during the grid integration of different types of renewable energy systems are outlined and discussed in this chapter. The different problems and solutions are highlighted in this chapter through detailed simulations and case studies.

© Springer International Publishing Switzerland 2015

S. Sumathi et al., *Solar PV and Wind Energy Conversion Systems*,
Green Energy and Technology, DOI 10.1007/978-3-319-14941-7_7

7.1.1 Integration of Small Scale Generation into Distribution Grids

Electricity generation using various renewable energy resources like small hydro, solar photovoltaic, biogas, biomass and small wind turbine based electricity generation are often taking place in small scale due to disperse nature of the resources and the generation varies between a few hundreds of kilowatts to several megawatts. Distributed generation (DG) or distributed resources (DR) are the one where these small scale electricity generators are generally connected to the grid either at the primary or secondary distribution level. Distributed resources include both renewable and non-renewable small scale generation as well as energy storage.

7.1.2 Different Types of Grid Interfaces

The energy generated through small renewable energy generators cannot be directly connected to grid. Some kind of interface is required between the generation and utility distribution grid. For example, power electronics based dc -to –ac converter is required between the grid and the solar photovoltaic's (PV) panel generator. Though the direct connection to the ac grid is possible through induction generator based small hydro or wind a power electronic converter is used to avoid concerns regarding starting transients, energy conversion efficiency and power quality. The common types of energy generation and their preferred interfacing technologies are summarized in Table 7.1.

7.1.3 Issues Related to Grid Integration of Small Scale Generation

Conventional electric distribution system has a single voltage source on each distribution feeder. But this is not the case when small scale renewable energy generations are interconnected to the distribution grid. Hence in order to ensure safe and reliable operation of the grid certain special requirements are to be satisfied during interconnection. Major protection related problems are fault clearance, reclosing and inadvertent islanded operation. In many cases, the grid –DG interface

Table 7.1 Interfacing technologies

Type	Interfacing technology
Fuel cells	Power electronic converter
Wind	Induction generator/power electronic converter
Photovoltaics	Power electronic converter
Small hydro	Synchronous or induction generator, power electronic converter

is based on power electronics inverters or asynchronous generators. The utilities are concerned about their impact on power quality and the impact includes harmonics, voltage dips, over voltages, and voltage flicker. Several studies in literature have identified that the technical requirements imposed by utilities to address these concerns as a major technical barrier for grid integration of DG. The general technical requirements for interconnection of small scale generation uses IEEE P1547 standards as guideline.

7.1.3.1 Protection Issues

The most serious issue related to the interconnection of distributed generation is Protection. Usually radial type distribution network configuration is used with time graded over current protection scheme. When a DG is interconnected it may alter the coordination of the existing protection scheme and can lead to malfunction of the protection equipment. The protection issues related to the interconnection of DG are briefly discussed below.

(a) Change of Short Circuit Levels

The main parameter used in the selection of fuses, reclosers. circuit breakers and currents transformers, and the coordination between over current relays are based on Short circuit level. The equivalent system fault point impedance and the expected fault current level are decided by the short circuit level. Rotating machine characteristics around the surroundings also decides the time variation in the fault current. Initially most distribution systems are designed as passive networks but the interconnection of DG made the equivalent network impedance to decrease which results in increase in the fault level. Therefore if fault occurs the existing circuit breakers may not withstand to the sudden high fault currents which also lead to CT saturation. Also the changed fault levels may upset the synchronisation among the over current relays which leads to unacceptable protection system operation. To explain the problem, consider the distribution system in Fig. 7.1. During the absence of DG the fault currents seen by the feeder breaker BK ($\mathbf{I_s}$) and the recloser RC ($\mathbf{I_r}$) are approximately equal to the fault current $\mathbf{I_f}$ ($I_s = I_r = I_f$). But when the DG is connected, $I_r = I_s + I_{dg}$ and $I_r > I_s$. This condition is not normally observed in passive radial network. This is not a concern if the interrupting capacity of the recloser is sufficient to handle the increased fault current. But, it is likely that coordination between the recloser and any downstream fuses is lost. During higher fault currents the recloser and fuses operate faster which makes the coordination to lose, due to reduction in the required margin between the recloser fast curve and the fuse melting curve.

(b) Reverse Power Flow

The power flows are unidirectional in radial distribution systems. Initially depending upon the power flow the protection schemes are designed. When a DG is connected, the coordination among the protection relays may get altered due to reversal in power.

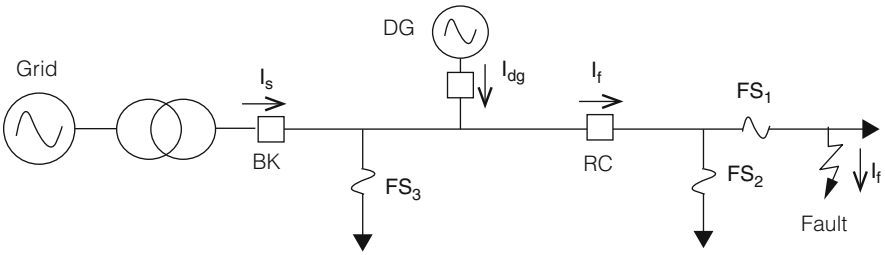


Fig. 7.1 Change of fault currents due to DG interconnection

(c) Lack of Sustained Fault Current

If fault occurs the protection relays may detect and discriminate the fault currents only if the measured fault current by the relays is significantly high when compared to the normal load current. When the DG fault current contribution is limited, the effective detection of faults by over current based protection relays is difficult. Normally, induction generators, small synchronous generators or power electronic converters are employed in renewable based energy generation. Supply of continual fault currents to three phase faults is not possible by the induction generators and fault current contribution to the asymmetrical faults is also limited. In small synchronous generators sustained fault current supply which is significantly higher than the rated current is not possible. Power electronic converters are designed to limit the output current internally since the power semiconductor devices cannot resist the significant over current for long period. The ability of the relays to detect faults is compromised by the lack of sustained fault.

(d) Islanding

When a part of utility network is disconnected from the main grid and if the network is operated as an independent system supplied with one or more generators then it is called Islanding. Islanding may leads to abnormal voltage and frequency variations. During a fault, if an auto recloser is opened then two independent systems are formed which are operated at two different frequencies. Disastrous results may occur when the auto recloser is made to reclose during out of phase of two systems. In addition to that the islanding operation may create an ungrounded system which depends on the transformer connection. An unidentified island would be hazardous for the repair crews. Owing to aforesaid reasons, islanding is accepted as unsafe situation and upon formation of an island immediate disconnection of DGs from the grid is recommended.

7.1.3.2 Voltage Control

In low load or high (DG) production conditions, interconnection of DG results in over voltages and results in changes in power flows and the voltage profile of the

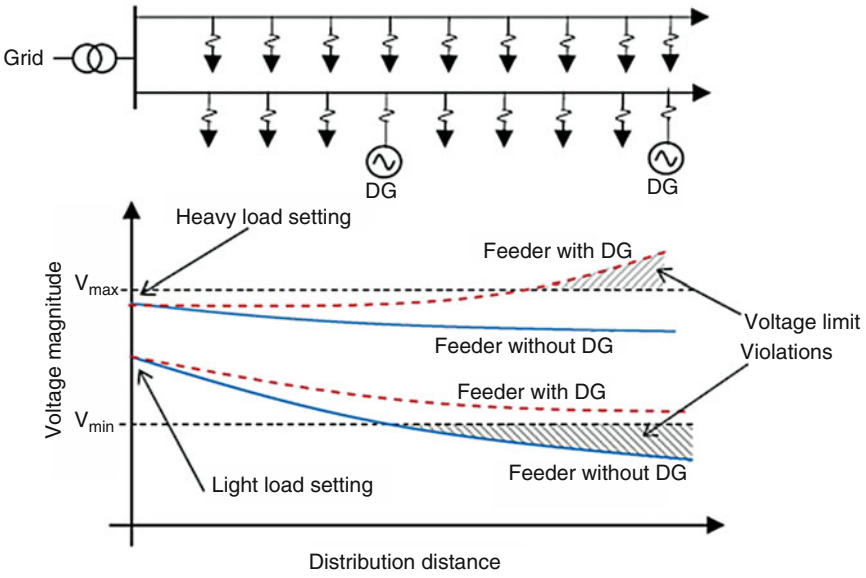


Fig. 7.2 Possible DG interconnection configurations

feeder. The voltage limit usually determines the DG capacity in weak networks and in addition to that the utility does not control the connection status of DG. Over voltages or under voltages may occur during the reconnection of DG under low load conditions or while during the disconnection of a DG during high load conditions. This may results in the operation of over/under voltage relays due to poor power quality situation. The increased penetration of DG made the selection of appropriate tap settings for the distribution transformer becomes difficult. The situation becomes more difficult when the DGs are not equally distributed among the feeders supplied by the same transformer. Figure 7.2 explains the concentration of DG on only one out of two feeders which are being supplied by a same transformer. Usually, the connection of DGs provides power to the nearby loads which results in reduction of net current flow through the transformer. Accordingly the transformer tap needs to be changed to the light load settings. As shown in Fig. 7.2 the decline in sending end voltage can cause a voltage violation at the far end of the feeder without DGs. Leaving the transformer tap at the heavy load setting risks over voltages on the feeder with DGs. The feeder voltages can be controlled by using switched capacitors and static VAr compensators, but it is too expensive. Unbalanced voltage profile also affects the operation of DGs at distribution level. As shown in Fig. 7.3, both the loads as well as DGs can be either three phase or single-phase. There will be an increase in system unbalance due to the interconnection of single phase sources. In addition to that, unbalanced distribution systems can pose problems for the three-phase DGs which are connected to it: causes overheating and frequent shutdowns due to unbalance currents in DGs.

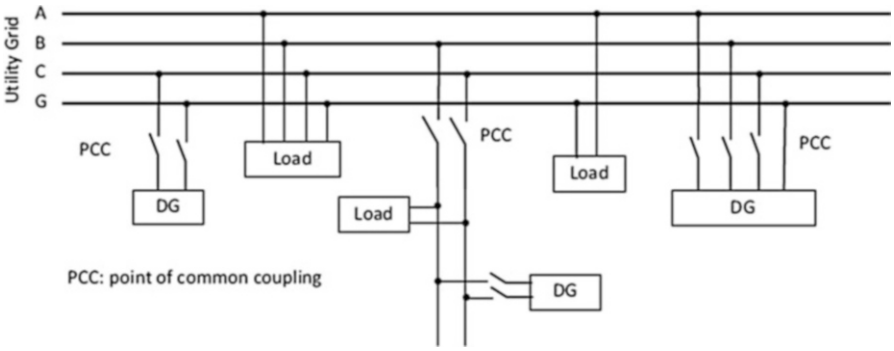


Fig. 7.3 Possible DG interconnection configurations

7.1.3.3 Harmonics and Flicker

One of the major concerns of service providers is to supply quality power to customers. Power electronic converters are used to interface most of the DGs, but this will injects harmonics into the system which results in poor power quality for the consumers. Harmonic filters can be used to overcome this. Based on the requirement hybrid filters can be selected appropriately and filters can be active, passive or hybrid. In addition to that voltage flickers may occur when connected induction generators are directly started. These voltage fluctuations can be reduced by some soft-starting mechanisms. Tower shadow effect may generate periodic voltage fluctuations in wind generators.

7.1.3.4 Interconnection Standards and Examples of Grid Codes

DG interconnection standards and guidelines have been introduced to address protection and safety issues. IEEE Std. 1547–2003, "IEEE Standards for Interconnecting Distributed Recourses (DR) with Electric Power Systems 2003" is the most commonly applied standard. Most utilities have accepted IEEE Std. 1547–2003 standard as a guideline/rule for interconnecting DG to their networks. The salient feature of IEEE Std. 1547–2003 is described below. Due to faults and other disturbances, when the voltage and/or frequency at the point of interconnection is deviated from their base values then the IEEE Std. 1547–2003 recommends to disconnect the distributed energy resources. Tables 7.2 and 7.3 define the allowable deviations. In Table 7.2, base voltages are the nominal system voltages stated in ANSI C84.1-1995. bDR 5 30 kW, maximum clearing times; In Table 7.3, if $DR \leq 30$ kW, maximum clearing times occur, and if $DR > 30$ kW, default clearing times occur.

Also, for an unintentional island where a DG energizes a portion of the network, within 2 s of the formation of island the DG interconnection system must detect the island and should disconnect the DG.

Table 7.2 Interconnection system response to abnormal voltages

Voltage range (% of base voltage)	Clearing time
$V < 50\ \%$	0.16
$50\ \% \leq V < 88\ \%$	2.00
$110\ \% \leq V < 120\ \%$	1.00
$V \geq 120\ \%$	0.16

Table 7.3 Interconnection system response to abnormal frequencies

DR size	Frequency range (Hz)	Clearing time
≤ 30 kW	>60.5	0.16
	<59.3	0.16
>30 kW	>60.5	0.16
	<{59.8–57.0} (adjustable set point)	0.16–300 (adjustable)
	<57.0	0.16

7.1.4 Integration of Large Scale Renewable Energy Generation

Based on synchronous generators conventional large scale renewable energy generations like hydro, steam turbines operated with biomass or geothermal energy uses conventional technologies. The utilities are very familiar with this conventional technology. But large scale wind farm integration poses completely different set of challenges, mainly due to interest of variable speed of generators and irregular nature of wind.

7.1.4.1 Issues Related to Grid Integration of Large Wind Farms

Current growths of wind energy generation have results in the development of large wind farms with more than 100 MW capacities and are usually interconnected to the transmission grid. The installed wind generation capacity has reached several thousand megawatts in few countries like Germany and Spain and is still increasing. But, the wind generators cannot dispatch the output power. Though there are many advances in short-term (and long-term) wind forecasting technology, accurate forecast of wind speed is still difficult. Hence, to cover the fluctuations in wind farm production a significant amount of spinning reserve and stand by capacity is required. Even though, there exist some moderating effect in wide geographic area distribution of wind forms, the chance of simultaneous low energy generation from all wind farms cannot be completely neglected. Short circuit in high voltage transmission network causes short duration voltage dip which results in disconnection of several thousand megawatts of wind generation from the grid and leads to severe stability problems within the power system. So, many system operators introduce new connection requirements for large wind farms. New connection

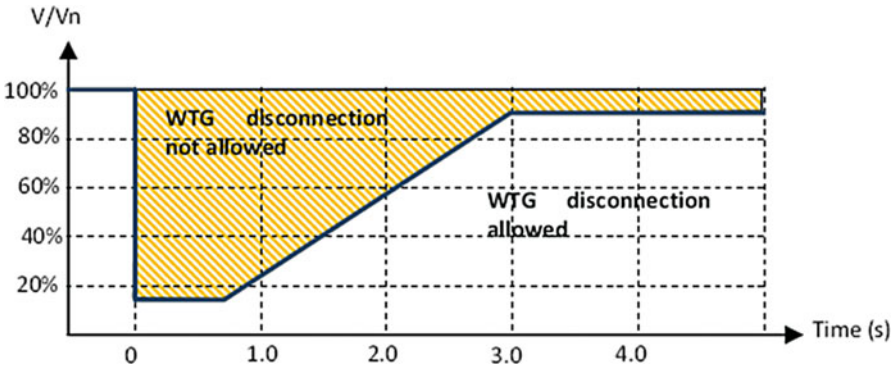


Fig. 7.4 Typical fault ride through requirements. The actual fault ride through curve can vary depending on the transmission operator

regulations like fault ride through capabilities force wind turbine to have a supporting effect on grid operations. Figure 7.4 shows the expected requirement of fault ride through capability in large, modern wind farms. The figure describes different levels of voltage depressions in wind farm and its connection time duration. This is a try to guarantee that the system will maintain stability after the clearance of fault and the wind farm is capable and ready to supply power immediately.

Serious challenges faced by the wind turbine system designer through 'strict' fault ride through standards are presented.

- The power transfer capability of the wind turbine generator (WTG) is reduced during fault. This will results in mechanical stress on blades and other rotating parts due to over speeding.
- The WTG may draw increased amount of reactive power from the system during fault and it depends on the employed generator technology which results in a poor fault recovery response.
- WTG technology decides the nature and the magnitude of the fault current. A good knowledge in this helps in designing equipment ratings for protection and control settings.
- The input mechanical power has to be regulated by the pitch control of turbine blades. During faults, the mechanical over speeding of rotating elements can be limited by the fast pitch control of blades.
- The overall performance of the wind farm can be improved by applying the appropriate FACTS based reactive power compensation device. One of the key issues related to wind power generation is the requirement of reactive power for voltage support. Induction generators are mostly used in wind generation systems. Induction machines do not have reactive power supply capability as synchronous machines. As per interconnection regulation the wind farms have to maintain the power factor within ± 0.95. Dynamic reactive supports like combination of capacitor bank and static var compensators (SVCs)/STATCOM are provided if the wind generators are not capable of meeting the aforesaid

requirements. The major protection problems related to the large wind farms is the over voltage due to the disconnection of the wind turbine generators while the capacitor bank is still connected. The performance of the wind farm immediately after the clearance of a system fault depends on the type of reactive power compensation method and devices. 'Available' terminal voltage of a capacitor banks (and SVCs) is decided by the reactive power capability. Owing to this reason, during fault recovery capacitor banks have a degraded reactive power capability which is also most needed. According to reactive power capability point of view FACTS based voltage source converters (e.g. STATCOM) are generally superior option and does not have this inherent drawback. Careful evaluation has to be done while selecting the reactive power compensation and its control strategy. Large wind farms can also use synchronous condensers as reactive power compensator they also provide inertia to the system but it has slower response when compared to STATCOM. This may be advantageous particularly when a weak ac system with dynamic stability concerns is interconnected. Detailed investigation which may be required on other possible challenges are as follows:

- Optimization of turbine power electronic design and controller.
- Protection and filter system design.
- Numerous turbine interaction.
- Wind farm issues which are connected into series compensated systems.
- Voltage flickers and other power quality problems.
- Wind farms starting and synchronization to the grid.
- Interaction of the electric network and the complex shaft/gear system of wind turbine leads to sub synchronous resonance problems.

To identify possible interconnection problems and its optimal solution, a detailed study on electromagnetic based transient program is essential.

7.2 MATLAB Model of Grid Integration

Solar grid-tie inverters are designed to quickly disconnect from the grid if the utility grid goes down. This is an NEC requirement that ensures that in the event of a blackout, the grid tie inverter will shut down to prevent the energy it produces from harming any line workers who are sent to fix the power grid. This section focuses on a MATLAB/SIMULINK model of a solar PV grid connected system. This model is developed to obtain solar panel output power and present it to an utility grid through a boost converter and an inverter. The boost converter is to step up the voltage obtained from the solar panel and the inverter is to convert the DC into AC. This section discusses the solar panel module, boost converter design and also design of the inverter. The solar PV grid connected system was tested using MATLAB/SIMULINK and the results are shown. During grid connection harmonic reduction, power factor corrections are taken into account.

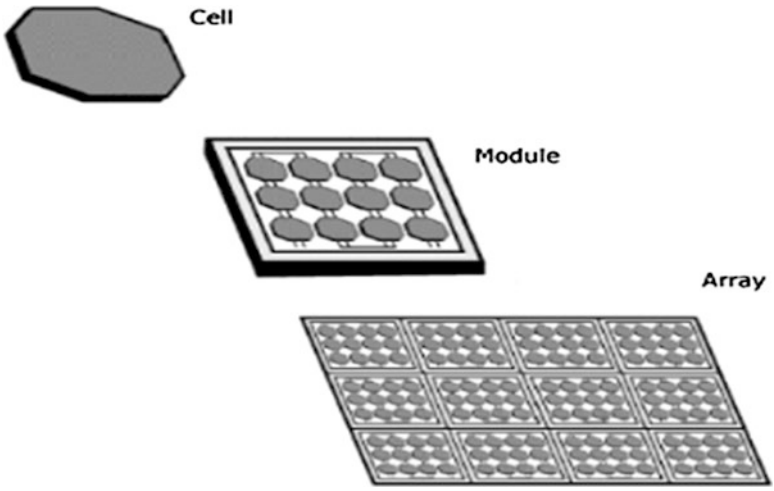


Fig. 7.5 Photovoltaic system

7.2.1 Photovoltaic Module

To produce the desired output, several low voltage PV cells (around 0.5 V) are connected in series (for high voltage) and in parallel (for high current) to form a PV module. A typical photovoltaic system is shown in Fig. 7.5. During partial or total shading, and at night, separate diodes may be needed to avoid reverse currents. These are not necessary for mono-crystalline silicon cells as they have sufficient reverse current characteristics. Reverse current can also leads to waste of power and overheating of shaded cells. At higher temperatures solar cells become less efficient and installers may provide good air circulation behind solar panels. Since a single module is not sufficient to produce the required power for home and business, Inverters are mostly used with PV arrays to convert the DC power into alternating current which can power motors, loads, lights etc. To produce desired voltage and current the modules in a PV array are first connected in series and then the individual modules in parallel. The MATLAB/SIMULINK model of a solar PV array is available in Sect. 2.4.1 of Chap. 2.

7.2.2 Boost Converter

DC-to-DC power converter whose output voltage is greater than its input voltage is known as step-up converter or boost converter. Boost converter shown in Fig. 7.6 is a type of SMPS (Switched Mode Power Supply) which consists of at least two semiconductor switches (a diode and a transistor) and one energy storage element like a capacitor, inductor or the combination of two. To reduce the output voltage

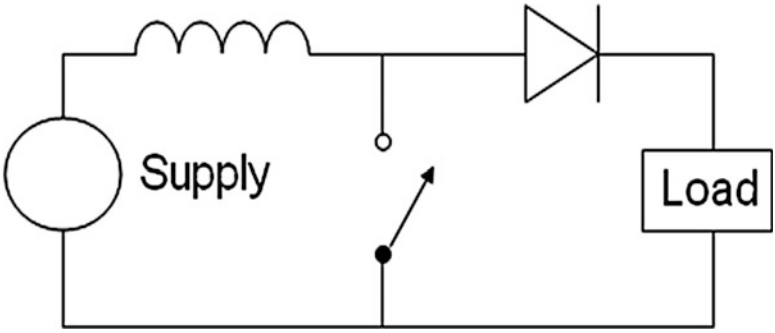


Fig. 7.6 Boost converter

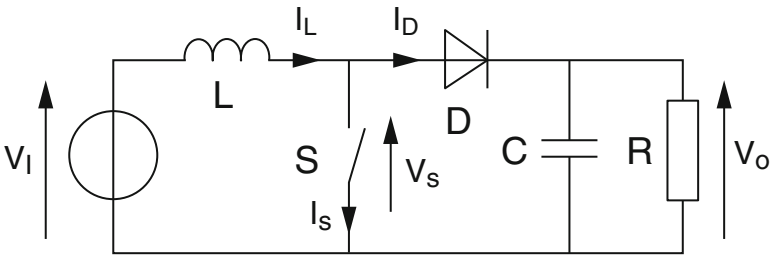


Fig. 7.7 Boost converter schematic

ripple a capacitor filter (sometimes in combination with inductor) is added at the output of converter.

DC sources like batteries, solar panels, rectifiers or DC generators can be used to power the boost converter. DC to DC conversion is the process of changing one voltage to other voltage. A converter with an output DC voltage greater than source DC voltage is known as boost converter or step-up converter. Since power must be conserved, the output current is lower than the source current.

The tendency of an inductor to resist changes in current is the key driving principle of the boost converter. The output voltage is higher than the input voltage in boost converter. Figure 7.7 shows the schematic boost power stage.

(a) Current flows through the inductor in clockwise direction and inductor stores energy when the switch is closed. Inductor left side polarity is positive.
(b) Impedance is higher and so the current is reduced when the switch is opened. Hence the inductor opposes the change or reduction in current. Now the left side of the inductor is negative and thus the polarity is reversed. The diode D made the capacitor to charge to higher voltage as a result of two sources in series.

The inductor will not discharge fully in between charging stages if the switching cycle is fast. Only when the switch is opened the load will always see a voltage greater than that of the input source. The capacitor parallel with the load is charged

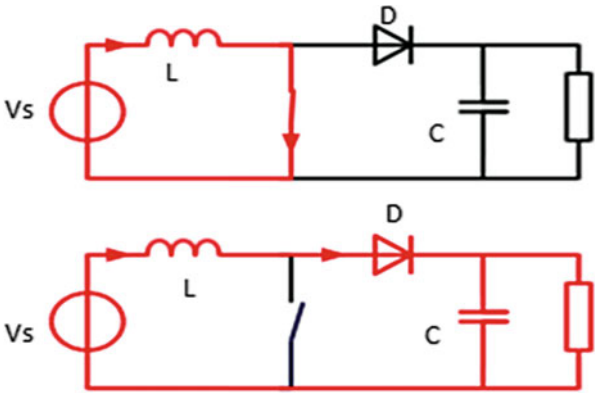


Fig. 7.8 The two configurations of a boost converter, depending on the state of the switch S

to the combined voltage. The capacitor provides voltage and energy to the load only when the switch is closed and the right hand side is shorted out from the left hand side. In the course of this time, the discharging of capacitor through the switch is prevented by the blocking diode. To prevent the capacitor from discharging too much, the switch must be opened fastly again.

Two distinct states of principle of boost converter are:

- The inductor current is increased when the switch is closed and is in on- state.
- The inductor current is flowed through the fly back diode D, the capacitor C and the load R when the switch is open and is in off-state. The energy accumulated during the on-state is transferred into the capacitor.

Figure 7.8 infers that the input current is same as the conductor current. Hence it is not discontinuous as in the buck converter. The input filter requirements are also relaxed when compared to buck converter.

7.2.3 SIMULINK Model of Boost Converter

The output voltage of 272 V DC obtained from the 2 KW panel is stepped up to about 500 V DC by means of boost converter shown in Fig. 7.9.

7.2.3.1 Design Parameters

The parameters involved in the design of boost converters are shown below:

(i) $V_0 = \frac{V_S}{1-K}$

(ii) $L = \frac{K(1-k)R}{2f}$

(iii) $C = \frac{K}{2fR}$

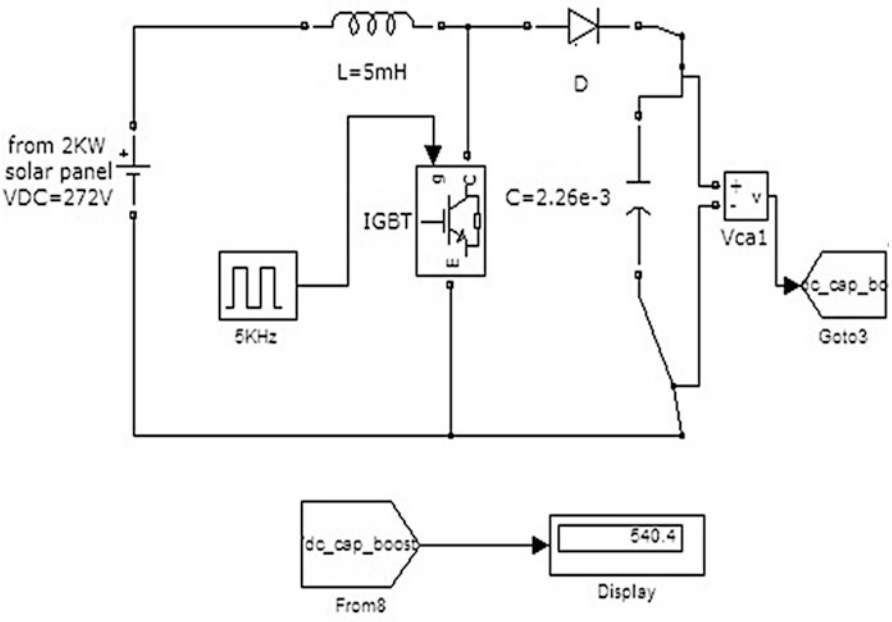


Fig. 7.9 SIMULINK model of boost converter

Table 7.4 Boost converter design values used in simulation

S. No.	Parameter	Value
1	Input voltage (V_s)	273 V
2	Output voltage (V_0)	500 V
3	Switching frequency (f)	5 KHz
4	Duty cycle (k)	0.456
5	Inductor (L)	5 mH
6	Capacitor (C)	0.226 μF

where

$V_0 =$ output voltage(V)
$V_s =$ input voltage(V)
K = duty cycle = Ton/T
F = switching frequency (Hz)

The parameters and their values are set in the simulation according to Table 7.4.

7.2.3.2 Voltage Source Inverter (VSI)

The VSI inverter is used in this grid integration model to regulate the DC 500 V from the boost converter. To achieve full control of the utility-grid current, the

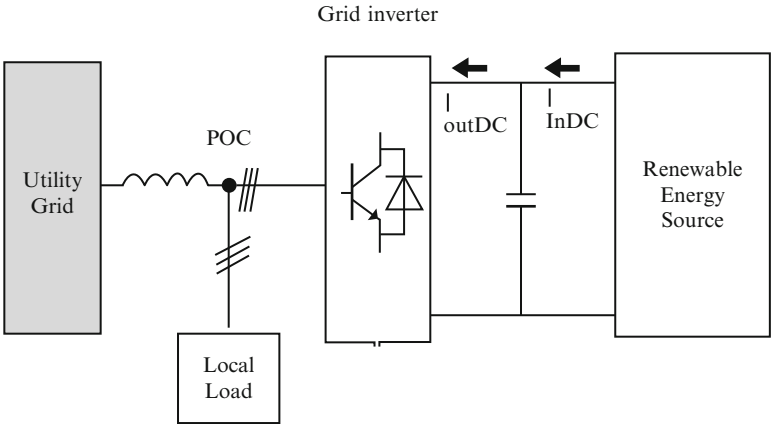


Fig. 7.10 Block diagram of grid inverter

DC-link voltage must be boosted to a level higher than the amplitude of the grid line voltage. In order to keep the DC-link voltage constant the power flow of the grid side inverter is controlled. Figure 7.10 shows the block diagram of grid inverter, with local load and grid interconnection.

The three- phase VSI is composed of a bridge with six reverse blocking switches (S1–S6) and each have IGBT and a series diode. The inductor is considered as the main storage component of the DC-link at the output. During unintended open circuit of bridge the transient voltage suppressor diode D provides a "freewheeling" path. The VSI is appropriate with IGBTs during commutation as their intrinsic body diodes are inactive. These have poor switching losses. Three phase inverters are commonly used in the application of AC motor drive and UPS. The circuit consists of six power semiconductor devices like transistors and six diodes. The change in firing from one switch to next in proper sequence for one cycle of 360° is known as step.

180 Degree Conduction

(i) Each switch conducts for 180°
(ii) Switch S1–S4 state change will occur after 180°
(iii) Upper arm switches S1, S3, S5 state change will occur at every 120°

At any instant of time, three devices conduct. Thus effective utilization of the switch is achieved. The switching sequence of VSI for 180° is shown in Fig. 7.11 and the states are shown in Table 7.5.

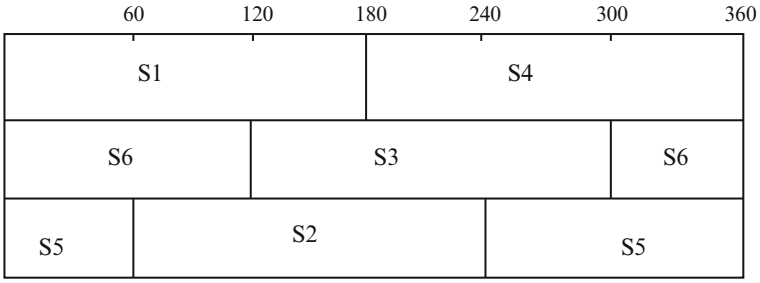


Fig. 7.11 Switching sequence of VSI for 180 conduction

Table 7.5 Switch states for three phase VSI

State		State no.	Switch state (binary)	V_{ab}	V_{bc}	V_{ca}	V_{an}
On	Off						
S6, S1, S5	S3, S4, S2	1	101	V_s	$-V_s$	0	$\frac{V_s}{3}$
S1, S2, S6	S4, S5, S3	2	100	V_s	0	$-V_s$	$\frac{2V_s}{3}$
S2, S3, S1	S5, S6, S4	3	110	0	V_s	$-V_s$	$\frac{V_s}{3}$
S3, S4, S2	S6, S1, S5	4	010	$-V_s$	V_s	0	$\frac{-V_s}{3}$
S4, S5, S3	S1, S2, S6	5	011	$-V_s$	0	V_s	$\frac{-2V_s}{3}$
S5, S6, S4	S2, S3, S1	6	001	0	$-V_s$	V_s	$\frac{-V_s}{3}$
S1, S3, S5	S4, S6, S2	7	111	0	0	0	0
S4, S6, S2	S1, S3, S5	8	000	0	0	0	0

7.2.4 Implementation of Grid Integration Using MATLAB

In the grid development shown in Fig. 7.12 using MATLAB/SIMULINK, first the generating station is represented by a programmable voltage source of 120 KV, 2,500 MVA capacity. Then the 120 KV is stepped down to 25 Kv by means of a star-delta transformer. In this type of connection, then primary is connected in star fashion while the secondary is connected in delta fashion as shown in the Fig. 7.13.

7.2.4.1 Grounding Transformers

A ground path is provided to an ungrounded "Y" or a delta connected system through a grounding transformer. Grounding transformers are usually used to:

1. The system neutral at or near ground potential is maintained by providing a relatively low impedance path to ground.
2. The transient over voltage magnitude is limited during the occurrence of re-striking ground faults.
3. A source of ground fault current is provided during line-to ground faults.
4. The connection of phase to neutral loads is permitted when required.

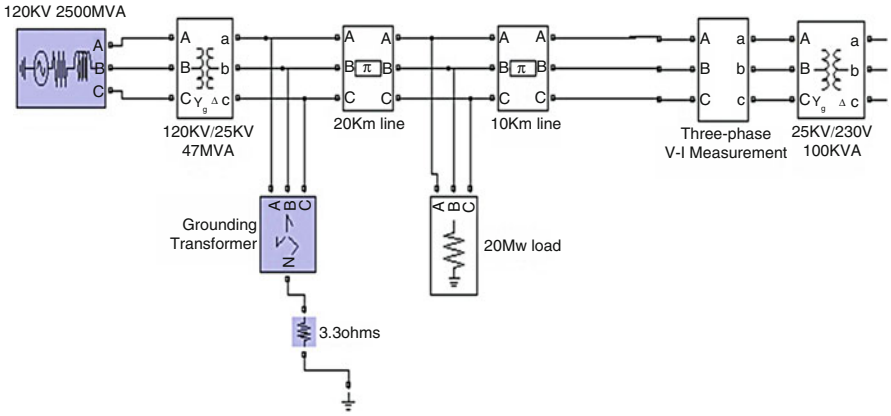


Fig. 7.12 SIMULINK model of grid development

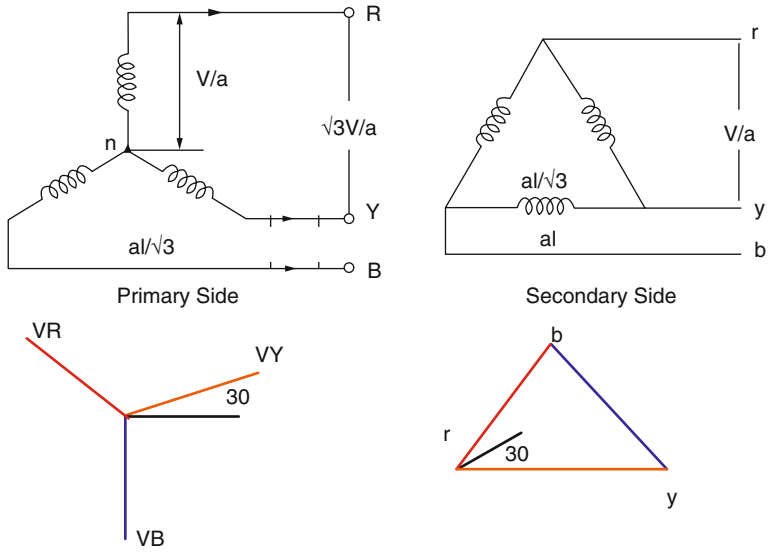


Fig. 7.13 Star – delta configuration of transformer

The transmission line is represented by a 'pi section line of 10 and 20 km. Then the 25 KV is stepped up to 230 V by means of a star-delta transformer. The setup as a whole forms the grid development. The SIMULINK Model of the grid integration using six IGBT switches is shown in Fig. 7.14. The model designed to generate pulses for the VSI inverter is shown in Fig. 7.15. Figure 7.16 shows the output voltage and current waveforms before 25 KV/230 V in the grid and Fig. 7.17 shows the output voltage of the inverter to the grid.

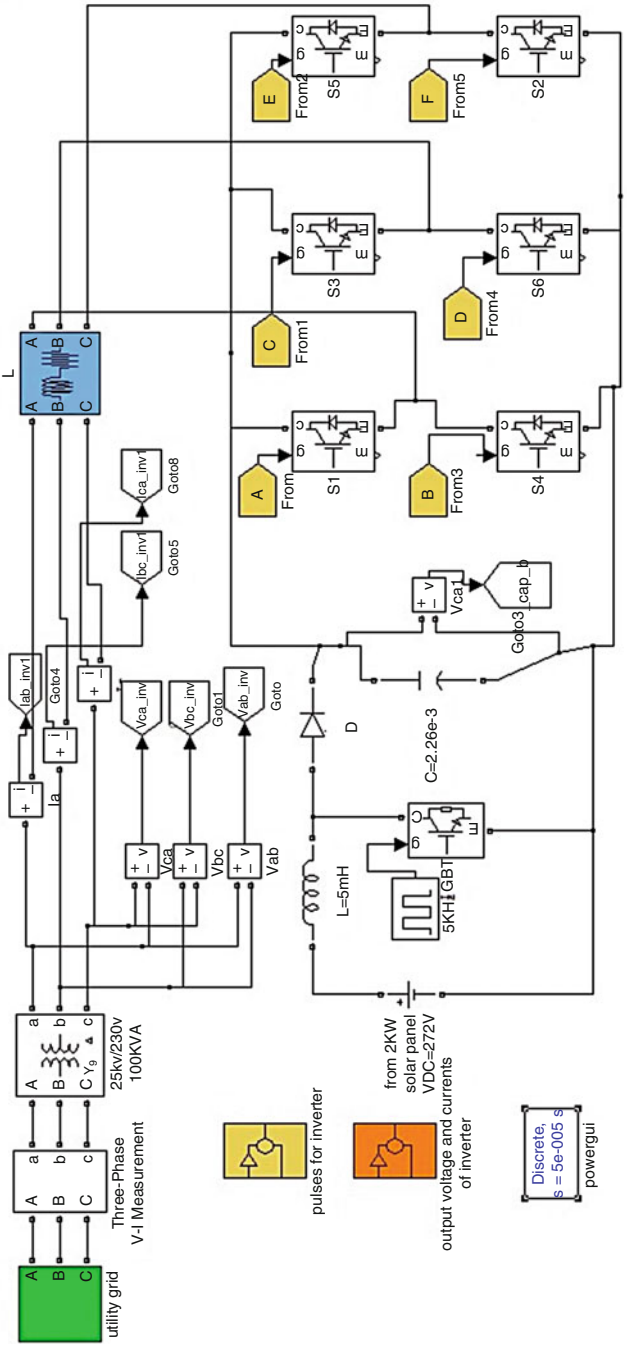


Fig. 7.14 SIMULINK model for solar PV grid integration

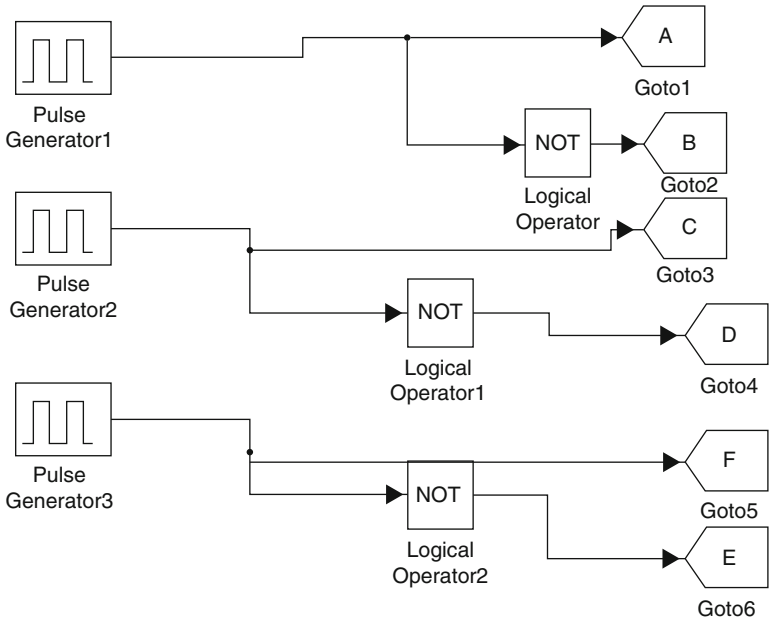


Fig. 7.15 SIMULINK model – pulses for inverter

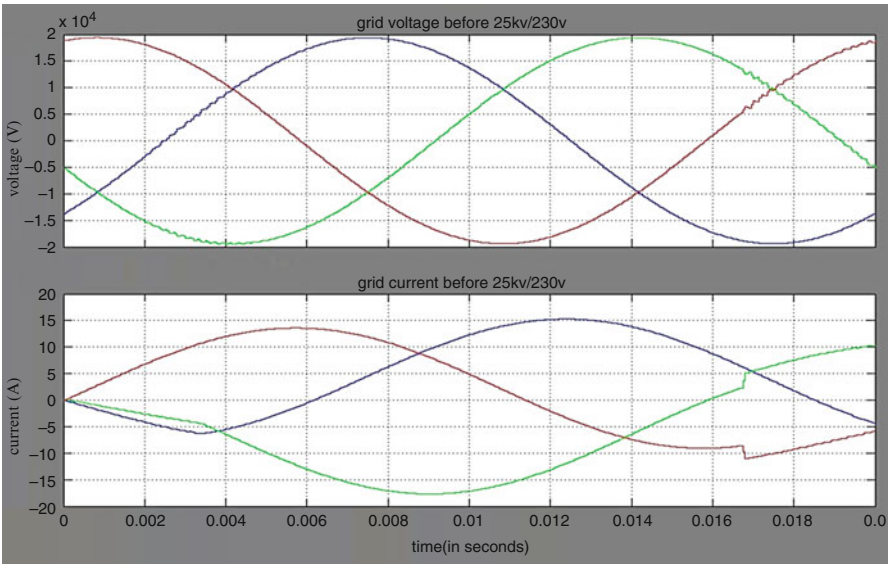


Fig. 7.16 Voltage and current waveforms before 25 KV/230 V in the grid

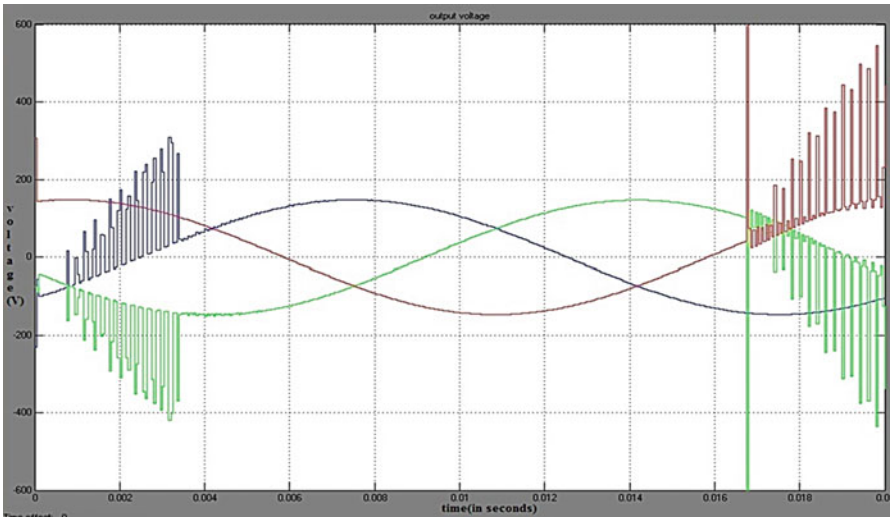


Fig. 7.17 Output voltage of the inverter to the grid

The MATLAB/SIMULINK is used to develop the solar PV grid integration models and their respective waveforms are shown. Certain technical requirements encouraged the utility industries with the deployment over 15–20 % range. Such work needed areas include:

- Integration of all characteristics from the transient to long-time domain and storage control.
- Sophisticated adaptive controls for combination and re-combination of PV resources.
- PV resources modeling and forecasting, from the feeder level to all the control areas.
- The nationwide grid is exploited to the fast response of inverter based generations by adapting the operating and reliable strategy.
- Adaptive techniques like advanced permissive signal anti-Islanding for self-identification of phase, feeder, and substation are exploited to low bandwidth requirement and for low-cost signal generators.

7.3 Phase Locked Loop for Grid Connected Power System

A Voltage Source Inverter (VSI) is connected to the supply network through a filter in many grid- connected power electronic systems like Static Synchronous Compensators (STATCOM), Unified Power Flow Controllers (UPFC) and Distributed Generation System (DGS). The switching harmonics entering the distribution network is reduced by this series inductance filters. LCL network is the alternative

filter which achieves the aforesaid requirement which has high potential benefits for high power applications. But more complex control strategies are required for the system which incorporates LCL filters and are not commonly presented in literature. A robust strategy for regulating the grid current entering a distribution network from a three phase VSI system connected via a LCL filter. An outer loop grid current regulator with inner capacitor current regulation strategy is integrated to stabilize the system. For the outer grid current control loop a synchronous frame PI current regulation strategy is used.

This section investigates and compares new control techniques to properly regulate the power flow between renewable source and the utility network. The control strategies are typically based on a fast and accurate detection of the phase angle of the grid voltage which may be estimated by using a Phase Locked Loop (PLL) control circuit. Here performances of four different PLLs that are investigated are Synchronous Reference Frame PLL (dq PLL), Stationary Reference Frame PLL (αβ PLL), Decoupled Synchronous Reference Frame PLL (DSRF PLL) and Decoupled Stationary Reference frame PLL (Dαβ PLL). The Decoupled Stationary Reference Frame PLL (Dαβ PLL) may be an appropriate solution to use in an interconnected RES with Fault Ride Through (FRT) capability, since it prevails the other PLLs with regards to its accuracy under unbalanced faults. Further, it has a lower deviation of the estimated phase after the fault occurs. The performance of the New Hybrid Dαβ PLL is verified through simulations and experiments. Further the new PLL is used in an interconnected RES through experiments under normal and FRT operation.

Special attention is given to systems which demand a third order Inductor-Capacitor-Inductor (LCL) filter as interface between converter and grid. This filter configuration is widely employed in high power systems, in which the switching frequency is typically limited by the switching devices. The LCL filter has the ability to reduce the level of harmonic distortion with less inductance, when compared to the first order Inductor (L) filter. Also, the evaluation of different current controllers employed for grid-connected distributed power generation systems are discussed. The MATLAB/SIMULINK models are developed to investigate the performance of the control strategies discussed in the literature.

The environmental regulations due to green house gas emission, the electricity business restructuring, and the recent development in small scale power generation are the main factors driving the energy sector into a new era, where large portions of increases in electrical energy demand will be met through wide spread installation of distributed resources or what's known as DGS. As a result, DGS can give commercial consumers various options in a wider range of high reliability-low price combinations.

The customer and utility requirements, such as compensation of reactive power and higher harmonic components, compensation of power quality events, power factor correction, peak saving, backup generation, and voltage reliability enhancement requirements are also meet in the DGS power system which is not possible with centralized generation. Within a micro-grid the DGS can operate either in Grid-connected mode or in an islanded mode. DC-AC Pulse Width Modulated

(PWM) Voltage Source Inverter (VSI) systems is used to interface the major distributed resources to the utility grid or to the customer load. Different sizes of DGS units ranging from few kW up to 1.6 MW can be interfaced through current power electronic technologies. When compared to the conventional rotary generators the inverter interface makes the energy sources more flexible and controllable.

7.3.1 Challenges Imposed on an Inverter-Based DG Interface

The dynamic and uncertain nature of a distribution network challenges the control and stability of the DGS interface system. The fact that a typical distribution system faces unavoidable disturbances and uncertainties complicates the design of a practical inverter-based DGS interface. In the Grid-connected mode, most of system disturbances are related to the main grid due to the relatively small size of DGS energy sources. Various grid disturbances can be imposed on the DGS interface. Difficulties occur in the following ways:

- Depending on the grid configuration, a large set of grid impedance values is yielded as DGS is commonly installed in weak grids with long radial distribution feeders. The interfacing impedance variations directly affect the stability of the inner controls of the DGS interface. With that, high frequency resonance dynamics might be excited due to the grid impedance interaction with the AC side filter of the DGS interface. Due to this, high distortion of injected current may propagate through the system which will drive other voltage and current harmonics.
- There is a strong trend toward the use of current control for PWM inverters in DGS, which offers the possibility of high power quality injection when it is properly designed. In this approach, it is commonly desired to design the inner current control loop with high bandwidth characteristics to ensure accurate current tracking, shorten the transient period as much as possible, and force the VSI to equivalently act as a current source amplifier within the current loop bandwidth. But, the sensitivity of the dominant poles of the closed loop current controller becomes very high to uncertainties in the total interfacing impedance (the impedance seen by the inverter at the point of common coupling, which is a function of the grid impedance) when the current control loop is designed with high bandwidth characteristics (e.g. Deadbeat control performance).
- The control performance of the DGS inverter is directly affected by the voltage at PCC. The grid voltage at the PCC is more distorted in weak grids with long radial distribution feeders due to the exposure to nonlinear loads.
- Grid faults, time- varying loads, non-dispatchable generation, voltage transients associated with parallel connected loads, and voltage transients caused by capacitor switching may cause severe and random voltage disturbances. Interfacing DGS should have high immunity and ability to override aforesaid disturbances especially in feeders with sensitive loads.

In the presence of the aforementioned system challenges, along with the reliability and cost enhancements, significant performance enhancements can be obtained by eliminating the grid voltage sensors in the Inverter-based DG interface. Among these are: (1) The elimination of the residual negative sequence and voltage feed-forward compensation errors, and (2) The positive contribution to the robustness of the power sharing mechanism.

The stability and control effectiveness of a grid-connected inverter-based DGS interface is affected by the uncertain and dynamic nature of the distribution network. Usually, grid impedance and interfacing parameter variations, grid voltage disturbances, and interaction with existing grid harmonics and unbalance are the possible challenges. A strong DGS interface should be developed to overcome these challenges and to make a safe integration and larger penetration of DGS. The characteristics which are offered by the DGS are as follows:

- Distribution system insensitivity and AC side filter parameters.
- Perfect current control performance with a strong capacity of eliminating the grid distortion and voltage disturbances caused by interfacing parameters mismatch and compensating for inverter system delays.

7.3.2 Requirements for Establishing a Grid Connection

The general grid code requirement for investigating the dynamic behavior of DGS is listed in this section. In countries like USA, Germany, Spain, Denmark, China and India which have substantial generation have imposed the grid codes. Main grid codes for operation and grid connection are listed as below:

7.3.2.1 Voltage Regulation

The voltage should not go outside the specified range at the Point of Common Coupling (PCC) during DGS connection.

7.3.2.2 System Frequency

The frequency variations should not go outside a specified range.

7.3.2.3 Synchronization

The voltage fluctuation due to synchronization of DGS with an area Electric Power System (EPS) should not be more than ± 5 % of the prevailing voltage level at the PCC.

7.3.2.4 Monitoring Provisions

250 kW or larger DGS rating will have provisions for monitoring connection status and real and reactive power output at the point of DGS connection.

7.3.2.5 Isolation Device

An isolation device shall be located between the DGS unit and the area EPS when required.

7.3.2.6 Grounding

Proper coordination is required among the grounding scheme and the grounding fault protection of DGSs with the EPS operators.

7.3.2.7 Voltage Disturbances

A DGS should cease to energize the EPS within a specified clearing time during abnormal voltage conditions.

7.3.2.8 Frequency Disturbances

A DGS should cease to energize the EPS within a specified time when the frequency is not within the limits.

7.3.2.9 Loss of Synchronization

The disconnection of 250 kW or larger DGS from the area EPS without intentional time delay can be made with synchronism loss protection.

7.3.2.10 Reconnection

The DGS will stop to energize the area EPS and remain disconnected until the area EPS voltage and frequency have returned to and maintained normal range for 5 min after an out-of-bound disturbance.

7.3.2.11 Anti-islanding

The DGS can detect the island condition and stop to energize the area EPS within 2 s from the formation of an Island.

7.3.2.12 Harmonics

The permissible voltage harmonic distortion is specified at the PCC. A maximum voltage total harmonic distortion of 5 % and maximum individual frequency voltage harmonics is 3 % of the fundamental component is usually required.

7.3.2.13 DC Current Injection

A DGS and its interconnection system will not inject dc current greater than 0.5 % of its rated output current into the area EPS at the PCC.

7.3.2.14 Flicker

The DGS will not create any objectionable drop for customers on the area EPS.

7.3.3 Grid Synchronization Algorithms

Some various grid synchronization algorithms that are presented in literature are discussed below:

7.3.3.1 Zero Crossing Detectors

Transition of AC voltage from one polarity to another is detected by the Zero Crossing Detector (ZCD). A pulse is generated showing 0° for a transition from positive to negative and 180° for the reverse case.

Drawbacks of Zero Crossing Detectors

The power quality phenomenon affects the performance of ZCD badly. Figure 7.18 shows the performance of ZCD during the presence of harmonics and notches.

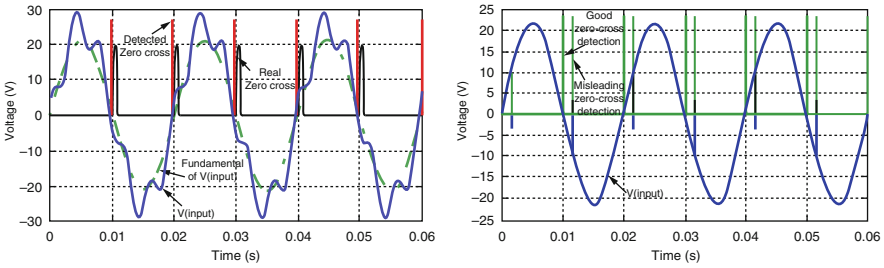


Fig. 7.18 Misleading zero cross detection due to harmonics and notches

Input wave transients also affect the performance of ZCD. The zero crossing detector detects the zero crosses once or twice during every cycle. This implies that even the phase jump occurrence is not estimated until the next zero cross. Frequency deviations may lead to severe malfunctioning of the system since the ZCD does not provide frequency estimation or adaptation.

The performance of the zero crossing detectors can be improved by applying some of the following improvement techniques. In three phase circuits the usual practice is to filter out the y-phase signals and to extrapolate the r-phase signals. Digital filters in discrete devices can provide better results when the fundamental component is extracted from noisy waveform. The performance of the normal ZCD can be improved by implementing suitable algorithm in discrete devices.

7.3.3.2 Phase Locked Loop

A system which synchronizes its output signal with a given input signal or reference signal both in frequency and in phase is known as Phase Locked Loop (PLL). It is a non-linear closed loop control which changes the frequency of a controlled oscillator automatically depending on the frequency and phase of the input signal such that the output is synchronized both in frequency and phase with the reference or the input signal.

The following are the main components of a PLL

(i) A **phase detector** generates an error signal by comparing the input/reference signal with the output signal.
(ii) A **loop filter** removes unwanted harmonics terms from the error signal.
(iii) A **voltage controlled oscillator (VCO)** which generates the output signal whose frequency varies around a central frequency depending on the output of the loop filter. Figure 7.19 shows the block diagram of a PLL.

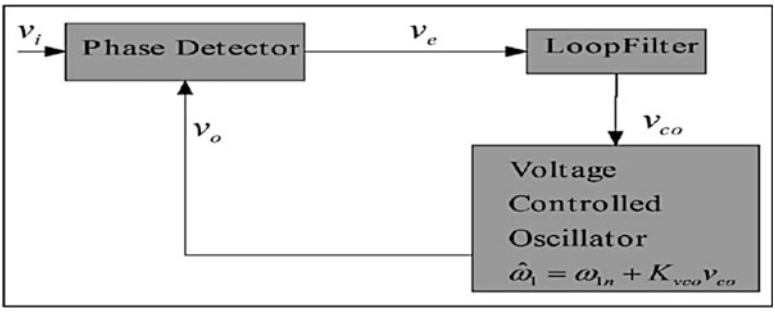


Fig. 7.19 3.2 block diagram of PLL

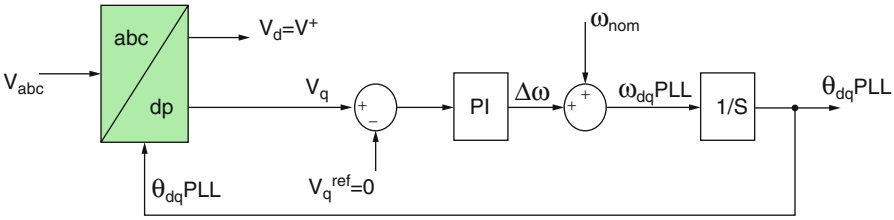


Fig. 7.20 The structure of a dq PLL

7.3.4 PLLs for Three Phase Systems

In this section, three different PLLs for three phase systems are presented in order to motivate the development of a hybrid PLL, Decoupled Stationary Reference Frame PLL (Dαβ PLL).They are:

- Synchronous Reference Frame PLL (dq PLL).
- Stationary Reference Frame PLL (αβ PLL).
- Decoupled Synchronous Reference Frame PLL (DSRF PLL).

7.3.4.1 Synchronous Reference Frame PLL (dq PLL)

The basic configuration is shown in Fig. 7.20. The dq PLL uses the equations of the Park's transformation, as shown in Eq. 7.1, to translate the abc natural rotating reference frame into the dq-Synchronous Reference Frame (SRF).

$$\begin{bmatrix} V_d \\ V_q \end{bmatrix}^{syn} = \frac{2}{3}\begin{bmatrix} \cos\theta & \cos(\theta-120) & \cos(\theta+120) \\ -\sin\theta & -\sin(\theta-120) & -\sin(\theta+120) \end{bmatrix}\begin{bmatrix} V_a \\ V_b \\ V_c \end{bmatrix} \tag{7.1}$$

In this PLL either direct axis component or quadrature axis component of voltage can be considered for the estimation of frequency or hence phase angle. A crucial aspect of the transformation is that the voltage of the d-axis (V_d) has to lie on the voltage of phase A. This is achieved by having the voltage of the q-axis (V_q) to track zero through a Proportional-Integral (PI) controller and therefore frequency, ω_{dqPLL} and phase, θ_{dqPLL} could be estimated as illustrated in Fig. 7.20. In this PLL, the PI controller performs the function of Loop filter in the basic PLL. The angle θ_{dqPLL} is found integrating the output ω_{dqPLL} which uses the error signal $V_q - V_q^{ref}$ in the dq frame.

When a balanced fault occurs, the dq PLL is operating well and can track the phase angle. However, when an unbalanced fault occurs, then the dq PLL fails to track accurately the phase angle because V_d does not perfectly match with the positive sequence voltage V^{+1} due to the oscillation which appears because of the existence of the negative sequence voltage V^{-1} under unbalanced disturbances.

7.3.4.2 Stationary Reference Frame PLL (αβPLL)

The basic configuration of a Stationary reference frame PLL is shown in Fig. 7.21. The αβ PLL sets $\theta = 0$ in that of dq PLL, in order to translate the αβ natural rotating reference frame into the αβ-stationary reference frame. Trigonometric equations are used in order to estimate the phase angle $\theta_{\alpha\beta PLL}$ as shown in Eqs. 7.2 and 7.3. It should be noticed that the below expression is valid if $\Delta\theta$ is small.

$$\Delta\theta = \theta_{gr} - \theta_{abPLL} \approx \sin\left(\theta_{gr} - \theta_{abPLL}\right) \tag{7.2}$$

$$\Leftrightarrow \Delta\theta \approx \sin\left(\theta_{gr}\right)\cos\left(\theta_{abPLL}\right) - \cos\left(\theta_{gr}\right)\sin\left(\theta_{abPLL}\right) \tag{7.3}$$

The objective of the closed loop control of αβPLL (Fig. 7.21) is to induce the difference $\Delta\theta$ to be controlled to zero by using a PI controller, where θ_{gr} is the actual phase angle of the voltage. The αβPLL in unbalanced operation has similar problems to those mentioned for the dq PLL.

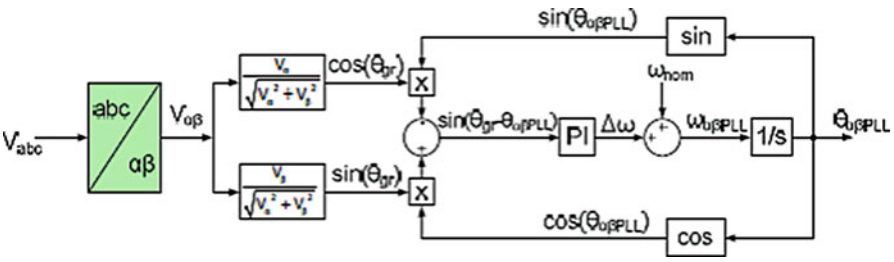


Fig. 7.21 The structure of αβ PLL

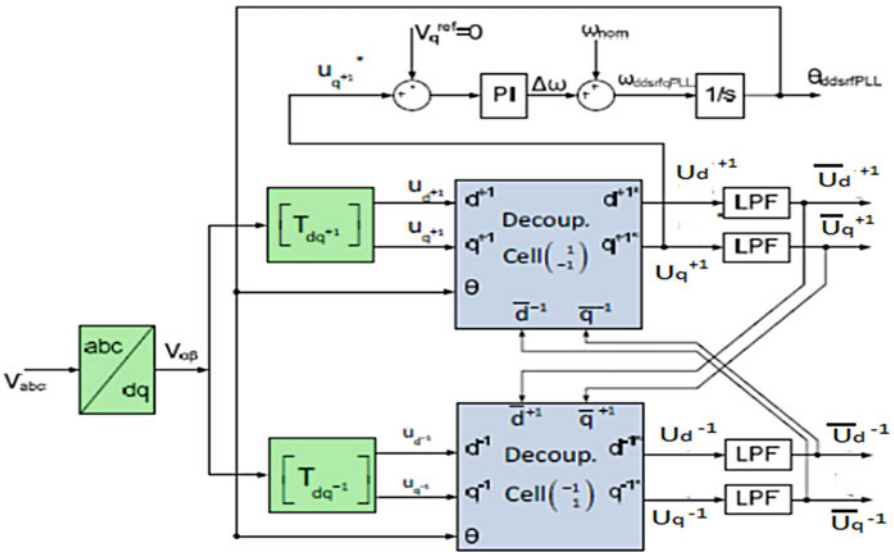


Fig. 7.22 The structure of a DSRF PLL

7.3.4.3 Decoupled Synchronous Reference Frame PLL (DSRFPLL)

The DSRFPLL stems from improving the conventional dq PLL. It consists of a decoupling network and phase locked loop operating on synchronous reference frame (dq PLL) as shown in Fig. 7.22. The decoupling network provides positive and negative sequence components from the input voltage vector. The synchronization to the positive sequence component of the grid voltage is achieved when the voltage positive sequence q-component is controlled to zero. This is done using dq PLL.

During the unbalanced three phase grid voltage, the fundamental positive-sequence voltage vector is appeared as a DC voltage on the dq^{+1} axes of the positive sequence SRF and ac voltages at twice the fundamental utility frequency on the dq^{-1} axes of the negative sequence SRF. Opposing to this the negative sequence voltage vector will cause a dc component on the negative sequence SRF and an ac oscillation on the positive sequence SRF. In order to cancel out the amplitude oscillation of the positive sequence SRF which matches to the DC level on the negative sequence SRF and vice versa, a decoupling network is applied to signals on the dq positive/negative SRF axes. DC component from the signal on the decoupled SRF axes can be extracted by using low pass filters. The information about the amplitude and phase angle of the positive and negative sequence components of the grid voltage vector can be collected by these DC components.

The DSRF PLL loop controller works on the decoupled q-axis signal of the positive sequence SRF (U_q^{+1}). Due to the effect of decoupling cells the signal is free from ac components and therefore the loop controller band width is increased.

7.3.4.4 Decoupling Network

The unbalanced grid voltage vector $u_{\alpha\beta}$ can be expressed in stationary reference frame as shown in Eq. 7.4.

$$u_{\alpha\beta} = \begin{matrix} u_\alpha \\ u_\beta \end{matrix} = U^+ \begin{bmatrix} \cos(\omega t + \varphi^+) \\ \sin(\omega t + \varphi^+) \end{bmatrix} + U^- \begin{bmatrix} \cos(-\omega t + \varphi^-) \\ \sin(-\omega t + \varphi^-) \end{bmatrix} \tag{7.4}$$

where U is the phase voltage peak value, ω is the grid angular frequency and φ is initial angle. The positive and negative sequences are represented by + and − superscripts. The positive sequence reference frame is assumed to rotate synchronously with the fundamental frequency positive sequence grid voltage component. Therefore, $\theta_{sync} = \omega t$. Angle θ_{sync} which is the output of the SRF-PLL of synchronous dq reference frame is used to express the positive and negative sequence components.

$$u_{dq}^+ = \begin{bmatrix} u_d^+ \\ u_q^+ \end{bmatrix} = T_{dq}^+ \begin{bmatrix} u_\alpha \\ u_\beta \end{bmatrix} = \begin{bmatrix} \cos(\theta_{sync}) & \sin(\theta_{sync}) \\ -\sin(\theta_{sync}) & \cos(\theta_{sync}) \end{bmatrix} \begin{bmatrix} u_\alpha \\ u_\beta \end{bmatrix} =$$
$$U^+ \begin{bmatrix} \cos(\varphi^+) \\ \sin(\varphi^+) \end{bmatrix} + U^- \cos(\varphi^-) \begin{bmatrix} \cos(2\omega t) \\ -\sin(2\omega t) \end{bmatrix} + U^- \sin(\varphi^-) \begin{bmatrix} \sin(2\omega t) \\ \cos(2\omega t) \end{bmatrix} \tag{7.5}$$

$$u_{dq}^- = \begin{bmatrix} u_d^- \\ u_q^- \end{bmatrix} = T_{dq}^- \begin{bmatrix} u_\alpha \\ u_\beta \end{bmatrix} = \begin{bmatrix} \cos(\varphi^-) \\ \sin(\varphi^-) \end{bmatrix} + U^+ \cos(\varphi^+) \begin{bmatrix} \cos(2\omega t) \\ \sin(2\omega t) \end{bmatrix}$$
$$+ U^+ \sin(\varphi^+) \begin{bmatrix} -\sin(2\omega t) \\ \cos(2\omega t) \end{bmatrix} \tag{7.6}$$

The left side terms and right side terms of the Eqs. 7.5 and 7.6 represents the DC and AC values respectively. The DC-values are solved in order to differentiate the positive and the negative sequence components from the grid voltage.

$$U^+ \begin{bmatrix} \cos(\varphi^+) \\ \sin(\varphi^+) \end{bmatrix} = \begin{bmatrix} U_d^+ \\ U_q^+ \end{bmatrix} = \begin{bmatrix} u_d^+ \\ u_q^+ \end{bmatrix} - U^- \cos(\varphi^-) \begin{bmatrix} \cos(2\omega t) \\ -\sin(2\omega t) \end{bmatrix}$$
$$- U^- \sin(\varphi^-) \begin{bmatrix} \sin(2\omega t) \\ \cos(2\omega t) \end{bmatrix} \tag{7.7}$$

$$U^- \begin{bmatrix} \cos(\varphi^-) \\ \sin(\varphi^-) \end{bmatrix} = \begin{bmatrix} U_d^- \\ U_q^- \end{bmatrix} = \begin{bmatrix} u_d^- \\ u_q^- \end{bmatrix} - U^+ \cos(\varphi^+) \begin{bmatrix} \cos(2\omega t) \\ \sin(2\omega t) \end{bmatrix}$$
$$- U^+ \sin(\varphi^-) \begin{bmatrix} -\sin(2\omega t) \\ \cos(2\omega t) \end{bmatrix} \tag{7.8}$$

Figure 7.23 represents the decoupling network based on Eqs. 7.7 and 7.8 which is used to cancel AC components from positive and negative sequence reference

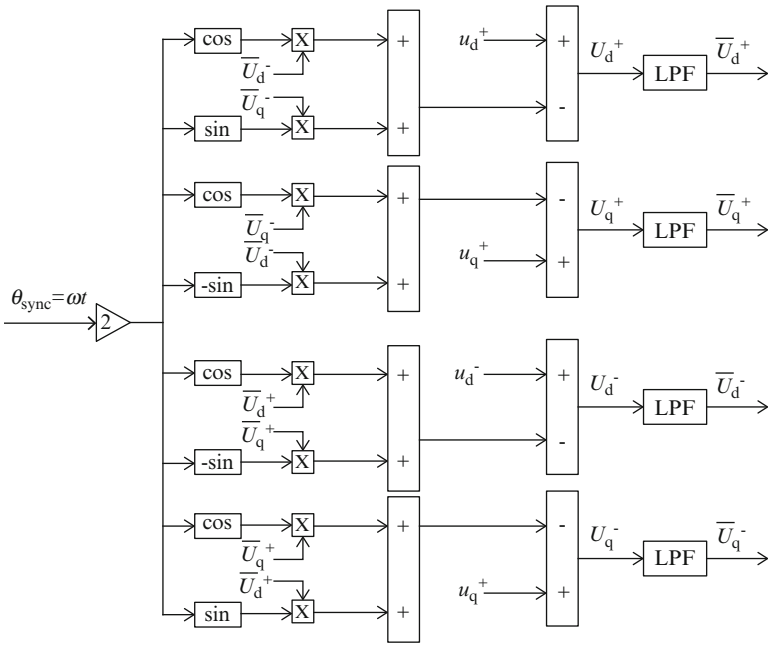


Fig. 7.23 Decoupling network

frames. The block LPF represents a simple first order low-pass filter with cut-off frequency of ω_f as shown in Eq. 7.9.

$$LPF(s) = \frac{\omega_f}{s + \omega_f} \tag{7.9}$$

The positive and negative sequence component from the input voltage vector is provided by the decoupling network. Hence, it is possible to synchronize the control system instead of GSC sub system to the grid voltage positive sequence component. When the positive sequence q axis voltage component U_q^+ is zero the synchronization of the grid voltage is achieved. In such case, the initial phase angle φ+ is zero and the positive sequence voltage component is aligned to d+ axis rotating with angular speed of ω. The positive sequence voltage component angle θ_{sync} is obtained using SRF-PLL.

The backward numerical approximation can be used to build the discrete controller and the integrator. As shown in the equation the frequency and phase can be then represented considering U_q^{+1} as the error to be minimized. ω_{nom} represents the feed forward nominal frequency as shown in Eqs. 7.10 and 7.11.

$$W(Z) = \frac{(K_p + K_i T_s)Z - K_p}{z - 1} . U_q^{+1}(Z) + w_{nom} \tag{7.10}$$

$$\theta^{+'} = \frac{T_s Z}{z - 1} . W(Z) \tag{7.11}$$

Finally the sample representation provides the equations whose expressions are to be programmed. The frequency feed forward has been included by introducing a initial condition to W′ in the Eqs. 7.12 and 7.13.

$$W'[n+1] = W'[n] + (K_p + K_i T_s) U_q^{+1}[n+1] \tag{7.12}$$

$$\theta^{+'}[n+1] = \theta^{+'}[n] + T_s W[n+1] \tag{7.13}$$

Even though the DSRF PLL is more complex than dq PLL, due to its excellent performance under unbalanced conditions of the network it is preferred for industrial applications. The performance of PLL is good even under distorted conditions when there is reduction in bandwidth.

A high overshoot in the phase angle and frequency estimation is appeared during the instant of fault occurrence. This is the only drawback of the DSRF PLL.

7.3.4.5 Decoupled Stationary Reference Frame PLL (DαβPLL)

The results of the investigation of the performance of the three PLLs motivate the development of a new hybrid PLL which is a combination of the abovementioned PLLs and uses the advantages of each PLL.

The effect of the time response of each PLL on the overshoot of the estimated phase angle is investigated and is shown in Fig. 7.24.

The simulation results in Fig. 7.24 show how the changing of the time response settings of each PLL affects the overshoot of the frequency estimation (f_{dqPLL}, $f_{\alpha\beta PLL}$ and $f_{DSRFPLL}$) when a 50 % balanced voltage sag occurs. Clearly the desired faster operation of a PLL causes undesirably higher overshoots in the frequency. An important conclusion from Fig. 7.24 is that the overshoot of αβ PLL is always

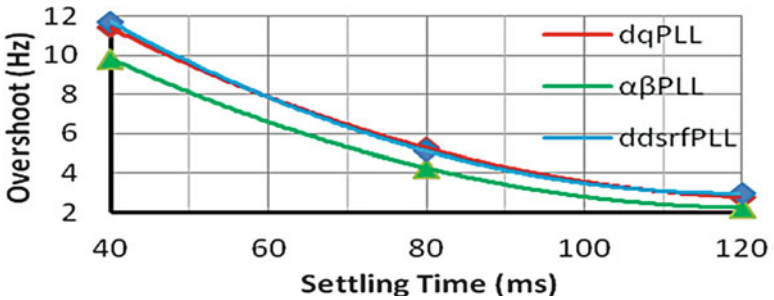


Fig. 7.24 Overshoot response of the three PLLs

lower (18 % lower overshoot on average) in comparison to the other two PLLs and also that dq PLL and DSRF PLL have very similar responses since the structure of the DSRFPLL is based on the dq PLL and on two decoupling cells.

The results in Fig. 7.24 show that the αβ PLL has lower overshoot on the frequency estimation when a fault occurs compared to the two other PLLs under investigation. In addition, the αβPLL faces a problem under unbalanced conditions, in contrast to the DSRF PLL, where the decoupling of the voltage sequence makes it very accurate under balanced and unbalanced conditions. The hybrid Dαβ PLL is a combination of the decoupling cells that are used in DSRF PLL to decouple the voltage sequence and the αβ PLL algorithm to estimate the phase angle of the grid voltage, which offers lower estimation overshoot instead of the algorithm that is used in dq PLL. The new hybrid Dαβ PLL aims at operating very accurately under balanced and unbalanced disturbances and also at having a lower phase angle and frequency overshoot than the DSRF PLL. Therefore, the desired faster operation could be achieved by the suggested Dαβ PLL within the same frequency limits. The structure of the hybrid DαβPLL is illustrated in Fig. 7.25.

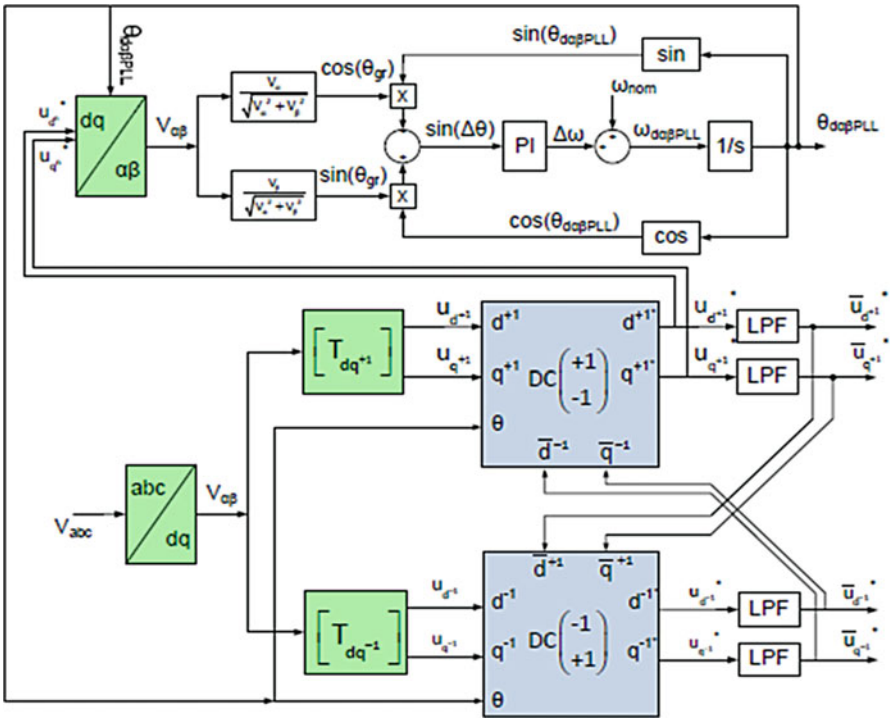


Fig. 7.25 The structure of the hybrid DαβPLL

7.4 Grid Connected Inverters

7.4.1 Inverters

Inverter is a power electronic device which converts the input DC source into an AC source. It is widely used in many applications which require the transportation of bulk power from source to load.

Power inverters produce one of three different types of wave output:

1. Square Wave.
2. Modified Square Wave or Modified Sine Wave.
3. Pure Sine Wave or True Sine Wave.

The three different wave signals represent three different qualities of power output.

7.4.1.1 Square Wave

Square wave inverters were first made but it is no longer used now a days. It delivers uneven power which cannot efficiently drive most devices. Modified square wave inverters came into existence which consistently delivers power and efficient to run devices. Sensitive equipment like medical equipments and variable rechargeable drives requires sine wave which shows great improvement over their predecessors.

7.4.1.2 Modified Sine Wave

Modified sine wave inverter has its own advantages over a true sine wave inverter which has lower efficiency and higher cost. These are the second generation of power inverters. It produces an approximate sine wave with low enough harmonics which do not cause problems with the household equipments. This inverter also has its own disadvantage as the peak voltage varies with the battery voltage. Battery voltage fluctuations may change the behavior of cheaper electronic devices fed by power supply without regulation.

7.4.1.3 True Sine Wave

True sine wave inverters are the recent trend inverters as the power delivered by them has no harmonics and all appliances operate properly. The problem arises with the implementation as the circuit is complex and costly.

Inverter operation depends mainly on the types of switches and their switching pattern which mainly depends on the configuration of the system and required output voltage. Conventionally transistors are used and it may vary as either IGBT (Insulated Gate Bipolar junction Transistor) or Power MOSFET (Metal Oxide

Silicon Field Effect Transistor) based on designer's requirement. IGBT is preferred for higher switching frequencies whereas MOSFET is preferred for little slower frequencies and high power demands.

7.4.2 Pulse Width Modulation Control

Pulse width modulation (PWM) control is used within inverters to obtain constant fundamental magnitude of the output voltage from inverter. PWM control eliminates the use of external circuitry for controlled output. By adjusting the on and off of the inverter components fixed input voltage can be converted to controlled ac voltage output.

The advantages of PWM control scheme are (i) no external circuit required to obtain desired output; (ii) Lower order harmonics are minimized by PWM itself whereas higher order harmonics are eliminated by filters.

Even though PWM scheme posses disadvantages as usage of expensive switching devices, this scheme is popularly used in all industrial equipment. PWM techniques use a constant amplitude pulse whose duty cycle can be varied as per the requirement for each period. Desired output voltage with reduced harmonic content can be obtained by modulating the width of these pulses. Based on the difference in the output harmonic content PWM techniques are classified into many types. Selection of particular PWM technique mainly depends on the acceptable harmonic content in the inverter output voltage.

7.4.2.1 Sinusoidal Pulse Width Modulation (SPWM)

SPWM is very popularly used in industrial applications. The different terminologies used for the same are the triangulation, sub-harmonic or sub-oscillation method.

The high-frequency triangular carrier wave, V_c is compared with a sinusoidal reference, V_r of the desired frequency to realize SPWM. In Figs. 7.27 and 7.28, V_c and V_r waves interact to determine the switching pattern of the modulated pulses. The magnitude and frequency of these signals are arbitrary. V_c represents the peak value of triangular carrier wave and V_r represents the peak value of the reference signal.

Comparator is used to mix reference control signal and the triangular wave which in turn controls the operation of the switches T_1 and T_6 (shown in Fig. 7.26). The logic behind this control is that when reference wave has higher magnitude than carrier wave the comparator output is high else it is low. The comparator output is processed in a trigger pulse generator such that the output voltage wave of the inverter has a pulse width in relation with the comparator output pulse width. The ratio of magnitude of reference wave to that of the carrier wave is termed as Modulation Index (M_i) i.e., $M_i = \frac{v_r}{v_c}$ and its value vary between 0 and 1. If the

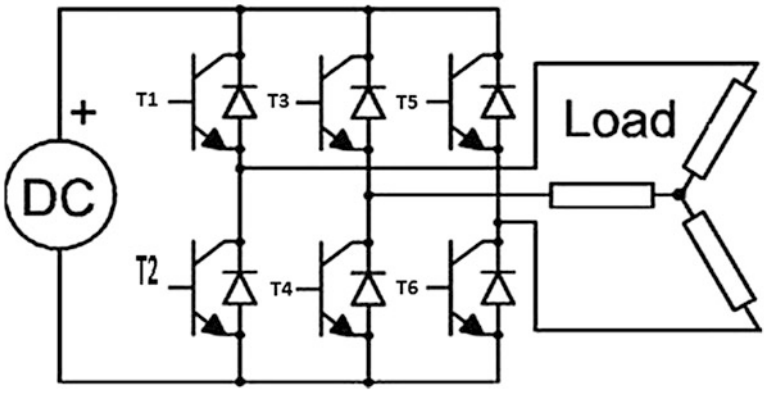


Fig. 7.26 Three phase inverter

triangular wave amplitude is kept constant, the magnitude of fundamental component of output voltage is proportional to the modulation index.

While designing inverters for grid connection designer should be aware of the current standards and regulations which apply in the target country. The National Renewable Energy Laboratory has published the American National Standard ANSI/IEEE 1547 in 2003. Additionally the International Electrotechnical Commission also published the standard IEC 61727.

7.4.2.2 Voltage

PV systems do not influence the grid voltage when it is connected to the grid. Their voltage operation range is more of a protection function that is used for detecting abnormal utility, rather than regulators. Such typical voltage detection may be as defined in and shown in Table 7.6. Trip time refers to the time between the abnormal condition and the inverter ceasing to energize the utility line. The inverter will actually remain connected to the utility to allow the inverter to sense utility electrical conditions for the reconnection process.

7.4.2.3 DC-Injection

The maximum rated output current injected into the power grid under any circumstances is not more than 0.5 % because large and durable DC currents will eventually saturate the transformer's iron core. Saturation leads to the selection of other paths outside the iron core by the magnetic flux and results in increasing leakage flux and lowering of the transformer ratio.

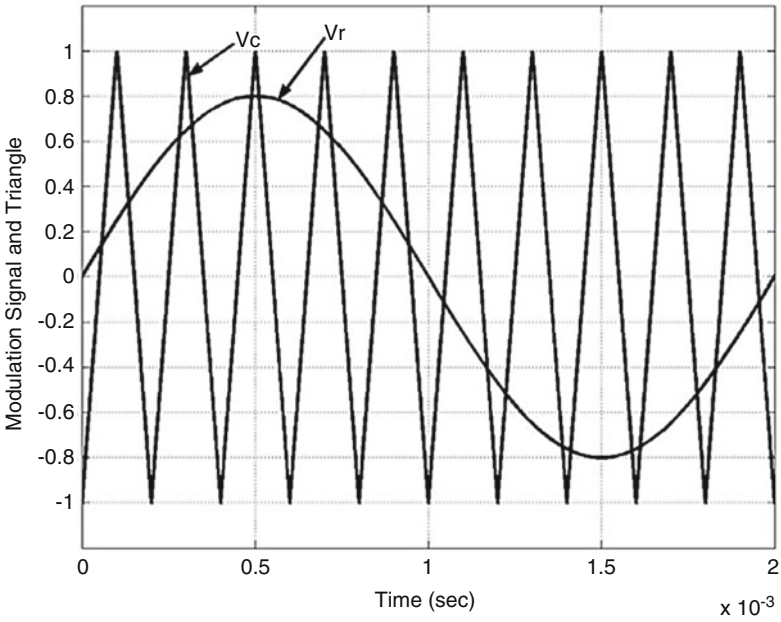


Fig. 7.27 Comparison of sinusoidal and triangular waveforms

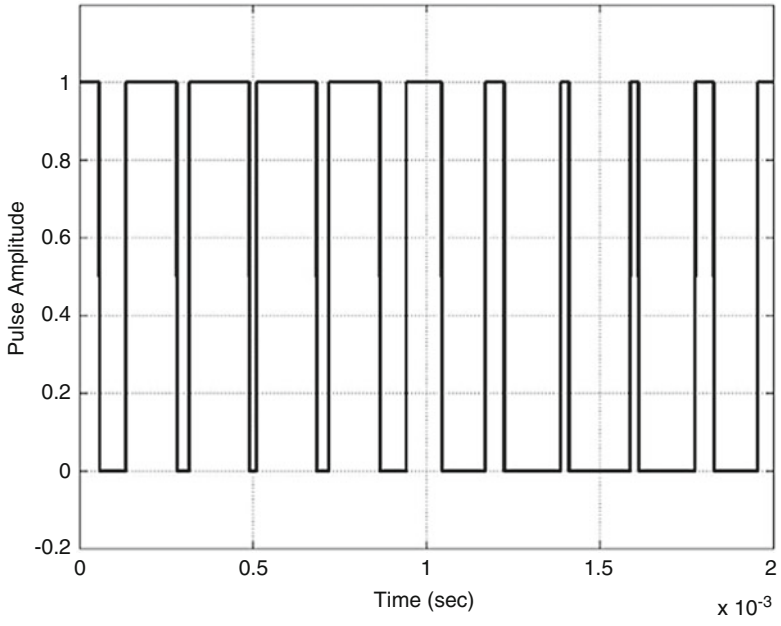


Fig. 7.28 Pulses generated

Table 7.6 Standards of grid-connected inverters

Issue	IEC 61727	IEEE 1547
Nominal power	10 kW	30 kW
Harmonic currents	(3–9) 4.0 %	(2–10) 4.0 %
	(11–15) 2.0 %	(11–16) 2.0 %
	(17–21) 1.5 %	(17–22) 1.5 %
	(23–33) 0.6 %	(23–34) 0.6 %
	Even harmonics shall be less than 25 % of the odd harmonics listed	(>35) 0.3 %
		Even harmonics shall be less than 25 % of the odd harmonics listed
Maximum current THD	5.0 %	5.0 %
Power factor at 50 % of rated power	0.90	–
DC current injection	Less than 1.0 % of rated output current	Less than 0.5 % of rated output current
Voltage range for normal operation	85–110 %	88–110 %
Frequency range for normal operation	50 ± 1 Hz	59.3–60.5 Hz

7.4.2.4 Flicker

Based on IEEE standard, flicker created by the PV system should not cross the acceptable limit. The percentage for this acceptance is not specified in the IEEE standard but it is specified in IEC as limits for the flicker for short term duration should be less than 1 s and for long term flickers the duration has to be less than 0.65 min.

7.4.2.5 Frequency

Inverter and power grid are always synchronized during the operating periods but if the grid itself goes outside some specified frequencies, then the PV system must stop providing power to the grid.

7.4.2.6 Current Distortion

Current distortion affects the grid connected devices in a negative manner and hence it should be avoided in any grid. An overview of the maximum allowed harmonic current distortion may be found in Table 7.6. The THD is limited to 5 % of the rated fundamental harmonic. Even harmonics are limited to 25 % of the odd harmonic limit.

7.4.2.7 Power Factor

The power factor can be larger than 0.85 (leading or lagging) in normal conditions when the load is larger than 10 % of the rated power. For reactive power compensation, the utility may allow lower power factors. For small systems the possible contribution of reactive power to the grid is very small that allows it to be excluded and only consider the given power factor provided by the grid.

7.4.2.8 Reconnection

Based on IEEE standards the inverter for some reason ceases to deliver power due to abnormal grid activity, then it may be reconnected to the grid only after the power voltage and frequency has been within normal voltage and frequency ranges for at least 5 min.

Table 7.6 summarizes the current standards dealing with interconnections of PV systems to a grid.

7.4.3 Grid Filter

Renewable power generation mainly depends on the control technology used in grid connected inverters. Fully-controlled power electronic devices IGBT and (Gate Turn-off Thyristor) GTO are to be used, which is modulated by the high frequency PWM.

Due to that the dv/dt and di/dt are ever large. The presence of some vagrant parameters made the harmonic pollution by inducing high order harmonic flow current into the power grid. The inductor filter is most commonly used in the grid-connected inverter. So as to decrease current ripple, the inductance have to be increased. As a result, the volume and weight of the filter increased. Even though the structure and the parameter of the LC filter are easy, the filtering effect is not good because of the uncertainty of network impedance. LCL filter had an inherently high cut-off frequency and strong penetrating ability in low frequency. So LCL filter has come into wide use in the inverter. The challenge arise in the selection of the parameter and control resonance. The structure of LCL filter is shown in Fig. 7.29.

7.4.3.1 Advantages of LCL Filters

The advantages of the LCL filters are listed below

- The LCL filters have the capability of attenuating harmonics at lower frequencies, which is a significant feature for high power applications.
- Precise control of the output current is possible.
- They provide a better decoupling between the filter and grid impedance (as it reduces the dependence of the filter on the grid parameters).
- A lower ripple of the current stress across the grid inductor is achieved.

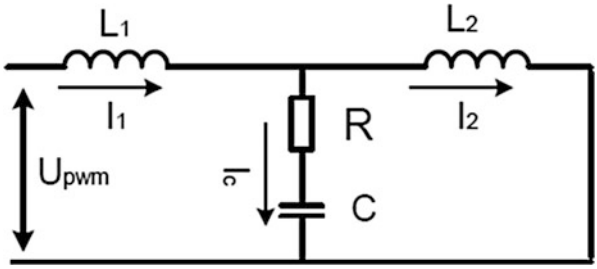


Fig. 7.29 LCL filter with series damping resistor

Table 7.7 Simulation parameters

Grid line-line voltage	Vg = 415 V
Rated active power	P = 5 kW
DC-link voltage	V_{dc} = 400 V
Frequency of grid voltage	f_g = 50 Hz
Switching frequency	f_s = 3 kHz

7.4.3.2 Filter Design

Factors which must be considered for the designing of LCL filter are current ripple, filter size and switching ripple attenuation. The reactive power requirements may cause a resonance of the capacitor interacting with the grid. Therefore, a resistor in series with the capacitor is included for passive or active damping. The required parameters are: V_{rated} – phase voltage (inverter output), P_{rated} – rated active power, V_{dc} – Dc link voltage, f_g – grid frequency, f_s – switching frequency. The selected values are given in Table 7.7.

7.4.3.3 Filter Inductance

Current ripple is the major consideration for the design of L. Smaller ripple results in lower switching and conduction losses. Typically the ripple current can be chosen as 10–15 % of rated current. Current ripples can be considered as 10 %. The value of inductor (L_1) in the system can be obtained from current ripples as given by Eq. 7.14.

$$\Delta I_{L\max} = \frac{\frac{1}{s}V_{dc}}{L_1 * f_s} \tag{7.14}$$

The inductance L_2 is calculated by multiplying the inductance L_1 with an attenuation factor as shown in Eq. 7.15. Here the attenuation factor is selected as 20 %.

$$L_2 = K_a * L_1 \tag{7.15}$$

Table 7.8 Filter values

Filter parameter	Value
L_1	6.6 mH
C	9.20 μF
L_2	1.32 mH
R_f	0.55 Ω

7.4.3.4 Filter Capacitance

Capacitor C selection is mainly based on the reactive power supplied by the capacitor at fundamental frequency. In this design reactive power is chosen as 15 % of the rated power is given by Eq. 7.16.

$$C = \frac{15\% * P_{rated}}{3 * 2\pi f * V_{rated}^2} \tag{7.16}$$

7.4.3.5 Damping Resistance

Because the LCL filter has resonance, the some order harmonic current that come from the grid-connected inverters may increase rapidly. For this reason, adding the damping resistance into filter to suppress the resonances. Generally, it is resistor.

The obtained LCL filter values are shown in the Table 7.8.

7.5 Current Controllers for PWM Inverters

Different reference frames such as synchronous rotating (dq), stationary (αβ), or reference (abc) frame can be used for the control strategy implementation for a distributed generation system. Designing mainly implies on different controller types and their implementation in different reference frames.

Each existing current control techniques have its own characteristics and strengths, which makes it suitable for specific applications. Properties associated to switching frequency, load current distortion and dynamic behavior usually contradict each other. Thus the most appropriate current control method can be selected based on the effective compromise between these characteristics and the nature of the application.

A few current control methods that are used for PWM inverters are shown in Fig. 7.30.

7.5.1 SRF PI Current Controller

The current controller of three-phase VSI plays a major role in controlling grid-connected inverters. The performance of the inverter system is highly affected by the quality of the applied current controller. Among many control mechanisms

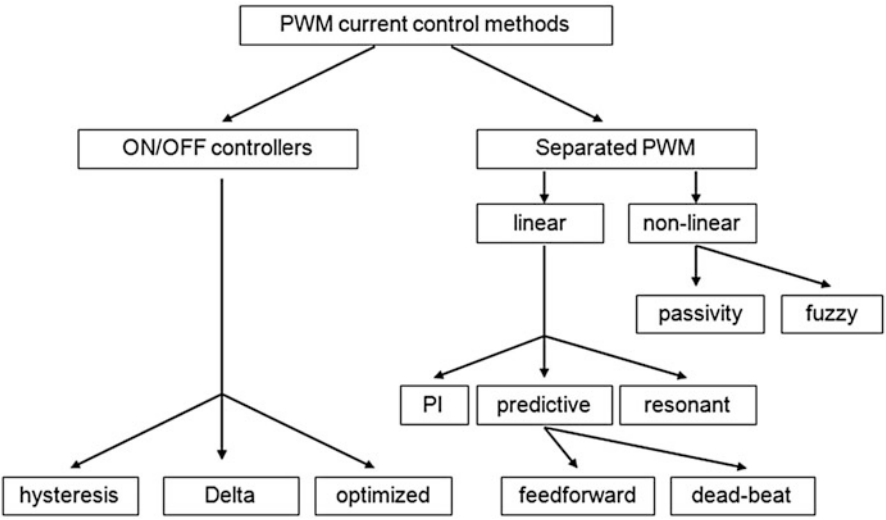


Fig. 7.30 Current controllers for PWM inverters

which have been developed to regulate the inverter output current that is injected into the utility grid, three major types of current controller have evolved: Hysteresis Controller, Predictive Controller and Linear Proportional-Integral (PI) controller. Predictive controller has a very good steady-state performance and provides a good dynamic performance. But, its performance is sensitive to system parameters. The Hysteresis Controller has a fast transient response, non-complex implementation and an inherent current protection. But it has some drawbacks such as variable switching frequency and high current ripples. These cause a poor current quality and introduce difficulties in the output filter design.

The PI controller is the most common control algorithm used for current error compensation. PI controller calculates an error value as the difference between a measured inverter output current and a desired injected current to the grid, then the controller attempts to minimize the error between them. The PI controller calculation algorithm involves two separate constant parameters, the proportional constant K_p and the integral constant K_i. The proportional term of the controller is formed by multiplying the error signal by a K_p gain. This tends to reduce the overall error with time. However, the effect of the proportional term will not reduce the error to zero, and there is some steady state error. The Integral term of the controller is used to fix small steady state errors. The Integral term integrates the error then multiplies it by a K_i constant and becomes the integral output term of the PI controller. This removes the steady state error and accelerates the movement of the process into the reference point.

The advantages of PI current control is that it offers an excellent steady-state response, low current ripple, constant switching frequency, in addition to well-defined harmonic content. Moreover, the controller is insensitive to system

parameters since the algorithm does not need system models. PI controllers can be applied either in the stationary (αβ) or in synchronous (dq) reference frame. When the synchronous PI controller is used, the control variables become DC and the PI compensators are able to reduce the stationary error of the fundamental component to zero whereas with PI controllers working in the stationary system, there is an inherent tracking error of phase and amplitude. Therefore, current control in a synchronous (rotating) reference frame, using PI controllers is the typical solution in the three-phase grid-connected inverters.

Based on the mathematical model of the grid-connected inverter, the output voltages of the inverter in the synchronous (dq) frame are given by Eq. 7.17.

$$\begin{bmatrix} u_d \\ u_q \end{bmatrix} = L\frac{d}{dt}\begin{bmatrix} i_d \\ i_q \end{bmatrix} + R\begin{bmatrix} i_d \\ i_q \end{bmatrix} + \omega L\frac{d}{dt}\begin{bmatrix} -i_q \\ i_d \end{bmatrix} + \begin{bmatrix} e_d \\ e_q \end{bmatrix} \tag{7.17}$$

where L is the inductance between the grid-connected inverter and the grid; R is the resistance between the grid-connected inverter and the grid; e_d and $e_{q.}$ are the components of the park transformation of the grid voltage; u_d and u_q are the components of the park transformation of the inverter output; ω is the angular frequency of the grid.

The block diagram of the synchronous controller for the grid-connected inverter is represented in Fig. 7.31. It is seen from the figure that the inverter has two PI controllers to compensate the current vector components that are defined in synchronous reference frame (dq). Because of coordinate transformations, i_q and i_d are DC components and therefore, PI compensators reduce the error(s) between the desired current I^*_d (I^*_q) and the actual current I_d (I_q) to zero The output energy

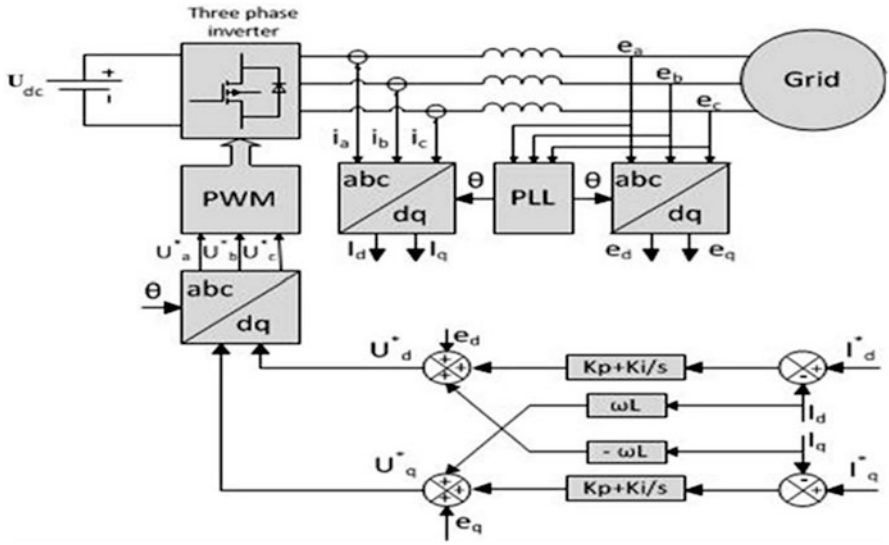


Fig. 7.31 SRF PI controller structure for a grid-connected inverter

and power factor can be controlled by changing d-axis current and q-axis current. The performance of PI controller can be improved by using cross-coupling terms and voltage feed forward.

7.5.2 *Cascaded Deadbeat and PI Controller*

A new effective control strategy named the Cascaded Deadbeat and PI current controller is used for DC-AC voltage source converters, connected to the grid via LCL filters as shown in Fig. 7.32. The advantage of the structure of this control system is intuitive, simple and straight forward. The output current is regulated via a PI controller. The output of PI controller determines the current reference for an inner-loop Deadbeat controller. Thus, the overall control is decomposed into two cascaded parts, facilitating the application of control analysis techniques for the design of a robust and well-damped control system.

Figure 7.32 shows the structure of the control system, which includes an external PI control loop for the output current regulation, stabilized by an inner loop Deadbeat controller for the inverter current. The control scheme is developed to regulate the output current by appropriately modulating the PWM inverter. This is achieved in two stages: the output current iL_2 error is fed to a PI controller, which generates the reference value iL_1^* for the inverter current. The PWM inverter is then modulated according to the output of the inner Deadbeat controller.

In Fig. 7.32, $Z_s = R_s + j\omega L_s$ is the grid impedance. This impedance is incorporated in the impedance L_2 of the filter for the derivation of transfer functions to yield $L = L_2 + L_s$, $R = R_s$.

The DC voltage input to the inverter is assumed to be constant when a reasonably large capacitor is connected at the inverter input. The output voltage of the modulator is modeled as a constant dc voltage per modulation period T_s (100 μs)

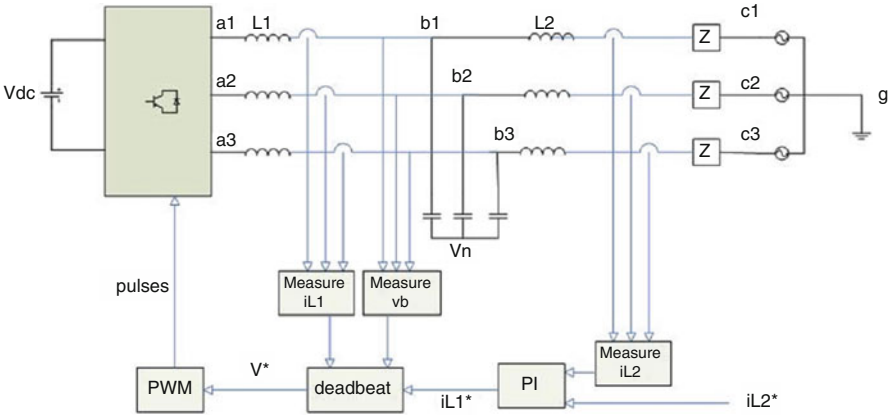


Fig. 7.32 Cascaded deadbeat PI control system

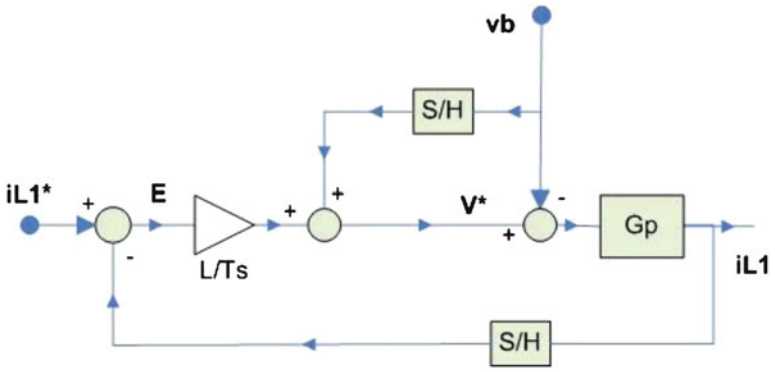


Fig. 7.33 The control diagram for iL_1 referring to d and q axis components

equal to the average value of the input dc voltage. The sampling period for the Deadbeat control is equal to T_s. Both the Deadbeat and PI controllers are analyzed in the synchronous dq frame, which significantly simplifies controller design and stability analysis.

7.5.2.1 Deadbeat and PI Controllers

For a sufficiently short PWM carrier period, T_s, it is possible to calculate the transfer function of the Deadbeat controller shown in Fig. 7.33 with difference equations in the z-plane. Z transform is applied to imply that the capacitor voltage is considered constant throughout T_s, which is valid for sufficiently high switching frequencies. The Principle of this controller is quite simple than other controllers. Feedback of iL_1 is amplified by L_1/T_s and added to the measured capacitor voltage v_b, thus yielding the voltage signal V^* which is fed to the modulator. Given that v_b remains constant over T_s, the transfer function of the above system is given by Eq. 7.18.

$$I_{L1}(z) = \left(I + G_p(z)\frac{L_1}{T_s}\right)^{-1} G_p(z)\frac{L_1}{T_s} {I_{L1}}^*(z) \tag{7.18}$$

where, the transfer function $G_p(z) = V_{ab}(z)/I_{L1}(z)$

Assuming a sufficiently small T_s, $G_p(z)$ is simplified and substituted in Eq. 7.18 yields Eq. 7.19,

$$I_{L1}(z) = \begin{bmatrix} \frac{1}{z} & 0 \\ 0 & \frac{1}{z} \end{bmatrix} {I_{L1}}^*(z) \tag{7.19}$$

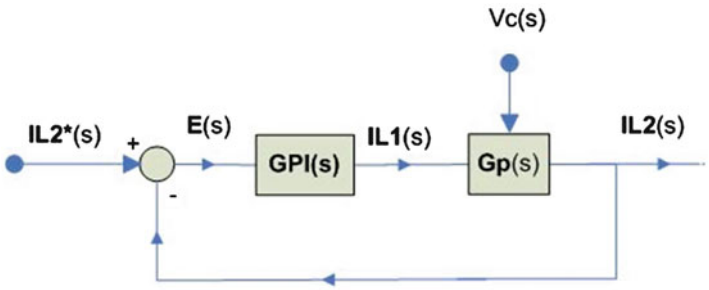


Fig. 7.34 The PI control of I referring to d and q axes components

Figure 7.34 shows the structure of the external PI control loop. The assumption is made that the output of the PI control is actually iL_1, not iL_1^*, for analysis because, as shown in Eq. 7.19, iL_1 follows iL_1^* with a lag of T_s, which is sufficiently small and can be ignored. The system is s-transformed on the dq frame. The transfer function of the PI controller is then given by Eq. 7.20; i.e., the d and q axes currents are controlled by independent regulators.

$$G_{pi}(s) = \begin{bmatrix} K_p + {}^{K_i}/_{s} & 0 \\ 0 & K_p + {}^{K_i}/_{s} \end{bmatrix} \tag{7.20}$$

$G_{pi}(s) = V_{ab}(s)/I_{L2}(s)^2$ is the transfer function of the network formed by C, L_2 and the grid impedance.

7.6 SIMULINK Model of PLL Grid Connected Power System

A comparison of the hybrid Dαβ PLL to the other PLLs is necessary in order to demonstrate its advantages. The comparison focuses especially on Dαβ PLL and DSRF PLL which are the only ones that are able to operate accurately under unbalanced disturbances.

7.6.1 SIMULINK Model of a Synchronous Reference Frame PLL

The SIMULINK Model of a Synchronous Reference Frame PLL is shown in Fig. 7.35. The tuning parameters of a PI controller are selected as kp = 180 ki = 3,200 calculated using Ziegler-Nichols method.

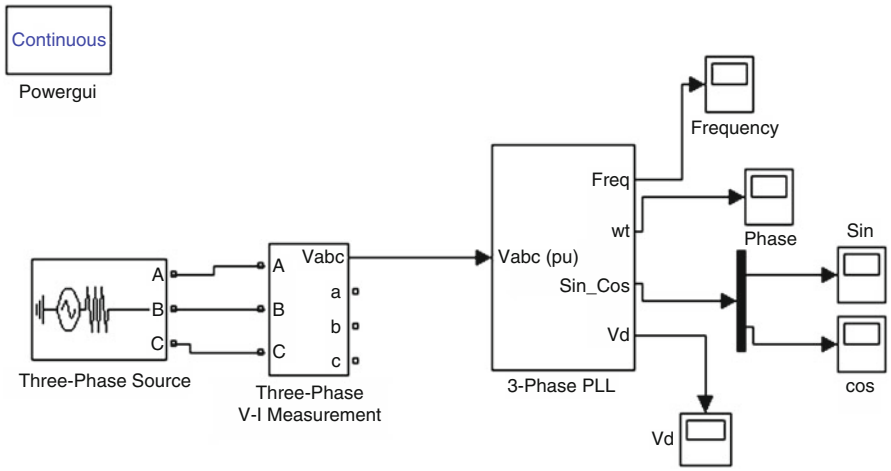


Fig. 7.35 SIMULINK model of a synchronous reference frame PLL

In the above SIMULINK diagram, the quadrature component of the voltage is taken for the frequency and hence the phase angle. The estimated phase angle is obtained by integrating the frequency. Practically this type of estimation results in $\theta = \text{infinity}$. As this type of design cannot be achieved in any discrete devices, the calculated value of the phase is made to fall between 0 and 2π using modulus operation.

7.6.1.1 Voltage and Phase Angle Tracked by SRF PLL

The output voltage Vd is obtained as 264.7 v for an input voltage of 325.26 v and the phase angle tracked by the SRF PLL is shown in Fig. 7.36.

7.6.2 SIMULINK Model of a Synchronous Reference Frame PLL During Unbalanced Fault

The SIMULINK Model of a Synchronous Reference Frame PLL during Unbalanced fault is shown in Fig. 7.37. Here an unbalanced fault is applied where there is a line to ground fault in two of the three phases.

7.6.2.1 Voltage and Phase Angle Tracked by SRF PLL During an Unbalanced Fault

The Voltage and Phase Angle Tracked by SRF PLL during an unbalanced fault are shown in Fig. 7.38.

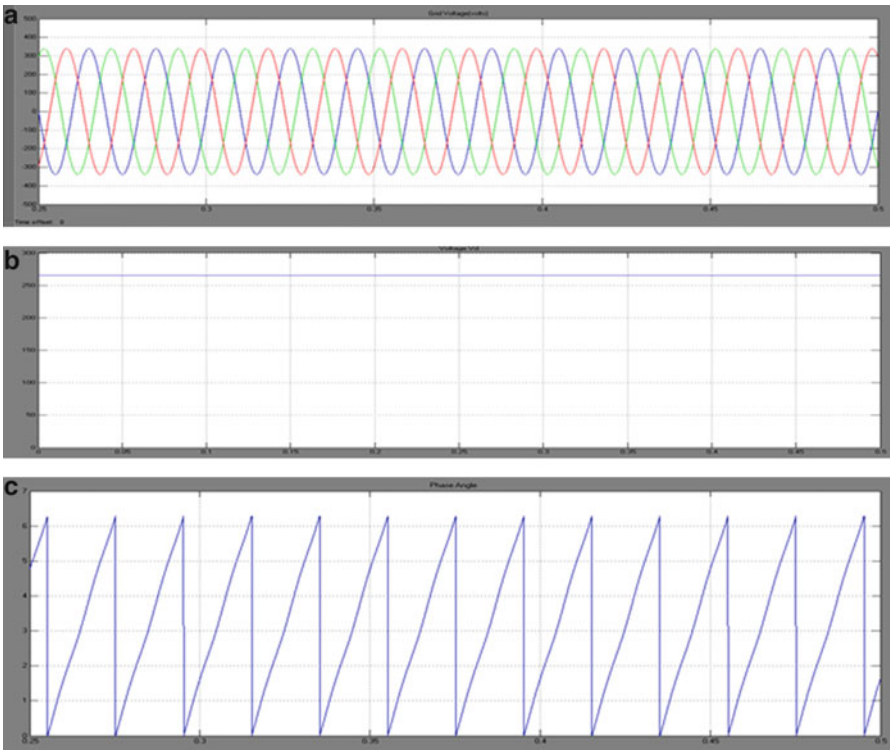


Fig. 7.36 (**a**) Grid voltage (**b**) voltage Vd obtained from PLL and (**c**) phase angle tracked by SRF PLL

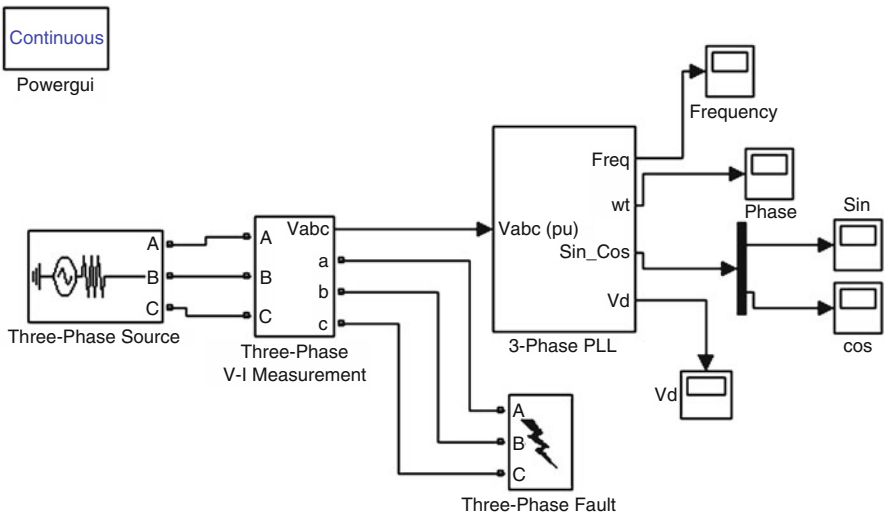


Fig. 7.37 SIMULINK model of a synchronous reference frame PLL during unbalanced fault

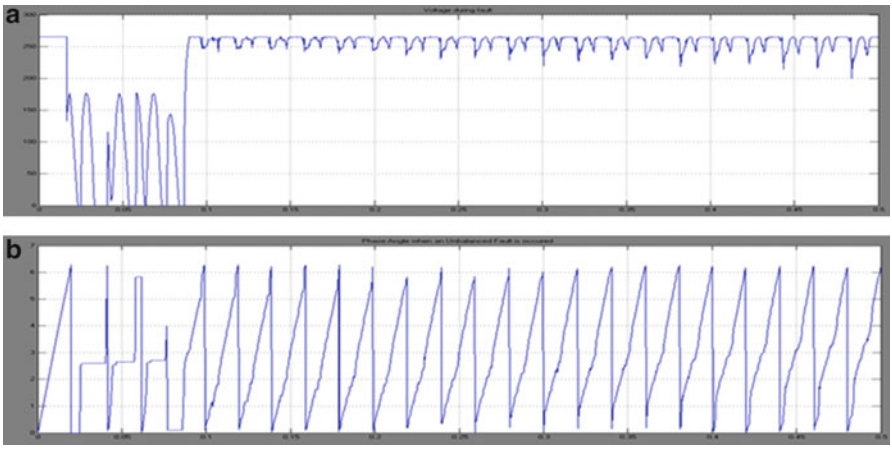


Fig. 7.38 (**a**) Voltage and (**b**) phase angle tracked by SRF PLL during an unbalanced fault

From the above two results, it is concluded that a synchronous reference frame PLL tracks the voltage and phase angle properly during normal conditions and under balanced faults

During an unbalanced fault, the voltage and phase angle are not tracked properly and are seen with many distortions.

7.6.3 SIMULINK Model of a DSRF PLL

The SIMULINK Model of a DSRF PLL is shown in Fig. 7.39. The tuning parameters of a PI controller are selected as $k_p = 2.2214$, $k_i = 246.74$ calculated using Ziegler-Nichols method.

7.6.3.1 Voltage and Phase Angle Tracked By DSRF PLL

The output voltage V_d, obtained as 420 V for an input voltage of 415 V, is shown in Fig. 7.40.

7.6.4 SIMULINK Model of a DSRF PLL Under an Unbalanced Fault

The SIMULINK Model of a DSRF PLL under an unbalanced fault is shown in Fig. 7.41. Here, an unbalanced fault is applied where there is a line to ground fault in two of the three phases.

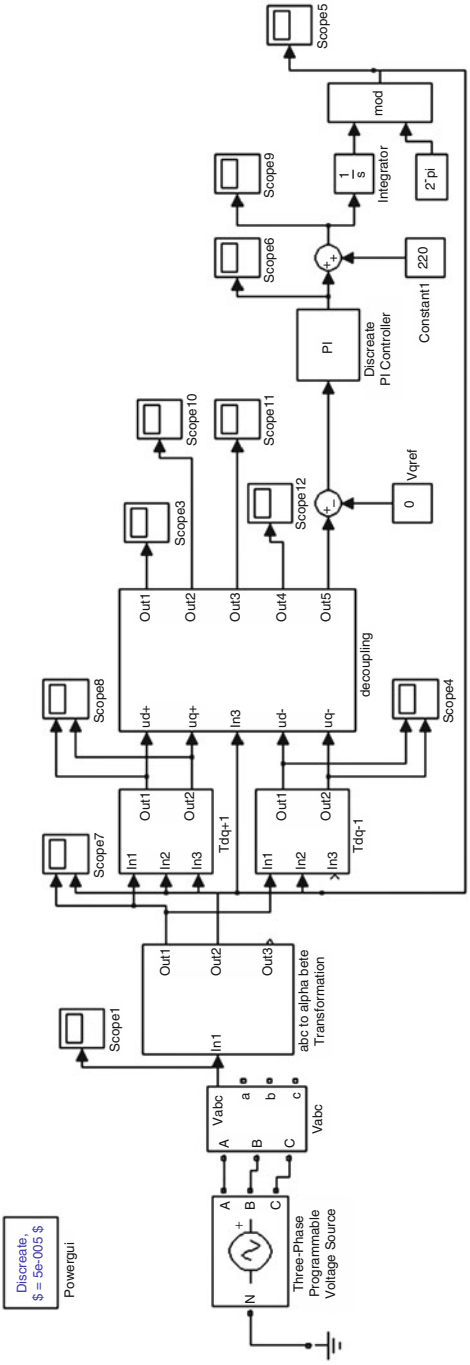


Fig. 7.39 SIMULINK model of a DSRF PLL

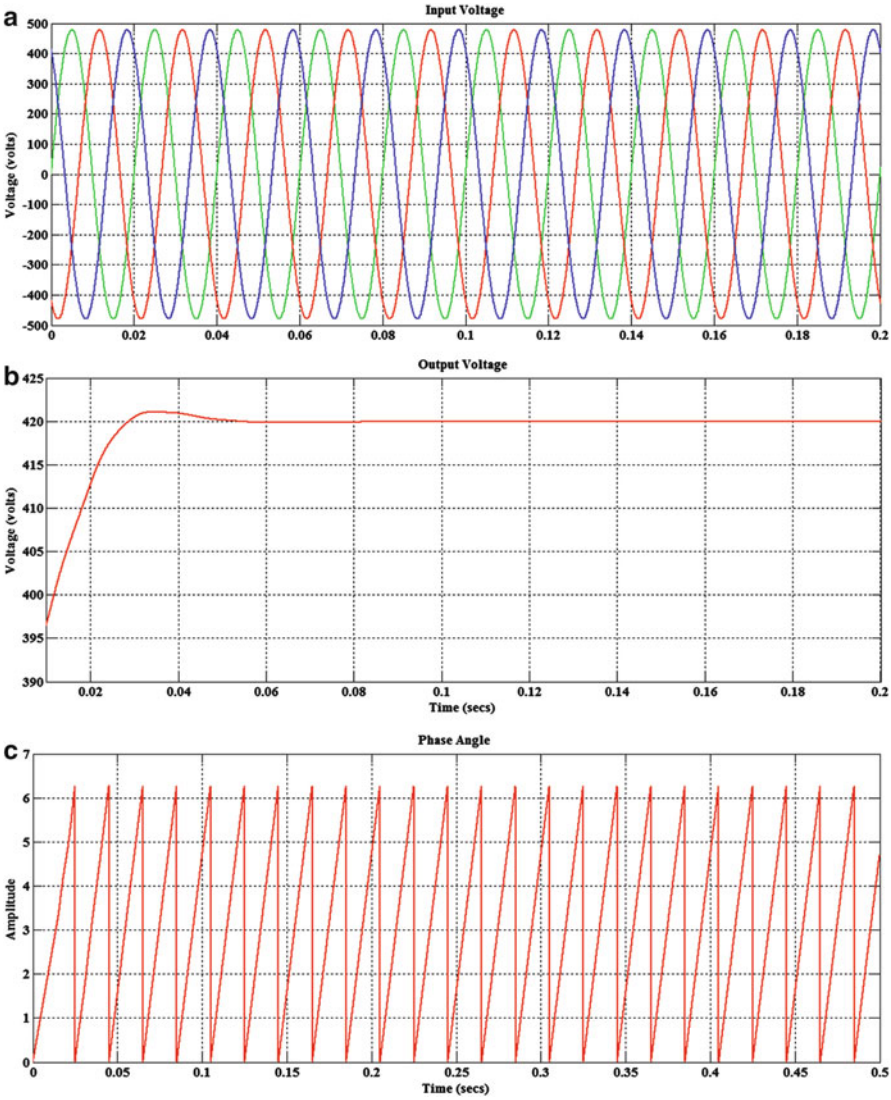


Fig. 7.40 Tracking by DSRF PLL – normal conditions (**a**) grid voltage (**b**) voltage V_d (**c**) phase angle

7.6.4.1 Voltage and Phase Angle Tracked By DSRF PLL During an Unbalanced Fault

The Voltage and Phase Angle Tracked by DSRF PLL during an unbalanced fault are shown in Fig. 7.42.

From the above results it is understood that when an unbalanced fault occurs, the DSRF PLL operates as same as under normal condition. Therefore it has an

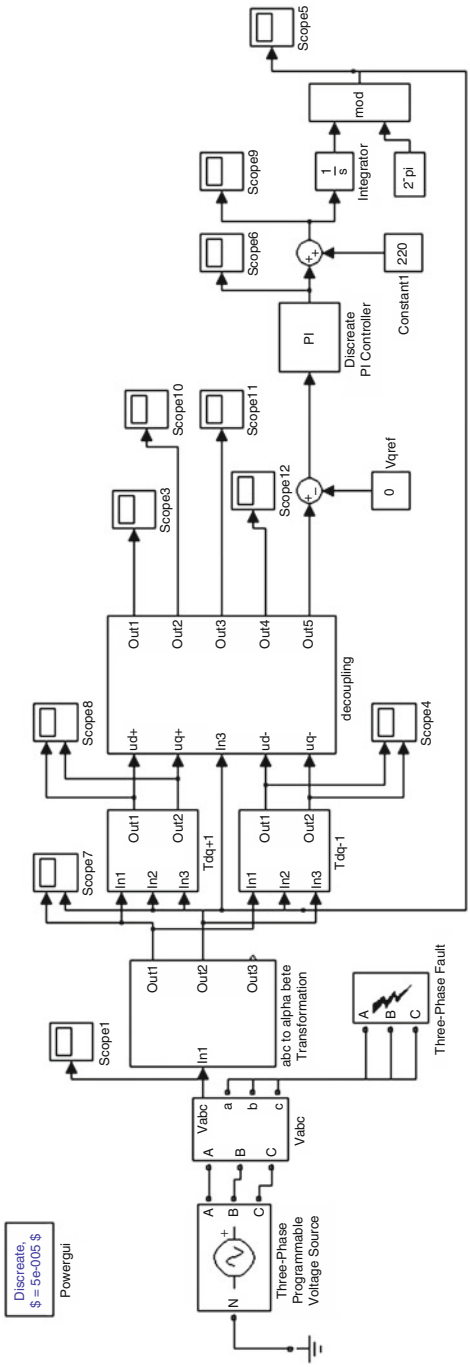


Fig. 7.41 SIMULINK model of a DSRF PLL under an unbalanced fault

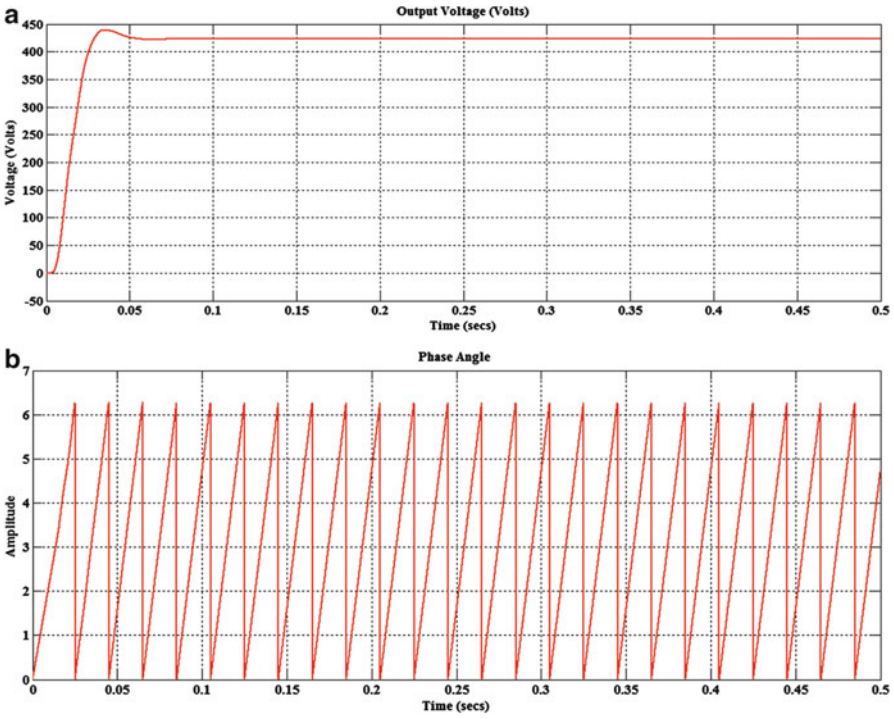


Fig. 7.42 Tracking by DSRF PLL -unbalanced fault (**a**) voltage (**b**) phase angle

improved result over the conventional dq PLL which cannot track the phase angle under fault conditions.

This is because of the decoupling of the positive and negative components present in the voltage and taking the positive component of the voltage as reference.

7.6.5 SIMULINK Model of αβPLL

The SIMULINK Model of an αβ Frame PLL is shown in Fig. 7.43. The tuning parametres of a PI controller are selected as kp = 180 ki = 3,200 calculated using Ziegler-Nichols method.

7.6.5.1 Voltage and Phase Angle Tracked by SRF PLL During an Unbalanced Fault

The voltage obtained by the PLL in d-q frame is shown in Fig. 7.44. The input voltage to the PLL is 325.26 V.

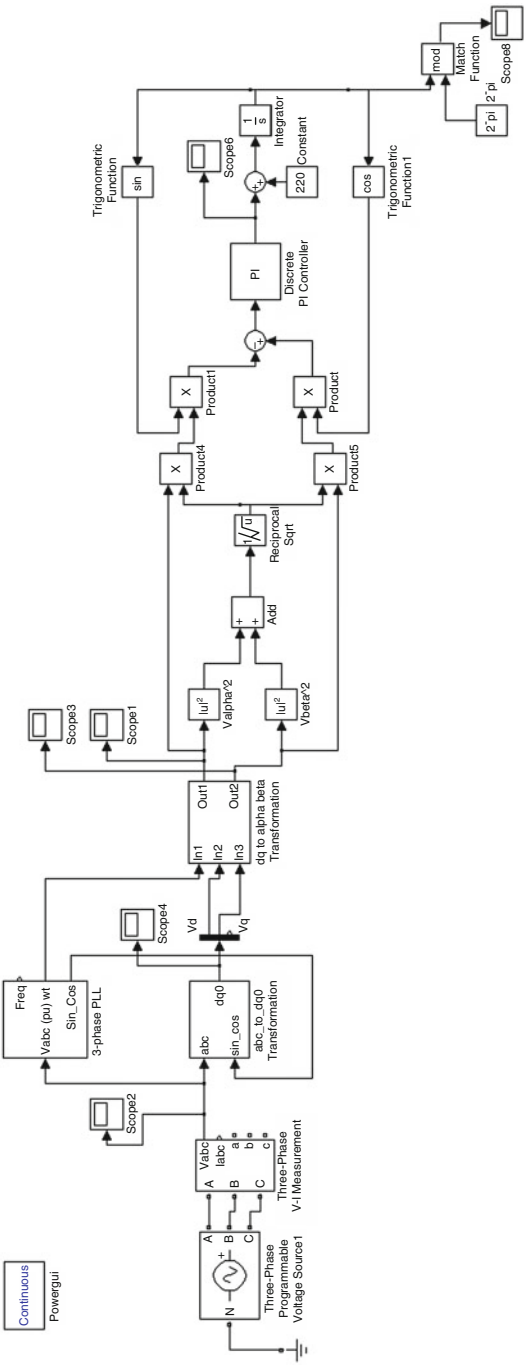


Fig. 7.43 SIMULINK model of an αβ PLL

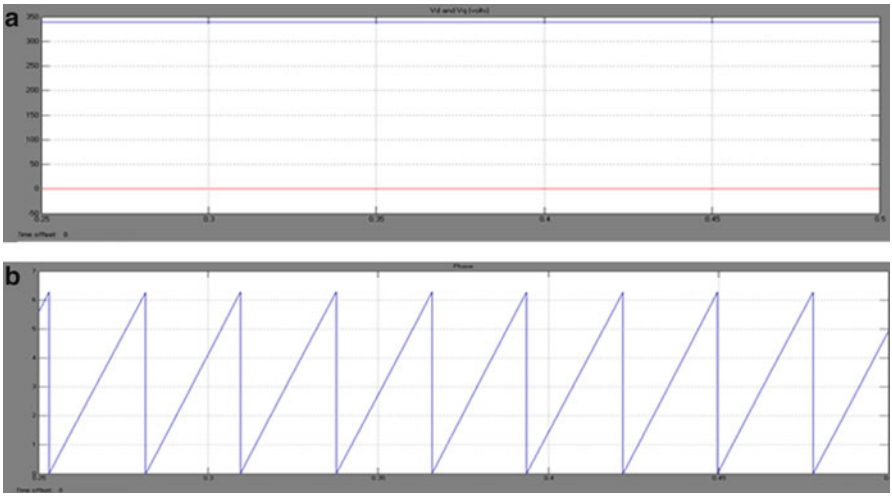


Fig. 7.44 (**a**) Voltage and (**b**) phase angle tracked by αβ PLL

7.6.6 SIMULINK Model of a αβPLL During Unbalanced Fault

The SIMULINK Model of a αβPLL during Unbalanced fault is shown in Fig. 7.45. Here an unbalanced fault is applied where there is a line to ground fault in two of the three phases.

7.6.6.1 Phase Angle Tracked by αβ PLL During an Unbalanced Fault

The phase angle tracked by αβ PLL during an unbalanced fault is shown in Fig. 7.46.

From the above two results, it can be inferred that the αβ PLL also exhibits the same behavior as that of the synchronous reference frame PLL. It also has a disturbed phase when an unbalanced fault occurs.

The advantage of the αβ PLL over the SRF PLL is that the peak over shoot in the phase angle tracked is less.

7.6.7 SIMULINK Model of a Dαβ PLL

The SIMULINK Model of a Decoupled αβ PLL (Dαβ PLL) is shown in Fig. 7.47. The tuning parameters of a PI controller are selected as $k_p = 180$, $k_i = 3{,}200$ calculated using Ziegler-Nichols method.

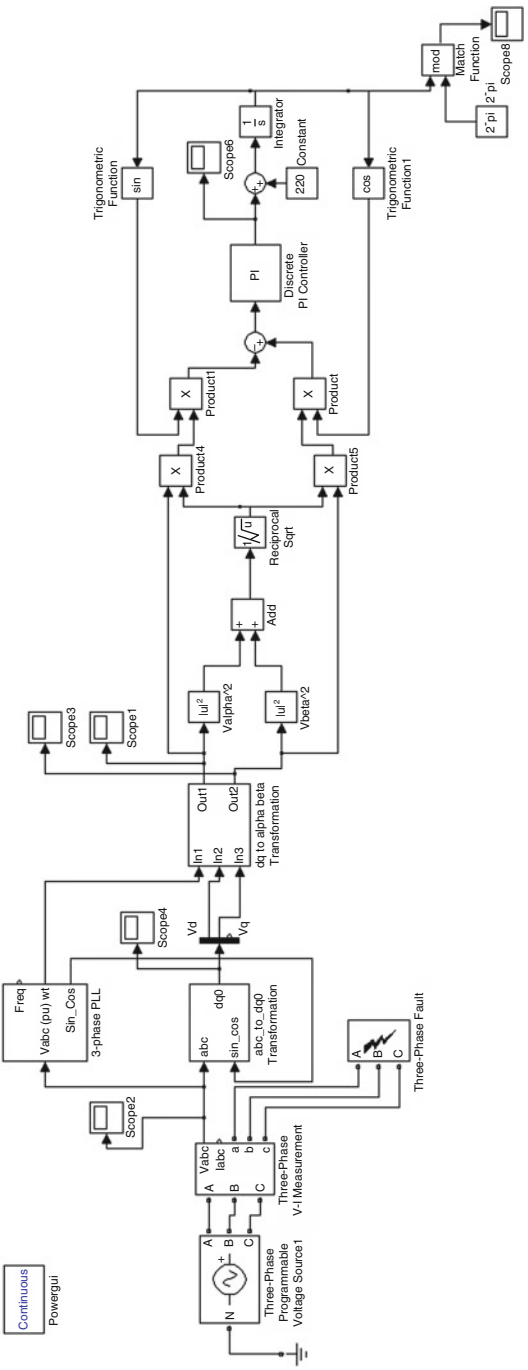


Fig. 7.45 SIMULINK model of an αβ PLL under an unbalanced fault

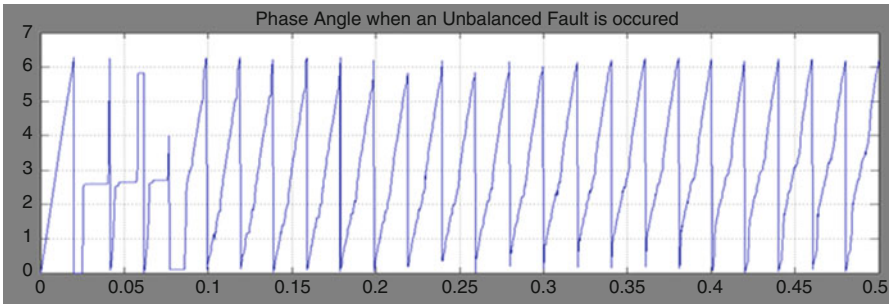


Fig. 7.46 Phase angle tracked by αβ PLL under an unbalanced fault

7.6.7.1 Voltage and Phase Angle Tracked Using Dαβ PLL

The Voltage and Phase angle tracked using Dαβ PLL is shown in Fig. 7.48. The output voltage V_d is 423.3 V for an input voltage of 415 V.

7.6.8 SIMULINK Model of a Dαβ PLL Under an Unbalanced Fault

The SIMULINK Model of a Decoupled αβ PLL (Dαβ PLL) under an Unbalanced Fault is shown in Fig. 7.49. Here an unbalanced fault is applied where there is a line to ground fault in two of the three phases.

7.6.8.1 Voltage and Phase Angle Tracked Using Dαβ PLL Under Unbalanced Fault

The Voltage and Phase angle tracked using Dαβ PLL under Unbalanced Fault are shown in Fig. 7.50.

From the above results it is found out that, the Dαβ PLL also efficiently tracks the phase even under unbalanced conditions.

The main difference between the DSRF PLL and Dαβ PLL is the peak overshoot that appears in the phase angle. The peak over shoot of DSRF PLL is more than that of the Dαβ PLL which is undesirable. The frequency response of two PLLs is shown in the Fig. 7.51.

Hence this PLL model has the better performance when compared to the other PLLs that are investigated under normal and unbalanced conditions.

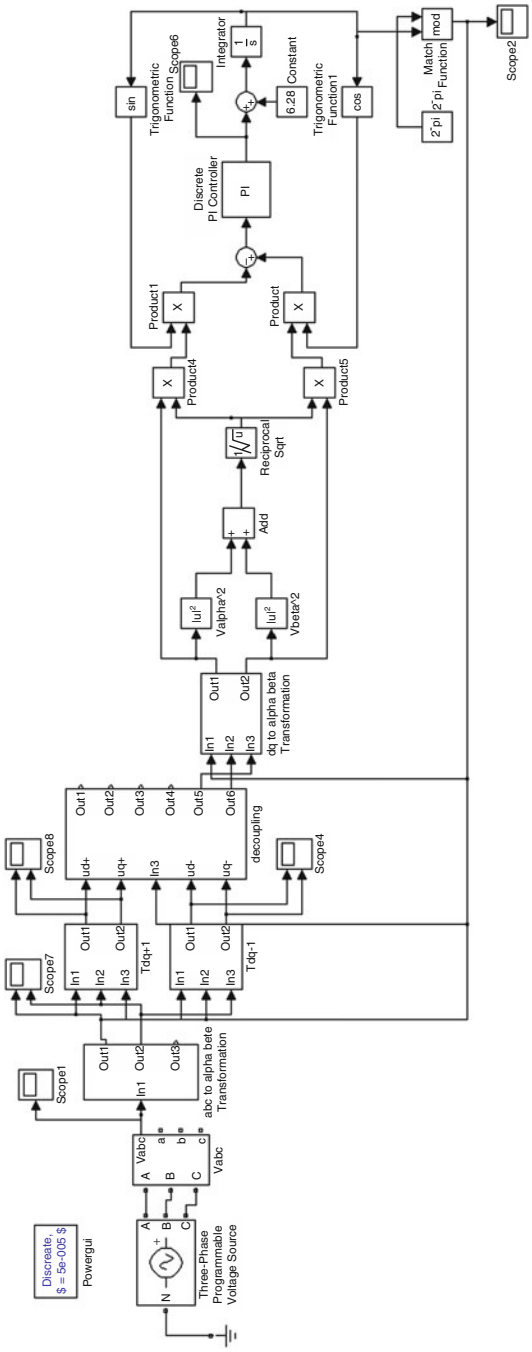


Fig. 7.47 SIMULINK model of a Dαβ PLL

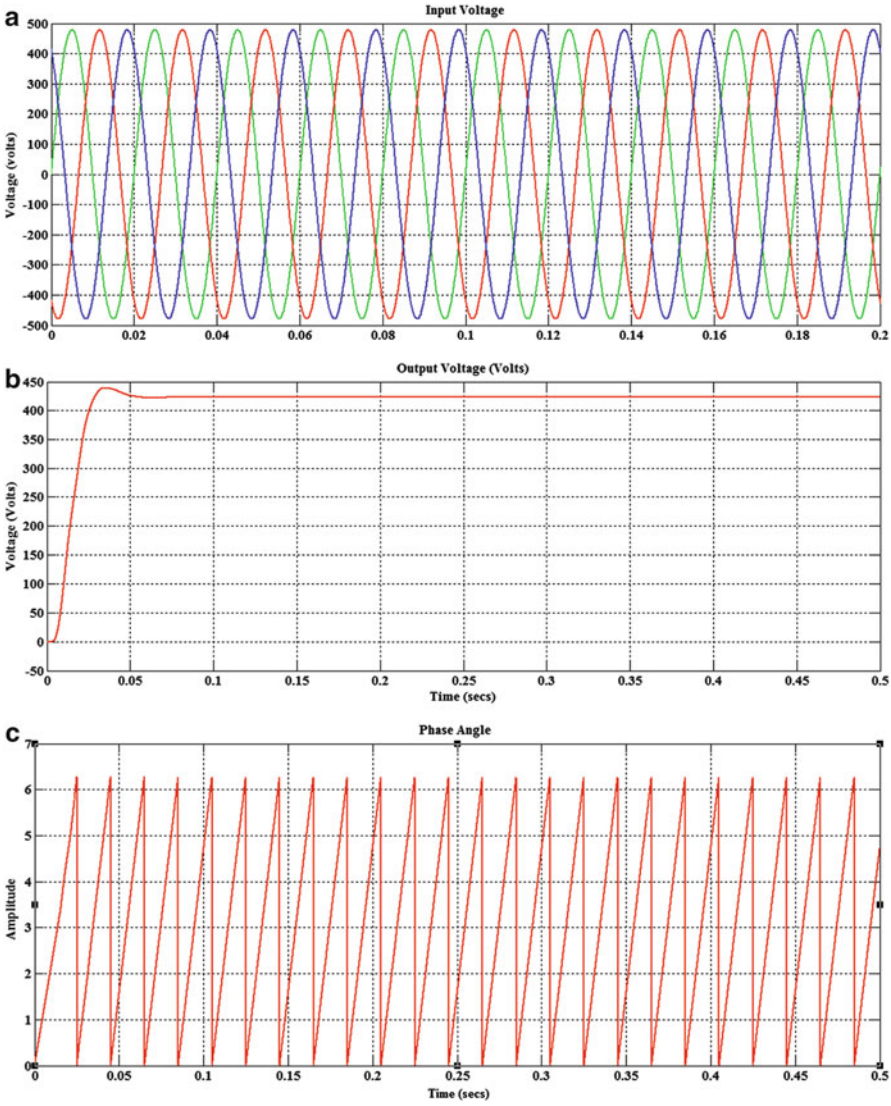


Fig. 7.48 Tracking by a Dαβ PLL – normal conditions (**a**) grid voltage (**b**) voltage (**c**) phase angle

7.6.9 SIMULINK Model of a Decoupled Double Synchronous Reference Frame PLL(DDSRF PLL)

The SIMULINK Model of a Decoupled Double Synchronous Reference Frame PLL(DDSRF PLL) is shown in Fig. 7.52. The tuning parameters of a PI controller are selected as kp = 2.2214 ki = 246.74 calculated using Ziegler-Nichols method.

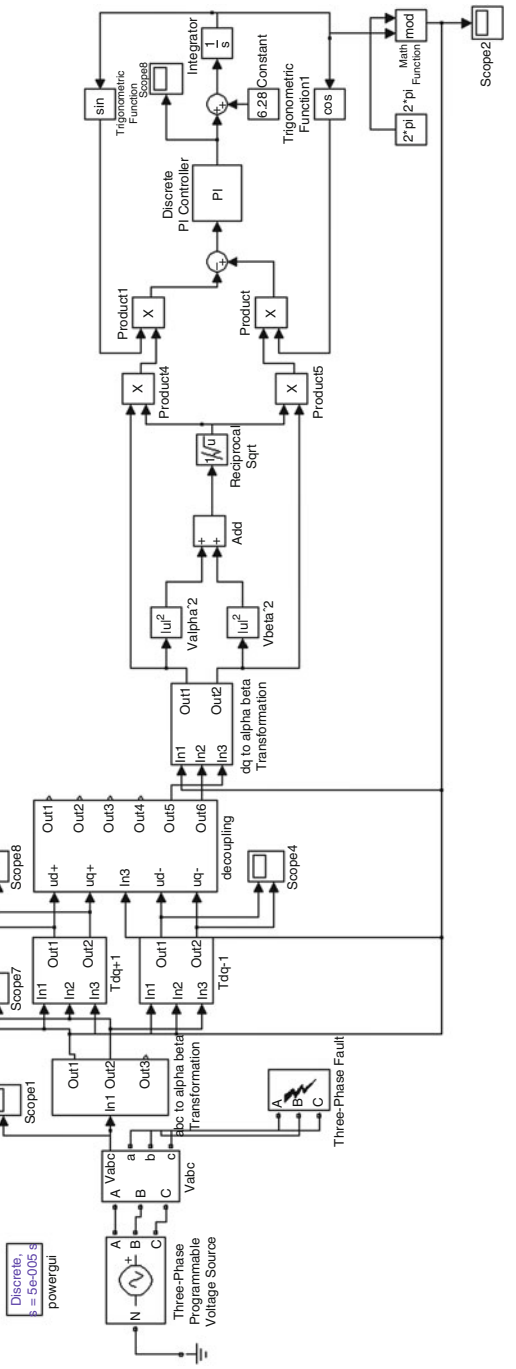


Fig. 7.49 SIMULINK model of a Dαβ PLL under unbalanced fault

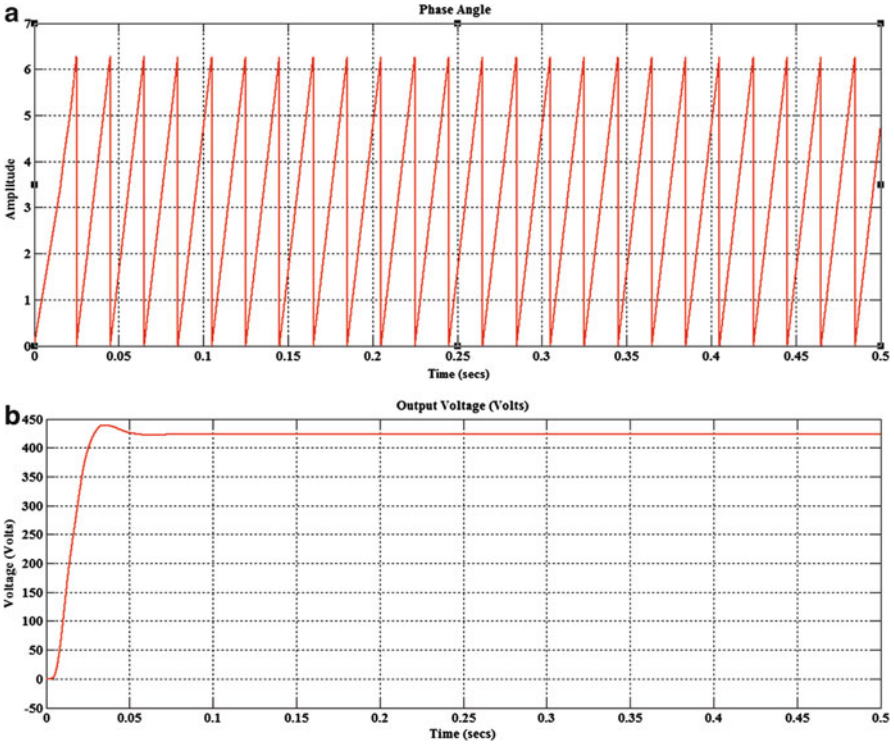


Fig. 7.50 Tracking by a Dαβ PLL -unbalanced fault (**a**) voltage (**b**) phase angle

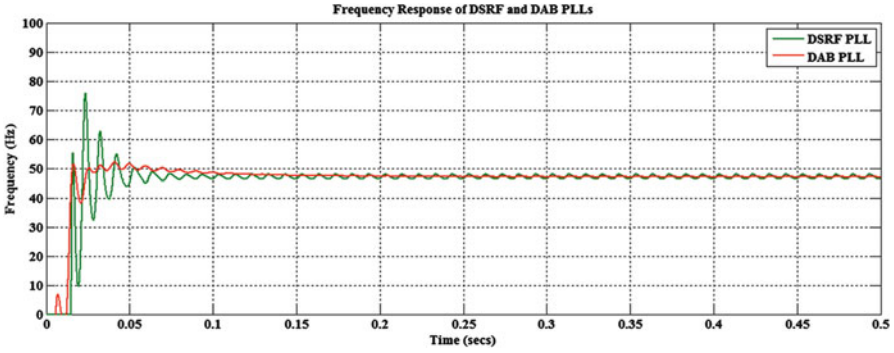


Fig. 7.51 Frequency response of DSRF and Dαβ PLLs

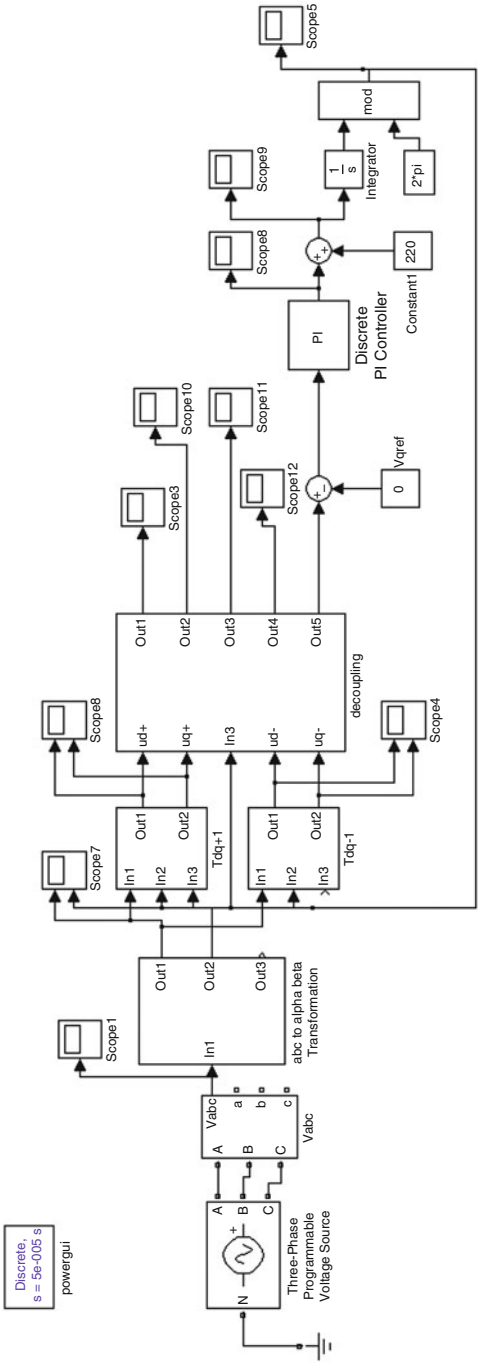


Fig. 7.52 SIMULINK model of a decoupled double synchronous reference frame PLL(DDSRF PLL)

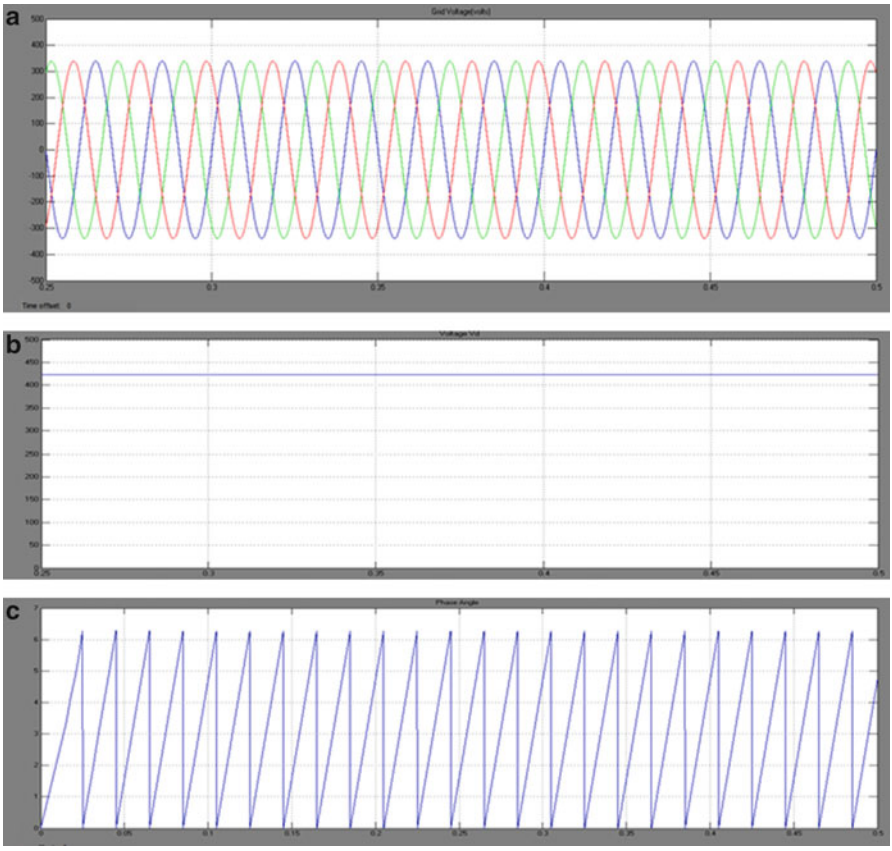


Fig. 7.53 (**a**) Grid voltage (**b**) voltage Vd and (**c**) phase angle tracked by DDSRF PLL

7.6.9.1 Voltage and Phase Angle Tracked by DDSRF PLL

The output voltage Vd is obtained as 423.3 v for an input voltage of 415 V is shown in Fig. 7.53.

7.6.10 SIMULINK Model of a DDSRF PLL During an Unbalanced Fault

The SIMULINK Model of a DDSRF PLL during an Unbalanced fault is shown in Fig. 7.54. Here an unbalanced fault is applied where there is a line to ground fault in two of the three phases.

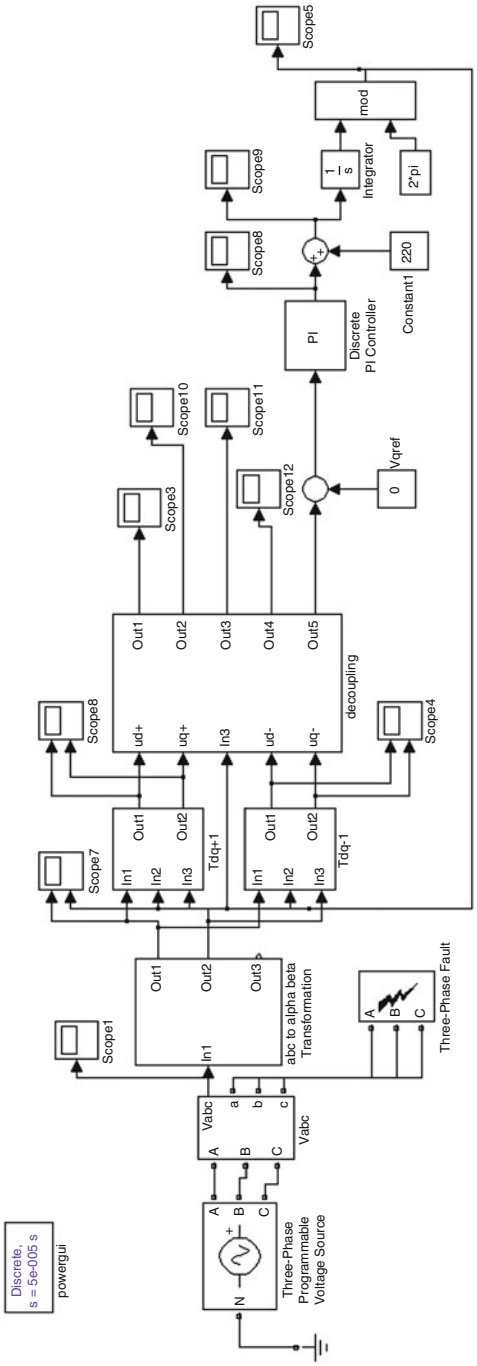


Fig. 7.54 SIMULINK model of a decoupled double synchronous reference frame PLL(DDSRF PLL) under an unbalanced fault

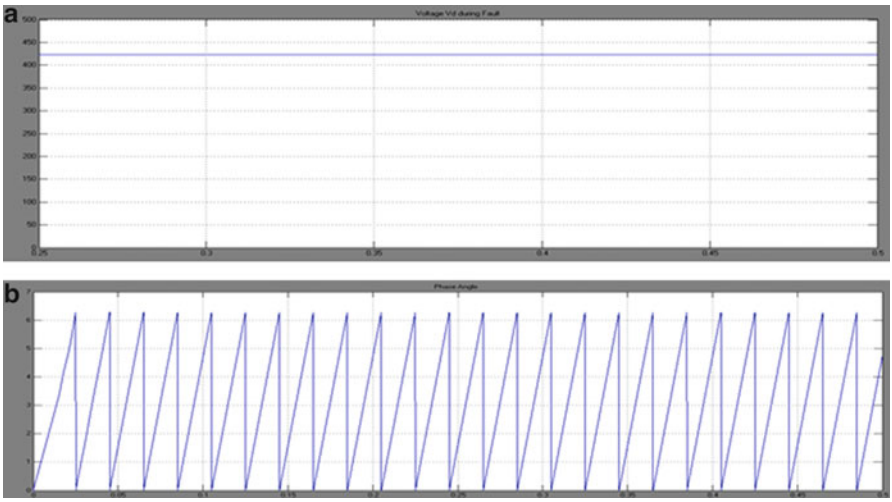


Fig. 7.55 (**a**) Voltage and (**b**) phase angle tracked by DDSRF PLL during an unbalanced fault

7.6.10.1 Voltage and Phase Angle Tracked by DDSRF PLL During an Unbalanced Fault

The Voltage and Phase Angle Tracked by DDSRF PLL during an unbalanced fault are shown in Fig. 7.55.

From the above results it is understood that when an unbalanced fault occurs, the DDSRF PLL operates as same as under normal condition. Therefore it has an improved result over the conventional SRF PLL which cannot track the phase angle under fault conditions. This is due to the decoupling of the positive and negative components present in the voltage and taking the positive component of the voltage as reference.

7.6.11 SIMULINK Diagram of Grid Synchronization of the Inverter Using the Hybrid Dαβ PLL

The hybrid Dαβ PLL is used to synchronize the inverter to grid using a current controller. The SIMULINK diagram is shown in Fig. 7.56. The current controller uses normal PI controller. To simulate the operation of the current control, a reference input active current Id whose amplitude is 2A is applied. Then followed by a reactive current reference component step Iq whose amplitude also is 2A. The simulated output inverter current of the inverter model is shown in Fig. 7.57. In this figure the output inverter current reaches its steady state value of 2A, which is exactly equal to the reference value. This proves that the current loop controller is

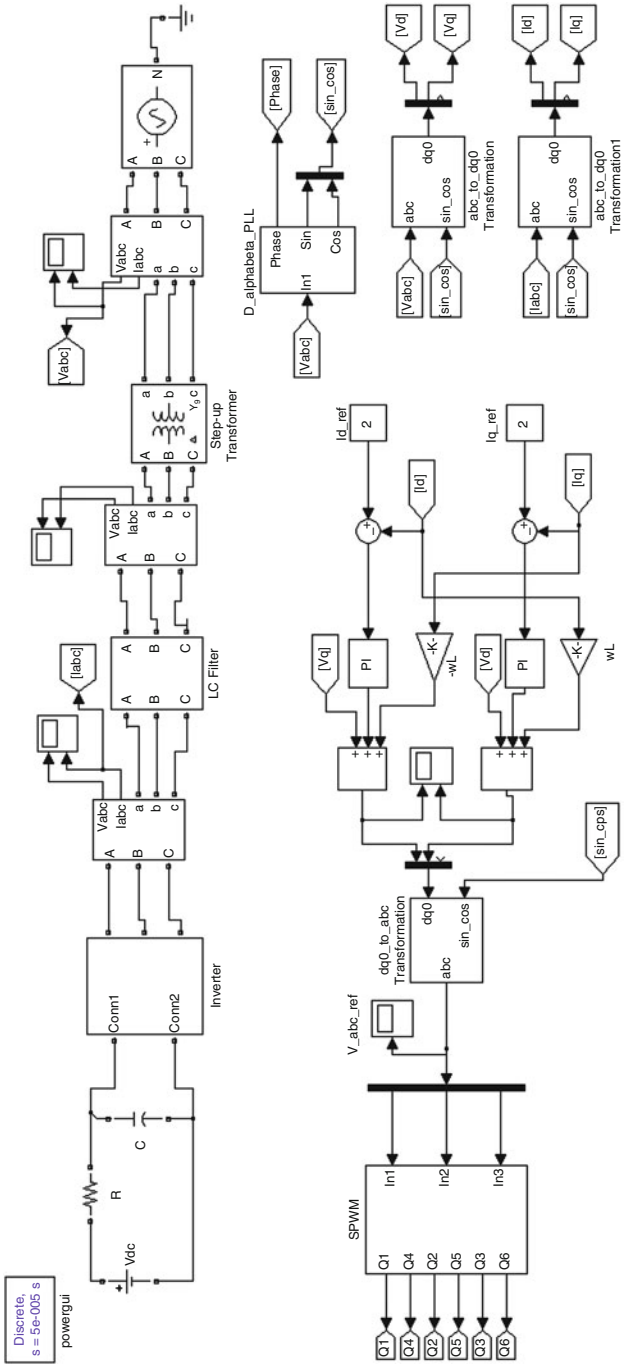


Fig. 7.56 Grid synchronization of the inverter using the hybrid PLL

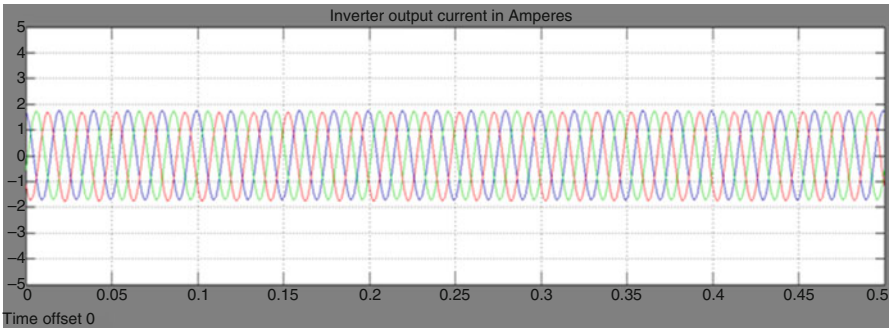


Fig. 7.57 Synchronized inverter output current in Amperes

effective such that measured currents track their references. In addition, its dynamic behavior is satisfactory.

The synchronized inverter output current is shown in Fig. 7.57. The current magnitude is almost near to that of the reference value 2A.

Thus, using the hybrid PLL the inverter is successfully synchronized to the grid.

7.6.12 SIMULINK Model of SRF PI Controlled Voltage Source Inverter

The SIMULINK model of the three phase grid connected inverter using a SRF PI controller is shown in Fig. 7.58. The above model consists of a SPWM inverter whose supply is assumed as a constant DC voltage (here 400 V). A LCL filter is connected at the output side of the inverter to attenuate the high frequency harmonics. Then the harmonic free current obtained from the inverter is given to the grid via step up transformer whose configuration is (delta-wye). A three phase programmable voltage source (available in Simpowersystems) is used as a three phase grid of 415 V. The Dαβ PLL is used to calculate the phase angle using the grid voltage.

The inverter output voltage and current is shown in Fig. 7.59.

7.6.13 SIMULINK Diagram of Grid Synchronization of the Inverter Using Cascaded Deadbeat and PI Controller

The SIMULINK model of the three phase Grid-connected inverter using a Deadbeat controller is shown in Fig. 7.60. The above model consists of a SPWM inverter whose supply is assumed as a constant DC voltage (here 400 V). A LCL filter is

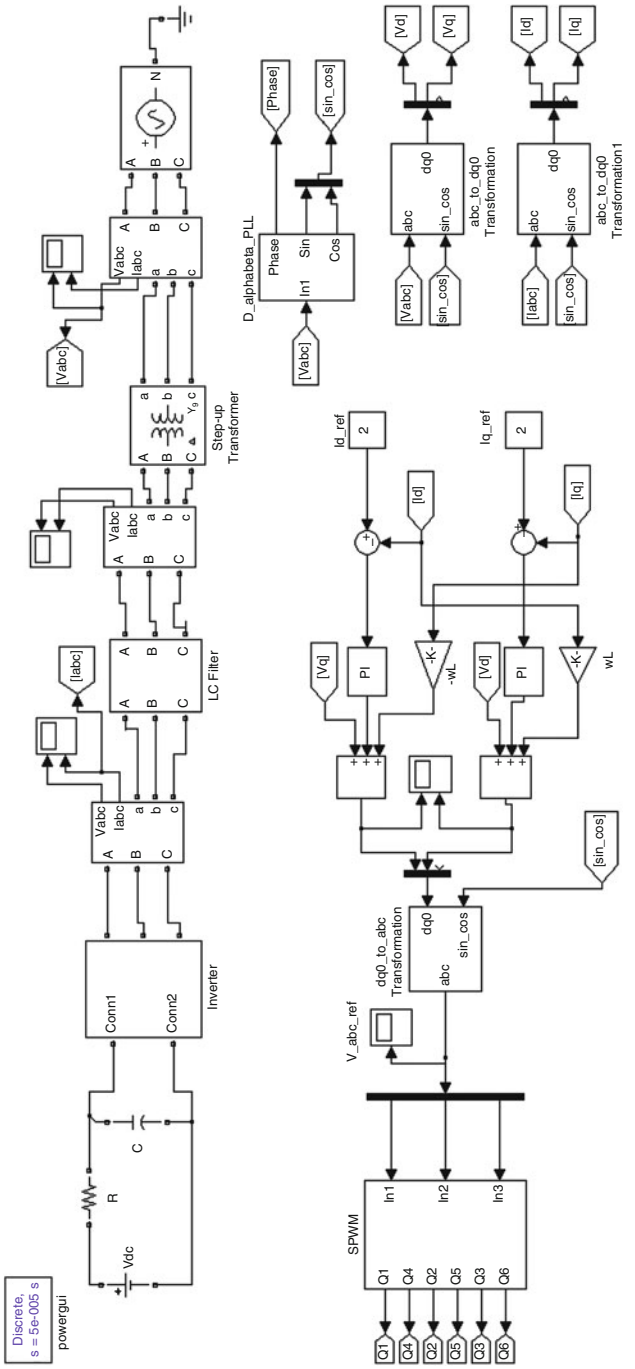


Fig. 7.58 SIMULINK diagram of a grid-connected inverter using SRF PI controller

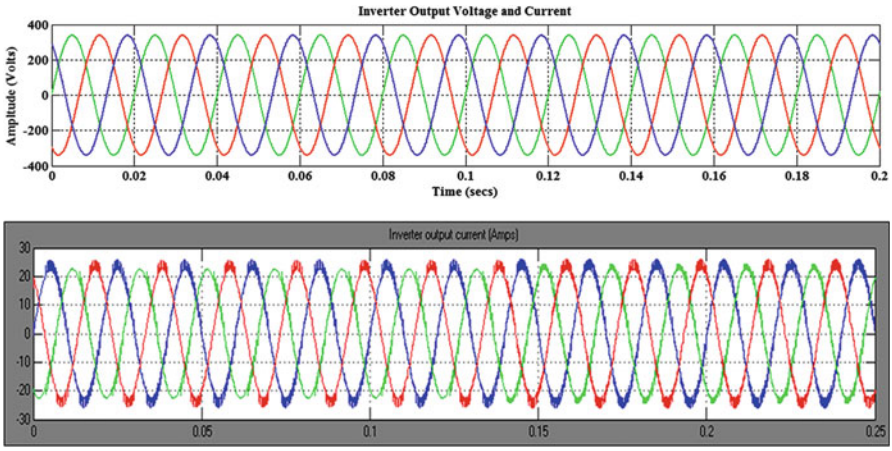


Fig. 7.59 Inverter output voltages and currents using SRF PI controller

connected at the output side of the inverter to attenuate the high frequency harmonics. Then the harmonic free current obtained from the inverter is given to the grid. A three phase programmable voltage source (available in Simpowersystems) is used as a three phase grid of 415 V. The Dαβ PLL is used to calculate the phase angle using the grid voltage and the plots are shown in Fig. 7.61.

7.6.14 Comparison of Current THD of SRF PI and Cascaded Deadbeat and PI Controllers

The THD Analysis of output inverter current of SRF PI controller is shown in Fig. 7.62. The THD is shown as 6.68 %.

The THD Analysis of output inverter current of the Deadbeat controller is shown in Fig. 7.63. The THD is shown as 0.02 %.

The above analysis shows that the cascaded Deadbeat and PI controller is more effective for integrating the inverter with the grid when compared to the SRF PI controller as the harmonics are almost negligible in the Cascaded Controller.

A benchmarking study of the effect of the time response on the overshoot of the estimated frequency and phase angle for three different PLLs is performed in this section. The investigation of dqPLL, αβPLL and ddsrfPLL motivates the proposal for a new PLL, which inherits the advantages of each PLL. The new hybrid dαβPLL is the most beneficial solution for grid synchronization compared to the other three PLLs under investigation, since it operates accurately under balanced and unbalanced conditions and also reduces the overshoot on the estimation of the phase angle and frequency, which is the main drawback of DDSRF PLL. The lower frequency overshoot of dαβPLL leads to a faster time response without any violation of the frequency limits of the grid codes. The hybrid dαβPLL could be

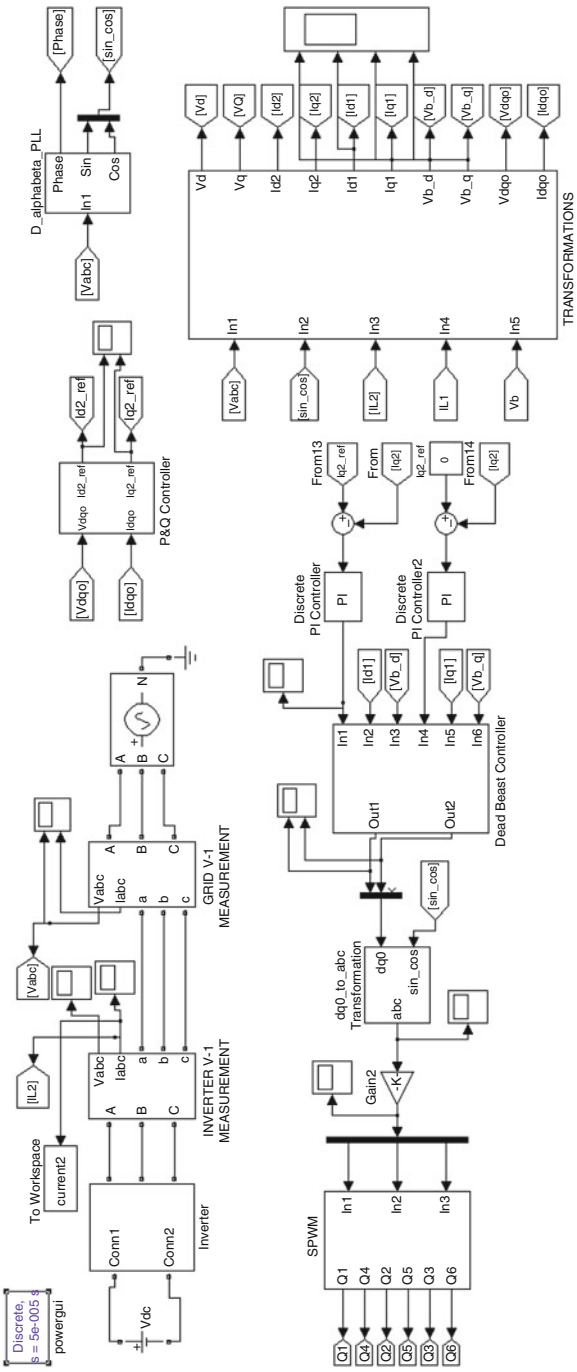


Fig. 7.60 SIMULINK diagram of a grid-connected inverter using cascaded deadbeat and PI controller

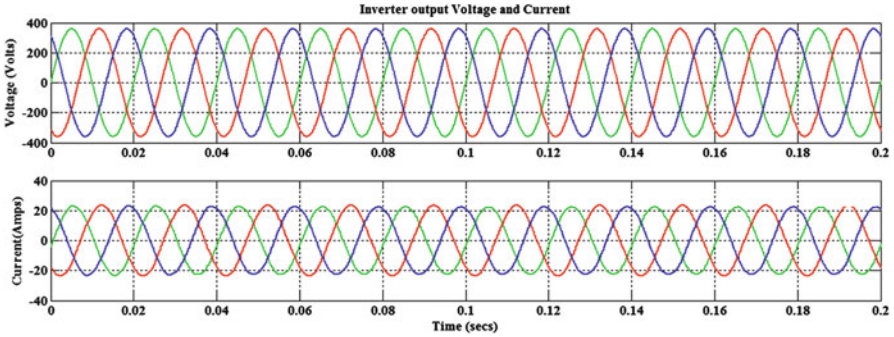


Fig. 7.61 Inverter output voltages and currents using cascaded deadbeat and PI controller

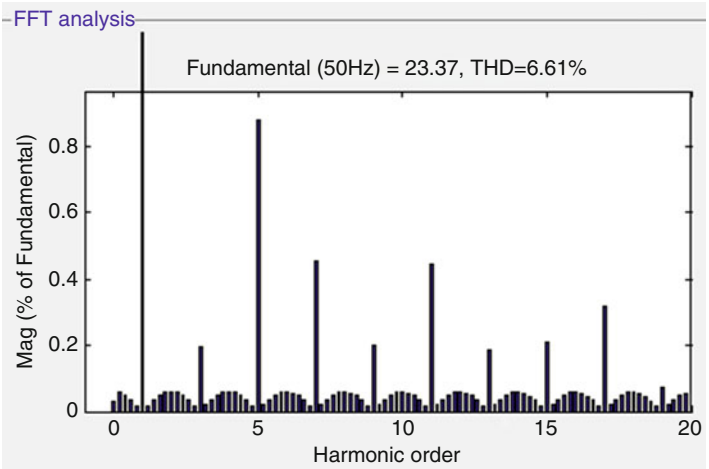


Fig. 7.62 THD analysis of SRF PI controller

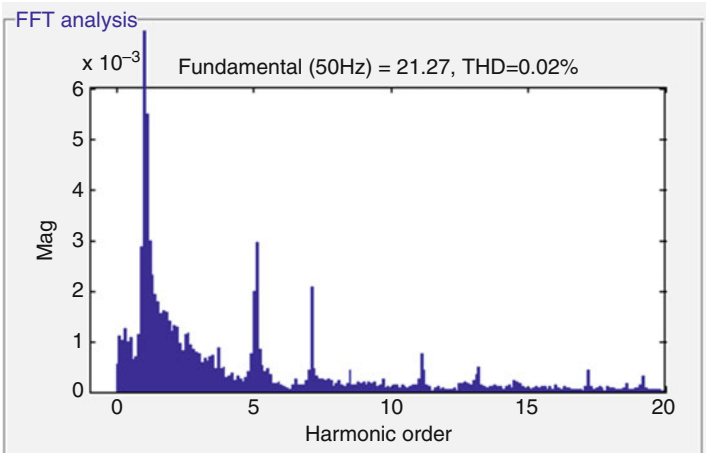


Fig. 7.63 THD analysis of cascaded deadbeat and PI controller

very useful in synchronizing the inverter to the grid. The performance of the dαβPLL in DGS is verified through results and its use is illustrated. Two control algorithms Synchronous PI control and Cascaded Dead-Beat and PI for the inverter-based DGS interface, in the Grid-connected and operation have been presented and compared in this project. The cascaded deadbeat and PI control algorithm is found appropriate to realize a robust DGS interface that guarantees stable and high power quality injection under the challenging uncertain nature of distribution systems. The Modeling and control of utility interactive inverters can be done more efficiently using the State of the art techniques that are available for Grid synchronization, anti-islanding control and current regulation. Control algorithms can be given in digital control format applicable to embedded control using digital signal processors.

7.7 Summary

Integration of renewable energy system to the grid and various problems and challenges that need to be addressed are discussed. Protection, voltage control and power quality are the major concerns related to the interconnection of the small scale renewable energy generation at the distribution level. Grid Issues in integrating renewable energy systems, converters used for grid integration techniques and its control strategy are discussed in this chapter. MATLAB/SIMULINK models of Synchronous Reference Frame PLL (dq PLL), Stationary Reference Frame PLL (αβ PLL), Decoupled Synchronous Reference Frame PLL (DSRF PLL), Decoupled Stationary Reference frame PLL (Dαβ PLL) and Hybrid Dαβ PLL are developed and the results are presented. Filters used for grid integration techniques and its control strategy is also explained in this chapter.

Review Questions

1. List the different types of interfacing technology used between renewable energy systems and grid unit.
2. What are the challenges involved in grid integration of renewable energy sources?
3. State the grid Interconnection standards.
4. Discuss the challenges imposed on an Inverter-Based DG Interface.
5. Mention the requirements for establishing a Grid Connection using PLL.
6. Discuss Grid Synchronization of Inverter Using Cascaded Deadbeat and PI Controller.
7. What are the advantages of using LCL filter in grid systems?
8. Mention the role of damping resistance in LCL filter.
9. Differentiate between SRF and DSRF PLL in Grid connected inverters.

Bibliography

Abella M, Chenlo F (2004) Choosing the right inverter for grid connected PV systems. Renew Energy World 7(2):132–147

Alepuz S, Busquets-Monge S, Bordonau J, Gago J, Gonzalez D, Balcells J (2006) Interfacing renewable energy sources to the utility grid using a three-level inverter. IEEE Trans Ind Electron 53:1504–1511

Basso TS, DeBlasio RD (2003) IEEE P1547-series of standards for interconnection. IEEE, New York

Bernal-Agustin J, Dufo-Lopez R (2005) Economical and environmental analysis of grid connected photovoltaic systems in Spain. Science Direct

Bryan J, Duke R, Round S (2003) Distributed generation – nanogrid transmission and control options. Int Power Eng Conf 1:341–346

Buso S, Malesani L, Mattavelli P (1998) Comparison of current control techniques for active filter applications. IEEE Trans Ind Electron 45(5):722–729

Cavalcanti MC, de Oliveira KC, Neves FAS, Azevedo GMS (2010) Modulation techniques to eliminate leakage currents in transformer less three-phase photovoltaic systems. IEEE Trans Ind Electron 57(4)

Chaudhari M, Frantzis L, Hoff TE (2004) PV grid connected market potential under a cost breakthrough scenario. Navigant Consulting, Sept 2004. http://www.ef.org/documents/EF-Final-Final2.pdf. Accessed June 2008

Chen Y-M, Liu Y-C, Lin S-H (2003) Double-input PWM DC/DC converter for high/low voltage sources. In: Proceedings of the IEEE international telecommunications energy conference, pp 27–32

Chen YM, Liu YC, Hung SC, Cheng CS (2007) Multi-input inverter grid-connected hybrid power system. IEEE Trans Power Electron 22:1070–1077

Dixon J, del Valle Y, Orchard M, Ortizar M, Moran L, Maffrand C (2003) A full compensating system for general loads based on a combination of thyristor binary compensator, and a PWM-IGBT active power filter. IEEE Trans Ind Electron 18(4):982–989

Dursun E, Kilic O (2012) Comparative evaluation of different power management strategies of a stand- alone PV/Wind/PEMFC hybrid power system. Electr Power Energy Syst 34:81–89, Elsevier

Gounden NA, Peter SA, Nallandula H, Krithiga S (2009) Fuzzy logic controller with MPPT using line-communicated inverter for three-phase grid-connected photovoltaic systems. Renew Energy 34:909–915

Grid-connected photovoltaic power systems: survey of inverter and related protection equipments, Task V, Report IEA PVPS T5-05: 2002

Hudson RM, Behnke MR, West R, Gonzalez S, Ginn J (2002) Design considerations for three-phase grid connected photovoltaic inverters. IEEE

IEC 61000-3-6:1996 Electromagnetic compatibility (EMC) – Part 3: Limits – Section 6: Assessment of emission limits for distorting loads in MV and HV power systems. Basic EMC publication

IEEE recommended practice for utility interface of photovoltaic system, IEEE Std. 929–2000

Jain S, Agarwal V (2008) An integrated hybrid power supply for distributed generation applications fed by nonconventional energy sources. IEEE Trans Energy Convers 23:622–631

Jeyraj S, Nasrudin AR (2009) Multilevel inverter for grid-connected PV system employing digital PI controller. IEEE Trans Ind Electron 56:149–158

Jiang Z (2006) Agent-based control framework for distributed energy resources micro grids. In: Proceedings of the IEEE International conference on intelligent agent technology, pp 646–652

Kalantar M, Mousavi SMG (2010) Dynamic behaviour of a stand-alone hybrid power generation system of wind turbine microturbine, solar array and battery storage. Appl Energy 87:3051–3064, Elsevier

Kawabata T, Miyashita T, Yamamoto Y (1990) Dead beat control of three phase PWM inverter. IEEE Trans Power Electron 5(1):21–28

Kazmierkowski MP, Malesani L (1998) Current control techniques for three-phase voltage-source PWM converters: a survey. IEEE Trans Ind Electron 45(5):691–703

Kern EC, Gulachenski EM, Kern GA (1989) Cloud effects on distributed photovoltaic generation: slow transients at the Gardner, Massachusetts photovoltaic experiment. IEEE Trans Energy Convers 4(2):184–190

Kjaer SB, Pedersen JK, Blaabjerg F (2005) A review of single-phase grid-connected inverters for photovoltaic modules. IEEE Trans Indus Appl 41(5):1292–1306

Kouro S, Bernal R, Miranda H, Silva CA, Rodriguez J (2007) High-performance torque and flux control for multilevel inverter fed induction motors. IEEE Trans Power Electron 22(6):2116–2123

Lara OA, Acha E (2002) Modelling and analysis of custom power systems by PSCAD/EMTDC. IEEE Trans Power Deliv 17(1):266–272

Leyva-Ramos J, Morales-Saldana JA (1998) A design criteria for the current gain in current programmed regulators. IEEE Trans Ind Electron 45(4):568–573

Pairodamonchai P, Sangwongwanich S (2009) Design and implementation of a hybrid output EMI filter for high frequency common-mode voltage compensation in PWM inverters. IEEE Trans Ind Appl 45(5):1647–1659

Pasterczyk RJ, Guichon JM, Schanen JL, Atienza E (2009) PWM inverter output filter cost-to-losses tradeoff and optimal design. IEEE Trans Ind Appl 45(2):887–897

Prodanovic M, Green TC (2003) Control and filter design of three-phase inverters for high power quality grid connection. IEEE Trans Power Electron 18(1):373–380

Rashid MH (2006) Power electronics devices, circuits and applications. Academic Press, San Diego

Saha S, Sundarsingh VP (1996) Novel grid-connected photovoltaic inverter. Proc Inst Elect Eng 143(2):143–156

Schekulin D (1999) Grid-connected photovoltaic system. Germany Patent DE197 32218 Cl; Mar 1999

Shathiand B, Natatajan SP (2009) Comparative study on various unipolar PWM strategies for single phase five level cascaded inverter. Int J Power Electron 2(1):36–50

Teodorescu R, Blaabjerg F, Pedersen JK, Cengelci E, Enjeti PN (2002) Multilevel inverter by cascaded industrial VSI. IEEE Trans Ind Electron 49(4):832–834

Thongprasri P (2011) A 5-level three-phase cascaded hybrid multilevel inverter. Int J Comput Electr Eng 3(6):789–794

Twining E, Holmes DG (2003) Grid current regulation of a three-phase voltage source inverter with an LCL input filter. IEEE Trans Power Electron 18(3):888–895

Wall CR, Performance of inverter interface distributed generation. IEEE Paper, 2001

Wood J, Wollenberg BF (1996) Power generation operation an control, 2nd edn. Wiley, New York

Xue Y, Chang L (2004) Closed-loop SPWM control for grid-connected buck–boost inverters. Proc IEEE PESC 5:3366–3371

Xue Y, Chang L, Kjaer S, Bordonau J, Shiminizu T (2004) Topologies of single-phase inverters for small distributed power generators: an overview. IEEE Trans Power Electron 19(5):1305–1314

Yaleinkaya G (1999) Characterization of voltage sags in industrial distribution systems. IEEE Trans Ind Appl 12(3)

Yi Wang, Heming Li, Xinchun Shi, Boqiang Xu (2004) A novel carrier-based PWM strategy for hybrid multilevel inverter. In: 35th annual IEEE power electronics specialists conference, ISSN: 0-7803-8399-0/04, pp 4233–4237

Youb L, Craciunescu A (2009) Direct torque control of induction motors with fuzzy minimization torque ripple. Proc WESCO 2:713–717

Youssef O, Kamal A-H, Luc AG (2011) Packed U cells multilevel converter topology: theoretical study and experimental validation. IEEE Trans Ind Electron 58:1294–1306

Yuan X, Zhang Y (2006) Status and opportunities of photovoltaic inverters in grid-tied and micro-grid systems. IEEE

Zeng Q, Chang L (2008) An advanced SVPWM-based predictive current controller for three-phase inverters in distributed generation systems. IEEE Trans Ind Electron 55(3):1235–1246

Zhang J, Zon Y, Zhang X, Ding K (2003) Study on a modified multilevel cascade inverter with hybrid modulation. IEEE Power Electronics Drives System, ISSN: 0-7803-7233-6/01, pp 379–383

Zhi Na, Zhang Hui, Xing Xiaowen (2013) Power control of DC micro grid with variable generation and energy storage. Int J Autom Power Eng 2(4)

Zmood DN, Holmes DG, Bode GH (2001) Frequency-domain analysis of three-phase linear current regulators. IEEE Trans Ind Appl 37(2):601–610

Chapter 8
Harmonic Reduction Techniques in Renewable Energy Systems

Learning Objectives
On completion of this chapter, the reader will have knowledge on:

- Basic concepts of harmonics and power quality issues.
- Reactive power compensation using custom power devices such as DSTATCOM, DVR and UPQC.
- Power quality problems and standards associated with power quality issues.
- Procedure for measurement of power quality in PV system.
- Harmonic reduction in Wind Energy Conversion Systems with power quality issues and a case study.

8.1 Introduction

During recent years, power system harmonics is a vital area which is seeking a great deal of attention. The reason behind this is mainly due to the non-linear (or maybe harmonic causing) loads. These loads consistently increase a portion on the total load for the typical industrial place. Such kind of an increase in load has provoked more strict recommendations in the IEEE Std. 519 and strict limits imposed by utilities. Incidence of harmonic related complications is low, merely awareness of harmonic issues cannot help to increase the reliability of power systems. The harmonics causes problems on occasions either due to the power system resonance or due to the magnitude of the harmonics produced.

Harmonics can be defined as a mathematical representation of distortion in a voltage or current waveform. More precisely, the term harmonic refers to a section of a waveform that occurs at an integer multiples of the fundamental frequency. Based on Fourier analysis, it is noted that any repetitive waveform can be represented as summing sinusoidal waves which in turn are integer multiples of

© Springer International Publishing Switzerland 2015

S. Sumathi et al., *Solar PV and Wind Energy Conversion Systems*,
Green Energy and Technology, DOI 10.1007/978-3-319-14941-7_8

the fundamental frequency. The Fourier series of a steady state waveform with equal positive and negative half-cycles can be represented according to Eq. 8.1,

$$f(t) = \sum_{n=1}^{\infty} A_n \sin\left(n \prod t/T\right) \tag{8.1}$$

where

f(t) is the time domain function.
n is the harmonic number (only odd values of n are required)
A_n is the amplitude of the nth harmonic component
T is the length of one cycle in seconds

In general harmonics should not be mistaken with spikes, dips, impulses, oscillations or other forms of transients. The important feature to be understood while dealing with harmonics is that harmonics are steady state event and they are repetitive in every cycle of 50 Hz. The terms Total Harmonic Distortion (THD) used in close relation with the harmonic theory is used to compute the voltage or current distortion according to Eq. 8.2,

$$THD(\%) = \sqrt{ID_1^2 + ID_2^2 + \ldots\ldots + ID_n^2} \tag{8.2}$$

where ID_n is the magnitude of the nth harmonic as a percentage of the fundamental.

Harmonics are mainly produced due to non-linear loads. The non-linear loads draw non-sinusoidal current from a sinusoidal voltage source. Loads such as electric arc furnaces, static VAR compensators, inverters, DC converters, switch-mode power supplies, and AC or DC motor drives are examples that cause harmonics. While using a motor drive, the AC current at the input to the rectifier looks more like a square wave than a sine wave as shown in Fig. 8.1.

Though power system problems based on harmonics are occasional, it is quite possible for a number of undesirable effects to occur. High degrees of harmonic distortion can cause effects as increased transformer heating, capacitor heating, motor or generator heating, malfunctioning of electronic equipment, error readings on meters, malfunctioning of protective relays, interference with telephone circuits, etc. The likelihood of such harmful effects occurring is greatly increased if the resonant condition occurs. Resonance occurs if a harmonic frequency produced by a non-linear load closely coincides using a grid natural frequency.

Power Quality (PQ) issues are of vital concern in most industries today because of the increased usage of sensitive and critical equipments such as communication networks, process industries, precise manufacturing processes and non-linear variable frequency drives. Power quality measurement and assessment was done as a case study on different solar PV generation systems such as 100, 80, and 60 kW located at PSG College of Technology. The analysis was carried out with the help of FLUKE 434 series II Energy analyzer reported as class-S meter according to IEC/IEEE standards. It was observed from the case study that power quality

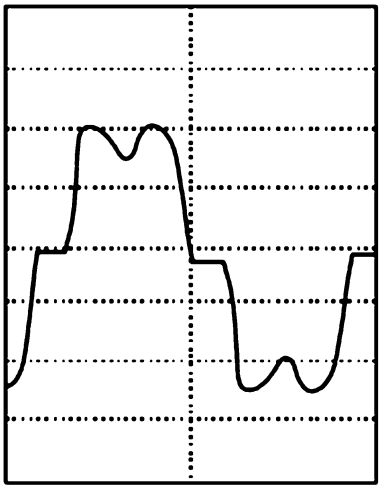


Fig. 8.1 Rectifier output

problems such as reactive power, 10 % sag/swell for duration of $\leq$1,000 μs, and 4 % of VTHD, 10 % ITHD in which 3rd, 5th and 7th harmonics are dominating and existing in system when connected to the load. To compensate these power quality problems, technologies like custom power devices have emerged. These are series-connected compensators known as Dynamic Voltage Restorer (DVR), shunt connected compensators such as Distribution STATic COMpensator (DSTATCOM) and a combination of series and shunt connected compensators known as Unified Power Quality Conditioner (UPQC).

In this chapter, the techniques for correcting the supply voltage sag/swell, harmonics and reactive power compensation in a distribution system by custom power devices such as DSTATCOM, DVR and UPQC are discussed. The custom power devices meet the power quality standards such as IEEE 519-1992 and IEC 61000-3-2/IEC 61000-3-4. A phase shift controlled voltage source converter based DSTATCOM has been implemented in the MATLAB/SIMULINK R2011a environment. DVR modeling, analysis and simulation has been done in MATLAB/SIMULINK environment to regulate voltage sag/swell, harmonics in supply voltage. The UPQC system is modeled using the elements of SIMULINK and it is simulated using MATLAB.

8.2 Power Quality Issues

Power quality issues are of vital concern generally in most industries today, due to surge in the quantity of loads sensitive to power disturbances. The electricity quality is usually an index to quality of current and voltage offered to industrial, commercial and household consumers of electricity. The condition regards both utilities and customers. With the utilities, to offer adequate power quality is really a

moving objective because of changes in user equipment as well as. For consumers, problems stemming on the sensitivity of electrical equipment to voltage quality have often very heavy consequences.

Power quality is usually a topic embracing a substantial field. On one side, several different events are going to complete power quality: spikes or surges, sags, swells, outages, under or higher voltages, harmonics, flicker, frequency deviations, and electrical noise. Accordingly, different measurements and analysis tools must investigate such phenomena, and various remedial actions could be adopted to pay them or reduce their effects. On the other side, many electronic devices (such as computers, process controls, adjustable speed drives, solid-state-relays, optical devices, to name a few) are sensitive to another touch power quality. Since a certain event may not be a serious issue for any given customer class, nevertheless it may represent a big problem for another class, it offers doubtful practical sense to rank the above mentioned events when it comes to importance without talking about an increasingly specific context. As far as industrial and commercial customers are involved, several recent studies acknowledge the statement that voltage sags has to be regarded as the most important concerns in power quality. This statement is especially true for producers, where even short duration voltage sags will often be accountable for a lot more long-lasting production downtimes and consequent large lost revenue. It is difficult to place a value about the impact of power quality problems, but it's reliable advice that unscheduled shutdowns could cost of countless rupees. Combined with tangible expense of lost production time (and therefore sales), wasted raw materials and damaged equipment, in addition there are indirect costs, for instance damaged to customer confidence brought on by missed delivery schedules.

Many times a custom power device offers probably the most economical solution by establishing the proper power quality level that is needed through the customer. Often this type of device would negate the necessity for the utility to set up additional feeders or substations or customer to run individual power conditioners on the load level. IEEE Standard 1100-1992 (IEEE Emerald Book) defines sag as "an rms cut in the AC voltage, with the power frequency, for durations from a half-cycle to some seconds". Note: The IEC terminology for sag is dip. They usually are followed by phase jumps. When the voltage is reduced to zero, the disturbance is said to be a momentary outage or micro interruption. Eat way to characterize a voltage sag was in the reduced voltage rms, duration and in all probability accompanied phase jump. The European Standard (EN50160-1994) defines adequately regarding the sags and it is indicative values; Voltage dips (sags) usually are due to faults occurring within the customers' installations on in the public distribution system. They're unpredictable, largely random events. The annular frequency varies depending on the sort of the provision systems additionally, on the point of observation. Moreover, the distribution over the year can be extremely irregular.

Voltage sags are sometimes generated by starting of large loads, like motors, transformer energizing, equipment faults, transmission and distribution system faults. Faults for the distribution and transmission systems can be due to numerous

sources like lightning strikes, conductors blowing together within a storm, experience of objects (e.g. tree branches, animals) or vandalism. These faults (70–80 %) are temporary as the name indicated; they're self-clearing in a few milliseconds. The fault which does not clear will result in a protective device/s (e.g. fuse, breaker, or recloser) to use it to get rid of current area of the system within the affected region.

8.3 Sources and Effects of Power Quality Problems

Power distribution systems, ideally, must provide their clients by having an uninterrupted flow of smooth sinusoidal voltage in the contracted magnitude level and frequency However, in practice, power systems, specially the distribution systems, have numerous nonlinear loads, which significantly affect the standard of power supplies. Caused by the nonlinear loads, the purity in the waveform of supplies is lost. This ultimately ends up producing many power quality problems.

While power disturbances occur on all electrical systems, the sensitivity nowdays sophisticated gadgets brings about weaker on the quality of power supply. For most sensitive devices, a momentary disturbance can cause scrambled data, interrupted communications, a frozen mouse, system crashes and equipment failure etc. An electric voltage spike damages valuable components. Power quality problems encompass a variety of disturbances such as voltage sags/swells, flicker, harmonics distortion, impulse transient, and interruptions, plus the definitions are listed below:

- Voltage dip: The short-term decrease in voltage of less than half a second is known as voltage dip.
- Voltage sag: The amplitudes of voltage sags occurring at any instant of time ranges from 10 % to 90 % and lasts for half a cycle to one minute.
- Voltage swell: An increase in rms voltage or current at the power frequency for durations from 0.5 cycles to 1 min is known as voltage swell.
- Voltage 'spikes', 'impulses' or 'surges': These are terms used to describe abrupt, very brief increases in voltage value.
- Voltage transients: They are temporary, undesirable voltages that appear on the power supply line. Transients are high over-voltage disturbances (up to 20 KV) that last for a very short time.
- Harmonics: The fundamental frequency of the AC electric power distribution system is 50 Hz. A harmonic frequency is any sinusoidal frequency, which is a multiple of the fundamental frequency. Harmonic frequencies can be even or odd multiples of the sinusoidal fundamental frequency.
- Flicker: Visual irritation and introduction of many harmonic components in the supply power and their associated ill effects.

Causes of Dips, Swell, Harmonics, Flicker, and Surges

(i) Rural location remote from power source.
(ii) Unbalanced load on a three phase system.
(iii) Switching of heavy loads.
(iv) Long distance from a distribution transformer with interposed loads.
(v) Unreliable grid systems.
(vi) Equipments not suitable for local supply.

Causes of Transients and Spikes

(i) Lightening.
(ii) Arc Welding.
(iii) Switching on reactive equipments such as motors, transformers, Variable Frequency Drives (VFDs).

8.4 Standards Associated with Power Quality

Standards regarding voltage sags are intended to be utilized for reference documents describing single components and systems in a power grid. The manufacturers as well as the buyers are using these standards to fulfill better power quality requirements. Manufacturers develop products meeting the needs of any standard, and buyers demand from your manufactures which the product stick to the standard. The most prevalent standards managing power quality are the types issued by Institute of Electrical and Electronics Engineers (IEEE), International Electro Chemical (IEC), Computer Business Equipment Manufacturing Association (CBEMA) and Semiconductor Equipment and Materials International (SEMI).

8.4.1 IEEE Standards

The Technical Committees in the IEEE societies along with the standards coordinating committees of IEEE standards board develop IEEE standards. The IEEE standards related to voltage sags are given below.

IEEE 446-1995, "IEEE recommended practice for emergency and standby power systems for industrial and commercial applications selection of sensibility loads." The standard discusses the effects of voltage sags on sensitive equipment. The principles and examples regarding how systems should be built to avoid voltage sags as well as other power quality problems when backup system operates.

IEEE 493-1990, "Recommended practice to the design of reliable industrial and commercial power systems." The normal proposes different techniques to predict voltage sag characteristics, magnitude, duration and frequency. You can find mainly three areas of interest for voltage sags. The several areas can be summarized the following:

(i) Calculating voltage sag magnitude by calculating voltage drop at critical load with expertise in the network impedance, fault impedance as well as placement of fault.
(ii) By studying protection equipment and fault clearing time it is achievable to estimate the duration of the voltage sag.
(iii) Dependant on reliable data to the neighborhood and knowledge of the system parameters an estimation of frequency of occurrence can be achieved.

IEEE 1100-1999, "IEEE recommended practice for powering and grounding Electronic equipment." This standard presents different monitoring criteria for voltage sags possesses a chapter explaining the fundamentals of voltage sags. It also explains the setting and putting on the CBEMA and I . t . Industry Council (ITIC) curves. It can be in some parts nearly the same as Std. 1159 but not as specific in defining various kinds of disturbances.

IEEE 1159-1995, "IEEE recommended practice for monitoring electrical energy quality." The aim of this standard is always to describe how you can interpret and monitor electromagnetic phenomena properly. It offers unique definitions for each kind of disturbance.

IEEE 1250-1995, "IEEE guide for service to equipment understanding of momentary voltage disturbances." This standard describes the effect of voltage sags on computers and sensitive equipment using solid-state power conversion. The key purpose would be to help identify potential problems. What's more, it aims to suggest techniques for voltage sag sensitive devices to operate safely during disturbances. It tries to categorize the voltage-related conditions that could be fixed from the utility and the ones that have for being addressed by the user or equipment designer. Second goal is usually to help designers of equipment to higher understand the planet by which their devices will operate. The typical explains different reasons behind sags, lists of examples of sensitive loads, and offers solutions to the problems.

8.4.2 SEMI International Standards

The SEMI international standards program is usually a service made available from Semiconductor Equipment and Materials Overseas (SEMI). Its purpose is always to supply the semiconductor and flat panel display industries with standards and advice to boost productivity and business. SEMI criteria are written documents as specifications, guides, test methods, lingo, and practices. The standards are usually voluntary technical agreements between apparatus manufacturer and end-user.

The actual standards ensure compatibility and interoperability of products and services. Considering voltage sags, two standards address the challenge to the equipment. SEMI F47-0200, "Specs for semiconductor processing equipment current sag immunity." The typical addresses specifications for semiconductor producing equipment voltage sag immunity. That only specifies voltage sags together

with duration from 50 ms approximately 1 s. It is usually limited by phase-to-phase and cycle-to-neutral voltage incidents, in addition to presents a voltage-duration graph, "Test method for semiconductor processing equipment voltage drop immunity."

This standard defines the test methodology employed to determine the susceptibility of semiconductor processing equipment and ways to qualify it from the specifications. It further describes test apparatus, test set-up, analyze procedure to look for the susceptibility of semiconductor processing equipment, and ultimately tips on how to report the results.

8.5 Measurement of Power Quality in Solar PV Systems

This section provides a discussion about the system under study, various measurement procedure involved in power quality monitoring, and PQ assessment techniques used in this work. The results of the case study performed on the system are given in Appendix IV. The power quality studies on different solar Photovoltaic (PV) systems have been done using FLUKE power analyzer referred in Appendix IV. Case Study-I: The case study done in 100 kW Solar PV system at PSG College of Technology K-block referred in Appendix IV. Case Study-II: The case study done in 100 kW Solar PV system at PSG College of Technology K-block load side referred in Appendix IV. Case Study-III: The power quality measurements done in 200 kW at Sarvajana Higher Secondary School, Peelamedu referred in Appendix IV.

8.5.1 System Description

In 100 kW Photovoltaic (PV) system each 20 kW is interfaced to a distribution system through parallel connection of 10 kHz PWM three phase inverter, a 750 μH three phase ac choke, a Δ-Δ (374–480) V, 250 kVA three phase isolation transformer, approximately 300 ft underground cable, and a grounded 11 kV-470 V, 500 kVA step-up transformer. The PWM inverter is an SMA Sunny Tripower of STP 20000TLEE-10 series specially designed for PV power conversion applications.

In Fig. 8.2 the single line diagram for Solar PV power system has been described. The 100 kW solar PV system is Connected to load through 10 kHz inverter. The grid power is synchronized with the Solar PV power generated with the help of synchronizing bus and fed to the load through an isolator switch. The Block diagram of solar PV generation system in PSG Tech, Coimbatore is shown in Fig. 8.3.

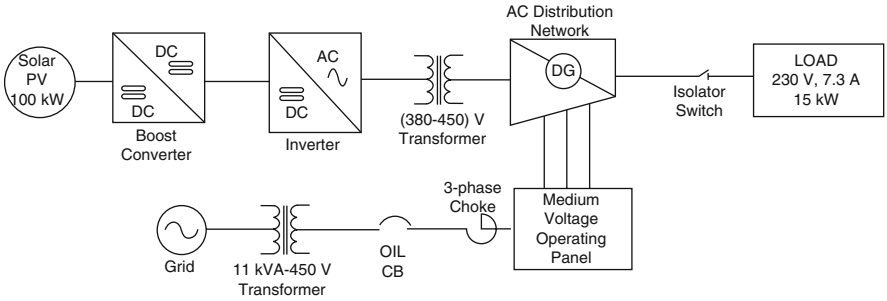


Fig. 8.2 Single line diagram of PSG Tech. power system

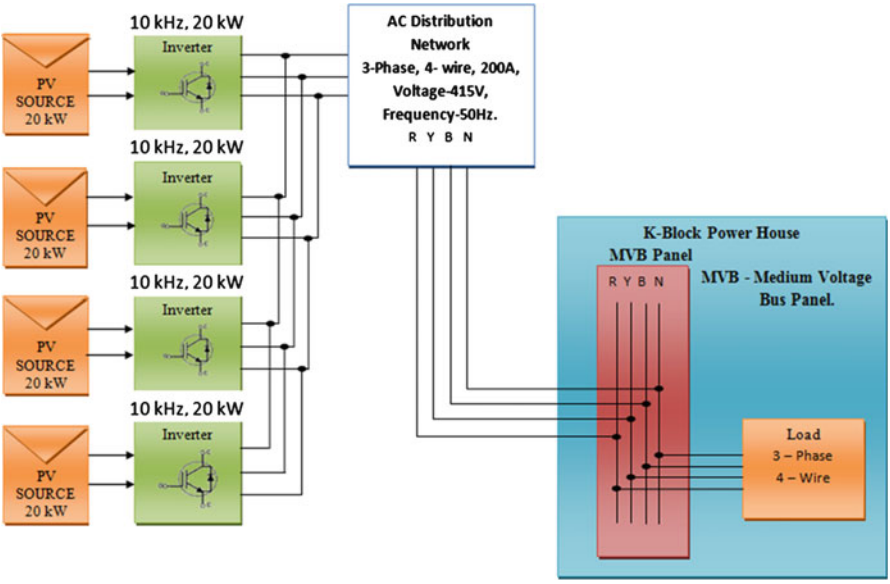


Fig. 8.3 Block diagram of solar PV generation system in PSG Tech, Coimbatore

8.5.2 Measurement Procedure for Power Quality in PV System

The actual measurement procedure includes test conditions, characteristics of the measurement equipment, and Power Quality (PQ) measurements. Test source conditions for small PV systems should agree with IEC 61000-3-2/12 and IEC 61000-3-3/11. Network conditions for large PV systems should be in accordance with IEC 61400-21.

Thus, the main requirements at Point of Common Coupling (PCC) when the PV unit is not generating are the following:

(i) THD of the voltage should be less than 4 %.
(ii) Voltage unbalance should be less than 2 %.
(iii) Measurement equipment should have class-A accuracy as defined by European standard IEC 61000-4-7.

The required PQ measurements for large PV systems are the following:

(i) 3-s/10-min harmonic currents up to the 50th order harmonic.
(ii) short-term/ long-term flicker.
(iii) A 3-s/10-min negative-sequence ratio of current unbalance, which should be raised to the 50th-order harmonic;
(iv) 1-min fundamental voltage.

Above all, measurements should be continuously recorded throughout the week so that PQ indices can be monitored for a period of time to know how changes are occurring. Measurements during hours without irradiance should be deleted to avoid distorting percentiles with measurements not determined by the PV unit.

The thermal effects of disturbances on the power system are presumably related to the disturbance level during 10-min periods. They are not related to the short time disturbance level, which affects the malfunction of relaying or electronic devices. Consequently, short time measurements should only be required when the PV unit has a significant impact on the power system.

8.5.3 Assessment Procedure for Power Quality in PV Systems

This section describes the procedure for assessing compliance with PQ requirements for PV systems based on PQ measurements. For small PV systems, the harmonic current emission should fulfill the objectives in IEC 61000-3-2/12. In contrast, the flicker emission should meet the objectives in IEC 61000-3-3/11. Focusing hence forth on large PV systems, the harmonic current emission from a PV unit (I_h, with h = 1–50) must be limited to comply with the harmonic current emission objective for the PV unit i at its PCC ($E_{I_h i}$) as in Eq. 8.3.

$$I_h \leq E_{I_h i} \tag{8.3}$$

According to, this assessment should be carried out for the ten intervals of nominal power of the PV unit. The flicker emission from a PV unit (P_{st}, P_{lt}) should be limited to comply with the flicker emission objective for the PV unit i at its PCC $\left(E_{p_{st}i}, E_{p_{lt}i}\right)$ expressed in Eqs. 8.4 and 8.5.

$$P_{st} \leq E_{p_{st}i} \tag{8.4}$$

$$P_{lt} \leq E_{p_{lt}i} \tag{8.5}$$

The emission of current unbalance from a PV unit must be limited so as to attain the voltage unbalance emission objective for the PV unit at its PCC. The steady-state voltage change resulting from a PV unit switching (ε) must be limited to comply with the voltage change objective resulting from the switching of the PV unit at its PCC ($E_{\varepsilon i}$) is given by Eq. 8.6.

$$\varepsilon \leq E_{\varepsilon i} = \frac{100}{U_n^2}(R_{sc,i} \cdot P_n + X_{sc,i} \cdot Q_n) \tag{8.6}$$

8.5.4 *Description of Case Studies*

The description of case studies used in this section is described below:

8.5.4.1 Case Study-I

The case study (Fig. 8.4) done in 100 kW Solar PV system at PSG College of Technology K-block referred in Appendix IV. In which a 100 kW PV source is divided into (5*20) kW. Each 20 kW is integrated to a distribution network through parallel connection of 10 kHz, 20 kW three-phase PWM inverter.

8.5.4.2 Case Study-II

The case study done in 100 kW Solar PV system at PSG College of Technology K-block load side referred in Appendix IV. In which the grid power and Solar PV power is synchronized and supplied to the load.

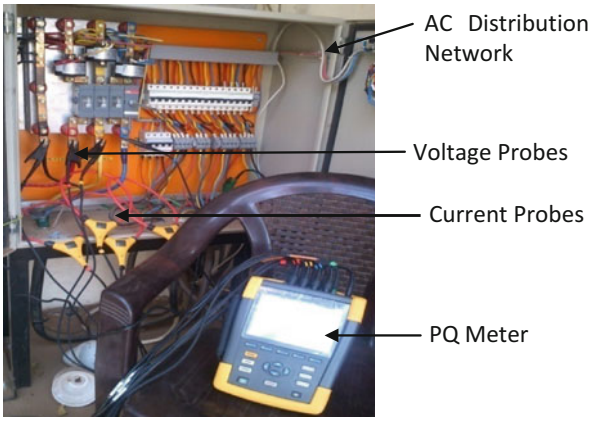


Fig. 8.4 PQ meter connections at load connected solar PV system

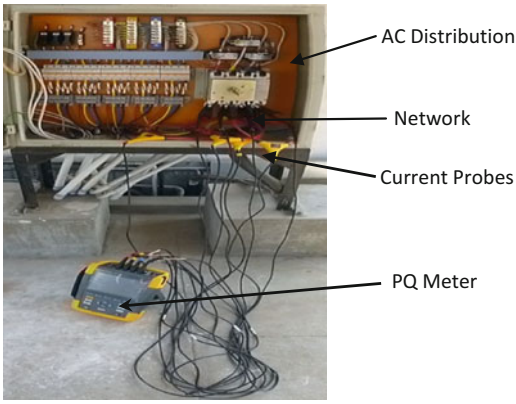


Fig. 8.5 PQ analyzer connected at AC choke in solar PV system

8.5.4.3 Case Study-III

The power quality measurements done in 200 kW at Sarvajana Higher Secondary School, Peelamedu (Fig. 8.5) referred in Appendix IV. In which the Solar PV power generated is directly connected to the lightning load.

8.5.5 Problem Evaluation and Solution Description

A complete analysis of the recorded data yielded the following results:

- The results taken from the case study-I done at "PSG College of Technology 100 kW system," as per Appendix IV shows that the current injected by the solar PV had a Total Harmonic Distortion (THD) of 5.2 % which is above 5 % limit set by the IEEE 519-1992. The average voltage THD at input and load side is 2.7 % which is below 3 % the limit set by the IEEE 519-1992. It is found that voltage injection profile of system is very satisfactory compared to current injection profile.
- When connected at the load side of 100 kW PV system at "PSG College of Technology K-Block," the results referred from Appendix IV, shows that voltage and current THD were 2.7 % and 5.1 % respectively. Also no voltage related problems noted, this confirms that PQ problems do not exist in the system. The wave shape of current is also purely sinusoidal no phase shift between voltage and current that shows reactive power flowing in system is zero.
- The results taken from the case study done at "SARVAJANA HIGHER SECONDARY SCHOOL, Peelamedu" as per Appendix IV, shows that PQ meter has recorded one voltage sag, four transients, and two interruptions. However, an analysis of the individual harmonic components revealed that 3rd, 5th, and 7th order harmonics are dominating because of the inductive load connected to the distributive system which may cause severe damage to sensitive equipments. In

that case, mitigation needs to be done by choosing custom power devices like Dynamic Voltage Restorer (DVR) to compensate voltage related problems as well as harmonics. For reactive power compensation, Distribution STATic COMpensator (DSTATCOM) was used.

8.6 Distribution Static Compensator

The problem of reactive power and harmonics in system are studied in the case study referred in Appendix IV. The phase shift controlled voltage source converter Distribution STATic COMpensator (DSTATCOM) is modelled in MATLAB for reducing harmonics in source side current and reactive power compensation. In this control algorithm the voltage regulation is achieved in a STATCOM by the measurement of the rms voltage at the load point and no reactive power measurements are required. Figure 8.6 shows the block diagram of the implemented scheme.

Sinusoidal PWM strategy is used since it is simple and offers a good response. The error signal obtained by comparing the measured system rms voltage along with the reference voltage. It really is fed into a PI controller which generates the angle which decides the mandatory phase shift between your output voltage on the VSC and also the AC terminal voltage. This angle is summed up with the phase on the balanced supply voltages that happen to be assumed to become equally spaced at 1,200 to create the required synchronizing signal forced to operate the PWM generator. The schematic diagram of phase shift control is shown in Fig. 8.7. In this method, the compensation is achieved by the measuring of the RMS voltage at the load point, whereas no reactive power measurements are required. Sinusoidal PWM technique is used with constant switching frequency. The error signal obtained by comparing the measured system rms voltage and the reference voltage is fed to a PI controller, which generates the angle for deciding the necessary phase shift between the output voltage of the VSC and the AC terminal voltage. This angle is summed with the phase angle of the balanced supply voltages, assumed to be equally spaced at 120° to produce the desired synchronizing signal required to operate the PWM generator. In this scheme, the DC voltage is maintained constant, using a separate battery source.

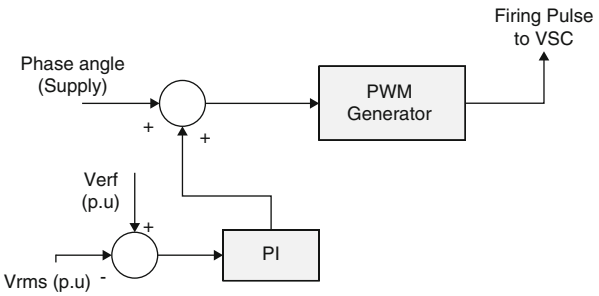


Fig. 8.6 Block diagram of phase shift control method

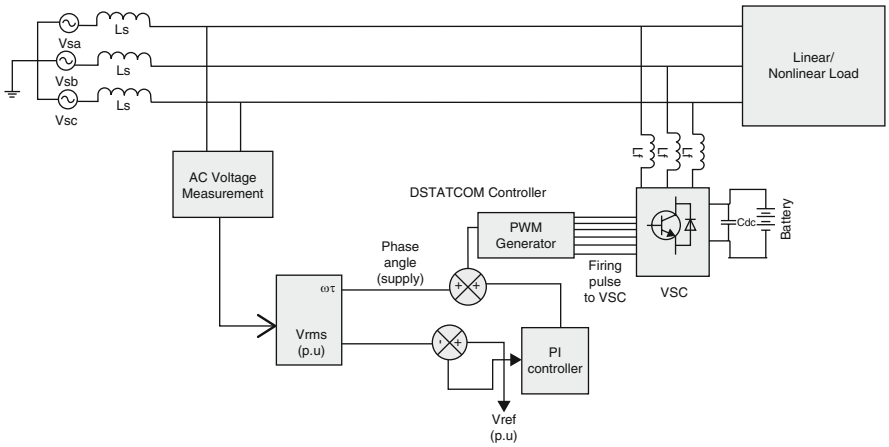


Fig. 8.7 Schematic of phase shift controlled DSTATCOM

8.6.1 SIMULINK Model of DSTATCOM

Figure 8.8 shows the SIMULINK model of the phase shift controlled DSTATCOM, in which a three-phase 230 V, 50 Hz system with line impedance of 0.1 + j3.5 mH is connected to the non-linear load of rectifier at 0.15 s and the DSTATCOM is connected via a circuit breaker with external control at 0.18 s to control the reactive power and current harmonics present in the system. Sinusoidal PWM technique is used with constant switching frequency. The error signal obtained by comparing the measured system rms voltage and the reference voltage is fed to a PI controller, which generates the angle for deciding the necessary phase shift between the output voltage of the VSC and the AC terminal voltage. This angle is summed with the phase angle of the balanced supply voltages, assumed to be equally spaced at 120̊ to produce the desired synchronizing signal required to operate the PWM generator.

8.6.2 Simulation Results

Figure 8.9 show the simulation results obtained using phase shift control for reactive power compensation and harmonic mitigation for a balanced varying linear load and for a non-linear load respectively. It is observed that the source current and the source voltage are in phase, correcting the power factor of the system in case of a linearly varying load; whereas, complete compensation is not achieved in case of non-linear load (source current THD 4.8 %) as can be seen in Fig. 8.10. The major disadvantages in this system of DSTATCOM are as follows:

- DC-link voltage is varying one but, it should be constant to make it constant some control techniques can be used like PI controller.
- The controller does not use a self supporting DC bus and thus requires a very large DC source to pre charge the capacitor.

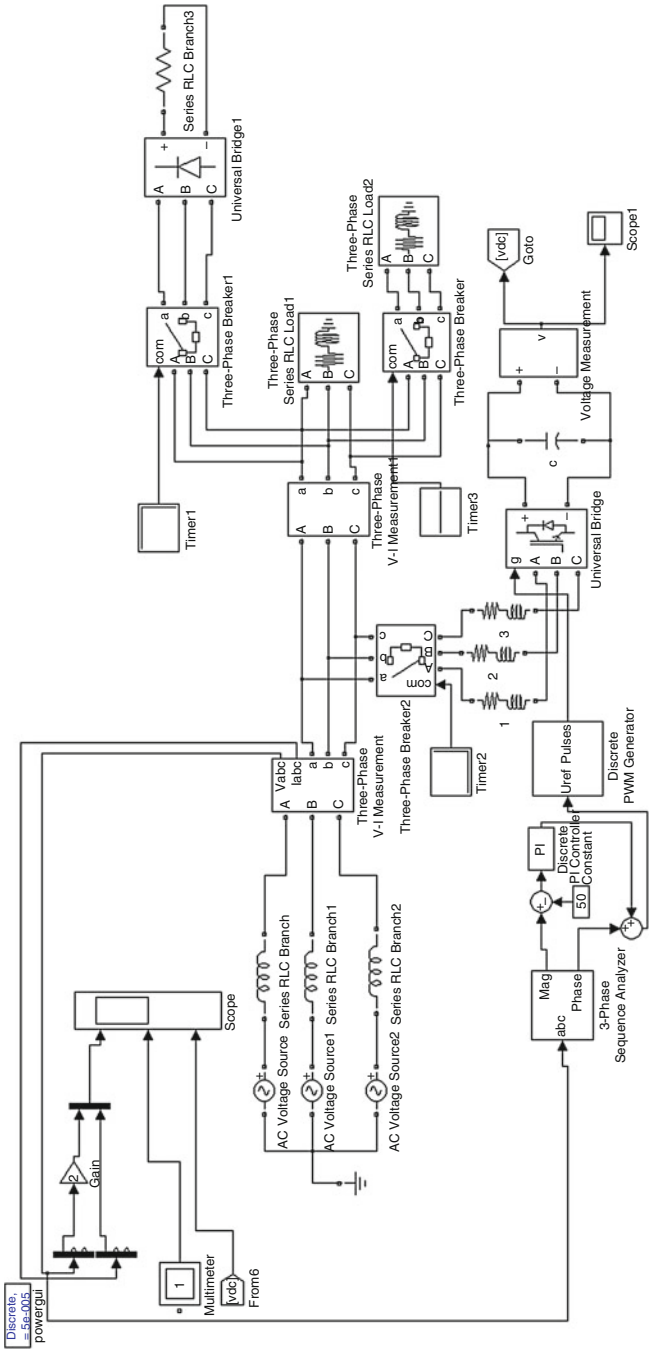


Fig. 8.8 SIMULINK model of DSTATCOM connected to a system with non-linear load

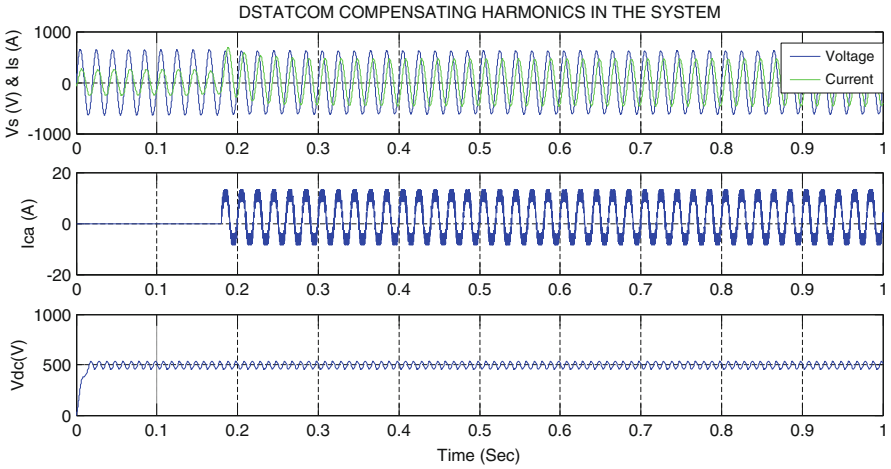


Fig. 8.9 Harmonics and reactive power compensation using DSTATCOM

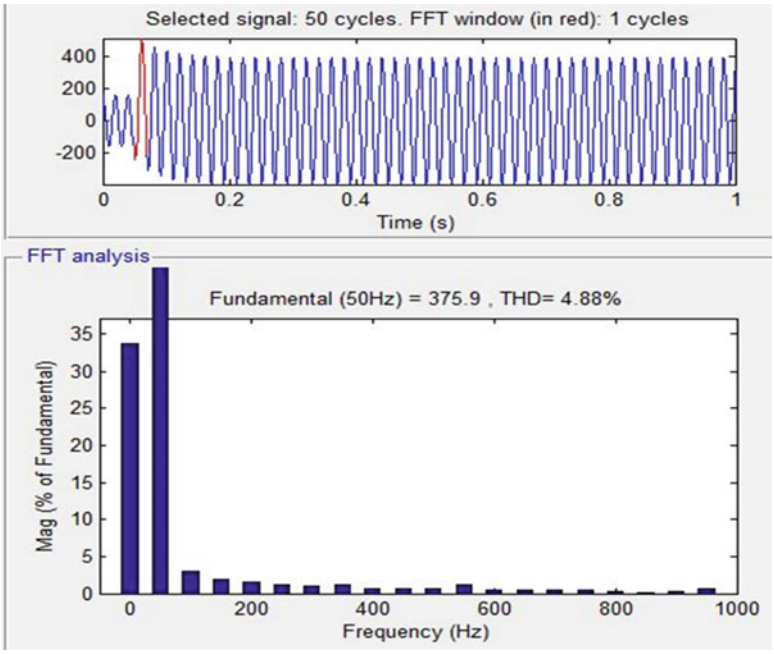


Fig. 8.10 THD% of source current waveform with DSTATCOM

- Balanced source supply as rms voltage is assumed and the supply phase angle are calculated over the fundamental only.
- No harmonic suppression and partial compensation is achieved in case of non-linear loads.

The phase shift controller for the DSTATCOM connected to a system with non-linear load compensating source side current harmonic %THD to 4.8 % which is less than 5 % limit specified by IEEE 519-1992.

8.7 Dynamic Voltage Restorer

This section discusses the modeling, simulation and analysis of Dynamic Voltage Restorer (DVR). Which is emerging custom power device to mitigate the power quality problems in distribution system. The DVR is similar to Static Synchronous Series Compensator (SSSC) a major difference involves the injection of harmonic currents and voltages to separate the source from load. A DVR can work as a harmonic isolator to prevent the harmonics in the source voltage reaching the load in addition to balancing the voltages and providing voltage regulation.

The results of case study referred from Appendix IV, yields that voltage sag/swell, interruptions, and transients are existed in the system. To compensate those problems DVR is modelled in MATLAB for providing constant voltage apart from disturbances in the supply voltage. The general configuration of the DVR shown in Fig. 8.11 consists of:

(i) An Injection/Booster transformer.
(ii) A Harmonic filter.
(iii) Storage Devices.
(iv) A Voltage Source Converter.
(v) DC charging circuit.
(vi) A Control and Protection system.

8.7.1 Equations Related to DVR

The system impedance Z_{TH} depends on the fault level of the load bus. When the system voltage (V_{TH}) drops, the DVR injects a series voltage V_{DVR} through the injection transformer so that the desired load voltage magnitude V_L can be

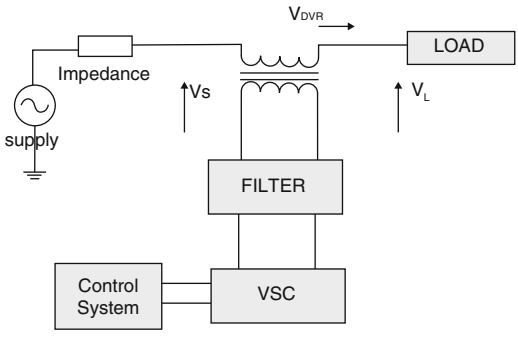


Fig. 8.11 Schematic diagram of DVR system

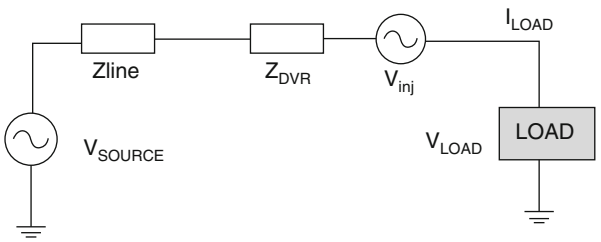


Fig. 8.12 Equivalent circuit diagram of DVR

maintained. The equivalent circuit diagram of DVR is shown in Fig. 8.12. The series injected voltage of the DVR can be written as Eq. 8.7.

$$V_{DVR} = V_L + Z_{TH} I_L - V_{TH} \tag{8.7}$$

where

V_L = The desired load voltage magnitude
Z_{TH} = The load impedance
I_L = The load current
V_{TH} = The system voltage during fault condition

The load current I_L is given by Eq. 8.8.

$$I_L = \frac{[P_L + jQ_L]}{V} \tag{8.8}$$

When V_L is considered as a reference equation can be rewritten as Eq. 8.9.

$$V^*_{DVR} = V_L^{\angle 0} + Z_{TH}^{\angle(\beta-\theta)} - V_{TH}^{\angle\delta} \tag{8.9}$$

α, β, δ are angles of V_{DVR}, Z_{TH}, V_{TH} respectively and is load power angle is given by Eq. 8.10.

$$\theta = \tan^{-1}\left(\frac{\theta_L}{P_L}\right) \tag{8.10}$$

The complex power injection of the DVR can be written as Eq. 8.11.

$$S_{DVR} = V_{DVR} I_L^* \tag{8.11}$$

It requires the injection of only reactive power and the DVR itself is capable of generating the reactive power.

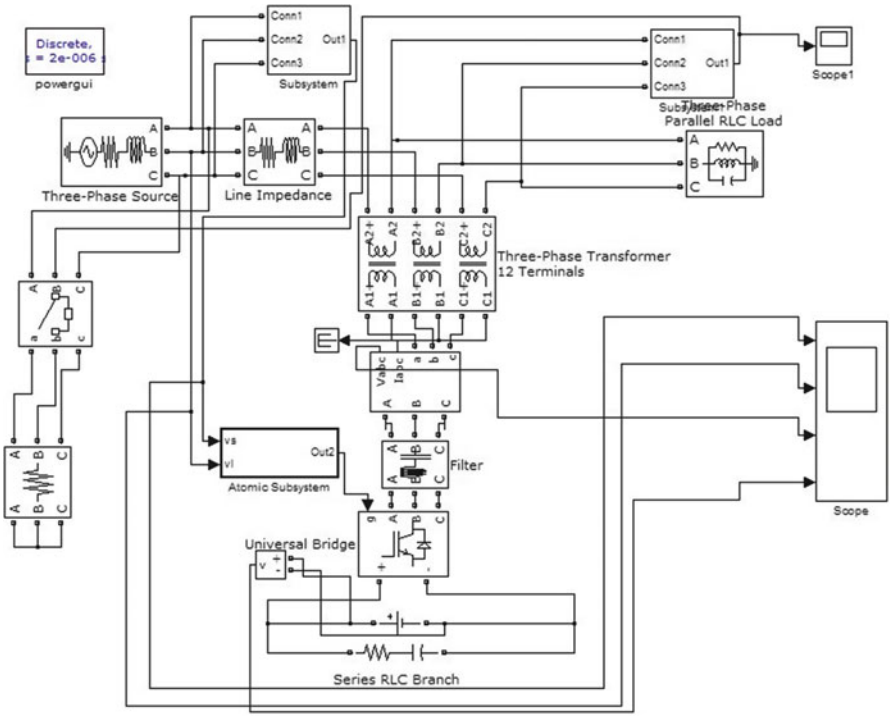


Fig. 8.13 SIMULINK model of dynamic voltage restorer

8.7.2 SIMULINK Model of DVR

Figure 8.13 shows the MATLAB model of the DVR connected system. The supply voltage is realized by using a three-phase voltage source and source impedance is connected in its series. In order to simulate the disturbances at the Point of Common Coupling (PCC) voltage, an additional load is switched on with a circuit breaker. The load considered is a lagging power factor load. The DVR is connected in series with the supply using an injection transformer. The VSC is connected to the transformer along with a ripple filter. The DC bus capacitor is selected based on the transient energy requirement and the DC bus voltage is selected based on the injection voltage level. The DC capacitor decides the ripple content in the DC voltage. The reference load terminal voltages are derived from the sensed supply voltages, supply currents, load terminal voltages and the DC bus voltage of DVR. The parameters used in SIMULINK are shown in Table 8.1.

Figure 8.13 shows a 415 V, 50 Hz three-phase source is connected to a linear load of 415 V, 10 kVA, 0.8 pf lag which will inject harmonics into the system to compensate this harmonics and voltage sag or swell created by connecting or

Table 8.1 List of parameters used in SIMULINK model of DVR

Symbol	Parameter	Value
V_s	**AC line voltage**	415 V
f	**System frequency**	50 Hz
R_S, L_S	**Source impedance**	0.01 + j 0.942
R_f, C_f	**Filter impedance**	4.8 + j 318.3
DVR with DC bus capacitor supported:		
V_{dcref}	**Reference DC-link voltage of DVR**	300 V
C_{dc}	**DC-link capacitance**	2,000 μF
K_{P1}, K_{i1}	**DC bus voltage PI controller**	0.5, 0.35
K_{p2}, K_{i2}	**AC load voltage PI controller**	0.1, 0.5
f_{sw}	**Switching frequency**	10 kHz
Three phase transformer 12 terminals	10 kVA, 200 V/300 V	

disconnecting a load in parallel to the existing load. The three-phase series injection transformer is used to inject voltage in series with the system to compensate voltage of sag/swell and supply constant voltage load. A ripple filter is used to filter out the voltage to inject into system. The three-phase circuit breaker is used to connect or disconnect load to create voltage sag/swell in system that the control feedback is given to the control circuit for controlling DVR system to compensate the voltage related problems. Voltage source converter based DVR system is simulated in the MATLAB which supported by the capacitor and battery storage system.

Figure 8.14 shows the control circuit for the Dynamic Voltage Restorer in which the synchronous reference frame theory is used for reference signal estimation of DVR voltages. The voltages at PCC and load voltages are converted to abc-dqo by using park's transformation. The unit vectors method is used to convert abc-dqo transformation unit vectors is provided by Phase Locked Loop (PLL) then, the reference voltages is obtained in rotating frame as Eqs. 8.12 and 8.13.

$$V_{Dd}^{*} = V_{Sd}^{*} - V_{Ld} \tag{8.12}$$

$$V_{Dq}^{*} = V_{Sq}^{*} - V_{Lq} \tag{8.13}$$

The error between the reference and actual DVR voltages in the rotating reference frame is regulated using two PI controllers. Reference DVR voltages ($V_{dvra}^{*}, V_{dvrb}^{*}, V_{dvrc}^{*}$) and actual DVR voltages ($V_{dvra}, V_{dvrb}, V_{dvrc}$) are used in a Pulse Width Modulated (PWM) controller to generate gating pulses to a VSC of the DVR.

8.7.2.1 Control Strategy

In the control algorithm the shunt compensator is controlled for harmonic current compensation, load current balancing and power factor correction. Here, the sag and swell in supply voltage are compensated by controlling the DVR. The control

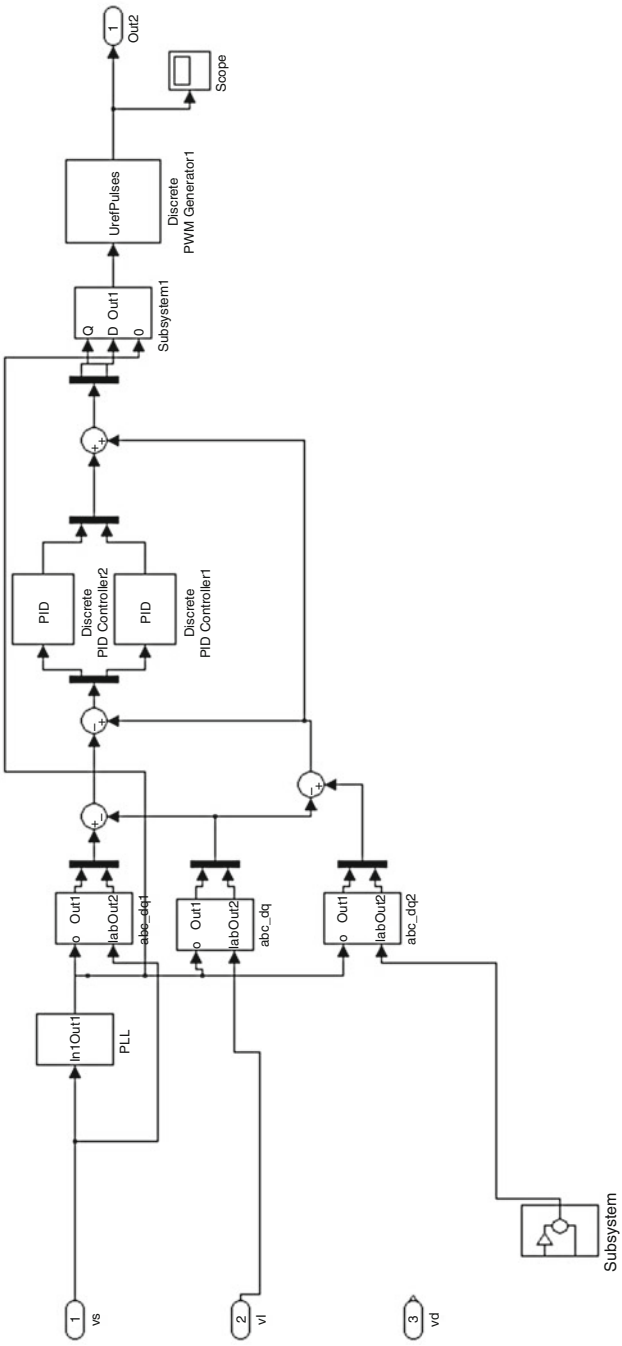


Fig. 8.14 SIMULINK model of control circuit for DVR

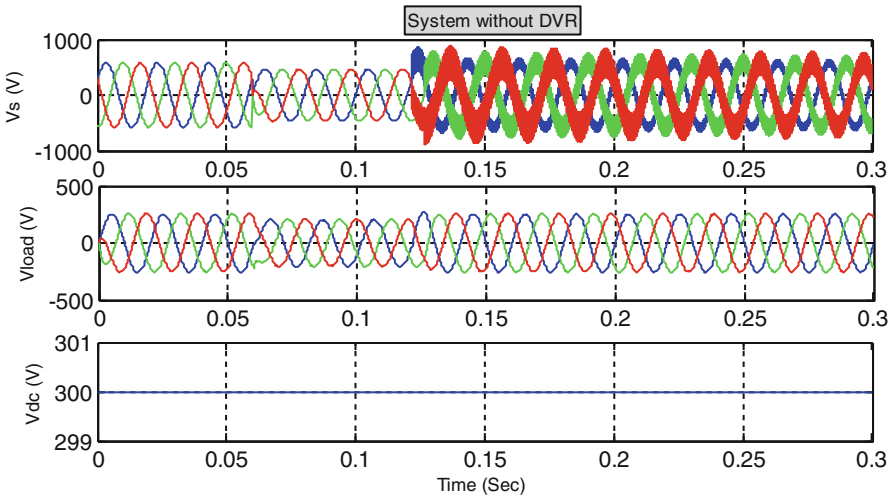


Fig. 8.15 3-Φ load and source voltages without DVR

technique used is developed with Synchronous Reference Frame theory (SRF) method. The actual voltage of DVR and estimated voltages of DVR are given to a specific voltage controlled PWM controller developed for generating pulses for triggering the IGBT's in VSC of DVR system.

8.7.3 Results and Discussion

Figure 8.15 shows the Supply voltage (V_S), load voltage (V_L), DVR voltages (V_{dvr}) and DC bus voltage without the operation of Dynamic Voltage Restorer in the system. From that we can observe that whenever a certain amount of load increases in parallel with the existing load, a sudden fall in supply voltage exists; i.e., followed in load voltage which may disturb and damage the sensitive equipments.

The dynamic performances of the DVR for a Voltage sag in supply voltage is given in Fig. 8.16 shows balanced sag of 30 % in supply voltage at 0.15 s and occur for 5 cycles of ac mains. The load voltage (V_L) is regulated at rated value, which shows the satisfactory performance of the DVR. The supply voltage (V_S), DVR voltage (V_{dvr}) and the DC bus voltage (V_{dc}) are also shown in the Fig. 8.16. The DC bus voltage is regulated at the reference value, though small fluctuation occurs during transients. The load voltage is maintained by DVR as constant value apart from disturbances caused in the supply voltages.

The dynamic performance of the DVR for a voltage swell in supply voltage is given in Fig. 8.17. The load voltage (V_L) is regulated at rated value, which shows the satisfactory performance of the DVR. The DVR voltage (V_C) supply current (i_s), the amplitude of load terminal voltage (V_{Lp}), the amplitude of supply voltage

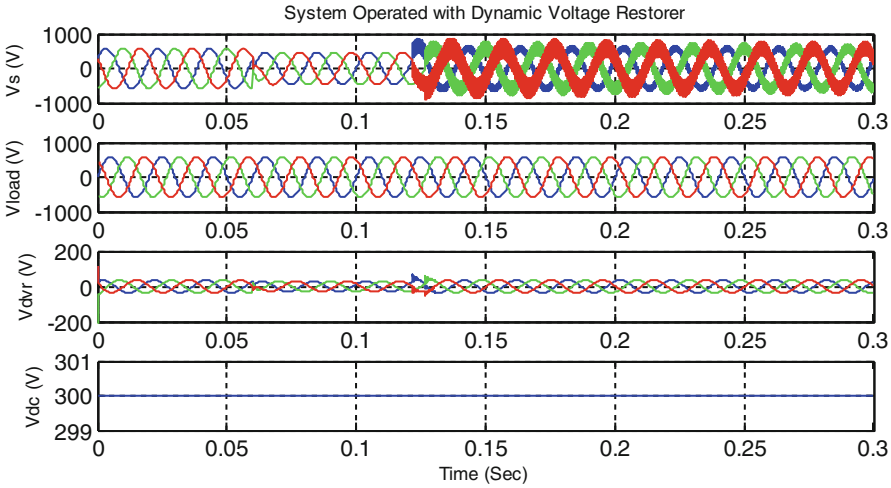


Fig. 8.16 DVR compensating voltage sag

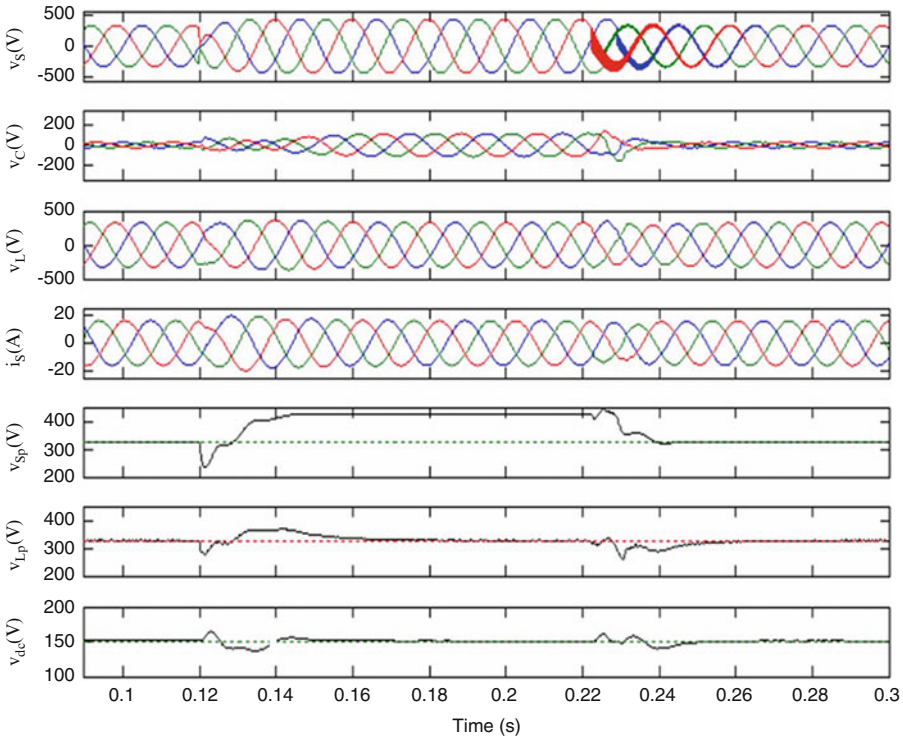


Fig. 8.17 DVR compensating voltage swell

(V_{Sp}) and the DC bus voltage (V_{dc}) are also shown in the Fig. 8.17. The DC bus voltage is regulated at the reference value, though small fluctuations occur during transients.

Power Quality (PQ) measurement and assessment was done as a case study on different solar PV generation systems such as 100, 80, and 60 kW located at PSG College of Technology. The Analysis was carried out with the help of FLUKE 434 series II Energy analyzer reported as Class-S meter according to IEC/IEEE standards. It was observed from the case study that power quality problems such as reactive power, 10 % sag/swell for duration of $\leq$1,000 μs, and 4 % of VTHD, 10 % ITHD in which 3rd, 5th, and 7th harmonics are dominating and existing in system when connected to the load. To mitigate these problems custom power devices Distribution STATic Compensator (DSTATCOM) and Dynamic Voltage Restorer (DVR) are simulated in MATLAB/SIMULINK.

The phase shift control scheme is described with the help of simulation results. The DSTATCOM shows better performance when connected to system by compensating the reactive power flow and harmonic mitigation in source side current waveform. The %THD of source current is 4.8 % after connecting DSTATCOM which is below the IEEE 519-1992 set limit.

The control scheme of DVR has been validated through computer simulation using MATLAB software along with SIMULINK and power system block set toolboxes. The simulation results of DVR show that compensation of voltage sag/swell is reduced to 3 % of nominal voltage. The IEC/IEEE standards are met by the system control technique developed by Synchronous Reference Frame (SRF) theory is efficient in compensating the voltage related problems and supplying constant load apart from disturbances created in supply side.

8.8 Unified Power Quality Conditioner

The Unified Power Quality Conditioner (UPQC) is used in a power transmission system to compensate supply voltage, flicker/imbalance, reactive power, negative sequence current and harmonics. The UPQC has the ease of improving power quality on the point of setting up power distribution systems. The UPQC is predicted to get probably the most powerful answers to large capacity loads that are sensitive to supply voltage sparkle/imbalance. The UPQC (Fig. 8.18) comprises of series active power filter (APF) and also a shunt APF which aid in compensating the interruption in voltage when energy storage or battery is present in the DC-link. The shunt APF is normally connected through the loads to meet all current-associated problems such as the reactive power compensation, power factor improvement, current harmonic compensation, and load unbalance compensation whereas the series APF can be connected in a series with the line through series transformers. It operates as controlled voltage source and can compensate all voltage related problems, for example voltage harmonics, potential difference sag, voltage swell, flicker, etc.

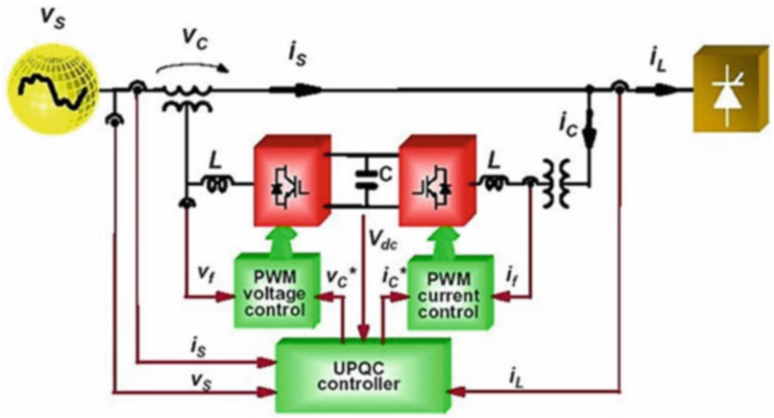


Fig. 8.18 General configuration of UPQC

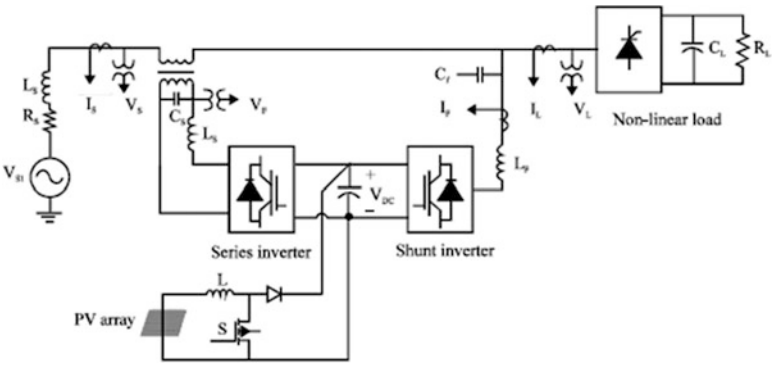


Fig. 8.19 UPQC system with PV array

8.8.1 UPQC with PV Array

The configuration of UPQC with PV array is shown in Fig. 8.19. The 3-phase 3-wire shunt inverters and series inverters are linked to a point of common coupling (PCC) by means of a shunt transformer. The series inverter lies between the source and coupling as a current source and it operates as a voltage source. By neglecting the resistance in the line, the real and reactive powers are given by Eqs. 8.14) and 8.15:

$$P = \frac{V_S V_R}{X} \sin(\delta_1 - \delta_2) \tag{8.14}$$

$$Q = \frac{V_R}{X}(V_S - V_R) \tag{8.15}$$

The boost converter is designed using Eq. 8.16,

$$V_o = \frac{V_i}{(1-\delta)} \tag{8.16}$$

The values of inductance and capacitance are calculated according to Eqs. 8.17 and 8.18,

$$L = \frac{V_i \delta}{f \Delta I} \tag{8.17}$$

$$C = \frac{\delta}{2fR} \tag{8.18}$$

8.8.2 SIMULINK Model of UPQC

The values of L and C are designed based on Eqs. 8.17 and 8.18, assuming $\Delta I = 0.4$ A, f = 3 kHz & R = 1 K Ω. For boost converter, the values of L and C are 8.8 mH and 0.147 μF with $T_{ON} = 0.29$ ms and $T_{OFF} = 0.04$ ms. The SIMULINK model of the UPQC system with PV array is shown in Fig. 8.20.

8.8.3 Simulation Results

The receiving end voltage, receiving end current, real power and reactive power are measured with scopes connected appropriately. The load on the receiving end is series combination of resistance 200 Ω and inductance of 100 mH. The parameters in the additional load are 50 Ω and 50 mH. DC required by UPQC is applied from the photo cell. The output of UPQC is injected utilizing a series transformer. The inverter of DVR employed in the UPQC is triggered at 50 Hz. Each of the switches are operated with pulses of width 10 ms. The pulses provided to additional two switches are displaced by 10 ms. The output of inverter is filtered by making use of LC filter. It will reduce heating since harmonics are reduced. The inverter switches of active filter are triggered at 250 Hz. The DC required by the DC-link is supplied using solar cell and boost converter. The output of solar cell is not sufficient to drive the capacitor at the input of the inverter. Therefore the output of solar cell is boosted by using a boost converter. The boost converter uses boost inductor, capacitor and blocking diode. The output voltage is controlled by using a MOSFET. An additional load is applied at t = 0.2 s. The total load current increases and the drop in the line impedance increases. The receiving end voltage is reduced. At t = 0.3 s, the voltage is injected by the UPQC to bring the receiving end voltage to the normal value. From the waveform of VL1, it can be seen that the sag is compensated by using the DVR part of UPQC. The voltage VL2 is zero up to 0.2 s, since the breaker is open. The real and reactive powers increase at t = 0.2 s due to the increase in the load. This increases further at t = 0.3 s, due to the injection of the voltage by UPQC.

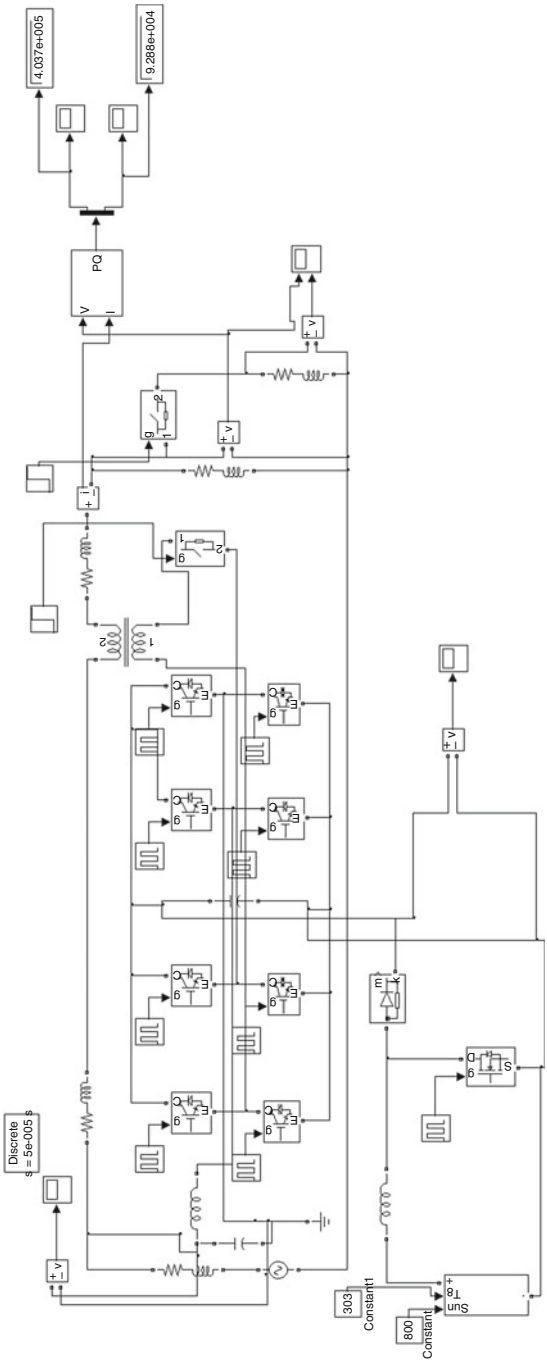


Fig. 8.20 SIMULINK model of UPQC

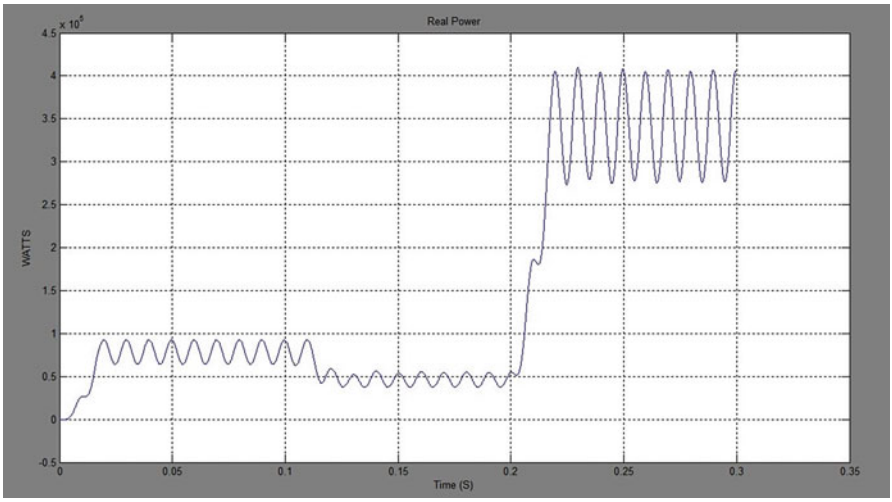


Fig. 8.21 Real power

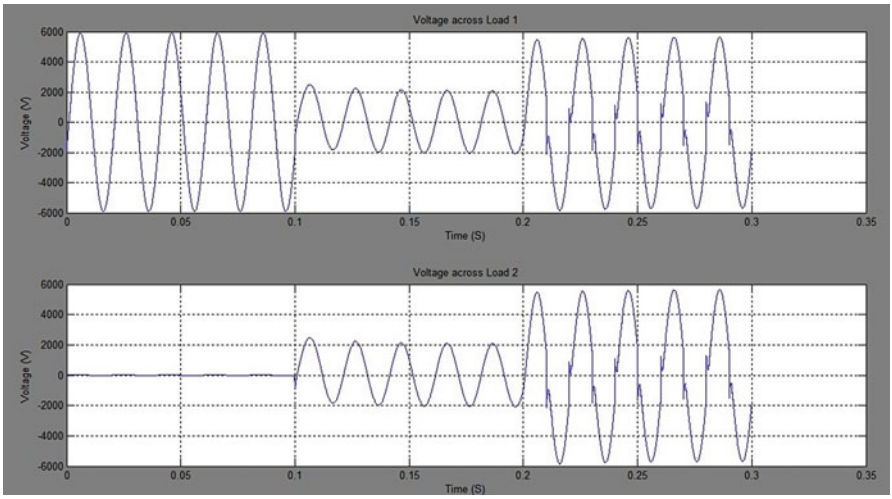


Fig. 8.22 Output voltage

The real power, output voltage and reactive power are shown in Figs. 8.21, 8.22, and 8.23 respectively. A nonlinear rectifier system with inductive load is connected in parallel with the linear load. This nonlinear load draws alternating square current which contains 5th harmonic. The THD is 8.6 %. The output of active filter is connected to the load. The inverter in the active filter is triggered at 250 Hz. FFT analysis is done for the receiving end current and the frequency spectrum is obtained. The THD is 1.6 %. Thus the THD is reduced to a minimum value by using active filter. Thus the quality of sending end current is improved by using UPQC.

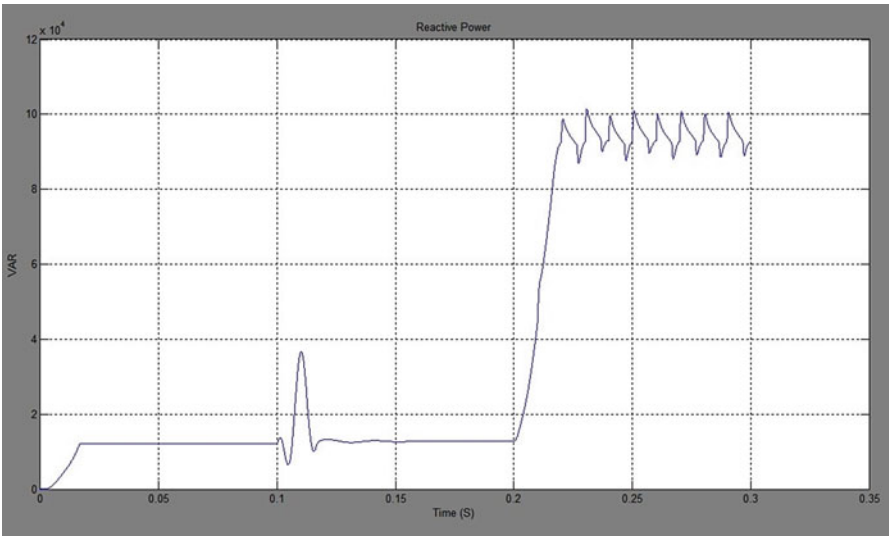


Fig. 8.23 Reactive power

Although the likelihood of harmonic problems is very low, the cases in which they do occur can result in decreasing power system reliability. An understanding of the causes, potential effects and mitigation means for harmonics can help to prevent harmonic related problems at the design stage and reduce the probability of undesired effects occurring on start-up. The UPQC system is successfully designed and modeled using the circuit elements of SIMULINK. The sag in the voltage is created by applying an additional heavy load at the receiving end. This sag is compensated by using DVR part of UPQC. The simulation results are in line with the predictions. The THD in the output is reduced by operating the inverter at 250 Hz.

8.9 Harmonic Reduction in WECS

To have sustainable growth and social progress, it is necessary to meet the energy need by utilizing the renewable energy resources like wind, biomass, hydro, co-generation, etc In sustainable energy system, energy conservation and the use of renewable source are the key paradigm. The need to integrate the renewable energy like wind energy into power system is to make it possible to minimize the environmental impact on conventional plant. The integration of wind energy into existing power system presents a technical challenges and that requires consideration of voltage regulation, stability, power quality problems. The power quality is an essential customer- focused measure and is greatly affected by the operation of a distribution and transmission network. The problem of power quality is of great importance towards the turbine. There is a substantial growth and quick rise in the exploitation of wind energy recently. From the fixed-speed turbine operation, all the fluctuation

within the wind speed are transmitted as fluctuations within the mechanical torque, energy around the grid and brings about large voltage fluctuations.

During the normal operation, wind mill creates a continuous variable output power. These power variations are generally attributable to the issue of turbulence, wind shear, and tower-shadow and of control system in the power system. Thus, the network needs to manage for such fluctuations. The power quality issues can be looked at based on the wind power, transmission and distribution network, for example voltage sag, swells, flickers, harmonics etc. However the wind generator introduces disturbances into the distribution network. One of many simple types of running a wind generating technique is to make use of the induction generator connected on to the grid system. The induction generator has inherent attributes of cost effectiveness and robustness. However; induction generators require reactive power for magnetization. When the generated active power of an induction generator is varied as a result of wind, absorbed reactive power and terminal voltage associated with an induction generator may be significantly affected. A correct control scheme in wind energy generation product is required under normal operating condition to permit the proper control in the active power production. In the case of increasing grid disturbance, an assortment energy storage system for wind energy generating strategy is generally necessary to compensate the fluctuation generated by wind generator.

8.9.1 Power Quality Standards and Issues

8.9.1.1 International Electro Technical Commission Guidelines

The policies are provided for measurement of power quality of wind mill. The International standards are produced by the working group of Technical Committee-88 from the International Electro-technical Commission (IEC), IEC standard 61400-21, describes the procedure for determining the electricity quality characteristics from the wind generator.

The standard norms are specified.

(a) IEC 61400-21: Wind turbine generating system, part-21. Measurement and Assessment of power quality characteristic of grid connected wind turbine.
(b) IEC 61400-13: Wind Turbine – measuring procedure in determining the power behavior.
(c) IEC 61400-3-7: Assessment of emission limits for fluctuating load IEC 61400-12: Wind Turbine performance.

8.9.1.2 Voltage Variation

The voltage variation issue results on the wind velocity and generator torque. The voltage variation is directly related to real and reactive power variations. The voltage variation is usually classified as Voltage Sag/Voltage Dips, Voltage Swells, Short

Interruptions, Long duration voltage variation. The voltage flicker issue describes dynamic variations within the network attributable to windmill or by varying loads. Thus the energy fluctuation from wind turbine occurs during continuous operation. The amplitude of voltage fluctuation is determined by grid strength, network impedance, and phase-angle and power factor on the wind turbines.

8.9.1.3 Harmonics

The harmonic results due to the operation of power electronic converters. The harmonic voltage and current ought to be restricted to the acceptable level for the point of wind generator link to the network. To ensure the harmonic voltage within limit, each method of obtaining harmonic current can allow only a limited contribution, as per the IEC-61400-36 guideline. The rapid switching gives a large cut in lower order harmonic current when compared to line commutated converter, even so the output current will have high frequency current which enables it to easily be filter-out.

8.9.1.4 Self Excitation of Wind Turbine Generating System

The self excitation of windmill generating system (WTGS) with an asynchronous generator takes place after disconnection of turbine generating system (WTGS) with local load. Potential risk of self excitation arises particularly when WTGS gives you compensating capacitor.

8.9.1.5 Consequences in the Issues

The voltage variation, flicker, harmonics causes the malfunction of equipments namely microprocessor based control system, programmable logic controller; adjustable speed drives, flickering of light and screen. It might brings about tripping of contractors, tripping of protection devices, stoppage of sensitive equipments like personal computer, programmable logic control system and will stop the process and in many cases can damage of sensitive equipments. Thus it degrades the electricity quality in the grid.

8.9.2 Power Curtailment or Wind Turbine Disconnection

In case of:

- grid capacity constraint resulting from a thermal constraint in a grid component,
- or an operating constraint,

- or security constraints, a possible solution would consist in limiting the active power delivered by the wind farm to the network. This could be:
  1. A permanent limitation defined prior to the connection and eventually modified during the life duration of the wind farm,
  2. A periodic limitation for a given duration if the constraint appears only during a forecasted time in the year (due to seasonal maximal external temperature, due to load and/or generation profile in the year).

8.9.3 Coordination with Other Generating Plants

The coordination of wind farms with one or several other generating plants (using other primary sources than wind) may allow:

- To compensate for the short term, midterm or long term power variations of the wind farm. This enables to limit the solicitation on the network, to facilitate the power system operation, and to improve the security.
- To share the frequency control participation between different generation units. In case of grid capacity constraints corresponding to a thermal constraint in a grid component, the true coordination of the wind farm with other generation plants (for instance hydro power plants) may provide a solution. The other generating units may adapt their production in order to allow the wind farm to deliver all the power it can provide while the grid thermal limits are respected. However this possibility is highly dependent of the location of the other production units regarding the grid equipment pieces under constraint. In the same way, if a wind farm and another production unit have their connection point close to each other; it could be envisaged to share the reactive power production or the voltage control. Different applications have been developed for the compensation of short term, midterm and long term power variations, for instance in:
  - isolated grids with diesel – wind coordination,
  - The Nordic Power Pool with Hydro electric – wind coordination.

8.9.4 Load Control

Local loads can be switched on or off to:

- Compensate slow active power variations of wind farms,
- Perform a frequency regulation with a load control,
- In order to facilitate the integration of wind farms to the grid,
- Solve a thermal constraint.

This can be achieved for instance by:

- the use of a remote control signal to shut on or off loads on the network,
- a automatic frequency control integrated directly at the load level,
- The use of an additional communication system.

Note that this requires that the loads can withstand an intermittent functioning and that the service associated to them is still acceptable. For instance, different applications are presently developed and tested with water heating (used for heating purposes or for domestic consumption), with water pumping or with different kinds of domestic loads which present "inertia" characteristics or a low priority for the consumers. In case of network congestions or when the power injected on the grid is limited, the wind power which cannot be supplied to the grid can be used for other applications. For instance, applications are presently considered with:

- Desalination plants,
- Hydrogen production,
- Water pumping.

8.9.5 Reactive Compensation and Voltage Control

Solutions to power quality issues are delineated in Table 8.2. A few of them are discussed below:

8.9.5.1 Wind Turbine Technology

Depending on the technology, the wind turbines can directly (without need of additional device) participate to the reactive compensation and voltage control. More precisely, doubly-fed and WTG connected to the grid through power electronics interfaces can be used to control the reactive power and the voltage. The reactive power provided or consumed by these WTGs is limited by the current limitation of the converters and so their rating. Depending on the technology, it generally enables to produce or consume a reactive power up to 30 % of the nominal active power. To perform the grid voltage control at the connection point of the wind farm, a coordinated voltage control strategy between the different wind turbines in the wind farm has to be defined. Classical squirrel cage induction WTGs and induction WTGs with dynamic slip control can only consume reactive power. They need additional devices to perform the reactive compensation and possibly contribute to the grid voltage control.

Table 8.2 Solutions for power quality issues

		Wind turbine technology	Wind farms and power system operation	Reactive compensation and voltage control	FRT systems	Energy storage system	Icc limitation devices	Other devices
Grid capacity	Steady state current	✓	✓			✓		
	Short circuit current	✓			✓		✓	
	Steady state voltage	✓		✓		✓		
Power quality	Voltage fluctuations	✓	✓	✓		✓		
	Flicker	✓		✓		✓		
	Harmonic	✓						
	Remote control disturbances							✓
Protection issues								✓
Dynamic behavior and ancillary services	Voltage dips	✓			✓	✓		
	Stability	✓	✓			✓		
	Voltage control	✓		✓		✓		
	Frequency control	✓ partially	✓			✓		

8.9.5.2 Thyristor-Switched Capacitor (TSC)

TSC are designed to insert the appropriate number of multi-stage power capacitors into the network, without transient effects. For that purpose, capacitors are switched into the circuit when the grid voltage and the capacitor voltage are both equal to the positive or negative peak voltage. Tow types of TSC systems may be found:

- the first one is based on 2 thyristors connected in back to back and
- the second one consists of a thyristor and diode connected in anti parallel for each valve.

A microprocessor-based system manages the measurements, calculates the amount of reactive power to compensate and the gating signals to the thyristors. TSC are often used to regulate voltage especially when it fluctuates slowly. The dynamic of a TSC is limited, as in any device including line commutated thyristors, at the double of the 50 Hz network frequency, i.e. 10 ms. Practically one should add to this time interval, the computation delay of the regulator (typically some milliseconds). Therefore the typical response time of a TSC is about 20 ms.

8.9.5.3 Static VAR Compensator (SVC)

Over the last three decades, utilization of large pulsed type loads such as arc furnaces, welding equipment, rolling mills has increased with the growing need of steel. The increasing number and size of those fluctuating loads caused power quality problems such as flicker, harmonics and unbalance. Static Var Compensators have been used in the factories to reduce flicker and unbalance. Some 900 SVC applications are running to date around the world. The technology, based on thyristor-controlled reactors (TCR) is mature. Its exploitation to improve reactive compensation and grid voltage control in wind farms can be envisaged. The device utilizes a Thyristor Controlled Reactor (TCR) and a Fixed Capacitor (C). Thanks to the semi-conductors, three branches of TCR are delta-connected to form a 3-phase variable inductance capable of absorbing continuously a amount of reactive power from -QL to QC.

8.9.5.4 STATCOM

The STATCOM (static compensator) and variant, the D-STATCOM, provide voltage sourced converters (VSC), and so are voltage sources where amplitude, period and frequency are entirely governable. The dc bus capacitor can be applied a dc voltage for the input in the inverter. Its output is connected to the AC grid via an inductance. While adjusting the converter potential drop (U2) depending on network Voltage (U1), the ripping tools can right away supply or absorb reactive power due to the gating signals set on the switches of the converter. The response time is influenced with the switching frequency (Typically 1–2 kHz) by how big the inductance.

8.9.5.5 Synchronous Condenser

Synchronous condensers are synchronous generators without prime mover, that can be controlled to soak up or provide reactive power and will perform a voltage control. They have been partly supplanted by static compensators. However developments by way of example on superconductor synchronous condensers (AMSC) may make them interesting for reactive settlement and voltage power over wind farms.

8.9.5.6 Rotary Phase Shifter (RPS)

By the end of the nineties, the study of a doubly-fed adjustable-speed flywheel generating system was initiated in Japan, with prospective applications in the stabilization of power in decentralized systems. Basically the system is an induction machine with a wound rotor. In the series type RPS with stator connected to the grid and rotor connected to a wind farm and no additional impedance element, thanks to the torque controller, the device works as a phase shifter, capable (in the same way as a phase shifting transformer) of controlling the power flowing between the stator and the rotor. Thanks to the slip of the induction machine, it can also acts as a frequency changer.

8.9.5.7 FRT Systems

The aim of a Fault Ride Through technique is to allow the wind energy facility (WF) to face up to a severe voltage dip with the connection point. Through the voltage dip, the active power provided to the grid by the WF is instantaneously reduced. This power becomes at least temporarily below the mechanical power available; hence the rotor speed of the generator increases. If the FRT capability is needed, the WTGs mustn't disconnect, for example caused by over speed or under voltage protections. Following the clearing with the fault that led to the voltage dip, the voltage at the wind turbine bus increases. The WTGs must resume their power supply towards network (but not lose stability). Risking potential a lack of stability after the fault clearing can be quite limited for induction or synchronous generators with full power electronics converters, and limited for doubly-fed WTG, with the control capabilities of the power electronic converters.

The WTGs never disconnect in case there is a voltage dip, due to the following:

- to limit the increase in the rotor speed so that it doesn't exceed the maximal permitted value,
- to hold the voltage with the generator bus inside permissible range,
- never to lose stability to be able to be capable of resume the energy supply following the fault clearing.

8.9.5.8 Energy Storage Systems

There are numerous forms of energy storage systems depending on different technologies and then for various time scales. Each one of these storage systems don't inevitably fit the specificities of blowing wind energy and don't essentially help with the grid integration of wind generation.

However, according to the technology and so on the rating with the energy storage systems, they will enable to:

- improve power high quality,
- smooth the voltage and energy variations on account of wind turbulences,
- smooth power versions these days scale of minutes, hours or even days,
- solve steady state current constraints,
- take part in voltage and frequency control,
- both help wind farms to resist voltage dips.

8.10 Power Quality in WECS- A Case Study

A PQ study was undertaken at the substation at incoming 110 kV and 11 kV feeder levels. Fluke Power Quality Analysers were positioned in 'A' substation specifically in 110 kV Group control in-comer breaker along with the 11 kV feeder.

Frequency dips as well as other electrical data were collected simultaneously in 110 kV level and 11 kV level and derived from one of wind mills also. The collected Information is analysed and lots of interesting inference could possibly be concluded.

From the above data (Figs. 8.24, 8.25, 8.26, 8.27, and 8.28), maybe it's inferred that severe dip in voltage is responsible for tripping in the wind mills. The dips inside the feeder originate from Tripping of adjacent feeder within the same substation. The fault within the feeders caused tripping from the feeders. In the study, it might be figured that the tripping of windmills result from severe voltage dips brought on by tripping of adjacent feeders due to feeder fault, mostly on the planet fault condition. Throughout the voltage dip, feeder current roseate abnormally creating severe stain for the aero generator, and related Transformers. Frequent pressure may ultimately damage the creator and Transformers also. There are numerous other occasions where dips saved minus the windmill Tripping. During the sort of condition on 5-6-'08 at 18.38 h there were dip in voltage in the feeder. On this condition there was clearly intense raise of feeder current in addition to feeder current increased by 400 %.

The windmill generator sustained your fault condition and the generator current increased by 209 %. This disorder will also be injurious to the generator if frequent dip throughout voltage and swell in insert current affects the generator. During one condition it absolutely was observed that there were an over voltage caused due to

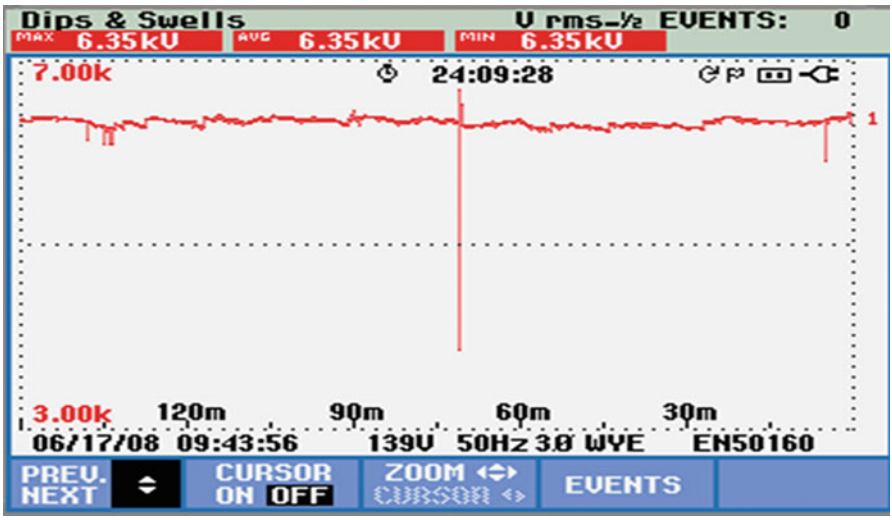


Fig. 8.24 Voltage dip in WM feeder

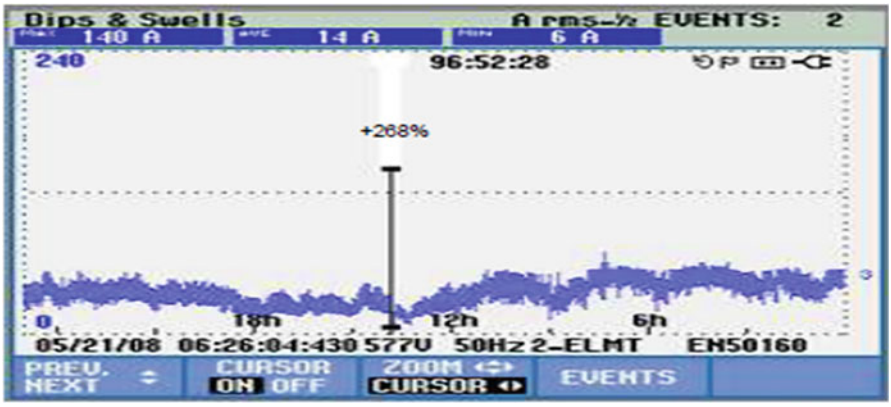


Fig. 8.25 Current rise in WM feeder

tripping in the feeders and before the voltage declined to zero economic value. Rrt had been observed the feeder voltage rose by 16.3 % before falling to absolutely no value. These phenomena may be due to discharge of stored energy with the Power factor correcting capacitors. This can be avoided by installing quick separate switches in case of voltage falling to zero importance. PQ analysis and recommendations Studies show that nearly 60 % of PQ issues are contributed by means of voltage sags and 29 % simply by voltage swells. Industrial customers are impacted 7–8 times by power electronic voltage sags than by means of outages.

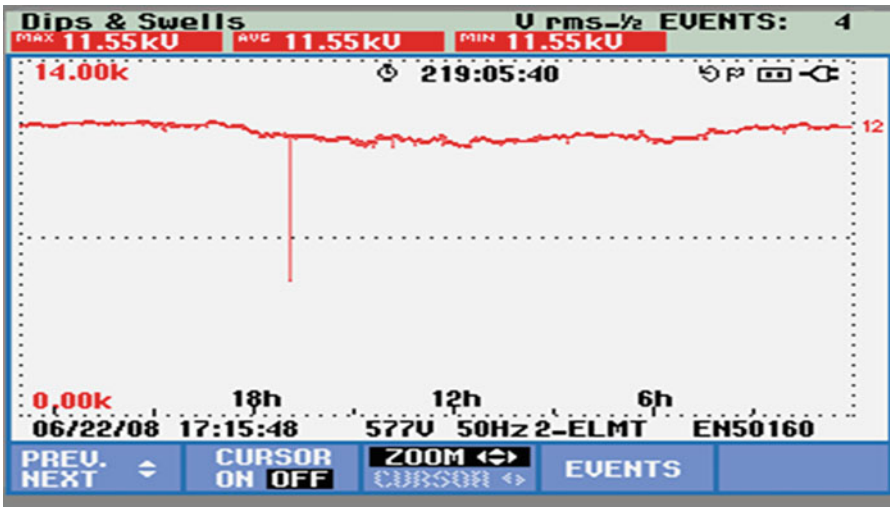


Fig. 8.26 Voltage dip

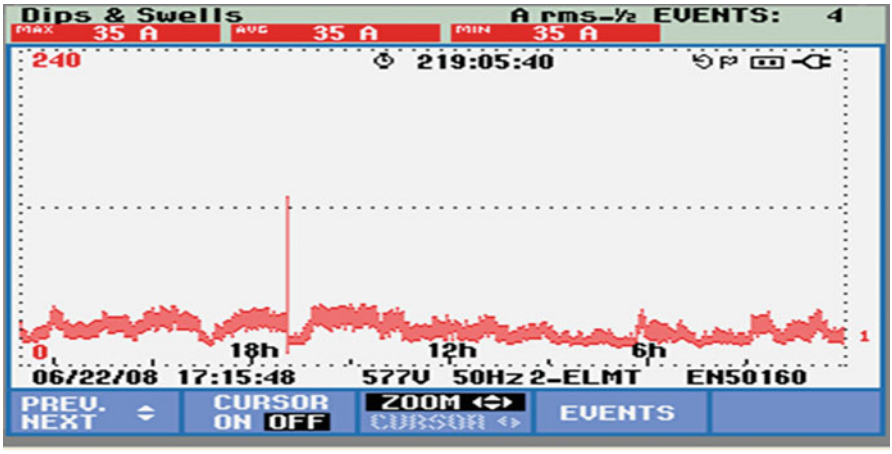


Fig. 8.27 Tripping of WM due to sag

To conquer these issues following recommendations were suggested:

1. To minimize the fault tripping from the feeders, it was recommended:
   (a) To pay off fouling trees.
   (b) To re also-sag the conductor within the feeders avoiding swinging of conductors during windy seasons.
   (c) Insulated conductors can be viewed in a few vulnerable areas.
   (d) Replace alleged insulators.

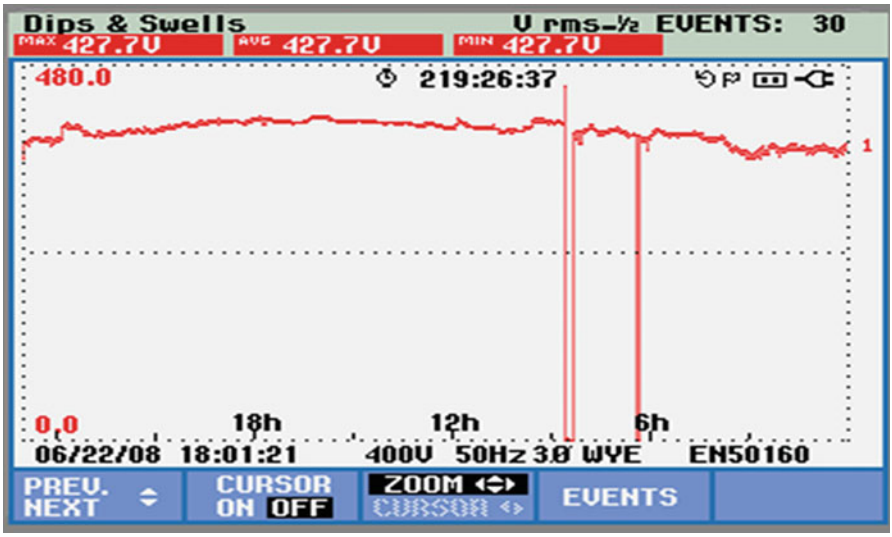


Fig. 8.28 Voltage rise in WM during supply failure

2. To setup improved version of relays inside feeder breaker to minimize the fault clearing time or otherwise prolonged fault condition could be injurious on the generator.
3. Certain kind of earth fault is not cleared or gets delayed reply through the relay caused by low fault current (due higher fault impedance). This type of situation might be overcome by installing improved variation of earth fault relay which may sense negative sequence/positive routine unbalance current and beneficial to detect weak earth faults. This would avoid persisting earth fault which often prolongs dip duration.
4. Around riding facility from the control circuit without injuring the generator/turbine.

8.10.1 Topology for Power Quality Improvement

The STATCOM based current manage voltage source inverter injects the actual in the grid so that this source current are harmonic free of charge and their phase-angle with respect to source voltage carries a desired value. The injected recent will block out the reactive part and harmonized the main load and induction generator latest, thus it improves the ability factor along with the power quality. To perform these goals, the grid voltages are sensed and are also synchronized in generating the existing command for the inverter. The grid linked strategy is implemented for power quality improvement at point of common coupling (PCC). The grid connected organization contains wind energy generation system as well as battery energy storage system having STATCOM.

Table 8.3 System parameters

S. No.	Parameters	Ratings
1	Grid voltage	3-phase, 415 V, 50 Hz
2	Induction motor/ generator	3.35 kVA, 415 V, 50 Hz, P = 4, Speed = 1,440 rpm, Rs = 0.01 Ω, Rr = 0.015 Ω, Ls = 0.06 H, Lr = 0.06 H
3	Line series inductance	0.05 mH
4	Inverter parameters	DC-link voltage = 800 V, DC-link capacitance = 100 μF, switching frequency = 2 kHz
5	IGBT rating	Collector voltage = 1,200 V, forward current = 50 A, Gate voltage = 20 V, Power dissipation = 310 W
6	Load parameter	Non-linear load 25 kW

8.10.1.1 Wind Energy Generating System

Within this configuration, wind generations provide constant speed topologies with pitch control turbine. The induction generator is needed within the scheme due to its simplicity, it doesn't require a separate field circuit, it could accept constant and variable loads, and contains natural protection against short. The system parameters are shown in Table 8.3.

8.10.1.2 BESS-STATCOM

The battery energy storage program (BESS) is used as a power storage element for the reason for voltage regulation. The BESS will naturally maintain dc capacitor voltage regular and is best suited with STATCOM since it rapidly inserts or absorbed reactive power for you to stabilize the grid system. It also control the distribution and transmission system in a very fast charge. When power fluctuation occurs inside the system, the BESS can be familiar with level the power fluctuation through charging and discharging operation. Battery is connected in parallel towards the dc capacitor of STATCOM.

The STATCOM is a three-period voltage source inverter having the particular capacitance on its DC and connected at the place of common coupling. The STATCOM injects a compensating existing of variable magnitude and regularity component at the bus involving common coupling.

8.10.1.3 System Operation

The shunt connected STATCOM with battery energy storage is connected with the port of the induction generator (Fig. 8.29) and also non-linear load at your PCC in the grid process. The STATCOM compensator output is actually varied according to the controlled strategy, so as to conserve the power quality norms in this grid system. The current command strategy is included in the actual control scheme that

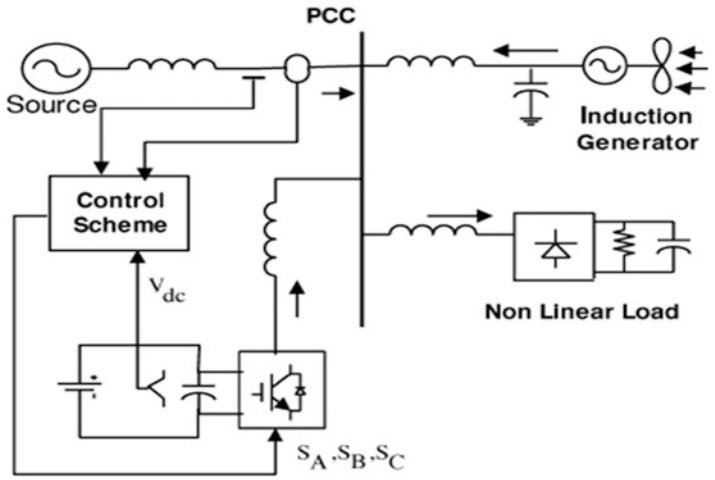


Fig. 8.29 System block diagram

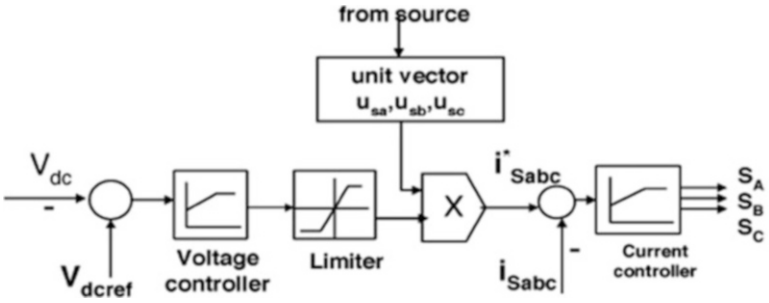


Fig. 8.30 Control system scheme

defines the actual functional operation of the STATCOM compensator in the grid. A single STATCOM using covered gate bipolar transistor is suggested to have a reactive strength support, to the induction generator and to the nonlinear weight in the grid system.

In three-phase balance system (Fig. 8.30), this RMS voltage resource amplitude is determined at the sampling frequency from the source phase electric potential and is also expressed, as test template Vsm, tried peak voltage is given in Eq. 8.19,

$$V_{sm} = \left\{ \frac{2}{3} \left(V_{sa}^2 + V_{sb}^2 + V_{sc}^2 \right) \right\}^{1/2} \tag{8.19}$$

The in-phase unit vectors are obtained from AC source – phase voltage and the RMS value of unit vector as shown in Eq. 8.20,

$$u_{sa} = \frac{V_{sa}}{V_{sm}}, u_{sb} = \frac{V_{sb}}{V_{sm}}, u_{sc} = \frac{V_{sc}}{V_{sm}} \tag{8.20}$$

The in-phase generated reference currents are derived using in-phase unit voltage vector is given by Eq. 8.21,

$$i^*_{Sa} = I.u_{Sa}, i^*_{Sb} = I.u_{Sb}, i^*_{Sc} = I.u_{Sc} \tag{8.21}$$

where I is proportional to magnitude of filtered source voltage for respective phases. This ensures that the source current is controlled to be sinusoidal. The unit vectors implement the important function in the grid connection for the synchronization for STATCOM. This method is simple, robust and favorable as compared with other methods.

8.10.2 SIMULINK Model of Grid Connected WECS

The wind energy generating system is connected with grid having the nonlinear load. The SIMULINK model is shown in Fig. 8.31. The source current and voltage waveforms without compensation is shown in Figs. 8.32 and 8.33.

8.10.3 SIMULINK Model of Grid Connected WECS with STATCOM

The control scheme is simulated using SIMULINK in power system block set as shown in Fig. 8.34.

The DC-link voltage regulates the source current in the grid system, so the DC-link voltage is maintained constant across the capacitor as shown in Fig. 8.35. The current through the dc link capacitor indicating the charging and discharging operation is as shown.

8.10.4 FFT Analysis

The FFT analysis of the Grid connected WECS is performed and the outputs are shown in Fig. 8.36 (without STATCOM controller) and Fig. 8.37 (with STATCOM controller).

In this simulation, various power quality issues related to grid connected WECS are studied. The major power quality issues, its causes and consequences are analyzed. The possible solutions for mitigating those issues were suggested. A grid connected WECS with SCIG is simulated using MATLAB/SIMULINK. The

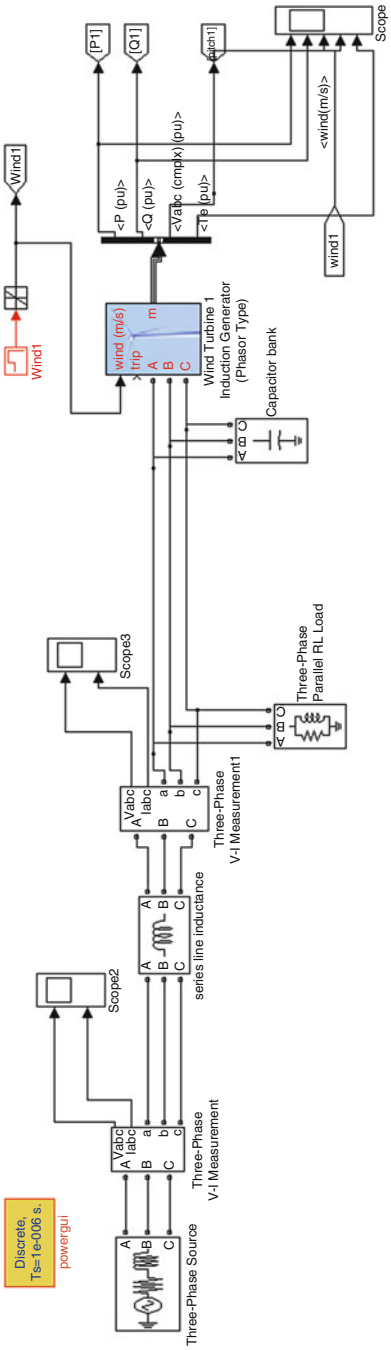


Fig. 8.31 Grid connected WECS

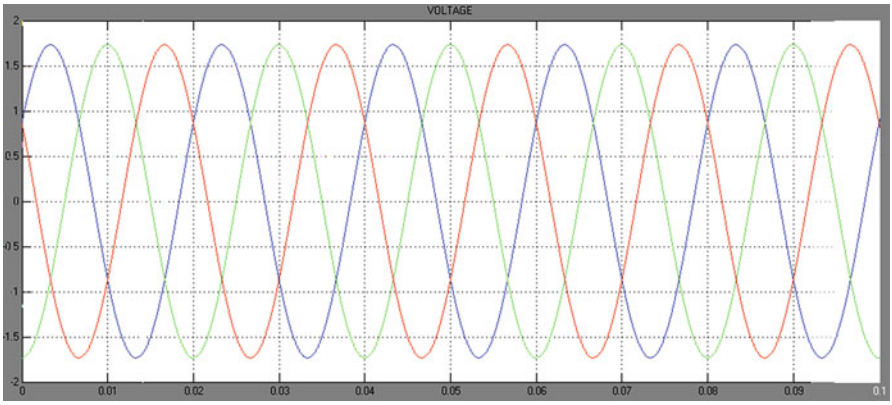


Fig. 8.32 Voltage at PCC (time v/s voltage (in pu))

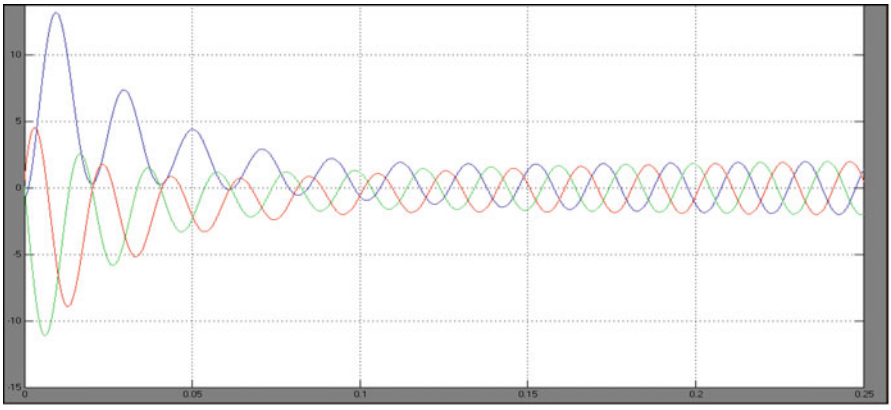


Fig. 8.33 Source current (time v/s current (in pu))

performance of the system is analyzed with a non linear load and during fault conditions. Any avoidance of downtime due to PQ related issue is direct contributor to revenue of the wind mill owner by avoiding the failure to supply to the grid. Reactive power draw during starting and voltage sag related events for grid connected wind mill are critical power quality areas that require attention. Also a STATCOM-based control scheme for power quality improvement in grid connected wind generating system is used for the comparative study on the system. The operation of the control system developed for the STATCOM in MATLAB/ SIMULINK for maintaining the power quality is simulated. It maintains the source

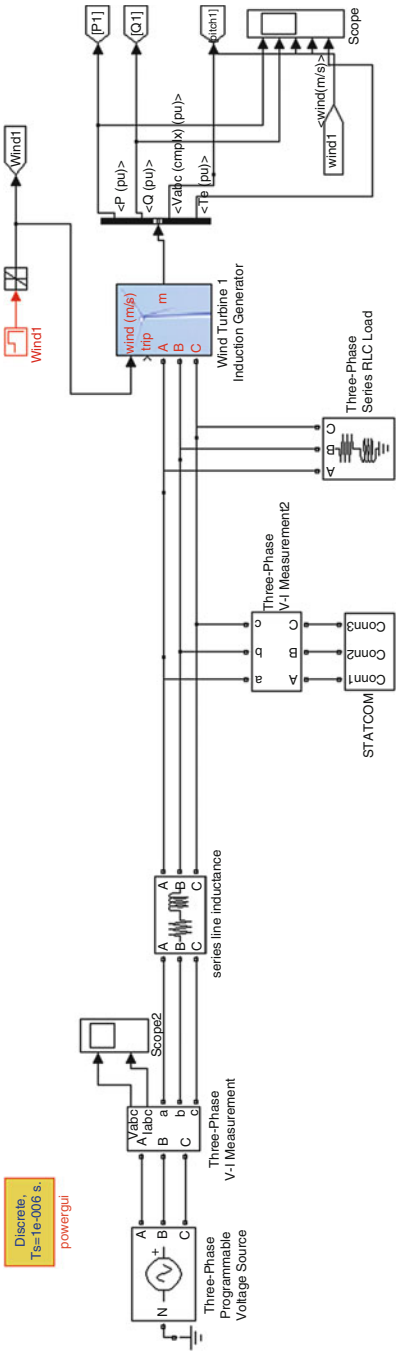


Fig. 8.34 Grid connected WECS with STATCOM

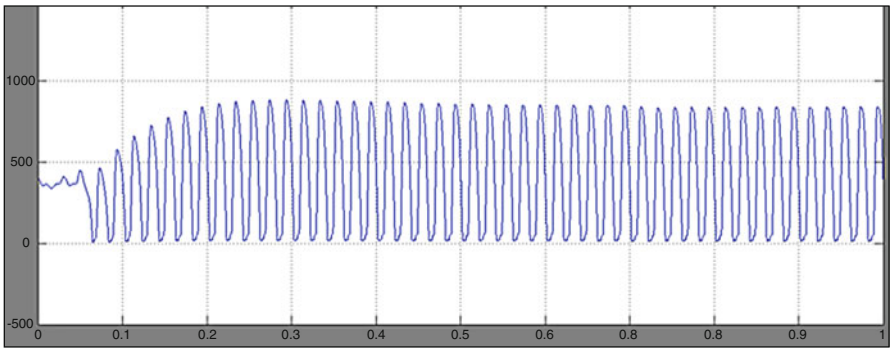


Fig. 8.35 Current through capacitor

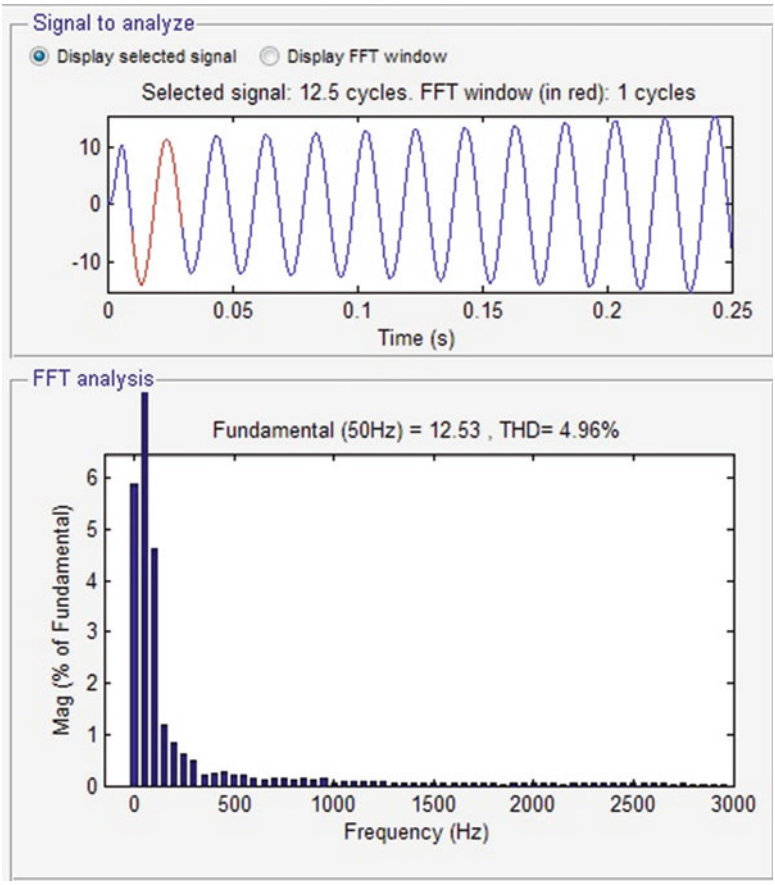


Fig. 8.36 FFT analysis without controller (THD = 4.96 %)

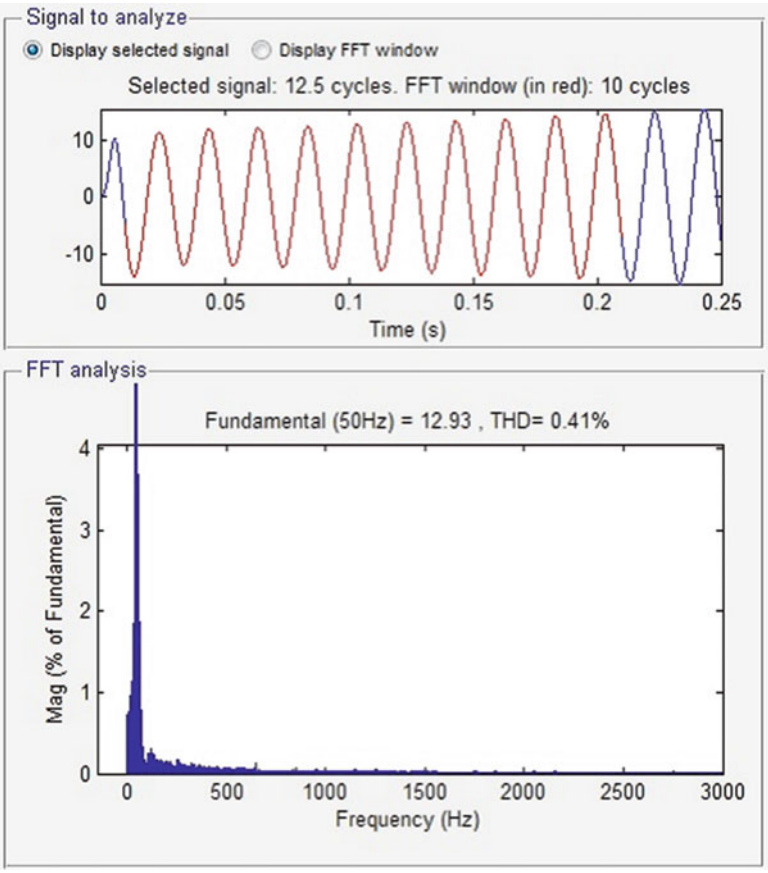


Fig. 8.37 FFT analysis with controller (THD = 0.41 %)

voltage and current in-phase and support the reactive power demand for the wind generator and load at PCC in the grid system, thus it gives an opportunity to enhance the utilization factor of transmission line.

8.11 Summary

In this chapter, the basic concepts of harmonics and power quality issues are discussed. The IEEE and SEMI standards associated with power quality are explained in detail. The measurement procedure for power quality in real time case studies is elaborated with suitable MATLAB/SIMULINK models. Reactive power compensation using custom power devices such as DSTATCOM, DVR and UPQC are given with relevant SIMULINK models. In addition, the power quality

problems and standards associated with power quality issues, and harmonic reduction in Wind Energy Conversion Systems with power quality issues and a case study are also described in detail.

Review Questions

1. Mention issues related to power quality.
2. What are the sources and effects of power quality problems?
3. State the suitable methods for reducing harmonics in renewable energy systems.
4. How is power quality measured in solar PV systems? Explain with a SIMULINK model.
5. Discuss the role of converters in reducing harmonics in renewable energy systems.
6. Address reactive power compensation using DSTATCOM, DVR and UPQC.
7. What is the role of Rotary Phase Shifter in reactive power compensation?
8. What do you mean by Fault Ride Through technique?
9. Discuss power curtailment with respect to wind energy conversion systems.

Bibliography

Ajami A, Taheri N, Younesi M (2009) A novel hybrid fuzzy/LQR damping oscillations controller using STATCOM. Second international conference on computer and electrical engineering

Akagi H. Instantaneous reaction power theory. Wiley

Akagi H (1996) Generalised instantaneous reactive power theory for three phase power systems. IEEE Proc 45(1)

AL-Ismail FS, Abido MA (2011) The impact of statcom based stabilizers on power system stability, using intelligent computational optimization approach. Innovative Smart Grid Technologies Asia (ISGT), 2011 IEEE PES, pp 1–13

Autoridad de Energía Eléctrica de Puerto Rico. Reglamento para la Interconexión de Generadores con el Sistema de Distribución Eléctrica (propuesta). http://www.prepa.com/. Accessed Apr 2008. [82] Puerto Rico Net Metering Law (Law 114), Aug 2007

Ayob SM, Yee CH, Muhamad ND, Jusoh A (2005) A new hybrid multilevel inverter topology with harmonics profile improvement. IEEE Trans Power Electron Drives Syst, ISSN: 0-7803-9296-5/05, pp 999–1002

Bode GH, Loh PC, Newman MJ, Holmes DG (2005) An improved robust predictive current regulation algorithm. IEEE Trans Ind Appl 41(6):1720–1733

Chakrabarti, Abhijith (2010) An introduction to reactive power control and voltage stability in power transmission systems. PHI, New Delhi

Dixon J, Moran L, Rodriguez J (2005) Reactive power compensation technologies: state of art review. Proc IEEE 93(12):2144–2164

Goel N, Patel RN, Chacko ST (2010) Genetically tuned STATCOM for voltage control and reactive power compensation. Int J Comput Theor Eng 2(3)

Hammad AE (1995) Comparing the voltage source capability of present and future var compensation techniques in transmission systems. IEEE Trans Power Deliv 1(1)

Hart DW (1997) Introduction to power electronics. Prentice Hall, New Jersey

Hingorani NG (2000) Understanding FACTS. IEEE press, New York

IEC 61000-3-6:1996 Electromagnetic compatibility (EMC) – Part 3: Limits – Section 6: Assessment of emission limits for distorting loads in MV and HV power systems. Basic EMC publication

Jin T, Li L, Smedley KM. A universal vector controller for four-quadrant three-phase power converter

Joos G (1991) Performance analysis of a PWM inverter VAr compensator. IEEE Trans Power Electron 6(3):380–391

Kalantar M, Mousavi SMG (2010) Dynamic behaviour of a stand-alone hybrid power generation system of wind turbine microturbine, solar array and battery storage. Appl Energy 87:3051–3064, Elsevier

Kouro S, Bernal R, Miranda H, Silva CA, Rodriguez J (2007) High-performance torque and flux control for multilevel inverter fed induction motors. IEEE Trans Power Electron 22(6):2116–2123

Kutkut NH, Divan DM, Novotny DW, Marion RH (1998) Design considerations and topology selection for a 120-kW IGBT converter for EV fast charging. IEEE Trans Power Electron 13:169–178

Leyva-Ramos J, Morales-Saldana JA (1998) A design criteria for the current gain in current programmed regulators. IEEE Trans Ind Electron 45(4):568–573

Lindgren M, Svensson J (1998) Control of a voltage-source converter connected to the grid through an LCL-filter – application to active filtering. Proc IEEE PESC 1:229–235

Maimone G (2010) Application note. Selecting L and C components in the power stage of the MC34700 switching regulators. Freescale Semiconductor, AN4067 Rev. 1.0, 11/2010

Mienski R, Pawelek R (2004) Shunt compensation for power quality improvement using a STATCOM controller: modeling and simulation. IEEE Proc Gener Trans Distrib 151(2):274

Miller TJE (2010) Reactive power control in electric systems. Wiley, New York

Mishra M, Ghosh A, Joshi A (2003) Operation of a DSTATCOM in voltage control mode. IEEE Trans Power Deliv 18(1):258–264

Moran LT, Ziogas PD, Joos G (1989) Analysis and design of a three phase current source solid state vary compensator. IEEE Trans Ind Appl 25(2):356–365

Moran LA, Dixon JW, Wallace RR (1995) A three phase active power filter with fixed switching frequency for reactive power and current harmonic compensation. IEEE Trans Ind Electron 42:402–408

Najafi E, Yatim AHM (2010) A D-STATCOM based on Goertzel algorithm for sag detection and a novel current mode controller. Industrial Electronics and Applications (ICIEA), June 2010, pp 1006–1011

Nastran J, Cajhen R, Seliger M, Jereb P (1994) Active power filters for nonlinear AC loads. IEEE Trans Power Electron 9(1):92–96

Poh CL, Donald GH (2005) Analysis of multiloop control strategies for LC/CL/LCL filtered voltage-source and current-Source inverters. IEEE Trans Ind Appl 41:644–654

Ranjith Kumar K, Sadanandam P (2011) GA for optimal PI in DC voltage regulation of D-STATCOM. Int J Electr Comput Eng 1(2):110–118

Rashid MH (2006) Power electronics devices, circuits and applications. Academic Press, San Diego

Schauder C, Mchta H (1993) Vector analysis and control of advanced static VAR compensators. IEE Proc C Gener Transm Distrib 140:299–306

Shen D, Lehn PW (2002) Modeling, analysis and control of a current source inverter based STATCOM. IEEE Trans Power Deliv 17:248–253

Singh B (2009) Static synchronous compensator (STATCOM): a review. IET Power Electron 2 (4):297–324

Singh B, Mishra V, Bhatt RKP (2003) Performance analysis of static condenser for article for copyediting voltage regulation, power factor correction and load balancing, Institution of Engineer's m, vol 84

Sun J, Czarkowski D, Zabar Z (2002) Voltage flicker mitigation using PWM-based distribution STATCOM. IEEE conference, pp 616–621

Voraphonpiput N (2005) STATCOM analysis and controller design for power system voltage regulation. Transmission and distribution conference and exhibition: Asia and Pacific, 1–6, IEEE/PES

Yaleinkaya G (1999) Characterization of voltage sags in industrial distribution systems. IEEE Trans Ind Appl 12(3)

Ye V, Kazerani M, Quintana V (2005) Current source converter based STATCOM: modeling and control. IEEE Trans Power Deliv 20(2):795–800

Youb L, Craciunescu A (2009) Direct torque control of induction motors with fuzzy minimization torque ripple. Proc WESCO 2:713–717

Zhang J, Zon Y, Zhang X, Ding K (2003) Study on a modified multilevel cascade inverter with hybrid modulation. IEEE Power Electronics Drives System, ISSN: 0-7803-7233-6/01, pp 379–383

Chapter 9
Fuel Cell and Converters

Learning Objectives
On completion of this chapter the reader will have knowledge on:

- Need for Fuel Cell and types of fuel cell.
- Comparative Analysis and Characteristic behaviour of fuel cells.
- MATLAB/SIMULINK implementation of fuel cell model.
- Types of converters and their implementation using MATLAB/SIMULINK.
- Series architecture, DC bus distribution architecture, High frequency AC (HFAC) distribution architecture, Multilevel architecture models for high power and high voltage applications.

9.1 Introduction

Depletion of fossil fuels, increasing energy consumption and rising public awareness for environmental pollution effects have turned the focus of research work towards alternative renewable energy sources. Fuel cells are one of the most promising sources of energy because of their high efficiency and low environmental impact. Fuel cell is a device which was invented in nineteenth century, but it took so long to turn our minds towards fuel cell due to several challenges in implementing it in various applications. As it is focussed only in recent years and considered as a relatively new technology, the perception of risk and lack of user experience are obstacles. The capital expense of fuel cell systems may have been the most significant barrier in the past, but as technology improves, this may no longer be the case. Some tedious obstacles are: (i) No acceptance of reverse current, (ii) Low output voltage and its degradation with age and current, (iii) Low efficiency with output ripple current, (iv) Limited overload capability and (v) Respond sluggishly to step variation in load. To overcome these technical challenges, power converters

© Springer International Publishing Switzerland 2015

S. Sumathi et al., *Solar PV and Wind Energy Conversion Systems*,
Green Energy and Technology, DOI 10.1007/978-3-319-14941-7_9

are often necessary to boost and regulate the output voltage to provide an applicable DC power source. In this chapter, the fuel cell technology, converter types and their MATLAB/SIMULINK models are discussed. Architecture for multiple fuel cell for applications with high power are also delineated.

9.2 Fuel Cell Technology

Fuel cells actually have been known to science for more than 150 years. Though generally considered a curiosity in the 1800s, fuel cells became the subject of intense research and development during the 1900s. The basic operation of fuel cell is very simple. In 1839, lawyer and scientist, William Groove discovered the reverse electrolysis of water. By combining hydrogen and oxygen in a particular configuration, electricity could be produced. A fuel cell is an electrochemical cell that derives electrical energy from spontaneous redox reaction taking place within the cell. It is similar to that of battery as it converts the chemical potential energy into electrical energy by means of electrochemical process. Both batteries and fuel cells convert chemical potential energy into electrical energy and also, as a by-product of this process, into heat energy. However, a battery holds a closed store of energy within it and once this is depleted the battery must be discarded, or recharged by using an external supply of electricity to drive the electrochemical reaction in the reverse direction. A fuel cell, on the other hand, uses an external supply of chemical energy and can run indefinitely, as long as it is supplied with a source of hydrogen and a source of oxygen (usually air). A basic schematic of fuel cell is shown in Fig. 9.1.

Fuel cell uses hydrogen-rich fuel and oxygen from air to produce electricity. It continues to generate electric power until these substances are fed into the cell. The process is implemented by using two electrodes. At one electrode, hydrogen fuel is oxidised and at the other electrode oxygen is reduced. Electrolyte which is in between two electrodes transmits ions from anode to cathode but does not allow movement of electrons. Thus the reactions exchange electrons through an external circuit which gives the electrical power to the load. The reactants flow into the cell and the reaction products flow out of it, while the electrolyte remains within it. The basic reactions involved in energy conversion of Hydrogen-Oxygen fuel cell are:

$$\text{At Anode} : 2H_2 \rightarrow 4H^+ + 4e^- \tag{9.1}$$

$$\text{At Cathode} : O_2 + 4H^+ + 4e^- \rightarrow 2H_2O \tag{9.2}$$

$$\text{Net reaction} : 2H_2 + O_2 \rightarrow 2H_2O \tag{9.3}$$

When pure hydrogen is used as fuel the products are thus water and energy which makes it advantageous. The fuel cell provides DC voltage which can be used for various applications directly or by converting to AC with the help of inverter. Pure Hydrogen can be obtained by using fuel reformer which consumes natural gas, coal and biomass to generate hydrogen.

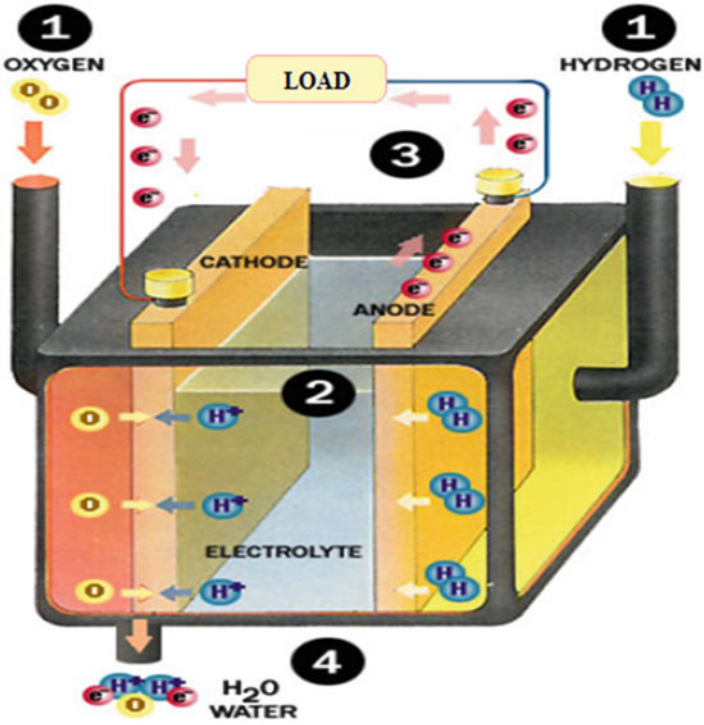


Fig. 9.1 Fuel cell process ((i)-Fuel supply inlet; (ii)-hydrogen through ion transfer electrolyte; (iii)-electron transfer through external circuit; (iv)- reaction product water outlet)

As per the required power rating fuel cells are bundled together in series and parallel combinations known as Stack. Its rating ranges from a few kilowatts to a hundred kilowatts (Fig. 9.2).

9.2.1 Importance of Fuel Cell

At present the entire world is in energy and environment crisis which forces people to go for a clean and more efficient renewable energy sources. Generating renewable electricity is an important way to reduce carbon dioxide (CO_2) emissions and many countries are installing wind and solar power plants to meet the targets for reducing CO_2 emission. One drawback of these energy sources is their variability: the wind tends to blow intermittently and solar power is only available during the daytime. Storing excess renewable energy generated during times of plenty is a difficult task. One of the alternative sources of power is fuel cell. Excess electricity can be fed into an electrolyser to split water into its constituent parts, oxygen and hydrogen. The hydrogen is then used in fuel cells to produce electricity when

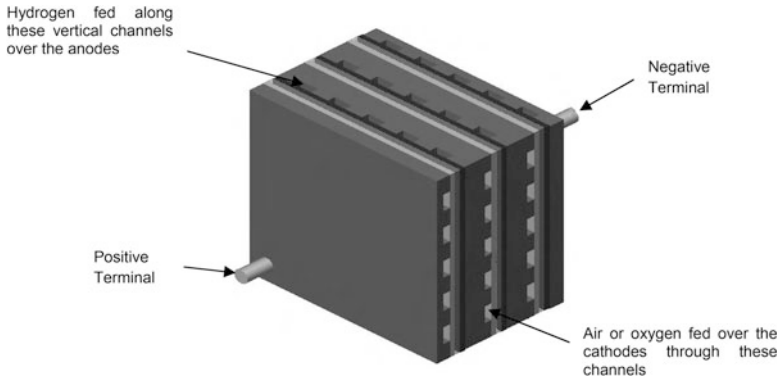


Fig. 9.2 Fuel cell stack connection using bipolar plates

needed, releasing the stored energy. Fuel cells also promise greater operating efficiency with lower emissions over conventional power sources used today. Unlike internal combustion engines, the fuel is not combusted the energy instead being released electro catalytically. This allows fuel cells to be highly energy efficient, especially if the heat produced by the reaction is also harnessed for cogeneration. The advantages of fuel cell are its high efficiency, low environmental impact, reliable and very quiet operation. But it has some technical challenges which includes expensiveness in manufacturing, production and storage of hydrogen-a difficult task and extreme heat generation in some models.

The major applications are: (i) Stationary (A.C. Applications)-Power plants, Residential use and Commercial use; (ii) Enclosed Environments (D.C. Applications)-Auxiliary power unit, Space Station, Space vehicles (space shuttle) and Underwater vehicles (submarine); (iii) Transportation and portable electronics (D.C. Applications)-Personal Vehicles (ZEV's -Zero Emission Vehicles), Public Transportation, Commercial and Military Vehicles.

9.2.2 Types of Fuel Cells

There are many different types of fuel cells which are mainly distinguished by the electrolyte/fuel that is used, though there are other important differences in performance parameter as well. The general classifications of fuel cells are: (i) Alkaline Fuel Cell (AFC); (ii) Proton Exchange Membrane Fuel Cell (PEMFC); (iii) Phosphoric Acid Fuel Cell (PAFC); (iv) Molten Carbonate Fuel Cell (MCFC); (v) Solid Oxide Fuel Cell (SOFC).

Table 9.1 shows the comparison of different fuel cells based on various parameters. The operating temperature of the fuel cell can be determined by the choice of electrolyte and the type of material used for it. Liquid electrolytes limits the operating temperature to about 250 °C or below because of the rapid degradation

Table 9.1 Comparison of different fuel cells

	AFC	PEMFC	PAFC	MCFC	SOFC
Electrolyte	Solution of KOH in water	Solid polymer (Nafion)	Liquid phosphoric acid in SiC matrix	Lithium and potassium carbonates in porous matrix	Solid oxide electrolyte (Yttria stabilised Zirconia)
Fuel	Pure H_2	Pure H_2	Pure H_2	H_2, CO, hydrocarbons	H_2, CO, hydrocarbons
Operating temperature, °C	50–100	30–80	160–220	600–700	600–1,000
Catalyst	Platinum	Platinum	Platinum	Electrode material (Nickel)	Nickel
Cell reaction	At anode: $2H_2 + 4OH^- \rightarrow 4H_2O + 4e^-$	At anode: $2H_2 \rightarrow 4H^+ + 4e^-$	At anode: $2H_2 \rightarrow 4H^+ + 4e^-$	At anode: $CO_3^{2-} + H_2 \rightarrow H_2O + CO_2 + 2e^-$	At anode: $O^{2-} + H_2 \rightarrow H_2O + 2e^-$
	At cathode: $O_2 + 2H_2O + 4e^- \rightarrow 4OH^-$	At cathode: $O_2 + 4H^+ + 4e^- \rightarrow H_2O$	At cathode: $O_2 + 4H^+ + 4e^- \rightarrow H_2O$	At cathode: $CO_2 + \frac{1}{2}O_2 + 2e^- \rightarrow CO_3^{2-}$	At cathode: $O_2 + 4e^- \rightarrow 2O^{2-}$
Mobile ion	OH^-	H^+	H^+	CO_3^{2-}	O^{2-}
Efficiency	About 55 %	40–50 %	Around 45 %	60–70 %	About 60 %
Advantages	High efficiency, low oxygen reduction reaction losses	Rapid start up, high hydrogen power density	Good quality waste heat, 1.5 % CO tolerance, simple and stable	Fuel flexibility, good quality waste heat, inexpensive nickel catalyst, CO tolerance	Fuel flexibility, CO_2 tolerance, waste heat can be recycled, inexpensive nickel catalyst

(continued)

Table 9.1 (continued)

	AFC	PEMFC	PAFC	MCFC	SOFC
Disadvantages	Small amount of CO and CO_2 in the atmosphere degrade the operation, expensive catalyst used	Expensive platinum catalyst used, fuel used must be purified from CO, poor quality waste heat	Expensive platinum catalyst used, internal parts must withstand corrosive acid, slow start up, loss of electrolyte	CO_2 injection necessary at the cathode, extremely long start up, electrolyte maintenance	Inactivity of electrolyte below 600 °C, long start up time
Applications	(i) Apollo space craft to provide both electricity and drinking water	(i) Mainly automotive applications	(i) Extraordinary premium stationary power system	(i) large stationary power plants	(i) Large stationary power plants
	(ii) Space missions	(ii) Portable applications	(ii) Waste heat used for cogeneration systems	(ii) Waste heat used for cogeneration systems	(ii) Waste heat used for cogeneration systems
					(iii) Auxiliary power

and vaporization of fluids at higher temperatures. Low temperature fuel cells include AFC, PAFC and PEMFC types. The rate of chemical reaction is too slow in low temperature fuel cells and hence it requires precious nobel metals such as platinum at any one electrode or both to catalyse the reaction. As low temperature fuel cells cannot tolerate CO concentration in the fuel which causes degradation of the operation, it requires external reformer to purify the hydrogen. Their applications are mainly focused on vehicle applications which requires quick start up and higher power density.

Higher temperatures fuel cells include MCFC and SOFC which has an operating temperature of 500 ° C and above typically promote faster reactions. As high temperature fuel cells react more readily and efficiently, it does not require the precious nobel metal catalyst. It is also fuel flexible and do not necessitate the use of external reformer as hydrocarbon fuels can be internally converted to hydrogen or even directly oxidized electrochemically during cell reaction.

Fuel cell is also classified based on the type of fuel used. Direct Methanol Fuel cell (DMFC) uses liquid form of Methanol or alcohol as fuel directly instead of pure hydrogen. So it operates without reforming. DMFC is a subtype of PEMFC which uses polymer as electrolyte and other operations are similar to that of it. It suits for some applications where the power density can be low but the energy density must be high such as portable electronic systems of low power and running for long times. It operates at a low temperature range of 20–60 °C.

9.2.3 Electrical Behaviour of Fuel Cell

The cell potential vs current density behaviour of the fuel cell predominantly determines the performance of fuel cell systems. The theoretical open circuit voltage (E) of a hydrogen fuel cell is given by the formula

$$E = (-\Delta G)/2F \tag{9.4}$$

where ΔG indicates the Gibbs free energy and F indicates the Faraday's constant.

The open circuit voltage value of a single fuel cell is about 1.2 V. When the amount of current is increased, the voltage drop is also increased. This drop in voltage is due to the losses such as activation losses, fuel crossover, ohmic losses and concentration losses at the electrode and in the electrolyte.

Activation losses are dominant when the current density is low. It is due to the slowness of the electrochemical reaction of hydrogen and oxygen at the surface of the electrode. Some of the voltage is lost in transferring electrons between the electrodes which makes this loss as highly non linear with the increase in current. Fuel crossover and internal currents contribute less to the voltage losses when the cell is operated at high temperature. It takes place due to the passing of fuels and electron conduction through the electrolyte. Ohmic losses take place due to the resistance offered by the electrode and various interconnections to the flow of

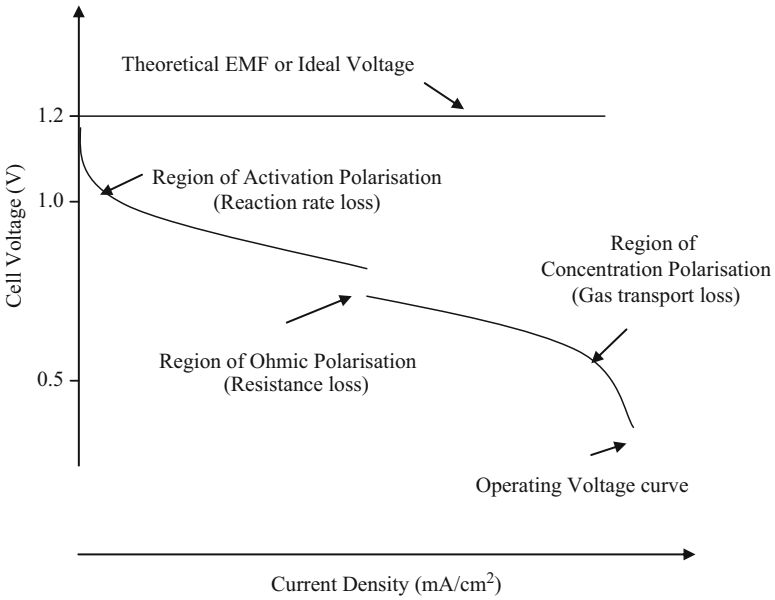


Fig. 9.3 Polarization curve of low temperature fuel cell, 70 °C

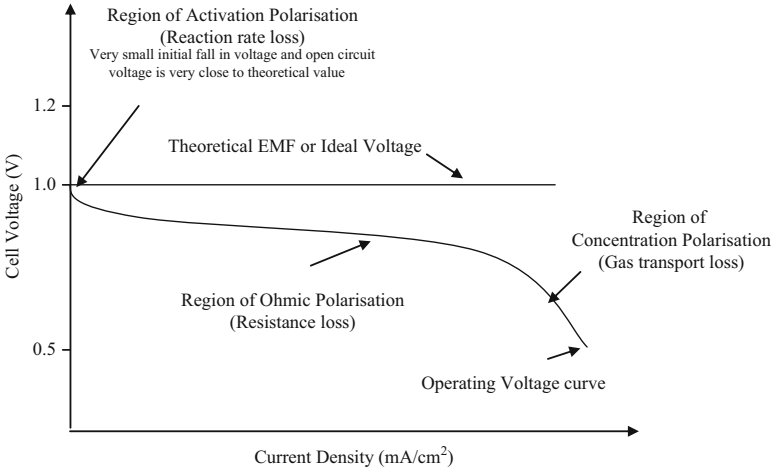


Fig. 9.4 Polarization curve of high temperature fuel cell, 800 °C

electron and also by the resistance to the flow of ions through the electrolyte. Ohmic losses are highly linear as it is purely dependent on the resistance. Concentration losses are due to the difference in the concentration of the reactants as the fuel is consumed. Only at high current densities, this loss will be dominant (Figs. 9.3 and 9.4).

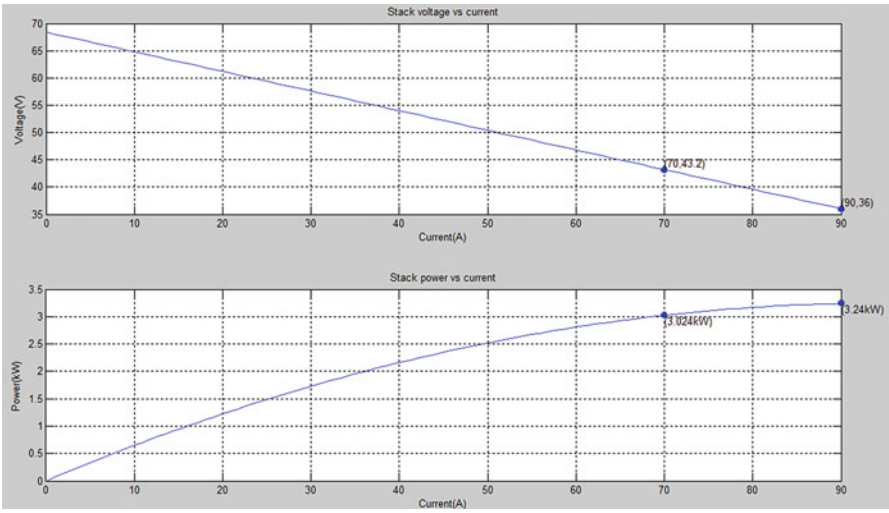


Fig. 9.5 Polarization curve of PEMFC

For low temperature fuel cell operating below 100 °C the open circuit voltage is less than the theoretical ideal value. When the current density increases the voltage decreases and losses will be high at high current densities.

For high temperature fuel cell operating about 800 °C the open circuit voltage is identical to its ideal value which is generally less than the ideal voltage value of low temperature fuel cell. But this is compensated when the fuel cell operates as the losses are less when compared with operating at low temperature. There will not be any sudden drop in voltage at the beginning which indicates no effect of activation losses.

Figure 9.5 shows the polarization curve of the selected PEM fuel cell stack using MATLAB/SIMULINK. The fuel cell stack produces an open circuit voltage of 68 V and 3 KW power at nominal operating point.

9.2.4 Need for Power Electronic Converters

All electrical power sources generate voltage which varies with time, temperature and other factors such as current. But fuel cells are badly regulated when compared to the other sources which is evident from its electrical characteristics (Figs. 9.3 and 9.4). Since the voltage of an elementary cell is only about 0.6–0.7 V at the rated current, the fuel cells are connected in series known as stack to produce a useful voltage. But higher stacking has a disadvantage of higher production cost, reducing the reliability and lifetime. Even when there is a small variation in one of its cell in stack the output will get heavily affected. Therefore the fuel cell stack output

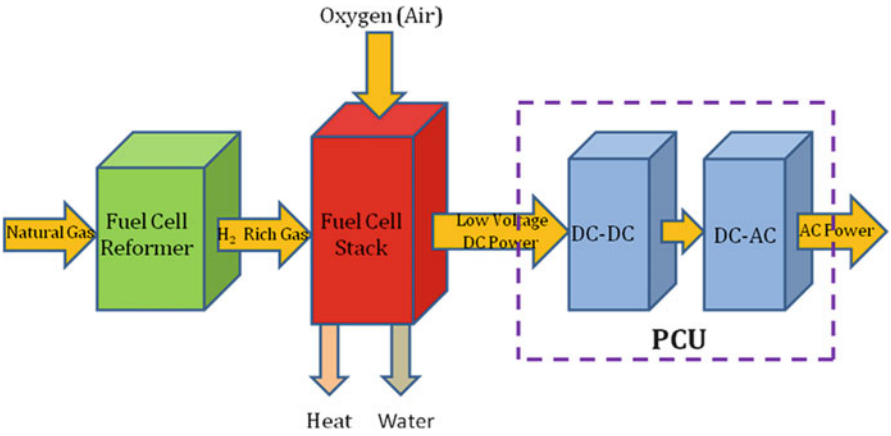


Fig. 9.6 Block diagram of fuel cell system

voltage is mostly limited to a maximum of 100 V to improve the lifetime and reliability. But various applications such as electric vehicles require high DC-bus voltage of few hundred volts to drive the power train. Therefore an effective DC-DC converter is needed to interface fuel cell stack with utility DC-bus (Fig. 9.6).

As fuel cell strongly varies with the load, the DC-DC converter should also serve as a voltage conditioning unit. The dynamic response of the fuel cell during load variations is very slow i.e. the output voltage cannot match the required demand and fluctuates. Typically, the cell voltage varies from 1 V to 400 mV, so a 60 % voltage variation must be managed. Then high stresses can be imposed on the switching devices. Also a diode is connected in series with the fuel cell module as fuel cells obstruct reverse current flow and do not absorb power back. Thus an additional energy storage system such as battery or super capacitor is required to store braking energy in vehicles and to manage high power transients. To implement this functionality Bidirectional DC-DC converter is linked in interfacing the energy storage system with the fuel cell system. One major problem with the DC-DC converter is the injection of ripple onto the fuel cell which affects the performance of the fuel cell. This ripple current is the result of switching characteristics of the electronic devices used in the power conditioning system which generates two components: a low frequency component and a high frequency component. The low frequency component has a frequency twice that of the output a.c frequency, generally in the range of 100 or 120 Hz. The high frequency component is in the range of kHz and is caused by the internal switching characteristics of the electronic devices. If the capacitor bank is added at the output of the fuel cell to absorb ripple current, the capacitor should be selected properly to avoid over stress on it. Moreover it increases the cost, size and reliability of the converter. The ripple factor must be lower than 5 % and switching frequencies must be greater than 1.25 kHz for the fuel cell output current to have mirror impact to the fuel cell operating conditions. The

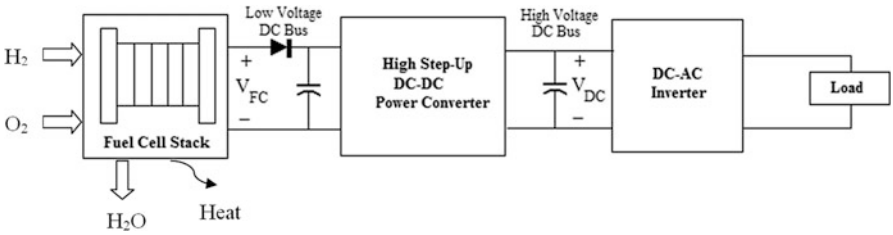


Fig. 9.7 General fuel cell power conditioning system

power electronic devices need to be thermally isolated from the fuel cell modules especially from high temperature fuel cells because power electronic units have high losses and it may even get failure under high temperature. Sometimes to provide electrical isolation between the low output voltage of the fuel cell and the high voltage DC-link, transformer will be added in DC-DC converters which protects the fuel cell. Thus the power conditioning unit plays an important role in all types of fuel cell applications. The basic power conditioning unit (Fig. 9.7) generally consists of a DC-DC converter to raise DC output voltage to DC bus voltage followed by a DC/AC inverter to convert DC bus voltage to AC voltage.

The power conditioning unit should be capable of controlling the fuel cell voltage and convert the fuel cell output to the appropriate type. It should be able to operate efficiently under all conditions which mainly depend upon the conduction losses and switching losses. To reduce the conduction losses, the number of components used in the converter and their operating ranges has to be reduced. The switching losses can be efficiently reduced by adapting soft switching techniques. Thus the configuration particularly number of stages and efficiency of individual components determine the overall efficiency of the power conditioning unit. It also depends on the mode of operation and it varies with the operating point of the system. Efficiencies close to 90 % can be achieved for a well-designed power conditioning system, and probably higher for single stage conversion without transformers. A limitation in power electronic interface is that it cannot perform efficiently beyond certain limit of voltage gain. Hence the fuel cell modules have to be designed in such a way to produce its minimum output voltage more than the least value required by the power electronics unit for the providing voltage gain during interfacing.

9.2.5 DC-DC Converters

DC-DC converters play an important role in fuel cell system to control and regulate the power output. Input to these converters is an unregulated DC voltage from fuel cell stack. It converts the unregulated DC voltage to a regulated voltage based on application.

The different DC-link voltage level based on its applications are 270 or 350 V for electric aircrafts, 270–540 V for electric vehicles, 350–750 V for locomotives, 48, 120 or 400–480 V for stand-alone or parallel grid connections. Therefore, a high step-up DC-DC converter is required to boost the low voltage output of the fuel cell stack into the high voltage at the DC bus. Due to non ideal characteristics of fuel cell the development and designing of power conditioning units play an important role to interface the fuel cell system with the end user. The main characteristics required for dc-dc converter are: (i) High efficiency in power conversion; (ii) High power density;(iii) Small size and light weight; (iv) Low electromagnetic interference (EMI); (v) Reduced ripple current to avoid the FC damage and increase its lifetime; (vi) Low cost.

The selection of proper switching devices also contributes to the efficient operation of the converter. Among all switching devices MOSFET and IGBT plays a wide role in efficient conversion especially the latter combines the advantages of MOSFET, BJT and GTO. Hence IGBT has a significant advantages such as fast switching, much less parasitic power to perform the switching function and reducing complexity by eliminating commutation circuits. But if the switching loss is the major constraint MOSFET is preferred than IGBT.

9.2.5.1 Types of DC-DC Converters

There are various topologies of unidirectional and bidirectional DC-DC converters suitable for fuel cell interface. Based on the existence of electrical barrier between the input and output, DC-DC converters are classified as Isolated and Non-Isolated Converters. The operation of a semiconductor device, during a given turn-on or turn-off switching transition, can be classified as hard switched, zero-current switched, or zero-voltage switched. Zero current switching (ZCS) and Zero voltage switching (ZVS) are the soft switching techniques in which zero-voltage switching comes at the expense of increased conduction loss. Based on switching topology used, DC-DC converters classified as soft and hard-switched converters. Soft switched converters are mainly adopted to reduce the switching losses over the device, to overcome the problems of switching stress and the EMI and to improve the efficiency at higher switching frequency.

9.2.6 Conventional Boost Converter

Among the DC-DC converters the efficiency of the conventional boost converter (Fig. 9.8) is always greater than the other converter topologies because it has reduced number of components and simplicity in control. It consists of an inductor for energy storage, a switch to control the output, a diode to isolate the output stage when the switch is on and a capacitor to reduce ripple. When the switch is closed (t_{on}) the input current flows through the inductor L and switch S. Hence inductor

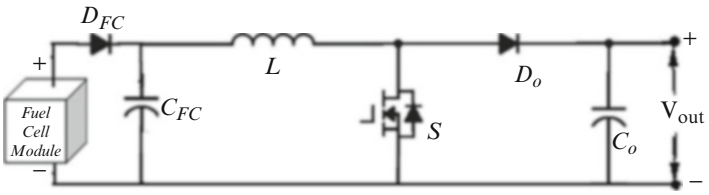


Fig. 9.8 DC-DC boost converter

stores some energy during this operating mode. When the switch is open (t_{off}) the current changes its path as inductor, diode, capacitor and load. The energy stored in the inductor is transferred to the load.

$$\text{During switching-on period } DT_s, \frac{di_L}{dt} = \frac{V_{in}}{L} \tag{9.5}$$

$$\text{During switching-off period } (1\text{-}D)T_s, \frac{di_L}{dt} = \frac{V_{in} - V_O}{L} \tag{9.6}$$

where i_L is the inductor current, V_{in} is the input voltage and V_o is the voltage across the load.

The output voltage for the selected duty cycle (D) is given by

$$V_o = \frac{V_{in}}{1 - D} \tag{9.7}$$

Some design parameters such as duty cycle, inductor values and design of output filter are to be considered for boosting the voltage to the required level.

Inductor selection is based on the changes in inductor current,

$$\Delta I_L = \frac{V_{in} D T_s}{2L} \tag{9.8}$$

Capacitor selection is based on the output ripple voltage,

$$\Delta V_o = \frac{V_o D T_s}{2RC} \tag{9.9}$$

where T_s is the switching time period.

The voltage gain of this boost converter is extremely high when the duty ratio is close to one. However, the switch turn-off period becomes short when the duty cycle increases and also large duty ratio leads to losses in power switches and diodes. It also cause reverse-recovery problem of diode. As the output voltage is very sensitive to changes in duty cycle it is difficult to stabilize the regulator. For high step-up conversion the current ripples on the devices are large which increases the power device conduction losses and turn-off current. The voltage stresses of the

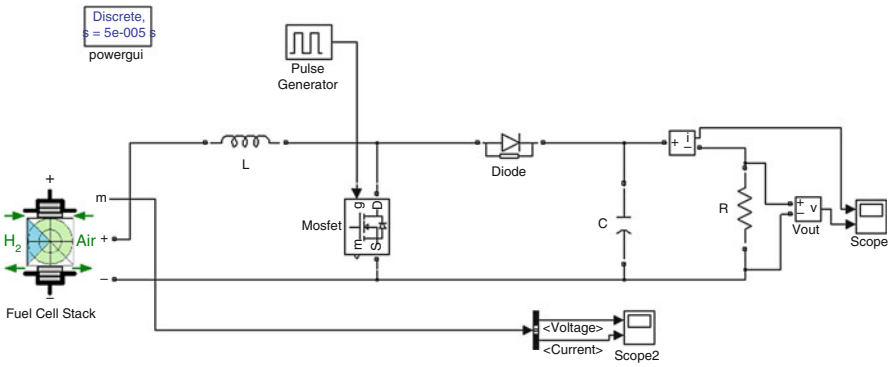


Fig. 9.9 MATLAB/SIMULINK model of the DC-DC boost converter

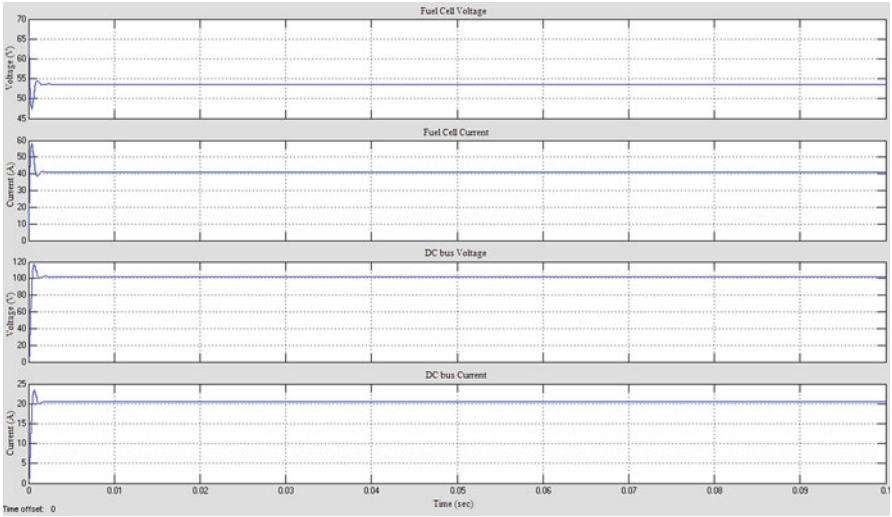


Fig. 9.10 Simulation results of DC-DC boost converter

switch and the diode are equal to the output voltage, which is large in high output voltage applications. Hence it requires high rating passive components. The cost of the switches with high voltage stress is rather higher than that of the switches with low voltage stress.

Figure 9.9 shows the MATLAB/SIMULINK model of the DC-DC boost converter.

Figure 9.10 shows the simulation results of the conventional DC-DC boost converter for 3 kW fuel cell stack input. For high conversion ratio greater than 5, the boost efficiency decreases drastically as a function of duty cycle. Thus conventional boost converter can be operated at reasonable duty cycle to achieve high efficiency and high voltage gain. Furthermore, the power level of the classical boost converter is limited and also it does not meet the criteria of electrical isolation.

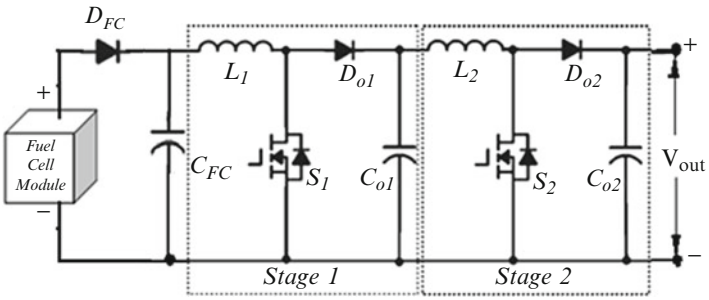


Fig. 9.11 Cascaded boost converter

9.2.7 Cascaded Boost Converter

The DC-DC converter should have a high voltage ratio to satisfy the requirements of various applications. The boost conversion ratio can be increased by connecting several boost components in series known as cascade connection. Important feature expected from the DC-DC converter is a low input current ripple. By cascading the current ripple can be significantly reduced to satisfy high step up requirements (Fig. 9.11). The first stage conversion is achieved with high switching frequency as the voltage stress on the devices is low. The second stage can be achieved with a low switching frequency to reduce the switching losses. The major limitation of cascade converters is the requirement of two sets of boost components, which is complex and expensive. However, the inductance requirement may be reduced if the switching frequency will increase, but this may be limited as semiconductor switching losses are increasing with frequency. Another issue in the cascade boost converters is the system stability which requires careful designing. Moreover, the output-diode reverse-recovery problem of the second stage is severe because a high voltage level should be sustained in the high output-voltage applications.

If the voltage across the capacitor C_1 is charged to V_1 and the voltage across the capacitor C_2 is charged to V_o, the current flowing through inductor L_2 increases with V_1 during the switching-on period DT_s and decreases with voltage $-(V_o-V_1)$ during the switching-off period $(1-D)\,T_s$. Thus the inductor selection is based on the ripple current ΔI_{L2} and ΔI_{L1} given by,

$$\Delta I_{L2} = \frac{I_{L2} D\left((1-D)^2\right) R}{f L_2} \tag{9.10}$$

$$\Delta I_{L1} = \frac{I_{L1} D\left((1-D)^4\right) R}{f L_1} \tag{9.11}$$

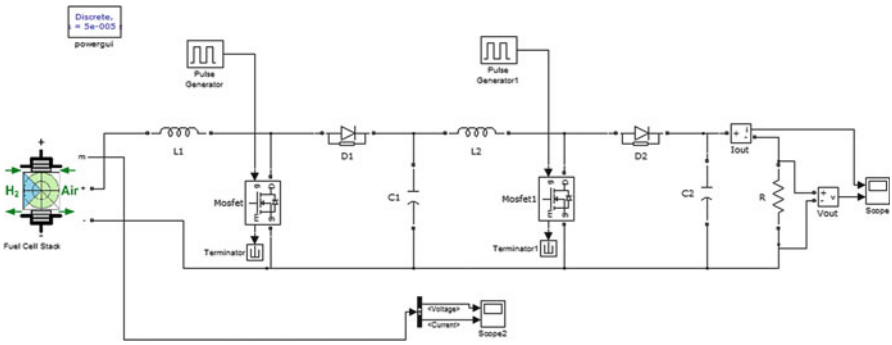


Fig. 9.12 MATLAB/SIMULINK model of cascaded boost converter

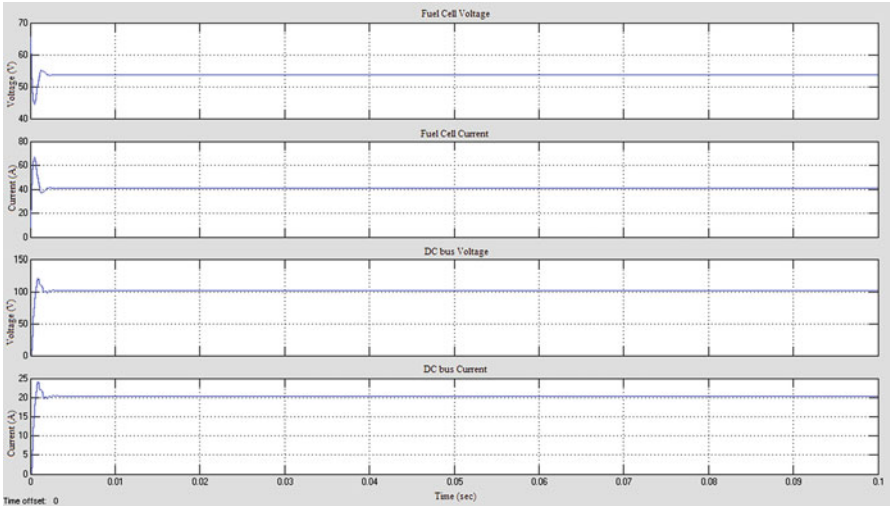


Fig. 9.13 Simulation results of cascaded boost converter

The capacitor selection is based on the ripple voltage

$$\Delta V_o = \frac{V_o(1-D)}{Rf\,C_2} \tag{9.12}$$

Figure 9.12 shows the MATLAB/SIMULINK model of the cascaded boost converter. The model is designed for 3 kW fuel cell stack input. Figure 9.13 shows the simulation results of cascaded boost converter obtained for the fuel cell input.

In order to reduce the circuit complexity the two switches can be integrated into one switch. The integrated cascade boost converter is shown in Fig. 9.14. When switch S turns on the inductors $L1$ and $L2$ stores energy. When switch S turns off $L1$

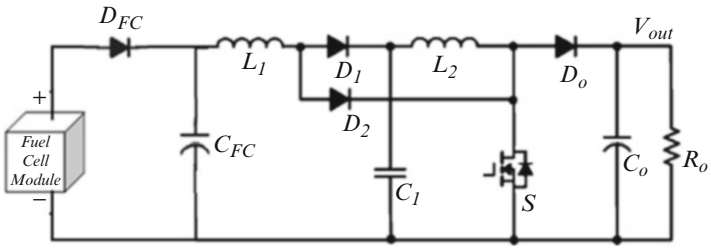


Fig. 9.14 Integrated cascaded boost converter

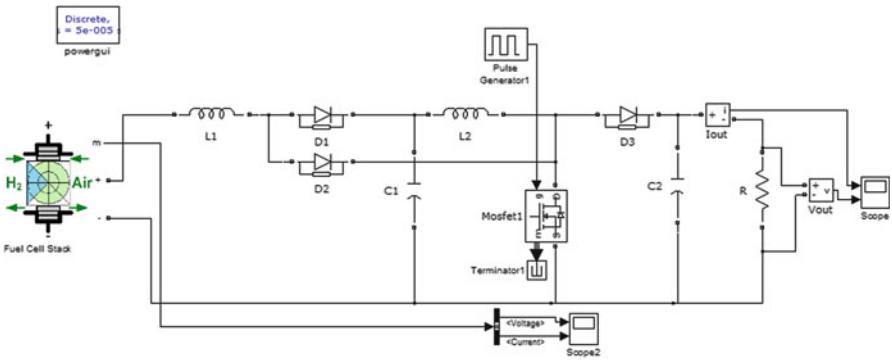


Fig. 9.15 MATLAB/SIMULINK model of the integrated cascaded boost converter

transfers stored energy through diode $D1$ to capacitor $C1$ and $L2$ transfers stored energy through diode $D0$ to the load. The circuit is simplified, and the instability caused by the cascade structure is avoided, compared with the cascade boost converter.

Figure 9.15 shows the MATLAB/SIMULINK model of the integrated cascaded boost converter. Figure 9.16 shows the simulation results of integrated cascaded boost converter obtained for 3 kW fuel cell stack input.

An integrated cascade boost converter with active clamping circuit is shown in Fig. 9.17. The auxiliary circuit is composed of a small inductor Ls, a resonant capacitor Cc, and a power MOSFET Sc, which is used to realize the soft switching (ZVS) for both main and clamp switches. The voltage stress of main switch can be effectively limited by the active clamp circuit. Therefore low-voltage stress of power switches with low Rds, on can be used to further reduce the conduction losses.

However, the switch voltage stress of the integrated cascade boost converters is equal to the high output voltage, and the current stress is large because the current of the inductors $L1$ and $L2$ flows through the switch when it turns on. These two factors increase the conduction losses and reduce the circuit efficiency. An auxiliary circuit is often necessary to improve the efficiency.

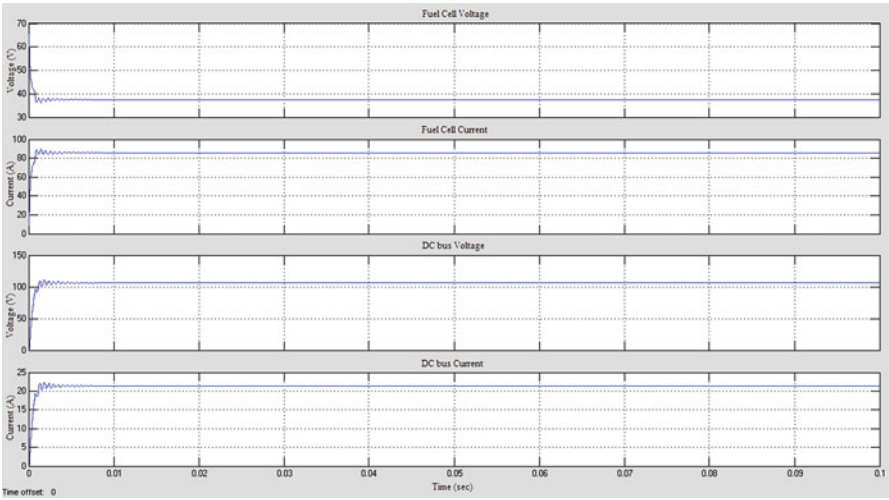


Fig. 9.16 Simulation results of integrated cascaded boost converter

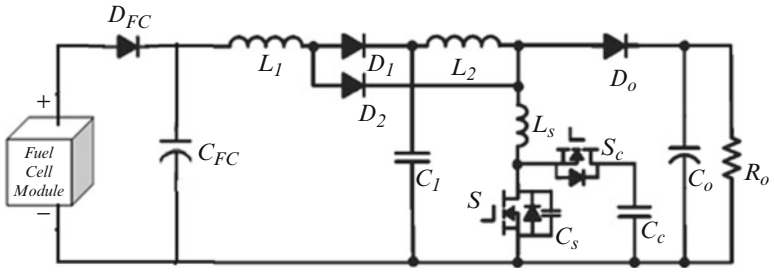


Fig. 9.17 Integrated cascaded boost converter with active clamping circuit

Figure 9.18 shows the MATLAB/SIMULINK model of the integrated cascaded boost converter along with the active clamping circuit. The model is designed to reduce the voltage stress. Figure 9.19 shows the simulation results of integrated cascaded boost converter along with the active clamping circuit obtained for 3 kW fuel cell input.

9.2.8 Interleaved Boost Converter

The interleaved boost converter structure is another effective solution for dc-dc power conversion. This structure can be used to increase the power level, minimize the current ripple, can reduce the passive component size, minimize the current stress on the power electronic devices, can improve the transient response, and can realize the thermal distribution.

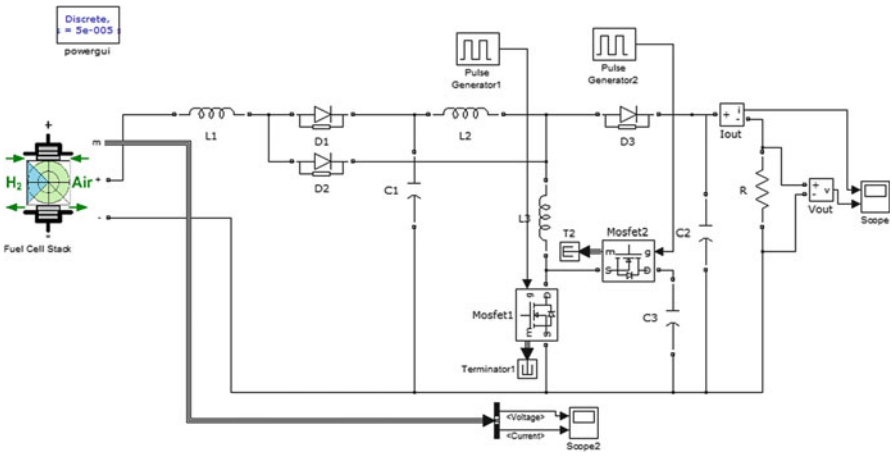


Fig. 9.18 MATLAB/SIMULINK model of the integrated cascaded boost converter with active clamping circuit

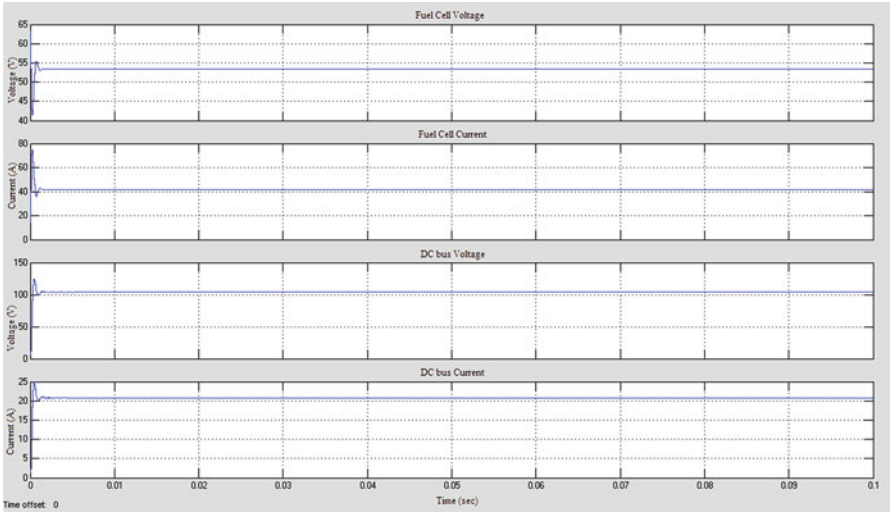


Fig. 9.19 Simulation results of integrated cascaded boost converter with active clamping circuit

The converters can be designed with multiple legs interleaving each other by means of input coupling inductors. It reduces the size and weight of the passive components and high efficiency can be obtained. For high-power applications, interleaved boost converters are preferable to increase the output current and to reduce the input current ripple. Since the currents through the switches are just fractions of the input current, current stress also can be minimized.

The Design parameters to be considered are decision of duty ratio and number of phases, selection of inductor values and the design of output filter. Ripple content is

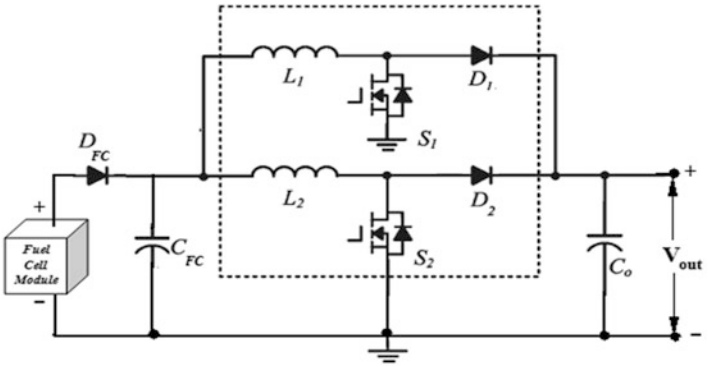


Fig. 9.20 Interleaved boost converter

inversely proportional to the number of phases (N). Ripple content decreases with increase in N. But if the number of phase is increased more the circuit complexity and cost increases so high without much decrease in ripple content. So the number of phase is limited to 2. Inductor values can be calculated based on the ripple current requirement which is given by

$$\Delta I_L = \frac{V_{in} D T_s}{L} \tag{9.13}$$

Capacitor serves the purpose of output voltage filtration. Thus its design calculation plays a major role in the elimination of ripples at the output which is based on the ripple voltage tolerable (ΔV_o).

$$\Delta V_o = \frac{V_o D T_s}{RC} \tag{9.14}$$

Figure 9.20 shows the conventional interleaved boost converter. However, the power devices still operate at hard switching which causes switching losses. The efficiency is limited because the output diode reverse-recovery problem is still serious in high-output voltage applications. Figure 9.21 shows the MATLAB/SIMULINK model of the conventional interleaved boost converter. Simulation results for the interleaved boost converter are shown in Fig. 9.22. The output is obtained for a fuel cell stack of 3 kW power.

By adding a set of auxiliary commutation circuit to each phase switch turn off which happens at maximum current conduction can be reduced. The auxiliary circuit consists of an active switch, a capacitor, and an inductor. The interleaved boost converter with auxiliary commutation circuits is introduced in Fig. 9.23. Turning on of the main switches occurs naturally at zero current, and the output-diode reverse-recovery problem is alleviated due to the critical discontinued current mode (DCM) operation. The auxiliary commutation circuits provide Zero Current

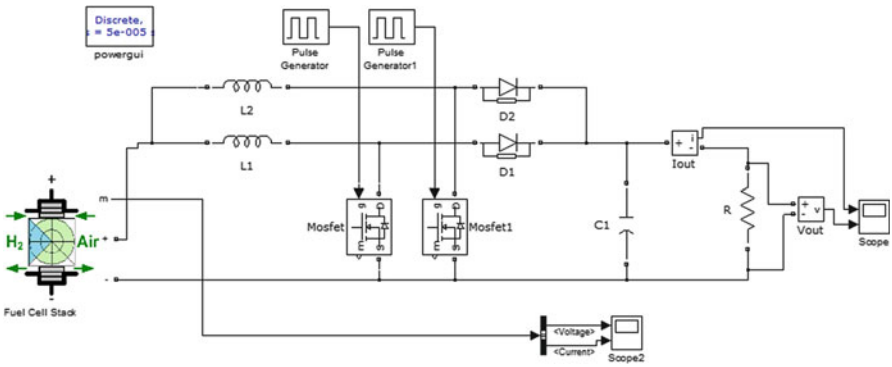


Fig. 9.21 MATLAB/SIMULINK model of the interleaved boost converter

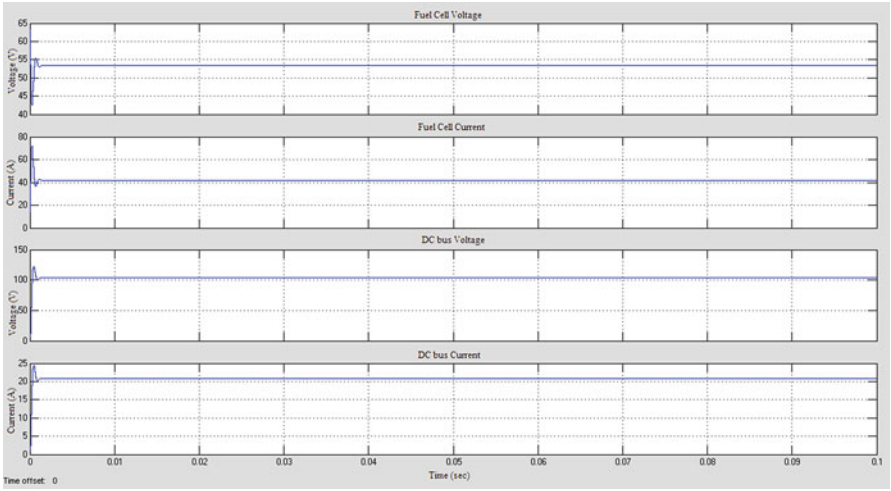


Fig. 9.22 Simulation results of interleaved boost converter

Transition (ZCT) when the main switch turns off. However, a variable frequency control is mandatory for this converter, which is difficult for the electromagnetic interference (EMI) filter design.

The MATLAB/SIMULINK model of the interleaved boost converter with auxiliary commutation circuit is shown in Fig. 9.24. Auxiliary commutation circuit reduces the maximum current conduction. Figure 9.25 shows the obtained simulation results for the interleaved boost converter with auxiliary commutation circuit.

To achieve the requirements of high efficiency and high power applications, an auxiliary circuit with an inductor and capacitor can be added along with the input filter inductor, a switch leg and diode leg. It reduces the voltage stresses of switches and diodes and enables soft switching which can eliminate losses and reverse recovery problem of Diode. Number of legs can be extended to desired voltage

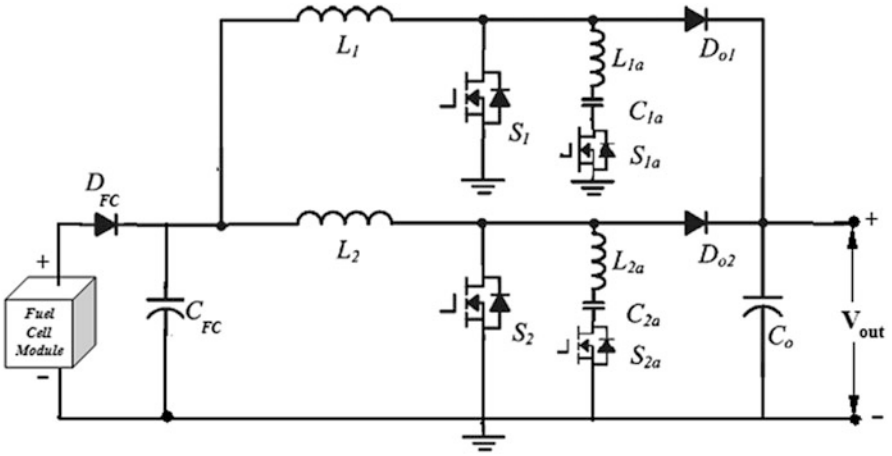


Fig. 9.23 Interleaved boost converter with an auxiliary commutation circuit

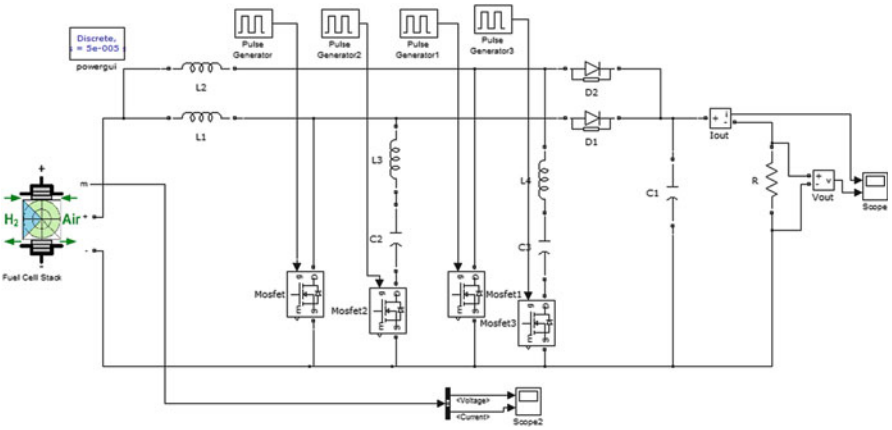


Fig. 9.24 MATLAB/SIMULINK model of the interleaved boost converter with auxiliary commutation circuit

gain and power level. However the converter circuit becomes complex and the overall cost increases. Two leg interleaving boost converter is shown in Fig. 9.26 and its MATLAB/SIMULINK model is shown in Fig. 9.27.

Figure 9.28 shows the simulation results of the interleaved boost converter which can be used for high step up applications with high efficiency. The input is given from the fuel cell stack of 3 kW power.

Integrated circuit methodology can be adapted to improve the performance of the interleaved converter. A high step-up converter shown in Fig. 9.29 consists of two phase circuits with interleaved operation. The first phase is a boost integrated Cuk-type converter, which includes a shared inductor $L1$ and switch $S1$ for the

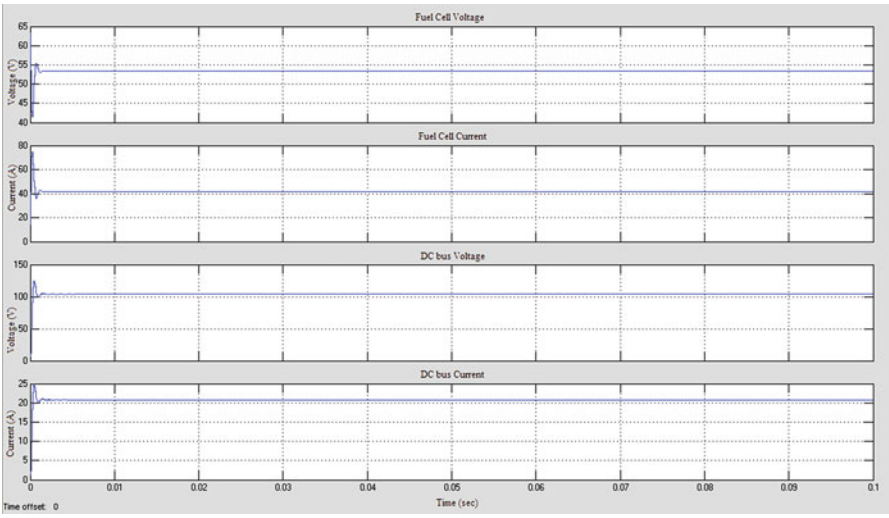


Fig. 9.25 Simulation results of interleaved boost converter with auxiliary commutation circuit

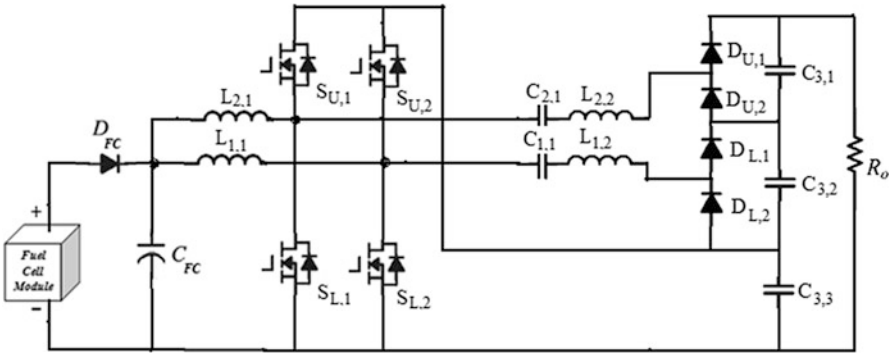


Fig. 9.26 Interleaved boost converter for high step up applications

boost and the isolated Cuk converter with turn ratio N to achieve a much higher voltage conversion ratio and avoid operating at extreme duty ratio. In addition, additional capacitors are added as voltage dividers for the two phases for reducing the voltage stress of active switches and diodes, which enables one to adopt lower voltage rating devices to further reduce both switching and conduction losses. The second phase of the proposed converter is a boost circuit which contains inductor $L2$, switch $S2$, blocking capacitor $C2$, and diode $D2$ followed by the common output capacitor Co.

However, current sharing among the parallel paths is a major design problem. Auxiliary circuits can be used but it increases the system cost and the overall converter circuit becomes bulky.

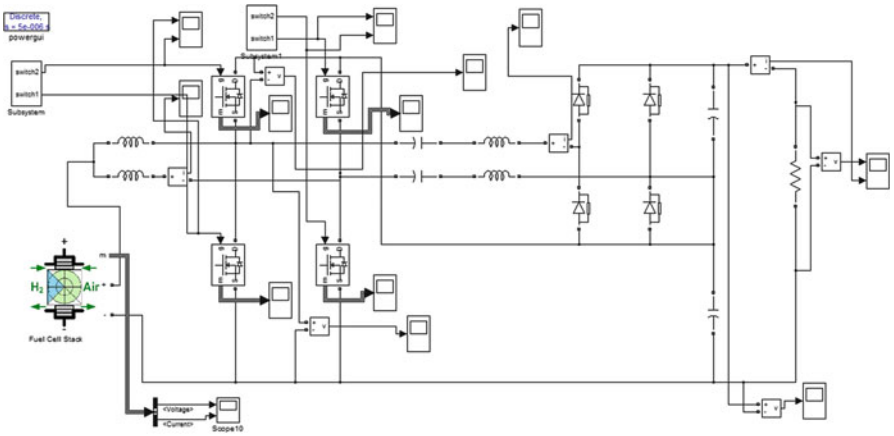


Fig. 9.27 MATLAB/SIMULINK model of the interleaved boost converter for high step up applications

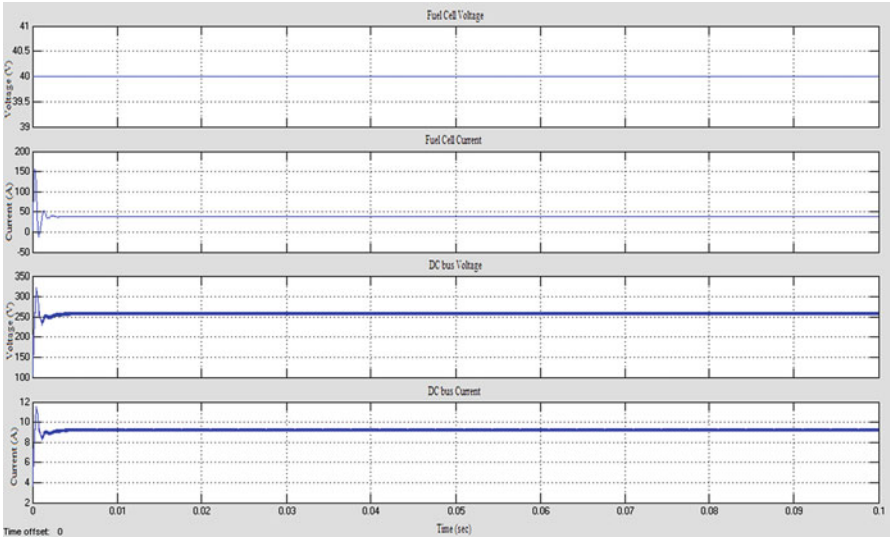


Fig. 9.28 Simulation results of interleaved boost converter for high step up applications

9.2.9 Isolated Converters

Both unidirectional and bidirectional DC-DC converters are preferred to be isolated to provide safety for the loading devices. In this view, most of the DC-DC converters incorporate a high frequency transformer. Isolated converters type of converters uses high frequency circuits with transformers which provide galvanic isolation. But inclusion of a transformer leads to the major issues such as high

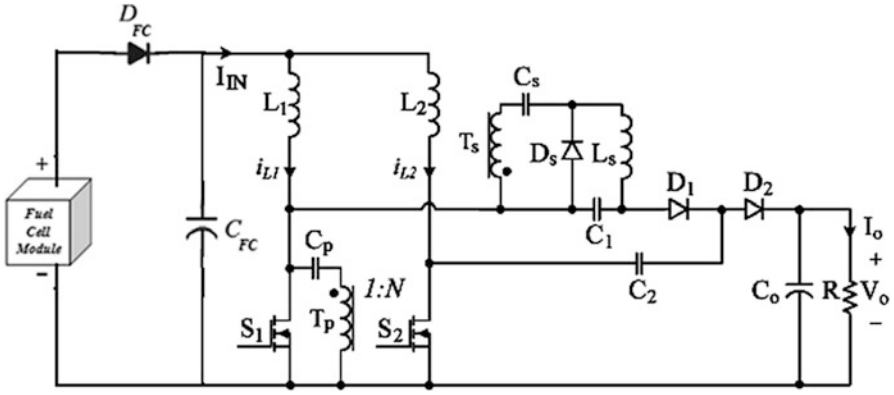


Fig. 9.29 Interleaved high step-up converter with low switch voltage stress

voltage stresses across the converter switches and diodes caused by the leakage inductance and the transistor/diode output capacitance, increase in converter area, volume, cost and increase in EMI. Most of the DC-DC converter designs are aimed to overcome these problems to yield highly efficient, cost effective converters. The current or voltage stresses imposed on the switches and diodes can be minimized by choosing appropriate transformer turns ratio, which may lead to an improved efficiency and lower cost. Various types of Isolated DC-DC converters are discussed below:

9.2.10 Flyback Converter

The topology of a flyback converter is shown in Fig. 9.30. This flyback converter has a large core size because of its single switch unipolar operation. It is an isolated version of the buck-boost and does not contain a transformer. It utilizes a coupled inductor arrangement. When the switch is turned on, current builds up in the primary and energy is stored in the core. This energy is then released to the output circuit through the secondary when the switch is turned off. All of the output power of the flyback has to be stored in the core as $\frac{1}{2}LI^2$ energy thus the core size and cost will be much greater than in the other topologies, where only the core excitation energy, which is normally small, is stored. This means that the transformer bulk is one of the major drawbacks of the flyback converter. In order to obtain sufficiently high stored energy, the flyback primary inductance has to be significantly lower than required for a true transformer, since high peak currents are needed. This is normally achieved by gapping the core. The gap reduces the inductance, and most of the high peak energy is then stored in the gap, thus avoiding transformer saturation. In the flyback converter, the secondary inductance is in series with the

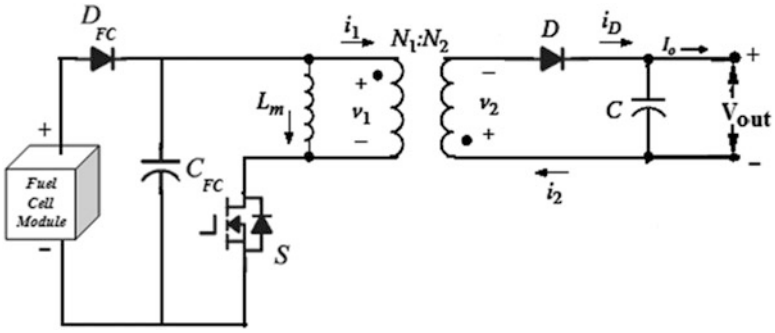


Fig. 9.30 Flyback converter

output diode when current is delivered to load. Hence, each output requires only one diode and output filter capacitor.

Flyback is the ideal choice for generating low cost, multiple output supplies. Flyback is also ideal for generating high voltage outputs. However, there is a voltage spike at turn-off due to the stored energy in the transformer leakage inductance. The switches must be capable of blocking approximately twice the supply voltage plus the leakage spike. Flyback converters have inherently much higher output ripples than other topologies. This, together with the higher peak currents, large capacitors, and transformer, limits the flyback to lower output power applications in the 20–200 W range. The flyback converter has a low number of components and a simple structure. The main drawbacks of this topology are high input current ripple, current and voltage stress on the power electronic devices, and discontinuous source current. However, such a topology is suitable for low power applications.

9.2.11 Forward Converter

The forward converter is also a single-switch isolated topology (Fig. 9.31). This is based on the buck converter. In contrast to the flyback, the forward converter has a true transformer action, where energy is transferred directly to the output through the inductor during the switch on time. When the switch turns off, the secondary voltage reverses, D1 goes from conducting to blocking mode, and the freewheel diode D2 then becomes forward biased and provides a path for the inductor current to continue to flow. This allows the energy stored in L to be released into the load during the switch off time. The forward converter is always operated in continuous mode, because this produces very low peak input and output currents and small ripple components. Since the transformer in this topology transfers energy directly, there is negligible stored energy in the core compared to the flyback. However, there is a small magnetization energy required to excite the core, allowing it to

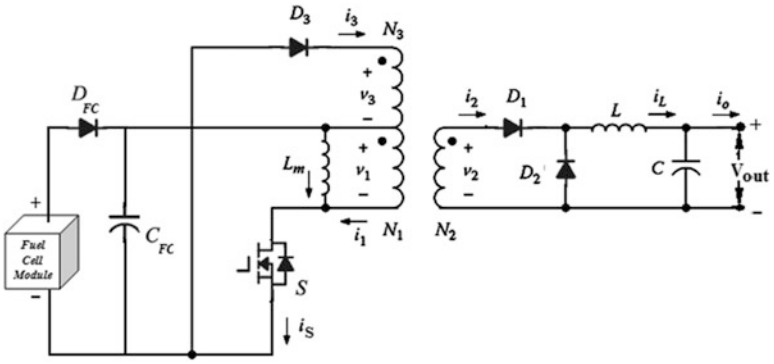


Fig. 9.31 Forward converter

become an energy transfer medium. This energy is very small and only a very small primary magnetization current is needed. This means that a high primary inductance is usually suitable, with no need for the core air gap required in the flyback. Standard ungapped ferrite cores with high permeability are ideal for providing the high inductance required. Negligible energy storage means that the forward converter transformer is considerably smaller than the flyback, and core loss is also much smaller for the same throughput power. However, the transformer is still operated asymmetrically, which means that power is only transferred during the switch on time, and this poor utilization means the transformer is still far bigger than in the symmetrical types. In addition, a major problem is how to remove the core magnetization energy by the end of each switching cycle. This path is provided by adding an additional reset winding of opposite polarity to the primary. If this did not happen, there would be a net DC flux build-up, leading to core saturation and possible destruction of power electronic devices.

For the forward topology a third winding is placed on the transformer core allowing for the demagnetization of the transformer due to any remaining energy in the core which may lead to saturation problems.

This topology has also a low number of components and a simple structure. Its main drawbacks are the presence of two magnetic components, misuse of the magnetic circuit of the transformer, and similar to flyback, current and voltage stress on the power electronic devices and discontinuous source current. This converter is also suitable for low power applications.

9.2.12 Push-Pull Converter

The primary concept of the push-pull converter (Fig. 9.32) is a center-tapped arrangement and each switch is driven alternately, driving the transformer in both directions. The push-pull transformer is typically half the size of that for the

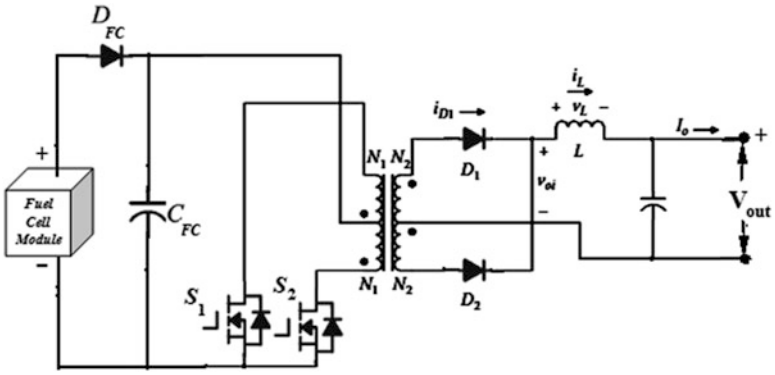


Fig. 9.32 Push-pull converter

single-ended types, resulting in a more compact design. This push-pull action produces core resetting during each half cycle hence, no clamp winding is required. Power is transferred to the buck type output circuit during each switch conduction period. The push-pull configuration is normally used for output power in the 100–500 W ranges. Push-pull converters are thus excellent for high power density, low ripple output. The push-pull offers very compact design of the transformer and output filter, while producing very low output ripple. So if space is a premium issue, the push-pull could be suitable. However, one of the main drawbacks of the push-pull converter is the fact that each switch must block twice the input voltage due to the doubling effect of the center-tapped primary, even though two switches are used. A further problem with the push-pull is that it is prone to flux symmetry imbalance. If the flux swing in each half cycle is not exactly symmetrical, the volt-second will not balance and this will result in transformer saturation, particularly for high input voltage. Symmetry imbalance can be caused by different characteristics in the two switches such as storage time in a bipolar and different on state losses. The center-tape arrangement also means that extra copper is needed and very good coupling between the two halves is necessary to minimize possible leakage spikes. It should also be noted that if snubbers are used to protect the device, the design must be very precise since they tend to interact with each other. This is true for all symmetrically driven converters. These advantages usually makes the push-pull to normally operated at lower voltage inputs such as 12, 28, or 48 V. DC-DC converters found in the automotive and telecommunication industries are often push-pull designs. At these voltage levels, transformer saturation is easier to avoid.

Push-pull converters use only one switch at any time to interface fuel cell stack voltage to DC bus which reduces the conduction loss. But the issue is that the device handles twice of the input voltage. This can be handled by the use of high voltage switching devices. The major problem with these types of converters is the transformer saturation which results in converter failure because the two half portions of the center tap transformer cannot be equal or symmetrically wound. Therefore these converters are suitable for low voltage and low power applications.

9.2.13 Half Bridge Converter

The half-bridge converter (Fig. 9.33) is also referred to as the single ended push-pull, and in principle is a balanced version of the forward converter. Again it is a derivative of the buck type. The half-bridge has some key advantages over the push-pull, which usually makes it first choice for higher power applications in the 500–1,000 W range. As shown in Fig. 9.17, the two main bulk capacitors C_1 and C_2 are connected in series, and an artificial input voltage mid-point is provided. The two switches are driven alternately, and this connects each capacitor across the single primary winding each half cycle. Vin/2 is super imposed symmetrically across the primary in a push-pull manner. A full wave buck output filter rather than a half wave filter is implemented. This again results in very efficient core utilization. The waveforms are identical to the push-pull, except that the voltage across the switches is halved. This means that the half-bridge is particularly suited to high voltage inputs, such as off-line applications. Another major advantage over the push-pull is that the transformer saturation problems due to flux symmetry imbalance do not occur. By using a small capacitor, DC build-up of flux in the transformer is blocked, and only symmetrical AC is drawn from the input. A less obvious exclusive advantage of the half-bridge is that the two series reservoir capacitors already exist, and this makes it ideal for implementing a voltage doubling circuit. The bridge circuits also have the same advantages over the single ended types that the push-pull possesses, including excellent transformer utilization, very low output ripple, and high output power capabilities. The limiting factor in the maximum output power available from the half bridge is the peak current handling capabilities of present day power switching devices. The upper power limit is typically 1,000 W. For higher output powers the four-switch full-bridge is normally used.

However, the need for two 50 or 60 Hz input capacitors in the half-bridge are a drawback because of their large size. The top switch must also have isolated drive, since the gate or base is at a floating potential. Furthermore, if snubbers are used

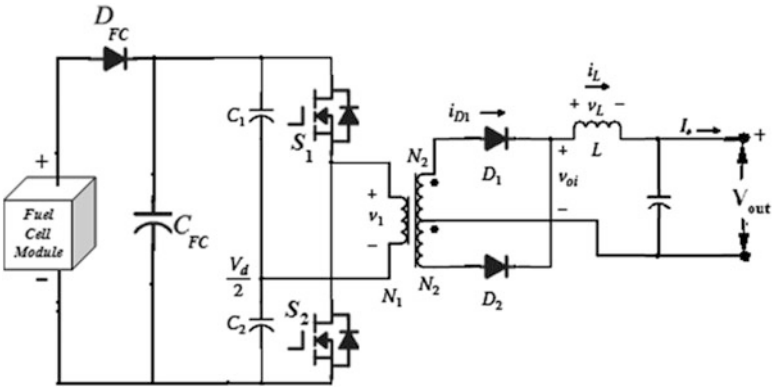


Fig. 9.33 Half bridge converter

across the power semiconductor switches, great care must be taken in their design because the symmetrical action means that they will interact with one another. The circuit cost and complexity have clearly increased and must be weighed against the advantage gained. In many cases, this normally excludes the use of the half-bridge at output power levels below 500 W. The two switches are driven alternately, and this half bridge converter is suitable for high power applications. The number of the active components is reduced, but the semiconductor devices have to handle twice of the current. Also split capacitors may cause some balancing issues. It also requires large value of transformation ratio to obtain the desired output voltage and large value of dc link capacitors to eliminate transformer saturation. This increases the cost of the converter. Single silicon device or transformer has to handle large value of current which causes current stress. In addition, interconnect and parasitic inductances will induce significant i^2R and Li^2 losses, which decreases the converter efficiency.

9.2.14 Full Bridge Converter

In the half-bridge converter, the maximum current rating of the switch will eventually determine the upper limit of the output power. The switches are driven alternately in pairs: T1 and T3 simultaneously, and then T2 and T4. The transformer primary is now subjected to the full input voltage. The current levels flowing are halved compared to the half-bridge for a given power level. Hence, the full-bridges will double the output power of the half-bridge using the same switch types (Fig. 9.34). The secondary circuit operates in exactly the same manner as the push-pull and half-bridge, producing very low ripple outputs at very high current levels. Therefore, the waveforms for the full-bridge are identical to the half-bridge waveforms, except for the voltage across the primary, which is effectively doubled. The full-bridge converter is ideal for the generation of very high output power level.

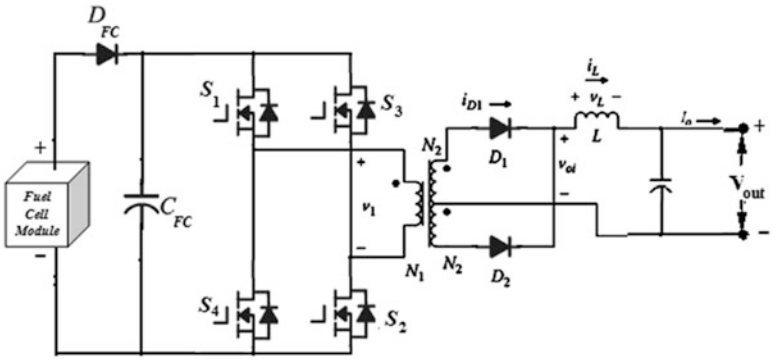


Fig. 9.34 Full bridge converter

The increased circuit complexity normally means that the full-bridge is reserved for applications with power output level of 1 kW and above. For such high power requirements, designers often select Darlington power, since its superior current rating and switching characteristics provide additional performance and in many cases a more cost-effective design. The full-bridge also has the advantage of only requiring one main smoothing capacitor compared to two for the half-bridge, hence saving space. Its other major advantages are the same as for the half-bridge. However, four switches and clamp diodes are needed instead of two for the other symmetrical types. The full-bridge has the most complex and costly design of any of the converters discussed, and should only be used where other types do not meet the requirements. Full bridge converters are suitable for high power applications. The main advantage of the full-bridge converter is reasonable device voltage and current ratings. It also has low transformer turns ratio and the voltage and current stress are minimum. It has more number of components which increases the cost and the control is also complex. But it has a good efficiency which makes this converter acceptable for suitable high power applications.

9.3 Inverters

In almost every application, AC power is required demanding the utilisation of an inverter in the power-conditioning system. The dc-ac converter, also known as the inverter, converts dc power to ac power at desired output voltage and frequency. The dc power input to the inverter is obtained from a fuel cell through dc-dc converter. The filter capacitor across the input terminals of the inverter provides a constant dc link voltage. The inverter therefore is an adjustable-frequency voltage constant dc link voltage. The inverter therefore is an adjustable-frequency voltage link converter.

Inverters can be broadly classified into two types, voltage source and current source inverters. A voltage–fed inverter (VFI) or more generally a voltage–source inverter (VSI) is one in which the dc source has small or negligible impedance. The voltage at the input terminals is constant. A current–source inverter (CSI) is fed with adjustable current from the dc source of high impedance that is from a constant dc source. A voltage source inverter employing thyristors as switches, some type of forced commutation is required, while the VSIs made up of using GTOs, power transistors, power MOSFETs or IGBTs, self commutation with base or gate drive signals for their controlled turn-on and turn-off.

9.3.1 Single Phase Inverter

A standard single phase voltage or current source inverter can be in half- bridge or full-bridge configuration. The single-phase units can be joined to have three-phase or multiphase topologies.

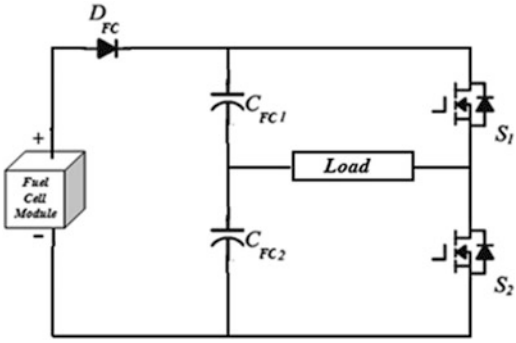


Fig. 9.35 Single phase half bridge inverter

9.3.2 Half-Bridge Configuration

Figure 9.35 shows the half-bridge or a single leg inverter, which is the simplest Topology. It is used to produce a two-level square wave output waveform using two semiconductor switches S1 and S2. A center tapped voltage source supply is needed; it may be possible to use a simple supply with two well-matched capacitors in series to provide the center tap.

9.3.3 Half Bridge with Resistive Load

A half-bridge voltage source-inverter with resistive load can be considered with representing load by only resistance. The circuit is operated by switching S1 (T1 & D1) and S2 (T2& D2) alternatively at 50 % duty cycle. It is seen that for $0 < t < \pi$ S1 conducts and the load is subjected Vs/2 due to the upper voltage source Vs/2. At $t = \pi$, switch S1 is commutated and S2 is gated on. During the period $\pi < t < 2\pi$, S2 conducts and the load is subjected to a voltage (–Vs/2) due to the lower voltage source Vs/2. Figure 9.36 shows simulation circuit by MATLAB/SIMULINK of a single phase half bridge inverter and Fig. 9.37 shows voltage and current waveforms.

9.3.4 Half Bridge with RL Load

A half-bridge voltage source-inverter with inductive-resistive load can be considered with representing load by only resistance and inductance. The circuit is operated by switching S1 and S2 alternatively at 50 % duty cycle. To understand the operation of the circuit, the inverter is started by giving signal to S1. There was no current in any part of the circuit earlier. A signal to S1 turns it on and connects

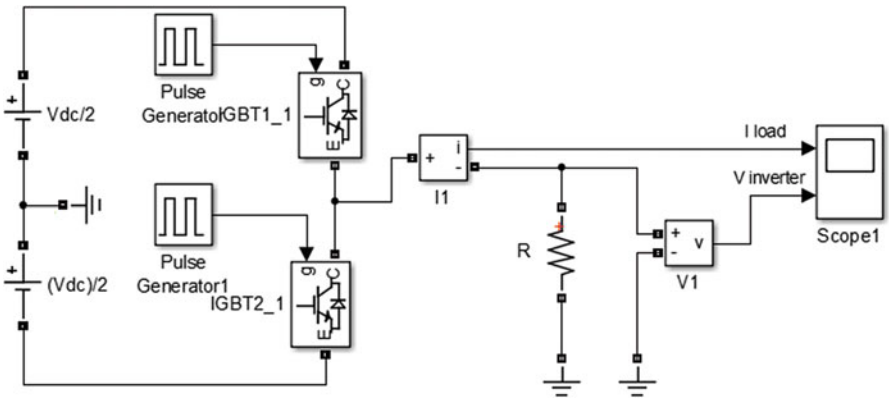


Fig. 9.36 MATLAB/SIMULINK model of single phase half bridge inverter with R load

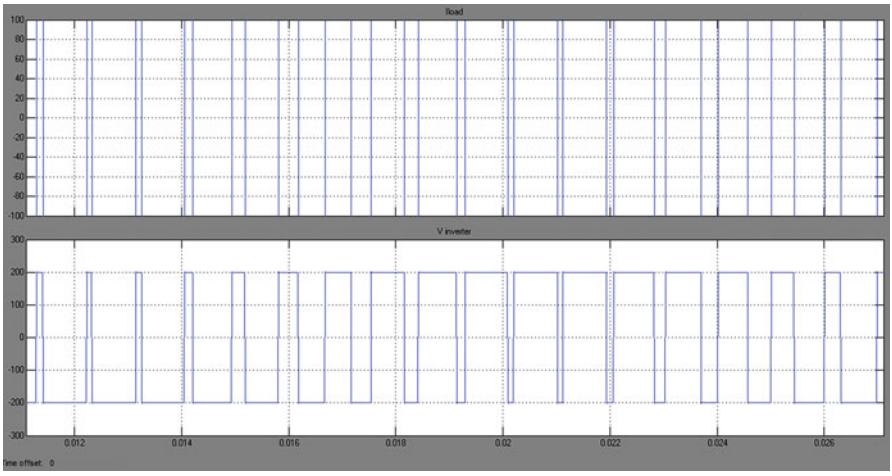


Fig. 9.37 Simulation results of single phase half bridge inverter with R load

the load to upper Vs/2. A positive current develops form upper Vs/2 through S1 to load. During the time period $0 < t < \pi$ current through the load (through S1 and upper Vs/2) has grown from zero to Imax. The current will be reduced to zero through D2. S2 is forward biased now; the current grows in the negative direction and the current flows through D2, load, lower Vs/2 until the current falls to zero. Similarly, when S2 is turned off at 2π, the load current flows through D1, load, and upper Vs/2. The energy will be fed back to DC source when D1 and D2 conduct. Figure 9.38 shows simulation circuit by MATLAB/SIMULINK and Fig. 9.39 shows the voltage and current waveforms.

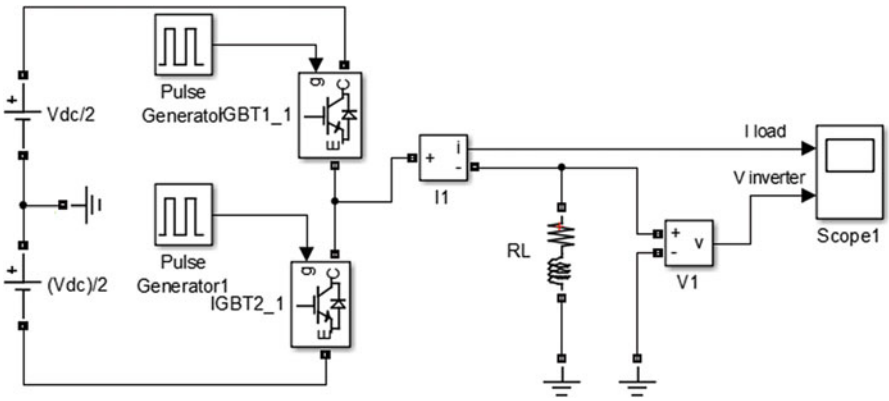


Fig. 9.38 MATLAB/SIMULINK model of single phase half bridge inverter with RL load

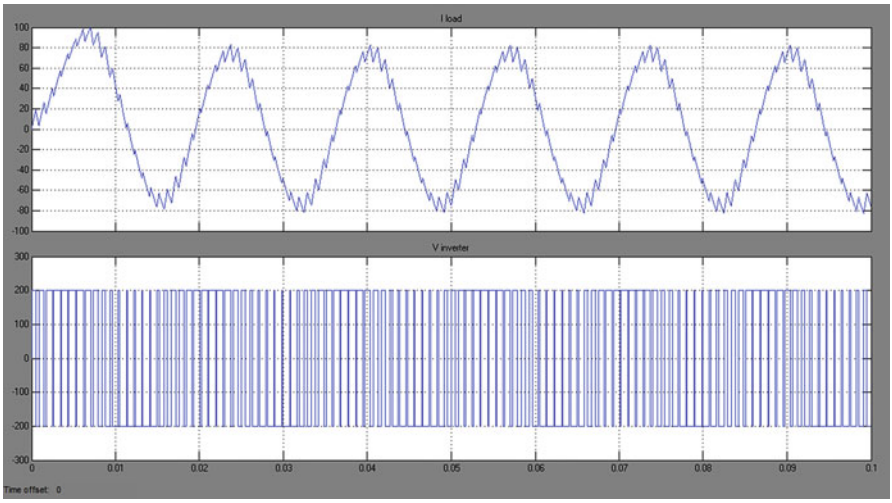


Fig. 9.39 Simulation results of single phase half bridge inverter with RL load

9.3.5 Full Bridge Configuration

The power circuit diagram of a single phase full bridge inverter is shown in Fig. 9.40. When S1 and S2 are connected, the input voltage Vs appears across the load. If S3 and S4 are connected the voltage across the load is –Vs. Table 9.2 shows the main principle of a single phase full bridge inverter.

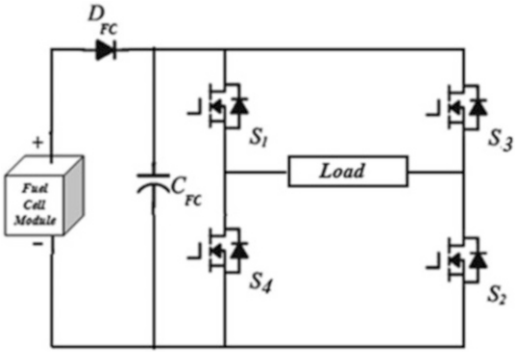


Fig. 9.40 Single phase full bridge inverter

Table 9.2 Switching sequence of single phase full bridge inverter

Switching states					Iout	
S1	S2	S3	S4	Vout	Iout > 0	Iout < 0
On	On	Off	Off	V_s	S1 and s2 conduct	D1 and D2 conduct
Off	Off	On	On	$-V_s$	D4 and D3 conduct	S3 and s4 conduct
On	Off	On	Off	0	S1 and D3 conduct	D1 and S3 conduct
Off	On	Off	On	0	D4 and S2 conduct	S4 and D2 conduct
Off	Off	Off	Off	$-V_s$	D4 and D3 conduct	–
Off	Off	Off	Off	V_s	–	D1 and D2 conduct

9.3.6 Full Bridge with Resistive Load

A full-bridge voltage source-inverter with resistive load can be considered with representing load by only resistance. The circuit is operated by switching S1, S2, S3, and S4. S1-S2 and S3-S4 are switched on and off at a 50 % duty cycle. When S1 and S2 are connected, the input voltage Vs appears across the load. If S3 and S4 are connected the voltage across the load is –Vs. Table 9.2 can be considered the operation table for a single-phase full-bridge Inverter with resistive load. Figure 9.41 shows simulation circuit by MATLAB/SIMULINK and Fig. 9.42 shows voltage and current waveforms.

9.3.7 Full Bridge with Resistive Load

A full-bridge voltage source-inverter with inductive-resistive load can be considered with representing load by only resistance and inductance. The circuit is operated by switching S1, S2, S3, and S4. S1–S3 and S2–S4 are switched on and off at a 50 % duty cycle. When S1 and S2 are connected, the input voltage Vs appears across the load. If S3 and S4 are connected the voltage across the load is –Vs. Fig. 9.43 shows simulation circuit by MATLAB/SIMULINK and Fig. 9.44 shows voltage and current waveforms.

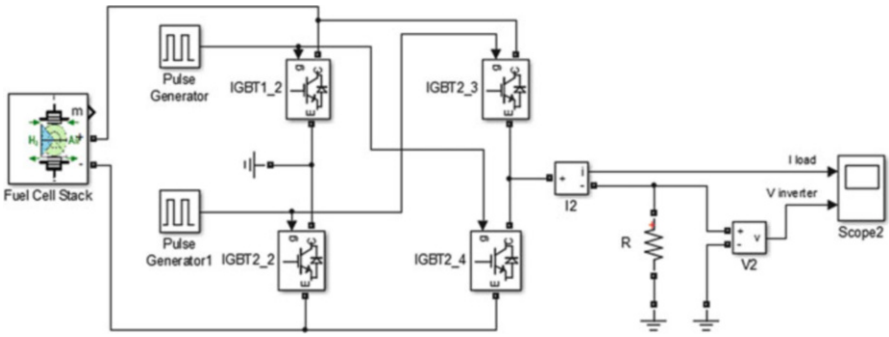


Fig. 9.41 MATLAB/SIMULINK model of single phase full bridge inverter with R load

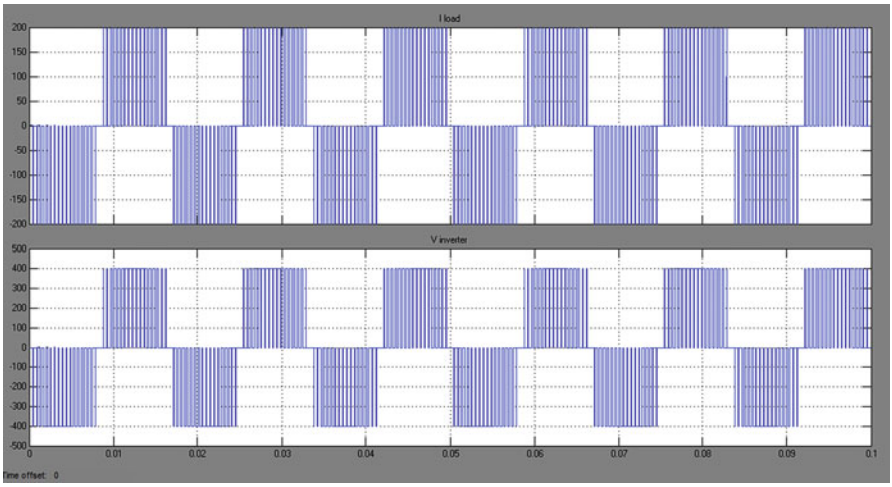


Fig. 9.42 Simulation results of single phase full bridge inverter with R load

9.3.8 Three Phase Inverter

A three phase inverters are used to provide industrial applications by adjustable frequency power. Three phase inverters are more common than single phase inverters. DC supply for three phase inverters is taken from a fuel cell or usually from DC-DC Converter. Three-phase counterparts of the single-phase half and full bridge voltage source inverters are shown in Figs. 9.45 and 9.46. Single-phase VSIs cover low-range power applications and three-phase VSIs cover medium to high power applications. The main purpose of these topologies is to provide a three-phase voltage source, where the amplitude, phase and frequency of the voltages can be controlled. The three-phase dc/ac voltage source inverters are extensively being used in motor drives, active filters and unified power flow controllers in power

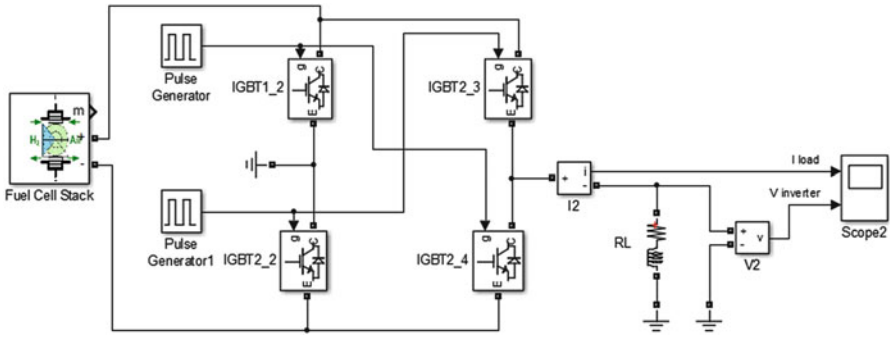


Fig. 9.43 MATLAB/SIMULINK model of single phase full bridge inverter with RL load

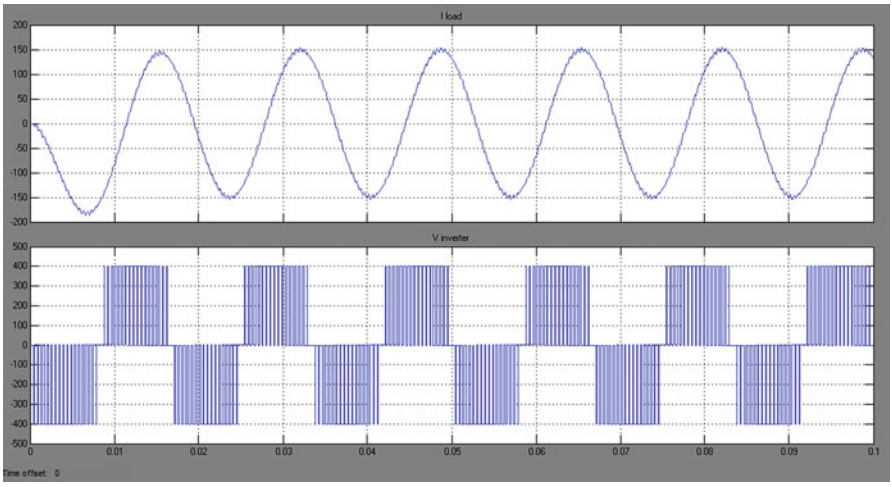


Fig. 9.44 Simulation results of single phase full bridge inverter with RL load

systems and uninterrupted power supplies to generate controllable frequency and ac voltage magnitudes using various pulse width modulation (PWM) strategies. The standard three-phase inverter has six switches the switching of which depends on the modulation scheme. A six steps bridge is used for three phase inverter by using six switches, two switches for each phase. Each step is defined as a change in the time operation for each transistor to the next transistor in proper sequence. For one cycle 360°, each step would be of 60° interval for a six step inverter. Figure 9.46 shows the power circuit diagram of a three phase bridge inverter using six IGBTs. Large capacitors are connected at the input terminal to make the DC input constant and also suppress the harmonics fed back to the source. The input dc is usually obtained from a single-phase or three phase utility power supply through a diode-bridge rectifier and LC or C filter. The nature of the two switches in the same leg is complementary.

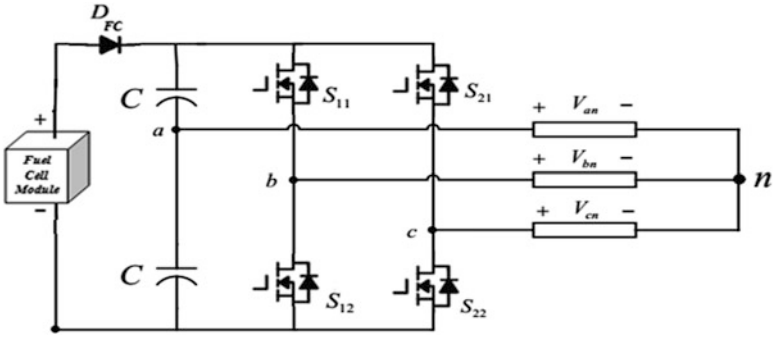


Fig. 9.45 Three phase half bridge inverter

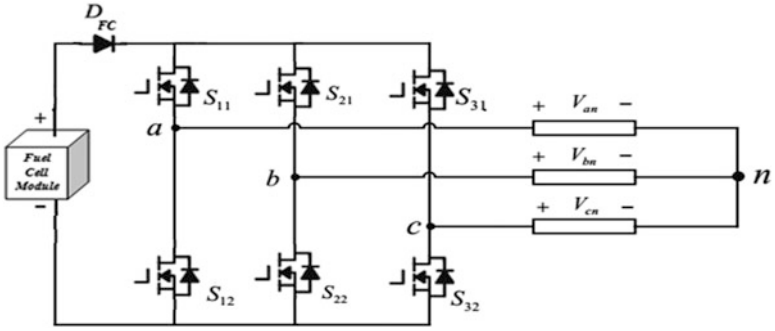


Fig. 9.46 Three phase full bridge inverter

Table 9.3 Switching sequence of three phase inverter

Switching states			Output voltage		
S11	S12	S31	Vab	Vbc	Vca
Off	Off	Off	0	0	0
Off	Off	On	0	$-V_S$	V_S
Off	On	Off	$-V_S$	V_S	0
Off	On	On	$-V_S$	0	$-V_S$
On	Off	Off	V_S	0	$-V_S$
On	Off	On	V_S	$-V_S$	0
On	On	Off	0	V_S	$-V_S$
On	On	On	0	0	0

Of the eight switching states as shown in Table 9.3 two of them produce zero ac line voltage at the output. In this case, the ac line currents freewheel through either the upper or lower components. The remaining states produce no zero ac output line voltages. In order to generate a given voltage waveform, the inverter switches from one state to another. Thus the resulting ac output line voltages consist of discrete values of voltages, which are $-V_{DC,}$ 0, and V_{DC}

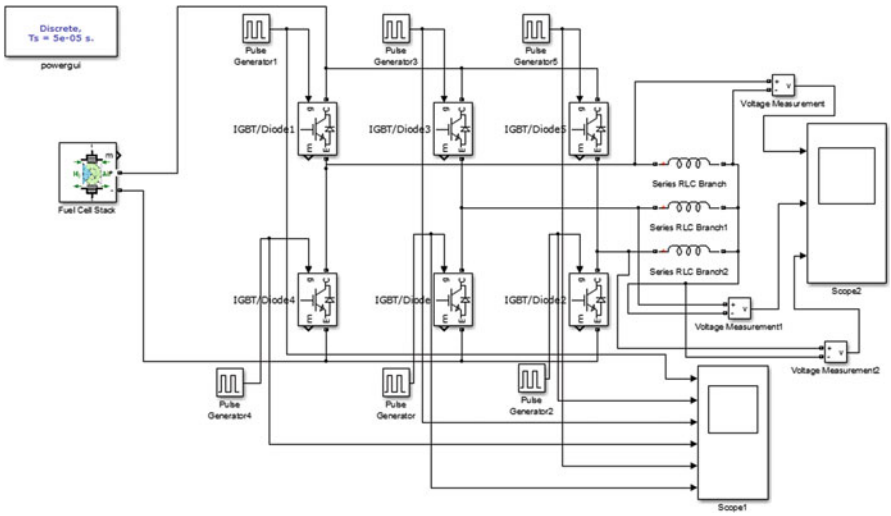


Fig. 9.47 MATLAB/SIMULINK model of three phase inverter

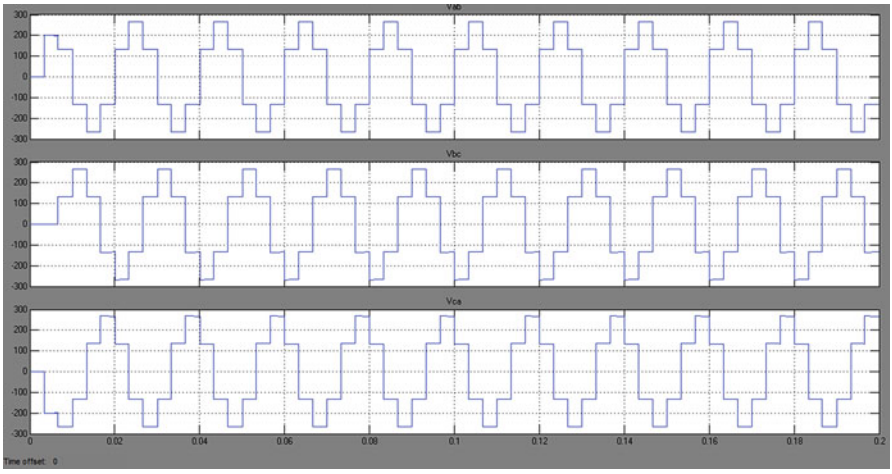


Fig. 9.48 Simulation results of three phase inverter

Figure 9.47 shows the MATLAB/SIMULINK Model of Three Phase Inverter and Fig. 9.48 shows the simulation results for three phase line-line voltage obtained for L load.

9.3.9 Z-Source Inverter

Impedance-source (or impedance-fed) power converter (abbreviated as Z-source converter) employs a unique impedance network (or circuit) to couple the converter

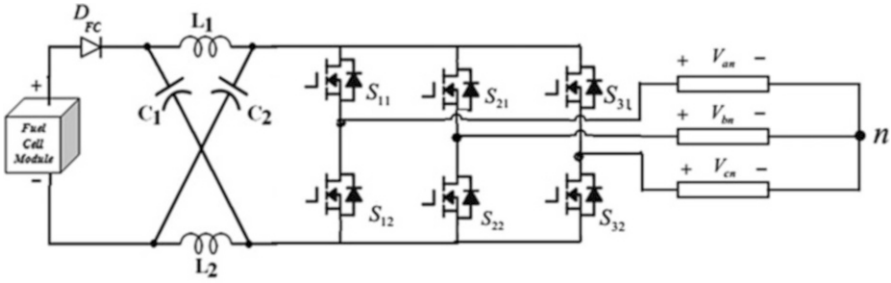


Fig. 9.49 Z-source inverter

main circuit to the power source, load, or another converter, for providing unique features that cannot be observed in the traditional V- and I-source converters where a capacitor and inductor are used, respectively. The Z-source converter overcomes the above-mentioned conceptual and theoretical barriers and limitations of the traditional V-source converter and I-source converter and provides a novel power conversion concept.

The Z-source concept can be applied to all dc-to-ac, ac-to-dc, ac-to-ac, and dc-to-dc power conversion. Because fuel cells usually produce a voltage that changes widely (2:1 ratio) depending on current drawn from the stack, for fuel-cell vehicles and distributed power generation, a boost dc–dc converter is needed as the V-source inverter cannot produce an ac voltage that is greater than the dc voltage. Figure 9.49 shows a Z-source inverter for such fuel-cell applications, which can directly produce an ac voltage greater and less than the fuel-cell voltage. The diode in series with the fuel cell is usually needed for preventing reverse current flow.

The unique feature of the Z-source inverter is that the output ac voltage can be any value between zero and infinity regard-less of the fuel-cell voltage. That is, the Z-source inverter is a buck–boost inverter that has a wide range of obtainable voltage. The traditional V- and I-source inverters cannot provide such feature. The three-phase Z-source inverter bridge has nine permissible switching states (vectors) unlike the traditional three-phase V-source inverter that has eight. The traditional three-phase V-source inverter has six active vectors when the dc voltage is impressed across the load and two zero vectors when the load terminals are shorted through either the lower or upper three devices, respectively.

However, the three-phase Z-source inverter bridge has one extra zero state (or vector) when the load terminals are shorted through both the upper and lower devices of any one phase leg (i.e., both devices are gated on), any two phase legs, or all three phase legs. This shoot-through zero state (or vector) is forbidden in the traditional V-source inverter, because it would cause a shoot-through. This third zero state (vector) is called as the shoot-through zero state (or vector), which can be generated by seven different ways: shoot-through via any one phase leg, combinations of any two phase legs, and all three phase legs. The Z-source network makes the shoot-through zero state possible. This shoot-through zero state provides the unique buck-boost feature to the inverter. All the traditional pulse

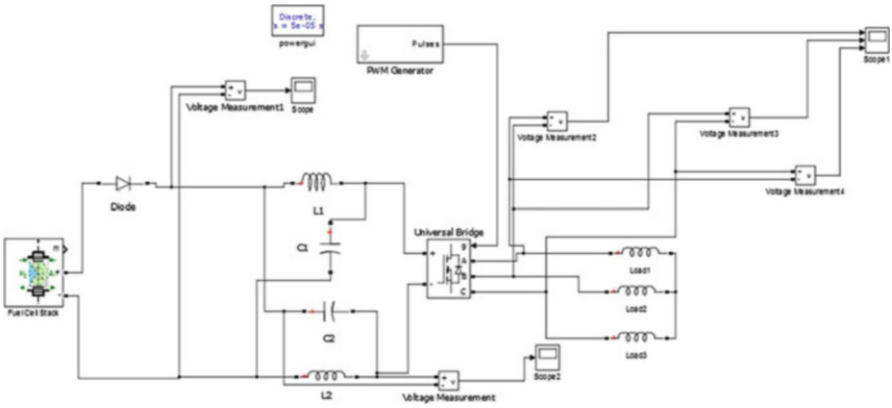


Fig. 9.50 MATLAB/SIMULINK model of Z-source inverter

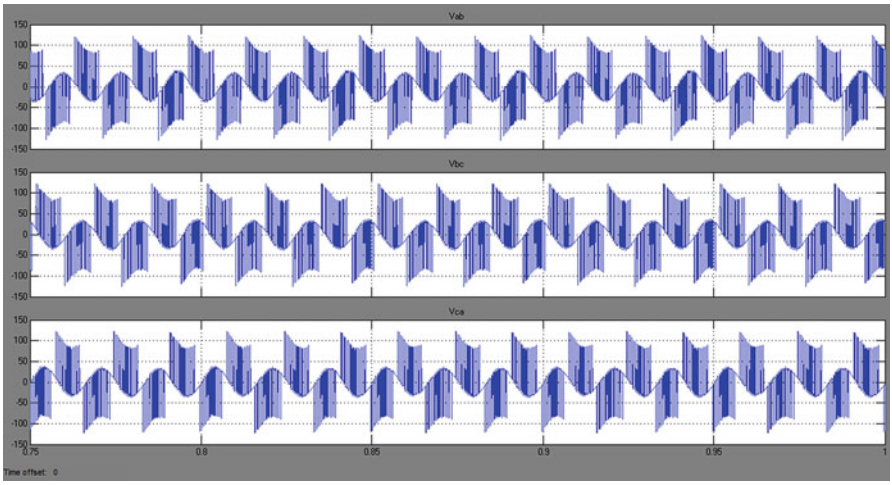


Fig. 9.51 Simulation results of Z-source inverter

width-modulation (PWM) schemes can be used to control the Z-source inverter and their theoretical input–output relationships still hold. Figure 9.50 shows the MATLAB/SIMULINK Model of Z-Source Inverter and Fig. 9.51 shows the simulation result of output voltage waveform.

9.3.10 LLCC Resonant Inverter

The diode at the output of the fuel-cell stack is necessary to prevent the negative current going into the stack. Due to the negative current, it is possible that the cell

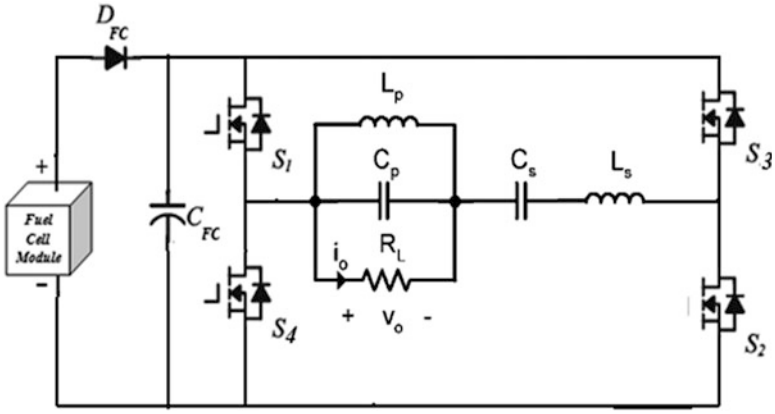


Fig. 9.52 LLCC resonant inverter

reversal could occur and damage the fuel-cell stack. The ripple current seen by the fuel-cell stack due to the switching of the boost converter has to be reduced. The power inverter circuit is composed of a boost dc/dc converter that uses PWM direct duty-cycle control and a newly designed LLCC resonant inverter. Because the output voltage of a fuel cell varies with the load variation, the boost dc/dc converter with dc voltage feedback control is utilized to provide the constant dc voltage for the inverter. The dc-link voltage amplitude is controlled by the boost dc/dc converter according to the control input. To provide stable sinusoid ac voltage output, the LLCC resonant circuit is operated at a geometric mean frequency such that the output voltage will not be influenced by the quality factor variation. This driving circuit has full-bridge switches (S1, S2, S3, S4), a series-resonant tank (Ls, Cs), and parallel-resonant tank (Lp, Cp, RL) as shown in Fig. 9.52. The LLCC inverter incorporates series and parallel combinations of inductors and capacitors otherwise known as a series-resonant tank (LS, CS) and parallel-resonant tank (LP, CP) to filter the voltage, remove some of the ripple current and provide a stable AC output. A half-bridge inverter converts the DC signal to AC using PWM with zero-voltage/zero-current switching. This reduces switching losses, thereby increasing the efficiency of the converter.

Unfortunately, the two capacitors and inductors increase the space and cost of the inverter. In addition, this resonant circuit highly depends on the parameters of the capacitors and inductances and may be influenced by their variation with operating conditions. Figure 9.53 shows the MATLAB/SIMULINK Model of LLCC Resonant Inverter and Fig. 9.54 shows the simulation result obtained using MATLAB.

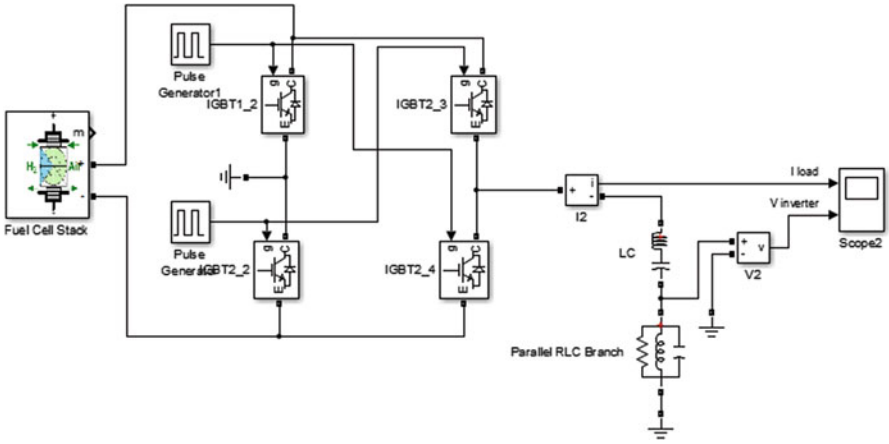


Fig. 9.53 MATLAB/SIMULINK model of LLCC resonant inverter

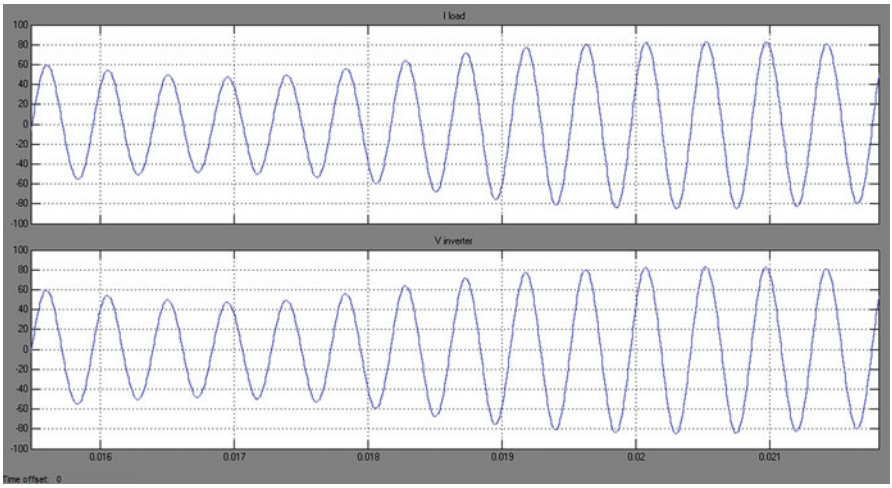


Fig. 9.54 Simulation results of LLCC resonant inverter

9.4 Fuel Cell System with Motor Load

As one of the most prominent sources of distributed energy in the future, fuel cells are under consideration for almost every application including both residential and industrial power generation. Yet, a power electronics interface must be incorporated between the fuel cell and output to provide flexibility due to the inherent

restrictions fuel cells produce, such as low voltage, large voltage variation, low efficiency when ripple current is high, slow load step responsibility and no acceptance of reverse current. The topology selection is not an easy process as it requires many constraints to be considered. The non isolated converters allows for the minimum size design. It is preferred for automotive applications. The converter must provide a high efficiency over the wide load range and maintain a high efficiency. The isolated converters are recommended for all applications where electrical isolation is required for a safety reason. It would be the automotive charging units or any grid-connected high power system. The isolated DC-DC converters are usually not considered for a vehicle power train as they require additional voltage conditioning systems. In general, high power converters tend to be multiphase for current sharing. Also, multiphase structure allows for increased part-load efficiency. The non-isolated converter is the most optimal solution for a low size converter in a low to medium voltage gain range. If a high voltage gain is required, the floating or transformer-based converters are the most optimum solution. The lowest input current ripple is available from multiphase converters due to current ripple cancelation. Selection of DC-AC converter plays a major role while using fuel cell output for AC loads and when connected to grid.

Apart from finding solutions to reduce device stresses and to improve the converter efficiency, many other challenges are posed for a power electronic circuit designer. Before selecting the converter topology, the efficiency of the converter must be evaluated in comparison with the overall efficiency of the system. Based on this evaluation, hard-switched or soft-switched topology must be chosen. Thorough investigation of DC-DC converters regarding EMI must be carried out to satisfy the standard regulations. Temperature effects must be considered to ensure a safe and reliable operation.

A fuel cell system with conventional boost converter and three phase inverter are used to feed an asynchronous machine. Figure 9.55 shows the MATLAB/SIMULINK model of the entire system and Fig. 9.56 shows the simulation result for speed, torque and stator current of asynchronous machine.

9.5 Architecture of Multiple Fuel Cells for High Voltage/High Power Applications

If more power is wanted than what is available from the standard size fuel cell, then modules need to be aggregated. There is more than one approach to aggregate numerous fuel cell modules for high-voltage/high-power applications. Four different approaches of these architectures are

- Series architecture.
- DC bus distribution architecture.
- High frequency AC (HFAC) distribution architecture.
- Multilevel architecture.

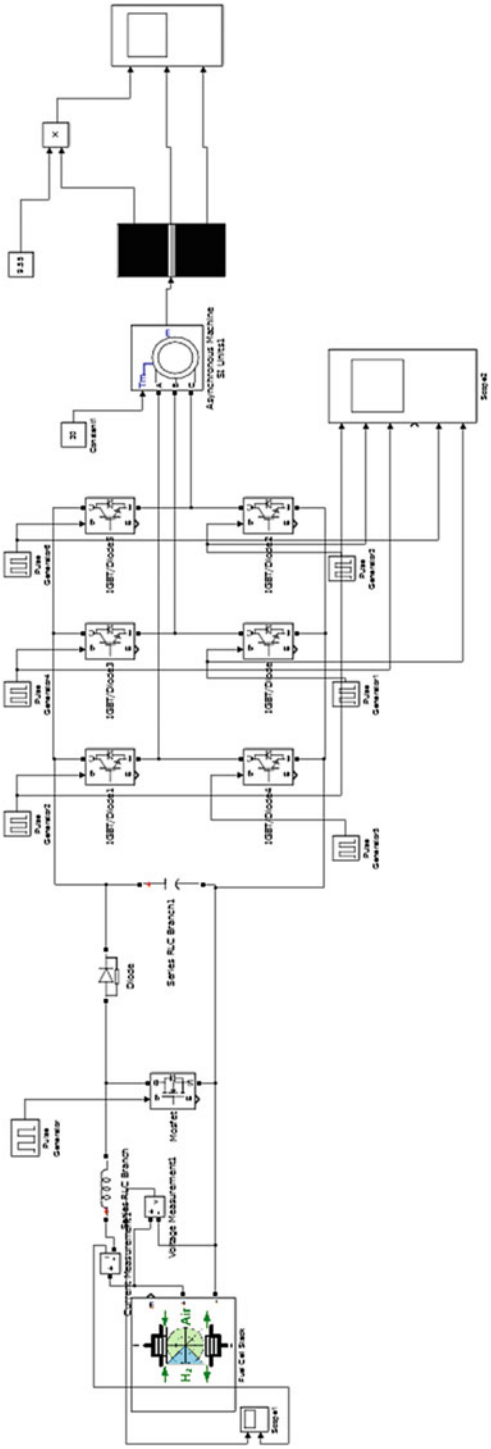


Fig. 9.55 MATLAB/SIMULINK model of fuel cell system to drive induction motor

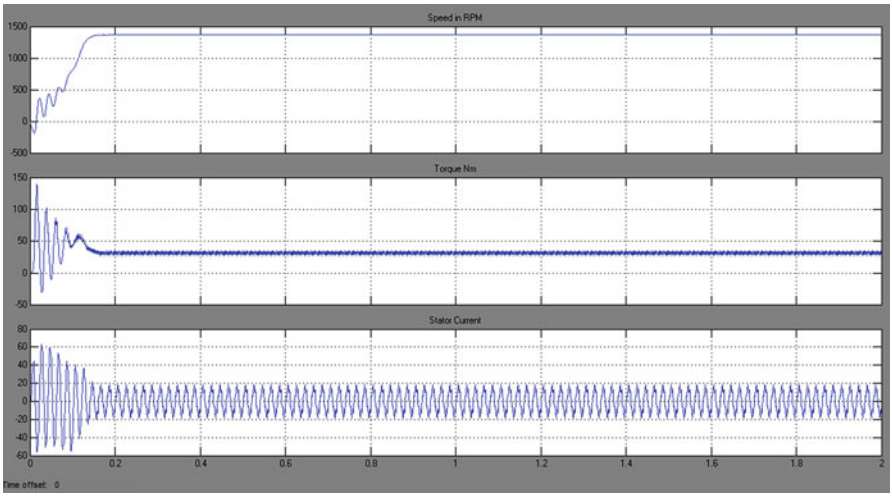


Fig. 9.56 Simulation results of the fuel cell system

9.5.1 Series Architecture

The series architecture, as shown in Fig. 9.57, simply connects all the fuel cell modules in series and interfaces the output with a power converter. The power converter can use any of the DC/DC converters and inverters. As the cumulative fuel cell module output voltage is enough for the inverter to produce AC grid level voltages, the DC/DC converter is used to regulate the DC voltage instead of boosting voltage. The DC/DC converter can also be removed and the modulation index of the inverter can be regulated to get a fixed output AC voltage. This architecture is the simplest of the topologies to be covered and is the most commonly used. The device count is low: only six power switches are required when no DC-DC regulator is used and sufficient fuel cell modules are aggregated. Three-phase inverter modules are commonly used and thus are inexpensive. Higher voltage- rated switches that need to handle no-load voltage levels would be more expensive. This is a modular architecture consisting of fuel cell modules, an inverter module, and a DC-DC converter module. To achieve the required power level, fuel cell modules can also be connected in parallel. The main quandary for this architecture is the failure mode. If one fuel cell module fails (open circuit), the whole system will stop working. The failing unit has to be replaced or bypassed externally. This causes reliability concerns.

But in paralleling fuel cell modules, extreme caution should be taken, since it is undesirable to feed current to the cells (unless a reversible fuel cell module is involved); a diode should be inserted as shown in Fig. 9.58 to block any possible circulating currents between the fuel cell modules.

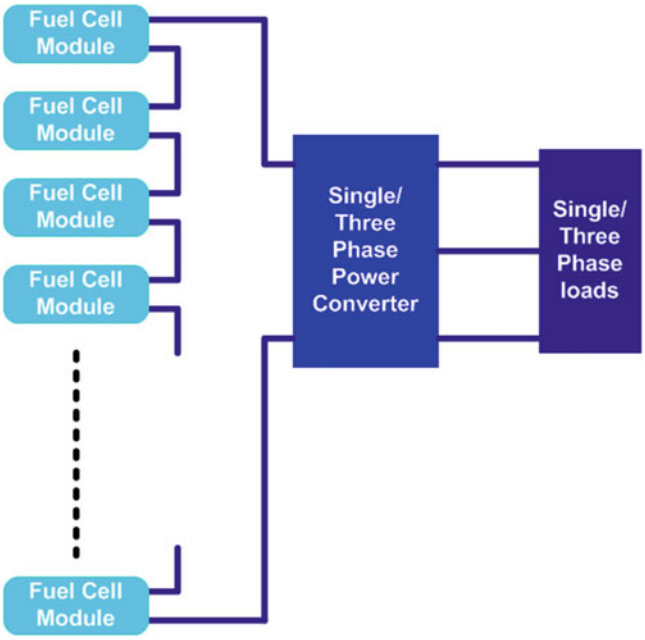


Fig. 9.57 Block diagram of series architecture

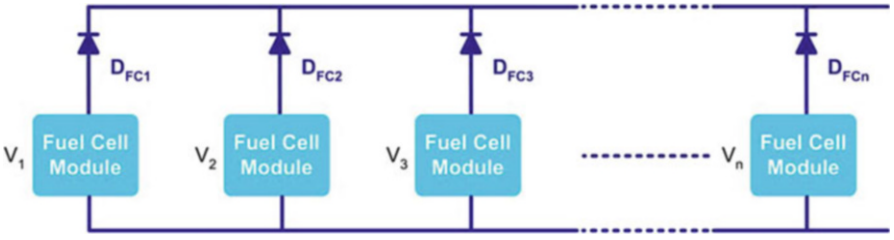


Fig. 9.58 Block diagram of parallel architecture

9.5.2 DC Bus Distribution Architecture

To overcome the disadvantages of the series architecture, a step-up DC-DC converter can connected to each fuel cell module; and the constant DC outputs of these converters can be connected in parallel, producing the DC bus distribution architecture shown in Fig. 9.59. In this architecture, each fuel cell module has its own power converter module. These DC-DC converters can be of the boost type if the fuel cell module voltage is less than the DC bus distribution voltage. The fuel cell module voltage can be equal to or greater than the DC bus distribution voltage if a sufficient number of cells are stacked together to form the fuel cell module. For such a scheme, a DC regulator should suffice to control the DC bus distribution voltage at a value best suited for the inverter. This architecture is inherently more reliable, as one individual fuel cell module's failure will not affect the whole system operation. Each subsystem can be designed as an individual module and stocked as

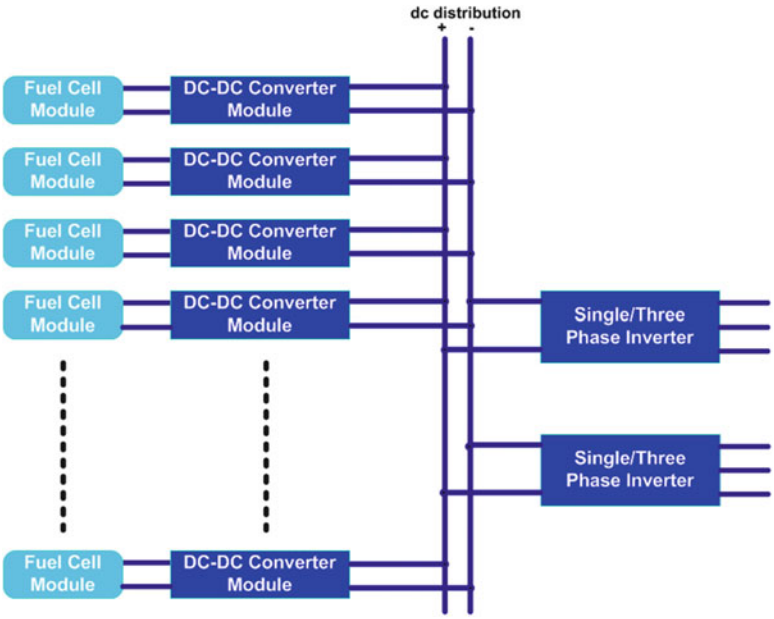


Fig. 9.59 Block diagram of DC bus distribution architecture

needed. The main dilemma of this converter is the higher device count. The addition of a DC-DC converter for every fuel cell multiplies the cost by a significant factor. In addition, each DC-DC converter's output voltage must be balanced with the other DC–DC converters to ensure that no circulating currents are present. To increase reliability, a redundant number of fuel cells can be connected in this architecture. Additionally, the constant voltage DC-link can also be used to feed one or several inverters, depending on the application.

The advantages of the DC Bus distribution architecture are: (i) each fuel cell can be controlled independently with the DC-DC converter module. The fuel cell modules can even be disconnected from the system for maintenance or replacement, and the rest of the system will continue the operation; (ii) Increased availability and fault-tolerant operation can be achieved by adding redundant fuel cell modules together with DC-DC converter modules. This architecture enhances the availability of fuel cell power, albeit at a reduced capacity while a fuel cell module is off-line for service or replacement; (iii) Each subsystem can be designed as an individual module, and they can be combined as needed. The list of modules would include the fuel cell module, the DC-DC converter module, and the inverter module. The inverter is already commercially available in a module. The disadvantages of the DC Bus distribution architecture are: (i) when the instantaneous voltages at the outputs of the DC-DC converters are not equal, circulating currents will occur. These will interfere with the operation of the system; therefore, they have to be prevented. Therefore, more complex control algorithms are required; (ii) This architecture requires a higher device count than the series architecture because of the DC-DC converters, but the devices have lower power ratings because more devices will be sharing the load current.

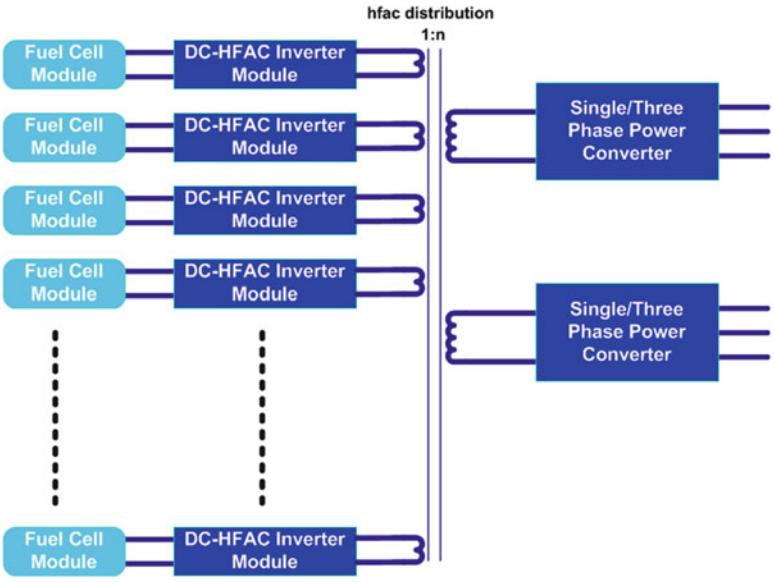


Fig. 9.60 Block diagram of HFAC distribution architecture

9.5.3 HFAC Distribution Architecture

The basic configuration of this architecture can be implemented through the use of the high-frequency link inverter as seen in Fig. 9.60. Each fuel cell is connected to a full-bridge inverter that converts the fuel cell DC voltage to a high-frequency AC. This AC is placed onto a small link and is shared among other fuel cells and their conditioning systems that are in parallel. Finally, a cycloconverter converts the high frequency link voltage to the appropriate output voltage. Unfortunately to place the converters in parallel, a strict control of the high-frequency output of the full-bridge converter must be in place adding severe complexity to this design.

The transformer brings the advantages of isolation, voltage boost, and the capability to add other power sources and loads through a power converter. Several converters can be connected to the extra primary and secondary taps, and the power can flow in different directions as required by the application. HFAC transformer is much smaller than a typical bulky 60 Hz transformer. As the frequency increases, the size of a transformer decreases. The challenge of fuel cell voltage variation with load also exists for the HFAC architecture. One solution to this problem is to insert a voltage regulator between fuel cell module and the DC-HFAC inverter. Another solution involves monitoring fuel cell voltages and modifying the control signals accordingly. The advantages of the HFAC distribution architecture are: (i) because of the high-frequency operation, the harmonics are at higher orders and it is easier to filter them with smaller, less-costly filters; (ii) The passive components required at high frequencies are smaller and lower cost just as in the case of the transformer;

(iii) Modularity is similar to the DC distribution case. The disadvantages of the HFAC distribution architecture are: (i) The HFAC transformer has to be specially designed; therefore, it will be expensive; (ii) If the transformer input voltage has a DC component, there will be a problem of transformer saturation. This can be eliminated with feedback control. Cycloconverters and matrix converters require AC switches, which are two switches connected back-to-back. They are not commonly available as modules. The control is complex because of the cycloconverter/matrix converter control and its interaction with the H-bridge high frequency inverters.

9.5.4 Multilevel Architecture

Fuel cell modules can be connected to one single/three-phase multilevel inverter as shown in Fig. 9.61. In this case, there might not be a need for a voltage regulator if fuel cell voltages are monitored.

There are many variations of multilevel architectures. One typical multilevel inverter, the diode clamped multilevel inverter, is shown in Fig. 9.62 for four fuel cell modules. The advantages of multilevel converter architecture are: (i) They are

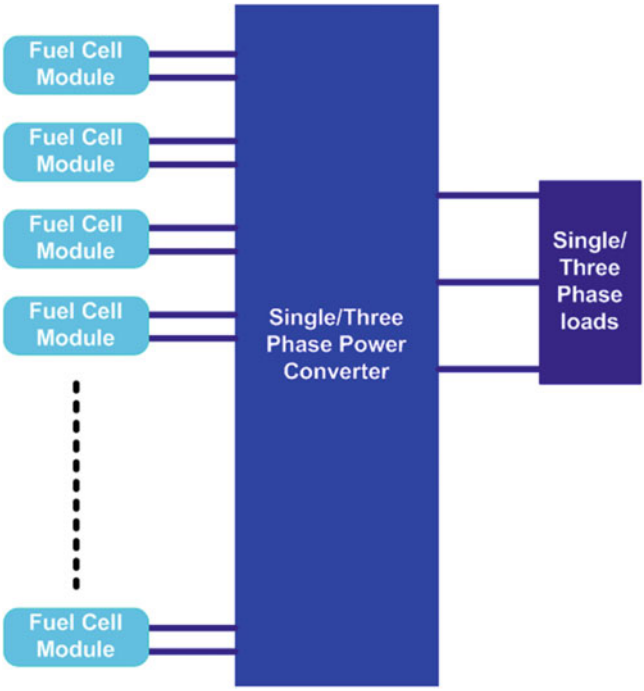


Fig. 9.61 Block diagram of the multilevel architecture

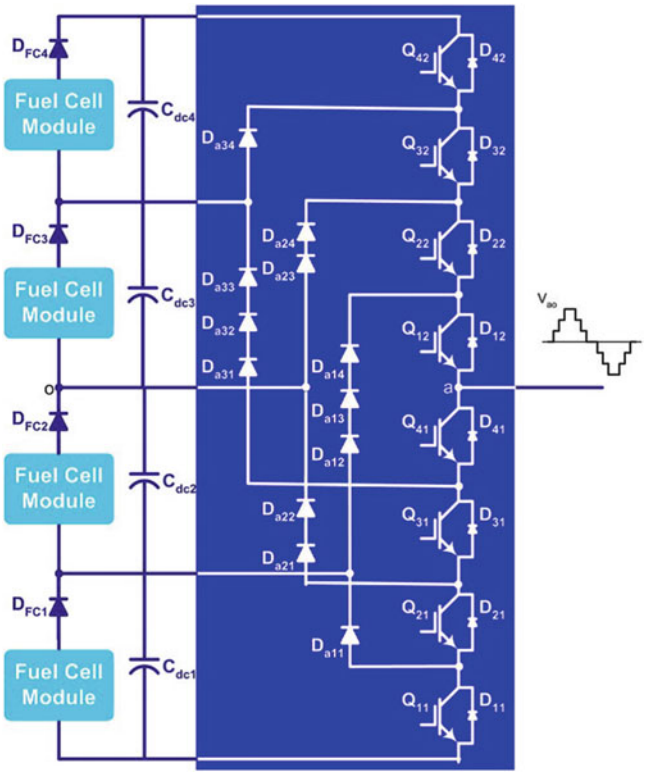


Fig. 9.62 One phase of a diode-clamped seven-level inverter

modular, lowering manufacturing costs. The cascaded multilevel converter is more modular than the other multilevel converters; (ii) Redundant levels can be added for increased reliability; (iii) Since each phase is built separately from the others, the final converter can be easily connected to be single-phase, multi-phase, or three-phase wye or delta; (iv) Fundamental frequency switching techniques can be applied to decrease the switching losses and to increase the converter efficiency; (v) Other control strategies, such as multilevel PWM or multilevel space vector PWM are possible. The disadvantages of multilevel converter architecture are: (i) the number of devices used in multilevel converters is high, but the voltage ratings of these devices are lower. An increased number of switches increase the price, but lower-rated switches are less-costly; (ii) Because of fundamental frequency switching, lower-order harmonics are higher; but there are techniques to reduce these harmonics. For example, the switching angles can be selected so that the required fundamental voltage is achieved with no 5th or 7th-order harmonics. Total harmonic distortion (THD) of 3 % has been achieved using fundamental frequency switching; (iii) for fuel cell applications, ripple current must be avoided. For a multilevel converter, care must be taken to reduce current ripple.

9.6 Summary

Uncertainty indeed remains as to the mix of technologies that will play the largest parts in meeting the challenges of global warming, energy security and economic efficiency in the longer term. Fuel cell could be a major and necessary source of energy within a decade. They have great potential as the basic elements of large and small stationary power plants and as the source of electricity for vehicles and smaller devices. Their shape and size are flexible and adaptable. They are modular having no moving parts, operate without combustion, are comparatively efficient and reliable, are nearly silent, generally do not pollute the environment and are quite safe. The technologies associated with hydrogen and with fuel cells are amongst those with the greatest potential, in particular, for the transport sector. Deployment of hydrogen infrastructure at this point would be premature, as some of the key technical issues that are still being worked on – such as fuel cell operating conditions and hydrogen on-board storage – may have a considerable impact on the choice of technologies for hydrogen production, distribution, and refuelling. As natural gas and coal are likely to remain the lowest-cost sources of hydrogen for many years to come, large-scale CO_2 capture and storage, already of the highest importance to mitigate emission in the power sector, is also a vital step towards the wider use of hydrogen. Fuel cells are under consideration for almost every application including both residential and industrial power generation. Yet, a power electronics interface must be incorporated between the fuel cell and output to provide flexibility due to the inherent restrictions fuel cells produce, such as low voltage, large voltage variation, low efficiency when ripple current is high, slow load step responsibility and no acceptance of reverse current. There are different types of fuel cell and based on the application the type of fuel cell has to be selected. Then the power electronic requirements of fuel cells have to be analysed and from various topologies of DC-DC boost converters and inverters best suited converters have to be used for fuel cells' power-conditioning system. Several architectures such as Series architecture, DC bus distribution architecture, High frequency AC (HFAC) distribution architecture, Multilevel architecture can be used to aggregate multiple fuel cells for high voltage/high-power applications.

Review Questions

1. What fuels can be used in a fuel cell?
2. How are fuel cells used to generate power for domestic purposes?
3. What is the present scenario of fuel cell energy?
4. Design a controller to control the fuel inputs to the fuel cell stack based on the feedback from the load output.
5. Develop a suitable power converter topology for efficient step up of voltage in fuel cells.
6. Mention the various switching techniques to control the switching operation with reduced switching losses.
7. Develop a MATLAB/SIMULINK model to implement the grid architectures using multiple fuel cells.

Bibliography

Bartok JW (2004) Approximate heating value of common fuels, Dec 2004
"Buck Converter Design Example", Microchip WebSeminor, Microchip Technology Incorporated. All Rights Reserved (2006). Microchip Web Sites: www.microchip.com/smps
Caceres RO, Barbi I (1999) A boost dc–ac converter: analysis, design, and experimentation. IEEE Trans Power Electron 14(1):134–141
Calais M, Agelidis V (1998) Multilevel converters for single phase grid connected photovoltaic systems, an overview. IEEE Int Symp Ind Electron 7–10:224–229
Chen A, He X (2006) Research on hybrid-clamped multilevel inverter topologies. IEEE Trans Ind Electron 53(6):1898–1906
Chen Y-M, Liu Y-C, Lin S-H (2003) Double-input PWM DC/DC converter for high/low voltage sources. In: Proceedings of the IEEE international telecommunications energy conference, pp 27–32
Chien-Ming W (2004) A novel single-stage full-bridge buck-boost inverter. IEEE Trans Power Electron 19(1):150–159
Chowdhury AA, Koval DO (2005) Impact of photovoltaic power sources on a power system's capacity reliability levels. I&CPS
Clean energy project analysis: RETSCREEN® engineering & cases textbook, [Online]. www.retscreen.net. Accessed June 2008
Corzine KA, Wielebski MW, Peng FZ, Wang J (2004) Control of cascaded multilevel inverter. IEEE Trans Power Electron 19(3):732–738
Haiwen Liu, Leon M Tolbert, Surin Khomfoi, Burak Ozpineci, Zhong Du (2008) Hybrid cascaded multievel inverter with PWM control method. IEEE, pp 162–166
Hart DW (1997) Introduction to power electronics. Prentice Hall, New Jersey
http://www.hrt.msu.edu/Energy/pdf/Heating%20Value%20of%20Common%20Fuels.pdf
http://www.solarbuzz.com/Technologies.htm
Institute of Electrical and Electronics Engineers (1987) IEEE recommended practice for installation and operation of lead-acid batteries for photovoltaic (PV) systems. ANSI/IEEE Std. 937–1987, New York
Institute of Electrical and Electronics Engineers (1990) IEEE recommended practice for installation and operation of nickel-cadmium batteries for photovoltaic (PV) systems. ANSI/IEEE Std. 1145–1990, New York
Khomfoi S, Aimsaard C (2009) A 5-level cascaded hybrid multilevel inverter for interfacing with renewable energy resources. IEEE, 978-1-4244-3388-9
Khomfoi S, Praisuwanna N (2010) A hybrid cascaded multilevel inverter for interfacing with renewable energy resources. IEEE, 978-1-4244-5393-1/10/2010
Kutkut NH, Divan DM, Novotny DW, Marion RH (1998) Design considerations and topology selection for a 120-kW IGBT converter for EV fast charging. IEEE Trans Power Electron 13:169–178
Linden D (1984) Handbook of batteries and fuel cells. McGraw Hill, New York
Musavi F, Eberle W, Dunford WG (2010) Efficiency evaluation of single-phase solutions for AC-DC PFC boost converters for plug-inhybrid electric vehicle battery chargers. In: Proceedings of IEEE VPPC, pp 1–6, Sept 2010
Navigant Consulting (2006) A review of PV inverter technology cost and performance projections NREL/SR-620-38771, Jan 2006. www.nrel.gov. Accessed June 2008
Orosco R, Vazquez N (2000) Discrete sliding mode control for DC/DC converters. Power Electronics Congress 231–236
Rashid MH (2006) Power electronics devices, circuits and applications. Academic Press, San Diego
Saravana Ilango G, Srinivasa Rao P, Karthikeyan A, Nagamani C Single-stage sine-wave inverter for an autonomous operation of solar Photo voltaic energconversion system
Teodorescu R, Blaabjerg F, Pedersen JK, Cengelci E, Enjeti PN (2002) Multilevel inverter by cascaded industrial VSI. IEEE Trans Ind Electron 49(4):832–834

Appendix I
Models Used to Assess the Performance of Solar PV Systems

The photovoltaic industry is poised to experience a period of fast development due to numerous factors, including but not bounded to the following: an increasing hope by public to cut down their carbon emissions, formation of state renewable portfolio standards (RPS), use of third-party power purchase agreements (PPAs), new federal tax incentives for constructing and installing, new PV cell, inverter and storage technologies, and a decrease in the cost of PV system components. When additional PV systems are installed, there will be an increase in need for software package that can be applied for plan, analysis and troubleshooting. A basic example outlining the importance of PV performance monitoring is that new regulatory devices are being put into place that make the amount of tax credit returned from an installation conditional on the amount of electricity generated by a PV system. An incomplete judgment of a PV system's capacities can underestimate system payback and affect potential funding. Once new PV technologies are deployed, anticipated and actual functioning data will be included in databases, and additional presumptions may postulate significant changes to the present empirical and analytical techniques. The utilization of batteries for both small and large-scale energy storage and power conditioning will also be important as PV grid penetration increases. A comprehensive perceptive of available models, capabilities, tradeoffs and shortcomings will be required to maintain with changes in technology and differing needs by end-users both at present and in the future. This new phase of PV deployment will be successful if the photovoltaic, hybrid simulation and battery modeling tools can handle these new challenges.

AI.1 PV Performance Models

Photovoltaic performance models are used to estimate the power output of a photovoltaic system, which typically includes PV panels, inverters, charge controllers and other "balance of system" (BOS) components. These models create a

© Springer International Publishing Switzerland 2015

S. Sumathi et al., *Solar PV and Wind Energy Conversion Systems*,
Green Energy and Technology, DOI 10.1007/978-3-319-14941-7

generation profile based on a specific geographic location which helps determine how much solar irradiance is available for harvesting. The meteorological inputs for any given location vary by latitude, season and changing weather patterns; being able to accurately determine the generation profile due to these changing variables results in better matching of system load with expected generation. Some models make general assumptions about system components and ratings while other more complex models take into account manufacturer parameters, derived parameters and empirically derived data. These models can also be used to evaluate system performance over time by providing a baseline to compare with if performance suddenly decreases and troubleshooting is necessary. Financial considerations are also important when considering PV; some models are considered "system" models due to the inclusion of capital and operating costs as well as expected benefits in terms of payback period, avoided costs, internal rate of return, levelized cost-of-energy (LCOE), cash flow and depreciable basis, just to name a few. System derate factors are also important as equipment degrades over time resulting in a power output decrease.

Following are some of the commonly used PV software models:

PVSS

The Photovoltaic System Simulation Program (PVSS) is a simple component model built in FORTRAN to simulate PV system performance by allowing the user to choose a variety of different system configurations for both on and off-grid PV systems. A plane of array (POA) radiation model was not used in this model. Array performance is based on a one-diode equivalent circuit equation for determining the current–voltage (I-V) curve. Temperature effects on irradiance are based on equation that is a function of the band-gap, a silicon specific constant, Boltzmann's constant and the cell temperature.

SOLCEL

SOLCEL is a system-level model used for both grid-tied and off-grid (battery storage) PV systems. It is implemented in FORTRAN and can run simulations down to an hourly time-step. A simple equivalent circuit model as described in PVSS is used to model array performance. Temperature effects on array performance are determined using a temperature-corrected efficiency model based on PVSS and modified based on different passive and active cooling configurations. The program can model both flat-plate and concentrating PV (CPV) incorporated onto trackers or fixed arrays. Weather and solar insolation data for the model is obtained using the SOLMET Typical Meteorological Year (TMY) database. SOLCEL is set up to look at different scenarios to determine the best system design for a desired range of costs including, but not limited to PV energy cost, total

system cost, life-cycle cost, and rate of return. The two economic-evaluation techniques the program implements are the life-cycle costing methodology and the Department of Energy (DOE)/Electric Power Research Institute (EPRI) required revenue methodology. SOLCEL can also find the optimal configuration with the lowest life-cycle cost

Evans and Facinelli Model

A photovoltaic performance model for PV systems was developed by Arizona State University under contract with Sandia National Laboratories. In the model, system performance is analyzed when using a battery or converted energy from the array for maximum power point tracking (MPPT). The assumption in this model is that the PV arrays only generate power at the maximum power point on the I-V curve. The model runs on a monthly time-step and is implemented in the TRNSYS environment. For POA irradiance, a tilt correction factor is used and the arrays are either tracking or moved monthly to optimize energy production. For array performance, a power temperature coefficient model considers the efficiency, temperature and tilt correction factor. Technologies modeled include cSi and CPV with weather and insolation data taken from the SOLMET TMY database.

PVForm

PVForm by Menicucci was one of the first "system" models for PV applications that can analyze and compare system performance in one or many locations with the benefit of incorporating system costs. The model has the ability to look at both grid-tied and stand-alone systems (with battery storage) and can allow a user to model system degradation, and the effects of load and component changes.

PVForm was also built to both simplify and improve the SOLCEL model. PVForm appears to only model flat plate cSi. For weather and solar insolation, the TMY dataset is utilized. For financial information, PVForm gives users the ability to understand important metrics such as LCOE for comparing the cost of other electricity generating technologies with PV.

PVSIM

PVSIM was developed better understand the electrical behavior between each module in an array. Specifically, it was built to take a look at module mismatch and shading loss. This analysis is done using a two-diode equivalent circuit model with empirically derived parameters from dark I-V measurements at a low (25 °C) and

high (50 °C) cell temperatures. The software program allows for users to enter their parameters to create cell I-V curves determined through testing. From there, users can see how an array would perform at a variety of different operating temperatures.

Sandia Photovoltaic Array Performance Model

The Sandia PV Array Performance Model utilizes a database of empirically derived PV module parameters developed by testing modules from a variety of manufacturers. The data can be used to evaluate the performance of PV systems in three ways:

1. Design a PV system to properly match desired generation with load information on timescales that vary from 1 h to 1 year;
2. Calculate the system power rating from module-specific empirically derived formulas developed at SNL, and
3. Provide long term analysis capabilities that are useful for measuring array performance and troubleshooting support.

Where other algorithms attempt to determine array performance in conditions that are not optimal (most of the time), using theoretical and semi-empirical methods, the Sandia PV Array Performance Model is a departure from many of the earlier equations used to derive power from a PV system as it is based on empirical measurements made for modules in conditions other than the manufacturer provided standard test conditions (STC). This model calculates the Isc, Imp, Vmp, Voc, and two other current values at intermediate points. This is accomplished with a curve-fitting process using coefficients derived from module testing. Empirical coefficients are also developed to calculate parameters that are temperature dependent (including a module specific thermal model), effects of air mass and angle of incidence on the short-circuit current, and type of mounting (whether rack mounted or BiPV). This model also allows for the determination of an "effective irradiance", which is the amount of irradiance that actually reaches the cells after other losses are taken into consideration.

Sandia Inverter Performance Model

The Sandia Inverter Performance Model for grid-tied systems characterizes efficiencies in the conversion process from dc-power to ac-power using an empirical method through the testing of operating inverters. Inverter performance is characterized as a function of input power and voltage, and coefficients are derived that can be used in the model. The results of the testing include an inverter parameter database with equations that can be utilized with the Sandia PV Array Performance Model.

PVDesignPro

PVDesignPro software is a commercially available software model developed by the Maui Solar Energy Software Corporation (MSESC) and SNL for photovoltaic systems modeling. The software incorporates algorithms from both of SNL's PV array and inverter performance models as well as SNL's database of PV module and inverter parameters. NIST uses a custom version of PVDesignPro for comparing different PV technologies and predicting PV module performance for BIPV applications. The program uses an hourly time-step for modeling system performance. If financial analysis is desired, the software will take system cost inputs to determine cash flow, payback period, internal rate of return, and utility

Solar Advisor Model

The Solar Advisor Model or SAM, as it is commonly referred to, is a stand-alone software program created in 2006 by a partnership with the National Renewable Energy Laboratory (NREL) and SNL through the DOE Solar Energy Technologies Program. The model is being continuously updated and improved and has an active user community that can be accessed at: http://groups.google.com/group/sam-user-group.

5-Parameter Array Performance Model

The 5-Parameter array performance model was developed from research conducted at the Wisconsin Solar Energy Laboratory (SEL). This model utilizes the well known one-diode array performance model for evaluating PV array performance.

PVWatts

PVWatts is a grid-connected photovoltaic modeling tool developed by NREL that is based on the PVForm algorithms developed at SNL. This includes the POA radiation model and the modified power temperature coefficient model for array performance. A hierarchy of programs that descended from PVForm and from its predecessor,

PVSYST

PVSYST is a photovoltaic system analysis software program developed by the Energy Group at the University of Geneva in Switzerland and can be used at any location that has meteorological and solar insolation data. It is widely used due to the many parameters available for the user to modify. The complexity of the input parameters makes it suitable for expert users.

Other interesting features include a 3-D shading tool that allows a user to draw a structure with PV arrays and see potential shading impacts from simulated obstructions. There is an option to analyze array mismatch to determine more specific Isc and Voc parameters, as well as look at cell/module shading and other voltage losses due to wiring, and soiling. Other useful features include an incident angle modifier and an air mass spectral correction for thin-film modules, as well as the ability for the user to input known parameters and coefficients if measured data is available for both PV modules and inverters.

PV F-Chart

PV F-Chart is a PV array performance modeling software developed at the University of Wisconsin SEL and licensed through F-Chart software. For POA radiation, it uses a simple isotropic sky model. Array performance of cSi modules is calculated as a function of cell temperature, efficiency, and incident angle. For weather and solar insolation, TMY2 data is utilized. Economic analysis results including life-cycle and equipment costs are also included in the analysis.

RETScreen Photovoltaic Project Model

RETScreen is a program developed by Natural Resources Canada for evaluating both financial and environmental costs and benefits for many different renewable energy technologies. RETScreen has a specific Photovoltaic Project Model that can model PV array performance for many locations around the world.

PVSol

PVSol is a photovoltaic systems analysis software program developed by Valentin Energy Software in Germany with an English language version distributed by the Solar Design Company based in the UK. The first version of PVSol was released in 1998. The Expert edition has the most features, including a 3-D shading program.

INSEL

The Integrated Simulation Environment Language (INSEL) solar electricity toolbox from Doppelintegral GmbH in Germany is a photovoltaic systems analysis program. It appears the software was initially developed in 1991. INSEL is modular in the sense that it can be linked to other programs and can be customized by an advanced user.

SolarPro

SolarPro software is a PV system simulation program from Laplace System based in Kyoto, Japan. The first version of the software appears to have been released in 1997. The user must first define the system in terms of mounting, array layout and orientation, then develop a 3-D layout that can have shading objects built-in. Interesting features include detailed analysis of module-specific shading within an array by looking at module I-V curves.

The user must first define the system in terms of mounting, array layout and orientation, then develop a 3-D layout that can have shading objects built-in. Interesting features include detailed analysis of module-specific shading within an array by looking at module I-V curves.

PVOptimize

PVOptimize is a software tool developed for the California market by KGA Associates and is geared towards installers for generating system quotes and design. The program uses PVWatts for solar resource data and array performance modeling. Modules available for analysis include cSi, CdTe, aSi, CPV and Ribbon. For weather and insolation, the program uses PVWatts (TMY2) data. There are many forms and inputs specific to the incentives and rebates offered by the State of California. Therefore the model may have limited utility to locations outside of California.

OnGrid

OnGrid is a software tool developed for use in the U.S. by Andy Black of OnGrid Solar in California and is focused on what installers need for system quotes and design. The program uses PVWatts for the array performance calculations. Module technologies available for analysis include cSi, aSi, CdTe and Ribbon. This

software consists of a macro-enabled Excel spreadsheet that can be customized for any incentive program available in the U.S. Incentives for the State of California are included by default. The spreadsheet can look at system cost, incentives, depreciation, cash flow, O&M costs, and internal rate of return.

CPF Tools

CPF Tools is a software program developed in 2007 by Energy Matters LLC for Clean Power Finance. The software is aimed towards system installers for system design, economics and financing. CPF tools also leverages the technology in RoofRay, which is an on-line interactive tool that allows a user to easily draw an outline of a potential PV array to explore the potential costs and benefits. RoofRay is similar to the IMBY tool developed by NREL for an interactive analysis of potential PV system size. CPF Tools was previously known as Solar Pro Tools

Solar Estimate

Solar Estimate is a web-based tool developed by Energy Matters LLC for both residential and commercial solar resource estimation. The user enters in a zip code and chooses the utility that they purchase power from. Assumptions include a total energy delivered of 78 %, which includes derates for panel, inverter, wiring and panel soiling. For POA radiation and array performance, PVWatts is used. The model does not specify a PV technology, although it is likely based on flat plate cSi modules. Because the model uses PVWatts for determining solar energy, it probably uses TMY2 data for weather and insolation measurements.

AI.2 Hybrid System Models

Hybrid system models are used to simulate the performance of "hybrid" or "distributed energy resource" systems that typically include one or more renewable sources of electricity combined with a traditional fossil based fuel source. These models were built initially to look at the use of PV or wind as a backup source for small and remote off-grid applications. Battery storage and lifetime (primarily from lead-acid) is simulated due to the need for a continuous source of power. More recent models can incorporate sources such as biomass, hydro, and other energy storage devices such as non lead-acid batteries, fuel cells, capacitors, flywheels and compressed air. These models discussed below can also look at grid-tied systems and attempt to capture interactions at the utility scale.

SOLSTOR

SOLSTOR is a model developed at SNL for looking at the overall economics and optimization strategies of different hybrid system configurations. Components include PV arrays, wind turbines and generators. Storage is in the form of batteries and flywheels. Power conditioning options are also available. The model can be run with a utility connection or stand-alone with a backup generator.

The program incorporates some of the PV array performance algorithms as described in SOLCEL. PV technologies that can be modeled include cSi and CPV. SOLSTOR uses the SOLMET database for weather and insolation data. Economic output includes capital costs, O&M costs, energy purchase costs, depreciation, investment tax credits, salvage value and financing.

HybSim

HybSim is a hybrid energy simulator developed and copyrighted at SNL for looking at the costs and benefits of adding renewable energy to a fossil fueled electrical generation system in a remote location. The model requires knowledge of the existing load profile, weather, battery characteristics and a few economic details. At the moment, solar PV is the only renewable energy source available for comparison however wind power will be another choice in a future versions of the model. Current license holders include the University of Michigan and a few corporate customers.

The system is designed to model cSi modules. For weather and insolation, HybSim can use data measured at 15-min intervals. Lifecycle costs are analyzed for system components including PV modules, generators and batteries. Capabilities include comparing cost and performance differences with a diesel only system with one using a combination of diesel, PV, wind and battery storage.

Hysim

Hysim is a hybrid energy simulation model developed at SNL for analyzing the combination of PV, diesel generators and battery storage for stand-alone systems in remote locations. The purpose of this model was to look at increasing overall system reliability by adding the PV and battery storage, as well as the economics associated with PV and batteries compared to existing generator only systems. Hysim uses a modified version of the battery model in SOLCEL. For POA radiation and PV array performance, Hysim uses PVForm. The only PV technology modeled in Hysim is cSi. For weather and insolation data, Hysim uses TMY2. Financial analysis includes LCOE, lifecycle, fuel and O&M costs, as well as cost comparisons between different configurations.

HOMER

HOMER is a hybrid system model developed at NREL in 1993 for both on-grid and off-grid systems. A unique capability that HOMER offers is the ability to find the optimal configuration based on price estimates as well as perform sensitivity analysis to help understand tradeoffs between different technologies and economic considerations. The software has the ability to compare multiple system configurations as well as different battery types. The model can incorporate the following components: PV, wind, hydro, fossil fuel generator, battery, AC/DC converter, electrolyzer, hydrogen tank and reformer. Temperature effects are not considered in the performance calculation, however they can be accounted for as a part of the total system derate. HOMER uses a generic module type for analysis. For weather and insolation, HOMER can use TMY2 formatted data or custom user inputs.

Hybrid2

Hybrid2 is described as a probabilistic time series computer model for evaluating the performance and economics of hybrid electricity generating systems. It was developed by the Renewable Energy Research Laboratory (RERL) at the University of Massachusetts Amherst with support from NREL. This program is an engineering design model for hybrid systems consisting of PV, wind, generators and battery storage for both on-grid and off-grid systems.

UW-Hybrid (TRNSYS)

The UW-Hybrid simulation model is described as a quasi-steady performance simulation tool for looking at hybrid systems consisting of solar, wind, diesel generators and battery storage. This hybrid simulator is part of the TRNSYS software program but can be run alone under a demonstration editor version called TRNSED.

RETScreen

RETScreen is a program developed by Natural Resources Canada for evaluating both financial and environmental costs and benefits for many different renewable energy technologies for any location in the world. The Photovoltaic Project Analysis module was covered in Sect. 2.4.1. Electricity generation options include solar,

wind, fuel cells, gas or diesel generators, gas turbines, geothermal, tidal power, wave power, hydro turbine, and ocean current power. For combustible fuels, fossil, biomass, waste and hydrogen are listed in terms of inputs for modeling. Energy storage options include batteries.

PVToolbox

PVToolbox is a hybrid system model developed for the Natural Resources Canada CANMET Energy Technology Centre – Varennes (CETC-Varennes). The program is written for use within Matlab Simulink and has been validated using bench tests which describe the model vs. measured performance under different load scenarios. The model looks specifically at PV, diesel generator and battery systems designed for Canadian latitudes and weather conditions.

RAPSIM

The Remote Area Power SIMulator (RAPSIM) is a hybrid system model developed in Australia at the Murdoch University Energy Research Institute (MUERI). This program simulates systems comprising of PV arrays, wind turbines and diesel generators with battery storage. The organization that currently houses the work at the university is called the Research Institute for Sustainable Energy (RISE).

SOMES

SOMES is also known as the Simulation and Optimization Model for Renewable Energy Systems. It was created at the Utrecht University in The Netherlands. The simulation program can look at hybrid systems that utilize PV arrays, wind turbines and generators for generating electricity and batteries for storage. Both technical and economic parameters can be modeled as well as an optimization model to help figure out the best configuration at a specific cost.

IPSYS

IPSYS is a hybrid simulation modeling tool for remote systems. The program has a component type library and can model electricity generation through PV arrays, wind turbines, diesel generators, fuel cells as well as natural gas. Energy storage

can be modeled using batteries, hydro reservoirs and hydrogen. The model is written in C++ and there is no current graphical user interface, however there are scripts that can be used to analyze model output within graphs.

HySys

The Hybrid Power System Balance Analyser, or HySys is a hybrid simulation tool developed at the Centro de Investigaciones Energeticas, Medioambientales y Technologicas (CIEMAT) institute in Spain by their wind technology group. The software is primarily for isolated systems and includes electricity from PV arrays, wind turbines and diesel generators. According to the IEA 2008 report as shown in the reference below, the software appears to be under development to operate primarily within Matlab.

Dymola/Modelica

The Fraunhofer Institute for Solar Energy (ISE) in Germany uses the Modelica/Dymola object oriented programming language for modeling PV-hybrid systems. The electricity sources include PV, wind turbines, generators and fuel cells along with storage in the form of batteries.

Battery Performance Models

Photovoltaic systems provide varying amounts of power throughout the day due to the intermittent nature of sunlight reaching PV panels. Cloudy days, varying temperatures, system latitude, module configuration and shading effects directly affect the amount and timing of photovoltaic energy that can be produced.

SIZEPV

The purpose of SIZEPV was to determine the optimal configuration of a PV system with battery storage using a loss-of-load probability model. The results of this model were by comparing with loss-of-load probabilities calculated with PVForm. The advantage of using SIZEPV for PV systems with battery storage is the ability to run multiple iterations much quicker than if set up using PVForm. The model is limited to lead-acid batteries. Required input data includes battery capacity, minimum allowable state-of-charge (SOC), equalization SOC, backup capacity, equalization schedule, beginning SOC, maximum charge efficiency and maximum discharge efficiency.

KiBaM

The Kinetic Battery Model (KiBaM) is a lead-acid battery modeling application developed by Manwell and McGowan (1993) at the University of Massachusetts RERL. KiBaM is considered a phenomenological model where many of the battery parameters are derived from extensive testing, and uses a modified amp-hour (Ah) cycle counting method to model battery performance and lifetime. The original version was built for wind/diesel systems with PV added in later versions. HOMER, as discussed above, uses a simplified version of the KiBaM model.

Appendix II
Research Projects

A brief description of research projects from various IEEE journals, Research centers and Universities are given in this appendix.

AII.1 A New Converter Topology for Hybrid Wind/ Photovoltaic Energy System

Renewable energy technologies offers clean, abundant energy gathered from self-renewing resources such as the sun, wind etc. As the power demand increases, power failure also increases. So, renewable energy sources can be used to provide constant loads. A new converter topology for hybrid wind/photovoltaic energy system can be proposed. Hybridizing solar and wind power sources provide a realistic form of power generation. The topology uses a fusion of Cuk and SEPIC converters. This configuration allows the two sources to supply the load separately or simultaneously depending on the availability of the energy sources. Renewable energy sources also called non-conventional type of energy are continuously replenished by natural processes. Hybrid systems are the right solution for a clean energy production. Hybridizing solar and wind power sources provide a realistic form of power generation. A hybrid wind and solar energy system with a converter topology can be proposed which makes use of Cuk and SEPIC converters in the design. This converter design overcomes the drawbacks of the earlier proposed converters. This topology allows the two sources to supply the load separately or simultaneously depending on the availability of the energy sources. The output voltage obtained from the hybrid system will be the sum of the inputs of the Cuk and SEPIC converters. This system has lower operating cost and finds applications in remote area power generation, constant speed and variable speed energy conversion systems and rural electrification. MATLAB/ SIMULINK software can be used to model the PV panel, wind turbine, DC-DC converters and the proposed hybrid system.

© Springer International Publishing Switzerland 2015

S. Sumathi et al., *Solar PV and Wind Energy Conversion Systems*,
Green Energy and Technology, DOI 10.1007/978-3-319-14941-7

AII.2 Energy Conversion Efficiency of a Novel Hybrid Solar System for Photovoltaic, Thermoelectric, and Heat Utilization

A novel hybrid solar system can be designed to utilize photovoltaic (PV) cells, thermoelectric (TE) modules, and hot water (HW) through a multilayered building envelope. Water pipelines are cast within a functionally graded material layer to serve as a heat sink, allowing heat to be easily transferred into flowing water through an aluminum-rich surface, while remaining insulated by a polymer rich bottom. The theoretical energy conversion efficiency limit of the system can be investigated for documenting the potential of this hybrid solar panel design. Given the material properties of each layer, the actual energy conversion efficiency depends on the solar irradiation, ambient temperature, and water flow temperature. Compared to the traditional solar panel, this design can achieve better overall efficiencies with higher electrical power output and thermal energy utilization. Based on theoretical conversion efficiency limits, the PV/TE/HW system is superior to PV/HW and traditional PV systems with 30 % higher output electrical power. However, the advantages of the PV/TE/HW system are not significant from experimental data due to the low efficiency of the bulk TE material. Thus, QW/QD TE materials are highly recommended to enhance the overall efficiency of the PV/TE/HW design. This design is general and open to new PV and TE materials with emerging nanotechnology for higher efficiencies. Hybrid solar panels integrated with Si solar cells, TE materials, and FGM water tube systems can be demonstrated. The FGM water tube systems have good cooling function, which can recover the PV cell efficiency by 30–50 % and 25–40 % for the PV/HW and PV/TE/HW system, respectively, by controlling the temperature and also enhance the TE output power by three times. Incorporation of bulk TE modules in the solar panel shows comparable performance as those of PV/FGM design. High-efficiency QW/QD TE materials could potentially contribute higher electric power and enhance the overall efficiency for PV/TE/HW design.

AII.3 Design and Implementation of Power Converters for Hybrid Wind-Solar Energy Conversion System with an Implementation of MPPT

The power converter can not only transfer the power from a wind generator, but also improve the stability and safety of the system. The proposed system consists of a Permanent magnet synchronous generator (PMSG); a DC/DC boosts converter, a bi-directional DC/DC converter and a full-bridge DC/AC inverter. The wind generator is the main power source of the system, and the battery can be used for

energy storage and power compensation to recover the natural irregularity of the wind power. A new system configuration of the front-end rectifier stage for a hybrid wind or photo voltaic energy system can be proposed. The configuration allows the two sources to supply the load separately or simultaneously, depending on the availability of energy sources. The inherent nature of this cuk-sepic fused converter, additional input filters are not necessary to filter out high frequency harmonic content is determinant for the generator life span, heating issue and efficiency. The fused multi-input rectifier stage also allows maximum power from the wind and sun. When it is available an adaptive MPPT algorithm will be used for photo voltaic (PV) system. Operational analysis of the proposed system can be simulated to highlight the merit of the proposed circuit. In this a new multi-input Cuk-SEPIC rectifier stage for hybrid wind/solar energy systems can be presented. The features of this circuit can be: (1) additional input filters are not necessary to filter out high frequency harmonics; (2) both renewable sources can be stepped up/down (supports wide ranges of PV and wind input); (3) MPPT can be realized for each source; (4) individual and simultaneous operation can be supported. By implementing this technique we can increase the power transfer efficiency. We can extract maximum power without any interruption. There is no need to depend upon non renewable energy sources and this could be eco friendly.

AII.4 Unit Sizing and Control of Hybrid Wind-Solar Power Systems

The aim is to provide the core of a CAD/CAA tool that can help designers determine the optimal design of a hybrid wind-solar power system for either autonomous or grid-link application. The analysis employs linear programming techniques to minimize average production cost of electricity while meeting the load requirements in a reliable manner, and takes environmental factors into consideration both in the design and operation phases. While in autonomous systems, the environmental credit gained as compared to diesel alternatives can be obtained through direct optimization, in grid-linked system emission is an another variable to be minimized such that the use of renewable energy can be justified. A controller that monitors the operation of the autonomous or grid-linked systems design can be used. Such a controller determines the energy available from each of the system components and the environmental credit of the systems. It gives details related to cost, unmet and spilled energies, and battery charge and discharge losses. It uses linear programming principle to reduce the cost of electricity. The use of renewable energy offers substantial environmental credit when compared to grid/diesel alternatives. This analysis will allow the user to study the interaction among economic, operational and environmental factors. It offers an useful tool for the design and analysis of hybrid wind-solar power systems.

AII.5 Application of Integrated Wind Energy Conversion System (WECS) and Photovoltaic (PV) Solar Farm as STATCOM to Regulate Grid Voltage During Night Time

The integration of wind energy conversion system (WECS) with photovoltaic (PV) solar farm (SF) can be proposed which could act as a flexible a.c transmission system controller-static synchronous compensator during night time, to regulate the point of common coupling voltage and to rectify faults when SF is not producing any active power. A novel concept of optimal utilization of a PV SF as a STATCOM can be proposed and validated through MATLAB/SIMULINK simulation. The proposed control will enable increased connections of WECS. The proposed strategy of PV SF control will facilitate integration of more wind plants in the system without needing additional voltage-regulating devices. PV Solar farm virtually inactive during night time in terms of active power generation can be used to regulate the distribution voltage at PCC within utility specified limits even during wide variations in WF output and rectifies the fault. This novel strategy implies operating PV solar plant as a generator during the day [providing megawatts (MW)] and ancillary services provider at night [providing mega volt amperes (MVARs)]. This may pose interesting questions on ownership/partnership/lease options, license to operate, etc., and possible code changes by the regulator.

AII.6 Application of Fuzzy Wavelet Transform to Smooth WindPV Hybrid Power System Output with Battery Energy Storage System

The battery energy storage system (BESS) is the current typical means of smoothing intermittent wind or solar power generation. The proposed system could present the results of a wind/PV/BESS hybrid power system simulation analysis undertaken to improve the smoothing performance of wind and Photo Voltaic (PV) power generation. A power smoothing control method can be proposed based on fuzzy logic and wavelet transform for reducing output power fluctuations of wind/PV/BESS hybrid power generation systems. Wind and PV power generation systems have the disadvantage of an unstable power output, which can impact negatively on utility- and micro-grid operations. One means of solving this problem is to integrate WPGS and PVGS with a battery energy storage system. For such hybrid generation systems, control strategies need to be developed to efficiently dispatch power. Therefore, a fuzzy-logic-based wavelet filtering control method can be proposed for smoothing the output fluctuation of the WPGS and PVGS hybrid power generation system. Simulation results demonstrate that the proposed control strategy can manage battery SOC within a specified target region while smoothing WPGS and PVGS output power.

AII.7 Night Time Application of PV Solar Farm as STATCOM to Regulate Grid Voltage

The concept of utilizing photovoltaic (PV) solar farm (SF) as flexible a.c transmission system controller-static synchronous compensator, to regulate the point of common coupling voltage during night time when the SF is not producing any active power can be proposed. The control will enable increased connections of Wind Energy Conversion System (WECS) to the grid on average wind energy which is the best at night when the atmosphere is stable. By combining the wind and solar PV on a utility scale the uncertainty of generation is greatly reduced and more reliable energy source can be created. Times of no energy production from either wind or solar dropped by 50 % or more for each time. Given one megawatt wind turbine and one mega watt of solar panels placed immediately south of the turbine they can both utilize the same pad mount transformer and electrical collection system reducing the initialized cost. MATLAB/simulink based simulation results can be presented for validation of the system. Thus by combining wind and solar power plants the whole is greater than the sum of its parts and the intermittency of renewable energy is significantly reduced by paring the two individual one-megawatt systems which have nearly opposite production phase gross capacity factor of 0.608 was attained when not curtailing either wind or solar.

AII.8 Micro Perspectives for Decentralized Energy Supply

To evaluate the electricity costs, of the PV-battery system, the progression of the power demand and electricity production can be evaluated and compared with cost and revenue of the resulting energy flow based on the electricity purchase prices and the EEG bonus for the feed in of renewable solar energy. But the high purchase price of the storage reduces the financial gain of the photovoltaic system. From the examined case it is revealed that the redox flow batteries are the most promising technology and lead acid batteries are more lucrative than lithium ion batteries due to their lower initial costs. The calculation can predict the cost effectiveness of a solar system with energy storage and therefore help to find the best battery size for a certain household. The high interest in storage systems is not surprising when considering the current, and the debate about rising electricity fees. Due to the high asset costs of storage systems, the cost effectiveness of a solar system is clearly reduced and one is risking a negative return if the application is not configured properly. Therefore, an individual technical and economical optimization is highly recommended, especially concerning the storage size. Redox flow batteries have a high financial potential and outrank the other two studied battery technologies. But it remains to be seen whether redox flow systems will be available for this application and whether the cost prediction is applicable. Despite poor efficiency, low operating life and high capacity loss, lead acid battery systems are surprisingly more profitable than lithium ion systems. Also the market incentive program for

storages of the German government improves the financial results clearly. But even with this support, the return of an installation without storage is about twice as large.

AII.9 Application of Photovoltaic (PV) Solar Farm in STATCOM to Regulate the Grid Voltage

A method of integrating the connections between photovoltaic (SF) and wind farm in the nearest surrounding place can be proposed. The energy distribution of both depends upon the storage batteries, which are one of the main advantageous of the distribution system. This method using point to common coupling to regulate voltage on the late night, when the solar farm is not generating any useful Power. The proposed method of Photovoltaic (SF) as elastic AC Transmission system controller-static synchronous compensator and wind farm as Flexible DC transmission must be enable improved connections of wind energy conversion system (WECS) to the grid. The entire system achieved to the reversible direction of grid voltage regulation using the Photovoltaic (SF) and storage energy to the batteries. A combination of Photovoltaic solar farm and wind energy conversion system (WECS) based on distribution of the production of energy system can be stored in to a battery. The two direction inverter acts as a switch of PV solar farm is using a battery charger especially during the late-night to charge the batteries and energy would be storage. The proposed method introduced concept of indirect feeder link paths to regulate the voltage control can be presented in which the voltage level increase, automatically the extensive amount of reverse power flow from WF is controlled by utilizing the solar farm inverter to charge the batteries and storage the power. The proposed system can be simulated using Simulink blocks in MATLAB. Simulation results could verify the achievement and efficiency of the proposed approach to regulate the feeder voltage by exchanging real active power through the storage batteries. In future work, the proposed approach will be expanded for a medium voltage large scale PV Solar- wind farm power based distribution system. This strategy implies operating PV solar plant and wind farm as a distributed generator [providing megawatts (MW)] and ancillary services provider at day time.

AII.10 Solar PV-Wind Hybrid Power Generation System

Renewable energy sources i.e. energy generated from solar, wind, biomass, hydro power, geothermal and ocean resources are considered as a technological option for generating clean energy. But the energy generated from solar and wind is much less than the production by fossil fuels, however, electricity generation by utilizing PV cells and wind turbine increased rapidly in recent years. The Solar-Wind hybrid Power system that control the renewable energy in Sun and Wind to generate electricity relies mainly on micro controller which ensures the optimum utilization

of resources and hence improves the efficiency as compared with their individual mode of generation. Also it increases the reliability and reduces the dependence on one single source. A portion of the energy required for a private house, farm house, a small company, an educational institution or an apartment depending on the need at the site where used has been supplied with the electricity generated from the wind and solar power. It reduces the dependence on one single source and has increased the reliability. Hence we could improve the efficiency of the system as compared with their individual mode of generation. This hybrid solar-wind power generating system suits for industries and domestic purposes also.

AII.11 Reliability Well-Being Assessment of PV-Wind Hybrid System Using Monte Carlo Simulation

The utilization of renewable energy has gained momentum nowadays due to the rapid decrease in fossil fuel resources and increased environmental concerns. But the amount of power available from these natural resources will vary continuously from place to place and time to time depending on its geographical locations, terrains, altitude, climatic conditions. So the energy supplied from these sources will be fluctuating in nature. Hybrid energy systems are excellent options for supplying small isolated power systems (SIPS) and remote villages where conventional grid cannot reach due to technical and economical reasons. It will discuss various components of hybrid energy systems involving photo voltaic (PV) and wind energy conversion systems (WECS) and their modeling for reliability studies. The reliability of supply can be the major concern in the hybrid energy systems. Several methods for reliability evaluation have been reported. The traditional methods for evaluating reliability evaluation like deterministic and probabilistic techniques have their own disadvantages. An improved method known as system well-being analysis which is the combination of deterministic and probabilistic techniques has been applied for evaluation of reliability of the system applying Monte Carlo simulation technique. Finally the renewable energy can be converted into useful electrical energy by making use of photovoltaic (PV) and wind energy conversion systems and all the designing are done according to Indian conditions and the cost is also reliable.

AII.12 Design of Off-Grid Home with Solar-Wind-Biomass Energy

Due to the limited reserves of fossil fuels and global environmental concerns for the production of electrical power generation and utilization, it is very necessary to use renewable energy sources. By use of hybrid systems we can implement renewable energy sources which are very economical for remote villages, homes etc. In

particular, rapid advances in wind-turbine generator, biomass generator and photovoltaic technologies have brought opportunities for the utilization of wind and solar resources for electric power generation world-wide. So by the use of hybrid systems consisting of Biomass, PV and also wind for production of electrical energy in these remote areas can be more economical. If the development of a computer-based approach for evaluating, the general performance of standalone hybrid PV- Biomass-wind generating systems are analyzed, then these results can be useful for developing and installing hybrid systems in remote areas. It focuses on the economical consideration and simulation approach for a standalone hybrid systems having PV, wind and Biomass for electrical production in remote areas. The average solar radiation, quantity of biomass, average wind speed for the remote area for prediction of general performance of the generating system have been taken into account. Simulation studies were carried out using HOMER software. Simulation results will be given for performance evaluation of a stand-alone hybrid wind-PV generating unit for a residential house which is to be located in a remote area. The system is a off grid one. Finally, the results obtained and methods can be suggested to enhance the performance of the proposed model.

AII.13 Modeling and Control of Hybrid Photovoltaic Wind Energy Conversion System

A hybrid energy conversion system combining photovoltaic and wind turbine can be as a small-scale alternative source of electrical energy where conventional generation is not practical. The hybrid system consists of photovoltaic panels, wind turbines and storage batteries. The wind and PV are used as main energy sources, while the battery can be used as back-up energy source. Two individual DC-DC boost converters can be used to control the power flow to the load. A simple and cost effective control with DC-DC converter is used for maximum power point tracking (MPPT) and hence maximum power is extracted from the turbine and the photo voltaic array. The modeling of hybrid system can be developed using MATLAB- SIMULINK. The proposed model takes sunlight irradiance and cell temperature as input parameters and outputs the I-V and P-V characteristics under various conditions. The masked icon makes the block model more user-friendly and a dialog box lets the users easily configure the PV model. It describes renewable energy hybrid Wind-PV with battery energy storage system. In Hybrid Wind-PV System, PV system acts as a main source. A simple and cost effective maximum power point tracking technique can be proposed for the photovoltaic and wind turbine without measuring the environmental conditions. This is based on controlling the photovoltaic terminal voltage or current according to the open circuit voltage or short circuit current and the control relationship between the turbine speed and the dc-link voltage can be obtained using simple calculations. A complete description of the hybrid system can be presented along with its detailed simulation results which ascertain its feasibility.

AII.14 Multi-Objective Optimization for Sizing of Solar-Wind Based Hybrid Power System

The concept of integrating photovoltaic (PV) and wind energy conversion system can be proposed. This hybrid technology could act as a flexible ac transmission system controller-static synchronous compensator, to regulate the point of common coupling voltage during night time when the Solar farm is not producing any active power. PV Solar farm (SF) is used to regulate the distribution voltage at point of common coupling (PCC) within utility specified limits even during wide variations in WF output and rectifies the fault. This implies operating PV solar plant as a generator during the day[providing megawatts (MW)] and ancillary services provider at night [providing mega volt amperes (MVARs)]. The capacitor banks can be used in parallel with other sources in order to reduce DC bus variation. A Fuel Cell-electrolyzer combination can be used as a backup and a long-term storage system. A simulation model for the hybrid energy system can be developed using MATLAB/Simulink. The system performance under different scenarios can be verified by carrying out simulation studies using a practical load demand profile and real weather data. This is based on controlling the photovoltaic terminal voltage or current according to the open circuit voltage or short circuit current and the control relationship between the turbine speed and the dc-link voltage can be obtained using simple calculations. For simulation, the data solar irradiance, temperature and wind speed can be used. The power fluctuation of the hybrid system is less dependent on the environmental conditions as compared to the power generated of individual PV and Wind energy generation systems.

AII.15 Design and Comparative Evaluation of a Hybrid Wind-Solar Power System

In today's world the rising rate of consumption and the price of fossil fuels and the environmental problems caused by the conventional power generation draw world-wide attention to renewable energy technologies. In fact, renewable energy systems are pollution free, takes low cost and less gestation period, user and social friendly. However, renewable power unit based on single source (wind or solar source) may not be effective in terms of cost, efficiency and reliability. A viable alternative solution is by combining these different renewable energy sources to form a hybrid energy system. An efficient hybrid model can be developed and compared with hybrid model which is using battery as its storage system instead of fuel cells. A complete hybrid power system of this nature may be too expensive and too labor intensive for many Industrial Technology Departments. In this hybrid system with using fuel cell is more efficiency, long life and cheapest compare to hybrid system with using battery. The enhancements to instruction, especially in making electrical power measurements more physical, intuitive, and real-world are substantial and the costs and labor involved in some adaptation to a smaller scale setup are reasonable. The use of solar/wind & FC hybrid power generation is an especially

vivid and relevant choice for as these are power sources of technological, political, and economic importance in their state. In other places, other power sources could be used. For example hybrid combinations of wind power, solar power, geothermal power, hydroelectric power, tidal power, biomass generated power, power from incineration of solid wastes, and many other technologies could be considered depending on local interests and resources.

AII.16 Analysis and Design of a Domestic Solar-Wind Hybrid Energy System for Low Wind Speeds

An application based system is designed on the basis of the solar and wind data for areas in Northern India. The power generated by the system can be intended for domestic use. The most common source of unconventional power in homes is battery based UPS (Uninterrupted Power Supply) inverter. The UPS inverter charges the battery with conventional grid power. This system will charge the battery of the UPS inverter by using only wind and solar power, which will make the system cost effective and more reliable. The reason for using both solar and wind is that the recent studies have proven that combined system can be more productive and consistent and the other thing is that neither of them can be used for continuous power generation. In the system illustrated, the solar-wind system provides power periodically which is controlled by electronic methods and a microcontroller is used to monitor the power from both the inputs. The switching action is provided from the microcontroller to the battery charging based on the power received from solar photovoltaic panel and wind generators. An efficient system has been proposed comprising of solar panel, wind generator, charge controller and charge storage unit(battery). Solar panel is selected as the main input and the wind resource will be used only in the absence of the solar photovoltaic (PV) output. Based on the above mentioned analysis the solar-wind hybrid systems can be used by any domestic user at a place where wind speeds are not that good. It will charge the battery even when there is no grid power. There is lots of space for improvement in this system like Maximum Power Point Tracking (MPPT) or other power enhancement methods. This improvement can be incorporated without any big increase in the system costing because there is only a little addition to the electronic components to the charge controller circuitry. This can prove a vital system in the field of renewable energy resources.

AII.17 Probabilistic Performance Assessment of Autonomous Solar-Wind Energy Conversion Systems

The development of a general probabilistic model of an autonomous solar-wind energy conversion system (SWECS) is composed of several wind turbines (wind farm), several photovoltaic (PV) modules (solar park), and a battery storage feeding

a load. The model takes into consideration outages due to the primary energy fluctuations and hardware failure. It allows the simulation of wind farms and solar parks containing either identical or different types of wind turbines and PV modules with the load being fed from either the renewable sources, or the battery storage, or both. A methodology can also be presented to determine an upper limit on the size of the battery storage required to satisfy a given load profile taking into consideration the charging/discharging of the batteries. The proposed strategy of PV SF control will facilitate integration of more wind plants in the system without needing additional voltage-regulating devices. PV Solar farm virtually inactive during night time in terms of active power generation can be used to regulate the distribution voltage at PCC within utility specified limits even during wide variations in WF output and rectifies the fault.

AII.18 Application of Off Grid Solar PV System for Power Processing Unit

A novel multi-functional power processing unit capable of extracting maximum power from solar photovoltaic panels can be described. It employs a combination of a voltage controlled voltage source inverter (VCVSI) and a current controlled voltage source inverter (CCVSI), connected in series on the DC side and in parallel on the AC side. The Power Processing Unit is able to provide an uninterruptible power supply feature, load voltage stabilization, unity power factor operation, maximum power point tracking, and higher efficiency for charging the battery from renewable energy sources and more reactive power support. The experimental results from the proto typed system confirm validity of the proposed topology. The fundamental concept and experimental results of a novel power conditioner for extracting maximum available energy of different renewable energy sources can be described. The proposed power conditioner employs two voltage source inverters connected in series on the DC side and in parallel on the AC side. The power conditioner provides unity power factor and maximum power point tracking as well as more reactive power support in all modes of operation through control of the instantaneous output parameter of inverters. It can be demonstrated that the proposed Power Processing Unit is an innovative solution to power conditioning for a weak grid, and suitable for application such as in hybrid power Systems.

AII.19 Application of APC Technique in a Unique Standalone Solar and Wind Hybrid Generation System

In India, more than 200 million people live in rural areas without access to grid-connected power. A convenient and cost-effective solution would be hybrid power systems which can reduce dependency on grid supply, improve reliability. An unique standalone hybrid power generation system can be, applying advanced

power control techniques(APC), fed by four power sources: wind power, solar power, storage battery, and fuel cell, and which is not connected to a commercial power system. One of the primary needs for socio-economic development in any nation in the world is the provision of reliable electricity supply systems. This work is a development of an indigenous technology hybrid Solar–Wind and fuel cell Power system that harnesses the renewable energies in Solar- Wind and fuel cell to generate electricity. Here, electric DC energies produced from photovoltaic and wind turbine systems are transported to a DC disconnect energy Mix controller. The controller is bidirectional connected to a DC-AC float charging-inverter system that provides charging current to a heavy duty storage bank of Battery and at the same time produces inverted AC power to AC loads. Under current acute power shortage scenario with increasing cost of natural gas, coal and turbine fuel and due to their impact on environment, there is a very urgent and great need of finding alternate source of energy to generate electricity. There are several ways by which electricity can be generated using renewable sources such as solar, wind, biogas, etc. Individual generation of solar and wind energy is costlier. Solar and wind energy integrated technologies have great potential to benefit our nation. They can diversify our energy supply, reduce our dependence on imported fuels, improve the quality of the air we breathe, offset greenhouse gas emissions, and stimulate our economy by creating jobs in the manufacturing and installation of solar and wind energy systems. By using solar and wind integrated system we can electrify remote area also it is applicable for metro cities in future to avoid unwanted load shedding.

AII.20 Hybrid Solar and Wind Power: An Essential for Information Communication Technology Infrastructure and People in Rural Communities

One of the primary needs for socio-economic development in any nation in the world is the provision of reliable electricity supply systems. This work is a development of an indigenous technology hybrid Solar -Wind Power system that harnesses the renewable energies in Sun and Wind to generate electricity. Here, electric DC energies produced from photovoltaic and wind turbine systems are transported to a DC disconnect energy Mix controller. The controller is bidirectional connected to a DC-AC float charging-inverter system that provides charging current to a heavy duty storage bank of Battery and at the same time produces inverted AC power to AC loads. The 2002–2009, 8 years wind velocity data for Abeokuta and its environs were collected. The two parameters distribution was used to simulate power in W/m^2 densities for the 8-years period. The step by step design of 1,000 W solar power supply system's was done as a sample case. Load estimates of a typical rural community and for rural ICT infrastructures were estimated. Simulation of wind power capacity in W/m^2 in Abeokuta, Ogun State Nigerian was done based on the obtained wind data. The results can predict that the

average exploitable wind power density between 4 and 14.97 W/m^2 is realizable and that development of hybrid wind-solar system for off- grid communities will go a long way to improve socio-economy lives of people. There is the need for the provision of an alternative sustainable electric power supply system to provide electricity to rural and the unreached communities. The importances of Information Communication Technology for e-service to rural communities are inevitable in order to achieve the MDGs objective. Also there is the need for rural banking and hospitals if the social and economic lives of rural citizens in Nigeria are to be improved. The provision of hybrid solar -wind energy system to power ICT infrastructures, banking and hospitals in rural and the unreached communities that are not connected to National Grid Power supply system is very important so as to maintain a continuous electricity supply. When considering the cost and overall efficiency, it is advisable for all the stakeholders who have concern for the rural community development to embrace solar and wind power.

AII.21 Renewable Hybrids Grid-Connection Using Converter Interferences

Use of Renewable Energy power sources is the best possible solution today to reduce increasingly risk of global warming and the most important type of renewable is Wind and Solar energies which are the most efficient. The green power generation resources are used power generators in Distributed Generation (DGs) sources that are in direct relation with the use of micro capacity power generating units of power system that are installed in distribution level of power systems or all segments that loads and energy consumers are located. Hybrid systems vary in models. The best hybrid model available today is combination of grid connected wind turbines and solar PV cells that can compensate each other in the grid connected state. In addition, solar cells provide electricity required in day-time while wind turbines compensate the power needed in the night period. Solar cells are consisted of a series of assembly of different cells together to form a flat photovoltaic system to absorb the photons and generate electricity by electrons energized in the circuit. On the other hand, Systems for conversion of energy of wind use PM Synchronous Generators. Recently, wind turbines are even enhanced to use VSD drives to provide the machine the ability of generation in cases that rotational speed varies with changes in speed of wind. The simplified version of the solar-wind hybrid system is provided and Simulations are done to confirm expectation outcomes of this connection. The connection considerations of wind and Solar hybrid systems that are connected to grid are discussed and working is done in ETAP. Wind turbines can be presented as changeable source by time and solar systems are simulated as DC systems connected to grid using DC-AC Inverters in ETAP. In Hybrid systems of Solar and wind, the capacity is compensated by each other in different cases.

AII.22 Hybrid (Solar and Wind) Energy Systems for Rural Electrification

Hybrid power system can be used to reduce energy storage requirements. The influence of the Deficiency of Power Supply Probability (DPSP), Relative Excess Power Generated (REPG), Energy to Load Ratio (ELR), fraction of PV and wind energy, and coverage of PV and wind energy against the system size and performance can be analyzed. The technical feasibility of PV-wind hybrid system in given range of load demand can be evaluated. The methodology of Life Cycle Cost (LCC) for economic evaluation of stand-alone photovoltaic system, stand-alone wind system and PV-wind hybrid system can be developed and simulated using the model. The optimum combination of solar PV-wind hybrid system lies between 0.70 and 0.75 of solar energy to load ratio and the corresponding LCC is minimum. The PV-wind hybrid system returns the lowest unit cost values to maintain the same level of DPSP as compared to standalone solar and wind systems. For all load demands the levelized energy cost for PV-wind hybrid system is always lower than that of standalone solar PV or wind system. The PV-wind hybrid option is techno-economically viable for rural electrification. There is the need for the provision of an alternative sustainable electric power supply system to provide electricity to rural and the unreached communities. The importances of Information Communication Technology for e-service to rural communities are inevitable in order to achieve the MDGs objective. Also there is the need for rural banking and hospitals if the social and economic lives of rural citizens in Nigeria are to be improved. The provision of hybrid solar -wind energy system to power ICT infrastructures, banking and hospitals in rural and the unreached communities that are not connected to National Grid Power supply system is very important so as to maintain a continuous electricity supply. When considering the cost and overall efficiency, it is advisable for all the stakeholders who have concern for the rural community development to embrace solar and wind power.

AII.23 Standalone Wind Energy

A procedure for the probabilistic treatment of solar irradiance and wind speed data is reported as a method of evaluating, at a given site, the electric energy generated by both a photovoltaic system and a wind system. It describes the development of a general probabilistic model of an autonomous solar-wind energy conversion system (SWECS) composed of several wind turbines (wind farm), several photovoltaic (PV) modules (solar park), and a battery storage feeding a load. The model takes into consideration outages due to the primary energy fluctuations and hardware failure. It allows the simulation of wind farms and solar parks containing either identical or different types of wind turbines and PV modules with the load being fed from either the renewable sources, or the battery storage, or both. A methodology

can also be presented to determine an upper limit on the size of the battery storage required to satisfy a given load profile taking into consideration the charging/discharging of the batteries. The combined utilization of renewables such as solar and wind energy is becoming increasingly attractive. Proper methods need to be employed that consider the inherent variability of these two technologies while determining the performance of a wind-solar hybrid energy conversion system (ECS). A stochastic approach has been utilized to develop the megawatt resource assessment model (MWRAM) of a wind-solar hybrid ECS at any selected location. The parameters required to define the probabilistic models can be computed from site-specific data using the maximum likelihood estimation method. The wind portion consists of several interconnected wind turbines while the solar component is a parabolic trough solar thermal electric generating system. Different applications of the model to assess resource benefits including capacity factors and reserve requirements from effective utilization of both wind and solar energy have been explored at different levels with varying wind-solar proportions. The integration of wind energy conversion system (WECS) with photovoltaic (PV) solar farm (SF) which acts as flexible a.c transmission system controller-static synchronous compensator during night time, to regulate the point of common coupling voltage and to rectify faults when SF is not producing any active power. The proposed control will enable increased connections of WECS. MATLAB/Simulink based simulation results can be presented for validation of the system.

AII.24 To Design Solar (Photovoltaic): Wind Hybrid Power Generation System

In recent year's generation of electricity using the different types of renewable sources are specifically evaluated in the economical performance of the overall equipment. Solar power & wind power has received considerable attention worldwide. The proposed methodology can be applied to evaluate the potential of Solar (photovoltaic) –wind hybrid system to produce electricity for a community and other state. Through this hybrid system we can reduce pollution and decrease the global warming. In this we can analyze the data of wind and solar energy and evaluate the average energy by using hybrid system we have fulfills the energy demand into the future. In future by using of better quality sensor can increase the potential. Because maintained cost becomes low using the better quality data logger is can increase the energy production. In future we have to install large solar and wind plant which are cheaper as compared to small plants. The Modeling and simulation of the Solar (photovoltaic) –wind hybrid system can be carried out using MATLAB/SIMULINK. The capitalization of renewable resources potential confers real premises to achieve some strategic aims, but also the durable development of energy sector and the protection of the environment. In order to exploit the economic potential of renewable resources in competitive conditions on the energy

market, it is necessary to adopt and implement some energy policies and specific resources. The promotion of energy production from renewable resources represents an imperative objective in present times justified by environment protection, the increase of energetic independence by supplying sources diversity and, of course, economic and social cohesion reasons.

AII.25 Increasing Efficiency of Solar PV and Windenergy Conversion Systems Using Pyroelectric Effect

To harvest solar micro-energy using the pyroelectric effect and low wind flow can be proposed. The basic concept can be presented and validated by laboratory experiments with controlled airflow. The measured temperature variation, subject to the intensity of radiation and wind speed in the environment was demonstrated to reach 16 °C. The time variation of temperature was 0.53 $°Cs^{-1}$ with the speed of airflow at 2 ms^{-1}. The power density with PZT as the pyroelectric material was 4.2 Wcm^{-3} in laboratory conditions. Both the thermodynamic model and electric model of the pyroelectric generator were established, and a numerical procedure was developed to predict the system performance which was proven to be reliable. The characteristics of such an energy harvesting system can be analyzed in detail by simulation. In this study, a new method of harvesting solar thermal energy was proposed. The time variation of temperature reached 0.23 $°Cs^{-1}$ with radiation of 1,000 Wm^{-2} and 0.53 $°Cs^{-1}$ with speed of airflow at 2 ms^{-1}. The corresponding average power density with PZT as the pyroelectric material was 4.2 Wcm^{-3}. The predicted Carnot efficiency of the PYEG reached 13.3 % with the proposed method. The measured time variation of temperature possible with wind flow under natural conditions could be higher than that achieved under laboratory conditions, and the equivalent power density under natural conditions was in the same order of magnitude as that measured under laboratory conditions. The detailed analysis on the PYEG was achieved by modeling the method. Both the thermodynamic and electric models were considered in an energy harvesting process aiming at driving low-power electronics. A numerical procedure was developed to predict the system performance. The characteristics of the proposed energy harvesting process could be estimated with the simulation. This proposal outlined the basic rules for the thermo dynamic design of the proposed PYEG. Although the power density of the proposed PYEG was much lower than that which a thermoelectric generator developed before (1.3 $mWcm^{-3}$), the inherent, simple structure of such a PYEG could be essential in some typical applications. The major cost of the PYEG included only the active material, and the cost-effectiveness is currently estimated as 15 W/euro (or 11 W/dollar) with PZT. Further work on this newly proposed energy harvesting method could inspect the thermal response of the PYEG to the complicated weather condition (sunny, windy, rainy, cloudy, snowy, etc.).

AII.26 Integrating Variable Energy Resources in Control Centers for Reliable Grid Operation

Wind power capacity has experienced tremendous growth in the past decade, thanks to wind benefits. A review of the interconnection issues of distributed resources including wind power with electric power systems, and reports the developments of interconnection standards in Canada and IEEE is accomplished. It describes the recent R&D programs in wind energy power's environmental benefits, technological advance, and government incentives. It presents the recent developments in wind energy conversion systems, and their social and environmental conversion system. A functional structure of a wind energy conversion system can be introduced, before making a comparison between the two typical wind turbine operating schemes in operation, namely constant-speed wind turbine and variable-speed wind turbine. In addition, the modeling and dynamic behavior of a variable speed wind turbine with pitch control capability is explained in detail and the turbine performance curves can be simulated in the MATLAB/Simulink.

AII.27 A Multifunctional Power Processing Unit for an Off-Grid PV Diesel Hybrid Power System

A novel multi-functional power processing unit capable of extracting maximum power from solar photovoltaic panels can be described. It employs a combination of a voltage controlled voltage source inverter (VCVSI) and a current controlled voltage source inverter (CCVSI), connected in series on the DC side and in parallel on the AC side. This Power Processing Unit can be able to provide an uninterruptible power supply feature, load voltage stabilization, unity power factor operation, maximum power point tracking, and higher efficiency for charging the battery from renewable energy sources and more reactive power support. The experimental results from the proto typed system confirm validity of the proposed topology. The fundamental concept and experimental results of a novel power conditioner for extracting maximum available energy of different renewable energy sources can be described. The proposed power conditioner employs two voltage source inverters connected in series on the DC side and in parallel on the AC side. The power conditioner provides unity power factor and maximum power point tracking as well as more reactive power support in all modes of operation through control of the instantaneous output parameter of inverters. It has demonstrated that the proposed Power Processing Unit is an innovative solution to power conditioning for a weak grid, and suitable for application such as in hybrid power Systems.

AII.28 Analysis, Design and Control of a Standalone Hybrid Renewable Energy Conversion System

This paper deals with the analysis, design and control of a proposed standalone hybrid renewable energy conversion system based on solar and wind energy sources employing a full bridge dc-dc converter and a Permanent Magnet Brush-Less DC (PMBLDC) generator. The proposed MPPT (Maximum Power Point Tracking) controllers of solar-PV (Photo-Voltaic) array and WECS (Wind Energy Conversion System) are operating on P&O (Perturb and Observation) based on FLC (Fuzzy Logic Control) method. It requires the sensing of the dc voltage and current output of solar-PV and the rectified output voltage of PMBLDC generator driven by a wind turbine. The power quality is maintained at the load end by using an output voltage controller of the VSI (Voltage Source Inverter) and the load leveling is implemented through the battery. The model of the system can be developed in Matlab and capability of designed MPPT control is investigated during varying solar insulation and wind speeds. Renewable energy sources also called non-conventional type of energy are continuously replenished by natural processes. Hybrid systems are the right solution for a clean energy proposed which makes use of Cuk and SEPIC converters in the design. This converter design overcomes the drawbacks of the earlier proposed converters. This topology allows the two sources to supply the load separately or simultaneously depending on the availability of the energy sources. The output voltage obtained from the hybrid system is the sum of the inputs of the Cuk and SEPIC converters. This system has lower operating cost and finds applications in remote area power generation, constant speed and variable speed energy conversion systems and rural electrification. MATLAB/ SIMULINK software can be used to model the PV panel, wind turbine, DC-DC converters and the proposed hybrid system.

AII.29 Modelling and Control of a Hybrid Renewable Energy System to Supply Demand of a Green-Building

Renewable energy sources are an "indigenous" environmental option, economically competitive with conventional power generation where good wind and solar resources are available. Hybrid plants can help in improving the economic and environmental sustainability of renewable energy systems to fulfil the energy demand. The aim is to present the architecture of a Decision Support System (DSS) that can be used for the optimal energy management at a local scale through the integration of different renewable energy sources. The integrated model representing a hybrid energy generation system connected to the grid can be developed. It consists of PV and solar thermal modules, wind turbine and biomass plant. Moreover, a framework can be presented for the optimization of the different ways to ensure the electrical and thermal energy demand of the micro grid as well as the water demand, with specific reference to two main cases for the real time energy

optimal control: the presence/absence of a storage system. Finally, the optimization model can be applied to a case study. A DSS for real time energy management can be proposed to define the optimal energy flows in a building characterized by a mix of renewable resources (solar plate collector, PV, biomass, wind and battery storage) to satisfy different energy demands. The model is applied to the case of Capo Vado (Liguria Region) and optimal results to satisfy all the energy demands are found for a testing day in the month of November.

AII.30 Renewable Energy Resources (Fuel Cell Technologies)

The recent severe energy crisis has forced the world to develop new and alternative methods of power generation, which could not be adopted so far due to various reasons. The magneto-hydro-dynamic (MHD) power generation is one of the examples of a new unique method of power generation. The other non-conventional methods of power generation may be such as solar cells, fuel cells, thermo-electric generator, thermionic converter, solar power generation, wind power generation, geothermal energy generation, tidal power generation etc. It elucidates about Different Energy sources, why we are going for non-conventional energy sources, Different non-conventional energy sources & comparison between them, about fuel cells and their applications. Starting with the current state of technology, the detailed R&D needs can be presented for the cell, stack, system, fuel and fuel processing for the proton exchange membrane. The PEMFC is being developed for automotive propulsion, portable power and distributed power applications. Toyota Prius (commercialized suv vehicle using PEMFC) is the first step in vehicles segment released in commercial market utilizing the fuel cell technology. At present, these fuel cells have gone through demonstration projects for performance levels and anticipated improvements. The major issues are the cost/kW, durability and reliability. Extensive efforts are being devoted to improve the performance with less costly materials, lower material content, more simplified systems/components, less number of parts, addressing transient and steady state performance issues, reducing the losses, etc.

AII.31 Modeling and Control for Smart Grid Integration with MPPT of Solar/Wind Energy Conversion System

Performance optimization, system reliability and operational efficiency are key characteristics of smart grid systems. A novel model of smart grid-connected PV/WT hybrid system can be developed. It comprises photovoltaic array, wind turbine, asynchronous (induction) generator, controller and converters. The model

can be implemented using MATLAB/SIMULINK software package. Perturb and observe (P&O) algorithm is used for maximizing the generated power based on maximum power point tracker (MPPT) implementation. The dynamic behavior of the proposed model is examined under different operating conditions. Solar irradiance, temperature and wind speed data is gathered from a grid connected, 28.8 kW solar power system located in central Manchester. Real-time measured parameters are used as inputs for the developed system. The proposed model and its control strategy offer a proper tool for smart grid performance optimization. A novel PV/WT hybrid power system is designed and modeled for smart grid applications. The developed algorithm comprises system components and an appropriate power flow controller. The model can be implemented using the MATLAB/SIMULINK software package, and designed with a dialog box like those used in the SIMULINK block libraries. The available power from the PV system is highly dependent on solar radiation. To overcome this deficiency of the PV system, the PV module was integrated with the wind turbine system. The dynamic behavior of the proposed model is examined under different operating conditions. Solar irradiance, temperature and wind speed data is gathered from a 28.8 kW grid connected solar power system located in central Manchester. The developed system and its control strategy exhibit excellent performance for the simulation of a complete day. The proposed model offers a proper tool for smart grid performance optimization.

AII.32 Augmented Horizontal Axis Wind Energy Systems

Solar PV cells are the devices which convert photons directly into electrical energy. Photovoltaic cells are made of special materials called semiconductors such as silicon. Basically, when light strikes the cell, a certain portion of it is absorbed within the semiconductor material and hence free electrons are created. It then needs to herd these stray electrons to electric current by creating an electrical imbalance. Creating the imbalance is achieved by adding small quantities of other elements. This creates two different type of silicon-n-type, which has spare electrons and p-type which has holes in the place of missing electrons. When these two materials are side by side, the n-type silicon's spare electrons rush to fill the gaps in the p-type silicon. This means the n-type silicon becomes positively charged and p-type silicon becomes negatively charged. This creates a potential difference causing the flow of electrons. Differential heating of the surface of the earth creates the movement of large masses of air on the surface of the earth i.e. the wind. The wind energy conversion system converts the kinetic energy of the wind to electricity or other forms of energy. The major components of wind energy convertors are wind turbine, generators, interconnection apparatus and control systems. Installing solar cells involves more initial cost. Apart from that, it also involves the cost of

inverters and charge storage elements. The efficiency of solar pv cells is about just 14–15 %. The efficiency depends on the purity of the silicon wafer. The cost of getting pure silicon is much higher. Although the solar pv cells have more constrains it is the best alternative for non-renewable resources and is more eco friendly. Advanced researches to implement hybrid, plastic and flexible solar PV cells should be carried. This also involves the role of the government to encourage the installment of solar pv cells. The efficiency of wind energy conversion is up to about 40–60 %. The cost of wind energy conversion has decreased due to extensive researches over the years. This should also be accompanied by giving incentives to encourage research.

AII.33 Hybrid (Solar and Wind) Energy Systems for Rural Electrification

Performance optimization, system reliability and operational efficiency are key characteristics of smart grid systems. Hybrid power system can be used to reduce energy storage requirements. The influence of the Deficiency of Power Supply Probability (DPSP), Relative Excess Power Generated (REPG), Energy to Load Ratio (ELR), fraction of PV and wind energy, and coverage of PV and wind energy against the system size and performance can be analyzed. The technical feasibility of PV-wind hybrid system in given range of load demand can be evaluated. The methodology of Life Cycle Cost (LCC) for economic evaluation of stand-alone photovoltaic system, stand-alone wind system and PV-wind hybrid system can be developed and simulated using the model. The optimum combination of solar PV-wind hybrid system lies between 0.70 and 0.75 of solar energy to load ratio and the corresponding LCC is minimum. The PV-wind hybrid system returns the lowest unit cost values to maintain the same level of DPSP as compared to standalone solar and wind systems. For all load demands the levelised energy cost for PV-wind hybrid system is always lower than that of standalone solar PV or wind system. The PV-wind hybrid option is techno-economically viable for rural electrification. In the present scenario standalone solar photovoltaic and wind systems have been promoted around the globe on a comparatively larger scale. These independent systems cannot provide continuous source of energy, as they are seasonal. The solar and wind energies are complement in nature. By integrating and optimizing the solar photovoltaic and wind systems, the reliability of the systems can be improved and the unit cost of power can be minimized. A PV wind hybrid systems is designed for rural electrification for the required load at specified Deficiency of Power Supply Probability (DPSP). A new methodology can be developed to determine the size of the PV wind hybrid system using site parameters, types of wind systems, types of solar photovoltaic system, number of days of autonomy of battery and life period of the system.

AII.34 Simulation and Harmonics Reduction of Wind-PV Hybrid System

A hybrid energy conversion system combining photo voltaic and wind turbine as a small-scale alternative source of electrical energy can be proposed. The set-up consists of a photo-voltaic solar-cell array, a mast mounted wind generator, lead-acid storage batteries, a PWM inverter unit to convert DC power to AC power, IGBT and three-phase loads, as the wind and sun shine is not available all the time, solar and wind power alone are poor power sources. Thus Hybridizing solar and wind power sources together with storage batteries is better option. Photo-Voltaic or solar cells, convert the energy from sunlight into DC electricity. PVs holds advantage over other renewable energy sources in that they give off no noise, and practically require no maintenance. Wind- turbines and PV cells provide DC power. A semiconductor-based device known as a power inverter is used to convert the DC power to AC power. The hybrid unit contains two complete generating plants, a PV solar cell plant and a wind-turbine system. These sources are connected in parallel to a 12 V DC line. The power is next connected to a DC to AC inverter and is then supplied from the inverter's output to a three phase load. A generalized PV model which is representative of the all PV cell, module, and array can be developed with Matlab/Simulink and verified with a PV cell and a commercial module. The proposed model takes sunlight irradiance and cell temperature as input parameters and outputs the I-V and P-V characteristics under various conditions. Such a generalized PV model is easy to be used for the implementation on Matlab/Simulink modeling and simulation platform. Especially, in the context of the Sim Power System tool, there is now a generalized PV model which can be used for the model and analysis in the field of solar PV power conversion system. The future work includes that dc output when converted to ac by inverter contains harmonics; these harmonics can be reduced by various technologies.

AII.35 Dead Band Method for Solar Irradiance and Power Ramp Detection Algorithms

Integration of solar photovoltaic (PV) power plants onto the electric utility grid can pose some challenges from the perspective of operating the power system (balancing load and demand) and in interconnecting a PV power plant (controlling distribution system voltage variations and thus power quality). An issue of particular importance is the rate at which the solar irradiance changes, and the consequent rate at which the power output changes, i.e. the ramp rates. Pertinent information describing the ramps is the frequency, duration, and magnitude of the ramps. It compares different methods of computing ramp rates in both irradiance and power. The "dead band" method, a historical data compression technique, is demonstrated for identifying fluctuations in the one second to several second timeframe. Ramp

calculation methods are presented along with the results describing ramp events for two case studies. A dead band technique was proposed to identify irradiance and power ramp rates. Two case studies were included; one for detecting irradiance ramps and one for detecting power ramps from a solar PV plant. This technique was found to sufficient in resolving rapid variations in power that can occur at a PV power plant. Ramp rates and ramp durations can be tabulated in histograms, tables, heat maps, envelope plots, and contour plots to characterize the ramping behavior of the solar resource or of a power plant. The dead band method is expected to be computationally similar to the swinging door method, and both are able to capture ramps at a variety of timescales. The dead band method (not unlike the swinging door method) requires pre-calibrating the algorithm to determine the sensitivity to ramp detection. This calibration requires judgment by the user in determining what type of ramp events are of interest for a particular application, making it tunable to the user's needs.

Appendix III
SIMULINK Block Sets

The MATLAB/SIMULINK blocks used in relation with solar PV, wind energy conversion systems and fuel cell are described in this section. The description of the block with block parameters and their setting is discussed below:

AIII.1 Series RLC Load

Implement linear series RLC load

Library

Elements

Description

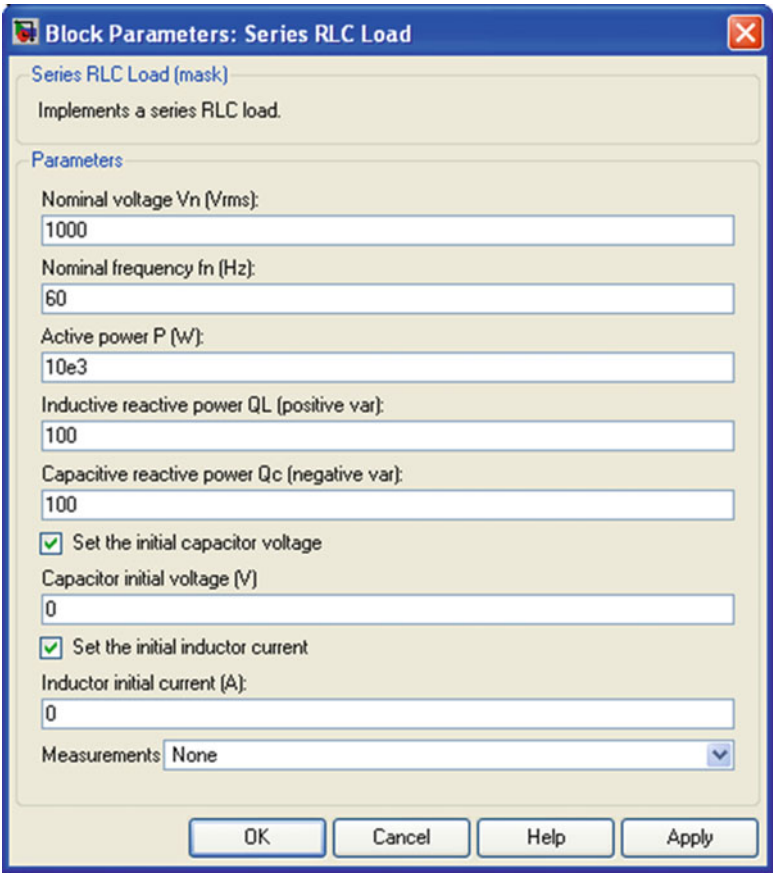


The Series RLC Load block implements a linear load as a series combination of R L C elements. At the specified frequency, the load exhibits a constant impedance. The active and reactive powers absorbed by the load are proportional to the square of the applied voltage. Only elements associated with nonzero powers are displayed in the block icon.

© Springer International Publishing Switzerland 2015

S. Sumathi et al., *Solar PV and Wind Energy Conversion Systems*,
Green Energy and Technology, DOI 10.1007/978-3-319-14941-7

Dialog Box and Parameters



Nominal Voltage Vn

The nominal voltage of the load, in volts RMS.

Nominal Frequency fn

The nominal frequency, in hertz.

Active Power P

The active power of the load, in watts.

Inductive Reactive Power QL

The inductive reactive power QL, in vars. Specify a positive value, or 0.

Capacitive Reactive Power QC

The capacitive reactive power QC, in vars. Specify a positive value, or 0.

Set the Initial Capacitor Voltage

If selected, the initial capacitor voltage is defined by the **Capacitor initial voltage** parameter. If not selected, the software calculates the initial capacitor voltage in order to start the simulation in steady-state.

The **Set the initial capacitor voltage** parameter have no effect on the block if the capacitive reactive power is equal to zero.

Capacitor Initial Voltage (V)

The initial capacitor voltage used at the start of the simulation. The **Capacitor initial voltage** parameter have no effect on the block if the capacitive reactive power is equal to zero and if the **Set the initial capacitor voltage** parameter is not selected.

Set the Initial Inductor Current

If selected, the initial inductor current is defined by the **Inductor initial current** parameter. If not selected, the software calculates the initial inductor current in order to start the simulation steady-state.

The **Set the initial inductor current** parameter have no effect on the block if the inductive reactive power is equal to zero.

Inductor Initial Current (A)

The initial inductor current used at the start of the simulation. The **Inductor initial current** parameter have no effect on the block if the inductive reactive power is equal to zero and if the **Set the initial inductor current** parameter is not selected.

AIII.2 Parallel RLC Load

Implement linear parallel RLC load

Library

Elements

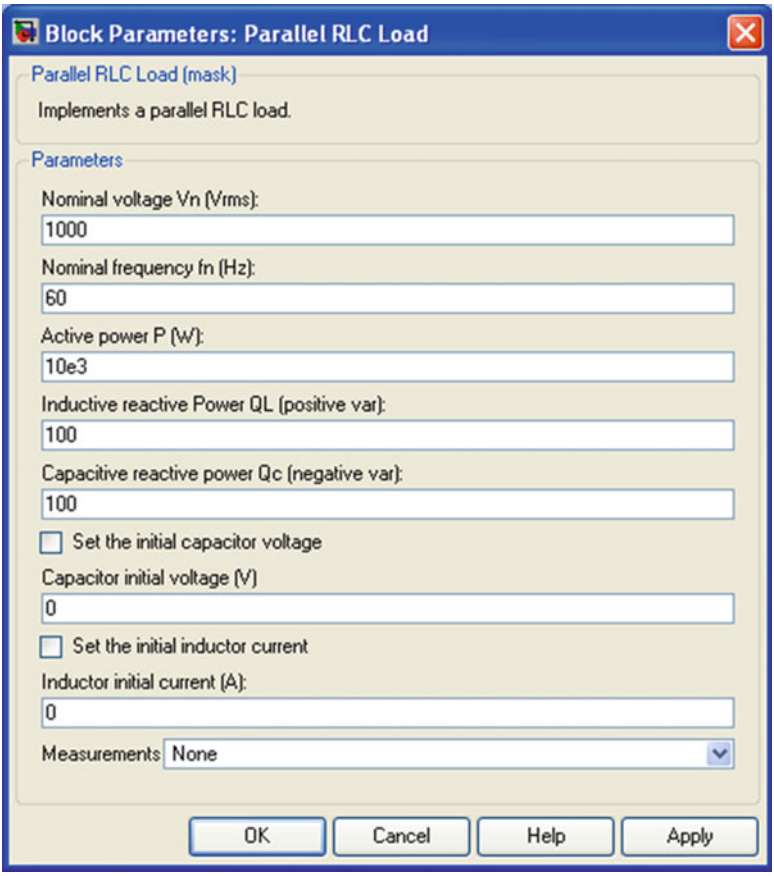
Description



The Parallel RLC Load block implements a linear load as a parallel combination of RLC elements. At the specified frequency, the load exhibits a constant impedance. The active and reactive powers absorbed by the load are proportional to the square of the applied voltage.

Only elements associated with nonzero powers are displayed in the block icon.

Dialog Box and Parameters



Nominal Voltage Vn

The nominal voltage of the load, in volts RMS (Vrms).

Nominal Frequency fn

The nominal frequency, in hertz (Hz).

Active Power P

The active power of the load, in watts.

Inductive Reactive Power QL

The inductive reactive power QL, in vars. Specify a positive value, or 0.

Capacitive Reactive Power QC

The capacitive reactive power QC, in vars. Specify a positive value, or 0.

Set the Initial Capacitor Voltage

If selected, the initial capacitor voltage is defined by the **Capacitor initial voltage** parameter. If not selected, the software calculates the initial capacitor voltage in order to start the simulation in steady-state.

The **Set the initial capacitor voltage** parameter have no effect on the block if the capacitive reactive power is equal to zero.

Capacitor Initial Voltage (V)

The initial capacitor voltage used at the start of the simulation. The **Capacitor initial voltage** parameter have no effect on the block if the capacitive reactive power is equal to zero and if the **Set the initial capacitor voltage** parameter is not selected.

Set the Initial Inductor Current

If selected, the initial inductor current is defined by the **Inductor initial current** parameter. If not selected, the software calculates the initial inductor current in order to start the simulation steady-state.

The **Set the initial inductor current** parameter have no effect on the block if the inductive reactive power is equal to zero.

Inductor Initial Current (A)

The initial inductor current used at the start of the simulation. The **Inductor initial current** parameter have no effect on the block if the inductive reactive power is equal to zero and if the **Set the initial inductor current** parameter is not selected.

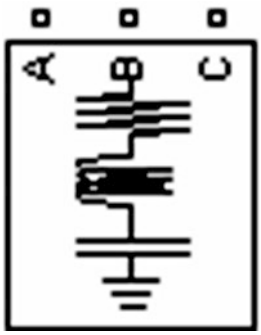
AIII.3 Three-Phase Series RLC Load

Implement three-phase series RLC load with selectable connection

Library

Elements

Description

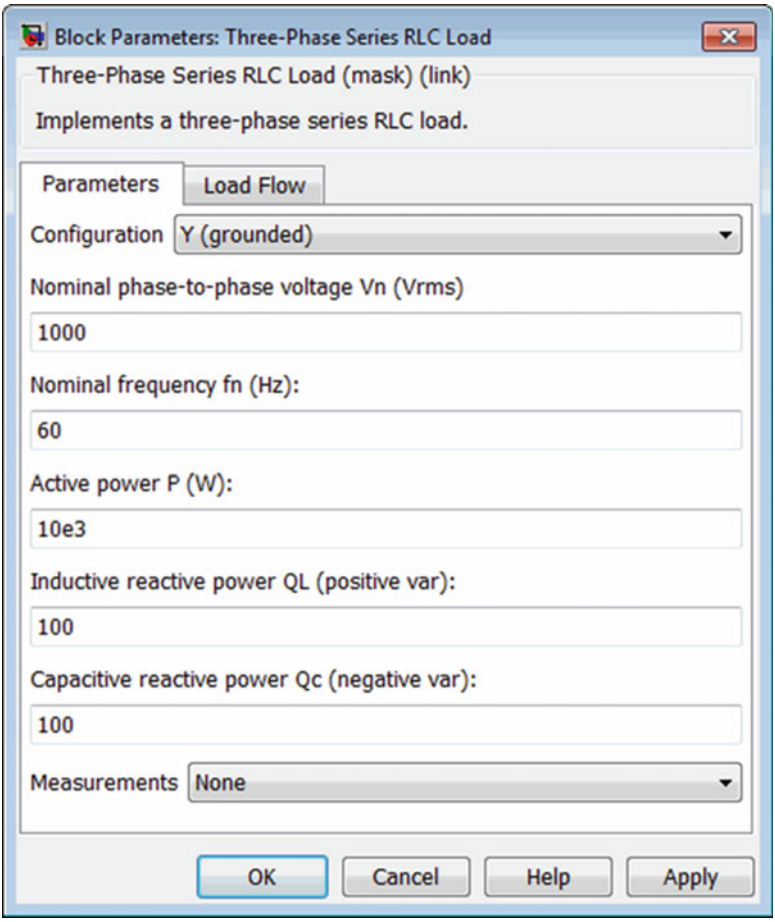


The Three-Phase Series RLC Load block implements a three-phase balanced load as a series combination of RLC elements. At the specified frequency, the load exhibits a constant impedance. The active and reactive powers absorbed by the load are proportional to the square of the applied voltage.

Only elements associated with nonzero powers are displayed in the block icon.

Dialog Box and Parameters

Parameters Tab



Configuration

The connection of the three phases. Select one of the following four connections:

`Y(grounded)`	Neutral is grounded
`Y(floating)`	Neutral is not accessible
`Y(neutral)`	Neutral is made accessible through a fourth connector
`Delta`	Three phases connected in delta

The block icon is updated according to the load connection.

Nominal Phase-to-Phase Voltage Vn

The nominal phase-to-phase voltage of the load, in volts RMS (Vrms).

Nominal Frequency fn

The nominal frequency, in hertz (Hz).

Active Power P

The three-phase active power of the load, in watts (W).

Inductive Reactive Power QL

The three-phase inductive reactive power QL, in vars. Specify a positive value, or 0.

Capacitive Reactive Power Qc

The three-phase capacitive reactive power QC, in vars. Specify a positive value, or 0.

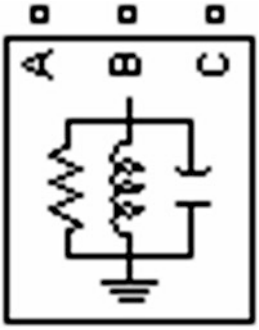
AIII.4 Three-Phase Parallel RLC Load

Implement three-phase parallel RLC load with selectable connection

Library

Elements

Description

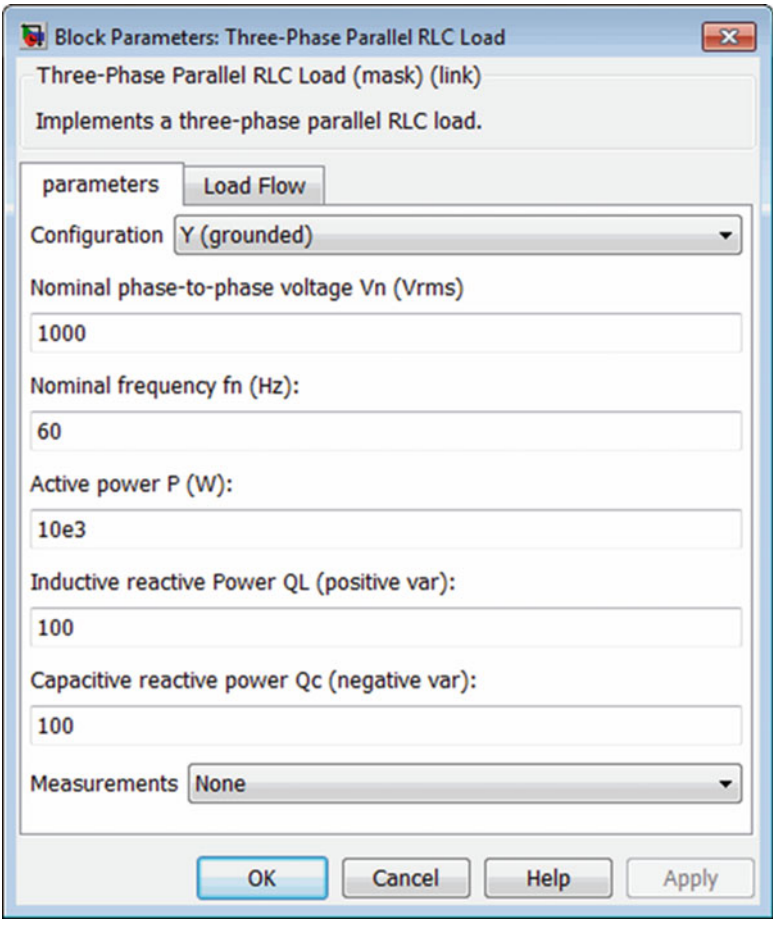


The Three-Phase Parallel RLC Load block implements a three-phase balanced load as a parallel combination of RLC elements. At the specified frequency, the load exhibits a constant impedance. The active and reactive powers absorbed by the load are proportional to the square of the applied voltage.

Only elements associated with nonzero powers are displayed in the block icon.

Dialog Box and Parameters

Parameters Tab



Configuration

The connection of the three phases. Select one of the following four connections:

`Y(grounded)`	Neutral is grounded
`Y(floating)`	Neutral is not accessible
`Y(neutral)`	Neutral is made accessible through a fourth connector
`Delta`	Three phases connected in delta

The block icon is updated according to the load connection.

Nominal Phase-to-Phase Voltage Vn

The nominal phase-to-phase voltage of the load, in volts RMS (Vrms).

Nominal Frequency fn

The nominal frequency, in hertz (Hz).

Active Power P

The three-phase active power of the load, in watts (W).

Inductive Reactive Power QL

The three-phase inductive reactive power QL, in vars. Specify a positive value, or 0.

Capacitive Reactive Power QC

The three-phase capacitive reactive power QC, in vars. Specify a positive value, or 0.

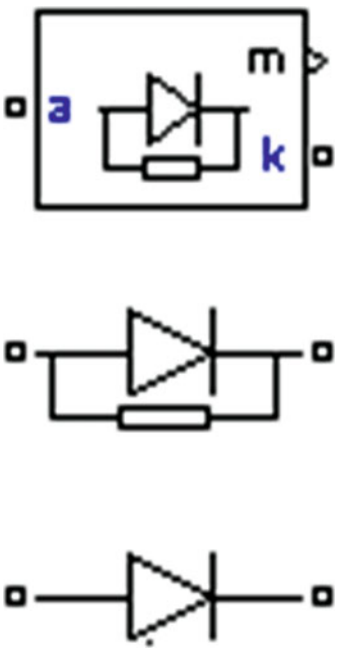
AIII.5 Diode

Implement diode model

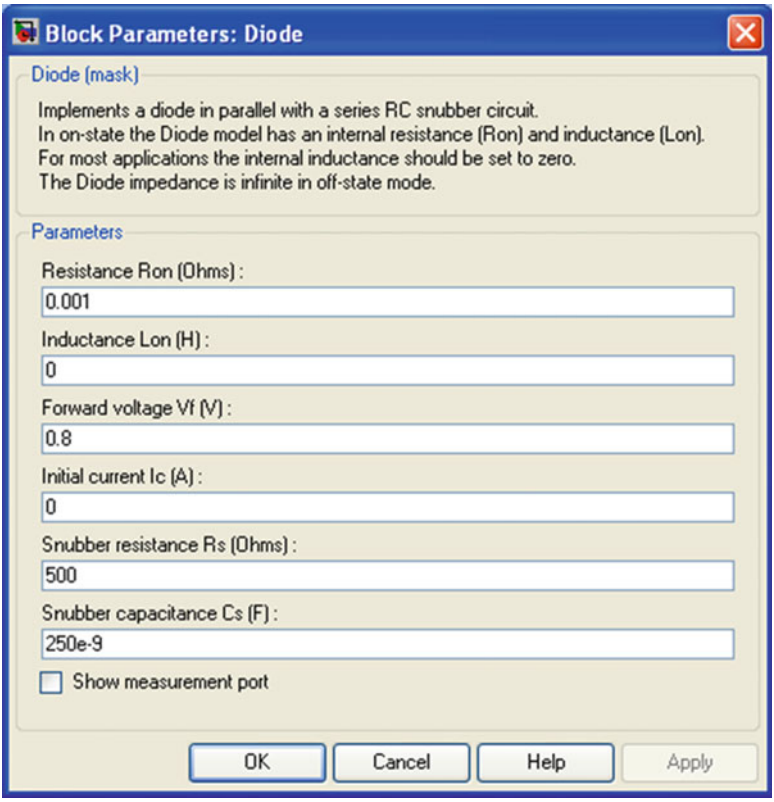
Library

Power Electronics

Description



Dialog Box and Parameters



Resistance Ron

The diode internal resistance Ron, in ohms (Ω). The **Resistance Ron** parameter cannot be set to 0 when the **Inductance Lon** parameter is set to 0.

Inductance Lon

The diode internal inductance Lon, in henries (H). The **Inductance Lon** parameter cannot be set to 0 when the **Resistance Ron** parameter is set to 0.

Forward Voltage Vf

The forward voltage of the diode device, in volts (V).

Initial Current Ic

Specifies an initial current flowing in the diode device. It is usually set to 0 in order to start the simulation with the diode device blocked. If the **Initial Current IC** parameter is set to a value greater than 0, the steady-state calculation considers the initial status of the diode as closed.

Initializing all states of a power electronic converter is a complex task. Therefore, this option is useful only with simple circuits.

Snubber Resistance Rs

The snubber resistance, in ohms (Ω). Set the **Snubber resistance Rs** parameter to inf to eliminate the snubber from the model.

Snubber Capacitance Cs

The snubber capacitance in farads (F). Set the **Snubber capacitance Cs** parameter to 0 to eliminate the snubber, or to inf to get a resistive snubber.

Show Measurement Port

If selected, adds a Simulink® output to the block returning the diode current and voltage.

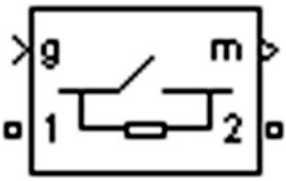
AIII.6 Ideal Switch

Implement ideal switch device

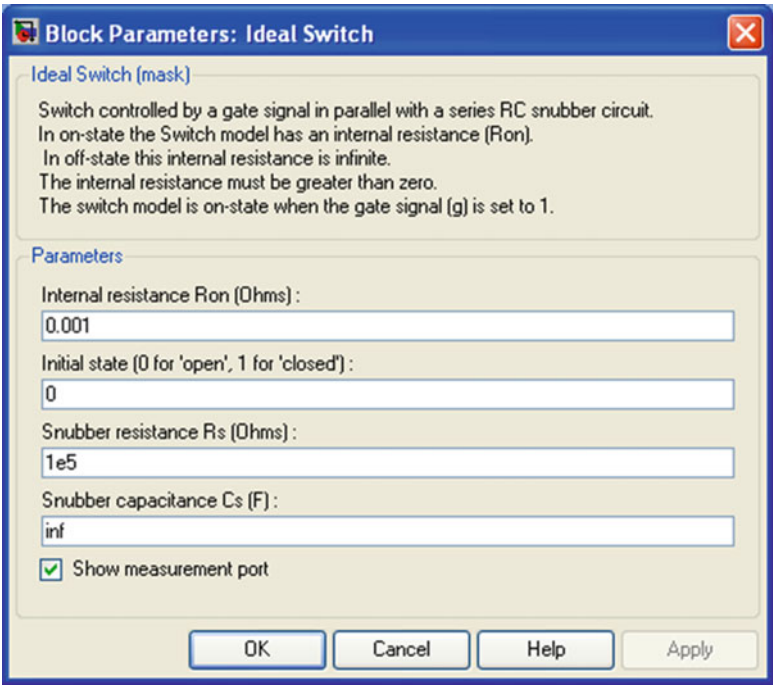
Library

Power Electronics

Description



Dialog Box and Parameters



Internal Resistance Ron

The internal resistance of the switch device, in ohms (Ω). The **Internal resistance Ron** parameter cannot be set to 0.

Initial State

The initial state of the Ideal Switch block. The initial status of the Ideal Switch block is taken into account in the steady-state calculation.

Snubber Resistance Rs

The snubber resistance, in ohms (Ω). Set the **Snubber resistance Rs** parameter to inf to eliminate the snubber from the model.

Snubber Capacitance Cs

The snubber capacitance in farads (F). Set the **Snubber capacitance Cs** parameter to 0 to eliminate the snubber, or to inf to get a resistive snubber.

Show Measurement Port

If selected, add a Simulink® output to the block returning the ideal switch current and voltage.

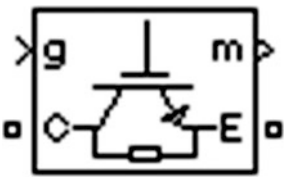
AIII.7 IGBT

Implement insulated gate bipolar transistor (IGBT)

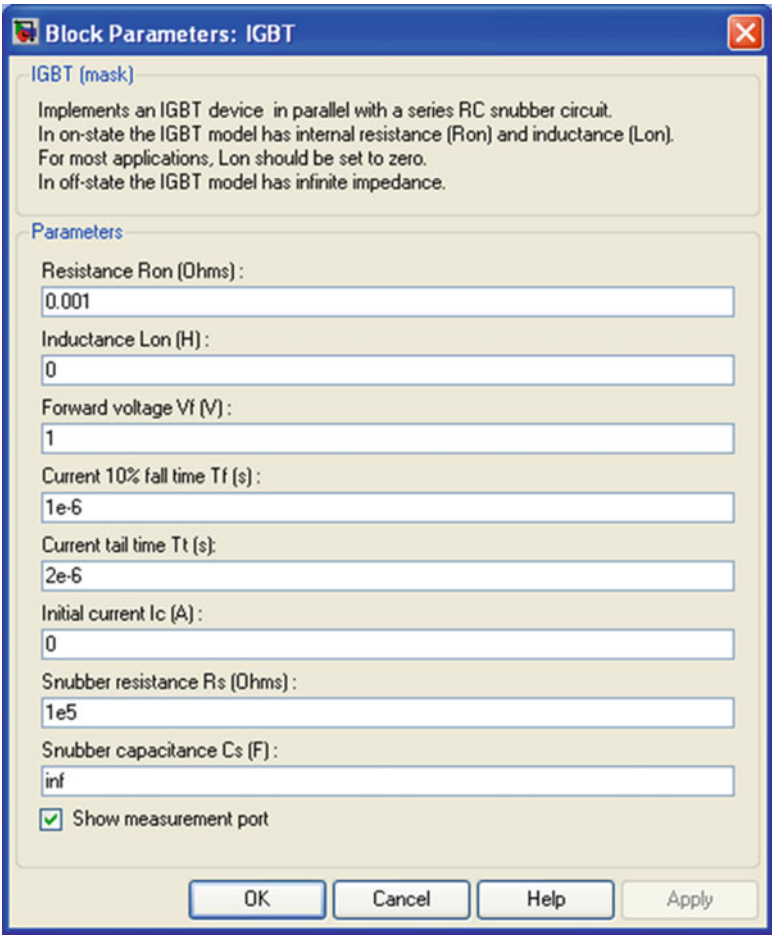
Library

Power Electronics

Description



Dialog Box and Parameters



Resistance Ron

The internal resistance Ron, in ohms (Ω). The **Resistance Ron** parameter cannot be set to 0 when the **Inductance Lon** parameter is set to 0.

Inductance Lon

The internal inductance Lon, in henries (H). The **Inductance Lon** parameter is normally set to 0 except when the **Resistance Ron** parameter is set to 0.

Forward Voltage Vf

The forward voltage of the IGBT device, in volts (V).

Current 10 % Fall Time

The current fall time Tf, in seconds (s). This parameter is not modeled when the **Enable use of ideal switching devices** parameter of the Powergui block is selected.

Current Tail Time

The current tail time Tt, in seconds (s). This parameter is not modeled when the **Enable use of ideal switching devices** parameter of the Powergui block is selected.

Initial Current Ic

You can specify an initial current flowing in the IGBT. It is usually set to 0 in order to start the simulation with the device blocked.

If the **Initial Current IC** parameter is set to a value greater than 0, the steady-state calculation considers the initial status of the IGBT as closed. Initializing all states of a power electronic converter is a complex task. Therefore, this option is useful only with simple circuits.

Snubber Resistance Rs

The snubber resistance, in ohms (Ω). Set the **Snubber resistance Rs** parameter to inf to eliminate the snubber from the model.

Snubber Capacitance Cs

The snubber capacitance in farads (F). Set the **Snubber capacitance Cs** parameter to 0 to eliminate the snubber, or to inf to get a resistive snubber.

Show Measurement Port

If selected, add a Simulink® output to the block returning the diode IGBT current and voltage.

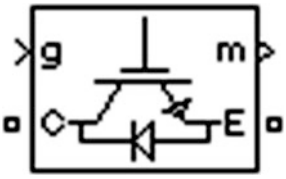
AIII.8 IGBT/DIODE

Implements ideal IGBT, GTO, or MOSFET and antiparallel diode

Library

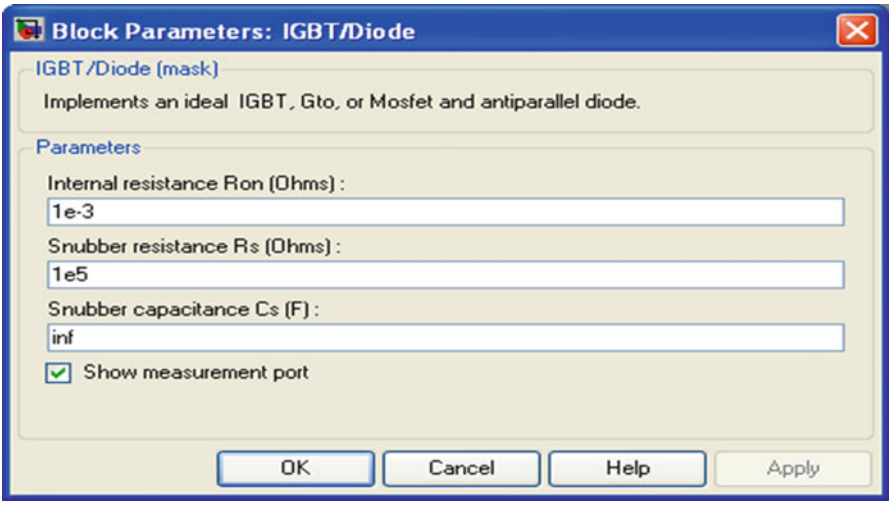
Power Electronics

Description



The IGBT/Diode block is a simplified mode of an IGBT (or GTO or MOSFET)/ Diode pair where the forward voltages of the forced-commutated device and diode are ignored.

Dialog Box and Parameters



Internal Resistance Ron

The internal resistance Ron of the IGBT device, in ohms (Ω).

Snubber Resistance Rs

The snubber resistance, in ohms (Ω). Set the **Snubber resistance Rs** parameter to inf to eliminate the snubber from the model.

Snubber Capacitance Cs

The snubber capacitance in farads (F). Set the **Snubber capacitance Cs** parameter to 0 to eliminate the snubber, or to inf to get a resistive snubber.

Show Measurement Port

If selected, add a Simulink® output to the block returning the diode IGBT current and voltage.

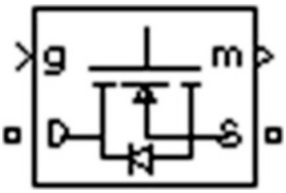
AIII.9 MOSFET

Implement MOSFET model

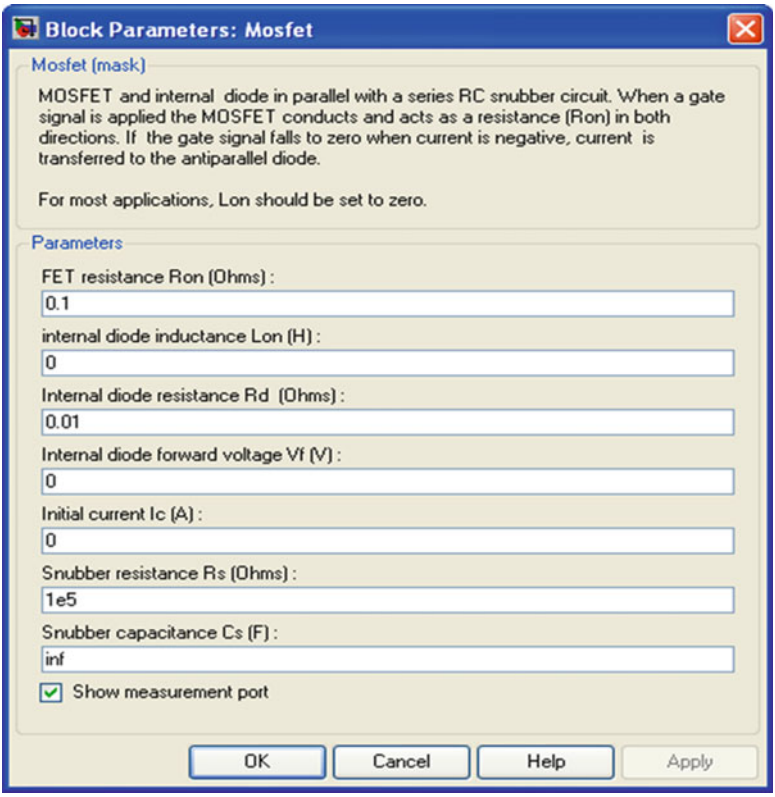
Library

Power Electronics

Description



Dialog Box and Parameters



FET Resistance Ron

The internal resistance Ron, in ohms (Ω). The **Resistance Ron** parameter cannot be set to `0` when the **Inductance Lon** parameter is set to 0.

Internal Diode Inductance Lon

The internal inductance Lon, in henries (H). The **Inductance Lon** parameter is normally set to `0` except when the **Resistance Ron** parameter is set to `0`.

Internal Diode Resistance Rd

The internal resistance of the internal diode, in ohms (Ω).

Internal Diode Forward Voltage Vf

The forward voltage of the internal diode, in volts (V).

Initial Current Ic

You can specify an initial current flowing in the MOSFET device. It is usually set to 0 in order to start the simulation with the device blocked.

If the **Initial current IC** parameter is set to a value greater than 0, the steady-state calculation considers the initial status of the MOSFET as closed. Initializing all states of a power electronic converter is a complex task. Therefore, this option is useful only with simple circuits.

Snubber Resistance Rs

The snubber resistance, in ohms (Ω). Set the **Snubber resistance Rs** parameter to `inf` to eliminate the snubber from the model.

Snubber Capacitance Cs

The snubber capacitance, in farads (F). Set the **Snubber capacitance Cs** parameter to `0` to eliminate the snubber, or to `inf` to get a resistive snubber.

Show Measurement Port

If selected, add a Simulink® output to the block returning the MOSFET current and voltage.

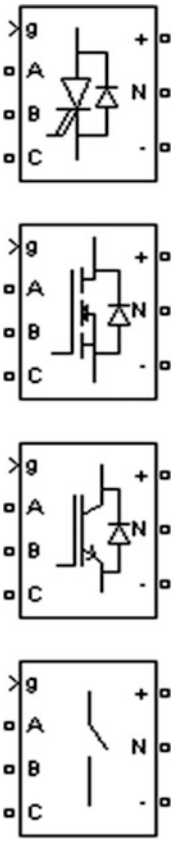
AIII.10 Three-Level Bridge

Implement three-level neutral point clamped (NPC) power converter with selectable topologies and power switching devices

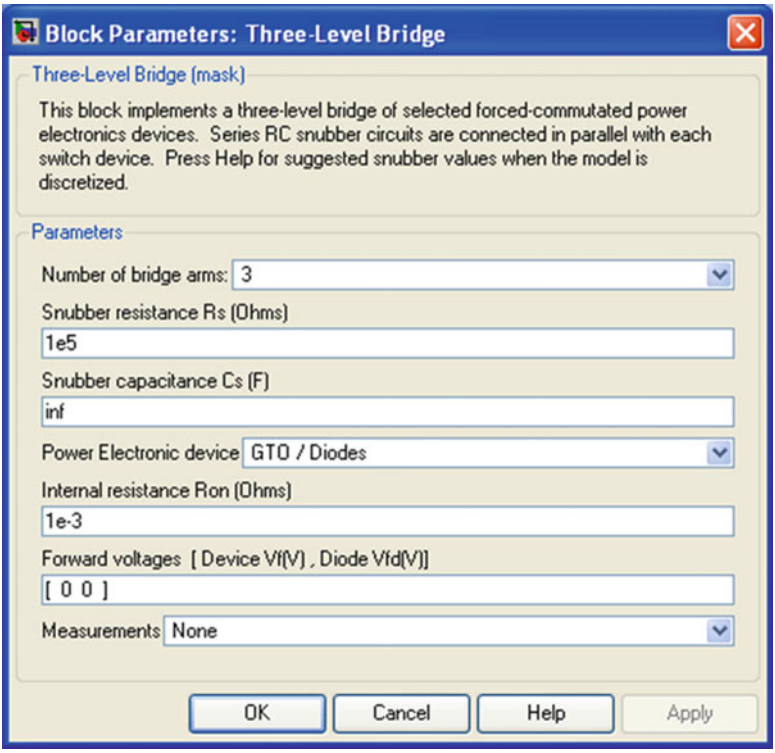
Library

Power Electronics

Description



Dialog Box and Parameters



Number of Bridge Arms

Determine the bridge topology: one, two, or three arms.

Snubber Resistance Rs

The snubber resistance, in ohms (Ω). Set the **Snubber resistance Rs** parameter to `inf` to eliminate the snubbers from the model.

Snubber Capacitance Cs

The snubber capacitance, in farads (F). Set the **Snubber capacitance Cs** parameter to `0` to eliminate the snubbers, or to `inf` to get a resistive snubber.

For forced-commutated devices (GTO, IGBT, or MOSFET) the Three-Level Bridge block operates satisfactorily with resistive snubbers as long as the firing pulses are sent to the switching devices.

If the firing pulses to forced-commutated devices are blocked, the bridge operates as a diode rectifier. In this condition, you must use appropriate values of

Rs and Cs. If the model is discretized, you can use the following formulas to compute approximate values of Rs and Cs:

$$Rs > 2\frac{Ts}{Cs}$$

$$Cs < \frac{Pn}{1000(2\pi f)Vn^2},$$

where

Pn = nominal power of single- or three-phase converter (VA)
Vn = nominal line-to-line AC voltage (Vrms)
f = fundamental frequency (Hz)
Ts = sample time (s)

These *Rs* and *Cs* values are derived from the following two criteria:

- The snubber leakage current at fundamental frequency is less than 0.1 % of nominal current when power electronic devices are not conducting.
- The RC time constant of snubbers is higher than two times the sample time Ts.

Note that the Rs and Cs values that guarantee numerical stability of the discretized bridge can be different from actual values used in the physical circuit.

Power Electronic Device

Select the type of power electronic device to use in the bridge.

Internal Resistance Ron

Internal resistance of the selected devices and diodes, in ohms (Ω).

Forward Voltages [Device Vf, Diode Vfd]

The forward voltage of the selected devices (for GTO or IGBT only) and of the antiparallel and clamping diodes, in volts.

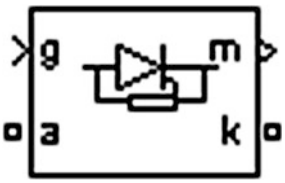
AIII.11 Thyristor

Implement thyristor model

Library

Power Electronics

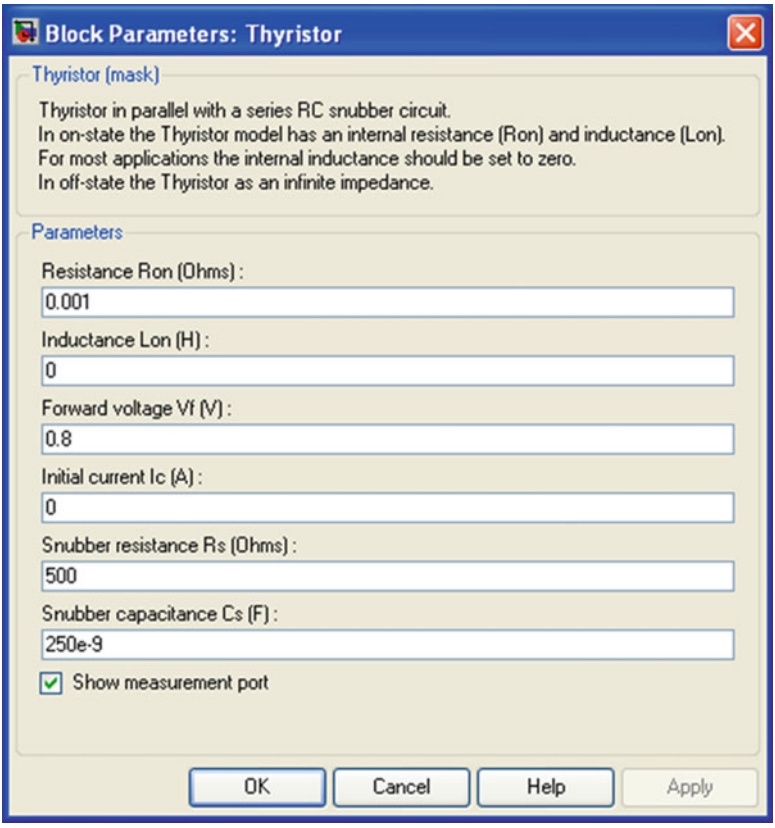
Description



Dialog Box and Parameters

Thyristor Model and Detailed Thyristor Model

In order to optimize simulation speed, two models of thyristors are available: the thyristor model and the detailed thyristor model. For the thyristor model, the latching current *Il* and recovery time *Tq* are assumed to be 0.



Resistance Ron

The thyristor internal resistance Ron, in ohms (Ω). The **Resistance Ron** parameter cannot be set to `0` when the **Inductance Lon** parameter is set to `0`.

Inductance Lon

The thyristor internal inductance Lon, in henries (H). The **Inductance Lon** parameter is normally set to 0 except when the **Resistance Ron** parameter is set to `0`.

Forward Voltage Vf

The forward voltage of the thyristor, in volts (V).

Initial Current Ic

When the **Inductance Lon** parameter is greater than 0, you can specify an initial current flowing in the thyristor. It is usually set to 0 in order to start the simulation with the thyristor blocked.

You can specify an **Initial current Ic** value corresponding to a particular state of the circuit. In such a case all states of the linear circuit must be set accordingly. Initializing all states of a power electronic converter is a complex task. Therefore, this option is useful only with simple circuits.

Snubber Resistance Rs

The snubber resistance, in ohms (Ω). Set the **Snubber resistance Rs** parameter to `inf` to eliminate the snubber from the model.

Snubber Capacitance Cs

The snubber capacitance in farads (F). Set the **Snubber capacitance Cs** parameter to `0` to eliminate the snubber, or to `inf` to get a resistive snubber.

Show Measurement Port

If selected, add a Simulink® output to the block returning the thyristor current and voltage.

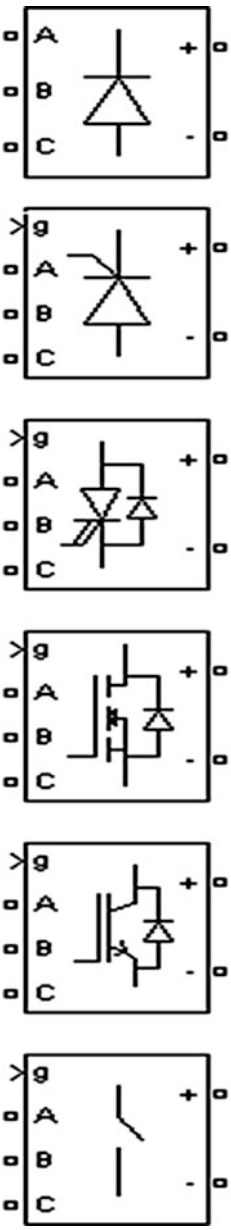
AIII.12 Universal Bridge

Implement universal power converter with selectable topologies and power electronic devices

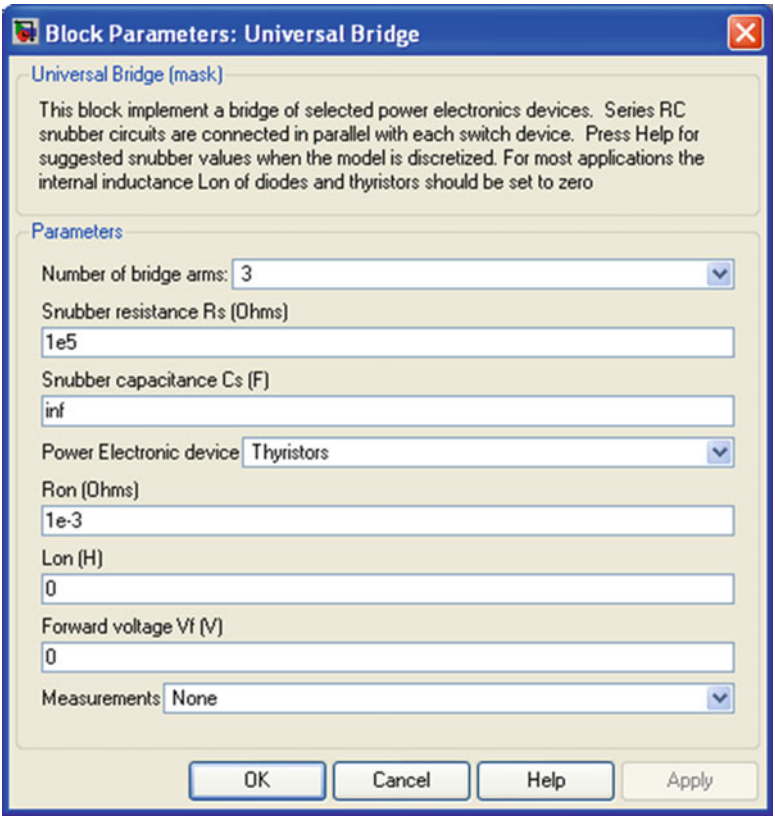
Library

Power Electronics

Description



Dialog Box and Parameters



Number of Bridge Arms

Set to `1` or `2` to get a single-phase converter (two or four switching devices). Set to `3` to get a three-phase converter connected in Graetz bridge configuration (six switching devices).

Snubber Resistance Rs

The snubber resistance, in ohms (Ω). Set the **Snubber resistance Rs** parameter to `inf` to eliminate the snubbers from the model.

Snubber Capacitance Cs

The snubber capacitance, in farads (F). Set the **Snubber capacitance Cs** parameter to `0` to eliminate the snubbers, or to `inf` to get a resistive snubber.

In order to avoid numerical oscillations when your system is discretized, you need to specify Rs and Cs snubber values for diode and thyristor bridges. For forced-commutated devices (GTO, IGBT, or MOSFET), the bridge operates satisfactorily with purely resistive snubbers as long as firing pulses are sent to switching devices.

If firing pulses to forced-commutated devices are blocked, only antiparallel diodes operate, and the bridge operates as a diode rectifier. In this condition appropriate values of Rs and Cs must also be used.

When the system is discretized, use the following formulas to compute approximate values of Rs and Cs:

$$Rs > 2\frac{T_s}{Cs}$$

$$Cs < \frac{P_n}{1000(2\pi f)V_n^2},$$

where

P_n = nominal power of single or three phase converter (VA)
V_n = nominal line-to-line AC voltage (V_{rms})
f = fundamental frequency (Hz)
T_s = sample time (s)

These Rs and Cs values are derived from the following two criteria:

- The snubber leakage current at fundamental frequency is less than 0.1 % of nominal current when power electronic devices are not conducting.
- The RC time constant of snubbers is higher than two times the sample time Ts.

These Rs and Cs values that guarantee numerical stability of the discretized bridge can be different from actual values used in a physical circuit.

Power Electronic Device

Select the type of power electronic device to use in the bridge.

When you select `Switching-function based VSC`, a switching-function voltage source converter type equivalent model is used, where switches are replaced by two voltage sources on the AC side and a current source on the DC side. This model uses the same firing pulses as for other power electronic devices and it correctly represents harmonics normally generated by the bridge.

When you select `Average-model based VSC`, an average-model type of voltage source converter is used to represent the power-electronic switches. Unlike the other power electronic devices, this model uses the reference signals (uref) representing the average voltages generated at the ABC terminals of the bridge. This model does not represent harmonics. It can be used with larger sample times while preserving the average voltage dynamics.

See `power_sfavg` for an example comparing these two models to an Universal Bridge block using IGBT/Diode device.

Ron

Internal resistance of the selected device, in ohms (Ω).

Lon

Internal inductance, in henries (H), for the diode or the thyristor device. When the bridge is discretized, the Lon parameter must be set to zero.

Forward Voltage Vf

This parameter is available only when the selected **Power electronic device** is `Diodes` or `Thyristors`.

Forward voltage, in volts (V), across the device when it is conducting.

Forward Voltages [Device Vf, Diode Vfd]

This parameter is available when the selected **Power electronic device** is `GTO/Diodes` or `IGBT/Diodes`.

Forward voltages, in volts (V), of the forced-commutated devices (GTO, MOSFET, or IGBT) and of the antiparallel diodes.

[Tf (s) Tt (s)]

Fall time Tf and tail time Tt, in seconds (s), for the GTO or the IGBT devices.

Measurements

Select `Device voltages` to measure the voltages across the six power electronic device terminals.

Select `Device currents` to measure the currents flowing through the six power electronic devices. If antiparallel diodes are used, the measured current is the total current in the forced-commutated device (GTO, MOSFET, or IGBT) and in the antiparallel diode. A positive current therefore indicates a current flowing in the forced-commutated device and a negative current indicates a current flowing in the diode. If snubber devices are defined, the measured currents are the ones flowing through the power electronic devices only.

Select `UAB UBC UCA UDC voltages` to measure the terminal voltages (AC and DC) of the Universal Bridge block.

Select `All voltages and currents` to measure all voltages and currents defined for the Universal Bridge block.

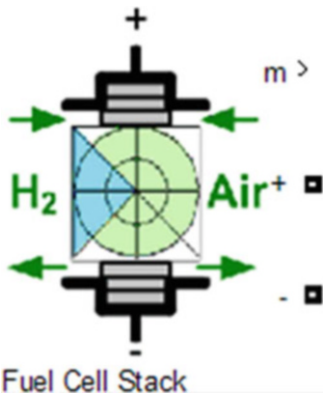
AIII.13 Fuel Cell Stack

Implement generic hydrogen fuel cell stack model

Library

Electric Drives/Extra Sources

Description

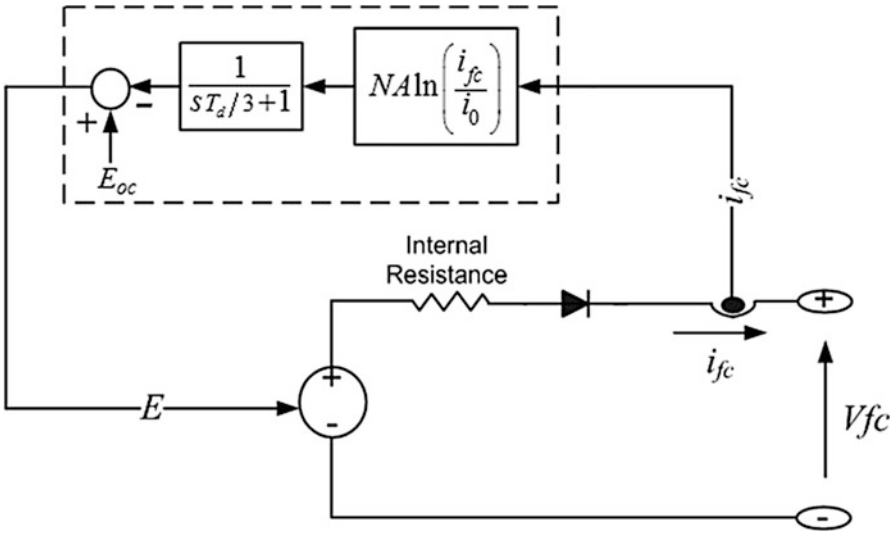


The Fuel Cell Stack block implements a generic model parameterized to represent most popular types of fuel cell stacks fed with hydrogen and air.

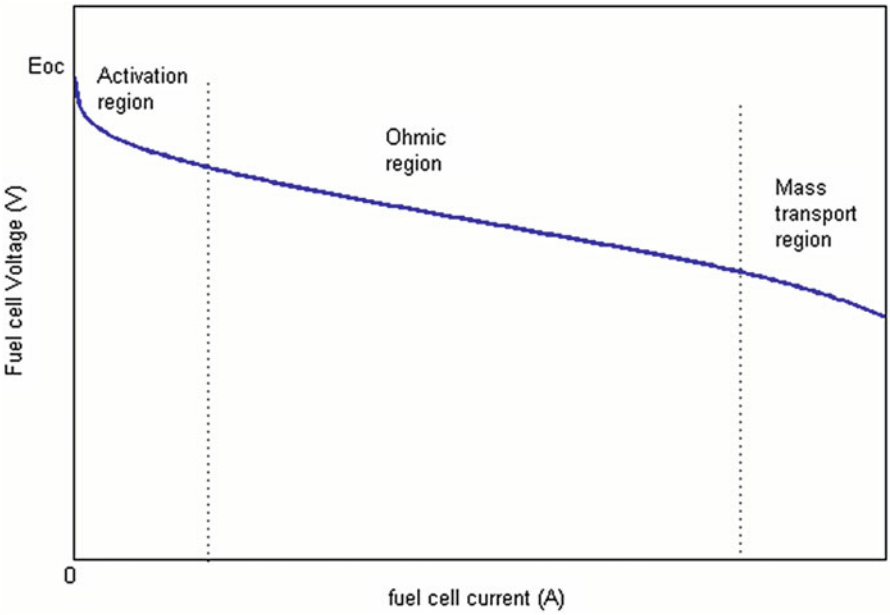
The block represents two versions of the stack model: a simplified model and a detailed model. You can switch between the two models by selecting the level in the mask under **Model detail level** in the block dialog box.

Simplified Model

This model is based on the equivalent circuit of a fuel cell stack shown below:



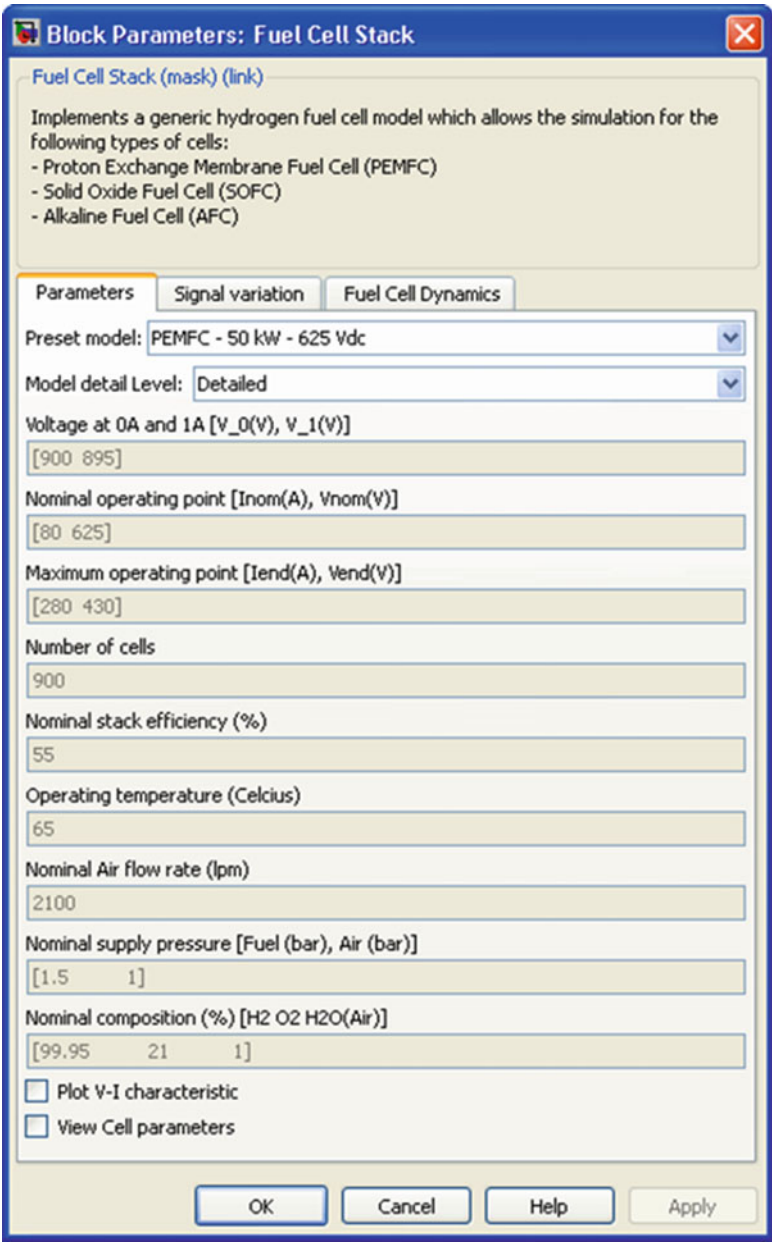
The simplified model represents a particular fuel cell stack operating at nominal conditions of temperature and pressure. The parameters of the equivalent circuit can be modified based on the polarization curve obtained from the manufacturer datasheet. You just have to input in the mask the value of the voltage at 0 and 1 A, the nominal and the maximum operating points, for the parameters to be calculated. A diode is used to prevent the flow of negative current into the stack. A typical polarization curve consists of three regions:



The first region represents the activation voltage drop due to the slowness of the chemical reactions taking place at electrode surfaces. Depending on the temperature and operating pressure, type of electrode, and catalyst used, this region is more or less wide. The second region represents the resistive losses due the internal resistance of the fuel cell stack. Finally, the third region represents the mass transport losses resulting from the change in concentration of reactants as the fuel is used.

Dialog Box and Parameters

Parameters Tab



Preset Model

Provides a set of predetermined polarization curves and parameters for particular fuel cell stacks found on the market:

- No (User-Defined).
- PEMFC – 1.26 kW – 24 Vdc.
- PEMFC – 6 kW – 45 Vdc.
- PEMFC – 50 kW – 625 Vdc.
- AFC – 2.4 kW – 48 Vdc.

Select one of these preset models to load the corresponding parameters in the entries of the dialog box. SelectNo (User-Defined) if you do not want to use a preset model.

Model Detail Level

Provide access to the two versions of the model:

- Simplified.
- Detailed.

When a simplified model is used, there is no variable under the **signal variation** pane

Voltage at 0 A and 1 A

The voltage at 0 A and 1 A of the stack (Volts). Assuming nominal and constant gases utilizations.

Nominal Operating Point

The rated current (Ampere) and rated voltage (Volts) of the stack. Assuming nominal and constant gases utilizations.

Maximum Operating Point

The current (Ampere) and voltage (Volts) of the stack at maximum power. Assuming nominal and constant gases utilizations.

Number of Cells

The number of cells in series in the stack. This parameter is available only for a detailed model.

Nominal Stack Efficiency

The rated efficiency of the stack relative to the low heating value (LHV) of water. This parameter is available only for a detailed model.

Operating Temperature

The nominal temperature of operation in degrees Celsius. This parameter is available only for a detailed model.

Nominal Air Flow Rate

The rated air flow rate (l/min). This parameter is available only for a detailed model.

Nominal Supply Pressure

Rated supply pressure (absolute) of fuel and air in bars. This parameter is available only for a detailed model.

Nominal Composition

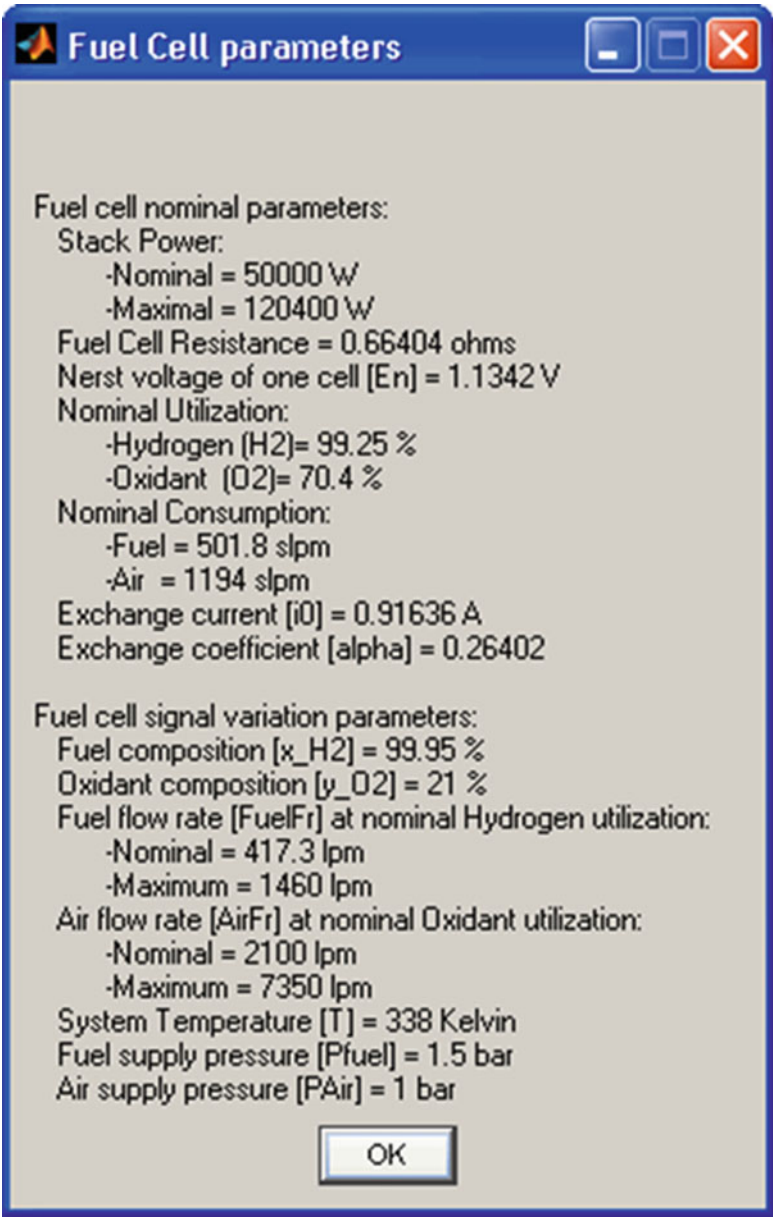
The rated percentage of hydrogen (x) in the fuel, oxygen (y) and water (w) in the oxidant. This parameter is available only for a detailed model.

Plot V-I Characteristic

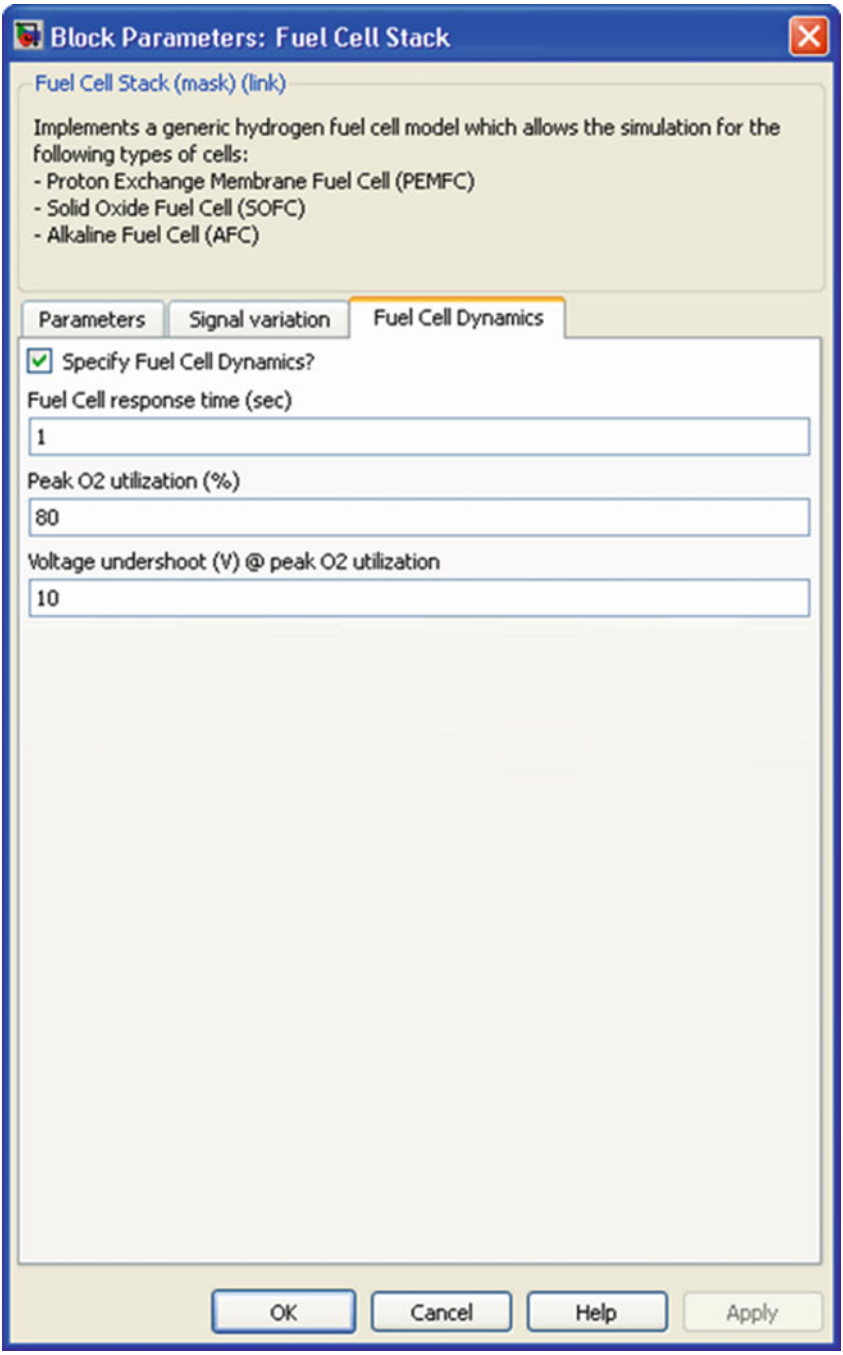
Plots a figure containing two graphs. The first graph represents the stack voltage (Volts) vs. current (A) and the second graph represents the stack power (kW) vs. current (A). To plot the graphs, select the checkbox. This checkbox is available only for a detailed model.

View Cell Parameters

Presents the overall parameters of the stack. This checkbox is available only for a detailed model. Select the checkbox to view the parameters. The dialog box is shown below.



Fuel Cell Dynamics Tab



Specify Fuel Cell Dynamics?

Asks whether you want to specify the fuel cell dynamics. Select the checkbox to enter the fuel cell response time in seconds.

Fuel Cell Response Time (Sec)

Enter the response time of the cell (at 95 % of the final value). This parameter becomes visible only when the **Specify Fuel Cell Dynamics?** checkbox is selected.

Peak O_2 Utilization (%)

Enter the peak oxygen utilization at nominal condition of operation. This parameter becomes visible only when the **Specify Fuel Cell Dynamics?** checkbox is selected and the **Air flow rate** checkbox is selected under the **Signal variation** pane.

Voltage Undershoot (V) @ Peak O_2 Utilization

Enter the voltage undershoot (Volts) at peak oxygen utilization at nominal condition of operation. This parameter becomes visible only when the **Specify Fuel Cell Dynamics?** checkbox is selected and the **Air flow rate** checkbox is selected under the **Signal variation** pane.

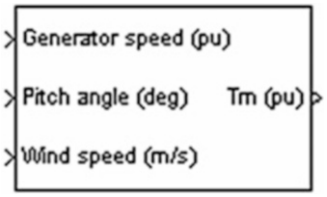
AIII.14 Wind Turbine

Implement model of variable pitch wind turbine

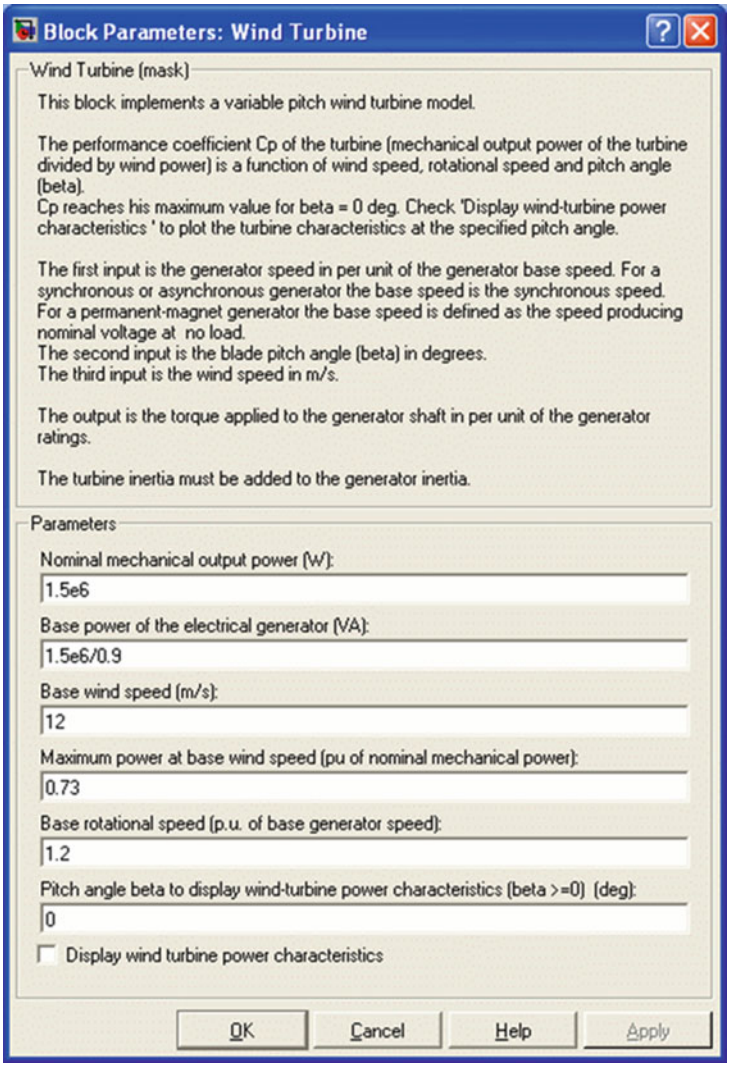
Library

Renewable Energy/Wind Generation

Description



Dialog Box and Parameters



Nominal Mechanical Output Power

The nominal output power in watts (W).

Base Power of the Electrical Generator

The nominal power of the electrical generator coupled to the wind turbine, in VA. This parameter is used to compute the output torque in pu of the nominal torque of the generator.

Base Wind Speed

The base value of the wind speed, in m/s, used in the per unit system. The base wind speed is the mean value of the expected wind speed. This base wind speed produces a mechanical power which is usually lower than the turbine nominal power.

Maximum Power at Base Wind Speed

The maximum power at base wind speed in pu of the nominal mechanical power. This parameter is the power gain k_p already defined.

Base Rotational Speed

The rotational speed at maximum power for the base wind speed. The base rotational speed is in pu of the base generator speed. For a synchronous or asynchronous generator, the base speed is the synchronous speed. For a permanent-magnet generator, the base speed is defined as the speed producing nominal voltage at no load.

Pitch Angle Beta to Display Wind Turbine Power Characteristics

The pitch angle beta, in degrees, used to display the power characteristics. Beta must be greater than or equal to zero.

Display Wind Turbine Power Characteristics

If this parameter is checked, the turbine power characteristics are displayed for different wind speeds and for the specified pitch angle beta.

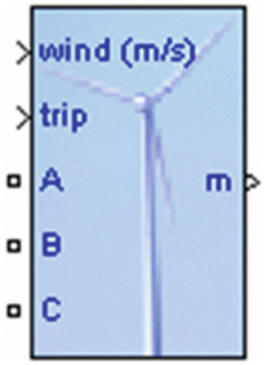
AIII.15 Wind Turbine Doubly-Fed Induction Generator (Phasor Type)

Implement phasor model of variable speed doubly-fed induction generator driven by wind turbine

Library

Renewable Energy/Wind Generation

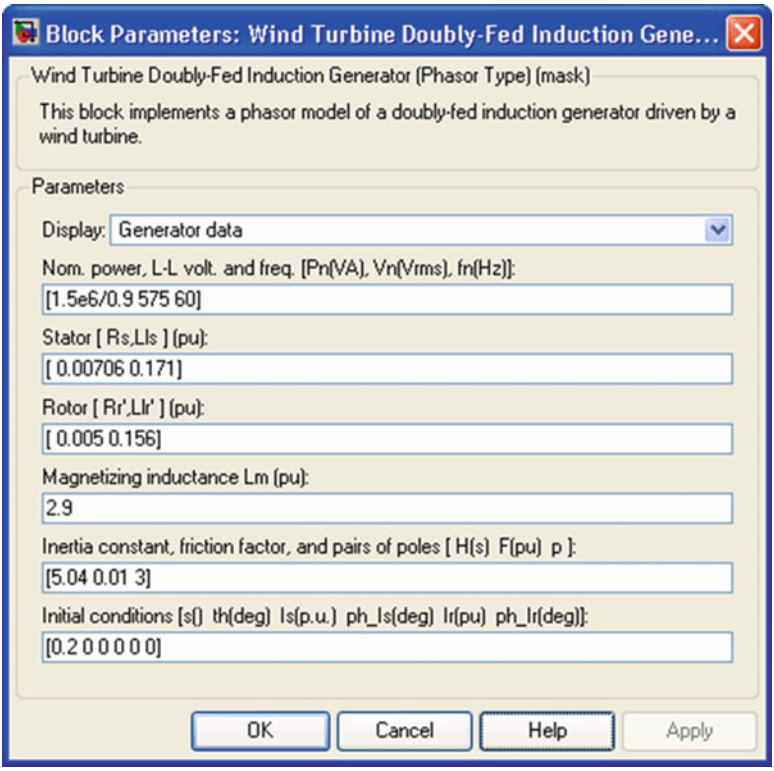
Description



Dialog Box and Parameters

The WTDFIG parameters are grouped in four categories: Generator data, Converters data, Turbine data, and Control parameters. Use the Display listbox to select which group of parameters you want to visualize.

Generator Data Parameters



WTDFIG Modeled Using Positive-Sequence Only

The WTDFIG is modeled by a three-wire system using two current sources. The WTDFIG does not generate any zero-sequence current, but it can generate negative-sequence currents during unbalanced system operation.

Nominal Power, Line-to-Line Voltage and Frequency

The nominal power in VA, the nominal line-to-line voltage in Vrms and the nominal system frequency in hertz.

Stator [Rs, Lls]

The stator resistance Rs and leakage inductance Lls in pu based on the generator rating.

Rotor [Rr', Llr']

The rotor resistance Rr' and leakage inductance Llr', both referred to the stator, in pu based on the generator rating.

Magnetizing Inductance Lm

The magnetizing inductance Lm in pu based on the generator rating.

Inertia Constant, Friction Factor and Pairs of Poles

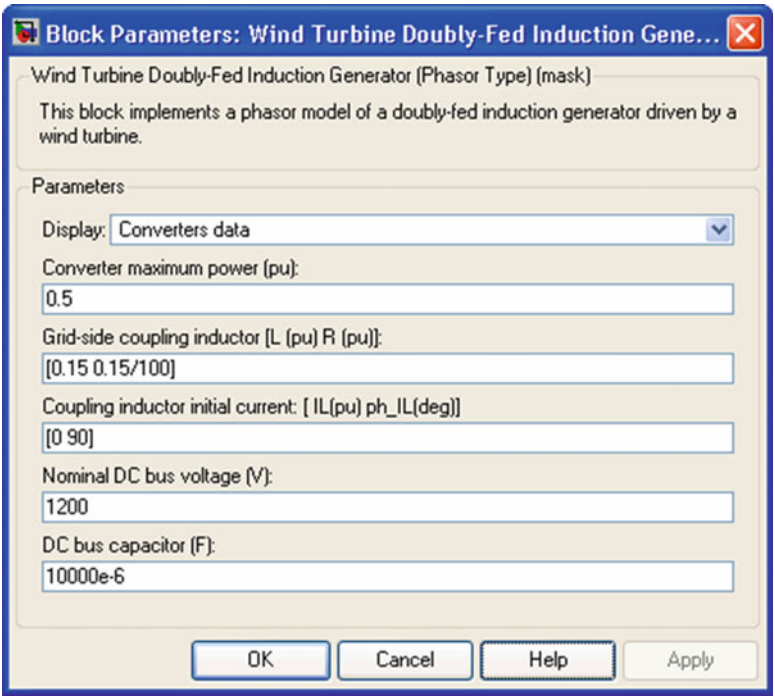
Combined generator and turbine inertia constant H in seconds, combined viscous friction factor F in pu based on the generator rating and number of pole pairs p.

You may need to use your own turbine model, in order for example, to implement different power characteristics or to implement the shaft stiffness. Your model must then output the mechanical torque applied to the generator shaft. If the inertia and the friction factor of the turbine are implemented inside the turbine model you specify only the generator inertia constant H and the generator friction factor F.

Initial Conditions

The initial slip s, electrical angle Θ in degrees, stator phasor current magnitude in pu, stator phasor current phase angle in degrees, rotor phasor current magnitude in pu and rotor phasor current phase angle in degrees.

Converters Data Parameters



Converter Maximum Power

The maximum power of both C_{grid} and C_{rotor} in pu of the nominal power. This parameter is used to compute the maximum current at 1 pu of voltage for C_{grid}. The maximum current for C_{rotor} is 1 pu.

Grid-Side Coupling Inductor [L R]

The coupling inductance L and its resistance R in pu based on the generator rating.

Coupling Inductor Initial Currents

The coupling inductor initial phasor current in positive-sequence. Enter magnitude IL in pu and phase ph_IL in degrees. If you know the initial value of the current corresponding to the WTDFIG operating point you may specify it in order to start simulation in steady state. If you don't know this value, you can leave [0 0]. The system will reach steady-state after a short transient.

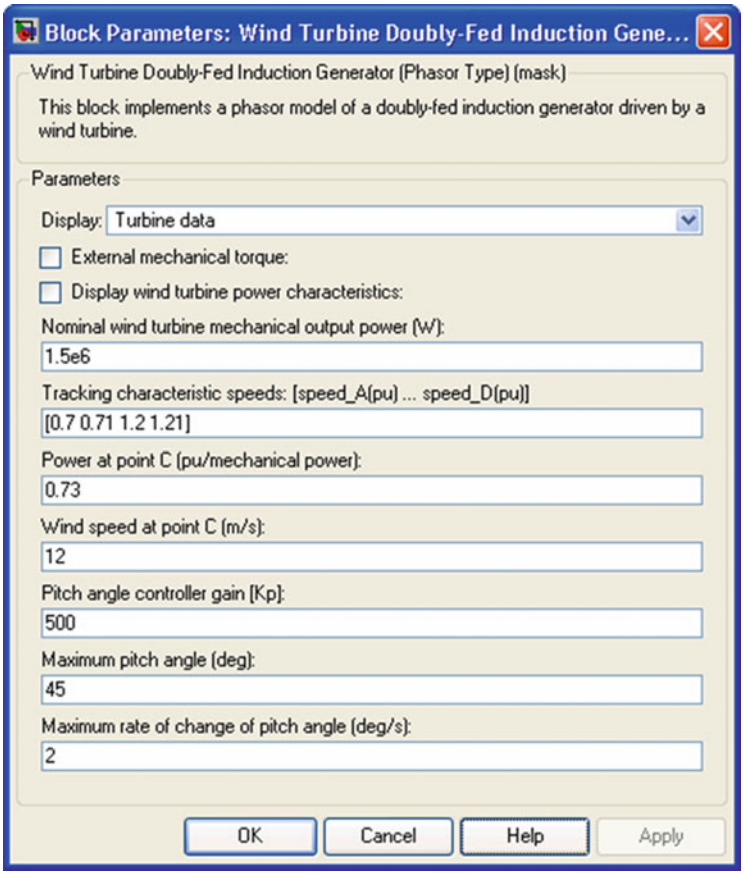
Nominal DC Bus Voltage

The nominal DC bus voltage in volts.

DC Bus Capacitor

The total capacitance of the DC-link in farads. This capacitance value is related to the WTDFIG rating and to the DC-link nominal voltage. The energy stored in the capacitance (in joules) divided by the WTDFIG rating (in VA) is a time duration which is usually a fraction of a cycle at nominal frequency. For example, for the default parameters, (C = 10,000 μF, Vdc = 1,200 V, Pn = 1.67 MVA) this ratio $1/2 \cdot C \cdot V_{dc}^2/P_n$ is 4.3 ms, which represents 0.26 cycle for a 60 Hz frequency. If you change the default values of the nominal power rating and DC voltage, you should change the capacitance value accordingly.

Turbine Data Parameters



External Mechanical Torque

If this parameter is checked, a Simulink® input named Tm appears on the block, allowing to use an external signal for the generator input mechanical torque. This external torque must be in pu based on the nominal electric power and synchronous speed. For example, the external torque may come from a user defined turbine model. Following the convention used in the induction machine, the torque must be negative for power generation.

Electric Power-Speed Characteristic

This parameter is visible only when the **External mechanical torque** parameter is checked. It is used to specify a series of speed-power pairs for the tracking characteristic. The speed is in pu based on synchronous speed and the power is in pu based on nominal generator power.

Display Wind Turbine Power Characteristics

If this parameter is checked, the turbine power characteristics at zero degree of pitch angle are displayed for different wind speeds. The tracking characteristic is also displayed on the same figure.

This parameter is not visible when the **External mechanical torque** parameter is checked.

Nominal Wind Turbine Mechanical Output Power

This parameter is not visible when the **External mechanical torque** parameter is checked.

The nominal turbine mechanical output power in watts.

Tracking Characteristic Speeds

This parameter is not visible when the **External mechanical torque** parameter is checked.

Specify the speeds of point A to point D of the tracking characteristic in pu of the synchronous speed. speed_B must be greater than speed_A and speed_D must be greater than speed_C.

Power at Point C

This parameter is not visible when the **External mechanical torque** parameter is checked.

Specify the power of point C of the tracking characteristic in pu of the **Nominal wind turbine mechanical output power.**

Wind Speed at Point C

This parameter is not visible when the **External mechanical torque** parameter is checked.

Specify wind speed in m/s for point C. The power at point C is the maximum turbine output power for the specified wind speed.

Pitch Angle Controller Gain [Kp]

This parameter is not visible when the **External mechanical torque** parameter is checked.

Proportional gain Kp of the pitch controller. Specify Kp in degrees/(speed deviation pu). The speed deviation is the difference between actual speed and speed of point D in pu of synchronous speed.

Maximum Pitch Angle

This parameter is not visible when the **External mechanical torque** parameter is checked.

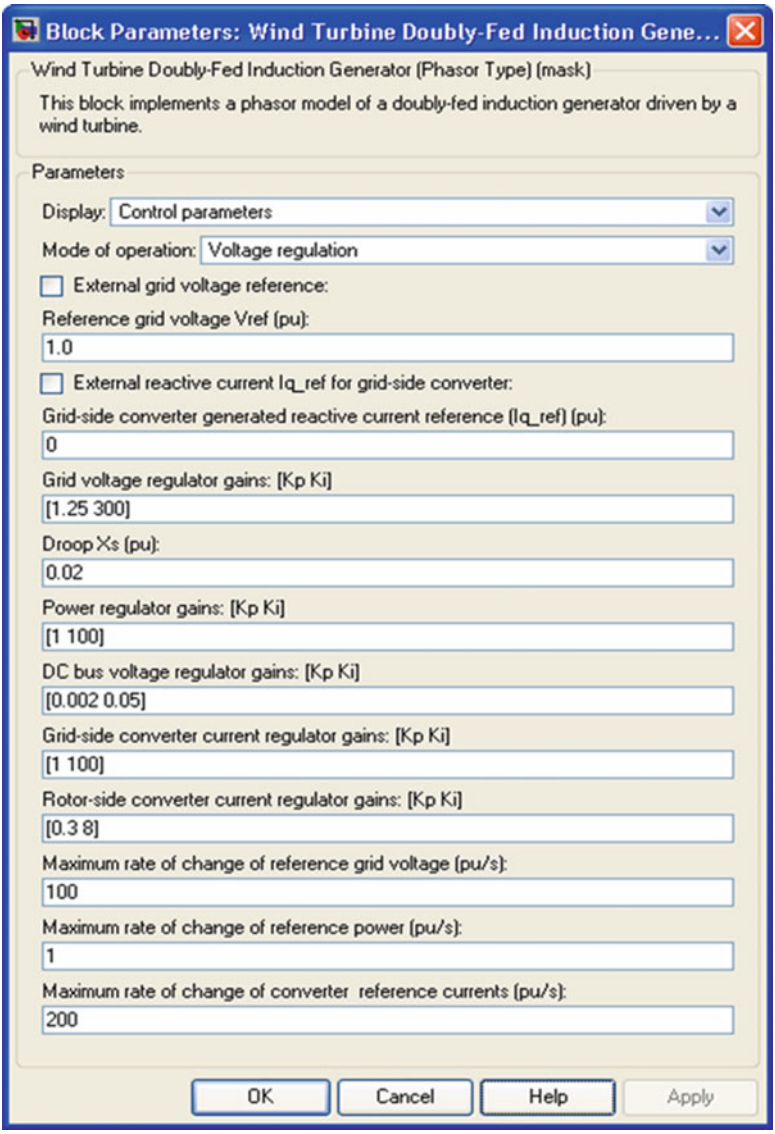
The maximum pitch angle in degrees.

Maximum Rate of Change of Pitch Angle

This parameter is not visible when the **External mechanical torque** parameter is checked.

The maximum rate of change of the pitch angle in degrees/s.

Control Parameters



Mode of Operation

Specifies the **WTDFIG** mode of operation. Select either `Voltage regulation` or `Var regulation`.

External Grid Voltage Reference

This parameter is not visible when the **Mode of operation** parameter is set to `Var regulation`.

If this parameter is checked, a Simulink input named Vref appears on the block, allowing to control the reference voltage from an external signal in pu. Otherwise a fixed reference voltage is used, as specified by the parameter below.

Reference Grid Voltage Vref

This parameter is not visible when the **Mode of operation** parameter is set to `Var regulation` or when the **External grid voltage reference** parameter is checked.

Reference voltage, in pu, used by the voltage regulator.

External Generated Reactive Power Reference

This parameter is not visible when the **Mode of operation** parameter is set to `Voltage regulation`.

If this parameter is checked, a Simulink input named Qref appears on the block, allowing to control the reference reactive power, at grid terminals, from an external signal in pu. Otherwise a fixed reference reactive power is used, as specified by the parameter below.

Generated Reactive Power Qref

This parameter is not visible when the **Mode of operation** parameter is set to `Voltage regulation` or when the **External generated reactive power reference** parameter is checked.

Reference generated reactive power at grid terminals, in pu, used by the var regulator.

External Reactive Current Iq_ref for Grid-Side Converter Reference

If this parameter is checked, a Simulink input named Iq_ref appears on the block, allowing to control the grid-side converter reactive current from an external signal in pu. Specify a positive value for Iq_ref for generated reactive power. Otherwise a fixed reactive current is used, as specified by the parameter below.

Grid-Side Converter Generated Reactive Current Reference (Iq_ref)

This parameter is not visible when the **External reactive current Iq_ref for grid-side converter reference** parameter is checked.

Reference grid-side converter reactive current, in pu, used by the current regulator. Specify a positive value of Iq_ref for generated reactive power.

Grid Voltage Regulator Gains [Kp Ki]

This parameter is not visible when the **Mode of operation** parameter is set to `Var regulation`.

Gains of the AC voltage regulator. Specify proportional gain Kp in (pu of I)/(pu of V), and integral gain Ki, in (pu of I)/(pu of V)/s, where V is the AC voltage error and I is the output of the voltage regulator.

Droop Xs

This parameter is not visible when the **Mode of operation** parameter is set to `Var regulation`.

Droop reactance, in pu/nominal power, defining the slope of the V-I characteristic.

Reactive Power Regulator Gains [Kp Ki]

This parameter is not visible when the **Mode of operation** parameter is set to `Voltage regulation`.

Gains of the var regulator. Specify proportional gain Kp in (pu of I)/(pu of Q), and integral gain Ki, in (pu of I)/(pu of Q)/s, where Q is the reactive power error and I is the output of the var regulator.

Power Regulator Gains [Kp Ki]

Gains of the power regulator. Specify proportional gain Kp in (pu of I)/(pu of P), and integral gain Ki, in (pu of I)/(pu of P)/s, where P is the power error and I is the output of the power regulator.

DC Bus Voltage Regulator Gains [Kp Ki]

Gains of the DC voltage regulator which controls the voltage across the DC bus capacitor. Specify proportional gain Kp in (pu of I)/(Vdc), and integral gain Ki, in (pu of I)/(Vdc)/s, where Vdc is the DC voltage error and I is the output of the voltage regulator.

Grid-Side Converter Current Regulator Gains [Kp Ki]

Gains of the grid-side converter current regulator.

Specify proportional gain Kp in (pu of V)/(pu of I) and integral gain Ki, in (pu of V)/(pu of I)/s, where V is the output Vgc of the current regulator and I is the current error.

Rotor-Side Converter Current Regulator Gains [Kp Ki]

Gains of the rotor-side converter current regulator.

Specify proportional gain Kp in (pu of V)/(pu of I) and integral gain Ki, in (pu of V)/(pu of I)/s, where V is the output Vr of the current regulator and I is the current error.

Maximum Rate of Change of Reference Grid Voltage

This parameter is not visible when the **Mode of operation** parameter is set to `Var regulation`.

Maximum rate of change of the reference voltage, in pu/s, when an external reference voltage is used.

Maximum Rate of Change of Reference Reactive Power

This parameter is not visible when the **Mode of operation** parameter is set to `Voltage regulation`.

Maximum rate of change of the reference reactive power, in pu/s, when an external reference reactive power is used.

Maximum Rate of Change of Reference Power

Maximum rate of change of the reference power in pu/s.

Maximum Rate of Change of Converters Reference Current

Maximum rate of change of the reference current in pu/s for both the rotor-side and the grid-side converters.

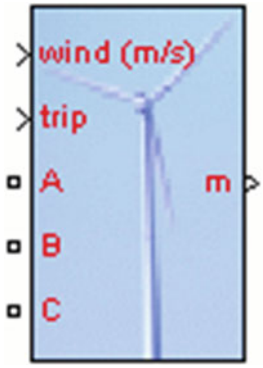
AIII.16 Wind Turbine Induction Generator (Phasor Type)

Implement phasor model of squirrel-cage induction generator driven by variable pitch wind turbine

Library

Renewable Energy/Wind Generation

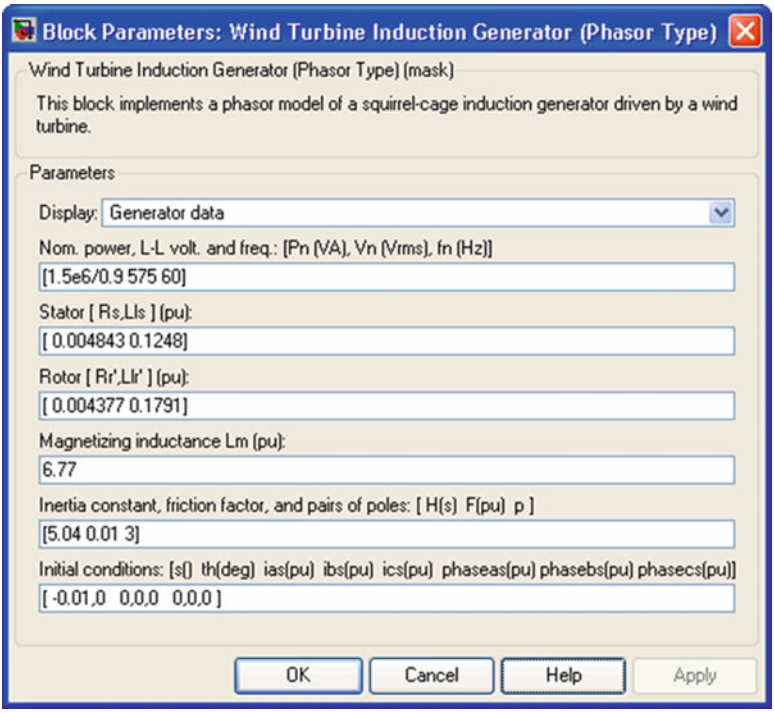
Description



Dialog Box and Parameters

The WTIG parameters are grouped in two categories: Generator `data` and Turbine data». Use the Display listbox to select which group of parameters you want to visualize.

Generator Data Parameters



Nominal Power, Line-to-Line Voltage and Frequency

The nominal power in VA, the nominal line-to-line voltage in Vrms and the nominal system frequency in hertz.

Stator [Rs, Lls]

The stator resistance Rs and leakage inductance Lls in pu based on the generator ratings.

Rotor [Rr', Llr']

The rotor resistance Rr' and leakage inductance Llr', both referred to the stator, in pu based on the generator ratings.

Magnetizing Inductance Lm

The magnetizing inductance Lm in pu based on the generator ratings.

Inertia Constant, Friction Factor and Pairs of Poles

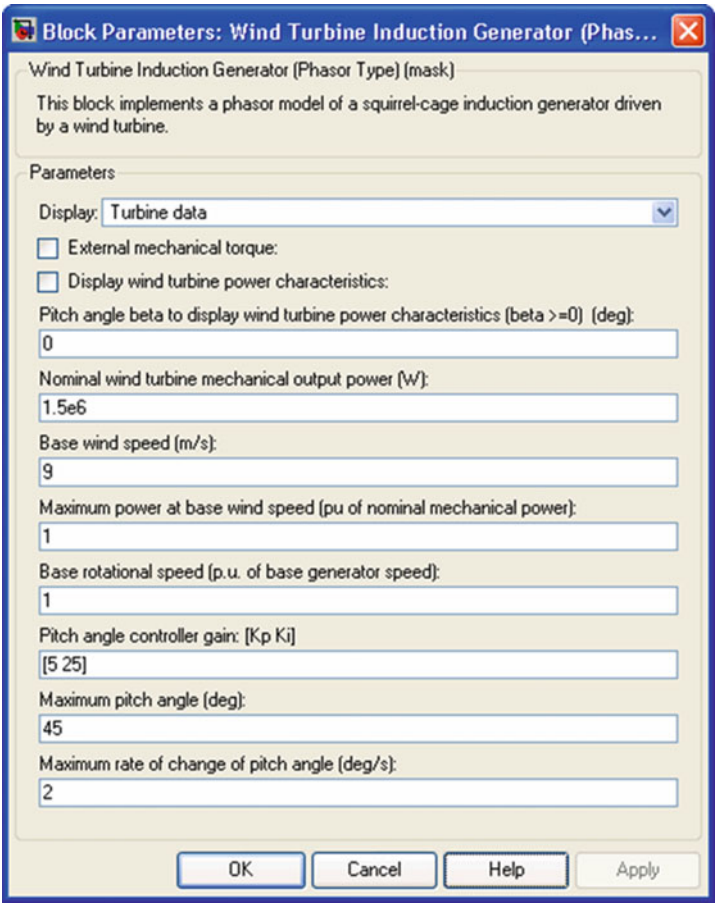
Combined generator and turbine inertia constant H in seconds, combined viscous friction factor F in pu based on the generator ratings and number of pole pairs p.

You may need to use your own turbine model, in order for example, to implement different power characteristics or to implement the shaft stiffness. Your model must then output the mechanical torque applied to the generator shaft. If the inertia and the friction factor of the turbine are implemented inside the turbine model you specify only the generator inertia constant H and the generator friction factor F.

Initial Conditions

The initial slip s, electrical angle Θ in degrees, stator current magnitude in pu and phase angle in degrees.

Turbine Data Parameters



External Mechanical Torque

If this parameter is checked, a Simulink® input named Tm appears on the block, allowing to use an external signal for the generator input mechanical torque. This external torque must be in pu based on the nominal electric power and synchronous speed of the generator. For example, the external torque may come from a user defined turbine model. By convention for the induction machine, the torque must be negative for power generation.

Display Wind Turbine Power Characteristics

If this parameter is checked, the turbine power characteristics at the specified pitch angle are displayed for different wind speeds.

This parameter is not visible when the **External mechanical torque** parameter is checked.

Nominal Wind Turbine Mechanical Output Power

This parameter is not visible when the **External mechanical torque** parameter is checked.

The nominal turbine mechanical output power in watts.

Base Wind Speed

This parameter is not visible when the **External mechanical torque** parameter is checked.

The base value of the wind speed, in m/s, used in the per unit system. The base wind speed is the mean value of the expected wind speed. This base wind speed produces a mechanical power which is usually lower than the turbine nominal power.

Maximum Power at Base Wind Speed

This parameter is not visible when the **External mechanical torque** parameter is checked.

The maximum power at base wind speed in pu of the nominal mechanical power.

Base Rotational Speed

This parameter is not visible when the **External mechanical torque** parameter is checked.

The rotational speed at maximum power for the base wind speed. The base rotational speed is in pu of the base generator speed.

Pitch Angle Controller Gain [Kp Ki]

This parameter is not visible when the **External mechanical torque** parameter is checked.

Proportional and Integral gains Kp and Ki of the pitch controller. Specify Kp in degrees/(power deviation pu) and Ki in degrees/(power deviation pu)/s. The power deviation is the difference between actual electrical output power and the nominal mechanical power in pu of the generator nominal power.

Maximum Pitch Angle (deg)

This parameter is not visible when the **External mechanical torque** parameter is checked.

The maximum pitch angle in degrees.

Maximum Rate of Change of Pitch Angle

This parameter is not visible when the **External mechanical torque** parameter is checked.

The maximum rate of change of the pitch angle in degrees/s.

Appendix IV
Data for Case Study

The Measurement of power quality is done in PSG College of Technology at k-block. Assessment and problem evaluation from the results in case study done has been described briefly in Chap. 8.

Table AIV.1 Solar panel details

Symbol	Parameter	Value
Standard test conditions		
V_{MMP}	**Maximum power point voltage**	30 V
I_{MMP}	**Maximum power point current**	8.33 A
V_{OC}	**Open circuit voltage**	36.8 V
I_{SC}	**Short circuit current**	8.83 A
Series fuse		20 A

Table AIV.2 SMA inverter details

Symbol	Parameter	Value
DC side		
V_{DCmax}	**Maximum DC voltage**	1,000 V
V_{DCMMP}	**Maximum power point DC voltage**	580–800 V
I_{DCmax}	**Maximum DC current**	36 A
AC side		
$V_{AC,r}$	**AC output voltage**	380/400/415 V
$P_{AC,r}$	**Power output at AC side**	20 kW
S_{max}	**Apparent power**	20 kVA
$f_{AC,r}$	**frequency**	50 Hz
I_{DCmax}	**Maximum current at AC side**	29 A
cosφ	**Power factor**	0.8 (Under/Over excited)

© Springer International Publishing Switzerland 2015

S. Sumathi et al., *Solar PV and Wind Energy Conversion Systems*,
Green Energy and Technology, DOI 10.1007/978-3-319-14941-7

AIV.1 Fluke Power Quality Analyzer

Fluke 430 Series II Three-phase power quality and energy analyzers pinpoint power quality problems and monetize energy Loss, The new 430 Series II analyzers offer the best in power quality analysis, and introduce, for the first time ever, the ability to monetarily quantify losses caused by power quality issues.

- Energy loss calculator: Classic active and reactive power measurements, unbalance and harmonic power, are quantified to pinpoint true system energy losses in rupees (other local currencies available).
- Power inverter efficiency: Simultaneously measure AC output power and DC input power for power electronics systems using optional DC clamp.
- Power Wave data capture: 435 and 437 Series II analyzers capture fast RMS data, show half-cycle and waveforms to characterize electrical system dynamics (generator start-ups, UPS switching).
- Waveform capture: 435 and 437 Series II models capture 50/60 cycles (50/60) Hz of each event that is detected in all modes, without set-up.
- Automatic Transient Mode: 435 and 437 Series II analyzers capture 200 kHz waveform data on all phases simultaneously up to 6 kV.
- Fully Class-A compliant: 435 and 437 Series II analyzers conduct tests according to the stringent international IEC 61000-4-30 Class-A standard.
- Mains signaling: 435 and 437 Series II analyzers measure interference from ripple control signals at specific frequencies.
- 400 Hz measurement: 437 Series II analyzer captures power quality measurements for avionic and military power systems.
- Troubleshoot: Analyze the trends using the cursors and zoom tools.
- Highest safety rating in the industry: 600 V CAT IV/1,000 V CAT III rated for use at the service entrance.
- Measure all three phases and neutral: With included four flexible current probes with enhanced thin flex designed to fit into the tightest places.
- Automatic Trending: Every measurement is always automatically recorded, without any set-up.
- System-Monitor: Ten power quality parameters on one screen according to EN50160 power quality standard.
- Logger function: Configure for any test condition with memory for up to 600 parameters at user defined intervals.
- View graphs and generate reports: With included analysis software.
- Battery life: Up to 8 h operating time per charge on Li-ion battery pack (Figs. AIV.1 and AIV.2).



Fig. AIV.1 Fluke 434 series II energy analyzer

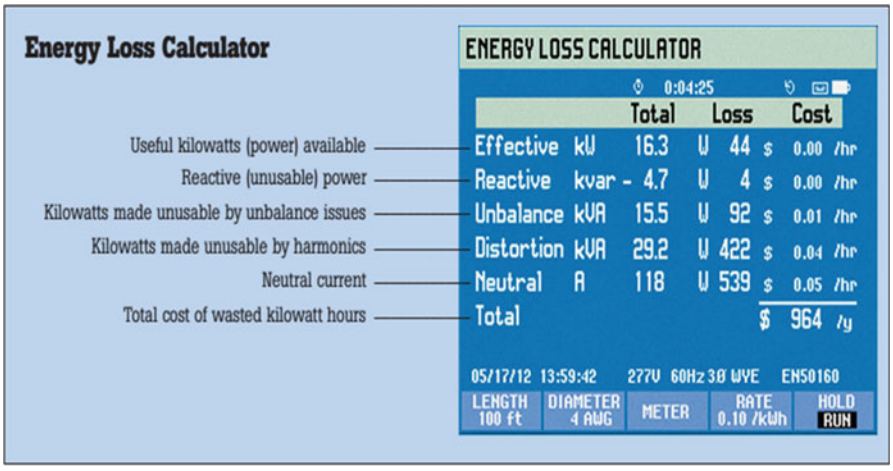


Fig. AIV.2 Special measurement included in FLUKE 434 series II

The meter can be used for:

- Frontline troubleshooting quickly diagnoses problems on-screen to get your operation back online.
- Energy loss management measure and quantify specific causes of energy losses to enable simple return-on-investment calculation of harmonics and unbalance mitigation equipment.
- Power inverter efficiency simultaneously measure AC input power and DC output power for power electronics systems.
- Capture fast Root Mean Square (RMS) data, show half-cycle and waveforms to characterize electrical system dynamics.
- Predictive maintenance detects and prevents power quality issues before they cause downtime.
- Qualities of service compliance validate incoming power quality at the service entrance.
- Long-term analysis Uncover hard-to-find or intermittent issues.
- Load studies Verify electrical system capacity before adding loads.
- Dynamic load testing capture instantaneous values to see the effect of load switch on generators and UPS systems.

Instrument Information

Model number	FLUKE 430-II
Serial number	24663010
Firmware revision	V04.01

Software Information

Power log version	4.1
FLUKE 345 DLL version	11.20.2006
FLUKE 430 DLL version	1.8.0.0
FLUKE 430-II DLL version	1.0.0.28

Measurement Summary

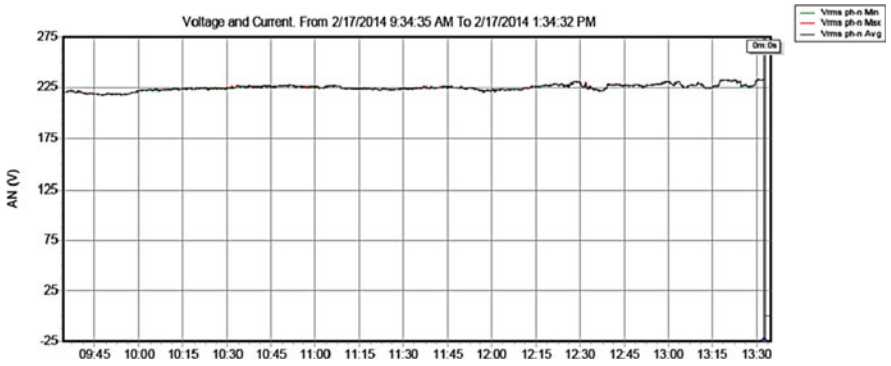
Measurement topology	Wye mode
Application mode	Logger
First recording	2/17/2014 9:34:35 AM
Last recording	2/17/2014 1:34:32 PM
Recording interval	0 h 0 m 3 s 0 m sec
Nominal voltage	230 V
Nominal current	300 A
Nominal frequency	50 Hz
File start time	2/17/2014 9:34:35 AM
File end time	2/17/2014 1:34:32 PM
Duration	0d 3 h 59 m 57 s 0 m sec
Number of events	7
Events downloaded	No
Number of screens	100
Screens downloaded	No
Power measurement method	Unified
Cable type	Copper
Harmonic scale	%H1
THD mode	THD 40
CosPhi/DPF mode	Cos Phi

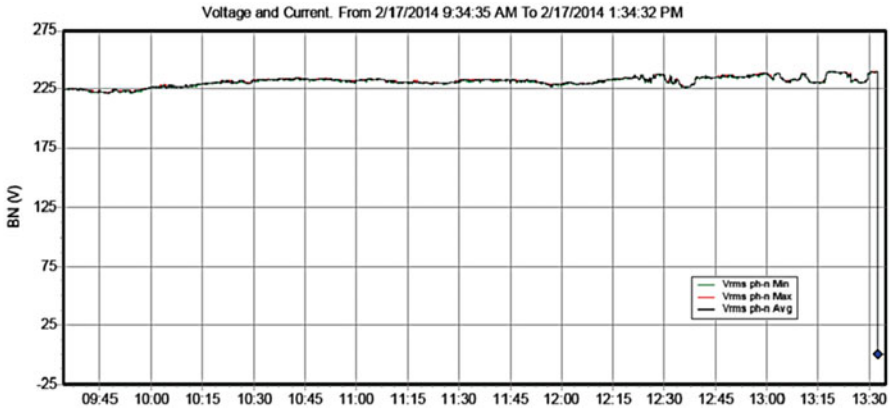
Recording Summary

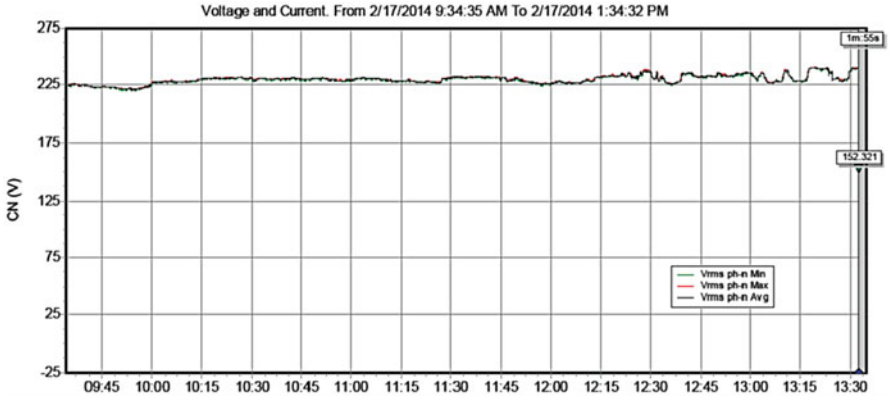
RMS recordings	4,800
DC recordings	0
Frequency recordings	4,800
Unbalance recordings	4,800
Harmonic recordings	4,800
Power harmonic recordings	0
Power recordings	4,800
Power unbalance recordings	0
Energy recordings	4,800
Energy losses recordings	0
Flicker recordings	0
Mains signaling recordings	0

Events Summary

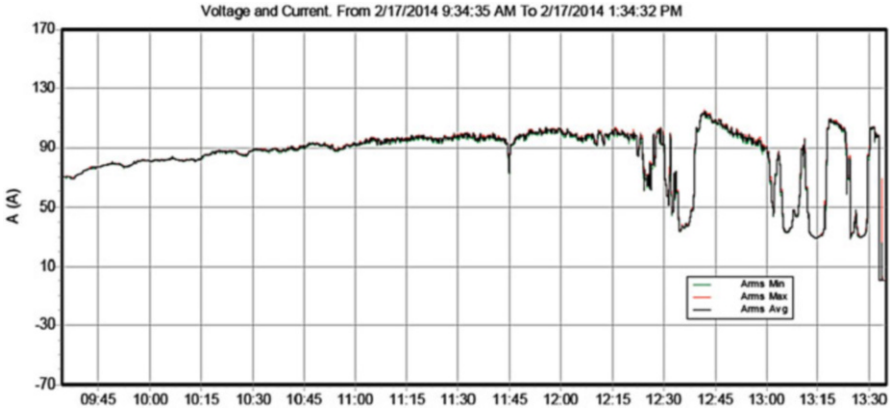
Dips	1
Swells	0
Transients	4
Interruptions	2
Voltage profiles	0
Rapid voltage changes	0
Screens	0
Waveforms	0
Intervals without measurements	0
Inrush current graphics	0
Wave events	0
RMS events	0



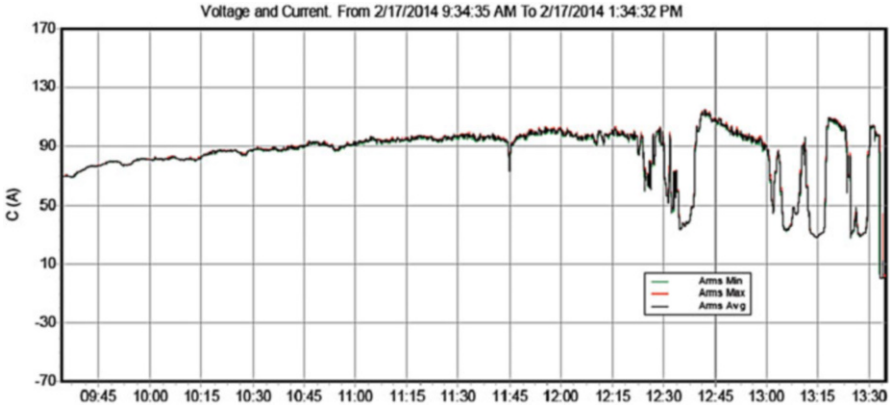


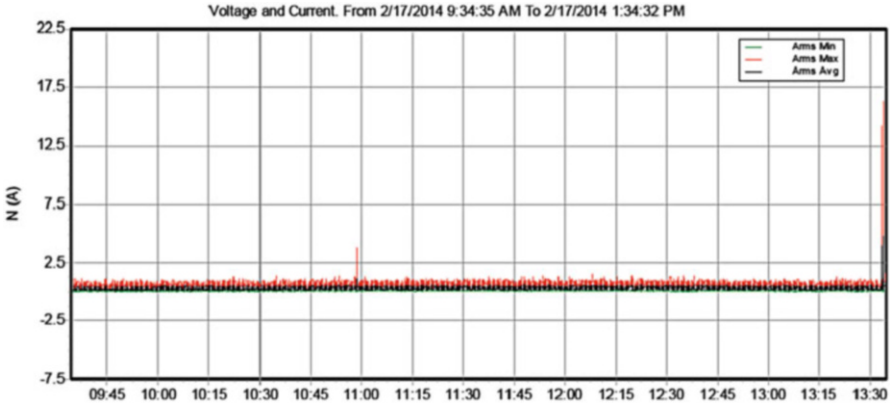

Voltage and Current. From 2/17/2014 9:34:35 AM To 2/17/2014 1:34:32 PM
CN (V)
275
225
175
125
75
25
-25
1m:55s
152.321
Vrms ph-n Min
Vrms ph-n Max
Vrms ph-n Avg
09:45 10:00 10:15 10:30 10:45 11:00 11:15 11:30 11:45 12:00 12:15 12:30 12:45 13:00 13:15 13:30

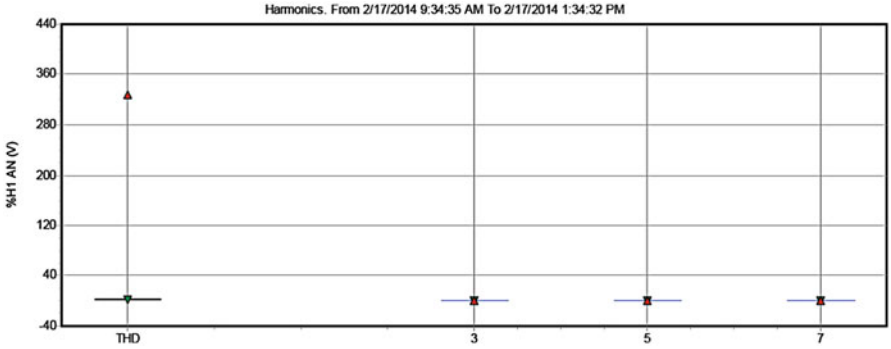

Voltage and Current. From 2/17/2014 9:34:35 AM To 2/17/2014 1:34:32 PM
NG (V)
165
135
105
75
45
15
-15
Vrms n-gnd Min
Vrms n-gnd Max
Vrms n-gnd Avg
09:45 10:00 10:15 10:30 10:45 11:00 11:15 11:30 11:45 12:00 12:15 12:30 12:45 13:00 13:15 13:30

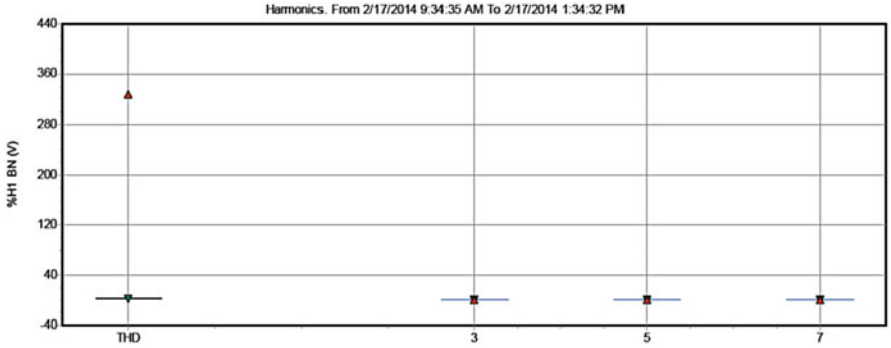

Voltage and Current. From 2/17/2014 9:34:35 AM To 2/17/2014 1:34:32 PM
A (A)
170
130
90
50
10
-30
-70
Arms Min
Arms Max
Arms Avg
09:45 10:00 10:15 10:30 10:45 11:00 11:15 11:30 11:45 12:00 12:15 12:30 12:45 13:00 13:15 13:30

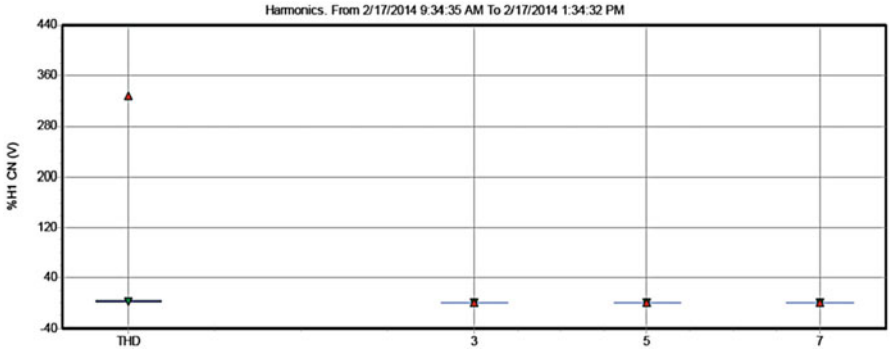

Voltage and Current. From 2/17/2014 9:34:35 AM To 2/17/2014 1:34:32 PM
B (A)
170
130
90
50
10
-30
-70
09:45
10:00
10:15
10:30
10:45
11:00
11:15
11:30
11:45
12:00
12:15
12:30
12:45
13:00
13:15
13:30
Arms Min
Arms Max
Arms Avg

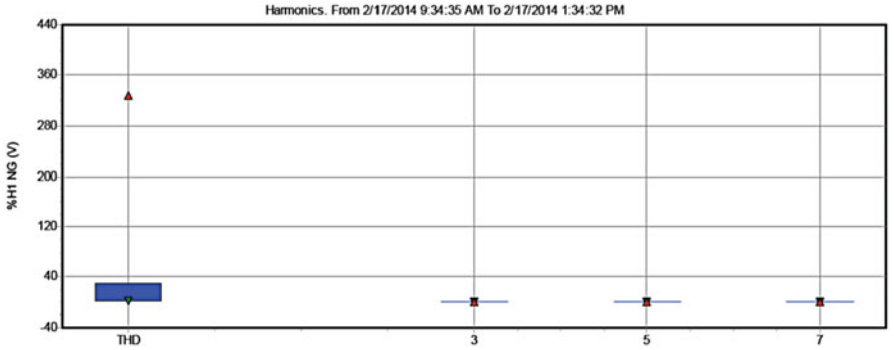

Voltage and Current. From 2/17/2014 9:34:35 AM To 2/17/2014 1:34:32 PM
C (A)
170
130
90
50
10
-30
-70
09:45
10:00
10:15
10:30
10:45
11:00
11:15
11:30
11:45
12:00
12:15
12:30
12:45
13:00
13:15
13:30
Arms Min
Arms Max
Arms Avg

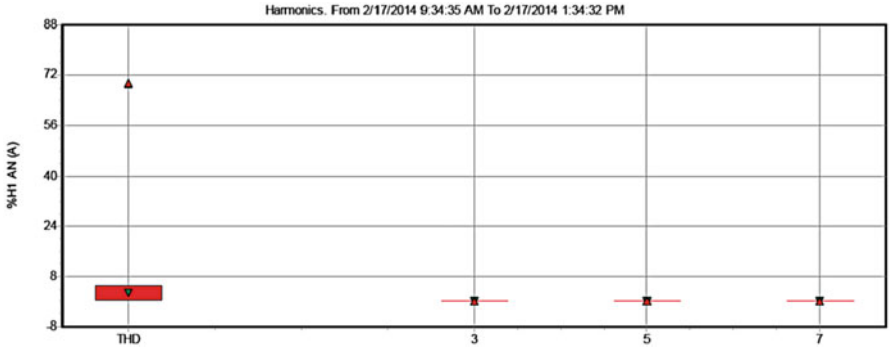

Voltage and Current. From 2/17/2014 9:34:35 AM To 2/17/2014 1:34:32 PM
N (A)
22.5
17.5
12.5
7.5
2.5
-2.5
-7.5
09:45
10:00
10:15
10:30
10:45
11:00
11:15
11:30
11:45
12:00
12:15
12:30
12:45
13:00
13:15
13:30
Arms Min
Arms Max
Arms Avg

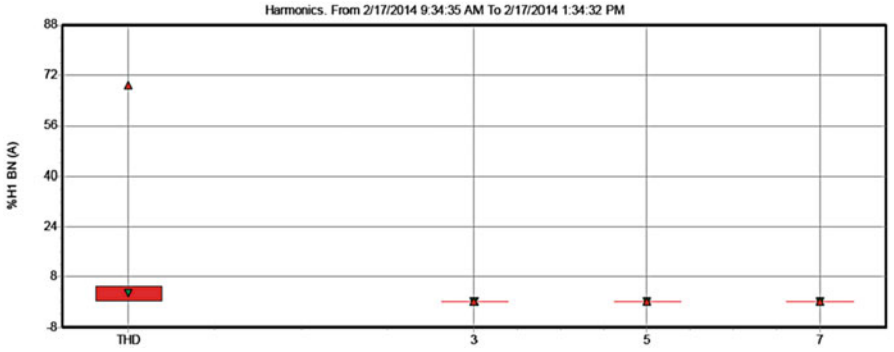

Harmonics. From 2/17/2014 9:34:35 AM To 2/17/2014 1:34:32 PM
%H1 AN (V)
440
360
280
200
120
40
-40
THD
3
5
7

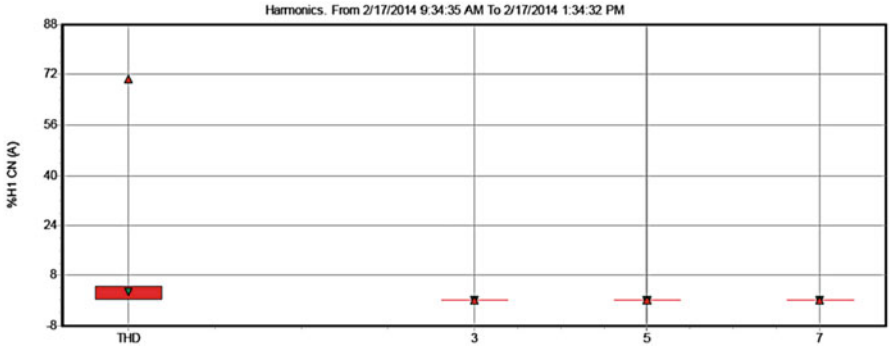

Harmonics. From 2/17/2014 9:34:35 AM To 2/17/2014 1:34:32 PM
%H1 BN (V)
440
360
280
200
120
40
-40
THD
3
5
7

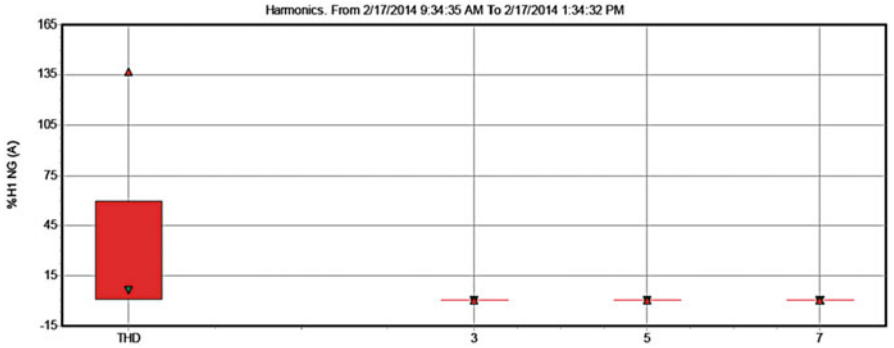

Harmonics. From 2/17/2014 9:34:35 AM To 2/17/2014 1:34:32 PM
%H1 CN (V)
440
360
280
200
120
40
-40
THD
3
5
7

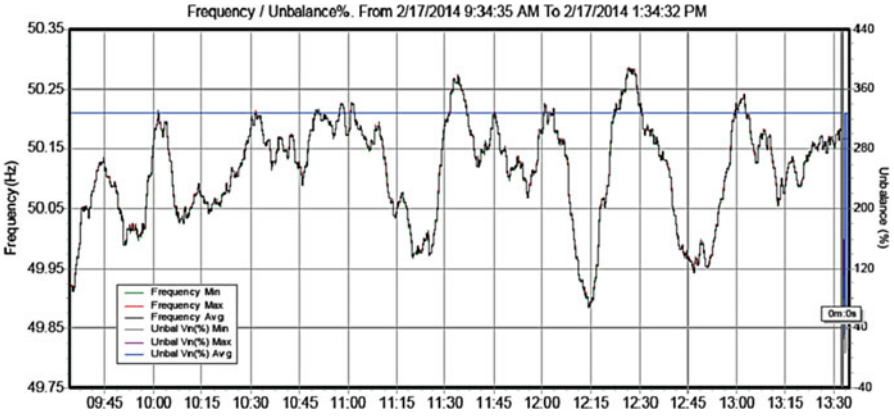

Harmonics. From 2/17/2014 9:34:35 AM To 2/17/2014 1:34:32 PM
%H1 NG (V)
440
360
280
200
120
40
-40
THD
3
5
7

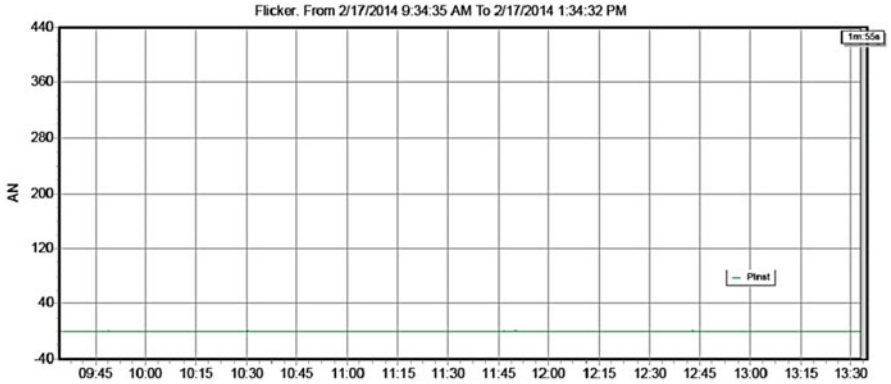

Harmonics. From 2/17/2014 9:34:35 AM To 2/17/2014 1:34:32 PM
%H1 AN (A)
88
72
56
40
24
8
-8
THD
3
5
7

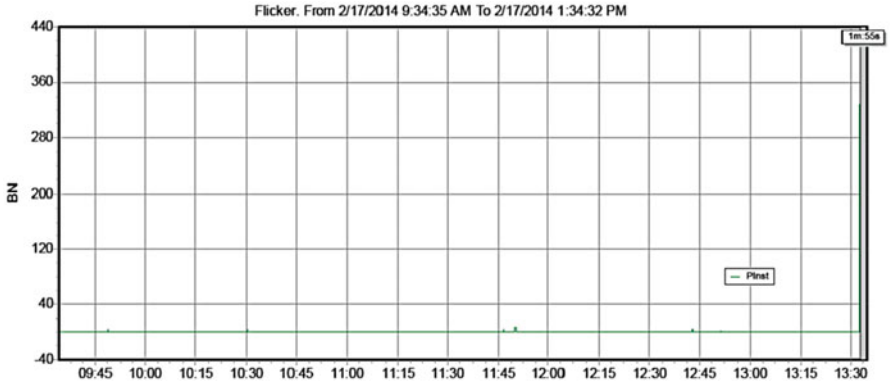

Harmonics. From 2/17/2014 9:34:35 AM To 2/17/2014 1:34:32 PM
%H1 BN (A)
88
72
56
40
24
8
-8
THD
3
5
7

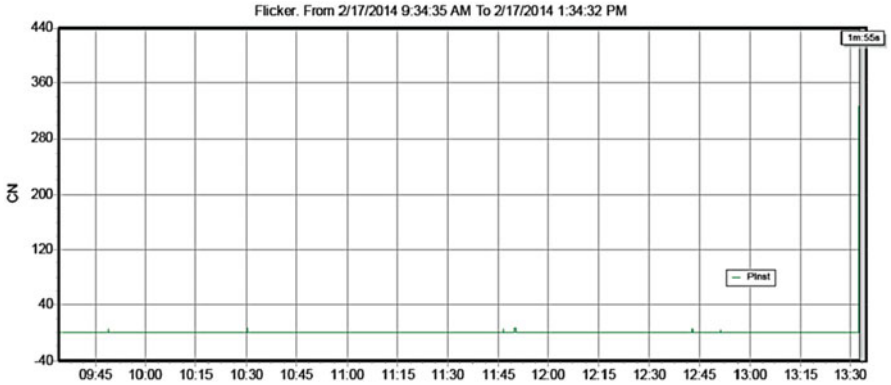

Harmonics. From 2/17/2014 9:34:35 AM To 2/17/2014 1:34:32 PM
%H1 CN (A)
88
72
56
40
24
8
-8
THD
3
5
7

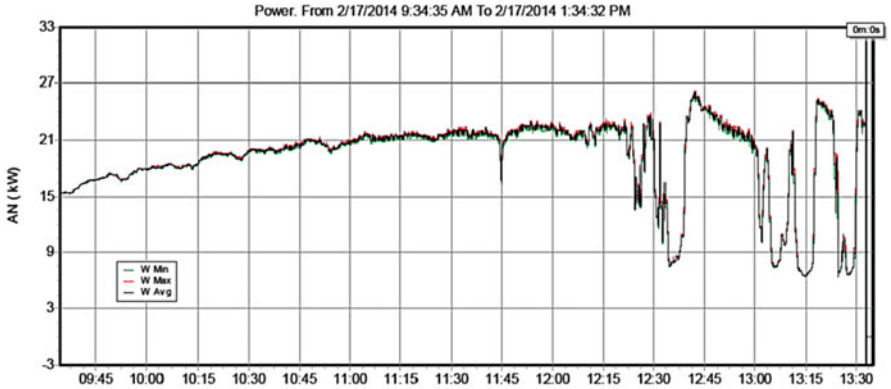

Harmonics. From 2/17/2014 9:34:35 AM To 2/17/2014 1:34:32 PM
%H1 NG (A)
165
135
105
75
45
15
-15
THD
3
5
7

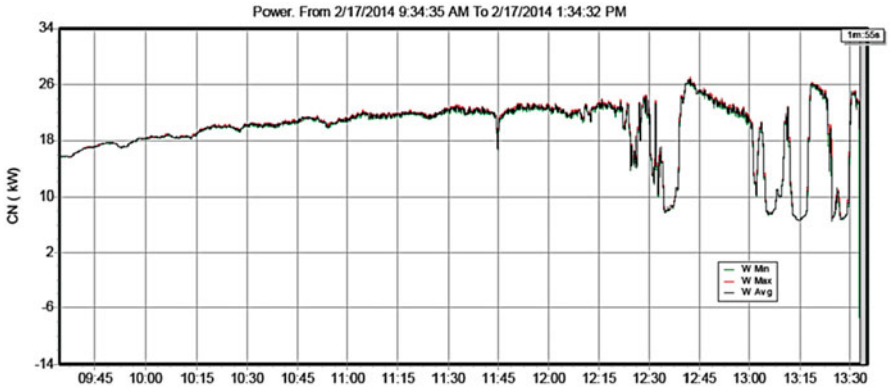

Frequency / Unbalance%. From 2/17/2014 9:34:35 AM To 2/17/2014 1:34:32 PM
Frequency (Hz)
50.35
50.25
50.15
50.05
49.95
49.85
49.75
Unbalance (%)
440
360
280
200
120
40
-40
Frequency Min
Frequency Max
Frequency Avg
Unbal Vn(%) Min
Unbal Vn(%) Max
Unbal Vn(%) Avg
09:45
10:00
10:15
10:30
10:45
11:00
11:15
11:30
11:45
12:00
12:15
12:30
12:45
13:00
13:15
13:30

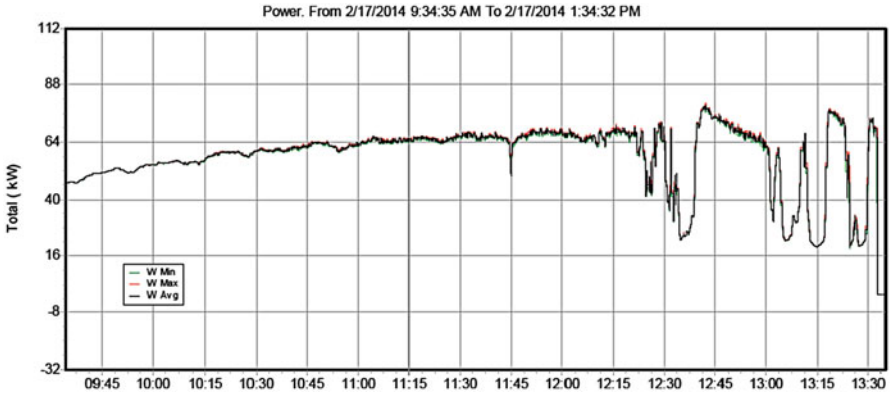

Flicker. From 2/17/2014 9:34:35 AM To 2/17/2014 1:34:32 PM
AN
440
360
280
200
120
40
-40
09:45 10:00 10:15 10:30 10:45 11:00 11:15 11:30 11:45 12:00 12:15 12:30 12:45 13:00 13:15 13:30
1m:55s
Plnst

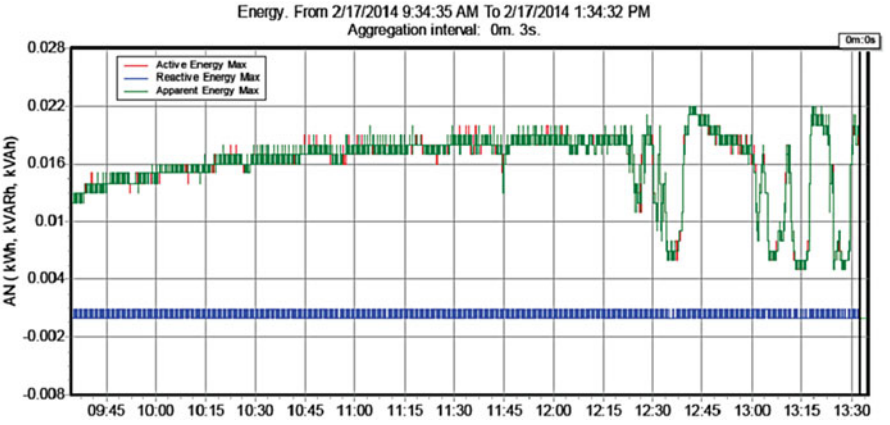

Flicker. From 2/17/2014 9:34:35 AM To 2/17/2014 1:34:32 PM
BN
440
360
280
200
120
40
-40
09:45 10:00 10:15 10:30 10:45 11:00 11:15 11:30 11:45 12:00 12:15 12:30 12:45 13:00 13:15 13:30
1m:55s
Plnst

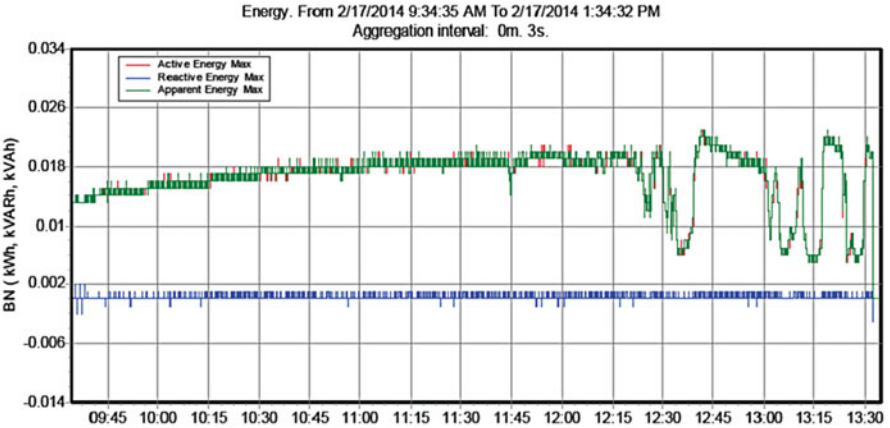

Flicker. From 2/17/2014 9:34:35 AM To 2/17/2014 1:34:32 PM
CN
440
360
280
200
120
40
-40
09:45 10:00 10:15 10:30 10:45 11:00 11:15 11:30 11:45 12:00 12:15 12:30 12:45 13:00 13:15 13:30
1m:55s
Plnst

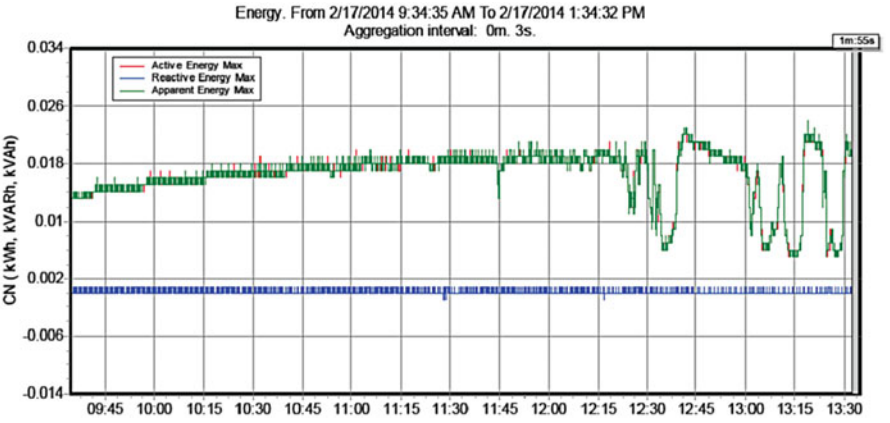

Power. From 2/17/2014 9:34:35 AM To 2/17/2014 1:34:32 PM
AN (kW)
33
27
21
15
9
3
-3
W Min
W Max
W Avg
09:45 10:00 10:15 10:30 10:45 11:00 11:15 11:30 11:45 12:00 12:15 12:30 12:45 13:00 13:15 13:30

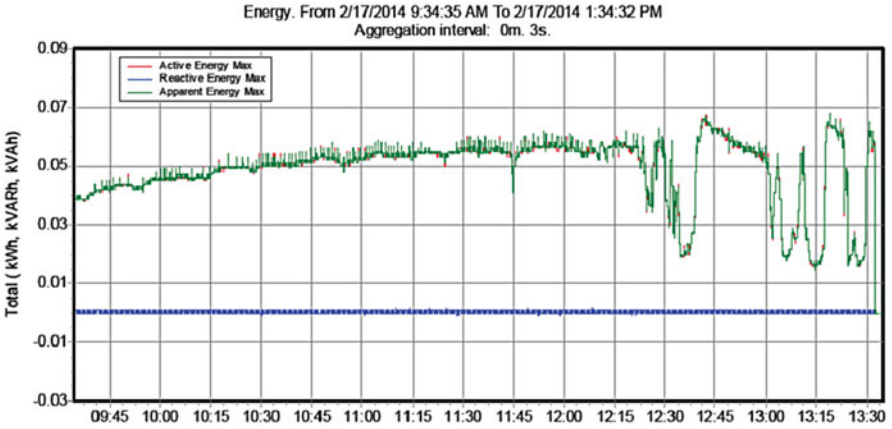

Power. From 2/17/2014 9:34:35 AM To 2/17/2014 1:34:32 PM
CN (kW)
34
26
18
10
2
-6
-14
W Min
W Max
W Avg
09:45 10:00 10:15 10:30 10:45 11:00 11:15 11:30 11:45 12:00 12:15 12:30 12:45 13:00 13:15 13:30

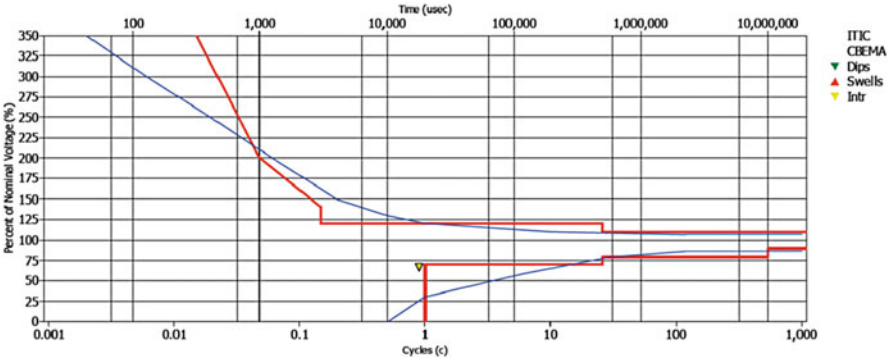

Power. From 2/17/2014 9:34:35 AM To 2/17/2014 1:34:32 PM
Total (kW)
112
88
64
40
16
-8
-32
W Min
W Max
W Avg
09:45 10:00 10:15 10:30 10:45 11:00 11:15 11:30 11:45 12:00 12:15 12:30 12:45 13:00 13:15 13:30

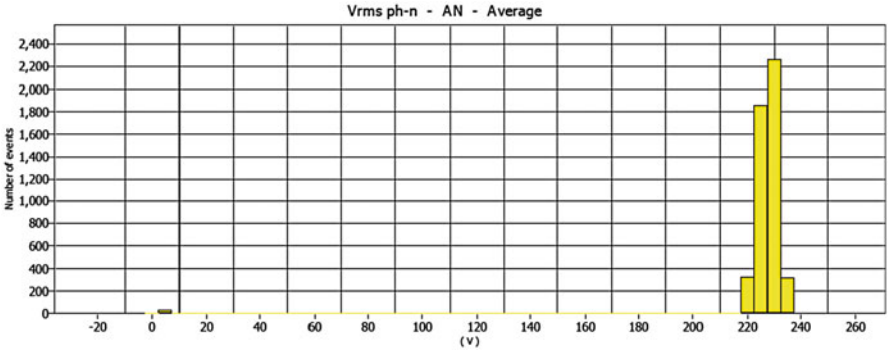

Energy. From 2/17/2014 9:34:35 AM To 2/17/2014 1:34:32 PM
Aggregation interval: 0m. 3s.
0m:0s
Active Energy Max
Reactive Energy Max
Apparent Energy Max
AN (kWh, kVARh, kVAh)
0.028
0.022
0.016
0.01
0.004
-0.002
-0.008
09:45 10:00 10:15 10:30 10:45 11:00 11:15 11:30 11:45 12:00 12:15 12:30 12:45 13:00 13:15 13:30

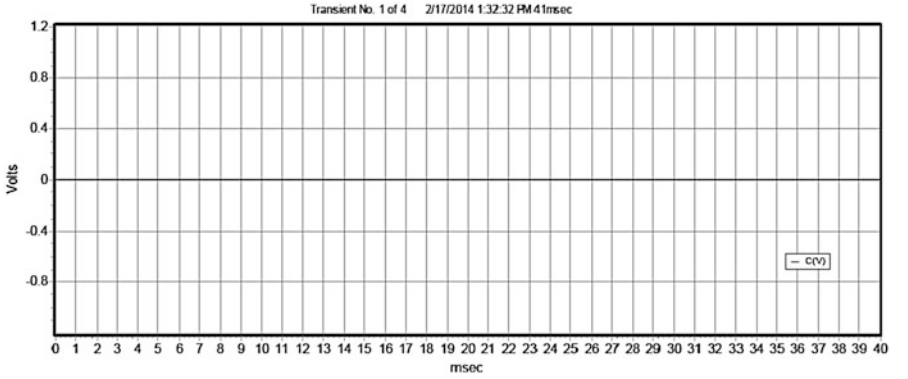

Energy. From 2/17/2014 9:34:35 AM To 2/17/2014 1:34:32 PM
Aggregation interval: 0m. 3s.
Active Energy Max
Reactive Energy Max
Apparent Energy Max
BN (kWh, kVARh, kVAh)
0.034
0.026
0.018
0.01
0.002
-0.006
-0.014
09:45 10:00 10:15 10:30 10:45 11:00 11:15 11:30 11:45 12:00 12:15 12:30 12:45 13:00 13:15 13:30

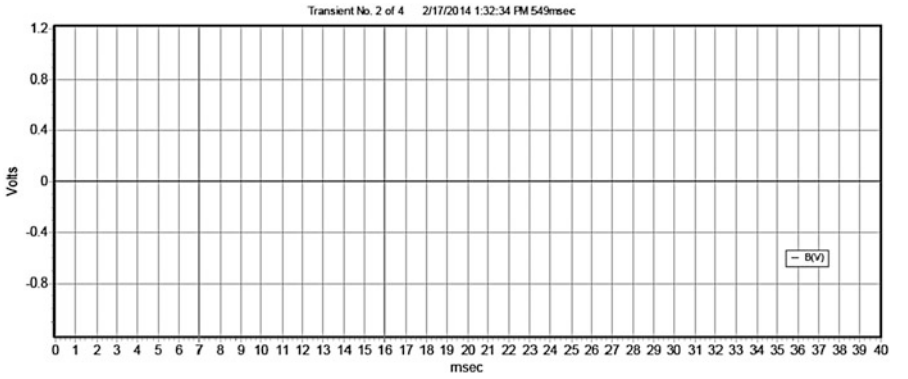

Energy. From 2/17/2014 9:34:35 AM To 2/17/2014 1:34:32 PM
Aggregation interval: 0m. 3s.
1m:55s
Active Energy Max
Reactive Energy Max
Apparent Energy Max
CN (kWh, kVARh, kVAh)
0.034
0.026
0.018
0.01
0.002
-0.006
-0.014
09:45 10:00 10:15 10:30 10:45 11:00 11:15 11:30 11:45 12:00 12:15 12:30 12:45 13:00 13:15 13:30

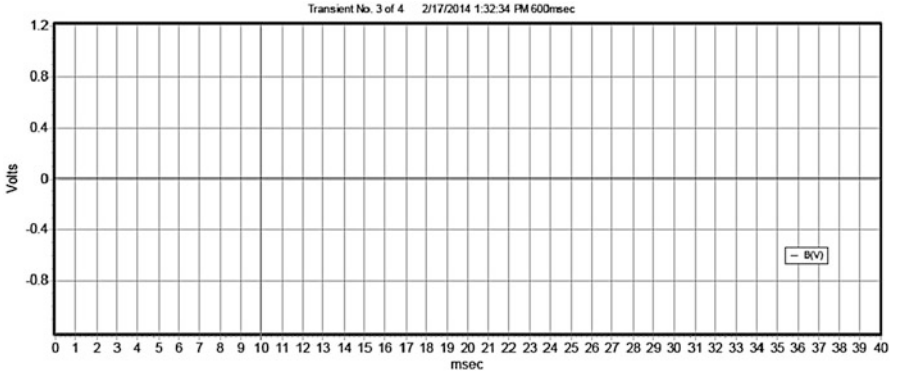

Energy. From 2/17/2014 9:34:35 AM To 2/17/2014 1:34:32 PM
Aggregation interval: 0m. 3s.
Active Energy Max
Reactive Energy Max
Apparent Energy Max
Total (kWh, kVARh, kVAh)
0.09
0.07
0.05
0.03
0.01
-0.01
-0.03
09:45 10:00 10:15 10:30 10:45 11:00 11:15 11:30 11:45 12:00 12:15 12:30 12:45 13:00 13:15 13:30

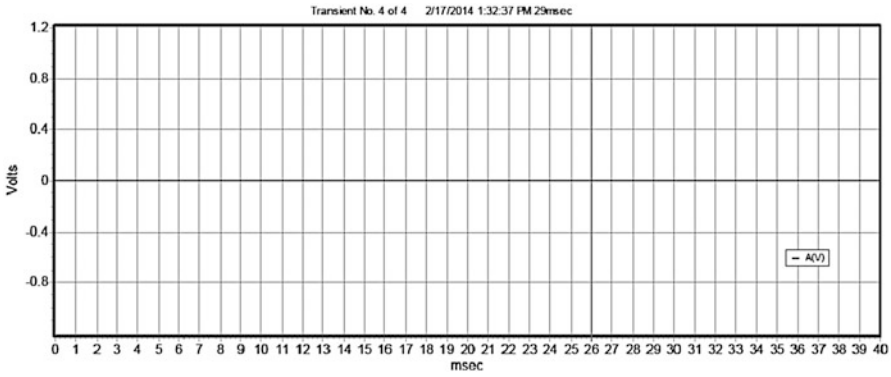

Time (usec)
100 1,000 10,000 100,000 1,000,000 10,000,000
ITIC
CBEMA
Dips
Swells
Intr
Percent of Nominal Voltage (%)
350 325 300 275 250 225 200 175 150 125 100 75 50 25 0
0.001 0.01 0.1 1 10 100 1,000
Cycles (c)


Vrms ph-n - AN - Average
Number of events
2,400 2,200 2,000 1,800 1,600 1,400 1,200 1,000 800 600 400 200 0
-20 0 20 40 60 80 100 120 140 160 180 200 220 240 260
(V)


Transient No. 1 of 4 2/17/2014 1:32:32 PM 41msec
1.2
0.8
0.4
0
-0.4
-0.8
Volts
C(V)
0 1 2 3 4 5 6 7 8 9 10 11 12 13 14 15 16 17 18 19 20 21 22 23 24 25 26 27 28 29 30 31 32 33 34 35 36 37 38 39 40
msec


Transient No. 2 of 4 2/17/2014 1:32:34 PM 549msec
1.2
0.8
0.4
0
-0.4
-0.8
Volts
B(V)
0 1 2 3 4 5 6 7 8 9 10 11 12 13 14 15 16 17 18 19 20 21 22 23 24 25 26 27 28 29 30 31 32 33 34 35 36 37 38 39 40
msec


Transient No. 3 of 4 2/17/2014 1:32:34 PM 600msec
1.2
0.8
0.4
0
-0.4
-0.8
Volts
B(V)
0 1 2 3 4 5 6 7 8 9 10 11 12 13 14 15 16 17 18 19 20 21 22 23 24 25 26 27 28 29 30 31 32 33 34 35 36 37 38 39 40
msec



Instrument Information

Model number	FLUKE 430-II
Serial number	24663010
Firmware revision	V04.00

Software Information

Power log version	4.1
FLUKE 345 DLL version	11.20.2006
FLUKE 430 DLL version	1.8.0.0
FLUKE 430-II DLL version	1.0.0.28

Measurement Summary

Measurement topology	Wye mode
Application mode	Logger
First recording	1/29/2014 10:50:01 PM
Last recording	1/30/2014 1:52:21 AM
Recording interval	0 h 0 m 10s 0 m sec
Nominal voltage	230 V
Nominal current	300 A
Nominal frequency	50 Hz
File start time	1/29/2014 10:50:01 PM
File end time	1/30/2014 1:52:21 AM

(continued)

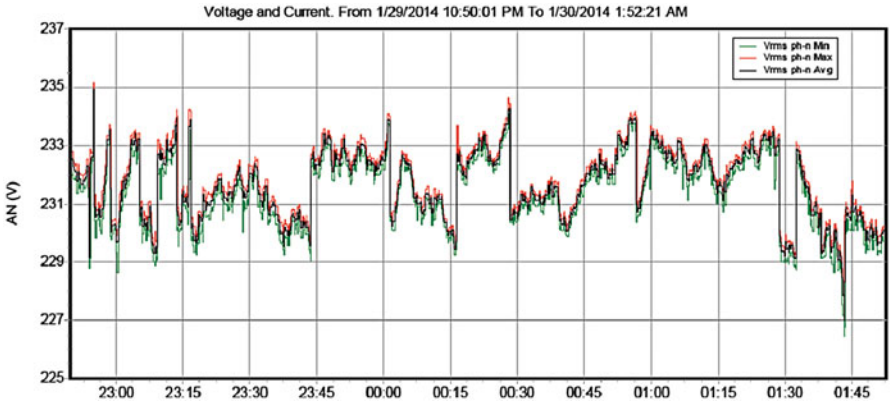
Duration	0 d 3 h 2 m 20 s 0 m sec
Number of events	0
Events downloaded	No
Number of screens	63
Screens downloaded	Yes
Power measurement method	Unified
Cable type	Copper
Harmonic scale	%H1
THD mode	THD 40
CosPhi/DPF mode	Cos Phi

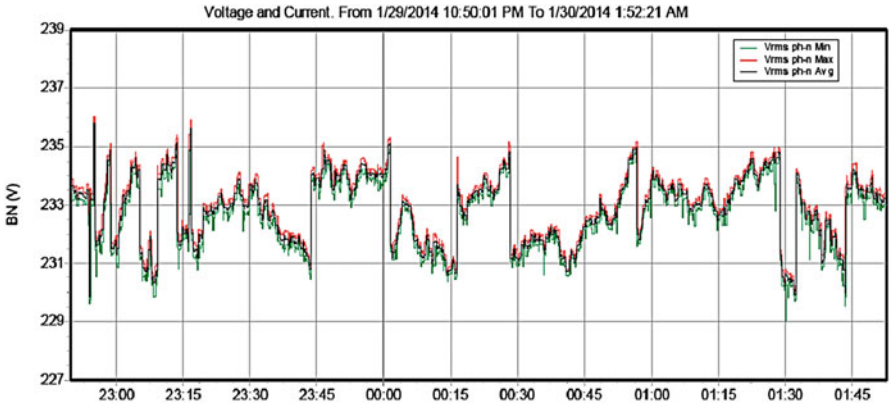
Recording Summary

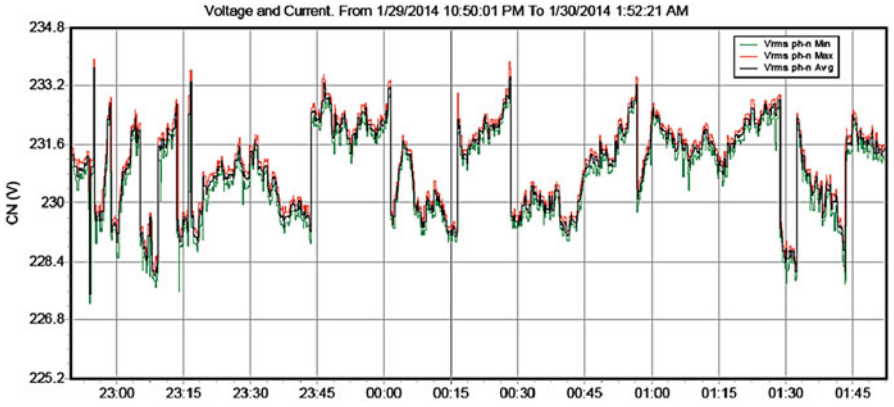
RMS recordings	1,095
DC recordings	0
Frequency recordings	1,095
Unbalance recordings	1,095
Harmonic recordings	0
Power harmonic recordings	0
Power recordings	1,095
Power unbalance recordings	0
Energy recordings	1,095
Energy losses recordings	0
Flicker recordings	0
Mains signaling recordings	0

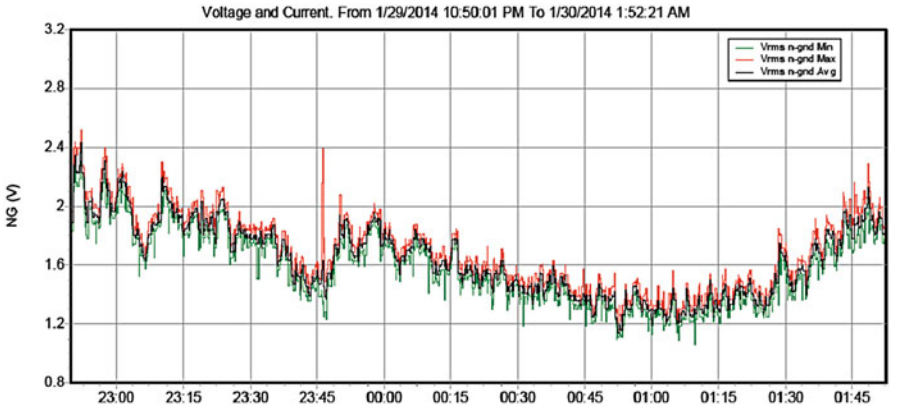
Events Summary

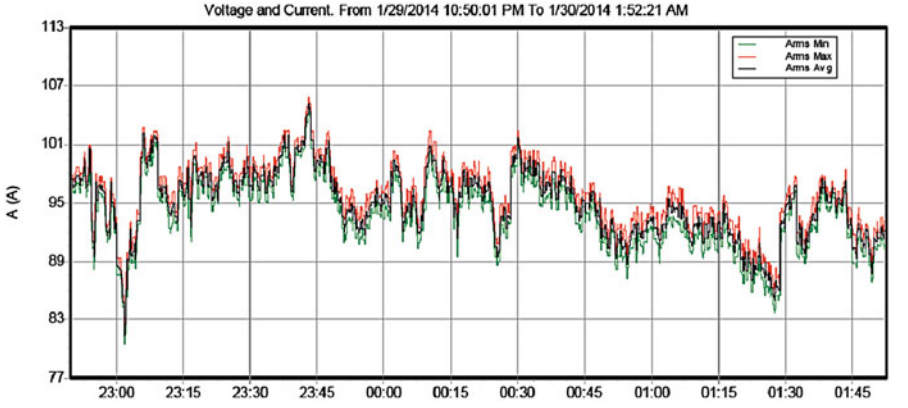
Dips	0
Swells	0
Transients	0
Interruptions	0
Voltage profiles	0
Rapid voltage changes	0
Screens	63
Waveforms	0
Intervals without measurements	0
Inrush current graphics	0
Wave events	0
RMS events	0

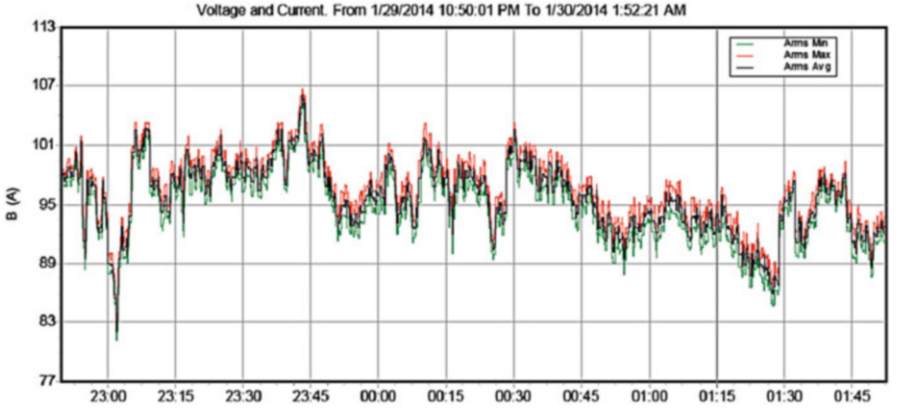

Voltage and Current. From 1/29/2014 10:50:01 PM To 1/30/2014 1:52:21 AM
Vrms ph-n Min
Vrms ph-n Max
Vrms ph-n Avg
AN (V)
237
235
233
231
229
227
225
23:00
23:15
23:30
23:45
00:00
00:15
00:30
00:45
01:00
01:15
01:30
01:45

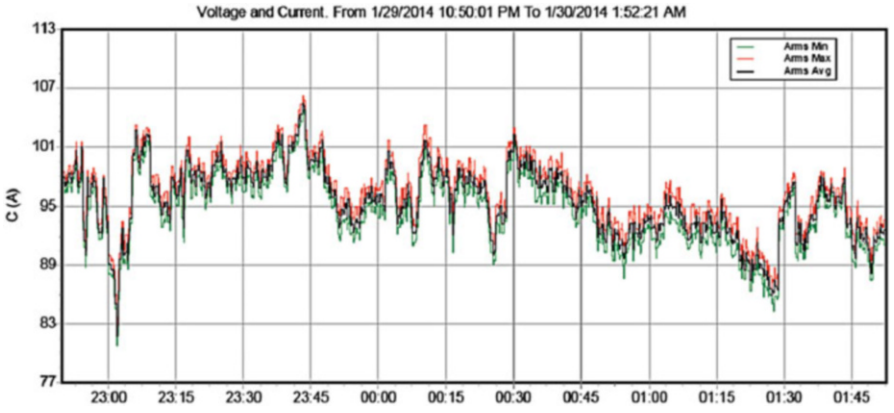

Voltage and Current. From 1/29/2014 10:50:01 PM To 1/30/2014 1:52:21 AM
Vrms ph-n Min
Vrms ph-n Max
Vrms ph-n Avg
BN (V)
239
237
235
233
231
229
227
23:00
23:15
23:30
23:45
00:00
00:15
00:30
00:45
01:00
01:15
01:30
01:45

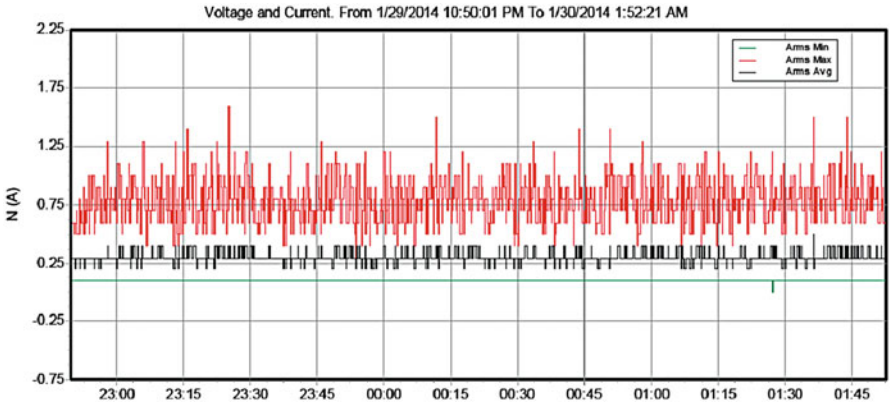

Voltage and Current. From 1/29/2014 10:50:01 PM To 1/30/2014 1:52:21 AM
Vrms ph-n Min
Vrms ph-n Max
Vrms ph-n Avg
CN (V)
234.8
233.2
231.6
230
228.4
226.8
225.2
23:00
23:15
23:30
23:45
00:00
00:15
00:30
00:45
01:00
01:15
01:30
01:45

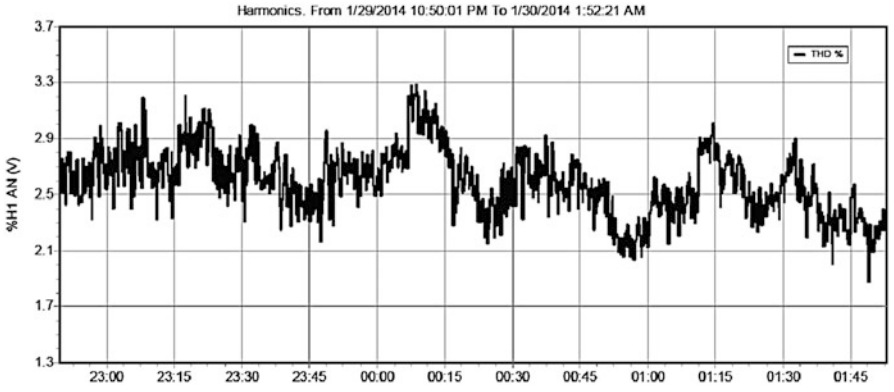

Voltage and Current. From 1/29/2014 10:50:01 PM To 1/30/2014 1:52:21 AM
Vrms n-gnd Min
Vrms n-gnd Max
Vrms n-gnd Avg
NG (V)
3.2
2.8
2.4
2
1.6
1.2
0.8
23:00
23:15
23:30
23:45
00:00
00:15
00:30
00:45
01:00
01:15
01:30
01:45

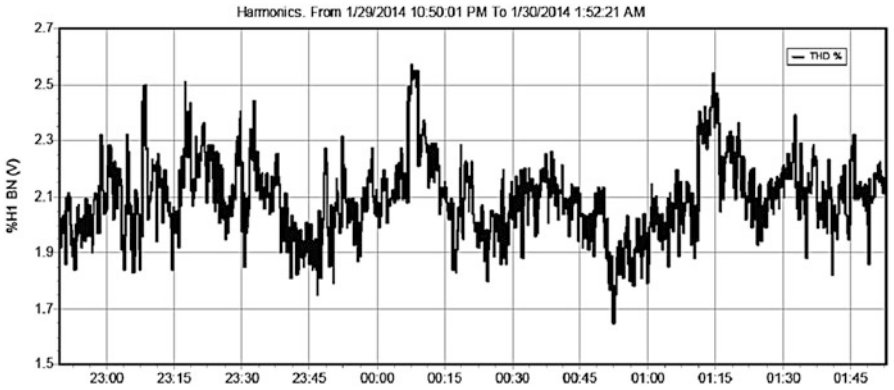

Voltage and Current. From 1/29/2014 10:50:01 PM To 1/30/2014 1:52:21 AM
Arms Min
Arms Max
Arms Avg
A (A)
113
107
101
95
89
83
77
23:00
23:15
23:30
23:45
00:00
00:15
00:30
00:45
01:00
01:15
01:30
01:45

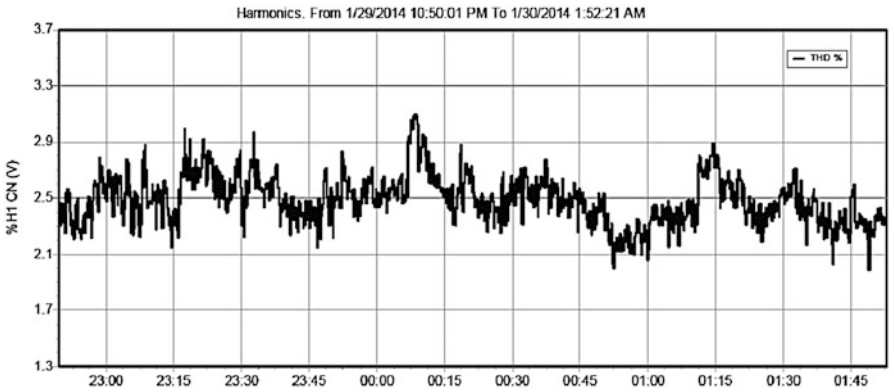

Voltage and Current. From 1/29/2014 10:50:01 PM To 1/30/2014 1:52:21 AM
Arms Min
Arms Max
Arms Avg
B (A)
113
107
101
95
89
83
77
23:00
23:15
23:30
23:45
00:00
00:15
00:30
00:45
01:00
01:15
01:30
01:45

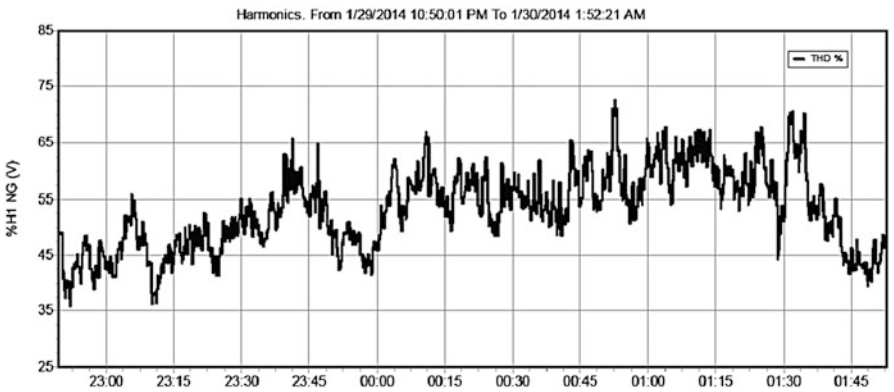

Voltage and Current. From 1/29/2014 10:50:01 PM To 1/30/2014 1:52:21 AM
Arms Min
Arms Max
Arms Avg
C (A)
113
107
101
95
89
83
77
23:00
23:15
23:30
23:45
00:00
00:15
00:30
00:45
01:00
01:15
01:30
01:45

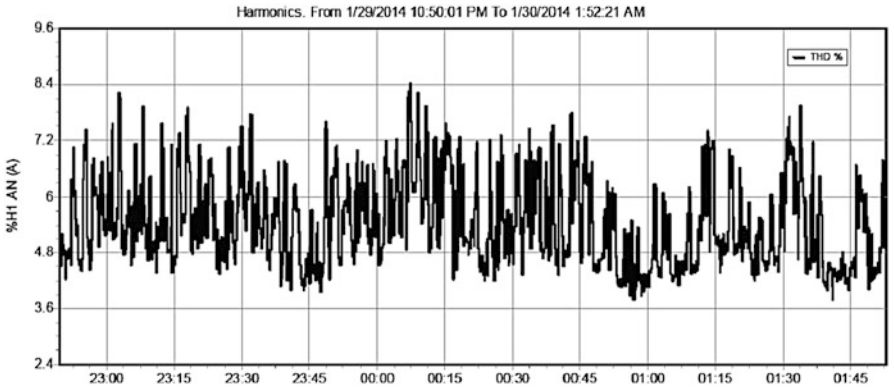

Voltage and Current. From 1/29/2014 10:50:01 PM To 1/30/2014 1:52:21 AM
Arms Min
Arms Max
Arms Avg
N (A)
2.25
1.75
1.25
0.75
0.25
-0.25
-0.75
23:00
23:15
23:30
23:45
00:00
00:15
00:30
00:45
01:00
01:15
01:30
01:45

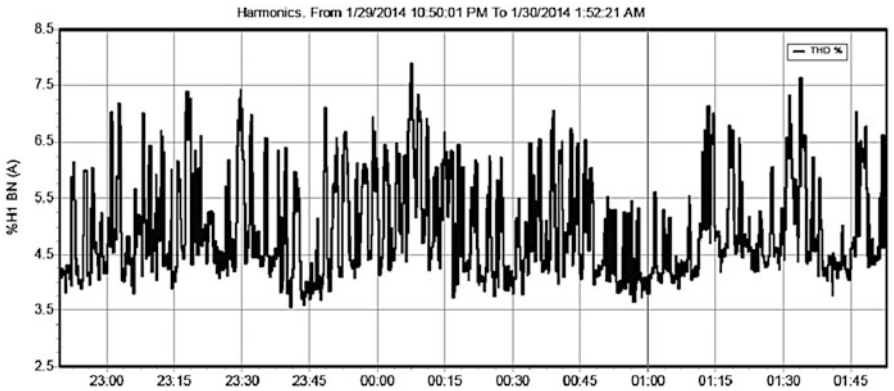

Harmonics. From 1/29/2014 10:50:01 PM To 1/30/2014 1:52:21 AM
THD %
%H1 AN (V)
3.7
3.3
2.9
2.5
2.1
1.7
1.3
23:00
23:15
23:30
23:45
00:00
00:15
00:30
00:45
01:00
01:15
01:30
01:45

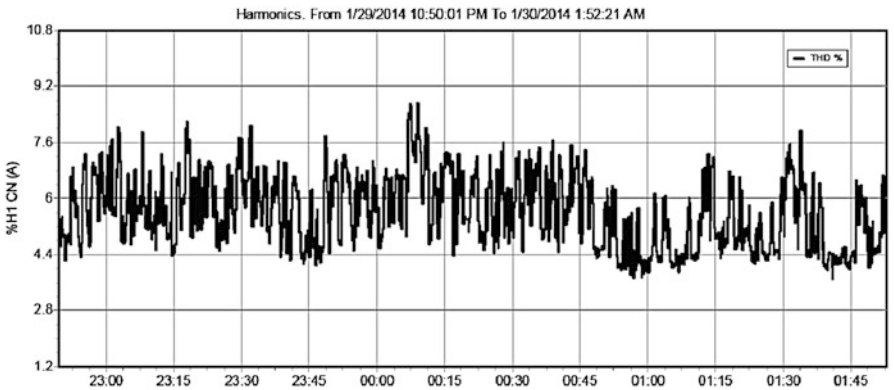

Harmonics. From 1/29/2014 10:50:01 PM To 1/30/2014 1:52:21 AM
THD %
%H1 BN (V)
2.7
2.5
2.3
2.1
1.9
1.7
1.5
23:00
23:15
23:30
23:45
00:00
00:15
00:30
00:45
01:00
01:15
01:30
01:45

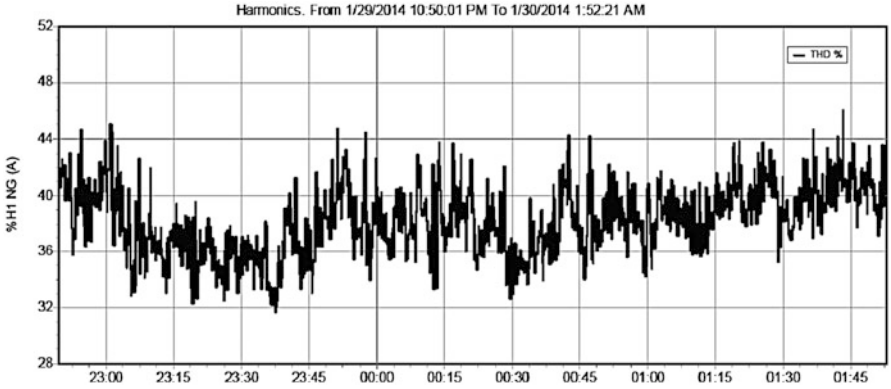

Harmonics. From 1/29/2014 10:50:01 PM To 1/30/2014 1:52:21 AM
THD %
%H1 CN (V)
3.7
3.3
2.9
2.5
2.1
1.7
1.3
23:00
23:15
23:30
23:45
00:00
00:15
00:30
00:45
01:00
01:15
01:30
01:45

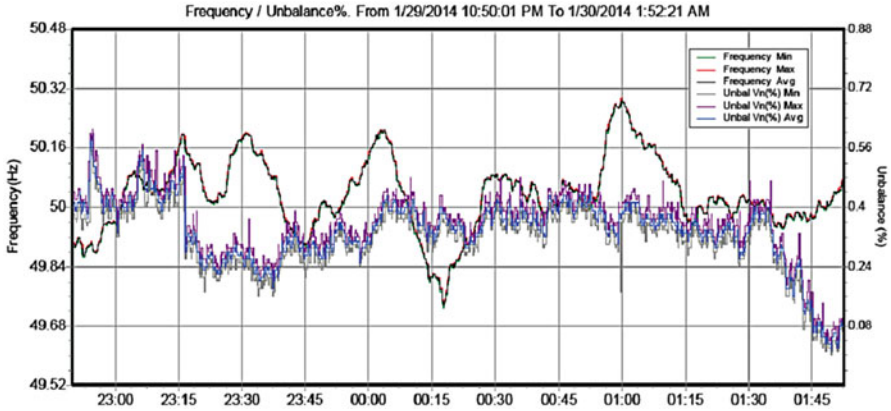

Harmonics. From 1/29/2014 10:50:01 PM To 1/30/2014 1:52:21 AM
THD %
%H1 NG (V)
85
75
65
55
45
35
25
23:00
23:15
23:30
23:45
00:00
00:15
00:30
00:45
01:00
01:15
01:30
01:45

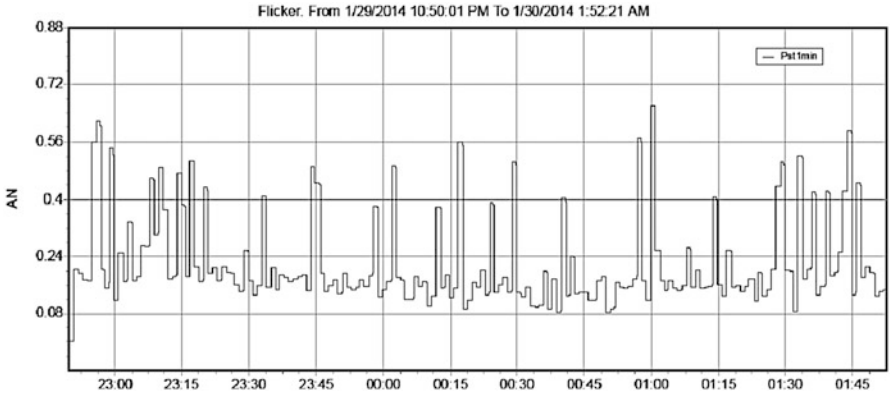

Harmonics. From 1/29/2014 10:50:01 PM To 1/30/2014 1:52:21 AM
THD %
%H1 AN (A)
9.6
8.4
7.2
6
4.8
3.6
2.4
23:00
23:15
23:30
23:45
00:00
00:15
00:30
00:45
01:00
01:15
01:30
01:45

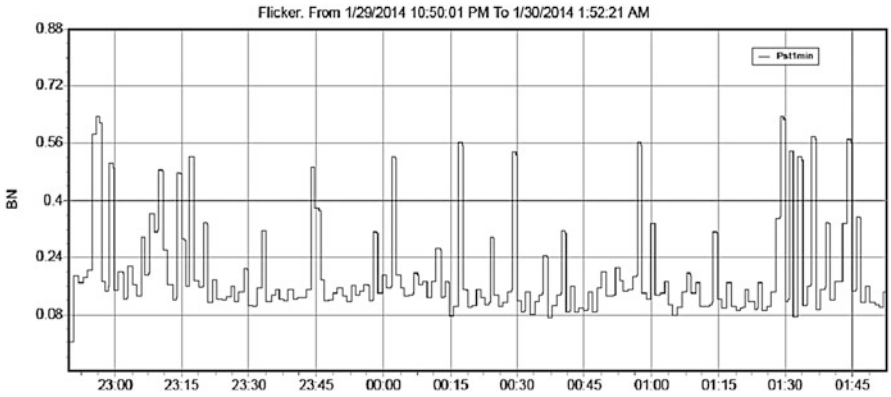

Harmonics. From 1/29/2014 10:50:01 PM To 1/30/2014 1:52:21 AM
THD %
%H1 BN (A)
8.5
7.5
6.5
5.5
4.5
3.5
2.5
23:00
23:15
23:30
23:45
00:00
00:15
00:30
00:45
01:00
01:15
01:30
01:45

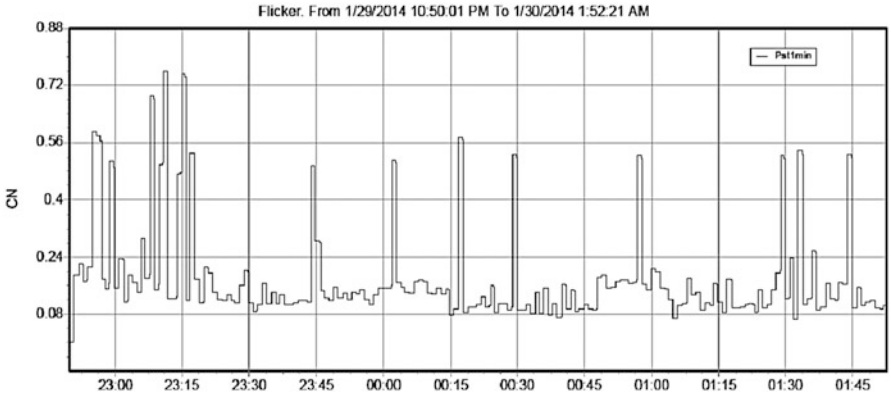

Harmonics. From 1/29/2014 10:50:01 PM To 1/30/2014 1:52:21 AM
THD %
%H1 CN (A)
10.8
9.2
7.6
6
4.4
2.8
1.2
23:00
23:15
23:30
23:45
00:00
00:15
00:30
00:45
01:00
01:15
01:30
01:45

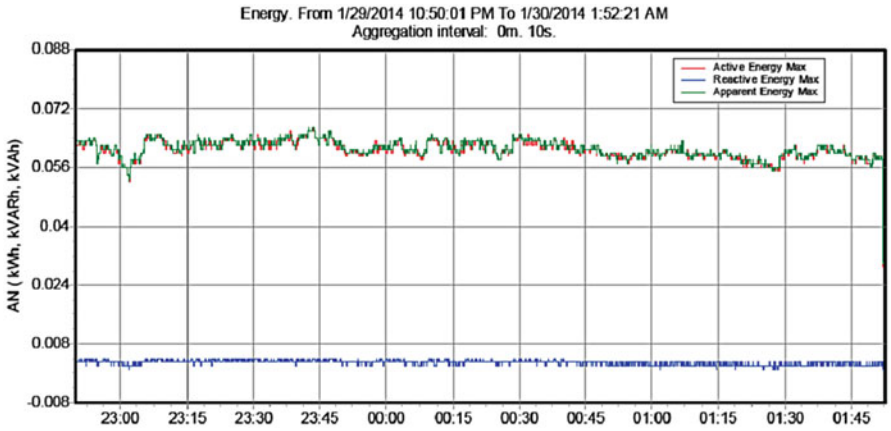

Harmonics. From 1/29/2014 10:50:01 PM To 1/30/2014 1:52:21 AM
THD %
%H1 NG (A)
52
48
44
40
36
32
28
23:00
23:15
23:30
23:45
00:00
00:15
00:30
00:45
01:00
01:15
01:30
01:45

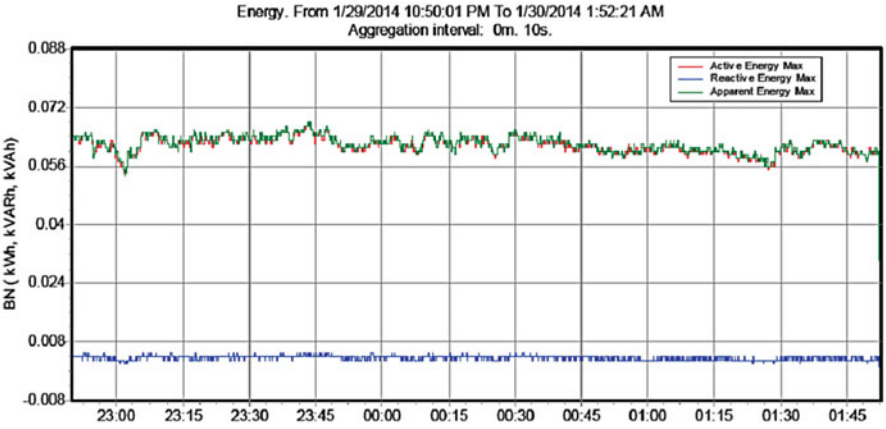

Frequency / Unbalance%. From 1/29/2014 10:50:01 PM To 1/30/2014 1:52:21 AM
Frequency Min
Frequency Max
Frequency Avg
Unbal Vn(%) Min
Unbal Vn(%) Max
Unbal Vn(%) Avg
Frequency(Hz)
Unbalance (%)
50.48
50.32
50.16
50
49.84
49.68
49.52
0.88
0.72
0.56
0.4
0.24
0.08
23:00
23:15
23:30
23:45
00:00
00:15
00:30
00:45
01:00
01:15
01:30
01:45

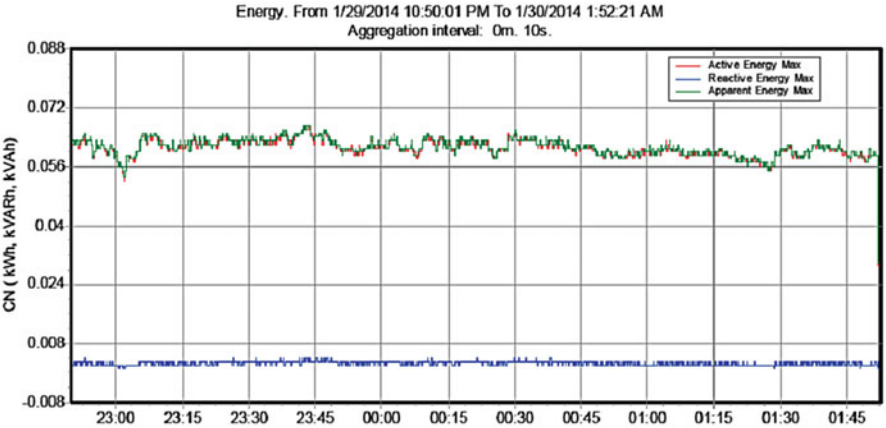

Flicker. From 1/29/2014 10:50:01 PM To 1/30/2014 1:52:21 AM
Pst1min
AN
0.88
0.72
0.56
0.4
0.24
0.08
23:00
23:15
23:30
23:45
00:00
00:15
00:30
00:45
01:00
01:15
01:30
01:45

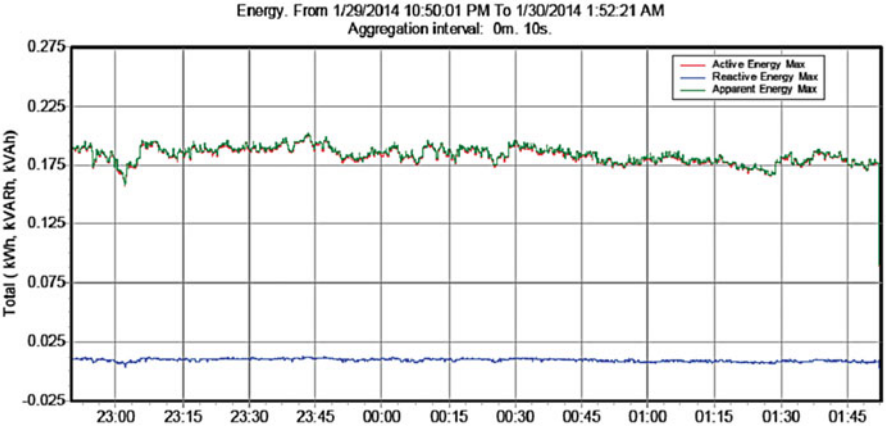

Flicker. From 1/29/2014 10:50:01 PM To 1/30/2014 1:52:21 AM
Pst1min
BN
0.88
0.72
0.56
0.4
0.24
0.08
23:00
23:15
23:30
23:45
00:00
00:15
00:30
00:45
01:00
01:15
01:30
01:45

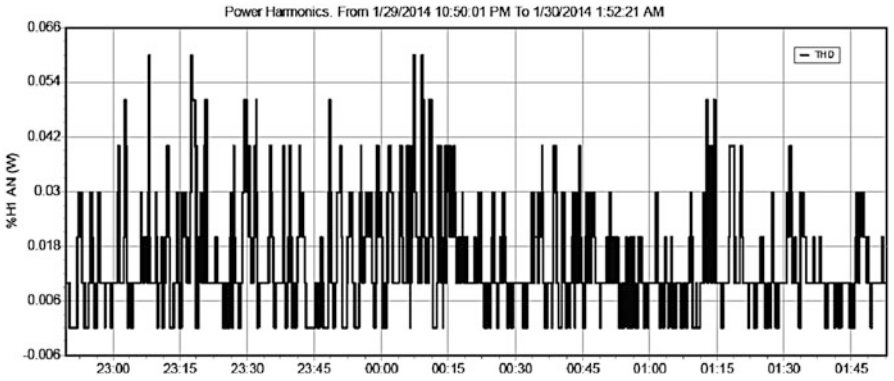

Flicker. From 1/29/2014 10:50:01 PM To 1/30/2014 1:52:21 AM
Pst1min
CN
0.88
0.72
0.56
0.4
0.24
0.08
23:00
23:15
23:30
23:45
00:00
00:15
00:30
00:45
01:00
01:15
01:30
01:45

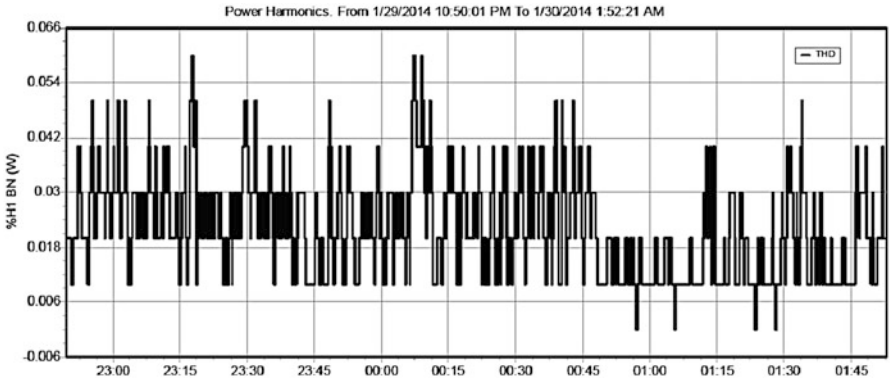

Energy. From 1/29/2014 10:50:01 PM To 1/30/2014 1:52:21 AM
Aggregation interval: 0m. 10s.
Active Energy Max
Reactive Energy Max
Apparent Energy Max
AN (kWh, kVARh, kVAh)
0.088
0.072
0.056
0.04
0.024
0.008
-0.008
23:00
23:15
23:30
23:45
00:00
00:15
00:30
00:45
01:00
01:15
01:30
01:45

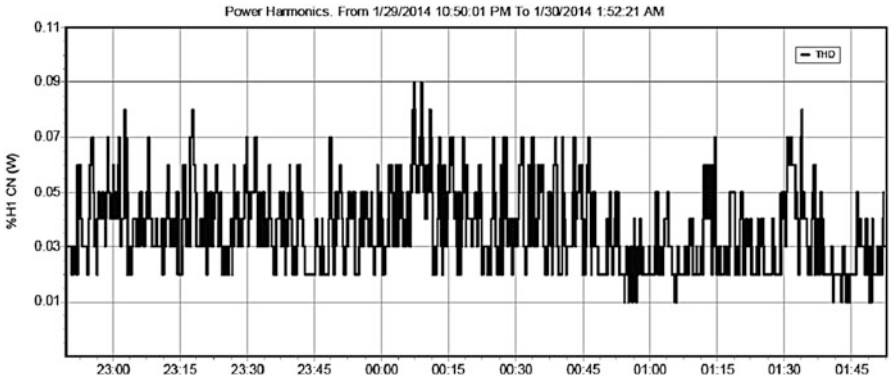

Energy. From 1/29/2014 10:50:01 PM To 1/30/2014 1:52:21 AM
Aggregation interval: 0m. 10s.
Active Energy Max
Reactive Energy Max
Apparent Energy Max
BN (kWh, kVARh, kVAh)
0.088
0.072
0.056
0.04
0.024
0.008
-0.008
23:00
23:15
23:30
23:45
00:00
00:15
00:30
00:45
01:00
01:15
01:30
01:45

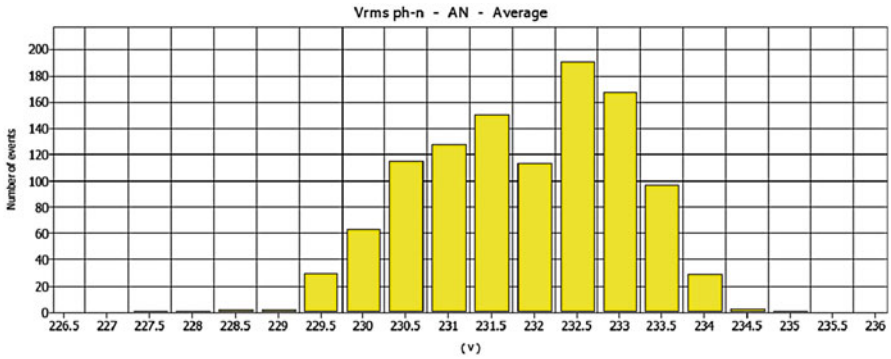

Energy. From 1/29/2014 10:50:01 PM To 1/30/2014 1:52:21 AM
Aggregation interval: 0m. 10s.
Active Energy Max
Reactive Energy Max
Apparent Energy Max
CN (kWh, kVARh, kVAh)
0.088
0.072
0.056
0.04
0.024
0.008
-0.008
23:00
23:15
23:30
23:45
00:00
00:15
00:30
00:45
01:00
01:15
01:30
01:45


Energy. From 1/29/2014 10:50:01 PM To 1/30/2014 1:52:21 AM
Aggregation interval: 0m. 10s.
Active Energy Max
Reactive Energy Max
Apparent Energy Max
Total (kWh, kVARh, kVAh)
0.275
0.225
0.175
0.125
0.075
0.025
-0.025
23:00
23:15
23:30
23:45
00:00
00:15
00:30
00:45
01:00
01:15
01:30
01:45


Power Harmonics. From 1/29/2014 10:50:01 PM To 1/30/2014 1:52:21 AM
THD
%H1 AN (W)
0.066
0.054
0.042
0.03
0.018
0.006
-0.006
23:00
23:15
23:30
23:45
00:00
00:15
00:30
00:45
01:00
01:15
01:30
01:45


Power Harmonics. From 1/29/2014 10:50:01 PM To 1/30/2014 1:52:21 AM
THD
%H1 BN (W)
0.066
0.054
0.042
0.03
0.018
0.006
-0.006
23:00
23:15
23:30
23:45
00:00
00:15
00:30
00:45
01:00
01:15
01:30
01:45


Power Harmonics. From 1/29/2014 10:50:01 PM To 1/30/2014 1:52:21 AM
THD
%H1 CN (W)
0.11
0.09
0.07
0.05
0.03
0.01
23:00
23:15
23:30
23:45
00:00
00:15
00:30
00:45
01:00
01:15
01:30
01:45



Instrument Information

Model number	FLUKE 430-II
Serial number	24663010
Firmware revision	V04.01

Software Information

Power log version	4.1
FLUKE 345 DLL version	11.20.2006
FLUKE 430 DLL version	1.8.0.0
FLUKE 430-II DLL version	1.0.0.28

Measurement Summary

Measurement topology	Wye mode
Application mode	Logger
First recording	2/5/2014 8:56:32 AM
Last recording	2/5/2014 9:00:52 AM
Recording interval	0 h 0 m 10 s 0 msec
Nominal voltage	230 V
Nominal current	300 A
Nominal frequency	50 Hz
File start time	2/5/2014 8:56:32 AM
File end time	2/5/2014 9:00:52 AM
Duration	0 d 0 h 4 m 20 s 0 msec
Number of events	0

(continued)

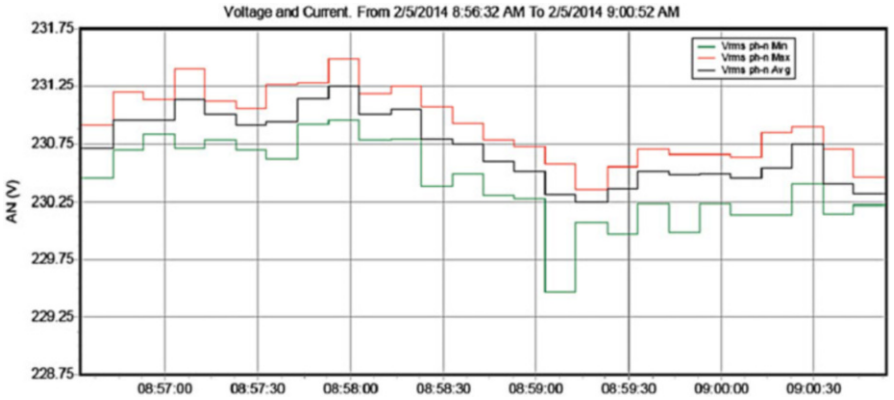
Events downloaded	No
Number of screens	100
Screens downloaded	No
Power measurement method	Unified
Cable type	Copper
Harmonic scale	%H1
THD mode	THD 40
CosPhi/DPF mode	Cos Phi

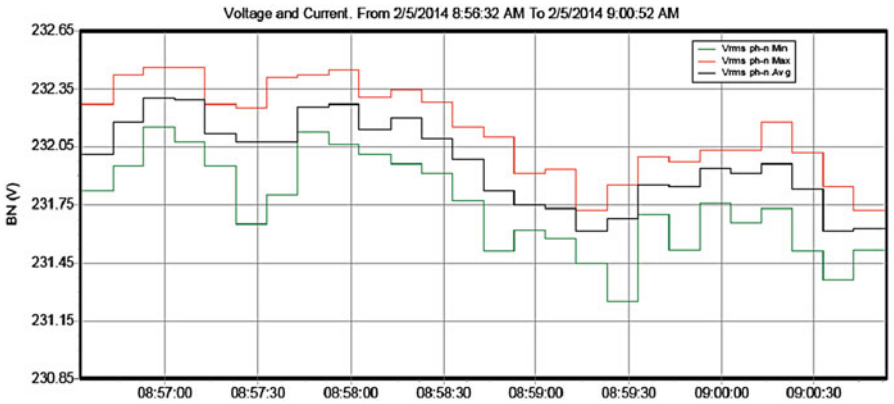
Recording Summary

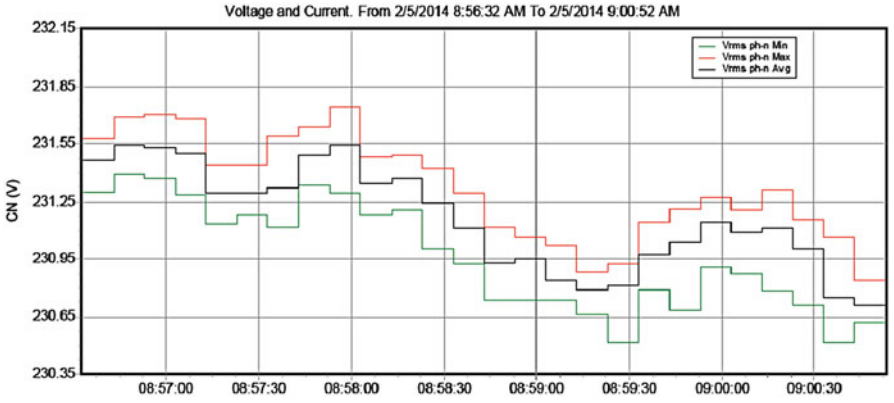
RMS recordings	27
DC recordings	0
Frequency recordings	27
Unbalance recordings	27
Harmonic recordings	0
Power harmonic recordings	0
Power recordings	0
Power unbalance recordings	0
Energy recordings	0
Energy losses recordings	0
Flicker recordings	0
Mains signaling recordings	0

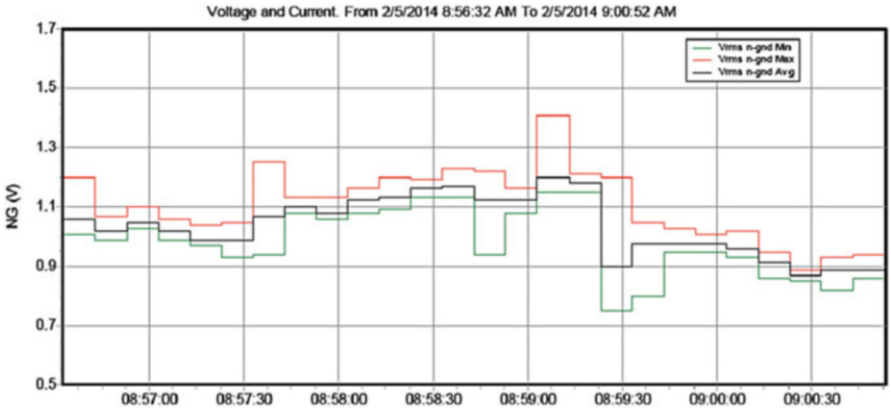
Events Summary

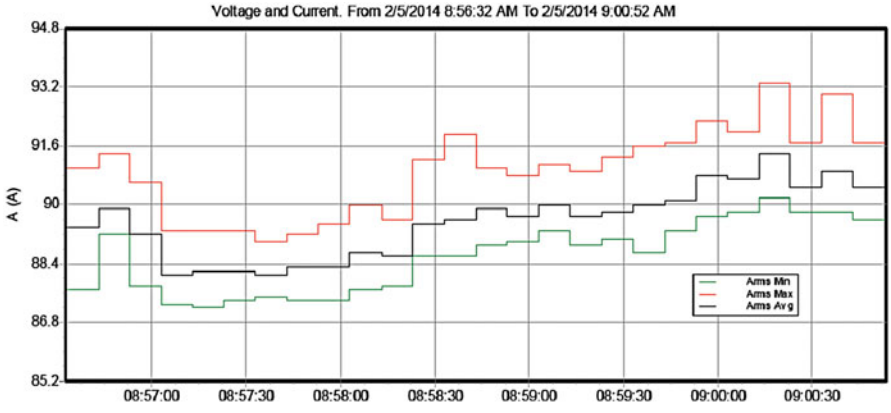
Dips	0
Swells	0
Transients	0
Interruptions	0
Voltage profiles	0
Rapid voltage changes	0
Screens	0
Waveforms	0
Intervals without measurements	0
Inrush current graphics	0
Wave events	0
RMS events	0

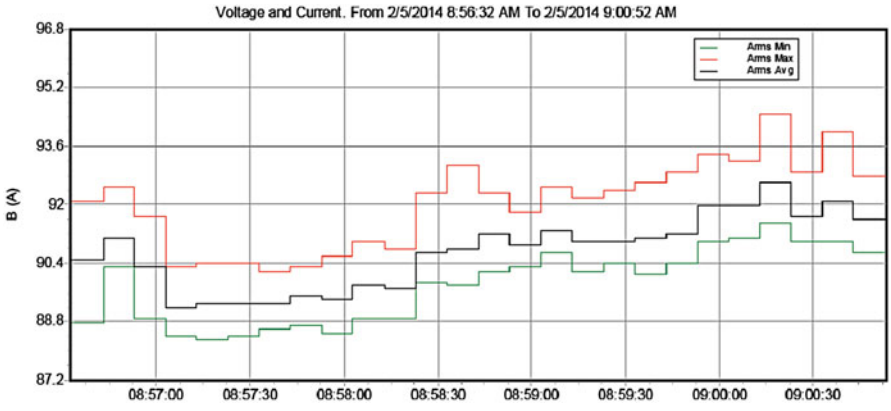

Voltage and Current. From 2/5/2014 8:56:32 AM To 2/5/2014 9:00:52 AM
Vrms ph-n Min
Vrms ph-n Max
Vrms ph-n Avg
AN (V)
231.75
231.25
230.75
230.25
229.75
229.25
228.75
08:57:00
08:57:30
08:58:00
08:58:30
08:59:00
08:59:30
09:00:00
09:00:30

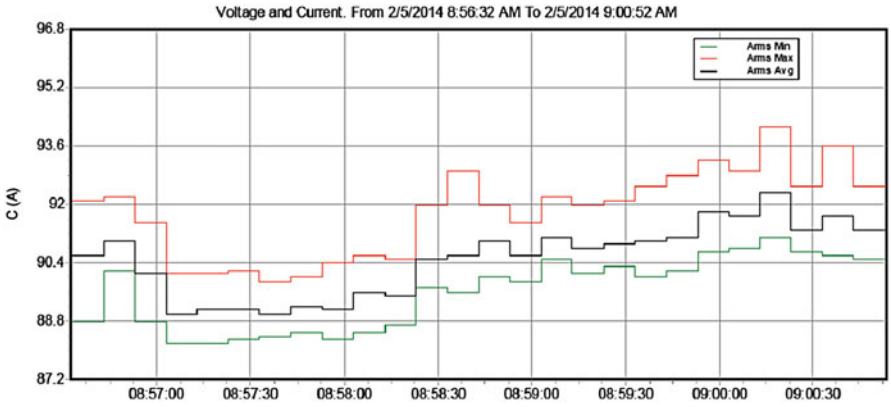

Voltage and Current. From 2/5/2014 8:56:32 AM To 2/5/2014 9:00:52 AM
Vrms ph-n Min
Vrms ph-n Max
Vrms ph-n Avg
BN (V)
232.65
232.35
232.05
231.75
231.45
231.15
230.85
08:57:00
08:57:30
08:58:00
08:58:30
08:59:00
08:59:30
09:00:00
09:00:30

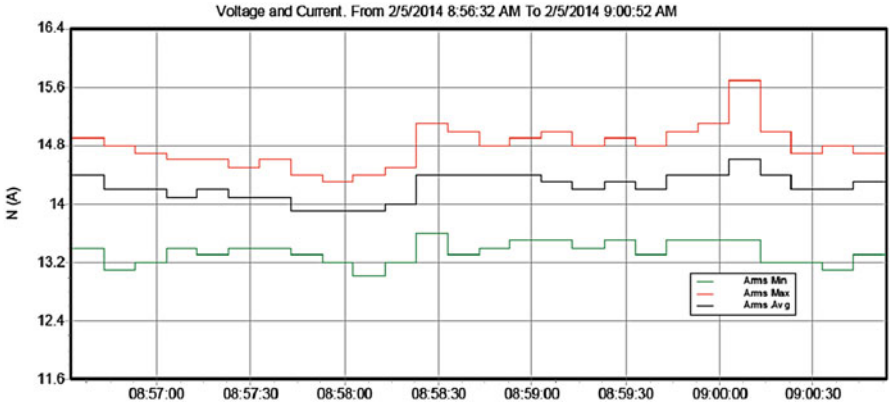

Voltage and Current. From 2/5/2014 8:56:32 AM To 2/5/2014 9:00:52 AM
Vrms ph-n Min
Vrms ph-n Max
Vrms ph-n Avg
CN (V)
232.15
231.85
231.55
231.25
230.95
230.65
230.35
08:57:00
08:57:30
08:58:00
08:58:30
08:59:00
08:59:30
09:00:00
09:00:30

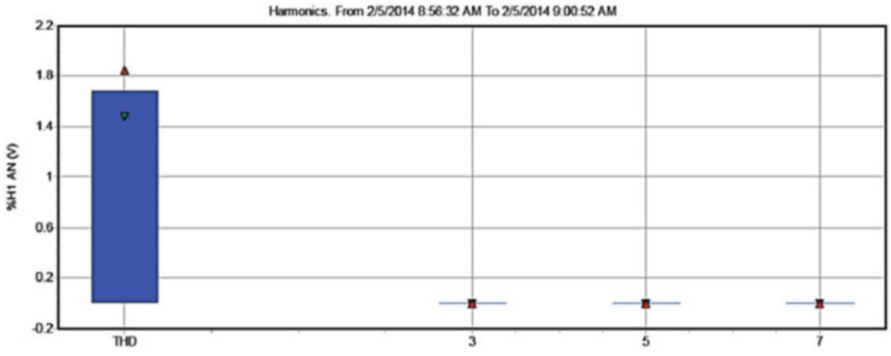

Voltage and Current. From 2/5/2014 8:56:32 AM To 2/5/2014 9:00:52 AM
Vrms n-gnd Min
Vrms n-gnd Max
Vrms n-gnd Avg
NG (V)
1.7
1.5
1.3
1.1
0.9
0.7
0.5
08:57:00
08:57:30
08:58:00
08:58:30
08:59:00
08:59:30
09:00:00
09:00:30

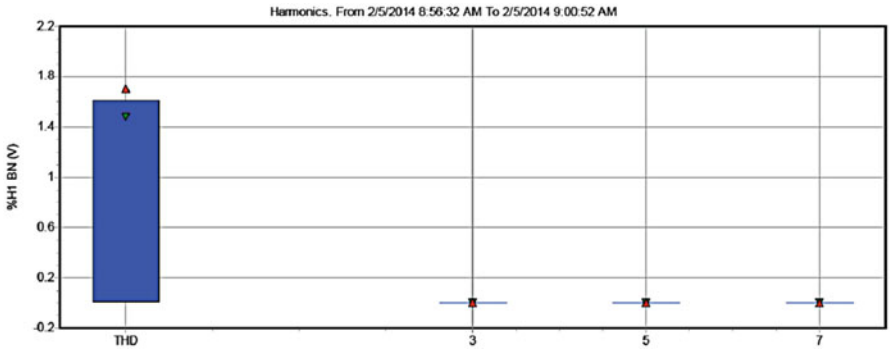

Voltage and Current. From 2/5/2014 8:56:32 AM To 2/5/2014 9:00:52 AM
A (A)
94.8
93.2
91.6
90
88.4
86.8
85.2
Arms Min
Arms Max
Arms Avg
08:57:00
08:57:30
08:58:00
08:58:30
08:59:00
08:59:30
09:00:00
09:00:30

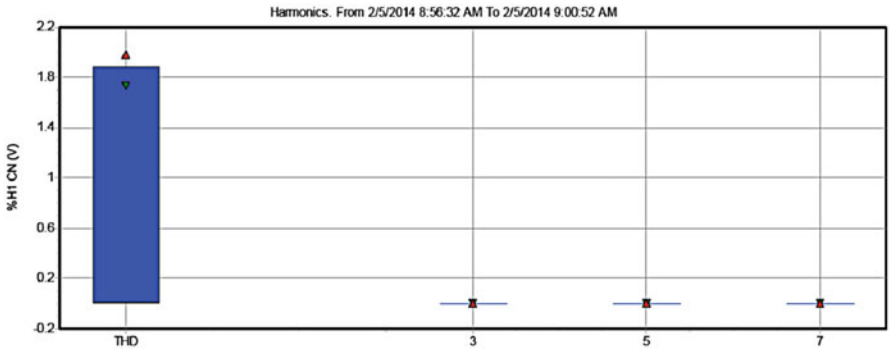

Voltage and Current. From 2/5/2014 8:56:32 AM To 2/5/2014 9:00:52 AM
B (A)
96.8
95.2
93.6
92
90.4
88.8
87.2
Arms Min
Arms Max
Arms Avg
08:57:00
08:57:30
08:58:00
08:58:30
08:59:00
08:59:30
09:00:00
09:00:30

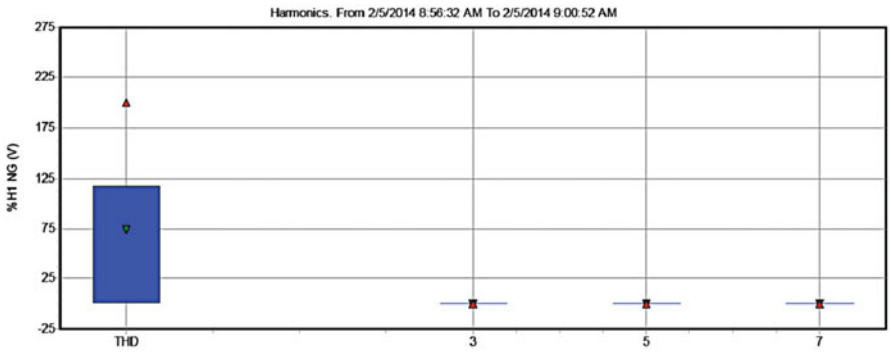

Voltage and Current. From 2/5/2014 8:56:32 AM To 2/5/2014 9:00:52 AM
C (A)
96.8
95.2
93.6
92
90.4
88.8
87.2
Arms Min
Arms Max
Arms Avg
08:57:00
08:57:30
08:58:00
08:58:30
08:59:00
08:59:30
09:00:00
09:00:30

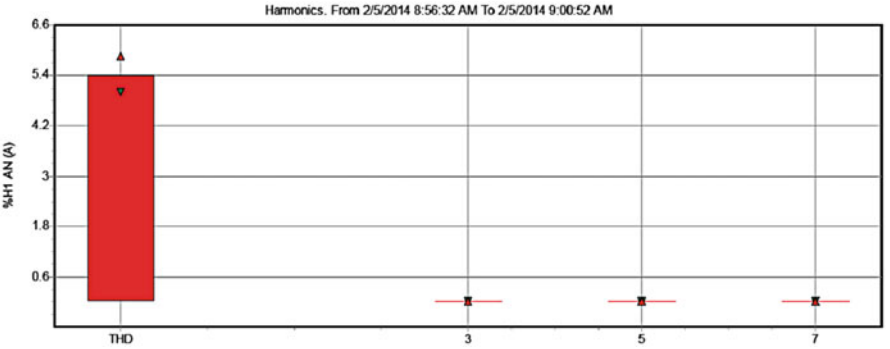

Voltage and Current. From 2/5/2014 8:56:32 AM To 2/5/2014 9:00:52 AM
N (A)
16.4
15.6
14.8
14
13.2
12.4
11.6
Arms Min
Arms Max
Arms Avg
08:57:00
08:57:30
08:58:00
08:58:30
08:59:00
08:59:30
09:00:00
09:00:30

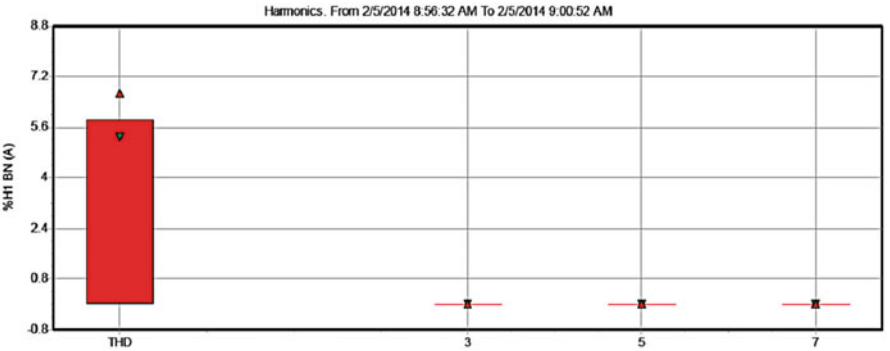

Harmonics. From 2/5/2014 8:56:32 AM To 2/5/2014 9:00:52 AM
%H1 AN (V)
2.2
1.8
1.4
1
0.6
0.2
-0.2
THD
3
5
7

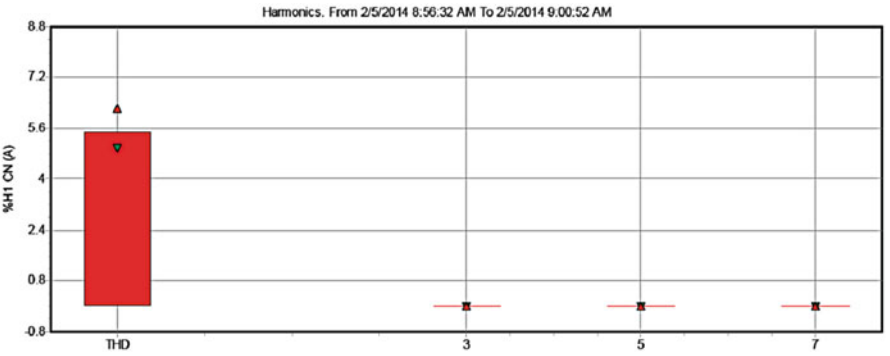

Harmonics. From 2/5/2014 8:56:32 AM To 2/5/2014 9:00:52 AM
%H1 BN (V)
2.2
1.8
1.4
1
0.6
0.2
-0.2
THD
3
5
7

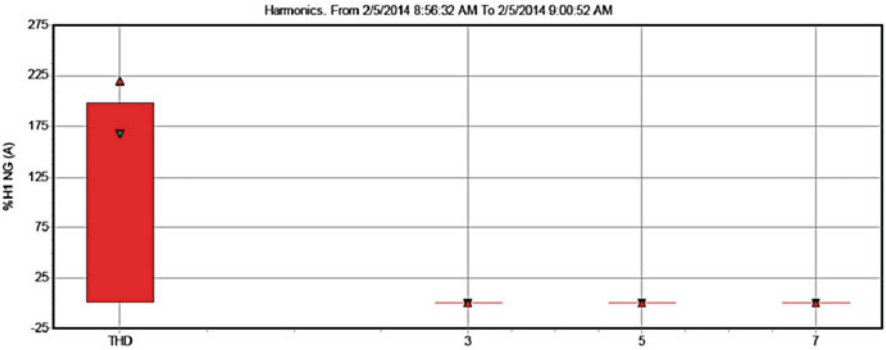

Harmonics. From 2/5/2014 8:56:32 AM To 2/5/2014 9:00:52 AM
%H1 CN (V)
2.2
1.8
1.4
1
0.6
0.2
-0.2
THD
3
5
7

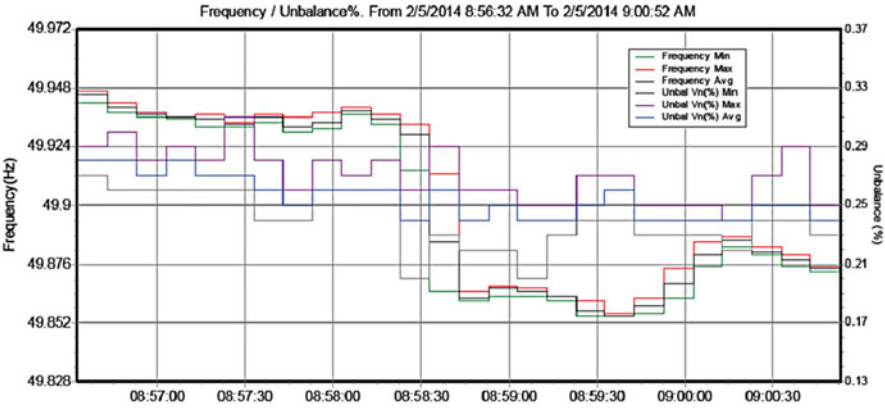

Harmonics. From 2/5/2014 8:56:32 AM To 2/5/2014 9:00:52 AM
%H1 NG (V)
275
225
175
125
75
25
-25
THD
3
5
7

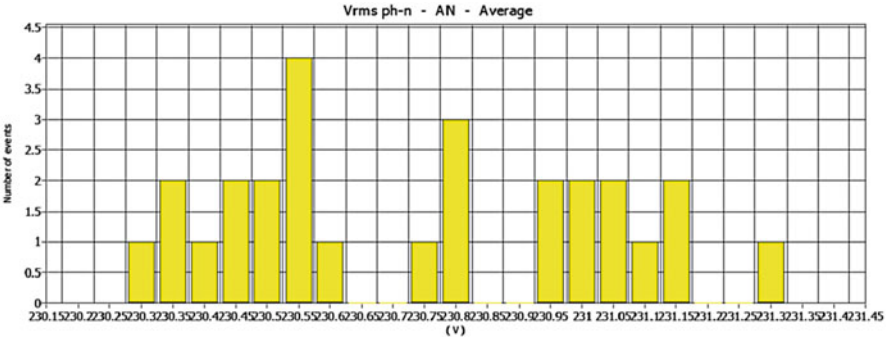

Harmonics. From 2/5/2014 8:56:32 AM To 2/5/2014 9:00:52 AM
%H1 AN (A)
6.6
5.4
4.2
3
1.8
0.6
THD
3
5
7


Harmonics. From 2/5/2014 8:56:32 AM To 2/5/2014 9:00:52 AM
%H1 BN (A)
8.8
7.2
5.6
4
2.4
0.8
-0.8
THD
3
5
7


Harmonics. From 2/5/2014 8:56:32 AM To 2/5/2014 9:00:52 AM
%H1 CN (A)
8.8
7.2
5.6
4
2.4
0.8
-0.8
THD
3
5
7


Harmonics. From 2/5/2014 8:56:32 AM To 2/5/2014 9:00:52 AM
%H1 NG (A)
275
225
175
125
75
25
-25
THD
3
5
7


Frequency / Unbalance%. From 2/5/2014 8:56:32 AM To 2/5/2014 9:00:52 AM
Frequency(Hz)
Unbalance (%)
Frequency Min
Frequency Max
Frequency Avg
Unbal Vn(%) Min
Unbal Vn(%) Max
Unbal Vn(%) Avg
49.972
49.948
49.924
49.9
49.876
49.852
49.828
0.37
0.33
0.29
0.25
0.21
0.17
0.13
08:57:00
08:57:30
08:58:00
08:58:30
08:59:00
08:59:30
09:00:00
09:00:30


Vrms ph-n - AN - Average
Number of events
4.5
4
3.5
3
2.5
2
1.5
1
0.5
0
230.15 230.2 230.25 230.3 230.35 230.4 230.45 230.5 230.55 230.6 230.65 230.7 230.75 230.8 230.85 230.9 230.95 231 231.05 231.1 231.15 231.2 231.25 231.3 231.35 231.4 231.45
(V)

Index

A
Accelerated depreciation profit, 16
AC-DC rectifier, 433
Active power control, 348
AC-type standby generator, 70
Adaptive neuro-fuzzy inference systems (ANFIS), 50, 163
Aerodynamical blades, 250
Aggregate Technical and Commercial (AT&C), 3
Agricultural practices, 43
Amager plant, 43
Anemometer, 264
ANFIS. *See* Adaptive neuro-fuzzy inference systems (ANFIS)
Animal based food consumption, 38
ANN. *See* Artificial neural networks (ANN)
Annual energy consumption, 24–25
Anti-islanding, 494
Arbitrary complexity, 49
Array power output, 62
Array reconnect voltage (ARV), 92–93
Artificial neural networks (ANN), 45–48
ARV. *See* Array reconnect voltage (ARV)
Availability based tariffs (ABT), 3
Average daily load, 86

B
Back-propagation (BP), 157
Back-to-back PWM converters, 266, 269–270
Backward pass, 171–173
  back-propagation method, 319–321
Balance-of-system (BoS), 60
Battery bank sizing, 69
Battery charging efficiency, 88
Battery energy storage program (BESS), 585
Battery gassing, 88
Battery lifetime, 87
Battery-powered device, 84
Biofuels, 18
Biomass energy, 35, 37, 38
Biomass powers, 4, 26
Blade number losses, 311
Blazing quality, 41
Boost converter, 108–111, 425–426, 480–482
BoS. *See* Balance-of-system (BoS)
BOS components, 63
Brushless Doubly-Fed induction generator (BDFIG), 278
Buck converter, 148, 443

C
Cable sizing, 64
Cabling, 64
Campbell–Stokes daylight recorder, 11
Carbon-zinc and lithium batteries, 85
Cascade boost converters, 611, 613
Cascaded deadbeat, 513–515
CEA. *See* Central Electricity Authority (CEA)
Cell voltage, 79
Central Electricity Authority (CEA), 14, 15, 32
Central Electricity Regulatory Commission (CERC), 17, 29
Centralized inverters, 104
Central Power Sector Unit, 4
Centre for Wind Energy Technology, 15
Centrifugal force, 249

© Springer International Publishing Switzerland 2015

S. Sumathi et al., *Solar PV and Wind Energy Conversion Systems*,
Green Energy and Technology, DOI 10.1007/978-3-319-14941-7

CERC. *See* Central Electricity Regulatory Commission (CERC)
Characteristic parameters for wind machine, 250
Characteristics required for dc-dc converter, 608
Charge controller, 83–96
Charge regulator, 84
Clamp-on meter, 6
Classifications of fuel cells, 600
CO_2 emissions, 18, 415, 416, 418, 599
Conventional electricity, 33
Convergence speed, 115, 129, 138
Conversion efficiency, 61, 62, 104
Coordinated energy policy, 27
Copenhagen heat network, 43
Coriolis force, 249
Correlation coefficient criterion, 241
Corrosion, 87
C-ratings, 64
CSI. *See* Current-source inverter (CSI)
Cuk converter, 405, 414
Cuk-SEPIC converters, 402, 403
Current distortion, 507
Current-source inverter (CSI), 627
Current sweep, 115, 124–125

D
Dαβ PLL. *See* Decoupled stationary reference frame PLL (Dαβ PLL)
Damping resistance, 510
Danish Energy Agency, 41
Daylight span, 11
DC-link capacitor, 266
DC-link capacitor droop control, 115, 125
DCM. *See* Discontinued current mode (DCM)
DDSRF PLL. *See* Decoupled double synchronous reference frame PLL (DDSRF PLL)
Decoupled double synchronous reference frame PLL (DDSRF PLL), 528
Decoupled stationary reference frame PLL (Dαβ PLL), 490, 501–502
Decoupled synchronous reference frame PLL (DSRF PLL), 490, 496, 498
Decoupling network, 499–501
Deep discharge protection, 93
Defuzzification, 185, 327–328, 375, 429
Defuzzifier, 49, 240
Degradation, 61
Depth of discharge (DOD), 64, 86
De-rating factor, 63, 65
DFAG. *See* Doubly fed asynchronous generator (DFAG)
DFIG. *See* Doubly fed induction generator (DFIG)
DG. *See* Distributed generation (DG)
DGS. *See* Distributed generation system (DGS)
Diesel genset, 417
Direct methanol fuel cell (DMFC), 603
DISCOMs. *See* Distribution companies (DISCOMs)
Discontinued current mode (DCM), 616
Dissect electronic circuits, 45
Distributed generation (DG), 472
Distributed generation system (DGS), 489
Distributed resources (DR), 472
Distribution companies (DISCOMs), 27, 29
DMFC. *See* Direct methanol fuel cell (DMFC)
DOD. *See* Depth of discharge (DOD)
Doubly fed asynchronous generator (DFAG), 260
Doubly fed induction generator (DFIG), 257, 260, 267
d–q components, 269
dq PLL. *See* Synchronous reference frame PLL (dq PLL)
dq-synchronous reference frame (SRF), 496
DR. *See* Distributed resources (DR)
Drive train, 253, 282, 460
DSRF PLL. *See* Decoupled synchronous reference frame PLL (DSRF PLL)
Dual DC cutoff, 68
Duty-cycle parameter, 220
Dynamic response of the fuel cell, 606
Dynamic voltage restorer (DVR), 547, 557, 561, 564, 568

E
Economic environmental dispatching (EED), 339
Eddy current, 67
Eddy losses, 311
EED. *See* Economic environmental dispatching (EED)
Effects of discharge rates, 87
Efficient energy use, 7
EIA. *See* Energy Information Administration (EIA)
EISPACK, 44
Electric voltage spike, 549
Electromagnetic energy, 11, 224
Electromagnetic torque, 269, 280
End losses, 311, 324
Energy crisis, 4–5

Energy efficiency, 2, 6–7
Energy Information Administration (EIA), 20
Energy poverty, 2
Energy storage capability and autonomy, 84
Environmentally friendly power energy corridors, 33
Equipment energy consumption, 6

F
FACTS. *See* Flexible AC transmission systems (FACTS)
Fault ride through (FRT) capability, 490
FCWT. *See* Full converter wind turbine (FCWT)
Filter capacitance, 510
Filter design, 509
Filter inductance, 509
Fire safety hazard, 62
Fitness function, 235, 237, 329
Five-layer feed-forward network, 317
Fixed capacitor, 579
Fixed-speed wind turbines, 251–252
Flexible AC transmission systems (FACTS), 355
Flicker, 476, 494, 507, 549
Fluke power quality analysers, 581
Flyback converter, 621
Footprint hypothesis, 31
Forward converter, 622
Forward pass, 170, 176
  least square estimator method, 319
Fractional open circuit voltage, 115, 119–120
Fractional short circuit current, 115, 120
Frequency disturbances, 493
FRT capability. *See* Fault ride through (FRT) capability
FRT systems, 580
Fuel cell, 597
Fuel cell stack, 600, 605, 606
Full-bridge converter, 626, 627, 645
Full converter wind turbine (FCWT), 296
Fuzzification, 49, 185, 358, 375, 429
Fuzzifier, 49, 197, 327
Fuzzy inference, 166, 168–169, 327
Fuzzy linguistic sets, 360
Fuzzy logic controller, 121–122, 197, 327–328, 331

G
GAs. *See* Genetic algorithms (GAs)
Gasification plans, 43
Gas-terminated force plants, 24
Gauging, 31
Gaussian fuzzy membership function, 168, 317
GBI. *See* Generation based incentive (GBI)
Generation based incentive (GBI), 15, 16, 28
Generator power, 329
Generator rotor speed, 329
Genetic algorithms (GAs), 51, 328–329
Gensim, 159
Gibbs free energy, 603
Global energy consumption, 19, 21
Global peak, 82
Global solar radiation, 52
Gradient descent method, 320
Gradient vector, 158, 320
Grading, 48
Green development, 13
Green energy corridor, 33
Grid-connected, 65, 66, 70
  HPS, 403
  WECS with STATCOM, 587
Grid filter, 508–510
Grid integration issues, 31–32
Grid integration of large wind farms, 477–479
Grid synchronization algorithms, 494
Grounding transformer, 303

H
Half-bridge converter, 625–626
Hard-switching supply-side inverter, 263–264
HCS control. *See* Hill-climb search (HCS) control
HDI. *See* Human Development Index (HDI)
Heat sink, 88, 666
HES. *See* Hybrid energy system (HES)
Hessian matrix, 157
High spatial variability, 223
High voltage disconnect (HVD), 92
Hill-climb search (HCS) control, 334
Horizontal-axis propeller, 250
Horizontal-axis wind turbine, 253
Horizontal turbine components, 253–254
HPS. *See* Hybrid power system (HPS)
Human Development Index (HDI), 3
HVD. *See* High voltage disconnect (HVD)
Hybrid power system (HPS), 403–404
Hydrogen-rich fuel, 598

I
Ideal switches, 103
IEA. *See* International Energy Agency (IEA)
IEEE 446-1995, 550

IEEE 465-1990, 550–551
IEEE 1100-1999, 551
IEEE 1159-1995, 551
IEEE 1250-1995, 551
IEGC. *See* Indian Electricity Grid Code (IEGC)
IG. *See* Induction machines (IG)
IGTB. *See* Insulated gate bipolar transistor (IGTB)
Incremental conductance method, 115, 117–119
Indian Electricity Grid Code (IEGC), 30
Indian Renewable Energy Development Agency (IREDA), 28
India Smart Grid Task Force (ISGTF), 33–34
Inductor-Capacitor-Inductor (LCL) filter, 490
Industrial loads, 417–418
Insolation, 10
Insulated gate bipolar transistor (IGTB), 106
Integrated cascade boost converter, 613
Interchange energy, 26
Interleaved boost converter, 614
Intermediate DC/DC converter stage, 264–266
International Electro-technical Commission (IEC), 574
International Energy Agency (IEA), 4
IREDA. *See* Indian Renewable Energy Development Agency (IREDA)
Irradiance conditions, 223, 458
ISGTF. *See* India Smart Grid Task Force (ISGTF)
Islanding, 474
Isolated converters, 620
Isolation device, 493

J
Jacobian matrix, 157

K
Kramer drive, 268

L
Land allocation policy, 31
Lawrence Berkeley National Laboratory (LBNL), 15
Laws of thought, 48
LCD. *See* Liquid crystal display (LCD)
LCL filter. *See* Inductor-Capacitor-Inductor (LCL) filter
LDR. *See* Light dependent resistors (LDR)
Lead-acid batteries, 85, 87, 89, 662
Learning process, 154
Light dependent resistors (LDR), 194
LINPACK, 44
Liquefied natural gas (LNG), 2, 3
Liquid biofuel, 38
LLCC resonant inverter, 638
Load reconnect voltage (LRV), 92–94
Local peaks, 82
Loop filter, 495
Low voltage load disconnect (LVD), 86, 92, 93
Low voltage load disconnect hysteresis (LVLH), 94
LRV. *See* Load reconnect voltage (LRV)
LVD. *See* Low voltage load disconnect (LVD)
LVLH. *See* Low voltage load disconnect hysteresis (LVLH)

M
Magneto-motive force (MMF), 272
Mamdani controller, 328
Matrix converter control, 271, 646
Matrix laboratory, 44
Maximum experimental peak output power (Pmax,e), 72
Maximum power point (MPP), 442
Maximum power point tracking (MPPT), 45, 60, 110, 403
  algorithms, 59
  controllers, 60, 334
Maximum-power remarkable points, 73
MDGs. *See* Millennium Development Goals (MDGs)
Mean square error (MSE), 157, 161
Membership functions (MFs), 51, 186, 323, 429
Metal oxide field effect transistors (MOSFET), 106, 152
MFs. *See* Membership functions (MFs)
Micro-inverters, 107–108
Millennium Development Goals (MDGs), 2
Ministry of Power (MOP), 15, 32, 34
MMF. *See* Magneto-motive force (MMF)
Modes of battery charging, 86
Modulation index, 356, 467
Module efficiency, 61
Module-level micro-inverters, 107
MOSFET. *See* Metal oxide field effect transistors (MOSFET)
Mounting structures, 63

MPP. *See* Maximum power point (MPP)
MPPT. *See* Maximum power point tracking (MPPT)
Multi-string inverters, 107

N
NAPCC. *See* National Action Plan on Climate Change (NAPCC)
NASA. *See* National Aeronautics and Space Administration (NASA)
National Action Plan on Climate Change (NAPCC), 16, 27
National Aeronautics and Space Administration (NASA), 248
National Clean Energy Fund (NCEF), 30
National Electricity Plan, 14
National Load Dispatch Centre, 29, 31
National Mission for Enhanced Energy Efficiency, 28, 34
National Sample Survey, 25
National Science Foundation (NSF), 248
NCEF. *See* National Clean Energy Fund (NCEF)
Net meters, 67
Neuro-fuzzy predictor (NFP), 238–241
Newff command, 156
New Policies Scenario, 8, 10, 13, 14, 18
NFP. *See* Neuro-fuzzy predictor (NFP)
Nickel-cadmium cells, 85
NOCT. *See* Nominal operating cell temperature (NOCT)
Nominal operating cell temperature (NOCT), 62
Nominal remarkable points, 73
Nominal short-circuit current (*I*sc,n), 72
Non conventional energy sources, 26, 33–34
NSF. *See* National Science Foundation (NSF)
Numerical weather predictions (NWP) models, 223

O
Off-grid inverter, 64
One-step control, 90
On-site electrical loads, 66
On-site load demand, 66
Open-circuit voltage/temperature coefficient (K_V), 72
Optimum point, 215, 219–221
Optional storage batteries, 417
Overcharge protection, 91

P
Pareto solutions, 345
PCC. *See* Point of common coupling (PCC)
PCC voltage, 563
PCU. *See* Power conditioning unit (PCU)
Per capita, 3, 5
Permanent magnet alternator (PMA), 297
Permanent magnet synchronous generator (PMSG), 262, 466
Perturb and observe (P&O) method, 115–117, 130, 684
Perturbation, 344
PGCIL. *See* Power Grid Corporation of India (PGCIL)
Phase detector, 495
Phase locked loop (PLL), 265, 489
Phase shift controller, 561
Phase shift control scheme, 568
Photo sensor, 194
Photosynthesis, 7
Photovoltaic diesel hybrid system, 415–416
Photovoltaics (PV)
  array, 417
  array voltage, 148
  exhibit power, 148
  inverters, 416–417
  show voltage, 148
  system costs, 65
Photovoltaic solar cells (PVSCs), 60, 201
Photovoltaic system, 65, 211
PI. *See* Proportional-Integral (PI)
PID. *See* Proportional integral derivative (PID)
PID controllers, 452–453
Pitch angle, 54
  control, 45, 290, 291, 326
Plant Load Factor (PLF), 3
PLL. *See* Phase locked loop (PLL)
αβ PLL. *See* Stationary reference frame PLL (αβ PLL)
PMA. *See* Permanent magnet alternator (PMA)
PMSG. *See* Permanent magnet synchronous generator (PMSG)
Point of common coupling (PCC), 298, 554
P&O method. *See* Perturb and observe (P&O) method
Potential electrical shock, 62
Power conditioning unit (PCU), 66, 607
Power contour, 251
Power conversion coefficient, 381
Power curves, 213, 333
Power distribution systems, 549
Power efficiency, 62

Power Grid Corporation of India (PGCIL), 15, 31, 33
Power quality (PQ)
  issues, 546
  measurement, 552
  problems, 549
Power signal feedback (PSF) control, 334
Power system harmonics, 545
Pre-set period, 90
Primary batteries, 85
Profile losses, 310–311
Proportional-Integral (PI), 291
Proportional integral derivative (PID), 54, 421
PSF control. *See* Power signal feedback (PSF) control
Pulse-width modulation (PWM) control, 91–93
Pulsing controllers, 89
Purelin, 156, 160
Push-pull converter, 623–624
PV. *See* Photovoltaics (PV)
PVSCs. *See* Photovoltaic solar cells (PVSCs)
PWM control. *See* Pulse-width modulation (PWM) control
Pyranometer, 11
Pyrheliometer, 11

Q
QGA. *See* Quantum genetic algorithm (QGA)
Quantum chromosome, 342
Quantum genetic algorithm (QGA), 339, 341–344
Quantum rotation gate, 343–344
Quasi-static model, 381–383

R
RCC. *See* Ripple correlation control (RCC)
REA. *See* Rural electric administration (REA)
Reactive power control, 261, 296, 347, 348
Real power control, 296
REC. *See* Renewable Energy Certificates (REC)
Recursive least-square method, 170, 319
Renewable Energy Certificates (REC), 16
Renewable Purchase Specification (RPS), 16, 27, 29
Renewable Regulatory Charge, 31
Renewable Regulatory Fund (RRF) mechanism, 30–31
Reverse electrolysis, 598
Reverse power flow, 473
Ripple content, 615–616
Ripple correlation control (RCC), 115, 122–123
Ripple factor, 606
Rotary phase shifter (RPS), 266, 580
Rotating mechanical power, 250
Rotor slot harmonics (RSH), 272
RPS. *See* Renewable Purchase Specification (RPS); Rotary phase shifter (RPS)
RSH. *See* Rotor slot harmonics (RSH)
Rule base, 121, 146, 149, 151, 185, 198, 204, 240, 429
Rural electric administration (REA), 248

S
SAF. *See* Sigmoid activation function (SAF)
SC. *See* Soft computing (SC)
Schmitz coefficient, 324, 325
SCIG. *See* Squirrel-cage induction generator (SCIG)
SCR. *See* Thyristor rectifier (SCR)
Seasonal efficiency, 6
Secondary batteries, 85
SEIG. *See* Self-excited induction generators (SEIG)
Selective harmonic elimination (SHE), 265
Self-commutated switching, 106
Self-discharge rate, 87
Self-excited induction generators (SEIG), 346
Self-regulating module, 95
Semiconductor Equipment and Materials International (SEMI), 551
Sensitive electronic loads, 104
Sensors, 127, 194–196
SEPIC converter, 405, 406
SERC. *See* State Electricity Regulatory Commission (SERC)
Series-interrupting, 90
SG. *See* Synchronous turbines (SG)
Shading levels, 63
SHE. *See* Selective harmonic elimination (SHE)
Short circuit current/temperature coefficient (K_I), 72
Shunt controllers, 88
Shunt-interrupting design, 89
Shunt-linear design, 89
Sigmoid activation function (SAF), 242
Single phase full-bridge inverter, 110, 631
Single-phase inverter, 109
Single switch unipolar operation, 621
Sinusoidal Pulse width modulation (SPWM), 504–505

Sliding mode control law, 268
SMPS. *See* Switched-mode power supply (SMPS)
SOC. *See* State of charge (SOC); State regarding battery charge (SOC)
SOC battery, 60
Socio-economic development, 2
Soft computing (SC), 44, 45, 52
Soft designing, 249
Solar air-conditioning system, 52
Solar arrays, 62, 211
Solar charge controllers, 84
Solar insolation, 11
Solar PV cell, 60
Solar tracking system, 53, 181
Solid-state current, 67
Solid-state switch, 89, 93
Space vector machine (SVM), 269
SPEA. *See* Strength Pareto Evolutionary Algorithm (SPEA)
SPSUs. *See* State power sector utilities (SPSUs)
SPWM. *See* Sinusoidal Pulse width modulation (SPWM)
Squirrel-cage induction generator (SCIG), 258, 276
Stable Kramer drive, 268
Stand alone/off-grid/islanding HPS, 403
Stand-alone renewable energy systems, 108
Standard Test Conditions (STC), 61, 747
STATCOM. *See* Static synchronous compensators (STATCOM)
State Electricity Regulatory Commission (SERC), 17
State Nodal Agencies, 33
State of charge (SOC), 87, 363
State power sector utilities (SPSUs), 4
State Transmission Utilities, 31
Static optimal dispatch, 339
Static synchronous compensators (STATCOM), 355, 489, 557, 579
Static synchronous series compensator (SSSC), 561
Static volt-ampere reactive compensator (SVC), 355, 579
Stationary reference frame PLL (αβ PLL), 490, 497
Stator voltage vector, 269
STC. *See* Standard Test Conditions (STC)
Strain gradient force, 249
Strategic commodity, 2
Strength Pareto Evolutionary Algorithm (SPEA), 339, 345–346
Sugarcane ethanol, 18
Superconductor synchronous condensers (AMSC), 580
Superhuman intelligence, 45
Supply surge currents, 84
Surge protectors, 60
SVC. *See* Static volt-ampere reactive compensator (SVC)
SVM. *See* Space vector machine (SVM)
Switched-mode power supply (SMPS), 425
Symmetric and asymmetric loads, 402, 404–405
Synchronization, 492
Synchronous condenser, 580
Synchronous reference frame PLL (dq PLL), 490, 496
Synchronous turbines (SG), 257
System frequency, 492

T

Takagi-Sugeno model, 174
Takagi-Sugeno type fuzzy inference system, 315
Tansig, 156, 160
TD. *See* Truth degree (TD)
Temperature, 159
  coefficient, $^{\circ}C^{-1}$, 212
  effects, 87
Terminal voltage error (eV), 351
THD. *See* Total harmonic distortion (THD)
Three phase inverters, 484, 632
Thyristor-controlled reactors (TCR), 579
Thyristor rectifier (SCR), 268
Thyristor supply-side inverter, 263
Thyristor-switched capacitor (TSC), 579
Tilting angle, 63
Tip speed ratio, 252, 327
Tip speed ratio (TSR) control, 334, 335
Topologies of unidirectional and bidirectional DC-DC converters, 608
Total harmonic distortion (THD), 410, 546, 556, 647
Tracking efficiency, 61
Tracking sensor, 194
Trainlm, 157
Trickle charging, 90
Trip time, 505
Truth degree (TD), 240
TSP. *See* Travelling salesman problem (TSP)
TSR control. *See* Tip speed ratio (TSR) control
Tweaking, 47

Twist angle, 54
Two blade systems, 250
Types of grid interfaces, 472

U
UL standards, 63
Unconventional schemes, 266–267
UNFCCC. *See* United Nations Climate Convention (UNFCCC)
Unified power flow controllers (UPFC), 355, 489
Unified Power Quality Conditioner (UPQC), 547, 568
Uninterrupted power supply, 69
United Nations Climate Convention (UNFCCC), 27
Universal bridge, 202, 298, 559
Unscheduled exchange charges, 3, 31
UPFC. *See* Unified power flow controllers (UPFC)

V
Variation of slip, 277
VCO. *See* Voltage controlled oscillator (VCO)
Vegetable food intake, 38
VFI. *See* Voltage-fed inverter (VFI)
V-I characteristics, 78
Voltage and current stabilization, 84
Voltage coefficient, 212
Voltage controlled oscillator (VCO), 495
Voltage dips (sags), 548, 549
Voltage-fed inverter (VFI), 627
Voltage ratio, 611
Voltage regulation hysteresis (VRH), 93
Voltage sags, 548, 549, 550
Voltage source converter (VSC), 263, 564
Voltage-source inverter (VSI), 264, 483–485, 489, 627
Voltage space vectors (VSV), 270
Voltage spikes, impulses/surges, 549
Voltage swells, 574–575, 582
Voltage transients, 549
V-P characteristics, 78
VR. *See* Voltage regulation (VR)
VRH. *See* Voltage regulation hysteresis (VRH)
VSC. *See* Voltage source converter (VSC)
VSI. *See* Voltage-source inverter (VSI)
VSV. *See* Voltage space vectors (VSV)

W
WECS. *See* Wind energy conversion systems (WECS)
Wind blade chord, 54
Wind capacity, 13
Wind flow speed, 251
Wind turbine technology, 3, 247
Wind velocity ratio, 252
World Energy Outlook, 14
Wound-rotor induction turbine (WRIG), 277
WRIG. *See* Wound-rotor induction turbine (WRIG)

Z
ZCD. *See* Zero crossing detector (ZCD)
ZCS. *See* Zero current switching (ZCS)
ZCT. *See* Zero current transition (ZCT)
Zero crossing detector (ZCD), 494–495
Zero current switching (ZCS), 608
Zero current transition (ZCT), 616–617
Zero voltage switching (ZVS), 608
Z-source converter, 635–636
ZVS. *See* Zero voltage switching (ZVS)